UNIVERSITÉ DE STRASBOURG

ÉCOLE DOCTORALE DES SCIENCES CHIMIQUES

UMR7200 – Laboratoire d'Innovation Thérapeutique

THÈSE présentée par :

Thiago MOREIRA PEREIRA

soutenue en co-tutelle avec UNIVERSITÉ FÉDÉRALE RURALE DE RIO DE JANEIRO le : **7 juin 2024**

pour obtenir le grade de : **Docteur de l'université de Strasbourg**

Discipline/ Spécialité : Chimie/ Chimie Biologique et Thérapeutique

Design and synthesis of trisubstituted 1,2,4-triazoles: structural exploration in the inhibition of GSK-3β for the treatment of Alzheimer's disease

THÈSE dirigée par :

Mme SCHMITT Martine	CRCE, Université de Strasbourg
M. EUGEN KÜMMERLE Arthur	Professeur, Université Fédérale Rurale de Rio de Janeiro

RAPPORTEURS :

M. SOTER DE MARIZ E MIRANDA Leandro	Professeur, Université Fédérale de Rio de Janeiro
M. DOS SANTOS FERNANDES João Paulo	Professeur, Université Fédérale de São Paulo

---

AUTRES MEMBRES DU JURY :

M. DANTAS PINHO Vagner	Professeur, Université Fédérale de Rio de Janeiro
Mme ECHEVARRIA Aurea	Professeur, Université Fédérale Rurale de Rio de Janeiro

Inventions are, above all, the result of stubborn work

Santos Dumont

To my parents, who have granted me the most precious teachings, for inspiring me and being my greatest example in life

This study was financed in part by Campus France and the Coordenação de Aperfeiçoamento de Pessoal de Nível Superior – Brasil (CAPES).

AKNOWLEDGMENTS

Before beginning the presentation of this thesis, I would like to thank everyone who has contributed in some way to making this work possible.

First and foremost, I would like to thank the members of the jury who accepted to read and evaluate this work: Mr. Leandro Soter de Mariz e Miranda, Mr. João Paulo dos Santos Fernandes, Mr. Vagner Dantas Pinho and Mrs. Aurea Echevarria.

I Thank Mr. Didier Rognan, director of the Laboratory for Therapeutic Innovation, for welcoming me to the lab. Mr. Frédéric Bihel, Director of research at the Medicinal Chemistry and Chemogenomics Group, for welcoming me to the group, and Mr. Jean-Jacques Bourguignon, Emeritus Research Director, for the warm reception and words of kindness.

A simple thank you will never be enough to express my gratitude to my advisor, Mrs. Martine Schmitt. Firstly, for accepting me to be her student in 2020 and since then being by my side throughout the entire thesis. I'm aware of how fortunate I've been to learn daily over the last almost 4 years from a researcher of the highest global level. Her knowledge, experiences, and unequivocal desire to make me a better professional are an inspiration. Moreover, she was able to guide and encourage me to move forward even in difficult times, both professionally and personally.

To my advisor, Mr. Arthur Eugen Kummerle, to whom I will be eternally grateful, I thank you for the opportunity to work alongside you over the past 11 years, for teaching me so much about the value of science, for the opportunities you provided me, for your professional excellence and multidisciplinarity, which are an example to be followed, for your patience, and, above all, for the friendship throughout this period.

I thank Mrs. Maria Laura Bolognesi and Mrs. Elisa Uliassi for the opportunity to work under their supervision during the sandwich internship at the University of Bologna.

To my colleagues at LIT, I express my gratitude, especially to Philippe Steinsoulz and Severine Schneider for their warm welcome and willingness to assist, to Patrick Wagner, Jacques Bricard, Camille Van Wesemael, Pauline Mornat, Laure Peilleron, Clothilde Le Guen, Kossi Soklou Efouako, Alexandra Hebert, Deniz Karabiyikli, and Johan Natter, for the always pleasant company.

To my colleagues at LaDMol-QM (Medicinal Chemistry and Molecular Diversity Laboratory), I extend my gratitude, especially to Natalia Nadur, for her availability to perform computational calculations, and to Lucas Caruso, Larissa Azevedo and Manuelle Cunha, for the good times shared, even though they were few during this thesis.

To my colleagues at BOMEDCHEM LAB (Bolognesi's Medicinal Chemistry Lab), I express my gratitude, especially to Bianca Martinengo, for the assistance and warm welcome, and to Anna Marta Pasieka, Aurora Gaza, Alessia Da Fermo, Rocio Chavés, Federico Sdei, Javier Recio Ramos, Viviana Mitarotonda, Diletta Perrone, Matteo Labate, Eleonora Diamanti, and Filippo Piazza for the shared moments and enjoyable conversations.

I thank Mrs. Delphine Garnier and Mrs. Estefania Oliva from the joint analysis service of the Faculty of Pharmacy of the University of Strasbourg for their availability and expertise in Nuclear Magnetic Resonance and Mass Spectrometry.

I express my gratitude to Mr. Vinicius Gomes and Mrs. Rosane Nora from the analytical center of UFRRJ for their availability to perform part of the Nuclear Magnetic Resonance and Mass Spectrometry analyses for this work.

I would like to thank Mr. Antonio Cellini and Francesca Bugamelli from the Faculty of Pharmacy of the University of Bologna for their availability to perform LC/MS analyses for this work.

I extend my gratitude to Mrs. Angela de Simone, professor at the University of Turin, for conducting the enzymatic inhibition assays against GSK-3β presented in this work.

To my friends, Kelton Rodrigues, Davi Malheiros, Beatrice Colcuc, Renato Neto, I'm grateful for the friendship and fun times.

To my parents, Selma Maria Moreira and Remi Pereira, I express my heartfelt gratitude for their love, affection, and for teaching me the importance of study and hard work. Both have always gone above and beyond to invest in my personal and professional development.

To my siblings, Thaiane Moreira Pereira and Remi Cunha, I thank you for your encouragement and for the long conversations about life and future aspirations.

To my relatives, Nicolas Pereira, Regina Rosa, Lara Pereira, Silma Moreira, Pedro Henrique, Celia Regina, Carol Pereira, Claudio Moreira, and all others, I express my gratitude for the peaceful and enjoyable family life we share.

I Thank CAPES, Campus France, UNISTRA and UFRRJ for the financial and academic support provided for the realization of this research.

Université de Strasbourg

Thiago MOREIRA PEREIRA

École doctorale Sciences chimiques | ED 222 Université de Strasbourg

Design and synthesis of trisubstituted 1,2,4-triazoles: structural exploration in the inhibition of GSK-3β for the treatment of Alzheimer's disease

Actuellement, 55 millions de personnes dans le monde vivent avec la démence, et près de 10 millions de nouveaux cas sont recensés chaque année. La démence résulte de maladies affectant le cerveau, la plus courante étant la maladie d'Alzheimer, liée à des phénomènes tels que la formation de filaments insolubles et d'agrégats protéiques. L'inhibition de la GSK-3β, une kinase impliquée dans ces processus délétères, a montré des résultats prometteurs *in vivo*, s'imposant ainsi comme une approche thérapeutique potentiellement modifiant l'évolution de la maladie. Dans cette étude, nous avons conçu trois séries de 1,2,4-triazoles en tant qu'inhibiteurs de la GSK-3β. Les voies de synthèse ont été optimisées avec succès, et les tests *in vitro* ont identifié un composé chef de file. La série présentant le meilleur profil a servi de base à la conception et à la synthèse de nouveaux dégradeurs de GSK-3β (PROTACs).

Nous avons aussi exploré la diversité des hétérocyles 1,2,4-triazoles par couplages croisés utilisant le Pd et le Cu et une cyanation écocompatible utilisant un complexe de cuivre.

Mots-clés : Alzheimer, 1,2,4-triazole, GSK-3β, couplage croisé, PROTAC, cyanation.

Currently 55 million people live with dementia worldwide with nearly 10 million new cases every year. Dementia results from various diseases affecting the brain, the most common being Alzheimer's disease (AD), which is caused by factors such as the formation of insoluble filaments and protein aggregates. Inhibition of GSK-3β, a kinase involved in many of these deleterious factors, has shown promising *in vivo* results, emerging as a potentially disease-modifying therapeutic class. In this work, we designed three series of 1,2,4-triazoles as GSK-3β inhibitors. The synthetic pathways were successfully developed, and the compounds tested *in vitro* revealed a hit compound. The series with the best profile was then used to design and synthesize new GSK-3β degraders (PROTACs).

We also explored the molecular diversity of the 1,2,4-triazole nucleus through various metal-catalyzed cross-coupling reactions and an eco-friendly copper-catalyzed cyanation reaction in aqueous medium.

Keywords: Alzheimer, 1,24-triazole, GSK-3β, Cross-coupling, PROTAC, cyanation.

ABREVIATION LIST

Acac	Acetylacetone
ACh	Acetylcholine
AChE	Acetylcholinesterase
EtOAc	Ethyl acetate
AD	Alzheimer's disease
ADP	Adenosine diphosphate
Ar	Aromatic
ATP	Adenosine triphosphate
Aβ	Amyloid β
BACE 1	β-secretase enzyme
BBB	Blood–brain barrier
BINAP	(*R*)-(+)-2,2′-Bis(diphenylphosphino)-1,1′-binaphthalene
BippyPhos	5-(Di-*tert*-butylphosphino)-1′, 3′, 5′-triphenyl-1′*H*-[1,4′]bipyrazole
Bn	Benzyl
Boc	Tert-butyloxycarbonyl
BoMedChem Lab	Bolognesi's Medicinal Chemistry Laboratory
br	Broad
Brettphos	2-(Dicyclohexylphosphino)3,6-dimethoxy-2′,4′,6′-triisopropyl-1,1′-biphenyl
BuChE	Butyrylcholinesterase
CAS	Catalytic site
Cat	Catalyst
ChaT	Colina Acetil Transferase
cPen	Cyclopentyl
d	Doublet
DCM	Dichloromethane
DIPEA	*N*-Ethyldiisopropylamine
DMCyDA	(1S,2S)-N1,N2-dimethylcyclohexane-1,2-diamine
DME	Dimethoxyethane
DMF	Dimethylformamide
DMSO	Dimethyl sulfoxide

Dppf	1,1′-Ferrocenediyl-bis(diphenylphosphine)
EDC.HCl	3-Dimethylamino-propyl)-ethyl-carbodiimide Hydrochloride
Eq.	Equivalent
ESI	Electrospray
EtOH	Ethanol
FDA	Food and Drug administration
FGI	Functional Group Interconversion
g	Grams
GSK	Glycogen Synthase Kinse
GSK-3β	Glycogen Synthas Kinase 3β
h	Hours
het	Heterocycle
HOBt	1-hydroxybenzotriazole
HPLC	High performance Liquid Chromatography
IC_{50}	Half maximal inhibitory concentration
IL	Interleukin
*i*Pr	Isopropyl
J	Coupling constant
LaDMol-QM	Medicinal Chemistry and Molecular Diversity Laboratory
LC-MS	Liquid chromatography/mass spectrometry
LIT	Laboratory for Therapeutic Innovation
MAO	Monoamine oxidase
MeCN	Acetonitrile
MeOH	Methanol
MePh	Toluene
min.	Minutes
mL	Milileter
mmol	Milimole
mol%	Mole percentage
MOMCl	Methoxymethyl chloride
nd	Not determinated
NFTs	Neurofibrillary tanlges
NMDA	N-methyl-D-aspartate
NMR	Nuclear Magnetic Resonance

Np	Nanoparticles
$Pd(OAc)_2$	Palladium (II) acetate
$Pd_2(dba)_3$	Tris(dibenzylideneacetone)dipalladium (0)
PDB	Protein Data Bank
PE	Petroleum ether
Ph	Phenyl
pH	Potential of Hydrongen
PM6	Parameterization Method 6
ppm	Parts per million
Ptau	Tau protein
q.	quadruplet
r.t.	Room temperature
ROS	Oxygen reactive species
SAR	Structure-Activity relationship
S_NAr	Aromatic Nucleophilic Substitution
S-Phos	2-Dicyclohexylphosphino-2′,6′-dimethoxybiphenyl
t	Triplet
*t*Bu	*tert*-butyl
t-BuxPhos	2-Di-*tert*-butylphosphino-2′,4′,6′-triisopropylbiphenyl
t-BuDavePhos	2′-(Di-tert-butylphosphino)-N,N-dimethylbiphenyl-2-amine
TFA	Trifluoroacetic acid
THF	Tetrahydrofuran
T*i*PSCl	2,4,6-Triisopropylbenzenesulfonyl chloride
TLC	Thin layer chromatography
TPGS	Tocopherol polyethylene glycol succinate
WHO	World and Health Organization
XantPhos	4,5-Bis(diphenylphosphino)-9,9-dimethylxanthene
$[(cinnamyl)PdCl]_2$	Palladium(1-phenylallyl)chloride dimer
°C	Degree Celsius
µL	Microliter
µW	Microwave

PREFACE

Nitrogen-containing heterocycles still remain the main source for the development of therapeutic tools. Among the major heterocycles are the triazoles, which occur in two forms: 1,2,3- and 1,2,4-triazole. Both possess one nitrogen similar to pyrrole and two nitrogens similar to pyridine. The 1,2,4-triazole is the most important of the two forms because it is the basis of the best modern agricultural fungicides, as well as medications for fungal diseases in humans.

Historically, the Laboratory of Therapeutic Innovation (LIT) at the University of Strasbourg (France) has been involved in the chemistry and pharmacology of nitrogen-containing heterocycles. At the same time, the laboratory is interested in metal-catalyzed cross-coupling reactions (Suzuki-Miyaura reaction, Sonagashira coupling, Buchwald-Hartwig reaction and Ullmann reaction) for the introduction of various substituents through the formation of CC and CN bonds. The use of these methodologies has revolutionized the tools available for drug development in the structural design, particularly in the structural optimization. In the last years, the LIT has developed studies on reactivity in molecular frameworks (mono and polycyclic) and its decoration (substitutions distributed throughout the molecular framework). Additionally, Dr. Martine Schmitt, researcher at LIT, idealized and carried out the transposition of many of these reactions commonly performed in organic solvents to water using surfactants. The micellar medium produced by the surfactants is consistently effective in conducting this type of reaction and is more in line with Green Chemistry principles.

For the rational design of new drug candidates, it is essential to start from knowledge about a molecule (endogenous ligand, inhibitor described in publication or patent, or molecule resulting from virtual screening) or about the biological target (enzymes, ion channels, or DNA). In recent years, Prof. Dr. Arthur Eugen Kummerle, coordinator of the Laboratory of Molecular Diversity and Medicinal Chemistry (LaDMol-QM) at the Federal Rural University of Rio de Janeiro (Brazil), has reported on the design, synthesis, and pharmacological evaluation of cholinesterase inhibitors for the treatment of Alzheimer's Disease (AD). Among the main types of inhibitors described are 3-amino-1,2,4-triazoles derivatives. Therefore, we decided to apply the same rational and effective approach for the design trisubstituted 1,2,4-triazoles as GSK-3β inhibitors.

GSK-3β is a kinase involved in many activities related to AD (Aβ protein deposition, p-Tau hyperphosphorylation and neuroinflammation) and up until 2022, only four research groups had reported pharmacological inhibition assays against GSK-3β (China (2), Germany

(1), Italy (1)) aiming to search new drug candidates for AD. The possibility of performing organic synthesis and concomitant inhibitory assays against GSK-3β motivated us to make a sandwich internship in Bologna's Medicinal Chemistry Lab (BOMEDCHEM), based at the University of Bologna (Italy) and coordinated by Prof. Dr. Maria Laura Bolognesi, who has extensive experience in searching for new drug candidates for AD. Currently, her research group has been centrally dedicated to the development of Proteolysis Targeting Chimeras (PROTACs) as protein degradation agents for the treatment of neurodegenerative and neglected diseases.

Summary plan of this thesis:

Chapter I: Development of synthesis procedure and molecular diversity exploration of the 1,2,4-triazole nucleus through metal-catalyzed cross-coupling reactions (Suzuki-Miyaura, Sonagashira, Buchwald-Hartwig, and Ullmann reactions).

Chapter II: Desing, synthesis and pharmacological evaluation of three series of trisubstituted 1,2,4-triazoles against GSK-3β.

Chapter III: Design and synthesis of a series of PROTACs as GSK-3β degraders.

Chapter IV: Development of a copper-catalyzed cyanation reaction using a non-toxic cyanide source in aqueous Medium.

CHAPTER I

SYNTHESIS AND MOLECULAR DIVERSITY EXPLORATION OF 1,2,4-TRIAZOLES

Although 1,2,4-triazoles are widely described in the literature with many applications in medicine and technology, the synthesis of polysubstituted 1,2,4-triazoles remains underexplored. One of the main reasons for this may be the lack of more convergent synthetic derivatization methodologies. In this chapter, we will describe the synthesis and exploration of the 1,2,4-triazole nucleus, mainly through metal-catalyzed cross-coupling reactions (Suzuki-Miyaura, Buchwald-Hartwig, and Ullmann reactions).

1. INTRODUCTION

Triazoles are aromatic heterocyclic compounds (molecular formula = $C_2H_3N_3$), which are characterized by a five-membered ring comprising three nitrogen and two carbon atoms.[1] Thus far, triazoles are exclusively obtained *via* synthesis because there are no indications of their natural occurrences.[2]

These compounds exhibit two isosteric forms (1,2,3-triazoles and 1,2,4-triazoles) based on the position of the three nitrogen atoms.[3] Each isosteric form exhibits three tautomers that differ according to the position of the hydrogen atom; however, the structures of the proton in the position five of the triazole core (**3** and **6**) are non-aromatic and are rarely mentioned in the literature (Figure 1).[4,5]

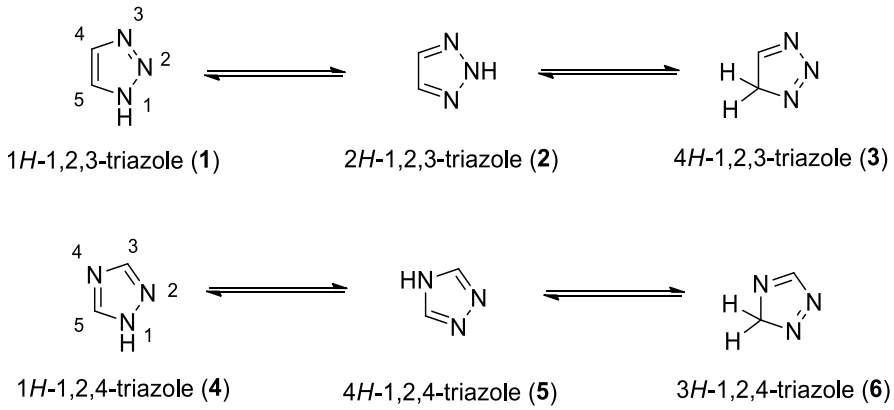

Figure 1. Chemical structures of 1,2,3-triazoles and 1,2,4-triazoles and their tautomers (**1**-**6**).

The aromaticity and high electron density of the triazole allow it to engage in various weak interactions, such as hydrogen bonding, ion-dipole, cation-π, hydrophobic effect, van der Waals force, and coordination, enabling its use in various fields of science.[6] Additionally, the triazole ring is also an important isostere of oxazole, thiazole, imidazole, pyrazole, and so forth.[7]

1,2,4-triazole derivatives exhibit a wide range of applications in medicinal, agricultural, supramolecular, and materials sciences. In medicinal chemistry, this heterocycle is used as an isostere of the cis amide bond both to mimic peptides and for drug development, resulting in the optimization of the pharmacological properties of the corresponding compound.[8,9] The triazole ring also allows its derivatives to easily interact with a variety of enzymes and receptors in the biological system, this results in a wide range of biological activities,[10] such as anti-inflammatory,[11–13] antibacterial,[14–17] antifungal,[18,19] antiviral,[20] anticancer,[21] antioxidant,[22–24] antitubercular,[25] anticonvulsants,[26] anti-nociceptive,[12] as well as CNS-stimulating, antidepressants,[27,28] and antianxiety properties.[29,30] To date, many drugs, including alprazolam (**7**), fluconazole (**8**), voriconazole (**9**), ribavirin (**10**), rizatriptan (**11**), estazolam (**12**), vorozole (**13**), anastrozole (**14**), and letrozole (**15**), containing the 1,2,4-triazole moiety have been extensively employed in clinics. In agriculture, 1,2,4-triazoles exhibit insecticidal and plant growth-regulating activities, as evidenced in cafenstrole (**16**), metosulam (**17**), azafenidin (**18**), carfentrazone-ethyl (**19**), and sulfentrazone (**20**) (Figure **2**).

Similarly, 1,2,3-triazole-based compounds have been extensively employed as agrochemicals,[31,32] dyes,[33,34] corrosion inhibitors, [35–37] photostabilizers,[38] dendrimers,[38–40] liquid crystals,[41–43] and metal chelators.[44,45] Additionally, 1,2,3-triazoles exist generally as the core structures of many compounds exhibiting broad biological activities,[10] such as anti-HIV,[46–48] anticancer,[49,50] antiprotozoal,[51,52] antimicrobial,[53,54] antifungal,[55,56] and neuroactive agents.[57,58] However, only a few molecules contain 1,2,3-triazole moieties in the market or the last phase of clinical trials. Cefatrizine (**21**) and tazobactam (**22**) account for some of the already commercialized drugs exhibiting such a ring system (Figure 2).

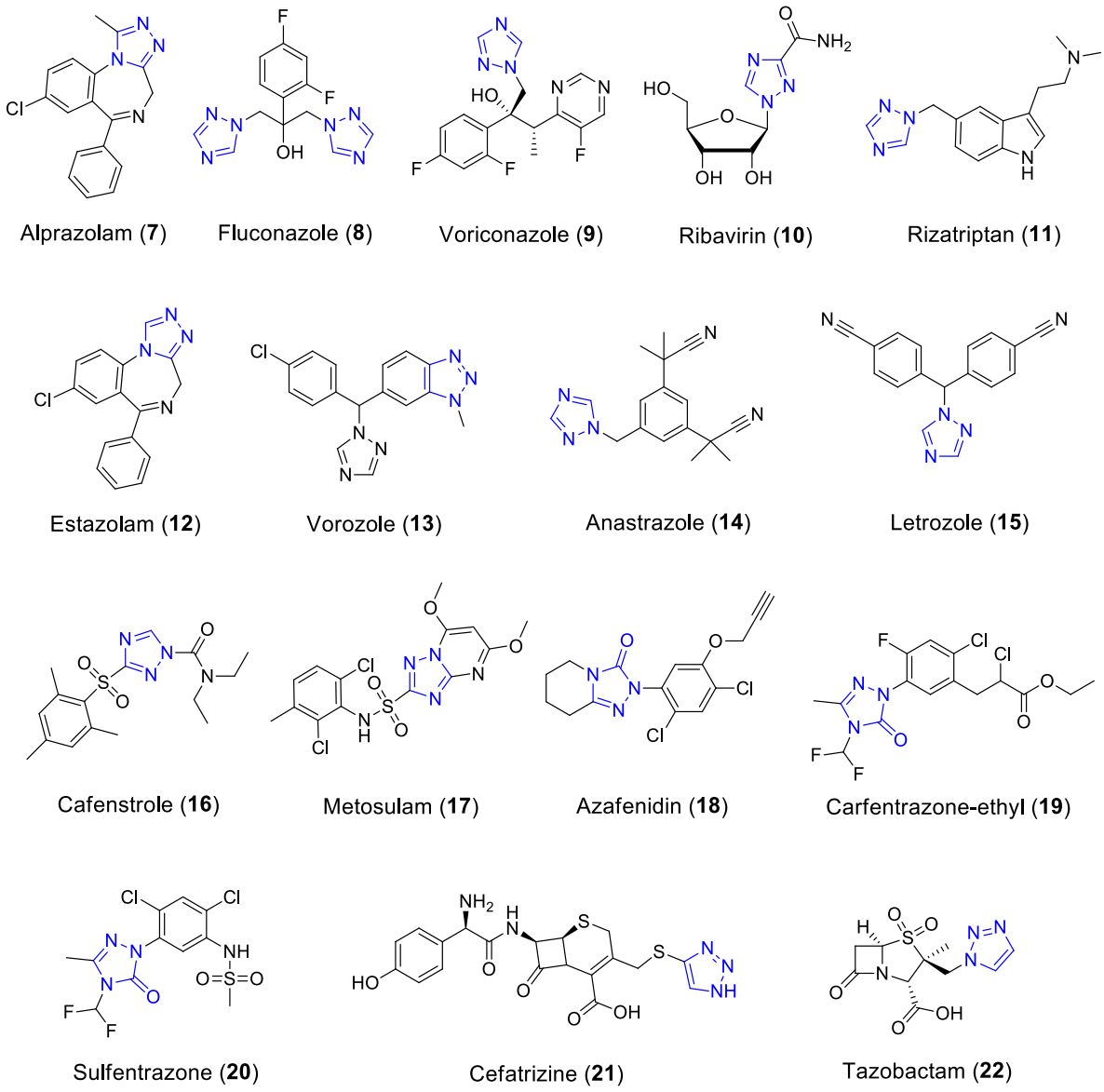

Figure 2. Approved drugs and agrochemicals containing triazole nucleus (**7-22**).

A literature search performed in Scopus® on June 20, 2021, revealed that the 1,2,4-triazole system with 14,002 publications (containing the keywords "1,2,4-triazole") is the most studied compared with the 8,333 publications related to the other system (containing the keywords "1,2,3-triazole"). However, there has been significantly increased research on 1,2,3-triazoles since the past 20 years[59] probably owing to the advent of "click chemistry."

1.1. 1,2,4-triazoles and bibliographical information on their synthesis

1,2,4-triazoles are heterocycles that have been increasingly considered owing to their potential applications in science and technology. Similar to the 1,2,3-triazole isomer, these

heterocycles are amphoteric (they are considered weak bases and acids (p*K*a = 10.26 and p*K*aH = 2.19). Both carbon atoms in 1H-1,2,4-triazoles are π-deficient because they are attached to electronegative nitrogen atoms. The low electron density on these carbon atoms makes them susceptible to nucleophilic substitution under mild conditions. On the other hand, electrophilic substitution occurs exclusively at the nitrogen atoms due to their high electron density.[60] These heterocycles occupy a central position in modern heterocyclic chemistry, principally because this heterocyclic ring is an important recognition element in biologically active molecules. Consequently, new and efficient methods for the preparation of this important heterocyclic ring system are of contemporary interest.[61]

The synthesis methods of 1,2,4-triazoles mainly uses amidine, amide, amidine amide, amidine hydrazones, aryldiazoniums salts and hydrazone as nitrogen sources. During the last few years, they have been excellent progress in copper-catalyzed cross couplings in the synthesis of 1,2,4 triazoles with inexpensive, low toxic, and goof functional tolerance. Some exemples of preparation of 1,2,4-triazoles are given below:

a) **Amidine as nitrogen source**

Amidine was widely used as an organic catalyst and ligand for the formation of nitrogen–carbon bonds due to the reactivity of nucleophilic nitrogen atoms. In 2011, a general method had been developed **via** one-pot, two-step process for the production of 1,3,5-trisubstituted-1,2,4-triazoles (**27**) with excellent yield (up to 90%). The sequence started with the *in situ* formation of acylamidine (**25**) from carboxylic acid (**23**) and primary amidine (**24**). Acylamidine (**25**) further reacted with monosubstituted hydrazine (**26**) and cyclized to trisubstituted triazole **(27**). This method had the advantages of high regioselectivity and good tolerance of functional groups (Scheme 1).[62]

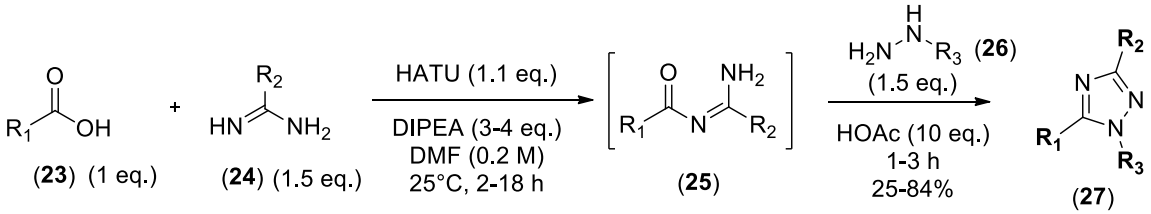

Scheme 1. Synthesis of trisubstituted 1,2,4-triazole series (**27**) with amidine (**24**) as nitrogen source.

In 2015, Huang described an $CuCl_2$ promoted synthesis 1,3-disubstituted-1,2,4-triazoles (**29**) in high yield (85%) under the presence of $CuCl_2$ and DMF using K_3PO_4 as base, O_2 as

oxidant, amidine (**28**) and DMF as raw materials. In fact, nitrogen atoms and methyl groups from DMF were incorporated into the triazole (Scheme 2).[63]

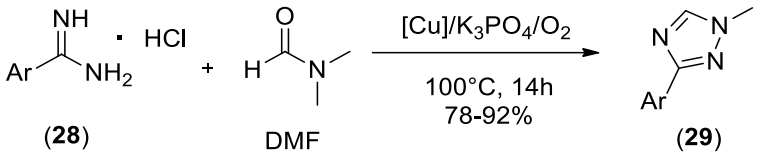

Scheme 2. Synthesis of 3-Ar-1,2,4-triazole series (**29**) with amidine (**28**) as nitrogen source.

More recently, in 2019, Xia developed a facile copper-catalyzed one-pot method to prepare 3,5-disubstituted-1,2,4-triazole (**32**) from amidine (**30**) and nitrile (**31**) by cascade addition oxidation cyclization. In this reaction, O_2 was used as an oxidant, and 1,10-phenanthroline-functionalized MCM-41-supported copper(I) complex [Phen-MCM-41-CuBr] with high yields (Scheme 3).[64]

Scheme 3. Synthesis of 1,2,4-triazole derivatives (**32**) using amidine (**30**) as nitrogen source.

b) Amide as nitrogen source

In 2016, Guirado proposed a simplified method for the synthesis of 3-aryl-1,2,4-triazole (**36**), which was obtained via the reaction of benzamide (**33**) with chloral hydrate in high yield.[65] When chloralamides (**34**) reacted with the mixture of phosphorus pentachloride/phosphorus oxychloride, almost quantitatively converted to *N*-(1,2,2,2-tetrachloroethyl)benzimidoyl chlorides (**35**), which were then handled with hydrazine hydrate to produce 3-aryl-1,2,4-triazoles (**36**) in high to quantitative yields (Scheme 4).[65]

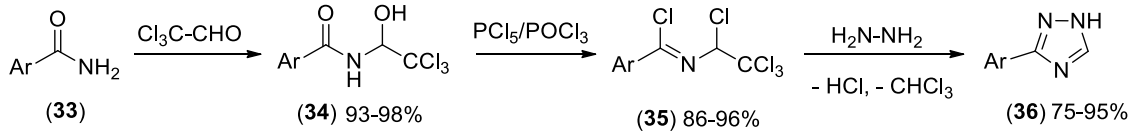

Scheme 4. Synthesis of 1,2,4-triazole derivatives (**36**) using amide (**33**) as nitrogen source.

c) Imidates as nitrogen source

Imidates are helpful precursors of triazoles, which have been extensive wielded in this field. In 2018, Azzouni et al. focused on the production of vinylimidates (**37**) that cyclize with hydrazines (**38**) for the synthesis of functionalized 1,2,4-triazoles (**39**). The method allowed a large array of substituents to be installed at (N_1, C_3, and C_5) positions of 1,2,4-triazole with good yield (98%) (Scheme 5).[66]

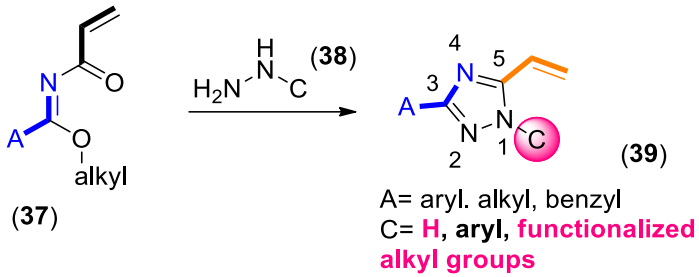

Scheme 5. Synthesis of 1,2,4-triazole derivatives (**39**) with imidate (**37**) as nitrogen source.

d) Amidrazone as nitrogen source

A series of 3,4,5-trisubstituted 1,2,4-triazoles have been synthesized from N 3-substituted amidrazones and anhydrides using $HClO_4$-SiO_2 at 80 °C under solvent-free conditions. The products were obtained with moderate to high yields (55-95%) (Scheme 6).[67]

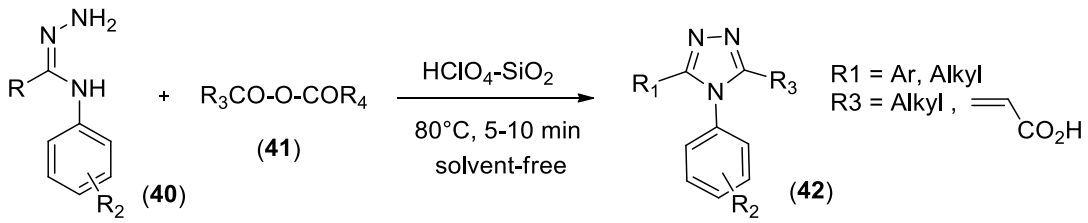

Scheme 6. Synthesis of 1,2,4-triazole derivatives (**42**) with amidrazone (**40**) as nitrogen source.

In 2014, Vidavalur et al. developed a similar method via using ceric ammonium nitrate (CAN) oxidative cyclization synthesis of 3,4,5-trisubstituted-1,2,4-triazole in polyethylene glycol (PEG) with good to excellent yield from 61% to 97%.[68] In this reaction, CAN was not only an oxidant, but also a Lewis acid (Scheme 7).

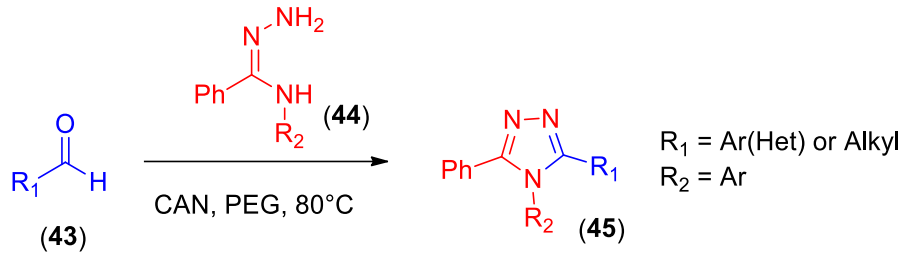

Scheme 7. Synthesis of 1,2,4-triazole derivatives (**45**) with amidrazone (**44**) as nitrogen source.

e) Aryl diazonium salts as nitrogen source

Aryldiazonium salts,[69–72] which are versatile and readily accessible 'N–N' synthons, have been utilized for the synthesis of 1,2,4-triazoles. As an illustration, a catalyst-dependent regioselective [3 + 2] cycloaddition of isocyanides with aryl diazonium salts was reported in 2018 by Liu and al in 2018. 1,3-Disubstituted 1,2,4-triazoles were selectively obtained in high yield under Ag(I) catalysis, whereas 1,5-disubstituted 1,2,4-triazoles were formed by Cu(II) catalysis (Scheme 8).[73]

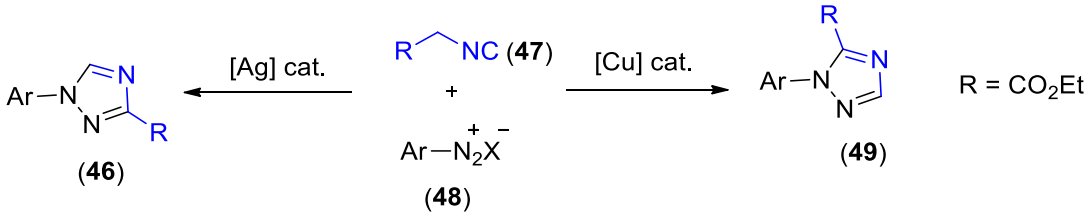

Scheme 8. Synthesis of 1,2,4-triazole derivatives (**49**) with Aryl diazonium (**48**) as nitrogen source.

More recently, in 2020, Tian and al developed the synthesis of 1,2,4-triazole by decarboxylation and cyclization of 2-aryl-2-isocyanate with aryl diazonium salts (Tian et al., 2020). In this metal-free reaction, the use of 1,4-diazocyclic [2.2.2]octane (DABCO) as a weak base was extremely critical (Scheme 9).[74]

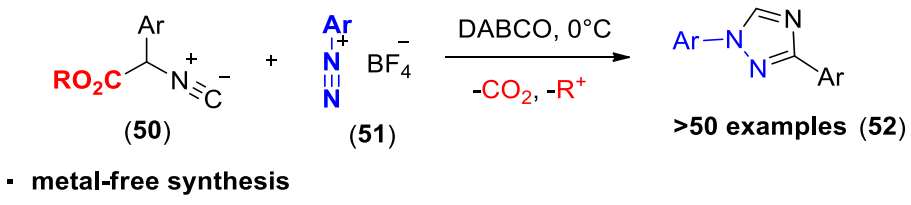

Scheme 9. Synthesis of 1,2,4-triazole derivatives (**52**) with Aryl diazonium (**51**) as nitrogen source.

f) Hydrazones as nitrogen source

In 2016, Chen *et al* developed a metal-free mediated synthesis of 1,3,5-trisubstituted 1,2,4-triazoles from hydrazones and aliphatic amines under aerobic oxidative conditions. The reaction proceeds through a cascade C–H functionalization, double C–N bonds formation, and oxidative aromatization sequence. A wide range of functional groups were well tolerated in hydrazone and amine fragments for the synthesis of multiple compounds (Scheme 10).[75]

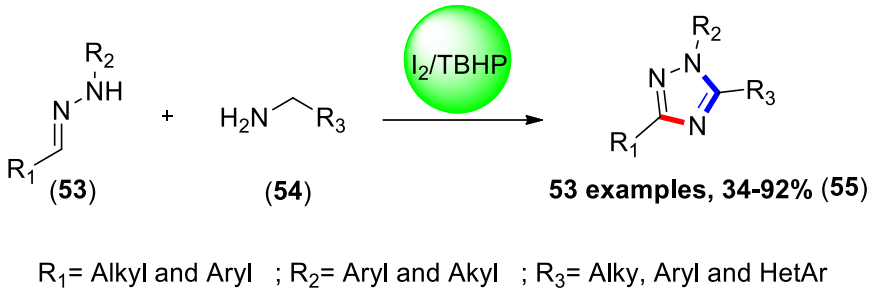

Scheme 10. Synthesis of 1,2,4-triazole derivatives (**55**) with hydrazones (**53**) as nitrogen source.

Finally, in 2019, Guru et al. described a metal-free catalytic method for dehydrogenation cyclization based on $B(C_6F_5)_3$ (Guru et al., 2019). $B(C_6F_5)_3$ activated the hydrazine portion nucleophilic attack in progress, following in proper order amination, intramolecular cyclization and dehydrogenation steps to prepare the 3,4,5-tsubstituted-1,2,4-triazole with up to 85% yield (Scheme 11).[76]

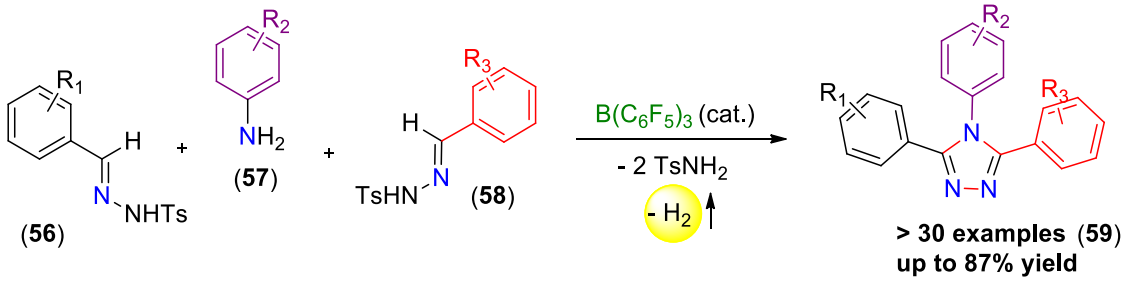

Scheme 11. Synthesis of 1,2,4-triazole derivatives (**59**) with hydrazones (**56**) as nitrogen source.

As we have already noted, these different synthetic methods lead to 1,2,4 mono, di- and even trisubstituted triazoles. The main substituents are alkyles, functionalized alkyles and aryles or heteroaryles.

Over the last few decades, the amino-triazole family of drugs has also been the subject of an increasing amount of research and two chemical families are to be considered: the 3-

amino-1,2,4-triazoles and 5-amino-1,2,4-triazoles. Biological evaluation and the main preparation methods known to date will be discussed in the following paragraphs.

1.1.1. 3-Amino-1,2,4-triazoles

Over the last decades, increased research has been devoted to amino triazoles drugs. 3-Amino-1,2,4-triazole and its derivatives have been the subject of numerous studies because of the many reported applications in the fields of medicinal and agrochemistry. Compounds containing the 3-amino-1,2,4-triazole core have been described in the literature MALT inhibitor (**60**),[77] a7nAChR alosteric receptor modulator (**61**),[78] DGAT1 inhibitor (**62**),[79] NPY receptor modulator (**63**),[80] antiinflammatory agent (**64**),[81] PDE10 inhibitor (**65**),[82] anti-lung-cancer (**66**),[83] OTR antagonist (**67**)[84] and antibiotic (**68**)[85] (Figure 3).

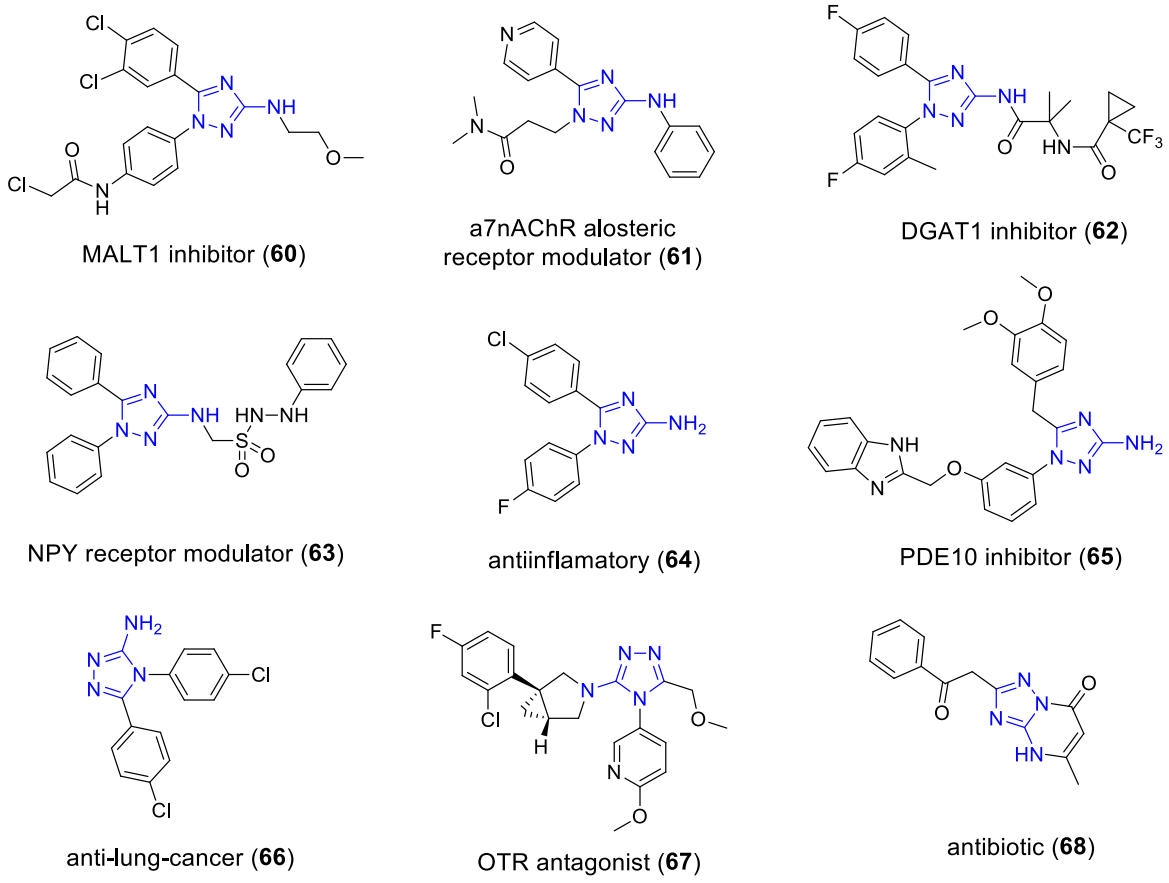

Figure 3. Examples of disubstituted 3-amino-1,2,4-triazoles with biological activities.

Several procedures have already been described for the synthesis of general 3-amino-1H-1,2,4-triazoles, with great attention to solid phase, microwaves and combinatorial synthesis.[86–89] However, the synthesis of the polyfunctionalized 3-amino-1,2,4-triazole is still underexplored. The first methodology described by Katritzky[90] and adapted for solid-phase synthesis by Houghten[91] involves the synthesis of 1,5-diaryl-3-amino-1,2,4-triazoles (**73**) through a cyclization reaction between an electrophilic species (N-acylguanidines derived from benzotriazole or N-acyl carbamidothioate) (**69**) and a nucleophilic one (substituted alkyl or aryl hydrazines) (**70**). However, this reaction requires long reaction times and low yields when both substrates carry aryl substituents. Moreover, in many cases, it is unable to produce unsubstituted 3-N,N-amino triazole derivatives (Scheme 12).

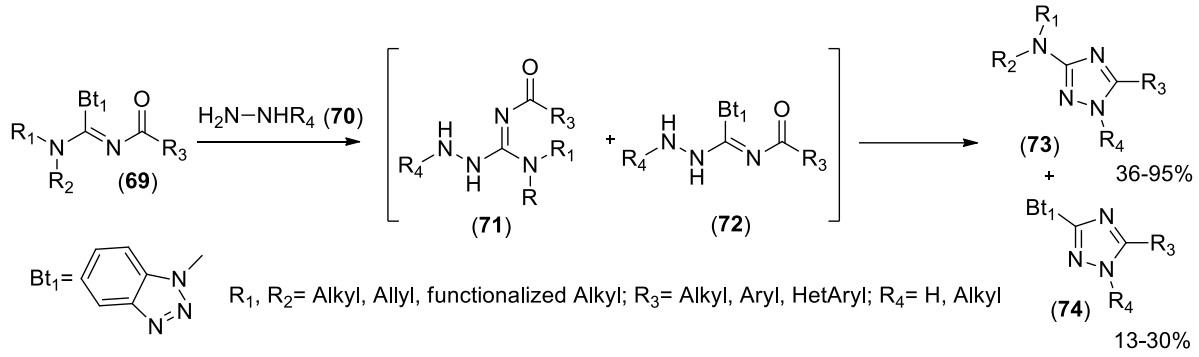

Scheme 12. Synthesis of 3-amino-1,2,4-triazole derivatives **73**.

The second methodology, described by Szilagyi, involves the reaction between the 1,3,4-oxadiazolium perchlorate (**75**) and cyanamide. Despite achieving better scope and reaction yields compared to the Katritzky method, the explosive nature of perchloric acid and perchlorate salts renders this methodology dangerous and unsuitable for synthesis on a larger scale (Scheme 13).[81]

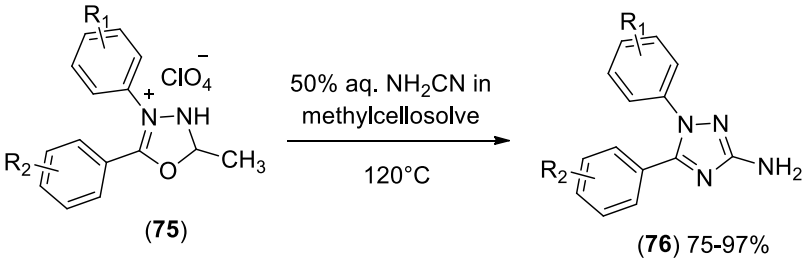

Scheme 13. Synthesis of 3-amino-1,2,4-triazole derivatives (**76**).

The third procedure was recently described by Shen, in which carbon arylation of amino-triazoles (**77**) is achieved through a Negishi coupling. Despite the good yields and described scope, the high cost of this reaction and its drastic conditions in the final deprotection (6 M H_2SO_4, 80°C, 16h) limit its applicability in some cases (Scheme 14).[92]

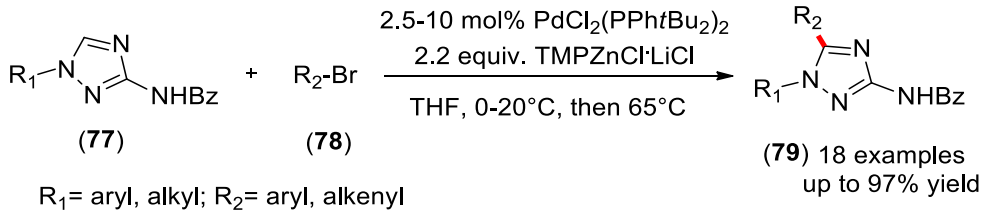

Scheme 14. Synthesis of 3-amino-1,2,4-triazole derivatives (**79**) through Negishi coupling.

Finally, our group in Brazil developed a simple regioselective synthesis protocol for obtaining N-protected or unprotected 1,5-diaryl-3-amino-1,2,4-triazoles (**82** and **83**), through the optimization of the Katritzky procedure using N-acyl-N-Boc-carbamidothioates (**80**) and phenylhydrazines (**81**) under microwave irradiation. This method yielded good yields and shorter reaction times for various aromatic compounds (Scheme 15).[93]

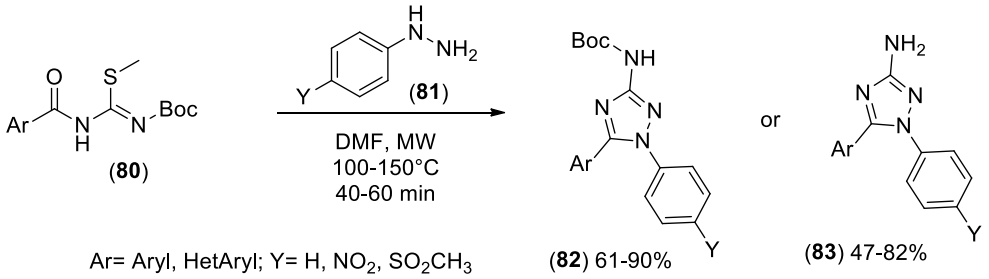

Scheme 15. Microwave-assisted synthesis of 1,5-diphenyl-3-amino-1,2,4-triazoles (**82** and **83**).

1.1.2. 5-Amino-1,2,4-triazoles

The most commonly used synthetic protocols for the preparation of amino-1,2,4-triazoles involve cyclization of hydrazonoyl derivatives and cyanamide, or equivalents,[94–96] condensation of N-cyanoimidates and mono-substituted hydrazines.[97,98]

An effective 1,3-dipolar cycloaddition was developed for the synthesis of 5-amino-1,2,4-triazoles (**85** and **86**) by reacting hydrazonoyl hydrochlorides (**84**) with carbodiimides in the presence of triethylamine as a base. Both symmetric and asymmetric carbodiimides are

compatible with this newly developed reaction; diphenyl carbodiimide is the one exception (Scheme 16).[99]

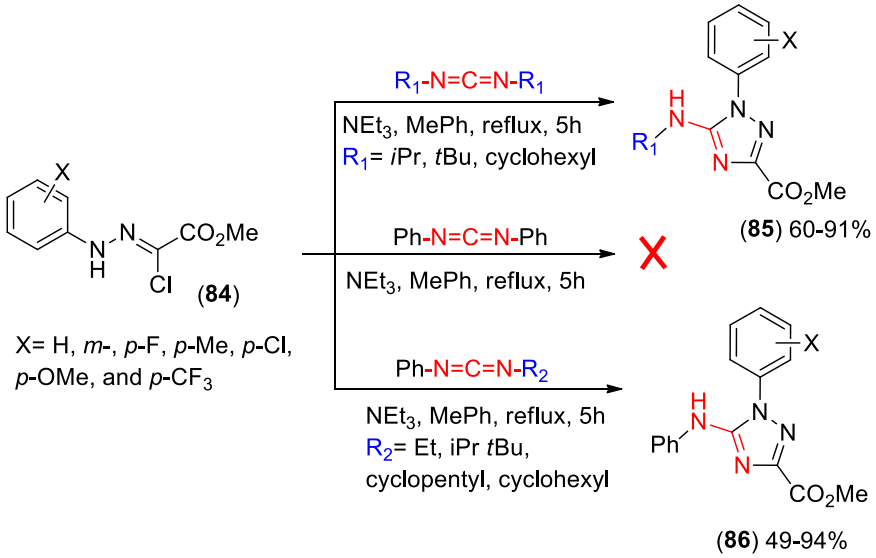

Scheme 16. Synthesis of 5-amino-1,2,4-triazoles (**85** and **86**).

In 1975, Wolkoff et al., described the cyclocondensation of hydrazonyl halide (**87**) with thiourea (**88**) in presence of triethylamine to give the 5-amino-1,2,4-triazoles in 59% (Scheme 17).[100]

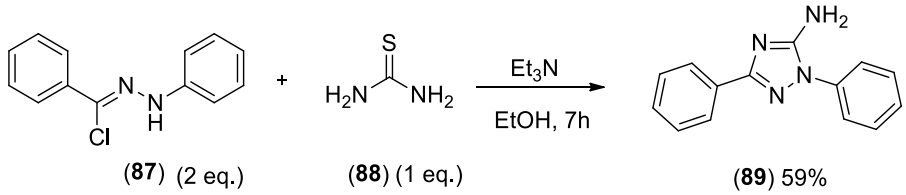

Scheme 17. Synthesis of 5-amino-1,2,4-triazoles (**89**).

Two series of compounds carrying 3-amino-1,2,4-triazole scaffold (**91** and **94**) were synthesized. The synthesis of the series **91** involves the cyclization of N-acylthioureas (**90**) with hydrazine hydroxide. For the synthesis of the pyridyl series **94**, the authors revisited the cyclization of S-methyl amidine (**92**) with nicotinohydrazide (**93**) (Scheme 18).[101]

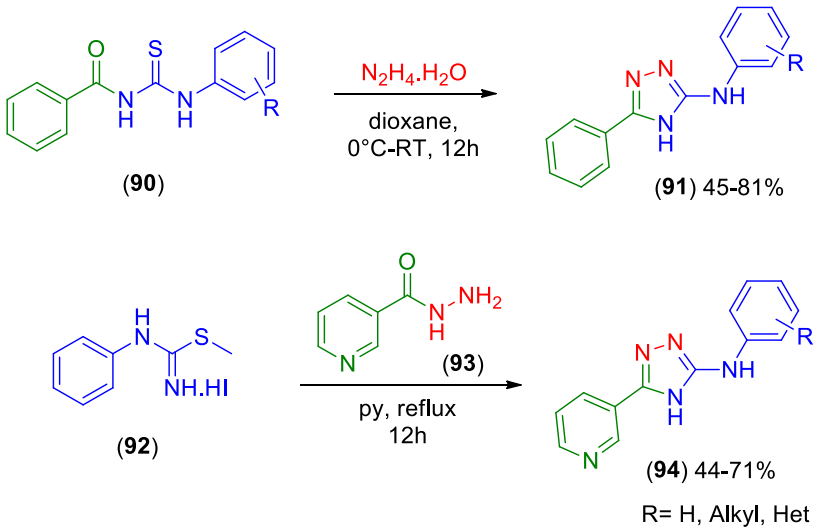

Scheme 18. Synthesis of 5-amino-1,2,4-triazoles (**91** and **94**).

An easy convenient one-step synthesis of variously substituted 5-amino-triazoles (**101**) was described based on the reaction of imidates (**95** and **98**) with hydrazine derivatives (**96** and **99**). The products were obtained in moderate to good yields and a general mechanism for the reactions was proposed (Scheme 19).[98]

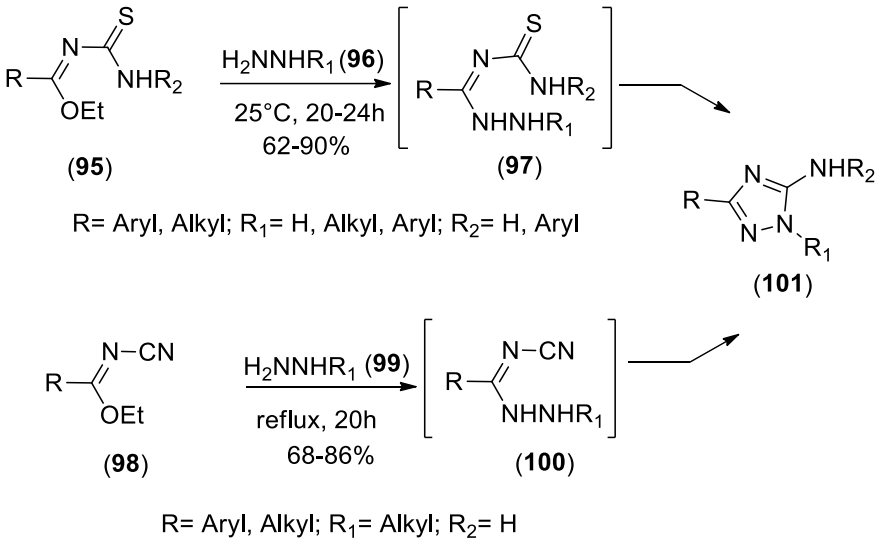

Scheme 19. Synthesis of 5-amino-1,2,4-triazoles (**101**).

Substituted *N*-cyanobenimidate compounds (**102**) were found to be capable of undergoing a cyclization reaction with phenylhydrazine to give l,2,4- triazole derivatives (**103**) in high yields. The method has several advantages, including mild conditions, simple workflow, high yields, and inexpensive reagents (Scheme 20).[97]

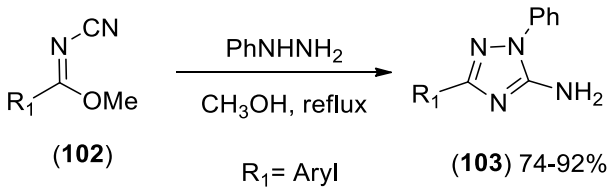

Scheme 20. Synthesis of 5-amino-1,2,4-triazoles (**103**).

Recently in 2021 a divergent efficient assembly of disubstituted 1,2,4-triazoles was established by cyclization of readily accessible N′-nitro-2-hydrocarbylidene-hydrazinecarboximidamides (**104**) with moderate yields under mild reaction conditions. Under acidic conditions, amino-1,2,4-triazoles (**105**) were obtained by an 1,3-hydride transfer pathway leading to HNO_2 elimination (Scheme 21).[102]

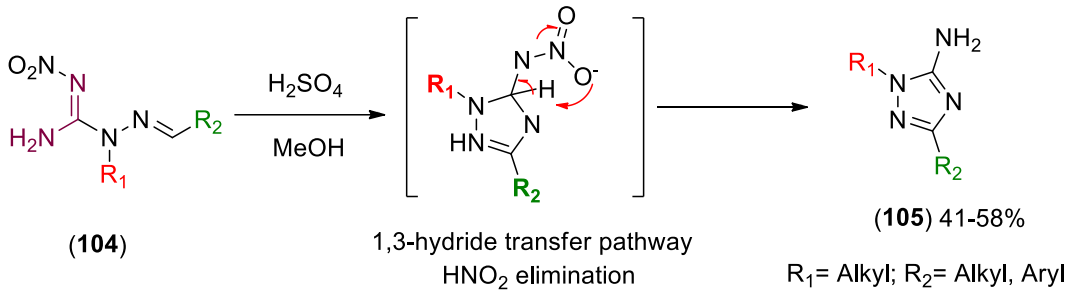

Scheme 21. Synthesis of 5-amino-1,2,4-triazoles (**105**).

All these procedures are focused on the construction of heterocycles from different nitrogen sources (hydrazine derivatives, cyanamides, etc.) and, to our knowledge, very few examples have been described starting from the triazoles ring already built. Only two examples are described in the literature. 3,5- dibromotriazole has been used by 2 different groups as a starting material for preparing in 2 steps 3-aryl 1*H*-1,2,4-triazol-5-amine derivatives by combining both amination and Suzuki cross coupling reactions.

The first group in collaboration with Bayer CropScience described a microwave assisted reaction for the preparation of both, the 5-amino-3-bromo-1,2,4-triazole analogs with the help of DBU and an excess of amine (3 equiv.) using anisole as solvent. The second step involved

Suzuki-Miyaura coupling with polymer-supported catalyst (Scheme 22).[103] Unfortunately no yields are available.

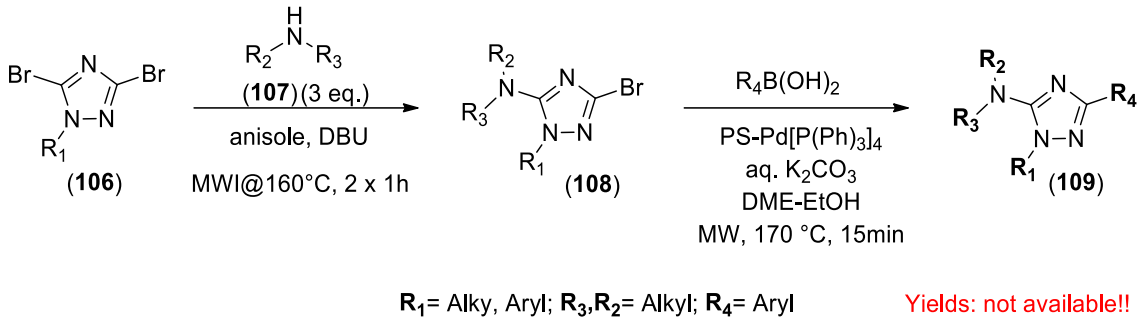

Scheme 22. Synthesis of 3-amino-1,2,4-triazoles starting from 3,5-dirbromo-1,2,4-triazole (**109**).

The second group also reported microwaves assisted synthesis but under more conventional conditions (K_2CO_3 in DMF, 45-90 min for the S_NAr reaction) and Tetrakis for the Suzuki Reaction. Yields are weak for both steps (Scheme 23).[104]

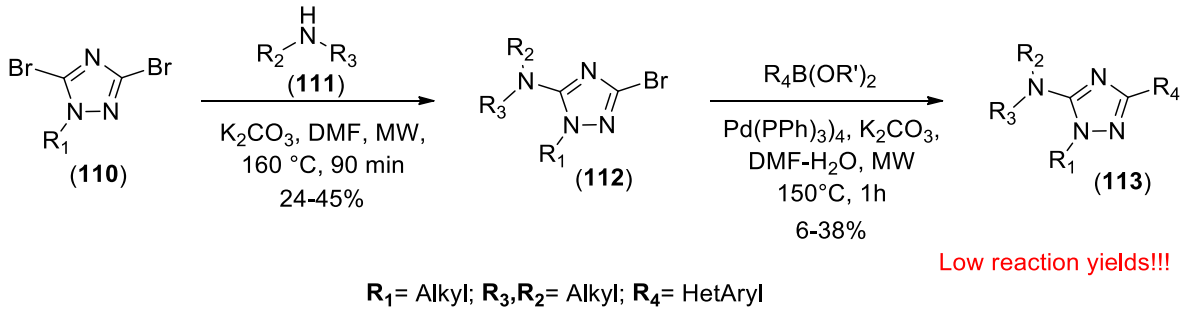

Scheme 23. Synthesis of 3-amino-1,2,4-triazoles starting from 3,5-dirbromo-1,2,4-triazole (**113**).

For both publications no experimental part is available. This lack of experimental details associated with harsh reaction conditions and the low yields of the second reference, encouraged us to reconsider these approaches.

2. OBJECTIVES

Accessing diverse libraries of potentially bioactive molecules in a cost-effective way remains one of the practical challenges of modern drug discovery. Supported by the growing potential of computational methods, the optimization of existing synthetic strategies and the development of new strategies leading to new drug-like molecules have become indispensable in medicinal chemistry. In the early stages, effective drug discovery often depends on the ability to identify active compounds from an extremely large, but virtual or readily available, set of structures. Despite the existence of well-established guidelines for providing these chemical structures, such as Lipinski's "rule of five" or similar criteria for fragment-based hit identification projects, a thorough exploration of chemical space remains a daunting challenge. (3,4) In this respect, a myriad of structurally and functionally diverse molecules, which are synthetically undemanding, remain unexplored solely due to the issue of availability. This obstacle is often due to tedious and unreliable synthesis protocols that can influence the pace of the active compound discovery process. Therefore, increasing the diversity and modularity of chemical synthesis can help overcome these limitations and provide medicinal chemists with a better ability to detect and evolve compounds of interest. In addition, a newly developed method must meet certain important criteria, such as the safety of chemical synthesis and economic feasibility.

1,2,4-triazoles are an important platform in medicinal chemistry and chemical biology, playing a key role in various biological mechanisms related to infections, cancer, seizures, inflammation, neurodegeneration, etc. Despite its importance for medicinal chemistry, there is a lack of convergent approaches for the preparation of polysubstituted triazoles. Our aim was to investigate a relevant strategy starting from readily available dihalogenated 1,2,4-triazoles and leading to versatile functionalized scaffolds to build libraries of triazoles. We therefore focused on developing synthetic strategies that allow us to control the substitution of the different triazole positions. In this context, we prioritized metallocatalyzed methods and demonstrated the efficacy of dibrominated triazole as the starting material of choice for the preparation of a set of 1,2,4-triazoles containing various entities (aliphatics, aromatics, heteroaromatics and amino groups, etc.).

3. RESULTS AND DICUSSION

Our initial objective in this work was to synthesize two families of 1,2,4-trisubstituted triazoles: 3-amino-1*H*-1,2,4-triazole (**117**) and 5-amino-1*H*-1,2,4-triazole (**119**) derivatives. The increasing interest for pharmacologically active 3(5)-amino-1H-1,2,4-triazoles (see figure 3) formally emphasis the two critical steps allowing introduction of both the aromatic ring and the amino function. As the result of the dramatic increase of palladium cross-coupling reaction (PCCR) applied to various heterocycles, the starting 3,5-dibromo-1*H*-1,2,4-triazole (**115**) constitute valuable intermediates in a sequential manner for combining both Suzuki and Amination reactions after a first alkylation or arylation reaction as illustrated in Figure 4.

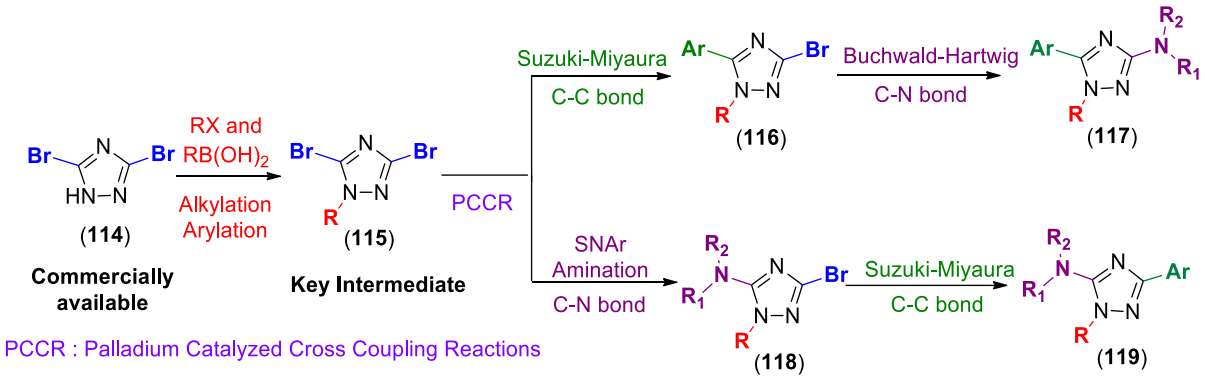

Figure 4. Convergent method to obtain functionalized amino-1*H*-1,2,4-triazole derivatives.

3.1. Alkylation and Arylation reactions

In the first step, we studied the synthetic feasibility for the preparation of 3,5-dibromo-1H-1,2,4-triazole (**114**) starting from 1*H*-1,2,4-triazole (**120**). This reaction was carried out in water using bromine as the reagent in presence of K_2CO_3 and led to the 3,5 dibromo triazole derivative (**114**) in 71% yield.[105] The results demonstrated that due to the high cost of bromine opting to commercially acquire the reagent 3,5-dibromo-1H-1,2,4-triazole (**114**) allowed us to save over 80% of the initial costs.

Starting from the commercially available dihalogenated triazole (**114**), we carried out alkylation reactions and also conducted a copper-catalyzed Chan-Lam arylation reaction, by using conventional methods from the literature (Table 1).[103,104] Different alkyles (**115a**, **115b**), functionalized alkyl groups (**115f**, **115h**), aryles (**115i**), heterocycle (**115e**) and aralkyles (**115c**, **115d**) were prepared in good to excellent yields (see table 1). With the use of bromoacetic acid

as the electrophile no reaction was observed (Table 1, Entry 7). However compound **115g** could be obtained easily by saponification of **115f**.

In the course of this work we were also interested in introducing protective groups on the triazole moiety and the use of THP or para methoxy benzyl bromide led to the desired products in respectively 71 % and 84 % yields.

Table 1. Protocols for Alkylation and Arylation reactions.

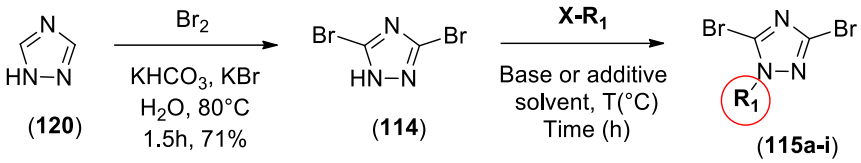

Entry	X-R_1	Base or additive	Solvent	T(°C)	Time (h)	Yield (%)
1[106]	I-Me	NaH	DMF	25	16	95
2[107]	I-i-Pr	NaH	DMF	40	3	83
3[103]	Br-Bn	DIPEA, KI	MeCN	82	16	85
4	Br-PMB	DIPEA, KI	MeCN	82	16	84
5[108]	THP	TFA	EtOAc	77	1	71
6	Br-CH_2COOEt	DIPEA	MeCN	82	15	85
7	Br-CH_2COOH	DIPEA	MeCN	82	16	0
8	Br-CH_2CN	DIPEA	MeCN	82	25	90
9[109]	4-Me-PhB$(OH)_2$	Pyridine, $Cu(OAc)_2$	DCM	25	16	62

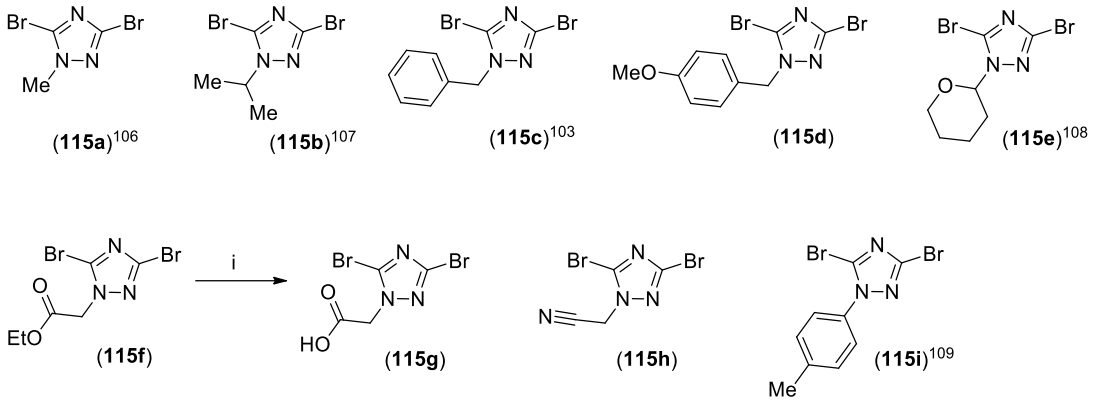

Figure 5. Alkylated and arylated products (**115a-i**). (i) LiOH, H_2O, MeOH, 0-25°C, 16h, 77%.

3.2. Preparation of trisubstituted 3-amino-1*H*-1,2,4-triazole

3.2.1. Suzuki-Miyaura reactions

3.2.1.1. State of the art

It was only in 2006 that the first cross coupling reaction using halogenated 1,2,4-triazoles was reported. In this work the authors explored di-halogenated 1-glycosyl-1,2,4-triazoles, 3,5-dichloro-1-(2,3,4-tri-O-pivaloyl-β-D-xylopyranosyl)-1,2,4-triazole (**120**) and 3,5-dibromo-1-(2,3,4-tri-O-pivaloyl-β-D-xylopyranosyl)-1,2,4-triazole (**121**), as starting materials for transition PCCR . Arylations of the triazole rings **120** and **121** were successful in 5-position with phenylboronic acids under Suzuki cross-coupling conditions with a modified Pd-catalyst (**L**$_1$),[110] which is in accordance with results of nucleophilic substitutions on similar substrates, where substitution at the 5-position was reported to occur fast, while at the 3-position it was considerably slower.[111]

Some secondary products were found in the arylation of nucleosides **120** and **121** with 4-methoxyphenylboronic acid. Thus, compound **120** yielded 9% of the 3-arylated product **123** and 12% of the 3,5-diarylated product **124**, in addition to the main product **122** (44%). The analogous conversion of the brominated derivative **121** was even less selective. The result was a yield of 25% of the slightly contaminated 3-bromo derivative **125**, in addition to mixtures containing the 3-arylated derivatives **126** and **128**, the 3,5-diaryl compound **124**, and 3-bromo-1-(2,3,4-tri-O-pivaloyl-b-D-xylopyranosyl)-1,2,4-triazole (**127**), respectively. According to the authors, these products could not be fully characterized (Scheme 24).[110]

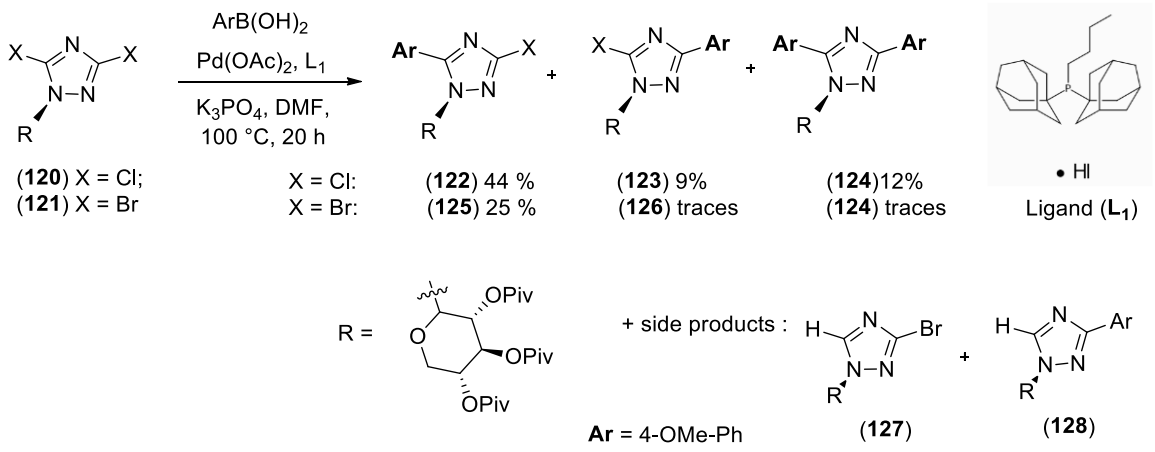

Scheme 24. First Suzuki cross coupling reactions on halogenated 1H-1,2,4-triazoles.

In 2010, the carboxylic acid anion moiety has been used as a tunable directing group for effective PCCR involving 3,5-dibromo-1*H*-1,2,4-triazole derivatives producing 5-substituted triazoles which were obtained under a variety of conditions (Scheme 25).

The authors studied the regioselectivity of the Suzuki-Miyaura reaction on the 1,2,4-triazolic ring. It was observed that in all cases, the reaction exhibited a higher selectivity for substitution at C-5, similar to the case of 2,5-dihalo-4-glycosidyl-1,2,4-triazoles previously described.[110] The authors argue that electronic factors predominate, rendering the C-5 of the triazole electronically deficient and thus promoting substitution at C-5, as proposed by Miethchen. However, experimental results indicate that the carboxylate may have a profound effect on site selectivity. For example, the propionic acid derivative (**129**), which would have electronic properties similar to those of **115f**, but would involve a 7-membered palladacycle transition state, provides only a 2:1 ratio of isomers favoring position 5, whereas **115f** provides a 73:3 ratio (Scheme 25).[112]

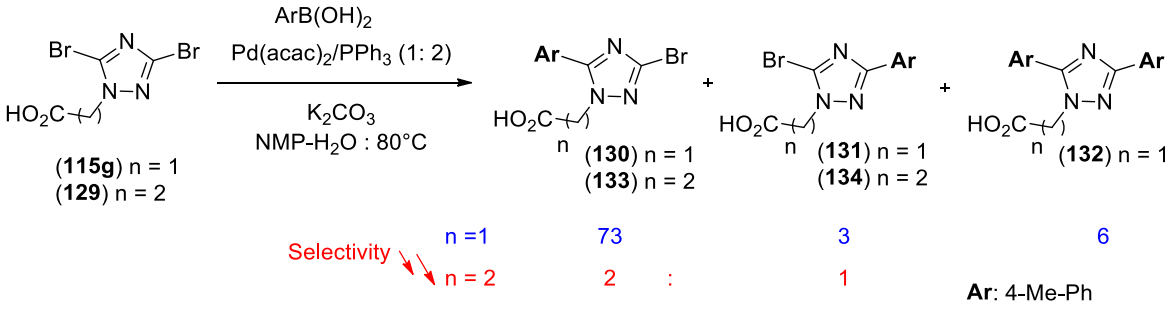

Scheme 25. Regioselective Suzuki cross coupling reactions on halogenated 1*H*-1,2,4-triazoles.

3.2.1.2. Theoretical study of regioselectivity between the two iminobromines

In order to investigate the difference of reactivity in both iminobromides in the 3,5-dibromo-1-methyl-1H-1,2,4-triazole ring, as described in the literature, we have opted to conduct theoretical studies employing quantum calculation methods in collaboration with M. Bruno Henrique from Molecular Modeling Laboratory of UFRRJ.

The resonance forms of **115a** show, in most of cases, N_1 with a positive charge, generating a strongly electron-withdrawing group. The presence of N_1^+ adjacent to C-5 may be the predominant factor for the higher reactivity of C-5 as illustrated bellow (Figure 6).

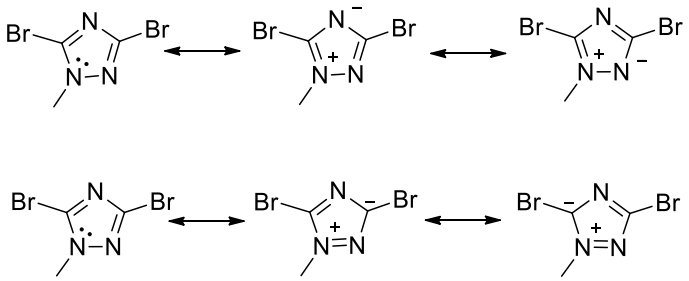

Figure 6. Resonance forms of 3,5-dibromo-1-methyl-1*H*-1,2,4-triazole (**115a**).

The structure of the molecule 3,5-dibromo-1-methyl-1H-1,2,4-triazole (**115a**) was initially built and then subjected to energy minimization using the Density Functional Theory (DFT) method [113,114] with the B3LYP functional [115] and 6-31G* basis set,[116–118] employing the Spartan'14 program (Wavefunction, Inc.) under vacuum conditions.

The graphical representation of the molecular electrostatic potential surface (MEP or ESP), as described by Kollman and Singh[119] is a series of values representing the evaluation of the interaction energy between a positively charged (proton) probe and points on a solvent accessible surface as defined by Connollyx.[120] As implemented within the SPARTAN program, areas of high electron density, representing a strong attraction between the proton and the points on the molecular surface, have the brightest red color and areas of lowest electron density, have deep blue to indigo color, indicating the regions of maximum repulsion (Figure 7 – MEP).

The Local Ionization Potential (IP) is intended to reflect the relative ease of electron removal at any location around a molecule.[121] Thus, it is a measure of the susceptibility of a molecular region to electrophilic attack (reactivity). The surface-mapped values of the IP, obtained from SPARTAN'14 and shown in Figure 7, used the program's default values throughout. The graphical convention used indicates a range of relative values, with red representing regions of higher likelihood of electrophilic attack, and blue, at the other extreme, areas of lower likelihood (more nucleophilic regions) (Figure 7 - IP).

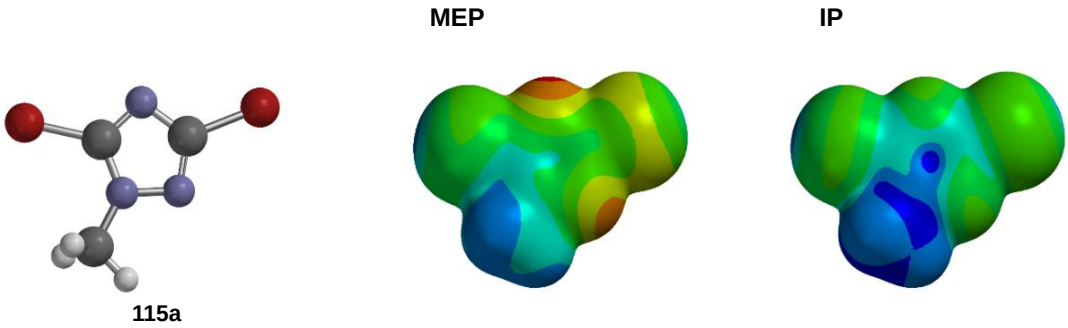

Figure 7. Electrostatic Potential Map (MEP) and Ionization Potential Map (IPM) of the molecule 3,5-dibromo-1-methyl-1H-1,2,4-triazole (**115a**).

Representative plots of local ionization potentials show interesting trends in regions most susceptible to nucleophilic attacks. An analysis of structure **115a**, Figure 7, reveals that the surface region of N_1-methyl group is more electron-deficient compared to the structure as a whole. From these data, we conclude that C_5-Br, immediately in the vicinity of the electron-deficient group, renders it more susceptible to nucleophilic attack. Surface IP analysis suggests that the optimal charge distribution for a nucleophilic attack on the surface of **115a** is best at C_5-Br immediately near N-methyl, which is shown as blue on the surface (Figure 7).

Historically, HOMO/LUMO and energy gap values, as calculated by the Simple Hückel Molecular Orbital Theory (SHMO), have provided insights into the interactions of molecular orbitals and understanding the reactivity of unsaturated and aromatic hydrocarbons.[122,123] The HOMO/LUMO/HOMO-1/LUMO+1 values and energy gap for **115a** are presented in Table 2.

Tabela 2. Total energy, dipole moment, energy of frontier orbitals (HOMO and LUMO), and the energy gap, as well as the HOMO-1 and LUMO+1 orbitals of the molecule 3,5-dibromo-1-methyl-1H-1,2,4-triazole (**115a**).

Energia (Hartree)	Dipolo (debye)	E. LUMO (eV)	E. HOMO (eV)	E. LUMO+1 (eV)	E. HOMO-1 (eV)	GAP (eV)
-5.428,13	4,02	-1,2	-7,2	-0,8	-8,3	6

The contribution to HOMO is distributed throughout the triazolic ring, while the C_3-Br group significantly contributes to HOMO-1. On the other hand, the C_5-Br group contributes significantly to LUMO, whereas for LUMO+1, the contribution is distributed throughout the ring (Figure 8). Thus, a general interpretation of the data suggests that the greater contribution

of C_3-Br to HOMO and HOMO+1, along with the greater contribution of C_5-Br to LUMO, makes C_5-Br a more attractive target for reactions with a nucleophilic species.

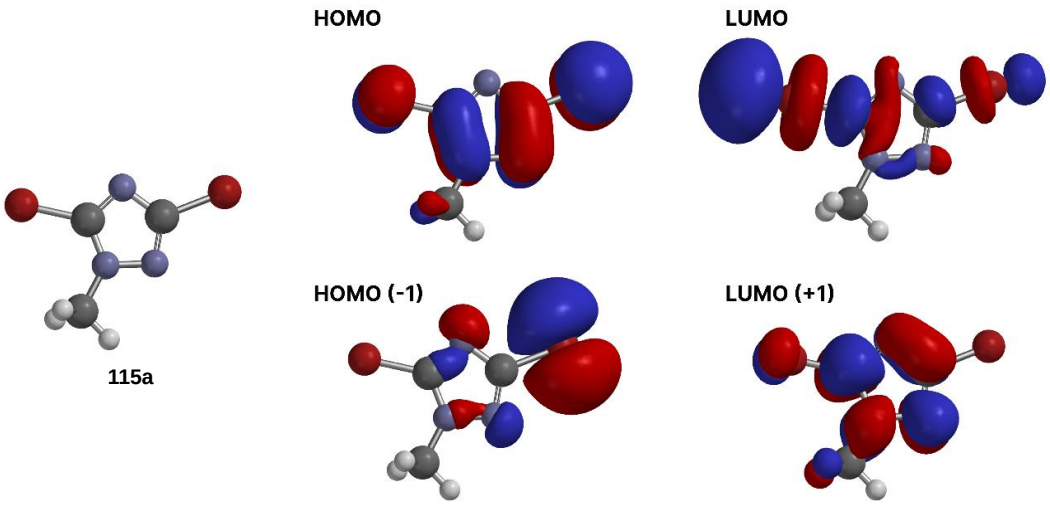

Figure 8. HOMO, HOMO-1, LUMO, and LUMO+1 orbitals of the molecule 3,5-dibromo-1-methyl-1H-1,2,4-triazole (**115a**).

Therefore, after the analyses by resonance, MEP, IP, HOMO/LUMO/HOMO-1/LUMO+1, the intrinsic differences between C_3-Br and C_5-Br become clear, and these differences have significant chemical relevance. In our opinion, the results of the theoretical study, even though conducted only in the ground state, provide support for explaining the experimental results, where C_5-Br is more susceptible to nucleophilic attacks and PCCR-type reactions.

3.2.1.3. Personal work: Optimization of the Suzuki reaction

Due to the absence of an effective regioselective arylation method in halogenated 1,2,4-triazoles, it was necessary to conduct a study of the Suzuki-Miyaura reaction in order to establish a scope.

Using N-alkyl and N-aryl triazoles **115a** and **115i** as model systems, we initiated the optimization of reaction conditions for the Suzuki-Miyaura reaction under classical conditions: sodium carbonate as the base, toluene, ethanol and water (5:1:1) as solvents and Palladium-tetrakis(triphenylphosphine) as the catalyst at 130°C. The desired C-5 arylated product (**116a**) was observed as the major compound; however, the presence of the regioisomer (**135a**) and the diadduct (**136**) were also detected in HPLC. Even after several attempts of purification by

chromatography on silica gel, it was not possible to separate the regioisomer **116a** from the diadduct (**136**).

Even with the exchange of base, solvent, and catalytic system, a mixture of products was still observed (see table 3). However, only by increasing the number of equivalents of triazole relative to boronic acid, it was possible to avoid the formation of the diadduct and obtain the desire compounds **116a** with a 75% yield and the regioisomer **135a** with a 4% yield after purification.

For the N-aryl triazole (**115i**), we also attempted classical conditions at low temperature and alteration of the catalytic system. In both cases, low selectivity and product mixtures were observed, but increasing the number of equivalents of the N-arylated triazole also proved to be a more efficient strategy, providing the desired regioisomer (**116b**) with excellent yield (90%) after purification.

Table 3. Optimization conditions for Suzuki-Miyaura reaction.

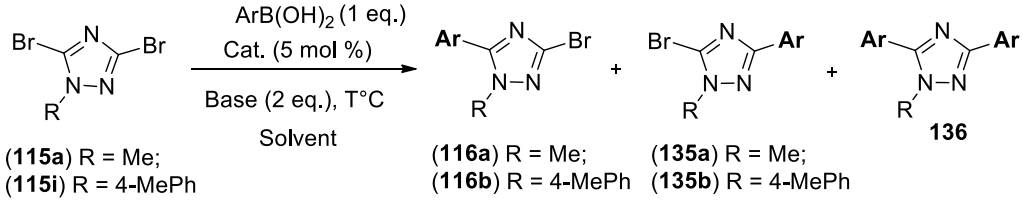

Entry	R	Ar	115 (n. eq.)	T(°C)	Time (h)	Yield (%)	Ratio 116/135/136 (HPLC, 210nm) ***
1[a]*	Me	4-Me-Ph	1	130	3	77 (**116**+**136**)	116/135/136: 4/0/1
2[b]	Me	4-Me-Ph	1.2	120 (μw)	0.2	69 (**116**+**136**) 5 (**135**)	116/136: 2.7/1
3[a]	Me	4-Me-Ph	2	105	3	75 (**116**) 4 (**135**)	-
4[a]	4-Me-Ph	Ph	1	75	5	nd	116/135/136: 2/0/1**
5[c]	4-Me-Ph	Ph	1	100	1	nd	116/135/136: 1/1.2/6.2
6[a]	4-Me-Ph	Ph	2	105	1	90 (**116**)	-

[a] $NaCO_3$ (2 eq.), ($Pd(PPh_3)_4$ (5 mol%), PhMe:EtOH:H_2O (5:1:1); [b] K_2CO_3 (2 eq.), $PdCl_2(PPh_3)_2$ (5 mol%), MeCN:H_2O (1:2); [c] K_2CO_3 (2 eq.), $Pd(OAc)_2$ (7 mol%), SPhos (15 mmol %), i-PrOAc; *$ArB(OH)_2$ (1.1 eq.); ** Presence of SM. *** Ratio was determined by HPLC/UV using caffeine as internal standard.

In 2008, Lipshutz and Gorai first reported the use of surfactants to conduct metal-catalyzed reactions in water.[124] Indeed, due to their amphiphilic nature, surfactants in water undergo

spontaneous transformation into micelles, which then act as nanoreactors, with their hydrophobic cores serving as reaction vessels where organic transformations involving water-insoluble reagents can take place. Interestingly, as organic reagents are brought together in a confined volume, reactions occur more readily and at lower temperatures. Furthermore, reactions under micellar conditions are generally straightforward to carry out, as everything can be performed exposed to air (without an inert atmosphere), and the micellar aqueous solution can be efficiently reused multiple times after extraction of the organic products. Since 2008, many significant contributions have been reported in the literature, with particular focus on palladium-catalyzed cross-coupling reactions (Suzuki-Miyaura, Stille, Heck, etc.).[124–134] Our team in Strasbourg has contributed to this field by developing an efficient and nearly "universal" catalytic system (t-BuXPhos / [(cinnamyl)$PdCl_2$,NaOt-Bu, TPGS 2%, 50°C), for the Buchwald-Hartwig cross-coupling reaction under micellar conditions.[134,135]

Based on our group's expertise, we explored the use of the TPGS surfactant in aqueous medium at low temperature for the Suzuki-Miyaura reaction using Pd(dtbpf)Cl_2 as the catalytic system and Et_3N as the base.[136] However, the reaction did not exhibit selectivity. Beside the starting material we observed the formation of the 2 regioisomers and also the di-adduct in a ratio of 2.4/1.6/1. Attempting to replace water by ethanol did not show any reactivity, and only the formation of the 4,4'-dimethyl-1,1'-biphenyl was observed, while employing toluene led to low conversion of the triazole **115a**.

Table 4. Suzuki-Miyaura reaction under eco-friendly conditions.[136]

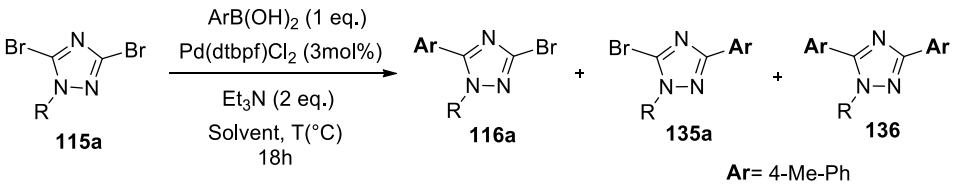

Entry	115a (n. eq.)	Solvent	Conc. (M)	T(°C)	Yield (%)	Ratio: 115a/116a/135a/136 (HPLC)*
1	1.5	TPGS-750M/H_2O 2% w/w	0.14	25-50	nd	2.4/2.4/1.6/1[a]
2	1.5	EtOH	0.14	25	nr	a
3	1.5	PhMe	0.14	25	nd	40/20/6/1[a]
4	1.6	PhMe	0.052	50	nd	5/1.1/0/1[a]

nr: no reaction; nd: not determined; a= 4,4'-dimethyl-1,1'-biphenyl (homocoupling); * Ratio was determined by HPLC/UV using caffeine as internal standard.

Next, under our optimized conditions, a small scope of six compounds was obtained. Compounds **116a** and **116b** were obtained in good and excellent yields, respectively. For the synthesis of compound **116c**, complete consumption of the starting material was observed; however, the yield of 49% could be explained by the compound's precipitation during purification by column chromatography using DCM as the eluent. Finally, compound **116d** was obtained in low yield after purification due to a higher presence of regioisomer (**135d**) and diadduct (**136**) in a ratioof **116**/**135**/**136** (4/2/1), possibly facilitated by the presence of the methyl ester and isopropyl group, which induce steric hindrance. In addition, the methyl ester group hydrolyzes readily to carboxylic acid in basic aqueous media, which may have contributed to the formation of the corresponding carboxylic acid and explains the reaction's poor yield. To answer this question, it would have been interesting to carry out the reaction using a tert-butyl ester (Figure 9).

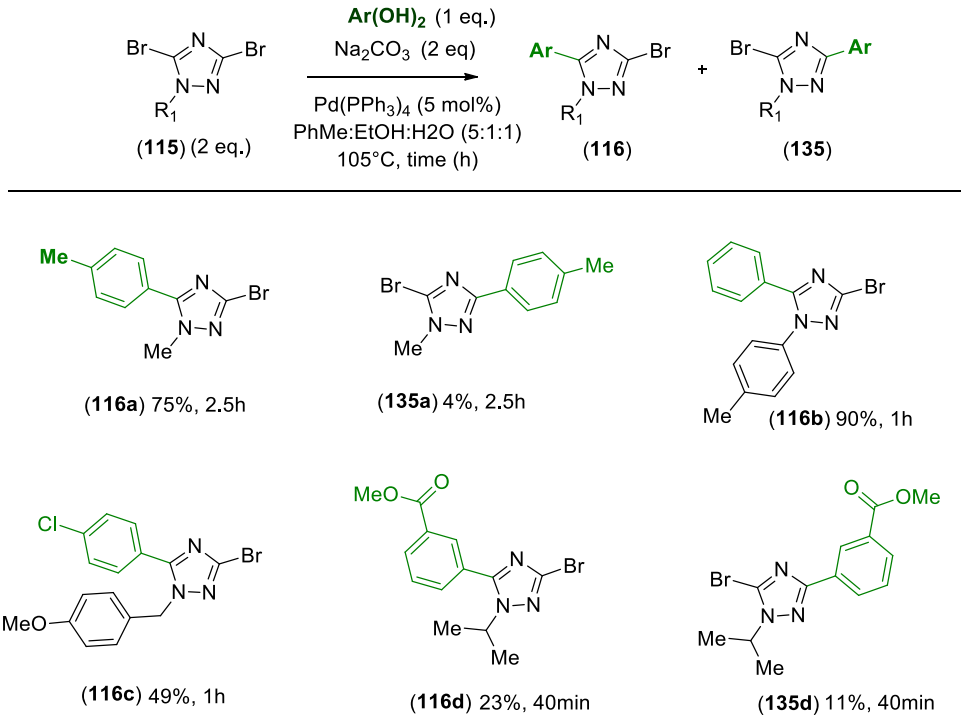

Figure 9. Substrate Scope of Arylated 1,2,4-triazoles.

We decided to confirm whether the structure of the isolated regioisomer was in accordance with the literature description for the predominant arylation at C-5. For this purpose, we used NOESY 2D analysis. It was possible to observe for the compound **116c** the spatial

coupling of the methylenic hydrogens (H_1) with the aromatic hydrogens (H_5), confirming that the isolated regioisomer is in accordance with the literature description that the arylation reaction predominantly occurs at position C-5 of the triazolic ring (Figure 10).

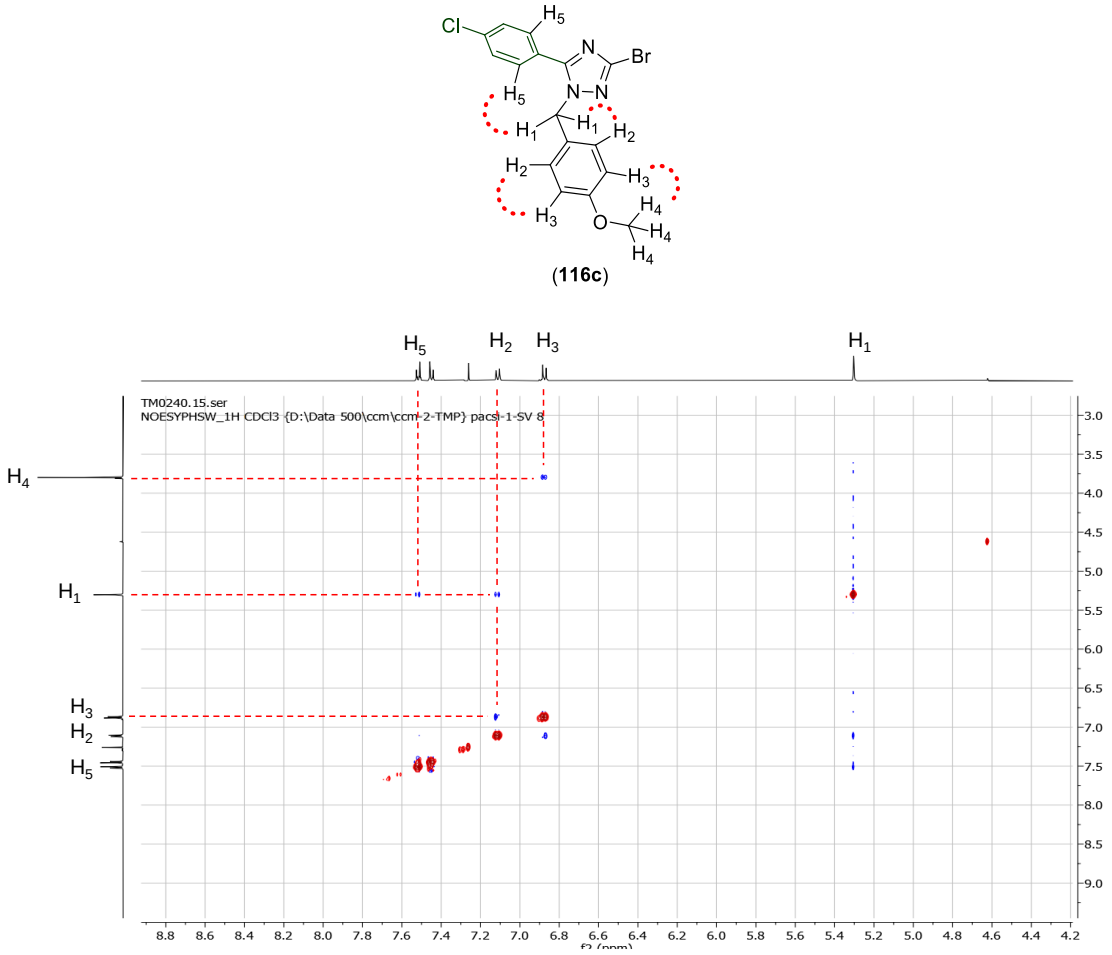

Figure 10. NOESY analysis of the compound **116c** in $CDCl_3$.

3.2.2. Buchwald-Hartwig reaction

3.2.2.1. State of the art

Conversely to 6-membered rings, triazole derivatives are particularly difficult to use for Buchwald cross-coupling reactions, due to their low reactivity. Only a few examples are available in the literature: no paper only patents.[137-143] For the majority of reactions involving cyclic primary or secondary amines, no reaction yields have been reported. However, when yields are specified, they are low (~ 25%). Conversely, the use of aromatic amines was more successful for C-N cross-coupling, leading to yields ranging from 51% to 90% (see Table 5).

These patents lack a general method, and in most of cases, the authors employed bulky electron rich t-Bu ligands (Table 5). This encouraged us to re-examine this reaction.

Table 5. State of the art of Buchwald-Hartwig reaction in disubstituted 3-bromo-1*H*-1,2,4-triazoles.

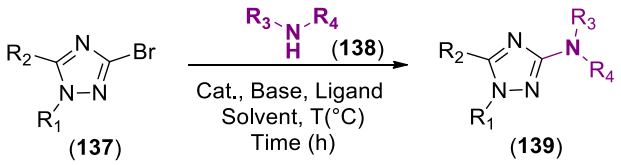

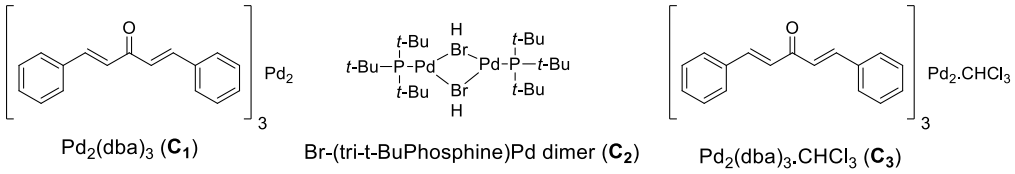

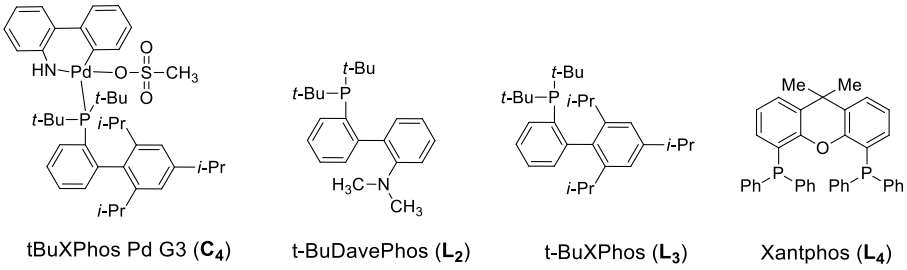

Ref	NR_3R_4	Base	Catalyst	Ligand	Solvent	T(°C)	Time (h)	Yield (%)
			Primary amines					
137	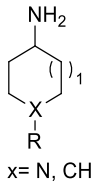 x= N, CH	NaOt-Bu	C_1	L_2	Dioxane	80	2	nd
138		NaOt-Bu	C_2	L_3	Dioxane	100	2	nd
139		NaOt-Bu	C_1	L_3	Dioxane	80	2	nd
			Secondary amines					
140	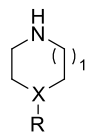 x= N, CH	NaOPh	C_3	L_4	Dioxane	140	1	27
141		NaOt-Bu	C_4	-	THF	90	16	nd
			Aromatic amines					
142	$Ar(Het)NH_2$	NaOPh	C_1	L_4	Dioxane	150	2	90
143		Cs_2CO_3	C_1	L_4	Toluene	100	3	51

3.2.2.2. Personal work: Optimization of the Buchwald-Hartwig reaction

These limited data in the literature have encouraged us to re-examine the Buchwald cross coupling reaction in order to find more effective conditions. For this purpose, we intend to implement a model system.

In our initial screening experiments, 3-bromo-1H-1,2,4-triazole and phenethylamine were used as the prototypical substrates to establish the most suitable reaction conditions.

First, we applied standard Buchwald-Hartwig coupling conditions using K_2CO_3, $Pd_2(dba)_3$ (**C_1**), Xantphos (**L_4**) and toluene at 100°C. When these conditions were applied, only around 20% of the desired product was observed in HPLC; however, still remained high amount of starting material (**116a**) (Table 6 - Entry 1). Improvements in Buchwald–Hartwig reactions have relied on the increased reactivity and stability of the metal catalyst using more effective ligands. A set of four ligands (**L_3 –L_6**) were evaluated in combination with different Pd catalyst (**C_1**, **C_5** and **C_6**).[144,145] In addition, in the Buchwald–Hartwig reaction, the choice of the base can also significantly influence the efficiency of the coupling. All the results obtained for our optimization study were reported in table 5. Using JosiPhos (**L_5**), a ferrocenyl diphosphine[146,147] as ligand in combination with $Pd(OAc)_2$ and $CsCO_3$ in DMF at 75°C was unsuccessful (Table 6 - Entry 2) as no trace of product was observed in HPLC, only the substrate. Further, we turned our attention to the use of the reported catalytic system(([(cinnamyl]PdCl]$_2$ /t-BuXPhos) which was developed in our group in Strasbourg for the Buchwald Hartwig reaction in water.[134,135] The reaction was carried in toluene using NaOt-Bu at different temperature. At 50°C, the presence of the product was observed, however significant amount of starting material (**116a**) still remained. Following purification, the product was isolated with a 15% yield (Table 6 - Entry 3). Subsequently, we decided to increase the temperature to 100°C, resulting in a higher conversion of the expected compound with a ratio **116a**/**117a** of 1/3. As a result, the desired product (**117a**) was isolated in 68% yield after purification by chromatography on silica gel (Table 6 - Entry 4). Compared to the two catalytic previous system the (([(cinnamyl]PdCl]$_2$ /t-BuXPhos) system provided much better efficacy. Next, we evaluated the effect of counter ion of the base, KOt-Bu versus NaOt-Bu, but no change in term of yield was observed (Table 6, entry 6). Furthermore, the replacement of ligand tBuXPhos (**L_3**) by BippyPhos (**L_6**), which had

been previously employed for coupling weakly nucleophilic amines,[148,149] resulted in a significant drop in **116a** conversion (Table 6 entry 5 versus entry 4).

Table 6. Optimization conditions for Buchwald-Hartwig reaction.

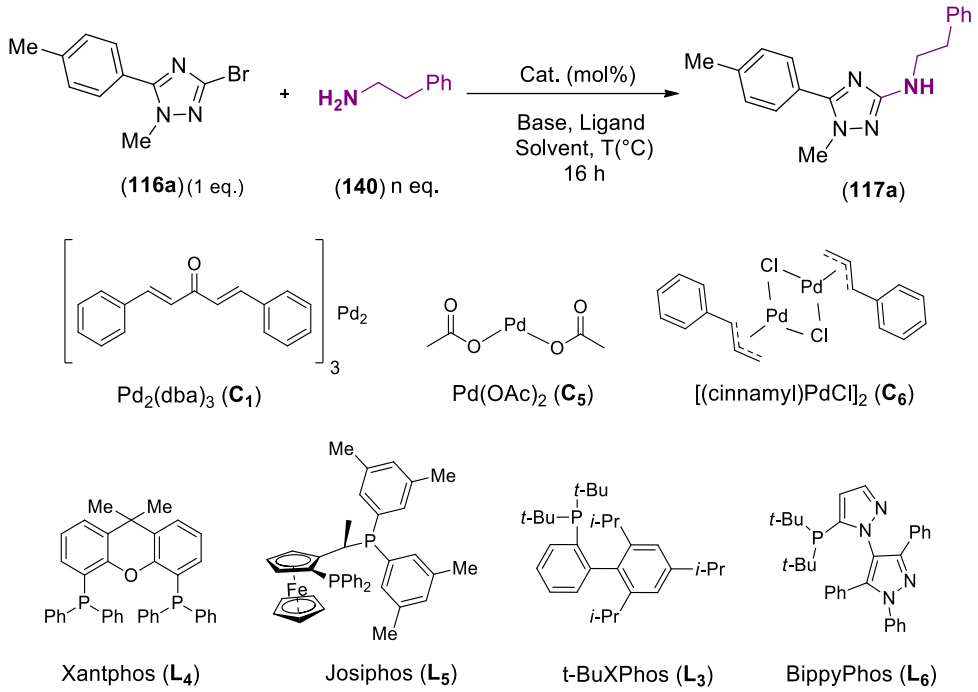

Entry	140 (n° eq.)	Base (1.5 equiv)	Catalyst	Ligand	Solvent	T(°C)	Yield (%)	Ratio 116a/117a (HPLC)*
1[a]	2	K_2CO_3	C_1	L_4	PhMe	100	nd	3.8/1
2[b]	1.2	$CsCO_3$	C_5	L_5	DMF	75	-	nr
3[c]	1.7	NaOt-Bu	C_6	L_3	PhMe	50	15	5.1/1
4[c]	1.3	NaOt-Bu	C_6	L_3	PhMe	100	68	1/3
5[c]	1.3	NaOt-Bu	C_6	L_6	PhMe	100	nd	6/1
6[c]	1.3	KOt-Bu	C_6	L_3	PhMe	100	67	1/3

nd: not determined; nr: no reaction; [a] Cat. (1 mol%); Ligand (2 mol%); [b] Cat. (5 mol%); Ligand (5 mol%). [c] Cat. (5 mol%); Ligand (10 mol%). * Ratio was determined by HPLC/UV using caffeine as internal standard.

Based on all these results, a combination of [(cinnamyl)PdCl]$_2$ (5 mol%), t-BuXPhos (10mol%) and NaOt-Bu (1.5 equiv.) was selected as the catalyst system of choice. Its efficacy in facilitating Buchwald–Hartwig coupling between a set of amines or amides coupling partners was evaluated (Figure 11). Under our optimized conditions we were able to couple the bromo-triazole **116a** with benzylamine in excellent yield (92 %). A complete conversion was observed

using aniline by HPLC, however, due to the lack of time, the product could not be isolated. Finally, and unfortunately, no and low conversion using benzamide and secondary amines (morpholine and phenylpiperazine) were observed, respectively. Due to limited time, an optimization for these last two amine classes could not be carried out. However, it would be interesting to see the efficiency of other enriched ligands (BrettPhos, RuPhos, BippyPhos, t-BuBrettPhos) or to carry out these reactions with different palladacycles.

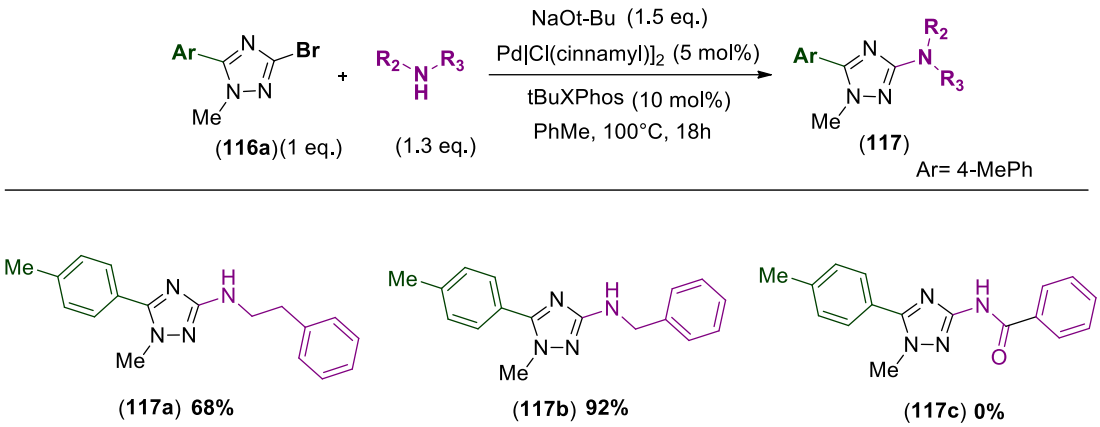

Figure 11. Substrate Scope of 5-Aryl-1,2,4-triazoles-3-amine.

3.3. Preparation of trisubstituted 5-amino-1*H*-1,2,4-triazole

We next focused on the preparation of the trisubstituted 5-amino-1H-1,2,4-triazole derivatives (**119**). As reported before, for the synthesis of the second family, we plan to invert the order of functionalization, starting with the amination reaction of the alkylated intermediate (**115a**) and then proceeding with the Suzuki-Miyaura arylation reaction.

3.3.1. Optimization of the amino reaction using Buchwald- Hartwig conditions

In initial screening experiments, 3,5-dibromo-1-methyl-1H-1,2,4-triazole (**115a**) and phenethylamine (**140**) were used as prototypical substrates to establish suitable conditions. In a first experiment we assessed our optimal conditions obtained previously (([(cinnamyl]PdCl]$_2$ /t-BuXPhos, NaOt-Bu) in toluene with a temperature reduction to 50°C due to the presence of two iminobromides in the starting material (**115a**). After 16 hours, beside the starting material, we observed in HPLC the formation of two new compounds: the expected amino triazoles (**118**) and the diarylation product (**141**) resulting from an additional N-heteroarylation of **118a** in a

1/2 ratio, (Table 7 – Entry 1). To avoid the formation of this diarylation product we decided to replace t-BuXPhos by a less enriched ligand. Using classical conditions Buchwald-Hartwig arene amination such as $Pd(OAc)_2$, BINAP, cesium carbonate, and toluene at 100°C only traces of the side product **141** was observed by HPLC, however, starting material still remained (Table 7 – Entry 2). Even with an increased reaction time, we still observed the presence of the starting material (**115a**) in a 1:1 ratio with the product (**118a**) (Table 7 – Entry 3). Changing the solvent to dioxane (Table 7 – Entry 4) and the base to sodium carbonate (Table 7 – Entry 5), only the starting material (**115a**) was observed as a major compound in both cases. By replacement of Cs_2CO_3 to NaOt-Bu we still observed the formation of the desired product (**118a**), however low conversion of the starting material (**115a**) and the secondary N-heteroarylated product (**141**) appeared in a significant manner (Table 7 – Entry 6).

Table 7. Optimization conditions for Buchwald-Hartwig reaction.

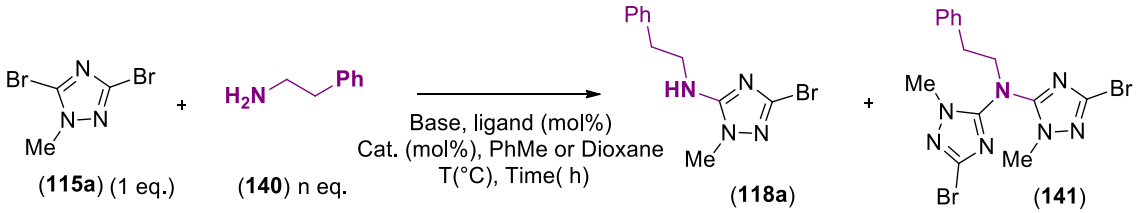

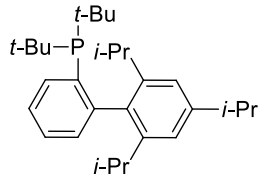

t-BuXPhos (L_3)

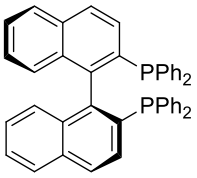

BINAP (L_7)

Entry	140 n° equiv	Base (1.5 equiv)	ligand	T(°C)	Time (h)	Ratio 115a/118a/141 (HPLC, 210nm)**
1[a] 135	1.2	NaOt-Bu	L_3	50	16	2.2/1/2.2
2[b]	1.2	Cs_2CO_3	L_7	100	4	1.3/1/trace
3[b]	1.3	Cs_2CO_3	L_7	100	16	1/1/ trace
4[b*]	1.3	Cs_2CO_3	L_7	100	16	115a: major cpd 118,141: traces
5[c]	1.3	Na_2CO_3	L_7	100	16	115a: major cpd
6[c]	1.3	NaOt-Bu	L_7	100	16	5.5/1/2.2

[a] Cat.: $PdCl_2$ (cinnamyl)$_2$ (5 mol%), Ligand (10 mol%); [b]Cat.: $Pd(OAc)_2$ (3 mol%); Ligand (6 mol%); [c]Cat.: $Pd(OAc)_2$ (5 mol%); Ligand (10 mol%) ; *The only reaction in Dioxane. ** Ratio was determined by HPLC/UV using caffeine as internal standard.

During all the tests conducted, we consistently observed a mixture of products that led us to abandon this reaction.

3.3.2. Aromatic nucleophilic substitution reaction (S_NAr): optimization conditions

Due to the less selectivity in the Buchwald-Hartwig reaction, we decided to explore an alternative method using the aromatic nucleophilic substitution reaction (S_NAr) as reported previously in the literature.[110,112]

As previously, 3,5-dibromo-1-methyl-1H-1,2,4-triazole (**115a**) and phenethylamine (**140**) were used as prototypical substrates. Using microwave-assisted synthesis with K_2CO_3 in DMF in a concentration of 0.10M at 160°C, we obtained the desired compound with a yield of 23% after purification, consistent with the literature. This may be attributed to the presence of diarylated (**141**) and other side products, which could not be identified, yet (Table 8 – Entry 1).

Changing for a low-basicity and low-polarity aprotic solvent (MeCN), decreasing the temperature and increasing both the reaction time and the concentration of our medium (0.20 M instead 0.10 M), we observed the desired product (**118a**) in a ratio of 2:1 over the starting material (Table 8 – Entry 2). Aiming the higher consumption of the starting material (**115a**) we increased the concentration of the reaction to 0.4 M. Under these conditions, the desired product was obtained in 53% of yield after purification by column chromatography on silica gel. (Table 8 – Entry 3). Finally, we also tested to replace the mineral base (K_2CO_3) by an organic base (DIPEA); however, the presence of the desired product was lower compared to the previous conditions (Table 8, compare entry 4 with entry3).

Table 8. Optimization conditions for S_NAr starting from N-Me triazole **115a**.

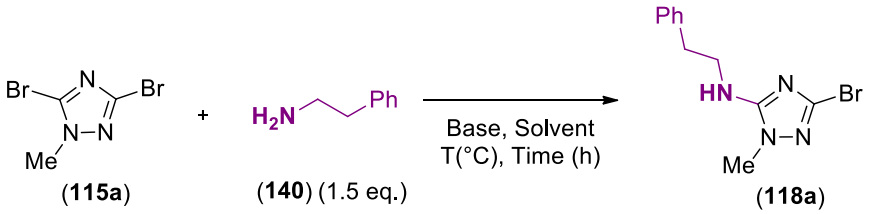

Entry	Base (2 equiv)	Solvent	Conc. (M)	T(°C)	Time (h)	Yield (%)	Ratio 115a/118a (HPLC, 210 nm)*

1	K_2CO_3	DMF	0.10	160 (µw)	1.5	23[a]	1/6.5
2	K_2CO_3	MeCN	0.20	110	20	nd	1/2
3	K_2CO_3	MeCN	0.42	110	15	53	1/5
4	DIPEA	MeCN	0.42	110	20	nd	1/2.5

[a] diarylated product (**141**); * Ratio was determined by HPLC/UV using caffeine as internal standard.

Next, we carried out a similar study to optimize the SNAr conditions starting from N-aryl-bromo triazole (**115i**). First by using the best conditions described previously (K_2CO_3, MeCN, 110°C, 15h), we observed the total consumption of our starting material. However, beside the expected amino triazoles derivative (**118b**) we observed the presence of the diarylation product (**142**) in a ratio of 8:1. Additionally, we also detected by HPLC traces of the hydrolysis (**143**) of our starting material (Table 9 – Entry 1).

By using an organic base and lowering the temperature to 82°C instead of 110°C, we observed by HPLC the formation of the target product in a 1:1 ratio with regard to the starting material. Under these conditions only traces of diarylation product (**142**) was detected (Table 9 – Entry 2). With the increase in temperature, the desired product was observed in greater quantity by HPLC and isolated in 63% yield after purification by column chromatography on silica gel (Table 9 – Entry 3).

Additionally, we used a stronger organic base like DBU; however, the dimer appeared significantly, along with the presence of hydrolysis product (**143**) (Table 9 – Entry 4). Moreover, the replacement of MeCN with n-BuOH in presence of K_2CO_3 at 160°C, led to a single compound; in this case, the solvent acted as a nucleophile, providing the alkoxytriazole (**144**) in 90% yield (Table 9 – Entry 5).

Table 9. Optimization conditions for Aromatic nucleophilic substitution reaction starting from N-Me triazole **115i**.

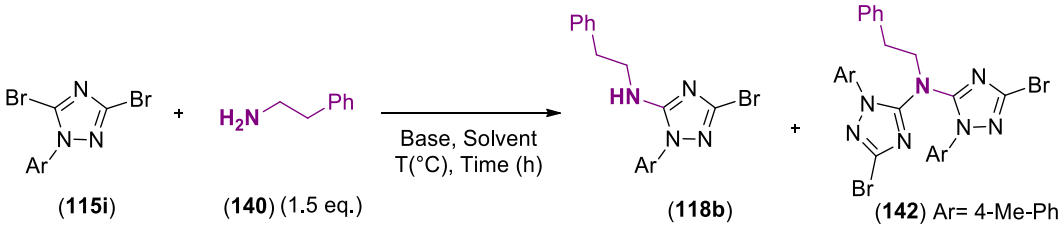

Entry	Base (2 equiv)	Solvent	T(°C)	Time (h)	Yield (%)	Ratio 4/5/6 (HPLC, 210 nm)*

1	K_2CO_3	MeCN	110	15	nd	0/8/1 [a]
2	DIPEA	MeCN	82	24	nd	1/1/traces
3	DIPEA	MeCN	110	20	63	1/8/traces
4	DBU	DMSO	80	2.5	nd	0/1.7/1 [a]
5	K_2CO_3	n-BuOH	160	1.5	0 [b]	-

a 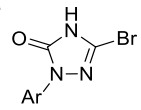
(**143**) trace

b 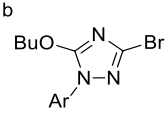
(**144**) 90%

* Ratio was determined by HPLC/UV using caffeine as internal standard.

Using our best reaction conditions, a set of amines was investigated and the results are shown in Figure 9. When the reaction was performed with amines with a low boiling point (morpholine), the reaction was performed with four equivalents of amines, (i.e **118f-g**). Six compounds were isolated with moderate to good yields, ranging from 48 to 84% and fully characterized (Figure 12).

In the presence of a less nucleophilic amine (i.e p-toluidine) it was necessary to use a stronger base as LiHMDS to obtain the expected N-aryl triazoles (**118h**). However, the yield was low (35%) after purification by column flash chromatography. Using ammonia as the nucleophile, we obtained the N-arylated amination product (**118i**) in 62% yield (Figure 12 – Miscellaneous).

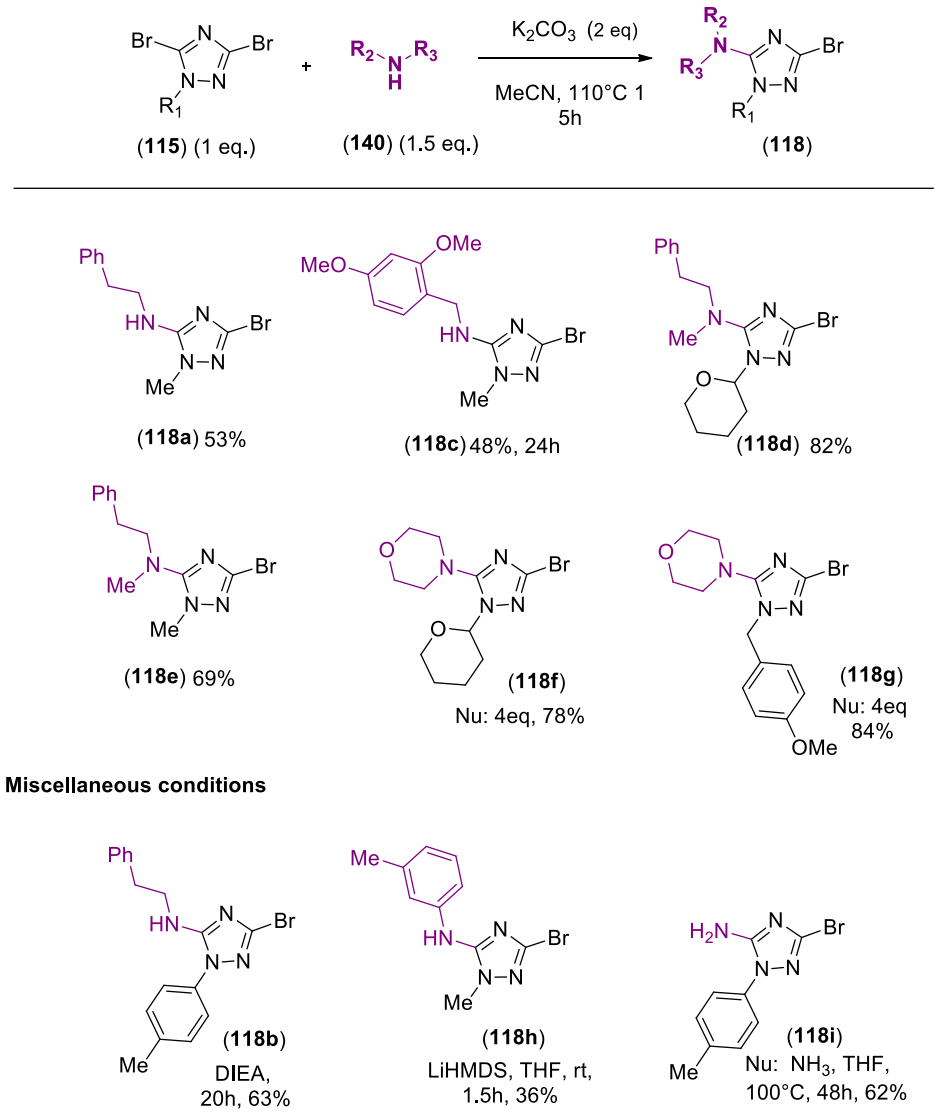

Figure 12. Substrate Scope of 5-amino-1,2,4-triazoles (**118a-i**).

We also decided to confirm whether the structure of the isolated regioisomer was in accordance with the literature description for the predominant amination at C-5 of the triazole core. For this purpose, we used NOESY 2D analysis. It was possible to observe the spatial coupling of the methyl hydrogens (H_1) with the NH + -CH_2, confirming that the isolated regioisomer is in accordance with the literature description. (Figure 13).

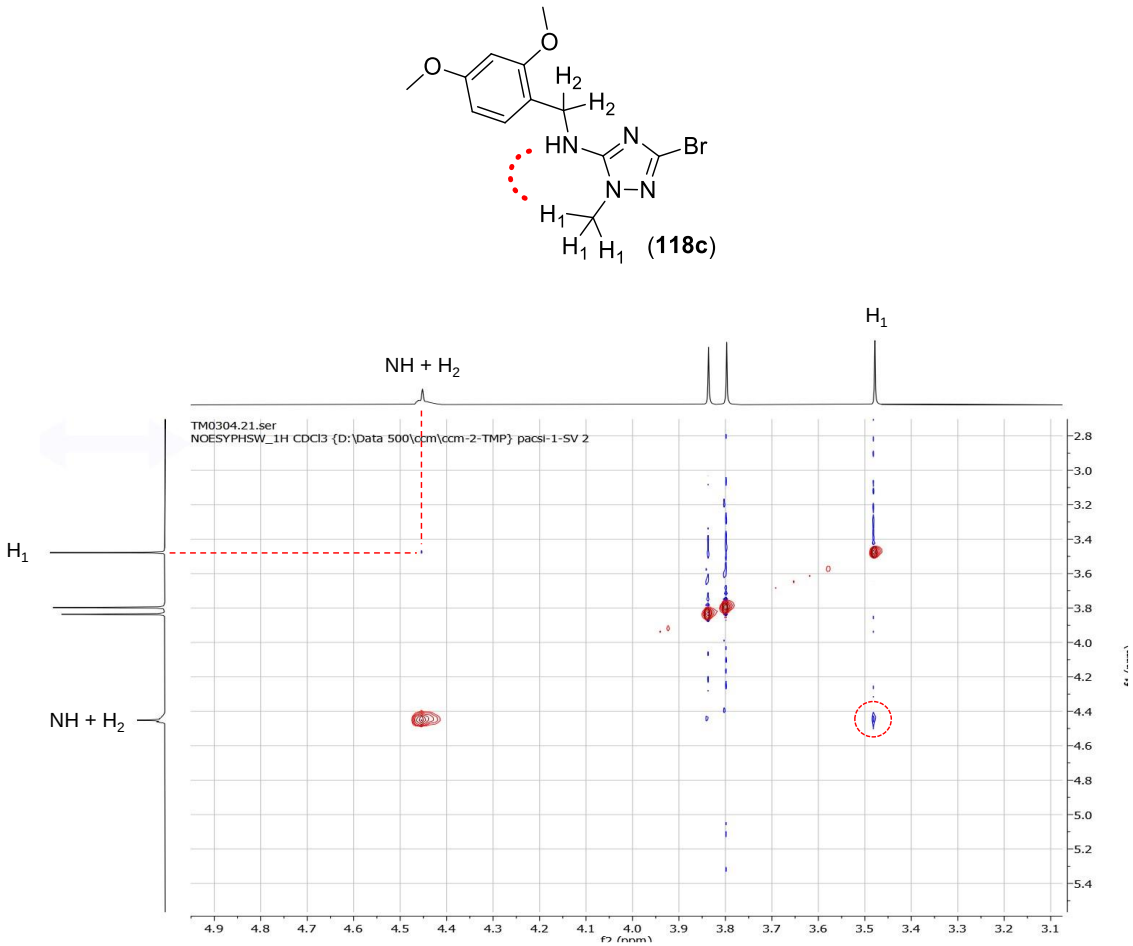

Figure 13. NOESY analysis of the compound **118c** in $CDCl_3$.

The amination reaction employing morpholine as the nucleophile utilized a large excess of amine (4 equiv.) due to its volatile nature. The significant excess of morpholine, its increased nucleophilic character, steric hindrance provided by the THP protecting group, and conflicting data regarding the preferential formation of regioisomers in patents[150,151] led us to structure **118f** using NOESY experiment (Figure 14). It was possible to observe the spatial coupling of the methyl hydrogens (H_1) with H_2 and H_3, confirming that the amination reaction predominantly occurs at position C-5 of the triazole ring (Figure 14).

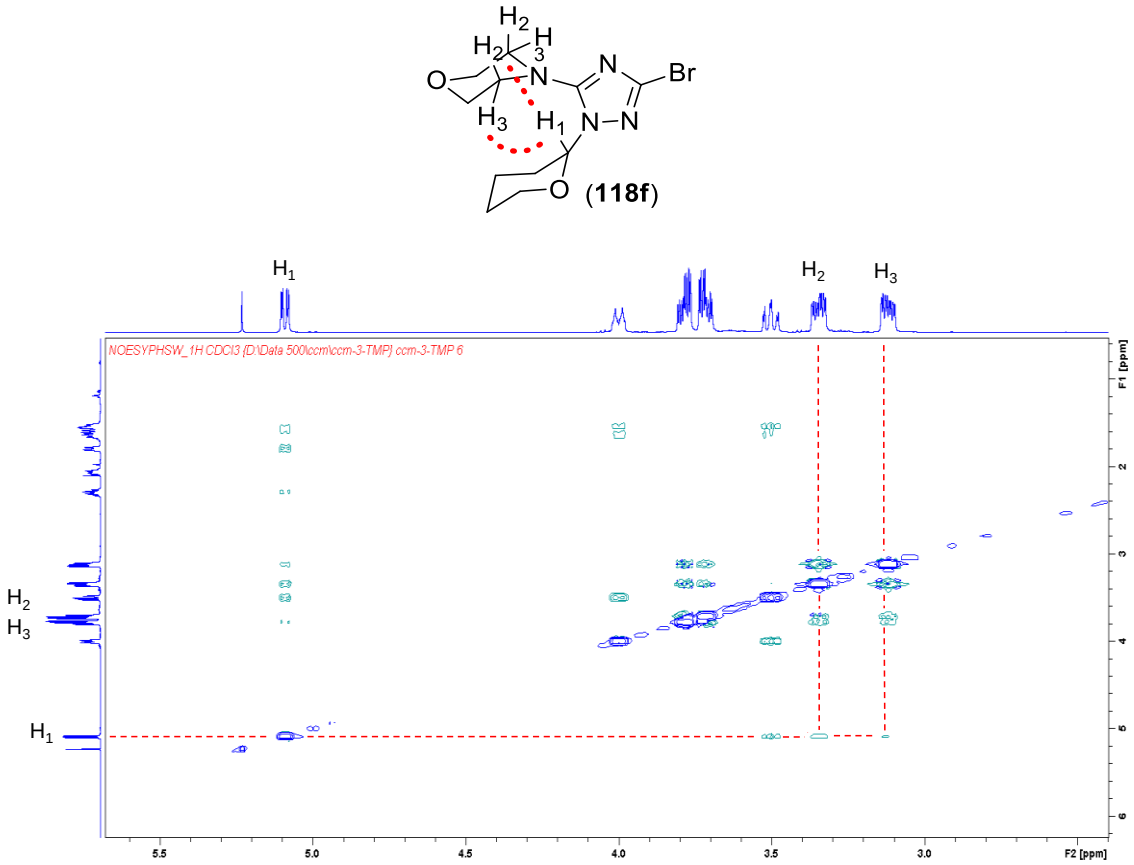

Figure 14. NOESY analysis of the compound **118f** in $CDCl_3$.

3.3.3. Suzuki-Miyaura reaction: C-3 arylation

Next we performed a Suzuki-Miyaura reaction using classical conditions ($ArB(OH)_2$ (1.3 eq.), Na_2CO_3 (2 eq.), $Pd(PPh_3)_4$ (5 mol%), PhMe:EtOH:H_2O (5:1:1), 105°C, 1 h). The compounds were obtained in good to excellent yields varying from 88 to 90%. Only for aminotriazole (**118i**) no reaction was observed, but we were able to obtain the desired compound by PMB deprotection in acid medium in excellent yield (Figure 15).

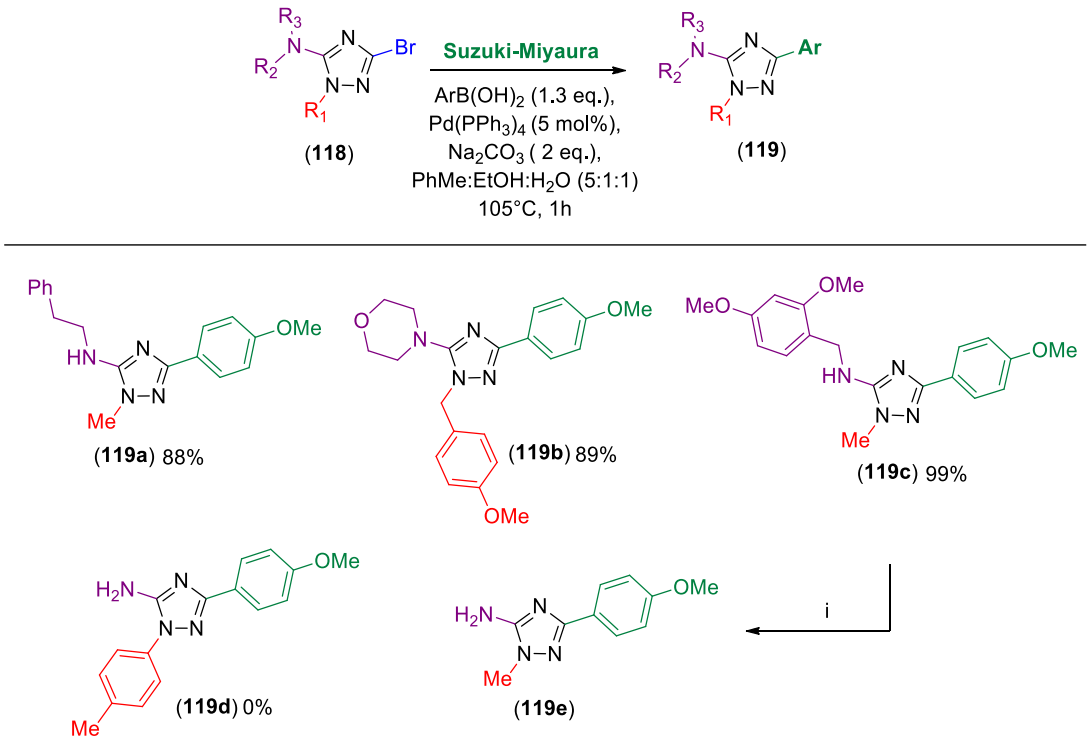

Figure 15. Substrate Scope of 5-amine-1,2,4-triazoles-3-Aryl (**119a-e**). (i) TFA, 100°C, 10 min., μ-waves, 90% yield.

3.4. Desymmetrization strategy for the regioselective functionalization of 3,5-dibromo-1,2,4-triazole

The commercially available 3,5-dibromo-1,2,4-triazole (**114**) showed to be a useful starting material for a quick introduction to structural diversity by means of PCCR. However, as found with other dihalogenated heteroarenes,[110,112] the first PCCR performed on the 3,5-dibromo-1,2,4-triazoles produced a mixture of mono and disubstituted-adducts.

In order to differentiate the reactivity of the both iminobromides in 3,5-dibromo-1,2,4-triazoles (**115**), we investigated the differentiation of the two positions of substitution with the introduction of an *O*-tosyl group (Table 8), as valuable leaving groups for both aminations and Suzuki reactions. Therefore, the 3,5-dibromo-1,2,4-triazoles (**115a-d, i**) were first refluxed in an aqueous sodium hydroxide solution to give the 3-bromo-1,2,4-triazol-5-ones (**143a-e**) in 83-95% (Figure 16).

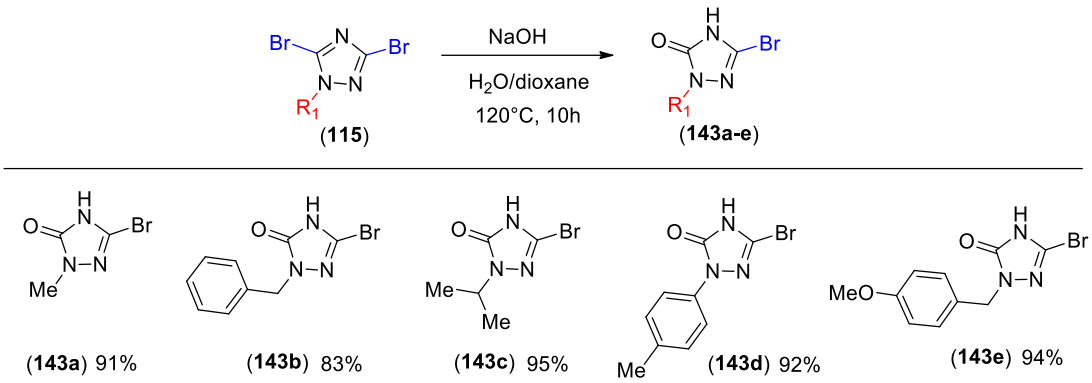

Figure 16. Substrate Scope of N_1-substituted 3-bromo-1,2,4-triazol-5-one (**143a-e**).

Then, the 3-bromo-1,2,4-triazol-5-ones (**143**) was firstly reacted with tosylchoride using pyridine as solvent. However, no reaction occurred (Table 10, Entry 1). Treatment with NaH in THF led to a mixture of *N*- and *O*- tosylation products. The mixture was purified by silica gel chromatography and we identified and distinguished the two isomers by ^{1}H NMR analysis. Due to the possible cone anisotropy produced by the carbonyl group over the -CH_2 in **147**, we attributed it as the corresponding *N*-benzylated product (δ CH_2= 4.74 ppm) while **146** as the *O*-benzylated product (δ CH_2= 5.12 ppm) (Table 10, Entry 2).

The use of K_2CO_3 in DMF resulted in the formation of product **147** but with low reagent consumption (Table 10, Entry 3).

Kim et al. reported efficient *O*-sulfonylation conditions starting from 3-aryl-1-methyl-1,2,4-triazolin-5-ones using pyridine or Et_3N in DCM.[152] By following their reported conditions (4 equiv. of TsCl) the use of pyridine provided the *N*-benzylated product, whereas Et_3N provided a *O*-benzylated in 58% (Table 10, Entry 4 and 5).

In order to optimize the reaction protocol, we reduced the amount of sulfonyl chloride and the reaction time, obtaining the desired O-tosylated product in excellent yields (Table 10, Entry 6).

Table 10. Preparation of 3-bromo-5-*O*-tosyl-1,2,4-triazol (**146**).

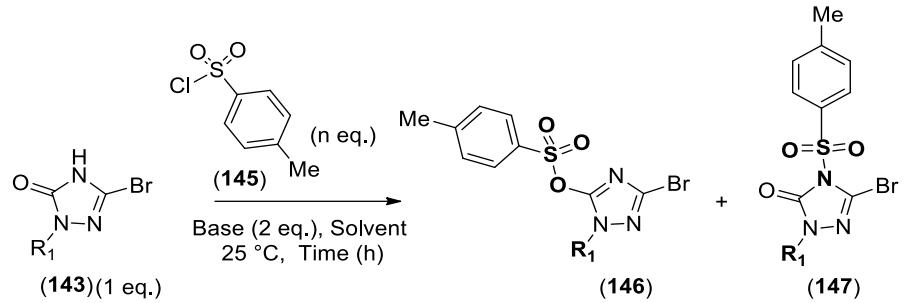

Entry	R_1	145 (n eq.)	Base	Solvent	Time (h)	Yield 146 (%)	Ratio 143/146/147 (HPLC, 210 nm)*
1	4-MePh	1.2	Pyridine	-	1-20	-	no reaction
2	4-MeOBn	1.1	NaH	THF	4	43	147: 28% isolated yield
3	4-MeOBn	1.1	K_2CO_3	DMF	18	-	143/146/147: 2.5/0/1*
4 [152]	4-MeOBn	4	Pyridine	DCM	18	-	143/146/147: 0/0/1*
5[152]	Me	4	Et_3N	DCM	18	58	143/146/147: 0/1/0
6	Me	2	Et_3N	DCM	3	84	143/146/147: 0/1/0

* Not isolated

3.4.1. Suzuki-Miyaura reaction: C-3 arylation

Unfortunately, the standard Suzuki PCCR conditions ($ArB(OH)_2$, Na_2CO_3 (2 eq.), $Pd(PPh_3)_4$ (5 mol%), PhMe:EtOH:H_2O (5:1:1), 105°C, 1 h) were unsuccessfully applied to produce compound **148a** as sole compound. We observed the formation of 3 products **148a**, **149**, **143a** by HPLC, with the compound 3-(4-methoxyphenyl)-1-methyl-1H-1,2,4-triazol-5(4H)-one (**149**) as the major product. This compound was isolated in 54% yield after reaction treatment and purification by silica column chromatography. The high temperature (≥100°C), together with the basic conditions are not suitable for basic-sensitive functional groups like O-tosyl group. For this reason, we subsequently modified our reaction conditions by varying the nature of the base and the solvent, but all these variations were unsuccessful. Under micellar conditions, only the desulfonylated starting material **143a** was observed (Table 11).

Table 11. 3-Bromo-1*H*-1,2,4-triazol-5-aryl sulfonate derivative (**146**) in Suzuki-Miyaura reaction.

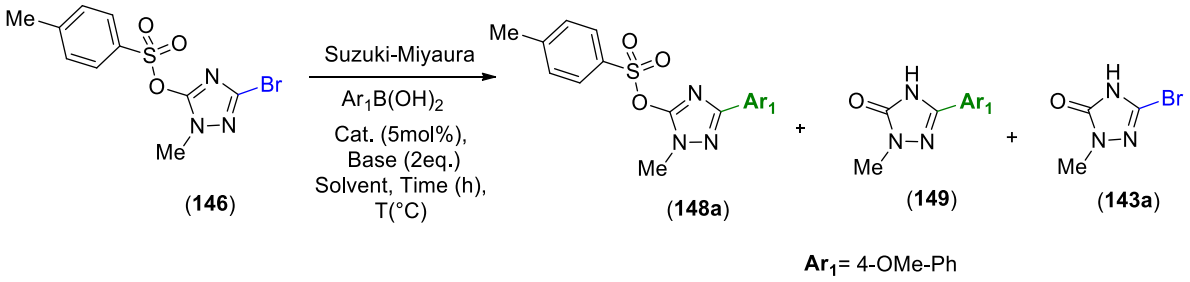

Entry	146 (n eq.)	$Ar_2B(OH)$ (n eq.)	Base	Solvent	T(°C)	Time (h)	Ratio 148a/149/143a (HPLC, 210 nm)**
1[a]	1.2	1	Na_2CO_3	PhMe:EtOH:H_2O	105	1	1.5/37*/1
2[a]	1.2	1	Cs_2CO_3	PhMe:EtOH:H_2O	105	1	1/3.7/0
3[a]	1.2	1	K_3PO_4	PhMe:EtOH:H_2O	105	1	1/8.8/21
4[a]	1	1.05	Na_2CO_3	DME:H_2O	100	0.3	0/1/1.6
5[b]	1	1.3	KF	MeOH	120 (μW)	0.3	4.4/1/11.7
6[c]	1	1.1	Et_3N	H_2O	25	15	0/0/1

[a] catalyst: $Pd(PPh_3)_4$; [b] catalyst: Pd(OAc); [c] catalyst: TPGS (20% v/v), 3 eq. of Et_3N; * obtained in 54% yield; * Ratio was determined by HPLC/UV using caffeine as internal standard.

Although PCCR performed on the intermediate **146** did not allow to recover the monosubstituted adduct in good yield, it was determined that the substitution firstly occurred on the bromine.

With the aim of finding suitable reaction conditions to prevent the desulfonylation of compound **146** during the Suzuki-Miyaura arylation reaction, we conducted a stability assay by varying the base, solvent, temperature, and reaction time. Except for toluene or methanol as sole solvents in short time periods, the presence of water or even the prolonged use of alcoholic solvent demonstrated the formation of desulfonylated products (Table 12).

Table 12. Stability assay for compound **146**.

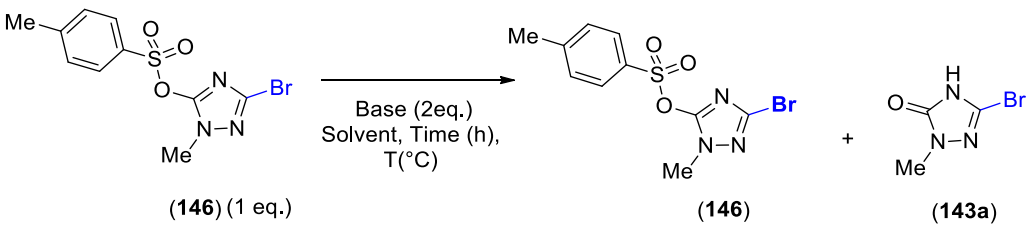

Entry	Base (2 equiv.)	Solvent	T(°C)	Time (h)	Ratio 146/143a (HPLC, 210 nm)
1	Na_2CO_3	PhMe	100	1.5	1/0
2	Na_2CO_3	PhMe:H_2O (5:1)	100	1.5	1/1
3	Na_2CO_3	PhMe:H_2O (5:1)	25	1.5	10/1
4	KF	MeOH	120(μW)	0.3	0/1
5	Et_3N	MeOH	110	0.5	1/0
7	Et_3N	MeOH	110	16	1/3.3

In order to prevent desulfonylation during PCCR reactions, we investigated a sterically hindered arylsulfonylchloride, O-Tri-O-4,6-triisopropylbenzenesulfonylgroup (T*i*PSCl). Using the optimized conditions (T*i*PSCl (1 eq.), Et_3N (2 eq.), DCM, r.t., 2h) for the sulfonation reaction and starting from N-Me and N-Bn triazolones **143a-b**, the TiPSO-triazoles **151a** and **151b** were obtained respectively in 89 % and 91% yields after purification (See table 8). Finally, as illustrated in scheme 9, the Suzuki procedure was successfully applied under our conventional conditions ($ArB(OH)_2$ (1.3 eq.), Na_2CO_3 (2 eq.), $Pd(PPh_3)_4$ (5 mol%), PhMe:EtOH:H_2O (5:1:1), 105°C, 1 h) to yield the expected monosubstituted adducts **152a** and **152b** in 98% and 73% yield respectively (Scheme 26).

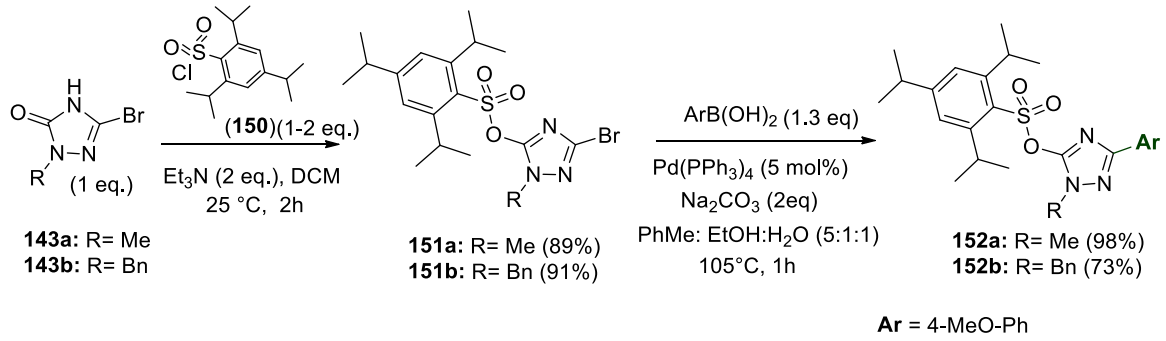

Scheme 26. Sequential Sulfonylation and Suzuki-Miyaura reaction.

Next, we involved compound **152a** and **152b** in a second Suzuki reaction using 4-MePh-$(BOH)_2$ as the coupling partner. Various conditions were tested. At 105°C under our conventional conditions over an extended period ($ArB(OH)_2$ (1.3 eq.), Na_2CO_3 (2 eq.), $Pd(PPh_3)_4$ (5 mol%), PhMe:EtOH:H_2O (5:1:1), 105°C, overnight), the aromatic insertion did not take place and we obtained only desulfonylation. Similar results were obtained by microwave heating ($PhB(OH)_2$ (1.3 equiv), $Pd(PPh_3)_4$, 155°C, 30 min , DME-H_2O 3:1). It's

worth noting that these last conditions were effective starting from O^6-TiPS-4-bromo-pyridazine 3-one (**155**) which offers two chemically different functionalities for sequential PCCR.[153] Finally, we introduced a bulky and electron-enriched dialkyl-biaryl phosphines such as BrettPhos[154] (**L_8**) ($Pd(OAc)_2$ (5 mol%), **L_8** (10mol%), K_3PO_4, 2Me-2-BuOH, 100°C); ($Pd(OAc)_2$ (5 mol%), L(10mol%), K_3PO_4, i-PrOH, 80°C) and ($Pd(OAc)_2$ (5 mol%), **L_8** (10mol%), K_3PO_4, MePh, 100°C) which should increasing the rate of oxidative addition. Despite numerous attempts to functionalize the O-Tri-O-4,6-triisopropylbenzenesulfonyl group through Suzuki reaction conditions, all efforts proved unsuccessful (Scheme 27).

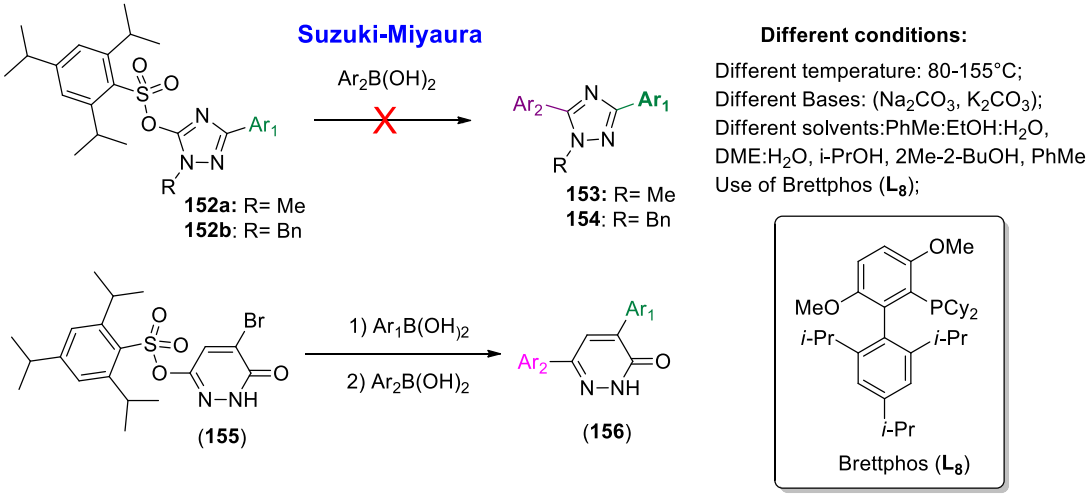

Scheme 27. Reactivity of OTiPS pyridazine versus OTiPS triazole.

In view of these negative results, we turned to an alternative which involves hydrolyzing the sulfonyl function to obtain triazolone (**149**) and then converting it to the corresponding iminochoride (**157**) with the help of $POCl_3$ as illustrated in scheme 28. Starting from **152a**, treatment with sodium hydroxide led to the triazolone **149** in 90% yield. Subsequent treatment with $POCl_3$ afforded the chlorotriazole **157** in 92%. Finally, the activated compound (**157**) was arylated through the Suzuki reaction in 72% after purification (Scheme 28).

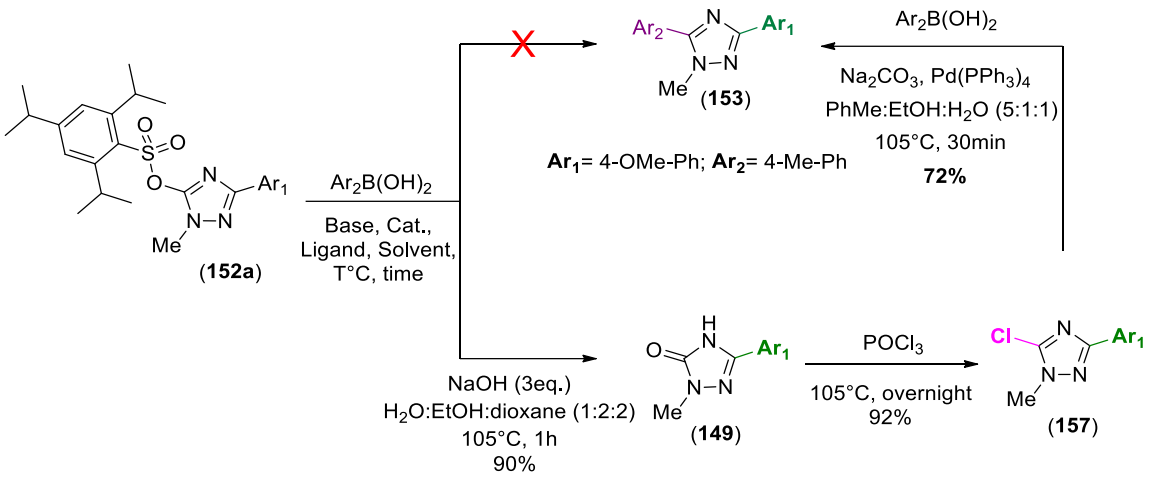

Scheme 28. Sequentiel Suzuki-Miyaura reaction starting from **152a**.

3.4.2. Amination reaction

As expected, and following the negative results obtained for the Suzuki reaction, both SNAr and Buchwald reactions yielded identical results when reacting O-Tri-O-4,6-triisopropylbenzenesulfonyl-1,2,4-triazole (**152a**) with phenethylamine (**140**). The nucleophile reacted with the benzenesulfonyl group, producing **159** and **143a** (Scheme 29).

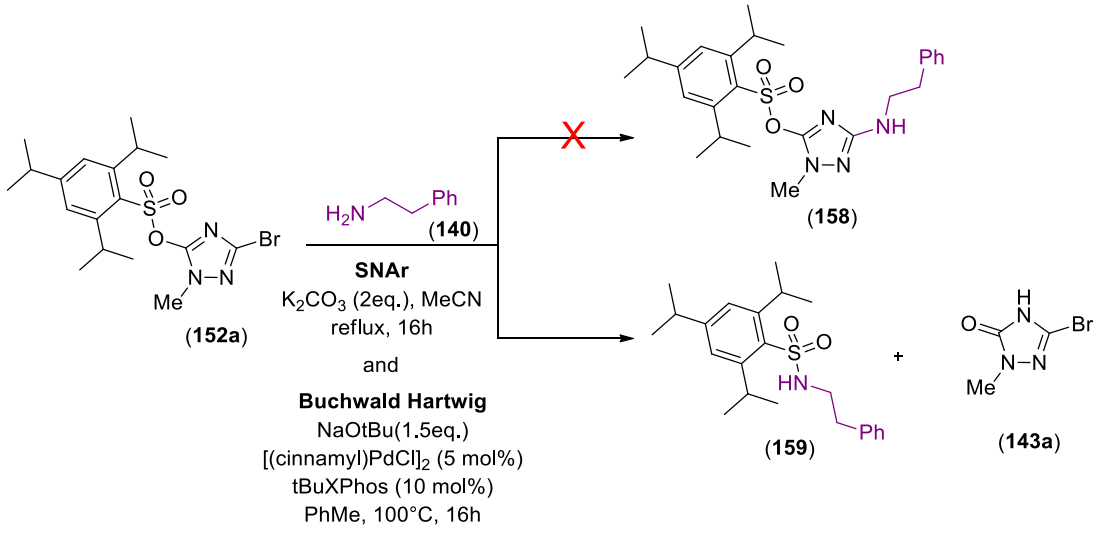

Scheme 29. SNAr and Buchwald Hartwig amination reactions.

3.5. Miscelaneous reactions: introduction of C-5 protecting groups

The discrimination of reactivity in the triazolic ring with the introduction of *O*-sulfonate groups showed no reactivity at C-5 for Suzuki reaction and lability of the sulfonate group in the

presence of phenetylamine. For these reasons, to discern the reactivity of iminobromides, we chose alternative approaches involving the introduction of the methoxymethyl ether (MOM) and benzyl protection groups.

3.5.1. Introduction of MOM group as "protecting group"

The bromotriazolones **143a** and **143b** were protected with 2-methoxyethoxymethyl chloride in the presence of NEt_3 in dichloromethane (DCM) at room temperature, affording **160a** and **160b** in 82% and 64% of yield, respectively. Subsequently, the arylated product (**161**) was successfully obtained from **160a** using the Suzuki protocol with a 82% yield, followed by deprotection under acidic conditions to yield the triazolone (**149**), which was then activated phosphorus trichloride ($POCl_3$) medium. We addressed the reactivity of iminochloride (**157**) through the Suzuki-Miyaura reaction, resulting in **153** with a yield of 72% using 4-Me-phenylboronic acid (Scheme 30).

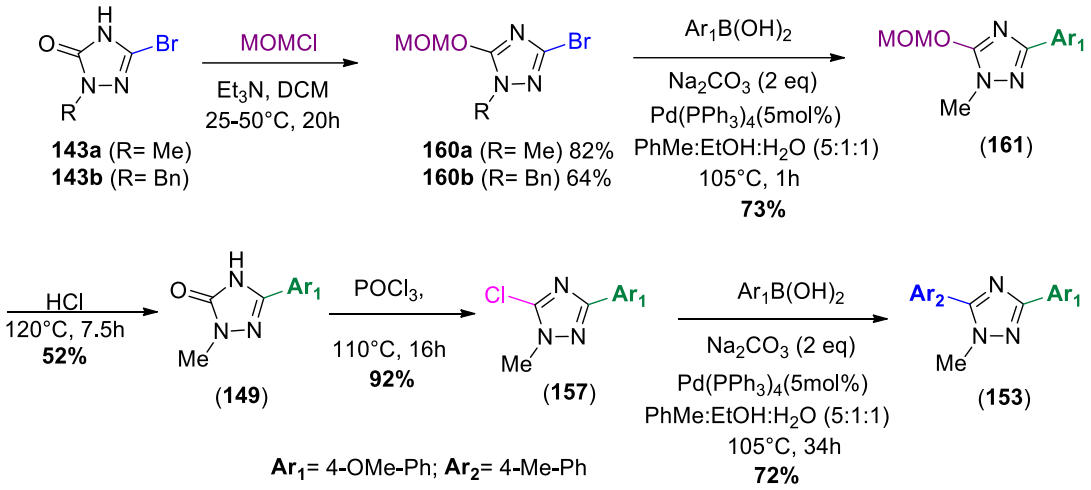

Scheme 30. Synthetic route with **160a-b** as key intermediates.

We further investigated the reactivity of iminochloride **157** through the PCCR Buchwald-Hartwig and SNAr reactions using 2-phenethylamine as a nucleophile. No reaction was observed under SNAr conditions, while the Buchwald-Hartwig reaction yielded **119a** in 80% yield after purification (Scheme 31).

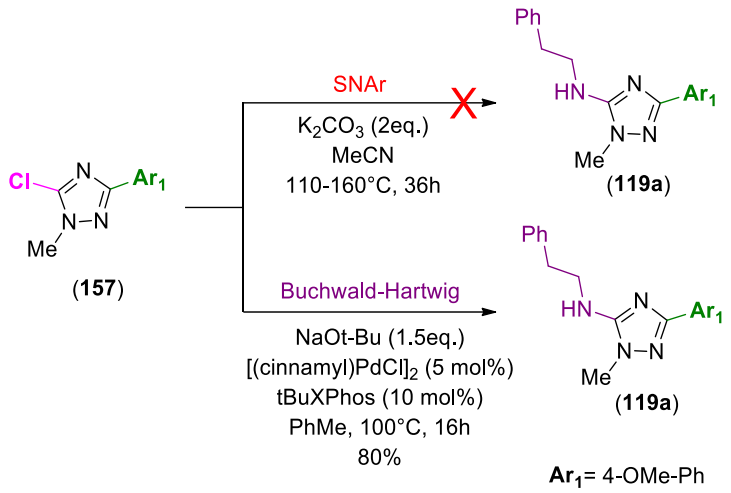

Scheme 31. Amination reaction of iminochloride **157**.

3.5.2. Introduction of Bn group as "protecting group"

In order to introduce a -OBn moiety in position 3 of the triazol ring, dibromotriazole (**115**) was initially heated at 120°C with benzyl alcohol and potassium carbonate in tert-butanol medium. After 1 hour, the formation of a product was observed, although a significant amount of starting material remained. Increasing the temperature to 160°C for an additional 3 hours resulted in complete consumption of the reagent and the formation of a new major and more polar product was observed. The mixture of products was isolated and obtained with 27% and 54% yields respectively after purification (Scheme 32). Analysis by ^{1}H NMR of the isolated compounds revealed the formation of two regioisomers. Unfortunately, the use of NOESY technique did not show spatial coupling of -CH_2 (δ 4.9 or 5.5 ppm) with the N-aryl hydrogens for both regioisomers. Additionally, the HMBC analysis did not show correlation of the *o*-N-aryl hydrogens (δ 7.7 or 7.5 ppm) with the quaternary C_5, however, the -CH_2 from one of them showed more correlation with the carbons (Figure 17 and Figure 18) which is expected for the C_5 substituted regioisomer, with the possible correlation between -CH_2 with the quaternary phenolic N_1-C_1. This, in our opinion, suggest that the regioisomer isolated in 54% is compound **162**, whereas **163** was obtained in 27% (Scheme 32), which is consistent with the results obtained previously for the arylation and amination reactions. A more detailed analysis is ongoing to confirm the proposed regioisomers 162 and 163.

Using less drastic conditions by refluxing gently benzylalcoolate in presence of **115b-c**, similar conditions then described by Khaliunllin et al., (dibromo-1,2,4-triazole in presence of

alcoolate)[155] presumably afforded the 5-OBn derivatives as the sole product and in quantitative yield (Scheme 32).

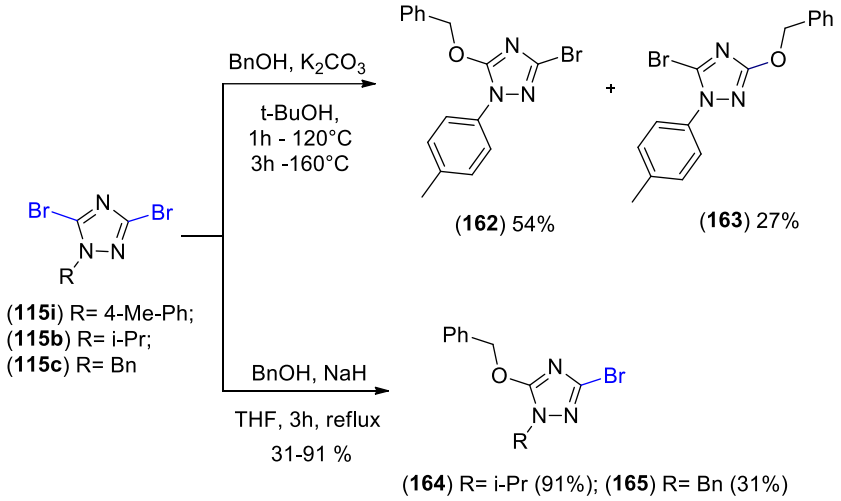

Scheme 32. Benzylation of 3,5-dibromo-1-alkyl-1*H*-1,2,4-triazol.

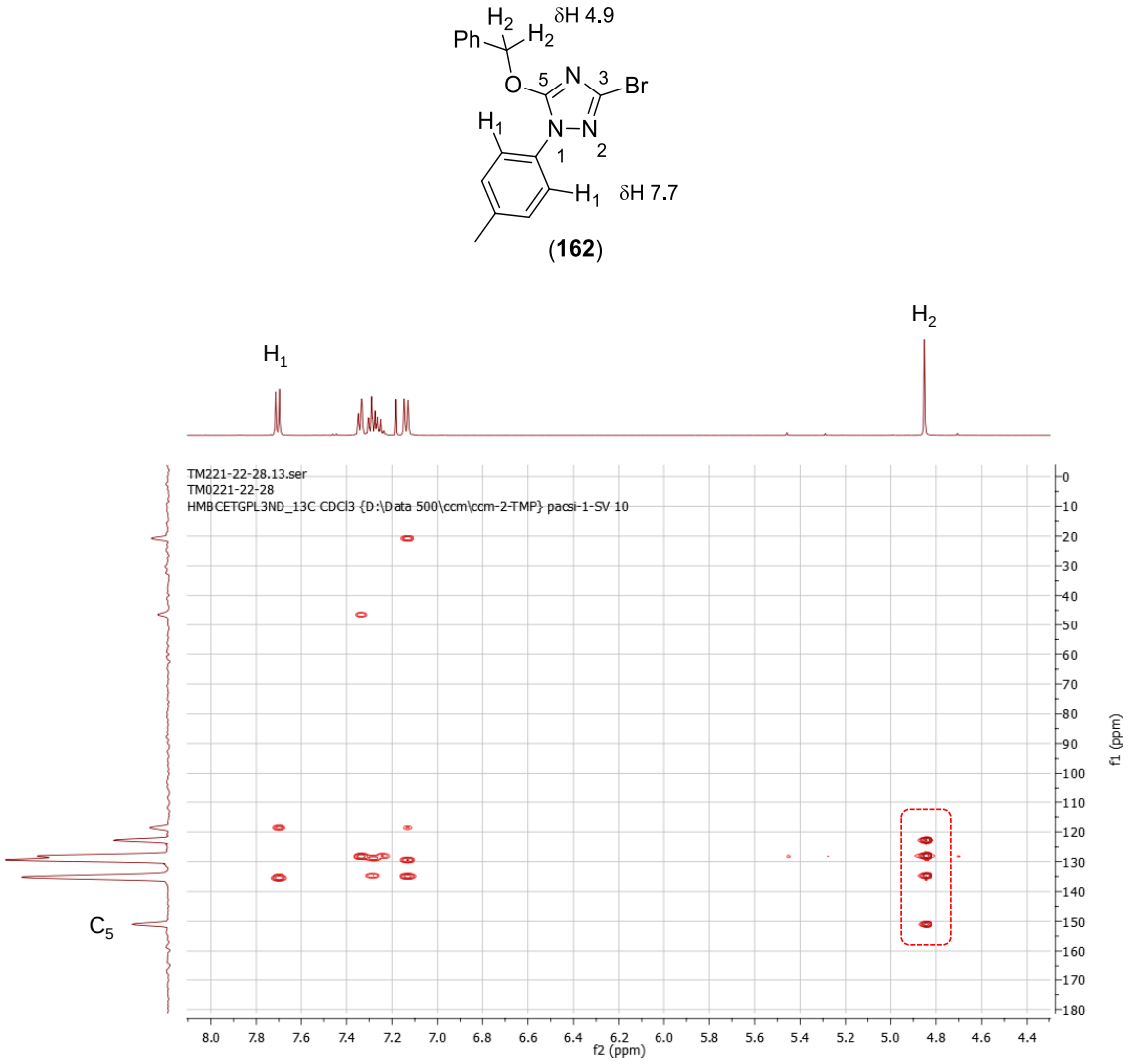

Figure 17. HMBC analysis of the compound **162** in $CDCl_3$.

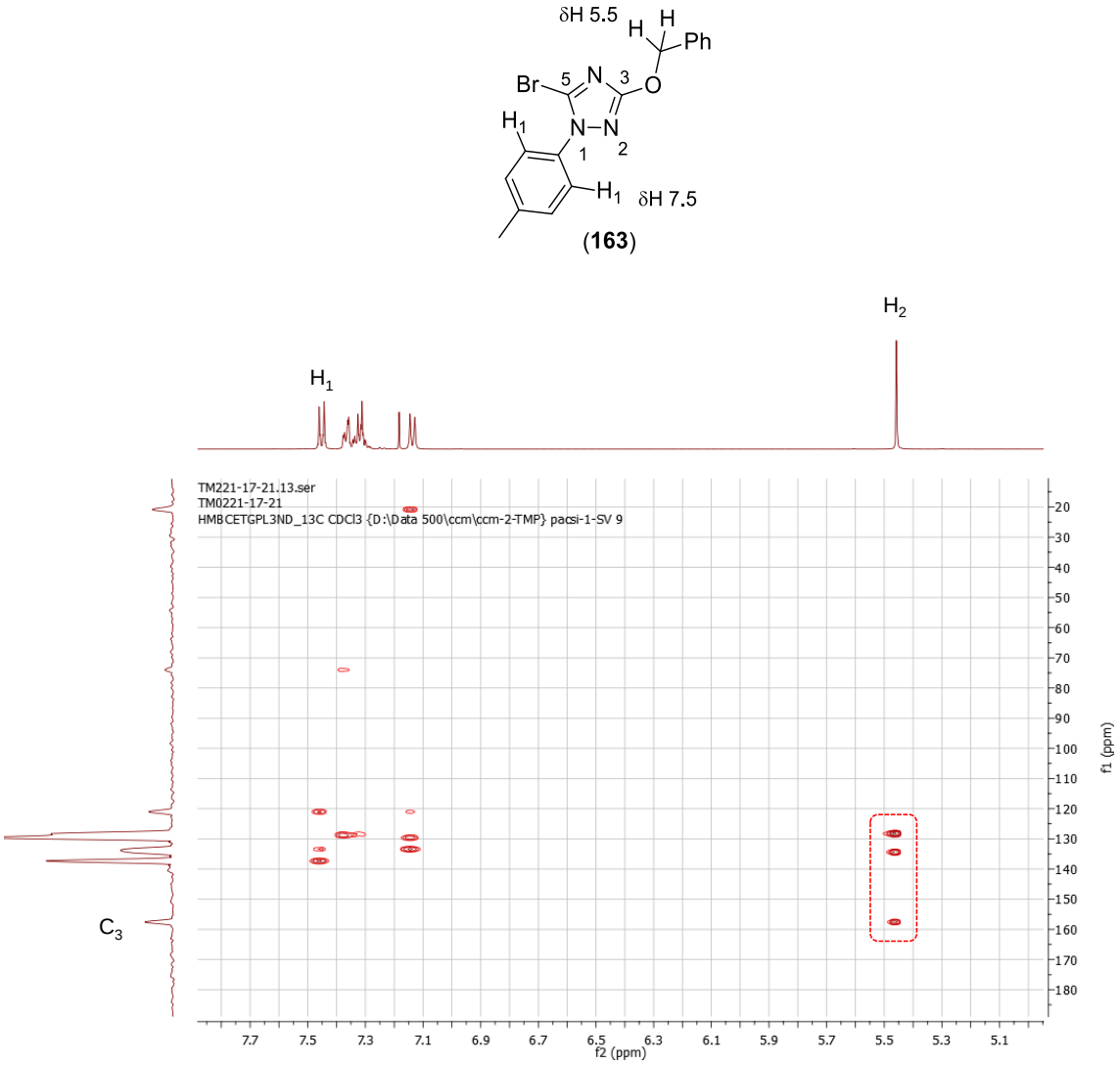

Figure 18. HMBC analysis of the compound **163** in $CDCl_3$.

Subsequently, O-benzyl triazole (**164**) was subjected to a Suzuki-Miyaura reaction. Surprisingly, a mixture of 2 products was observed, including the expected product **166** but also the unprotected arylated product **167** in a ratio of 1:3.5 after purification. In addition, we were able to functionalize the triazolone (**143b**) by Suzuki arylation without the need of protecting group. The compound **167** was then activated with $POCl_3$ under reflux, leading to the iminochloride **168** in 86% yield. The behavior of **168** under PCCR conditions is currently on going in the lab (Scheme 33).

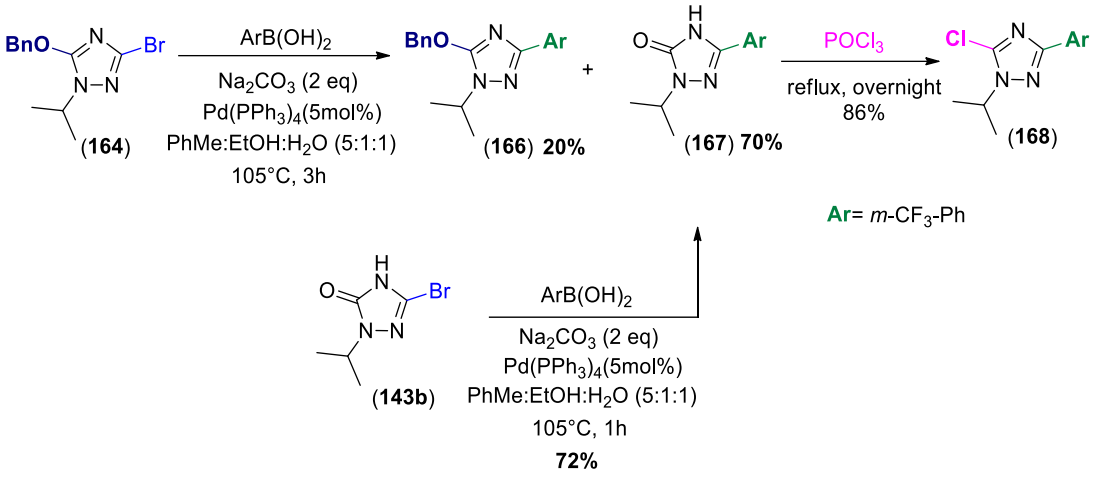

Scheme 33. Sequential functionalization of *O*-benzylated-1,2,4-triazole (**164**).

The compound **164** was subjected to two stability assays to assess the stability of the O-Bn bond. In the first assay, **164** was exposed to the same reaction conditions as the Suzuki reaction, but without boronic acid. Even after 3 hours, no changes were observed. For the second trial, we omitted the catalyst $Pd(PPh_3)_4$ and observed the same result. Both boronic acid and the $Pd(PPh_3)_4$ were omitted in a third trial. Despite being heated at 105°C for 17 hours, no debenzylation of compound **164** was observed.

In another hand, the OBn derivative **165**, was also subjected to a Buchwald-Hartwig-type amination reaction, yielding only the desired protected products **169-170**. Compound **169** was then activated with $POCl_3$ under reflux, leading to the correspondent iminochloride **171** in 89 % yield. The behavior of **171** under Suzuki –Miyaura conditions is actually on going in the lab (Scheme 34).

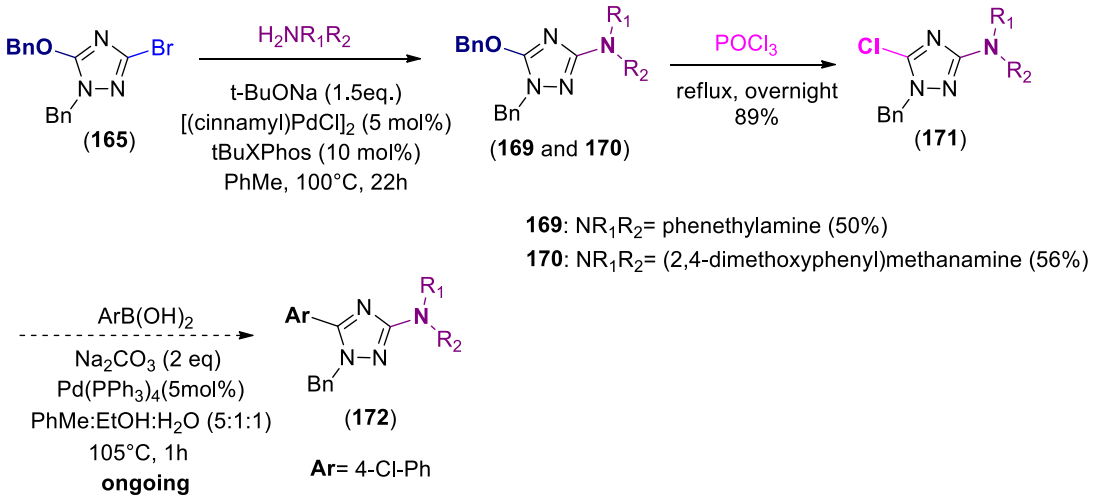

Scheme 34. Sequential Buchwald-Hartwig reaction and deprotection.

We also investigated the N-benzylation of the triazole as a protection strategy. Compound **143b** was refluxed with benzyl bromide and potassium carbonate in acetonitrile for 3 hours. The benzylated compound obtained was analyzed by ^{1}H NMR to verify whether we obtained the N- or O-benzylated product. Two -CH_2 peaks at 4.86 and 4.96 ppm and one multiplet at the aromatic region 7.27-7.40 ppm were observed, while the previously obtained *O*-benzylated (**165**) product possess two -CH_2 peaks at 5.05 and 5.43 ppm and three multiplets at the aromatic region. These differences indicate that the expected N-benzylated compound (**173**) was obtained in 63% yield, and we are currently studying the reactivity of the iminobromides by addressing the Buchwald-Hartwig reaction (**174**). The expected product formation was detected after 22 hours via LC/MS, with a ratio of 3:1 compared to the reactant (Scheme 35).

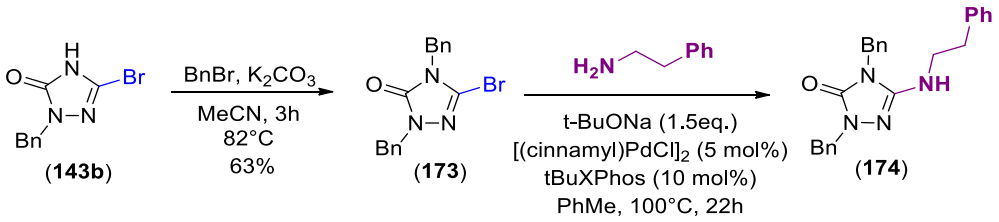

Scheme 35. Sequential protection and Buchwald-Hartwig reaction.

3.6. Ullmann-type functionalization

In addition to the palladium-catalyzed study, we became interested in the Ullmann reaction for introducing primary aliphatic amines onto 1,2,4-triazoles. Thanks to S. Buchwald, this reaction was revisited in the early 21st century with the provision of efficient and versatile ligands, enabling the formation of a C-N bond under milder reaction conditions.[156] This significant discovery allows for the use of copper in catalytic quantities. Furthermore, this metal is less expensive and less toxic than palladium. Subsequently, several groups became interested in developing new ligands (Figure 19) to design simple and effective procedures.

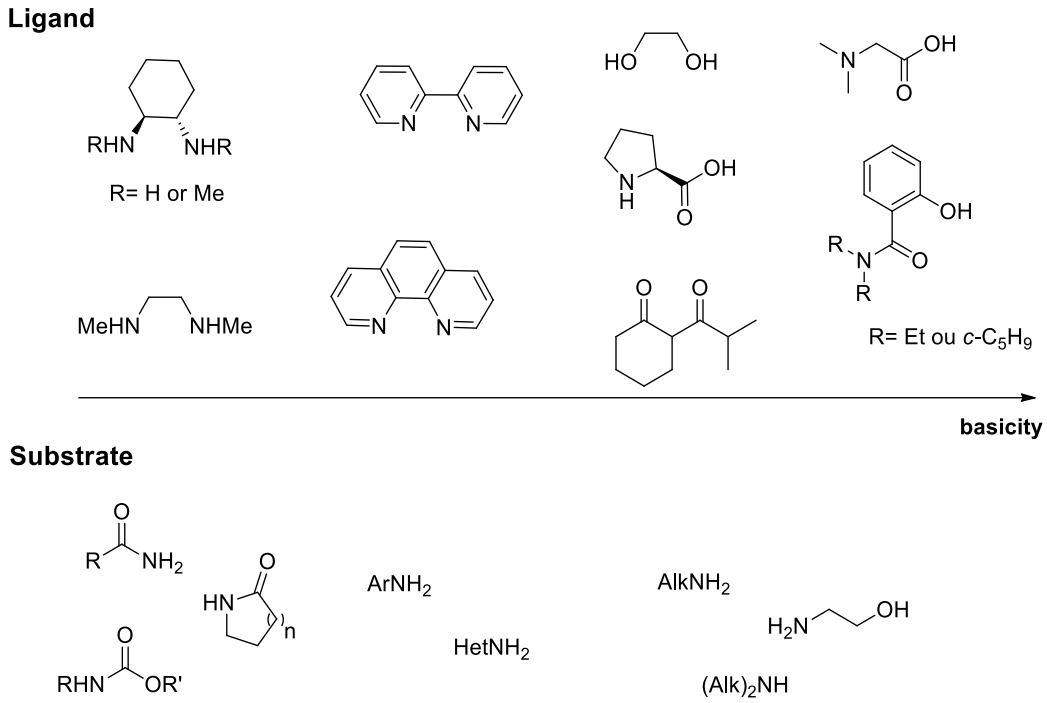

Figure 19. Ranking of copper ligands used for the Ullmann reaction based on the basicity of the amine.[156]

Among these ligands, there are diamine chelating ligands that have shown their importance for the arylation of amides, lactams, and carbamates. For example, we can also mention 2,2'-bipyridine or 1,10-phenanthroline, used for the arylation of anilines or aminoheterocycles. Finally, bidentate ligands such as ethylene glycol,[157] proline,[158] N,N-dimethylglycine, but also dicarbonyl compounds such as iso-butyrylcyclohexanone,[159] have proven to be very useful for N-arylation selectivity versus O-arylation (Figure 20 and Scheme 36).

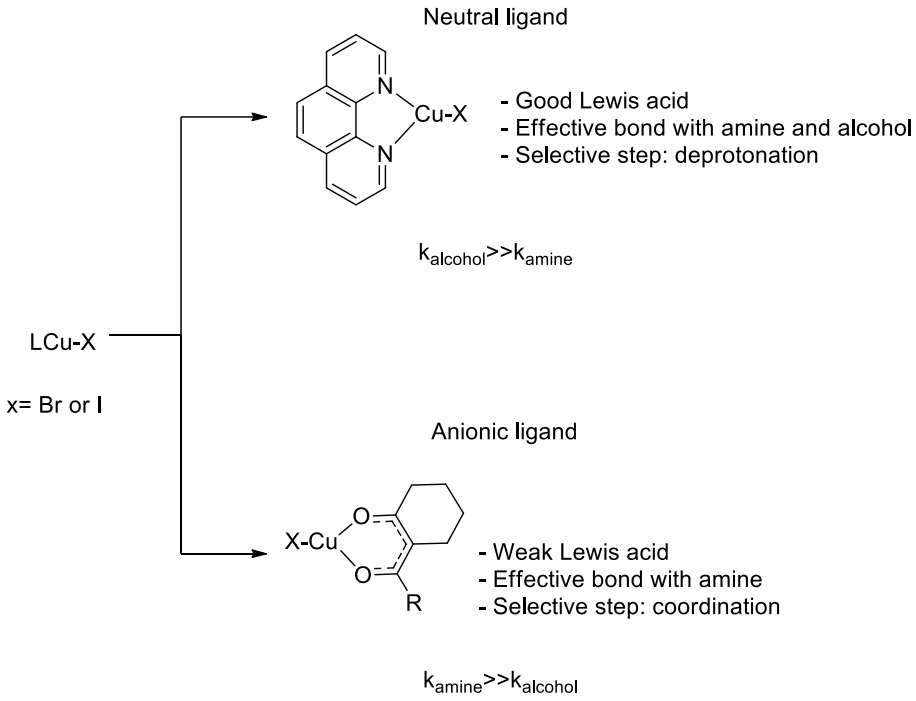

Figure 20. Difference in selectivity for the arylation of an amine between a neutral ligand and an anionic ligand.[160]

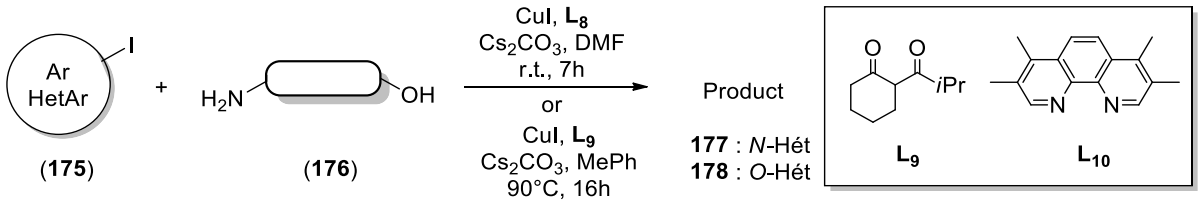

***N*-arylation (L_9)**			***O*-arylation (L_{10})**		
Cpd	**Product**	**Yield %**	**Cpd**	**Product**	**Yield %**
177	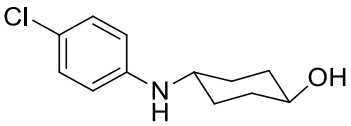	80	**178**	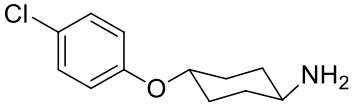	80

Scheme 36. N- vs O-arylation selectivity.[161]

Finally, a comparative study of bidentate ligands was conducted by the group of S. Buchwald starting from 3,5-dimethyliodobenzene.[159] This study highlighted the high efficiency of iso-butyrylcyclohexanone (**L_{11}**) as a ligand for primary amines (Figure 21).

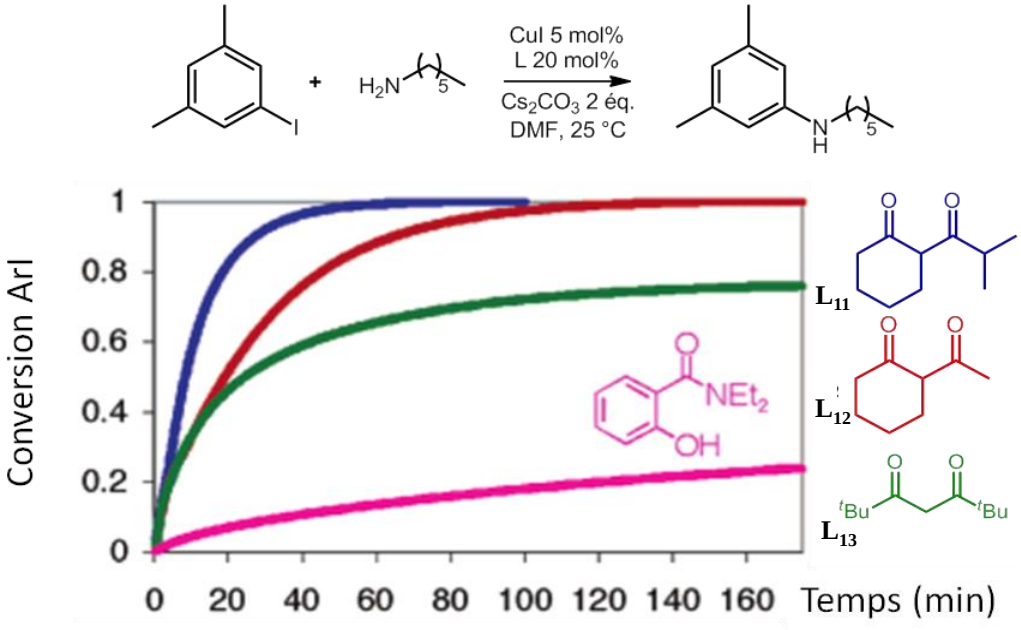

Figure 21. Efficient diketone ligands for the N-arylation of primary amines.[159]

3.6.1. Personal work

To our knowledge, the Ullmann reaction has never been applied to halogenated 1,2,4-triazoles. Three tests were carried out with cyclopropanecarboxamide and azide as nucleophiles towards MOMO- and BnO-triazole (**160b** and **165**) employing the method described by Andersen et *al*. in 2005.[162] The authors described a rapid synthesis of aryl azides from the corresponding aryl halides catalyzed by CuI/diamine (**L_{14}**). In addition, they noted that sodium ascorbate positively influenced the stabilization of the catalyst system. The reactions were performed under mild conditions generally with high yields.

The first reaction with cyclpropanecarboxamide led to the formation of many products, but the LC/MS analysis made it possible to identify the product with the expected mass corresponding to 24% of the total area (Table 13, entry 1). In the presence of azide, we performed two reaction. In both, the major products identified by LC/MS, **180** and **181**, showed NR_1R_2= NH_2 and corresponding areas of 40% and 52%, respectively (Table 13, entry 2 and 3).

Table 13. Reaction conditions for Ullmann-type functionalization.

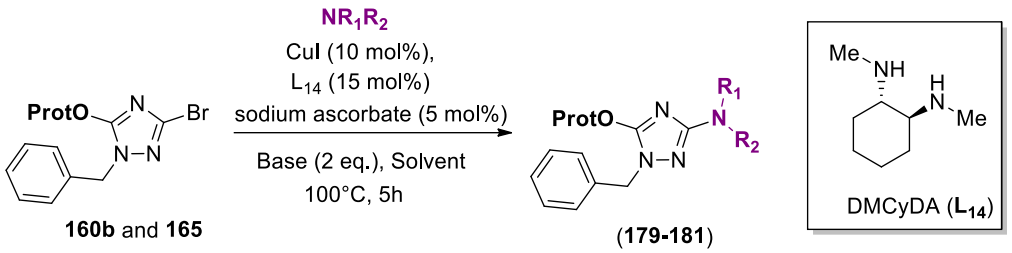

Entry	Prot	NR_1R_2	NR_1R_2 (n° eq.)	Base	Solvent	Comments (LC/MS % area)
1	MOM	H_2NCOc-Pr	2	K_3PO_4	MePh	**179**: 24%
2	MOM	N_3	3	-	H_2O:EtOH (1:2)	**180**: 40%*
3	Bn	N_3	3	-	H_2O:EtOH (1:2)	**181**: 52% *

***** NR_1R_2= NH_2

Due to the schedule of this thesis work, it was not possible to isolate the above products. Therefore, the development of a scope for the Ullmann-type reaction in 1,2,4-triazoles using different ligand sources, bases and solvents will be performed soon.

3.7. Cyanation of 3,5-dibromo-1,2,4-triazole

Aryl nitriles are important building blocks for numerous pharmaceuticals, herbicides, natural products, and dyes. The compact nature of the nitrile, along with its hydrogen-accepting ability and in vivo metabolic stability, has made this functional group significant for medicinal chemistry research.[124] Currently, there are more than 30 approved drugs, along with 20 drug candidates in clinical testing stages, that contain one or more nitrile substituents in their chemical composition. The nitrile function serves as an excellent synthetic precursor to a variety of functional groups, such as amides, ketones, amines, and alcohols. For these reasons, significant attention has been devoted to the development of efficient and practical methodologies for the synthesis of aryl nitriles.

Recently, Peng and colleagues reported on the synthesis and pharmacological evaluation of a series of triazole-based Sigma 1 antagonists.[163] The synthetic pathway for obtaining these antagonists lacks convergence with functionalization in the initial stages of the route (Scheme 37).

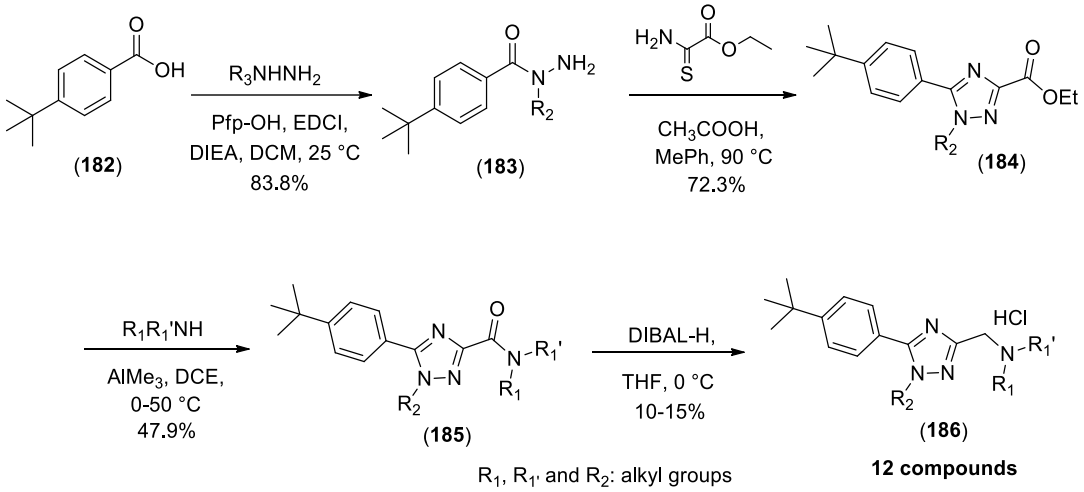

Scheme 37. Non-convergent synthetic route to obtain the triazole-based sigma 1 antagonist.[163]

As an alternative, we propose a new synthetic route illustrated in scheme 38. Introducing the cyano group to the triazole ring will allow greater molecular diversity in a more convergent synthetic approach. The optimization of the cyannation reaction conditions with different CN sources will be performed soon.

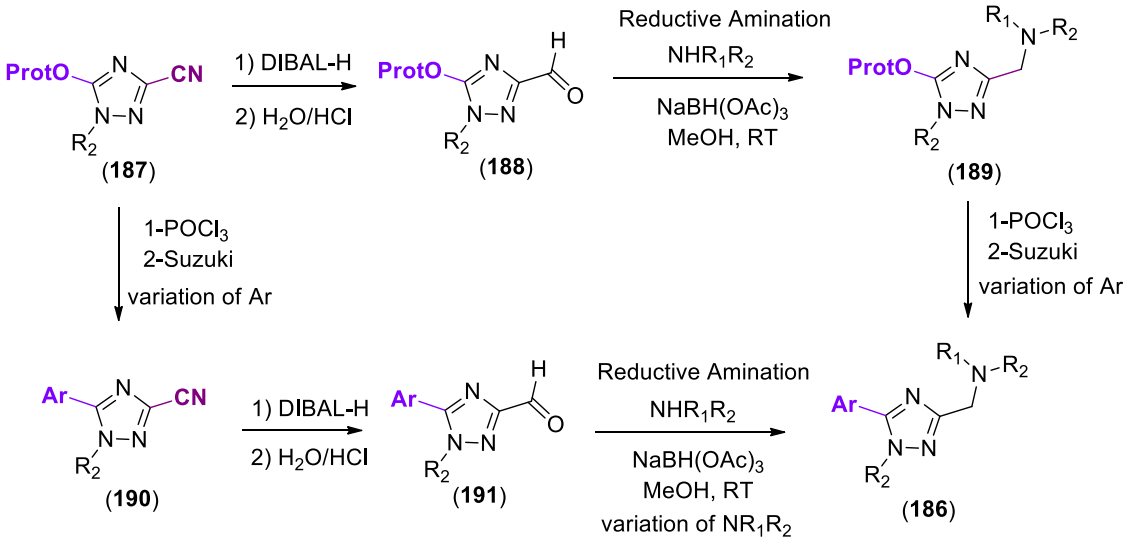

Scheme 38. New synthetic route to obtain the triazole-based sigma 1 antagonist.

3.7.1. Personal work

In order to investigate the feasibility of introducing a cyano group to dibromotriazole (**115i**), we intend to initially study the reactivity through aromatic nucleophilic substitution reactions.

By employing NaCN in DMF at 110°C, the cyano triazole (**192**) was obtained in quantitative yield, subsequently leading to the corresponding ester (**193**), amide (**194**) and acid (**195**) derivatives through methanolysis with $SOCl_2$ at room temperature (Scheme 39).

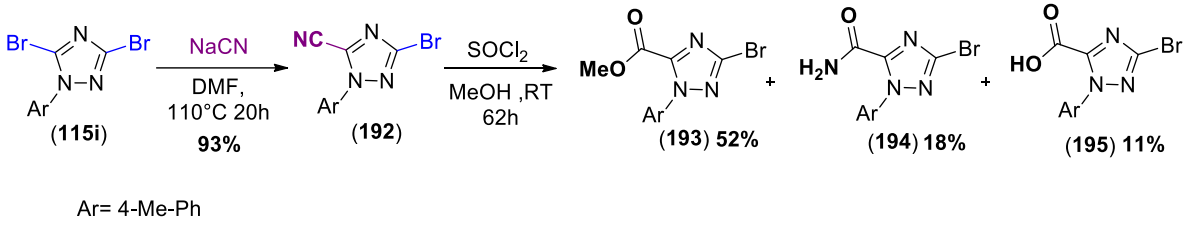

Ar= 4-Me-Ph

Scheme 39. Sequential Cyanation and methanolysis reactions.

4. CONCLUSION AND PERSPECTIVES

In this work, we synthesized a small library of novel polysubstituted 1,2,4-triazoles. For this, we employed pertinent strategies of chemo- and regioselective synthesis starting from the readily available 3,5-dibromo-1*H*-1,2,4-triazole.

Through collaboration, we conducted a Theoretical DFT study of N-methyl-dibromo-1,2,4-triazole aiming to explain the difference in reactivity between the two iminobromines. After analyzing the HOMO/LUMO/HOMO-1/LUMO+1 orbitals, ionization potential map (IP), and electrostatic potential map (MEP), the reactivity differences became evident, showing that C_3-Br is more susceptible to nucleophilic attack and PCCR reactions.

We employed the desymmetrization strategy by introducing sulfonyl groups, less reactive in PCC. The presence of the electron withdrawing group T*i*PSO increased the reaction constant of the Suzuki reaction at C_5-Br. Unfortunately, our efforts to functionalize the T*i*PSO-C_5 group proved to be unsuccessful, but through a simple and fast hydrolysis, followed by activation with $POCl_3$, we were able to functionalize C_5-Cl by means Suzuki and Buchwald reactions, altering the initial functionalization sequence. Additionally, we successfully applied the protection of the triazole C_3 position with MOM and benzyl protecting groups.

We efficiently applied the 2d NMR techniques NOESY, for spatial coupling, and HMBC to determine the regioselectivity of the isolated compounds.

The commercially available 3,5-dibromo-1*H*-1,2,4-triazole showed to be a versatile starting material, ensuring a straightforward exploration of structural diversity.

As a perspective, we intend to optimize the Buchwald-Hartwig reaction for secondary amines and amides, as well as explore the Ullmann-type functionalization reaction for the same purpose. We also aim to investigate the mechanisms involved in debenzylation during the Suzuki-Miyaura reaction and explore the copper-catalyzed cyanation reaction at C_3-Br, which could enable the introduction of a wide variety of functional groups. Additionally, we aim to increase the scope of synthesized compounds for publication in a scientific journal.

5. EXPERIMENTAL

5.1. Materials and instruments

All commercial reagents were used without purification. Analytical TLC was performed using Merck 60 F254 silica gel plates, and visualized by exposure to ultraviolet light (254 and 365 nm). Compounds were purified on silica gel Merck 60 (particle size 0.040−0.063 nm). NMR spectra were recorded on Bruker Avance III spectrometers. Operating at 500, 400, or 300 MHz for ^{1}H, 125, 101, or 75 MHz for ^{13}C. All chemical shift values δ and coupling constants J are quoted in ppm and in Hz, respectively, multiplicity (s= singlet, d= doublet, t= triplet, q= quartet, m= multiplet, and br = broad). Analytical RP-HPLC-MS was performed using a LC 1200 Agilent with quadrupole-time-of-flight (QTOF) (Agilent Accurate Mass QToF 6520) with a ZORBAX Agilent C18-column (C18, 50 mm × 2.1 mm; 1.8 μm) using the following parameters: (1) the solvent system: A (0.05% of formic acid in acetonitrile) and B (0.05% of formic acid in H_2O); (2) a linear gradient: t = 0 min, 98% B; t = 8 min, 0% B; t = 12.5 min, 0% B; t = 12.6 min, 98% B; t = 13 min, 98% B; (3) flow rate of 0.5 mL/min; (4) column temperature: 35 °C; (5) DAD scan from 190 to 700 nm; and (6) ionization mode: ESI+. HPLC were performed using a Dionex UltiMate 3000 using the following parameters: column temperature: 40°C, from t = 0 min to t = 3.80 min the flow rate goes from 0.650 mL/min to 0.900 ml/min with the solvent system: A (0.05% of TFA in H_2O) and B (MeCN) with 5 to 100% of B, then after t = 3.80 min to the end of the run t = 5.50 min: 100% of B at 0.900 ml/min.

5.2. Synthetic Methodology

5.2.1. Synthesis of 3,5-dibromo-1*H*-1,2,4-triazole (114)[105]

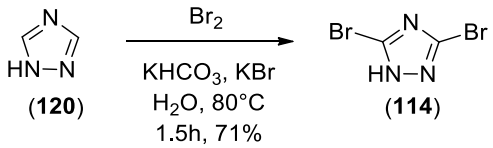

A 100 mL round bottom flask containing a Teflon stirrer bar was charged with 1,2,4-triazole (1 eq., 1 g, 14.48 mmol) and water (25 mL) followed by the addition of $KHCO_3$ (2.35 eq., 3.4 g, 33.96 mmol). The reaction mixture was stirred and heated to 80°C for 30-40min. To this solution, Br_2 (2.14 eq., 4.95 g, 1.59 mL, 31 mmol) diluted in aqueous solution of KBr (0.7 eq., 1.2 g, 10.084 mmol) was added dropwise with constant stirring. The reaction mixture was stirred for further 15-20 min to eliminate the excess of bromine. The reaction mixture was

cooled to room temperature and acidified. The resulting precipitate was filtered off and washed with ice cold water. The dry precipitate was recrystallized from hot H_2O (35ml) and filtered off under reduced pressure to give the desired product as white solid (2.33 g, 10.28 mmol, 71%). ^{1}H NMR (400 MHz, DMSO): δ 15.24 (bs, 1H).

5.2.2. Synthesis of 3,5-dibromo-1-methyl-1H-1,2,4-triazole (115a)[106]

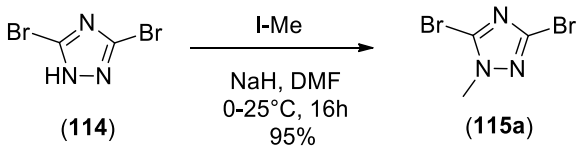

A 100 mL round bottom flask containing a Teflon stirrer bar was charged with 3,5-dibromo-1,2,4-triazole (1 eq., 3.0 g, 13.22 mmol) and solubilized in 40 ml of anhydrous DMF under stirring. The solution was cooled to 0°C and then NaH (1.202 eq., 636 mg, 15.9 mmol) was added slowly in small portions. After 30 minutes MeI (2 eq., 3.75 g, 1.64 mL, 26.41 mmol) was added dropwise and the reaction was stirred 18h at room temperature. The progress of the reaction was monitored by HPLC. The reaction mixture was solubilized with 100 ml of saturated solution of NaCl and extracted with EtOAc (3 x 100 mL). The organic layers were collected, washed with H_2O (3 x 100 mL), dried with anhydrous Na_2SO_4 and concentrated under reduced pressure to give the desired product as yellow solid (3.03 g, 12.6 mmol, 95%). ^{1}H NMR (400 MHz, $CDCl_3$): δ 3.87 (s, 3H); ^{13}C NMR (101 MHz, $CDCl_3$): δ 37.1, 130, 140.

5.2.3. Synthesis of 3,5-dibromo-1-isopropyl-1H-1,2,4-triazole (115b)[107]

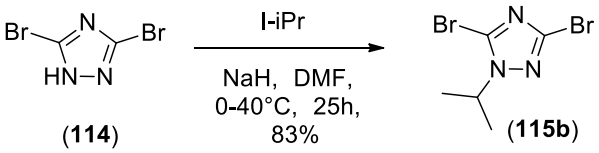

A 100 mL two neck round bottom flask containing a Teflon stirrer bar was charged with 3,5-dibromo-1,2,4-triazole (1 eq., 1 g, 4.4 mmol) and solubilized with anhydrous DMF (15 mL) under stirring. The solution was cooled to 0°C and then, NaH (1.5 eq., 0.263 g, 6.6 mmol) was added in small portions. After 30 min, 2-iodopropane (1.2 eq., 0.9 g, 0.53 mL, 5.3 mmol) was added dropwise. The reaction mixture was stirred at room temperature overnight. It was observed that still remained starting material by HPLC. Then, the temperature was increased to

50°C for 4h and the HPLC analysis showed the same pattern. More 1.2 eq. of 2-iodopropane was added and, after 5h the starting material was completely consumed. Approximately 100g of ice was added to the reaction mixture which was extracted 3x with iPr_2O. The organic layers were collected and washed with H_2O (3 x 100ml), dried with Na_2SO_4 and concentrated under reduced pressure to afford the desired compound as a colorless oil (0.989 g, 3.68 mmol, 83%). ^{1}H NMR (400 MHz, $CDCl_3$): δ 1.49-1.50 (d, *J*= 6.65 Hz, 6H), 4.61-4.71 (m, 1H); ^{13}C NMR (101 MHz, $CDCl_3$): δ 22, 52.9, 128.1, 140.

5.2.4. Synthesis of 1-benzyl-3,5-dibromo-1H-1,2,4-triazole (115c)

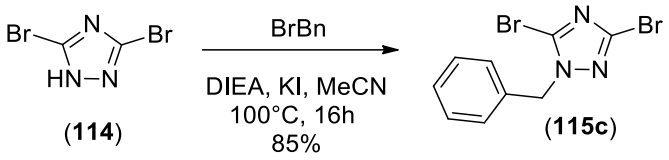

A 100 mL round bottom flask containing a Teflon stirrer bar was charged with 3,5-dibromo-1,2,4-triazole (1 eq., 3 g, 13.22 mmol), benzyl bromide (1 eq., 2.23 g, 1.58 mL, 13.22 mmol), DIPEA (2.0 eq., 3.42 g, 4.38 mL, 26.508 mmol) and dissolved in MeCN (30 mL). The reaction mixture was refluxed for 16h. The progress of the reaction was monitored by HPLC. The reaction mixture was then concentrated under reduced pressure and the crude product was purified by chromatography on silica gel using *n*-heptane/EtOAc (80/20) to give the desired product as a white solid (3.54 g, 11.17 mmol, 85%). ^{1}H NMR (400 MHz, $CDCl_3$): δ 5.31 (s, 2H), 7.29-7.33 (m, 2H), 7.34-7.40 (m, 3H).

5.2.4. Synthesis of 3,5-dibromo-1-(4-methoxybenzyl)-1*H*-1,2,4-triazole (115d)

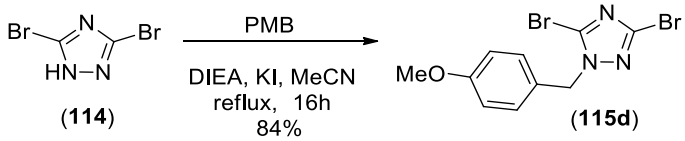

A 100 mL round bottom flask containing a Teflon stirrer bar was charged with 3,5-dibromo-1,2,4-triazole (1 eq., 1 g, 4.408 mmol), 4-methoxybenzylchloride (1.3 eq., 0.90 g, 0.78 mL, 5.73 mmol), DIPEA (2 eq., 1.14 g, 1.46 mL, 8.84 mmol) and MeCN (20 mL). Then KI (0.5 eq., 0.367 g, 0.24 mL, 2.204 mmol) was added. The reaction mixture was refluxed overnight. The progress of the reaction was monitored by HPLC. The reaction mixture was then

concentrated under reduced pressure and the crude product was purified by chromatography on silica gel using *n*-heptane/EtOAc (80/20) to give the desired product as a white solid (1.28 g, 3.71 mmol, 84%). ^{1}H NMR (400 MHz, $CDCl_3$): δ 3.8 (s, 3H), 5.24 (s, 2H), 6.87-6.90 (d, *J* = 8.74 Hz, 2H), 7.27-7.29 (d, *J* = 8.74 Hz, 2H); ^{13}C NMR (101 MHz, $CDCl_3$): δ 53.5, 55.5, 114.5, 125.9, 129.2, 129.8, 140.4, 160.1.

5.2.5. Synthesis of 3,5-dibromo-1-(tetrahydro-2H-pyran-2-yl)-1H-1,2,4-triazole (115e)[108]

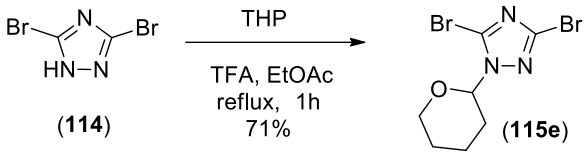

A 100 mL round bottom flask containing a Teflon stirrer bar was charged with 3,5-dibromo-1,2,4-triazole (1 eq., 2 g, 0.0088 mol), EtOAc (20 mL) and 3 drops of TFA. The mixture was heated to 50°C under stirring and then, DHP (2.38 eq., 1.76 g, 1.9 mL, 0.021 mol) was added over a period of 10 min. The temperature of the reaction mixture was increased to reflux and stirred for more 1h. The progress of the reaction was monitored by HPLC. The reaction mixture was cooled to room temperature and concentrated under reduced pressure to give the desired compound as a white solid (1.94 g, 6.24 mmol, 71%). ^{1}H NMR (400 MHz, $CDCl_3$): δ 1.75-1.59 (m, 3H), 1.92-1.96 (m, 1H), 2.11-2.45 (m, 1H), 2.28-2.37 (m, 1H), 3.7-3.65 (m, 1H), 4.03-4.06 (d, *J* = 11.2 Hz, 1H), 5.45-5.48 (dd, *J* = 2.98 Hz, *J* = 9.24 Hz, 1H); ^{13}C NMR (101 MHz, $CDCl_3$): δ 22, 24.62, 29.15, 67.89, 84.85, 130.14, 140.73.

5.2.6. Synthesis of 2-(3,5-dibromo-1H-1,2,4-triazol-1-yl)acetonitrile (115h)

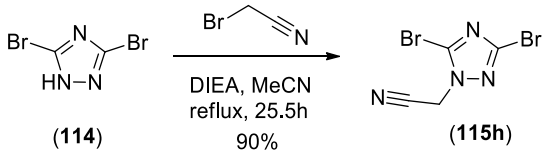

A 100 mL round bottom flask containing a Teflon stirrer bar was charged with 3,5-dibromo-1,2,4-triazole (1 eq., 0.1 g, 4.41 mmol), MeCN (20 mL), $BrCH_2CN$ (1 eq., 0.53 g, 0.30 mL, 4.4 mmol), DIPEA (2 eq., 1.14 g, 1.46 mL, 8.84 mmol). The reaction mixture was refluxed for 25.5 h and the progress of the reaction was monitored by HPLC. The reaction mixture cooled to r.t. and concentrated under reduced pressure. The crude was solubilized with

20mL of EtOAc and washed with H_2O (3 x 20mL). The organic layer was collected, dried with Na_2SO_4 and concentrated to give the desired product (1.05 g, 3.95 mmol, 90%). ^1H NMR (400 MHz, $CDCl_3$): δ 5.09 (s, 2H)

5.2.7. Synthesis of ethyl 2-(3,5-dibromo-1H-1,2,4-triazol-1-yl)acetate (115f)

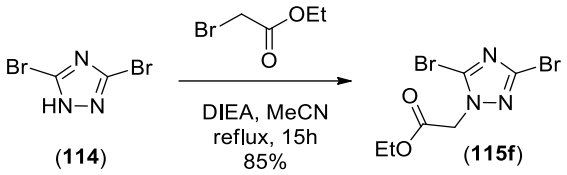

(**114**) (**115f**)

A 100 mL round bottom flask containing a Teflon stirrer bar was charged with 3,5-dibromo-1,2,4-triazole (1 eq., 2 g, 8.82 mmol), MeCN (30 mL), ethyl bromoacetate (1 eq., 1.47 g, 0.98 mL, 8.82 mmol) and DIPEA (2.005 eq., 2.28 g, 2.9 mL, 17.67 mmol). The reaction mixture was refluxed for 15h. The progress of the reaction was monitored by HPLC. The reaction mixture was concentrated under reduced pressure and 20mL of EtOAc was added. The solution was washed with H_2O (4 x 20 mL). The organic layer was collected, dried with Na_2SO_4 and concentrated to give the desired product (2.33 g, 7.46 mmol, 85%). ^1H NMR (400 MHz, $CDCl_3$): δ 1.28 (t, 3H), 4.24-4.26 (m, 2H), 4.88 (s, 2H).

5.2.8. Synthesis of 2-(3,5-dibromo-1H-1,2,4-triazol-1-yl)acetic acid (115g)

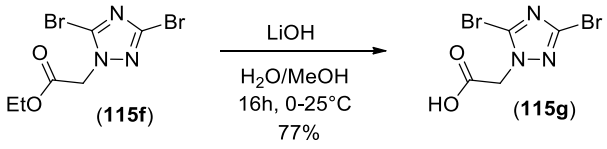

(**115f**) (**115g**)

A 100 mL round bottom flask containing a Teflon stirrer bar was charged with ethyl 2-(3,5-dibromo-1H-1,2,4-triazol-1-yl)acetate (**115f**) (1 eq., 1.8 g, 5.75 mmol) and LiOH (3.3 eq., 0.8 g, 18.98 mmol) followed by the addition of the mixture H_2O/MeOH (20/ 80 mL). The reaction mixture was stirred at r.t. for 16h. The progress of the reaction was monitored by HPLC. The reaction volume was concentrated until the half and then extracted with DCM (3 x 50 mL). The pH of the aqueous phase was adjusted to ~1 with drops of HCl and then extracted with DCM (3 x 50ml). The organic layers were collected, dried with Na_2SO_4 and concentrated under reduced pressure to give the desired product (1.27 g, 4.44 mmol, 77%). ^1H NMR (400 MHz, DMSO): δ 5.09 (s, 2H), 13.62 (bs, 1H).

5.2.9. Synthesis of 3,5-dibromo-1-(p-tolyl)-1H-1,2,4-triazole (115i)[109]

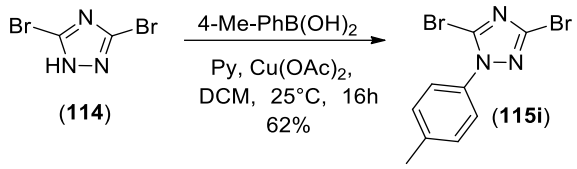

A 100 mL round bottom flask containing a Teflon stirrer bar was charged with 4-MePhB(OH)$_2$ (1.33 eq., 0.4 g, 2.94 mmol), Py (1.33 eq., 0.23 g, 0.24 mL, 2.94 mmol), Cu(OAc)$_2$ (1 eq., 0.4 g, 2.208 mmol), 3A molecular sieves and dry DCM (10 mL) followed by the addition of 3,5-dibromo-1,2,4-triazole (**114**) (1 eq., 0.5 g, 2.20 mmol). The reaction mixture was stirred at r.t. for 16h. The progress of the reaction was monitored by HPLC. The reaction mixture was then filtered using celite. H_2O (10 mL) was added to the filtered solution and the mixture extracted with DCM (3 x 10 mL). The organic layers were collected, dried and concentrated under reduced pressure. The crude product was purified by chromatography on silica gel using *n*-heptane/EtOAc (90/10) to give the desired product as a white solid (0.43 g, 1.36 mmol, 62%). ^{1}H NMR (400 MHz, $CDCl_3$): δ 2.44 (s, 3H), 7.31-7.33 (d, *J* = 8.1 Hz, 2H), 7.39-7.41 (d, *J* = 8.4 Hz, 2H); ^{13}C NMR (101 MHz, $CDCl_3$): δ 21.3, 125, 129.3, 130, 133.5, 140.4, 141.

5.2.10. General procedure for the C-3 Suzuki-Miyaura functionalization.

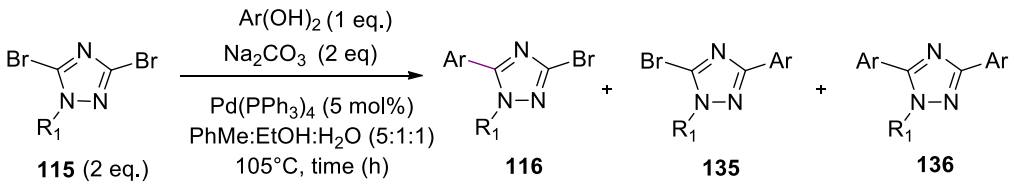

A microwave vial containing a Teflon stirrer bar was charged with compounds **115** (2 eq.), corresponding boronic acids (1 eq.), Na_2CO_3 (2 eq.) and $Pd(PPh_3)_4$ (0.05 eq.). The vessel was then capped properly, evacuated and backfilled with argon (this process was repeated a total of three times). A second microwave vial was charged with MePh, EtOH and H_2O (5:1:1) capped properly, evacuated and backfilled with argon (this process was repeated a total of three times). This solvent mixture was then added to the mixture of solids. The reaction mixture was then placed in a preheated oil bath at 105°C. The progress of the reaction was

evaluated by HPLC. The reaction mixture was concentrated, and the crude product was purified by chromatography on silica gel to give the desired product.

5.2.10.1. Synthesis of 3-bromo-1-methyl-5-(p-tolyl)-1H-1,2,4-triazole (116a) and 5-bromo-1-methyl-3-(p-tolyl)-1H-1,2,4-triazole (135a)

The synthesis followed the general procedure using compound **115a** (2 eq., 0.1 g, 0.42 mmol), 4-tolylboronic acid (1 eq., 0.028 g, 0.2 mmol), Na_2CO_3 (2 eq., 0.044 g, 0.42 mmol), $Pd(PPh_3)_4$ (0.05 eq., 0.012 g, 0.01 mmol), MePh (1.8 mL), EtOH (0.4 mL) and H_2O (0.4 mL) in 2.5h. The crude product was purified by chromatography on silica gel using *n*-heptane/EtOAc (80/20) to give the desired products **116a** (0.039 g, 0.15 mmol, 75%) and **135a** (0.002 g, 0.0079 mmol, 4%).

5.2.10.1.1. 3-bromo-1-methyl-5-(p-tolyl)-1H-1,2,4-triazole (116a)

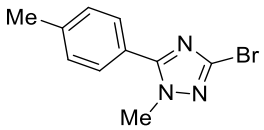

^{1}H NMR (400 MHz, $CDCl_3$): δ 2.42 (s, 3H), 3.95 (s, 3H), 7.30-7.32 (d, *J* = 8 Hz, 2H), 7.54-7.56 (d, *J* = 8 Hz, 2H).

5.2.10.1.2. 5-bromo-1-methyl-3-(p-tolyl)-1H-1,2,4-triazole (135a)

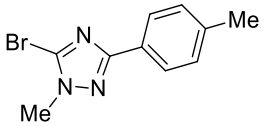

^{1}H NMR (400 MHz, $CDCl_3$): δ 2.39 (s, 3H), 3.88 (s, 3H), 7.23-7.24 (d, *J* = 8 Hz, 2H), 7.91-7.93 (d, *J* = 8 Hz, 2H).

5.2.10.2. Synthesis of 3-bromo-5-phenyl-1-(p-tolyl)-1H-1,2,4-triazole (116b)

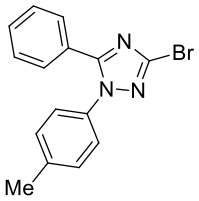

The synthesis followed the general procedure using compound **115b** (2 eq., 0.4 g, 1.2 mmol), phenylboronic acid (1 eq., 0.077 g, 0.63 mmol), Na_2CO_3 (2 eq., 0.134 g, 1.3 mmol), $Pd(PPh_3)_4$ (0.05 eq., 0.037 g, 0.032 mmol), MePh (10 mL), EtOH (2 mL) and H_2O (2 mL) in 2.5h. The reaction was monitoreb by TLC (Hex/EtOAc (95/5), RF= 0.24). The crude product was purified by chromatography on silica gel using Hex/EtOAc (95/5) to give the desired products **116b** (0.178 g, 0.57 mmol, 90%). ^{1}H NMR (500 MHz, DMSO): δ 2.36 (s, 3H), 7.30 (bs, 4H), 7.38-7.43 (m, 4H), 7.45-7.48 (m, 4H);^{13}C NMR (125 MHz, DMSO): δ 21.2, 126.1, 126.8, 129, 129.2, 130.5, 131.1, 135, 139.9, 140.1, 155.8.

5.2.10.3. Synthesis of 3-bromo-5-(4-chlorophenyl)-1-(4-methoxybenzyl)-1H-1,2,4-triazole (116c)

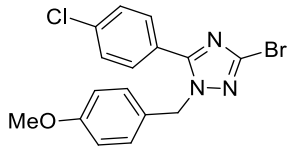

The synthesis followed the general procedure using compound **115d** (2 eq., 0.2 g, 0.58 mmol), 4-chlorophenylboronic acid (1 eq., 0.045 g, 0.29 mmol), Na_2CO_3 (2 eq., 0.061 g, 0.58 mmol), $Pd(PPh_3)_4$ (0.05 eq., 0.017 g, 0.014 mmol), MePh (2.5 mL), EtOH (0.5 mL) and H_2O (0.5 mL) in 1h. The crude product was purified by chromatography on silica gel using DCM to give the desired product (0.053 g, 0.14 mmol, 49%). ^{1}H NMR (400 MHz, $CDCl_3$): δ 3.8 (s, 3H), 5.3 (s, 2H), 6.86-6.89 (d, *J* = 8.8 Hz, 2H), 7.10-7.13 (d, *J* = 8.8 Hz, 2H), 7.44-7.46 (d, *J* = 8.75 Hz, 2H), 7.51-7.53 (d, *J* = 8.73 Hz, 2H).

5.2.10.4. Synthesis of methyl 3-(3-bromo-1-isopropyl-1H-1,2,4-triazol-5-yl)benzoate (116d) and 3-(5-bromo-1-isopropyl-1H-1,2,4-triazol-3-yl)benzoate (135b)

The synthesis followed the general procedure using compound **115b** (2 eq., 0.2 g, 0.74 mmol), 3-methoxycarbonylphenylboronic acid (1 eq., 0.067 g, 0.37 mmol), Na_2CO_3 (2 eq.,

0.079 g, 0.74 mmol), $Pd(PPh_3)_4$ (0.05 eq., 0.022 g, 0.019 mmol), MePh (3.2 mL), EtOH (0.65 mL) and H_2O (0.65 mL) in 40 min. The crude product was purified by chromatography on silica gel using *n*-heptane/EtOAc (70/30) to give the desired products **116d** (0.028 g, 0.087 mmol, 24%) and **135d** (0.014 g, 0.042 mmol, 11%).

5.2.10.4.1. methyl 3-(3-bromo-1-isopropyl-1H-1,2,4-triazol-5-yl)benzoate (116d)

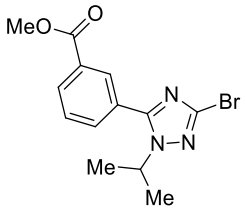

^{1}H NMR (400 MHz, $CDCl_3$): δ 1.52 (d, *J* = 6.6 Hz, 6H), 3.94 (s, 3H), 4.59-4.69 (m, 1H), 7.58-7.62 (t, *J* = 7.8 Hz, 1H), 7.78-7.77 (dt, *J* = 1.3 Hz, *J* = 7.7 Hz, 1H), 8.18-8.2 (dt, *J* = 1.3 Hz, *J* = 7.9 Hz, 1H), 8.24-8.23 (t, *J* = 1.7 Hz, 1H).

5.2.10.4.2. methyl 3-(5-bromo-1-isopropyl-1H-1,2,4-triazol-3-yl)benzoate (135d)

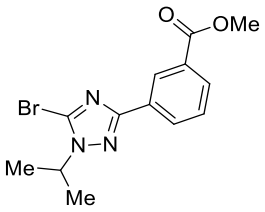

^{1}H NMR (400 MHz, $CDCl_3$): δ 1.55-1.57 (d, *J* = 6.6 Hz, 6H), 3.94 (s, 3H), 4.69-4.75 (m, 1H), 7.49-7.53 (t, *J* = 7.8 Hz, 1H), 8.06-8.08 (dt, *J* = 1.3 Hz, *J* = 7.7 Hz, 1H), 8.25-8.28 (dt, *J* = 1.3 Hz, *J* = 7.9 Hz, 1H), 8.72-8.73 (t, *J* = 1.7 Hz, 1H).

5.2.11. General procedure for the synthesis of 117a-b.

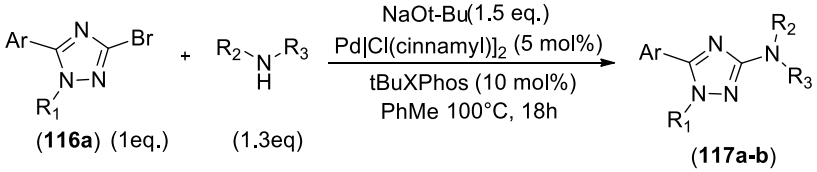

A microwave vial containing a Teflon stirrer bar was charged with 3-bromo-1H-1,2,4-triazoles (**116a**) (1 eq.), NaOtBu (1.5 eq.), t-BuXPhos (0.1 eq.) and [(cinnamyl)PdCl]$_2$ (0.05

eq.). The reaction vessel was evacuated and backfilled with argon (this process was repeated a total of three times) and then, the mixture of toluene and the corresponding amines (1.5 eq.) was bubbled with argon for 1 minute and added. The reaction mixture was then capped properly and placed in a preheated oil bath at 100 °C until complete conversion of the starting material was detected. The reaction mixture was monitored by HPLC analysis. The reaction mixture was concentrated, and the crude product was purified by chromatography on silica gel using *n*-heptane/EtOAc to give the desired product.

5.2.10.1. 1-methyl-N-phenethyl-5-(p-tolyl)-1H-1,2,4-triazol-3-amine (117a)

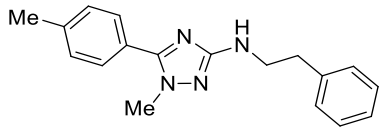

The synthesis followed the general procedure using compound **116a** (1 eq., 0.025 g, 0.069 mmol), phenethylamine (1.3 eq, 0.011 g, 0.0902 mmol), NaOt-Bu (1.5 eq., 0.010 g, 0.1 mmol), t-BuXPhos (0.1 eq., 0.003 g, 0.007 mmol) and $[(cinnamyl)PdCl]_2$ (0.05 eq., 0.002 g, 0.0035 mmol). The crude product was purified by chromatography on silica gel using *n*-heptane/EtOAc (50/50) to give the desired product (0.014 g, 0.047 mmol, 68%). ^{1}H NMR (400 MHz, $CDCl_3$): δ 2.41 (s, 3H), 2.92-2.96 (t, *J* = 6.8 Hz, 2H), 3.55-3.60 (q, 2H), 3.8 (s, 3H), 4.12 (t, *J* = 6.8 Hz, 1H), 7.19-7.32 (m, 7H), 7.49-7.51 (d, *J* = 8.1 Hz, 2H). ^{13}C NMR (101 MHz, $CDCl_3$): δ 21.5, 36.1, 36.5, 44.9, 125.5, 126.4, 128.6, 128.7, 129, 129.5, 139.4, 140.1, 141.9, 163.5**.**

5.2.10.2. N-benzyl-1-methyl-5-(p-tolyl)-1H-1,2,4-triazol-3-amine (117b)

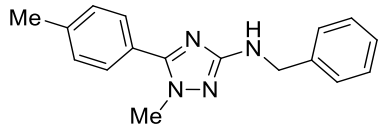

The synthesis followed the general procedure using compound **116a** (1 eq, 0.025 g, 0.069 mmol), benzylamine (1.3 eq, 0.010 g, 0.0902 mmol), NaOt-Bu (1.5 eq., 0.010 g, 0.1 mmol), t-BuXPhos (0.1 eq., 0.003 g, 0.007 mmol) and $[(cinnamyl)PdCl]_2$ (0.05 eq., 0.002 g, 0.0035 mmol). The crude product was purified by chromatography on silica gel using gradient elution *n*-heptane/EtOAc (70/30 to 50/50) to give the desired product (0.018 g, 0.065 mmol,

92%). ^{1}H NMR (400 MHz, $CDCl_3$): δ 2.41 (s, 3H), 3.8 (s, 3H), 4.58 (bs, 3H), 7.27-7.29 (m, 3H), 7.32-7.35 (t, *J* = 7.1 Hz, 2H), 7.40-7.41 (d, *J* = 7.1 Hz, 2H), 7.50-7.52 (d, *J* = 8.1 Hz, 2H). ^{13}C NMR (101 MHz, $CDCl_3$): δ 21.5, 29.8, 36.5, 47.8, 125.1, 127.2, 127.6, 128.5, 128.6, 129.6, 139.6, 140.2, 153.9, 163.3.

5.2.11. General procedure for the synthesis of 118.

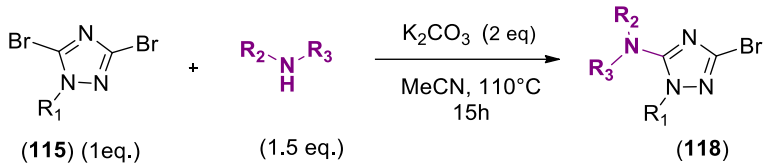

A microwave vial containing a Teflon stirrer bar was charged with the corresponding 3,5-dibromo-1H-1,2,4-triazoles (**115**) (1 eq.), K_2CO_3 (2 eq.) and MeCN (0.5 mL), followed by the addition of the corresponding amine (1.5 eq.). The reaction mixture was then capped properly and placed in a preheated oil bath at 110 °C for 15h. The reaction mixture was monitored by HPLC analysis. The reaction mixture was concentrated, and the crude product was purified by chromatography on silica gel using *n*-heptane/EtOAc.

5.2.11.1. 3-bromo-1-methyl-N-phenethyl-1H-1,2,4-triazol-5-amine (118a)

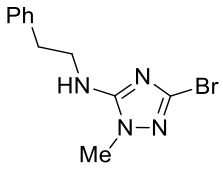

The synthesis followed the general procedure using compound **115a** (1 eq., 0.050 g, 0.21 mmol), phenethylamine (1.5 eq., 0.038 g, 0.039 mL, 0.31 mmol), K_2CO_3 (2 eq., 0.057 g, 0.42 mmol) and MeCN (0.5 mL). The crude product was purified by chromatography on silica gel using gradient elution *n*-heptane/EtOAc (65/35 to 60/40) to give the product (0.031 g, 0.11 mmol, 53%). ^{1}H NMR (400 MHz, $CDCl_3$): δ 2.85-2.88 (t, *J* = 6.7 Hz, 2H), 3.37 (s, 3H), 3.57-3.52 (q, 2H), 3.87 (bs, 1H), 7.11-7.13 (d, *J* = 6.9 Hz, 2H), 7.16-7.20 (t, *J* = 7.6 Hz, 1H), 7.24-7.28 (t, *J* = 7.5 Hz, 2H).

5.2.11.2. 3-bromo-N-(3-bromo-1-methyl-1H-1,2,4-triazol-5-yl)-1-methyl-N-phenethyl-1H-1,2,4-triazol-5-amine (141)

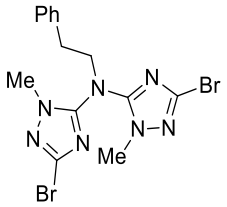

A microwave vial containing a Teflon stirrer bar was charged with the 3,5-dibromo-1H-1,2,4-triazole (**115a**) (1 eq., 0.050 g, 0.21 mmol), K_2CO_3 (2 eq., 0.057 g, 0.42 mmol) and DMF (2 mL), followed by the addition of phenethylamine (1 eq., 0.025 g, 0.026 mL, 0.20 mmol). The reaction mixture was then capped properly and placed in a preheated oil bath at 160 °C for 1.5h. The reaction mixture was monitored by HPLC analysis. The reaction mixture was concentrated, and the crude product was purified by chromatography on silica gel using gradient elution *n*-heptane/EtOAc (50/50) to give the product (0.002 g, 0.0045 mmol, 2%). ^{1}H NMR (400 MHz, $CDCl_3$): δ 3.09-3.12 (t, *J* = 7 Hz, 2H), 3.23 (s, 3H), 4.06-4.10 (t, *J* = 7 Hz, 2H), 7.15-7.15 (d, *J* = 6.8 Hz, 2H), 7.22-7.24 (m, 1H), 7.27-7.30 (m, 2H).

5.2.11.3. 3-bromo-N-(2,4-dimethoxybenzyl)-1-methyl-1H-1,2,4-triazol-5-amine (118c)

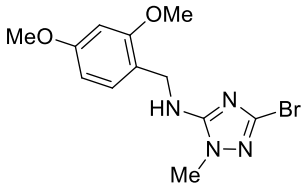

The synthesis followed the general procedure using compound **115a** (1 eq., 0.2 g, 0.83 mmol), 2,4-dimethoxybenzylamine (1.5 eq., 0.208 g, 0.187 mL, 1.25 mmol), K_2CO_3 (2 eq., 0.23 g, 1.66 mmol) and MeCN (2 mL). The crude product was purified by chromatography on silica gel using gradient elution *n*-heptane/EtOAc (60/40 to 50/50) to give the product (0.131 g, 0.40 mmol, 48%). ^{1}H NMR (400 MHz, $CDCl_3$): δ 3.48 (s, 3H), 3.80 (s, 3H), 3.84 (s, 3H), 4.45 (bs, 3H), 6.43-6.47 (m, 2H), 7.23-7.27 (m, 2H). ^{13}C NMR (101 MHz, $CDCl_3$): δ 33.2, 44, 55.4, 98.77, 104, 118.5, 130.9, 136.3, 156, 158.6, 160.8.

5.2.11.4. 3-bromo-N,1-dimethyl-N-phenethyl-1H-1,2,4-triazol-5-amine (118e)

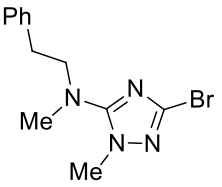

The synthesis followed the general procedure using compound **115a** (1 eq., 0.05 g, 0.20 mmol), N-methylphenethylamine (1.5 eq., 0.042 g, 0.045 mL, 0.31 mmol), K_2CO_3 (2 eq., 0.057 g, 0.42 mmol) and MeCN (1 mL). The crude product was purified by chromatography on silica gel using *n*-heptane/EtOAc (70/30) to give the desired product (0.042 g, 0.14 mmol, 69%). ^{1}H NMR (400 MHz, $CDCl_3$): δ 2.82–2.86 (t, *J* = 7.2 Hz, 2H), 2.88 (s, 3H), 3.35-3.39 (t, *J* = 7.2 Hz, 2H), 3.47 (s, 3H), 7.12-7.14 (d, *J* = 6.8 Hz, 2H), 7.17-7.20 (m, 1H), 7.23-7.28 (m, 2H). ^{13}C NMR (101 MHz, $CDCl_3$): δ 33.7, 35.6, 39.4, 55.6, 126.5, 128.5, 128.8, 136.6, 138.7, 159.7.

5.2.11.5. 4-(3-bromo-1-(tetrahydro-2H-pyran-2-yl)-1H-1,2,4-triazol-5-yl)morpholine (118f)

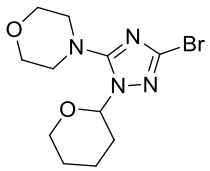

A microwave vial containing a Teflon stirrer bar was charged with the 3,5-dibromo-1H-1,2,4-triazole **115e** (1 eq., 0.2 g, 0.64 mmol), morpholine (4 eq., 0.224 g, 0.226 mL, 2.57 mmol) and MeCN (3 mL). The reaction mixture was then capped properly and placed in a preheated oil bath at 110 °C for 14.5 h. The reaction mixture was monitored by HPLC analysis. The reaction mixture was concentrated under reduced pressure and solubilized in DCM (10 mL). The solution was washed with H_2O (3 x 10 mL). The organic layer was dried with Na_2SO_4 and concentrated to give the desire product (0.160 g, 0.50 mmol, 78%). ^{1}H NMR (400 MHz, $CDCl_3$): δ 1.58–1.72 (m, 3H), 1.84-1.87 (dd, *J* = 3.5 Hz, *J* = 13.6 Hz, 1H), 2.09-2.14 (m, 1H), 2.32-2.40 (m, 1H), 3-16-3.20 (m, 2H), 3.39-3.43 (m, 2H), 3.54-3.59 (dt, *J* = 2.6 Hz, *J* = 11.3 Hz, 1H), 3.76-3.80 (m, 2H), 3.83-3.87 (m, 2H), 4.05-4.07 (d, *J* = 11.5 Hz, 1H), 5.14.5.17 (dd, *J* = 2.8 Hz, *J* = 9.4 Hz, 1H).

5.2.11.6. 4-(3-bromo-1-(4-methoxybenzyl)-1H-1,2,4-triazol-5-yl)morpholine (118g)

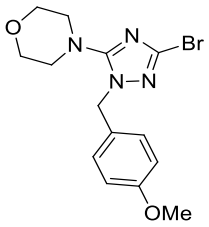

A microwave vial containing a Teflon stirrer bar was charged with the 3,5-dibromo-1H-1,2,4-triazole **115d** (1 eq., 0.05 g, 0.14 mmol), morpholine (4 eq., 0.050 g, 0.051 mL, 0.58 mmol) and MeCN (0.15 mL). The reaction mixture was then capped properly and placed in a preheated oil bath at 110 °C for 15 h. The reaction mixture was monitored by HPLC analysis. The reaction mixture was cooled to r.t. and solubilized in 7 mL of EtOAc. This solution was washed with H_2O (3 x 7 mL) and brine (1 x 7 mL), dried with Na_2SO_4 and concentrated to give the desired product (0.043 g, 0.12 mmol, 84%). ^{1}H NMR (400 MHz, $CDCl_3$): δ 3.08-3.11 (t, *J* = 4.7 Hz, 4H), 3.74-3.76 (t, *J* = 4.7 Hz, 4H), 3.8 (s, 3H), 5.11 (s, 2H), 6.86-6.88 (d, *J* = 8.7 Hz, 2H), 7.16-7.18 (d, *J* = 8.7 Hz, 2H).

5.2.11.7. 3-bromo-N-methyl-N-phenethyl-1-(tetrahydro-2H-pyran-2-yl)-1H-1,2,4-triazol-5-amine (118d)

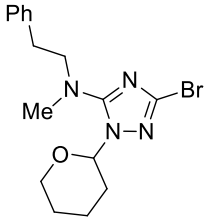

The synthesis followed the general procedure using compound **115e** (1 eq., 0.2 g, 0.64 mmol), N-methylphenethylamine (1.5 eq., 0.130 g, 0.140 mL, 0.96 mmol), K_2CO_3 (2 eq., 0.178 g, 1.29 mmol) and MeCN (3 mL). The crude product was purified by chromatography on silica gel using gradient elution *n*-heptane/EtOAc (60/40 to 50/50) to give the product (0.194 g, 0.53 mmol, 82%). ^{1}H NMR (400 MHz, $CDCl_3$): δ 1.41−1.53 (m, 2H), 1.62-1.72 (m, 2H), 1.99-2.04 (m, 2H), 2.24-2.34 (m, 2H), 2.8-2.94 (m, 2H), 2.98 (s, 3H), 3.39-3.56 (m, 3H), 3.99-4.04 (m, 1H), 4.87-4.90 (dd, *J* = 2.7 Hz, *J* = 9.8 Hz, 1H), 7.17-7.31 (m, 5H). ^{13}C NMR (101 MHz, $CDCl_3$): δ 22.5, 24.6, 29.5, 33.6, 39.5, 56, 67.7, 82.9, 126.5, 128.5, 128.9, 137.6, 138.9, 159.8.

5.2.11.8. 3-bromo-N-phenethyl-1-(p-tolyl)-1H-1,2,4-triazol-5-amine (118b)

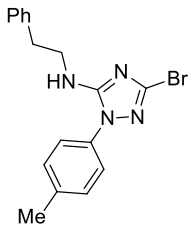

A microwave vial containing a Teflon stirrer bar was charged with the 3,5-dibromo-1H-1,2,4-triazole **115i** (1 eq., 0.050 g, 0.16 mmol), DIPEA (2 eq., 0.041 g, 0.055 mL, 0.32 mmol) and MeCN (0.5 mL) followed by the addition of phenethylamine (1.5 eq., 0.041 g, 0.030 mL, 0.24 mmol). The reaction mixture was then capped properly and placed in a preheated oil bath at 110 °C for 20h. The reaction mixture was monitored by HPLC analysis. The reaction mixture was concentrated, and the crude product was purified by chromatography on silica gel using gradient elution *n*-heptane/EtOAc (50/50) to give the product (0.036 g, 0.099 mmol, 63%). ^{1}H NMR (400 MHz, $CDCl_3$): δ 2.46 (s, 3H), 2.99-3.03 (t, *J* = 6.8 Hz, 2H), 3.72-3.77 (q, *J* = 6.7 Hz, 2H), 4.49-4.52 (t, *J* = 5.7 Hz, 1H), 7.24-7.40 (m, 9H).

5.2.11.9. 3-bromo-1-methyl-N-(p-tolyl)-1H-1,2,4-triazol-5-amine (118h).

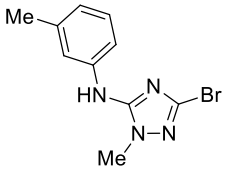

LiHMDS (1M in THF, 0.400 mL) was added dropwise to a cooled (ice bath) solution of 3,5-dibromo-1H-1,2,4-triazole **115a** (1 eq., 0.050 g, 0.21 mmol), *m*-toluidine (2 eq., 0.045 g, 0.42 mmol) in dry THF (0.5 mL). The reaction mixture was stirred at r.t. for 30 min. A satured aqueous NH_4Cl solution was added slowly. The reaction mixture was extracted with DCM (3 x 5 mL). The organic layers were collected, dried with Na_2SO_4 and concentrated under reduced pressured. The crude product was purified by chromatography on silica gel using *n*-heptane/EtOAc (70/30) to give the desired product (0.020 g, 0.074 mmol, 36%). ^{1}H NMR (400 MHz, $CDCl_3$): δ 2.33 (s, 3H), 3.63 (s, 3H), 6.35 (bs, 1H), 6.85-6.87 (d, *J* = 7.5 Hz, 1H), 7.02-7.04 (m, 2H), 7.17-7.21 (m, 1H). ^{13}C NMR (101 MHz, $CDCl_3$): δ 21.5, 34.5, 115.1, 118.7, 124, 129.3, 136.7, 139.2, 139.5.

5.2.11.10. 3-bromo-1-(p-tolyl)-1H-1,2,4-triazol-5-amine (118i)

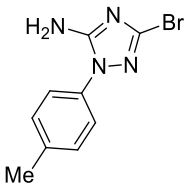

A microwave vial containing a Teflon stirrer bar was charged with the 3,5-dibromo-1H-1,2,4-triazole **115i** (1 eq., 0.050 g, 0.16 mmol) and NH_4OH 8M (50 eq., 0.986 mL, 7.89 mmol). The reaction mixture was then capped properly and placed in a preheated oil bath at 110 °C for 20h. The reaction mixture was monitored by HPLC analysis. The reaction mixture was concentrated, solubilized in EtOAc (10 mL) and washed with H_2O (2 x 10 mL). The organic layer was concentrated and purified by chromatography on silica gel using *n*-heptane/EtOAc (50/50) to give the desired product (0.024 g, 0.096 mmol, 62%). ^1H NMR (500 MHz, $CDCl_3$): δ 2.4 (s, 3H), 5.5 (bs, 2H), 7.29-7.30 (d, *J* = 7.4 Hz, 2H), 7.36-7.37 (d, *J* = 7.5 Hz, 2H).

5.2.12. General procedure for the synthesis of aminotriazole family 119.

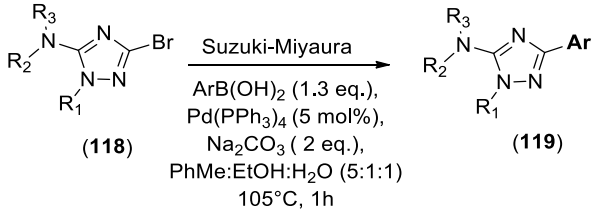

A microwave vial containing a Teflon stirrer bar was charged with the correspondenting aminotriazoles **118** (1 eq.) , 4-methoxyphenylboronic acid (1.34 eq.) , Na_2CO_3 (2 eq.) and $Pd(PPh_3)_4$ (0.05 eq.). The vessel was then capped properly, evacuated and backfilled with argon (this process was repeated a total of three times). A second microwave vial was charged with MePh, EtOH and H_2O (5:1:1) capped properly, evacuated and backfilled with argon (this process was repeated a total of three times). This solvent mixture was then added to the mixture of solids. The reaction mixture was then placed in a preheated oil bath at 105°C for 1h. The progress of the reaction was evaluated by HPLC. The reaction mixture was concentrated, and the crude product was purified by chromatography on silica gel using *n*-heptane/EtOAc to give the desired product.

5.2.12.1. 3-(4-methoxyphenyl)-1-methyl-N-phenethyl-1H-1,2,4-triazol-5-amine (119a)

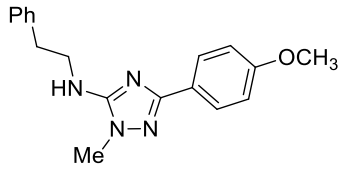

The synthesis followed the general procedure using aminotriazole **118a** (1 eq., 0.025 g, 0.089 mmol), 4-metoxyphenylboronic acid (1.34 eq., 0.018 g, 0.12 mmol), Na_2CO_3 (2 eq., 0.019 g, 0.18 mmol) and $Pd(PPh_3)_4$ (0.05 eq., 0.005 g, 0.0044 mmol), MePh (0.8 mL), EtOH (0.16 mL) and H_2O (0.16 mL). The crude product was purified by chromatography on silica gel using gradient elution *n*-heptane/EtOAc (50/50) to give the product (0.024 g, 0.078 mmol, 88%). ^{1}H NMR (400 MHz, $CDCl_3$): δ 2.97-3.0 (t, *J* = 6.7 Hz, 2H), 3.49 (s, 3H), 3.7-3.75 (q, *J* = 6.7 Hz, 2H), 3.81 (bs, 1H), 3.83 (s, 3H), 6.92-6.94 (d, *J* = 8.9 Hz, 2H), 7.22-7.27 (m, 3H), 7.31-7.35 (m, 2H), 7.95-7.97 (d, *J* = 8.9 Hz, 2H). ^{13}C NMR (101 MHz, $CDCl_3$): δ 33, 35.8, 42.2, 55.3, 113.8, 124.44, 126.6, 127.4, 128.7, 128.9, 138.9, 155.6, 158.5, 160.

5.2.12.2. 4-(1-(4-methoxybenzyl)-3-(4-methoxyphenyl)-1H-1,2,4-triazol-5-yl)morpholine (119b)

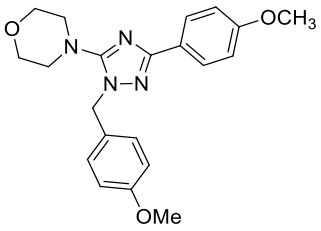

The synthesis followed the general procedure using aminotriazole **118g** (1 eq., 0.023 g, 0.065 mmol), 4-metoxyphenylboronic acid (1.34 eq., 0.013 g, 0.087 mmol), Na_2CO_3 (2 eq., 0.014 g, 0.13 mmol) and $Pd(PPh_3)_4$ (0.05 eq., 0.004 g, 0.0033 mmol), MePh(0.6 mL), EtOH (0.11 mL) and H_2O (0.11 mL). The crude product was purified by chromatography on silica gel using gradient elution *n*-heptane/EtOAc (50/50) to give the product (0.022 g, 0.058 mmol, 89%). ^{1}H NMR (400 MHz, $CDCl_3$): δ 3.11-3.14 (t, *J* = 4.7 Hz, 4H), 3.77-3.79 (m, 7H), 3.84 (s, 3H), 5.19 (s, 2H), 6.85-6.87 (d, *J* = 8.7 Hz, 2H), 6.92-6.94 (d, *J* = 8.9 Hz, 2H), 7.19-7.21 (d, *J* = 8.7 Hz, 2H), 7.98-8.0 (d, *J* = 8.9 Hz, 2H). ^{13}C NMR (101 MHz, $CDCl_3$): δ 50.7, 50.8, 55.3,

66.5, 113.8, 114.1, 124.4, 127.5, 128, 128.3, 159.1, 159.2, 159.4, 160.2. LC/MS m/z $[M + H]^+$ 381.15.

5.2.12.3. N-(2,4-dimethoxybenzyl)-3-(4-methoxyphenyl)-1-methyl-1H-1,2,4-triazol-5-amine (119c)

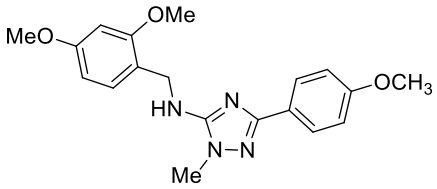

The synthesis followed the general procedure using aminotriazole **118c** (1 eq., 0.050 g, 0.15 mmol), 4-metoxyphenylboronic acid (1.34 eq., 0.031 g, 0.2 mmol), Na_2CO_3 (2 eq., 0.032 g, 0.30 mmol) and $Pd(PPh_3)_4$ (0.05 eq., 0.009 g, 0.008 mmol), MePh (1.4 mL), EtOH (0.3 mL) and H_2O (0.3 mL). The crude product was purified by chromatography on silica gel using gradient elution *n*-heptane/EtOAc (50/50 to 0/100) to give the product (0.054 g, 0.15 mmol, 99%). %). ^{1}H NMR (400 MHz, $CDCl_3$): δ 3.35 (s, 3H), 3.79 (s, 3H), 3.83 (s, 3H), 3.84 (s, 3H), 4.31-4.34 (t, *J* = 5.9 Hz, 1H), 4.54-4.56 (d, *J* = 5.9 Hz, 2H), 6.43-6.46 (dd, *J* = 2.4 Hz, *J* = 8.2 Hz, 1H), 6.48 (d, *J* = 2.3 Hz, 1H), 6.91-6.93 (d, *J* = 8.9 Hz, 2H), 7.32-7.34 (d, *J* = 8.2 Hz, 1H), 7.95-7.97 (d, *J* = 8.9 Hz, 2H). ^{13}C NMR (101 MHz, $CDCl_3$): δ 33.2, 44.1, 55.3, 55.4, 76.7, 77, 77.4, 98.7, 104, 113.7, 119.2, 124.6, 127.4, 131, 156, 158.3, 158.7, 160, 160.7.

5.2.13. Synthesis of 3-(4-methoxyphenyl)-1-methyl-1H-1,2,4-triazol-5-amine (119e)

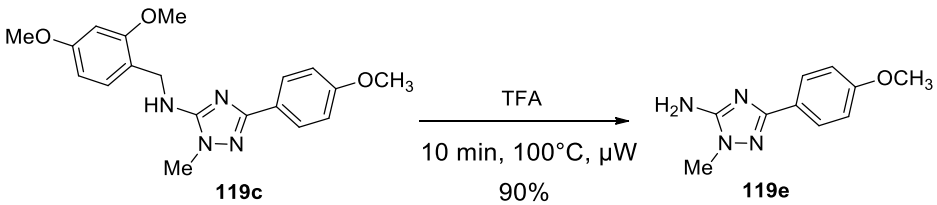

A microwave vial containing a Teflon stirrer bar was charged with compound **119c** (1 eq., 0.054 mg, 0.15 mmol) and TFA (54 eq., 0.934 g, 0.608 mL, 8.19 mmol). The reaction mixture was then capped with a Teflon septum. The mixture was irradiated at 100°C in a microwave (3bar) for 10min and after cooled to 40°C. The trifluoracetic acid was concentrated in vacuum, and the crude sample was triturated with a mixture *n*-heptane/EtOAc (50/50) to

provide the desired product as the triflate salt. The solid was dissolved in H_2O (5 mL) and then $NaHCO_3$ aqueous solution was added until the pH= 7. The aqueous solution was extracted with DCM (3 x 5 mL). The organic layers were collected, dried with Na_2SO_4 and concentrated under reduced pressure providing the product (0.028 g, 0.14 mmol, 90%). The product was used in the further step without purification.

5.2.14. Boc protection of compound 119e

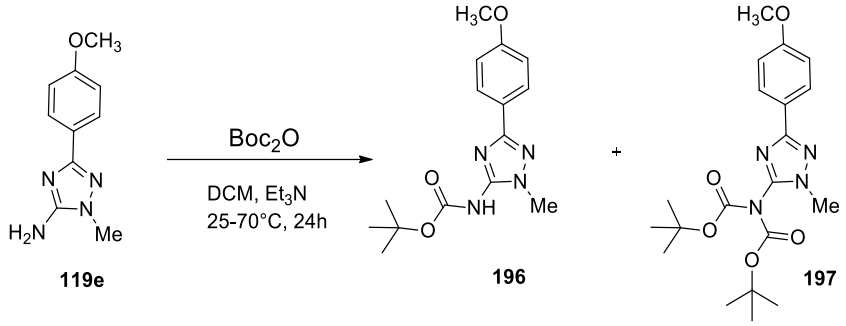

A microwave vial containing a Teflon stirrer bar was charged with compound **119e** (1 eq., 0.028 mg, 0.14 mmol), Et_3N (2 eq., 0.028 g, 0.038 mL, 0.27 mmol) and DCM (1 mL). The reaction mixture was then capped with a Teflon septum. The mixture was stirred at 70 °C for 2h. Then, DMF (1 mL) was added and the reaction mixture remained stirring at 70°C for 48h. The progress of the reaction was monitored by TLC (*n*-heptane/EtOAc (70/30), RF= 0.39). The reaction mixture was cooled to r.t. and concentrated under reduced pressure. The crude product was purified by chromatography on silica gel using *n*-heptane/EtOAc (75/25) to give the products **196** (0.004 g, 0.013 mmol, 10%) and **197** (0.008 g, 0.02 mmol, 15%).

5.2.14.1. tert-butyl (3-(4-methoxyphenyl)-1-methyl-1H-1,2,4-triazol-5-yl)carbamate (196)

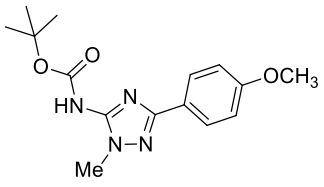

^{1}H NMR (400 MHz, $CDCl_3$): δ 1.47 (s, 9H), 3.68 (s, 3H), 3.8 (s, 3H), 6.99-7.02 (d, *J* = 8.9 Hz, 2H), 7.84-7.86 (d, *J* = 8.9 Hz, 2H), 9.84 (s, 1H).

5.2.14.2. bis-tert-butyl (3-(4-methoxyphenyl)-1-methyl-1H-1,2,4-triazol-5-yl)carbamate (197)

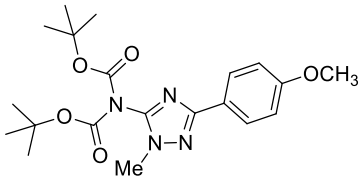

^{1}H NMR (400 MHz, $CDCl_3$): δ 1.44 (s, 18H), 3.74 (s, 3H), 3.85 (s, 3H), 6.94-6.97 (d, *J* = 8.9 Hz, 2H), 7.98-8 (d, *J* = 8.9 Hz, 2H).

5.2.15. General procedure for the synthesis of triazolones 143a-e.

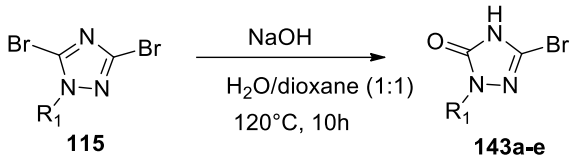

115 **143a-e**

A round bottom flask containing a Teflon stirrer bar was charged with the corresponding 3,5-dibromo-1,2,4-triazoles (**115**) (1 eq.) and NaOH (3 eq.) followed by the addition of H_2O and dioxane. The reaction mixture was then placed in a preheated oil bath at 120 °C until complete conversion of the starting material was detected. The reaction mixture was monitored by HPLC analysis and was usually complete within 10 h. The reaction mixture was cooled to r.t. and concentrated under reduced pressure. The pH of the reaction mixture was adjusted to ~1 with drops of concentrated HCl. Part of compounds were isolated by filtration and for other part the aqueous solution was extracted, dried and concentrated under reduced pressure.

5.2.15.1. 3-bromo-1-methyl-1H-1,2,4-triazol-5(4H)-one (143a)

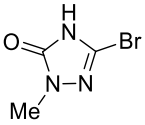

The synthesis followed the general procedure using 3,5-dibromo-1,2,4-triazole (**115a**) (1 eq., 0.39 g, 1.62 mmol) and NaOH (3 eq., 0.194 g, 4.86 mmol), H_2O (5 mL) and dioxane (5

mL). After the addition of drops of HCl, the volume of the reaction mixture was reduced and then extracted with EtOAc (5 x 10 mL). The organic layers were collected, dried with Na_2SO_4 and concentrated under reduced pressure to give the product (0.261 g, 1.47 mmol, 91%). ^{1}H NMR (400 MHz, $CDCl_3$): δ 3.26 (s, 3H), 12.45 (bs, 1H).

5.2.15.2. 1-benzyl-3-bromo-1H-1,2,4-triazol-5(4H)-one (143b)

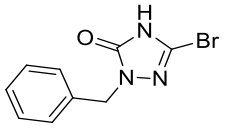

The synthesis followed the general procedure using 3,5-dibromo-1,2,4-triazole (**115c**) (1 eq., 1 g, 3.15 mmol) and NaOH (3 eq., 0.379 g, 9.46 mmol), H_2O (22 mL) and dioxane (22 mL). After the addition of drops of HCl, a white precipitate formed in the solution was filtered off to give the desired product (0.666 g, 2.62 mmol, 83%). ^{1}H NMR (400 MHz, $CDCl_3$): δ 4.84 (s, 2H), 7.24-7.38 (m, 5H), 12.58 (bs, 1H).

5.2.15.3. 3-bromo-1-isopropyl-1H-1,2,4-triazol-5(4H)-one (143c)

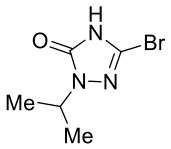

The synthesis followed the general procedure using 3,5-dibromo-1,2,4-triazole (**115b**) (1 eq., 0.3 g, 4.46 mmol) and NaOH (3 eq., 0.134 g, 3.35 mmol), H_2O (6 mL) and dioxane (6 mL). After the addition of drops of HCl, the volume of the reaction mixture was reduced and then extracted with EtOAc (3 x 10 mL). The organic layers were collected, dried with Na_2SO_4 and concentrated under reduced pressure to give the product (0.218 g, 1.061 mmol, 95%). ^{1}H NMR (400 MHz, $CDCl_3$): δ 1.20-1.22 (d, J = 6.7 Hz, 6H), 4.20-4.30 (m, J = 6.7 Hz, 1H), 12.38 (bs, 1H).

5.2.15.4. 3-bromo-1-(p-tolyl)-1H-1,2,4-triazol-5(4H)-one (143d)

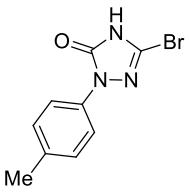

The synthesis followed the general procedure using 3,5-dibromo-1,2,4-triazole (**115i**) (1 eq., 0.2 g, 0.63 mmol) and NaOH (3 eq., 0.076 g, 1.89 mmol), H_2O (3.4 mL) and dioxane (3.4 mL). After the addition of drops of HCl, the volume of the reaction mixture was reduced and then extracted with EtOAc (3 x 10 mL). The organic layers were collected, dried with Na_2SO_4 and concentrated under reduced pressure to give the product (0.147 g, 0.58 mmol, 92%). ^{1}H NMR (400 MHz, $CDCl_3$): δ 2.28 (s, 3H), 7.20-7.22 (d, *J* = 8.4 Hz, 2H), 7.66-7.68 (d, *J* = 8.4 Hz, 2H).

5.2.15.5. 3-bromo-1-(4-methoxybenzyl)-1H-1,2,4-triazol-5(4H)-one (143e)

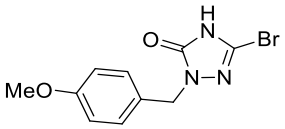

The synthesis followed the general procedure using 3,5-dibromo-1,2,4-triazole (**115d**) (1 eq., 0.3 g, 0.86 mmol), NaOH (3 eq., 0.103 g, 2.59 mmol), H_2O (6 mL) and dioxane (6 mL). After the addition of drops of HCl, a white precipitate formed in the solution was filtered off to give the desired product (0.230 g, 0.81 mmol, 94%). ^{1}H NMR (400 MHz, $CDCl_3$): δ 3.73 (s, 3H), 4.74 (s, 2H), 6.89-6.91 (d, *J* = 8.7 Hz, 2H), 7.17-7.20 (d, *J* = 8.7 Hz, 2H), 12.53 (bs, 1H).

5.2.16. Synthesis of O- and N- tosyl N-alkyl-3-bromo-1,2,4-triazol (146b and 147b).

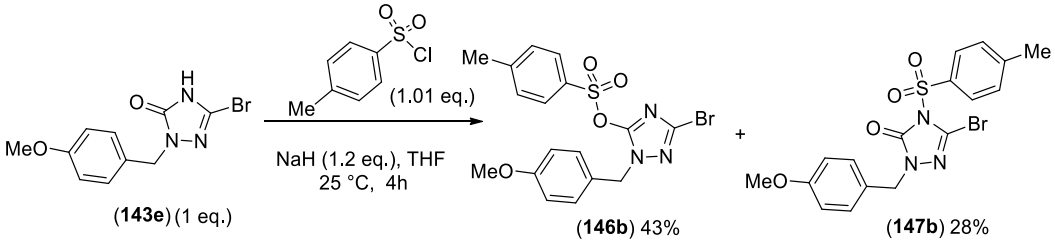

A microwave vial containing a Teflon stirrer bar was charged with 3-bromo-1-[(4-methoxyphenyl)methyl]-1H-1,2,4-triazol-5-ol (**143e**) (1 eq., 0.050 g, 0.18 mmol) and THF (0.72 mL) followed by the addition of small portions of NaH (1.25 eq., 0.009 mg, 0.22 mmol).

After 15 minutes, a solution of tosyl chloride (1.091 eq., 0.037 mg, 0.19 mmol) in THF (0.72 mL) was added dropwise to the reaction mixture. The reaction stirred at r.t. for 4h and the progress of the reaction was monitored by HPLC. The reaction mixture was diluted with 5 mL of H_2O and extracted with EtOAc (4 x 5 mL). The organic layers were collected, dried with Na_2SO_4 and concentrated under reduced pressure. The crude was triturated in EtOH and a solid formation was observed. This solid was filtered off and dried open air to give the crude product **147b** (0.021 g, 0.049 mmol, 28%). The filtered solution was concentrated to give the crude product **146b** (0.033 g, 0.076 mmol, 43%).

5.2.16.1. 3-bromo-1-(4-methoxybenzyl)-1H-1,2,4-triazol-5-yl 4-methylbenzenesulfonate (146b)

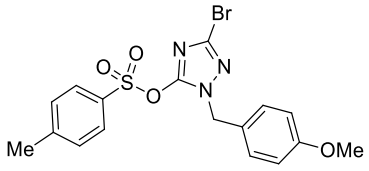

^{1}H NMR (400 MHz, $CDCl_3$): δ 2.49 (s, 3H), 3.8 (s, 3H), 5.12 (s, 2H), 6.86-6.89 (d, *J* = 8.7 Hz, 2H), 7.26-7.28 (d, *J* = 8.7 Hz, 2H), 7.39-7.42 (d, *J* = 8.3 Hz, 2H), 7.92-7.94 (d, *J* = 8.4 Hz, 2H). ^{13}C NMR (101 MHz, $CDCl_3$): δ 20.9, 50.3, 54.3, 113.3, 124.6, 128.2, 128.9, 129.1, 135.9, 146.2, 158.9.

5.2.16.2. 3-bromo-1-(4-methoxybenzyl)-4-tosyl-1H-1,2,4-triazol-5(4H)-one (147b)

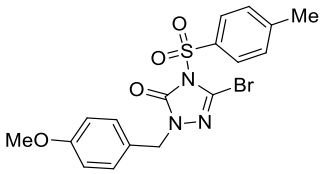

^{1}H NMR (400 MHz, $CDCl_3$): δ 2.47 (s, 3H), 3.78 (s, 3H), 4.74 (s, 2H), 6.82-6.85 (d, *J* = 8.7 Hz, 2H), 7.23-7.25 (d, *J* = 8.7 Hz, 2H), 7.39-7.41 (d, *J* = 8.1 Hz, 2H), 8.02-8.04 (d, *J* = 8.4 Hz, 2H). ^{13}C NMR (101 MHz, $CDCl_3$): δ 21.9, 49.2, 55.3, 114.2, 115.5, 126.8, 128.7, 130, 130.2, 133.8, 147, 148.9, 159.7.

5.2.17. Synthesis of 3-bromo-1-methyl-1H-1,2,4-triazol-5-yl 4-methylbenzenesulfonate (146a).

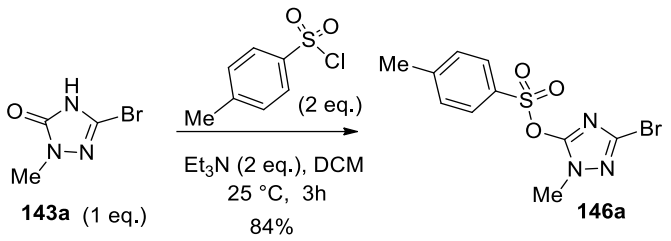

A 100 mL round botton flask containing a Teflon stirrer bar was charged with 3-bromo-1-methyl-1H-1,2,4-triazol-5(4H)-one (**143a**) (1 eq., 0.160 g, 0.9 mmol) and dry DCM (13 mL) followed by the addition of Et_3N (2 eq., 0.182 g, 0.25 mL, 1.8 mmol) under stirring. TsCl (2 eq., 0.343 g, 1.8 mmol) dissolved in 5 mL of dry DCM, was added dropwise to the reaction mixture. The reaction remained under stirring for 3h at r.t. The progress of the reaction was monitored by HPLC. The reaction mixture was concentrated, and the crude was purified by chromatography on silica gel using *n*-heptane/EtOAc (80/20) to give the desired product (0.252 g, 0.76 mmol, 84%). ^{1}H NMR (400 MHz, $CDCl_3$): δ 2.49 (s, 3H), 3.76 (s, 3H), 7.41-7.43 (d, *J* = 8 Hz, 2H), 7.91-7.93 (d, *J* = 8.5 Hz, 2H). ^{13}C NMR (101 MHz, $CDCl_3$): δ 21.9, 34.7, 129.2, 130.2, 136.8, 147.3.

5.2.18. Synthesis of 3-bromo-1-methyl-1H-1,2,4-triazol-5-yl 2,4,6-triisopropylbenzenesulfonate (151a).

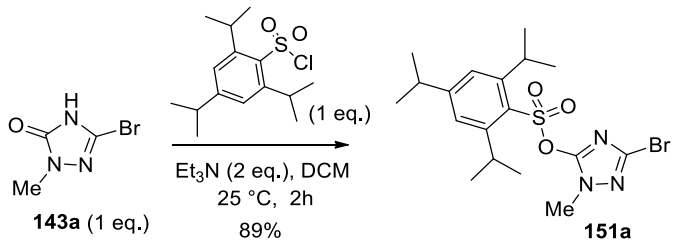

A microwave vial containing a Teflon stirrer bar was charged with 3-bromo-1-methyl-1H-1,2,4-triazol-5-ol (**143a**) (1 eq., 0.080 g, 0.45 mmol), dry DCM (6 mL) followed by the addition of Et_3N (2 eq., 0.091 g, 0.12 mL, 0.9 mmol) under stirring. T*i*PSCl (2 eq., 0.272 g, 0.9 mmol) dissolved in 3 ml of dry DCM was added dropwise to the reaction mixture. The reaction remained under stirring for 2h at r.t. The progress of the reaction was evaluated by HPLC. The reaction mixture was concentrated, and the crude product purified by chromatography on silica gel using gradient elution *n*-heptane/EtOAc (97.5/2.5 to 90/10) to give the desired product **151a** (0.178 g, 0.4 mmol, 89%). ^{1}H NMR (400 MHz, $CDCl_3$): δ 1.25-1.29 (t, *J* = 6.8 Hz, 18H), 2.89-

3.0 (m, *J* = 6.8 Hz, 1H), 3.81 (s, 3H), 3.92-4.02 (m, *J* = 6.8 Hz, 2H), 7.24 (s, 2H). ^{13}C NMR (101 MHz, $CDCl_3$): δ 23.4, 24.5, 30.1, 34.4, 34.6, 124.4, 136.8, 151.8, 155.6.

5.2.19. Synthesis of 1-benzyl-3-bromo-1H-1,2,4-triazol-5-yl 2,4,6-triisopropylbenzenesulfonate (151b).

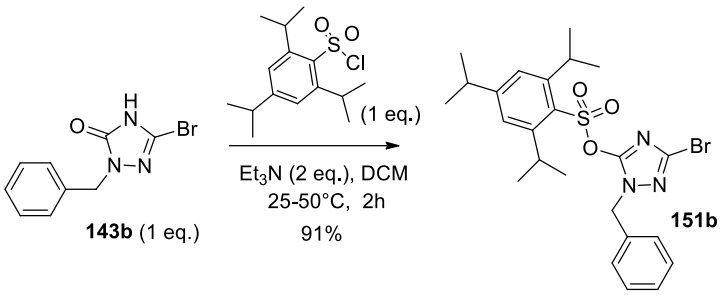

A 100 mL round botton flask containing a Teflon stirrer bar was charged with 1-benzyl-3-bromo-1H-1,2,4-triazol-5-ol (**143b**) (1 eq., 0.300 g, 1.18 mmol), dry DCM (20 mL) followed by the addition of Et_3N (2 eq., 0.239 g, 0.33 mL, 2.36 mmol) under stirring. T*i*PSCl (1 eq., 0.358 g, 1.18 mmol) dissolved in 10 ml of DCM was added dropwise to the reaction mixture. The reaction remained under stirring for 1h at r.t. and 1h at 50°C. The progress of the reaction was evaluated by HPLC. The reaction mixture was concentrated, and the crude product was dissolved in H_2O (20 mL) and extracted with EtOAc (2 x 20 mL). The organic layers were collected, dried with Na_2SO_4 and concentrated to give the product **151b** (0.560 g, 1.07 mmol, 91%). ^{1}H NMR (400 MHz, $CDCl_3$): δ 1.24-1.26 (d, *J* = 6.7 Hz, 12H), 1.27-1.29 (d, *J* = 6.9 Hz, 6H), 2.89-2.98 (m, *J* = 6.9 Hz, 1H), 3.95-4.05 (m, *J* = 6.7 Hz, 2H), 5.24 (s, 2H), 7.24 (s, 2H), 7.31-7.39 (m, 5H).

5.2.20. Synthesis of 3-(4-methoxyphenyl)-1-methyl-1H-1,2,4-triazol-5(4H)-one (149).

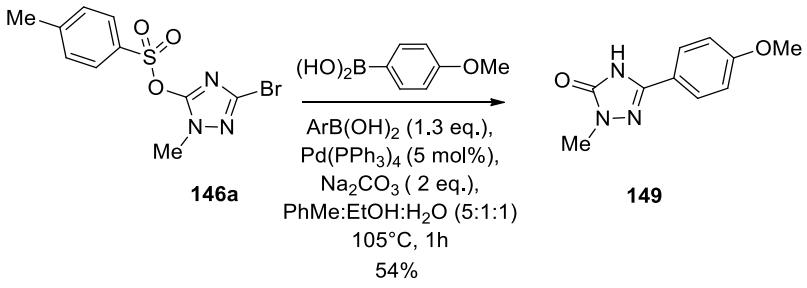

A microwave vial containing a Teflon stirrer bar was charged with 3-bromo-1-methyl-1H-1,2,4-triazol-5-yl 4-methylbenzene-1-sulfonate (**146b**) (1.2 eq., 0.025 g, 0.075 mmol), 4-methoxyphenylboronic acid (1 eq., 0.0096 g, 0.063 mmol), Na_2CO_3 (2 eq., 0.013 g, 0.13

mmol) and $Pd(PPh_3)_4$ (0.05 eq., 0.0036 g, 0.0031 mmol). The vessel was then capped properly, evacuated and backfilled with argon (this process was repeated a total of three times). A second microwave vial was charged with MePh (0.56 mL), EtOH (0.11 mL) and H_2O (0.11 mL) capped properly, evacuated and backfilled with argon (this process was repeated a total of three times). This solvent mixture was then added to the mixture of solids. The reaction mixture was placed in a preheated oil bath at 105°C for 1h. The progress of the reaction was evaluated by HPLC. The reaction mixture was cooled to r.t., concentrated under reduced pressure and the crude product was solubilized with EtOAc (5 mL) and washed with H_2O (3 x 5 mL). The organic layer was concentrated and purified by chromatography on silica gel using *n*-heptane/EtOAc (35/65) to give the product **149** (0.007 g, 0.034 mmol, 54%). ^{1}H NMR (400 MHz, $CDCl_3$): δ 3.56 (s, 3H), 3.86 (s, 3H), 6.98-7.0 (d, *J* = 8.9 Hz, 2H), 7.77-7.8 (d, *J* = 8.9 Hz, 2H), 12.84 (bs, 1H). ^{13}C NMR (101 MHz, $CDCl_3$): δ 32.2, 55.4, 114.5, 119.1, 126.7, 161.2.

5.2.21. Synthesis of 3-(4-methoxyphenyl)-1-methyl-1H-1,2,4-triazol-5-yl 2,4,6-triisopropylbenzenesulfonate (152a).

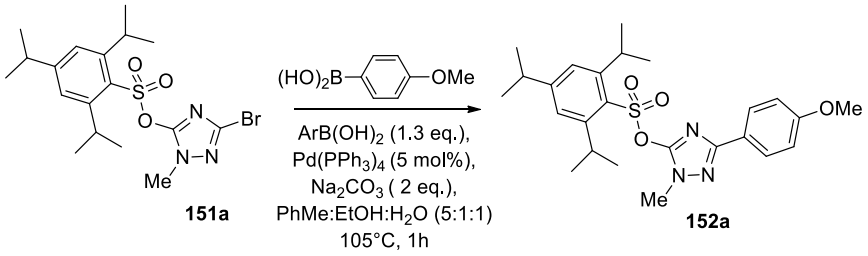

A microwave vial containing a Teflon stirrer bar was charged with 3-bromo-1-methyl-1H-1,2,4-triazol-5-yl 2,4,6-tris(propan-2-yl)benzene-1-sulfonate (**151a**) (1.1 eq., 0.050 g, 0.11 mmol), 4-methoxyphenylboronic acid (1 eq., 0.016 g, 0.102 mmol), Na_2CO_3 (2 eq., 0.022 g, 0.205 mmol) and $Pd(PPh_3)_4$ (0.05 eq., 0.006 g, 0.0051 mmol). The vessel was then capped properly, evacuated and backfilled with argon (this process was repeated a total of three times). A second microwave vial was charged with MePh (0.92 mL), EtOH (0.18 mL) and H_2O (0.18 mL) capped properly, evacuated and backfilled with argon (this process was repeated a total of three times). This solvent mixture was then added to the mixture of solids. The reaction mixture was then placed in a preheated oil bath at 105°C for 1h. The progress of the reaction was evaluated by HPLC. The reaction mixture was concentrated, and the crude product was purified by chromatography on silica gel using *n*-heptane/EtOAc (90/10) to give the desired product **152a** (0.047 g, 0.1 mmol, 98%). ^{1}H NMR (400 MHz, $CDCl_3$): δ 1.25-1.26 (d, *J* = 6.7 Hz, 12H), 1.28-1.30 (d, *J* = 6.9 Hz, 6H), 2.91-3.01 (m, *J* = 6.9 Hz, 1H), 3.81 (s, 3H), 3.83 (s, 3H), 4.04-

4.11 (m, *J* = 6.7 Hz, 2H), 6.84-6.86 (d, *J* = 8.9 Hz, 2H), 7.25 (s, 2H), 7.75-7.77 (d, *J* = 8.9 Hz, 2H). ^{13}C NMR (101 MHz, $CDCl_3$): δ 23.5, 24.5, 30.1, 34.2, 34.4, 55.3, 113.7, 123.4, 124, 127.3, 129.2, 151, 151.7, 155.2, 158.9, 160.5.

5.2.22. Synthesis of 1-benzyl-3-(4-methoxyphenyl)-1H-1,2,4-triazol-5-yl 2,4,6-triisopropylbenzenesulfonate (152b).

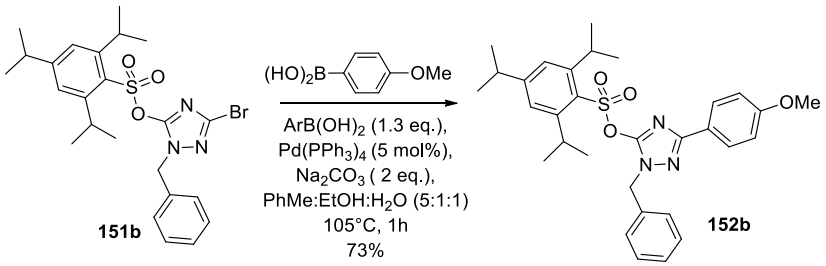

A microwave vial containing a Teflon stirrer bar was charged with 3-bromo-1-methyl-1H-1,2,4-triazol-5-yl 2,4,6-tris(propan-2-yl)benzene-1-sulfonate (**151b**) (1 eq., 0.080 g, 0.15 mmol), 4-methoxyphenylboronic acid (1.34 eq., 0.031 g, 0.2 mmol), Na_2CO_3 (2 eq., 0.032 g, 0.3 mmol) and $Pd(PPh_3)_4$ (0.05 eq., 0.009 g, 0.008 mmol). The vessel was then capped properly, evacuated and backfilled with argon (this process was repeated a total of three times). A second microwave vial was charged with MePh (3.6 mL), EtOH (0.7 mL) and H_2O (0.7 mL) capped properly, evacuated and backfilled with argon (this process was repeated a total of three times). This solvent mixture was then added to the mixture of solids. The reaction mixture was then placed in a preheated oil bath at 105°C for 1h. The progress of the reaction was evaluated by HPLC. The reaction mixture was concentrated, and the crude product was purified by chromatography on silica gel using *n*-heptane/EtOAc (90/10) to give the desired product **152b** (0.061 g, 0.11 mmol, 73%). ^{1}H NMR (400 MHz, $CDCl_3$): δ 1.16-1.17 (d, *J* = 6.7 Hz, 12H), 1.21-1.22 (d, *J* = 6.9 Hz, 6H), 2.83-2.92 (m, *J* = 6.9 Hz, 1H), 3.72 (s, 3H), 3.99-4.05 (m, *J* = 6.7 Hz, 2H), 5.22 (s, 2H), 6.75-6.78 (d, *J* = 9 Hz, 2H), 7.17 (s, 2H), 7.21-7.27 (m, 2H), 7.69-7.71 (d, *J* = 9 Hz, 2H).

5.2.23. Synthesis of 3-(4-methoxyphenyl)-1-methyl-1H-1,2,4-triazol-5(4H)-one (149)

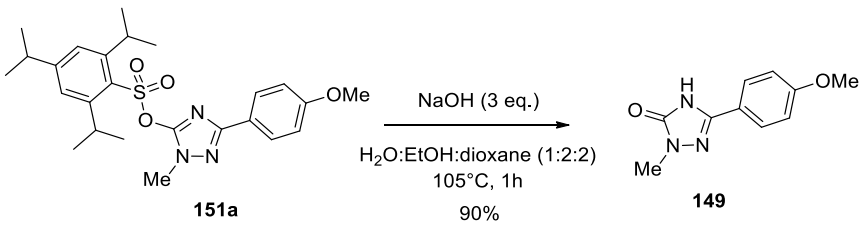

A microwave vial containing a Teflon stirrer bar was charged with compound **151a** (1 eq., 0.329 g, 0.74 mmol) and NaOH (3 eq., 0.083 g, 2.0 mmol) followed by the addition of H_2O (2.5 mL), dioxane (5 mL) and EtOH (5 mL). The reaction mixture was capped properly and stirred at 105°C for 1h. After cooling to r.t., the mixture was acidified with HCl, concentrated under reduced pressure and purified by chromatography on silica gel using EtOAc to give the product **149** (0.128 g, 0.63 mmol, 90%). ^{1}H NMR (400 MHz, $CDCl_3$): δ 3.56 (s, 3H), 3.86 (s, 3H), 6.98-7.0 (d, *J* = 8.9 Hz, 2H), 7.77-7.8 (d, *J* = 8.9 Hz, 2H), 12.84 (bs, 1H). ^{13}C NMR (101 MHz, $CDCl_3$): δ 32.2, 55.4, 114.5, 119.1, 126.7, 161.2.

5.2.24. Synthesis of 5-chloro-3-(4-methoxyphenyl)-1-methyl-1H-1,2,4-triazole (157)

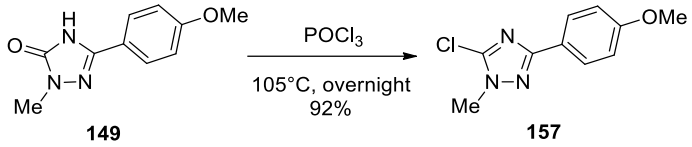

A microwave vial containing a Teflon stirrer bar was charged with compound **149** (1 eq., 0.025 g, 0.12 mmol) and solubilized with $POCl_3$ (88.073 eq., 1.6 g, 1 mL, 10.73 mmol). The reaction mixture was then capped properly and placed in a preheated oil bath at 110°C until complete conversion of the starting material was detected. The reaction mixture was concentrated under reduced pressure, diluted with 5ml of EtOAc and then washed with H_2O (5 mL), aqueous satured $NaHCO_3$ (5 mL) and brine (5 mL). The organic layer was then dried over anhydrous Na_2SO_4 and concentrated to give the desired product **157** (0.025 g, 0.11 mmol, 92%). ^{1}H NMR (400 MHz, $CDCl_3$): δ 3.84 (s, 3H), 3.87 (s, 3H), 6.93-6.95 (d, *J* = 8.9 Hz, 2H), 7.94-7.97 (d, *J* = 8.9 Hz, 2H). ^{13}C NMR (101 MHz, $CDCl_3$): δ 35.5, 55.3, 114, 123, 127.4, 160.8, 161.3.

5.2.25. Synthesis of 3-(4-methoxyphenyl)-1-methyl-5-(p-tolyl)-1H-1,2,4-triazole (153)

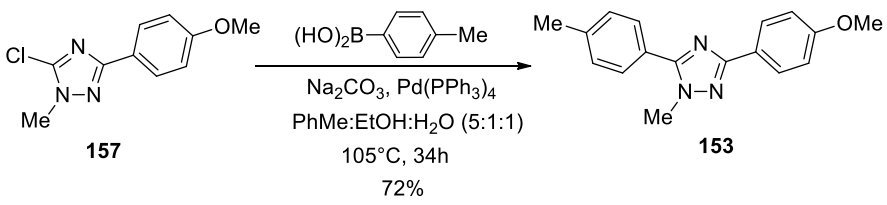

A microwave vial containing a Teflon stirrer bar was charged with 5-chloro-3-(4-methoxyphenyl)-1-methyl-1H-1,2,4-triazole (**157**) (1 eq., 0.020 g, 0.089 mmol), 4-tolylboronic acid (1.34 eq., 0.016 g, 0.12 mmol), Na_2CO_3 (2 eq., 0.019 g, 0.18 mmol) and $Pd(Ph_3)_4$ (0.05 eq., 0.005 g, 0.0045 mmol). The vessel was then capped properly, evacuated and backfilled with argon (this process was repeated a total of three times). A second microwave vial was charged with MePh (1.97 mL), EtOH (0.39 mL) and H_2O (0.39 mL) capped properly, evacuated and backfilled with argon (this process was repeated a total of three times). This solvent mixture was then added to the mixture of solids. The reaction mixture was then placed in a preheated oil bath at 105°C for 34h. The progress of the reaction was evaluated by HPLC. The reaction mixture was concentrated, and the crude product was purified by chromatography on silica gel using *n*-heptane/EtOAc (30/70) to give the desired product **153** (0.018 g, 0.064 mmol, 72%). ^{1}H NMR (400 MHz, $CDCl_3$): δ 2.43 (s, 3H), 3.85 (s, 3H), 3.98 (s, 3H), 6.95-6.97 (d, *J* = 8.9 Hz, 2H), 7.31-7.33 (d, *J* = 7.9 Hz, 2H), 7.60-7.62 (d, *J* = 8.1 Hz, 2H), 8.06-8.08 (d, *J* = 8.9 Hz, 2H). ^{13}C NMR (101 MHz, $CDCl_3$): δ 21.4, 36.9, 55.3, 113.9, 123.8, 125.2, 127.8, 128.6, 129.5, 140.2, 155.6, 160.4, 160.9.

5.2.26. Synthesis of 2,4,6-triisopropyl-N-phenethylbenzenesulfonamide (159)

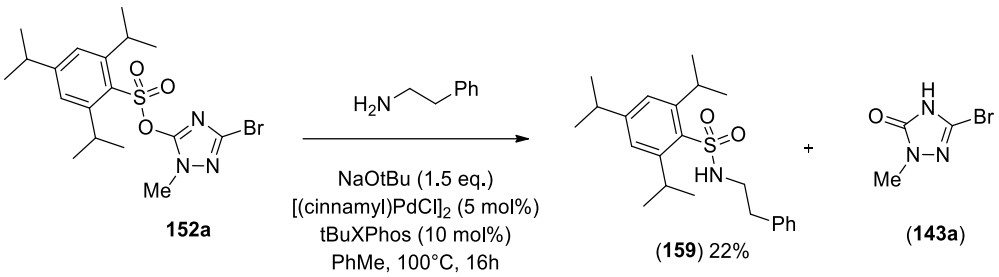

A microwave vial containing a Teflon stirrer bar was charged with compound **152a** (1 eq., 0.025 g, 0.056 mmol), NaOtBu (1.5 eq., 0.0095 g, 0.084 mmol), tBuXPhos (0.1 eq., 0.0024 g, 0.0056 mmol) and [(cinnamyl)PdCl]$_2$ (0.05 eq., 0.0015 g, 0.0028 mmol). The reaction vessel was capped properly, evacuated and backfilled with argon (this process was repeated a total of three times). A mixture of MePh (0.25 mL) and phenethylamine (1.3 eq., 0.009 g, 0.009 mL, 0.073 mmol) was bubbled with argon for 5 minute and added to the reaction vessel. The reaction mixture was then placed in a preheated oil bath at 100 °C until complete conversion of the starting material was detected. The reaction mixture was monitored by HPLC analysis. The reaction mixture was cooled to r.t. and concentrated under reduced pressure. The crude product was purified by chromatography on silica gel using *n*-heptane/EtOAc (50/50) to give the

product **159** (0.011 g, 0.029 mmol, 22%). ^{1}H NMR (400 MHz, $CDCl_3$): δ 1.20-1.21 (d, *J* = 6.8 Hz, 12H), 1.24-1.26 (d, *J* = 6.9 Hz, 6H), 2.82-2.85 (t, *J* = 6.8 Hz, 2H), 2.87-2.98 (m, *J* = 6.9 Hz, 1H), 3.20-3.25 (q, *J* = 6.8 Hz, 2H), 4.05-4.15 (m, *J* = 6.8 Hz, 2H), 4.26-4.30 (t, *J* = 6.4 Hz, 1H), 7.11-7.13 (m, 4H), 7.20-7.24 (m, 1H), 7.26-7.29 (m, 2H).

5.2.27. Synthesis of 3-bromo-5-(methoxymethoxy)-1-methyl-1H-1,2,4-triazole (160a)

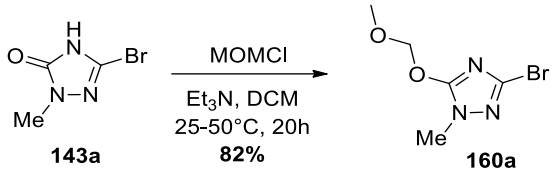

A Bioshake vial was charged with 3-bromo-1-methyl-1H-1,2,4-triazol-5-ol (**143a**) (1 eq., 0.050 g, 0.28 mmol), DCM (1 mL) and Et_3N (3 eq., 0.085 g, 0.117 mL, 0.84 mmol). The mixture was stirred at r.t. for 10 min. Then, MOMCl (3 eq., 0.068 g, 0.064 mL, 0.84 mmol) was added. The reaction mixture was stirred at 50°C for 20h in a Bioshake reactor. The progress of the reaction was monitored by HPLC. After cooling to r.t. a saturated aqueous solution of NH_4Cl (5 mL) was added to the reaction mixture. The aqueous solution was extracted with DCM (3 x 5 mL). The organic layers were combined, dried over Na_2SO_4 and concentrated under reduced pressure to give the desired product **160a** (0.051 g, 0.23 mmol, 82%). ^{1}H NMR (400 MHz, $CDCl_3$): δ 3.4 (s, 3H), 3.46 (s, 3H), 5.01 (s, 2H). ^{13}C NMR (101 MHz, $CDCl_3$): δ 32.7, 57.2, 73.4, 120.8.

5.2.28. Synthesis of 1-benzyl-3-bromo-5-(methoxymethoxy)-1H-1,2,4-triazole (160b)

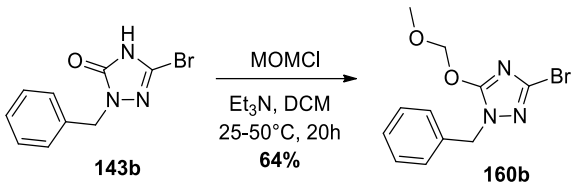

A Bioshake vial was charged with 1-benzyl-3-bromo-1H-1,2,4-triazol-5(4H)-one (**143b**) (1 eq., 0.276 g, 0.37 mmol), DCM (1.5 mL) and Et_3N (3 eq., 0.112 g, 0.153 mL, 1.10 mmol). The mixture was stirred at r.t. for 10 min. Then, MOMCl (3 eq., 0.089 g, 1.10 mL, 0.84 mmol) was added. The reaction mixture was stirred at 50°C for 20h in a Bioshake reactor. The progress of the reaction was monitored by HPLC. After cooling to r.t. a saturated aqueous

solution of NH_4Cl (5 mL) was added to the reaction mixture. The aqueous solution was extracted with DCM (3 x 5 mL). The organic layers were combined, dried over Na_2SO_4 and concentrated under reduced pressure to give the desired product **160b** (0.206 g, 0.69 mmol, 64%). ^{1}H NMR (400 MHz, $CDCl_3$): δ 3.41 (s, 3H), 4.95 (s, 2H), 5.03 (s, 2H), 7.30-7.37 (m, 5H).

5.2.29. Synthesis of 5-(methoxymethoxy)-3-(4-methoxyphenyl)-1-methyl-1H-1,2,4-triazole (161)

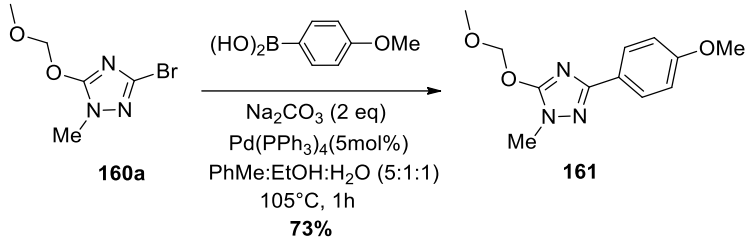

A microwave vial containing a Teflon stirrer bar was charged with 3-bromo-5-(methoxymethoxy)-1-methyl-1H-1,2,4-triazole (**160a**) (1 eq., 0.049 g, 0.22 mmol), 4-methoxyphenylboronic acid (1.34 eq., 0.045 g, 0.29 mmol), Na_2CO_3 (2 eq., 0.047 g, 0.44 mmol) and $Pd(Ph_3)_4$ (0.05 eq., 0.013 g, 0.011 mmol). The vessel was then capped properly, evacuated and backfilled with argon (this process was repeated a total of three times). A second microwave vial was charged with MePh (1.97 mL), EtOH (0.39 mL) and H_2O (0.39 mL) capped properly, evacuated and backfilled with argon (this process was repeated a total of three times). This solvent mixture was then added to the mixture of solids. The reaction mixture was then placed in a preheated oil bath at 105°C for 1h. The progress of the reaction was evaluated by HPLC. After cooling to r.t., the reaction mixture was concentrated under reduced pressure and the crude product was purified by chromatography on silica gel using *n*-heptane/EtOAc (50/50) to give the desired product **161** (0.040 g, 0.16 mmol, 73%). ^{1}H NMR (400 MHz, $CDCl_3$): δ 3.52 (s, 3H), 3.53 (s, 3H), 5.04 (s, 2H), 6.97-6.99 (d, J = 8.9 Hz, 2H), 7.73-7.76 (d, J = 8.9 Hz, 2H). ^{13}C NMR (101 MHz, $CDCl_3$): δ 32.4, 55.4, 57, 72.8, 114.4, 118.9, 129.6, 146.1, 154.5, 161.3.

5.2.30. Synthesis of 3-(4-methoxyphenyl)-1-methyl-1H-1,2,4-triazol-5(4H)-one (149)

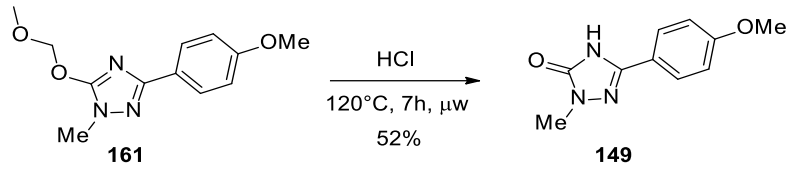

A microwave vial containing a Teflon stirrer bar was charged with compound **161** (0.37 eq., 0.020 g, 0.0802 mmol) and 2 mL of HCl (4 M in 1,4-dioxane). The reaction mixture was heated to 120 °C for 7h under microwave irradiation. The progress of the reaction was monitored by HPLC analysis. The reaction mixture was diluted with 5mL of H_2O and extracted with EtOAc (3 x 10ml). The organic layers were combined, dried with Na_2SO_4 and concentrated under reduced pressure to give the product **149** (0.009 g, 0.042 mmol, 52%). ^{1}H NMR (400 MHz, $CDCl_3$): δ 3.56 (s, 3H), 3.86 (s, 3H), 6.98-7.0 (d, *J* = 8.9 Hz, 2H), 7.77-7.8 (d, *J* = 8.9 Hz, 2H), 12.84 (bs, 1H). ^{13}C NMR (101 MHz, $CDCl_3$): δ 32.2, 55.4, 114.5, 119.1, 126.7, 161.2.

5.2.31. Synthesis of 3-(4-methoxyphenyl)-1-methyl-N-phenethyl-1H-1,2,4-triazol-5-amine (119a)

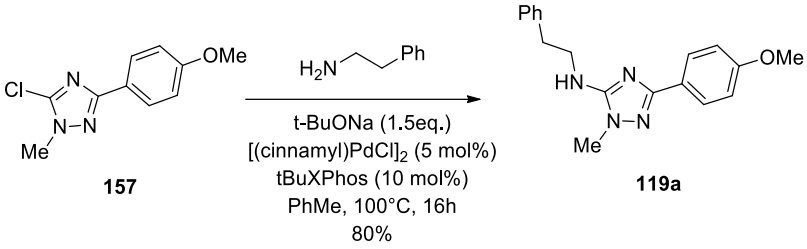

A microwave vial containing a Teflon stirrer bar was charged with 5-chloro-3-(4-methoxyphenyl)-1-methyl-1H-1,2,4-triazole (**157**) (1 eq., 0.025 g, 0.11 mmol), KOtBu (1.5 eq., 0.019 g, 0.17 mmol), tBuXPhos (0.1 eq., 0.005 g, 0.011 mmol) and $[(cinnamyl)PdCl]_2$ (0.05 eq., 0.003 g, 0.0056 mmol). The reaction vessel was evacuated and backfilled with argon (this process was repeated a total of three times). A mixture of MePh (0.5 mL) and phenethylamine (1.3 eq., 17.609 mg, 0.018 mL, 0.15 mmol) was bubbled with argon for 1 minute and added to the reaction vessel. The reaction mixture was then capped properly and placed in a preheated oil bath at 100 °C until complete conversion of the starting material was detected. The reaction mixture was monitored by HPLC analysis. Afte cooling to r.t., the reaction mixture was concentrated, and the crude product was purified by chromatography on silica gel using *n*-heptane/EtOAc 50/50 to give expected product **119a** (0.028 g, 0.089 mmol, 80%). ^{1}H NMR (400 MHz, $CDCl_3$): δ 2.97-3.0 (t, *J* = 6.7 Hz, 2H), 3.49 (s, 3H), 3.7-3.75 (q, *J* = 6.7 Hz, 2H), 3.81 (bs, 1H), 3.83 (s, 3H), 6.92-6.94 (d, *J* = 8.9 Hz, 2H), 7.22-7.27 (m, 3H), 7.31-7.35 (m, 2H),

7.95-7.97 (d, *J* = 8.9 Hz, 2H). ^{13}C NMR (101 MHz, $CDCl_3$): δ 33, 35.8, 42.2, 55.3, 113.8, 124.44, 126.6, 127.4, 128.7, 128.9, 138.9, 155.6, 158.5, 160.

5.2.32. Synthesis of 5-(benzyloxy)-3-bromo-1-(p-tolyl)-1H-1,2,4-triazole and 3-(benzyloxy)-5-bromo-1-(p-tolyl)-1H-1,2,4-triazole (162 and 163)

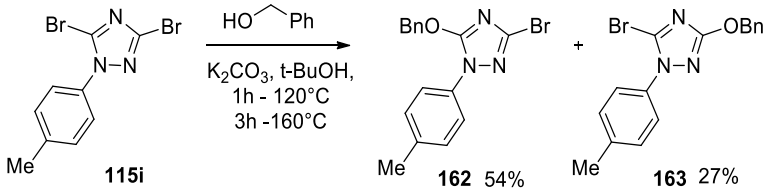

A microwave vial containing a Teflon stirrer bar was charged with 3,5-dibromo-1-(4-methylphenyl)-1H-1,2,4-triazole (**115i**) (1 eq., 0.050 g, 0.16 mmol), K_2CO_3 (2 eq., 0.044 g, 0.32 mmol), tBuOH (1 mL), followed by the addition of benzyl alcohol (2 eq., 0.034 g, 0.033 mL, 0.32 mmol). The reaction mixture was stirred for 1h at 120°C and 3h at 160°C. The progress of the reaction was evaluated by HPLC. After cooling to r.t., the reaction mixture was diluted with H_2O (10 mL) and extracted with EtOAc (3 x 10 mL). The organic layers were combined, dried with Na_2SO_4 and concentrated. The crude was purified by using gradient elution *n*-heptane/EtOAc (100/0 to 90/10) to give **162** (0.029 g, 0.085 mmol, 54%) and **163** (0.014 g, 0.042 mmol, 27%).

5.2.32.1. 5-(benzyloxy)-3-bromo-1-(p-tolyl)-1H-1,2,4-triazole (162)

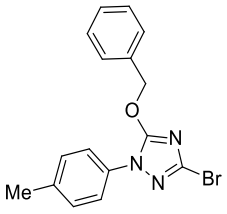

^{1}H NMR (400 MHz, $CDCl_3$): δ 2.35 (s, 3H), 4.93 (s, 2H), 7.21-7.23 (d, *J* = 8.3 Hz, 2H), 7.33-7.43 (m, 5H), 7.77-7.79 (d, *J* = 8.5 Hz, 2H).

5.2.32.2. 3-(benzyloxy)-3-bromo-1-(p-tolyl)-1H-1,2,4-triazole (163)

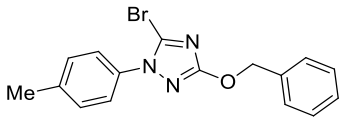

^{1}H NMR (400 MHz, $CDCl_3$): δ 2.36 (s, 3H), 5.53 (s, 2H), 7.20-7.22 (d, *J* = 8.5 Hz, 2H), 7.37-7.46 (m, 5H), 7.52-7.54 (d, *J* = 8.5 Hz, 2H).

5.2.33. Synthesis of 5-(benzyloxy)-3-bromo-1H-1,2,4-triazoles (164)

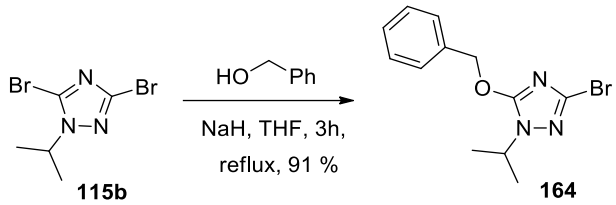

A microwave vial containing a Teflon stirrer bar was charged with NaH (1.1 eq., 0.025 g, 0.94 mmol) and then flamed, evacuated and backfilled (this process was repeated a total of three times). The reaction vessel was cooled to r.t., then THF anhydrous and benzyl alcohol (1.2 eq., 0.111 g, 0.106 mL, 1.03 mmol) were added and the mixture stirred for 20 min at r.t. The 3,5-dibromo-1H-1,2,4-triazole (**115b**) (1 eq.) was then added and the reaction mixture heated to 85°C for 3h. After cooling to r.t., the reaction mixture was versed over ice (10 g). The aqueous phase was extracted with EtOAc (3 x 20 mL). The organic layers were combined and washed with H_2O (2 x 20 mL), dried with Na_2SO_4 and concentrated under reduced pressure to give the product **164** (0.230 g, 0.78 mmol, 91%). ^{1}H NMR (400 MHz, $CDCl_3$): δ 1.38-1.4 (d, *J* = 6.7 Hz, 6H), 4.37-4.47 (m, *J* = 6.7 Hz, 1H), 5.42 (s, 2H), 7.35-7.44 (m, 5H).

5.2.34. Synthesis of 1-benzyl-5-(benzyloxy)-3-bromo-1H-1,2,4-triazole (165)

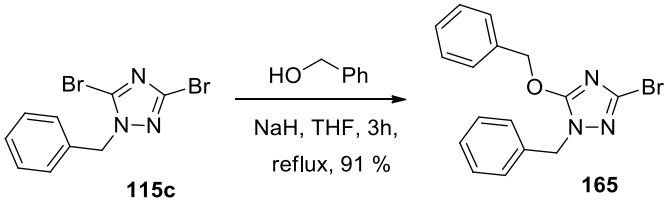

A microwave vial containing a Teflon stirrer bar was charged with NaH (1.1 eq., 0.043 g, 1.6 mmol) and then flamed, evacuated and backfilled (this process was repeated a total of three times). The reaction vessel was cooled to r.t., then anhydrous THF and benzyl alcohol (1.2 eq., 0.189 g, 0.181 mL, 1.75 mmol) were added and the mixture stirred for 20 min at r.t. The 3,5-dibromo-1H-1,2,4-triazole (**115c**) (1 eq.) was then added and the reaction mixture heated to

85°C for 3h. After cooling to r.t., the reaction mixture was versed over ice (10 g). The aqueous phase was extracted with EtOAc (3 x 20 mL). The organic layers were combined and washed with H_2O (2 x 20 mL), dried with Na_2SO_4 and concentrated under reduced pressure to give the product **165** (0.157 g, 0.46 mmol, 31%). ^{1}H NMR (400 MHz, $CDCl_3$): δ 5.05 (s, 2H), 5.43 (s, 2H), 7.22-7.24 (m, 2H), 7.30-7.38 (m, 8H).

5.2.35. Suzuki-Miyaura arylation of 5-(benzyloxy)-3-bromo-1-isopropyl-1H-1,2,4-triazole

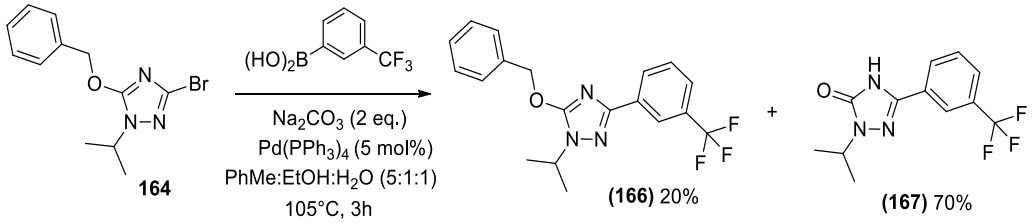

A microwave vial containing a Teflon stirrer bar was charged with 5-(benzyloxy)-3-bromo-1-(propan-2-yl)-1H-1,2,4-triazole (**164**) (1 eq., 0.058 g, 0.2 mmol), 3-(trifluoromethyl)phenylboronic acid (1.34 eq., 0.050 g, 0.26 mmol), Na_2CO_3 (2 eq., 0.042 g, 0.39 mmol) and $Pd(Ph_3)_4$ (0.05 eq., 0.011 g, 0.0098 mmol). The vessel was then capped properly, evacuated and backfilled with argon (this process was repeated a total of three times). A second microwave vial was charged with MePh (1.72 mL), EtOH (0.34 mL) and H_2O (0.34 mL) capped properly, evacuated and backfilled with argon (this process was repeated a total of three times). This solvent mixture was then added to the mixture of solids. The reaction mixture was placed in a preheated oil bath at 105°C for 3h. The progress of the reaction was evaluated by HPLC. After cooling to r.t., the reaction mixture was concentrated, and the crude product was purified by chromatography on silica gel using EtOAc to give **166** (0.014 g, 0.039 mmol, 20%) and **167** (0.037 g, 0.13 mmol, 70%).

5.2.35.1. 5-(benzyloxy)-1-isopropyl-3-(3-(trifluoromethyl)phenyl)-1H-1,2,4-triazole (166)

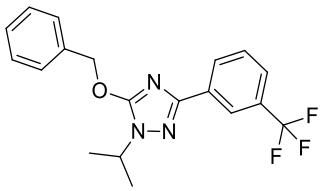

^{1}H NMR (400 MHz, $CDCl_3$): δ 1.45-1.46 (d, *J* = 6.7 Hz, 6H), 4.45-4.53 (m, *J* = 6.7 Hz, 1H), 5.52 (s, 2H), 7.29-7.34 (m, 9H).

5.2.35.2. 1-isopropyl-3-(3-(trifluoromethyl)phenyl)-1H-1,2,4-triazol-5(4H)-one (167)

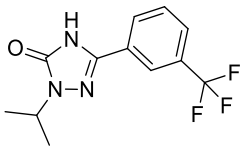

^{1}H NMR (400 MHz, $CDCl_3$): δ 1.47-1.48 (d, *J* = 6.7 Hz, 6H), 4.55-4.65 (m, *J* = 6.7 Hz, 1H), 7.59-7.63 (t, *J* = 7.8 Hz, 1H), 7.68-7.7 (d, *J* = 7.8 Hz, 1H), 8.05-8.07 (d, *J* = 7.8 Hz, 1H), 8.23 (s, 1H), 13.38 (bs, 1H). LC/MS m/z $[M + H]^+$ 272.12.

5.2.36. Synthesis of 1-isopropyl-3-(3-(trifluoromethyl)phenyl)-1H-1,2,4-triazol-5(4H)-one

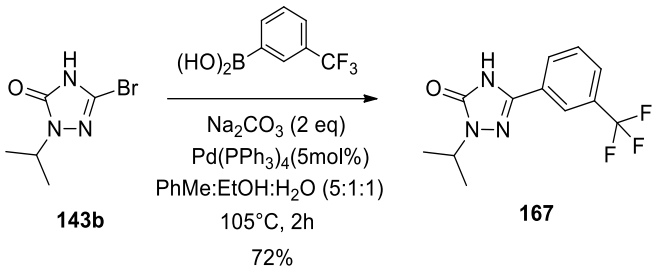

A microwave vial containing a Teflon stirrer bar was charged with 3-bromo-1-(propan-2-yl)-1H-1,2,4-triazol-5-ol (**143b**) (1 eq., 0.050 g, 0.24 mmol), 3-(trifluoromethyl)phenylboronic acid (1.34 eq., 0.062 g, 0.33 mmol), Na_2CO_3 (3 eq., 0.077 g, 0.73 mmol) and $Pd(Ph_3)_4$ (0.05 eq., 0.014 g, 0.012 mmol). The vessel was then capped properly, evacuated and backfilled with argon (this process was repeated a total of three times). A second microwave vial was charged with MePh (2.14 mL), EtOH (0.43 mL) and H_2O (0.43 mL) capped properly, evacuated and backfilled with argon (this process was repeated a total of three times). This solvent mixture was then added to the mixture of solids. The reaction mixture was placed in a preheated oil bath at 105°C for 2h. The progress of the reaction was evaluated by HPLC. After cooling to r.t., the reaction mixture was concentrated, and the crude product was purified by chromatography on silica gel using EtOAc to give the product **167** (0.047 g, 0.17 mmol, 72%). ^{1}H NMR (400 MHz, $CDCl_3$): δ 1.47-1.48 (d, *J* = 6.7 Hz, 6H), 4.55-4.65 (m, *J* = 6.7 Hz, 1H), 7.59-7.63 (t, *J* = 7.8 Hz, 1H), 7.68-7.7 (d, *J* = 7.8 Hz, 1H), 8.05-8.07 (d, *J* = 7.8 Hz, 1H), 8.23 (s, 1H), 13.38 (bs, 1H).

5.2.37. Synthesis of 5-chloro-1-isopropyl-3-(3-(trifluoromethyl)phenyl)-1H-1,2,4-triazole (168)

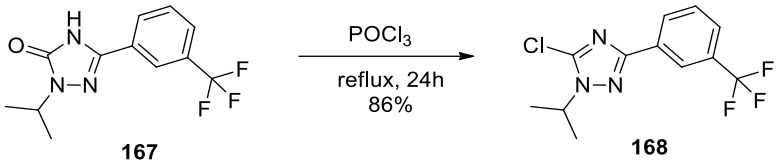

167 168

A microwave vial containing a Teflon stirrer bar was charged with 1-isopropyl-3-(3-(trifluoromethyl)phenyl)-1H-1,2,4-triazol-5(4H)-one (**167**) (1 eq., 0.057 g, 0.208 mmol) and solubilized with $POCl_3$ (88 eq., 2.8 g, 1.71 mL, 18.35 mmol). The reaction mixture was then capped and placed in a preheated oil bath at 110°C until complete conversion of the starting material was detected. The reaction mixture was concentrated under reduced pressure, diluted with 5ml of EtOAc and then washed with H_2O (5 mL), aqueous satured $NaHCO_3$ (5 mL) and brine (5 mL). The organic layer was then dried over anhydrous sodium sulfate and concentrated under reduced pressure to give the crude product. The crude product was purified by chromatography on silica gel using DCM to give expected product **168** (0.052 g, 0.18 mmol, 86%). ^{1}H NMR (400 MHz, $CDCl_3$): δ 1.54-1.56 (d, *J* = 6.7 Hz, 6H), 4.67-4.73 (m, *J* = 6.7 Hz, 1H), 7.52-7.56 (t, *J* = 7.8 Hz, 1H), 7.63-7.65 (d, *J* = 7.8 Hz, 1H), 8.23-8.25 (d, *J* = 7.8 Hz, 1H), 8.34 (s, 1H).

5.2.38. Buchwald-Hartwig of 1-benzyl-5-(benzyloxy)-3-bromo-1H-1,2,4-triazole

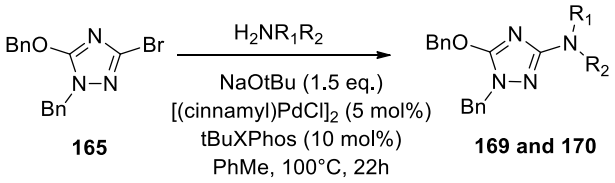

165 169 and 170

A microwave vial containing a Teflon stirrer bar was charged with 1-benzyl-5-(benzyloxy)-3-bromo-1H-1,2,4-triazole (**165**) (1 eq.), NaOtBu (1.5 eq.), t-BuXPhos (0.1 eq.) and $[(cinnamyl)PdCl]_2$ (0.05 eq.). The mixture vessel was evacuated and backfilled with argon (this process was repeated a total of three times), and then the mixture of Toluene and phenethylamine (1.5 eq., 14.57 mg, 0.013 mL, 0.087 mmol) was bubbled with argon for 1 minute and added. The reaction mixture was then capped properly and placed in a preheated oil bath at 100 °C until complete conversion of the starting material was detected. The reaction mixture was monitored by HPLC analysis. The reaction mixture was concentrated, and the crude product was purified by chromatography on silica gel to give the products **169** and **170**.

5.2.38.1. 1-benzyl-5-(benzyloxy)-N-phenethyl-1H-1,2,4-triazol-3-amine (169)

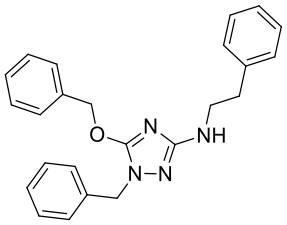

The synthesis followed the general procedure using 1-benzyl-5-(benzyloxy)-3-bromo-1H-1,2,4-triazole (**165**) (1 eq., 0.030 g, 0.087 mmol), NaOtBu (1.5 eq., 0.013 g, 0.13 mmol), tBuXPhos (0.1 eq., 0.004 g, 0.009 mmol), [(cinnamyl)PdCl]$_2$ (0.05 eq., 0.003 g, 0.004 mmol), MePh (0.4 mL). The crude product was purified by chromatography on silica gel using gradient elution *n*-heptane/EtOAc (30/70 to 50/50) to give the product **169** (0.017 g, 0.044 mmol, 50%). ^{1}H NMR (400 MHz, $CDCl_3$): δ 2.87-2.91 (t, *J* = 6.9 Hz, 2H), 3.47-3.52 (m, 2H), 3.92-3.95 (t, 1H), 4.95 (s, 2H), 5.35 (s, 2H), 7.23-7.21 (m, 5H), 7.27-7.3 (m, 5H), 7.35 (s, 5H).

5.2.38.2. 1-benzyl-5-(benzyloxy)-N-(2,4-dimethoxybenzyl)-1H-1,2,4-triazol-3-amine (170)

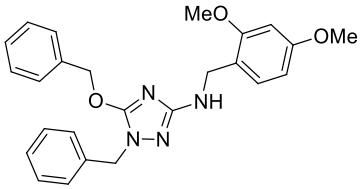

The synthesis followed the general procedure using 1-benzyl-5-(benzyloxy)-3-bromo-1H-1,2,4-triazole (**165**) (1 eq., 0.020 g, 0.058 mmol), NaOtBu (1.5 eq., 0.008 g, 0.087 mmol), tBuXPhos (0.1 eq., 0.0025 g, 0.006 mmol), [(cinnamyl)PdCl]$_2$ (0.05 eq., 0.0015 g, 0.003 mmol), MePh (0.27 mL). The crude product was purified by chromatography on silica gel using gradient elution *n*-heptane/EtOAc (30/70 to 50/50) to give the product **170** (0.014 g, 0.033 mmol, 56%). ^{1}H NMR (400 MHz, $CDCl_3$): δ 3.8 (s, 3H), 3.8 (s, 3H), 4.31-4.33 (d, *J* = 6 Hz, 2H), 4.42-4.45 (t, *J* = 6.2 Hz, 1H), 4.94 (s, 2H), 5.35 (s, 2H), 6.38-6.41 (dd, *J* = 2.4 Hz, *J* = 8.2 Hz, 1H), 6.44-6.45 (d, *J* = 2.4 Hz, 1H), 7.18-7.29 (m, 6H), 7.35 (s, 5H).

5.2.39. Synthesis of 1-benzyl-5-chloro-N-phenethyl-1H-1,2,4-triazol-3-amine (171)

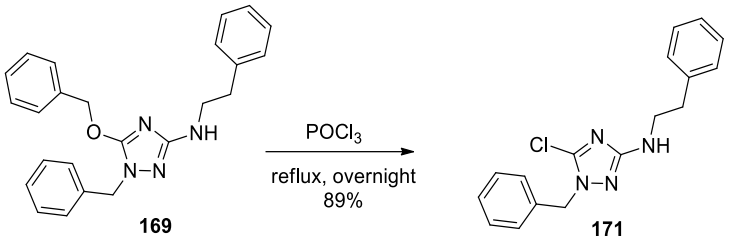

A microwave vial containing a Teflon stirrer bar was charged with 1-benzyl-5-(benzyloxy)-N-(2-phenylethyl)-1H-1,2,4-triazol-3-amine (**169**) (1 eq., 0.015 g, 0.039 mmol) and solubilized with $POCl_3$ (88 eq., 0.527 g, 0.32 mL, 3.44 mmol). The reaction mixture was then capped and placed in a preheated oil bath at 110°C until complete conversion of the starting material was detected. The reaction mixture was concentrated under reduced pressure, diluted with 5ml of EtOAc and then washed with H_2O (5 mL), aqueous satured $NaHCO_3$ (5 mL) and brine (5 mL). The organic layer was then dried over anhydrous Na_2SO_4 and concentrated to give the desired product **171** (0.011 g, 0.035 mmol, 89%). ^1H NMR (400 MHz, $CDCl_3$): δ 2.86-2.90 (t, *J* = 6.8 Hz, 2H), 3.36 (bs, 1H), 3.48-3.52 (t, *J* = 6.8 Hz, 2H), 5.14 (s, 2H), 7.21-7.36 (m, 10 H).

5.2.40. Synthesis of 1-benzyl-5-(4-chlorophenyl)-N-phenethyl-1H-1,2,4-triazol-3-amine (172)

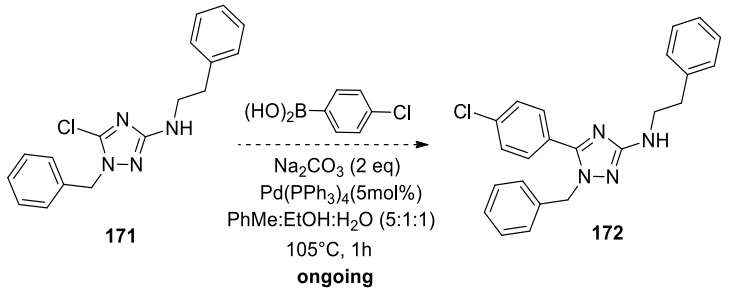

A microwave vial (oven-dried and under nitrogen) containing a Teflon stirrer bar was charged with 4-chlorophenylboronic acid (1.3 eq., 0.007 g, 0.045 mmol), Na_2CO_3 (2 eq., 0.0074 g, 0.07 mmol) and $Pd(Ph_3)_4$ (0.05 eq., 0.002 g, 0.0017 mmol). The vessel was then capped properly, evacuated and backfilled with argon (this process was repeated a total of three times). A second microwave vial was charged with MePh (0.307 mL), EtOH (0.061 mL), H_2O (0.061 mL) and 1-benzyl-5-chloro-N-(2-phenylethyl)-1H-1,2,4-triazol-3-amine (**171**) (1 eq., 0.0011 g, 0.035 mmol), capped, evacuated and backfilled with argon (this process was repeated a total of three times). This mixture was then added to the mixture of solids. The reaction mixture was

then placed in a preheated oil bath at 105°C for 1h. The progress of the reaction was evaluated by HPLC.

5.2.41. Synthesis of 1,4-dibenzyl-3-bromo-1H-1,2,4-triazol-5(4H)-one (173)

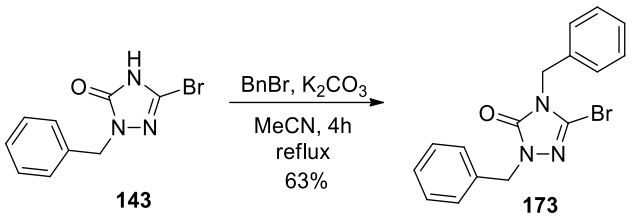

A microwave vial containing a Teflon stirrer bar was charged with 1-benzyl-3-bromo-4,5-dihydro-1H-1,2,4-triazol-5-one (**143**) (1 eq., 0.050 g, 0.2 mmol), K_2CO_3 (2 eq., 0.054 g, 0.39 mmol) and dry MeCN (0.5 mL) followed by the addition of benzyl bromide (1.5 eq., 0.050 g, 0.035 mL, 0.3 mmol). The reaction mixture was then capped properly and placed in a preheated oil bath at 90 °C until complete conversion of the starting material was detected. The reaction mixture was monitored by HPLC analysis and was usually complete within 4 h. H_2O (10 mL) was added to the mixture, and extracted by EtOAc (3 x 10 mL). The organic layers were combined, dried over Na_2SO_4 and concentrated to give a crude product **173** (0.043 g, 0.12 mmol, 63%). ^{1}H NMR (400 MHz, $CDCl_3$): δ 4.86 (s, 2H), 4.96 (s, 2H), 7.29-7.38 (m, 10H).

5.2.42. Buchwald-Hartwig reaction of 1,4-dibenzyl-3-bromo-1H-1,2,4-triazol-5(4H)-one (174)

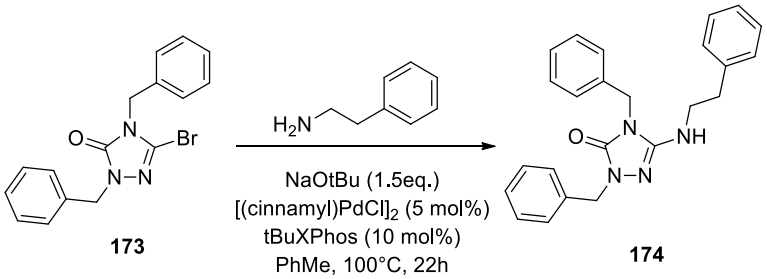

A microwave vial (oven-dried and under nitrogen) containing a Teflon stirrer bar was charged with 1,4-dibenzyl-3-bromo-4,5-dihydro-1H-1,2,4-triazol-5-one (**173**) (1 eq., 0.030 g, 0.087 mmol), NaOtBu (1.5 eq., 0.013 g, 0.13 mmol), tBuXPhos (0.1 eq., 0.0037 mg, 0.0087 mmol) and [(cinnamyl)PdCl]$_2$ (0.05 eq., 0.003 g, 0.0044 mmol). The mixture was then capped properly, evacuated and backfilled with argon (this process was repeated a total of three times). A second microwave vial (oven-dried and under nitrogen) containing a Teflon stirrer bar was

charged with phenethylamine (1.3 eq., 0.014 g, 0.014 mL, 0.11 mmol) and MePh (0.4 mL). This solution was then capped properly, evacuated and backfilled with argon (this process was repeated a total of three times) and subsequently, added to the microwave vial containing the mixture of solids. The reaction mixture was then placed in a preheated oil bath at 100 °C for 22h. The progress of the reaction was evaluated by LC/MS.

5.2.43. Synthesis of N-(1-benzyl-5-(methoxymethoxy)-1H-1,2,4-triazol-3-yl)cyclopropanecarboxamide (179)

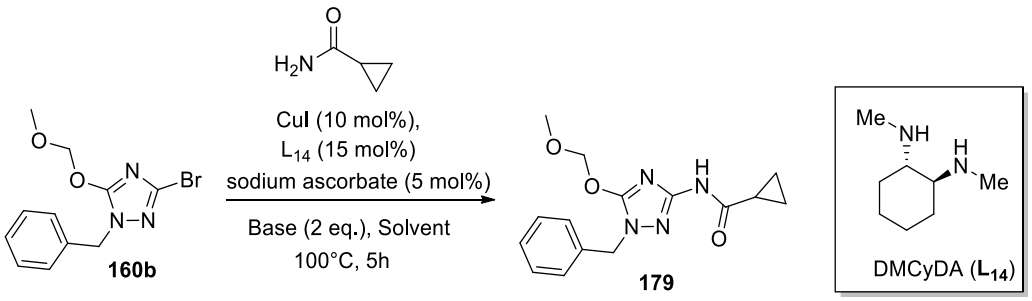

A microwave vial (oven-dried and under nitrogen) containing a Teflon stirrer bar was charged with 1-benzyl-3-bromo-5-(methoxymethoxy)-1H-1,2,4-triazole (**160b**) (1 eq., 0.0125 g, 0.042 mmol), cyclopropanecarboxamide (2 eq., 0.007 g, 0.084 mmol), sodium ascorbate (0.05 eq., 0.00042 g, 0.0021 mmol), K_2CO_3 (2 eq., 0.012 g, 0.084 mmol), CuI (0.1 eq., 0.0008 g, 0.0042 mmol), (1S,2S)-N1,N2-dimethylcyclohexane-1,2-diamine (**L_{14}**) (0.15 eq., 0.0009 g, 0.0063 mmol), followed by the addition of MePh (0.1 mL). The reaction mixture was then capped properly, evacuated and backfilled with argon (this process was repeated a total of three times) and then placed in a preheated oil bath at 110 °C for 5h. The reaction mixture was concentrated under vacuum, and the progress of the reaction was evaluated by LC/MS.

5.2.44. Synthesis of 1-benzyl-5-(methoxymethoxy)-1H-1,2,4-triazol-3-amine (180)

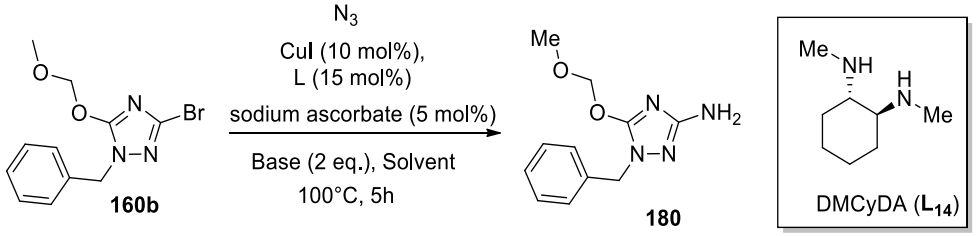

A microwave vial (oven-dried and under nitrogen) containing a Teflon stirrer bar was charged with 1-benzyl-3-bromo-5-(methoxymethoxy)-1H-1,2,4-triazole (**160b**) (1 eq., 0.013 g,

0.042 mmol), azide (3 eq., 0.0053 g, 0.13 mmol), sodium ascorbate (0.05 eq., 0.00042 g, 0.0021 mmol), CuI (0.1 eq., 0.0008 g, 0.0042 mmol), (1S,2S)-N1,N2-dimethylcyclohexane-1,2-diamine (**L_{14}**) (0.15 eq., 0.0009 g, 0.0063 mmol), followed by the addition of EtOH (0.059 mL) and H_2O (0.025 mL). The reaction mixture was then capped properly, evacuated and backfilled with argon (this process was repeated a total of three times) and then placed in a preheated oil bath at 110 °C for 5h. The reaction mixture was concentrated under vacuum, and the progress of the reaction was evaluated by LC/MS.

5.2.45. Synthesis of 1-benzyl-5-(benzyloxy)-1H-1,2,4-triazol-3-amine (181)

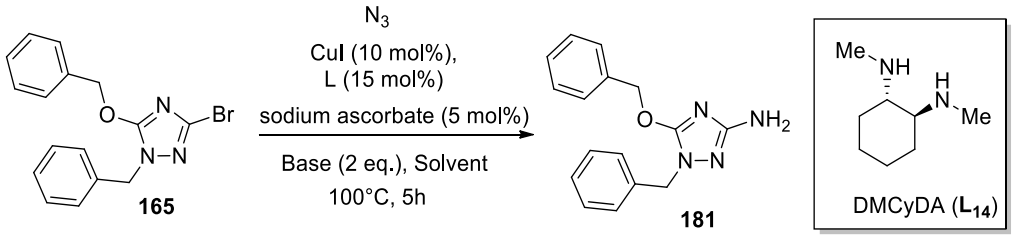

A microwave vial (oven-dried and under nitrogen) containing a Teflon stirrer bar was charged with 1-benzyl-3-bromo-5-(methoxymethoxy)-1H-1,2,4-triazole (**165**) (1 eq., 0.030 g, 0.087 mmol), azide (3 eq., 0.011 g, 0.26 mmol), sodium ascorbate (0.05 eq., 0.00086 g, 0.0044 mmol), CuI (0.1 eq., 0.0016 g, 0.0087 mmol), (1S,2S)-N1,N2-dimethylcyclohexane-1,2-diamine (**L_{14}**) (0.15 eq., 0.0019 g, 0.013 mmol), followed by the addition of EtOH (0.122 mL) and H_2O (0.052 mL). The reaction mixture was then capped properly, evacuated and backfilled with argon (this process was repeated a total of three times) and then placed in a preheated oil bath at 110 °C for 5h. The reaction mixture was concentrated under vacuum, and the progress of the reaction was evaluated by LC/MS.

5.2.46. Synthesis of 3-bromo-1-(p-tolyl)-1H-1,2,4-triazole-5-carbonitrile (192)

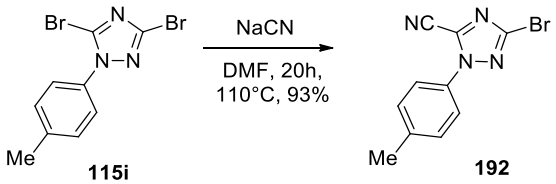

A microwave vial containing a Teflon stirrer bar was charged with 3,5-dibromo-1-(4-methylphenyl)-1H-1,2,4-triazole (**115i**) (1 eq., 0.025 g, 0.079 mmol) and NaCN (1 eq., 0.004

g, 0.079 mmol) followed by the addition of dry DMF (1 mL). The reaction mixture was then capped properly and placed in a preheated oil bath at 110 °C for 20h. The reaction mixture was monitored by HPLC analysis. The reaction mixture was kept under stirring at 110°C for 20h. After cooling to room temperature, 10 ml of H_2O was added and extracted with EtOAc (3 x 10 mL). The organic layers were collected and washed with H_2O (2 x 10mL) and brine (10 mL). The organic phase was dried with Na_2SO_4 and concentrated under reduced pressure to provide the desired compound (**192**) as a white solid (0.019 g, 0.073 mmol, 93%). ^{1}H NMR (400 MHz, $CDCl_3$): δ 2.46 (s, 3H), 7.37-7.39 (d, *J* = 8.3 Hz, 2H), 7.56-7.58 (d, *J* = 8.5 Hz, 2H). ^{13}C NMR (101 MHz, $CDCl_3$): δ 21.3, 108.1, 122.6, 122.7, 130.6, 132.8, 141.2, 141.5.

5.2.47. Methanolisys of 3-bromo-1-(p-tolyl)-1H-1,2,4-triazole-5-carbonitrile

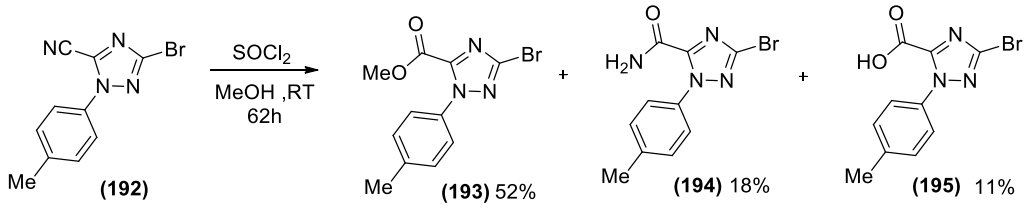

A microwave vial containing a Teflon stirrer bar was charged with 3-bromo-1-(4-methylphenyl)-1H-1,2,4-triazole-5-carbonitrile (**192**) (1 eq., 0.019 g, 0.073 mmol), and MeOH (0.32 mL) followed by the addition of Cs_2CO_3 (1.88 eq., 0.045 g, 0.14 mmol). The reaction mixture was then capped properly and maintained under stirring at room temperature for 62 h. After stirring at r.t. for 62 h, the crude was concentrated and aqueous acetic acid was added until pH ~ 4. The aqueous phase was extracted with DCM (3 x 5 mL). The organic layers were collected, dried with Na_2SO_4 and concentrated. The crude was purified by chromatography on silica gel using gradient elution *n*-heptane/EtOAc (80/20 to 0/100) to give **193** (0.011 g, 0.038 mmol, 52%), **194** (0.0037 g, 0.013 mmol, 18%) and **195** (0.0022 g, 0.0078 mmol, 11%).

5.2.46.1. methyl 3-bromo-1-(p-tolyl)-1H-1,2,4-triazole-5-carboxylate (193)

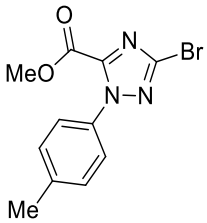

^{1}H NMR (400 MHz, $CDCl_3$): δ 2.38 (s, 3H), 4.19 (s, 3H), 7.23-7.25 (d, *J* = 8.2 Hz, 2H), 7.5-7.53 (d, *J* = 8.5 Hz, 2H).

5.2.46.2. 3-bromo-1-(p-tolyl)-1H-1,2,4-triazole-5-carboxamide (194)

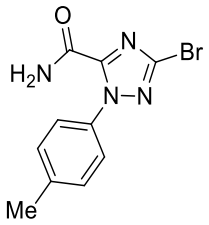

^{1}H NMR (400 MHz, $CDCl_3$): δ 2.42 (s, 3H), 5.67 (bs, 1H), 7.10 (bs, 1H), 7.27-7.29 (d, *J* = 8.5 Hz, 2H), 7.35-7.37 (d, *J* = 8.5 Hz, 2H).

5.2.46.3. 3-bromo-1-(p-tolyl)-1H-1,2,4-triazole-5-carboxylic acid (195)

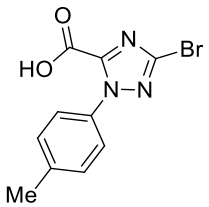

^{1}H NMR (400 MHz, $CDCl_3$): δ 2.37 (s, 3H), 7.22-7.24 (d, *J* = 8.4 Hz, 2H), 7.72-7.74 (d, *J* = 8.5 Hz, 2H).

6. BIBLIOGRAPHY

(1) Portella, D.; Caruso, L.; Nadur, N.; Moreira, T.; Lacerda, R.; Kummerle, A. Recent Advances in Microwave-Assisted Synthesis and Functionalization of 1,2,3- and 1,2,4-Triazoles. *Curr. Org. Chem.* **2021**, *25*. https://doi.org/10.2174/1385272825666211011111408.

(2) Hudson, J. From Alchemy to Chemistry. In *The History of Chemistry*; Hudson, J., Ed.; Springer US: Boston, MA, 1992; pp 35–46. https://doi.org/10.1007/978-1-4684-6441-2_3.

(3) Joule, J. A. *Heterocyclic Chemistry, 3rd Edition*, 3rd ed.; CRC Press: London, 2020. https://doi.org/10.1201/9781003072850.

(4) Balaban, A. T.; Oniciu, D. C.; Katritzky, A. R. Aromaticity as a Cornerstone of Heterocyclic Chemistry. *Chem. Rev.* **2004**, *104* (5), 2777–2812. https://doi.org/10.1021/cr0306790.

(5) Bean, G. P. Application of Natural Bond Orbital Analysis and Natural Resonance Theory to Delocalization and Aromaticity in Five-Membered Heteroaromatic Compounds. *J. Org. Chem.* **1998**, *63* (8), 2497–2506. https://doi.org/10.1021/jo971725x.

(6) Katritzky, A. R.; Ramsden, C. A.; Joule, J. A.; Zhdankin, V. V. *Handbook of Heterocyclic Chemistry*; Elsevier, 2010.

(7) Song, M.-X.; Deng, X.-Q. Recent Developments on Triazole Nucleus in Anticonvulsant Compounds: A Review. *J. Enzyme Inhib. Med. Chem.* **2018**, *33* (1), 453–478. https://doi.org/10.1080/14756366.2017.1423068.

(8) Chen, C.; Dagnino, R.; Huang, C. Q.; McCarthy, J. R.; Grigoriadis, D. E. 1-Alkyl-3-Amino-5-Aryl-1*H*-[1,2,4]Triazoles: Novel Synthesis via Cyclization of *N*-Acyl-*S*-Methylisothioureas with Alkylhydrazines and Their Potent Corticotropin-Releasing Factor-1 (CRF1) Receptor Antagonist Activities. *Bioorg. Med. Chem. Lett.* **2001**, *11* (24), 3165–3168. https://doi.org/10.1016/S0960-894X(01)00657-6.

(9) Boeglin, D.; Cantel, S.; Heitz, A.; Martinez, J.; Fehrentz, J.-A. Solution and Solid-Supported Synthesis of 3,4,5-Trisubstituted 1,2,4-Triazole-Based Peptidomimetics. *Org. Lett.* **2003**, *5* (23), 4465–4468. https://doi.org/10.1021/ol035778e.

(10) Morais, P. A. B.; Francisco, C. S.; Paula, H. de; Ribeiro, R.; Eloy, M. A.; Javarini, C. L.; Neto, Á. C.; Júnior, V. L. Semisynthetic Triazoles as an Approach in the Discovery of Novel

Lead Compounds. *Curr. Org. Chem.* *25* (10), 1097–1179. https://doi.org/10.2174/1385272825666210126100227.

(11) Palaska, E.; Sahin, G.; Kelicen, P.; Durlu, N. T.; Altinok, G. Synthesis and Anti-Inflammatory Activity of 1-Acylthiosemicarbazides, 1,3,4-Oxadiazoles, 1,3,4-Thiadiazoles and 1,2,4-Triazole-3-Thiones. *Farm. Soc. Chim. Ital. 1989* **2002**, *57* (2), 101–107. https://doi.org/10.1016/s0014-827x(01)01176-4.

(12) Upmanyu, N.; Gupta, J. K.; Shah, K.; Mishra, P. Anti-Inflammatory and Antinociceptive Evaluation of Newly Synthesized 4-(Substituted Ethanoyl) Amino-3-Mercapto-5-(4-Methoxy) Phenyl-1,2,4-Triazoles. *J. Pharm. Bioallied Sci.* **2011**, *3* (2), 259–265. https://doi.org/10.4103/0975-7406.80783.

(13) Amir, Mohd.; Kumar, S. Anti-inflammatory and Gastro Sparing Activity of Some New Indomethacin Derivatives. *Arch. Pharm. (Weinheim)* **2005**, *338* (1), 24–31. https://doi.org/10.1002/ardp.200400891.

(14) Demirbas, N.; Karaoglu, S. A.; Demirbas, A.; Sancak, K. Synthesis and Antimicrobial Activities of Some New 1-(5-Phenylamino-[1,3,4]Thiadiazol-2-Yl)Methyl-5-Oxo-[1,2,4]Triazole and 1-(4-Phenyl-5-Thioxo-[1,2,4]Triazol-3-Yl)Methyl-5-Oxo- [1,2,4]Triazole Derivatives. *Eur. J. Med. Chem.* **2004**, *39* (9), 793–804. https://doi.org/10.1016/j.ejmech.2004.06.007.

(15) Atia, A. J. K. Synthesis and Antibacterial Activities of New Metronidazole and Imidazole Derivatives. *Molecules* **2009**, *14* (7), 2431–2446. https://doi.org/10.3390/molecules14072431.

(16) Sahoo, P. K.; Sharma, R.; Pattanayak, P. Synthesis and Evaluation of 4-Amino-5-Phenyl-4H-[1,2,4]-Triazole-3-Thiol Derivatives as Antimicrobial Agents. *Med. Chem. Res.* **2010**, *19* (2), 127–135. https://doi.org/10.1007/s00044-009-9178-8.

(17) Sumangala, V.; Poojary, B.; Chidananda, N.; Arulmoli, T.; Shenoy, S. Synthesis and Biological Evaluation of Some Schiff Bases of 4-Amino-5-(4-Methylsulfonyl)Benzyl-2,4-Dihydro-3H-[1,2,4]-Triazole-3-Thione. *Med. Chem. Res.* **2013**, *22* (6), 2921–2928. https://doi.org/10.1007/s00044-012-0294-5.

(18) Shalini, K.; Kumar, N.; Drabu, S.; Sharma, P. K. Advances in Synthetic Approach to and Antifungal Activity of Triazoles. *Beilstein J. Org. Chem.* **2011**, *7*, 668–677. https://doi.org/10.3762/bjoc.7.79.

(19) Kocyigit-Kaymakcioglu, B.; Celen, A. O.; Tabanca, N.; Ali, A.; Khan, S. I.; Khan, I. A.; Wedge, D. E. Synthesis and Biological Activity of Substituted Urea and Thiourea Derivatives Containing 1,2,4-Triazole Moieties. *Molecules* **2013**, *18* (3), 3562–3576. https://doi.org/10.3390/molecules18033562.

(20) Küçükgüzel, İ.; Tatar, E.; Küçükgüzel, Ş. G.; Rollas, S.; De Clercq, E. Synthesis of Some Novel Thiourea Derivatives Obtained from 5-[(4-Aminophenoxy)Methyl]-4-Alkyl/Aryl-2,4-Dihydro-3H-1,2,4-Triazole-3-Thiones and Evaluation as Antiviral/Anti-HIV and Anti-Tuberculosis Agents. *Eur. J. Med. Chem.* **2008**, *43* (2), 381–392. https://doi.org/10.1016/j.ejmech.2007.04.010.

(21) Li, Y.-H.; Zhang, B.; Yang, H.-K.; Li, Q.; Diao, P.-C.; You, W.-W.; Zhao, P.-L. Design, Synthesis, and Biological Evaluation of Novel Alkylsulfanyl-1,2,4-Triazoles as Cis-Restricted Combretastatin A-4 Analogues. *Eur. J. Med. Chem.* **2017**, *125*, 1098–1106. https://doi.org/10.1016/j.ejmech.2016.10.051.

(22) Aswathanarayanappa, C.; Bheemappa, E.; Bodke, Y. D.; Krishnegowda, P. S.; Venkata, S. P.; Ningegowda, R. Synthesis and Evaluation of Antioxidant Properties of Novel 1,2,4-Triazole-Based Schiff Base Heterocycles. *Arch. Pharm. (Weinheim)* **2013**, *346* (12), 922–930. https://doi.org/10.1002/ardp.201300202.

(23) Khan, I.; Ali, S.; Hameed, S.; Rama, N. H.; Hussain, M. T.; Wadood, A.; Uddin, R.; Ul-Haq, Z.; Khan, A.; Ali, S.; Choudhary, M. I. Synthesis, Antioxidant Activities and Urease Inhibition of Some New 1,2,4-Triazole and 1,3,4-Thiadiazole Derivatives. *Eur. J. Med. Chem.* **2010**, *45* (11), 5200–5207. https://doi.org/10.1016/j.ejmech.2010.08.034.

(24) Karayel, A.; Özbey, S.; Ayhan-Kılcıgil, G.; Kuş, C. Crystal Structures and Intermolecular Interactions of Two Novel Antioxidant Triazolyl-Benzimidazole Compounds. *Crystallogr. Rep.* **2015**, *60* (7), 1084–1088. https://doi.org/10.1134/S1063774515070111.

(25) Nandikolla, A.; Srinivasarao, S.; Kumar, B. K.; Murugesan, S.; Aggarwal, H.; Major, L. L.; Smith, T. K.; Sekhar, K. V. G. C. Synthesis, Study of Antileishmanial and Antitrypanosomal Activity of Imidazo Pyridine Fused Triazole Analogues. *RSC Adv.* **2020**, *10* (63), 38328–38343. https://doi.org/10.1039/D0RA07881F.

(26) Siddiqui, N.; Ahsan, W. Triazole Incorporated Thiazoles as a New Class of Anticonvulsants: Design, Synthesis and in Vivo Screening. *Eur. J. Med. Chem.* **2010**, *45* (4), 1536–1543. https://doi.org/10.1016/j.ejmech.2009.12.062.

(27) Khan, I.; Tantray, M. A.; Hamid, H.; Alam, M. S.; Kalam, A.; Hussain, F.; Dhulap, A. Synthesis of Pyrimidin-4-One-1,2,3-Triazole Conjugates as Glycogen Synthase Kinase-3β Inhibitors with Anti-Depressant Activity. *Bioorganic Chem.* **2016**, *68*, 41–55. https://doi.org/10.1016/j.bioorg.2016.07.007.

(28) Chelamalla, R.; Akena, V.; Manda, S. Synthesis of N′-Arylidene-2-(5-Aryl-1H-1, 2, 4-Triazol-3-Ylthio) Acetohydrazides as Antidepressants. *Med. Chem. Res.* **2017**, *26* (7), 1359–1366. https://doi.org/10.1007/s00044-017-1854-5.

(29) Reed, C. W.; Yohn, S. E.; Washecheck, J. P.; Roenfanz, H. F.; Quitalig, M. C.; Luscombe, V. B.; Jenkins, M. T.; Rodriguez, A. L.; Engers, D. W.; Blobaum, A. L.; Conn, P. J.; Niswender, C. M.; Lindsley, C. W. Discovery of an Orally Bioavailable and Central Nervous System (CNS) Penetrant mGlu7 Negative Allosteric Modulator (NAM) in Vivo Tool Compound: N-(2-(1H-1,2,4-Triazol-1-Yl)-5-(Trifluoromethoxy)Phenyl)-4-(Cyclopropylmethoxy)-3-Methoxybenzamide (VU6012962). *J. Med. Chem.* **2019**, *62* (3), 1690–1695. https://doi.org/10.1021/acs.jmedchem.8b01810.

(30) Reed, C. W.; McGowan, K. M.; Spearing, P. K.; Stansley, B. J.; Roenfanz, H. F.; Engers, D. W.; Rodriguez, A. L.; Engelberg, E. M.; Luscombe, V. B.; Loch, M. T.; Remke, D. H.; Rook, J. M.; Blobaum, A. L.; Conn, P. J.; Niswender, C. M.; Lindsley, C. W. VU6010608, a Novel mGlu7 NAM from a Series of N-(2-(1H-1,2,4-Triazol-1-Yl)-5-(Trifluoromethoxy)Phenyl)Benzamides. *ACS Med. Chem. Lett.* **2017**, *8* (12), 1326–1330. https://doi.org/10.1021/acsmedchemlett.7b00429.

(31) Silva, R. A. da; Quintela, E. D.; Mascarin, G. M.; Barrigossi, J. A. F.; Lião, L. M. Compatibility of Conventional Agrochemicals Used in Rice Crops with the Entomopathogenic Fungus Metarhizium Anisopliae. *Sci. Agric.* **2013**, *70*, 152–160. https://doi.org/10.1590/S0103-90162013000300003.

(32) Borgati, T. F.; Alves, R. B.; Teixeira, R. R.; Freitas, R. P. de; Perdigão, T. G.; Silva, S. F. da; Santos, A. A. dos; Bastidas, A. de J. O. Synthesis and Phytotoxic Activity of 1,2,3-Triazole Derivatives. *J. Braz. Chem. Soc.* **2013**, *24*, 953–961. https://doi.org/10.5935/0103-5053.20130121.

(33) Kishorekumar, A.; Jaleel, C. A.; Manivannan, P.; Sankar, B.; Sridharan, R.; Panneerselvam, R. Comparative Effects of Different Triazole Compounds on Growth, Photosynthetic Pigments and Carbohydrate Metabolism of *Solenostemon Rotundifolius*.

Colloids Surf. B Biointerfaces **2007**, *60* (2), 207–212. https://doi.org/10.1016/j.colsurfb.2007.06.008.

(34) Yen, Y.-S.; Hsu, J.-L.; Ni, J.-S.; Lin, J. T. Influence of Various Dithienoheterocycles as Conjugated Linker in Naphtho[2,3-*d*] [1,2,3]Triazole-Based Organic Dyes for Dye-Sensitized Solar Cells. *Dyes Pigments* **2021**, *188*, 109220. https://doi.org/10.1016/j.dyepig.2021.109220.

(35) Mostafa, M. A.; Ashmawy, A. M.; Reheim, M. A. M. A.; Bedair, M. A.; Abuelela, A. M. Molecular Structure Aspects and Molecular Reactivity of Some Triazole Derivatives for Corrosion Inhibition of Aluminum in 1 M HCl Solution. *J. Mol. Struct.* **2021**, *1236*, 130292. https://doi.org/10.1016/j.molstruc.2021.130292.

(36) Hrimla, M.; Bahsis, L.; Boutouil, A.; Laamari, M. R.; Julve, M.; Stiriba, S.-E. Corrosion Inhibition Performance of a Structurally Well-Defined 1,2,3-Triazole Derivative on Mild Steel-Hydrochloric Acid Interface. *J. Mol. Struct.* **2021**, *1231*, 129895. https://doi.org/10.1016/j.molstruc.2021.129895.

(37) Finšgar, M. The influence of the amino group in 3-amino-1,2,4-triazole corrosion inhibitor on the interface properties for brass studied by ToF-SIMS. *Rapid Commun. Mass Spectrom.* **2021**, *35* (7), e9056. https://doi.org/10.1002/rcm.9056.

(38) Katritzky, A. R.; Song, Y.; Sakhuja, R.; Gyanda, R.; Meher, N. K.; Wang, L.; Duran, R. S.; Ciaramitaro, D. A.; Bedford, C. D. Synthesis of Boltorn 1,2,3-Triazole Dendrimers by Click Chemistry. *J. Polym. Sci. Part Polym. Chem.* **2009**, *47* (15), 3748–3756. https://doi.org/10.1002/pola.23427.

(39) Johnson, J. A.; Finn, M. G.; Koberstein, J. T.; Turro, N. J. Construction of Linear Polymers, Dendrimers, Networks, and Other Polymeric Architectures by Copper-Catalyzed Azide-Alkyne Cycloaddition "Click" Chemistry. *Macromol. Rapid Commun.* **2008**, *29* (12–13), 1052–1072. https://doi.org/10.1002/marc.200800208.

(40) Arseneault, M.; Wafer, C.; Morin, J.-F. Recent Advances in Click Chemistry Applied to Dendrimer Synthesis. *Molecules* **2015**, *20* (5), 9263–9294. https://doi.org/10.3390/molecules20059263.

(41) Tsuei, M.; Shivrayan, M.; Kim, Y.-K.; Thayumanavan, S.; Abbott, N. L. Optical "Blinking" Triggered by Collisions of Single Supramolecular Assemblies of Amphiphilic Molecules with Interfaces of Liquid Crystals. *J. Am. Chem. Soc.* **2020**, *142* (13), 6139–6148. https://doi.org/10.1021/jacs.9b13360.

(42) Al-shargabi, A.; Yeap, G.-Y.; Mahmood, W. A. K.; Han, C.-C.; Lin, H.-C.; Ito, M. M. Liquid Crystal Dimers Containing Cholesteryl and Triazole-Containing Mesogenic Units. *Liq. Cryst.* **2020**, *47* (2), 219–230. https://doi.org/10.1080/02678292.2019.1641637.

(43) Srividhya, D.; Manjunathan, S.; Thirumaran, S.; Saravanan, C.; Senthil, S. Synthesis and Characterization of [1,2,3]-Triazole Containing Liquid Crystals through Click Reaction. *J. Mol. Struct.* **2009**, *927* (1), 7–13. https://doi.org/10.1016/j.molstruc.2009.01.035.

(44) Xiao, D.; Do, L. H. Triazolecarboxamidate Donors as Supporting Ligands for Nickel Olefin Polymerization Catalysts. *Organometallics* **2018**, *37* (2), 254–260. https://doi.org/10.1021/acs.organomet.7b00807.

(45) McCarney, E. P.; Hawes, C. S.; Blasco, S.; Gunnlaugsson, T. Synthesis and Structural Studies of 1,4-Di(2-Pyridyl)-1,2,3-Triazole Dpt and Its Transition Metal Complexes; a Versatile and Subtly Unsymmetric Ligand. *Dalton Trans.* **2016**, *45* (25), 10209–10221. https://doi.org/10.1039/C6DT01416J.

(46) Feng, L.-S.; Zheng, M.-J.; Zhao, F.; Liu, D. 1,2,3-Triazole Hybrids with Anti-HIV-1 Activity. *Arch. Pharm. (Weinheim)* **2021**, *354* (1), 2000163. https://doi.org/10.1002/ardp.202000163.

(47) Brai, A.; Riva, V.; Saladini, F.; Zamperini, C.; Trivisani, C. I.; Garbelli, A.; Pennisi, C.; Giannini, A.; Boccuto, A.; Bugli, F.; Martini, M.; Sanguinetti, M.; Zazzi, M.; Dreassi, E.; Botta, M.; Maga, G. DDX3X Inhibitors, an Effective Way to Overcome HIV-1 Resistance Targeting Host Proteins. *Eur. J. Med. Chem.* **2020**, *200*, 112319. https://doi.org/10.1016/j.ejmech.2020.112319.

(48) Sun, L.; Huang, T.; Dick, A.; Meuser, M. E.; Zalloum, W. A.; Chen, C.-H.; Ding, X.; Gao, P.; Cocklin, S.; Lee, K.-H.; Zhan, P.; Liu, X. Design, Synthesis and Structure-Activity Relationships of 4-Phenyl-1*H*-1,2,3-Triazole Phenylalanine Derivatives as Novel HIV-1 Capsid Inhibitors with Promising Antiviral Activities. *Eur. J. Med. Chem.* **2020**, *190*, 112085. https://doi.org/10.1016/j.ejmech.2020.112085.

(49) Li, N.; Chen, C.; zhu, H.; Shi, Z.; Sun, J.; Chen, L. Discovery of Novel Celastrol-Triazole Derivatives with Hsp90-Cdc37 Disruption to Induce Tumor Cell Apoptosis. *Bioorganic Chem.* **2021**, *111*, 104867. https://doi.org/10.1016/j.bioorg.2021.104867.

(50) Zhang, X.-H.; Kang, H.-Q.; Tao, Y.-Y.; Li, Y.-H.; Zhao, J.-R.; Ya-Gao; Ma, L.-Y.; Liu, H.-M. Identification of Novel 1,3-Diaryl-1,2,4-Triazole-Capped Histone Deacetylase 6

Inhibitors with Potential Anti-Gastric Cancer Activity. *Eur. J. Med. Chem.* **2021**, *218*, 113392. https://doi.org/10.1016/j.ejmech.2021.113392.

(51) Pertino, M. W.; F. de la Torre, A.; Schmeda-Hirschmann, G.; Vega, C.; Rolón, M.; Coronel, C.; Rojas de Arias, A.; Leal López, K.; Carranza-Rosales, P.; Viveros Valdez, E. Synthesis, Trypanocidal and Anti-Leishmania Activity of New Triazole-Lapachol and nor-Lapachol Hybrids. *Bioorganic Chem.* **2020**, *103*, 104122. https://doi.org/10.1016/j.bioorg.2020.104122.

(52) Sahu, A.; Agrawal, R. K.; Pandey, R. Synthesis and Systemic Toxicity Assessment of Quinine-Triazole Scaffold with Antiprotozoal Potency. *Bioorganic Chem.* **2019**, *88*, 102939. https://doi.org/10.1016/j.bioorg.2019.102939.

(53) Phatak, P. S.; Bakale, R. D.; Kulkarni, R. S.; Dhumal, S. T.; Dixit, P. P.; Krishna, V. S.; Sriram, D.; Khedkar, V. M.; Haval, K. P. Design and Synthesis of New Indanol-1,2,3-Triazole Derivatives as Potent Antitubercular and Antimicrobial Agents. *Bioorg. Med. Chem. Lett.* **2020**, *30* (22), 127579. https://doi.org/10.1016/j.bmcl.2020.127579.

(54) Gondru, R.; Kanugala, S.; Raj, S.; Ganesh Kumar, C.; Pasupuleti, M.; Banothu, J.; Bavantula, R. 1,2,3-Triazole-Thiazole Hybrids: Synthesis, *in Vitro* Antimicrobial Activity and Antibiofilm Studies. *Bioorg. Med. Chem. Lett.* **2021**, *33*, 127746. https://doi.org/10.1016/j.bmcl.2020.127746.

(55) Blokhina, S. V.; Sharapova, A. V.; Ol'khovich, M. V.; Doroshenko, I. A.; Levshin, I. B.; Perlovich, G. L. Synthesis and Antifungal Activity of New Hybrids Thiazolo[4,5-*d*]Pyrimidines with (1*H*-1,2,4)Triazole. *Bioorg. Med. Chem. Lett.* **2021**, *40*, 127944. https://doi.org/10.1016/j.bmcl.2021.127944.

(56) Zoidis, G.; Kritsi, E.; Lecinska, P.; Ivanov, M.; Zoumpoulakis, P.; Sokovic, M.; Catto, M. The Triazole Ring as a Privileged Scaffold for Putative Antifungals: Synthesis and Evaluation of a Series of New Analogues. *ChemMedChem* **2021**, *16* (1), 134–144. https://doi.org/10.1002/cmdc.202000312.

(57) Jahani, R.; Reza Abtahi, S.; Nematpour, M.; Fasihi Dastjerdi, H.; Chamanara, M.; Hami, Z.; Paknejad, B. Design, Synthesis, and Pharmacological Evaluation of Novel 1,2,4-Triazol-3-Amine Derivatives as Potential Agonists of GABAA Subtype Receptors with Anticonvulsant and Hypnotic Effects. *Bioorganic Chem.* **2020**, *104*, 104212. https://doi.org/10.1016/j.bioorg.2020.104212.

(58) Ouach, A.; Pin, F.; Bertrand, E.; Vercouillie, J.; Gulhan, Z.; Mothes, C.; Deloye, J.-B.; Guilloteau, D.; Suzenet, F.; Chalon, S.; Routier, S. Design of A7 Nicotinic Acetylcholine Receptor Ligands Using the (Het)Aryl-1,2,3-Triazole Core: Synthesis, *in Vitro* Evaluation and SAR Studies. *Eur. J. Med. Chem.* **2016**, *107*, 153–164. https://doi.org/10.1016/j.ejmech.2015.11.001.

(59) *Scopus preview - Scopus - Welcome to Scopus*. https://www.scopus.com/home.uri (accessed 2021-06-20).

(60) Eicher, T.; Hauptmann, S.; Speicher, A. *The Chemistry of Heterocycles: Structures, Reactions, Synthesis, and Applications*; John Wiley & Sons, 2013.

(61) Dai, J.; Tian, S.; Yang, X.; Liu, Z. Synthesis Methods of 1,2,3-/1,2,4-Triazoles: A Review. *Front. Chem.* **2022**, *10*. https://doi.org/10.3389/fchem.2022.891484.

(62) Castanedo, G. M.; Seng, P. S.; Blaquiere, N.; Trapp, S.; Staben, S. T. Rapid Synthesis of 1,3,5-Substituted 1,2,4-Triazoles from Carboxylic Acids, Amidines, and Hydrazines. *J. Org. Chem.* **2011**, *76* (4), 1177–1179. https://doi.org/10.1021/jo1023393.

(63) Huang, H.; Guo, W.; Wu, W.; Li, C.-J.; Jiang, H. Copper-Catalyzed Oxidative C(Sp3)–H Functionalization for Facile Synthesis of 1,2,4-Triazoles and 1,3,5-Triazines from Amidines. *Org. Lett.* **2015**, *17* (12), 2894–2897. https://doi.org/10.1021/acs.orglett.5b00995.

(64) Xia, J.; Huang, X.; Cai, M. Heterogeneous Copper(I)-Catalyzed Cascade Addition–Oxidative Cyclization of Nitriles with 2-Aminopyridines or Amidines: Efficient and Practical Synthesis of 1,2,4-Triazoles. *Synthesis* **2019**, *51* (9), 2014–2022. https://doi.org/10.1055/s-0037-1611712.

(65) Guirado, A.; López-Caracena, L.; López-Sánchez, J. I.; Sandoval, J.; Vera, M.; Bautista, D.; Gálvez, J. A New, High-Yield Synthesis of 3-Aryl-1,2,4-Triazoles. *Tetrahedron* **2016**, *72* (49), 8055–8060. https://doi.org/10.1016/j.tet.2016.10.045.

(66) Azzouni, S.; Abdelli, A.; Gaucher, A.; Arfaoui, Y.; Efrit, M. L.; Prim, D. From Imidates to Vinyl-1,2,4-Triazoles: Synthesis, Mechanistic Aspects and First Issues of Their Reactivity. *Tetrahedron* **2018**, *74* (49), 6972–6978. https://doi.org/10.1016/j.tet.2018.10.050.

(67) Siddaiah, V.; Basha, G. M.; Srinuvasarao, R.; Yadav, S. K. HClO4-SiO2: An Efficient Reusable Catalyst for the Synthesis of 3,4,5-Trisubstituted 1,2,4-Triazoles Under Solvent-Free Conditions. *Catal. Lett.* **2011**, *141* (10), 1511–1520. https://doi.org/10.1007/s10562-011-0665-4.

(68) Nakka, M.; Tadikonda, R.; Rayavarapu, S.; Sarakula, P.; Vidavalur, S. A Simple and Efficient Synthesis of 3,4,5-Trisubstituted/N-Fused 1,2,4-Triazoles via Ceric Ammonium Nitrate Catalyzed Oxidative Cyclization of Amidrazones with Aldehydes Using Polyethylene Glycol as a Recyclable Reaction Medium. *Synthesis* **2015**, *47* (4), 517–525. https://doi.org/10.1055/s-0034-1378909.

(69) Chen, Z.; Fan, S.-Q.; Zheng, Y.; Ma, J.-A. Silver-Catalyzed Regioselective [3+2] Cycloaddition of Arene-Diazonium Salts with 2,2,2-Trifluorodiazoethane (CF3CHN2): A Facile Access to 2-Aryl-5-Trifluoromethyltetrazoles. *Chem. Commun.* **2015**, *51* (92), 16545–16548. https://doi.org/10.1039/C5CC07324C.

(70) *One-Pot Reactions for Synthesis of 2,5-Substituted Tetrazoles from Aryldiazonium Salts and Amidines | Organic Letters*. https://pubs.acs.org/doi/10.1021/acs.orglett.5b03068 (accessed 2024-05-06).

(71) Matsumoto, K.; Suzuki, M.; Tomie, M.; Yoneda, N.; Miyoshi, M. A New Synthesis of 1-Aryl-1H-1, 2, 4-Triazole-3-Carboxylic Acid Esters. *Synthesis* **1975**, *1975* (09), 609–610. https://doi.org/10.1055/s-1975-23855.

(72) Zhang, F.-G.; Chen, Z.; Cheung, C. W.; Ma, J.-A. Aryl Diazonium Salt-Triggered Cyclization and Cycloaddition Reactions: Past, Present, and Future. *Chin. J. Chem.* **2020**, *38* (10), 1132–1152. https://doi.org/10.1002/cjoc.202000270.

(73) Liu, J.-Q.; Shen, X.; Wang, Y.; Wang, X.-S.; Bi, X. [3 + 2] Cycloaddition of Isocyanides with Aryl Diazonium Salts: Catalyst-Dependent Regioselective Synthesis of 1,3- and 1,5-Disubstituted 1,2,4-Triazoles. *Org. Lett.* **2018**, *20* (21), 6930–6933. https://doi.org/10.1021/acs.orglett.8b03069.

(74) Tian, Y.-T.; Zhang, F.-G.; Nie, J.; Cheung, C. W.; Ma, J.-A. Metal-Free Decarboxylative Annulation of 2-Aryl-2-Isocyano-Acetates with Aryldiazonium Salts: General Access to 1,3-Diaryl-1,2,4-Triazoles. *Adv. Synth. Catal.* **2021**, *363* (1), 227–233. https://doi.org/10.1002/adsc.202001016.

(75) Chen, Z.; Li, H.; Dong, W.; Miao, M.; Ren, H. I2-Catalyzed Oxidative Coupling Reactions of Hydrazones and Amines and the Application in the Synthesis of 1,3,5-Trisubstituted 1,2,4-Triazoles. *Org. Lett.* **2016**, *18* (6), 1334–1337. https://doi.org/10.1021/acs.orglett.6b00277.

(76) Mohan Guru, M.; De, S.; Dutta, S.; Koley, D.; Maji, B. B(C 6 F 5) 3 -Catalyzed Dehydrogenative Cyclization of N -Tosylhydrazones and Anilines via a Lewis Adduct: A Combined Experimental and Computational Investigation. *Chem. Sci.* **2019**, *10* (34), 7964–7974. https://doi.org/10.1039/C9SC02492A.

(77) Wu, G.; Wang, H.; Zhou, W.; Zeng, B.; Mo, W.; Zhu, K.; Liu, R.; Zhou, J.; Chen, C.; Chen, H. Synthesis and Structure–Activity Relationship Studies of MI-2 Analogues as MALT1 Inhibitors. *Bioorg. Med. Chem.* **2018**, *26* (12), 3321–3344. https://doi.org/10.1016/j.bmc.2018.04.059.

(78) Winterer, G.; Gallinat, J.; Brinkmeyer, J.; Musso, F.; Kornhuber, J.; Thuerauf, N.; Rujescu, D.; Favis, R.; Sun, Y.; Franc, M. A.; Ouwerkerk-Mahadevan, S.; Janssens, L.; Timmers, M.; Streffer, J. R. Allosteric Alpha-7 Nicotinic Receptor Modulation and P50 Sensory Gating in Schizophrenia: A Proof-of-Mechanism Study. *Neuropharmacology* **2013**, *64*, 197–204. https://doi.org/10.1016/j.neuropharm.2012.06.040.

(79) Nakajima, K.; April, M.; Brewer, J. T.; Daniels, T.; Forster, C. J.; Gilmore, T. A.; Jain, M.; Kanter, A.; Kwak, Y.; Li, J.; McQuire, L.; Serrano-Wu, M. H.; Streeper, R.; Szklennik, P.; Thompson, J.; Wang, B. Discovery of Diamide Compounds as Diacylglycerol Acyltransferase 1 (DGAT1) Inhibitors. *Bioorg. Med. Chem. Lett.* **2016**, *26* (4), 1245–1248. https://doi.org/10.1016/j.bmcl.2016.01.025.

(80) Fauchere, J.-L.; Ortuno, J.-C.; Duhault, J.; Boutin, J. A.; Levens, N. Aminotriazole Compounds, Process for Their Preparation and Pharmaceutical Compositions Containing Them. EP1044970A1, October 18, 2000.

(81) Bozó, E.; Szilágyi, G.; Janáky, J. 1,2,4-Triazoles, III: New 1,5-Diaryl-3-(Substituted Amino)-1H-1,2,4-Triazoles as Anti-Inflammatory Agents. *Arch. Pharm. (Weinheim)* **1989**, *322* (10), 583–587. https://doi.org/10.1002/ardp.19893221003.

(82) Shipps, G. W. J.; Sauvagnat, B.; Bracken, J.; Mcelroy, W. T.; Cox, C. D.; Ho, G.; Mcgaughey, G.; Deng, Y.; Zhu, L.; Dudkin, V.; Steele, T. G.; Steen, J. T. Substituted Amino-Triazolyl Pde10 Inhibitors. WO2012054366A2, April 26, 2012.

(83) Liu, X.; Liang, X.; LeCouter, J.; Ubhayakar, S.; Chen, J.; Cheng, J.; Lee, T.; Lubach, J.; Nonomiya, J.; Shahidi-Latham, S.; Quiason, C.; Solon, E.; Wright, M.; Hop, C. E. C. A.; Heffron, T. P. Characterization of Anti-Neovascularization Activity and Ocular Pharmacokinetics of PI3K/mTOR Inhibitor GNE-947. *Drug Metab. Dispos.* **2020**. https://doi.org/10.1124/dmd.119.089763.

(84) Li, X.; Zhang, Z.; Chen, Y.; Wan, H.; Sun, J.; Wang, B.; Feng, B.; Hu, B.; Shi, X.; Feng, J.; Zhang, L.; He, F.; Bai, C.; Zhang, L.; Tao, W. Discovery of SHR1653, a Highly Potent and Selective OTR Antagonist with Improved Blood–Brain Barrier Penetration. *ACS Med. Chem. Lett.* **2019**, *10* (6), 996–1001. https://doi.org/10.1021/acsmedchemlett.9b00186.

(85) Tee, E. H. L.; Karoli, T.; Ramu, S.; Huang, J. X.; Butler, M. S.; Cooper, M. A. Synthesis of Essramycin and Comparison of Its Antibacterial Activity. *J. Nat. Prod.* **2010**, *73* (11), 1940–1942. https://doi.org/10.1021/np100648q.

(86) Maddila, S.; Pagadala, R.; Jonnalagadda, S. 1,2,4-Triazoles: A Review of Synthetic Approaches and the Biological Activity. *Lett. Org. Chem.* **2013**, *10* (10), 693–714. https://doi.org/10.2174/15701786101010131126115448.

(87) Meng, J.; Kung, P.-P. Rapid, Microwave-Assisted Synthesis of N1-Substituted 3-Amino-1,2,4-Triazoles. *Tetrahedron Lett.* **2009**, *50* (15), 1667–1670. https://doi.org/10.1016/j.tetlet.2008.12.042.

(88) Makara, G. M.; Ma, Y.; Margarida, L. Solid-Phase Synthesis of 3-Alkylamino-1,2,4-Triazoles. *Org. Lett.* **2002**, *4* (10), 1751–1754. https://doi.org/10.1021/ol025821i.

(89) Bogolyubsky, A. V.; Savych, O.; Zhemera, A. V.; Pipko, S. E.; Grishchenko, A. V.; Konovets, A. I.; Doroshchuk, R. O.; Khomenko, D. N.; Brovarets, V. S.; Moroz, Y. S.; Vybornyi, M. Facile One-Pot Parallel Synthesis of 3-Amino-1,2,4-Triazoles. *ACS Comb. Sci.* **2018**, *20* (7), 461–466. https://doi.org/10.1021/acscombsci.8b00060.

(90) Katritzky, A. R.; Rogovoy, B. V.; Vvedensky, V. Y.; Kovalenko, K.; Steel, P. J.; Markov, V. I.; Forood, B. Synthesis of N,N-Disubstituted 3-Amino-1,2,4-Triazoles. *Synthesis* **2001**, *2001* (6), 897–903. https://doi.org/10.1055/s-2001-13400.

(91) Yu, Y.; Ostresh, J. M.; Houghten, R. A. Solid-Phase Synthesis of 3-Amino-1,2,4-Triazoles. *Tetrahedron Lett.* **2003**, *44* (42), 7841–7843. https://doi.org/10.1016/j.tetlet.2003.08.074.

(92) Shen, J.; Wong, B.; Gu, C.; Zhang, H. Negishi Approach to 1,5-Disubstituted 3-Amino-1H-1,2,4-Triazoles. *Org. Lett.* **2015**, *17* (19), 4678–4681. https://doi.org/10.1021/acs.orglett.5b02021.

(93) Santos, S. N.; Souza, G. A. de; Pereira, T. M.; Franco, D. P.; Cistia, C. de N. D.; Sant'Anna, C. M. R.; Lacerda, R. B.; Kümmerle, A. E. Regioselective Microwave Synthesis and Derivatization of 1,5-Diaryl-3-Amino-1,2,4-Triazoles and a Study of Their Cholinesterase

Inhibition Properties. *RSC Adv.* **2019**, *9* (35), 20356–20369. https://doi.org/10.1039/C9RA04105B.

(94) Kakwani, M. D.; Palsule Desai, N. H.; Lele, A. C.; Ray, M.; Rajan, M. G. R.; Degani, M. S. Synthesis and Preliminary Biological Evaluation of Novel *N*-(3-Aryl-1,2,4-Triazol-5-Yl) Cinnamamide Derivatives as Potential Antimycobacterial Agents: An Operational Topliss Tree Approach. *Bioorg. Med. Chem. Lett.* **2011**, *21* (21), 6523–6526. https://doi.org/10.1016/j.bmcl.2011.08.076.

(95) Chernyshev, V. M.; Chernysheva, A. V. Recyclization of 2-(2,5-Dioxopyrrolidin-1-Yl)-Guanidine under the Action of Aliphatic Amines. a Novel Method for the Synthesis of 3-(5-Amino-1h-1,2,4-Triazol-3-Yl)Propanoic Acid Amides. *Chem. Heterocycl. Compd.* **2010**, *46* (5), 627–628. https://doi.org/10.1007/s10593-010-0559-1.

(96) Chernyshev, V. M.; Chernysheva, A. V.; Taranushich, V. A. Optimization of the Synthesis of 5-Amino-1,2,4-Triazol-3-Ylacetic Acid and Bis(5-Amino-1,2,4-Triazol-3-Yl)Methane. *Russ. J. Appl. Chem.* **2009**, *82* (2), 276–281. https://doi.org/10.1134/S1070427209020219.

(97) Yin, P.; Ma, W.-B.; Chen, Y.; Huang, W.-C.; Deng, Y.; He, L. Highly Efficient Cyanoimidation of Aldehydes. *Org. Lett.* **2009**, *11* (23), 5482–5485. https://doi.org/10.1021/ol902207h.

(98) Zarguil, A.; Boukhris, S.; El Efrit, M. L.; Souizi, A.; Essassi, E. M. Easy Access to Triazoles, Triazolopyrimidines, Benzimidazoles and Imidazoles from Imidates. *Tetrahedron Lett.* **2008**, *49* (41), 5883–5886. https://doi.org/10.1016/j.tetlet.2008.07.134.

(99) Yen, W.-P.; Kung, F.-C.; Wong, F. F. 1,3-Dipolar Cycloaddition of Carbodiimides and Nitrilimines: Synthesis and Mechanistic Study of 5-Amino-1,2,4-Triazoles. *Eur. J. Org. Chem.* **2016**, *2016* (13), 2328–2335. https://doi.org/10.1002/ejoc.201600240.

(100) Wolkoff, P.; Nemeth, S. T.; Gibson, M. S. Reaction of Hydrazonyl Halides with Derivatives of Thiourea and Thiosemicarbazide; A New Source of C-Amino- and C-Hydrazino-1,2,4-Triazoles. *Can. J. Chem.* **1975**, *53* (21), 3211–3215. https://doi.org/10.1139/v75-458.

(101) Grytsai, O.; Valiashko, O.; Penco-Campillo, M.; Dufies, M.; Hagege, A.; Demange, L.; Martial, S.; Pagès, G.; Ronco, C.; Benhida, R. Synthesis and Biological Evaluation of 3-Amino-1,2,4-Triazole Derivatives as Potential Anticancer Compounds. *Bioorganic Chem.* **2020**, *104*, 104271. https://doi.org/10.1016/j.bioorg.2020.104271.

(102) Zhao, F.; Singh, T.; Xiao, Y.; Su, W.; Yang, D.; Jia, C.; Li, J.-Q.; Qin, Z. Divergent Synthesis of Substituted Amino-1,2,4-Triazole Derivatives. *Synthesis* **2021**, *53* (11), 1901–1910. https://doi.org/10.1055/a-1477-4630.

(103) Szommer, T.; Lukács, A.; Kovács, J.; Szabó, M. J.; Hoffmann, M. G.; Schmitt, M. H.; Gerencsér, J. Parallel Synthesis of 1,2,4-Triazole Derivatives Using Microwave and Continuous-Flow Techniques. *Mol. Divers.* **2012**, *16* (1), 81–90. https://doi.org/10.1007/s11030-012-9357-2.

(104) Velter, A. I.; Bischoff, F. P.; Berthelot, D.; De Cleyn, M.; Oehlrich, D.; Jaroskova, L.; Macdonald, G.; Minne, G.; Pieters, S.; Rombouts, F.; Van Brandt, S.; Van Roosbroeck, Y.; Surkyn, M.; Trabanco, A. A.; Tresadern, G.; Wu, T.; Borghys, H.; Mercken, M.; Masungi, C.; Gijsen, H. Anilinotriazoles as Potent Gamma Secretase Modulators. *Bioorg. Med. Chem. Lett.* **2014**, *24* (24), 5805–5813. https://doi.org/10.1016/j.bmcl.2014.10.024.

(105) Patel, B. D.; Bhadada, S. V.; Ghate, M. D. Design, Synthesis and Anti-Diabetic Activity of Triazolotriazine Derivatives as Dipeptidyl Peptidase-4 (DPP-4) Inhibitors. *Bioorganic Chem.* **2017**, *72*, 345–358. https://doi.org/10.1016/j.bioorg.2017.03.004.

(106) Glunz, P. W.; Wurtz, N.; Cheng, X. Heterocyclic Compounds as Inhibitors of Factor Viia. WO2006062972A2, June 15, 2006. https://patents.google.com/patent/WO2006062972A2/en?oq=2006062972 (accessed 2024-05-07).

(107) Brandt, S. F. A. V.; Cleyn, M. A. J. D.; Gijsen, H. J. M.; Berthelot, D. J.-C.; Surkyn, M. Novel Substituted Triazole Derivatives as Gamma Secretase Modulators. WO2011086099A1, July 21, 2011. https://patents.google.com/patent/WO2011086099A1/en?oq=2011086099 (accessed 2024-05-07).

(108) Tolstyakov, V. V. Synthesis of 1-Alkyl-5-Amino-1,2,4-Triazoles Based on Nucleophilic Substitution and Reduction Reactions. *Russ. J. Org. Chem.* **2018**, *54* (10), 1537–1547. https://doi.org/10.1134/S1070428018100160.

(109) JONES, C. D.; BUNYARD, P.; Pitt, G.; BYRNE, L.; Pesnot, T.; GUISOT, N. E. S. Heterocyclylamino-Substituted Triazoles as Modulators of Rho-Associated Protein Kinase. WO2019145729A1, August 1, 2019. https://patents.google.com/patent/WO2019145729A1/en (accessed 2024-05-06).

(110) Wille, S.; Hein, M.; Miethchen, R. First Cross-Coupling Reactions on Halogenated 1*H*-1,2,4-Triazole Nucleosides. *Tetrahedron* **2006**, *62* (14), 3301–3308. https://doi.org/10.1016/j.tet.2006.01.053.

(111) Zumbrunn, A. The First Versatile Synthesis of 1-Alkyl-3-Fluoro-1H-[1,2,4]Triazoles. *Synthesis* **1998**, *1998* (9), 1357–1361. https://doi.org/10.1055/s-1998-6080.

(112) Houpis, I. N.; Liu, R.; Wu, Y.; Yuan, Y.; Wang, Y.; Nettekoven, U. Regioselective Cross-Coupling Reactions of Boronic Acids with Dihalo Heterocycles. *J. Org. Chem.* **2010**, *75* (20), 6965–6968. https://doi.org/10.1021/jo101223z.

(113) Labanowski, J. K.; Andzelm, J. W. *Density Functional Methods in Chemistry*; Springer Science & Business Media, 2012.

(114) Andzelm, J.; Wimmer, E. Density Functional Gaussian-type-orbital Approach to Molecular Geometries, Vibrations, and Reaction Energies. *J. Chem. Phys.* **1992**, *96* (2), 1280–1303. https://doi.org/10.1063/1.462165.

(115) Becke, A. D. Density-functional Thermochemistry. III. The Role of Exact Exchange. *J. Chem. Phys.* **1993**, *98* (7), 5648–5652. https://doi.org/10.1063/1.464913.

(116) Hariharan, P. C.; Pople, J. A. The Influence of Polarization Functions on Molecular Orbital Hydrogenation Energies. *Theor. Chim. Acta* **1973**, *28* (3), 213–222. https://doi.org/10.1007/BF00533485.

(117) Francl, M. M.; Pietro, W. J.; Hehre, W. J.; Binkley, J. S.; Gordon, M. S.; DeFrees, D. J.; Pople, J. A. Self-consistent Molecular Orbital Methods. XXIII. A Polarization-type Basis Set for Second-row Elements. *J. Chem. Phys.* **1982**, *77* (7), 3654–3665. https://doi.org/10.1063/1.444267.

(118) Petersson, G. A.; Al-Laham, M. A. A Complete Basis Set Model Chemistry. II. Open-shell Systems and the Total Energies of the First-row Atoms. *J. Chem. Phys.* **1991**, *94* (9), 6081–6090. https://doi.org/10.1063/1.460447.

(119) Singh, U. C.; Kollman, P. A. An Approach to Computing Electrostatic Charges for Molecules. *J. Comput. Chem.* **1984**, *5* (2), 129–145. https://doi.org/10.1002/jcc.540050204.

(120) Connolly, M. L. Solvent-Accessible Surfaces of Proteins and Nucleic Acids. *Science* **1983**, *221* (4612), 709–713. https://doi.org/10.1126/science.6879170.

(121) Sjoberg, P.; Murray, J. S.; Brinck, T.; Politzer, P. Average Local Ionization Energies on the Molecular Surfaces of Aromatic Systems as Guides to Chemical Reactivity. *Can. J. Chem.* **1990**, *68* (8), 1440–1443. https://doi.org/10.1139/v90-220.

(122) Rauk, A. *Orbital Interaction Theory of Organic Chemistry*; John Wiley & Sons, 2004.

(123) Streitwieser, A. Molecular Orbital Theory for Organic Chemists. In *Pioneers of Quantum Chemistry*; ACS Symposium Series; American Chemical Society, 2013; Vol. 1122, pp 275–300. https://doi.org/10.1021/bk-2013-1122.ch009.

(124) Lipshutz, B.; Ghorai, S. Transition-Metal-Catalyzed Cross-Couplings Going Green: In Water at Room Temperature. *Aldrichimica Acta* **2008**, *41*.

(125) Krasovskiy, A.; Duplais, C.; Lipshutz, B. H. Zn-Mediated, Pd-Catalyzed Cross-Couplings in Water at Room Temperature Without Prior Formation of Organozinc Reagents. *J. Am. Chem. Soc.* **2009**, *131* (43), 15592–15593. https://doi.org/10.1021/ja906803t.

(126) Lipshutz, B. H.; Taft, B. R.; Abela, A. R.; Ghorai, S.; Krasovskiy, A.; Duplais, C. Catalysis in the Service of Green Chemistry: Nobel Prize-Winning Palladium-Catalysed Cross-Couplings, Run in Water at Room Temperature. *Platin. Met. Rev.* **2012**, *56* (2), 62–74. https://doi.org/10.1595/147106712X629761.

(127) Isley, N. A.; Gallou, F.; Lipshutz, B. H. Transforming Suzuki–Miyaura Cross-Couplings of MIDA Boronates into a Green Technology: No Organic Solvents. *J. Am. Chem. Soc.* **2013**, *135* (47), 17707–17710. https://doi.org/10.1021/ja409663q.

(128) Lipshutz, B. H.; Isley, N. A.; Fennewald, J. C.; Slack, E. D. On the Way Towards Greener Transition-Metal-Catalyzed Processes as Quantified by E Factors. *Angew. Chem. Int. Ed.* **2013**, *52* (42), 10952–10958. https://doi.org/10.1002/anie.201302020.

(129) Lu, G.; Cai, C.; H. Lipshutz, B. Stille Couplings in Water at Room Temperature. *Green Chem.* **2013**, *15* (1), 105–109. https://doi.org/10.1039/C2GC36042J.

(130) Isley, N. A.; Dobarco, S.; Lipshutz, B. H. Installation of Protected Ammonia Equivalents onto Aromatic & Heteroaromatic Rings in Water Enabled by Micellar Catalysis. *Green Chem.* **2014**, *16* (3), 1480–1488. https://doi.org/10.1039/C3GC42188K.

(131) Handa, S.; Wang, Y.; Gallou, F.; Lipshutz, B. H. Sustainable Fe–Ppm Pd Nanoparticle Catalysis of Suzuki-Miyaura Cross-Couplings in Water. *Science* **2015**, *349* (6252), 1087–1091. https://doi.org/10.1126/science.aac6936.

(132) Fennewald, J. C.; Landstrom, E. B.; Lipshutz, B. H. Reductions of Aryl Bromides in Water at Room Temperature. *Tetrahedron Lett.* **2015**, *56* (23), 3608–3611. https://doi.org/10.1016/j.tetlet.2015.02.066.

(133) Bhonde, V. R.; O'Neill, B. T.; Buchwald, S. L. An Improved System for the Aqueous Lipshutz–Negishi Cross-Coupling of Alkyl Halides with Aryl Electrophiles. *Angew. Chem.* **2016**, *128* (5), 1881–1885. https://doi.org/10.1002/ange.201509341.

(134) Salomé, C.; Wagner, P.; Bollenbach, M.; Bihel, F.; Bourguignon, J.-J.; Schmitt, M. Buchwald–Hartwig Reactions in Water Using Surfactants. *Tetrahedron* **2014**, *70* (21), 3413–3421. https://doi.org/10.1016/j.tet.2014.03.083.

(135) Wagner, P.; Bollenbach, M.; Doebelin, C.; Bihel, F.; Bourguignon, J.-J.; Salomé, C.; Schmitt, M. T-BuXPhos: A Highly Efficient Ligand for Buchwald–Hartwig Coupling in Water. *Green Chem.* **2014**, *16* (9), 4170–4178. https://doi.org/10.1039/C4GC00853G.

(136) Lipshutz, B. H.; Abela, A. R. Micellar Catalysis of Suzuki−Miyaura Cross-Couplings with Heteroaromatics in Water. *Org. Lett.* **2008**, *10* (23), 5329–5332. https://doi.org/10.1021/ol801712e.

(137) Amberg, W.; Pohlki, F.; Lange, U.; Wang, Y. X.; Zhao, H. H.; Li, H.-Q.; Brewer, J. T.; Zanze, I.; DIETRICH, J.; Vasudevan, A.; Djuric, S. W.; Lao, Y.; Hutchins, C. W. Pyrrolidine Derivatives, Pharmaceutical Compositions Containing Them, and Their Use in Therapy. WO2014140310A1, September 18, 2014. https://patents.google.com/patent/WO2014140310A1/zh (accessed 2024-02-24).

(138) Bartels, B.; COOK, X. A. F.; Ratni, H.; REUTLINGER, M.; Vifian, W. Triazolo-Azepine Derivatives. WO2019121434A1, June 27, 2019. https://patents.google.com/patent/WO2019121434A1/en?oq=WO2019121434 (accessed 2024-05-07).

(139) Ratni, H. Triazolo-Azepine Derivatives. WO2019141832A1, July 25, 2019. https://patents.google.com/patent/WO2019141832A1/en?oq=WO2019141832 (accessed 2024-05-07).

(140) Flohr, A.; Zbinden, K. G.; Kuhn, B.; Lerner, C.; Rudolph, M.; Schaffhauser, H. Triazolo Compounds as Pde10 Inhibitors. WO2013178572A1, December 5, 2013. https://patents.google.com/patent/WO2013178572A1/en?oq=WO2013178572 (accessed 2024-05-07).

(141) LARSEN, M. A.; Ali, A.; Cumming, J.; Demong, D.; Deng, Q.; Graham, T. H.; HENNESSY, E.; HOOVER, A. J.; Liu, P.; Liu, K.; Mansoor, U. F.; Pan, J.; Plummer, C. W.; SATHER, A.; Swaminathan, U.; Wang, H.; Zhang, Y. 9-Substituted Amino Triazolo Quinazoline Derivatives as Adenosine Receptor Antagonists, Pharmaceutical Compositions and Their Use. WO2020112700A1, June 4, 2020. https://patents.google.com/patent/WO2020112700A1/en?oq=WO2020112700 (accessed 2024-05-07).

(142) Fader, L.; Bilodeau, F.; Poirier, M.; Parisien, M.; Kuhn, C.; Thibeault, C.; TRINH, T. Inhibitors of Cytomegalovirus. WO2014070978A1, May 8, 2014. https://patents.google.com/patent/WO2014070978A1/en?oq=WO2014070978 (accessed 2024-05-07).

(143) Rosa, M. A. D. L.; Kazmierski, W. M.; Samano, V. Modulators of Indoleamine 2,3-Dioxygenase. WO2018116107A1, June 28, 2018. https://patents.google.com/patent/WO2018116107A1/en?oq=WO2018116107 (accessed 2024-05-07).

(144) Maiti, D.; P. Fors, B.; L. Henderson, J.; Nakamura, Y.; L. Buchwald, S. Palladium-Catalyzed Coupling of Functionalized Primary and Secondary Amines with Aryl and Heteroaryl Halides: Two Ligands Suffice in Most Cases. *Chem. Sci.* **2011**, *2* (1), 57–68. https://doi.org/10.1039/C0SC00330A.

(145) Surry, D. S.; Buchwald, S. L. Biaryl Phosphane Ligands in Palladium-Catalyzed Amination. *Angew. Chem. Int. Ed.* **2008**, *47* (34), 6338–6361. https://doi.org/10.1002/anie.200800497.

(146) Shen, Q.; Shekhar, S.; Stambuli, J. P.; Hartwig, J. F. Highly Reactive, General, and Long-Lived Catalysts for Coupling Heteroaryl and Aryl Chlorides with Primary Nitrogen Nucleophiles. *Angew. Chem. Int. Ed.* **2005**, *44* (9), 1371–1375. https://doi.org/10.1002/anie.200462629.

(147) Roy, A. H.; Hartwig, J. F. Oxidative Addition of Aryl Tosylates to Palladium(0) and Coupling of Unactivated Aryl Tosylates at Room Temperature. *J. Am. Chem. Soc.* **2003**, *125* (29), 8704–8705. https://doi.org/10.1021/ja035835z.

(148) Singer, R. A.; Doré, M.; Sieser, J. E.; Berliner, M. A. Development of Nonproprietary Phosphine Ligands for the Pd-Catalyzed Amination Reaction. *Tetrahedron Lett.* **2006**, *47* (22), 3727–3731. https://doi.org/10.1016/j.tetlet.2006.03.132.

(149) Kotecki, B. J.; Fernando, D. P.; Haight, A. R.; Lukin, K. A. A General Method for the Synthesis of Unsymmetrically Substituted Ureas via Palladium-Catalyzed Amidation. *Org. Lett.* **2009**, *11* (4), 947–950. https://doi.org/10.1021/ol802931m.

(150) BELFIELD, A.; Jones, C. D.; MARGATHE, J.-F.; COLLETTO, C. Fused Bicyclic Raf Inhibitors and Methods for Use Thereof. WO2022023447A2, February 3, 2022. https://patents.google.com/patent/WO2022023447A2/en?oq=WO2022023447 (accessed 2024-05-07).

(151) Hattori, K.; Takaya, K.; Kawase, K.; Aoki, N.; Ishida, Y. Oxazolotriazole Derivative and Drug Composition Containing Same, October 31, 2013. https://patentscope.wipo.int/search/en/detail.jsf?docId=WO2013161928 (accessed 2024-05-07).

(152) Rae Kim, H.; Hwan Song, J.; Ryu, E. K. Study on the Alkylation and Sulfonylation of 3-Aryl-1-Methyl-1,2,4-Triazolin-5-Ones. *Synth. Commun.* **1994**, *24* (21), 3065–3071. https://doi.org/10.1080/00397919408011319.

(153) de Araújo-Júnior, J. X.; Schmitt, M.; Benderitter, P.; Bourguignon, J.-J. Sequential Regio and Chemoselective Cross-Coupling Reactions by Means of O6-Tri-Isopropylsulfonate of 4-Bromo-Pyridazine 3,6-Dione. *Tetrahedron Lett.* **2006**, *47* (34), 6125–6128. https://doi.org/10.1016/j.tetlet.2006.06.056.

(154) Tian, J.; Wang, G.; Qi, Z.-H.; Ma, J. Ligand Effects of BrettPhos and RuPhos on Rate-Limiting Steps in Buchwald–Hartwig Amination Reaction Due to the Modulation of Steric Hindrance and Electronic Structure. *ACS Omega* **2020**, *5* (34), 21385–21391. https://doi.org/10.1021/acsomega.0c01528.

(155) Khaliullin, F. A.; Klen, E. E.; Makarova, N. N. Thietanyl Protection in the Synthesis of 5-Aryloxy(Sulfonyl)-3-Bromo-1,2,4-Triazoles. *Russ. J. Org. Chem.* **2018**, *54* (12), 1856–1859. https://doi.org/10.1134/S1070428018120242.

(156) S. Surry, D.; L. Buchwald, S. Diamine Ligands in Copper -Catalyzed Reactions. *Chem. Sci.* **2010**, *1* (1), 13–31. https://doi.org/10.1039/C0SC00107D.

(157) Enguehard, C.; Allouchi, H.; Gueiffier, A.; Buchwald, S. L. Easy Access to Novel Substituted 6-Aminoimidazo[1,2-a]Pyridines Using Palladium- and Copper-Catalyzed Aminations. *J. Org. Chem.* **2003**, *68* (11), 4367–4370. https://doi.org/10.1021/jo0341463.

(158) Yeh, V. S. C.; Wiedeman, P. E. Practical Cu-Catalyzed Amination of Functionalized Heteroaryl Halides. *Tetrahedron Lett.* **2006**, *47* (34), 6011–6016. https://doi.org/10.1016/j.tetlet.2006.06.119.

(159) Shafir, A.; Buchwald, S. L. Highly Selective Room-Temperature Copper-Catalyzed C−N Coupling Reactions. *J. Am. Chem. Soc.* **2006**, *128* (27), 8742–8743. https://doi.org/10.1021/ja063063b.

(160) Hammoud, H. Conception, Synthèse et Activité Anti-Hyperalgésique de Dérivés de Guanidine Comme Antagonistes Des Récepteurs Du Neuropeptide FF (NPFF). These de doctorat, Strasbourg, 2012. https://theses.fr/2012STRAF008 (accessed 2024-05-06).

(161) Shafir, A.; Lichtor, P. A.; Buchwald, S. L. N- versus O-Arylation of Aminoalcohols: Orthogonal Selectivity in Copper-Based Catalysts. *J. Am. Chem. Soc.* **2007**, *129* (12), 3490–3491. https://doi.org/10.1021/ja068926f.

(162) Andersen, J.; Madsen, U.; Björkling, F.; Liang, X. Rapid Synthesis of Aryl Azides from Aryl Halides under Mild Conditions. *Synlett* **2005**, *2005* (14), 2209–2213. https://doi.org/10.1055/s-2005-872248.

(163) Peng, Y.; Zhang, Q.; Welsh, W. J. Novel Sigma 1 Receptor Antagonists as Potential Therapeutics for Pain Management. *J. Med. Chem.* **2021**, *64* (1), 890–904. https://doi.org/10.1021/acs.jmedchem.0c01964.

CHAPTER II

DESIGN, SYNTHESIS AND PHARMACOLOGICAL EVALUATION OF TRISUBSTITUTED 1,2,4-TRIAZOLES AS GSK-3β INHIBITORS

Given the expertise and contribution of the groups involved in this work in the search for new drug candidates for Alzheimer's disease. In this chapter, we will describe the design, synthesis, and pharmacological evaluation of 3 series of trisubstituted 1,2,4-triazoles against GSK-3β.

1. INTRODUCTION

1.1. Dementia and its impact on society

Dementia is a broad term that encompasses various diseases affecting memory, cognitive abilities, and behavior, significantly interfering with an individual's capacity to carry out daily activities. Over time, these diseases lead to the destruction of nerve cells and cause brain damage, resulting in a deterioration of the ability to process thoughts beyond what might be expected in natural biological aging. Impairment in cognitive function is often associated with, and in some cases preceded by, changes in mood, emotional control, motivation, and social behavior.[1]

Dementia entails a series of impacts not only for those affected by the disease but also for their caregivers, families, and society at large, encompassing areas such as physical, psychological, social, and economic dependence. Currently, a lack of awareness and understanding of dementia persists, leading to stigma and obstacles to diagnosis and treatment.[1]

According to the World Health Organization (WHO), dementia is currently the seventh leading cause of death worldwide, with over 55 million people living with this condition. This number is projected to nearly double every 20 years, reaching 82 million in 2030 and 152 million in 2050 (Figure 22). The increase will be primarily observed in developing countries. Currently, over 60% of individuals with dementia reside in middle and low-income countries, but it is expected that by 2050, this proportion will increase to 71% (Figure 22). Approximately 10 million new cases are recorded yearly, equivalent to a new case every 3.2 seconds.[2]

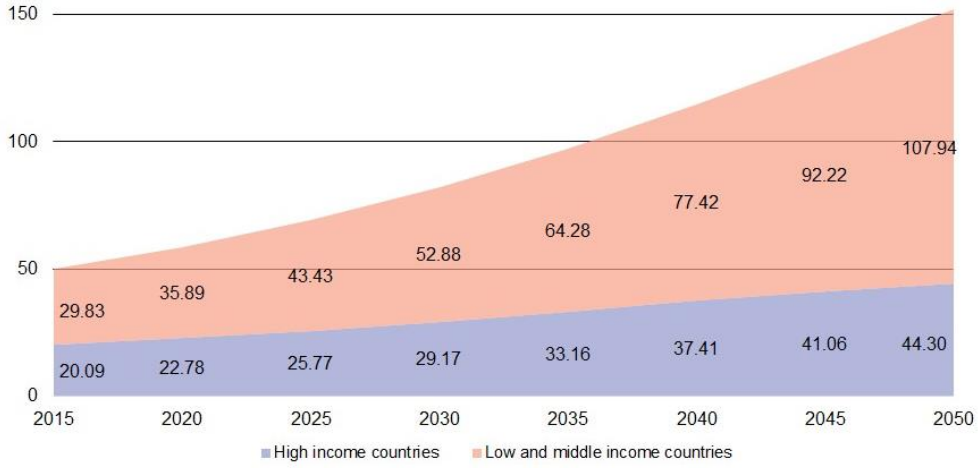

Figure 22. Number of people with dementia (millions) in low- and middle-income countries compared to high income countries. Reproduced from 2 (authors do not request permission). Copyright © Alzheimer's Disease International.

In 2015, the costs associated with dementia were estimated at 818 billion dollars, representing 1.1% of the global Gross Domestic Product (GDP). This proportion ranged from 0.2% for middle and low-income countries to 1.4% for high-income countries. The annual global cost of dementia already exceeds the 1.3 trillion dollar mark, and projections indicate it will reach 2.8 trillion dollars by 2030. This scenario raises concerns regarding the impact on global social and economic development, as well as the burden on healthcare and social assistance systems, including long-term care systems in particular.[1–3]

Among the most common forms of dementia are Alzheimer's Disease (AD), Vascular Dementia, Lewy Body Dementia (abnormal protein deposits inside nerve cells), and Frontotemporal Dementia (degeneration of the frontal lobe of the brain), with AD being the most prevalent form, contributing to 60-70% of cases.[2]

1.2. General aspects of Alzheimer's disease

Alois Alzheimer was the first researcher to describe a clinical picture of a neurodegenerative disease on November 4, 1906, later named Alzheimer's Disease (AD) by Emil Kraepelin. In this unique case, Alzheimer outlined typical clinical features of the disease, such as memory disturbances, language issues, disorientation, and hallucination. Additionally, he identified histopathological images in the cell bodies of the central nervous system, such as the formation of dense bundles of fibrils and amyloid plaques, which we now know are the main characteristics of the disease.[4]

In general, the initial symptoms of AD vary from person to person. For many, a decline in non-memory aspects of cognition, such as difficulty finding words, vision/spatial issues, and impaired judgment or reasoning, may indicate the very early stages of the disease. [5] As the disease progresses, individuals face more significant memory loss and other cognitive difficulties, including wandering and getting lost, difficulty handling money and paying bills, repeating questions, delays in performing daily tasks, and changes in personality and behavior. In the moderate stage, damage occurs in brain areas that control language, reasoning, conscious thought, and sensory processing, such as properly perceiving sounds and smells. Memory loss and confusion worsen, and individuals begin to struggle with recognizing family and friends, becoming unable to learn new things, perform complex tasks like dressing, or handle new situations. At this stage, individuals may experience hallucinations, delusions, and paranoia, and may act impulsively. In the severe stage, people with Alzheimer's cannot communicate and depend entirely on others for their care. In the end stages of life, the person may be in bed, most or all of the time as the body undergoes a gradual shutdown. [5]

Alzheimer's disease is a neurodegenerative disorder microscopically characterized by extracellular plaques containing β-amyloid peptide (Aβ) and intracellular neurofibrillary tangles containing tau protein.[6] Alternatively, AD can be characterized by the loss of synaptic homeostasis, neurons, or neural network integrity. Many pathogenic mechanisms involved in these changes are being studied, including hyperphosphorylation of tau protein, aggregation of Aβ peptides, neurovascular dysfunction, as well as other mechanisms such as inflammatory processes, oxidative stress, cell cycle alteration, and mitochondrial dysfunction.[7] These events predominantly occur in specific regions of the brain, such as the cerebral cortex, hippocampus, entorhinal cortex, and ventral striatum, which are responsible for cognitive functions.[8]

The comparison between a normal brain and one after considerable cell degeneration in the advanced stages of AD highlights the shrinkage of the cerebral cortex, damaging regions involved in thinking and memory. This shrinkage is particularly severe in the hippocampus, a cortex region responsible for forming new memories. Additionally, the ventricles, which are fluid-filled spaces within the brain, become larger with the progression of the disease (Figure 23).[9]

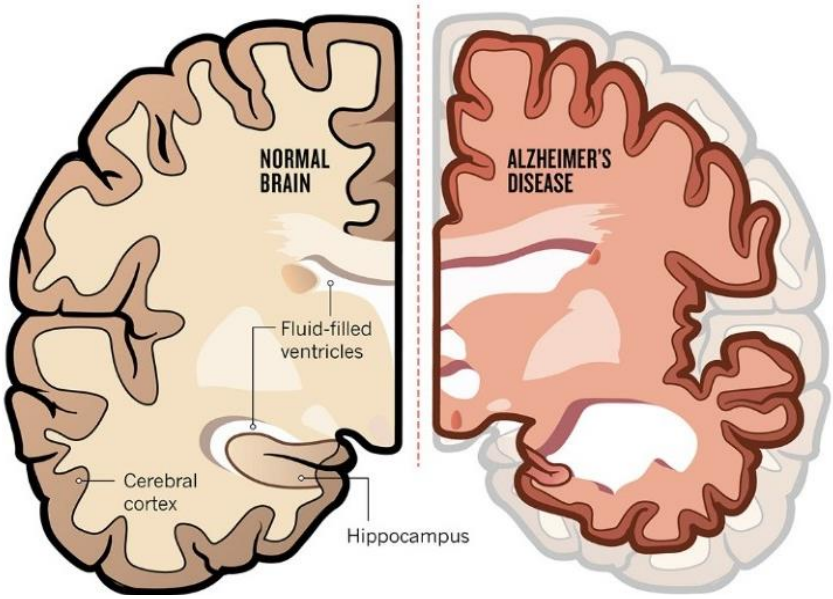

Figure 23. Illustration of the comparison between a normal brain and one after considerable cellular degeneration in an advanced stage of AD. Adapted from 10 (authors do not request permission). Copyright © Springer Nature Limited.

Until the 2000s, the only definitive way to confirm if a person had AD was through autopsy, a procedure performed after the patient's death. Currently, thanks to advances in research, the diagnosis of the disease relies on the use of various methods and tools to help determine if a person with cognitive dysfunction has AD. For diagnosis, it is necessary to gather information about the medical history and physical examination, conduct cognitive and neuropsychological tests, examine blood, scan the brain, analyze cerebrospinal fluid, perform genetic tests, and observe behavioral patterns. The definitive diagnosis of AD involves a more comprehensive assessment, and a combination of these methods can be used to arrive at a more accurate conclusion. Additionally, ongoing research is exploring new diagnostic approaches and biomarkers to enhance early detection and intervention.[11]

Among the main risk factors for developing dementia and AD, age is the most significant. In elderly populations worldwide, for example, aged 65 and older, the incidence of dementia is higher in women compared to men due to higher male mortality above the age of 45 from other causes.[12] Additionally, many studies indicate that the prevalence of dementia is either higher in women or does not show a significant difference between the sexes.[13]

Genetic risk factors for AD include rare dominant inherited mutations in APP (amyloid precursor protein) and presenilins (PSEN1 and PSEN2).[14] These presenilins are constituents of the γ-secretase enzyme complex responsible for degrading APP into Aβ. Additionally, more

common mutations in the isoforms of the cholesterol-carrying apolipoprotein (APOE) are also considered genetic risk factors.[15] Collectively, genetic contributions represent only a modest portion and are associated with rare cases known as familial Alzheimer's disease, accounting for about 5% of total cases.[16] Familial AD is characterized by an early onset, occurring before the age of 65, and is often referred to as early-onset AD.[17]

Several potentially modifiable risk factors that occur in midlife (40-60 years), primarily metabolic factors (diabetes mellitus, hypertension, obesity, and low HDL cholesterol), hearing loss, traumatic brain injuries, and alcohol abuse, are associated with an increased risk of dementia in old age.[18] Throughout life, smoking, depression, sedentary lifestyle, social isolation, diabetes mellitus, and air pollution are risk factors of similar magnitude for dementia, although in some cases, such as sedentary lifestyle and depression, they may have a bidirectional link and be part of the early stages of dementia.[19] Probably, the most common and important risk factors for dementia in older ages are diabetes mellitus and hypertension, especially when these risk factors are present from midlife.[20,21] Both diabetes mellitus and hypertension induce cerebrovascular diseases and are believed to affect the clinical manifestation of AD pathology through potentially modifiable effects on cerebrovascular diseases, rather than a direct effect on the pathophysiology of AD.[22]

Although there is no proven effective treatment or prevention for AD and related dementias, adopting a healthy lifestyle can generally help prevent or reduce the associated risk factors. Beneficial practices include controlling high blood pressure, properly managing blood sugar levels, maintaining a healthy weight, adopting a healthy diet, staying physically and mentally active, staying connected with family and friends, addressing hearing problems, taking care of both physical and mental health, getting adequate sleep, preventing head injuries, consuming less alcohol, and quitting tobacco use. However, more research is needed to find effective ways to prevent AD and other related dementias.[23]

1.3. The molecular basis of AD

AD is a heterogeneous disease driven by multiple deleterious factors. Its origin and how these factors exactly contribute to the progression of the disease remain undetermined at the moment. Different hypotheses regarding its molecular bases have emerged, based on observed molecular and pathophysiological changes in the brains of AD patients, attempting to explain the complexity and multifactorial nature of AD and evolving gradually with technological advances. The oldest theory is represented by the cholinergic hypothesis, postulated in the early

1980s. Following that, there is the emergence of the glutamatergic hypothesis. The “amyloid cascade” hypothesis was first proposed in 1992. Other conjectures, such as the oligomeric and metal hypotheses, which can be considered extensions of the amyloid hypothesis, hyperphosphorylation of tau protein, oxidative stress, and anti-inflammatory processes, began to gain more prominence during the 1990s.[24]

1.3.1. The cholinergic hypothesis

The cholinergic hypothesis of AD asserts that the degeneration of cholinergic neurons and the decrease in the concentration of choline acetyltransferase (ChAT), the enzyme responsible for the synthesis of the neurotransmitter acetylcholine (ACh), in the nuclei of the basal forebrain, lead to disturbances in presynaptic cholinergic terminals in the hippocampus and neocortex, regions of extreme importance for memory disorders and other cognitive symptoms.[25] As a result of neurodegeneration and the decrease in ChAT concentration, the activity of cholinergic neurons, those that utilize acetylcholine (ACh), is reduced.

Acetylcholine (AChE) is synthesized by choline acetyltransferase (ChAT) through the action of choline and acetyl CoA. This substance is then encapsulated by the synaptic vesicle and released into the synaptic cleft, where it is rapidly metabolized by acetylcholinesterase (AChE), yielding an acetate ion and a choline molecule as products. Subsequently, the choline molecule is transported back to the cholinergic neuron by axon terminals through a specific sodium-dependent transporter (choline transporter), being utilized to synthesize a new ACh molecule (Figure 24).

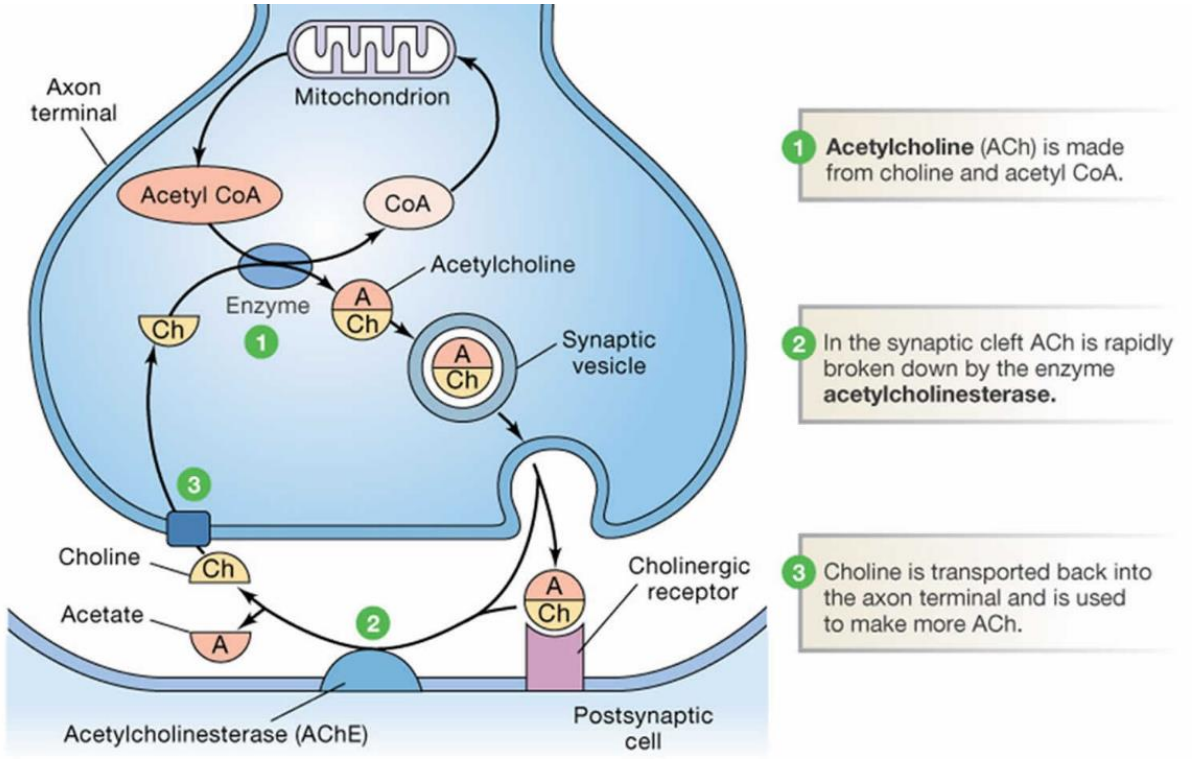

Figure 24. Representation of the acetylcholine cycle. Reproduced from 26. (authors do not request permission). Copyright © 2001, Sinauer Associates, Inc.

The cholinergic hypothesis provided a rational basis for the development of therapeutic approaches aimed at improving cholinergic transmission. Synaptic levels of acetylcholine can be increased by inhibiting AChE, using precursors, or enhancing acetylcholine release or muscarinic agonists. However, the only proven effective approach in treating the cognitive and functional symptoms of AD has been based on cholinesterase inhibitors.[27]

1.3.2. The glutamatergic dysfunction hypothesis

The glutamatergic hypothesis, also known as the "excitotoxic" hypothesis, of AD emerged in the 1980s.[28] Glutamate, the principal excitatory neurotransmitter in the central nervous system, has its activity mediated by three types of receptors: N-methyl-D-aspartate (NMDA), alpha-amino-3-hydroxy-5-methyl-4-isoxazolepropionic acid (AMPA), and 149ainite. The glutamatergic hypothesis predicts that, under specific conditions, such as alterations in cellular energy metabolism, there is an excessive activation of NMDA receptors, potentially disrupting calcium homeostasis, leading to an increase in intracellular calcium concentrations capable of initiating the process of neuronal apoptosis (degeneration and death).[29]

NMDA receptors have a complex structure with different binding sites for glutamate and various modulators. The physiological activation of these receptors results in a neuronal influx of Ca^{2+} ions. It is believed that released glutamate initially activates AMPA and cyanate receptors, which, despite low affinity, would promote rapid cell depolarization through the influx of Na^{+} and Ca^{2+}. The entry of these ions causes partial depolarization of the plasma membrane, removing the block exerted by Mg^{2+} ions within the NMDA receptor channel. Thus, glutamate could bind to a subunit of this receptor, promoting, in association with glycine bound to another subunit, the entry of more Na+ and Ca^{2+} into the neuron, contributing to its excitability.[30,31] It is postulated, therefore, that this glutamate-dependent "excitotoxicity" may constitute one of the necessary pathogenic mechanisms for maintaining and amplifying the neurodegenerative process. [32]

1.3.3. The amyloid cascade hypothesis

Since AD was discovered, it has been recognized that the symptoms of this disease may be associated with the development of numerous intraneuronal and extracellular filamentous lesions in the limbic cortex, as well as in the cerebral cortex. Abnormal aggregates of cytoplasmic fibers occur both in neuronal cell bodies, involving neurofibrillary tangles, and in axons and dendrites. Another important histopathological marker of AD is the presence of plaques and aggregates, primarily formed by the Aβ peptide, in the extracellular portion of brain tissue.[33–35] Figure 25 schematically presents the differences between a healthy neuron and neurons characteristic of an individual in the prodromal and advanced stages of AD.

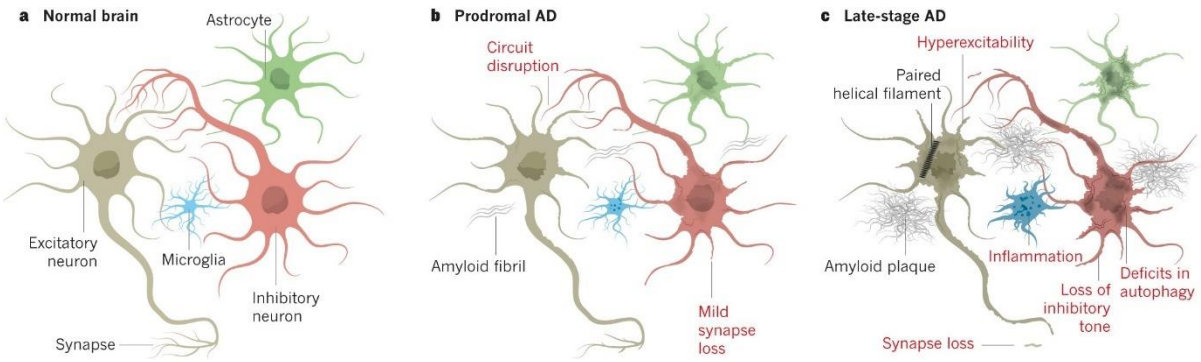

Figure 25. (**a**) Subpopulations of neurons and glial cells form functional circuits through synaptic connections. (**b**) In prodromal AD, amyloid-β fibrils begin to form in the extracellular space, possibly contributing to early circuit dysfunction that stimulates inhibitory sprouting and the initiation of inflammatory processes. (**c**) In late-stage AD, amyloid-β plaques grow as production of the peptide

outpaces its clearance. Reproduced from 36. Reprinted with permission from *Nature* **2016**, *539* (7628), 187–196. Copyright © 2016, Springer Nature Limited.

The amyloid cascade hypothesis was first published in the early 1990s following the identification of pathogenic mutations in the amyloid precursor protein (APP) gene on chromosome 21. These mutations were also found in individuals with Down syndrome, who exhibit Aβ deposits in late childhood or early adulthood and later develop the classic neuropathological characteristics of AD.[37] This observation suggested that the metabolism of APP and the deposition of Aβ were crucial events in AD. Therefore, it was postulated that the Aβ peptide plays a central role in the origin of the disease due to its neurotoxicity, capable of leading to the formation of senile plaques and triggering a sequence of events resulting in cell death.[38]

The Aβ peptides are formed through the cleavage of APP, a highly conserved integral membrane protein whose expression is mainly localized around the synapse of neuronal tissue. Although its primary role is not fully understood, its essential importance for neuronal plasticity and synapse formation is recognized. APP can be processed by the α-secretase enzyme, followed by the γ-secretase enzyme in the non-amyloidogenic pathway; this process does not produce insoluble Aβ. In the amyloidogenic pathway, APP is first cleaved by the β-secretase and then by the γ-secretase, producing fibrillogenic Aβ peptides of different sizes, ranging from 38 to 42 amino acids (Figure 26).[38,39] In healthy brains, the Aβ peptide is also produced but undergoes proteolytic degradation by Aβ-degrading peptide proteases (AβDPs), which are responsible for regulating Aβ peptide levels in the brain, highlighting the existence of an imbalance in this natural process in patients with AD.[40]

There are two main types of Aβ peptides that play a direct role in plaque formation and induced neurotoxicity, with 40 and 42 amino acid residues, respectively: $A\beta_{1\text{-}40}$ and $A\beta_{1\text{-}42}$. Despite the first fragment being more common, the second, considered more hydrophobic, currently has a higher amyloidogenic potential, although both are capable of aggregating and giving rise to protofibrils, fibrils, and ultimately insoluble plaques.[38,39,41]

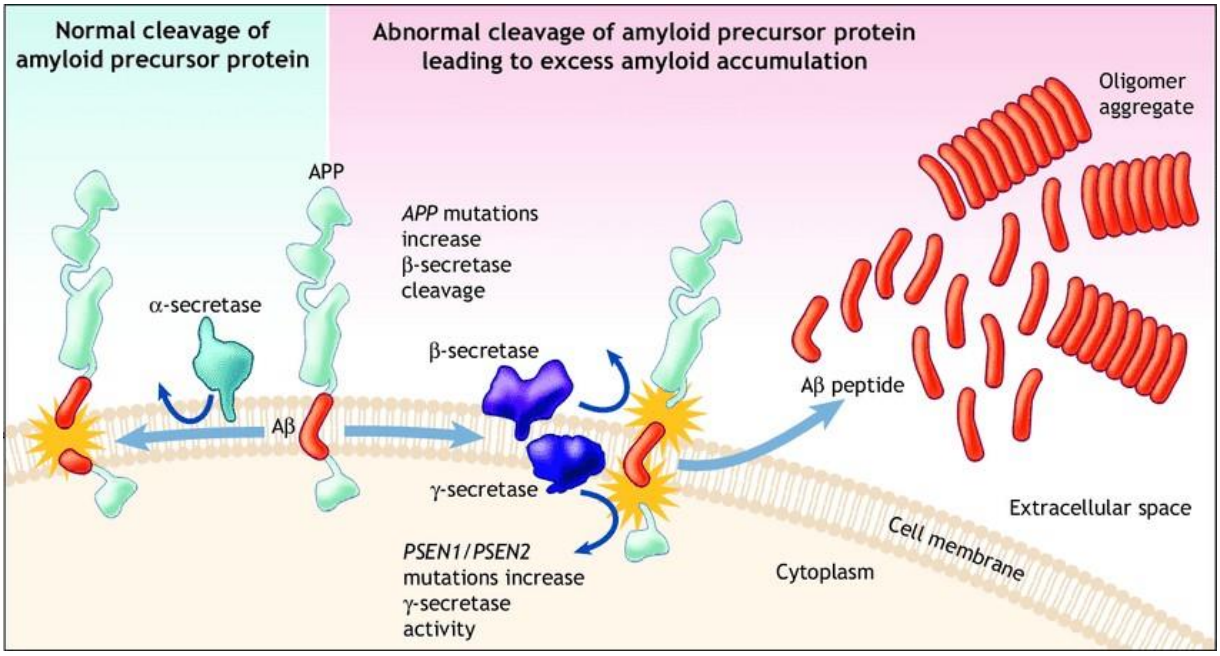

Figure 26. Formation of Aβ peptides followed by their accumulation, leading to the formation of insoluble Aβ plaques in the brains of individuals with AD. Reproduced from 42 (authors do not request permission) Copyright © 2008 Canadian Medical Association.

The progressive accumulation of Aβ peptides leads to a sequence of pathological events, including synaptic signaling blockade and altered neuronal activity; activation of microglia and reactive astrocytes, leading to a local inflammatory response; neuronal damage; oxidative stress; activation of kinases, resulting in hyperphosphorylation of the tau protein, leading to neurofibrillary tangle formation; and ultimately, neuronal death and synaptic loss.[43]

1.3.4. Correlation between the amyloid and cholinergic hypotheses

The regulatory mechanism of APP cleavage through the amyloidogenic pathway is still under investigation. Different studies suggest that cholinergic inputs are involved in this process,[44] as evidenced by the presence of cholinesterases in neuritic plaques. The formation of extracellular aggregates appears to induce an inflammatory response capable of damaging cholinergic system cells[45] On the other hand, the cholinergic system, in addition to its catalytic function, has the ability to exert regulatory control over amyloid peptide processing, reinforcing the neurodegenerative process.[46] Therefore, it is natural to assume that both aspects may have mutual influence, making it difficult to understand which event could be the triggering factor in the pathology.[44]

1.3.5. The tau protein hypothesis

The presence of neurofibrillary tangles inside neurons is a crucial marker of AD.[47,48] Immunocytochemical and biochemical analyses demonstrate that these tangles are primarily composed of tau protein (p-tau), which is associated with microtubules, mainly found in axons. The binding of this protein to microtubules promotes their stabilization, allowing for the transport of essential substances (Figure 27a).[49]

Under normal conditions, there is a constant dynamic balance between the phosphorylation of p-tau by kinases, promoting its dissociation from microtubules, and dephosphorylation, thereby maintaining the neuron's morphology. However, excessive phosphorylation of p-tau results in its dissociation from microtubules, leading to the gradual loss of microtubule function, axonal transport dysfunction, followed by synaptic dysfunction, and neuronal loss. Hyperphosphorylated p-tau aggregates to form paired helical filaments (PHF) that cluster into neurofibrillary tangles (NFTs) and deposit within the neuron, imparting additional toxic damage and leading to neuronal death (Figure 27b).[50]

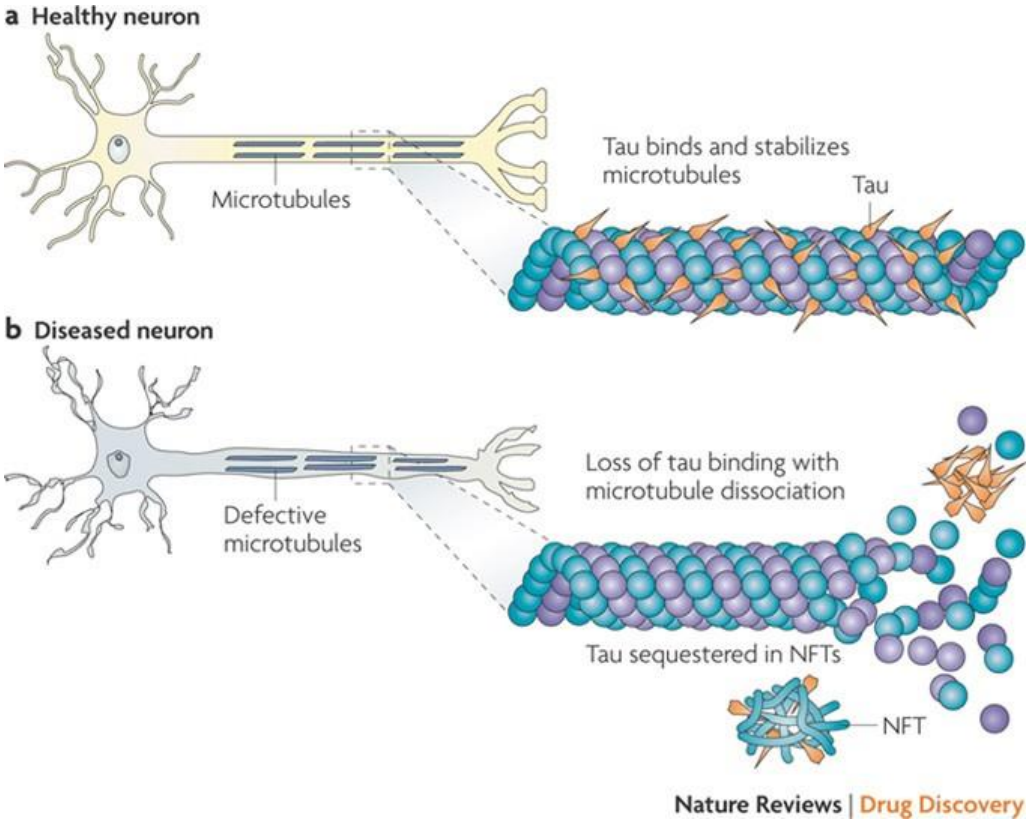

Figure 27. (a) Normal neurons in which Tau proteins are bound to microtubules, stabilizing them. (b) Neurons of individuals with AD in which Tau protein undergoes hyperphosphorylation, resulting in the dissociation of microtubules and the formation of neurofibrillary filaments. Reproduced from 51.

The hypothesis of p-tau propagation argues that tau pathology typically appears first in specific areas and then results in the autocatalytic spread of the p-tau aggregation cascade to all interconnected neurons.[52] Although p-tau plays a crucial role, the p-tau hypothesis alone is not sufficient to explain all the symptomatic conditions observed in AD.[53]

There is no consensus on identifying the event that initiates AD, but it is known the hyperphosphorylation of p-tau and the aggregation of Aβ peptides play important roles in its pathophysiology. Several studies indicate that the accumulation of Aβ peptides may be the event that triggers the hyperphosphorylation of p-tau, although the factors that trigger this imbalance are not yet fully understood.[53,54] Neurofibrillary tangles containing hyperphosphorylated tau proteins are also found in other neurological diseases, strongly suggesting that these cytoskeletal changes may be a secondary response, albeit of vital importance, to various brain injuries.[7,55,56]

1.3.6. Neuroinflammation

Neuroinflammation is a prominent characteristic in AD, primarily characterized by a high number of leukocytes and mononuclear macrophages in the central nervous system (CNS), including glial cells such as astrocytes and microglia. Microglial cells are CNS-specific macrophages, constituting 10-15% of all brain cells.[57] These cells are crucial because they perform immune functions, which, under physiological conditions, involve recognizing pathogens, debris, damaged and misfolded proteins, and damaged cells, initiating their controlled degradation and removal. However, under pathophysiological conditions, such as neuronal death, they elicit exacerbated reactions in the medium term. Thus, in neurodegenerative diseases, a positive feedback loop is established between neuronal death and neuroinflammation.[58]

In AD, senile plaques, neurofibrillary tangles (NFTs), and damaged or dead neurons activate microglia to initiate inflammation, inducing pro-inflammatory mediators such as interleukin-1 beta (IL-1), interleukin-6 (IL-6), tumor necrosis factor-alpha (TNF-α), interleukin-8 (IL-8) chemotactic factor, macrophage inflammatory protein, prostaglandins, leukotrienes, coagulation factor, proteases, and protease inhibitors. These mediators activate

neuronal death pathways,[58,59] causing localized damage in the brain and further contributing to neuronal death.[60]

Studies demonstrate that microglia exhibit higher activity in patients with AD than in the control group.[61] Additionally, it has also been described that the concentration of clusters of microglial cells near senile plaques and neurons containing neurofibrillary tangles (NFTs) in individuals with AD is generally 2-5 times higher than in normal individuals.[62]

1.3.7. Oxidative stress

Oxidative stress, a process that intensifies in the brain with aging, occurs due to an imbalance in the redox state, involving the excessive production of reactive oxygen species (ROS) or dysfunction of the antioxidant system.[63] The brains of patients with AD exhibit a substantial extent of oxidative damage associated with the marked abnormal accumulation of Aβ peptide and the formation of neurofibrillary tangles.[64]

Some studies demonstrate that there is evidence that oxidative stress is crucial for the progression of AD,[65] acting both as a cause and a consequence in the inflammatory processes generally characteristic of neurodegenerative diseases.[66]

The brain is an organ with high energy activity and requires a substantial oxygen supply, accounting for 20% of the body's oxygen consumption, rendering neuronal cells more vulnerable to oxidative stress.[67] Energy demand is met through mitochondrial oxidative phosphorylation, a process that leads to the generation of reactive oxygen species (ROS). These ROS, at low concentrations, play a crucial role in maintaining cellular redox state, proper immune system function, and appropriate cellular signaling.[68]

Under normal conditions, reactive oxygen species (ROS) do not exhibit particularly high oxidative damage, as protective mechanisms are in place. These mechanisms include enzymes such as superoxide dismutase (SOD), catalase, and glutathione peroxidase (GPx), along with oxidant compounds like vitamins C and E. Oxidative stress occurs when antioxidant protection mechanisms become overwhelmed, a result of excessive ROS production.[69] Generally, oxidative stress in the brains of AD patients is manifested by increased protein oxidation, lipid peroxidation, DNA and messenger RNA oxidation, and excessive ROS formation, leading to deleterious consequences for cellular function.[70]

1.3.8. Metal ion hypothesis

Metal ions play a crucial role in maintaining homeostasis, acting as essential cofactors in metalloproteins, mitochondrial function, and neuronal function.[71]

In healthy brains, metal ions are maintained at very low levels, and their concentration is strictly regulated through the blood-brain barrier.[72] When an imbalance occurs in the metal ion regulation system, it can lead to cytotoxic consequences for cell survival, such as an increased response to oxidative stress and incorrect protein folding, contributing to the progression of neurodegenerative diseases.[73] The homeostatic imbalance of biometals such as iron, copper, and zinc in the brain, their roles in the formation of reactive oxygen species (ROS) and oxidative stress, and their interactions with Aβ plaques leading to the production of toxic aggregates, have been demonstrated as significant factors contributing to the development of Alzheimer's pathology. Copper and zinc ions are known to accelerate the aggregation of Aβ peptides, leading to the formation of senile plaques.[74] The interaction of metals (Cu, Fe, and Zn) with the Aβ peptide and the toxicity related to this phenomenon are at the core of the metal hypothesis.[75]

The increased concentration of metals is also involved in inflammatory processes potentially associated with neurodegenerative diseases. Metal chelators can block metal-related oxidative stress, modulate the formation of β-amyloid plaques or neurofibrillary tangles, as well as interfere with inflammatory processes. Thus, disrupting Aβ-metal peptide interactions using appropriately designed chelating small molecules has been an active area of research. In recent years, this strategy has led to the development of molecules that target the chelation of Cu^{2+} and Zn^{2+} in the Aβ-Cu^{2+} or Aβ-Zn^{2+} complex, modulating metal-induced toxicity.[76]

1.4. Treatment and therapeutic strategies for AD

Based on the different molecular hypotheses of AD, various treatments are currently available in the market. These include those targeting cholinergic, glutamatergic, and amyloid cascade hypotheses, as well as those assisting in the partial control of various symptoms, particularly agitation, depression, hallucinations, and delusions, which become more frequent as the disease progresses. The current therapy is not capable of curing the disease. Commercially available medications focus on managing cognitive disorders and reducing the progression of the disease.[77]

1.4.1. Cholinesterase inhibitors

As described before in the "cholinergic hypothesis," individuals with AD exhibit low levels of acetylcholine, a crucial neurotransmitter. Acetylcholinesterase inhibitors slow down the metabolic degradation of acetylcholine, increasing the availability of this substrate in the synaptic cleft, enhancing communication between cells. This helps delay the progression of cognitive dysfunction and may be effective for some patients in the early and intermediate stages of the disease.[78] Currently, four drugs belonging to this class have been approved by the Food and Drug Administration (FDA): tacrine (**198**), donepezil (**199**), rivastigmine (**200**), and galantamine (**201**) (Figure 28). Among them, only donepezil was approved for the treatment of severe symptoms in 2006.[79,80]

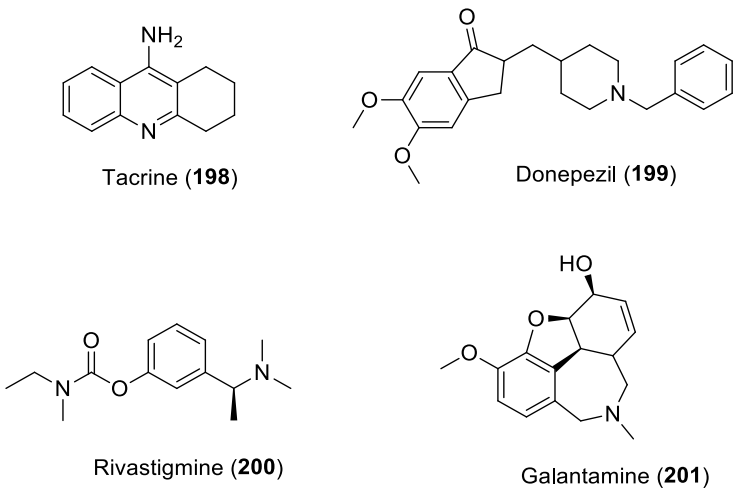

Figure 28. Commercially available acetylcholinesterase inhibitors for the treatment of AD.

Tacrine (**198**) (trade name: Cognex®) was the first drug approved for the treatment of AD in 1993 by the FDA. It is considered a non-selective, reversible, and non-competitive AChE inhibitor. Due to a high incidence of adverse effects, such as constipation, diarrhea, gas, loss of appetite, muscle pain, nausea, stomach pain, stuffy nose, vomiting, weight loss, and potential hepatotoxicity, tacrine is no longer commercially available.[78]

Donepezil (**199**) (trade name Aricept®) was the second drug approved by the FDA for the treatment of AD in 1996. It is a highly selective, reversible, non-competitive AChE inhibitor. Besides being the only one approved for the treatment of severe symptoms, it has advantages such as not being hepatotoxic and having a long half-life, approximately 70 hours, allowing for a once-daily dose.[81]

Rivastigmine (**200**) (trade name: Exelon®) was approved in the year 2000. This drug prevents acetylcholine degradation by inhibiting AChE and butyrylcholinesterase (BuChE), a

cholinesterase that plays a minor role in acetylcholine breakdown in the human body. The most common side effects include nausea, diarrhea, vomiting, muscle weakness, loss of appetite, weight loss, dizziness, drowsiness, and stomach pain. In 2007, the FDA approved Exelon®Patch, a transdermal system for rivastigmine, to deliver the medication through a skin patch as an alternative to oral capsules.[78]

Galantamine (**201**) (trade name: Razadyne®) is a tertiary alkaloid discovered accidentally in 1950, but it was only approved in 2001 for the treatment of mild to moderate AD. This drug prevents the degradation of acetylcholine and stimulates nicotinic receptors to release larger amounts of this neurotransmitter in the brain. The most common side effects include nausea, vomiting, diarrhea, weight loss, dizziness, headache, and fatigue.[78]

Several studies have indicated that, besides inhibiting the hydrolysis of acetylcholine (ACh), AChE inhibitors (AChEIs) available in the market have a range of neuroprotective effects that go beyond symptomatic improvement in cognition. This suggests that these medications may have the ability to positively influence the progression of AD, challenging the predominant view that they are merely a symptomatic treatment. Among the marketed AChEIs, donepezil demonstrates the ability to inhibit *in vitro* the first two events in the neurotoxic cascade of AD, specifically the formation of beta-amyloid (Aβ) and Aβ aggregation. This ability may explain the apparent superiority of donepezil in neuroprotection studies compared to other medications of this type.[82]

1.4.2. NMDA receptor antagonists

Memantine (**202**) (trade name: Namenda®, Figure 29) was the first drug approved by the FDA to treat symptoms of AD in moderate to severe stages. It is also the first and, so far, the only representative of the NMDA receptor antagonist's class. It regulates the activity of glutamate, which is released in large quantities by cells damaged by AD and some other neurological disorders. When glutamate reaches NMDA-type receptors on the cell surface, calcium flows freely into the cell, which can lead to cell degeneration. Memantine has the ability to interrupt this destructive sequence.[24]

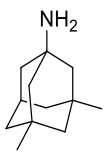

Memantine (**202**)

Figure 29. N-methyl-D-aspartate (NMDA) receptor antagonist available for the treatment of AD.

1.5. New therapeutic strategies for AD

In recent decades, significant scientific and economic efforts have been dedicated to understanding the mechanisms underlying AD. The goal has been to identify biological targets and crucial pathological events to discover new, more effective medications to combat the progression of the disease. In this context, various therapeutic strategies have emerged, based on different molecular hypotheses of AD, as previously mentioned. These approaches have resulted in clinical studies involving numerous disease-modifying agents, approximately 221 between the years 2002 and 2012, with 65.6% of them targeting beta-amyloid (Aβ) therapeutically.[83]

1.5.1. Aβ aggregation inhibitor

Due to the progressive accumulation of beta-amyloid (Aβ) peptide in individuals with AD, the strategy of inhibiting the aggregation of Aβ and/or the toxic forms generated by it has emerged as a valid disease-modifying therapy for AD.[84]

In recent years, research has advanced in the development of drugs capable of removing beta-amyloid (Aβ) plaques from the brains of patients with AD; these drugs act as immunotherapies.[85] Immunotherapy involves the intervention of the immune system to achieve the necessary immune response for disease treatment. Several immunotherapies have been developed and tested in clinical studies to remove neurotoxic protein aggregates, Aβ peptide, or tau protein. So far, two drugs belonging to this class have been approved by the FDA: aducanumab and lecanemab.

Aducanumab (trade name: Aduhelm®) was the first drug to receive FDA approval for the treatment of AD since 2003. This drug is a monoclonal antibody with the ability to remove beta-amyloid (Aβ) peptide from the brain in the early stages of AD. Aducanumab received accelerated FDA approval in June 2021 for the treatment of early-stage AD based on data demonstrating a reduction in the presence of Aβ plaques. However, this approval sparked controversy due to the lack of clear evidence of improvements in clinical symptoms. Additionally, concerns related to side effects, including edema and cerebral bleeding, arose during clinical trials.[86]

Lecanemab (trade name: Leqembi®) became the second monoclonal antibody approved by the FDA for the treatment of AD. This medication has demonstrated efficacy in removing beta-amyloid (Aβ) peptide, as evidenced in clinical trials involving patients with AD. The FDA granted accelerated approval to Lecanemab for the treatment of early-stage AD. However, reports indicate that three individuals enrolled in the Lecanemab phase III study have died, and the cause is directly associated with treatment with this monoclonal antibody. There are suspicions that the medication may have weakened blood vessels in the brain that were coated with amyloid plaques.[87]

Even with the recent approval of monoclonal antibodies by the FDA for the treatment of AD, immunotherapy targeting beta-amyloid (Aβ) peptide is associated with a considerable number of side effects, including severe allergic reactions, bleeding points inside or on the surface of the brain, dizziness, nausea, confusion, altered vision, among others. Additionally, controversial data from clinical trials emphasize the urgent need to explore new therapeutic approaches for the treatment of AD.[88]

1.5.2. GSK-3β inhibitors

Kinases are key enzymes at the intersection of multiple intracellular pathways, and the dysregulation of their activity is associated with various pathologies. For this reason, kinases have been intensively investigated as therapeutic targets, and 52 kinase inhibitors have been approved by the FDA. Recent evidence highlights that kinases in the Central Nervous System (CNS) are emerging as important therapeutic targets in AD, with Glycogen Synthase Kinase-3 beta (GSK-3β) likely being the most well-known among them.[89]

In the Central Nervous System, GSK-3β is the most abundant isoform, and its expression levels increase with age.[90] The activity of this kinase is crucial for cellular signaling and for controlling brain functions related to development, metabolic homeostasis, neuronal growth and differentiations, as well as cell polarity, fate, and modulation of apoptotic potential.[91,92] In patients with AD, GSK-3β is hyperactivated, and consistent evidence supports that it is the primary tau kinase involved in AD pathology (Figure 30).[89,93] GSK-3β is responsible for the hyperphosphorylation of the tau protein, which, as mentioned earlier, is responsible for the formation of neurofibrillary tangles, conferring it a fundamental role in the pathogenesis of AD.[94] Several reports in the literature indicate that the inhibition of GSK-3β reduces taupathy and degeneration in vivo.[90]

GSK-3β is also involved in the toxicity induced by the Aβ peptide through different mechanisms (Figure 30).[95] It regulates the production of Aβ peptide by affecting the function of presenilin 1 (PS1),[96] a component of the γ-secretase complex, and the enzymatic cleavage of APP mediated by BACE-1.[97] Additionally, the overexpression of NF-kB in patients with AD mediates the GSK-3β-induced expression of BACE-1.[98] It has also been observed that the Aβ peptide blocks the Wnt-mediated inhibition of GSK-3β, leading to an increase in Aβ peptide formation and hyperphosphorylation of the tau protein.[99]

GSK-3β is expressed in both microglia and astrocytes, where it promotes the production of cytokines such as IL-1, IL-6, and TN-α, and may contribute to the development and progression of neurological disorders, including AD, by regulating the neuroinflammatory process.[100–102]

Data from the literature indicates that GSK-3β plays a critical role in synaptic plasticity and memory formation. Indeed, GSK-3β phosphorylates and regulates the function of a large number of transcription factors that play critical roles in neuronal plasticity, such as NF-kB,[103] heat shock factor 1 (HSF1),[104] MYC,[105] and cAMP element-binding protein (CREB).[106] Additionally, GSK-3β is a critical regulator of the balance between long-term potentiation (LTP) and long-term depression (LTD).[92] In particular, it has been observed that the induction of LTP prevented LTD through the inhibition of GSK-3β, and GSK-3β inhibitors blocked the induction of LTD.[107]

GSK-3β also negatively regulates the β-catenin signaling that influences the size and strength of synapses. In fact, it phosphorylates β-catenin, leading to its degradation by the proteasome.[108] Additionally, the overexpression of GSK-3β impairs hippocampal neurogenesis in adults. GSK-3β is also involved in the degeneration of neurons due to the hyperactivation of NMDA receptors and subsequent accumulation of intracellular calcium.[109]

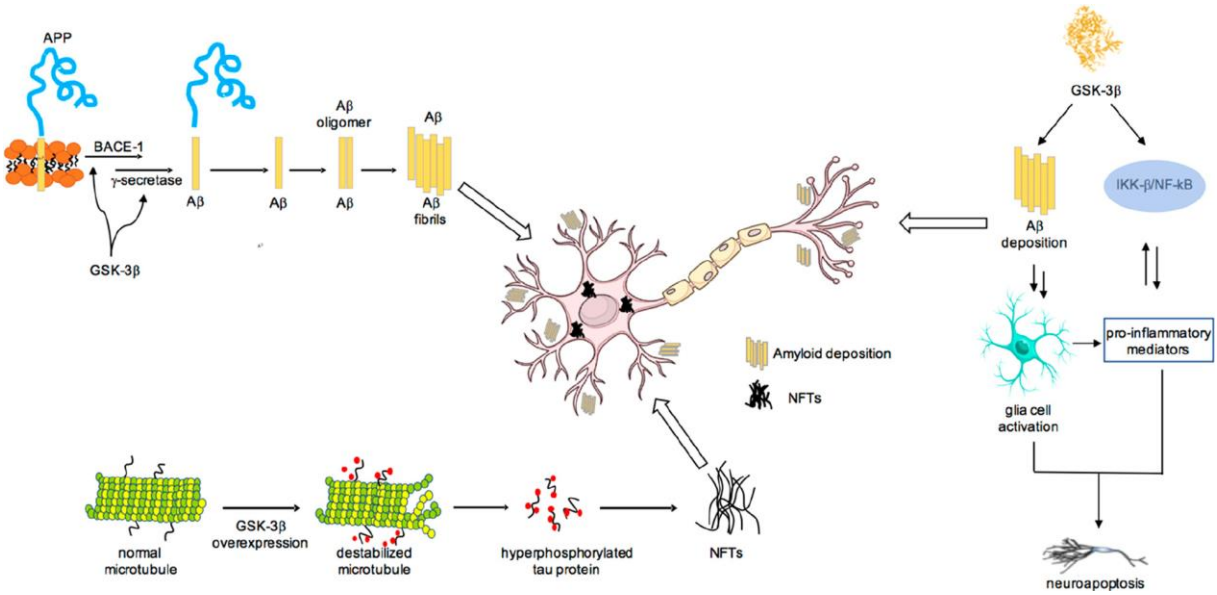

Figure 30. The involvement of GSK-3β in AD results from various activities, with the most significant ones reported in this figure. GSK-3β contributes to the production of amyloid deposits by affecting the function of presenilin 1 (PS1) and enzymatic cleavage of APP mediated by BACE-1; senile plaques derive from the abnormal extracellular accumulation and deposition of the Aβ peptide. GSK-3β is responsible for the hyperphosphorylation of tau protein and, consequently, the formation of neurofibrillary tangles (NFTs). GSK-3β is involved in neuroinflammation, promoting the production of cytokines in astrocytes and microglia. Reproduced from 110 (authors do not request permission) Copyright © 2020 American Chemical Society.

Among GSK-3β inhibitors, both small cations and organic compounds can be found. Lithium was the first GSK-3β inhibitor used in clinical practice to treat bipolar disorder and major depression.[111] Lithium prevents Aβ-induced toxicity and tau phosphorylation in cellular and in vivo models of AD and improves cognition in transgenic mice.[112] Different clinical trials have produced positive results in patients with mild cognitive impairment (MCI), where long-term treatment with lithium significantly reduced phospho-tau levels in cerebrospinal fluid and improved cognitive parameters.[112]

Organic inhibitors of GSK-3β can be of natural or synthetic origin and, in general, they vary widely in structure, spanning a broad range of chemical spaces.[113,114] Based on their inhibition mechanisms, they are commonly classified as either ATP competitive or non-competitive with ATP. Most inhibitors belong to the former group, acting by blocking the enzyme and competing with ATP for its binding site. These classes of compounds are often characterized by very high affinity, typically in the nanomolar concentration range. Selectivity over other kinases represents one of the main challenges associated with these compounds. Many competitive ATP inhibitors have been co-crystallized with GSK-3β, and their structures

resolved by X-ray crystallography. Therefore, designing new, highly selective competitive ATP inhibitors can be achieved using ligand-based and structure-based methodologies (LBDD and SBDD) based on the ligand's structure and resolved structures.

In relation to ATP competitive inhibitors, the class of amino/amido-azaheterocycles is widely described. Among these, acylaminopyridines have systematically explored their chemical space around the central spacer, leading to potent GSK-3β inhibitors in the single to subnanomolar range.[115] When orally administered in a transgenic mouse model of AD, compound **203** (IC_{50} = 1.1 nM) (Figure 31A) showed a significant reduction in Tau phosphorylation. This class can also be represented by compounds **204**, **205**, and **206**, which always have aminopyridine as the main core linked to substituted heterocycles (Figure 31A). This characteristic is based on the ability of aminopyridines to mimic ATP adenine binding to the catalytic site of GSK-3β through H-bonds with Val135 and Asp133, while their substituents seek to interact with Lys85 and Gln185, the triphosphate interaction region (Figure 31B).

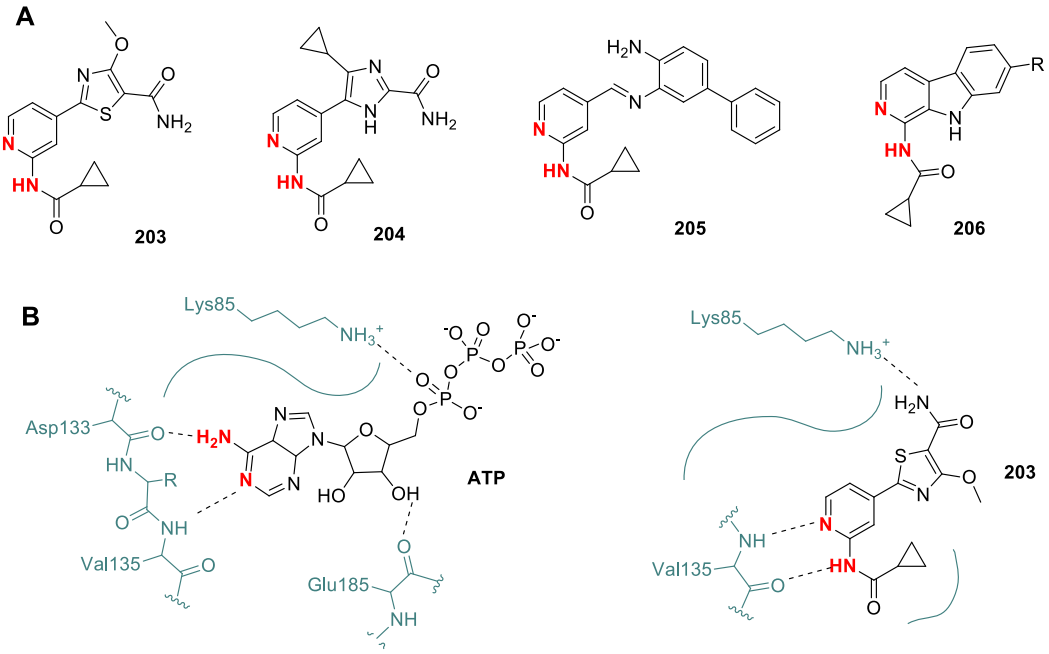

Figure 31. A- Competitive GSK-3β inhibitors of the aminopyridine class. B- Comparison of **ATP** and **203** interaction modes with the active site of GSK-3β.

Other classes, such as maleimides (**207**), have also been extensively explored as GSK-3β inhibitors[113] The maleimide scaffold can form key H-bonds with amino acids located within the enzymatic hinge region (the same site of ATP adenine interaction). Specifically, the nitrogen atom interacts with the carbonyl oxygen of Asp133, while one of the two carbonyl oxygens interacts with the nitrogen of the primary chain of Val135 (Figure 32).[116] Natural products from

the Paullone class, such as alsterpaullone (**208**), are another interesting class of competitive ATP inhibitors.[117] The crystal structure revealed that alsterpaullone can also establish H-bonds with Val135, while the nitro group forms additional H-bond interactions with Lys85.

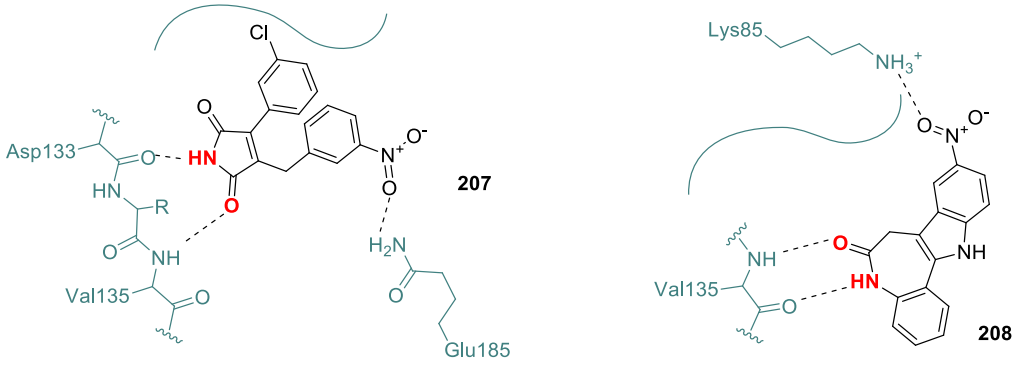

Figure 32. Competitive inhibitors of GSK-3β from the maleimide class (**207**) and paullones (**208**) and their modes of interaction with the active site of GSK-3β.

Comparing the interactions made by selective inhibitors highlights residues in the ATP binding site that can be targeted for inhibitor selectivity. The information obtained from these structures provides essential requirements for generating new GSK-3β inhibitors.

1.6. Contribution to Alzheimer's disease by Molecular Diversity and Medicinal Chemistry Laboratory (LaDMol-QM)

A series of alkylamino-indanones has been described in the literature and tested to assess their potential as anti-Alzheimer's disease agents. Most compounds in the series exhibited good inhibitory activity against AChE, with IC_{50} values in the nanomolar range, particularly **209** (IC_{50} = 17nM), showing significantly higher inhibitory activity than tacrine and similar to donepezil. Additionally, compound **209** significantly inhibited Aβ aggregation (85% inhibition rate), catalyzed the disassembly of Aβ fibrils, and exhibited antioxidant activity. Moreover, it demonstrated the ability to cross the blood-brain barrier in vitro.[118]

Based on the structural requirements for the selective inhibition of mixed-type AChE present in the alkylamino-indanone inhibitor (**209**), as well as the widespread use of coumarins as cholinesterase inhibitors,[119] our group designed new alkylamino-coumarin derivatives (Figure 33).[120] The design was based on: 1 – maintenance of the cyclic alkylamino group, responsible for interaction with the catalytic anionic site (CAS) of AChE, exploring ligands of

different lengths (2-6); 2 – replacement of the indanone core with coumarin through non-classical ring expansion isosterism; 3 – the use of hydrophobic groups at position 3 of coumarin, aiming for interactions with the peripheral anionic site (PAS) of AChE (Figure 33).

All planned compounds (**210a-d**) were effective for AChE inhibition, with potencies in the nanomolar range. The compound 3-(4-(dimethylamino)phenyl)-7-aminoethoxy-coumarin (**210c**) showed good AChE inhibition potency (IC_{50}= 20 nM) and selectivity (IC_{50} BuChE/AChE= 354), very similar to the reference drug donepezil (IC_{50}= 6 nM; IC_{50} BuChE/AChE= 365), in addition to having antioxidant properties, low cytotoxicity, and good predicted ADMET properties.[120]

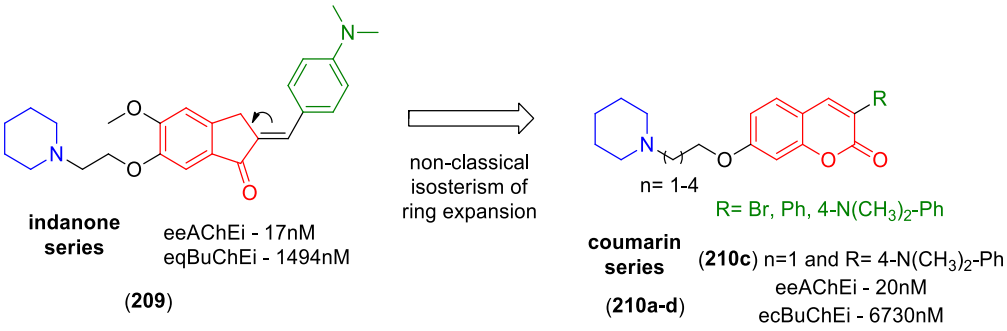

Figure 33. Design of alkylamino-coumarin cholinesterase inhibitors series.[120]

Derivatives of vicinal diaryl triazine have been described in the literature as suppressors of ROS generation and cell death induced by oxidative stress, as well as inhibitors of cholinesterases (ChEs) and potent neuroprotective agents.[121]

Based on the literature, our group developed a series of 3-amino-1,2,4-triazole-N-1,5-trisubstituted compounds (**213a-d**) planned through the bioisosterism strategy,[122] which allowed the isosteric exchange of the triazine core (**211**) for the 1,2,4-triazole; and molecular hybridization,[123] which united the benzylpiperazine subunit (purple) (**212**), capable of mimicking the pharmacophoric group of the drug donepezil, responsible for interacting with the catalytic anionic site (CAS) of the AChE enzyme; and the vicinal diaryl group (blue) (**211**), described as capable of interacting with the peripheral anionic site (PAS) of AChE. Additionally, the exploration of the distance between the triazole and the cyclic amine in the hydrophobic cavity of acetylcholinesterase was proposed. This study resulted in a series of compounds (**213a-d**) capable of inhibiting cholinesterases with good IC_{50} values of up to 1 μM, showing a mixed-type enzymatic inhibition mode, i.e., proving the simultaneous interaction of the CAS and PAS sites, with the compound containing 3 methylene carbons as a spacer being the most active (**213a**) (Figure 34).[57]

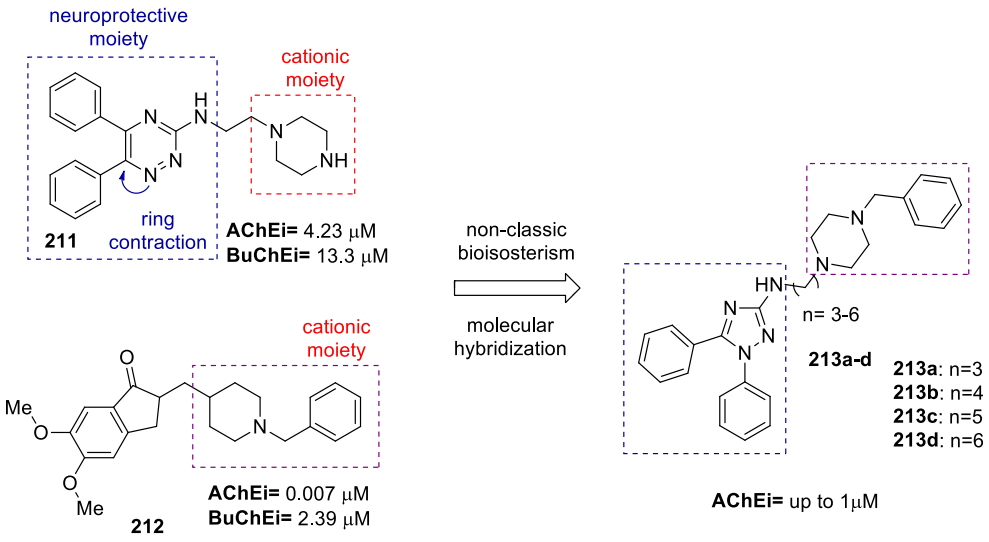

Figure 34. Design of the series of 3-amino-1,2,4-triazole-N-1,5-trisubstituted compounds (**213a-d**).[57]

These interesting results with trisubstituted 1,2,4-triazoles led us to propose this less commonly used structure from a pharmacological perspective over other enzymes.

2. OBJECTIVES

2.1. General objective

This project aims at the design, synthesis and pharmacological evaluation of three series of new trisubstituted 1,2,4-triazoles as competitive inhibitors of GSK-3β.

2.2. Specific objectives

- Synthesis development and characterization of the three designed series of 1,2,4-triazole compounds;
- *In vitro* evaluation of the designed compounds on GSK-3β inhibition model;
- Comparison of the *in vitro* results versus molecular modeling analyses aiming to understand how the compounds interact with the enzyme.

3. RESULTS AND DICUSSION

3.1. Structural Design of 1,2,4-triazoles as GSK-3β inhibitors

Our structural design was based on the three series previously described (amino-pyridines – **203-206**, maleimides **- 207**, and paullones – **208**, see Figure 31 and Figure 32), aiming at the design of new classes of iGSK-3β compounds.

The first series of compounds (**A**) (Figure 35A) was based on two classical bioisosterism: (**a**) of amino-pyridine (pyridine → 1,2,4-triazole), and (**a'**) of imidazole (imidazole → phenyl). In this case, the 3-amino-1,2,4-triazoles could mimic interactions with the adenine site, similar to amino-pyridines (**204**). In red, potential interaction sites with Val135 are highlighted. The transposition of the functional group in **b** was guided by synthetic route principles and the possible exploration of a hydrophobic cavity in the region. The R group in this case could be alkyl and aromatic groups.

The second series (**B**) focused on the class of maleimides (**207**), which exhibit interactions at the adenine site with Val135 and Asp133 through hydrogen bonds. For series **B**, the modification of maleimide by 1,2,4-triazole was envisaged, aiming at maintaining exactly the same interactions highlighted by the atoms in red with Val135 and Asp133. Additionally, the transposition of the functional group in **e** would maintain interactions with the same hydrophobic cavity as the prototype **207**.

Finally, the third series (**C**) was proposed based on alsterpaullone (**208**), through classical bioisosteric substitutions of pyrrole by 1,2,4-triazole in **c**, and non-classical ring-opening in **d**. With the potential spatial difference between the rings in **d**, functional groups such as amides, nitro, and carboxylic acid can be explored at positions 2, 3, and 4 of the ring, aiming for interactions via hydrogen bonding with Lys85.

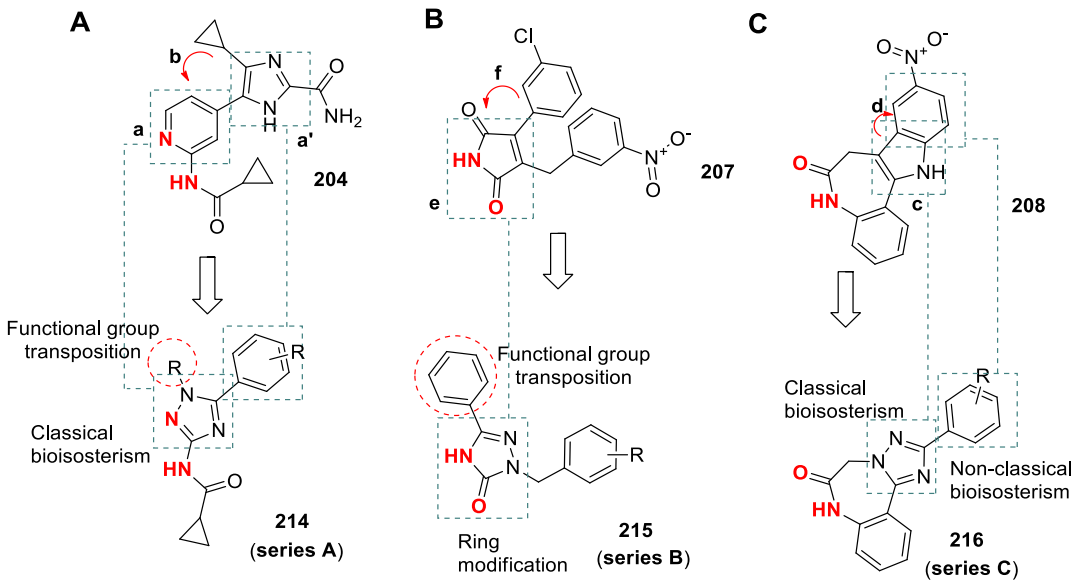

Figure 35. Structural planning of 1,2,4-triazoles as GSK-3β inhibitors.

To corroborate the structural design, molecular *docking* analyses were used to theoretically verify whether the interaction prerequisites with the active site of GSK-3β, discussed above, could be observed. For the analyses, compounds **214**, **215**, and **216** were used, in addition to their corresponding prototypes **204**, **207**, and **208**.

The *docking* results indicated that the designed planned compounds can make the main interactions of their prototypes, as predicted by the structural planning. Additionally, the score values obtained for compounds **215** and **216** were quite similar to their direct prototypes, while compound **214** showed a significantly higher value, suggesting that perhaps the transposition of the functional group could lead to better interactions in the hydrophobic cavity.

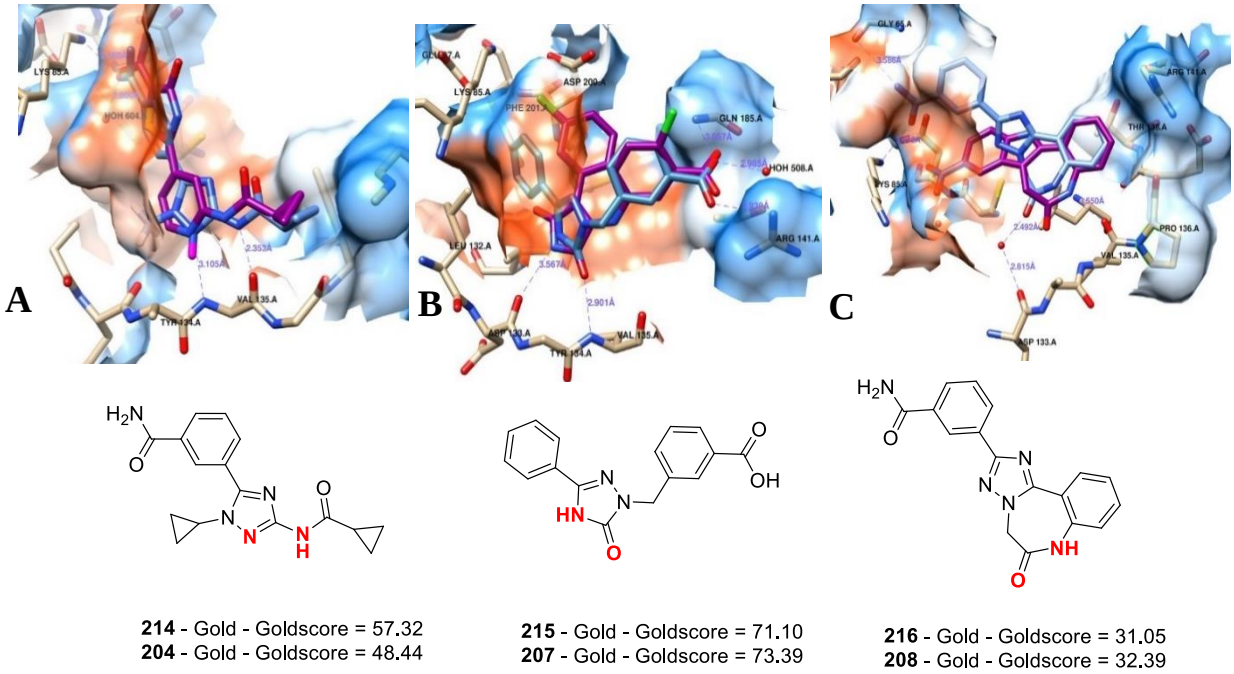

Figure 36. Comparison of molecular dockings at the active site of GSK-3β between the prototypes amino-pyridine (**204**), maleimide (**207**) and alsterpaullone (**208**) with compounds **214** (**A**), **215** (**B**), and **216** (**C**). Results obtained using Gold software and PDBs 4PTC (**A**), 1Q4L (**B**), and 1Q3L (**C**).

3.2. Synthetic Design of the series A (214)

To obtain the series A, we envisioned the Buchwald-Hartwig or Ullmann reactions as an efficient way for the introduction of amides in position 3 of the key intermediate **217** (Scheme 40). The Buchwald-Hartwig reaction ([(cinnamyl)PdCl]$_2$, t-BuXPhos, t-BuONa in MePh or [Pd(Cl)(C$_3$H$_5$)]$_2$, AdBrettPhos, CsCO$_3$ in 2-Me-2-BuOH at 100°C for 20h) did not show reaction, while the Ullmann procedure (CuI, DMCyDA, K$_3$PO$_4$ and sodium ascorbate in toluene or H$_2$O:EtOH at 100°C for 5h) showed the formation of the expected compound **218** in the presence of a mixture of products by HPLC (see chapter 1, Table 10).

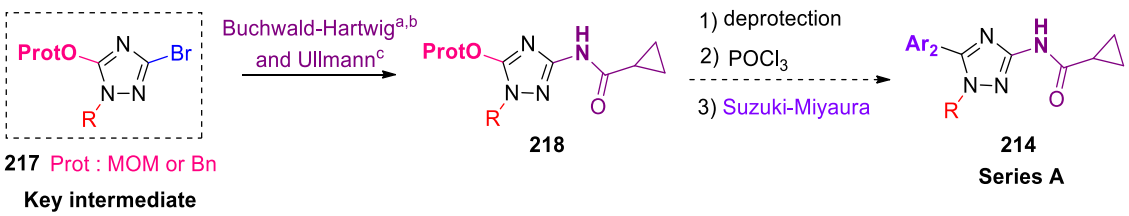

Scheme 40. Proposed synthesis of the **series A**. Buchwald-Hartwig conditions: (a) [(cinnamyl)PdCl]$_2$, t-BuXPhos, t-BuONa in MePh for 20h, Prot: Bn; (b) [Pd(Cl)(C$_3$H$_5$)]$_2$, AdBrettPhos, CsCO$_3$ in 2-Me-2-BuOH at 100°C for 20h, Prot: Bn; Ulmmann conditions: (c) CuI, DMCyDA, K$_3$PO$_4$ and sodium ascorbate in MePh at 100°C for 5h, Prot: Bn.

Due to the need to improve the cross-coupling procedure to react 3-bromo-1,2,4-triazole with amides, but facing the lack of catalysts and properly conditions to work with this type of reaction during the internship in Italy, we decided to work with a classical and non-convergent synthetic route to obtain the series A. The synthetic route was based on previous results from LaDMol-QM, which described the development of an efficient protocol for regioselective synthesis of 1,5-diaryl-3-amino-1,2,4-triazoles derivatives (**214**), starting from N-acyl-N-Boc-carbaimidothiates with low reaction times and moderate yields.[57] These studies demonstrated the importance of the labile *tert*-butoxycarbonyl (Boc) group, also electron-withdrawing, attached to the subunit -C=NH(S-CH_3), for regioselectivity and increased reactivity.

Therefore, starting from an amide coupling (step a) and followed by a hydrolysis reaction (step b) and subsequent C-N disconnection (step c), the compound 3-amino-1,2,4-triazole (**220**) and cyclopropanecarbonyl chloride (**219**) are identified as precursors, with this step being provided by the carbonyl substitution reaction.

The precursor 3-amino-1,2,4-triazole N-Boc (**221**) was identified with the presence of the -Boc protecting group through FGI. This step occurs through the deprotection reaction (step d). Thanks to a C-N disconnection (step e) and a C=N disconnection (step f) of the five membered triazole, it was possible to identify the two key intermediates: the N-acyl-S-methylisothiourea (**223**) as an 1, 3-dielectrophile and the commercially available p-tolylhydrazine as the 1, 2-dinucleophile. However, to significantly increase the reactivity of the electrophile, the introduction of a Boc group is required leading under basic medium to a carbodiimide (**224**).

Next, through another C-N disconnection (step g), the precursors identified were N-Boc-2-methylisothiourea (**227**) and benzoyl chloride (**225**), this step being obtained via acylation reaction. Through FGI, commercial p-cyanobenzoic acid (**226**) was identified as a precursor to acid chloride (**225**).

Starting from a C-N disconnection, 2-methylisothiourea (**228**) was identified as a precursor, obtained through protection reaction with the Boc group via a conventional acylation reaction. Finally, an S-C disconnection (step j) highlights thiourea (**229**) and methyl iodide (**230**) as precursors of 2-methylisothiourea, by exploring the bimolecular nucleophilic substitution reaction (Scheme 41).

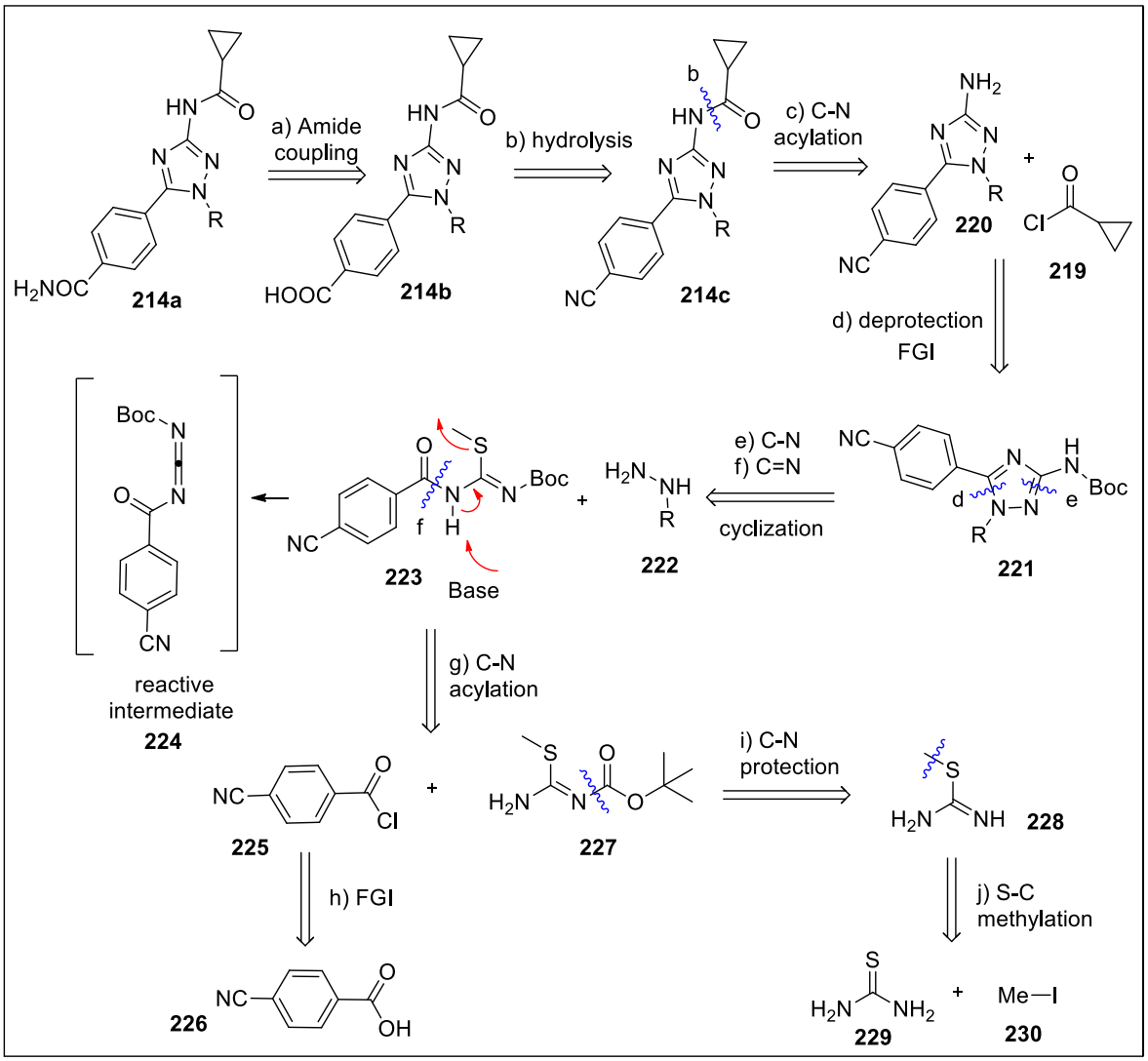

Scheme 41. Initial retrosynthetic analysis for the preparation of series A.

3.3 Synthesis of the series A (214)

3.3.1. Use of Aryl hydrazine derivatives

The first step for the synthesis of series A started with the synthesis of S-methylisothiourea (**228**) according to the procedure described by Hickey et al.,[124] by means the alkylation of thiourea (**229**) with methyl iodide followed by precipitation and filtration (99% yield). The second step was the synthesis of N-Boc-S-methylisothiourea (**227**) reacting **228** with di-tert-butyl dicarbonate in DCM at room temperature, furnishing a white solid in 83%. The presence of the Boc protecting group is essential for the following steps, since as described by our group in Brazil, this o t-Bu residue not only increases reactivity and regioselectivity, but is also easily deprotected to lead to the free amine.[57] Subsequently, N-Boc-2-methylisothiourea

(**227**) was reacted with 4-cyanobenzoyl chloride in DCM at r.t. for 24 hours, leading to the desired intermediate **223** in 82% yield (characteristic NMR peaks from aromatic AB system at 7.7 and 8.3 ppm were found). We started the cyclocondensation step with appropriate aromatic hydrazine derivatives (tolyl-hydrazine) using the literature procedure (same temperature: 100°C; and solvent: i.e. MeCN, same time: 2h).[57] In our hands, these conditions were not efficient. Beside a large amount of the starting material, we observed the formation of the expected Boc-triazole but also the deprotected triazole (**220**). Aiming the complete consumption of **221**, the reaction time was increased to more 14 hours leading directly to the deprotected products **220** (79%). The acylation of **220** was performed with cyclopropanecarbonyl chloride, pyridine as base and DCM as solvent at room temperature. After 7.5 hours the complete consumption of **220** was observed furnishing **214c** in 46% yield (characteristic NMR peaks from aromatic AB system at 7.6 and 7.2 ppm, methyl group at 2.4 ppm, -NH at 8.4 ppm and cyclopropyl at 0.8-1.3 pmm were found).

In a first attempt of the conversion of the nitrile group to carboxylic acid, cpd **214c** was treated with a large excess of base at reflux. The reaction medium was able to hydrolyze the nitrile but, unfortunately, also the cyclopropanecarboxamide group, leading to **231** in 89% yield. Finally, due to the low solubility of **231**, the first attempt of acetylation using the same conditions describe before (cyclopropanecarboxamide (1.2 eq.), Py (2.5 eq.), DCM at r.t for 7.5 h) was unsuccessful. Consequently, the reaction was performed with cyclopropanecarbonyl chloride in pyridine at reflux, leading to **214b** in 35% yield after purification (Scheme 42).

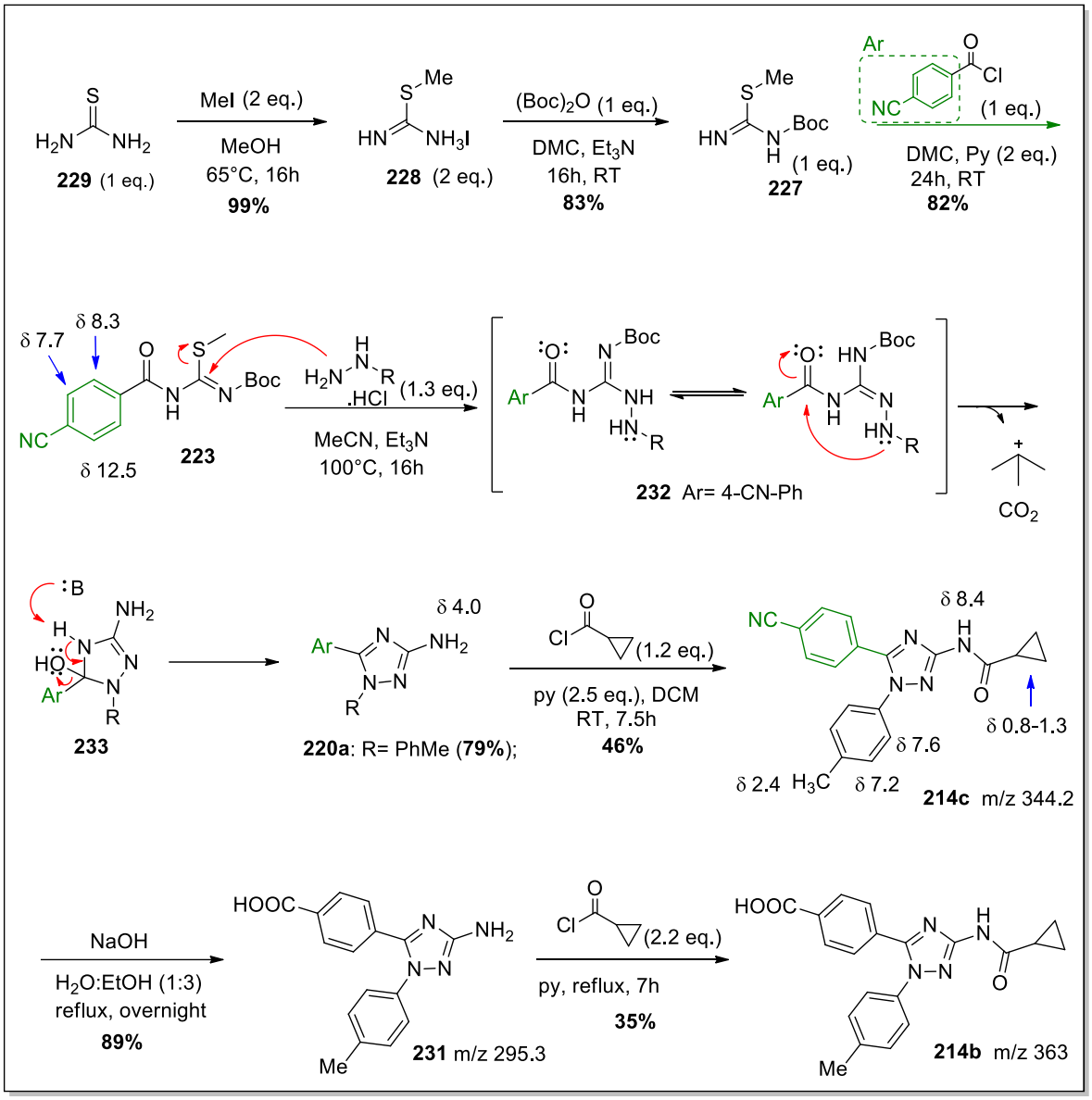

Scheme 42. Synthesis and scheme of intermediates to obtain series A.

3.3.2. Use of aliphatic hydrazine derivatives

The use of aliphatic hydrazine for the construction of N_1-alkyltriazole-amine is much less investigated in the literature; to our knowledge, only one paper and a few patents are available.[125–128] In the first example, the authors described the cyclocondensation reaction of symmetric S-methyl thiourea (**234**) with benzyl hydrazine (**235**), unfortunately the yield is not available (Scheme 43, A)[127]; Bartolozzi et al.[126] described the use of ethyl hydrazine oxalate (**238**) starting from 1-benzyloxycarbonyl-3-(4-methoxy-benzoyl)-2-methyl-isothiourea (**237**) in DMF with the help of DIPEA, the target N_1-ethyl triazole was obtained in 95% yield.

Unfortunately, the deprotection of the benzyloxycarbonyl group was much more laborious as the free amino triazole was only reached in 25% yield (Scheme 43, B(1)). The use of Hydroxyethylhydrazine (**241**) in scheme 43, B(2) allowed the formation of the corresponding N_1-substituted triazoles (**242**) in 55% yield.[128] Finally, from a more hindered hydrazine, isopropyl hydrazine hydrochloride (**244**), the expected aminotriazole (**245**) was isolated in 49% yield (Scheme 43 B(3)).[129] It should be noted that in all these examples, the reaction is regioselective, none of the papers mention the presence of a second regioisomer. Examples of cyclocondensation reaction of S-methylthiourea with methyl hydrazine were not found.

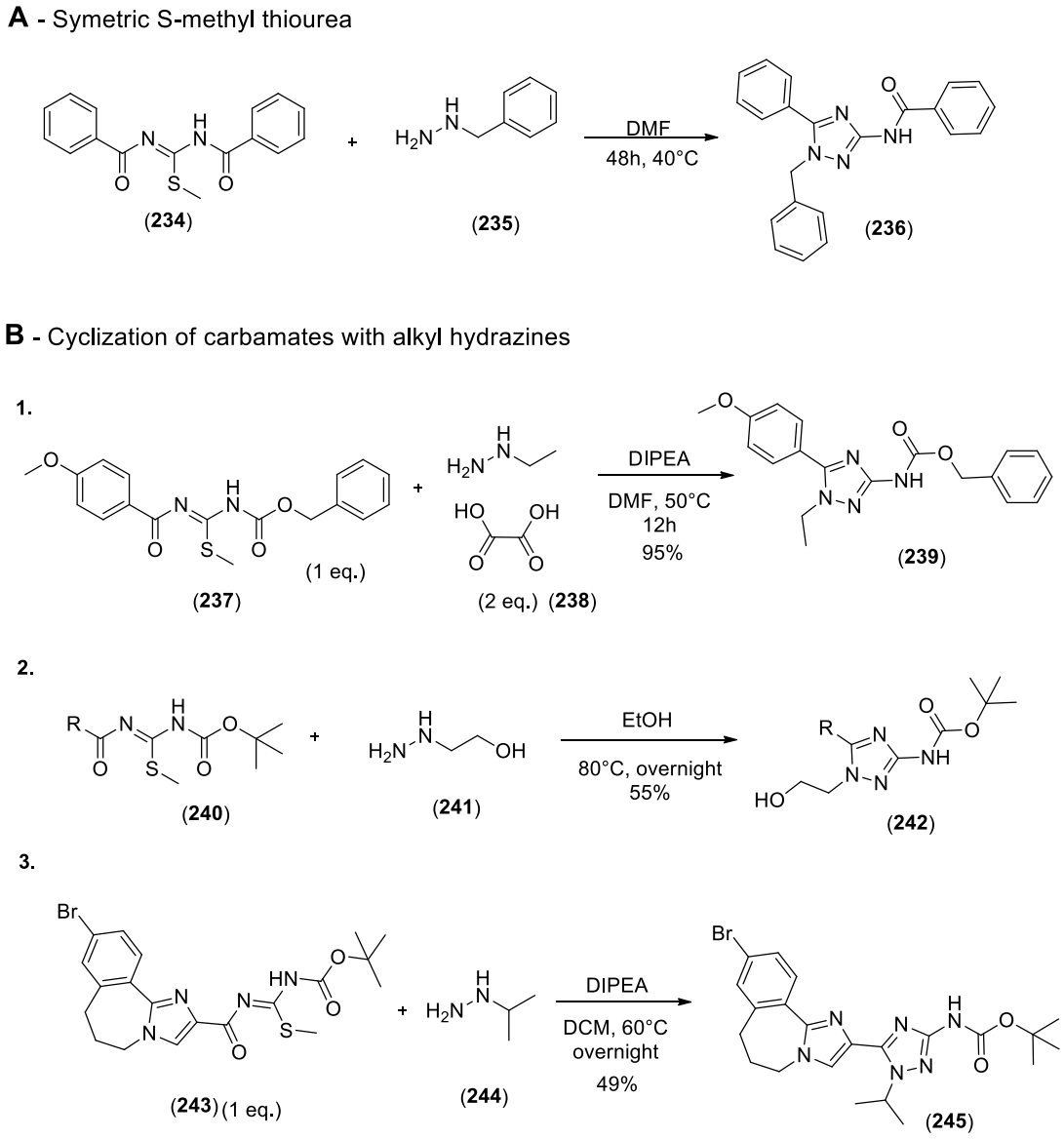

Scheme 43. State of the art of the synthesis of 1,2,4-triazoles using alkylhydrazines.

As mentioned in chap I, another route for the preparation of 1-phenyl-3-Aryl-1H-1,2,4-triazol-5-amine (**248**) is highlighted in the literature involving a cyclisation reaction of N-cyanobenzimidates (**246**) with arylhydrazine derivatives (Scheme 44). This method has several advantages, including efficient one-pot procedure for the cyanoimidation of aldehydes, mild conditions for the cyclisation and high yields.[125] However, only one example described the preparation of 1-Methyl-5-phenyl-1H-1,2,4-triazol-3-amine (**249**) by refluxing N-Methylhydrazine in MeOH with Methyl N-cyanobenzimidate (**246**).[130] Formation of the latter product results from the attack of the secondary amine (NHMe) on N-cyanobenzimidate and leads to the N-Me triazole derivative in 50% yield. However, the authors do not report the formation of a regioisomer.

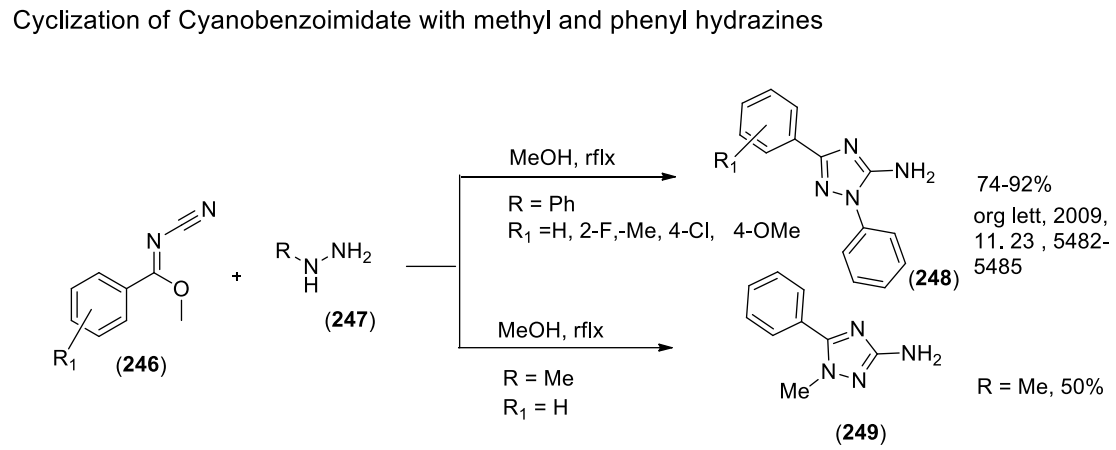

Scheme 44. Synthesis of 1,2,4-triazoles by cyclization reaction of N-cyanobenzimidates with alkyl- and arylhydrazines.

The lack of data encouraged us to conducted tests on the cyclocondensation reaction of compound **223** with alkyllhydrazines. We choose two alkylhydrazine derivatives: the cyclopentyl hydrazine and methylhydrazine.

We started the cyclocondensation step with appropriate alkyl hydrazine (cyclopentyl hydrazine hydrochloride (1.5 eq.)) using our optimized procedure (i.e. Et_3N (2.2 eq.), MeCN, reflux, 13h). We observed the formation of the expected deprotected triazole (**220**) by LC/MS. The desired product was obtained in 40% after purification by chromatograph column (Scheme 45). Given the size of hydrazine's cyclopentyl group, it seems obvious that hydrazine will react with its primary amine function.

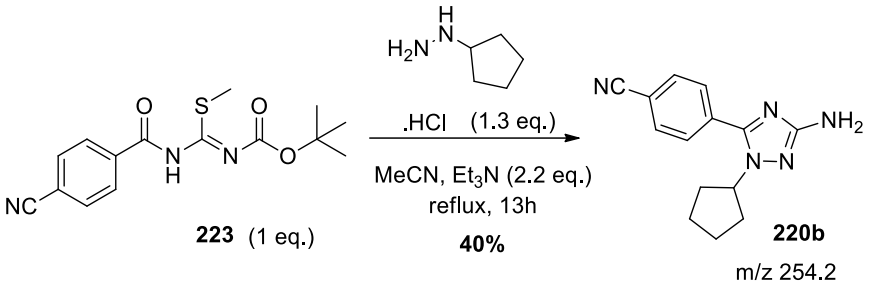

Scheme 45. Synthesis of amino-1,2,4-triazoles by cyclization reaction of S N-Boc-S-methylisothiourea **223** with cyclopentyl hydrazine.

In the first assay for cyclocondensation of N-Boc-S-methylisothiourea (**223**) with methylhydrazine, we applied reaction conditions similar to the previous described by our group in Brazil (Figure 34); however, after 1 hour, the formation of a non-cyclized major product was observed by TLC (RF= 0.23, PE/EtOAc – 50/50) (Table 14, Entry 1). The isolated product demonstrated low solubility and was characterized as **250** or **251** by LC/MS and NMR. The NMR characterization revealed the presence of hydrazine protons as broad singlets at 7.86 and 8.41 ppm, which may indicate that methyl hydrazine reacted first with the secondary amine function to give of the regioisomer **250**. In a second assay, we increased the reaction time to 16 hours, the Et_3N concentration and the temperature to 120°C, which promoted greater formation of the cyclization product. Due to the presence of a mixture of products, the crude material was subjected to a deprotection reaction in TFA for 3 hours. The cyclization product **220c** or **251** was isolated in 36% yield after purification (Table 14, Entry 2). NOESY analyses, will be conducted soon to determine which regioisomer was obtained. Subsequently, we performed new tests using the protocol described in Scheme 43 (Table 14, Entry 3) (methyl hydrazine (2.5 eq.), DIPEA (2.5 eq,), DMF, 50°C, 12h); however, a large mixture of products was observed by LC/MS. Due to the absence of acid in our system, which was present in the reference (Scheme 43, B(1))[126] we added 10 mol% of PTSA and increased the temperature to 100°C for an additional 30 hours (Table 14, Entry 3). Unfortunately, due to the presence of a mixture of compounds with the same RF, we were unable to adequately separate the desired product.

Table 14. Optimization conditions for cyclocondensation with methyl hydrazine.

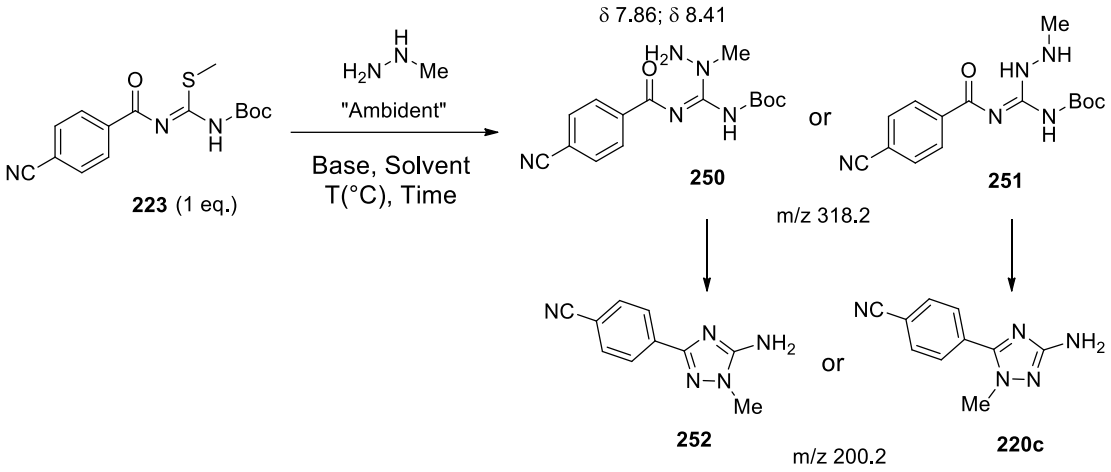

Entry	$CH_3(NH)NH_2$	Base	Eq. Base	Solvent	T(°C)	Time (h)	Yield 250 or 251 (%)	Yield 252 or 220c (%)
1	1.1	Et_3N	1	MeCN	100	1	60	-
2[a]	1.3	Et_3N	2.1	MeCN	120	16	-	36
3[b]	2.5	DIPEA	2.5	DMF	50	12	-	-

[a] TFA, 3h, RT; [b] PTSA (10 mol%), 100°C, 30h.

In the next step, regardless of the regioisomer **252** or **220c** formed, we were interested in the corresponding acylation product **253 or 214c** with cyclopropanecarbonyl chloride. Due to the low solubility of the nucleophile, we adopted the same acylation protocol used for amino triazole **231**, employing pyridine as the solvent at 120°C for 16 hours (Table 15, Entry 1). The use of basic solvents such as DMF and DMSO was also investigated (Table 15, Entry 2 and 3); however, unfortunately, all attempts to acylate **252** or **220c** were unsuccessful.

Table 15. Acylation reaction attempts.

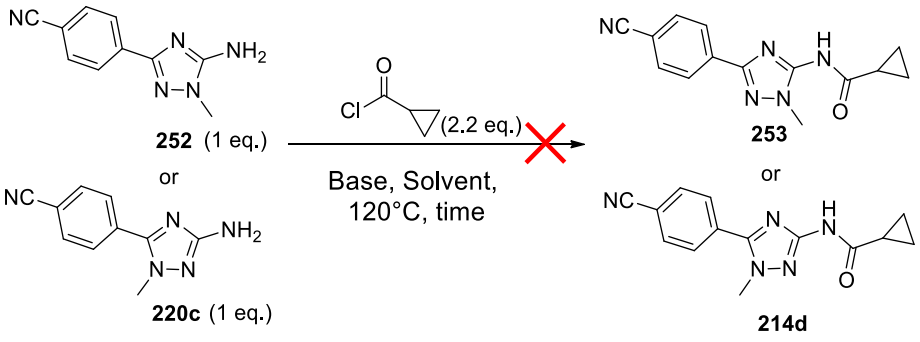

Entry	Base (2.5 eq.)	Solvent	Time (h)
1	-	Py/dioxane	16
2	Py	DMF	16
3	Py	DMSO	2

Due to challenges encountered during the acylation reaction of **252** or **220c**, we decided to modify the synthetic route in an attempt to obtain the acyl-triazole (**214d**). The synthesis was carried out via two different synthetic routes starting from N-Boc-S-methyl thiourea (**227**) (Scheme 46). In both routes, the first step involved the acylation of **227** with *p*-cyanophenyl and cyclopropane carbonyl chlorides. The second step consisted of deprotecting the Boc group using TFA, followed by a new acylation step with *p*-cyanophenyl and cyclopropane carbonyl chlorides. Finally, compound **257** underwent cyclization reaction with methylhydrazine. After 5 hours of reaction, we observed the predominant presence of the unreacted **258** or **259** product by LC/MS. The crude product was refluxed in toluene for an additional 16 hours, and even after this period, we observed the presence of **214d** or **253**/**258** or **259** in a ratio of 1/12 by LC/MS.

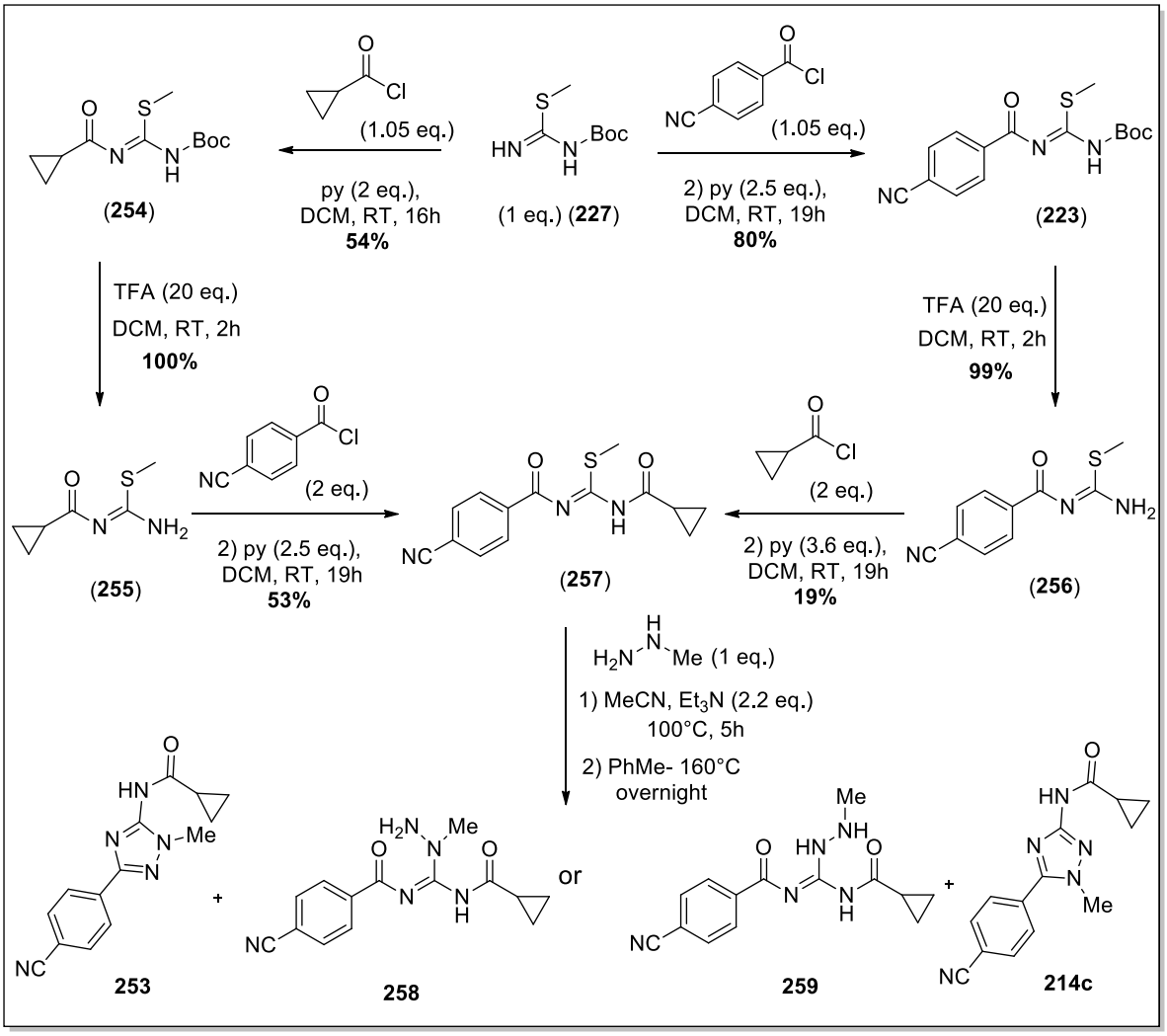

Scheme 46. Synthetic route to obtain **253** or **214c**.

Therefore, using the classical and non-convergent synthetic route to obtain series A, we have so far obtained only 2 final compounds, **214a** and **214b**. We intend to invest in the synthesis of this series using cross-coupling reactions in the future. We plan to abandon the desymmetrization strategy involving the introduction of MOM or Bn protecting group. We prefer a more convergent method, utilizing a common intermediate, compound **260**, resulting from the Suzuki-Miyaura reaction using (3-(tert-butoxycarbonyl)phenyl)boronic acid, and conducting the Ullmann reaction with cyclopropanecarboxamide followed by deprotection and amine coupling with NH_3 in methanolic medium (Scheme 47).

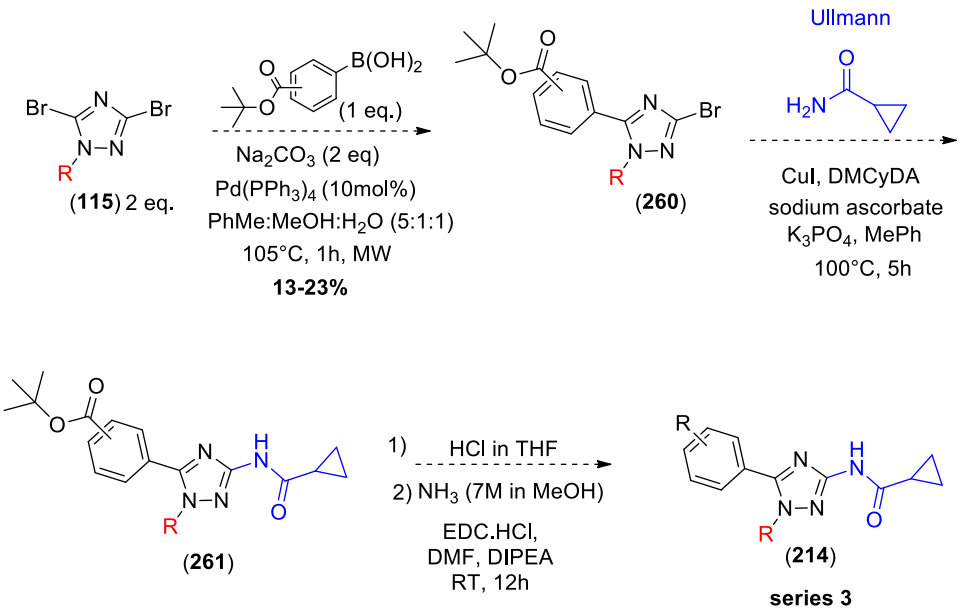

Scheme 47. Designed synthetic route to obtain series 3.

3.4. Synthetic design of the series B (215)

The good results obtained for the regio- and chemoselective derivatization of 1,2,4-trisubstituted triazoles encouraged us to prepare the compounds of the series B starting from commercially available 3,5-dibromo-1,2,4-triazole. To achieve this, we applied the desymetrization method discussed in Chapter I, introducing a triisopropyl sulfonyl group (TIPS) onto the triazole ring via the formation of N-substituted 3-bromo-1,2,4-triazol-5-one as the key intermediate **265**. The latter **215** is readily obtained by SNAr using NaOH. We have chosen to use the cyano group as a carboxylic group precursor as the 2-bromomethylbenzonitrile could be converted easily to the corresponding ethyl carboxylate or carboxylic acid (Scheme 48).

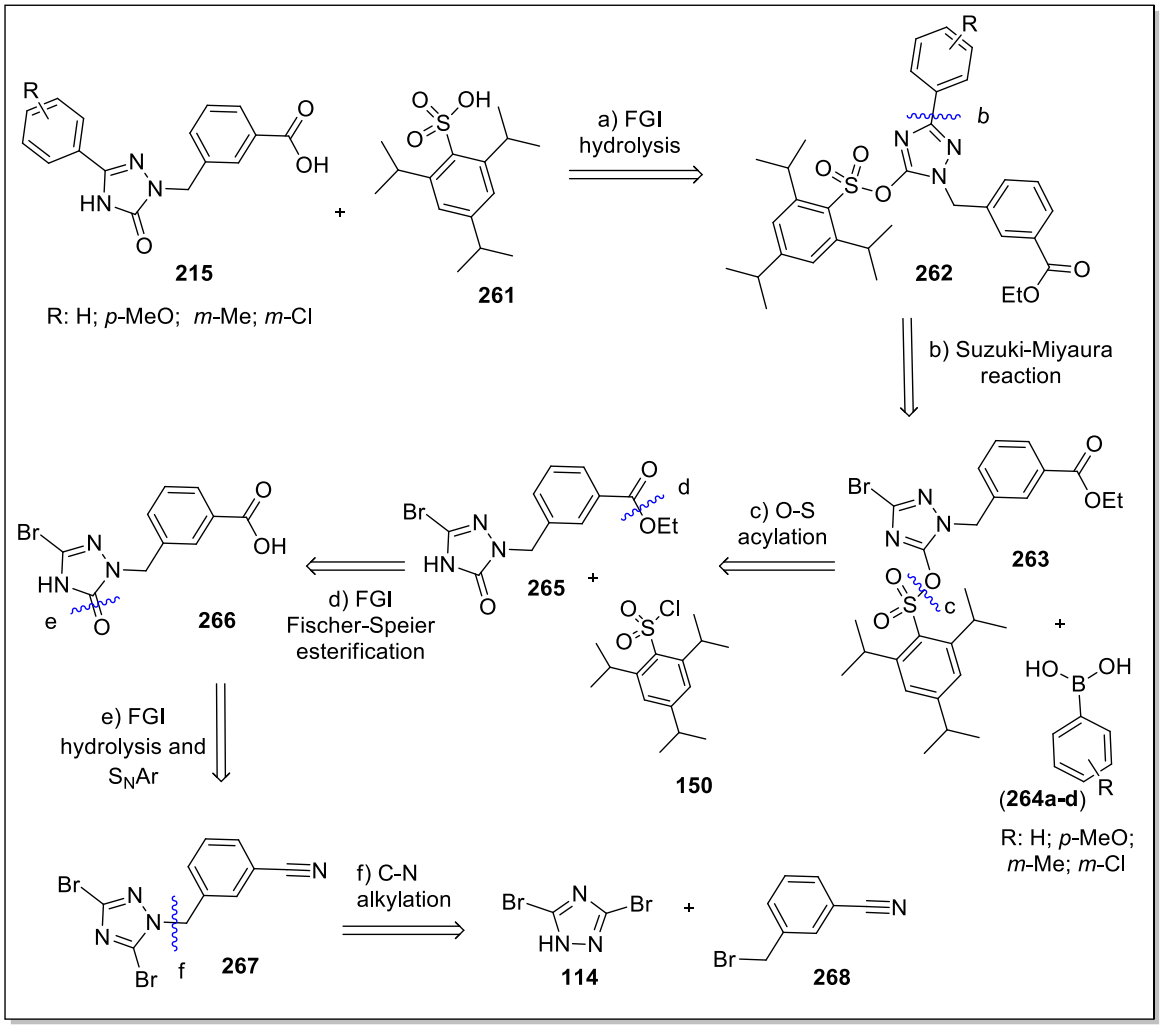

Scheme 48. Retrosynthetic analysis for the synthesis of series B.

3.5. Synthesis of the series B (215)

The synthesis of the series B started with the N-alkylation of **114** with 3-(bromomethyl)benzonitrile to give **267** in 79% yield (characteristic NMR peaks from -CH_2 at 5.3 ppm and aromatic ring between 7.50-7.68 ppm were found). Under reflux in an aqueous NaOH solution, we envisioned that compound **267** might undergo 2 simultaneous transformations: hydrolysis of iminobromide and conversion of the cyano group to carboxylic acid. However, even after 19h, a mixture of products **269** and **266** in a 1:1 ratio was observed. Both showed hydrolysis of the iminobromide, but only **266** underwent conversion of the cyano group to carboxylic acid. Then, Fischer-Speier esterification was applied to the mixture to obtain **265** in 94% (characteristic NMR peaks from ethyl group at 1.4 and 4.4 ppm and -OH at 11-13 ppm were found). The TIPSO derivative **263** was obtained in 84% yield using the same

procedure then described before in chapter I (TIPSCl and NEt_3 in DCM at room temperature). The Suzuki procedure was successfully applied in presence of various aryl boronic acids using tetrakis(triphenylphosphine)palladium(0) as the catalyst in a mixture of toluene-ethanol and water to afford **262a-d** in good yields ranging from 55-98% followed by the final stage of the synthesis which involves both the cleavage of the tri-isopropyl sulfone group and the saponification of the ester function (characteristic NMR peaks from carboxylic acid and N=C-OH at 12.4 and 13 ppm were found from). To achieve these goals, we used an aqueous solution of NaOH in dioxane-ethanol leading to **215a-d** in good to excellent yield (83-99%) (Scheme 49).

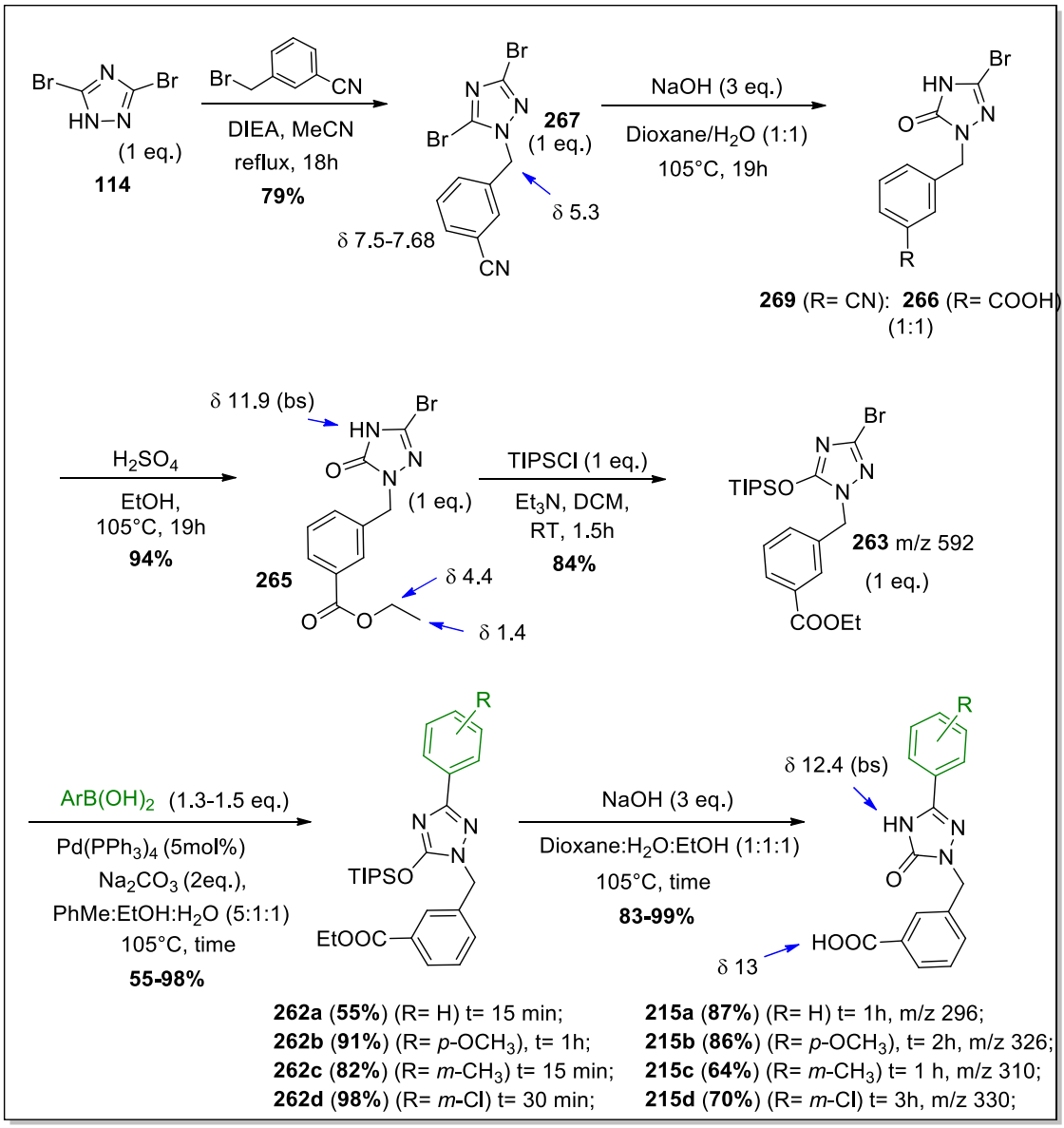

Scheme 49. Synthetic route and scheme of intermediates to obtain series B.

3.6. Synthetic Design of the series C (216)

From a retrosynthetic point of view, starting from the diazepine series (**216a-e**), sequential saponification (b) and amide coupling (a) could result in the derivatives **246h-i** and **216j-k**, as well as the demetilation reaction (c) in **216f-g**. The 2-aryltriazolo diazepinone series (**216a-e**) could result from a Suzuki-Miyaura reaction involving 2-bromotriazolo diazepinone (**271)** and variously substituted boronic acids (step d). This reaction intermediate **272** itself could result from a Suzuki-Miyaura reaction involving 2 -aminophenyl boronic acid (step f).

Given that the molecular diversity is driven by the aryl in position 3, the use of the desymetrization method involving the introduction of a tri-isopropylsulfonyl is less suitable. We preferred a more convergent method, using a common intermediate, compound **271**, resulting from the Suzuki -Miyaura reaction using 2-amino boronic acid, and conducting the 2nd Suzuki reaction using various boronic aryls just prior to the cyclization step (Scheme 50).

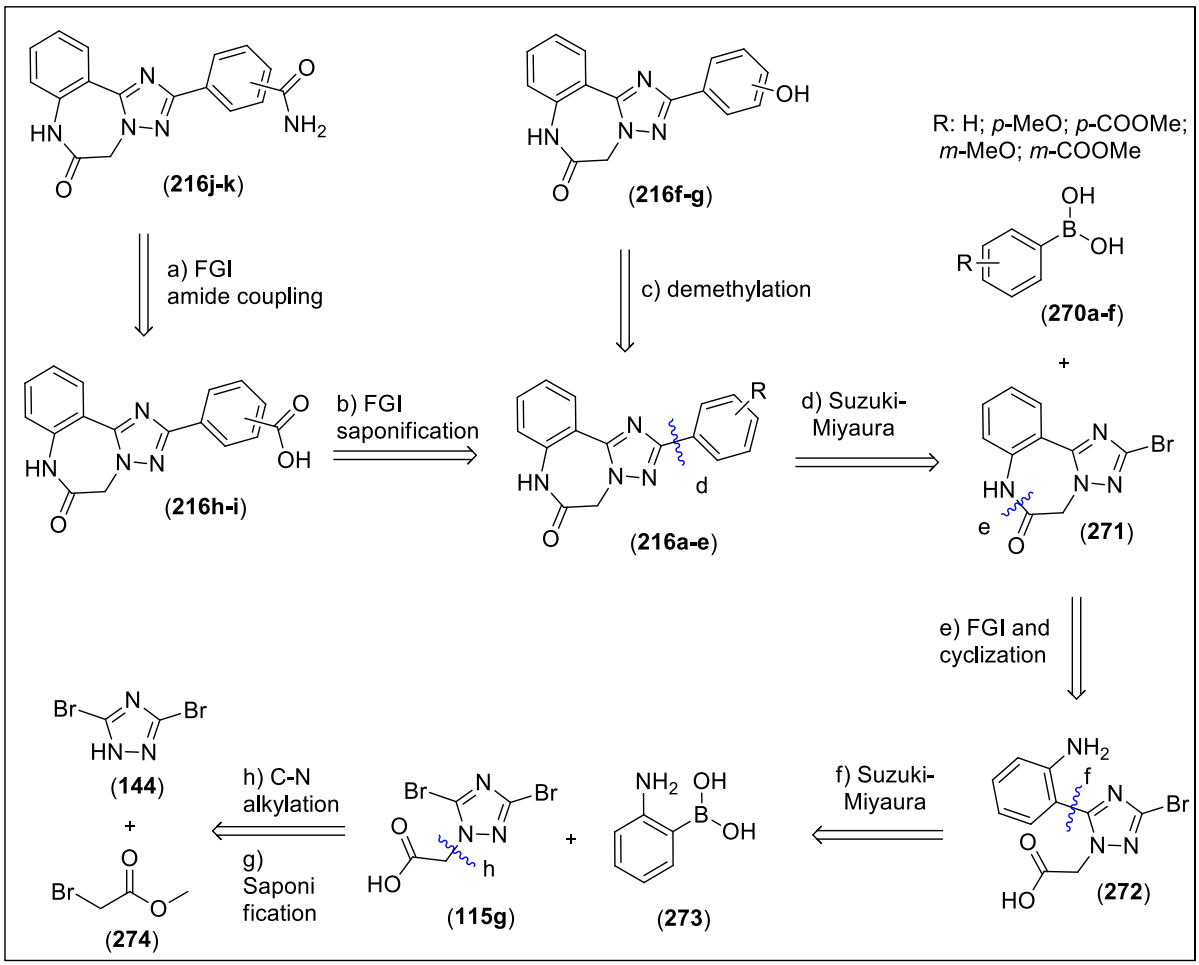

Scheme 50. Retrosynthetic analysis for the synthesis of compounds in series C (**216a-k**).

The Suzuki procedure involving 2-amino boronic acid (step f), an *ortho*-substituted boronic acid, led us to imagine the possibility of higher selectivity for the formation of the C-3 substituted product (**275**) compared to the desired arylated product at C-5 (**272**) due to steric hindrance. Therefore, we conducted a test using compound **115g**, described in the literature for the formation of a palladacycle that generates a favorable effect for C-5 arylation (see chapter 1, Scheme 25) using the same protocol described by the authors,[131] and comparing it to the classical protocol we previously used, but with stoichiometric amounts of reagents (Table 16).

Table 16. Optimization conditions for Suzuki-Miyaura reaction.

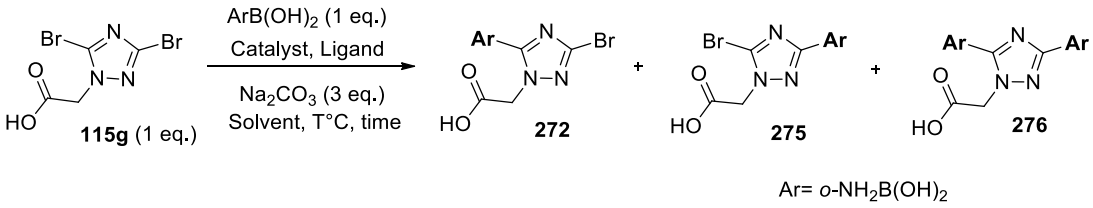

Entry	Catalyst	Ligand	Solvent	T (°C)	Time (h)	Ratio 272/275/276 (HPLC, 254 nm)
1[a]	$Pd(acac)_2$	PPh_3	NMP:H_2O (1:1)	80	18	272/275: 2.1/1
2[b]	$Pd(PPh_3)_4$	-	MePh:EtOH:H_2O (5 :1 :1)	105	3	272/275: 2.5/1

[a] Cat. (3 mol%), Ligand (6 mol%); [b] Cat (5 mol%).

Both reactions showed similar results with the predominant formation of the C-5 substituted regioisomer. Additionally, we subjected the crude to an intramolecular cyclization reaction protocol using H_2SO_4 methanolic medium, but high quantity of reagent **115g** and a mixture of products was observed by HPLC after 4h.

3.7 Synthesis of the series C (216)

The synthesis of the series C started under the same conditions described previously but replacing 2-bromomethylbenzonitrile by *tert*-butyl-2-bromoacetate led to the N-alkyl 3.5-dibromotriazole (**277**) in 96 % yield yield (characteristic NMR peaks from -CH_2 at 4.8 ppm and *tert*-butyl group at 1.50 ppm were found). Since the Suzuki reaction takes place in the presence of a base, we chose to use 2-bromo *tert*-butylacetate instead of 2-bromo carboxylic acid for the N-alkylation step to avoid saponification, which would complicate the purification by chromatography column. To avoid the mixture of mono and di-adducts in the Suzuki procedure, an excess (2 equiv.) of the alkylated intermediate (**277**) over boronic acid was successfully applied to obtain the mono adduct **278** as the main product in 80% yield (characteristic NMR peak from -NH_2 at 4.7 ppm was found). The 2-bromotriazolo diazepinone (**271**) was obtained in 68% after conversion of *tert*-butyric ester to methyl ester using $SOCl_2$ in MeOH followed by subsequent cyclization in refluxing toluene (characteristic NMR peak from -NH at 10.8 ppm was found). Finally, in the last step, we performed the Suzuki-Miyaura reaction using the classical protocol (Entry 1). However, even after 3 hours, we did not observe reagent

consumption due to the low solubility of diazepinone (**271**). In a new attempt using DMF:H_2O (1:1) as solvent (Entry 2), we observed complete consumption of the reagent and formation of the desired product **216a** by HPLC (Scheme 51).

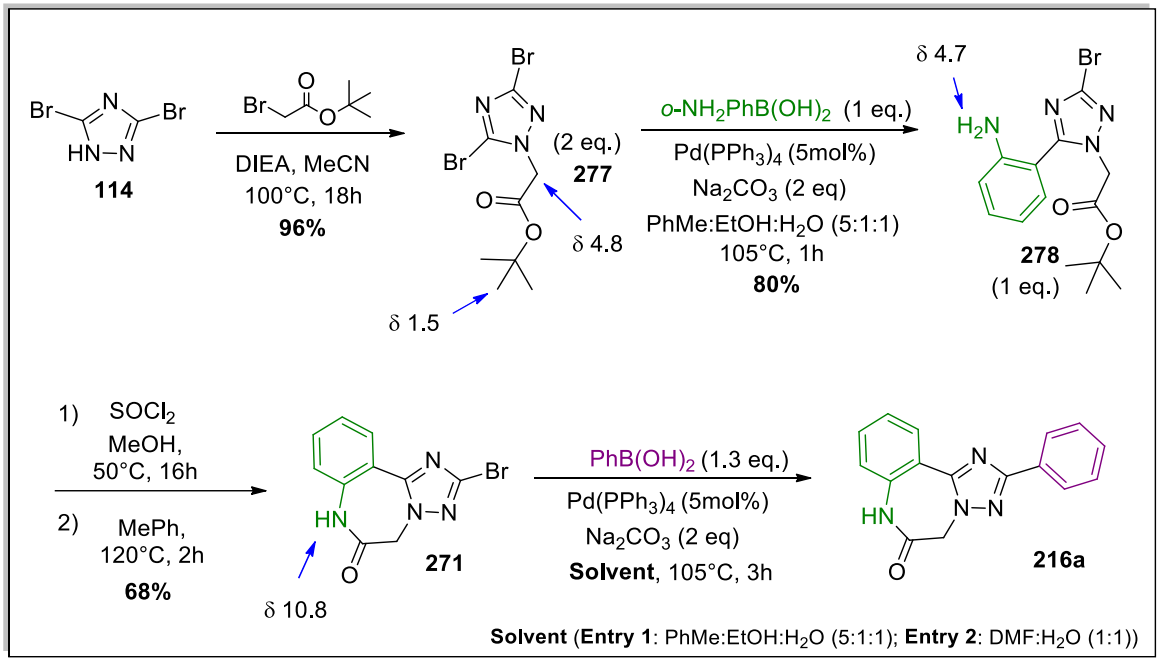

Scheme 51. Synthetic pathway to obtain series C.

The low solubility of **271**, even in alcoholic medium, and the need to perform purification by column chromatography in the subsequent step, prompted us to alter the synthetic route and carry out the Suzuki-Miyaura reaction with intermediate **278** due to its higher lipophilicity. The Suzuki procedure allowed the introduction of aromatic moiety at the position 3 of the triazole core leading to **279a-e** in reasonable to excellent yields varying from 49-94%. Finally, in the last step, compounds **216a-e** were obtained in good to moderate yields (67-91%) after transesterification followed by subsequent cyclization in refluxing toluene (characteristic NMR peak from -NH at 10.7 ppm was found) (Scheme 52).

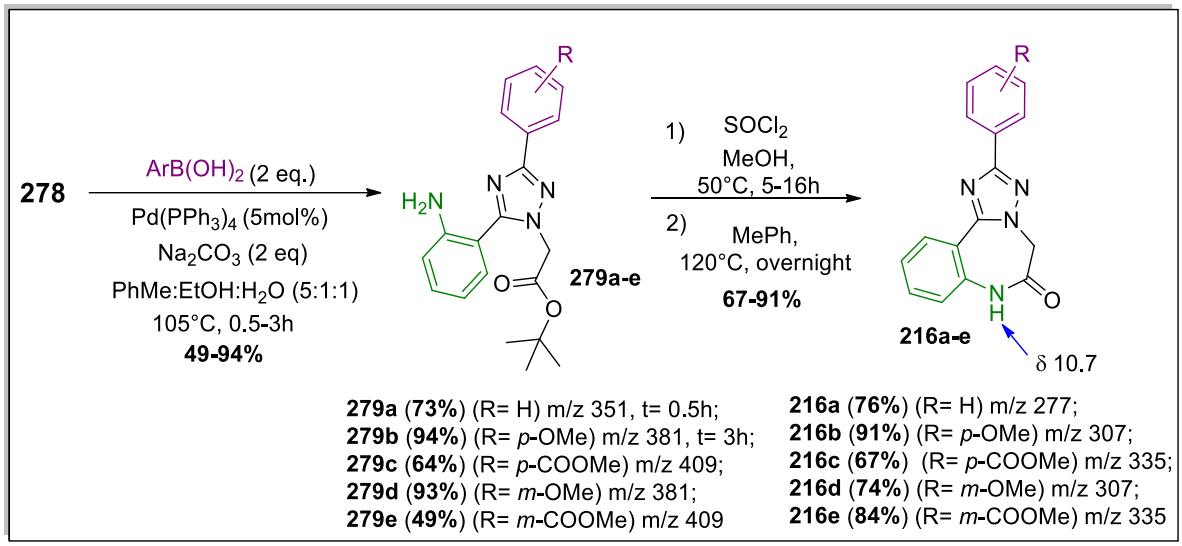

Scheme 52. Synthetic pathway to obtain series C.

Compounds **216b** and **216d** were demethylated in the presence of BBr_3 (6.5 equiv.) in DCM under reflux as illustrated in Scheme 53A. The *p*- and *m*-OH derivatives (**216f-g**) were obtained in 83 and 76% yield, respectively, after purification (characteristic NMR peak from -OH at 9.8 ppm (**216f**) and 9.6 ppm (**216g**) was found). Saponification of compounds **216c** and **216e** with LiOH led after hydrolysis to the expected carboxylic acids. However, we observed by LC/MS the formation of a by-product (**280-281**) resulting from δ-lactam ring opening in a ratio of 1:1 with the expected product at room temperature, whereas heating to reflux overnight provided only the ring opening product. The crude mixture was finally refluxed in toluene to provide **216h** (90%) and **216i** (91%) (m/z 321). The *p*-amide derivative (**216j**) was obtained in two different ways. Treatment of the *p*-COOMe cpd (**216c**) with NH_3 (7M in MeOH) at reflux led to the benzamide derivative **216j** in only 25% of yield after purification. As previously, we observed the formation of side products (**282-283**) resulting from the δ-lactam ring opening in a ratio of 1.2:1:1:1.5 for **216c**:**216j**:**282**:**283** by LC/MS. Cpd **216j** was obtained in 25% after purification. The *m*- and *p*-amide derivatives (**216j-k**) were successfully obtained from the reaction of NH_3 (7M in MeOH) with an activated benzotriazole intermediate, previously obtained from the *in situ* reaction of the benzoic acid derivative (**216i**) with N-(3-dimethylaminopropyl)-N'-ethylcarbodiimide hydrochloride (EDC.HCl) and 1-hydroxybenzotriazole (HOBt) (characteristic NMR peaks from NH_2 at 7.4 and 8.1 ppm were found). (Scheme 53B).

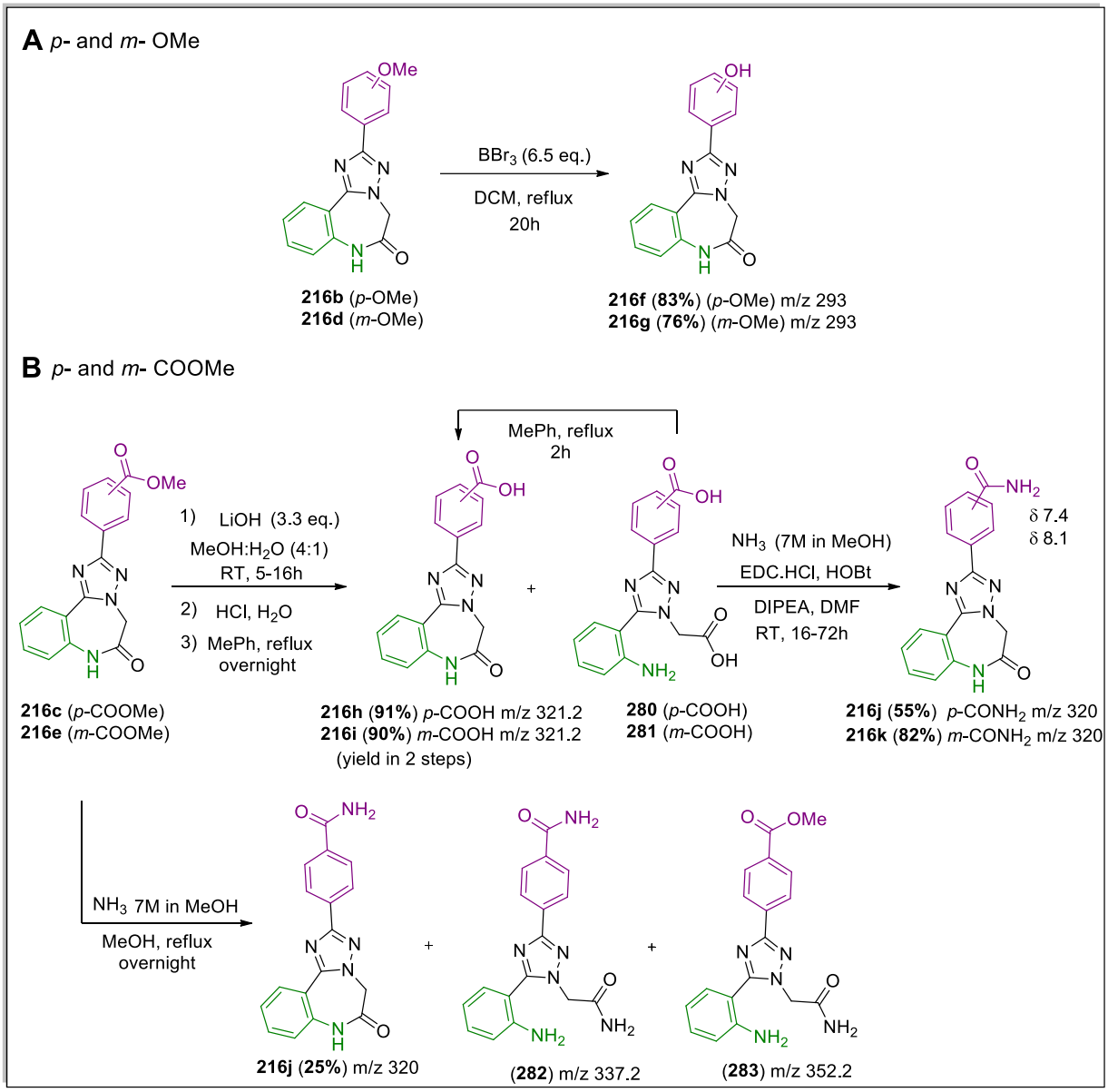

Scheme 53. Synthesis of final compounds **216f-k**.

3.8. *In vitro* evaluation of the inhibitory activity against GSK-3β of the derivatives.

During this thesis, we also established a close relationship with the University of Bologna and particularly developed a strong collaboration with Professor Angela de Simone. As a result, we were able to benefit from the evaluation of the inhibitory activity of compounds **214c**, **215a-d**, **216a-j** for GSK-3β. The inhibition assays against GSK-3β of the compounds (**214c**, **215a-d**, **216a-j**) were conducted using the luminescence detection method, Baki method,[132] with SB415286 (IC_{50}= 70nM) as the reference compound. This assay is based on detecting GSK-3β activity by measuring the luminescence intensity generated by the enzymatic reaction. The reaction is initiated by adding ATP and a specific substrate for GSK-3β to a

solution containing the enzyme. GSK-3β phosphorylates the substrate, consuming ATP and generating ADP. Then, a solution containing the commercial reagent Kinase-GloTM is added to the mixture, resulting in the release of light proportional to the amount of ATP present in the solution. Luminescence is measured in a plate reader, and the signal intensity is inversely proportional to the activity of GSK-3β (as illustrated in Figure 37).[132]

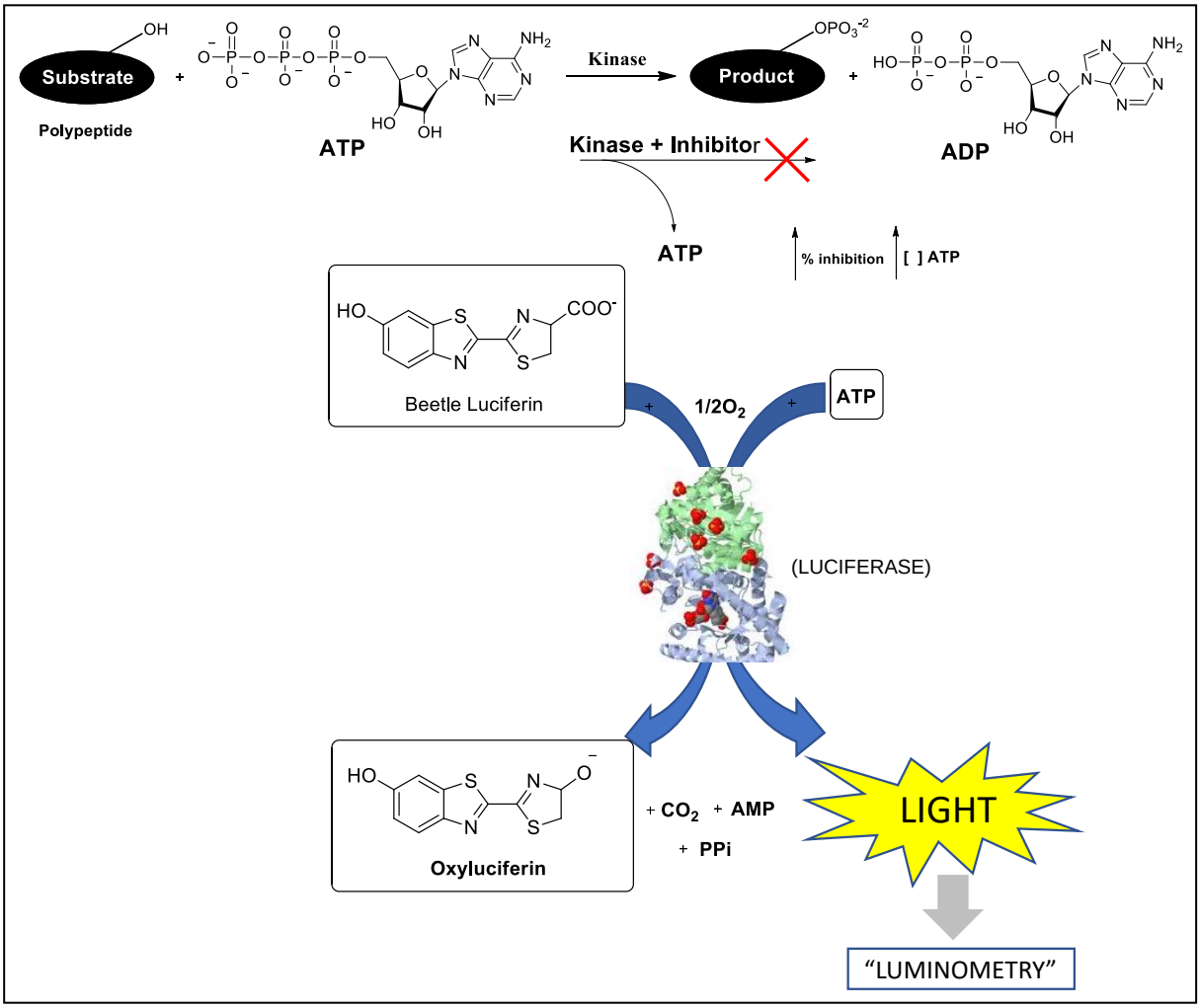

Figure 37. GSK-3β inhibition assay.

The results of the inhibitory activity showed that the designed series B (**215a-d)** and compound **214c** did not show any inhibition against GSK-3β. The results obtained for the designed series C (**216a-j**) were promising, and the pattern of substitution of the aromatic moieties appeared to have an important role for the GSK-3β inhibition, with compound **216g** showing the best inhibitory profile. The respective IC_{50} results obtained in the inhibition assays against GSK-3β are presented in Table 17.

Table 17. Effects of compounds **214c**, **215a-d** and **216a-j** on GSK-3β activity.

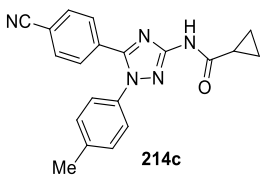

214c

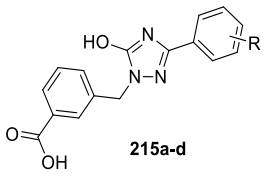

215a-d

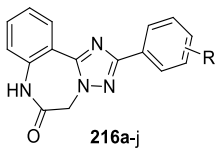

216a-j

Cpd	R	%Inhibition @10 μM	IC_{50} [μM]
214c	-	n.i.	-
215a	H	n.i.	-
215b	*p*-OMe	n.i.	-
215c	*m*-Me	n.i.	-
215d	*m*-Cl	n.i.	-
216a	H	42.3	-
216b	*p*-OMe	9	-
216c	*p*-COOMe	14.3	-
216d	*m*-OMe	15.2	-
216[e]	*m*-COOMe	52	44
216f	*p*-OH	49.7	15
216g	*m*-OH	71.2	2.5
216h	*p*-COOH	4	-
216i	*m*-COOH	42	21
216j	*p*-$CONH_2$	15.7	-
SB415286	-	-	70nM

Reference compound SB415286 IC_{50}= 70nM. The results represent the mean value ± SEM of at least two independent experiments each carried out in duplicate. N.i.: no inhibition.

Trying to understand all the obtained inhibitory activity results, we conducted further molecular docking studies using the GOLD 5.6 software (CCDC Software Ltd., Cambridge, UK) and crystallographic structures of the GSK-3β enzyme (4PTC, 1Q4L, 1Q3L) obtained from the Protein Data Bank (PDB). The Goldscore function was employed to quantify the prediction of compound interaction with the enzyme.

Therefore, the triazolic compounds **214c**, **215a-e**, and **216a-j** were initially subjected to energy minimization using the semi-empirical PM6 method and subsequently docked into the active site of GSK-3β.

In the GOLD program, docking functions produce dimensionless score values, referred to as "fitness scores." The score of each identified pose is calculated as the negative sum of a

series of energy terms involved in the protein-ligand interaction process, so the more positive the score, the better the interaction. The score values serve as a guide to how good the docking position could be, meaning that a higher score indicates a better interaction between the ligand and the binding site.

The analysis of compound **214c** planned for series A indicated a good overlap with the reference inhibitor from the literature **204**, and the possibility of making the same intermolecular interactions with the amino acid residues. The results also showed the possibility of exploring different substituents on the triazole ring, seeking new intermolecular interactions with GSK-3β by exploration of a lipophilic cavity in this enzyme (Figure 38). Unfortunately, we couldn't obtain this compound to confirm this hypothesis. An in deep analysis of this cavity showed that its size is not sufficient to accommodate large groups such as aromatic rings, making it more suitable for the introduction of smaller groups such as methyl or cyclopropyl (Figure 38). Therefore, we believe that the presence of the *p*-Tolyl group in **214c** did not allow the fitting into the enzyme's catalytic site, which could explain its absence of *in vitro* inhibitory activity.

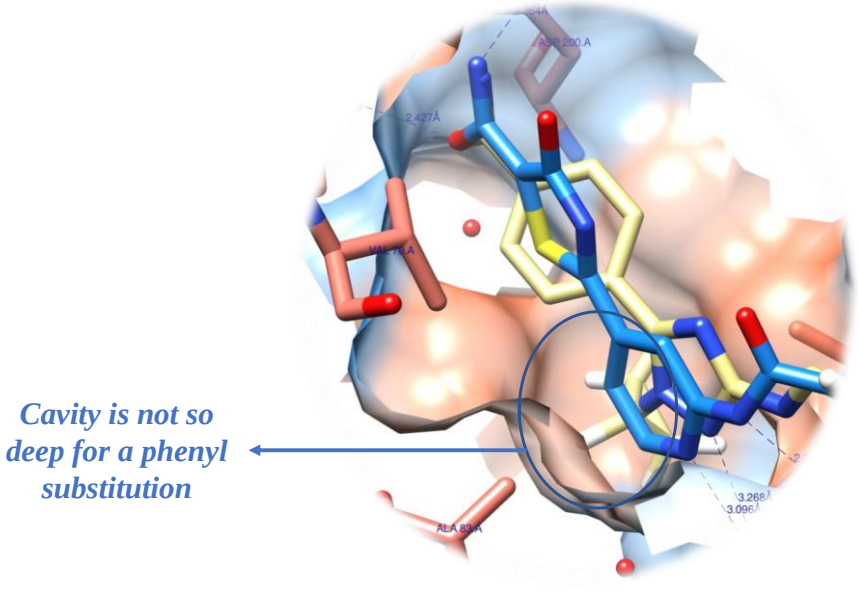

Figure 38. Analysis of the docking position of compounds **204** (blue) and **214c** (yellow) in the access cavity to the catalytic site of GSK-3β (PDBs – 4PTC). Figure generated with UCSF Chimera.

The analysis of compound **215a** from series B also indicated good overlap with the reference inhibitor from the literature, maleimide (**207**). The result also suggested the possibility of exploring different substitutions on the aromatic ring attached to position 3 of the triazole

ring of the designed compound **215a**, with the intention of seeking new intermolecular interactions with nearby amino acids (Figure 39).

Upon analyzing the theoretical model, the interactions of maleimide (**207**) and **215a** with valine and aspartic acid were observed and highlighted in Figure **39**. This interaction model predicts that the designed compound **215a** should be in the amidic tautomeric form for the interactions to occur as designed (Figure 39).

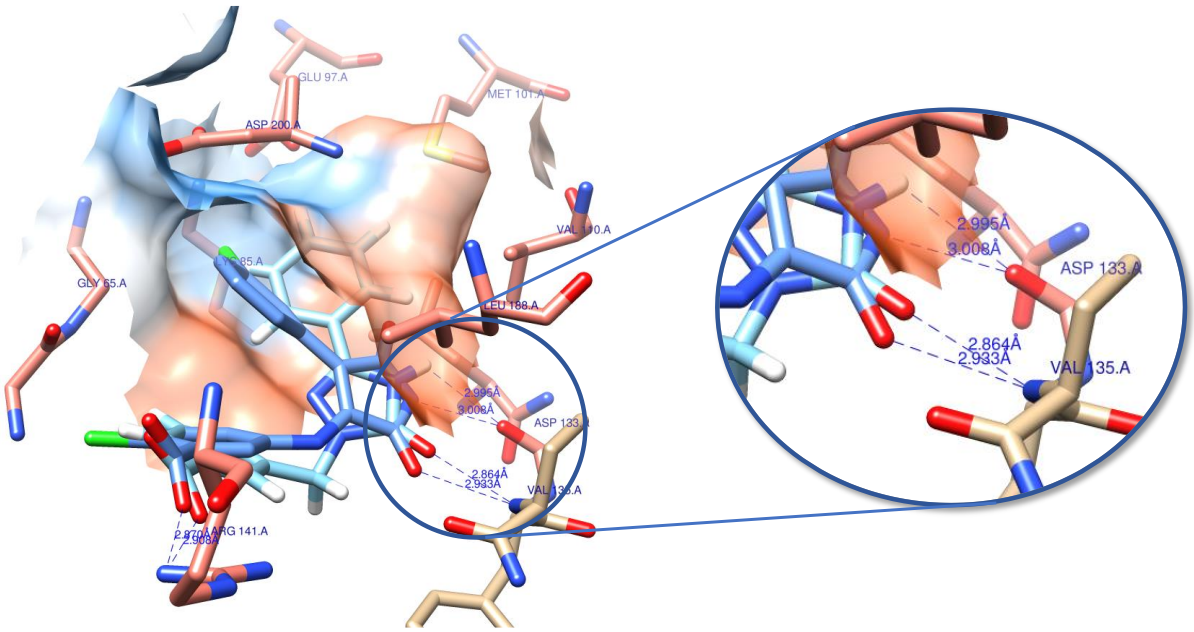

Figure 39. Analysis of the docking position of compounds **207** (dark blue) and **215a** (light blue) in the access cavity to the catalytic site of GSK-3β (PDBs - 1Q4L). Figure generated with UCSF Chimera.

The NOESY spectroscopic analysis for compound **215d** showed strong spatial coupling between the proton of the carboxylic acid (δ 13 ppm) and the proton originated from the triazole core (δ 12.3 ppm). Spatial analysis of **215d** indicates that only the triazolone (**215d”**) or triazolol (**215d”’**) tautomers could perform a spatial coupling with the carboxylic acid group (Figure 40). This, in our opinion, may account for the lack of inhibitory activity of series B against GSK-3β. Additionally, the low solubility of the compounds in most organic solvents and in water is another important factor that may explain the absence of inhibitory activity against GSK-3β.

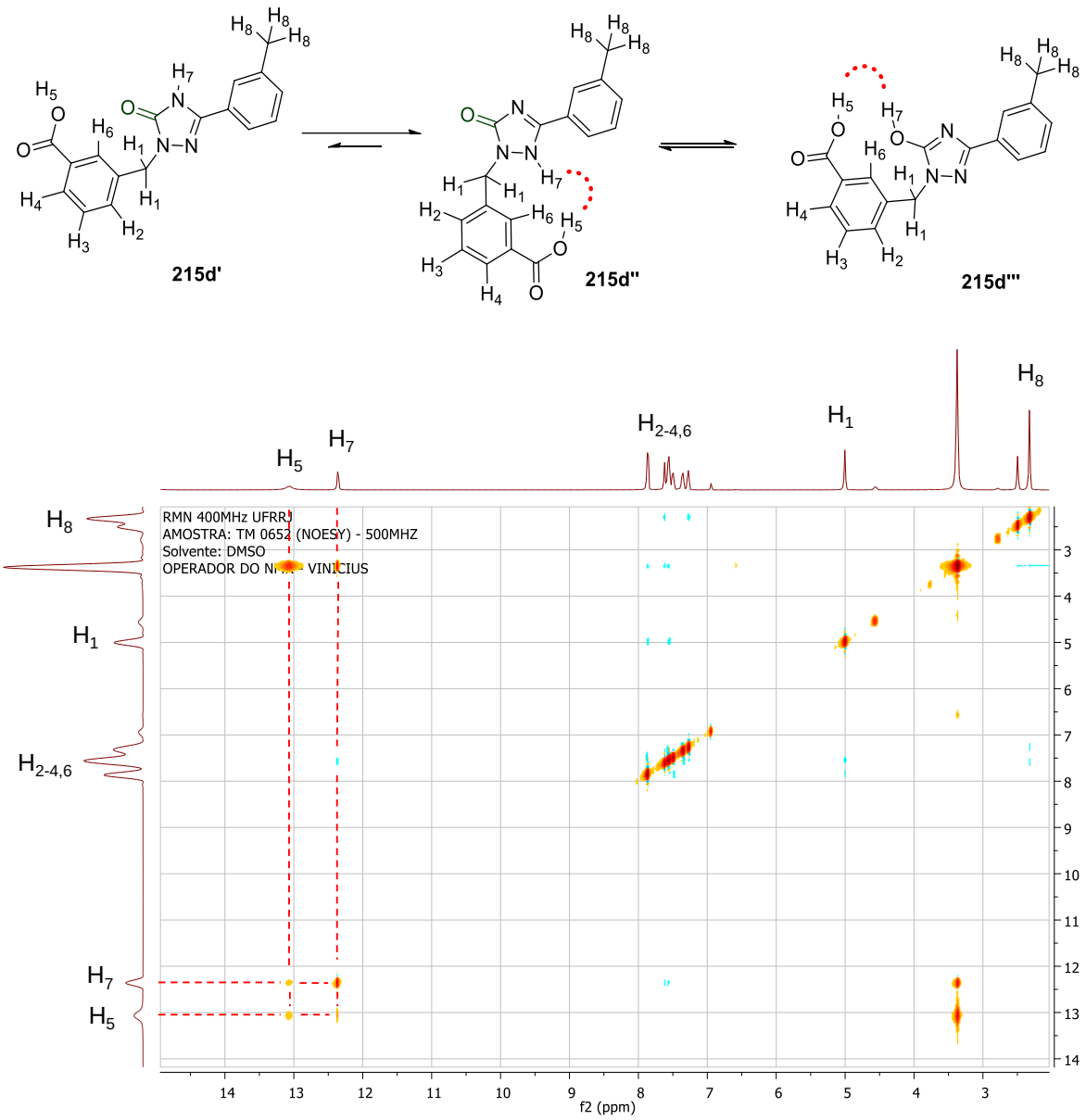

Figure 40. NOESY analysis of the compound **215d** in DMSO.

Finally, we performed molecular modeling calculations to understand if the inhibitory activity results of series C were in accordance with the theoretical model previously used for the series design. For this purpose, the meta-substituted compounds were compared (Figure 41), and according to the docking calculations, compound **216g**, which showed the best inhibitory activity in vitro against GSK-3β (IC_{50}= 2.5 μM), also exhibited the best profile, with a higher score (Table 18). The observed reason for this best score came from two hydrogen bonds that compound **216g** can perform with Lys85 and Asp200. This result inspired us, motivating further investigations on the structure-activity relationship and optimizations currently underway.

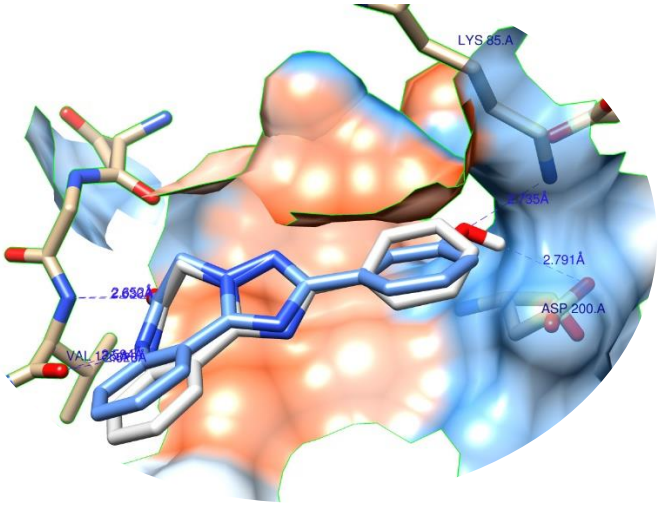

Figure 41. Docking analysis of compound **216g** binding in the catalytic site cavity of GSK-3β (PDB - 1Q3L). Figure generated with UCSF Chimera.

Table 18. Molecular mechanics calculations

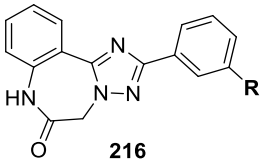

216

Cpd	R	Score
216a	H	29.1
216d	OMe	32.0
216g	OH	32.2
216i	$CONH_2$	31.5
Alsterpaullone	-	32.4

4. CONCLUSION AND PERSPECTIVES

In this work, 17 novel trisubstituted 1,2,4-triazole compounds (**214b-c**, **215a-d**, **216a-k**) were synthesized. All final compounds were characterized by ^{1}H and ^{13}C NMR spectroscopy, as well as LC/MS.

The proposed synthesis methodologies for the planned B and C series proved to be efficient, yielding good to excellent reaction yields. The synthesis methodology for the compounds in series A needs to be optimized, requiring the development of a more convergent route.

The enzymatic inhibition assays of **214c**, **215a-d,** and **216a-j** against GSK-3β demonstrated that the compounds in series C were able to inhibit this kinase at 10 μM, especially **216g**, which proved to be the most active (IC50= 2.5 μM). These results are promising for the development of a new hit compound and prompt further optimizations.

The *in silico* assays were consistent with the in vitro results and indicated that the meta substitution of the aromatic ring with -OH in **216g** showed the best profile, validating the model used for the series planning.

As perspectives include increasing the number of compounds in series C, mainly exploring new derivatives with substitution patterns in the ortho and meta positions of the aromatic ring; conducting a structure-activity relationship study based on the new modifications; and developing a convergent synthesis route for obtaining the compounds in series A.

5. EXPERIMENTAL

5.1. Materials and instruments – LIT (Laboratory for Therapeutic Innovation)

All commercial reagents were used without purification. Analytical TLC was performed using Merck 60 F254 silica gel plates, and visualized by exposure to ultraviolet light (254 and 365 nm). Compounds were purified on silica gel Merck 60 (particle size 0.040−0.063 nm). NMR spectra were recorded on Bruker Avance III spectrometers. Operating at 500, 400, or 300 MHz for ^{1}H, 126, 101, or 75 MHz for ^{13}C. All chemical shift values δ and coupling constants J are quoted in ppm and in Hz, respectively, multiplicity (s= singlet, d= doublet, t= triplet, q= quartet, m= multiplet, and br = broad). Analytical RP-HPLC-MS was performed using a LC 1200 Agilent with quadrupole-time-of-flight (QTOF) (Agilent Accurate Mass QToF 6520) with a ZORBAX Agilent C18-column (C18, 50 mm × 2.1 mm; 1.8 μm) using the following parameters: (1) the solvent system: A (0.05% of formic acid in acetonitrile) and B (0.05% of formic acid in H_2O); (2) a linear gradient: t = 0 min, 98% B; t = 8 min, 0% B; t = 12.5 min, 0% B; t = 12.6 min, 98% B; t = 13 min, 98% B; (3) flow rate of 0.5 mL/min; (4) column temperature: 35 °C; (5) DAD scan from 190 to 700 nm; and (6) ionization mode: ESI+. HPLC were performed using a Dionex UltiMate 3000 using the following parameters: column temperature: 40°C, from t = 0 min to t = 3.80 min the flow rate goes from 0.650 mL/min to 0.900 ml/min with the solvent system: A (0.05% of TFA in H2O) and B (MeCN) with 5 to 100% of B, then after t = 3.80 min to the end of the run t = 5.50 min: 100% of B at 0.900 ml/min.

5.2. Materials and instruments – BOMEDCHEM LAB (Bolognesi's Medicinal Chemistry Laboratory)

All chemicals were purchased from Aldrich Chemistry (Milan, Italy), Alfa Aesar (Milan, Italy) and FluoroChem (Cambridge, UK) were of the highest purity. Solvents were of analytical grade. Reaction progress was followed by thin layer chromatography on precoated silica gel 60 F254 plates (Merck, Darmstad, Germany). Chromatographic separations were performed on 0.040- to 0.063-mm silica gel 40 columns via the flash method (Merck). The ^{1}H nuclear magnetic resonance (NMR) and ^{13}C NMR spectra were recorded on a Varian Gemini spectrometer (Varian Medical System Italia, Milan, Italy) at 400 and 101 MHz, respectively, in $CDCl_3$ solutions unless otherwise indicated. Chemical shifts (δ) were reported as parts per million relative to tetramethylsilane, used as internal standard; coupling constants (*J*) are reported in Hertz (Hz). Standard abbreviations indicating spin multiplicities are given as

follows: s (singlet), d (doublet), dd (double doublet), t (triplet), q (quartet) and m (multiplet). Ultra-HPLC–mass spectrometry analyses were run on a Waters ACQUITY Arc system (Milan, Italy) consisting of a QDa mass spectrometer equipped with an electrospray ionization interface and a 2489 UV/VIS detector. The detected wavelengths were 254 and 365 nm. Analyses were performed on an XBridge BEH C18 column with a 10 × 2.1 mm internal diameter (particle size 2.5 μm) with an XBridge BEH C18 VanGuard Cartridge precolumn with a 5 × 2.1-mm internal diameter (particle size 1.8 μm) (Waters). The mobile phases were H_2O (0.1% formic acid) and MeCN (0.1% formic acid). Electrospray ionization in positive and negative mode was applied in the mass scan range of 50–1200 Da. The authors used a generic method and linear gradient: 0–0.78 min, 20% B; 0.78–2.87 min, 20–95% B; 2.87–3.54 min, 95% B; 3.54–3.65 min, 95–20% B; 3.65–5.73, 20% B. The flow rate was 0.8 ml/min. HRMS spectra were recorded on a Waters Xevo G2-XS quadrupole time-of-flight apparatus operating in electrospray mode. Compounds were named based on the naming algorithm developed by CambridgeSoft and used in ChemBioDraw Ultra (PerkinElmer, Milan, Italy, version 20.0). All tested compounds were found to have >95% purity.

5.3. Materials and instruments – LaDMol-QM (Medicinal Chemistry and Molecular Diversity Laboratory)

The reactions were monitored using the thin-layer chromatography (TLC) technique, in which Kieselgel 60 aluminum plates (HF-254, Merck) with 0.2 mm thickness were used. Visualization of substances on TLC was performed under ultraviolet lamp (254-365 nm). Compounds purification was conducted using flash column chromatography technique, Isolera Biotage, model ISO-4SV (IQ-UFRRJ). Silica gel 70-230 mesh (Merck) was used for column packing. As the mobile phase, solvents were selected based on the physicochemical properties of each compound. The ^{1}H NMR spectra were obtained using Bruker Avance-500 and Bruker Avance-400 instruments (IQ-UFRRJ), operating at 500MHz and 400MHz, respectively. Samples were dissolved in CDCl3, DMSO-d6, or acetone-d6, containing tetramethylsilane as an internal reference, and placed in 5 mm diameter tubes. The ^{13}C NMR spectra were obtained operating at 125 MHz and 100MHz, using Bruker Avance-500 and Bruker Avance-400 instruments (IQ-UFRRJ), respectively. Samples were dissolved in CDCl3, DMSO-d6, or acetone-d6, containing TMS as an internal reference. Signal areas were obtained through electronic integration and their multiplicity described as follows: s-singlet / bs-broad singlet / d-doublet / t-triplet / q-quartet / m-multiplet / dd-double doublet.

5.4. Synthetic methodology

5.4.1. Synthesis of 1-iodo-2-methylisothiouronium (228)[124]

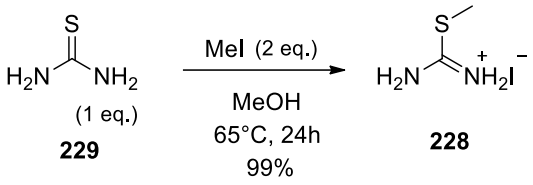

To a 25 mL round bottom flask, thiourea (1 equiv., 0.68 g, 8.8 mmol) was dissolved in methanol (6.7 mL) and methyl iodide (2 equiv., 2.5 g, 1.1 mL, 17.64 mmol) was added. The resulting reaction mixture was refluxed at 65°C for 24 h then cooled to r.t., and finally concentrated under reduced pressure to yield a yellow solid (1.89 g, 8.69 mmol, 99%). The product was used directly for the next step without further purification. The analytical data are identical to the literature.

5.4.2. Synthesis of 2-methylisothiouronium-N-Boc (227)

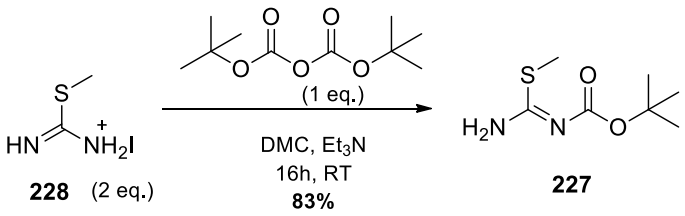

1-iodo-2-methylisothiouronium (2 equiv., 1 g, 4.59 mmol) was added to a 50 mL round bottom flask and dissolved in DCM (10 mL). The temperature of the reaction mixture was lowered to 0°C, and then triethylamine (2.35 equiv., 0.54 g, 0.75 mL, 5.39 mmol) was added. Boc_2O (1 equiv., 0.5 g, 0.49 mL, 2.29 mmol) was dissolved in DCM (5 mL) and added dropwise to the reaction mixture. After some time, the ice bath was removed, and the reaction mixture was allowed to stir at r.t. overnight. The progression of the reaction was monitored by TLC (Hex/EtOAc – 80/20, RF= 0.69). The crude reaction mixture was then dissolved in 15 mL of DCM and washed twice with 10 mL of water. After drying with anhydrous Na_2SO_4, the solution was concentrated under reduced pressure. Initially, the product was in the form of an oil, but it eventually precipitated as a white solid (0.36 g, 1.9 mmol, 83%). ^1H NMR (400 MHz, $CDCl_3$) δ 1.50 (s, 9H), 2.45 (s, 3H), 7.41 (bs, 2H). LC/MS m/z $[M + H]^+$ 135.09

5.4.3. Synthesis of N-acyl-2-methylisothiouronium-N-Boc (223)

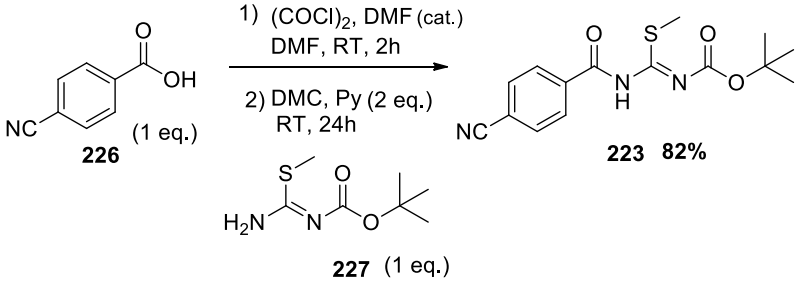

4-cyanobenzoic acid (1 equiv., 0.40 g, 2.76 mmol was added to a 125 mL round-bottom flask and dissolved in DCM (15 mL). Then, oxalyl chloride (4 equiv., 1.36 g, 0.92 mL, 10.51 mmol) and 3 drops of DMF were added. The reaction mixture was stirred for 2 hours. Afterward, the crude mixture was concentrated and dissolved in DCM (8 mL). This resulting solution was then added dropwise to a solution of *tert*-butyl N-[(1Z)-amino(methylsulfanyl)methylidene]carbamate (**227**) (1 equiv., 0.50 g, 2.63 mmol) and pyridine (2 equiv., 0.41 g, 0.42 mL, 5.26 mmol) in DCM (20 mL). The progression of the reaction was monitored by TLC (PE/EtOAc – 80/20, RF= 0.41). After 20 hours, the reaction mixture was concentrated under reduced pressure. The crude product was then purified by chromatography column using gradient elution with PE/EtOAc (90/10 - 80/20) to yield the desired product as a white solid (0.68 g, 2.15 mmol, 82%). ^{1}H NMR (400 MHz, $CDCl_3$) δ 1.53 (s, 9H), 2.58 (s, 3H), 7.73-7.75 (d, *J* = 8.2 Hz, 2H), 8.33-8.35 (d, *J* = 8.3 Hz, 2H), 12.51 (bs, 1H). LC/MS m/z $[M + H]^+$ 220.11.

5.4.4. Synthesis of 4-(3-amino-1-(p-tolyl)-1H-1,2,4-triazol-5-yl)benzonitrile (220a)

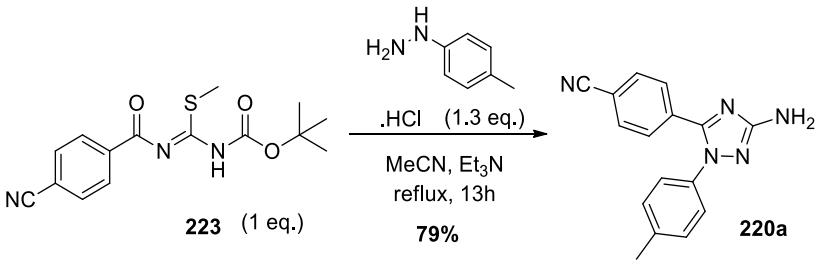

A microwave vial containing a Teflon stirrer bar was charged with *tert*-butyl N-[(1Z)-{[(Z)-4-cyanobenzoyl]imino}(methylsulfanyl)methyl]carbamate (**223**) (1 equiv., 0.14 g, 0.45

mmol) dissolved in MeCN (3 mL) was combined with p-tolylhydrazine hydrochloride (1.33 equiv., 95.12 mg, 0.6 mmol) and Et_3N (2.1 equiv., 95.81 mg, 0.131 mL, 0.95 mmol). The reaction mixture was refluxed for 13 hours. The progression of the reaction was monitored by TLC (PE/EtOAc - 50/50, RF= 0.19). The crude reaction mixture was concentrated under reduced pressure and purified by chromatography column using gradient elution with PE/EtOAc (30/70 to 0/100) to give the desired compound **220a** as a white solid (0.098 g, 0.38 mmol, 79%). ^{1}H NMR (400 MHz, $CDCl_3$) δ 2.41 (s, 3H), 3.94 (bs, 2H), 7.16-7.23 (m, 4H), 7.56-7.62 (m, 4H).

5.4.5. Synthesis of 4-(3-amino-1-cyclopentyl-1H-1,2,4-triazol-5-yl)benzonitrile (220b)

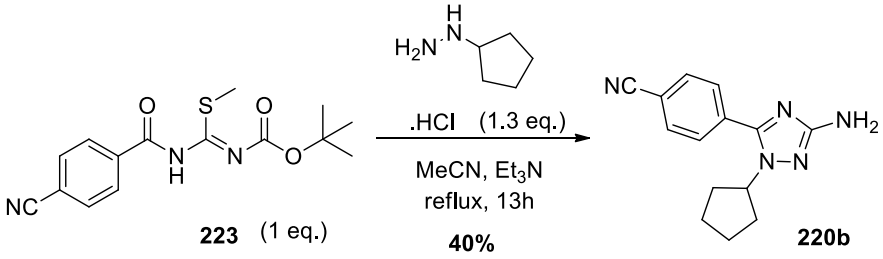

In a sealed borosilicate tube, 4-(3-amino-1-cyclopentyl-1H-1,2,4-triazol-5-yl)benzonitrile (1 equiv., 0.023 g, 0.074 mmol) dissolved in MeCN (1.6 mL) was combined with cyclopentylhydrazine (1.5 equiv., 15.2 mg, 0.11 mmol) and Et_3N (2.2 equiv., 0.016 mg, 0.022 mL, 0.16 mmol). The reaction mixture was refluxed for 13 hours. The progression of the reaction was monitored by TLC (PE/EtOAc - 50/50, RF= 0.14). The crude reaction mixture was concentrated under reduced pressure and purified by chromatography column using PE/EtOAc (30/70) to afford the desired compound as white solid (0.0075 g, 0.03 mmol, 40%). LC/MS m/z $[M + H]^+$ 254.22.

5.4.6. Synthesis of N-(5-(4-cyanophenyl)-1-(p-tolyl)-1H-1,2,4-triazol-3-yl)cyclopropanecarboxamide (214c)

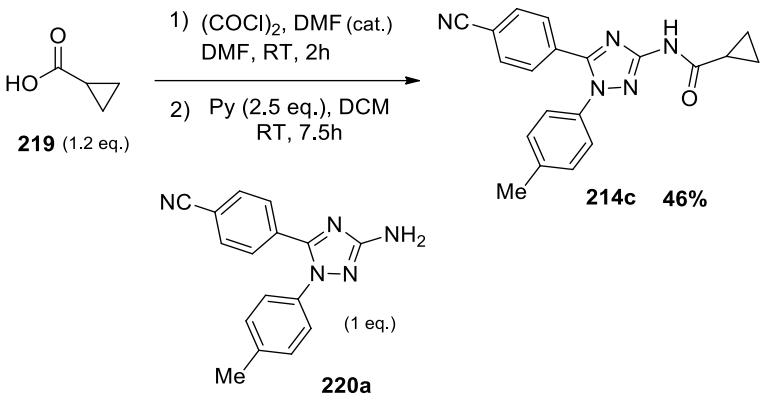

Cyclopropane carboxylic acid (1.2 equiv., 0.044 g, 0.040 µL, 0.51 mmol) was dissolved in 3 mL of DCM in a 50 mL round bottom flask containing a Teflon stirrer bar. Then, oxalyl chloride (5 equiv., 0.27 g, 0.18 mL, 2.1 mmol) and 3 drops of DMF were added. The reaction mixture was stirred at r.t. for 2 hours and then, the crude reaction mixture was concentrated, dissolved in DCM (5 mL), and added dropwise to a solution of 4-[3-amino-1-(4-methylphenyl)-1H-1,2,4-triazol-5-yl]benzonitrile (1 equiv., 0.12 mg, 0.42 mmol), pyridine (2.51 equiv., 0.084 g, 85.54 µL, 1.058 mmol) and DCM (6 mL) in a 50 mL round bottom flask containing a Teflon stirrer bar. The reaction mixture was maintained under stirring for 7.5 hours at room temperature and the progress of the reaction was monitored by TLC (PE/EtOAc - 30/70, RF= 0.47). The reaction mixture was concentrated under reduced pressure, and the crude product was purified by chromatography column using PE/EtOAc (30/70) to yield the desired product as a white solid (0.066 g, 0.19 mmol, 46%). ^{1}H NMR (400 MHz, $CDCl_3$) δ 0.87 (m, 2H), 1.16 (m, 2H), 1.78 (m, 1H), 2.42 (s, 3H), 7.22 (m, 4H), 7.60 (m, 4H), 8.45 (bs, 1H). ^{13}C NMR (101 MHz, $CDCl_3$) δ 21.3, 118, 125.5, 129.4, 130.3, 131.5, 132.3, 134.8, 139.8. LC/MS m/z $[M + H]^+$ 344.24.

5.4.7. Synthesis of 4-(3-amino-1-(p-tolyl)-1H-1,2,4-triazol-5-yl)benzoic acid (231)

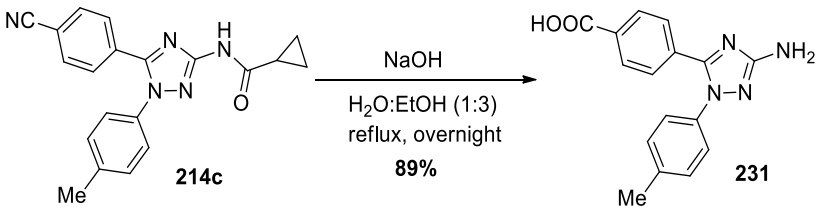

Compound **214c** (1 equiv., 0.0046 g, 0.13 mmol) and NaOH (226.42 equiv., 1.2 g, 30.33 mmol) were dissolved in Ethanol (15 mL) and H_2O (15 mL) in a 100 mL round bottom flask containing a Teflon stirrer bar. The reaction mixture was stirred at 120°C overnight. The reaction mixture was cooled to r.t., concentrated under reduced pressure and then, extracted with DCM (3 x 15 mL). The pH of the aqueous phase was decreased to ~1 with drops of concentrated HCl, and then extracted with Ethyl acetate (3 x 15mL). The organic layers were collected, dried with anhydrous Na_2SO_4 and concentrated under reduced pressure to give **231** as white solid (0.035 g, 0.12 mmol, 89%). ^{1}H NMR (400 MHz, DMSO): δ 2.34 (s, 3H), 5.64 (s, 2H), 7.18-7.20 (d, *J* = 8.4 Hz, 2H), 7.24-7.26 (d, *J* = 8.2 Hz, 2H), 7.47-7.49 (d, *J* = 8.4 Hz, 2H), 7.89-7.91 (d, *J* = 8.4 Hz, 2H). LC/MS m/z $[M + H]^+$ 295.23

5.4.8. Synthesis of 4-(3-(cyclopropanecarboxamido)-1-(p-tolyl)-1H-1,2,4-triazol-5-yl)benzoic acid (214b)

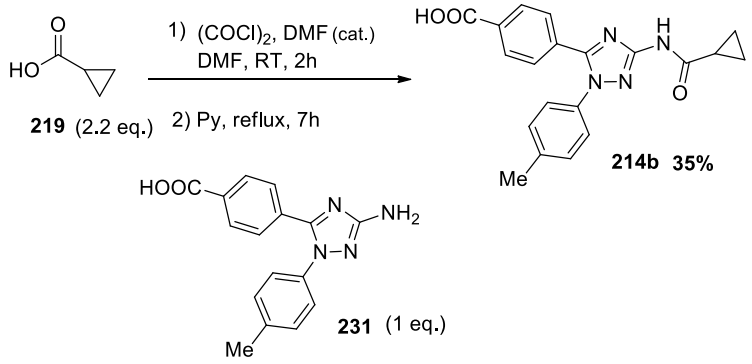

Cyclopropane carboxylic acid (2.2 equiv., 0.011 mg, 0.010 mL, 0.13 mmol) was dissolved in 1 mL of DCM in a 25 mL round bottom flask containing a Teflon stirrer bar. Then, oxalyl chloride (5 equiv., 0.037 g, 0.025 mL, 0.29 mmol) and 3 drops of DMF were added. The reaction mixture was stirred at r.t. for 2 hours and then, the crude reaction mixture was concentrated, dissolved in dioxane (1 mL), and added dropwise to a solution of 4-[3-amino-1-(4-methylphenyl)-1H-1,2,4-triazol-5-yl]benzoic acid (**231**) (1 eq., 0.017 g, 0.058 mmol) in pyridine (1 mL) in a 25 mL round bottom flask containing a Teflon stirrer bar. The reaction mixture was maintained under stirring at 120°C for 7h and the progress of the reaction was monitored by LC/MS. The reaction mixture was cooled to r.t., diluted with HCl 2N and then extracted with Ethyl acetate (3 x 5 mL). The organic layers were collected, dried with Na_2SO_4 and then purified by chromatography column using gradient elution EtOAc/MeOH (90/10) - EtOAc/MeOH/NH_4OH (89.5/9.5/1) to yield the desired product (0.0074 g, 0.020

mmol, 35%). ^{1}H NMR (400 MHz, $CDCl_3$): δ 0.73-0.79 (m, 2H), 0.93-0.97 (m, 2H), 2.32 (s, 3H), 7.13 (s, 4H), 7.44-7.46 (d, *J* = 8.4 Hz, 2H), 7.87-7.90 (d, *J* = 8.4 Hz, 2H). LC/MS m/z $[M + H]^+$ 363.25.

5.4.9. Synthesis of (Z)-tert-butyl (((4-cyanobenzoyl)imino)(1-methylhydrazinyl)methyl)carbamate (250 or 251)

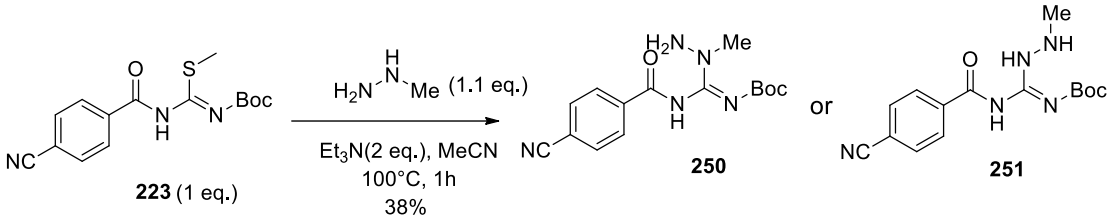

In a microwave vial with a Teflon stirrer bar, compound **223** (1 equiv., 0.050 g, 0.16 mmol) dissolved in MeCN (0.5 mL) was combined with methylhydrazine (1.1 equiv., 0.008 g, 0.009 mL, 0.17 mmol) and Et_3N (1 equiv., 0.016 g, 0.021 mL, 0.16 mmol). The vial was capped properly and the reaction mixture was stirred at 100°C for 1 hours. The progression of the reaction was monitored by TLC (PE/EtOAc - 50/50, RF= 0.24). The crude reaction mixture was concentrated under reduced pressure and purified by chromatography column using gradient elution with PE/EtOAc (50/50 to 0/100) to give the compound **250** or **251** as white solid (0.030 g, 0.095 mmol, 60%). ^{1}H NMR (400 MHz, DMSO) δ 1.40 (s, 9H), 3.14 (s, 3H), 7.73 (bs, 1H), 8.01-8.03 (d, *J* = 8.6 Hz, 2H), 8.08-8.09 (d, *J* = 8.6 Hz, 2H), 8.37 (bs, 1H), 10.95 (s, 1H). LC/MS m/z $[M + H]^+$ 318.24.

5.4.10. Synthesis of 4-(5-amino-1-methyl-1H-1,2,4-triazol-3-yl)benzonitrile (252 or 220c)

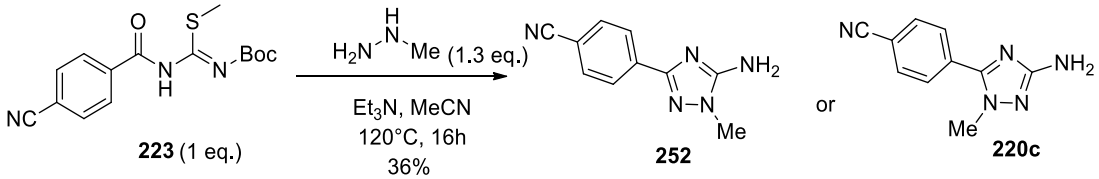

In a microwave vial with a Teflon stirrer bar, compound **223** (1 equiv., 0.2 g, 0.63 mmol) dissolved in MeCN (4 mL) was combined with methylhydrazine (1.3 equiv., 0.038 g, 0.045 mL, 0.83 mmol) and Et_3N (2.1 equiv., 0.133 g, 0.182 mL, 1.32 mmol). The vial was capped properly and the reaction mixture was stirred at 120°C for 16 hours. The progression of the reaction was monitored by TLC (PE/EtOAc - 50/50, RF= 0.32). The crude reaction mixture was

concentrated under reduced pressure, solubilized with DCM (3 mL) and TFA (20 equiv., 0.714 g, 0.46 mL, 6.26 mmol) and stirred at r.t. for 3h. The reaction mixture was concentrated under reduced pressure and diluted with water and the pH was adjusted to 8-9. The aqueous solution was extracted with DCM (3x 10 mL) and EtOAc (1 x 15 mL). The organic layers were collected, concentrated and purified by chromatography column using gradient elution with EtOAc to EtOAc/MeOH 90/10) to give the desired compound as white solid (0.045 g, 0.22 mmol, 36%). ^{1}H NMR (400 MHz, DMSO) δ 3.60 (s, 3H), 6.42 (s, 2H), 7.84-7.86 (d, *J* = 8.6 Hz, 2H), 7.99-8.01 (d, *J* = 8.6 Hz, 2H). LC/MS m/z $[M + H]^+$ 200.2.

5.4.11. Synthesis of (Z)-tert-butyl (cyclopropanecarboxamido(methylthio)methylene)carbamate (254)

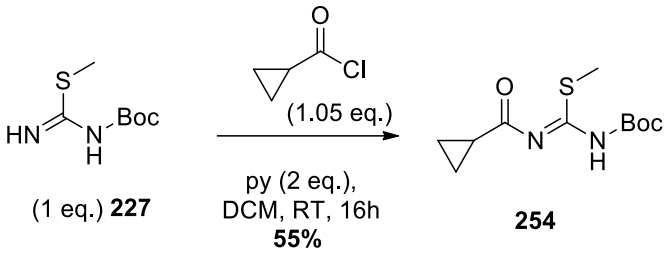

A 25 mL round bottom flask containing a Teflon stirrer bar was charged with compound **227** (1 equiv., 0.1 g, 0.53 mmol), py (2 equiv., 0.083 g, 0.085 mL, 1 mmol) and DCM (4 mL), followed by the dropwise addition of cyclopropanecarbonyl chloride (1.05 eq, 0.55 mmol) solution in DCM (3 mL). The reaction mixture was stirred for 16 hours at r.t. and the progress of the reaction was monitored by LC/MS. The reaction mixture was concentrated under reduced pressure, and the crude product was purified by chromatography column using PE/EtOAc (70/30) to give the desired product (0.073 g, 0.28 mmol, 54%). LC/MS m/z $[M + H]^+$ 259.22.

5.4.12. Synthesis of (Z)-methyl N'-cyclopropanecarbonylcarbamimidothioate (255)

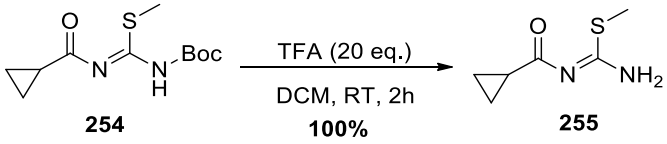

A microwave vial with a Teflon stirrer bar was charged with compound **254** (0.68 equiv., 0.074 g, 0.29 mmol), followed by the addition of DCM (4 mL) and TFA (20 equiv., 0.956 g,

0.62 mL, 8.39 mmol). The reaction mixture was stirred at r.t. for 3h. The reaction mixture was then basified with 30 mL of satured solution of $NaHCO_3$ and extracted with DCM (3 x 30 mL). The organic layers were collected, dried with Na_2SO_4 and concentrated under reduced pressure to give the product (0.046 g, 0.29 mmol, 100%).

5.4.13. Synthesis of (Z)-methyl N'-(4-cyanobenzoyl)-N-(cyclopropanecarbonyl)carbamimidothioate (257)

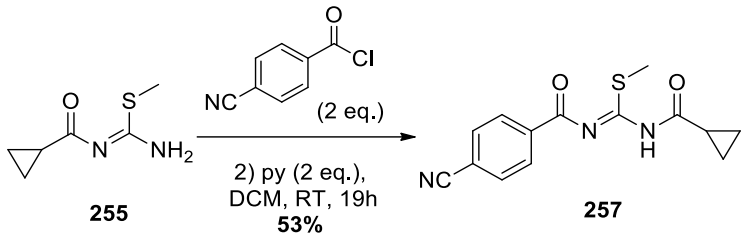

A 25 mL round bottom flask containing a Teflon stirrer bar was charged with compound **255** (1 equiv., 0.046 g, 0.29 mmol), py (2 equiv., 0.046 g, 0.059 mL, 1 mmol) and DCM (2.1 mL), followed by the dropwise addition of p-cyanobenzoic acid (1.05 eq, 0.309 mmol) solution in DCM (1.6 mL). The reaction mixture was stirred for 19 hours at r.t. and the progress of the reaction was monitored by LC/MS. The reaction mixture was concentrated under reduced pressure, and the crude product was purified by chromatography column using PE/EtOAc (70/30) to give the desired product (0.045 g, 0.15 mmol, 53%). LC/MS m/z $[M + H]^+$ 288.23.

5.4.14. Synthesis of (Z)-methyl N'-(4-cyanobenzoyl)carbamimidothioate (256)

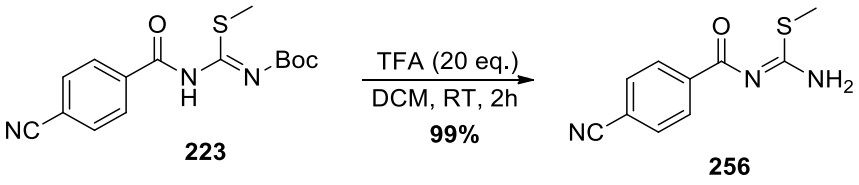

A microwave vial with a Teflon stirrer bar was charged with compound **223** (1 equiv., 0.134 g, 0.42 mmol), followed by the addition of DCM (4 mL) and TFA (20 equiv., 0.956 g, 0.62 mL, 8.39 mmol). The reaction mixture was stirred at r.t. for 3h. The reaction mixture was then basified with 30 mL of satured solution of $NaHCO_3$ and extracted with DCM (3 x 30 mL). The organic layers were collected, dried with Na_2SO_4 and concentrated under reduced pressure to give the desired product (0.090 g, 0.41 mmol, 99%). LC/MS m/z $[M + H]^+$ 220.11.

5.4.15. Synthesis of (Z)-methyl N'-(4-cyanobenzoyl)-N-(cyclopropanecarbonyl)carbamimidothioate (257)

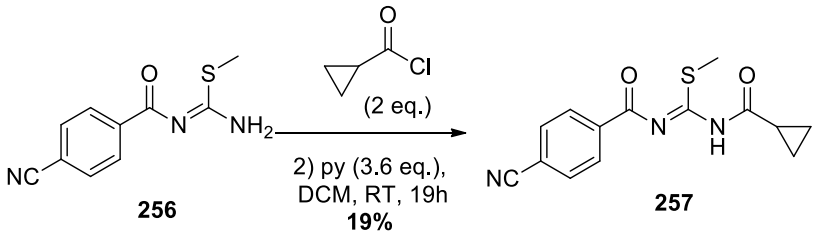

A 25 mL round bottom flask containing a Teflon stirrer bar was charged with compound **256** (1 equiv., 0.091 g, 0.41 mmol), py (3.6 equiv., 0.118 g, 0.120 mL, 1.49 mmol) and DCM (3 mL), followed by the dropwise addition of cyclopropanecarbonyl chloride (2 eq, 0.83 mmol) solution in DCM (1.6 mL). The reaction mixture was stirred for 19 hours at r.t. and the progress of the reaction was monitored by LC/MS. The reaction mixture was concentrated under reduced pressure, and the crude product was purified by chromatography column using PE/EtOAc (70/30) to give the desired product (0.022 g, 0.077 mmol, 19%). LC/MS m/z $[M + H]^+$ 288.23.

5.4.16. Synthesis of 3-((3,5-dibromo-1H-1,2,4-triazol-1-yl)methyl)benzonitrile (267)

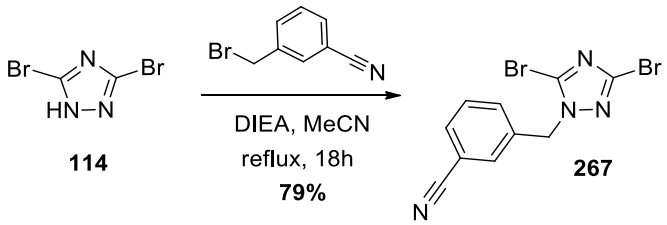

In a 100 mL round bottom flask containing a Teflon stirrer bar, 3,5-dibromo-1,2,4-triazole (1 equiv., 1 g, 4.4 mmol), 3-cyanobenzyl bromide (1 equiv., 0.87 g, 4.4 mmol), and DIPEA (2 equiv., 1.14 g, 1.46 mL, 8.84 mmol) were combined and dissolved in anhydrous MeCN (20 mL). The reaction mixture was maintained under stirring at reflux for 18 h and the progress of the reaction was monitored by HPLC. The reaction mixture was concentrated under reduced pressure, diluted with ethyl acetate (20 mL) and then washed with H_2O (3 x 20 mL). The organic phase was dried with anhydrous Na_2SO_4 and concentrated under reduced pressure. The crude product was purified by chromatography column on silica gel using gradient elution Hex/EtOAc (75/5 to 50/50) to give the desired product as a colorless oil which slowly

crytallized (1.19 g, 3.49 mmol, 79%). ^{1}H NMR (400 MHz, $CDCl_3$) δ 5.34 (s, 2H), 7.50-7.57 (m, 2H), 7.62 (m, 1H), 7.66-7.68 (dt, *J* = 1.6 Hz, *J* = 7.3 Hz, 1H). ^{13}C NMR (125 MHz, $CDCl_3$) δ 52.4, 118.9, 130.6, 131.8, 132, 132.6, 133, 136.6, 140.2.

5.4.17. Synthesis of ethyl 3-((3-bromo-5-oxo-4,5-dihydro-1H-1,2,4-triazol-1-yl)methyl)benzoate (265)

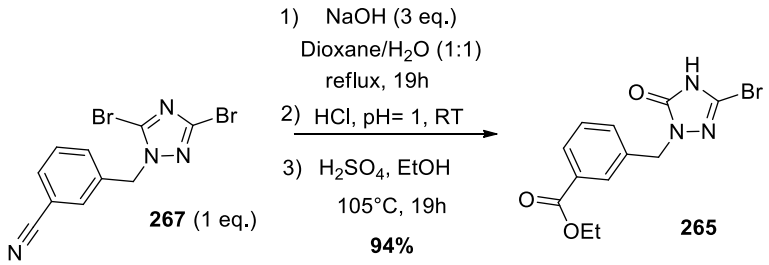

A 250 mL round bottom flask containing a Teflon stirrer bar was charged with 3-[(3,5-dibromo-1H-1,2,4-triazol-1-yl)methyl]benzonitrile (**267**) (1 equiv., 0.97 g, 2.85 mmol), NaOH (4 equiv., 0.45 g, 11.38 mmol), water (30 mL) and dioxane (30 mL). The reaction mixture stirred at reflux for 19 hours. After this time, the reaction mixture was cooled to r.t. and concentrated under reduced pressure. The pH of the mixture was adjusted to ~1 with drops of concentrated HCl. The mixture was then extracted with EtOAc (5 x 10 mL). The organic layers were collected, dried, and concentrated under reduced pressure. The crude product was then dissolved in EtOH (80 mL) and treated with H_2SO_4 (66 equiv., 18.7 g, 10 mL, 187.8 mmol). The mixture was stirred at reflux for 3 hours, and an additional H_2SO_4 (13 equiv., 3.72 g, 2 mL, 37 mmol) was added. The reaction mixture was stirred at reflux overnight. The progress of the reaction was monitored by HPLC. The reaction mixture was cooled to r.t. and concentrated under reduced pressure. The crude product was dissolved in 70 mL of H_2O, and the pH adjusted to 2. The aqueous solution was then extracted with DCM (3 x 70 mL). The organic layers were combined, dried with Na_2SO_4, and concentrated under reduced pressure to give the desire compound (0.87 g, 2.67 mmol, 94%). ^{1}H NMR (400 MHz, $CDCl_3$) δ 1.37-1.41 (t, *J* = 7.1 Hz, 3H), 4.35-4.40 (q, *J* = 7.1 Hz, 2H), 5.0 (s, 2H), 7.42-7.45 (t, *J* = 7.7 Hz, 1H), 7.53-7.55 (dt, *J* = 1.3 Hz, *J* = 7.7 Hz, 1H), 7.99-8.01 (dt, *J* = 1.3 Hz, *J* = 7.8 Hz, 1H), 8.02 (m, 1H), 12.19 (bs, 1H).

5.4.18. Synthesis of ethyl 3-((3-bromo-5-(((2,4,6-triisopropylphenyl)sulfonyl)oxy)-1H-1,2,4-triazol-1-yl)methyl)benzoate (263)

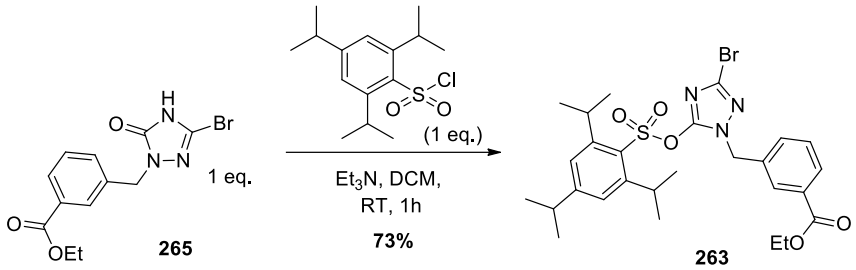

A 100 mL round bottom flask containing a Teflon stirrer bar was charged with ethyl 3-((3-bromo-5-oxo-4,5-dihydro-1H-1,2,4-triazol-1-yl)methyl)benzoate (**265**) (1 equiv., 0.43 g, 1.33 mmol), DCM (12 mL) and Et_3N (2 equiv., 0.27 g, 0.37 mL, 2.66 mmol). Afterwards, 2,4,6-triisopropylbenzenesulfonyl chloride (2 equiv., 0.8 g, 2.66 mmol) dissolved in 5 mL of dry DCM was added dropwise to the reaction mixture. The reaction mixture was stirred for 1 hour at r.t.. The progress of the reaction was monitored by HPLC and TLC (PE/EtOAc - 95/5, RF= 0.27). The reaction mixture was concentrated, and the crude product was purified on a silica gel column using PE/EtOAc (90/10) to give the desired product as a colorless oil (0.572 g, 0.97 mmol, 73%). ^{1}H NMR (400 MHz, $CDCl_3$) δ 1.24-1.26 (d, *J* = 6.7 Hz, 12H), 1.27-1.28 (d, *J* = 6.9 Hz, 6H), 1.38-1.42 (t, *J* = 7.1 Hz, 3H), 2.91-2.98 (m, *J* = 6.9 Hz, 1H), 3.94-4.04 (m, *J* = 6.7 Hz, 2H), 4.36-4.41 (q, *J* = 7.1 Hz, 2H), 5.29 (s, 2H), 7.24 (s, 2H), 7.44-7.47 (t, *J* = 7.9 Hz, 1H), 7.51-7.53 (d, *J* = 7.8 Hz, 1H), 8.03-8.04 (m, 1H). LC/MS m/z $[M + H]^+$ 592.20.

5.4.19. General procedure for the synthesis of ethyl 3-((3-Ar-5-(((2,4,6-triisopropylphenyl)sulfonyl)oxy)-1H-1,2,4-triazol-1-yl)methyl)benzoate (262a-d)

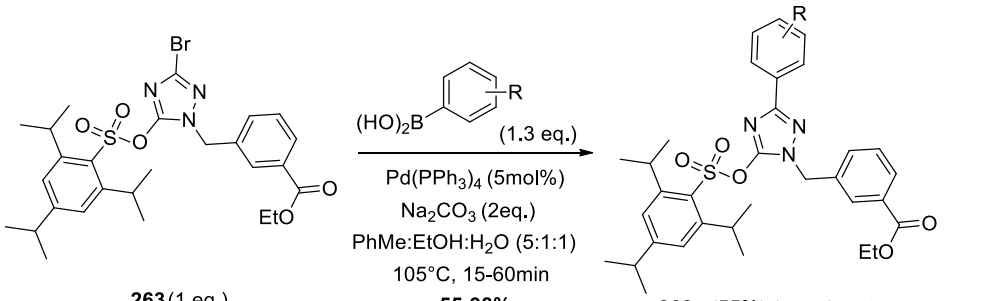

A microwave vial containing a Teflon stirrer bar was charged with compound (**263**) (1 equiv.), the corresponding boronic acid, Na_2CO_3 (2 equiv., 0.035 g, 0.34 mmol), and $Pd(PPh_3)_4$. The vessel was then capped properly, evacuated and backfilled with argon (this process was repeated a total of three times). A second microwave vial was charged

with toluene, ethanol and water capped properly, evacuated and backfilled with argon (this process was repeated a total of three times). This solvent mixture was then added to the mixture of solids. The reaction mixture was heated at 105°C for 15-60 min. The progress of the reaction was evaluated by TLC. The reaction mixture was concentrated, and the crude product was purified by chromatography on silica gel to give the desired products as viscous colorless oil.

5.4.19.1. Synthesis of ethyl 3-((3-phenyl-5-(((2,4,6-triisopropylphenyl)sulfonyl)oxy)-1H-1,2,4-triazol-1-yl)methyl)benzoate (262a)

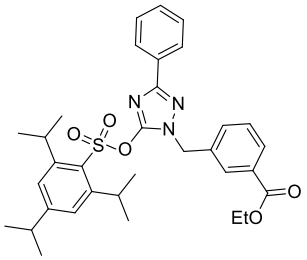

The synthesis followed the general procedure using compound **263** (1 equiv., 0.1 g, 0.17 mmol), phenylboronic acid (1.5 equiv., 0.030 g, 0.25 mmol), Na_2CO_3 (2 equiv., 0.035 g, 0.34 mmol), $Pd(PPh_3)_4$ (0.05 equiv., 0.010 g, 0.0084 mmol), MePh (2 mL), EtOH (0.4 mL) and H_2O (0.4 mL). The reaction mixture was placed in a microwave reactor and heated at 105°C for 15 min. The progress of the reaction was evaluated by LC/MS and TLC (PE/EtOAc - 90/10, RF= 0.42). The crude product was purified on a silica gel column using PE/EtOAc (90/10) to give the desired product as viscous colorless oil (0.055 g, 0.093 mmol, 55%).

5.4.19.2. Synthesis of ethyl 3-((3-(4-methoxyphenyl)-5-(((2,4,6-triisopropylphenyl)sulfonyl)oxy)-1H-1,2,4-triazol-1-yl)methyl)benzoate (262b)

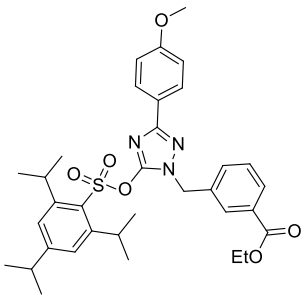

The synthesis followed the general procedure using compound **263** (1 equiv., 0.072 g, 0.12 mmol), *p*-methoxyphenylboronic acid (1.34 equiv., 0.024 g, 0.16 mmol), Na_2CO_3 (2 equiv., 0.026 g, 0.24 mmol), $Pd(PPh_3)_4$ (0.05 equiv., 0.007 g, 0.0061 mmol), MePh (2.8 mL), EtOH (0.6 mL) and H_2O (0.6 mL). The reaction mixture was placed in a microwave reactor and heated at 105°C for 1h. The progress of the reaction was evaluated by LC/MS and TLC

(PE/EtOAc - 95/5, RF= 0.39). The crude product was purified on a silica gel column using gradient elution PE/EtOAc (95/5 – 90/10) to give the desired product as viscous colorless oil (0.069 g, 0.11 mmol, 91%). ^{1}H NMR (400 MHz, $CDCl_3$) δ 1.25-1.26 (d, *J* = 6.7 Hz, 12H), 1.30-1.32 (d, *J* = 6.9 Hz, 6H), 1.39-1.43 (t, *J* = 7.1 Hz, 3H), 2.92-3.03 (m, *J* = 6.9 Hz, 1H), 3.82 (s, 3H), 4.05-4.17 (m, *J* = 6.7 Hz, 2H), 4.37-4.42 (q, *J* = 7.1 Hz, 2H), 5.36 (s, 2H), 6.86-6.84 (d, *J* = 8.9 Hz, 2H), 7.26-7.28 (d, *J* = 6.7 Hz, 2H), 7.43-7.47 (t, *J* = 7.7 Hz, 1H), 7.53-7.55 (d, *J* = 7.8 Hz, 1H), 7.77-7.79 (d, *J* = 8.9 Hz, 2H), 8.02-8.04 (d, *J* = 7.7 Hz, 1H), 8.09 (s, 1H). LC/MS m/z $[M + H]^+$ 622.5

5.4.19.3. Synthesis of ethyl 3-((3-(m-tolyl)-5-(((2,4,6-triisopropylphenyl)sulfonyl)oxy)-1H-1,2,4-triazol-1-yl)methyl)benzoate (262c)

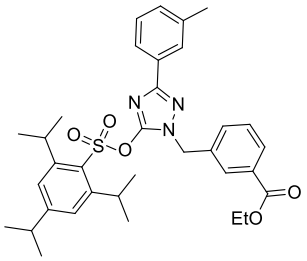

The synthesis followed the general procedure using compound **263** (1 equiv., 0.1 g, 0.17 mmol), *m*-tolylboronic acid (1.5 equiv., 0.035 g, 0.25 mmol), Na_2CO_3 (2 equiv., 0.035 g, 0.34 mmol), $Pd(PPh_3)_4$ (0.05 equiv., 0.010 g, 0.0084 mmol), MePh (2 mL), EtOH (0.4 mL) and H_2O (0.4 mL). The reaction mixture was placed in a microwave reactor and heated at 105°C for 15 min. The progress of the reaction was evaluated by LC/MS and TLC (PE/EtOAc – 90/10, RF= 0.41). The crude product was purified on a silica gel column using PE/EtOAc (90/10) to give the desired product as viscous colorless oil (0.083 g, 0.14 mmol, 82%). LC/MS m/z $[M + H]^+$ 604.9.

5.4.19.4. Synthesis of ethyl 3-((3-(3-chlorophenyl)-5-(((2,4,6-triisopropylphenyl)sulfonyl)oxy)-1H-1,2,4-triazol-1-yl)methyl)benzoate (262d)

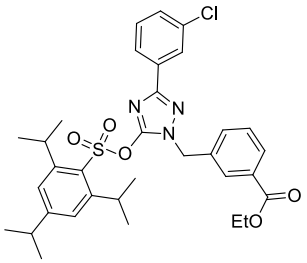

The synthesis followed the general procedure using compound **263** (1 equiv., 0.1 g, 0.17 mmol), *m*-chlorophenylboronic acid (1.3 equiv., 0.035 g, 0.23 mmol), Na_2SO_4 (2 equiv., 0.035 g, 0.34 mmol), $Pd(PPh_3)_4$ (0.05 equiv., 0.010 g, 0.0084 mmol), MePh (4 mL), EtOH (0.8 mL) and H_2O (0.8 mL). The reaction mixture was then placed in a preheated oil bath at 105°C for 1h. The progress of the reaction was evaluated by HPLC and TLC (PE/EtOAc - 90/10, RF= 0.41). The crude product was purified on a silica gel column using PE/EtOAc (90/10) to give the desired product as viscous colorless oil (0.103 g, 0.17 mmol, 98%). ^{1}H NMR (400 MHz, $CDCl_3$) δ 1.23-1.25 (d, *J* = 6.7 Hz, 12H), 1.29-1.30 (d, *J* = 6.9 Hz, 6H), 1.38-1.42 (t, *J* = 7.1 Hz, 3H), 2.91-3.02 (m, *J* = 6.9 Hz, 1H), 4.03-4.13 (m, *J* = 6.7 Hz, 2H), 4.36-4.41 (q, *J* = 7.1 Hz, 2H), 5.35 (s, 2H), 7.23-7.26 (m, 3H), 7.28-7.31 (m, 1H), 7.43-7.47 (t, *J* = 7.7 Hz, 1H), 7.52-7.54 (d, *J* = 7.8 Hz, 1H), 7.71-7.73 (dt, , *J* = 1.5 Hz, *J* = 7.5 Hz, 1H), 7.80-7.81 (t, *J* = 1.5 Hz, 1H), 8.01-8.03 (d, *J* = 7.7 Hz, 1H), 8.08 (s, 1H).

5.4.20. General procedure for the synthesis of 3-((5-oxo-3-Ar-4,5-dihydro-1H-1,2,4-triazol-1-yl)methyl)benzoic acid (215a-d)

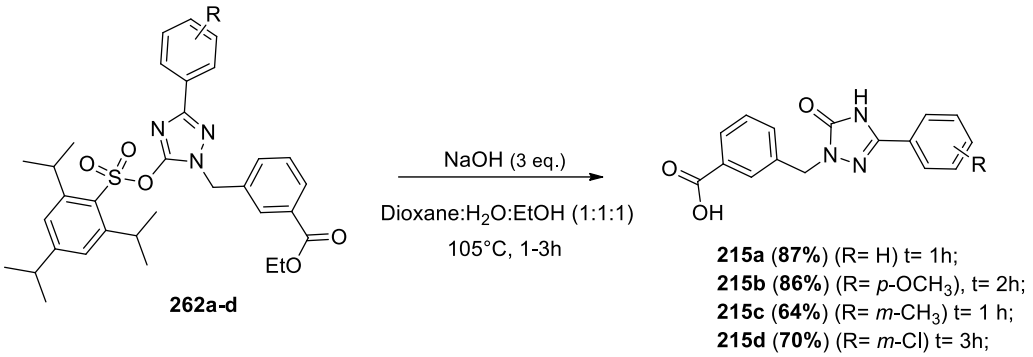

A 50 mL round-bottom flask containing a Teflon stirrer bar was charged with the corresponding compounds **262a-d** (1 equiv.), NaOH (3 equiv.) followed by the addition of water, ethanol, and dioxane. The reaction mixture was stirred at 105°C for 1-3h. After cooler to r.t., the amount of solvent was reduced under reduced pressure and the pH adjusted to ~2. The precipitate formed was then filtered off under reduced pressure to give the desire products **215a-d** as white solids.

5.4.20.1. 3-((5-oxo-3-phenyl-4,5-dihydro-1H-1,2,4-triazol-1-yl)methyl)benzoic acid (215a)

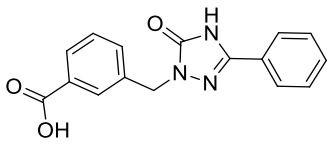

The synthesis followed the general procedure using compound **262a** (1 equiv., 0.055 g, 0.093 mmol), NaOH (3 equiv., 0.011 g, 0.28 mmol), H_2O (1 mL), EtOH (2 mL) and dioxane (2 mL). The reaction mixture was then placed in a preheated oil bath at 105°C for 1h. After cooler to r.t., the amount of solvent was reduced under reduced pressure and the pH adjusted to ~2. The precipitate formed was then filtered off under reduced pressure to give the desire product **215a** as white solids (0.023 g, 0.080 mmol, 87%). ^{1}H NMR (400 MHz, DMSO) δ 5.02 (s, 2H), 7.47-7.52 (m, 4H), 7.56-7.58 (d, *J* = 7.7 Hz, 1H), 7.77-7.80 (m, 2H), 7.86-7.88 (m, 2H), 12.39 (s, 1H), 13.03 (bs, 1H). ^{13}C NMR (125 MHz, DMSO) δ 47.8, 125.3, 126.9, 128.7, 128.9, 129.4, 129.5, 130.7, 131.5, 132.5, 138.3, 144.5, 154.6, 167.5. LC/MS m/z $[M + H]^+$ 296.13.

5.4.20.2. 3-((3-(4-methoxyphenyl)-5-oxo-4,5-dihydro-1H-1,2,4-triazol-1-yl)methyl)benzoic acid (215b)

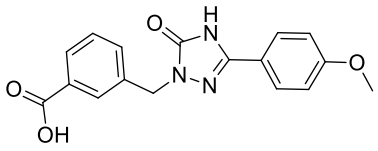

The synthesis followed the general procedure using compound **262b** (1 equiv., 0.068 g, 0.11 mmol), NaOH (3 equiv., 0.013 g, 0.33 mmol), H_2O (1.1 mL), EtOH (2.2 mL) and dioxane (2.2 mL). The reaction mixture was then heated using oil bath at 105°C for 2h. After cooler to r.t., the amount of solvent was reduced under reduced pressure and the pH adjusted to ~2. The precipitate formed was then filtered off under reduced pressure to give the desire product **215b** as white solids (0.030 g, 0.095 mmol, 86%). ^{1}H NMR (400 MHz, DMSO) δ 3.79 (s, 3H), 4.98 (s, 2H), 7.47-7.52 (m, 4H), 7.02-7.04 (d, *J* = 8.8 Hz, 1H), 7.47-7.51 (t, *J* = 7.8 Hz, 1H), 7.54-7.56 (d, *J* = 7.7 Hz, 2H), 7.71-7.73 (d, *J* = 8.8 Hz, 2H), 7.86 (m, 2H), 12.24 (s, 1H), 13.03 (bs, 1H). ^{13}C NMR (125 MHz, DMSO) δ 47.8, 55.8, 114.9, 119.4, 114.9, 119.4, 127, 128.7, 128.9, 129.4, 131.5, 132.5, 138.3, 144.5, 155, 161.1, 167.6.

5.4.20.3. 3-((5-oxo-3-(m-tolyl)-4,5-dihydro-1H-1,2,4-triazol-1-yl)methyl)benzoic acid (215c)

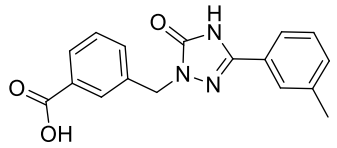

The synthesis followed the general procedure using compound **262c** (1 equiv., 0.084 g, 0.14 mmol), NaOH (3 equiv., 0.017 g, 0.42 mmol), H_2O (1.5 mL), EtOH (3 mL) and dioxane (3 mL). The reaction mixture was then heated using oil bath at 105°C for 1h. After cooler to r.t., the amount of solvent was reduced under reduced pressure and the pH adjusted to ~2. The precipitate formed was then filtered off under reduced pressure to give the desire product **215c** as white solids (0.027 g, 0.089 mmol, 64%). ^{1}H NMR (400 MHz, DMSO) δ 2.33 (s, 3H), 5.0 (s, 2H), 7.27-7.28 (d, *J* = 7.4 Hz, 1H), 7.34-7.38 (t, *J* = 7.5 Hz, 1H), 7.47-7.51 (t, *J* = 7.8 Hz, 1H), 7.55-7.58 (m, 2H), 7.62 (s, 1H), 7.86 (s, 2H), 12.32 (s, 1H), 13.02 (bs, 1H). ^{13}C NMR (125 MHz, DMSO) δ 21.4, 47.8, 122.6, 125.8, 126.9, 128.7, 128.9, 129.3, 129.4, 131.3, 131.6, 132.4, 138.3, 138.8, 144.6, 154.9, 167.5. LC/MS m/z $[M + H]^+$ 310.23.

5.4.20.4. 3-((3-(3-chlorophenyl)-5-oxo-4,5-dihydro-1H-1,2,4-triazol-1-yl)methyl)benzoic acid (215d)

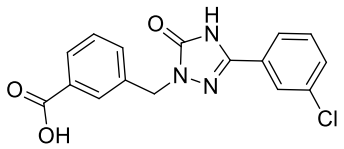

The synthesis followed the general procedure using compound **262d** (1 equiv., 0.081 g, 0.13 mmol), NaOH (3 equiv., 0.016 g, 0.39 mmol), H_2O (1.3 mL), EtOH (2.6 mL) and dioxane (2.6 mL). The reaction mixture was then heated using oil bath at 105°C for 3h. After cooler to r.t., the amount of solvent was reduced under reduced pressure and the pH adjusted to ~2. The precipitate formed was then filtered off under reduced pressure to give the desire product **215d** as white solids (0.030 g, 0.091 mmol, 70%). ^{1}H NMR (400 MHz, DMSO) δ 5.03 (s, 2H), 7.49-7.58 (m, 4H), 7.75-7.77 (dt, , *J* = 6.9 Hz, 1H), 7.83 (m, 2H), 7.87-7.89 (m, 2H), 12.46 (s, 1H), 13.04 (bs, 1H). ^{13}C NMR (125 MHz, DMSO) δ 47.9, 123.9, 125, 128.7, 128.9, 129, 129.5, 130.4, 131.5, 132.5, 134.3, 138, 143.3, 159.8, 167.5. LC/MS m/z $[M + H]^+$ 330.14.

5.4.21. tert-butyl 2-(3,5-dibromo-1H-1,2,4-triazol-1-yl)acetate (277)

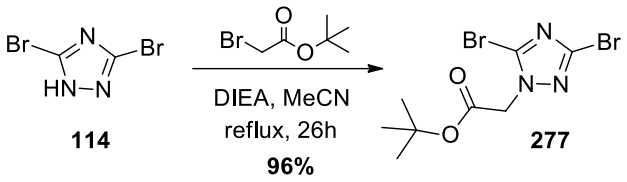

A 100 mL round bottom flask containing a Teflon stirrer bar was charged with 3,5-dibromo-1,2,4-triazole (1 equiv., 5 g, 22.04 mmol) (**114**) and dissolved in acetonitrile (100 mL). Then, *tert*-butyl bromoacetate (1 equiv., 4.3 g, 3.2 mL, 22.04 mmol) and DIPEA (2 equiv., 5.7 g, 7.3 mL, 44.18 mmol) were added, and the mixture was refluxed for 26 hours. The reaction mixture was then cooled to room temperature and concentrated under reduced pressure. The crude product was solubilized with EtOAc (70 mL) and washed with H_2O (3 x 70 mL). The organic phase was dried with anhydrous Na_2SO_4 and concentrated under reduced pressure to give the desired product (7.2 g, 21.2 mmol, 96%). ^{1}H NMR (400 MHz, $CDCl_3$) δ 1.48 (s, 3H), 4.81 (s, 2H).

5.4.22. tert-butyl 2-(5-(2-aminophenyl)-3-bromo-1H-1,2,4-triazol-1-yl)acetate (278)

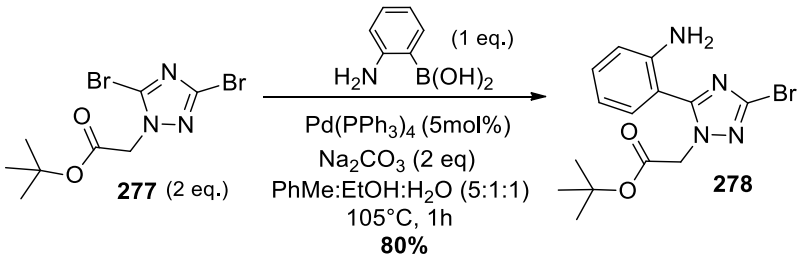

A 250 mL round-bottom flask containing a Teflon stirrer bar was charged with Tert-butyl 2-(3,5-dibromo-1H-1,2,4-triazol-1-yl)acetate (**277**) (2 equiv., 3.8 g, 11.056 mmol), (2-aminophenyl)boronic acid (1 equiv., 0.76 g, 5.53 mmol) and Na_2CO_3 (2 equiv., 1.2 g, 11.06 mmol) followed by the addition of MePh (48.6 mL), EtOH (9.7 mL), and H_2O (9.7 mL). The reaction mixture was then flushed with argon under stirring (this process was performed a total of 10 min.). The catalyst $Pd(PPh_3)_4$ (0.05 equiv., 322.62 mg, 0.28 mmol) was then added and the reaction mixture was placed in a preheated oil bath stirred at 105°C for 3 hours. The progress of the reaction was monitored by TLC. After cooling to r.t., the reaction mixture was concentrated, and the crude product was purified by chromatography on silica gel using gradiet elution PE/EtOAc (80/20 – 70/30) to give the desired product (1.56 g, 4.42 mmol, 80%). ^{1}H

NMR (400 MHz, $CDCl_3$) δ 1.45 (s, 9H), 4.69 (bs, 2H), 4.80 (s, 2H), 6.72-6.79 (m, 2H), 7.16-7.18 (dd, *J* = 1.3 Hz, *J* = 7.7 Hz, 1H), 7.23-7.27 (m, 1H). LC/MS m/z $[M + H]^+$ 353.1.

5.4.23. 2-bromo-5H-benzo[f][1,2,4]triazolo[1,5-d][1,4]diazepin-6(7H)-one (271)

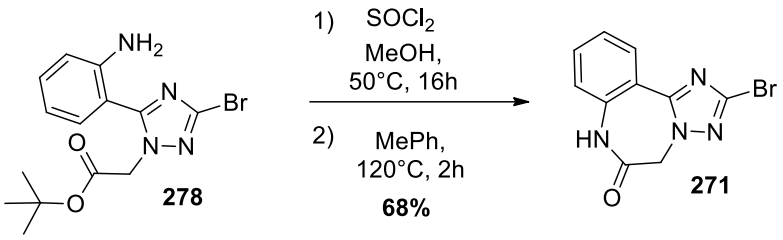

A 25 mL round-bottom flask containing a Teflon stirrer bar was charged with compound **278** (1 equiv., 0.030 g, 0.099 mmol) and MeOH (1 mL). The mixture was cooled to 0°C using ice bath and then $SOCl_2$ (4 equiv., 0.047 g, 0.029 mL, 0.4 mmol) was added dropwise. The temperature of the reaction mixture was increased to 50°C and maintained under stirring for 5h. The progress of the reaction was monitored by HPLC. The reaction mixture was then concentrated under reduced pressure. The crude product was solubilized with MePh (3 mL) in a microwave vial, capped properly and then stirred at 120°C for 2 h. The reaction was cooled to r.t., concentrated and the precipitate formed filtered off under reduced pressure to give the desire product as white solid (0.019 g, 0.067 mmol, 68%). ^{1}H NMR (400 MHz, DMSO) δ 4.96 (s, 2H), 7.30-7.33 (d, *J* = 8.2 Hz, 1H), 7.35-7.39 (t, *J* = 7.5 Hz, 1H), 7.61-7.65 (t, *J* = 8.5 Hz, 1H), 7.88-7.90 (dd, *J* = 1.4 Hz, *J* = 7.8 Hz, 1H), 10.87 (s, 1H).

5.4.24. General procedure for the synthesis of tert-butyl 2-(5-(2-aminophenyl)-3-Ar-1H-1,2,4-triazol-1-yl)acetate (279a-e)

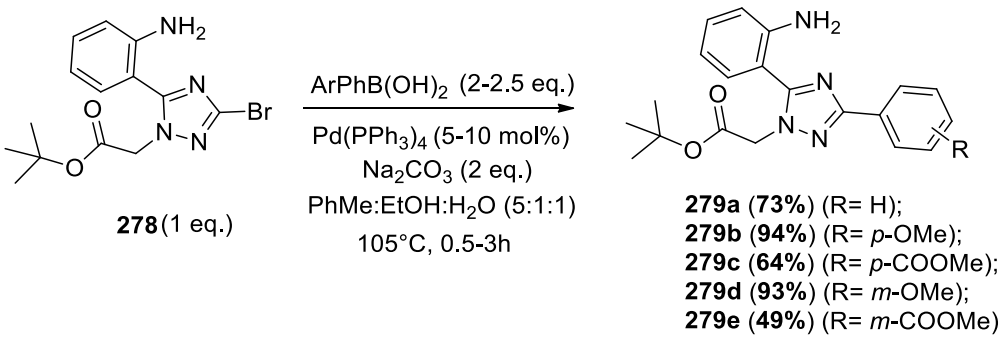

279a (**73%**) (R= H);
279b (**94%**) (R= *p*-OMe);
279c (**64%**) (R= *p*-COOMe);
279d (**93%**) (R= *m*-OMe);
279e (**49%**) (R= *m*-COOMe)

A microwave vial or 50 mL round-bottom flask containing a Teflon stirrer bar was charged with compound **278** (1 equiv.), the corresponding boronic acids and Na_2CO_3 (2 equiv.) followed by the addition of MePh, EtOH and H_2O. The mixture was flushed with N_2 under stirring for 10 min. and then, $Pd(PPh_3)_4$ was added. The reaction mixture was placed in a microwave reactor and stirred at 105°C for 1-3h. After cooling to r.t., the reaction mixture was concentrated, and the crude product was purified by chromatography on silica gel to give the desire product.

5.4.24.1. Synthesis of tert-butyl 2-(5-(2-aminophenyl)-3-phenyl-1H-1,2,4-triazol-1-yl)acetate (279a)

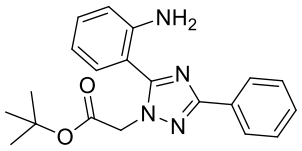

The synthesis followed the general procedure. A microwave vial containing a Teflon stirrer bar was charged with compound **278** (1 equiv., 0.05 g, 0.099 mmol), phenylboronic acid (2 equiv., 0.024, 0.2 mmol) and Na_2CO_3 (2 equiv., 0.021 g, 0.2 mmol) followed by the addition of MePh (0.87 mL), EtOH (0.17 mL) and H_2O (0.17 mL). The mixture was flushed with N_2 under stirring for 10 min. and then, $Pd(PPh_3)_4$ (0.05 equiv., 0.0057 g, 0.005 mmol) was added. The reaction mixture was placed in a microwave reactor and stirred at 105°C for 30 min. The progress of the reaction was monitored by TLC (PE/EtOAc (80/20), RF= 0.4). After cooling to r.t., the reaction mixture was concentrated, and the crude product was purified by chromatography on silica gel using PE/EtOAc (80/20) to give the desire product. LC/MS m/z $[M + H]^+$ 351.24.

5.4.24.2. Synthesis of tert-butyl 2-(5-(2-aminophenyl)-3-(4-methoxyphenyl)-1H-1,2,4-triazol-1-yl)acetate (279b)

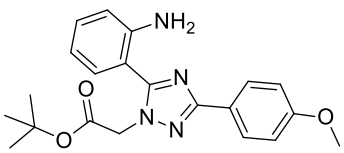

The synthesis followed the general procedure. A 50 mL round-bottom flask was charged with a Teflon stirrer bar was charged with compound **278** (1 equiv., 0.2 g, 0.57 mmol), 4-

methoxyphenylboronic acid (2 equiv., 0.172 g, 1.13 mmol) and Na_2CO_3 (2 equiv., 0.12 g, 1.13 mmol) followed by the addition of MePh (5 mL), EtOH (1 mL) and H_2O (1 mL). The mixture was flushed with N_2 under stirring for 10 min. and then, $Pd(PPh_3)_4$ (0.05 equiv., 0.033 g, 0.028 mmol) was added. The reaction mixture was heated using oil bath and stirred at 105°C for 3h. The progress of the reaction was monitored by TLC (PE/EtOAc (70/30), RF= 0.43). After cooling to r.t., the reaction mixture was concentrated, and the crude product was purified by chromatography on silica gel using PE/EtOAc (70/30) to give the desire product (0.203 g, 0.53 mmol, 94%). ^{1}H NMR (400 MHz, $CDCl_3$) δ 1.46 (s, 9H), 3.86 (s, 3H), 4.82 (bs, 1H), 4.86 (s, 1H), 6.76-6.82 (m, 2H), 6.95-6.97 (d, *J* = 8.9 Hz, 2H), 7.22-7.25 (m, 3H), 8.07-8.09 (d, *J* = 8.9 Hz, 2H).

5.4.24.3. Synthesis of methyl 4-(5-(2-aminophenyl)-1-(2-(tert-butoxy)-2-oxoethyl)-1H-1,2,4-triazol-3-yl)benzoate (279c)

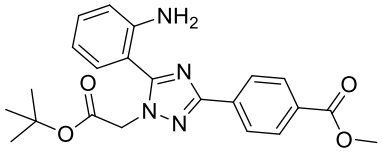

The synthesis followed the general procedure. A 50 mL round-bottom flask was charged with a Teflon stirrer bar was charged with compound **278** (1 equiv., 0.3 g, 0.85 mmol), 4-methoxycarbonylphenylboronic acid (2 equiv., 0.305 g, 1.7 mmol) and Na_2CO_3 (2 equiv., 0.18 g, 1.7 mmol) followed by the addition of MePh (7.5 mL), EtOH (1.5 mL) and H_2O (1.5 mL). The mixture was flushed with N_2 under stirring for 10 min. and then, $Pd(PPh_3)_4$ (0.1 equiv., 0.099 g, 0.085 mmol) was added. The reaction mixture was heated using oil bath and stirred at 105°C for 1h. The progress of the reaction was monitored by TLC (PE/EtOAc (80/20), RF= 0.31). After cooling to r.t., the reaction mixture was concentrated, and the crude product was purified by chromatography on silica gel using PE/EtOAc (80/20) to give the desire product (0.222 g, 0.54 mmol, 64%). LC/MS m/z $[M + H]^+$ 409.36.

5.4.24.4. Synthesis of tert-butyl 2-(5-(2-aminophenyl)-3-(3-methoxyphenyl)-1H-1,2,4-triazol-1-yl)acetate (279d)

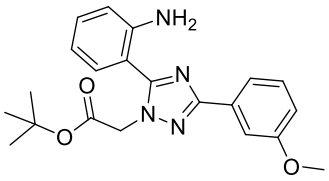

The synthesis followed the general procedure. A 50 mL round-bottom flask was charged with a Teflon stirrer bar was charged with compound **278** (1 equiv., 0.189 g, 0.54 mmol), 3-methoxyphenylboronic acid (2 equiv., 0.163, 1.07 mmol) and Na_2CO_3 (2 equiv., 0.11 g, 1.07 mmol) followed by the addition of MePh (5 mL), EtOH (1 mL) and H_2O (1 mL). The mixture was flushed with N_2 under stirring for 10 min. and then, $Pd(PPh_3)_4$ (0.05 equiv., 0.031 g, 0.027 mmol) was added. The reaction mixture was placed in a pre-heated reactor and stirred at 105°C for 3h. The progress of the reaction was monitored by TLC (PE/EtOAc (70/30), RF= 0.47). After cooling to r.t., the reaction mixture was concentrated, and the crude product was purified by chromatography on silica gel using PE/EtOAc (70/30) to give the desire product (0.156 g, 0.41 mmol, 77%). %). ^{1}H NMR (400 MHz, $CDCl_3$) δ 1.46 (s, 9H), 3.89 (s, 3H), 4.82 (bs, 2H), 4.89 (s, H), 6.77-6.82 (m, 2H), 6.95-6.98 (dd, *J* = 2.5 Hz, *J* = 7.6 Hz, 1H), 7.24-7.28 (m, 2H), 7.33-7.37 (t, *J* = 7.9 Hz, 1H), 7.69 (m, 1H), 7.74-7.76 (d, *J* = 7.7 Hz, 2H). LC/MS m/z $[M + H]^+$ 381.4.

5.4.24.5. Synthesis of methyl 3-(5-(2-aminophenyl)-1-(2-(tert-butoxy)-2-oxoethyl)-1H-1,2,4-triazol-3-yl)benzoate (279e)

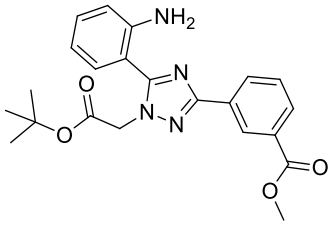

The synthesis followed the general procedure. A 50 mL round-bottom flask was charged with a Teflon stirrer bar was charged with compound **278** (1 equiv., 0.1 g, 0.28 mmol), 3-methoxyphenylboronic acid (2.5 equiv., 0.127, 0.7 mmol) and Na_2CO_3 (2 equiv., 0.06 g, 0.57 mmol) followed by the addition of MePh (2.5 mL), EtOH (0.5 mL) and H_2O (0.5 mL). The mixture was flushed with N_2 under stirring for 10 min. and then, $Pd(PPh_3)_4$ (0.1 equiv., 0.033 g, 0.028 mmol) was added. The reaction mixture was heated using oil bath and stirred at 105°C for 1h. The progress of the reaction was monitored by TLC (PE/EtOAc (80/20), RF= 0.31). After cooling to r.t., the reaction mixture was concentrated, and the crude product was purified

by chromatography on silica gel using PE/EtOAc (80/20) to give the desire product (0.108 g, 0.26 mmol, 93%). LC/MS m/z $[M + H]^+$ 409.4.

5.4.25. Synthesis of 2-Ar-5H-benzo[f][1,2,4]triazolo[1,5-d][1,4]diazepin-6(7H)-one (216a-e)

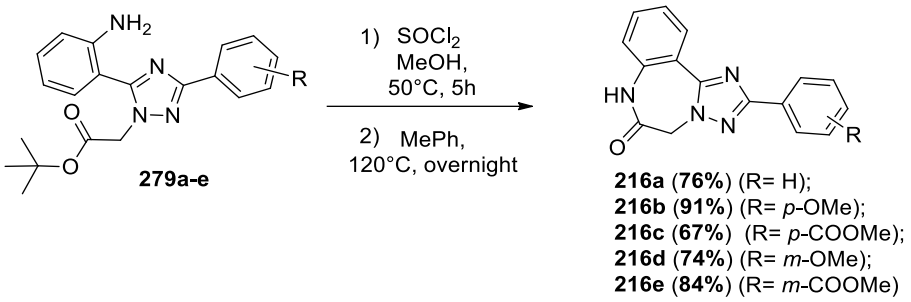

216a (**76%**) (R= H);
216b (**91%**) (R= *p*-OMe);
216c (**67%**) (R= *p*-COOMe);
216d (**74%**) (R= *m*-OMe);
216e (**84%**) (R= *m*-COOMe)

5.4.25.1. 2-phenyl-5H-benzo[f][1,2,4]triazolo[1,5-d][1,4]diazepin-6(7H)-one (216a)

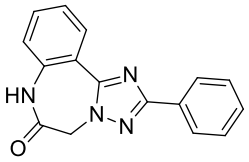

A 25 mL round-bottom flask containing a Teflon stirrer bar was charged with compound **279a** (1 equiv., 0.025 g, 0.071 mmol) and MeOH (1 mL). The mixture was cooled to 0°C using ice bath and then $SOCl_2$ (4 equiv., 0.034 g, 0.020 mL, 0.3 mmol) was added dropwise. The temperature of the reaction mixture was increased to 50°C and maintained under stirring for 5h. The progress of the reaction was monitored by HPLC. The reaction mixture was then concentrated under reduced pressure. The crude product was solubilized with MePh (3 mL) in a microwave vial, capped properly and then stirred at 120°C for 16 h. The reaction was cooled to r.t., concentrated and the precipitate formed filtered off under reduced pressure to give the desire product as white solid (0.015 g, 0.054 mmol, 76%). ^{1}H NMR (400 MHz, DMSO) δ 5.01 (s, 2H), 7.31-7.33 (d, *J* = 7.3 Hz, 1H), 7.40 (s, 1H), 7.48-7.51 (m, 3H), 7.62 (s, 1H), 8.0-8.02 (d, *J* = 6.7 Hz, 1H), 8.07-8.08 (d, *J* = 6.7 Hz, 2H), 10.85 (s, 1H). ^{13}C NMR (125 MHz, DMSO) δ 53.3, 118, 122.6, 125.3, 126.4, 129.3, 129.7, 130, 130.9, 132.3, 136.3, 153.15, 161.6, 167.5. LC/MS m/z $[M + H]^+$ 277.1.

5.4.25.2. 2-(4-methoxyphenyl)-5H-benzo[f][1,2,4]triazolo[1,5-d][1,4]diazepin-6(7H)-one (216b)

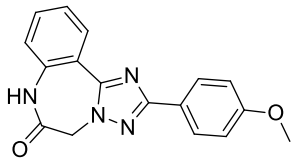

A 25 mL round-bottom flask containing a Teflon stirrer bar was charged with compound **279b** (1 equiv., 0.202 g, 0.53 mmol) and MeOH (7.5 mL). The mixture was cooled to 0°C using ice bath and then $SOCl_2$ (4 equiv., 0.252 g, 0.154 mL, 2.2 mmol) was added dropwise. The temperature of the reaction mixture was increased to 50°C and maintained under stirring for 14h. The reaction was cooled to r.t., concentrated and the precipitate formed was filtered off under reduced pressure to give the desire product as white solid (0.148 g, 0.48 mmol, 91%). ^{1}H NMR (400 MHz, DMSO) δ 3.82 (s, 3H), 4.98 (s, 2H), 7.05-7.07 (d, , *J* = 8.4 Hz, 2H), 7.31-7.33 (d, *J* = 8.2 Hz, 1H), 7.37-7.40 (t, , *J* = 7.6 Hz, 1H), 7.59-7.63 (t, *J* = 7.7 Hz, 1H), 7.99-8.01 (d, *J* = 8.4 Hz, 3H), 10.85 (s, 1H). ^{13}C NMR (125 MHz, DMSO) δ 53.2, 55.7, 114.7, 118, 122.6, 123.4, 125.2, 127.9, 129.6, 132.2, 136.3, 152.9, 160.7, 161.4, 167.5. LC/MS m/z $[M + H]^+$ 307.2.

5.4.25.3. methyl 4-(6-oxo-6,7-dihydro-5H-benzo[f][1,2,4]triazolo[1,5-d][1,4]diazepin-2-yl)benzoate (216c)

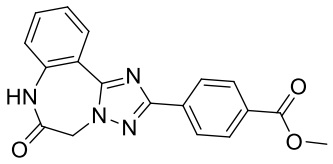

A 25 mL round-bottom flask containing a Teflon stirrer bar was charged with compound **279c** (1 equiv., 0.221 g, 0.54 mmol) and MeOH (7.6 mL). The mixture was cooled to 0°C using ice bath and then $SOCl_2$ (4 equiv., 0.257 g, 0.157 mL, 2.16 mmol) was added dropwise. The temperature of the reaction mixture was increased to 50°C and maintained under stirring for 16h. The reaction was cooled to r.t., concentrated and the precipitate formed filtered off under reduced pressure to give the desire product as white solid (0.120 g, 0.36 mmol, 67%). ^{1}H NMR (400 MHz, DMSO) δ 3.89 (s, 3H), 5.04 (s, 2H), 7.32-7.34 (d, *J* = 7.3 Hz, 1H), 7.41 (s, 1H), 7.63 (s, 1H), 8.01-8.02 (d, *J* = 6.8 Hz, 3H), 8.09-8.11 (d, *J* = 7.1 Hz, 2H), 8.21-8.22 (d, *J* = 7.1 Hz, 2H), 10.87 (s, 1H). ^{13}C NMR (125 MHz, DMSO) δ 52.7, 53.4, 117.8, 122.6, 125.3, 126.6,

129.7, 130.3, 130.6, 132.4, 135.1, 136.4, 153.5, 160.6, 166.4, 167.3. LC/MS m/z $[M + H]^+$ 335.24.

5.4.25.4. 2-(3-methoxyphenyl)-5H-benzo[f][1,2,4]triazolo[1,5-d][1,4]diazepin-6(7H)-one (216d)

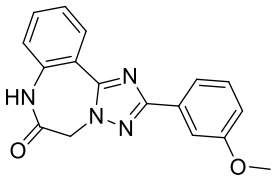

A 25 mL round-bottom flask containing a Teflon stirrer bar was charged with compound **279d** (1 equiv., 0.12 g, 0.32 mmol) and MeOH (4.5 mL). The mixture was cooled to 0°C using ice bath and then $SOCl_2$ (4 equiv., 0.15 g, 0.091 mL, 1.26 mmol) was added dropwise. The temperature of the reaction mixture was increased to 50°C and maintained under stirring for 15h. The reaction was cooled to r.t., concentrated and the precipitate formed filtered off under reduced pressure to give the desire product as white solid (0.071 g, 0.23 mmol, 74%). ^{1}H NMR (400 MHz, DMSO) δ 3.82 (s, 3H), 5.0 (s, 2H), 7.02-7.04 (d, , *J* = 8.2 Hz, 2H), 7.31-7.33 (d, *J* = 8.2 Hz, 1H), 7.37-7.43 (m, 2H), 7.57-7.66 (m, 3H), 7.99-8.01 (d, *J* = 7.7 Hz, 1H), 10.84 (s, 1H). ^{13}C NMR (125 MHz, DMSO) δ 53.3, 55.6, 111.2, 115.9, 117.9, 118.8, 122.6, 125.2, 129.7, 130.6, 132.2, 132.3, 136.3, 153.1, 160, 161.4, 167.4. LC/MS m/z $[M + H]^+$ 307.23.

5.4.25.5. methyl 3-(6-oxo-6,7-dihydro-5H-benzo[f][1,2,4]triazolo[1,5-d][1,4]diazepin-2-yl)benzoate (216e)

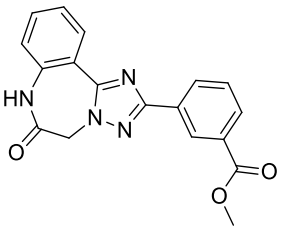

A 25 mL round-bottom flask containing a Teflon stirrer bar was charged with compound **279e** (1 equiv., 0.68 g, 0.17 mmol) and MeOH (2.3 mL). The mixture was cooled to 0°C using ice bath and then $SOCl_2$ (4 equiv., 0.080 g, 0.049 mL, 0.67 mmol) was added dropwise. The temperature of the reaction mixture was increased to 50°C and maintained under stirring for 16h. The reaction mixture was then concentrated under reduced pressure. The crude product was solubilized with MePh (5 mL) in a microwave vial, capped properly and then stirred at

120°C for 7h. The reaction was cooled to r.t., concentrated and the precipitate formed filtered off under reduced pressure to give the desire product as white solid (0.047 g, 0.014 mmol, 84%). ^{1}H NMR (400 MHz, DMSO) δ 3.91 (s, 3H), 5.04 (s, 2H), 7.32-7.34 (d, *J* = 8 Hz, 1H), 7.39-7.41 (t, *J* = 7.5 Hz, 1H), 7.62-7.65 (t, *J* = 7.7 Hz, 1H), 7.67-7.70 (t, *J* = 6.7 Hz, 1H), 8.03-8.05 (m, 2H), 8.32-8.33 (d, *J* = 7.6 Hz, 1H), 8.66 (s, 1H), 10.86 (s, 1H). ^{13}C NMR (125 MHz, DMSO) δ 52.9, 53.3, 117.8, 122.6, 125.3, 126.8, 129.7, 130, 130.5, 130.7, 130.8, 131.4, 132.4, 136.4, 153.4, 160.6, 166.4, 167.4. LC/MS m/z $[M + H]^+$ 335.24.

5.4.26. Synthesis of 2-(3- and 4-hydroxyphenyl)-5H-benzo[f][1,2,4]triazolo[1,5-d][1,4]diazepin-6(7H)-one (216f-g)

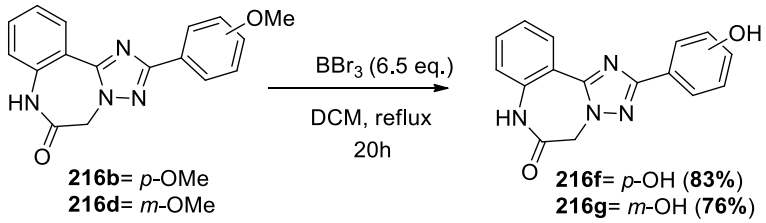

216b= *p*-OMe
216d= *m*-OMe

216f= *p*-OH (**83%**)
216g= *m*-OH (**76%**)

5.4.26.1. 2-(4-hydroxyphenyl)-5H-benzo[f][1,2,4]triazolo[1,5-d][1,4]diazepin-6(7H)-one (216f)

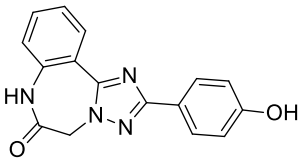

A microwave vial with a Teflon stirrer bar was charged with compound **216b** (1 equiv., 0.025 g, 0.082 mmol) and dissolved in DCM (1 mL). The mixture was cooled to 0°C using ice bath and stirred for 10 minutes. Then, BBr_3 (6.5 equiv., 0.133 mg, 0.050 mL, 0.53 mmol) was added, the vial was capped properly and the reaction mixture stirred at refluxed overnight. The progress of the reaction was monitored by LC/MS. The reaction mixture was then cooled to room temperature, and the crude product was purified by chromatography column using DCM/MeOH (98/2) to yield the desired product as white solid (0.020 g, 0.067 mmol, 83%). ^{1}H NMR (400 MHz, DMSO) δ 4.95 (s, 2H), 6.86-6.88 (d, , *J* = 7.7 Hz, 2H), 7.30-7.32 (d, *J* = 7.7 Hz, 1H), 7.37-7.40 (t, , *J* = 7 Hz, 1H), 7.59-7.62 (t, *J* = 7 Hz, 1H), 7.88-7.89 (d, *J* = 7.7 Hz, 2H), 7.98-7.99 (d, *J* = 7.3 Hz, 1H), 9.82 (s, 1H), 10.82 (s, 1H). ^{13}C NMR (125 MHz, DMSO) δ 53.13,

116, 118.1, 122, 122.6, 125.2, 128, 129.6, 132.1, 136.2, 152.8, 159, 161.9, 167.6. LC/MS m/z $[M + H]^+$ 293.23.

5.4.26.2. 2-(3-hydroxyphenyl)-5H-benzo[f][1,2,4]triazolo[1,5-d][1,4]diazepin-6(7H)-one (216g)

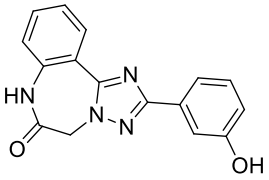

A microwave vial with a Teflon stirrer bar was charged with compound **216d** (1 equiv., 0.025 g, 0.082 mmol) and dissolved in DCM (1 mL). The mixture was cooled to 0°C using ice bath and stirred for 10 minutes. Then, BBr_3 (6.5 equiv., 0.133 mg, 0.050 mL, 0.53 mmol) was added, the vial was capped properly and the reaction mixture stirred at refluxed overnight. The progress of the reaction was monitored by LC/MS. The reaction mixture was then cooled to room temperature, and the crude product was purified by chromatography column using DCM/MeOH (98/2) to yield the desired product as white solid (0.018 g, 0.062 mmol, 76%). ^{1}H NMR (400 MHz, DMSO) δ 5.0 (s, 2H), 6.84-6.85 (d, , *J* = 7.7 Hz, 2H), 7.28-7.33 (m, 2H), 7.38-7.41 (t, , *J* = 7.5 Hz, 1H), 7.51 (m, 2H), 7.60-7.63 (t, *J* = 7.4 Hz,12H), 7.98-8.0 (d, *J* = 7.6 Hz, 1H), 9.66 (s, 1H), 10.84 (s, 1H). ^{13}C NMR (125 MHz, DMSO) δ 53.25, 113, 117, 118, 122.6, 125.2, 129.6, 130.4, 132.1, 132.2, 136.3, 153, 158.1, 161.2, 167.5. LC/MS m/z $[M + H]^+$ 293.23.

5.4.27. Synthesis of 3- and 4-(6-oxo-6,7-dihydro-5H-benzo[f][1,2,4]triazolo[1,5-d][1,4]diazepin-2-yl)benzoic acid (216h-i)

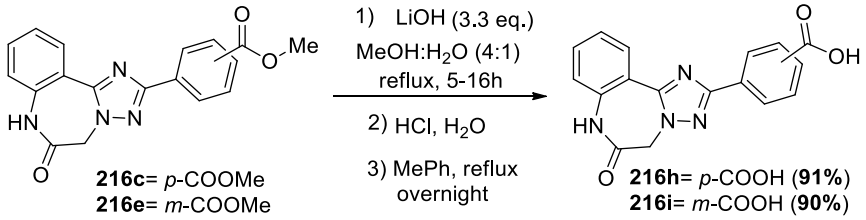

5.4.27.1. 4-(6-oxo-6,7-dihydro-5H-benzo[f][1,2,4]triazolo[1,5-d][1,4]diazepin-2-yl)benzoic acid (216h)

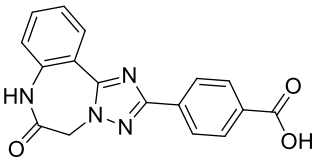

A 25 mL round-bottom flask with a Teflon stirrer bar was charged with compound **216c** (1 equiv., 0.025 g, 0.075 mmol), LiOH (3.3 equiv., 0.010 g, 0.25 mmol) followed by the addition of water (2 mL) and MeOH (8 mL). The reaction mixture was stirred at reflux for 5h. The progress of the reaction was monitored by LC/MS. The reaction mixture was cooled to r.t. and the pH adjusted to ~1. The reaction mixture was then extracted with EtOAc (3 x 20 mL). The organic layers were collected, dried with Na_2SO_4 and concentrated under reduced pressure. The crude product was dissolved in MePh (20 mL) and stirred at 150°C overnight. After cooling, the mixture was concentrated, and the resulting solid was filtered off to yield the desired products as a white solid (0.022 g, 0.068 mmol, 91%). ^{1}H NMR (400 MHz, DMSO) δ 5.05 (s, 2H), 7.32-7.34 (d, *J* = 8.1 Hz, 1H), 7.41 (bs, 1H), 7.64 (bs, 1H), 8.03-8.08 (m, 3H), 8.18-8.20 (d, *J* = 8.2 Hz, 2H), 10.87 (s, 1H), 13.2 (s, 1H). LC/MS m/z $[M + H]^+$ 321.24.

5.4.27.2. 3-(6-oxo-6,7-dihydro-5H-benzo[f][1,2,4]triazolo[1,5-d][1,4]diazepin-2-yl)benzoic acid (216i)

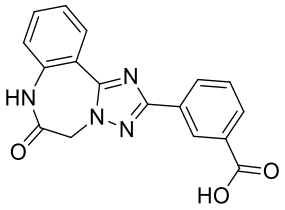

A 25 mL round-bottom flask with a Teflon stirrer bar was charged with compound **216e** (1 equiv., 0.060 g, 0.18 mmol), LiOH (3.3 equiv., 0.025 g, 0.60 mmol) followed by the addition of water (4.8 mL) and MeOH (19.2 mL). The reaction mixture was stirred at reflux overnight. The progress of the reaction was monitored by LC/MS. The reaction mixture was cooled to r.t. and the pH adjusted to ~1. The reaction mixture was then extracted with EtOAc (3 x 20 mL). The organic layers were collected, dried with Na_2SO_4 and concentrated under reduced pressure. The crude product was dissolved in MePh (20 mL) and stirred at 150°C overnight. After cooling, the mixture was concentrated, and the resulting solid was filtered off to yield the desired products as a white solid (0.052 g, 0.016 mmol, 90%). ^{1}H NMR (400 MHz, DMSO) δ 5.03 (s, 2H), 7.31-7.33 (d, *J* = 8 Hz, 1H), 7.38-7.41 (t, *J* = 7.5 Hz, 1H), 7.60-7.66 (m, 2H), 8.02 (m, 2H), 8.28-8.29 (d, *J* = 7.6 Hz, 1H), 8.65 (s, 8.66), 10.86 (s, 1H). ^{13}C NMR (125 MHz,

DMSO) δ 56.32, 117.9, 122.6, 125.3, 127.1, 129.7, 129.9, 130.4, 130.6, 131.2, 131.9, 132.4, 136.3, 153.4, 160.8, 167.4, 167.5. LC/MS m/z $[M + H]^+$ 321.22.

5.4.28. Synthesis of 3- and 4-(6-oxo-6,7-dihydro-5H-benzo[f][1,2,4]triazolo[1,5-d][1,4]diazepin-2-yl)benzamide (216j-k)

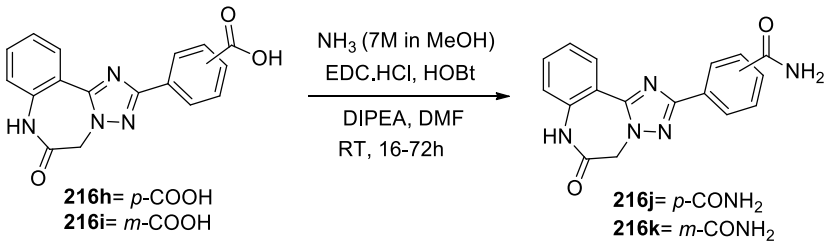

5.4.28.1. 4-(6-oxo-6,7-dihydro-5H-benzo[f][1,2,4]triazolo[1,5-d][1,4]diazepin-2-yl)benzamide (216j)

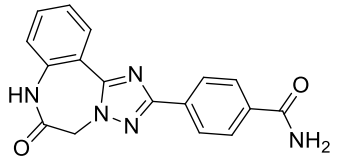

A 25 mL round-bottom flask containing a Teflon stirrer bar was charged with compound **216h** (1 equiv., 0.010 g, 0.031 mmol), EDC.HCl (2 equiv., 0.012 g, 0.062 mmol) and HOBt (1 equiv., 0.0042 g, 0.031 mmol) followed by the addition of dry DMF (0.27 mL) and DIPEA (3 equiv., 0.012 g, 0.016 mL, 0.094 mmol). The temperature was adjusted to 0°C using ice bath. The solution was then stirred and flushed with N_2 for 30 min. NH_3 (4 equiv., 0.018 mL, 0.12 mmol) dissolved in methanol (7M) was added, and the reaction mixture was maintained under stirring at r.t. for 16h. The crude product was then concentrated under reduced pressure and solubilized with MeOH (5 mL). The resulting precipitate was filtered off under reduced pressure to give the desired product as white solid (0.0055 g, 0.017 mmol, 55%). ^{1}H NMR (400 MHz, DMSO) δ 5.03 (s, 2H), 7.32-7.47 (m, 3H), 7.63 (s, 1H), 8.01-8.14 (m, 6H), 10.87 (s, 1H). LC/MS m/z $[M + H]^+$ 320.24.

5.4.28.2. 3-(6-oxo-6,7-dihydro-5H-benzo[f][1,2,4]triazolo[1,5-d][1,4]diazepin-2-yl)benzamide (216k)

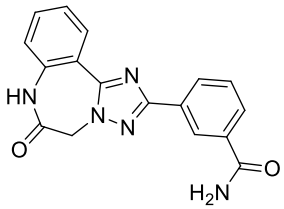

A 25 mL round-bottom flask containing a Teflon stirrer bar was charged with compound **216i** (1 equiv., 0.052 g, 0.16 mmol), EDC.HCl (2 equiv., 0.062 g, 0.32 mmol) and HOBt (1 equiv., 0.022 mg, 0.16 mmol) followed by the addition of dry DMF (1.4 mL) and DIPEA (3 equiv., 0.063 g, 0.084 mL, 0.48 mmol). The temperature was adjusted to 0°C using ice bath. The solution was then stirred and flushed with N_2 for 30 min. NH_3 (1 equiv., 0.023 mL, 0.16 mmol) dissolved in methanol (7M) was added, and the reaction mixture was maintained under stirring at r.t. for 72h. The crude product was then concentrated under reduced pressure and solubilized with MeOH (5 mL). The resulting precipitate was filtered off under reduced pressure to give the desired product as white solid (0.040 g, 0.13 mmol, 80%). ^{1}H NMR (400 MHz, DMSO) δ 5.03 (s, 2H), 7.33-7.34 (d, *J* = 8.1 Hz, 1H), 7.39-7.41 (t, *J* = 7.2 Hz, 1H), 7.45 (bs, 1H), 7.57-7.64 (m, 2H), 7.95-7.96 (d, *J* = 7.7 Hz, 1H), 8.03-8.04 (d, *J* = 6.7 Hz, 1H), 8.14 (bs, 1H), 8.19-8.21 (d, *J* = 7.8 Hz, 1H), 8.58 (s, 1H), 10.83 (s, 1H). ^{13}C NMR (125 MHz, DMSO) δ 53.3, 117.9, 122.6, 125.2, 125.7, 128.8, 128.9, 129.3, 129.7, 131, 132.3, 135.4, 136.4, 153.3, 161.2, 167.4, 168. LC/MS m/z $[M + H]^+$ 320.22.

5.5. GSK-3β inhibition assay[132]

Kinase Glo assays were performed in assay buffer containing 50mM 4-(2-hydroxy-ethyl)-1-piperazineethanesulfonic acid (HEPES) (pH= 7.5), 1 mM ethylenediaminetetraacetic acid (EDTA), 1 mM ethylene glycol tetra acetic acid (EGTA), and 15 mM magnesium acetate, using white 96-well plates. The following procedure was carried out, 10 µL of each compound solution, and 10µL ATP (1µM) were added to each well followed by 20 µL of assay buffer containing 25µM substrate and (20ng) of enzyme. The final DMSO concentration in the reaction mixture did not exceed 5%. After 30-min incubation at 37°C the enzymatic reaction was stopped by 40 µL of Kinase-Glo reagent. Glow-type luminescence was registered after 10 min using a multiwells plate reader Victor X3 PerkinElmer. The activity is proportional to the difference of the total and consumed ATP. The inhibitory activities were calculated based on

maximal kinase (average positive) and luciferase (average negative) activities measured in the absence of inhibitor and in the presence of reference compound inhibitor (SB415286 Merck Millipore, IC_{50}= 70nM) at total inhibition concentration (5μM), respectively. All the compounds were preliminarily tested at 10μM concentration. Then, a dose-response curve was obtained for those compounds showing a percentage of inhibition higher than 20%. Once the percentages have been obtained at different concentrations, the results were plotted versus the logarithm of inhibitor concentrations tested. The IC_{50} values were extrapolated after determining the linear regression parameters.

5.6. *In silico* enzymatic interaction study

The Spartan 14 program (Wavefunction Inc.) was used for the construction and optimization of three-dimensional models of the chemical structures of the inhibitors. For this purpose, the semi-empirical Parameterization Method 6 (PM6) calculation method was utilized.[133]

The GOLD 5.6 program (CCDC Software Ltd., Cambridge UK) was used to evaluate the *in silico* interactions between the compounds and the active sites of the enzyme GSK-3β. Initially, molecular docking studies were performed with GSK-3β, using three available GSK-3β structures from the Protein Data Bank (PDB), with codes 4PTC, 1Q4L, and 1Q3L. Hydrogen atoms were added to the protein crystallographic structures based on ionization and tautomeric states defined by GOLD. The binding site radius of the enzymes was tested at 15 °A and 20 °A around amino acid residue atoms, present in the CAS and using the GoldScore function.

The docking study for each evaluated compound generated several binding positions, which were quantitatively analyzed according to their adimensional scoring (Score) and qualitatively according to their interaction position with amino acid residues.

6. BIBLIOGRAPHY

(1) *Dementia*. https://www.who.int/news-room/fact-sheets/detail/dementia (accessed 2024-02-06).

(2) International, A. D.; Guerchet, M.; Prince, M.; Prina, M. Numbers of People with Dementia Worldwide: An Update to the Estimates in the World Alzheimer Report 2015. **2020**.

(3) *ADI - Dementia statistics*. https://www.alzint.org/about/dementia-facts-figures/dementia-statistics/ (accessed 2023-12-04).

(4) Maurer, K.; Volk, S.; Gerbaldo, H. Auguste D and Alzheimer's Disease. *The Lancet* **1997**, *349* (9064), 1546–1549. https://doi.org/10.1016/S0140-6736(96)10203-8.

(5) *Alzheimer's Disease Fact Sheet*. National Institute on Aging. https://www.nia.nih.gov/health/alzheimers-and-dementia/alzheimers-disease-fact-sheet (accessed 2024-05-07).

(6) Knopman, D. S.; Amieva, H.; Petersen, R. C.; Chételat, G.; Holtzman, D. M.; Hyman, B. T.; Nixon, R. A.; Jones, D. T. Alzheimer Disease. *Nat. Rev. Dis. Primer* **2021**, *7* (1), 1–21. https://doi.org/10.1038/s41572-021-00269-y.

(7) Blennow, K.; Leon, M. J. de; Zetterberg, H. Alzheimer's Disease. *The Lancet* **2006**, *368* (9533), 387–403. https://doi.org/10.1016/S0140-6736(06)69113-7.

(8) Whitesell, L.; Lindquist, S. L. HSP90 and the Chaperoning of Cancer. *Nat. Rev. Cancer* **2005**, *5* (10), 761–772. https://doi.org/10.1038/nrc1716.

(9) *Cérebro saudável vs. cérebro com Alzheimer | Alzheimer's Association*. https://www.alz.org/brain_portuguese/09.asp (accessed 2024-05-07).

(10) Drew, L. An Age-Old Story of Dementia. *Nature* **2018**, *559* (7715), S2–S3. https://doi.org/10.1038/d41586-018-05718-5.

(11) *How Is Alzheimer's Disease Diagnosed?* National Institute on Aging. https://www.nia.nih.gov/health/alzheimers-symptoms-and-diagnosis/how-alzheimers-disease-diagnosed (accessed 2023-12-22).

(12) Wu, Y.-T.; Beiser, A. S.; Breteler, M. M. B.; Fratiglioni, L.; Helmer, C.; Hendrie, H. C.; Honda, H.; Ikram, M. A.; Langa, K. M.; Lobo, A.; Matthews, F. E.; Ohara, T.; Pérès, K.; Qiu, C.; Seshadri, S.; Sjölund, B.-M.; Skoog, I.; Brayne, C. The Changing Prevalence and Incidence

of Dementia over Time - Current Evidence. *Nat. Rev. Neurol.* **2017**, *13* (6), 327–339. https://doi.org/10.1038/nrneurol.2017.63.

(13) Mielke, M. M.; Vemuri, P.; Rocca, W. A. Clinical Epidemiology of Alzheimer’s Disease: Assessing Sex and Gender Differences. *Clin. Epidemiol.* **2014**, *6*, 37–48. https://doi.org/10.2147/CLEP.S37929.

(14) Levy-Lahad, E.; Wasco, W.; Poorkaj, P.; Romano, D. M.; Oshima, J.; Pettingell, W. H.; Yu, C.; Jondro, P. D.; Schmidt, S. D.; Wang, K.; Crowley, A. C.; Fu, Y.-H.; Guenette, S. Y.; Galas, D.; Nemens, E.; Wijsman, E. M.; Bird, T. D.; Schellenberg, G. D.; Tanzi, R. E. Candidate Gene for the Chromosome 1 Familial Alzheimer's Disease Locus. *Science* **1995**, *269* (5226), 973–977. https://doi.org/10.1126/science.7638622.

(15) Mattson, M. P. Pathways towards and Away from Alzheimer's Disease. *Nature* **2004**, *430* (7000), 631–639. https://doi.org/10.1038/nature02621.

(16) Wollmer, M. A. Cholesterol-Related Genes in Alzheimer's Disease. *Biochim. Biophys. Acta BBA - Mol. Cell Biol. Lipids* **2010**, *1801* (8), 762–773. https://doi.org/10.1016/j.bbalip.2010.05.009.

(17) Monczor, M. Diagnosis and Treatment of Alzheimer's Disease. *Curr. Med. Chem. - Cent. Nerv. Syst. Agents* **2005**, *5* (1), 5–13. https://doi.org/10.2174/1568015053202723.

(18) Livingston, G.; Huntley, J.; Sommerlad, A.; Ames, D.; Ballard, C.; Banerjee, S.; Brayne, C.; Burns, A.; Cohen-Mansfield, J.; Cooper, C.; Costafreda, S. G.; Dias, A.; Fox, N.; Gitlin, L. N.; Howard, R.; Kales, H. C.; Kivimäki, M.; Larson, E. B.; Ogunniyi, A.; Orgeta, V.; Ritchie, K.; Rockwood, K.; Sampson, E. L.; Samus, Q.; Schneider, L. S.; Selbæk, G.; Teri, L.; Mukadam, N. Dementia Prevention, Intervention, and Care: 2020 Report of the Lancet Commission. *The Lancet* **2020**, *396* (10248), 413–446. https://doi.org/10.1016/S0140-6736(20)30367-6.

(19) Singh-Manoux, A.; Dugravot, A.; Fournier, A.; Abell, J.; Ebmeier, K.; Kivimäki, M.; Sabia, S. Trajectories of Depressive Symptoms Before Diagnosis of Dementia. *JAMA Psychiatry* **2017**, *74* (7), 712–718. https://doi.org/10.1001/jamapsychiatry.2017.0660.

(20) Gottesman, R. F.; Albert, M. S.; Alonso, A.; Coker, L. H.; Coresh, J.; Davis, S. M.; Deal, J. A.; McKhann, G. M.; Mosley, T. H.; Sharrett, A. R.; Schneider, A. L. C.; Windham, B. G.; Wruck, L. M.; Knopman, D. S. Associations Between Midlife Vascular Risk Factors and

25-Year Incident Dementia in the Atherosclerosis Risk in Communities (ARIC) Cohort. *JAMA Neurol.* **2017**, *74* (10), 1246–1254. https://doi.org/10.1001/jamaneurol.2017.1658.

(21) Samieri, C.; Perier, M.-C.; Gaye, B.; Proust-Lima, C.; Helmer, C.; Dartigues, J.-F.; Berr, C.; Tzourio, C.; Empana, J.-P. Association of Cardiovascular Health Level in Older Age With Cognitive Decline and Incident Dementia. *JAMA* **2018**, *320* (7), 657–664. https://doi.org/10.1001/jama.2018.11499.

(22) Vemuri, P.; Lesnick, T. G.; Przybelski, S. A.; Knopman, D. S.; Preboske, G. M.; Kantarci, K.; Raman, M. R.; Machulda, M. M.; Mielke, M. M.; Lowe, V. J.; Senjem, M. L.; Gunter, J. L.; Rocca, W. A.; Roberts, R. O.; Petersen, R. C.; Jack, C. R. Vascular and Amyloid Pathologies Are Independent Predictors of Cognitive Decline in Normal Elderly. *Brain J. Neurol.* **2015**, *138* (Pt 3), 761–771. https://doi.org/10.1093/brain/awu393.

(23) *Can I Prevent Dementia? | Alzheimers.gov*. https://www.nia.nih.gov/life-with-dementia/can-i-prevent-dementia (accessed 2023-12-23).

(24) Falco, A. D.; Cukierman, D. S.; Hauser-Davis, R. A.; Rey, N. A. DOENÇA DE ALZHEIMER: HIPÓTESES ETIOLÓGICAS E PERSPECTIVAS DE TRATAMENTO. *Quím. Nova* **2016**, *39*, 63–80. https://doi.org/10.5935/0100-4042.20150152.

(25) Terry, A. V.; Buccafusco, J. J. The Cholinergic Hypothesis of Age and Alzheimer's Disease-Related Cognitive Deficits: Recent Challenges and Their Implications for Novel Drug Development. *J. Pharmacol. Exp. Ther.* **2003**, *306* (3), 821–827. https://doi.org/10.1124/jpet.102.041616.

(26) *Acetylcholine (ACh) | Raleighe's Intro Neuroscience Study Blog*. https://sites.psu.edu/rbo5016neurostudyblog/2014/02/26/acetylcholine-ach/ (accessed 2024-05-07).

(27) Ferri, C. P.; Prince, M.; Brayne, C.; Brodaty, H.; Fratiglioni, L.; Ganguli, M.; Hall, K.; Hasegawa, K.; Hendrie, H.; Huang, Y.; Jorm, A.; Mathers, C.; Menezes, P. R.; Rimmer, E.; Scazufca, M. Global Prevalence of Dementia: A Delphi Consensus Study. *The Lancet* **2005**, *366* (9503), 2112–2117. https://doi.org/10.1016/S0140-6736(05)67889-0.

(28) Greenamyre, J. T.; Maragos, W. F.; Albin, R. L.; Penney, J. B.; Young, A. B. Glutamate Transmission and Toxicity in Alzheimer's Disease. *Prog. Neuropsychopharmacol. Biol. Psychiatry* **1988**, *12* (4), 421–430. https://doi.org/10.1016/0278-5846(88)90102-9.

(29) Danysz, W.; Parsons, C. G.; Mobius, H. J.; Stoffler, A.; Quack, G. Neuroprotective and Symptomatological Action of Memantine Relevant for Alzheimer's Disease--a Unified Glutamatergic Hypothesis on the Mechanism of Action. *Neurotox. Res.* **2000**, *2* (2–3), 85–97. https://doi.org/10.1007/BF03033787.

(30) Sucher, N. J.; Awobuluyi, M.; Choi, Y. B.; Lipton, S. A. NMDA Receptors: From Genes to Channels. *Trends Pharmacol. Sci.* **1996**, *17* (10), 348–355.

(31) Dingledine, R.; Borges, K.; Bowie, D.; Traynelis, S. F. The Glutamate Receptor Ion Channels. *Pharmacol. Rev.* **1999**, *51* (1), 7–61.

(32) Greenamyre, J. T.; Young, A. B. Excitatory Amino Acids and Alzheimer's Disease. *Neurobiol. Aging* **1989**, *10* (5), 593–602. https://doi.org/10.1016/0197-4580(89)90143-7.

(33) Nie, Q.; Du, X.; Geng, M. Small Molecule Inhibitors of Amyloid β Peptide Aggregation as a Potential Therapeutic Strategy for Alzheimer's Disease. *Acta Pharmacol. Sin.* **2011**, *32* (5), 545–551. https://doi.org/10.1038/aps.2011.14.

(34) Jenkins, E. C.; Devine-Gage, E. A.; Robakis, N. K.; Yao, X. L.; Brown, W. T.; Houck, G. E.; Wolfe, G.; Ramakrishna, N.; Silverman, W. P.; Wisniewski, H. M. Fine Mapping of an Alzheimer Disease-Associated Gene Encoding Beta-Amyloid Protein. *Biochem. Biophys. Res. Commun.* **1988**, *151* (1), 1–8. https://doi.org/10.1016/0006-291x(88)90551-7.

(35) Selkoe, D. J. Amyloid Beta-Protein and the Genetics of Alzheimer's Disease. *J. Biol. Chem.* **1996**, *271* (31), 18295–18298. https://doi.org/10.1074/jbc.271.31.18295.

(36) Canter, R. G.; Penney, J.; Tsai, L.-H. The Road to Restoring Neural Circuits for the Treatment of Alzheimer's Disease. *Nature* **2016**, *539* (7628), 187–196. https://doi.org/10.1038/nature20412.

(37) Hardy, J.; Allsop, D. Amyloid Deposition as the Central Event in the Aetiology of Alzheimer's Disease. *Trends Pharmacol. Sci.* **1991**, *12*, 383–388. https://doi.org/10.1016/0165-6147(91)90609-V.

(38) Hardy, J.; Selkoe, D. J. The Amyloid Hypothesis of Alzheimer's Disease: Progress and Problems on the Road to Therapeutics. *Science* **2002**, *297* (5580), 353–356. https://doi.org/10.1126/science.1072994.

(39) Rajasekhar, K.; Govindaraju, T. Current Progress, Challenges and Future Prospects of Diagnostic and Therapeutic Interventions in Alzheimer's Disease. *RSC Adv.* **2018**, *8* (42), 23780–23804. https://doi.org/10.1039/C8RA03620A.

(40) Saido, T.; Leissring, M. A. Proteolytic Degradation of Amyloid β-Protein. *Cold Spring Harb. Perspect. Med.* **2012**, *2* (6), a006379. https://doi.org/10.1101/cshperspect.a006379.

(41) Cheignon, C.; Tomas, M.; Bonnefont-Rousselot, D.; Faller, P.; Hureau, C.; Collin, F. Oxidative Stress and the Amyloid Beta Peptide in Alzheimer's Disease. *Redox Biol.* **2018**, *14*, 450–464. https://doi.org/10.1016/j.redox.2017.10.014.

(42) Patterson, C.; Feightner, J. W.; Garcia, A.; Hsiung, G.-Y. R.; MacKnight, C.; Sadovnick, A. D. Diagnosis and Treatment of Dementia: 1. Risk Assessment and Primary Prevention of Alzheimer Disease. *CMAJ* **2008**, *178* (5), 548–556. https://doi.org/10.1503/cmaj.070796.

(43) Panek, D.; Wichur, T.; Godyń, J.; Pasieka, A.; Malawska, B. Advances toward Multifunctional Cholinesterase and β-Amyloid Aggregation Inhibitors. *Future Med. Chem.* **2017**, *9* (15), 1835–1854. https://doi.org/10.4155/fmc-2017-0094.

(44) Parikh, V.; Bernard, C. S.; Naughton, S. X.; Yegla, B. Interactions between Aβ Oligomers and Presynaptic Cholinergic Signaling: Age-Dependent Effects on Attentional Capacities. *Behav. Brain Res.* **2014**, *274*, 30–42. https://doi.org/10.1016/j.bbr.2014.07.046.

(45) Mohandas, E.; Rajmohan, V.; Raghunath, B. Neurobiology of Alzheimer's Disease. *Indian J. Psychiatry* **2009**, *51* (1), 55. https://doi.org/10.4103/0019-5545.44908.

(46) Inestrosa, N. C.; De Ferrari, G. V.; Garrido, J. L.; Alvarez, A.; Olivares, G. H.; Barría, M. I.; Bronfman, M.; Chacón, M. A. Wnt Signaling Involvement in β-Amyloid-Dependent Neurodegeneration. *Neurochem. Int.* **2002**, *41* (5), 341–344. https://doi.org/10.1016/S0197-0186(02)00056-6.

(47) Braak, H.; Braak, E. Evolution of the Neuropathology of Alzheimer's Disease. *Acta Neurol. Scand.* **1996**, *94* (S165), 3–12. https://doi.org/10.1111/j.1600-0404.1996.tb05866.x.

(48) Braak, E.; Griffing, K.; Arai, K.; Bohl, J.; Bratzke, H.; Braak, H. Neuropathology of Alzheimer's Disease: What Is New since A. Alzheimer? *Eur. Arch. Psychiatry Clin. Neurosci.* **1999**, *249* (3), S14–S22. https://doi.org/10.1007/PL00014168.

(49) Iqbal, K.; Liu, F.; Gong, C.-X.; Grundke-Iqbal, I. Tau in Alzheimer Disease and Related Tauopathies. *Curr. Alzheimer Res.* **2010**, *7* (8), 656–664. https://doi.org/10.2174/156720510793611592.

(50) Jakob-Roetne, R.; Jacobsen, H. Alzheimer's Disease: From Pathology to Therapeutic Approaches. *Angew. Chem. Int. Ed.* **2009**, *48* (17), 3030–3059. https://doi.org/10.1002/anie.200802808.

(51) Brunden, K. R.; Trojanowski, J. Q.; Lee, V. M.-Y. Advances in Tau-Focused Drug Discovery for Alzheimer's Disease and Related Tauopathies. *Nat. Rev. Drug Discov.* **2009**, *8* (10), 783–793. https://doi.org/10.1038/nrd2959.

(52) Frost, B.; Jacks, R. L.; Diamond, M. I. Propagation of Tau Misfolding from the Outside to the Inside of a Cell *. *J. Biol. Chem.* **2009**, *284* (19), 12845–12852. https://doi.org/10.1074/jbc.M808759200.

(53) Lansdall, C. J. An Effective Treatment for Alzheimer's Disease Must Consider Both Amyloid and Tau. *Biosci. Horiz. Int. J. Stud. Res.* **2014**, *7*, hzu002. https://doi.org/10.1093/biohorizons/hzu002.

(54) Bloom, G. S. Amyloid-β and Tau: The Trigger and Bullet in Alzheimer Disease Pathogenesis. *JAMA Neurol.* **2014**, *71* (4), 505–508. https://doi.org/10.1001/jamaneurol.2013.5847.

(55) Weiner, M. W.; Veitch, D. P.; Aisen, P. S.; Beckett, L. A.; Cairns, N. J.; Green, R. C.; Harvey, D.; Jack, C. R.; Jagust, W.; Liu, E.; Morris, J. C.; Petersen, R. C.; Saykin, A. J.; Schmidt, M. E.; Shaw, L.; Shen, L.; Siuciak, J. A.; Soares, H.; Toga, A. W.; Trojanowski, J. Q. The Alzheimer's Disease Neuroimaging Initiative: A Review of Papers Published since Its Inception. *Alzheimers Dement.* **2013**, *9* (5), e111–e194. https://doi.org/10.1016/j.jalz.2013.05.1769.

(56) Mudher, A.; Lovestone, S. Alzheimer's Disease – Do Tauists and Baptists Finally Shake Hands? *Trends Neurosci.* **2002**, *25* (1), 22–26. https://doi.org/10.1016/S0166-2236(00)02031-2.

(57) Santos, S. N.; Souza, G. A. de; Pereira, T. M.; Franco, D. P.; Cistia, C. de N. D.; Sant'Anna, C. M. R.; Lacerda, R. B.; Kümmerle, A. E. Regioselective Microwave Synthesis and Derivatization of 1,5-Diaryl-3-Amino-1,2,4-Triazoles and a Study of Their Cholinesterase Inhibition Properties. *RSC Adv.* **2019**, *9* (35), 20356–20369. https://doi.org/10.1039/C9RA04105B.

(58) Tuppo, E. E.; Arias, H. R. The Role of Inflammation in Alzheimer's Disease. *Int. J. Biochem. Cell Biol.* **2005**, *37* (2), 289–305. https://doi.org/10.1016/j.biocel.2004.07.009.

(59) Town, T.; Nikolic, V.; Tan, J. The Microglial "Activation" Continuum: From Innate to Adaptive Responses. *J. Neuroinflammation* **2005**, *2* (1), 24. https://doi.org/10.1186/1742-2094-2-24.

(60) Halliday, G.; Robinson, S. R.; Shepherd, C.; Kril, J. Alzheimer's Disease And Inflammation: A Review Of Cellular And Therapeutic Mechanisms. *Clin. Exp. Pharmacol. Physiol.* **2000**, *27* (1–2), 1–8. https://doi.org/10.1046/j.1440-1681.2000.03200.x.

(61) McGeer, P. L.; Itagaki, S.; McGeer, E. G. Expression of the Histocompatibility Glycoprotein HLA-DR in Neurological Disease. *Acta Neuropathol. (Berl.)* **1988**, *76* (6), 550–557. https://doi.org/10.1007/BF00689592.

(62) McGeer, E. G.; McGeer, P. L. Neuroinflammation in Alzheimer's Disease and Mild Cognitive Impairment: A Field in Its Infancy. *J. Alzheimers Dis.* **2010**, *19* (1), 355–361. https://doi.org/10.3233/JAD-2010-1219.

(63) Andreyev, A. Yu.; Kushnareva, Yu. E.; Starkov, A. A. Mitochondrial Metabolism of Reactive Oxygen Species. *Biochem. Mosc.* **2005**, *70* (2), 200–214. https://doi.org/10.1007/s10541-005-0102-7.

(64) Christen, Y. Oxidative Stress and Alzheimer Disease12. *Am. J. Clin. Nutr.* **2000**, *71* (2), 621S-629S. https://doi.org/10.1093/ajcn/71.2.621s.

(65) Liu, J.; Liu, Z.; Zhang, Y.; Yin, F. A Novel Antagonistic Role of Natural Compound Icariin on Neurotoxicity of Amyloid β Peptide. *Indian J. Med. Res.* **2015**, *142* (2), 190. https://doi.org/10.4103/0971-5916.164254.

(66) Schwab, C.; McGeer, P. L. Inflammatory Aspects of Alzheimer Disease and Other Neurodegenerative Disorders. *J. Alzheimers Dis.* **2008**, *13* (4), 359–369. https://doi.org/10.3233/JAD-2008-13402.

(67) Mohsenzadegan, M.; Mirshafiey, A. The Immunopathogenic Role of Reactive Oxygen Species in Alzheimer Disease. *Iran. J. Allergy Asthma Immunol.* **2012**, 203–216.

(68) Rang, H. P.; Dale, M. M.; Ritter, J. M.; Flower, R. J.; Henderson, G. *Rang & Dale's Pharmacology*; Elsevier Health Sciences, 2011.

(69) Valko, M.; Leibfritz, D.; Moncol, J.; Cronin, M. T. D.; Mazur, M.; Telser, J. Free Radicals and Antioxidants in Normal Physiological Functions and Human Disease. *Int. J. Biochem. Cell Biol.* **2007**, *39* (1), 44–84. https://doi.org/10.1016/j.biocel.2006.07.001.

(70) Nunomura, A.; Castellani, R. J.; Zhu, X.; Moreira, P. I.; Perry, G.; Smith, M. A. Involvement of Oxidative Stress in Alzheimer Disease. *J. Neuropathol. Exp. Neurol.* **2006**, *65* (7), 631–641. https://doi.org/10.1097/01.jnen.0000228136.58062.bf.

(71) Gh Popescu, B. F.; Nichol, H. Mapping Brain Metals to Evaluate Therapies for Neurodegenerative Disease. *CNS Neurosci. Ther.* **2011**, *17* (4), 256–268. https://doi.org/10.1111/j.1755-5949.2010.00149.x.

(72) Zheng, W.; Monnot, A. D. Regulation of Brain Iron and Copper Homeostasis by Brain Barrier Systems: Implication in Neurodegenerative Diseases. *Pharmacol. Ther.* **2012**, *133* (2), 177–188. https://doi.org/10.1016/j.pharmthera.2011.10.006.

(73) Jomova, K.; Vondrakova, D.; Lawson, M.; Valko, M. Metals, Oxidative Stress and Neurodegenerative Disorders. *Mol. Cell. Biochem.* **2010**, *345* (1), 91–104. https://doi.org/10.1007/s11010-010-0563-x.

(74) Faller, P.; Hureau, C.; La Penna, G. Metal Ions and Intrinsically Disordered Proteins and Peptides: From Cu/Zn Amyloid-β to General Principles. *Acc. Chem. Res.* **2014**, *47* (8), 2252–2259. https://doi.org/10.1021/ar400293h.

(75) Savelieff, M. G.; Lee, S.; Liu, Y.; Lim, M. H. Untangling Amyloid-β, Tau, and Metals in Alzheimer's Disease. *ACS Chem. Biol.* **2013**, *8* (5), 856–865. https://doi.org/10.1021/cb400080f.

(76) Robert, A.; Liu, Y.; Nguyen, M.; Meunier, B. Regulation of Copper and Iron Homeostasis by Metal Chelators: A Possible Chemotherapy for Alzheimer's Disease. *Acc. Chem. Res.* **2015**, *48* (5), 1332–1339. https://doi.org/10.1021/acs.accounts.5b00119.

(77) Fish, P. V.; Steadman, D.; Bayle, E. D.; Whiting, P. New Approaches for the Treatment of Alzheimer's Disease. *Bioorg. Med. Chem. Lett.* **2019**, *29* (2), 125–133. https://doi.org/10.1016/j.bmcl.2018.11.034.

(78) Anand, P.; Singh, B. A Review on Cholinesterase Inhibitors for Alzheimer's Disease. *Arch. Pharm. Res.* **2013**, *36* (4), 375–399. https://doi.org/10.1007/s12272-013-0036-3.

(79) Cunningham, E. L.; Passmore, A. P. Drug Development in Dementia. *Maturitas* **2013**, *76* (3), 260–266. https://doi.org/10.1016/j.maturitas.2013.04.013.

(80) Ellul, J.; Archer, N.; Foy, C. M. L.; Poppe, M.; Boothby, H.; Nicholas, H.; Brown, R. G.; Lovestone, S. The Effects of Commonly Prescribed Drugs in Patients with Alzheimer's Disease on the Rate of Deterioration. *J. Neurol. Neurosurg. Psychiatry* **2007**, *78* (3), 233–239. https://doi.org/10.1136/jnnp.2006.104034.

(81) Sugimoto, H.; Ogura, H.; Arai, Y.; Iimura, Y.; Yamanishi, Y. Research and Development of Donepezil Hydrochloride, a New Type of Acetylcholinesterase Inhibitor. *Jpn. J. Pharmacol.* **2002**, *89* (1), 7–20. https://doi.org/10.1254/jjp.89.7.

(82) Munoz-Torrero, D. Acetylcholinesterase Inhibitors as Disease-Modifying Therapies for Alzheimer's Disease. *Curr. Med. Chem.* **2008**, *15* (24), 2433–2455. https://doi.org/10.2174/092986708785909067.

(83) Cummings, J. L.; Morstorf, T.; Zhong, K. Alzheimer's Disease Drug-Development Pipeline: Few Candidates, Frequent Failures. *Alzheimers Res. Ther.* **2014**, *6* (4), 37. https://doi.org/10.1186/alzrt269.

(84) Estrada, L. D.; Soto, C. Disrupting β-Amyloid Aggregation for Alzheimer Disease Treatment. *Curr. Top. Med. Chem.* **2007**, *7* (1), 115–126. https://doi.org/10.2174/156802607779318262.

(85) *Three promising drugs for treating Alzheimer's disease bring fresh hope | Alzheimer's Society*. https://www.alzheimers.org.uk/blog/three-promising-drugs-for-treating-alzheimers-disease-bring-fresh-hope (accessed 2024-05-07).

(86) Aschenbrenner, D. S. Controversial Approval of New Drug to Treat Alzheimer's Disease. *AJN Am. J. Nurs.* **2021**, *121* (10), 22. https://doi.org/10.1097/01.NAJ.0000794244.40800.99.

(87) Reardon, S. FDA Approves Alzheimer's Drug Lecanemab amid Safety Concerns. *Nature* **2023**, *613* (7943), 227–228. https://doi.org/10.1038/d41586-023-00030-3.

(88) *Medications for Memory, Cognition and Dementia-Related Behaviors*. Alzheimer's Disease and Dementia. https://alz.org/alzheimers-dementia/treatments/medications-for-memory (accessed 2024-01-22).

(89) Lauretti, E.; Dincer, O.; Praticò, D. Glycogen Synthase Kinase-3 Signaling in Alzheimer's Disease. *Biochim. Biophys. Acta BBA - Mol. Cell Res.* **2020**, *1867* (5), 118664. https://doi.org/10.1016/j.bbamcr.2020.118664.

(90) Lee, S. J.; Chung, Y. H.; Joo, K. M.; Lim, H. C.; Jeon, G. S.; Kim, D.; Lee, W. B.; Kim, Y. S.; Cha, C. I. Age-Related Changes in Glycogen Synthase Kinase 3β (GSK3β) Immunoreactivity in the Central Nervous System of Rats. *Neurosci. Lett.* **2006**, *409* (2), 134–139. https://doi.org/10.1016/j.neulet.2006.09.026.

(91) Luo, J. The Role of GSK3beta in the Development of the Central Nervous System. *Front. Biol.* **2012**, *7* (3), 212–220. https://doi.org/10.1007/s11515-012-1222-2.

(92) Giese, K. P. GSK-3: A Key Player in Neurodegeneration and Memory. *IUBMB Life* **2009**, *61* (5), 516–521. https://doi.org/10.1002/iub.187.

(93) Llorens-Marítin, M.; Jurado, J.; Hernández, F.; Ávila, J. GSK-3β, a Pivotal Kinase in Alzheimer Disease. *Front. Mol. Neurosci.* **2014**, *7*. https://doi.org/10.3389/fnmol.2014.00046.

(94) Hanger, D. P.; Hughes, K.; Woodgett, J. R.; Brion, J.-P.; Anderton, B. H. Glycogen Synthase Kinase-3 Induces Alzheimer's Disease-like Phosphorylation of Tau: Generation of Paired Helical Filament Epitopes and Neuronal Localisation of the Kinase. *Neurosci. Lett.* **1992**, *147* (1), 58–62. https://doi.org/10.1016/0304-3940(92)90774-2.

(95) Vanleuven, F. GSK3 and Alzheimer's Disease: Facts and Fiction…. *Front. Mol. Neurosci.* **2011**, *4*. https://doi.org/10.3389/fnmol.2011.00017.

(96) Uemura, K.; Kuzuya, A.; Shimozono, Y.; Aoyagi, N.; Ando, K.; Shimohama, S.; Kinoshita, A. GSK3β Activity Modifies the Localization and Function of Presenilin 1*. *J. Biol. Chem.* **2007**, *282* (21), 15823–15832. https://doi.org/10.1074/jbc.M610708200.

(97) Ly, P. T. T.; Wu, Y.; Zou, H.; Wang, R.; Zhou, W.; Kinoshita, A.; Zhang, M.; Yang, Y.; Cai, F.; Woodgett, J.; Song, W. Inhibition of GSK3β-Mediated BACE1 Expression Reduces Alzheimer-Associated Phenotypes. *J. Clin. Invest.* **2013**, *123* (1), 224–235. https://doi.org/10.1172/JCI64516.

(98) Chen, C.-H.; Zhou, W.; Liu, S.; Deng, Y.; Cai, F.; Tone, M.; Tone, Y.; Tong, Y.; Song, W. Increased NF-κB Signalling up-Regulates BACE1 Expression and Its Therapeutic Potential in Alzheimer's Disease. *Int. J. Neuropsychopharmacol.* **2012**, *15* (1), 77–90. https://doi.org/10.1017/S1461145711000149.

(99) Magdesian, M. H.; Carvalho, M. M. V. F.; Mendes, F. A.; Saraiva, L. M.; Juliano, M. A.; Juliano, L.; Garcia-Abreu, J.; Ferreira, S. T. Amyloid-β Binds to the Extracellular Cysteine-Rich Domain of Frizzled and Inhibits Wnt/β-Catenin Signaling*. *J. Biol. Chem.* **2008**, *283* (14), 9359–9368. https://doi.org/10.1074/jbc.M707108200.

(100) Spangenberg, E. E.; Green, K. N. Inflammation in Alzheimer's Disease: Lessons Learned from Microglia-Depletion Models. *Brain. Behav. Immun.* **2017**, *61*, 1–11. https://doi.org/10.1016/j.bbi.2016.07.003.

(101) Green, H. F.; Nolan, Y. M. GSK-3 Mediates the Release of IL-1β, TNF-α and IL-10 from Cortical Glia. *Neurochem. Int.* **2012**, *61* (5), 666–671. https://doi.org/10.1016/j.neuint.2012.07.003.

(102) Kinney, J. W.; Bemiller, S. M.; Murtishaw, A. S.; Leisgang, A. M.; Salazar, A. M.; Lamb, B. T. Inflammation as a Central Mechanism in Alzheimer's Disease. *Alzheimers Dement. Transl. Res. Clin. Interv.* **2018**, *4* (1), 575–590. https://doi.org/10.1016/j.trci.2018.06.014.

(103) Steinbrecher, K. A.; Wilson III, W.; Cogswell, P. C.; Baldwin, A. S. Glycogen Synthase Kinase 3β Functions To Specify Gene-Specific, NF-κB-Dependent Transcription. *Mol. Cell. Biol.* **2005**, *25* (19), 8444–8455. https://doi.org/10.1128/MCB.25.19.8444-8455.2005.

(104) Xavier, I. J.; Mercier, P. A.; McLoughlin, C. M.; Ali, A.; Woodgett, J. R.; Ovsenek, N. Glycogen Synthase Kinase 3β Negatively Regulates Both DNA-Binding and Transcriptional Activities of Heat Shock Factor 1*. *J. Biol. Chem.* **2000**, *275* (37), 29147–29152. https://doi.org/10.1074/jbc.M002169200.

(105) Gregory, M. A.; Qi, Y.; Hann, S. R. Phosphorylation by Glycogen Synthase Kinase-3 Controls c-Myc Proteolysis and Subnuclear Localization*. *J. Biol. Chem.* **2003**, *278* (51), 51606–51612. https://doi.org/10.1074/jbc.M310722200.

(106) Grimes, C. A.; Jope, R. S. CREB DNA Binding Activity Is Inhibited by Glycogen Synthase Kinase-3β and Facilitated by Lithium. *J. Neurochem.* **2001**, *78* (6), 1219–1232. https://doi.org/10.1046/j.1471-4159.2001.00495.x.

(107) Hooper, C.; Markevich, V.; Plattner, F.; Killick, R.; Schofield, E.; Engel, T.; Hernandez, F.; Anderton, B.; Rosenblum, K.; Bliss, T.; Cooke, S. F.; Avila, J.; Lucas, J. J.; Giese, K. P.; Stephenson, J.; Lovestone, S. Glycogen Synthase Kinase-3 Inhibition Is Integral to Long-Term Potentiation. *Eur. J. Neurosci.* **2007**, *25* (1), 81–86. https://doi.org/10.1111/j.1460-9568.2006.05245.x.

(108) Hui, J.; Zhang, J.; Pu, M.; Zhou, X.; Dong, L.; Mao, X.; Shi, G.; Zou, J.; Wu, J.; Jiang, D.; Xi, G. Modulation of GSK-3β/β-Catenin Signaling Contributes to Learning and Memory Impairment in a Rat Model of Depression. *Int. J. Neuropsychopharmacol.* **2018**, *21* (9), 858–870. https://doi.org/10.1093/ijnp/pyy040.

(109) Chen, P.; Gu, Z.; Liu, W.; Yan, Z. Glycogen Synthase Kinase 3 Regulates N-Methyl-d-Aspartate Receptor Channel Trafficking and Function in Cortical Neurons. *Mol. Pharmacol.* **2007**, *72* (1), 40–51. https://doi.org/10.1124/mol.107.034942.

(110) De Simone, A.; Tumiatti, V.; Andrisano, V.; Milelli, A. Glycogen Synthase Kinase 3β: A New Gold Rush in Anti-Alzheimer's Disease Multitarget Drug Discovery? *J. Med. Chem.* **2021**, *64* (1), 26–41. https://doi.org/10.1021/acs.jmedchem.0c00931.

(111) Tondo, L.; Alda, M.; Bauer, M.; Bergink, V.; Grof, P.; Hajek, T.; Lewitka, U.; Licht, R. W.; Manchia, M.; Müller-Oerlinghausen, B.; Nielsen, R. E.; Selo, M.; Simhandl, C.; Baldessarini, R. J.; International Group for Studies of Lithium (IGSLi). Clinical Use of Lithium Salts: Guide for Users and Prescribers. *Int. J. Bipolar Disord.* **2019**, *7* (1), 16. https://doi.org/10.1186/s40345-019-0151-2.

(112) Forlenza, O. V.; De-Paula, V. J. R.; Diniz, B. S. O. Neuroprotective Effects of Lithium: Implications for the Treatment of Alzheimer's Disease and Related Neurodegenerative Disorders. *ACS Chem. Neurosci.* **2014**, *5* (6), 443–450. https://doi.org/10.1021/cn5000309.

(113) Kramer, T.; Schmidt, B.; Lo Monte, F. Small-Molecule Inhibitors of GSK-3: Structural Insights and Their Application to Alzheimer's Disease Models. *Int. J. Alzheimers Dis.* **2012**, *2012*, 381029. https://doi.org/10.1155/2012/381029.

(114) Xu, M.; Wang, S. L.; Zhu, L.; Wu, P. Y.; Dai, W. B.; Rakesh, K. P. Structure-Activity Relationship (SAR) Studies of Synthetic Glycogen Synthase Kinase-3β Inhibitors: A Critical Review. *Eur. J. Med. Chem.* **2019**, *164*, 448–470. https://doi.org/10.1016/j.ejmech.2018.12.073.

(115) Sivaprakasam, P.; Han, X.; Civiello, R. L.; Jacutin-Porte, S.; Kish, K.; Pokross, M.; Lewis, H. A.; Ahmed, N.; Szapiel, N.; Newitt, J. A.; Baldwin, E. T.; Xiao, H.; Krause, C. M.; Park, H.; Nophsker, M.; Lippy, J. S.; Burton, C. R.; Langley, D. R.; Macor, J. E.; Dubowchik, G. M. Discovery of New Acylaminopyridines as GSK-3 Inhibitors by a Structure Guided in-Depth Exploration of Chemical Space around a Pyrrolopyridinone Core. *Bioorg. Med. Chem. Lett.* **2015**, *25* (9), 1856–1863. https://doi.org/10.1016/j.bmcl.2015.03.046.

(116) Bertrand, J. A.; Thieffine, S.; Vulpetti, A.; Cristiani, C.; Valsasina, B.; Knapp, S.; Kalisz, H. M.; Flocco, M. Structural Characterization of the GSK-3beta Active Site Using Selective and Non-Selective ATP-Mimetic Inhibitors. *J. Mol. Biol.* **2003**, *333* (2), 393–407. https://doi.org/10.1016/j.jmb.2003.08.031.

(117) Leost, M.; Schultz, C.; Link, A.; Wu, Y. Z.; Biernat, J.; Mandelkow, E. M.; Bibb, J. A.; Snyder, G. L.; Greengard, P.; Zaharevitz, D. W.; Gussio, R.; Senderowicz, A. M.; Sausville, E. A.; Kunick, C.; Meijer, L. Paullones Are Potent Inhibitors of Glycogen Synthase Kinase-3beta

and Cyclin-Dependent Kinase 5/P25. *Eur. J. Biochem.* **2000**, *267* (19), 5983–5994. https://doi.org/10.1046/j.1432-1327.2000.01673.x.

(118) Huang, L.; Miao, H.; Sun, Y.; Meng, F.; Li, X. Discovery of Indanone Derivatives as Multi-Target-Directed Ligands against Alzheimer's Disease. *Eur. J. Med. Chem.* **2014**, *87*, 429–439. https://doi.org/10.1016/j.ejmech.2014.09.081.

(119) Pereira, T. M.; Franco, D. P.; Vitorio, F.; Kummerle, A. E. Coumarin Compounds in Medicinal Chemistry: Some Important Examples from the Last Years. *Curr. Top. Med. Chem.* **2018**, *18* (2), 124–148. https://doi.org/10.2174/1568026618666180329115523.

(120) de Souza, G. A.; da Silva, S. J.; Del Cistia, C. de N.; Pitasse-Santos, P.; Pires, L. de O.; Passos, Y. M.; Cordeiro, Y.; Cardoso, C. M.; Castro, R. N.; Sant'Anna, C. M. R.; Kümmerle, A. E. Discovery of Novel Dual-Active 3-(4-(Dimethylamino)Phenyl)-7-Aminoalcoxy-Coumarin as Potent and Selective Acetylcholinesterase Inhibitor and Antioxidant. *J. Enzyme Inhib. Med. Chem.* **2019**, *34* (1), 631–637. https://doi.org/10.1080/14756366.2019.1571270.

(121) Sinha, A.; Tamboli, R. S.; Seth, B.; Kanhed, A. M.; Tiwari, S. K.; Agarwal, S.; Nair, S.; Giridhar, R.; Chaturvedi, R. K.; Yadav, M. R. Neuroprotective Role of Novel Triazine Derivatives by Activating Wnt/β Catenin Signaling Pathway in Rodent Models of Alzheimer's Disease. *Mol. Neurobiol.* **2015**, *52* (1), 638–652. https://doi.org/10.1007/s12035-014-8899-y.

(122) Lima, L. M.; Barreiro, E. J. Bioisosterism: A Useful Strategy for Molecular Modification and Drug Design. *Curr. Med. Chem.* **2005**, *12* (1), 23–49. https://doi.org/10.2174/0929867053363540.

(123) Barreiro, E. J.; Fraga, C. A. M. *Química Medicinal - 3.Ed.: As bases moleculares da ação dos fármacos*; Artmed Editora, 2014.

(124) Hickey, S. M.; Ashton, T. D.; Khosa, S. K.; Pfeffer, F. M. An Optimised Synthesis of 2-[2,3-Bis(Tert-Butoxycarbonyl)Guanidino]Ethylamine. *Synlett* **2012**, *23* (12), 1779–1782. https://doi.org/10.1055/s-0031-1290698.

(125) Yin, P.; Ma, W.-B.; Chen, Y.; Huang, W.-C.; Deng, Y.; He, L. Highly Efficient Cyanoimidation of Aldehydes. *Org. Lett.* **2009**, *11* (23), 5482–5485. https://doi.org/10.1021/ol902207h.

(126) Bartolozzi, A.; Hickey, E. R.; Riether, D.; Wu, L.; Zindell, R. M.; East, S. P.; Ermann, M. Compounds Which Selectively Modulate The CB2 Receptor. US20100076029A1, March

25, 2010. https://patents.google.com/patent/US20100076029A1/en?oq=US20100076029 (accessed 2024-05-07).

(127) Forster, C. J.; Kwak, Y.-S.; Nakajima, K.; Wang, B. Organic Compounds. WO2010007046A2, January 21, 2010. https://patents.google.com/patent/WO2010007046A2/en?oq=WO2010007046+A2 (accessed 2024-05-08).

(128) Novel pyrrolo[2,3-d]pyrimidine compound. WO2011145718A1, November 24, 2011. https://patents.google.com/patent/WO2011145718A1/en?oq=WO2011145718A1 (accessed 2024-05-07).

(129) Hanan, E. J.; Braun, M.-G.; Heald, R. A.; MacLeod, C.; Chan, C.; Clausen, S.; Edgar, K. A.; Eigenbrot, C.; Elliott, R.; Endres, N.; Friedman, L. S.; Gogol, E.; Gu, X.-H.; Thibodeau, R. H.; Jackson, P. S.; Kiefer, J. R.; Knight, J. D.; Nannini, M.; Narukulla, R.; Pace, A.; Pang, J.; Purkey, H. E.; Salphati, L.; Sampath, D.; Schmidt, S.; Sideris, S.; Song, K.; Sujatha-Bhaskar, S.; Ultsch, M.; Wallweber, H.; Xin, J.; Yeap, S.; Young, A.; Zhong, Y.; Staben, S. T. Discovery of GDC-0077 (Inavolisib), a Highly Selective Inhibitor and Degrader of Mutant PI3Kα. *J. Med. Chem.* **2022**, *65* (24), 16589–16621. https://doi.org/10.1021/acs.jmedchem.2c01422.

(130) Multi-Azole linked spirorenone compound and preparation method and application thereof. CN102850337A, January 2, 2013. https://patents.google.com/patent/CN102850337A/en?oq=CN102850337+A+2013-01-02 (accessed 2024-05-07).

(131) Houpis, I. N.; Liu, R.; Wu, Y.; Yuan, Y.; Wang, Y.; Nettekoven, U. Regioselective Cross-Coupling Reactions of Boronic Acids with Dihalo Heterocycles. *J. Org. Chem.* **2010**, *75* (20), 6965–6968. https://doi.org/10.1021/jo101223z.

(132) Baki, A.; Bielik, A.; Molnár, L.; Szendrei, G.; Keserü, G. M. A High Throughput Luminescent Assay for Glycogen Synthase Kinase-3beta Inhibitors. *Assay Drug Dev. Technol.* **2007**, *5* (1), 75–83. https://doi.org/10.1089/adt.2006.029.

(133) Nakata, M.; Maeda, T. PubChemQC B3LYP/6-31G*//PM6 Data Set: The Electronic Structures of 86 Million Molecules Using B3LYP/6-31G* Calculations. *J. Chem. Inf. Model.* **2023**, *63* (18), 5734–5754. https://doi.org/10.1021/acs.jcim.3c00899.

CHAPTER III

SYNTHESIS OF PROTHEOLYSIS TARGETING CHIMERAS (PROTACs) DESIGNED TO MODULATE GSK-3β DEGRADATION

With the recent approval of PROTACs for clinical trials, many research groups are focusing their efforts on identifying new drug candidates using this tool. In addition to the significant expertise in Alzheimer's disease and, more recently, in PROTACs for neurodegenerative disorders, by the research group led by Professor Maria Laura Bolognesi at the University of Bologna, where most of this chapter was developed, in this chapter we will describe the design and synthesis of a new series of PROTACs targeting GSK-3β.

1. INTRODUCTION

In the last 20 years, the drug discovery process has seen a groundbreaking paradigm shift with the discovery of **T**argeted **P**rotein **D**egradation (TPD), a therapeutical strategy of inducing the depletion and/or reduction of a disease-causing protein via hijacking the endogenous protein degradation machineries.[1–3] During this period, the focus has changed from complete attention to the classical targets of traditional therapies (e.g. enzymes, ion channels, protein kinases, G protein-coupled receptors (GPCRs)), to also include those “unreachable” of high biological function interests, such as targets considered "undruggable”.[4]

These “undruggable” targets are molecular entities that have proven challenging to modulate with traditional small-molecule therapies but that remained of great therapeutic interest.[1,5] Generally, they include proteins without enzymatic function, such as scaffolding proteins and transcription factors,[6,7] and play crucial roles in various diseases, such as cancer, neurodegenerative disorders, and inflammatory and infectious diseases. Estimative counts that nearly 400 human “undruggable” proteins are disease-related.[8,9] As characteristics, these targets have broad active sites and functional interfaces that are flat and lacking defined pockets, which make it difficult for small molecules to bind to.[8]

The traditional and well-succeeded design of occupancy-driven small molecule compounds, for single or multitarget compounds, has been used during the last several decades in drug discovery.[10,11] This strategy is focused on inhibiting target proteins' function by occupying their active or allosteric sites. However, occupancy-driven drug discovery is not feasible and efficient for all drug targets, needing well-defined binding sites and high affinity.[1] From this point, the TPD approach emerges as innovative and key therapeutic modality to exploit current known targets (in a more selective way or overcoming potential resistances, for example) as well as those “undruggables” by means of an event-driven new **M**ode **O**f **A**ction (MOA).[5,12,13]

Probably the main class of small molecules acting as TPD are **PRO**teolysis-**T**argeting **C**himeras (PROTACs), first described in 2001 by Craig M. Crews and Raymond J. Deshaies.[14] Since many protein levels are regulated by **U**biquitin-dependent **P**roteassome **S**ystem (UPS), they designed these compounds as TPD aiming at hijacking the cellular machinery to degrade a **P**rotein **O**f **I**nterest (POI), as an effective way to modulate the protein abundance of normal and / or diseased cells. Indeed, the PROTACs were designed to be hetero-bifunctional compounds able to bring together a POI and the UPS degradation machinery, which do not usually form such a complex.

In this review, we will briefly address the PROTACs discovery process, MOA, evolution, current stage, their design, applications to modulating inflammatory conditions and the future directions of this promising drug discovery modality, including problems that still need to be overcome.

1.1. The UPS System Behind the Discovery of PROTACs

The proteostasis process, which is indeed protein homeostasis, denotes the intricate and interrelated cellular processes employed to control the concentration, conformation, and subcellular localization of proteins.[15] This complex system encompasses a wide array of pathways governing protein synthesis, folding, transport, and disposal.[16] In eukaryotic cells, damaged proteins or organelles can be effectively eliminated through proteasomes,[17] which manage the degradation of short-lived proteins and soluble misfolded proteins through the UPS,[18] a major pathway that degrades intracellular proteins.

In this pathway, proteins are targeted for degradation by the proteasome in a three-step process involving ubiquitin-activating enzymes (E1), ubiquitin-conjugating enzymes (E2) and ubiquitin protein ligases (E3), which coordinate the transfer of ubiquitin molecules to the target protein (substrate) with high specificity (Figure 42).[19] There are seven different lysin polyubiquitin chains (K6, K11, K27, K29, K33, K48, K63; and one methionine residue) depending on the residue number of the ubiquitin molecule that is conjugated.[20] Poly-ubiquitinated proteins in K48 (one of the most abundant) are often targeted to proteasome for degradation (Figure 42). The human genome is estimated to encode more than 600 E3 ligases,[21,22] each one with specificity for a different subset of proteins.

The utilization of this protein degradation system for therapeutic applications drew inspiration from researches conducted on viruses and plants. More than 20 different viruses can

hijack the human UPS system to promote their own survival and replication.[23] For example, human papillomavirus types 16 (HPV-16) and 18 (HPV-18) possess the E6 protein that recruits the human E3 ligase to ubiquitylate p53, resulting in its degradation.[24] Due to the fast degradation of ubiquitinated proteins within cells and nature inspiration, Craig M. Crews and Raymond J. Deshaies raised the idea that manipulating the UPS pathway could serve as an effective method for regulating the protein levels in both healthy and diseased cells. This approach led to the discovery of PROTACs.

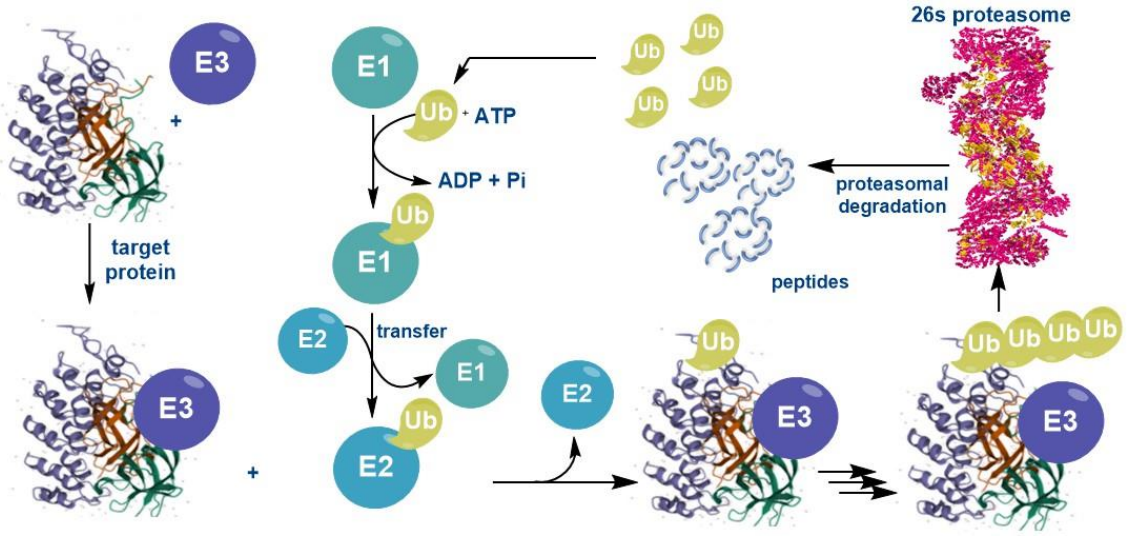

Figure 42. Schematic representation of Ubiquitin–Proteasome System (UPS) process of protein degradation. The ubiquitin molecule is linked to E1 through an ATP-dependent process that is subsequently transferred to E2 through interaction with E2. In a parallel process, E3 recognizes and binds to the target protein. After, the complexed E3 catalyzes the transfer of the ubiquitin molecule from E2 to the protein target. Thus, a sequential process results in the polyubiquitination of the substrate, targeting it for the subsequent proteasome degradation.

1.2. Discovery and Mode of Action of PROTACs

Despite the occupancy-driven pharmacology MOA has been successful for many biological targets, it is not applicable for all targets. Specifically, it is less effective for proteins lacking enzymatic activity, such as scaffolding proteins or those that rely on **P**rotein-**P**rotein **I**nteractions (PPIs).[25] Drugs that work by occupying a target site are most effective when the target site remains occupied, often requiring high drug doses that can lead to unwanted side effects due to off-target binding at higher drug concentrations.[26] Additionally, resistance to inhibition by occupancy-driven therapies can be develop in many diseases, including cancer

and bacterial infections.[27,28] As a result, many researchers have been explored new drug classes that use alternatives MOA.

Under this perspective, in the early 2000s, PROTACs were developed as a novel class of small molecules with a new MOA, being designed to harness the cellular machinery responsible for protein degradation. The first PROTAC (named **Protac-1**), synthesized in 2001, was the *in vitro* proof of concept for the biological application of this class of compounds, and confirmed the expectations for its MOA.[14] **Protac-1** was specifically designed to target methionyl aminopeptidase 2 (MetAp-2), identified as the potential target of the potent angiogenesis inhibitors ovalicin and fumagillin. It comprised two different components: ovalicin and a 10-amino acid phosphopeptide DRHDSGLDSM derived from nuclear factor-κB inhibitor-α (NF-κBIα, also known as IκBα), which is recognized by the E3 ligase β-transducin repeat-containing E3 ubiquitin–protein ligase (β-TRCP) (Figure 2A). **Protac-1** acted as a molecular bridge, promoting the interaction between MetAp-2 and β-TRCP, allowing the ligase to ubiquitylate METAP2 and inducing its degradation.[14]

As for **Protac-1**, the development of PROTAC technology was based on its hetero-bifunctional nature, which includes a ligand for the protein of interest (POI), a ligand for recruiting ubiquitin E3 ligase, and a linker (Figure 2B).[2,29] This unique heterobifunctional character allows simultaneously binding to both the POI and a ubiquitin E3 ligase, forming a ternary complex that activates the ubiquitin-proteasome system (UPS) for the degradation of the POI (Figure 43).[2,29,30]

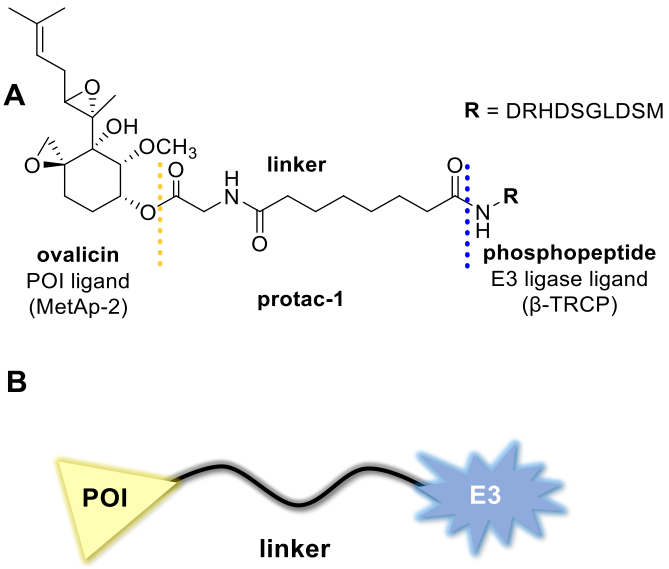

Figure 43. A- Structure of first described PROTAC (**protac-1**); **B-** PROTACs hetero-bifunctional nature including POI ligand, a linker, and a ligand for E3 ligase.

The event-driven nature of PROTACs allows them to act catalytically (considered sub-stoichiometric and an innovative pharmacodynamic modality), triggering the degradation of multiple molecules of the POI with just one PROTAC molecule (Figure 44). This distinctive ability to induce protein degradation and the event-driven MOA distinguish PROTACs as having unique therapeutic potential when compared to classical occupancy-driven therapeutics (Figure 44).[31,32]

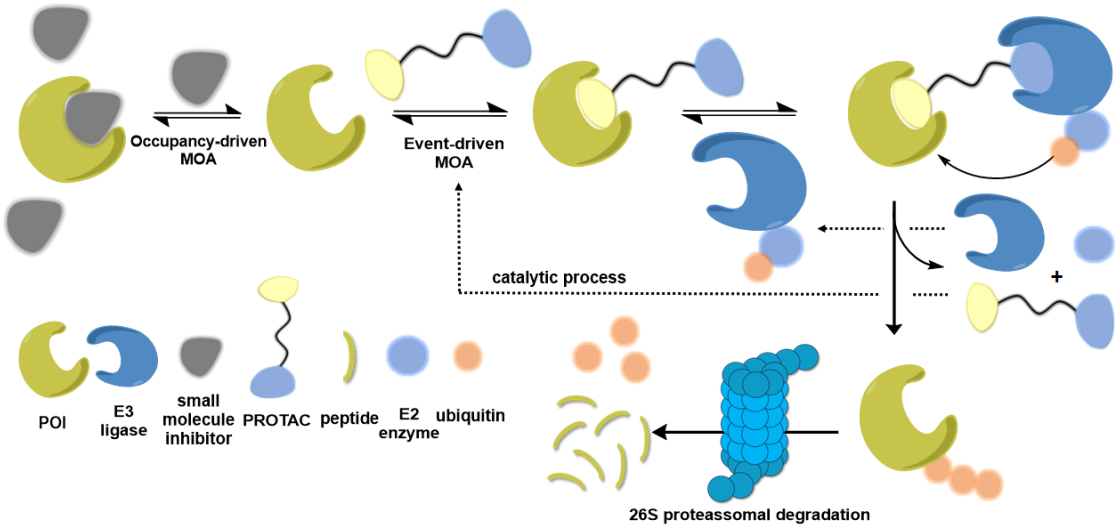

Figure 44. Illustration comparing occupancy- and event-driven MOA: In occupancy-driven MOA the small molecule modulates the POI by means of an association-dissociation occupancy of active site (non-catalytic). In event-driven MOA (catalytic), protein function is modulated by degradation, with PROTAC initiating a degradation cascade involving POI ubiquitination followed by its 26S proteasomal degradation.

Indeed, while both inhibitors and degraders share the common objective of diminishing functional proteins, their mechanisms differ: inhibition governs protein function, while degradation manages protein abundance. The main advantage of PROTACs MOA, like in **Protac-1**, is depletes the entire target and thereby disrupts both enzymatic activity and nonenzymatic functions. This comprehensive approach enables PROTACs to tackle potential resistance encountered in current therapeutic treatments.[33–36] Moreover, PROTACs are also less affected by increases in target expression and mutations in the target protein, as their catalytic action requires only low doses.[37,38]

1.3. PROTACs Mechanistic highlights

The main point of PROTAC-induced degradation MOA resides in the ternary complex (POI-PROTAC-E3) formation, enabling POI polyubiquitination and subsequent proteasomal degradation (Figure 44). Established mathematical models applied to this ternary complex formation[39,40] predict a bell-shaped dependency on PROTAC concentration (Figure 45A).[41] Compared to the classical occupancy-driven MOA, in which the occupancy and activity increase with concentration, for PROTACs a phenomenon called "hook effect" occurs due to the formation of an unproductive binary complex (Figure 45A).[42] Furthermore, interactions between the POI and E3 may stabilize or destabilize ternary complex formation (Figure 45B). A cooperative factor ($\alpha = K_{d\ binary} / K_{d\ ternary}$) provides a measure of susceptibility to ternary complex formation and can be positive or negative. Positive cooperativity ($\alpha > 1$) occurs when stabilizing PPIs between the POI and E3 promote the ternary complex formation, in which the hook effect can be effectively minimized, which ultimately leads to an amplified production of ternary complex. On the other hand, negative values ($\alpha < 1$) mean that destabilizing factors are abrogating the ternary complex formation.[43]

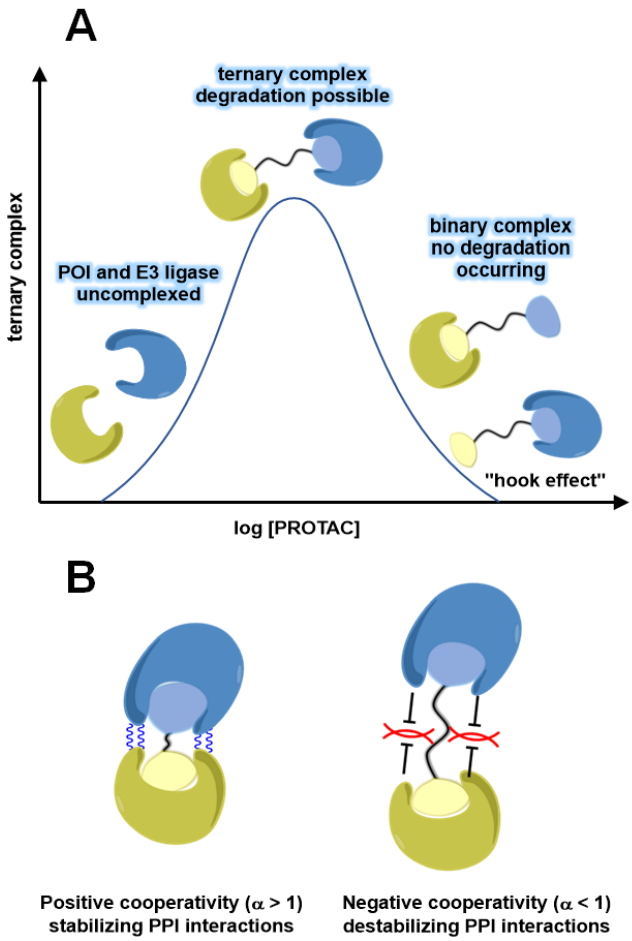

Figure 45. A- Increasing concentration of PROTAC leading to formation of ternary complex (ideal concentration), and the binary complex and "hook effect" (when concentration is too high). PROTAC compound; POI ligand (yellow), E3 ligase (blue); **B-** Positive and negative cooperativity working on stabilizing or destabilizing, respectively, PPIs interactions. Favorable interactions (blue wave line), unfavorable interactions like charge repulsion and/or steric clashes (red curves).

The first experimentally demonstration of the ternary complex was only described in 2017 by Ciulli laboratory from a complex involving MZ1 (PROTAC) and both the bromodomain of BRD4BD2 and VHL.[44] The crystal structure provided insights into the interactions between BRD4 and VHL, along with the interactions between the PROTAC linker and BRD4. Through assessments using diverse biophysical methods, the study demonstrated positive cooperativity. This cooperative effect was found to enhance the potency and selectivity of PROTAC, leading to the induced degradation of specific members within the BRD family (Figure 46).[44]

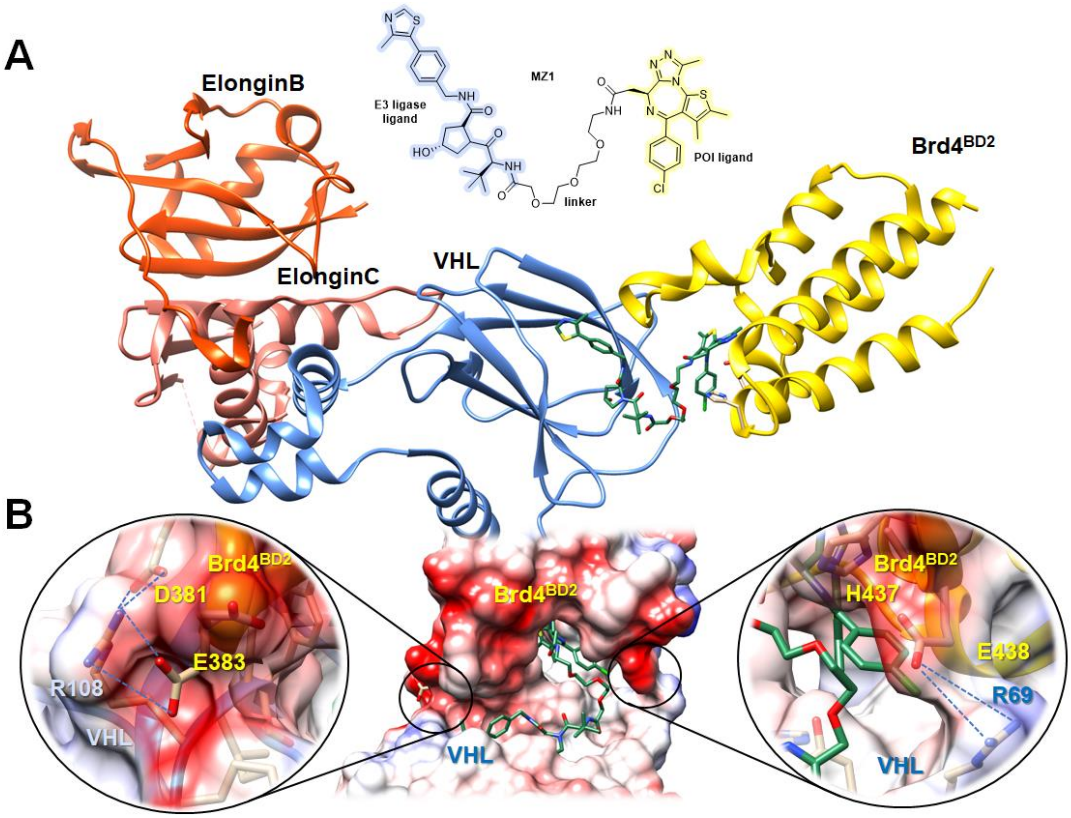

Figure 46. A- Crystal structure of the complex PROTAC MZ1 (POI ligand – linker – E3 ligase ligand) and Brd4 (PDB5T35). B- Electrostatic potential map showing the charged zipper contacts between $Brd4^{BD2}$ residues D381 and E383 with VHL residues R108; and E438 with VHL residue R69. Blue dashed lines indicate hydrogen bonds.

Many times, one can hear that the good affinity of a given PROTAC for its POI is not the most important point for a good degradation. Indeed, because of occupancy-driven MOA, Medicinal Chemists are used to thinking that good affinities can be converted into good activities. However, the event-driven nature of PROTACs is completely associated with the ternary complex formation. As described above, its formation can occurs with positive cooperativity due to favorable/stabilizing PPIs,[44] which can ultimately lead to better activities and potencies. As example, an ibrutinib PROTAC derivative (**284**) exhibiting a low binary binding affinity (K_d = 11 μM) towards the kinase BTK demonstrated potent induction of its degradation, with a DC_{50} of 1.1 nM and a Dmax of 87% (Figure 47). Important though, is bear in mind that positive cooperativity is not a rule for good PROTACs, as demonstrated for some examples in which cooperativity appears to be less important for efficient degradation.[45]

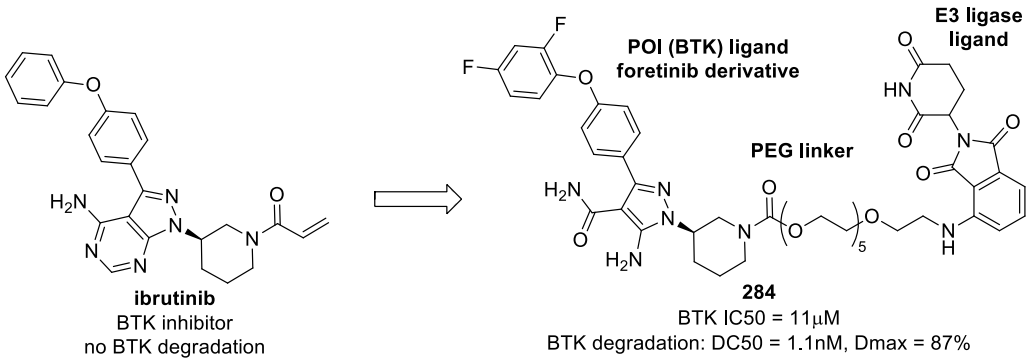

Figure 47. Ibrutinib and PROTAC (**284**) structures. Comparison between binary (IC_{50}) and ternary (DC_{50}) potencies of **284**.

1.4. Evolution of PROTACs until the Present

Since the discovery and first description of PROTACs by Crews group, the technology has hugely expanded from molecules studied in cell lysates and cell culture to studies in animals and animal disease models, finally reaching clinical trials in humans. PROTACs have also spread from an exclusive academic universe at the beginning to the pharmaceutical and biotechnological industries (Figure 48).

Regarding publications in PROTACs and based on the Scopus database, we analyzed the period from 2001 to the end of 2023. Curiously, the entry "PROTAC" was not the most precise since some articles described this acronym for fields other than the Proteolysis Target Chimeras. Thus, our analysis was made with the entries "PROTAC" or "PROTACs" and "proteolysis" or "E3".

After the discovery of **Protac-1** in 2001, a clear gap with minor publications was observed until 2015, when an inflection point started, with an impressive increase from 2017. This first period was marked by peptidic PROTACs (e.g. **285**) targeting the degradation of the androgen and estrogen nuclear receptors (AR and ER, respectively), expanding the target scope.[46] A proof of concept that PROTACs could modulate protein degradation intracellularly was achieved when microinjections of these AR- and ER targeting PROTACs demonstrated that they could function in an intact cell. However, these PROTACs lacked good cell permeability (Figure 48).

The subsequent development of PROTACs involved incorporating a peptide from hypoxia-inducible factor 1 subunit-α (HIF1α), a fragment able to recruit the Von Hippel-Lindau disease tumor-suppressor protein (VHL) E3 ligase in intact cells, eliminating the need for

microinjection.[47] A shorter peptide fragment of HIF-1α was later incorporated into a PROTAC targeting aryl hydrocarbon receptor nuclear translocator (ARNT).[48] Despite this PROTAC's "first generation" (indeed considered "bioPROTACs" today) confirmed promising applications inducing specific degradation of desired targets, the peptide nature of these compounds led to poor cell permeability that summed to the low micromolecular activities, hampered their use as therapeutic products (Figure 48).[7]

The undesirable cell penetration parameters led to efforts to overcome this problem and in 2008 Crew and coworkers developed the first small-molecule PROTAC targeting AR (**287**),[49] increasing dramatically the targets reported to be degraded by PROTACs,[50] consisting of nonsteroidal AR ligand (SARM), a ligand targeting E3 ligase from murine double minute 2 (MDM2-p53 PPI inhibitor, nutlin), and a PEG-based linker.[49] These compounds were more readily taken up by cells than previous peptide-based PROTACs and more likely to be developed into drugs (Figure 48).[29]

During the next years, the discovery of multiple other E3 ligases, including cereblon (CRBN) (**288**),[51,52] cell inhibitor of apoptosis protein (cIAP) (**289**).[52–54] and later the Von-Hippel-Lindau (VHL) (**290**),[55,56] led to a significant advancement of the PROTAC technology. Special attention and development have been made to VHL and CRBN ligands. While many peptidomimetics of VHL with high affinity for the VHL E3 were developed,[57–59] as well as further structure-activity relationship (SAR) performed to improve physical-chemical properties maintaining similar affinities towards VHL, the immunomodulatory drugs (IMiDs), including thalidomide, pomalidomide, and lenalidomide, were found to target the E3 cereblon (CRBN) at the molecular level (Figure 48).[60–65]

Much evidence showed promising applications for PROTACs. However, no evidence of in vivo activity was reported until 2013 when PhosphoPROTACs were described as the first in vivo proof of concept of PROTACs, being able to inhibit tumor growth in murine models.[66] Moreover, PhosphoPROTACs have distinguished between receptor tyrosine kinase (RTK) signaling pathways by incorporating different peptide sequencers as POI recruiting moiety (Figure 48).

The following years experienced the increase on PROTACs interesting and development. In the year 2014, the first peptide based antiviral PROTACs against HBV was developed;[67] and in 2015, CRBN- and VHL E3 recruiting ligands were used to develop CRBN- and VHL-based PROTACs such as the Halo-PROTACs,[68] and PROTACs targeting the bromodomain and extra-terminal (BRD/BET) family of epigenetic proteins.[69] In 2016, a new PROTAC class was discovered by Astex Pharmaceuticals,[70] the CLIPTACs (in cell

CLIckformed **P**roteolysis **TA**rgeting **C**himeras). These PROTACs could be formed intracellularly by biocompatible reactions such as an inverse electron demand Diels–Alder reaction after treating cells, sequentially, with cell permeable compounds.

Probably, the year 2019 was a landmark in which PROTACs shifted from laboratory proof of concepts to a translational exploration when compounds ARV-110 (NCT03888612) and ARV-471 (NCT04072952) entered in clinical trial phase 1 targeting the androgen receptor (AR) and estrogen receptor (ER), respectively (Figure 48). The interest for PROTACs as pharmaceutical products also had a considerable increase after 2019 when analyzed the number of patents with the term "PROTAC" in Scifinder. For instance, the number of patents since the first Crew's patent in 2002 until 2019 was 57. Only in 2020, 48 patents were registered while this number grew to 176 registers last year. Worth of note, antitumoral and anti-inflammatory compounds correspond to the major applications described inside the patents, with anticancer responding to 61%, though.

For sure, the increasing interest of pharmaceutical companies accelerated the translation process of PROTACs from the basic research to the clinical trials and it is reflected in the increase in patents number. Furthermore, the clinical significance of the PROTAC approach became evident through the initiation of many clinical trials with PROTAC-based molecules until today (data shown in a next section).

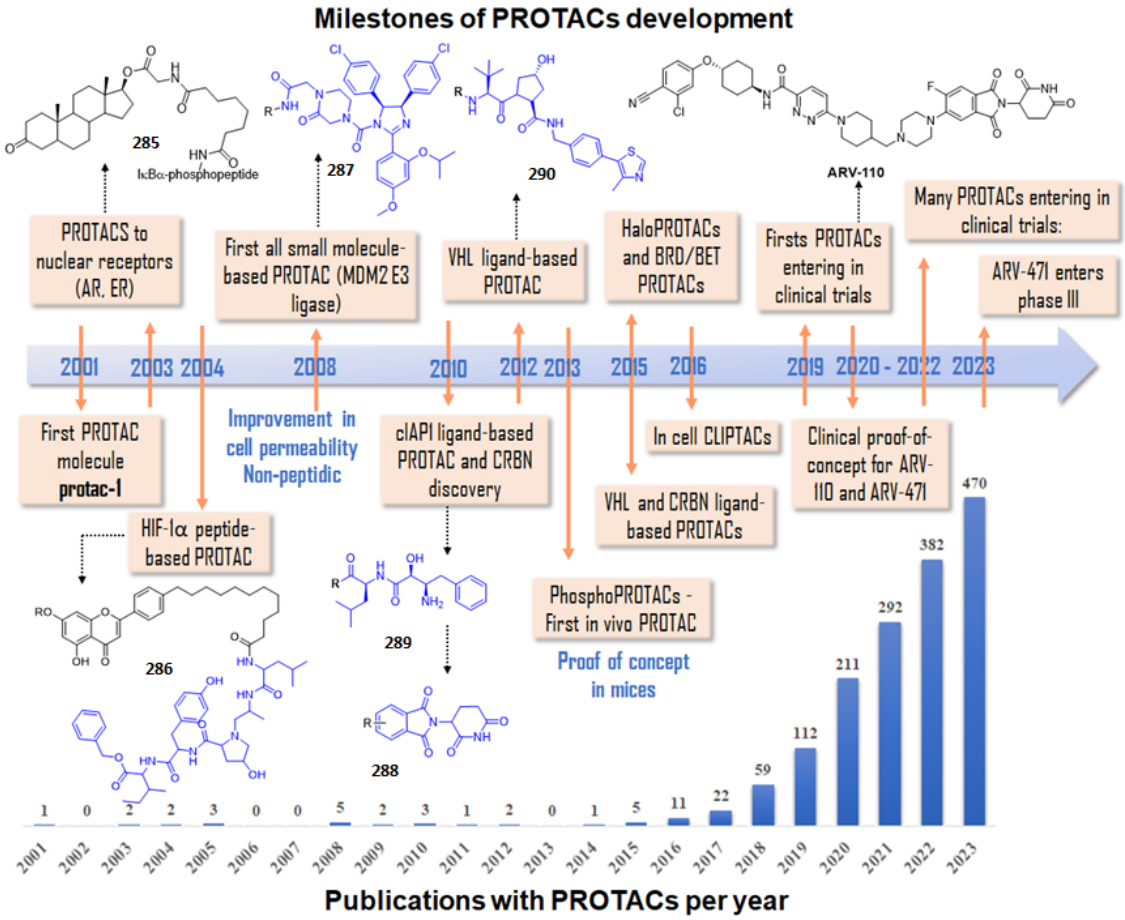

Figure 48. Milestones of the PROTACs' discovery and development and publications about PROTACs since the first relate in 2001.

1.4.1. Present

The total number of 470 publications in PROTACs last year and 1467 in a 5-years period (2019-2023) shows how this field has grown since its first description in 2001 (Figure 7). The importance of PROTACs is measured not only by the number of publications, but also the high-impact journals in which we can find these publications: Journal of Medicinal Chemistry (149), European Journal of Medicinal Chemistry (110), Cell Chemical Biology (46), ACS Medicinal Chemistry Letters (36), and Journal of the American Chemical Society (36).

Regarding targets reached, in 2019, a review from Sun and colleagues described that around 40 proteins could be degraded by PROTACs at that time.[37] The same group updated this number for about 130 degradable targets in 2021, showing an impressive increase of 90 targets from 2020-2021.[38] Currently, consulting the PROTAC-DB (a repository of structural and experimental data about PROTACs with POI and chemical structures of POI ligands, along

with biological activities and physicochemical properties), the number of these targeted proteins has increased to 323 (an increase of 70 % in degradable targets in only 2 years),[71] indicating that the era of protein degradation has indeed arrived.

Maybe one of the main appeals to PROTACs is the possibility of reaching "undruggable" targets. Indeed, some compounds were developed as degraders of proteins lacking a catalytic site or a small-molecule binding site like aberrant Tau, present in frontotemporal dementia,[72–74] and RAS (KRAS, NRAS and HRAS), the most frequently mutated gene family in cancers,[75–78] both considered "undruggable" targets. Nevertheless, the use of PROTAC for degrading these proteins, particularly those engaged in PPIs, remains somehow restricted due to challenges in identifying small-molecule binders for these proteins.[79] New techniques are welcome to identify new chemical entities that bind to the these "undruggable" POI, like the recently described site-specific and fragment-based covalent ligand screening using liquid chromatography-tandem mass spectrometry (LC-MS/MS).[79]

In contrast, PROTACs are widely used for targeting kinases (n = 195 kinases), today representing around 60% of all described PROTACs' targeted proteins. At a first sight, it appears to be countersense since kinases are already explored target by the classical occupancy-driven pharmacology MOA. The main point here is that many kinases possess well-established and potent inhibitors or high affinity ligands. These compounds can be readily modified to incorporate linkers, keeping adequate binding affinity. Furthermore, kinases exhibit deep binding pockets, facilitating the binding of PROTACs, prompting interaction between the kinases and the E3 ligases, leading to ubiquitination and eventual degradation.

Additionally, PROTACs may solve one of the main problems of ATP-competitive kinase inhibitors, that is the lack of selectivity coming from the high degree of homology of ATP binding site between kinases.[38] When nonselective inhibitors are used as POI ligands for designing new PROTACs, both the protein ligands and the degraders can binding to the corresponding kinases. However, in the case of PROTACs this recognition induces specific protein–protein interactions between the POI and E3 ligase, forming a specific ternary complex. This two-step recognition mechanisms contributes to the selective degradation of targets.[38] An interesting example was described by Bondeson and colleagues. From a high-throughput competitive binding assay, they discovery that foretinib at 10 μM could bind to more than 130 different kinases (Figure 49). Taking foretinib as model for the POI ligand, they designed and synthesized two PROTACS (**291** and **292**) using different E3 ligase ligands (CRBN (**291**) and VHL (**292**)). PROTACs (**291** and **292)**, at the same concentration, significantly changed the binding profile, in which **291** retained binding to 52 kinases while **292** bounded 62 kinases and

were able to only degrade less than 10 kinases. Additionally, they demonstrated that PROTAC **291** effectively degraded the therapeutically relevant protein p38a/MAPK14, despite weak binding affinity (Figure 49).[80]

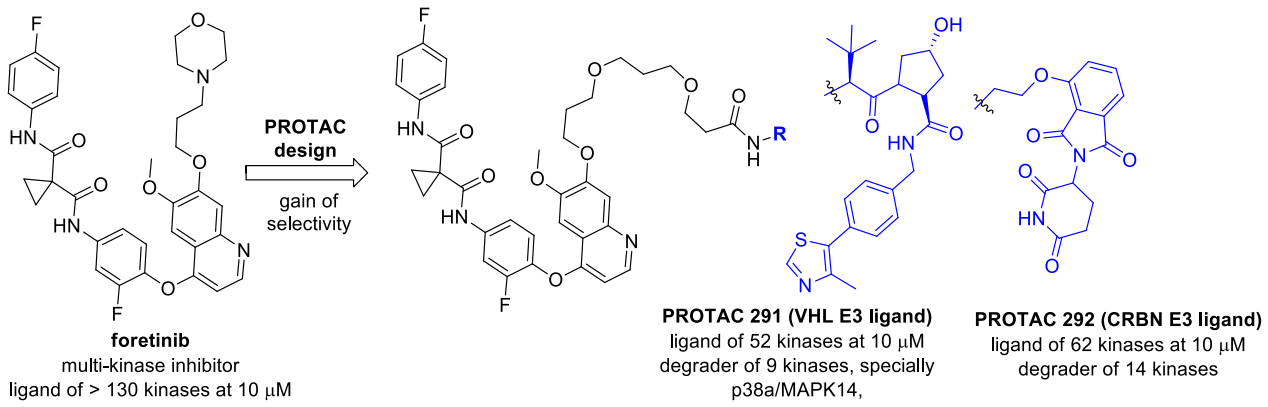

Figure 49. Use of non-selective inhibitor foretinib as POI ligand for designing new selective PROTACs.

Common observed drug resistance via mutations (close to the inhibitor binding pockets), gain of scaffolding function or overexpression of drug targets in long term treatments with traditional kinase inhibitors are explanations to the current option for new PROTACs. The event-driven MOA of PROTACs, resulting in catalytic removal of POI, can evade drug resistance from long-term selection pressure by degrading target proteins.[81] Furthermore, studies have revealed that PROTACs can induced the degradation of many mutated kinases like Bruton's Tyrosine Kinase (BTK). This highlights the potential of TPD for treating diseases, e.g. **C**hronic **L**ymphocytic **L**eukemia (CLL), resulting from kinase resistance to ibrutinib due to mutations.[82–84] While the ibrutinib MOA is to covalently binding to cysteine in the ATP binding pocket of BTK, exactly where the mutation occurs (C481S), PROTAC derivatives were not designed to covalently bind to BTK, inducing the degradation of both wildtype and mutant (C418S) forms.[34,45,45,82,85]

1.4.2. Clinical Proof-of-Concept

All the attractive characteristics of PROTACs described herein had their clinical validation when ARV-110 (AR) and ARV-471 (ER) entered in clinical trials in 2009. The oral efficacy and safety of ARV-110 have been proven in managing metastatic castrated prostate cancer (mCRPC),[86–88] while ARV-471 has demonstrated promising results in treating breast cancer.[89] Since them, an increasing number of protein targets have emerged to develop clinical

degraders and 21 new PROTACs entering in clinical trials as single chemical entities or as pharmaceutical combination with other know drugs, and nowadays, 20 clinical trials are still running. These PROTACs degraders are based on different E3 ligands, but mainly on CRBN-based ligands.

While the first two PROTACs modulated androgen (AR) and estrogen (ER) receptors, many other targets raised such as B-cell lymphoma-extra large (BCL-X_L), bromodomain-containing protein 9 (BRD9), signal transducer and activator of transcription 3 (STAT3) (Table 19 and disclosed structures in Figure 50). Currently, almost all clinical trials are focused on research for anticancer PROTACs. However, recently (2021) the first clinical degrader of IRAK4 for autoimmune inflammation-diseases entered in clinical trials, the KYMERA's degrader KT-474.[90] Worth of note, KT-474 is already in phase 2 clinical trials and maybe is showing that degraders for inflammatory conditions would be an interesting and promising field.

Table 19. Status and characteristics of PROTACs currently under clinical trial evaluations.

Year	Comp	PROTAC	ROA	Target	Main Indications	E3	CP	NCT numbers	Status *
2019	Arvinas	ARV-110	oral	AR	Metastatic Castration Resistant Prostate Cancer	CRBN	I/II, Ib	NCT03888612	A, NR
							Ib	NCT05177042	A, NR
2019	Arvinas / Pfizer	ARV-471	oral	ER	ER+/HER2- Locally Advanced or Metastatic Breast Cancer	CRBN	I	NCT05538312 NCT05930925 NCT05652660 NCT05673889 NCT06005688	C
								NCT05463952 NCT05501769 NCT05732428	A, NR
							I/II	NCT05548127 NCT04072952	R
								NCT06206837	NYR
							II	NCT05549505	A, NR
								NCT06125522 NCT05573555 NCT01042379	R
							III	NCT05909397 NCT05654623	R
2020	Bristol Myers Squibb	CC-94676	oral	AR	Metastatic castration-resistant prostate cancer	CRBN	I	NCT03554993 NCT04958291	C
2021	BeiGene	BGB-16673		BTK	B-Cell malignancies	CRBN	I	NCT05294731 NCT05006716	R

2021	Nurix Therap.	NX-2127	oral	BTK	Relapsed/ refractory B-cell malignancies	CRBN	I	NCT04830137	A, NR
2021	Nurix Therap.	NX-5948	oral	BTK	Relapsed/ refractory B-cell malignancies	CRBN	I	NCT05131022	R
2021	Haisco	HSK29116		BTK	Relapsed/ refractory B-cell malignancies	CRBN	I	NCT04861779	R
2021	Lynk	LNK-01002		Ras GTP-ase	Myelofibrosis (PV-MF, ET-MF) or acute myeloid leukemia	CRBN	I	NCT04896112	W
2021	Accutar Biotech	AC682	oral	ER	Locally advanced or metastatic ER+ breast cancer	CRBN	I	NCT05489679	T
							I	NCT05080842	A, NR
2021	Arvinas	ARV-766	oral	AR	Metastatic castration-resistant prostate cancer	Undis-closed	I / II	NCT05067140	R
2021	Dialectic Therap.	DT2216	i.v.	BCL-X_L	Solid tumor, hematologic malignancy	VHL	I	NCT04886622	C
2021	Foghorn Therap.	FHD-609	i.v.	BRD9	Advanced synovial sarcoma	Undis-closed	I	NCT04965753	A, NR
2021	Kymera / Sanofi	KT-474	oral	IRAK4	Autoimune diseases, atopic dermatitis (AD) or hidradenitis suppurativa (HS)	CRBN -based	I	NCT04772885	C
							II	NCT06058156 , NCT06028230	R
2022	Hinova	HP518		AR	Metastatic castration-resistant prostate cancer	CRBN	I	NCT05252364	C
							I	NCT06155084	NYR
2022	Kintor	GT-20029		AR	Prostate cancer	CRBN	I	NCT05428449	C
2022	Arvinas	ARV-110		AR	ARV-110 in combination with abiraterone	CRBN	I	NCT05177042	A, NR
							I / II	NCT03888612	A, NR
2022	Kymera	KT-413	i.v.	IRAK4	Relapsed or refractory B-cell NHL	CRBN	I	NCT05233033	S
2022	Kymera	KT-333	ND	STAT3	Lymphoma, large granular lymphocytic leukemia, solid tumors	undis-closed	I	NCT05225584	R
2022	C4 Therap.	CFT8634	oral	BRD9	Synovial sarcoma	CRBN	I / II	NCT05355753	T
2022	C4 Therap.	CFT8919	oral	EGFR-L858R	Non-small-cell lung cancer	CRBN	I	FDA permission, not yet started	-

2022	Accutar Biotech	AC176	oral	AR	Prostate cancer	undis-closed	I	NCT05241613	A, NR
2022	Cullgen	CG 001419	oral	TRK	Cancer and other indications	CRBN	I / II	FDA permission, not yet started	-
2022	Astellas Pharma	ASP3082	i.v.	KRAS G12D	Solid tumor	undis-closed	I	NCT05382559	R

ROA – route of administration; *A – active, NR – not recruiting, C – completed, R – recruiting, NYR – not yet recruiting, W – withdrawal, T – terminated, S – suspended.

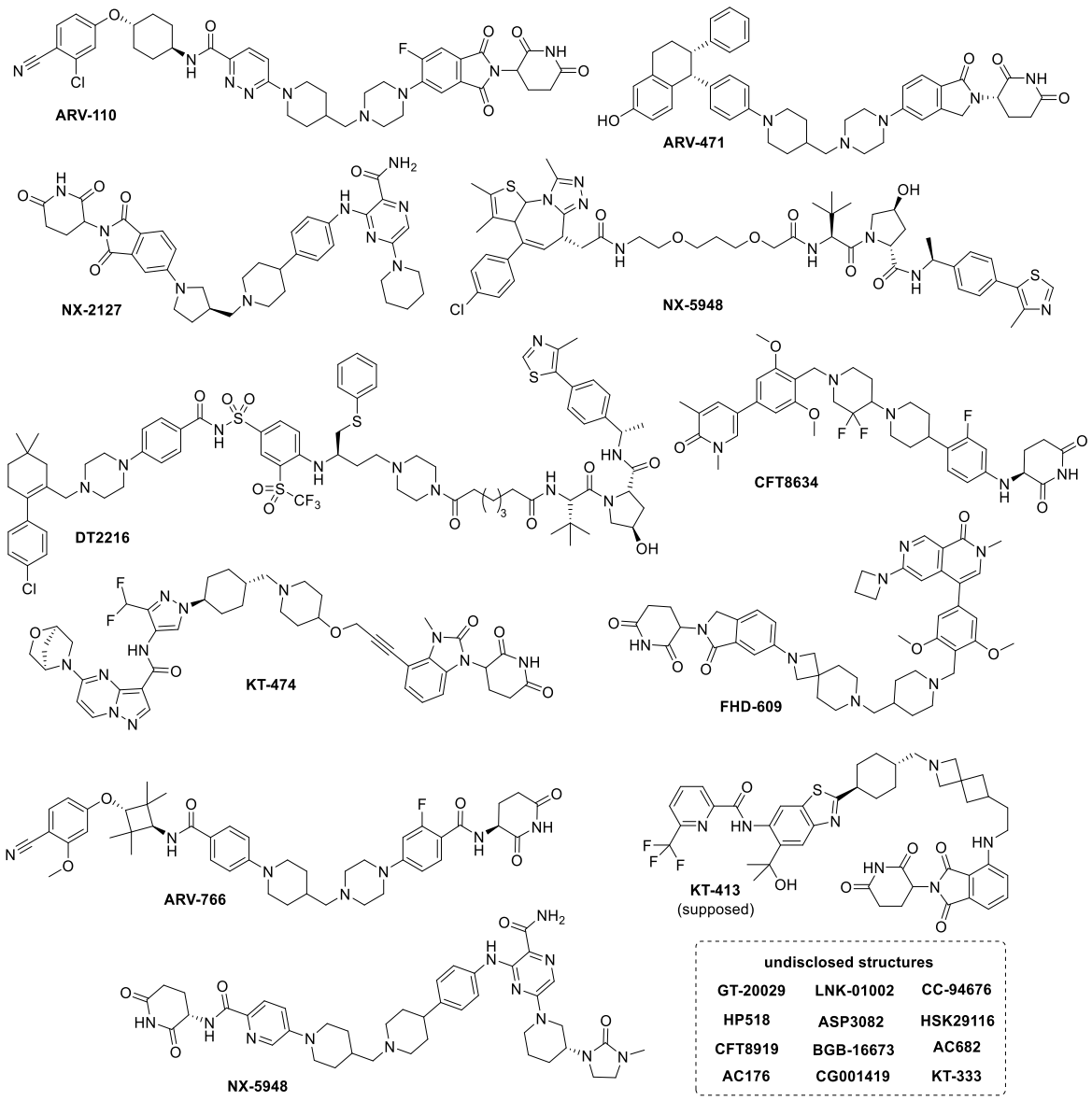

Figure 50. All disclosed structures of PROTACs under clinical evaluations.

1.5. Current drawbacks of PROTACs and possible avenues to improvements

Despite many advantages above discussed in this review, PROTACs still have space for improvement in some areas that can be considered disadvantageous,[91] as discussed:

1- PROTACs have some drawbacks in terms of potential toxicities, stemming from either on-target or off-target protein degradation. PROTACs may lack selectivity, leading to the degradation of other proteins (off-target effect) or causing unselective degradation of the POIs in undesired tissues (on-target effect). This challenge can be partially addressed using other administration ways, like topical PROTACs that have proven to mitigate systemic exposure and associated side effects. A recent illustration is compound GT20029 (structure not yet disclosed), targeting AR and currently undergoing Phase I clinical trials in China.[92] However, in cases where systemic administration is necessary, targeted delivery systems can potentially overcome issues related to poor selectivity. In contrast to conventional small molecules, PROTACs typically present greater complexities in terms of drug metabolism and pharmacokinetics (DMPK) and need more comprehensive safety evaluations.[93] The metabolites of PROTACs, particularly those formed through linker cleavage, have the potential to competitively bind to the POI or the E3 ligase. This competitive binding may "antagonize" the degradation of the POI, consequently diminishing the efficacy of the original PROTAC. Hence, there is a necessity to develop innovative approaches for characterizing pharmacokinetics and metabolite profiling.[93]

2- PROTACs are molecules with properties lying outside Lipinsk's rule of five that can negatively affect their pharmaceutical effects.[94–96] As an illustration, PROTACs possess a higher molecular weight (MW) in comparison to conventional small-molecule inhibitors, potentially posing a pharmacokinetic challenge to their cellular permeability.[97] However, upon oral administration, PROTACs have demonstrated the ability to induce degradation of the POIs in any accessible cells as proved in clinical trials. Recent studies reveal an intriguing aspect of PROTACs, indicating that their properties can somehow contribute to their cell-permeability. An example from a PEG-linker PROTAC demonstrated varying conformations in different environments. In aqueous solvents like extra- and intra-cellular compartments, the PROTAC assumed elongated and polar conformations. Conversely, in apolar solvents such as chloroform, simulating the cell membrane interior, the PROTAC adopted conformations with a smaller polar surface area. It suggests that the flexibility of PROTACs could facilitate a kind of chameleonic behavior, allowing the PROTAC surface to adapt to the solvent, ensuring good

solubility in both polar and apolar compartments and, consequently, enabling cellular permeability.[98,99]

3- A current obstacle in advancing proteolysis targeting chimeras (PROTACs) lies in the empirical nature of structure–activity relationships (SARs) associated with linker length as well as the flexibility, that is a crucial parameter to be considered during design and development. More than only influencing PK properties,[100,101] length and flexibility plays an important role in inducing the ternary complex formation. In this context, employing macrocyclization or conformational restriction strategies to rigidify the linkers, and so fixing POI and E3 ligands in the bioactive conformation, may promote the formation of ternary complexes and improve the degradation profile of the PROTAC.[93]

4- At elevated concentrations, PROTACs exhibit "hook effects", wherein the competitive formation of a target POI-PROTAC or E3 ligase-PROTAC binary complex occurs, leading to diminished efficacy. This phenomenon has been observed in various studies and can lead to problems regarding differences in metabolic capabilities between populations.[91,94,102]

5- Despite previous theories, it is already possible to identify PROTACs' resistance emerging through genomic alterations in the core components of E3 ligase complexes.[103] This is an additional challenge for PROTAC development arising from the potential development of resistance in cells treated with degraders containing CRBN and VHL E3 ligase recruiters.[103] Thus far, a limited number of E3 ligases (e.g., CRBN, VHL, MDM2, IAP) are used for PROTAC development (discussed in a next session). CRBN and VHL E3 ligases are generally considered to be ubiquitously expressed in humans, showing limited selectivity of PROTACs in cancer cells over normal cells. There are some exceptions when tumor enrichment of an E3 ligase coincides with the dependence of the tumor on expression of that ligase. An analysis with CERES scores in DepMap of E3 ligases across multiple tumor cell lines indicated these correlations.[104] This discovery has enabled the recognition of E3 ligases and other genes associated with the UPS, with some better-characterized than others (e.g WD repeat-containing protein 82 (WDR82) and cell division cycle 20 (CDC20)), that demonstrate significant tumor essentiality across various cancer cell types.[105] Ligases exhibiting these profiles offer the advantage of reducing the likelihood of tumor cells developing resistance to PROTACs through ligase-based mechanisms.

6- New E3 ligase scaffolds must be developed. CRBN-based structures (the most used scaffold) are thalidomide like derivatives that are known as possible degradation inducer of

GSTP1, IKZF1 and IKZF3. From this optics, PROTACs must be as selective as possible to prevent the degradation of proteins caused by the CRBN ligands themselves.[63,106]

7- As explained before, the number of targets that can be degraded by PROTACs has greatly expanded. However, most of them are "druggable" targets while some others are still challenge to tackle via small-molecule degraders.[1] For instance, modulation of targets lacking well defined binding sites and hydrophobic pockets have received growing attention with the use of new potential strategies as oligonucleotide-based PROTACs.[1,93,107,108]

1.6. Design of PROTACs

From a structural perspective, the success of designing PROTACs for targeting different proteins, as quickly discussed above, depends on integrating three distinct chemical moieties: a ligand for POI, an E3 ligase binder, and a linker connecting these two components.[12,37,102] In a Medicinal Chemistry point of view, the design strategy of PROTACs is not different from the so called "Molecular Hybridization", which is a strategy that aims to combine two or more molecules (or parts of them) in a new, single chemical entity.[109,110] Identifying the proper combination of these three elements is the first and pivotal step, needing a thorough examination of the structural features of both the E3 ligase and the POI. The formation of a ternary complex is completely dependent on the spatial orientation and alignment of both elements (POI and E3 ligase ligands), which plays a pivotal role in conducting the ubiquitin-protein knockdown process. As so, the design is specially influenced by the attachment position used to link the E3 ligase and POI ligands, a parameter that can be anticipated based, for example, on the binding mode of the POI and its ligand from a co-crystallized structure or by using computational tools. Additionally, the length and flexibility of the linker connecting the two moieties, i.e. POI and E3 ligase, can markedly impact potency and selectivity.[55,80,102,111,112]

1.7. The POI Ligand Requirements

The structural requirements for the POI ligand choice / exploration always depends on which target is supposed to be used. Regarding these ligands, a diverse range of warheads has been documented,[113] encompassing non-covalent, irreversible, and reversible covalent ligands, as well as allosteric variants.[114] Good consultation sources of POI ligands are the PROTAC-DB database and PROTACpedia.[71,115] Both serve as valuable resources for PROTAC development by gathering the chemical structures, biological activities, and physicochemical properties of POI ligands.

As described within topic 2.1, most of the current proteins targeted by PROTACs are "druggable" targets. For these POI, structural information can many times be found, such as crystal structures with bounded ligands or their structure-activity relationship (SAR), guiding the design of new degraders. Based on these data, it is possible to discover / propose the best linker attachment points in regions that are both exposed to the solvent and not involved with the POI binding. Two examples of degraders starting from co-crystallized ligands are described below in Figure 10. The potent IRAK4 (enzyme involved in inflammatory processes) degrader **PROTAC 293** was designed based on the crystal structure of **PF-06650833** (a phase II IRAK4 inhibitor) inside the IRAK4 kinase domain, showing solvent exposed vector at 4-position of isoquinoline scaffold. This position was selected to the linker attachment and led to the **PROTAC 293** with a DC_{50} of 151 nM (Figure 51A).[116] The second example describes a similar approach for the discovery of the GPX4 degrader, the **GDC-11**. From the covalent inhibitor **ML 162**, crystalized with GPX4, three sites were observed turned to the solvent and able to be modified. To the original anisole moiety, an amide linker and a pomalidomide based E3 ligase ligand were attached giving the PROTAC **GDC-11**, which presented a moderate GPX4 degradation efficacy of 33% at 10μM (Figure 51B).[117]

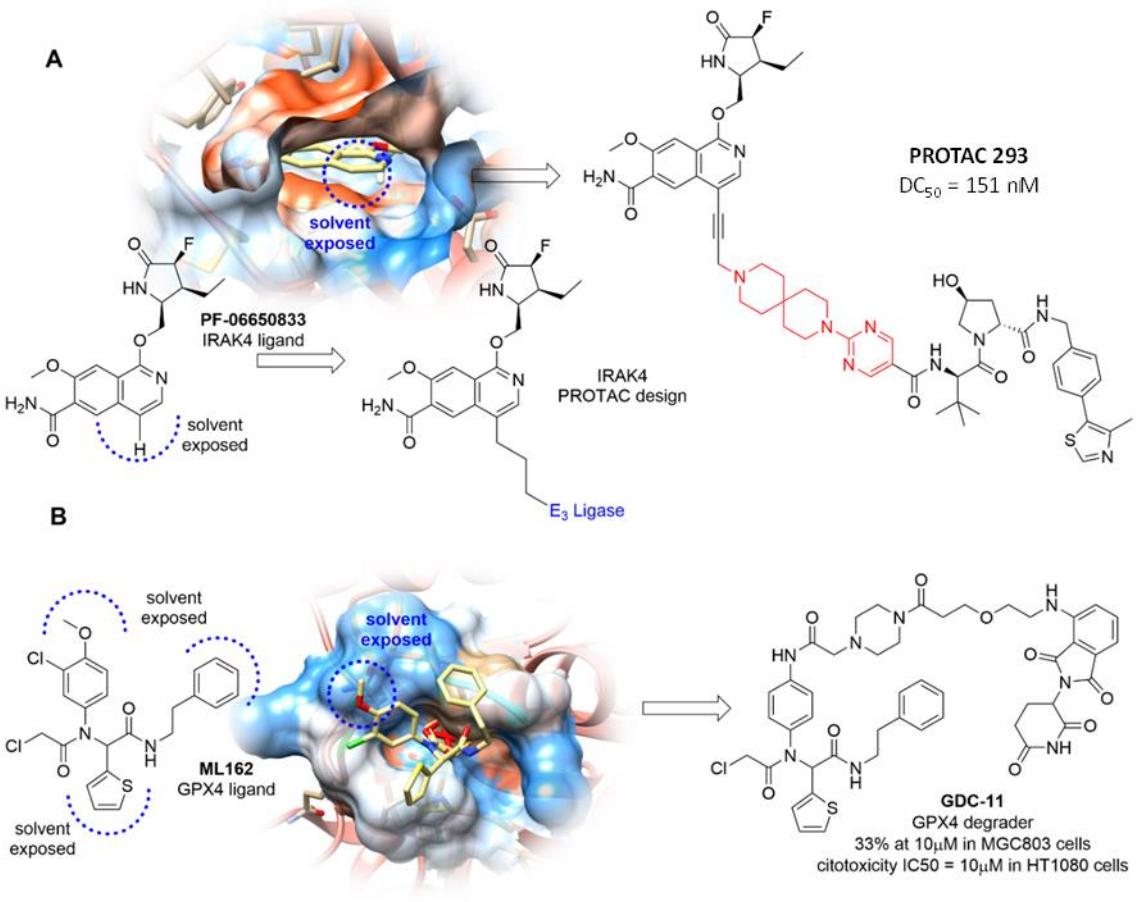

Figure 51. A- Design of **PROTAC 293** based on the crystal structure of phase II IRAK4 inhibitor **PF-06650833**. B- Discovery of the GPX4 degrader **GDC-11** from the co-crystallized covalent inhibitor **ML 162**.

Nevertheless, the absence of a well-defined ligand capable of engaging the intended target limits early-stage drug discovery initiatives, particularly those focused on novel biological targets characterized by poorly understood pharmacology. These "undruggable targets" needs more technologies helping the discovery of new compounds useful as POI ligands. However, important to remember, the affinity of the ligand to the POI is not the main focus on PROTACs, since their mechanism of action is based on an event-driven sub-stoichiometric catalytic MOA (Figure 44).[5,12,13] Thus, techniques like **F**ragment **B**ased **D**rug **D**iscovery (FBDD), which is frequently used to discover new ligands (usually with low affinities) can be a valuable tool for the discovery of new POI ligands. Indeed, many successful examples of PROTACs used the FBDD in their discovery process including **CST905** ($BRAF^{V600E}$-PROTAC), **SIAIS100** (BCR-ABL-PROTAC) and **294** (CDK9-PROTAC) (Figure 52).[118–120]

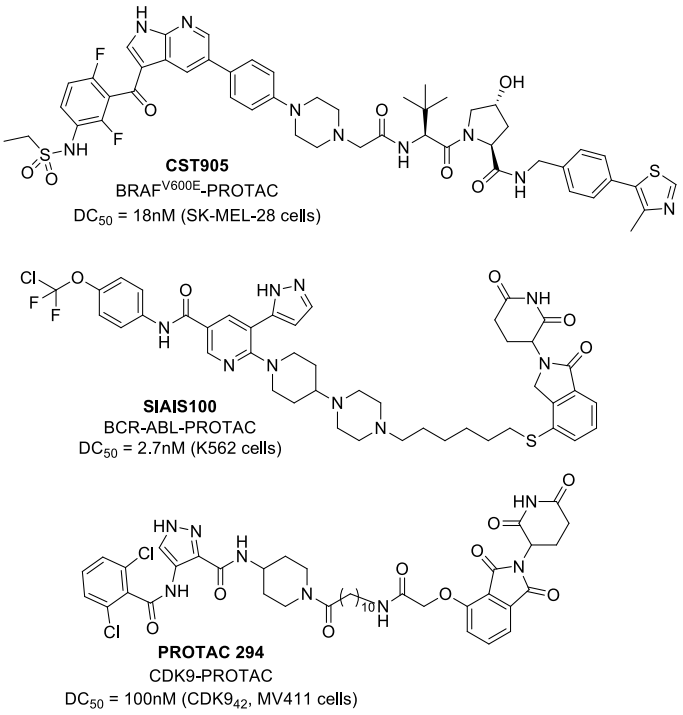

Figure 52. Discovered of PROTACs by means of the FBDD process.

Maybe the most successful example of FBDD in the drug discovery process is the BCL-X_L-PROTAC **DT2216**, that is currently in phase 1 clinical trials (Table 19 and Figure 49, and 53).[121] This PROTAC was developed from an NMR-based screening that furnished two active fragments (**295** (300 μM) and **296** (4300 μM)) binding in adjacent sites. Both fragments were linked by the sulfonamide group, leading to compound **297** (IC_{50} = 93 nM) (Figure 53). A lead optimization process was carried out with further modifications in this structure, specifically outside the active pocket, aiming at improving hydrophobic interaction and π-π stacking with BCL-XL resulted in compound **ABT-737** (**298**) (IC_{50} = 83 pM). Due to low solubility and high lipophilicity, resulted in poor pharmacokinetics properties, optimization of compound **298** was continued by replacing the hydrophobic groups with hydrophilic ones. Furthermore, crystal structure of compound **298** indicated that the tertiary amine was turned to an open space and to this group the linker and VHL E3 Ligase were attached, giving the compound **DT2216** (Figure 53).

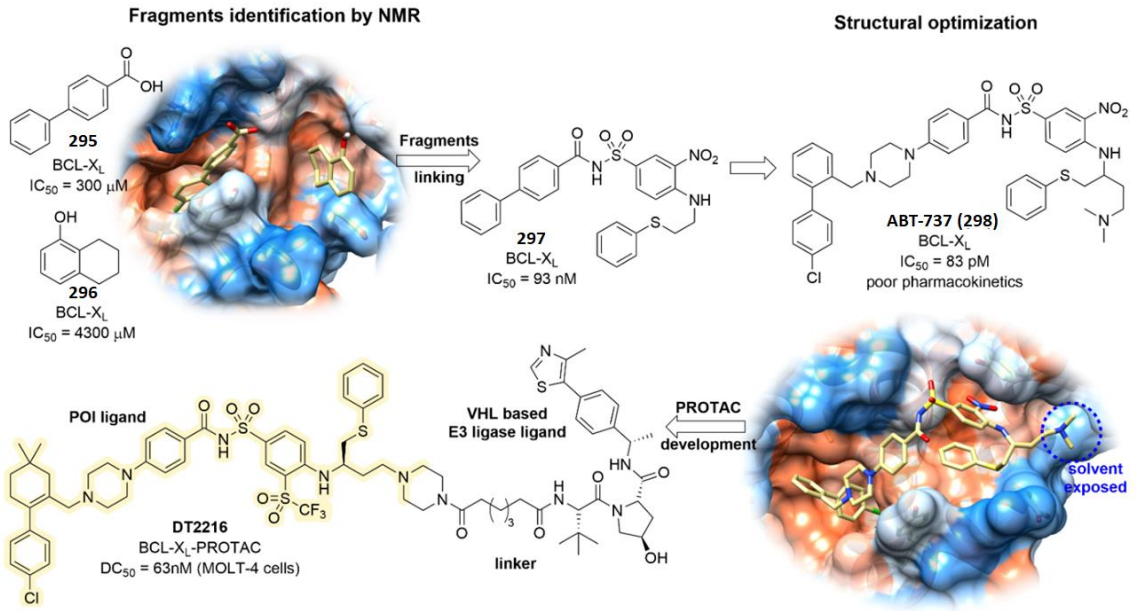

Figure 53. FBDD applied to the discovery of the BCL-X_L-PROTAC **DT2216** (Phase 1 clinical trials) from the two fragment hits (**295** and **296**) identified by NMR.

1.8. The Linkers as Fundamental Moieties

Linkers play a crucial role in the activities of PROTACs. The adaptability of the linkers significantly influences the overall degradation efficiency of a specific PROTAC. Parameters such as the distance between the POI and the UPS, and the presentation and accessibility of reactive lysine residues on the POI to the E2 are vital factors, ultimately determined by the characteristics of the linker unit. Nonetheless, the connection between the spatial arrangement of lysine residues on the POI surface, the structure, and interconnection of poly-Ub chains, and the effectiveness of degradation remains inadequately comprehended.[111,122] Guidelines for formulating potent PROTAC linker designs, from scratch, are regrettably absent and to date, studies on the SAR of linkers are predominantly empirical, and the design of linkers still poses a bottleneck.

The appropriate combination of length, hydrophilicity, and rigidity in ligand-connecting linkers has been demonstrated to influence various properties of PROTACs such as pharmacodynamic (PD), and pharmacokinetic (PK) characteristics such as cellular permeability, metabolic stability, solubility, and, of course, biological activity.[111,123] This combination forms the basis for the successful design of effective PROTACs. Optimization of linker composition is crucial for each ligand pair (POI and E3 ligase), especially concerning the length and conjugating sites on each ligand.[45,111] A commonly employed strategy involves

creating a library of PROTACs that incorporate linear unsaturated aliphatic linkers of variable lengths, typically ranging from a few atoms to 29 atoms. This process continues until a suitable spatial orientation is identified, proving productive for ternary complex formation between the target POI and the E3 ubiquitin ligase.[1,100,111] The most potent PROTAC linkers are selected through systematic and extensive iterations, incorporating different chemical motifs.

Typically, longer aliphatic linkers, including polyethylene glycol and other glycol chains, have produced substantial contributions to protein–ligand interactions within the ternary complex. They have played a role in stabilizing the orientation of the complex through cooperative binding. However, there are cases where the energy gained in the ternary complex from new PPIs is counteracted by the entropic cost associated with reduced PROTAC flexibility.[100] Recently, there has been a shift from flexible, linear alkyl- and PEG linkers to more rigid structures, including alkyne, and cyclic scaffolds like piperazine, piperidine, and triazole (Figure 54). This sentence is particularly true if we have a look to the disclosed structures from compounds in clinical trials in Figure 50, in which nine of eleven PROTACs have more rigid linkers.

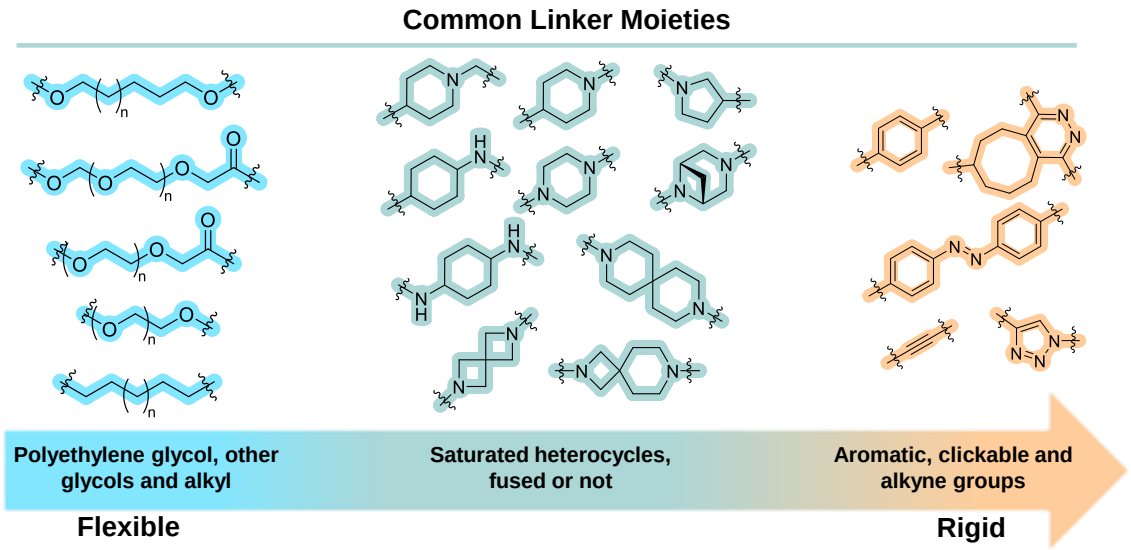

Figure 54. The most common linker moieties used in PROTAC design according to chain flexibility.

One prevalent approach to combine POI and an E3 ligase binders involves the utilization of click chemistry, such as the copper-catalyzed Huisgen 1,3-dipolar cycloaddition reaction described by Carolyn R. Bertozzi, Morten Meldal and K. Barry Sharpless, which incorporates an azide and an alkyne moiety given an 1,2,3-triazol.[124–126] An extensive and insightful review

on this technique applied to PROTACs was provided by Pasieka and colleagues, covering a wide range of aspects related to the topic.[127] Beyond the broad applicability and excellent compatibility of this linking strategy, the resultant triazole ring may offer a metabolic advantage compared to linear linkers being more susceptible to oxidative metabolism *in vivo*, as highlighted by Xia and coworkers,[128] Furthermore, improve the rigidification of the linker, potentially leading to reduced entropy loss within the system.

The first two articles introducing the utilization of **Cu**-Catalyzed **A**zide-**A**lkyne **C**ycloaddition (CuAAC) to PROTAC synthesis were concurrently published in a special issue of the Journal of Medicinal Chemistry.[129] The research conducted by Jung's group focused on the synthesis of triazole-based PROTACs targeting sirtuins (Sirt), a family of histone deacetylases implicated in the pathogenesis of various diseases, including inflammation.[130] A Sirt2-selective and potent compound (**SirReal**) was chosen as the ligand for the POI, while the well-established CRBN ligand thalidomide was selected as the E3 ligase binder. For the first time the use of a triazole linker led to novel degraders and induced the degradation process of Sirt by facilitating the formation of a ternary complex (Figure 55).[129] In the second work, Wurz and colleagues developed PROTACs targeting BRD4. Utilizing the well-known **JQ-1** moiety, which binds to BRD4,[131] and E3 ligase binders of both VHL and CRBN class connected by PEG linkers. Proximity and protein degradation assays confirmed the capability of the triazole-based PROTACs **299**-**301** to form the ternary complex, thus inducing proteasome-mediated degradation (Figure 55).[132]

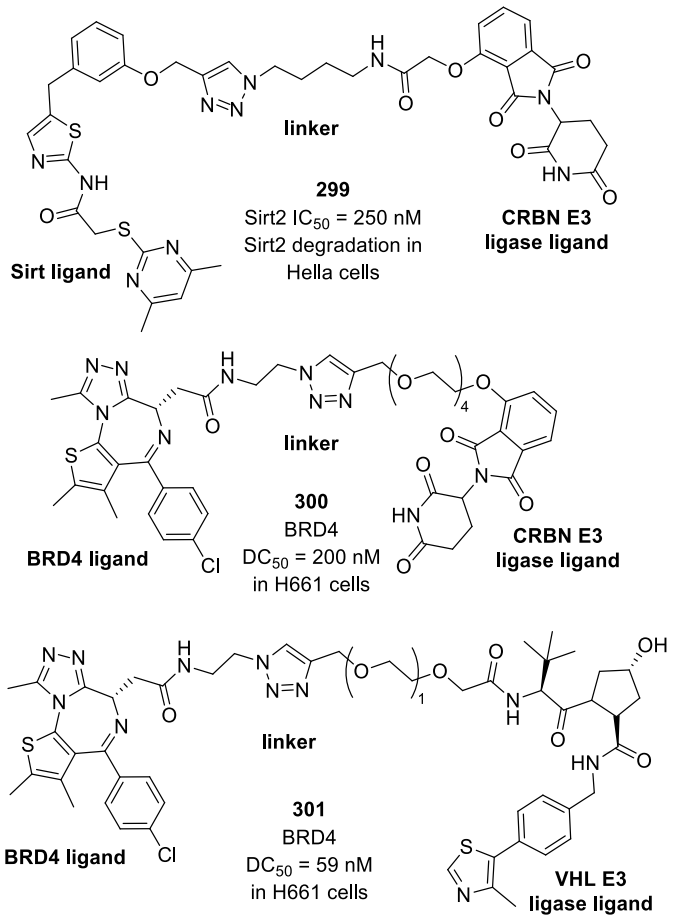

Figure 55. Synthesis of first-in-class 1,2,3-triazole-based **PROTACs 299** as Sirt2 degraders and **300** and **301**, as BRD4 degraders.

Another interesting feature involved with linkers is the possible photochemical modulation of PROTACs activity, enabling spatiotemporal control of PROTAC-mediated protein degradation, which has potential to avoid side effects.[133] Two possible Photochemically Controllable PROTACs (PHOTACs) are know: 1- Photocaged, that is a modified PROTAC designed by caging the PROTAC, thus leading to an inactive degrader, in which the light irradiation can remove the substituent leading to an active PROTAC able to conduct the protein degradation.[134] This approach, despite applied to linkers, can be also used in POI and E3 ligase binders; and 2- Photoswitchable PROTACs, that is applied specially to linkers. This photochemical modulation is an alternative approach to locally activate PROTACs by means of a photoisomerization.

Pfaff et al. designed the photoswitchable **PROTAC 302** by integrating a bistable *ortho*-tetrafluoroazobenzenes (*ortho*-F_4-azobenzenes) linker between the POI ligand and the E3 ligase ligand. So far, azobenzenes are the most common class of photoswitches used for the photo-

control of biomolecules.[135] The lead PROTAC structure chosen was **ARV-771**, where the linker's length between the POI ligand and the E3 ligase ligand is approximately 11 Å. As illustrated in Figure 15, substituting the PEG-based linker in **ARV-771** with *ortho*-F_4-azobenzene resulted in an anisomeric photo PROTAC pair.[136] The ***trans*-PROTAC 302** (active form) maintained an optimal distance of 11 Å between both ligands, while ***cis*-PROTAC 302** (inactive form) presented a shorter distance of only 8 Å. Photoswitch occurred upon exposure to 530 nm irradiation (visible light), in which ***trans*-PROTAC 302** could be converted into ***cis*-PROTAC 302**. Conversely, under 415 nm irradiation, ***cis*-PROTAC 302** could be transformed into ***trans*-PROTAC 302**. Intriguingly, ***trans*-PROTAC 302** induced the degradation of BRD2 but not BRD4 in Ramos cells after 18 hours, while no apparent degradation was observed with ***cis*-PROTAC 302**. In contrast to photocaged PROTACs, photoswitchable PROTACs provide a reversible on/off switch for targeted protein degradation.[136]

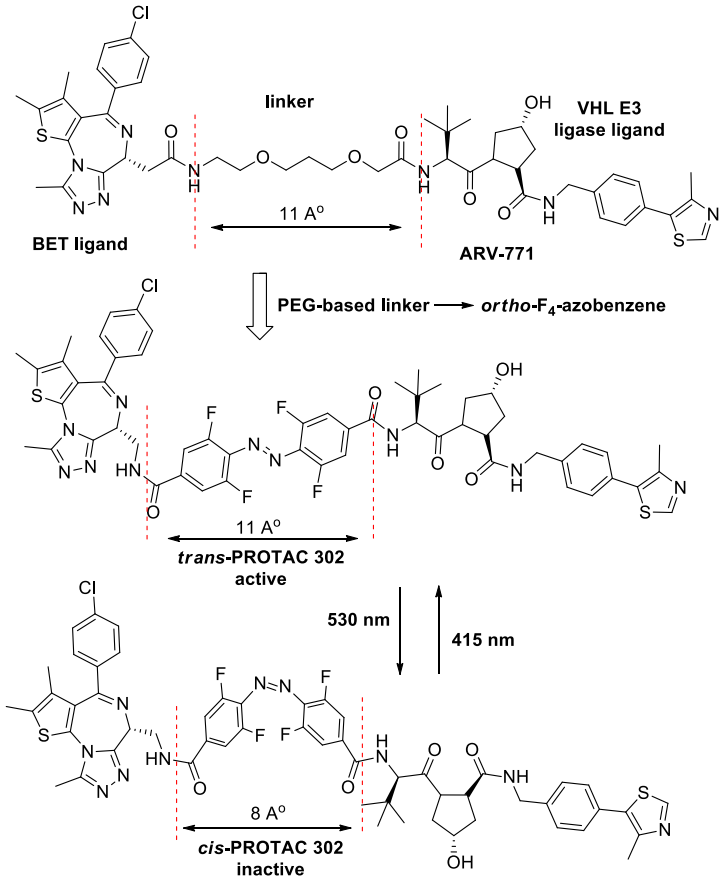

Figure 56. Photoswitchable BET PROTAC design: substitution of the PEG linker in **ARV-771** by an *ortho*-F_4-azobenzene generating anisomeric photo-**PROTAC 302** pair of isomers with considerable changing in the distance between POI ligand and E3 ligase binder moieties.

1.9. The E3 Ligase Universe in Expansion

Likewise, the selection of the E3 ligase ligand plays a crucial role in determining the ultimate success of PROTACs, since they are the "responsible moiety" to recruit the degrader machinery.

The human genome contains two members of the E1 enzyme family, approximately 40 E2s, and over 600 E3 ubiquitin ligases.[137] While our comprehension of substrate recognition and the regulation of ubiquitination remains incomplete, the genome's choice of approximately 600 E3 ligases demonstrates the capacity to ubiquitinate a significantly larger number of protein substrates in a controlled manner, exhibiting considerable specificity.[138] Playing a vital role in protein ubiquitination, E3 ligases contribute to substrate selection and influence the efficiency of the ubiquitin cascade.[22] The success of a protein knockdown depends directly on the selection of the best E3 ligase. Different degradation profiles can be observed on a specific target based on the recruited E3 ligase.[139]

A beautiful example of this specificity was demonstrated by Ciulli group,[140] when they reported the development of a **L**eucine-**R**ich **R**epeat **K**inase **2** (LRRK2) (implicated in Parkinson's disease and inflammatory processes) **PROTAC XL01126**,[141] as an alternative LRRK2-targeting strategy. Initial design and screenings of PROTACs based on ligands for the E3 ligases von VHL, CRBN, and cIAP identified the best degraders, always containing a thioether-conjugated VHL ligand, while other E3 ligase ligands presented none or insipient activity (Figure 57). A structural optimization in a second step led to the discovery of **XL01126** as a fast and potent degrader of LRRK2 in multiple cell lines, with DC_{50} varying within 15−72 nM, high cell permeability, positively cooperative ternary complex with VHL and LRRK2 ($\alpha = 5.7$) (Figure 57). Also presented interesting PK properties being orally bioavailable (F = 15%) and penetrating to the blood−brain barrier (BBB) after either oral or parenteral dosing in mice.[140]

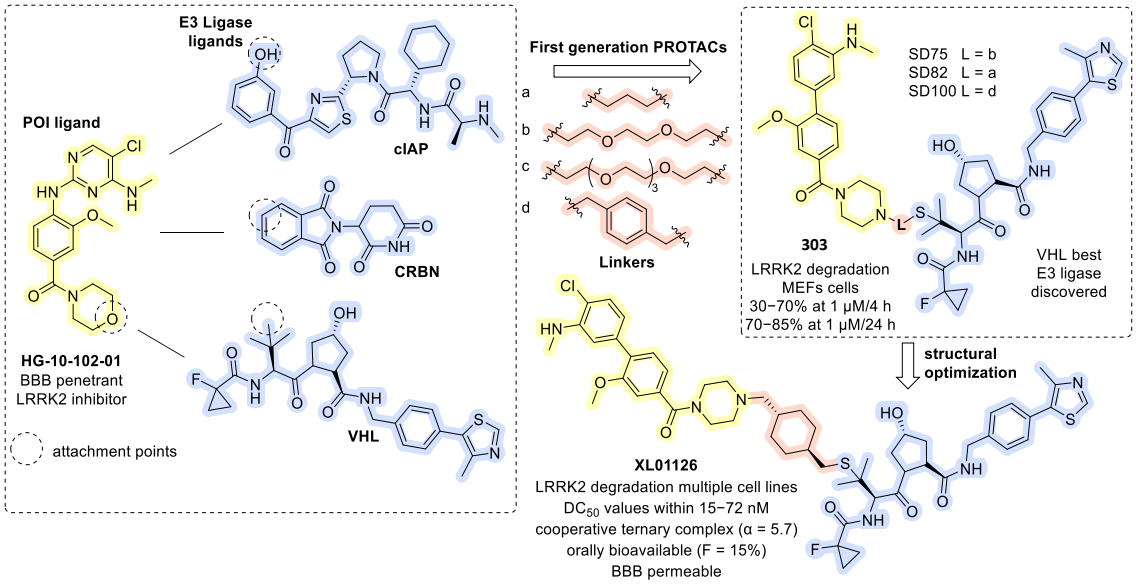

Figure 57. Development of the LRRK2 **PROTAC XL01126** by screening different ligands for the E3 ligases: von VHL, CRBN, and cIAP.

Each E3 ligase has its own specificities and, despite the vast number of known E3 ligases, until now not many of them have been successfully used for PROTACs' construction as exemplified until here in this review: e.g., von Hippel Lindau (VHL), mouse double minute 2 homologue (MDM2), cellular inhibitor of apoptosis protein (cIAP), and Cereblon (CRBN). Thus, a substantial universe of E3 ligases is still unexplored, holding promise for targeted protein degradation. Consequently, E3 ubiquitin ligases are garnering attention as appealing drug targets, given their implication and dysregulation in various diseases.[52,93] A significant amount of the initial efforts has focused on pairing VHL or CRBN with various target proteins to optimize resource utilization and accelerate advancement of PROTACs and indeed, these are the most common E3 ligase ligands found in "PROTACs' world".

We proceeded with an analysis on PROTAC-DB[71] to mapping the relevance of each E3 ligase ligand to the PROTACs' development until today. CRBN (65%, n = 3530) is so far the most used ligand, followed by VHL (29%, n = 1578), the IAP family (XIAP, cIAP, and IAPs; 4%, n = 190) and MDM2 (1%, n = 56) (Figure 58). Main representants of these E3 ligase ligand families are illustrated in Figure 59. The most used E3 ligases explored (CRBN and VHL) are considered to have low tissue-specific expression and already presented punctual relates of mutation in cancer models. This demonstrates the importance of developing new ligands for E3 ligase and some ones are already on going, like DCAF11, DCAF15, DCAF16, FEM1B, RNF114, RNF4,[142–146] that are depicted as "others" in Figure 18, still representing an incipient 1% of total examples, within 34 PROTACs. Despite few examples, the main structures of these

new E3 ligase ligands are disclosed in Figure 60. The same analysis applied to PROTACs under clinical trial evaluations was affected by 5 compounds (22%) that still haven't had their structures disclosed. Within the disclosed structures, again CRBN is for sure the most applied (74%, n = 17), with VHL presenting only 1 compound (4%) (Figure 58).

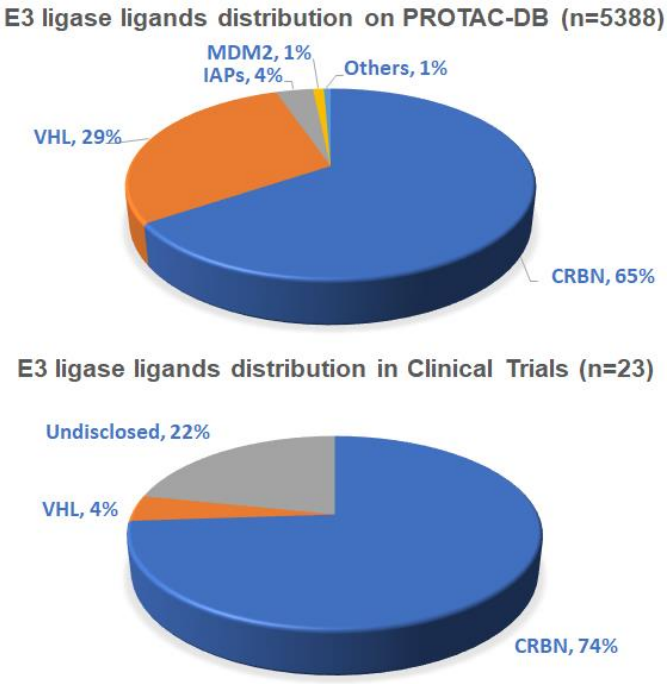

Figure 58. Representative analysis of E3 ligase ligand families described on PROTAC-DB (accessed in 02-19-2024) and under current clinical trials.

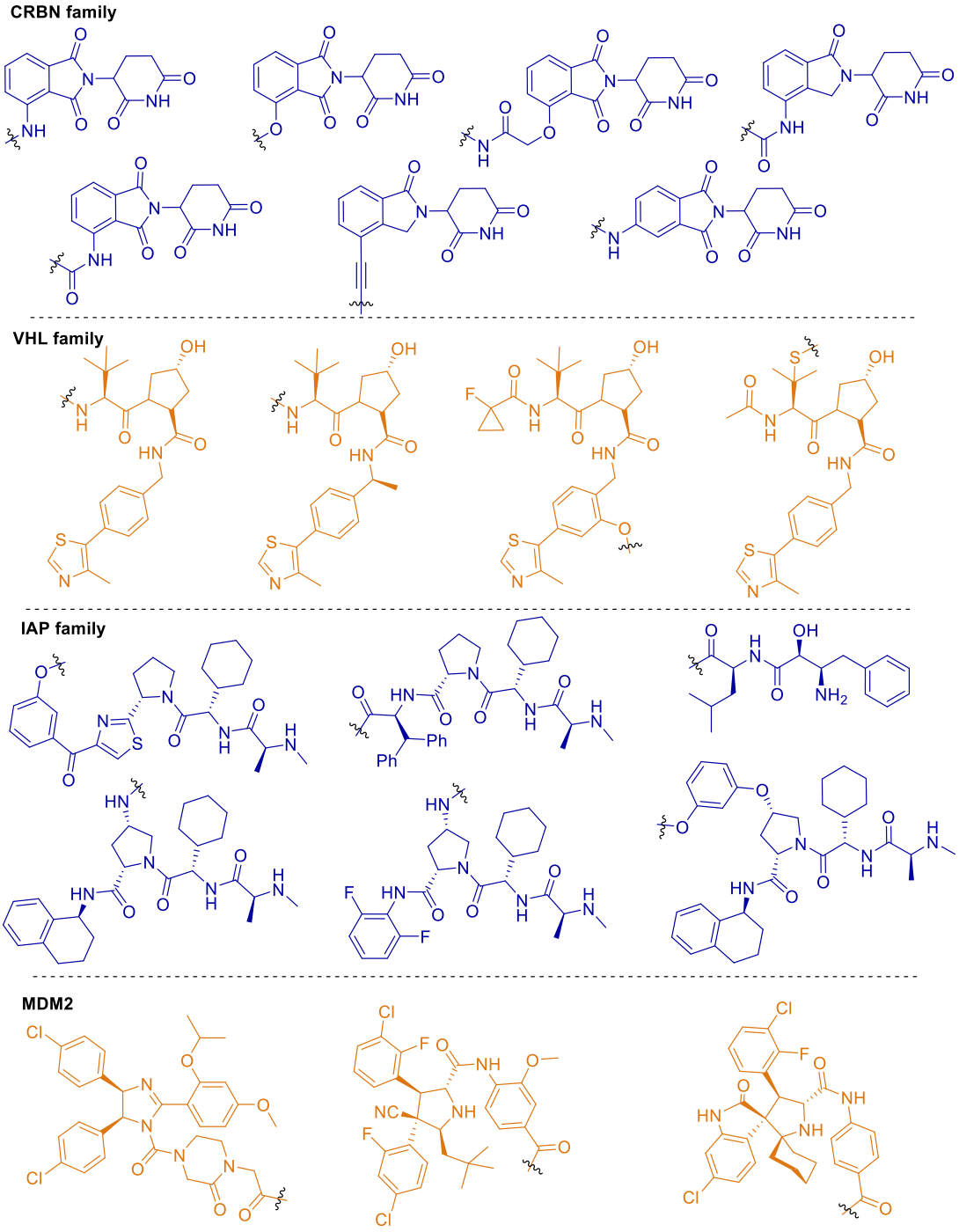

Figure 59. Main representants of the most used E3 ligase ligands families. The black wave line represents the point of attachment to the linker.

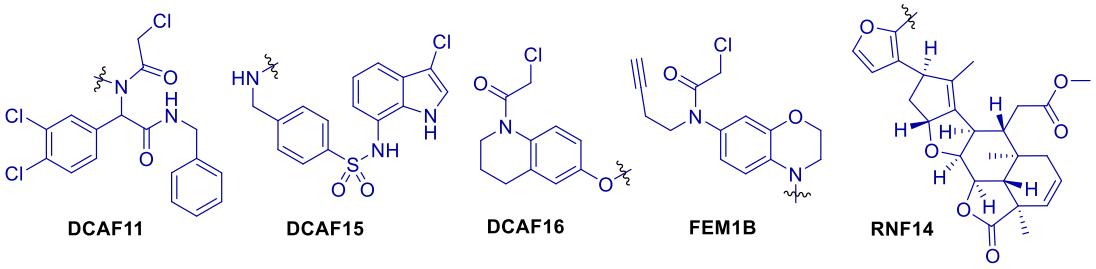

Figure 60. Representants of the "other" used E3 ligase ligands families.

Nowadays there is increasing interest in academia and industry for identifying E3 ligases with unique expression profiles to enable tissue- and cell- type-specific target degradation.[1] Recent discoveries suggested that E3 ligases with tissue-selective expression profiles may present unique therapeutic opportunities, even though their mechanisms have not yet been fully elucidated.[147] For example, specific E3 ligases from the central nervous system (CNS) have emerged, including RNF182 and tripartite motif-containing protein 9 (TRIM9).[148,149] These ligases are particularly noteworthy for addressing targets associated with neuronal diseases, possible allowing CNS-specific therapeutic targeting, and avoiding systemic off-target and toxicity effects, despite no PROTAC has been developed until now for these ligases. The same idea can be used to treatments focusing on degrading specific proteins in cells with improvement of a determined E3 ligase, such as the F-box protein 44 (FBXO44) that is enriched in some tissues but not specific to any.[150,151]

1.10. PROTACs developed for GSK-3β

Recently, three independent research groups published about PROTACs targeting GSK-3β due to its critical roles in cellular homeostasis and in a multitude of neurodegeneration specific signaling pathways.[152–154] These three PROTACs were able to induce GSK-3β degradation in cells, and one of them was also effective in AD mouse model.[152]

In 2021, Jiang et al. described the first example of a PROTAC to degrade the GSK-3β protein (Figure 61). In this study, the design, synthesis, and evaluation of a series of PROTAC GSK-3β degraders, through tethering the GSK-3β inhibitor **G1** and CRBN ligand thalidomide, were reported. Most of the PROTACs displayed good inhibitory activity, with IC_{50} values in the tens of nanomolar range and moderate protein degradation ability against GSK-3β. Western blot data showed that the compound **PG21** could effectively degrade GSK-3β in a dose-

dependent manner, inducing a 44.2% protein degradation at 2.8 μM. Additional pharmacological experiments revealed that the ability of **PG21** to degrade GSK-3β is mediated by the ubiquitin-proteasome system (UPS). Furthermore, preliminary in vitro cytotoxicity experiments show that **PG21** has neuroprotective effects (Figure 62). Due to its good kinase selectivity, it is expected that the **PG21** degrader will serve as a new tool for analyzing the role of GSK-3β in various pathological states.[153]

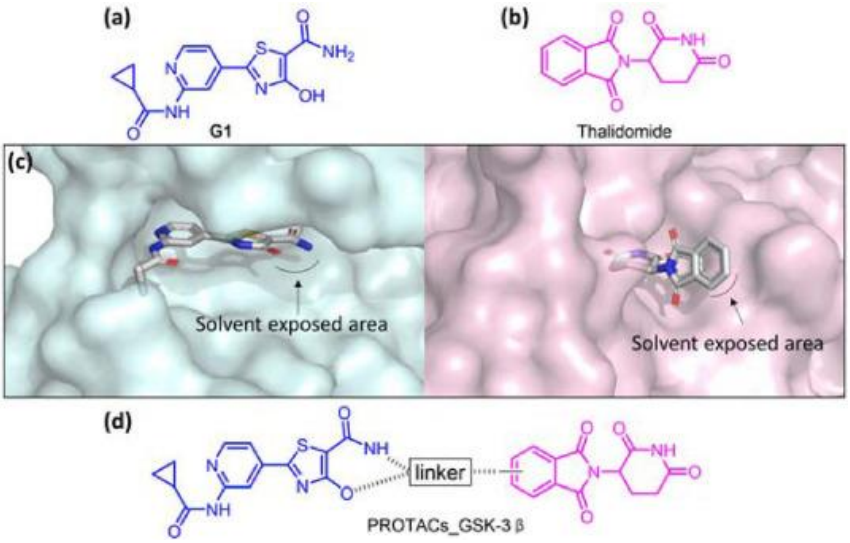

Figure 61. Design of PROTACs for GSK-3β. (a) Chemical structures of **G1** (GSK-3β ligand). (b) Chemical structures of thalidomide (CRBN ligand). (c) X-ray cocrystal structures of GSK-3β with **G1** (left, PDB: 4PTC) and thalidomide with CRBN (right, PDB: 4CI1). (d) Construction of PROTAC candidates targeting GSK-3β from solvent-exposed areas of ligands. Reproduced from 153. Reprinted with permission from *European Journal of Medicinal Chemistry* **2021**, *210*, 112949. Copyright © 2020 Elsevier Masson SAS.

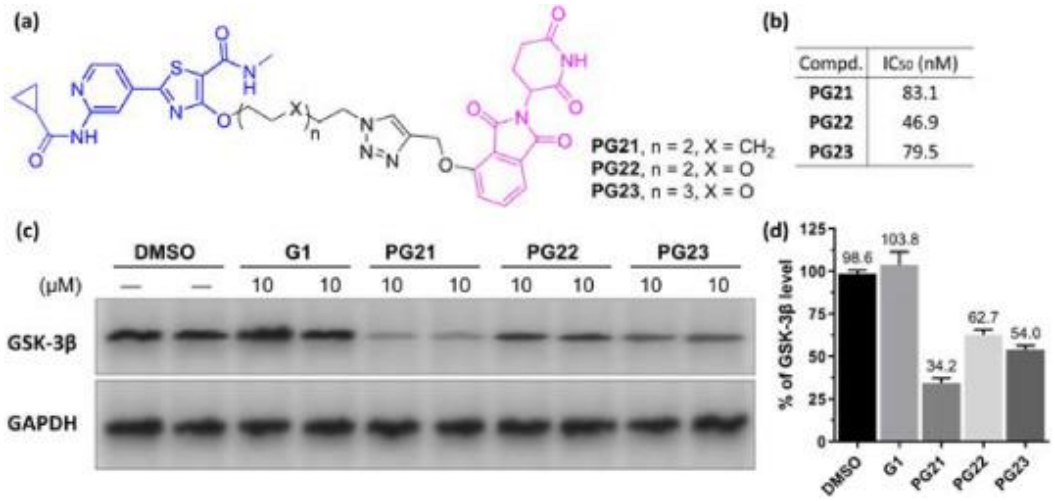

Figure 62. The degradation of GSK-3β by PROTACs PG21–23. (a) Chemical structures of PROTACs. (b) IC50 values of PROTACs against GSK-3β. (c) Degradation of GSK-3β by PROTACs with different linker lengths in PC12 cells for 10 h at 10 μM. (c) GSK-3β protein levels in cells. Numbers were calculated by the GSK-3β/GAPDH ratio with normalization by the DMSO control as 100. The bars in the graphs show the means ± standard deviations from two biological replicates. Reproduced from 153. Reprinted with permission from *European Journal of Medicinal Chemistry* **2021**, *210*, 112949. Copyright © 2020 Elsevier Masson SAS.

The design and synthesis of a series of highly potent GSK-3 degraders based on a click chemistry platform was described by Wang et al. (Figure 63). Among them, **304n** exhibited most potent degradation potency against GSK-3α (DC_{50} = 28.3 nM) and GSK-3β (DC_{50} = 34.2 nM) in SH-SY5Y cells. SPR assay confirmed that PT-65 binds to GSK-3β with high affinity (K_D = 12.41 nM). The proteomic study indicated that PT-65 could selectively induced GSK-3 degradation. Moreover, **304n** could effectively suppress GSK-3β and Aβ mediated tau hyperphosphorylation in a dose-dependent manner and protect SH-SY5Y cells from Aβ caused cell damage. The authors also showed that **304n** could suppress Okadaic Acid (OA) induced tau hyperphosphorylation and ameliorate learning and memory impairments *in vivo* model of AD.[152]

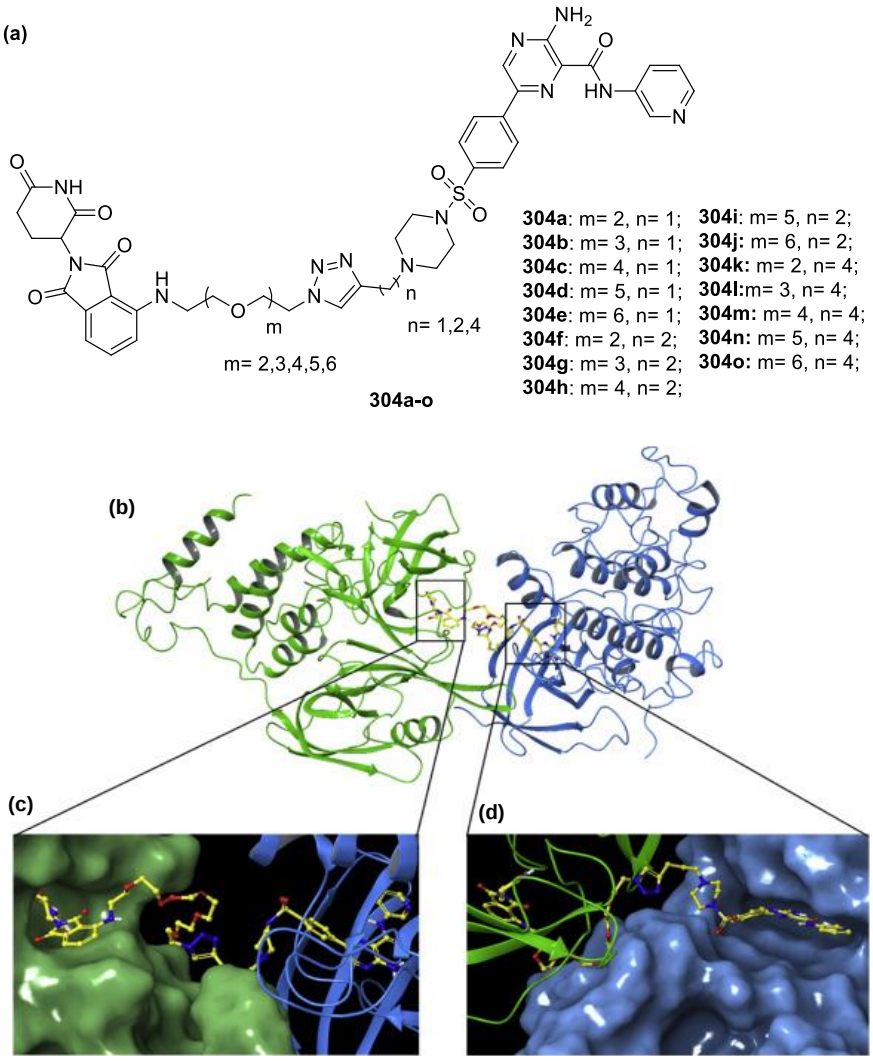

Figure 63. (a) Series of highly potent GSK3 degraders based on a click chemistry. **(b)** Computational modeling conformation of the ternary CRBN−**304n**−GSK3β complex. **(c, d)** Predicted binding mode for **304n** in the CRBN−GSK3β complex. PDB: 4CI3 for CRBN, green; PDB: 4ACD for GSK-3β, blue; **304n**, yellow. Reproduced from 152. Reprinted with permission from *Eur J Med Chem* **2021**, *226*, 113889. Copyright © 2021 Elsevier Masson SAS.

A small set of novel GSK-3β degraders was designed and synthesized by linking two different GSK-3β inhibitors, **SB-216763** and tideglusib, to pomalidomide, as E3 recruiting element, through linkers of different lengths (Figure 64). Compound **305** emerged as the most effective PROTAC being nontoxic up to 20 μM to neuronal cells and already able to induce significant GSK-3β degradation starting from 0.5 μM in a dose-dependent manner. PROTAC **305** significantly reduced the neurotoxicity induced by Aβ25−35 peptide and $CuSO_4$ in SH-SY5Y cells in a dose-dependent manner.[154]

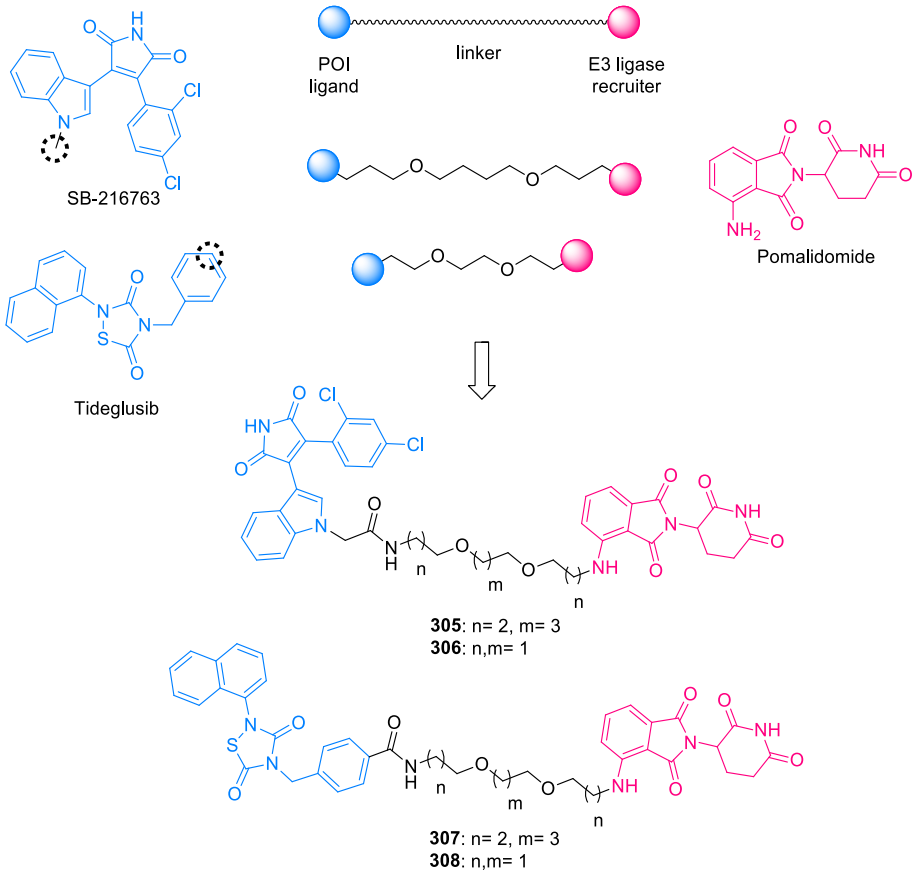

Figure 64. Design strategy leading to GSK-3β-directed PROTAC **305-308**. Black dashed circles represent tethering points.[154]

2. OBJECTIVES

2.1. General objective

This project aims at the design and synthesis of a new series of PROTACs able to induce GSK-3β degradation.

2.2. Specific objectives

- Structural and *in silico* design of new series of PROTACs;
- Synthesis and characterization of the designed series of PROTACs;

3. RESULTS AND DICUSSION

3.1. Structural Design of PROTACs for GSK-3β

Owing to the availability of a new series of GSK-3β inhibitors (**216a-k**) described in Chapter II, we sought to develop new PROTACs characterized by different types of linkers tethering our unexplored GSK-3β series and a E3 ligase recruiter. Analyzing the molecular docking result performed with our compound **216a** and a crystallographic structure of GSK-3β (PDB 1QL3), depicted in Figure 65, it is clear that indicated positions **a**, **b** and **c** of **216a** are turned out through solvent and may be good choices for introducing modifications aiming at constructing the PROTACs. Moreover, these positions do not present essencial functional groups for GSK-3β activity, what is a good start point for linker attachement connecting positions **a**, **b** or **c** of the 1,2,4-triazole (**216a**) to the E3 ligase recruiting element (Figure 65).

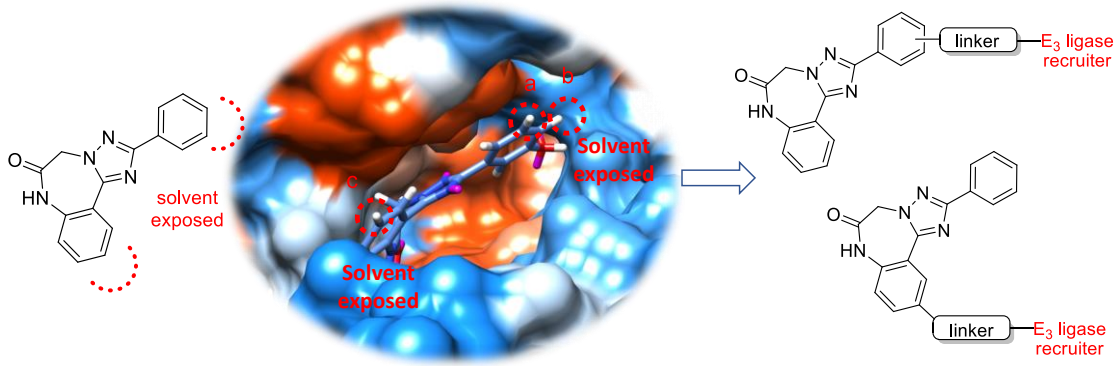

Figure 65. A - Molecular docking of **216a** and GSK-3b catalytic site.

Since the degrading potential of PROTACs depends on their ability to form ternary complex with the POI and the E3 ligase, we were interested, particularly, to evaluate whether any difference could be observed between the different types of linkers and then, we hypothesized the use of six linkers of different lengths and shapes. For the POI ligand attachment point, we have chosen to explore only the solvent-exposed position **a** of the GSK-3β inhibitor. In addition to the better GSK-3β inhibition profile shown by the *m*-substituted compounds, according to the docking studies, position **a** is more exposed to the solvent region compared to position **b**. Reinforcing this postulated, a 2D superposition between the GSK-3β PROTACs **PG21-23** and our compound *m*-substituted **216** demonstrated that the linker point

attachment is in the same region (Figure 66). As for the derivatization of the **c** position, since it poses a greater synthetic challenge, we intend to explore it in forthcoming works.

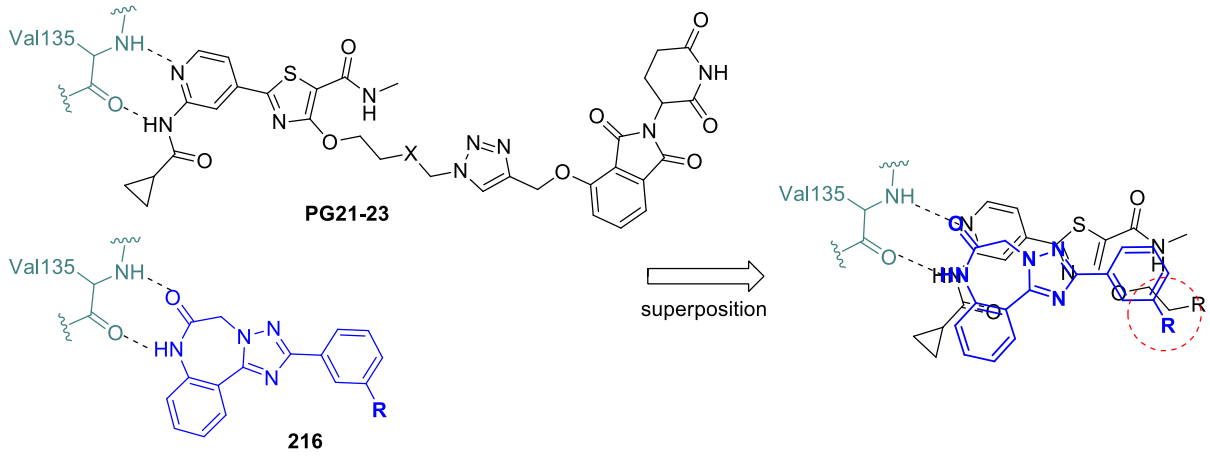

Figure 66. 2D superposition of PROTACs **PG21-23** and *m*-substituted compound **216** based on their docking models

As E3 ligase recruiting element we have selected the CRBN ligand pomalidomide. Common motifs (PEG and alkyl) were selected to be incorporated into the PROTACs due to their favorable properties, in terms of flexibility, availability and physicochemical profile. Seeking for more rigidity, we also selected linkers with cyclic rings such as piperidine and piperazine. The proposed structures to be built can be found in the figure 67.

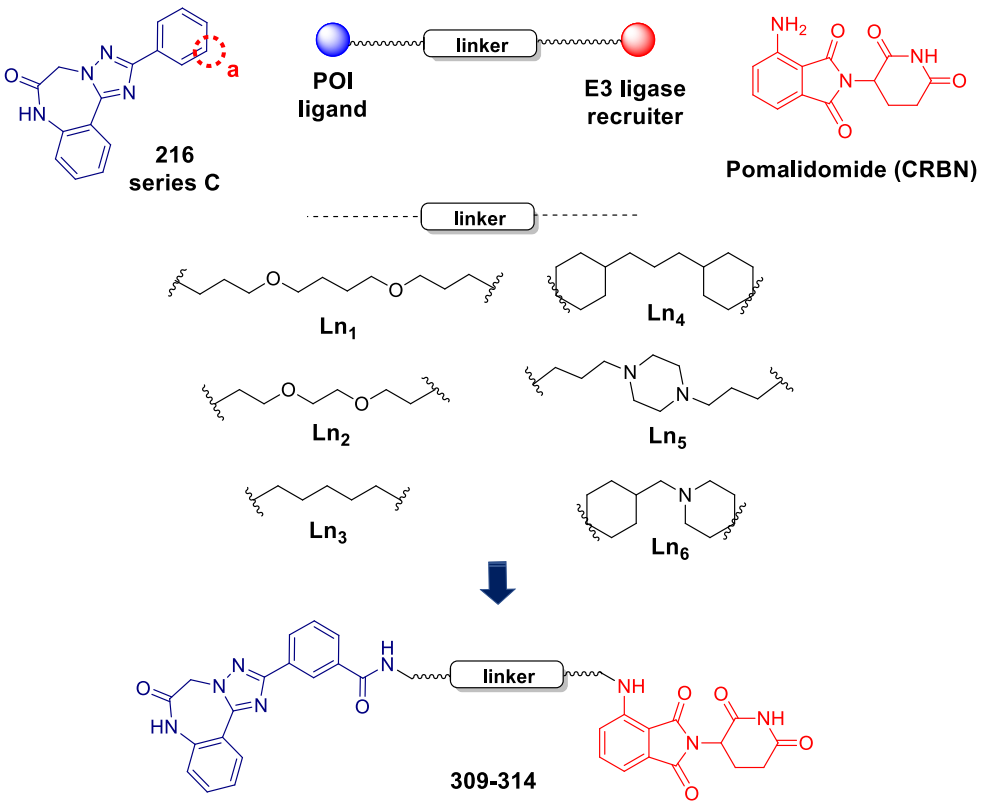

Figure 67. Design of PROTACs **309-314**.

To corroborate the structural design, molecular *docking* analyses were performed to theoretically verify whether the interaction prerequisites with the active site of GSK-3β, could be observed. For the analyses, compounds **309** and **310** were selected, in order to verify whether the E3 ligase recruiter pomalidomide is positioned facing the external region of GSK-3β.

The *docking* results indicated that the POI recruiter could make the same interactions as the 1,2,4-triaole GSK-3β inhibitors, as predicted by the structural planning. Additionally, we observed that the pomalidomide is directed towards the outer area of the enzyme, interacting with halosteric cavities. Since the docking study was conducted only with the enzyme GSK3β and the designed 1,2,4-triazol PROTACs (**309-310**), the interactions of pomalidomide on the external face of the enzyme were already theoretically predicted due to the program forcing these interactions with the nearby amino acid residues, which favors the reduction of the enthalpy energy of the enzyme-ligand complex (Figure 68 and 69).

Docking calculation results also showed that PROTAC **310**, with shorter linker, has higher score value than **309**, which suggests that exploring different sizes and shapes of linkers

that tether the POI to E3 ligase recruiters is a good starting point for the development of new degraders (Figure 68 and 69).

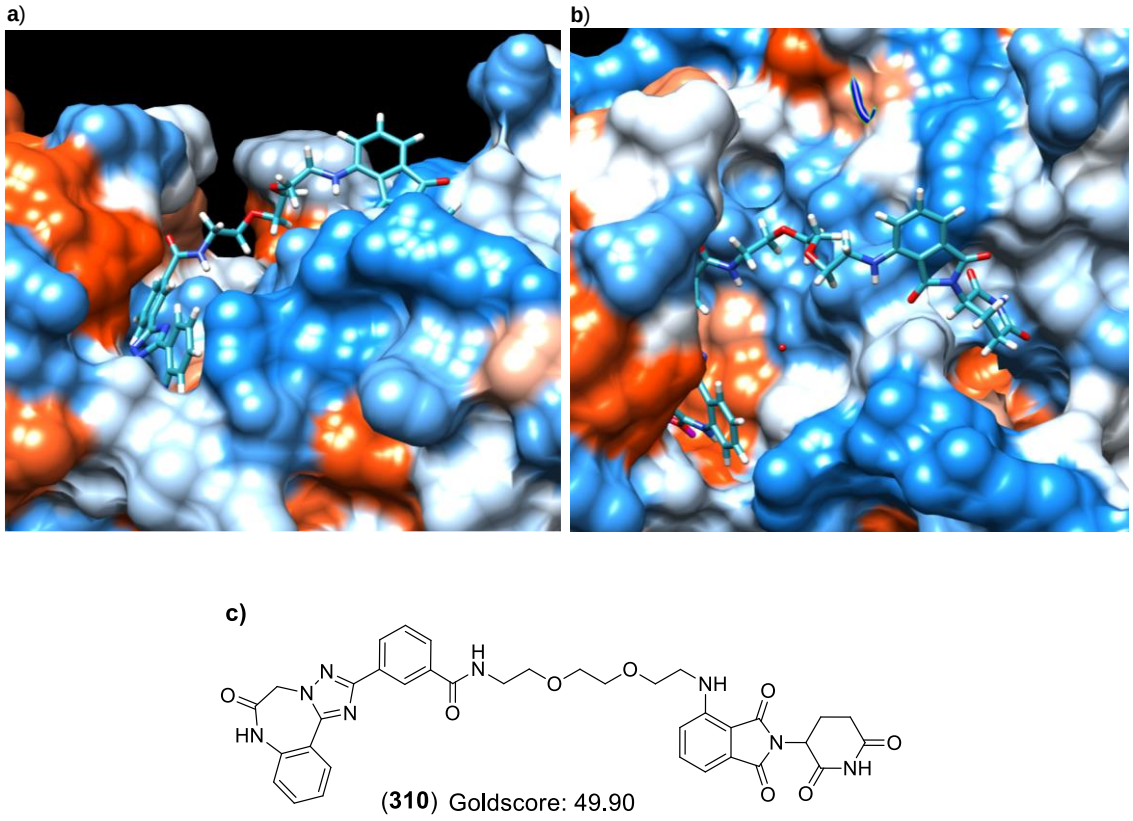

Figure 68. **(a, b)** Molecular dockings at the active site of GSK-3β with the designed PROTAC **310**. **(c)** Structure of the PROTAC **310**. Results obtained using Gold software and PDBs 1Q3L.

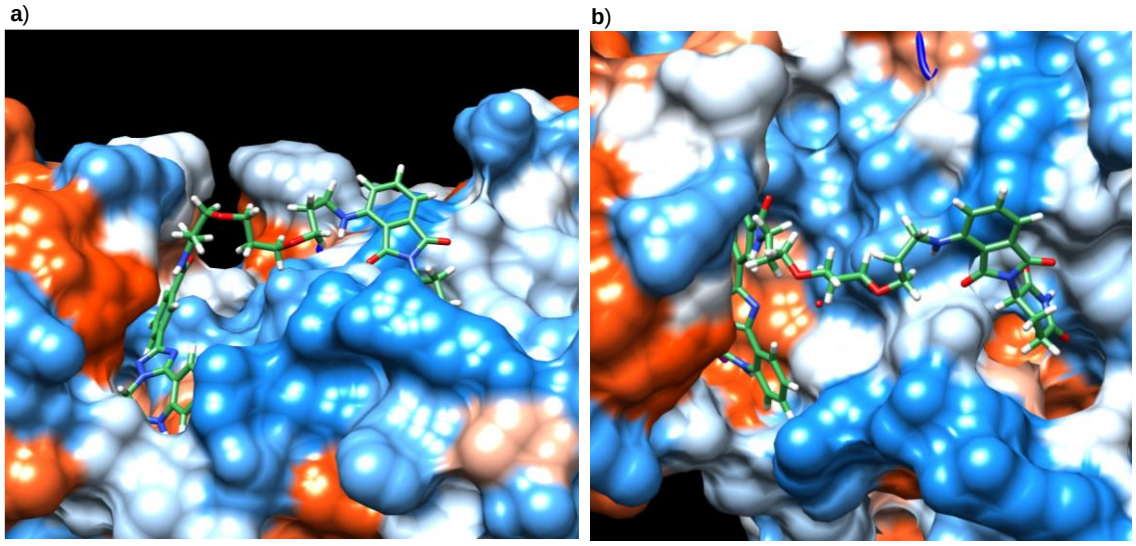

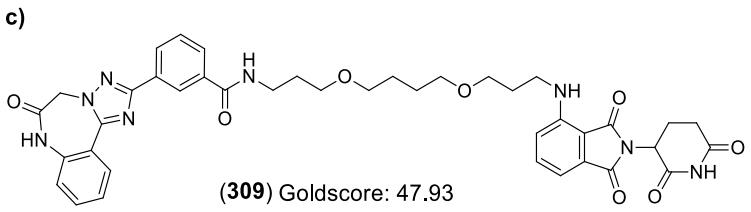

Figure 69. **(a, b)** Molecular dockings at the active site of GSK-3β with the designed PROTAC **309** (green). **(c)** Structure of the PROTAC **309**. Results obtained using Gold software and PDBs 1Q3L.

3.2. Synthetic design of PROTACs (309-314)

From a retrosynthetic perspective, the PROTAC series could be synthesized via amide coupling starting from compound **216i** and the pomalidomide series (**315-320**). This series could be originated from Boc deprotection of **321-326**, which, in turn, might be derived from an aromatic nucleophilic substitution involving 4-fluorothalidomide (**327**) and Boc-protected amines (**328-333**). The protected amine could be obtained through protection of commercially available bis(amines) (**334-338**). Finally, the N-Boc amine **333** could results from the nucleophilic substitution of piperazine and bromomethyl-N-Boc-piperazine (**339**) (Scheme 54).

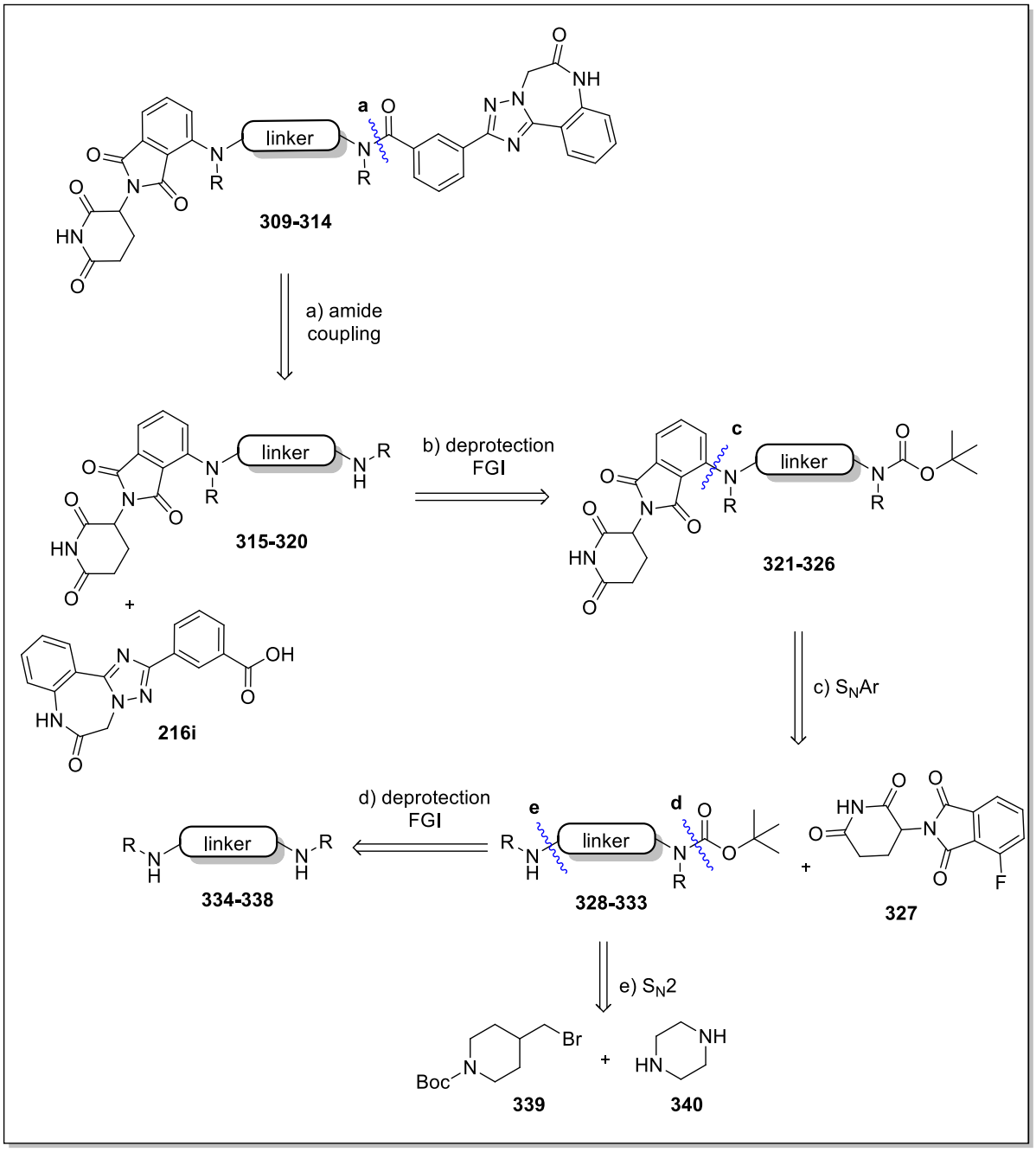

Scheme 54. Retrosynthetic analysis for the synthesis of compounds **309-314**.

3.3 Synthesis of the designed PROTACs (309-314)

The synthesis of the designed PROTACs started with a N-Boc monoprotection of the diamines **334-338**. The protection was carried out with di-*tert*-butyldicarbonate in DCM at r.t. for 3 hours, yielding **328-332** in 68-95% (Scheme 55A). Through nucleophilic substitution (S_N2), the N-Boc-4-(bromomethyl)piperidine (**339**) underwent reaction with a large excess of

piperazine (10 eq.) at reflux for 16 hours resulting in **333** in 88% yield after precipitation and filtration (Scheme 55B).

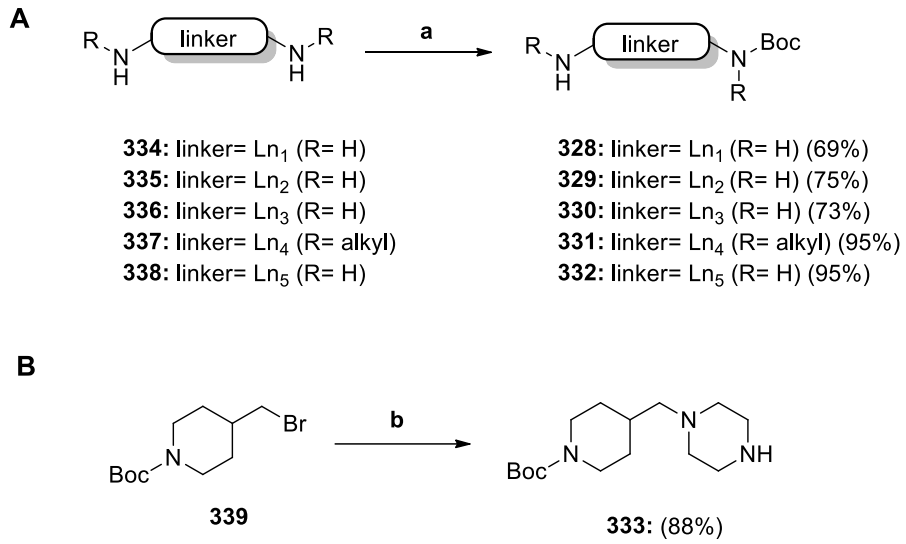

Scheme 55. Synthesis of N-Boc derivatives **328-333**. Reagents and conditions: (a) Boc_2O, DCM, 0-25°C, 3h; (b) Piperazine (10 eq.), MeCN, 80°C, 16h.

The pomalidomide derivatives **321-326** were synthesized through SN_{Ar} reactions involving 4-Fluorothalidomide (**327**) and the previously synthesized amines **328-333**. The reactions followed a standardized protocol utilizing dimethylsulfoxide (DMSO) as the solvent, with diisopropylethylamine (DIPEA) serving as the base at 90°C for 16 hours. Purification procedures by chromatograph column yielded the compounds in the range of 33-92% yield. (Scheme 56). The pomalidomide compounds (**321-326**) were deprotected in trifluoroacetic acid (TFA) at room temperature for 2 hours. They were subsequently used in the next step without an additional purification step. Finally, for the synthesis of the designed series of PROTACs (**309-314**), solutions of the deprotected compounds were prepared with an excess of DIPEA and stirred at room temperature. Then, a solution of compound **216i**, EDC.HCl, HOBt, and DIPEA in DMF was prepared at 0°C, stirred at r.t. for 30 minutes, and after this period, it was added to the previously prepared solutions and kept under stirring overnight. The desired PROTACs **309-314** were obtained in yields ranging from 37-66% after purification by chromatograph column (Scheme 56). ^{1}H NMR signals at 5.04-5.12 ppm, containing 3H from -CH_2 of **216i** and -CH from thalidomide were detected. Additionally, two singlets were observed at 10.8 and 11.1 ppm, corresponding to N-H signals from both thalidomide and **216i**. Currently, the designed PROTACs **309-314** are being evaluated for inhibition and degradation of GSK-3β in

collaboration with Professor Angela de Simone and Professor Andrea Milelli at the University of Bologna.

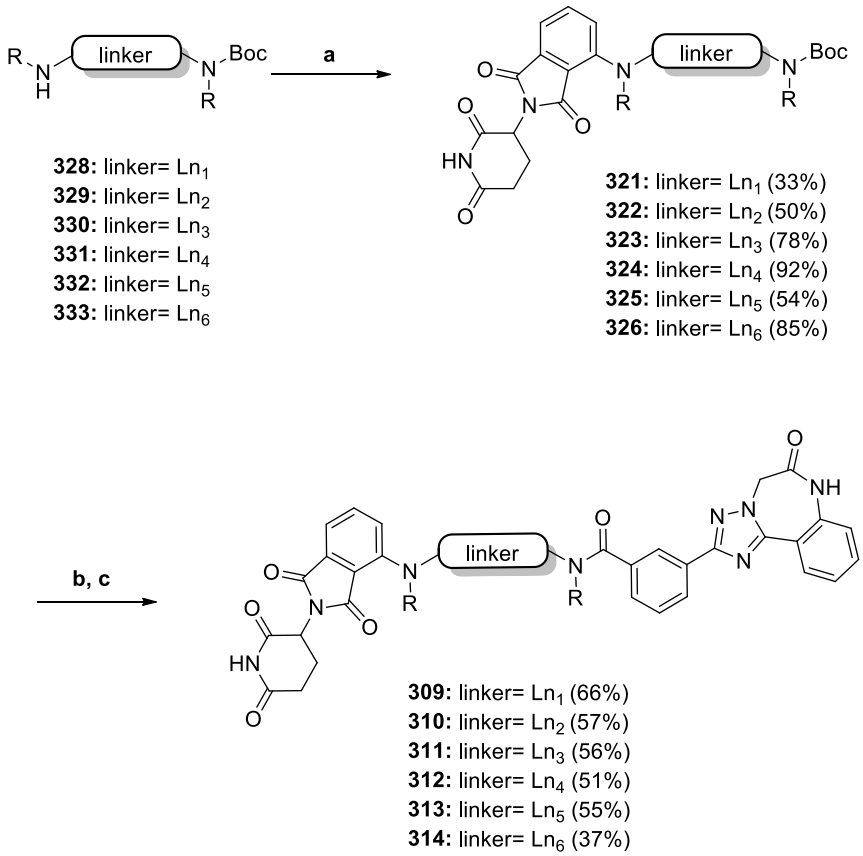

Scheme 56. Synthesis of the designed PROTACs. Reagents and conditions: (a) **328-333** (1.3 eq.), 4-Fluorothalidomide (1 eq.), DIPEA (3 eq.), DMSO, 90°C, 16h; (b) TFA (20 eq.), DCM, RT, 2h; (c) **216i** (1 eq.), EDC.HCl, HOBt, DMF, DIPEA (3-4 eq.), r.t., 12h.

4. CONCLUSION AND PERSPECTIVES

GSK-3β has become one of the most investigated AD targets by both companies and academia, due to its critical roles in cellular homeostasis and in a multitude of neurodegeneration specific signaling pathways. Despite this, up to now, no GSK3β inhibitor has been approved for clinical practice. In recent years, the PROTAC paradigm has emerged as a compelling strategy for modulating challenging or traditionally considered "undruggable" targets. In this work, we were able to design and synthesize a novel series of PROTACs. To achieve this, we utilized a novel GSK-3β inhibitor (**216i**) that we developed in Chapter II of this thesis. This establishes a potentially new structural profile for PROTACs, as all references so far have described PROTACs with the POI ligand containing GSK-3β inhibitors already described in the literature. We linked **216i** to the CRBN ligand pomalidomide, an E3 recruiting element, through linkers of different lengths and shapes. Currently, the designed PROTACs **309-314** are being evaluated for their ability to inhibit and degrade GSK-3β at the University of Bologna.

5. EXPERIMENTAL

5.1. Materials and instruments - BOMEDCHEM

All chemicals were purchased from Aldrich Chemistry (Milan, Italy), Alfa Aesar (Milan, Italy) and FluoroChem (Cambridge, UK) were of the highest purity. Solvents were of analytical grade. Reaction progress was followed by thin layer chromatography on precoated silica gel 60 F254 plates (Merck, Darmstad, Germany). Chromatographic separations were performed on 0.040- to 0.063-mm silica gel 40 columns via the flash method (Merck). The ^{1}H nuclear magnetic resonance (NMR) and ^{13}C NMR spectra were recorded on a Varian Gemini spectrometer (Varian Medical System Italia, Milan, Italy) at 400 and 101 MHz, respectively, in $CDCl_3$ solutions unless otherwise indicated. Chemical shifts (δ) were reported as parts per million relative to tetramethylsilane, used as internal standard; coupling constants (*J*) are reported in Hertz (Hz). Standard abbreviations indicating spin multiplicities are given as follows: s (singlet), d (doublet), dd (double doublet), t (triplet), q (quartet) and m (multiplet). Ultra-HPLC–mass spectrometry analyses were run on a Waters ACQUITY Arc system (Milan, Italy) consisting of a QDa mass spectrometer equipped with an electrospray ionization interface and a 2489 UV/VIS detector. The detected wavelengths were 254 and 365 nm. Analyses were performed on an XBridge BEH C18 column with a 10 × 2.1 mm internal diameter (particle size 2.5 μm) with an XBridge BEH C18 VanGuard Cartridge precolumn with a 5 × 2.1-mm internal diameter (particle size 1.8 μm) (Waters). The mobile phases were H_2O (0.1% formic acid) and MeCN (0.1% formic acid). Electrospray ionization in positive and negative mode was applied in the mass scan range of 50–1200 Da. The authors used a generic method and linear gradient: 0–0.78 min, 20% B; 0.78–2.87 min, 20–95% B; 2.87–3.54 min, 95% B; 3.54–3.65 min, 95–20% B; 3.65–5.73, 20% B. The flow rate was 0.8 ml/min. HRMS spectra were recorded on a Waters Xevo G2-XS quadrupole time-of-flight apparatus operating in electrospray mode. Compounds were named based on the naming algorithm developed by CambridgeSoft and used in ChemBioDraw Ultra (PerkinElmer, Milan, Italy, version 20.0). All tested compounds were found to have >95% purity.

5.2. Materials and instruments – LaDMol-QM

The reactions were monitored using the thin-layer chromatography (TLC) technique, in which Kieselgel 60 aluminum plates (HF-254, Merck) with 0.2 mm thickness were used. Visualization of substances on TLC was performed under ultraviolet lamp (254-365 nm).

Compounds purification was conducted using flash column chromatography technique, Isolera Biotage, model ISO-4SV (IQ-UFRRJ). Silica gel 70-230 mesh (Merck) was used for column packing. As the mobile phase, solvents were selected based on the physicochemical properties of each compound. The ^{1}H NMR spectra were obtained using Bruker Avance-500 and Bruker Avance-400 instruments (IQ-UFRRJ), operating at 500MHz and 400MHz, respectively. Samples were dissolved in CDCl3, DMSO-d6, or acetone-d6, containing tetramethylsilane as an internal reference, and placed in 5 mm diameter tubes. The ^{13}C NMR spectra were obtained operating at 125 MHz and 100MHz, using Bruker Avance-500 and Bruker Avance-400 instruments (IQ-UFRRJ), respectively. Samples were dissolved in CDCl3, DMSO-d6, or acetone-d6, containing TMS as an internal reference. Signal areas were obtained through electronic integration and their multiplicity described as follows: s-singlet / bs-broad singlet / d-doublet / t-triplet / q-quartet / m-multiplet / dd-double doublet.

5.3. Synthetic Methodology

5.3.1. General procedure for the synthesis of 328-332

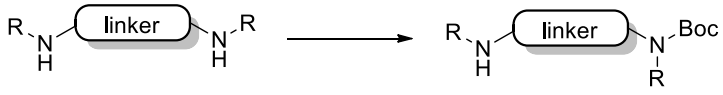

334: linker= Ln_1 (R= H)
335: linker= Ln_2 (R= H)
336: linker= Ln_3 (R= H)
337: linker= Ln_4 (R= alkyl)
338: linker= Ln_5 (R= H)

328: linker= Ln_1 (R= H) (69%)
329: linker= Ln_2 (R= H) (75%)
330: linker= Ln_3 (R= H) (73%)
331: linker= Ln_4 (R= alkyl) (95%)
332: linker= Ln_5 (R= H) (95%)

A 250 mL round bottom flask containing a Teflon stirrer bar was charged with the corresponding bis(amine) **334-338** (3-5 eq.) and DCM (10-35 mL). The mixture was kept under stirring at 0°C using ice bath and then, Boc_2O (1 eq.), solubilized in 25 mL of DCM, was added dropwise to the bis(amine) solution. The reaction mixture remained under stirring for 3-15 h at room temperature. The progress of the reaction was monitored by TLC using DCM/MeOH/NH_4OH (80/20/2) and Bromocresol green as indicator.

5.3.1.1. tert-butyl (3-(4-(3-aminopropoxy)butoxy)propyl)carbamate (328)

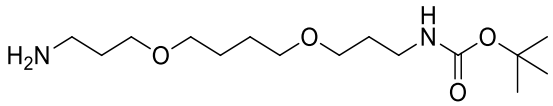

The synthesis followed the general procedure in 3h (RF= 0.4) using compound **334** (3 eq., 0.450 g, 0.47 mL, 2.2 mmol), DCM (10 mL) and Boc_2O (1 eq., 0.160 g, 0.16 mL, 0.73 mmol). Part of the solvent was removed under reduced pressure. The crude was washed with H_2O (5 x 25 mL). The organic layer was dried with Na_2SO_4 and concentrated under reduced pressure. The crude was solubilized with DCM (10 mL) and then, extracted with $KHSO_4$ aqueous solution (pH= 3) (3 x 10 mL). The aqueous layers were collected and then NaOH 10% solution was added util pH= 12-13. The aqueous phase was then extracted with DCM (7 x 50 mL). The organic layers were collected, dried with Na_2SO_4 and concentrated under reduced pressure to give the desire compound (0.154 g, 0.5 mmol, 69%). ^{1}H NMR (400 MHz, $CDCl_3$) δ 1.43 (s, 9H), 1.61-1.63 (m, 4H), 1.68-1.74 (m, 4H), 2.77-2.80 (t, *J* = 6.8 Hz, 2H), 3.21-3.23 (m, 2H), 3.42 (m, 5H), 3.46-3.49 (m, 5H), 4.94 (bs, 1H).

5.3.1.2. tert-butyl (2-(2-(2-aminoethoxy)ethoxy)ethyl)carbamate (329)

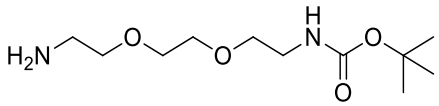

The synthesis followed the general procedure in 7h (RF= 0.33) using compound **335** (5 eq., 2 g, 1.93 mL, 13.5 mmol), DCM (30 mL) and Boc_2O (1 eq., 0.590 g, 0.58 mL, 2.7 mmol). Part of the solvent was removed under reduced pressure. The crude was washed with H_2O (5 x 25 mL). The organic layer was then extracted with $KHSO_4$ aqueous solution (pH= 3) (3 x 10 mL). The aqueous layers were collected and then NaOH 10% solution was added util pH= 12-13. The aqueous phase was then extracted with DCM (7 x 50 mL). The organic layers were collected, dried with Na_2SO_4 and concentrated under reduced pressure to give the desire compound (0.502 g, 2.02 mmol, 75%).

5.3.1.3. tert-butyl (5-aminopentyl)carbamate (330)

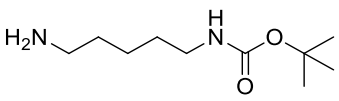

The synthesis followed the general procedure in 4h (RF= 0.42) using compound **336** (5 eq., 2 g, 2.3 mL, 19.6 mmol), DCM (35 mL) and Boc_2O (1 eq., 0.854 g, 0.84 mL, 3.9 mmol). Part of the solvent was removed under reduced pressure. The crude was washed with water (5 x 25 mL). The organic layer was then extracted with $KHSO_4$ aqueous solution (pH= 3) (3 x 10 mL). The aqueous layers were collected and then NaOH 10% solution was added util pH= 12-13. The aqueous phase was then extracted with DCM (7 x 50 mL). The organic layers were collected, dried with Na_2SO_4 and concentrated under reduced pressure to give the desire compound in (0.576 g, 2.84 mmol, 73%). ^{1}H NMR (400 MHz, $CDCl_3$) δ 1.31-1.36 (m, 2H), 1.43-1.53 (m, 17H), 2.68 (t, *J* = 6.9 Hz, 2H), 3.10 (m, 2H), 4.56 (bs, 1H).

5.3.1.4. tert-butyl 4-(3-(piperidin-4-yl)propyl)piperidine-1-carboxylate (331)

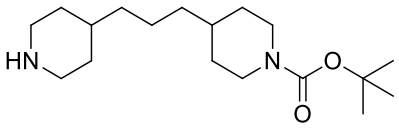

The synthesis followed the general procedure in 3h (RF= 0.68) using compound **337** (5 eq., 2 g, 9.5 mmol), DCM (35 mL) and Boc_2O (1 eq., 0.414 g, 0.4 mL, 1.9 mmol). The reaction mixture was concentrated under reduced pressure and then, purified by chromatography on silica gel using DCM/MeOH/ NH_4OH (79/19/2) to give the desired compound (0.563 g, 1.81 mmol, 95%). ^{1}H NMR (400 MHz, $CDCl_3$) δ 1.05-1.15 (m, 4H), 1.18-1.22 (m, 4H), 1.28-1.34 (m, 4H), 1.45 (s, 9H), 1.62-1.68 (m, 4H), 2.44 (bs, 2H), 2.57-2.61 (t, *J* = 12 Hz, 2H), 3.08-3.1 (d, *J* = 12 Hz, 2H), 4.06 (bs, 1H).

5.3.1.5. tert-butyl (3-(4-(3-aminopropyl)piperazin-1-yl)propyl)carbamate (332)

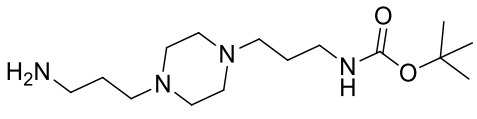

The synthesis followed the general procedure in 15h (RF= 0.13) using compound **338** (5 eq., 2 g, 2 mL, 9.98 mmol), DCM (35 mL) and Boc_2O (1 eq., 0.435 g, 0.43 mL, 2 mmol). The reaction mixture was concentrated under reduced pressure and the crude was purified by

chromatography on silica gel using DCM/MeOH/NH_4OH (79/19/2) to give the desired compound (0.570 g, 1.9 mmol, 95%).

5.3.2. Synthesis of tert-butyl 4-(piperazin-1-ylmethyl)piperidine-1-carboxylate (333)

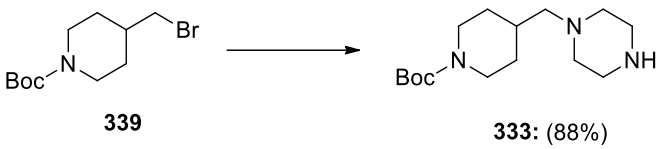

A 50 mL microwave vial containing a Teflon stirrer bar was charged with tert-butyl 4-(bromomethyl)piperidine-1-carboxylate (**339**) (1 eq., 1 g, 3.59 mmol), MeCN (20 mL) and piperazine (10 eq., 3096.37 mg, 35.95 mmol). The reaction mixture remained under stirring at 80°C for 16h. The progress of the reaction was monitored by TLC using DCM/MeOH/NH_4OH (79/19/2) (RF= 0.31). The reaction mixture was concentrated under reduced pressure and the crude was purified by chromatography on silica gel using DCM/MeOH/NH_4OH (79/19/2) to give the product (0.9 g, 3.18 mmol, 88%).

5.3.3. General procedure for the synthesis of 321-326[155]

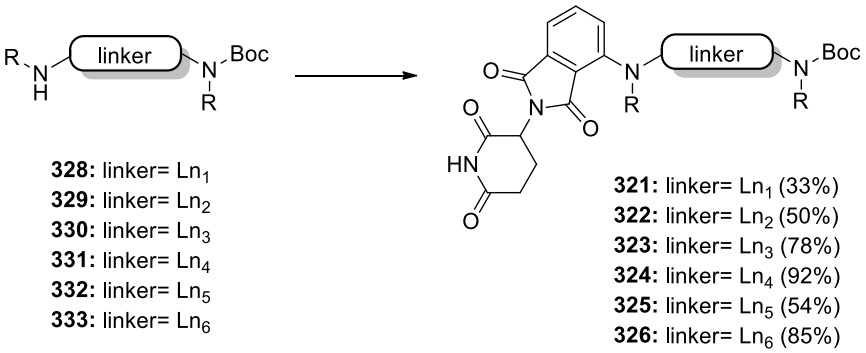

A microwave flask containing a Teflon stirrer bar was charged with 4-Fluorothalidomide (1 eq.), the corresponding amine **328-333** (1.2 - 1.3 eq.), DMSO (1-2 mL) and DIPEA (3 eq). The reaction mixture was capped properly and stirred at 90°C for 16h. The progress of the reaction was monitored by TLC. The reaction mixture was concentrated under reduced pressure and the crude products were purified by chromatography on silica gel.

5.3.3.1. tert-butyl (3-(4-(3-((2-(2,6-dioxopiperidin-3-yl)-1,3-dioxoisoindolin-4-yl)amino)propoxy)butoxy)propyl)carbamate (321)

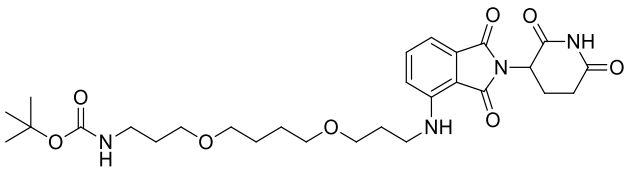

The synthesis followed the general procedure using 4-Fluorothalidomide (1 eq., 0.050 g, 0.18 mmol), compound **328** (1.2 eq., 0.066 g, 0.22 mmol), DMSO (1 mL) and DIPEA (3 eq., 0.070 g, 0.095 mL, 0.54 mmol). The progress of the reaction was monitored by TLC using PE/EtOAc (40/60) (RF= 0.33). The reaction mixture was concentrated under reduced pressure and then, purified by chromatography on silica gel using PE/EtOAc (40/60) to give the desire product (0.033 g, 0.059 mmol, 33%). LC/MS m/z $[M + H]^+$ 561.4

5.3.3.2. tert-butyl (2-(2-(2-((2-(2,6-dioxopiperidin-3-yl)-1,3-dioxoisoindolin-4-yl)amino)ethoxy)ethoxy)ethyl)carbamate (322)

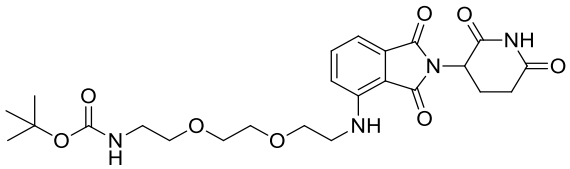

The synthesis followed the general procedure using 4-Fluorothalidomide (1 eq., 0.1 g, 0.36 mmol), compound **329** (1.2 eq., 0.108 g, 0.43 mmol), DMSO (2 mL) and DIPEA (3 eq., 0.14 g, 0.189 mL, 1.09 mmol). The progress of the reaction was monitored by TLC using PE/EtOAc (40/60) (RF= 0.31). The reaction mixture was concentrated under reduced pressure and the crude was purified by chromatography on silica gel using PE/EtOAc (40/60) to give the desire product (0.092 g, 0.18 mmol, 50%). LC/MS m/z $[M + H]^+$ 505.3.

5.3.3.3. tert-butyl (5-((2-(2,6-dioxopiperidin-3-yl)-1,3-dioxoisoindolin-4-yl)amino)pentyl)carbamate (323)

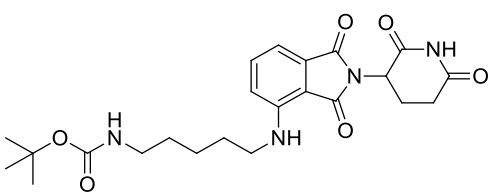

The synthesis followed the general procedure using 4-Fluorothalidomide (1 eq., 0.1 g, 0.36 mmol), compound **330** (1.3 eq., 0.95 g, 0.47 mmol), DMSO (2 mL) and DIPEA (3 eq., 0.14 g, 0.189 mL, 1.09 mmol). The progress of the reaction was monitored by TLC using PE/EtOAc (40/60) (RF= 0.66). The reaction mixture was concentrated under reduced pressure and the crude was purified by chromatography on silica gel using PE/EtOAc (50/50) to give the desire product (0.130 g, 0.28 mmol, 78%). LC/MS m/z $[M + H]^+$ 459.4.

5.3.3.4. tert-butyl 4-(3-(1-(2-(2,6-dioxopiperidin-3-yl)-1,3-dioxoisoindolin-4-yl)piperidin-4-yl)propyl)piperidine-1-carboxylate (324)

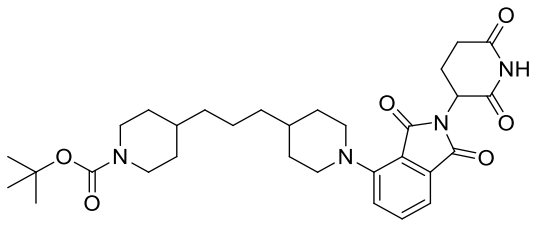

The synthesis followed the general procedure using 4-Fluorothalidomide (1 eq., 0.1 g, 0.36 mmol), compound **331** (1.2 eq., 0.108 g, 0.43 mmol), DMSO (2 mL) and DIPEA (3 eq., 0.14 g, 0.189 mL, 1.09 mmol). The progress of the reaction was monitored by TLC using PE/EtOAc (40/60) (RF= 0.65). The reaction mixture was concentrated under reduced pressure and the crude was purified by chromatography on silica gel using PE/EtOAc (50/50) to give the desire product (0.188 g, 0.33 mmol, 92%). LC/MS m/z $[M + H]^+$ 567.5.

5.3.3.5. tert-butyl (3-(4-(3-((2-(2,6-dioxopiperidin-3-yl)-1,3-dioxoisoindolin-4-yl)amino)propyl)piperazin-1-yl)propyl)carbamate (325)

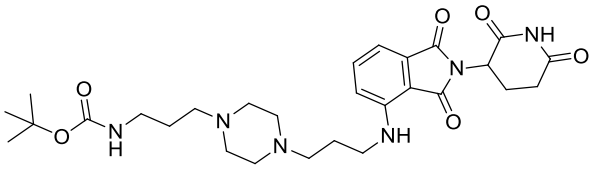

The synthesis followed the general procedure using 4-Fluorothalidomide (1 eq., 0.1 g, 0.36 mmol), compound **332** (1.3 eq., 0.141 g, 0.47 mmol), DMSO (2 mL) and DIPEA (3 eq., 0.14 g, 0.189 mL, 1.09 mmol). The progress of the reaction was monitored by TLC using DCM/MeOH/NH_4OH (89.5/9.5/1) (RF= 0.36). The reaction mixture was concentrated under reduced pressure and the crude was purified by chromatography on silica gel using gradient

elution DCM/MeOH/NH_4OH (97/3/0 to 94.7/4.7/0.5) to give the desire product (0.108 g, 0.19 mmol, 54%). LCMS m/z $[M + H]^+$ 557.5.

5.3.3.6. tert-butyl 4-((1-(2-(2,6-dioxopiperidin-3-yl)-1,3-dioxoisoindolin-4-yl)piperidin-4-yl)methyl)piperazine-1-carboxylate (326)

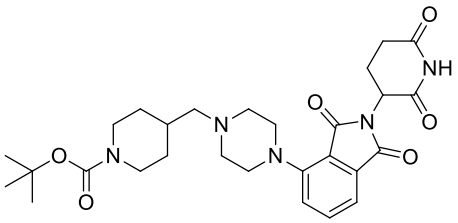

The synthesis followed the general procedure using 4-Fluorothalidomide (1 eq., 0.1 g, 0.36 mmol), compound **333** (1.3 eq., 0.141 g, 0.47 mmol), DMSO (2 mL) and DIPEA (3 eq., 0.14 g, 0.189 mL, 1.09 mmol). The progress of the reaction was monitored by TLC using PE/EtOAc (40/60) (RF= 0.66). The reaction mixture was cooled to r. t. and then MeOH was added. A yellow precipitate formed in solution was filtered off under reduced pressure to give the desire product (0.166 g, 0.3 mmol, 85%). ^{1}H NMR (400 MHz, DMSO) δ 0.95-0.97 (m, 2H), 1.39 (s, 9H), 1.68-1.70 (d, *J* = 11.9 Hz, 3H), 2.01-2.03 (m, 1H), 2.18-2.19 (d, *J* = 6.8 Hz, 2H), 2.53-2.60 (m, 6H), 2.71 (bs, 2H), 2.85-2.89 (m, 1H), 3.29 (bs, 4H), 3.92 (bs, 2H), 5.07-5.10 (dd, *J* = 5.5 Hz, *J* = 12.9 Hz, 1H), 7.32-7.34 (d, *J* = 8.4 Hz, 1H), 7.35-7.36 (d, *J* = 7.1 Hz, 1H), 7.69-7.71 (t, *J* = 7.6 Hz, 1H), 11.08 (bs, 1H). ^{13}C NMR (125 MHz, DMSO) δ 22.5, 28.6, 31.4, 33, 49.3, 51, 53.5, 64.2, 78.9, 115.3, 117, 124.2, 134.1, 136.3, 150.2, 154.4, 166.8, 167.5, 170.5, 173.3. LC/MS m/z $[M + H]^+$ 540.4.

5.3.4. General procedure for the synthesis of 309-314.[154]

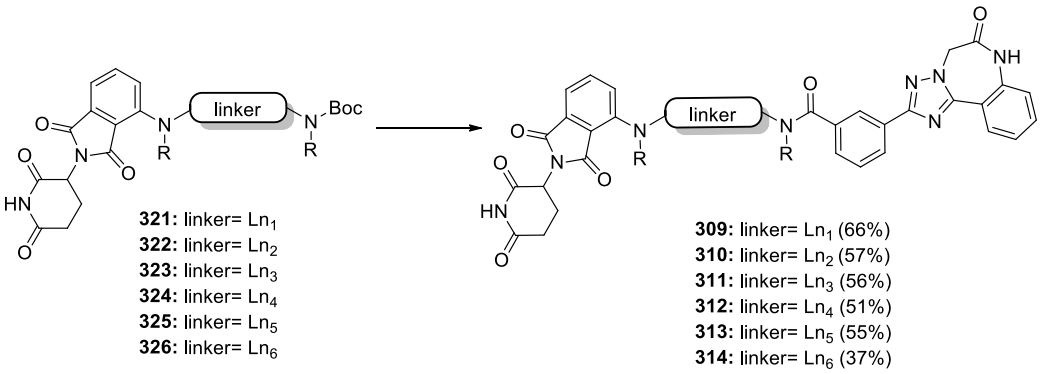

1. A 50 mL sealed tube containing a Teflon stirrer bar was charged with the corresponding pomalidomide derivative (**321-326**) (1 eq.) and DCM, followed by the addition of TFA (280 eq.) The reaction mixture remained under stirring at r.t. for 8h. The reaction mixture was concentrated under reduced pressure and then resolubilized with Hex (this process was repeated three times), to give the deprotected products (**315-320**). The crude products were used in the next step without further purification.

2. A microwave flask containing a Teflon stirrer bar was charged with compound **216i** (1 eq.), EDC.HCl (2 eq.), HOBt (1 eq.), DMF, followed by the addition of DIPEA (3 eq.). The vessel was then capped properly, evacuated and backfilled with argon for 1 minute and then the reaction mixture was cooled to 0°C using water bath. The reaction mixture was kept under stirring for 30 min. A solution of the corresponding deprotected pomalidomide derivative (**315-320**) in DMF (1 mL) and DIPEA (2-4 eq.) was added to the reaction mixture. The reaction mixture remained under stirring at r.t. overnight. The reaction mixture was concentrated under reduced pressure and the crude was purified by chromatography on silica gel to give the desire products **309-314**.

5.3.4.1. N-(3-(4-(3-((2-(2,6-dioxopiperidin-3-yl)-1,3-dioxoisoindolin-4-yl)amino)propoxy)butoxy)propyl)-3-(6-oxo-6,7-dihydro-5H-benzo[f][1,2,4]triazolo[1,5-d][1,4]diazepin-2-yl)benzamide (309)

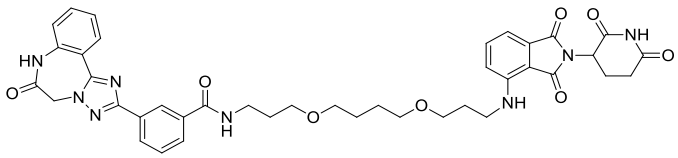

The synthesis followed the general procedure using compound **216**i (1 eq., 0.010 g, 0.031 mmol), EDC.HCl (2 eq., 0.012 g, 0.062 mmol), HOBt (1 eq., 0.004 g, 0.031 mmol), DMF (1 mL), DIPEA (3 eq., 0.012 g, 0.016 mL,0.094 mmol) and a solution of compound **315** (1 eq., 0.018 g, 0.031 mmol) in DMF (1 mL) and DIPEA (2 eq., 0.008 g, 0.011 mL, 0.062 mmol). The progress of the reaction was monitored by TLC using EtOAc (RF= 0.52). The reaction mixture was concentrated under reduced pressure and the crude was purified by flash chromatography on silica gel using gradient elution Hex/EtOAc (25/75 to 0/100) to give the desired product as yellow solid (0.016 g, 0.020 mmol, 66%). ^{1}H NMR (400 MHz, DMSO) δ 0.85-0.86 (d, *J* = 6.3 Hz, 1H), 1.24 (bs, 1H), 1.56 (s, 4H), 1.79 (s, 4H), 2.02 (bs, 1H), 2.56-2.64 (m, 2H), 2.86-2.94

(m, 1H), 3.4 (m, 10H), 5.04 (bs, 3H), 6.67 (bs, 1H), 7.01-7.02 (d, *J* = 6 Hz, 1H), 7.07-7.09 (d, *J* = 8.4 Hz, 1H), 7.32-7.34 (d, *J* = 7.4 Hz, 1H), 7.40 (bs, 1H), 7.57-7.63 (m, 3H), 7.91-7.92 (d, *J* = 6.9 Hz, 1H), 8.03-8.04 (d, *J* = 5.3 Hz, 1H), 8.19-8.20 (d, *J* = 6 Hz, 1H), 8.54 (bs, 1H), 8.65 (bs, 1H), 10.86 (s, 1H), 11.12 (s, 1H). ^{13}C NMR (125 MHz, DMSO) δ 22.6, 26.5, 26.6, 29.3, 29.8, 31.4, 37.3, 49, 53.3, 68.3, 68.4, 70.4, 70.5, 110.8, 117.5, 122.6, 125.2, 128.5, 128.8, 129.4, 129.7, 132.3, 132.7, 136.7, 146.9, 161.1, 167.4, 173.3. LC/MS m/z [M - 2H]$^-$ 760.

5.3.4.2. N-(2-(2-(2-((2-(2,6-dioxopiperidin-3-yl)-1,3-dioxoisoindolin-4-yl)amino)ethoxy)ethoxy)ethyl)-3-(6-oxo-6,7-dihydro-5H-benzo[f][1,2,4]triazolo[1,5-d][1,4]diazepin-2-yl)benzamide (310)

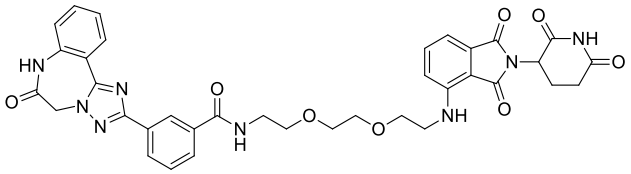

The synthesis followed the general procedure using compound **216**i (1 eq., 0.030 g, 0.094 mmol), EDC.HCl (2 eq., 0.036 g, 0.019 mmol), HOBt (1 eq., 0.013 g, 0.094 mmol), DMF (1 mL), DIPEA (3 eq., 0.036 g, 0.049 mL,0.028 mmol) and a solution of compound **316** (1 eq., 0.048 g, 0.094 mmol) in DMF (1 mL) and DIPEA (2 eq., 0.024 g, 0.033 mL, 0.19 mmol). The progress of the reaction was monitored by TLC using EtOAc (RF= 0.28). The reaction mixture was concentrated under reduced pressure and the crude was purified by flash chromatography on silica gel using EtOAc to give the desired product as yellow solid (0.038 g, 0.054 mmol, 57%). ^{1}H NMR (400 MHz, DMSO) δ 1.99-2.03 (m, 1H), 2.51-2.59 (m, 4H), 2.83-2.89 (m, 1H), 3.59-3.62 (m, 10H), 5.03 (s, 2H), 5.03-5.07 (m, 1H), 6.58-6.60 (t, *J* = 5.1 Hz, 1H), 7.01-7.02 (d, *J* = 7 Hz, 1H), 7.08-7.09 (d, *J* = 8.6 Hz, 1H), 7.32-7.34 (d, *J* = 8.2 Hz, 1H), 7.34-7.42 (t, *J* = 7.5 Hz, 1H), 7.52-7.64 (m, 3H), 7.91-7.93 (d, *J* = 7.8 Hz, 1H), 8.02-8.03 (d, *J* = 7.7 Hz, 1H), 8.18-8.20 (d, *J* = 7.7 Hz, 1H), 8.55 (s, 1H), 8.70-8.73 (t, *J* = 5.3 Hz, 1H), 10.86 (s, 1H), 11.12 (s, 1H). ^{13}C NMR (125 MHz, DMSO) δ 22.6, 31.4, 42.1, 49, 53.3, 69.3, 70.1, 111.1, 122.6, 125.2, 128.6, 128.9, 129.4, 129.7, 132.4, 136.7. LC/MS m/z [M - 2H]$^-$ 704.

5.3.4.3. N-(5-((2-(2,6-dioxopiperidin-3-yl)-1,3-dioxoisoindolin-4-yl)amino)pentyl)-3-(6-oxo-6,7-dihydro-5H-benzo[f][1,2,4]triazolo[1,5-d][1,4]diazepin-2-yl)benzamide (311)

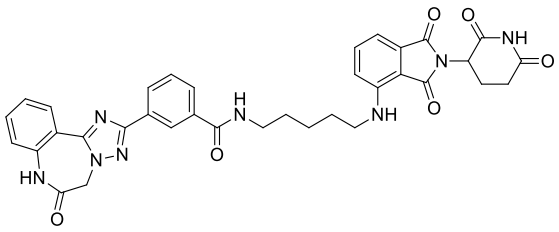

The synthesis followed the general procedure using compound **216**i (1 eq., 0.030 g, 0.094 mmol), EDC.HCl (2 eq., 0.036 g, 0.019 mmol), HOBt (1 eq., 0.013 g, 0.094 mmol), DMF (1 mL), DIPEA (3 eq., 0.036 g, 0.049 mL,0.028 mmol) and a solution of compound **317** (1 eq., 0.044 g, 0.094 mmol) in DMF (1 mL) and DIPEA (2 eq., 0.024 g, 0.033 mL, 0.19 mmol). The progress of the reaction was monitored by TLC using EtOAc (RF= 0.49). The reaction mixture was concentrated under reduced pressure and the crude was purified by flash chromatography on silica gel using gradient elution Hex/EtOAc (25/75 to 0/100) to give the desired product as yellow solid (0.035 g, 0.052 mmol, 56%). ^{1}H NMR (400 MHz, DMSO) δ 1.23 (bs, 1H), 1.42 (bs, 2H), 1.62 (bs, 4H), 2.02 (bs, 1H), 2.60 (m, 1H), 2.89 (m, 1H), 3.32 (m, 4H), 5.04 (s, 3H), 6.56 (bs, 1H), 7.01 (bs, 1H), 7.11-7.12 (d, *J* = 6.9 Hz, 1H), 7.32-7.34 (d, *J* = 5.9 Hz, 1H), 7.40 (s, 1H), 7.58-7.63 (m, 3H), 7.91 (bs, 1H), 8.04 (bs, 1H), 8.19 (bs, 1H), 8.54 (bs, 1H), 8.68 (bs, 1H), 10.86 (s, 1H), 11.12 (s, 1H). ^{13}C NMR (125 MHz, DMSO) δ 22.6, 24.3, 28.9, 29.3, 31.4, 42.3, 49, 53.3, 110.9, 117.7, 122.6, 128.6, 128.8, 129.4, 129.7, 132.4, 136.8. LC/MS m/z [M - 2H]$^{-}$ 658.

5.3.4.4. 2-(2,6-dioxopiperidin-3-yl)-4-(4-(3-(1-(3-(6-oxo-6,7-dihydro-5H-benzo[f][1,2,4]triazolo[1,5-d][1,4]diazepin-2-yl)benzoyl)piperidin-4-yl)propyl)piperidin-1-yl)isoindoline-1,3-dione (312)

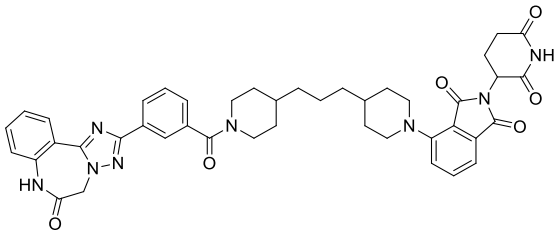

The synthesis followed the general procedure using compound **216**i (1 eq., 0.030 g, 0.094 mmol), EDC.HCl (2 eq., 0.036 g, 0.019 mmol), HOBt (1 eq., 0.013 g, 0.094 mmol), DMF (1 mL), DIPEA (3 eq., 0.036 g, 0.049 mL,0.028 mmol) and a solution of compound **318** (1 eq., 0.054 g, 0.094 mmol) in DMF (1 mL) and DIPEA (2 eq., 0.024 g, 0.033 mL, 0.19 mmol). The

progress of the reaction was monitored by TLC using EtOAc (RF= 0.59). The reaction mixture was concentrated under reduced pressure and the crude was purified by flash chromatography on silica gel using gradient elution Hex/EtOAc (50/50 to 30/70) to give the desired product as a yellow solid (0.037 g, 0.048 mmol, 51%). ^{1}H NMR (400 MHz, DMSO) δ 0.85-0.86 (d, *J* = 6.5 Hz, 1H), 1.06-1.42 (m, 14H), 1.52 (bs, 1H), 1.63 (bs, 1H), 1.74-1.77 (d, *J* = 11 Hz, 3H), 2.0-2.03 (m, 1H), 2.61 (m, 1H), 2.73-2.89 (m, 4H), 3.60 (bs, 1H), 3.66-3.68 (d, *J* = 10.6 Hz, 2H), 4.37-4.5 (m, 1H), 5.03 (s, 2H), 5.07-5.10 (dd, *J* = 5.3 Hz, *J* = 12.5 Hz, 1H), 7.32-7.33 (d, *J* = 6.8 Hz, 3H), 7.39-7.42 (t, *J* = 7.6 Hz, 1H), 7.45-7.46 (d, *J* = 7.4 Hz, 1H), 7.57-7.68 (m, 3H), 8.02 (s, 2H), 8.12-8.13 (d, *J* = 7.6 Hz, 1H), 10.86 (s, 1H), 11.11 (s, 1H). ^{13}C NMR (125 MHz, DMSO) δ 22.5, 23.5, 31.4, 32.4, 35.1, 35.8, 36.5, 36.6, 49.2, 51.7, 53.3, 112, 114.8, 116.7, 117.9, 122.6, 124.4, 124.5, 125.3, 127, 128, 129.6, 129.7, 131, 132.3, 132.6, 134.1, 136.2, 136.4, 137.6, 150.7, 153.3, 157.9, 161, 167.4, 167.6, 168.9, 170.5, 173.3. LC/MS m/z $[M - 2H]^-$ 766.

5.3.4.5. N-(3-(4-(3-((2-(2,6-dioxopiperidin-3-yl)-1,3-dioxoisoindolin-4-yl)amino)propyl)piperazin-1-yl)propyl)-3-(6-oxo-6,7-dihydro-5H-benzo[f][1,2,4]triazolo[1,5-d][1,4]diazepin-2-yl)benzamide (313)

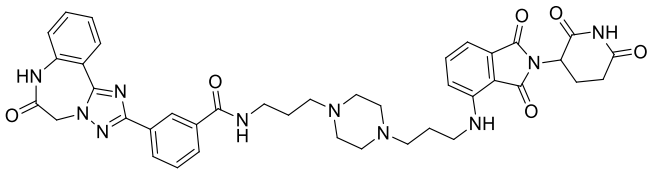

The synthesis followed the general procedure using compound **216**i (1 eq., 0.030 g, 0.094 mmol), EDC.HCl (2 eq., 0.036 g, 0.019 mmol), HOBt (1 eq., 0.013 g, 0.094 mmol), DMF (1 mL), DIPEA (3 eq., 0.036 g, 0.049 mL,0.028 mmol) and a solution of compound **319** (1 eq., 0.075 g, 0.094 mmol) in DMF (1 mL) and DIPEA (6 eq., 0.073 g, 0.098 mL, 0.56 mmol). The progress of the reaction was monitored by TLC using EtOAc/MeOH/Et_3N (8.95/0.95/0.1) (RF= 0.2). The reaction mixture was concentrated under reduced pressure and the crude was purified by flash chromatography on silica gel using gradient elution EtOAc/MeOH/Et_3N (90/10/0 to 79/19/2) to give the desired product as a yellow solid (0.039 g, 0.052 mmol, 55%). ^{1}H NMR (400 MHz, DMSO) δ 1.26-1.27 (d, *J* = 6.6 Hz, 6H), 1.29-1.30 (d, *J* = 6.6 Hz, 6H), 3.07 (bs, 4H), 3.12 (bs, 4H), 3.60 (bs, 4H), 5.04 (s, 3H), 7.0-7.05 (m, 1H), 7.14-7.48 (m, 3H), 7.60-7.63 (m, 3H), 7.96-7.97 (d, *J* = 6.9 Hz 1H), 8.03-8.04 (d, *J* = 7.5 Hz, 1H), 8.21-8.23 (d, *J* = 7.7 Hz,

1H), 8.56 (s, 1H), 8.85 (bs, 1H), 9.11 (bs, 1H), 10.88 (s, 1H), 11.14 (s, 1H). ^{13}C NMR (125 MHz, DMSO) δ 17.2, 18.4, 42, 45.9, 53.8, 122.7, 125.3. LC/MS m/z [M - 2H]$^{-}$ 756

5.3.4.6. 2-(2,6-dioxopiperidin-3-yl)-4-(4-((1-(3-(6-oxo-6,7-dihydro-5H-benzo[f][1,2,4]triazolo[1,5-d][1,4]diazepin-2-yl)benzoyl)piperidin-4-yl)methyl)piperazin-1-yl)isoindoline-1,3-dione (314)

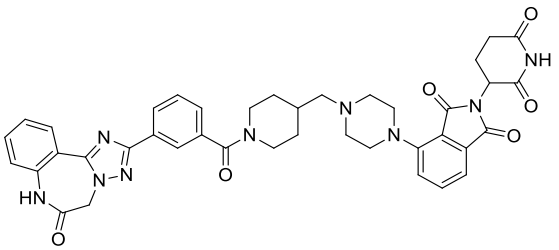

The synthesis followed the general procedure using compound **216**i (1 eq., 0.030 g, 0.094 mmol), EDC.HCl (2 eq., 0.036 g, 0.019 mmol), HOBt (1 eq., 0.013 g, 0.094 mmol), DMF (1 mL), DIPEA (3 eq., 0.036 g, 0.049 mL,0.028 mmol) and a solution of compound **320** (1 eq., 0.062 g, 0.094 mmol) in DMF (1 mL) and DIPEA (4 eq., 0.048 g, 0.065 mL, 0.37 mmol). The progress of the reaction was monitored by TLC using EtOAc (RF= 0.42). The reaction mixture was concentrated under reduced pressure and the crude was purified by flash chromatography on silica gel using gradient elution DCM/MeOH (99/1 to 90/10). The product precipitate during the purification and then, the crude was concentrated and recrystallized with EtOH. The precipitate was filtered off under reduced pressure to give the desired product as yellow solid in (0.026 g, 0.035 mmol, 37%). ^{1}H NMR (400 MHz, DMSO) δ 1.10 (bs, 2H), 1.69 (bs, 1H), 1.87 (bs, 2H), 2.02 (bs, 1H), 2.24 (s, 2H), 2.54-2.61 (m, 4H), 2.84-2.88 (m, 2H), 3.09 (bs, 1H), 3.29 (s, 6H), 3.61 (bs, 1H), 4.50 (bs, 1H), 5.03 (s, 2H), 5.08-5.12 (dd, *J* = 4.5 Hz, *J* = 7.4 Hz, *J* = 12.3 Hz, 1H), 7.32-7.42 (m, 4H), 7.46-7.47 (d, *J* = 7 Hz, 1H), 7.57-7.64 (m, 2H), 7.69-7.71 (t, *J* = 7.2 Hz, 1H), 8.03 (s, 2H), 8.12-8.13 (d, *J* = 7.4 Hz, 1H), 10.86 (s, 1H), 11.12 (s, 1H). ^{13}C NMR (125 MHz, DMSO) δ 22.5, 31.4, 32.2, 49.2, 51, 53.3, 53.5, 64, 115.3, 117, 117.9, 122.6, 124.2, 124.5, 125.2, 127, 128, 129.6, 129.7, 131, 132.4, 134.1, 136.4, 137.6, 150.2, 153.3, 161, 165.7, 166.8, 167.4, 167.5, 168.9, 170.5, 173.3. LC/MS m/z [M - 2H]$^{-}$ 739.

5.4. *In silico* enzymatic interaction study of PROTACs

The Spartan 14 program (Wavefunction Inc.) was used for the construction and optimization of three-dimensional models of the chemical structures of the inhibitors. For this purpose, the semi-empirical Parameterization Method 6 (PM6) calculation method was utilized.[156]

The GOLD 5.6 program (CCDC Software Ltd., Cambridge UK) was used to evaluate the *in silico* interactions between the compounds (**309-310**) and the active sites of the enzyme GSK-3β. Initially, molecular docking studies were performed with GSK-3β, using the available GSK-3β structures from the Protein Data Bank (PDB), with code 1Q3L. Hydrogen atoms were added to the protein crystallographic structures based on ionization and tautomeric states defined by GOLD. The binding site radius of the enzymes was tested at 15 °A and 20 °A around amino acid residue atoms, present in the CAS and using the GoldScore function.

The docking study for each evaluated compound generated several binding positions, which were qualitatively analyzed according to their interaction position with amino acid residues.

6. BIBLIOGRAPHY

(1) Békés, M.; Langley, D. R.; Crews, C. M. PROTAC Targeted Protein Degraders: The Past Is Prologue. *Nat Rev Drug Discov* **2022**, *21* (3), 181–200. https://doi.org/10.1038/s41573-021-00371-6.

(2) Luh, L. M.; Scheib, U.; Juenemann, K.; Wortmann, L.; Brands, M.; Cromm, P. M. Prey for the Proteasome: Targeted Protein Degradation—A Medicinal Chemist's Perspective. *Angewandte Chemie International Edition* **2020**, *59* (36), 15448–15466. https://doi.org/10.1002/anie.202004310.

(3) Dale, B.; Cheng, M.; Park, K.-S.; Kaniskan, H. Ü.; Xiong, Y.; Jin, J. Advancing Targeted Protein Degradation for Cancer Therapy. *Nat Rev Cancer* **2021**, *21* (10), 638–654. https://doi.org/10.1038/s41568-021-00365-x.

(4) Valeur, E.; Guéret, S. M.; Adihou, H.; Gopalakrishnan, R.; Lemurell, M.; Waldmann, H.; Grossmann, T. N.; Plowright, A. T. New Modalities for Challenging Targets in Drug Discovery. *Angewandte Chemie International Edition* **2017**, *56* (35), 10294–10323. https://doi.org/10.1002/anie.201611914.

(5) Samarasinghe, K. T. G.; Crews, C. M. Targeted Protein Degradation: A Promise for Undruggable Proteins. *Cell Chemical Biology* **2021**, *28* (7), 934–951. https://doi.org/10.1016/j.chembiol.2021.04.011.

(6) Hopkins, A. L.; Groom, C. R. The Druggable Genome. *Nat Rev Drug Discov* **2002**, *1* (9), 727–730. https://doi.org/10.1038/nrd892.

(7) Pettersson, M.; Crews, C. M. PROteolysis TArgeting Chimeras (PROTACs) — Past, Present and Future. *Drug Discovery Today: Technologies* **2019**, *31*, 15–27. https://doi.org/10.1016/j.ddtec.2019.01.002.

(8) Dang, C. V.; Reddy, E. P.; Shokat, K. M.; Soucek, L. Drugging the "undruggable" Cancer Targets. *Nat Rev Cancer* **2017**, *17* (8), 502–508. https://doi.org/10.1038/nrc.2017.36.

(9) Xie, X.; Yu, T.; Li, X.; Zhang, N.; Foster, L. J.; Peng, C.; Huang, W.; He, G. Recent Advances in Targeting the "Undruggable" Proteins: From Drug Discovery to Clinical Trials. *Sig Transduct Target Ther* **2023**, *8* (1), 1–71. https://doi.org/10.1038/s41392-023-01589-z.

(10) Pedreira, J. G. B.; Franco, L. S.; Barreiro, E. J. Chemical Intuition in Drug Design and Discovery. *Curr Top Med Chem* **2019**, *19* (19), 1679–1693. https://doi.org/10.2174/1568026619666190620144142.

(11) Bolognesi, M. L. Harnessing Polypharmacology with Medicinal Chemistry. *ACS Med. Chem. Lett.* **2019**, *10* (3), 273–275. https://doi.org/10.1021/acsmedchemlett.9b00039.

(12) Paiva, S.-L.; Crews, C. M. Targeted Protein Degradation: Elements of PROTAC Design. *Curr Opin Chem Biol* **2019**, *50*, 111–119. https://doi.org/10.1016/j.cbpa.2019.02.022.

(13) Zhao, L.; Zhao, J.; Zhong, K.; Tong, A.; Jia, D. Targeted Protein Degradation: Mechanisms, Strategies and Application. *Sig Transduct Target Ther* **2022**, *7* (1), 1–13. https://doi.org/10.1038/s41392-022-00966-4.

(14) Sakamoto, K. M.; Kim, K. B.; Kumagai, A.; Mercurio, F.; Crews, C. M.; Deshaies, R. J. Protacs: Chimeric Molecules That Target Proteins to the Skp1–Cullin–F Box Complex for Ubiquitination and Degradation. *Proceedings of the National Academy of Sciences* **2001**, *98* (15), 8554–8559. https://doi.org/10.1073/pnas.141230798.

(15) Anfinsen, C. B. Principles That Govern the Folding of Protein Chains. *Science* **1973**, *181* (4096), 223–230. https://doi.org/10.1126/science.181.4096.223.

(16) Hanley, S. E.; Cooper, K. F. Sorting Nexins in Protein Homeostasis. *Cells* **2021**, *10* (1), 17. https://doi.org/10.3390/cells10010017.

(17) Dikic, I. Proteasomal and Autophagic Degradation Systems. *Annual Review of Biochemistry* **2017**, *86* (1), 193–224. https://doi.org/10.1146/annurev-biochem-061516-044908.

(18) Pohl, C.; Dikic, I. Cellular Quality Control by the Ubiquitin-Proteasome System and Autophagy. *Science* **2019**, *366* (6467), 818–822. https://doi.org/10.1126/science.aax3769.

(19) Ciechanover, A.; Orian, A.; Schwartz, A. L. Ubiquitin-Mediated Proteolysis: Biological Regulation via Destruction. *Bioessays* **2000**, *22* (5), 442–451. https://doi.org/10.1002/(SICI)1521-1878(200005)22:5<442::AID-BIES6>3.0.CO;2-Q.

(20) Tracz, M.; Bialek, W. Beyond K48 and K63: Non-Canonical Protein Ubiquitination. *Cellular & Molecular Biology Letters* **2021**, *26* (1), 1. https://doi.org/10.1186/s11658-020-00245-6.

(21) Jeong, Y.; Oh, A.-R.; Jung, Y. H.; Gi, H.; Kim, Y. U.; Kim, K. Targeting E3 Ubiquitin Ligases and Their Adaptors as a Therapeutic Strategy for Metabolic Diseases. *Exp Mol Med* **2023**, *55* (10), 2097–2104. https://doi.org/10.1038/s12276-023-01087-w.

(22) Zheng, N.; Shabek, N. Ubiquitin Ligases: Structure, Function, and Regulation. *Annual Review of Biochemistry* **2017**, *86* (1), 129–157. https://doi.org/10.1146/annurev-biochem-060815-014922.

(23) Verma, R.; Mohl, D.; Deshaies, R. J. Harnessing the Power of Proteolysis for Targeted Protein Inactivation. *Mol Cell* **2020**, *77* (3), 446–460. https://doi.org/10.1016/j.molcel.2020.01.010.

(24) Lou, Z.; Wang, S. E3 Ubiquitin Ligases and Human Papillomavirus-Induced Carcinogenesis. *J Int Med Res* **2014**, *42* (2), 247–260. https://doi.org/10.1177/0300060513506655.

(25) Fuller, J. C.; Burgoyne, N. J.; Jackson, R. M. Predicting Druggable Binding Sites at the Protein–Protein Interface. *Drug Discovery Today* **2009**, *14* (3), 155–161. https://doi.org/10.1016/j.drudis.2008.10.009.

(26) Adjei, A. A. What Is the Right Dose? The Elusive Optimal Biologic Dose in Phase I Clinical Trials. *JCO* **2006**, *24* (25), 4054–4055. https://doi.org/10.1200/JCO.2006.07.4658.

(27) Holohan, C.; Van Schaeybroeck, S.; Longley, D. B.; Johnston, P. G. Cancer Drug Resistance: An Evolving Paradigm. *Nat Rev Cancer* **2013**, *13* (10), 714–726. https://doi.org/10.1038/nrc3599.

(28) Blair, J. M. A.; Webber, M. A.; Baylay, A. J.; Ogbolu, D. O.; Piddock, L. J. V. Molecular Mechanisms of Antibiotic Resistance. *Nat Rev Microbiol* **2015**, *13* (1), 42–51. https://doi.org/10.1038/nrmicro3380.

(29) Toure, M.; Crews, C. M. Small-Molecule PROTACS: New Approaches to Protein Degradation. *Angewandte Chemie International Edition* **2016**, *55* (6), 1966–1973. https://doi.org/10.1002/anie.201507978.

(30) Hershko, A. The Ubiquitin System for Protein Degradation and Some of Its Roles in the Control of the Cell-Division Cycle (Nobel Lecture). *Angewandte Chemie International Edition* **2005**, *44* (37), 5932–5943. https://doi.org/10.1002/anie.200501724.

(31) Bondeson, D. P.; Mares, A.; Smith, I. E. D.; Ko, E.; Campos, S.; Miah, A. H.; Mulholland, K. E.; Routly, N.; Buckley, D. L.; Gustafson, J. L.; Zinn, N.; Grandi, P.; Shimamura, S.; Bergamini, G.; Faelth-Savitski, M.; Bantscheff, M.; Cox, C.; Gordon, D. A.; Willard, R. R.; Flanagan, J. J.; Casillas, L. N.; Votta, B. J.; den Besten, W.; Famm, K.; Kruidenier, L.; Carter, P. S.; Harling, J. D.; Churcher, I.; Crews, C. M. Catalytic in Vivo Protein

Knockdown by Small-Molecule PROTACs. *Nat Chem Biol* **2015**, *11* (8), 611–617. https://doi.org/10.1038/nchembio.1858.

(32) Burslem, G. M.; Smith, B. E.; Lai, A. C.; Jaime-Figueroa, S.; McQuaid, D. C.; Bondeson, D. P.; Toure, M.; Dong, H.; Qian, Y.; Wang, J.; Crew, A. P.; Hines, J.; Crews, C. M. The Advantages of Targeted Protein Degradation Over Inhibition: An RTK Case Study. *Cell Chemical Biology* **2018**, *25* (1), 67-77.e3. https://doi.org/10.1016/j.chembiol.2017.09.009.

(33) Yang, Y.; Gao, H.; Sun, X.; Sun, Y.; Qiu, Y.; Weng, Q.; Rao, Y. Global PROTAC Toolbox for Degrading BCR–ABL Overcomes Drug-Resistant Mutants and Adverse Effects. *J. Med. Chem.* **2020**, *63* (15), 8567–8583. https://doi.org/10.1021/acs.jmedchem.0c00967.

(34) Sun, Y.; Zhao, X.; Ding, N.; Gao, H.; Wu, Y.; Yang, Y.; Zhao, M.; Hwang, J.; Song, Y.; Liu, W.; Rao, Y. PROTAC-Induced BTK Degradation as a Novel Therapy for Mutated BTK C481S Induced Ibrutinib-Resistant B-Cell Malignancies. *Cell Res* **2018**, *28* (7), 779–781. https://doi.org/10.1038/s41422-018-0055-1.

(35) Sun, X.; Rao, Y. PROTACs as Potential Therapeutic Agents for Cancer Drug Resistance. *Biochemistry* **2020**, *59* (3), 240–249. https://doi.org/10.1021/acs.biochem.9b00848.

(36) Martín-Acosta, P.; Xiao, X. PROTACs to Address the Challenges Facing Small Molecule Inhibitors. *European Journal of Medicinal Chemistry* **2021**, *210*, 112993. https://doi.org/10.1016/j.ejmech.2020.112993.

(37) Sun, X.; Gao, H.; Yang, Y.; He, M.; Wu, Y.; Song, Y.; Tong, Y.; Rao, Y. PROTACs: Great Opportunities for Academia and Industry. *Sig Transduct Target Ther* **2019**, *4* (1), 1–33. https://doi.org/10.1038/s41392-019-0101-6.

(38) He, M.; Cao, C.; Ni, Z.; Liu, Y.; Song, P.; Hao, S.; He, Y.; Sun, X.; Rao, Y. PROTACs: Great Opportunities for Academia and Industry (an Update from 2020 to 2021). *Sig Transduct Target Ther* **2022**, *7* (1), 1–64. https://doi.org/10.1038/s41392-022-00999-9.

(39) Douglass, E. F. Jr.; Miller, C. J.; Sparer, G.; Shapiro, H.; Spiegel, D. A. A Comprehensive Mathematical Model for Three-Body Binding Equilibria. *J. Am. Chem. Soc.* **2013**, *135* (16), 6092–6099. https://doi.org/10.1021/ja311795d.

(40) Lu, C.; Wang, Z.-X. Quantitative Analysis of Ligand Induced Heterodimerization of Two Distinct Receptors. *Anal. Chem.* **2017**, *89* (13), 6926–6930. https://doi.org/10.1021/acs.analchem.7b01274.

(41) Hughes, S. J.; Ciulli, A. Molecular Recognition of Ternary Complexes: A New Dimension in the Structure-Guided Design of Chemical Degraders. *Essays in Biochemistry* **2017**, *61* (5), 505–516. https://doi.org/10.1042/EBC20170041.

(42) Tate, J.; Ward, G. Interferences in Immunoassay. *Clin Biochem Rev* **2004**, *25* (2), 105–120.

(43) Roy, R. D.; Rosenmund, C.; Stefan, M. I. Cooperative Binding Mitigates the High-Dose Hook Effect. *BMC Systems Biology* **2017**, *11* (1), 74. https://doi.org/10.1186/s12918-017-0447-8.

(44) Gadd, M. S.; Testa, A.; Lucas, X.; Chan, K.-H.; Chen, W.; Lamont, D. J.; Zengerle, M.; Ciulli, A. Structural Basis of PROTAC Cooperative Recognition for Selective Protein Degradation. *Nat Chem Biol* **2017**, *13* (5), 514–521. https://doi.org/10.1038/nchembio.2329.

(45) Zorba, A.; Nguyen, C.; Xu, Y.; Starr, J.; Borzilleri, K.; Smith, J.; Zhu, H.; Farley, K. A.; Ding, W.; Schiemer, J.; Feng, X.; Chang, J. S.; Uccello, D. P.; Young, J. A.; Garcia-Irrizary, C. N.; Czabaniuk, L.; Schuff, B.; Oliver, R.; Montgomery, J.; Hayward, M. M.; Coe, J.; Chen, J.; Niosi, M.; Luthra, S.; Shah, J. C.; El-Kattan, A.; Qiu, X.; West, G. M.; Noe, M. C.; Shanmugasundaram, V.; Gilbert, A. M.; Brown, M. F.; Calabrese, M. F. Delineating the Role of Cooperativity in the Design of Potent PROTACs for BTK. *Proc Natl Acad Sci U S A* **2018**, *115* (31), E7285–E7292. https://doi.org/10.1073/pnas.1803662115.

(46) Sakamoto, K. M.; Kim, K. B.; Verma, R.; Ransick, A.; Stein, B.; Crews, C. M.; Deshaies, R. J. Development of Protacs to Target Cancer-Promoting Proteins for Ubiquitination and Degradation*. *Molecular & Cellular Proteomics* **2003**, *2* (12), 1350–1358. https://doi.org/10.1074/mcp.T300009-MCP200.

(47) Schneekloth, J. S. Jr.; Fonseca, F. N.; Koldobskiy, M.; Mandal, A.; Deshaies, R.; Sakamoto, K.; Crews, C. M. Chemical Genetic Control of Protein Levels: Selective in Vivo Targeted Degradation. *J. Am. Chem. Soc.* **2004**, *126* (12), 3748–3754. https://doi.org/10.1021/ja039025z.

(48) Lee, H.; Puppala, D.; Choi, E.-Y.; Swanson, H.; Kim, K.-B. Targeted Degradation of the Aryl Hydrocarbon Receptor by the PROTAC Approach: A Useful Chemical Genetic Tool. *ChemBioChem* **2007**, *8* (17), 2058–2062. https://doi.org/10.1002/cbic.200700438.

(49) Schneekloth, A. R.; Pucheault, M.; Tae, H. S.; Crews, C. M. Targeted Intracellular Protein Degradation Induced by a Small Molecule: En Route to Chemical Proteomics. *Bioorg Med Chem Lett* **2008**, *18* (22), 5904–5908. https://doi.org/10.1016/j.bmcl.2008.07.114.

(50) Zou, Y.; Ma, D.; Wang, Y. The PROTAC Technology in Drug Development. *Cell Biochemistry and Function* **2019**, *37* (1), 21–30. https://doi.org/10.1002/cbf.3369.

(51) Wang, C.; Zhang, Y.; Wu, Y.; Xing, D. Developments of CRBN-Based PROTACs as Potential Therapeutic Agents. *European Journal of Medicinal Chemistry* **2021**, *225*, 113749. https://doi.org/10.1016/j.ejmech.2021.113749.

(52) Bricelj, A.; Steinebach, C.; Kuchta, R.; Gütschow, M.; Sosič, I. E3 Ligase Ligands in Successful PROTACs: An Overview of Syntheses and Linker Attachment Points. *Frontiers in Chemistry* **2021**, *9*.

(53) Yang, X.-D.; Sun, S.-C. Targeting Signaling Factors for Degradation, an Emerging Mechanism for TRAF Functions. *Immunological Reviews* **2015**, *266* (1), 56–71. https://doi.org/10.1111/imr.12311.

(54) Itoh, Y.; Ishikawa, M.; Naito, M.; Hashimoto, Y. Protein Knockdown Using Methyl Bestatin−Ligand Hybrid Molecules: Design and Synthesis of Inducers of Ubiquitination-Mediated Degradation of Cellular Retinoic Acid-Binding Proteins. *J. Am. Chem. Soc.* **2010**, *132* (16), 5820–5826. https://doi.org/10.1021/ja100691p.

(55) Diehl, C. J.; Ciulli, A. Discovery of Small Molecule Ligands for the von Hippel-Lindau (VHL) E3 Ligase and Their Use as Inhibitors and PROTAC Degraders. *Chem. Soc. Rev.* **2022**, *51* (19), 8216–8257. https://doi.org/10.1039/D2CS00387B.

(56) Setia, N.; Almuqdadi, H. T. A.; Abid, M. Journey of Von Hippel-Lindau (VHL) E3 Ligase in PROTACs Design: From VHL Ligands to VHL-Based Degraders. *European Journal of Medicinal Chemistry* **2024**, *265*, 116041. https://doi.org/10.1016/j.ejmech.2023.116041.

(57) Buckley, D. L.; Gustafson, J. L.; Van Molle, I.; Roth, A. G.; Tae, H. S.; Gareiss, P. C.; Jorgensen, W. L.; Ciulli, A.; Crews, C. M. Small-Molecule Inhibitors of the Interaction between the E3 Ligase VHL and HIF1α. *Angewandte Chemie International Edition* **2012**, *51* (46), 11463–11467. https://doi.org/10.1002/anie.201206231.

(58) Buckley, D. L.; Van Molle, I.; Gareiss, P. C.; Tae, H. S.; Michel, J.; Noblin, D. J.; Jorgensen, W. L.; Ciulli, A.; Crews, C. M. Targeting the von Hippel–Lindau E3 Ubiquitin

Ligase Using Small Molecules To Disrupt the VHL/HIF-1α Interaction. *J. Am. Chem. Soc.* **2012**, *134* (10), 4465–4468. https://doi.org/10.1021/ja209924v.

(59) Van Molle, I.; Thomann, A.; Buckley, D. L.; So, E. C.; Lang, S.; Crews, C. M.; Ciulli, A. Dissecting Fragment-Based Lead Discovery at the von Hippel-Lindau Protein:Hypoxia Inducible Factor 1α Protein-Protein Interface. *Chemistry & Biology* **2012**, *19* (10), 1300–1312. https://doi.org/10.1016/j.chembiol.2012.08.015.

(60) Ito, T.; Ando, H.; Suzuki, T.; Ogura, T.; Hotta, K.; Imamura, Y.; Yamaguchi, Y.; Handa, H. Identification of a Primary Target of Thalidomide Teratogenicity. *Science* **2010**, *327* (5971), 1345–1350. https://doi.org/10.1126/science.1177319.

(61) Lopez-Girona, A.; Mendy, D.; Ito, T.; Miller, K.; Gandhi, A. K.; Kang, J.; Karasawa, S.; Carmel, G.; Jackson, P.; Abbasian, M.; Mahmoudi, A.; Cathers, B.; Rychak, E.; Gaidarova, S.; Chen, R.; Schafer, P. H.; Handa, H.; Daniel, T. O.; Evans, J. F.; Chopra, R. Cereblon Is a Direct Protein Target for Immunomodulatory and Antiproliferative Activities of Lenalidomide and Pomalidomide. *Leukemia* **2012**, *26* (11), 2326–2335. https://doi.org/10.1038/leu.2012.119.

(62) Fischer, E. S.; Böhm, K.; Lydeard, J. R.; Yang, H.; Stadler, M. B.; Cavadini, S.; Nagel, J.; Serluca, F.; Acker, V.; Lingaraju, G. M.; Tichkule, R. B.; Schebesta, M.; Forrester, W. C.; Schirle, M.; Hassiepen, U.; Ottl, J.; Hild, M.; Beckwith, R. E. J.; Harper, J. W.; Jenkins, J. L.; Thomä, N. H. Structure of the DDB1–CRBN E3 Ubiquitin Ligase in Complex with Thalidomide. *Nature* **2014**, *512* (7512), 49–53. https://doi.org/10.1038/nature13527.

(63) Krönke, J.; Udeshi, N. D.; Narla, A.; Grauman, P.; Hurst, S. N.; McConkey, M.; Svinkina, T.; Heckl, D.; Comer, E.; Li, X.; Ciarlo, C.; Hartman, E.; Munshi, N.; Schenone, M.; Schreiber, S. L.; Carr, S. A.; Ebert, B. L. Lenalidomide Causes Selective Degradation of IKZF1 and IKZF3 in Multiple Myeloma Cells. *Science* **2014**, *343* (6168), 301–305. https://doi.org/10.1126/science.1244851.

(64) Petzold, G.; Fischer, E. S.; Thomä, N. H. Structural Basis of Lenalidomide-Induced CK1α Degradation by the CRL4CRBN Ubiquitin Ligase. *Nature* **2016**, *532* (7597), 127–130. https://doi.org/10.1038/nature16979.

(65) Gandhi, A. K.; Kang, J.; Havens, C. G.; Conklin, T.; Ning, Y.; Wu, L.; Ito, T.; Ando, H.; Waldman, M. F.; Thakurta, A.; Klippel, A.; Handa, H.; Daniel, T. O.; Schafer, P. H.; Chopra, R. Immunomodulatory Agents Lenalidomide and Pomalidomide Co-Stimulate T Cells by Inducing Degradation of T Cell Repressors Ikaros and Aiolos via Modulation of the E3

Ubiquitin Ligase Complex CRL4CRBN. *British Journal of Haematology* **2014**, *164* (6), 811–821. https://doi.org/10.1111/bjh.12708.

(66) Hines, J.; Gough, J. D.; Corson, T. W.; Crews, C. M. Posttranslational Protein Knockdown Coupled to Receptor Tyrosine Kinase Activation with phosphoPROTACs. *Proceedings of the National Academy of Sciences* **2013**, *110* (22), 8942–8947. https://doi.org/10.1073/pnas.1217206110.

(67) Montrose, K.; Krissansen, G. W. Design of a PROTAC That Antagonizes and Destroys the Cancer-Forming X-Protein of the Hepatitis B Virus. *Biochemical and Biophysical Research Communications* **2014**, *453* (4), 735–740. https://doi.org/10.1016/j.bbrc.2014.10.006.

(68) Buckley, D. L.; Raina, K.; Darricarrere, N.; Hines, J.; Gustafson, J. L.; Smith, I. E.; Miah, A. H.; Harling, J. D.; Crews, C. M. HaloPROTACS: Use of Small Molecule PROTACs to Induce Degradation of HaloTag Fusion Proteins. *ACS Chem. Biol.* **2015**, *10* (8), 1831–1837. https://doi.org/10.1021/acschembio.5b00442.

(69) Zengerle, M.; Chan, K.-H.; Ciulli, A. Selective Small Molecule Induced Degradation of the BET Bromodomain Protein BRD4. *ACS Chem. Biol.* **2015**, *10* (8), 1770–1777. https://doi.org/10.1021/acschembio.5b00216.

(70) Lebraud, H.; Wright, D. J.; Johnson, C. N.; Heightman, T. D. Protein Degradation by In-Cell Self-Assembly of Proteolysis Targeting Chimeras. *ACS Cent. Sci.* **2016**, *2* (12), 927–934. https://doi.org/10.1021/acscentsci.6b00280.

(71) Weng, G.; Cai, X.; Cao, D.; Du, H.; Shen, C.; Deng, Y.; He, Q.; Yang, B.; Li, D.; Hou, T. PROTAC-DB 2.0: An Updated Database of PROTACs. *Nucleic Acids Research* **2023**, *51* (D1), D1367–D1372. https://doi.org/10.1093/nar/gkac946.

(72) Silva, M. C.; Ferguson, F. M.; Cai, Q.; Donovan, K. A.; Nandi, G.; Patnaik, D.; Zhang, T.; Huang, H.-T.; Lucente, D. E.; Dickerson, B. C.; Mitchison, T. J.; Fischer, E. S.; Gray, N. S.; Haggarty, S. J. Targeted Degradation of Aberrant Tau in Frontotemporal Dementia Patient-Derived Neuronal Cell Models. *Elife* **2019**, *8*, e45457. https://doi.org/10.7554/eLife.45457.

(73) Silva, M. C.; Nandi, G.; Donovan, K. A.; Cai, Q.; Berry, B. C.; Nowak, R. P.; Fischer, E. S.; Gray, N. S.; Ferguson, F. M.; Haggarty, S. J. Discovery and Optimization of Tau Targeted Protein Degraders Enabled by Patient Induced Pluripotent Stem Cells-Derived Neuronal Models of Tauopathy. *Frontiers in Cellular Neuroscience* **2022**, *16*.

(74) Wang, W.; Zhou, Q.; Jiang, T.; Li, S.; Ye, J.; Zheng, J.; Wang, X.; Liu, Y.; Deng, M.; Ke, D.; Wang, Q.; Wang, Y.; Wang, J.-Z. A Novel Small-Molecule PROTAC Selectively Promotes Tau Clearance to Improve Cognitive Functions in Alzheimer-like Models. *Theranostics* **2021**, *11* (11), 5279–5295. https://doi.org/10.7150/thno.55680.

(75) Moore, A. R.; Rosenberg, S. C.; McCormick, F.; Malek, S. RAS-Targeted Therapies: Is the Undruggable Drugged? *Nat Rev Drug Discov* **2020**, *19* (8), 533–552. https://doi.org/10.1038/s41573-020-0068-6.

(76) Yang, F.; Wen, Y.; Wang, C.; Zhou, Y.; Zhou, Y.; Zhang, Z.-M.; Liu, T.; Lu, X. Efficient Targeted Oncogenic KRASG12C Degradation via First Reversible-Covalent PROTAC. *European Journal of Medicinal Chemistry* **2022**, *230*, 114088. https://doi.org/10.1016/j.ejmech.2021.114088.

(77) Bond, M. J.; Chu, L.; Nalawansha, D. A.; Li, K.; Crews, C. M. Targeted Degradation of Oncogenic KRASG12C by VHL-Recruiting PROTACs. *ACS Cent. Sci.* **2020**, *6* (8), 1367–1375. https://doi.org/10.1021/acscentsci.0c00411.

(78) Li, L.; Wu, Y.; Yang, Z.; Xu, C.; Zhao, H.; Liu, J.; Chen, J.; Chen, J. Discovery of KRas G12C-IN-3 and Pomalidomide-Based PROTACs as Degraders of Endogenous KRAS G12C with Potent Anticancer Activity. *Bioorganic Chemistry* **2021**, *117*, 105447. https://doi.org/10.1016/j.bioorg.2021.105447.

(79) Lee, H.; Lee, J. Y.; Jang, H.; Cho, H. Y.; Kang, M.; Bae, S. H.; Kim, S.; Kim, E.; Jang, J.; Kim, J. Y.; Jeon, Y. H. Discovery of Proteolysis-Targeting Chimera Targeting Undruggable Proteins Using a Covalent Ligand Screening Approach. *European Journal of Medicinal Chemistry* **2024**, *263*, 115929. https://doi.org/10.1016/j.ejmech.2023.115929.

(80) Bondeson, D. P.; Smith, B. E.; Burslem, G. M.; Buhimschi, A. D.; Hines, J.; Jaime-Figueroa, S.; Wang, J.; Hamman, B. D.; Ishchenko, A.; Crews, C. M. Lessons in PROTAC Design from Selective Degradation with a Promiscuous Warhead. *Cell Chemical Biology* **2018**, *25* (1), 78-87.e5. https://doi.org/10.1016/j.chembiol.2017.09.010.

(81) Burke, M. R.; Smith, A. R.; Zheng, G. Overcoming Cancer Drug Resistance Utilizing PROTAC Technology. *Frontiers in Cell and Developmental Biology* **2022**, *10*.

(82) Buhimschi, A. D.; Armstrong, H. A.; Toure, M.; Jaime-Figueroa, S.; Chen, T. L.; Lehman, A. M.; Woyach, J. A.; Johnson, A. J.; Byrd, J. C.; Crews, C. M. Targeting the C481S Ibrutinib-Resistance Mutation in Bruton's Tyrosine Kinase Using PROTAC-Mediated

Degradation. *Biochemistry* **2018**, *57* (26), 3564–3575. https://doi.org/10.1021/acs.biochem.8b00391.

(83) Bueno, C.; Velasco-Hernandez, T.; Gutiérrez-Agüera, F.; Zanetti, S. R.; Baroni, M. L.; Sánchez-Martínez, D.; Molina, O.; Closa, A.; Agraz-Doblás, A.; Marín, P.; Eyras, E.; Varela, I.; Menéndez, P. CD133-Directed CAR T-Cells for MLL Leukemia: On-Target, off-Tumor Myeloablative Toxicity. *Leukemia* **2019**, *33* (8), 2090–2125. https://doi.org/10.1038/s41375-019-0418-8.

(84) Woyach, J. A.; Furman, R. R.; Liu, T.-M.; Ozer, H. G.; Zapatka, M.; Ruppert, A. S.; Xue, L.; Li, D. H.-H.; Steggerda, S. M.; Versele, M.; Dave, S. S.; Zhang, J.; Yilmaz, A. S.; Jaglowski, S. M.; Blum, K. A.; Lozanski, A.; Lozanski, G.; James, D. F.; Barrientos, J. C.; Lichter, P.; Stilgenbauer, S.; Buggy, J. J.; Chang, B. Y.; Johnson, A. J.; Byrd, J. C. Resistance Mechanisms for the Bruton's Tyrosine Kinase Inhibitor Ibrutinib. *New England Journal of Medicine* **2014**, *370* (24), 2286–2294. https://doi.org/10.1056/NEJMoa1400029.

(85) Huang, H.-T.; Dobrovolsky, D.; Paulk, J.; Yang, G.; Weisberg, E. L.; Doctor, Z. M.; Buckley, D. L.; Cho, J.-H.; Ko, E.; Jang, J.; Shi, K.; Choi, H. G.; Griffin, J. D.; Li, Y.; Treon, S. P.; Fischer, E. S.; Bradner, J. E.; Tan, L.; Gray, N. S. A Chemoproteomic Approach to Query the Degradable Kinome Using a Multi-Kinase Degrader. *Cell Chemical Biology* **2018**, *25* (1), 88-99.e6. https://doi.org/10.1016/j.chembiol.2017.10.005.

(86) Neklesa, T.; Snyder, L. B.; Willard, R. R.; Vitale, N.; Pizzano, J.; Gordon, D. A.; Bookbinder, M.; Macaluso, J.; Dong, H.; Ferraro, C.; Wang, G.; Wang, J.; Crews, C. M.; Houston, J.; Crew, A. P.; Taylor, I. ARV-110: An Oral Androgen Receptor PROTAC Degrader for Prostate Cancer. *JCO* **2019**, *37* (7_suppl), 259–259. https://doi.org/10.1200/JCO.2019.37.7_suppl.259.

(87) Neklesa, T.; Snyder, L. B.; Willard, R. R.; Vitale, N.; Raina, K.; Pizzano, J.; Gordon, D.; Bookbinder, M.; Macaluso, J.; Dong, H.; Liu, Z.; Ferraro, C.; Wang, G.; Wang, J.; Crews, C. M.; Houston, J.; Crew, A. P.; Taylor, I. Abstract 5236: ARV-110: An Androgen Receptor PROTAC Degrader for Prostate Cancer. *Cancer Research* **2018**, *78* (13_Supplement), 5236. https://doi.org/10.1158/1538-7445.AM2018-5236.

(88) Gao, X.; Burris III, H. A.; Vuky, J.; Dreicer, R.; Sartor, A. O.; Sternberg, C. N.; Percent, I. J.; Hussain, M. H. A.; Rezazadeh Kalebasty, A.; Shen, J.; Heath, E. I.; Abesada-Terk, G.; Gandhi, S. G.; McKean, M.; Lu, H.; Berghorn, E.; Gedrich, R.; Chirnomas, S. D.; Vogelzang, N. J.; Petrylak, D. P. Phase 1/2 Study of ARV-110, an Androgen Receptor (AR) PROTAC

Degrader, in Metastatic Castration-Resistant Prostate Cancer (mCRPC). *JCO* **2022**, *40* (6_suppl), 17–17. https://doi.org/10.1200/JCO.2022.40.6_suppl.017.

(89) Snyder, L. B.; Flanagan, J. J.; Qian, Y.; Gough, S. M.; Andreoli, M.; Bookbinder, M.; Cadelina, G.; Bradley, J.; Rousseau, E.; Chandler, J.; Willard, R.; Pizzano, J.; Crews, C. M.; Crew, A. P.; Houston, J.; Moore, M. D.; Peck, R.; Taylor, I. Abstract 44: The Discovery of ARV-471, an Orally Bioavailable Estrogen Receptor Degrading PROTAC for the Treatment of Patients with Breast Cancer. *Cancer Research* **2021**, *81* (13_Supplement), 44. https://doi.org/10.1158/1538-7445.AM2021-44.

(90) Ackerman, L.; Acloque, G.; Bacchelli, S.; Schwartz, H.; Feinstein, B. J.; La Stella, P.; Alavi, A.; Gollerkeri, A.; Davis, J.; Campbell, V.; McDonald, A.; Agarwal, S.; Karnik, R.; Shi, K.; Mishkin, A.; Culbertson, J.; Klaus, C.; Enerson, B.; Massa, V.; Kuhn, E.; Sharma, K.; Keaney, E.; Barnes, R.; Chen, D.; Zheng, X.; Rong, H.; Sabesan, V.; Ho, C.; Mainolfi, N.; Slavin, A.; Gollob, J. A. IRAK4 Degrader in Hidradenitis Suppurativa and Atopic Dermatitis: A Phase 1 Trial. *Nat Med* **2023**, *29* (12), 3127–3136. https://doi.org/10.1038/s41591-023-02635-7.

(91) Moreau, K.; Coen, M.; Zhang, A. X.; Pachl, F.; Castaldi, M. P.; Dahl, G.; Boyd, H.; Scott, C.; Newham, P. Proteolysis-Targeting Chimeras in Drug Development: A Safety Perspective. *British Journal of Pharmacology* **2020**, *177* (8), 1709–1718. https://doi.org/10.1111/bph.15014.

(92) *Kintor Pharmaceutical Announces AR-PROTAC (GT20029) Approved for Acne and Androgenic Alopecia Clinical Trials in China_Kintor Pharmaceutical Limited*. https://en.kintor.com.cn/news/171.html (accessed 2024-02-24).

(93) Salerno, A.; Seghetti, F.; Caciolla, J.; Uliassi, E.; Testi, E.; Guardigni, M.; Roberti, M.; Milelli, A.; Bolognesi, M. L. Enriching Proteolysis Targeting Chimeras with a Second Modality: When Two Are Better Than One. *J Med Chem* **2022**, *65* (14), 9507–9530. https://doi.org/10.1021/acs.jmedchem.2c00302.

(94) Kostic, M.; Jones, L. H. Critical Assessment of Targeted Protein Degradation as a Research Tool and Pharmacological Modality. *Trends in Pharmacological Sciences* **2020**, *41* (5), 305–317. https://doi.org/10.1016/j.tips.2020.02.006.

(95) Edmondson, S. D.; Yang, B.; Fallan, C. Proteolysis Targeting Chimeras (PROTACs) in 'beyond Rule-of-Five' Chemical Space: Recent Progress and Future Challenges. *Bioorganic &*

Medicinal Chemistry Letters **2019**, *29* (13), 1555–1564. https://doi.org/10.1016/j.bmcl.2019.04.030.

(96) Lipinski, C. A.; Lombardo, F.; Dominy, B. W.; Feeney, P. J. Experimental and Computational Approaches to Estimate Solubility and Permeability in Drug Discovery and Development Settings. *Advanced Drug Delivery Reviews* **1997**, *23* (1), 3–25. https://doi.org/10.1016/S0169-409X(96)00423-1.

(97) Matsson, P.; Kihlberg, J. How Big Is Too Big for Cell Permeability? *J. Med. Chem.* **2017**, *60* (5), 1662–1664. https://doi.org/10.1021/acs.jmedchem.7b00237.

(98) Jimenez, D. G.; Sebastiano, M. R.; Caron, G.; Ermondi, G. Are We Ready to Design Oral PROTACs®? *ADMET and DMPK* **2021**, *9* (4), 243–254. https://doi.org/10.5599/admet.1037.

(99) Atilaw, Y.; Poongavanam, V.; Svensson Nilsson, C.; Nguyen, D.; Giese, A.; Meibom, D.; Erdelyi, M.; Kihlberg, J. Solution Conformations Shed Light on PROTAC Cell Permeability. *ACS Med. Chem. Lett.* **2021**, *12* (1), 107–114. https://doi.org/10.1021/acsmedchemlett.0c00556.

(100) Bemis, T. A.; Clair, J. J. L.; Burkart, M. D. Unraveling the Role of Linker Design in Proteolysis Targeting Chimeras. *Journal of Medicinal Chemistry* **2021**, *64* (12), 8040–8052. https://doi.org/10.1021/acs.jmedchem.1c00482.

(101) Chen, S.; Chen, Z.; Lu, L.; Zhao, Y.; Zhou, R.; Xie, Q.; Shu, Y.; Lin, J.; Yu, X.; Wang, Y. Discovery of Novel BTK PROTACs with Improved Metabolic Stability via Linker Rigidification Strategy. *Eur J Med Chem* **2023**, *255*, 115403. https://doi.org/10.1016/j.ejmech.2023.115403.

(102) Cecchini, C.; Pannilunghi, S.; Tardy, S.; Scapozza, L. From Conception to Development: Investigating PROTACs Features for Improved Cell Permeability and Successful Protein Degradation. *Frontiers in Chemistry* **2021**, *9*.

(103) Zhang, L.; Riley-Gillis, B.; Vijay, P.; Shen, Y. Acquired Resistance to BET-PROTACs (Proteolysis-Targeting Chimeras) Caused by Genomic Alterations in Core Components of E3 Ligase Complexes. *Molecular Cancer Therapeutics* **2019**, *18* (7), 1302–1311. https://doi.org/10.1158/1535-7163.MCT-18-1129.

(104) Pacini, C.; Dempster, J. M.; Boyle, I.; Gonçalves, E.; Najgebauer, H.; Karakoc, E.; van der Meer, D.; Barthorpe, A.; Lightfoot, H.; Jaaks, P.; McFarland, J. M.; Garnett, M. J.;

Tsherniak, A.; Iorio, F. Integrated Cross-Study Datasets of Genetic Dependencies in Cancer. *Nat Commun* **2021**, *12* (1), 1661. https://doi.org/10.1038/s41467-021-21898-7.

(105) Shirasaki, R.; Matthews, G. M.; Gandolfi, S.; Simoes, R. de M.; Buckley, D. L.; Vora, J. R.; Sievers, Q. L.; Brüggenthies, J. B.; Dashevsky, O.; Poarch, H.; Tang, H.; Bariteau, M. A.; Sheffer, M.; Hu, Y.; Downey-Kopyscinski, S. L.; Hengeveld, P. J.; Glassner, B. J.; Dhimolea, E.; Ott, C. J.; Zhang, T.; Kwiatkowski, N. P.; Laubach, J. P.; Schlossman, R. L.; Richardson, P. G.; Culhane, A. C.; Groen, R. W. J.; Fischer, E. S.; Vazquez, F.; Tsherniak, A.; Hahn, W. C.; Levy, J.; Auclair, D.; Licht, J. D.; Keats, J. J.; Boise, L. H.; Ebert, B. L.; Bradner, J. E.; Gray, N. S.; Mitsiades, C. S. Functional Genomics Identify Distinct and Overlapping Genes Mediating Resistance to Different Classes of Heterobifunctional Degraders of Oncoproteins. *Cell Reports* **2021**, *34* (1). https://doi.org/10.1016/j.celrep.2020.108532.

(106) Matyskiela, M. E.; Lu, G.; Ito, T.; Pagarigan, B.; Lu, C.-C.; Miller, K.; Fang, W.; Wang, N.-Y.; Nguyen, D.; Houston, J.; Carmel, G.; Tran, T.; Riley, M.; Nosaka, L.; Lander, G. C.; Gaidarova, S.; Xu, S.; Ruchelman, A. L.; Handa, H.; Carmichael, J.; Daniel, T. O.; Cathers, B. E.; Lopez-Girona, A.; Chamberlain, P. P. A Novel Cereblon Modulator Recruits GSPT1 to the CRL4CRBN Ubiquitin Ligase. *Nature* **2016**, *535* (7611), 252–257. https://doi.org/10.1038/nature18611.

(107) Zhong, Y.; Chi, F.; Wu, H.; Liu, Y.; Xie, Z.; Huang, W.; Shi, W.; Qian, H. Emerging Targeted Protein Degradation Tools for Innovative Drug Discovery: From Classical PROTACs to the Novel and Beyond. *European Journal of Medicinal Chemistry* **2022**, *231*, 114142. https://doi.org/10.1016/j.ejmech.2022.114142.

(108) Ghidini, A.; Cléry, A.; Halloy, F.; Allain, F. H. T.; Hall, J. RNA-PROTACs: Degraders of RNA-Binding Proteins. *Angewandte Chemie International Edition* **2021**, *60* (6), 3163–3169. https://doi.org/10.1002/anie.202012330.

(109) Viegas-Junior, C.; Danuello, A.; Bolzani, V. da S.; Barreiro, E. J.; Fraga, C. A. M. Molecular Hybridization: A Useful Tool in the Design of New Drug Prototypes. *Current Medicinal Chemistry* **2007**, *14* (17), 1829–1852.

(110) Ivasiv, V.; Albertini, C.; Gonçalves, A. E.; Rossi, M.; Bolognesi, M. L. Molecular Hybridization as a Tool for Designing Multitarget Drug Candidates for Complex Diseases. *Current Topics in Medicinal Chemistry* **2019**, *19* (19), 1694–1711.

(111) Troup, R. I.; Fallan, C.; Baud, M. G. J. Current Strategies for the Design of PROTAC Linkers: A Critical Review. *Explor Target Antitumor Ther.* **2020**, *1* (5), 273–312. https://doi.org/10.37349/etat.2020.00018.

(112) Zheng, S.; Tan, Y.; Wang, Z.; Li, C.; Zhang, Z.; Sang, X.; Chen, H.; Yang, Y. Accelerated Rational PROTAC Design via Deep Learning and Molecular Simulations. *Nat Mach Intell* **2022**, *4* (9), 739–748. https://doi.org/10.1038/s42256-022-00527-y.

(113) Fisher, S. L.; Phillips, A. J. Targeted Protein Degradation and the Enzymology of Degraders. *Current Opinion in Chemical Biology* **2018**, *44*, 47–55. https://doi.org/10.1016/j.cbpa.2018.05.004.

(114) Nalawansha, D. A.; Crews, C. M. PROTACs: An Emerging Therapeutic Modality in Precision Medicine. *Cell Chemical Biology* **2020**, *27* (8), 998–1014. https://doi.org/10.1016/j.chembiol.2020.07.020.

(115) *PROTACpedia*. https://protacpedia.weizmann.ac.il/ptcb/main (accessed 2024-02-19).

(116) Nunes, J.; McGonagle, G. A.; Eden, J.; Kiritharan, G.; Touzet, M.; Lewell, X.; Emery, J.; Eidam, H.; Harling, J. D.; Anderson, N. A. Targeting IRAK4 for Degradation with PROTACs. *ACS Med. Chem. Lett.* **2019**, *10* (7), 1081–1085. https://doi.org/10.1021/acsmedchemlett.9b00219.

(117) Cai, M.; Ma, F.; Hu, C.; Li, H.; Cao, F.; Li, Y.; Dong, J.; Qin, J.-J. Design and Synthesis of Proteolysis-Targeting Chimeras (PROTACs) as Degraders of Glutathione Peroxidase 4. *Bioorganic & Medicinal Chemistry* **2023**, *90*, 117352. https://doi.org/10.1016/j.bmc.2023.117352.

(118) Miller, D. S. J.; Voell, S. A.; Sosič, I.; Proj, M.; Rossanese, O. W.; Schnakenburg, G.; Gütschow, M.; Collins, I.; Steinebach, C. Encoding BRAF Inhibitor Functions in Protein Degraders. *RSC Med. Chem.* **2022**, *13* (6), 731–736. https://doi.org/10.1039/D2MD00064D.

(119) Liu, H.; Mi, Q.; Ding, X.; Lin, C.; Liu, L.; Ren, C.; Shen, S.; Shao, Y.; Chen, J.; Zhou, Y.; Ji, L.; Zhang, H.; Bai, F.; Yang, X.; Yin, Q.; Jiang, B. Discovery and Characterization of Novel Potent BCR-ABL Degraders by Conjugating Allosteric Inhibitor. *European Journal of Medicinal Chemistry* **2022**, *244*, 114810. https://doi.org/10.1016/j.ejmech.2022.114810.

(120) Tokarski, R. J.; Sharpe, C. M.; Huntsman, A. C.; Mize, B. K.; Ayinde, O. R.; Stahl, E. H.; Lerma, J. R.; Reed, A.; Carmichael, B.; Muthusamy, N.; Byrd, J. C.; Fuchs, J. R. Bifunctional Degraders of Cyclin Dependent Kinase 9 (CDK9): Probing the Relationship

between Linker Length, Properties, and Selective Protein Degradation. *European Journal of Medicinal Chemistry* **2023**, *254*, 115342. https://doi.org/10.1016/j.ejmech.2023.115342.

(121) Khan, S.; Zhang, X.; Lv, D.; Zhang, Q.; He, Y.; Zhang, P.; Liu, X.; Thummuri, D.; Yuan, Y.; Wiegand, J. S.; Pei, J.; Zhang, W.; Sharma, A.; McCurdy, C. R.; Kuruvilla, V. M.; Baran, N.; Ferrando, A. A.; Kim, Y.; Rogojina, A.; Houghton, P. J.; Huang, G.; Hromas, R.; Konopleva, M.; Zheng, G.; Zhou, D. A Selective BCL-XL PROTAC Degrader Achieves Safe and Potent Antitumor Activity. *Nat Med* **2019**, *25* (12), 1938–1947. https://doi.org/10.1038/s41591-019-0668-z.

(122) Churcher, I. Protac-Induced Protein Degradation in Drug Discovery: Breaking the Rules or Just Making New Ones? *J. Med. Chem.* **2018**, *61* (2), 444–452. https://doi.org/10.1021/acs.jmedchem.7b01272.

(123) Zografou-Barredo, N. A.; Hallatt, A. J.; Goujon-Ricci, J.; Cano, C. A Beginner's Guide to Current Synthetic Linker Strategies towards VHL-Recruiting PROTACs. *Bioorganic & Medicinal Chemistry* **2023**, *88–89*, 117334. https://doi.org/10.1016/j.bmc.2023.117334.

(124) Rostovtsev, V. V.; Green, L. G.; Fokin, V. V.; Sharpless, K. B. A Stepwise Huisgen Cycloaddition Process: Copper(I)-Catalyzed Regioselective "Ligation" of Azides and Terminal Alkynes. *Angewandte Chemie International Edition* **2002**, *41* (14), 2596–2599. https://doi.org/10.1002/1521-3773(20020715)41:14<2596::AID-ANIE2596>3.0.CO;2-4.

(125) Tornøe, C. W.; Christensen, C.; Meldal, M. Peptidotriazoles on Solid Phase: [1,2,3]-Triazoles by Regiospecific Copper(I)-Catalyzed 1,3-Dipolar Cycloadditions of Terminal Alkynes to Azides. *J. Org. Chem.* **2002**, *67* (9), 3057–3064. https://doi.org/10.1021/jo011148j.

(126) Agard, N. J.; Prescher, J. A.; Bertozzi, C. R. A Strain-Promoted [3 + 2] Azide−Alkyne Cycloaddition for Covalent Modification of Biomolecules in Living Systems. *J. Am. Chem. Soc.* **2004**, *126* (46), 15046–15047. https://doi.org/10.1021/ja044996f.

(127) Pasieka, A.; Diamanti, E.; Uliassi, E.; Laura Bolognesi, M. Click Chemistry and Targeted Degradation: A Winning Combination for Medicinal Chemists? *ChemMedChem* **2023**, *18* (20), e202300422. https://doi.org/10.1002/cmdc.202300422.

(128) Xia, L.-W.; Ba, M.-Y.; Liu, W.; Cheng, W.; Hu, C.-P.; Zhao, Q.; Yao, Y.-F.; Sun, M.-R.; Duan, Y.-T. Triazol: A Privileged Scaffold for Proteolysis Targeting Chimeras. *Future Medicinal Chemistry* **2019**, *11* (22), 2919–2973. https://doi.org/10.4155/fmc-2019-0159.

(129) Schiedel, M.; Herp, D.; Hammelmann, S.; Swyter, S.; Lehotzky, A.; Robaa, D.; Oláh, J.; Ovádi, J.; Sippl, W.; Jung, M. Chemically Induced Degradation of Sirtuin 2 (Sirt2) by a Proteolysis Targeting Chimera (PROTAC) Based on Sirtuin Rearranging Ligands (SirReals). *J. Med. Chem.* **2018**, *61* (2), 482–491. https://doi.org/10.1021/acs.jmedchem.6b01872.

(130) Wu, Q.-J.; Zhang, T.-N.; Chen, H.-H.; Yu, X.-F.; Lv, J.-L.; Liu, Y.-Y.; Liu, Y.-S.; Zheng, G.; Zhao, J.-Q.; Wei, Y.-F.; Guo, J.-Y.; Liu, F.-H.; Chang, Q.; Zhang, Y.-X.; Liu, C.-G.; Zhao, Y.-H. The Sirtuin Family in Health and Disease. *Sig Transduct Target Ther* **2022**, *7* (1), 1–74. https://doi.org/10.1038/s41392-022-01257-8.

(131) Filippakopoulos, P.; Qi, J.; Picaud, S.; Shen, Y.; Smith, W. B.; Fedorov, O.; Morse, E. M.; Keates, T.; Hickman, T. T.; Felletar, I.; Philpott, M.; Munro, S.; McKeown, M. R.; Wang, Y.; Christie, A. L.; West, N.; Cameron, M. J.; Schwartz, B.; Heightman, T. D.; La Thangue, N.; French, C. A.; Wiest, O.; Kung, A. L.; Knapp, S.; Bradner, J. E. Selective Inhibition of BET Bromodomains. *Nature* **2010**, *468* (7327), 1067–1073. https://doi.org/10.1038/nature09504.

(132) Wurz, R. P.; Dellamaggiore, K.; Dou, H.; Javier, N.; Lo, M.-C.; McCarter, J. D.; Mohl, D.; Sastri, C.; Lipford, J. R.; Cee, V. J. A "Click Chemistry Platform" for the Rapid Synthesis of Bispecific Molecules for Inducing Protein Degradation. *J. Med. Chem.* **2018**, *61* (2), 453–461. https://doi.org/10.1021/acs.jmedchem.6b01781.

(133) Reynders, M.; Trauner, D. Optical Control of Targeted Protein Degradation. *Cell Chemical Biology* **2021**, *28* (7), 969–986. https://doi.org/10.1016/j.chembiol.2021.05.010.

(134) Li, W.; Elhassan, R. M.; Fang, H.; Hou, X. Photopharmacology-Based Small-Molecule Proteolysis Targeting Chimeras: Optical Control of Protein Degradation. *Future Medicinal Chemistry* **2020**, *12* (22), 1991–1993. https://doi.org/10.4155/fmc-2020-0210.

(135) Bléger, D.; Schwarz, J.; Brouwer, A. M.; Hecht, S. O-Fluoroazobenzenes as Readily Synthesized Photoswitches Offering Nearly Quantitative Two-Way Isomerization with Visible Light. *J. Am. Chem. Soc.* **2012**, *134* (51), 20597–20600. https://doi.org/10.1021/ja310323y.

(136) Pfaff, P.; Samarasinghe, K. T. G.; Crews, C. M.; Carreira, E. M. Reversible Spatiotemporal Control of Induced Protein Degradation by Bistable PhotoPROTACs. *ACS Cent. Sci.* **2019**, *5* (10), 1682–1690. https://doi.org/10.1021/acscentsci.9b00713.

(137) Kleiger, G.; Mayor, T. Perilous Journey: A Tour of the Ubiquitin–Proteasome System. *Trends in Cell Biology* **2014**, *24* (6), 352–359. https://doi.org/10.1016/j.tcb.2013.12.003.

(138) Fisher, S. L.; Phillips, A. J. Targeted Protein Degradation and the Enzymology of Degraders. *Current Opinion in Chemical Biology* **2018**, *44*, 47–55. https://doi.org/10.1016/j.cbpa.2018.05.004.

(139) Steinebach, C.; Ng, Y. L. D.; Sosič, I.; Lee, C.-S.; Chen, S.; Lindner, S.; Vu, L. P.; Bricelj, A.; Haschemi, R.; Monschke, M.; Steinwarz, E.; Wagner, K. G.; Bendas, G.; Luo, J.; Gütschow, M.; Krönke, J. Systematic Exploration of Different E3 Ubiquitin Ligases: An Approach towards Potent and Selective CDK6 Degraders. *Chem. Sci.* **2020**, *11* (13), 3474–3486. https://doi.org/10.1039/D0SC00167H.

(140) Liu, X.; Kalogeropulou, A. F.; Domingos, S.; Makukhin, N.; Nirujogi, R. S.; Singh, F.; Shpiro, N.; Saalfrank, A.; Sammler, E.; Ganley, I. G.; Moreira, R.; Alessi, D. R.; Ciulli, A. Discovery of XL01126: A Potent, Fast, Cooperative, Selective, Orally Bioavailable, and Blood–Brain Barrier Penetrant PROTAC Degrader of Leucine-Rich Repeat Kinase 2. *J. Am. Chem. Soc.* **2022**, *144* (37), 16930–16952. https://doi.org/10.1021/jacs.2c05499.

(141) Dwyer, Z.; Rudyk, C.; Thompson, A.; Farmer, K.; Fenner, B.; Fortin, T.; Derksen, A.; Sun, H.; Hayley, S.; CLINT (Canadian LRRK2 in inflammation team). Leucine-Rich Repeat Kinase-2 (LRRK2) Modulates Microglial Phenotype and Dopaminergic Neurodegeneration. *Neurobiol Aging* **2020**, *91*, 45–55. https://doi.org/10.1016/j.neurobiolaging.2020.02.017.

(142) Tong, B.; Spradlin, J. N.; Novaes, L. F. T.; Zhang, E.; Hu, X.; Moeller, M.; Brittain, S. M.; McGregor, L. M.; McKenna, J. M.; Tallarico, J. A.; Schirle, M.; Maimone, T. J.; Nomura, D. K. A Nimbolide-Based Kinase Degrader Preferentially Degrades Oncogenic BCR-ABL. *ACS Chem. Biol.* **2020**, *15* (7), 1788–1794. https://doi.org/10.1021/acschembio.0c00348.

(143) Henning, N. J.; Manford, A. G.; Spradlin, J. N.; Brittain, S. M.; Zhang, E.; McKenna, J. M.; Tallarico, J. A.; Schirle, M.; Rape, M.; Nomura, D. K. Discovery of a Covalent FEM1B Recruiter for Targeted Protein Degradation Applications. *J. Am. Chem. Soc.* **2022**, *144* (2), 701–708. https://doi.org/10.1021/jacs.1c03980.

(144) Zhang, X.; Crowley, V. M.; Wucherpfennig, T. G.; Dix, M. M.; Cravatt, B. F. Electrophilic PROTACs That Degrade Nuclear Proteins by Engaging DCAF16. *Nat Chem Biol* **2019**, *15* (7), 737–746. https://doi.org/10.1038/s41589-019-0279-5.

(145) Zhang, X.; Luukkonen, L. M.; Eissler, C. L.; Crowley, V. M.; Yamashita, Y.; Schafroth, M. A.; Kikuchi, S.; Weinstein, D. S.; Symons, K. T.; Nordin, B. E.; Rodriguez, J. L.; Wucherpfennig, T. G.; Bauer, L. G.; Dix, M. M.; Stamos, D.; Kinsella, T. M.; Simon, G. M.; Baltgalvis, K. A.; Cravatt, B. F. DCAF11 Supports Targeted Protein Degradation by

Electrophilic Proteolysis-Targeting Chimeras. *J. Am. Chem. Soc.* **2021**, *143* (13), 5141–5149. https://doi.org/10.1021/jacs.1c00990.

(146) Zoppi, V.; Hughes, S. J.; Maniaci, C.; Testa, A.; Gmaschitz, T.; Wieshofer, C.; Koegl, M.; Riching, K. M.; Daniels, D. L.; Spallarossa, A.; Ciulli, A. Iterative Design and Optimization of Initially Inactive Proteolysis Targeting Chimeras (PROTACs) Identify VZ185 as a Potent, Fast, and Selective von Hippel–Lindau (VHL) Based Dual Degrader Probe of BRD9 and BRD7. *J. Med. Chem.* **2019**, *62* (2), 699–726. https://doi.org/10.1021/acs.jmedchem.8b01413.

(147) Schapira, M.; Calabrese, M. F.; Bullock, A. N.; Crews, C. M. Targeted Protein Degradation: Expanding the Toolbox. *Nat Rev Drug Discov* **2019**, *18* (12), 949–963. https://doi.org/10.1038/s41573-019-0047-y.

(148) Liu, Q. Y.; Lei, J. X.; Sikorska, M.; Liu, R. A Novel Brain-Enriched E3 Ubiquitin Ligase RNF182 Is up Regulated in the Brains of Alzheimer's Patients and Targets ATP6V0C for Degradation. *Molecular Neurodegeneration* **2008**, *3* (1), 4. https://doi.org/10.1186/1750-1326-3-4.

(149) Menon, S.; Goldfarb, D.; Ho, C. T.; Cloer, E. W.; Boyer, N. P.; Hardie, C.; Bock, A. J.; Johnson, E. C.; Anil, J.; Major, M. B.; Gupton, S. L. The TRIM9/TRIM67 Neuronal Interactome Reveals Novel Activators of Morphogenesis. *Mol Biol Cell* **2021**, *32* (4), 314–330. https://doi.org/10.1091/mbc.E20-10-0622.

(150) Kumanomidou, T.; Nishio, K.; Takagi, K.; Nakagawa, T.; Suzuki, A.; Yamane, T.; Tokunaga, F.; Iwai, K.; Murakami, A.; Yoshida, Y.; Tanaka, K.; Mizushima, T. The Structural Differences between a Glycoprotein Specific F-Box Protein Fbs1 and Its Homologous Protein FBG3. *PLOS ONE* **2015**, *10* (10), e0140366. https://doi.org/10.1371/journal.pone.0140366.

(151) Glenn, K. A.; Nelson, R. F.; Wen, H. M.; Mallinger, A. J.; Paulson, H. L. Diversity in Tissue Expression, Substrate Binding, and SCF Complex Formation for a Lectin Family of Ubiquitin Ligases *. *Journal of Biological Chemistry* **2008**, *283* (19), 12717–12729. https://doi.org/10.1074/jbc.M709508200.

(152) Qu, L.; Li, S.; Ji, L.; Luo, S.; Ding, M.; Yin, F.; Wang, C.; Luo, H.; Lu, D.; Liu, X.; Peng, W.; Kong, L.; Wang, X. Discovery of PT-65 as a Highly Potent and Selective Proteolysis-Targeting Chimera Degrader of GSK3 for Treating Alzheimer's Disease. *Eur J Med Chem* **2021**, *226*, 113889. https://doi.org/10.1016/j.ejmech.2021.113889.

(153) Jiang, X.; Zhou, J.; Wang, Y.; Liu, X.; Xu, K.; Xu, J.; Feng, F.; Sun, H. PROTACs Suppression of GSK-3β, a Crucial Kinase in Neurodegenerative Diseases. *European Journal of Medicinal Chemistry* **2021**, *210*, 112949. https://doi.org/10.1016/j.ejmech.2020.112949.

(154) Guardigni, M.; Pruccoli, L.; Santini, A.; Simone, A. D.; Bersani, M.; Spyrakis, F.; Frabetti, F.; Uliassi, E.; Andrisano, V.; Pagliarani, B.; Fernández-Gómez, P.; Palomo, V.; Bolognesi, M. L.; Tarozzi, A.; Milelli, A. PROTAC-Induced Glycogen Synthase Kinase 3β Degradation as a Potential Therapeutic Strategy for Alzheimer's Disease. *ACS Chem. Neurosci.* **2023**, *14* (11), 1963–1970. https://doi.org/10.1021/acschemneuro.3c00096.

(155) Qi, M.; Zhong, H.; Cheng, Z.; Chen, S.; Xiao, H.; Shang, J.; Chen, L.; Sun, J. Discovery of NAFLD-Improving Agents by Promoting the Degradation of Keap1. *J. Med. Chem.* **2023**, *66* (13), 9184–9200. https://doi.org/10.1021/acs.jmedchem.3c00822.

(156) Nakata, M.; Maeda, T. PubChemQC B3LYP/6-31G*//PM6 Data Set: The Electronic Structures of 86 Million Molecules Using B3LYP/6-31G* Calculations. *J. Chem. Inf. Model.* **2023**, *63* (18), 5734–5754. https://doi.org/10.1021/acs.jcim.3c00899.

CHAPTER IV

COPPER-CATALYZED CYANATION REACTION IN WATER

Given the expertise and contribution of our team in Strasbourg in metal catalyzed reactions in aqueous medium, with the development of efficient catalytic systems for Buchwald-Hartwig and Ullmann reactions, in this chapter, we will describe the optimization of the synthesis protocol for cyanation reaction in water.

1. INTRODUCTION

Aromatic nitriles are important building blocks in many pharmaceuticals, herbicides, natural products, and dyes.[1] The compact nature of the nitrile fragment (eight times smaller than a methyl group), along with its ability to accept hydrogen bonds, its metabolic stability in in vivo studies, and its use as a hydroxyl or carbonyl isostere, have made it an important functional group in medicinal chemistry research.[2] Currently, there are over 30 approved drugs and 20 others in advanced clinical trials that contain one or more nitrile substituents. These bioactive molecules containing nitriles have been shown to treat a wide range of conditions, such as depression, breast cancer, HIV, and Parkinson's disease, etc. (Figure 70).

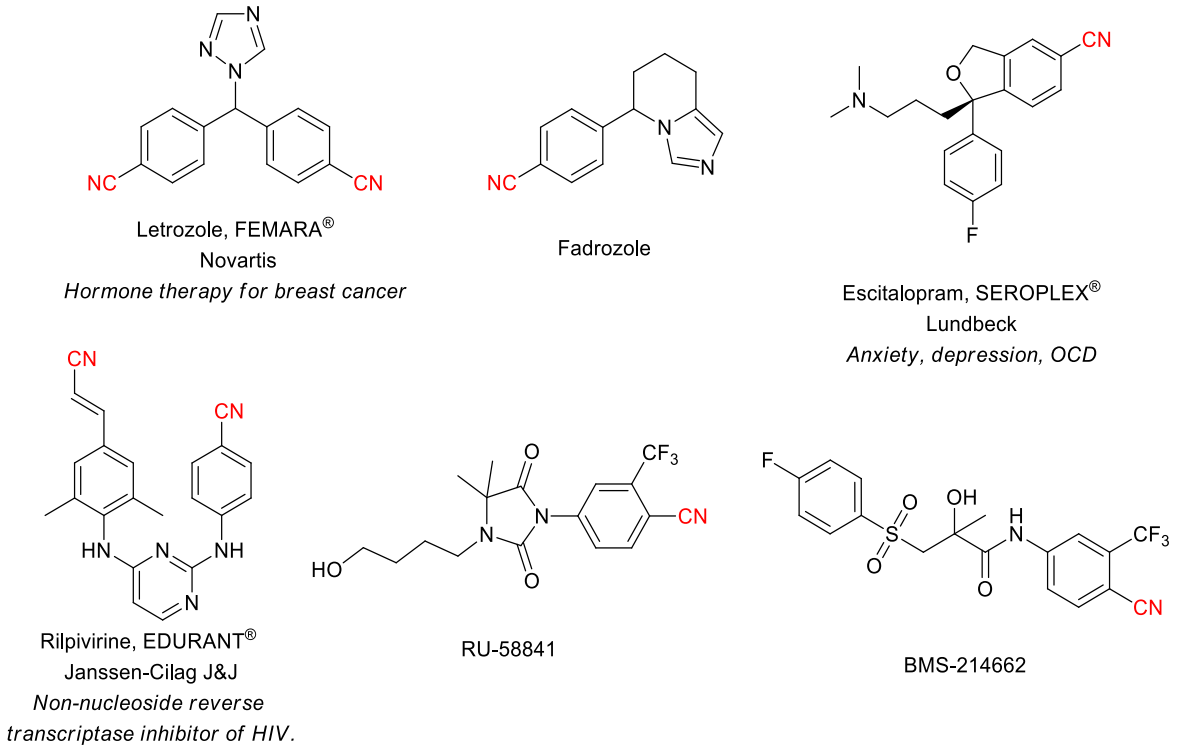

Figure 70. Examples of active substances whose structure includes a cyano group and associated therapeutic applications.

Aromatic nitriles are among the most versatile synthetic intermediates due to their easy conversion into benzoic acid/ester, aldehyde, ketone, amide, amidine, imidoester, amine, and a

variety of heterocycles (thiazoles, oxazolidinones, thiazoles, tetrazoles), etc.[3] Consequently, the development of efficient and practical routes for the synthesis of aromatic nitriles has been a long-standing objective.

Typically, the introduction of a cyanide group is the most direct and versatile route for the preparation of functionalized benzonitriles. For over a century, the synthesis of benzonitriles through stoichiometric methods using copper cyanide (CuCN) has been prevalent in both laboratory and industrial settings (Scheme 57). Among these methods, the Rosenmund-von Braun reaction from aryl halides,[4,5] and the diazotization of aniline derivatives combined with the Sandmeyer reaction,[6] were the most popular. However, due to the production of (over)stoichiometric amounts of metallic waste, these processes no longer meet current criteria for sustainable synthesis. For the production of benzonitriles on a ton scale, the method of choice in the industry is ammoxidation,[7] wherein corresponding toluene derivatives react with oxygen and ammonia at high temperatures (300-550°C) in the presence of fixed-bed heterogeneous catalysts. However, the lack of functional group tolerance and extreme reaction conditions make this method less suitable for the synthesis of functionalized benzonitriles.

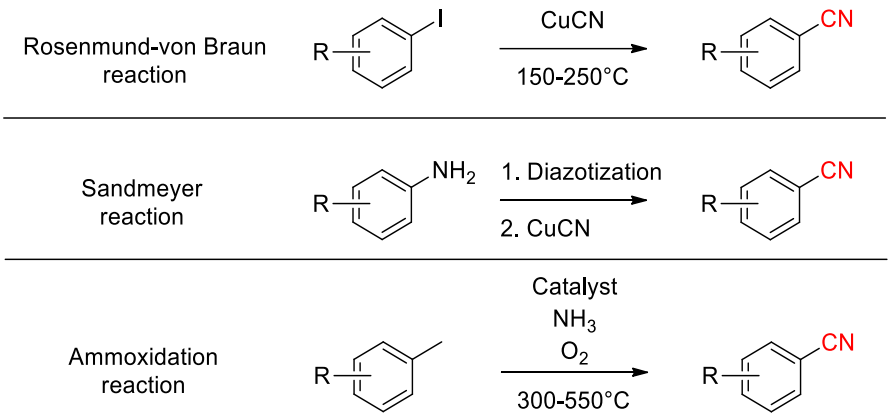

Scheme 57. Traditional preparation of benzonitriles.

The past four decades have witnessed significant advances in the field of transition metal-catalyzed cyanation of aryl halides. Most of these efforts have been based on catalytic procedures involving palladium or copper. The success of these processes relies on the implementation of several key strategies designed to address catalyst deactivation phenomena observed in these reactions.

1.1. Palladium-Catalyzed Cyanation Reactions

1.1.1. Use of Metal Cyanides

In the early 1970s, the introduction and development of transition metal-catalyzed carbon-carbon coupling reactions radically changed the method of functionalizing arenes. Indeed, catalysis allows for the limitation of waste quantities and presents a significant interest for the production of large quantities of cyanated compounds. In this context, the first palladium-catalyzed cyanation of aryl halides was introduced in 1973 by Takagi et al., reacting aryl bromides and iodides with potassium cyanide as the cyanating agent.[8] This reaction involved palladium(II) acetate in DMF at 140-150°C for 2-12 hours. Later on, various sources of CN have been explored using KCN,[9] NaCN,[10] TMSCN,[11] $Zn(CN)_2$[12] as cyanation agents. Since then, palladium-catalyzed cyanation procedures, mainly using $Zn(CN)_2$, have found numerous applications in the pharmaceutical industry (Figure 71) due to their favorable characteristics: better functional group tolerance, greater catalyst stability to air and moisture, and especially superior catalytic activity compared to copper.

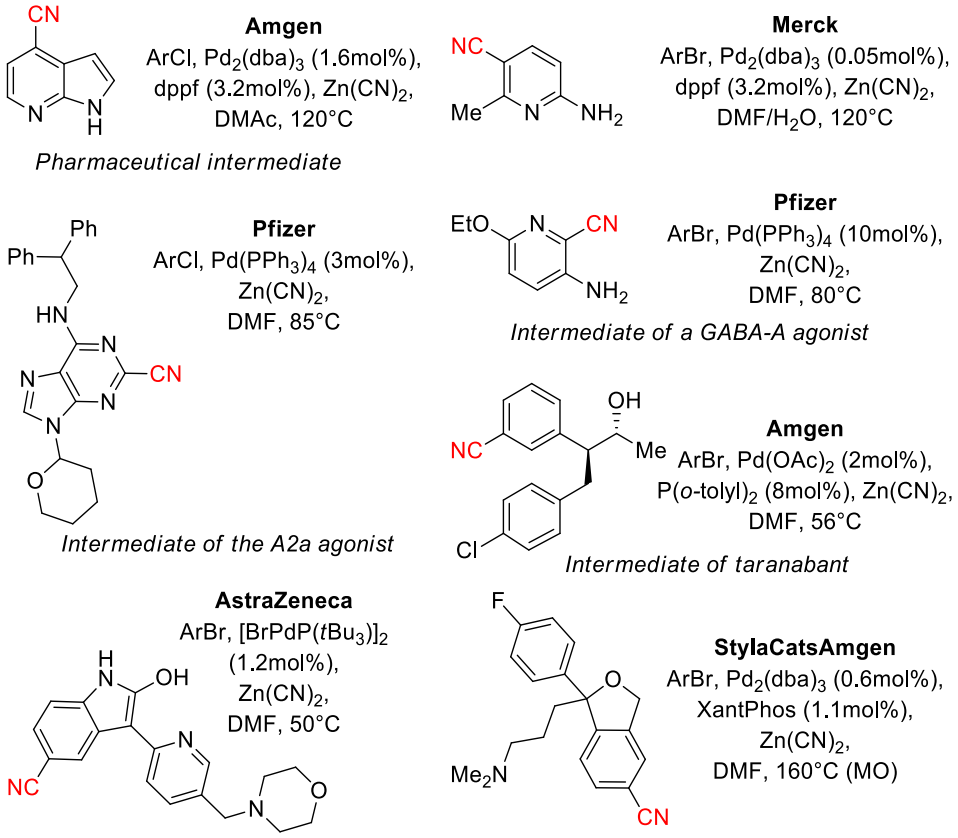

Figure 71. Examples of palladium-catalyzed cyanation in the pharmaceutical industry.

This cyanation reaction using $Zn(CN)_2$ was extended in the early 2000s to aryl chlorides by employing $Pd_2(dba)_3$ (2 mol%), dppf (4 mol%), and a reducing agent, Zn (12 mol%) in DMA (Scheme 58).[13] Besides the harsh heating conditions (120-150°C), another drawback of this procedure is the use of an almost stoichiometric amount (0.6 eq.) of zinc cyanide, resulting in the formation of heavy metal salt wastes.

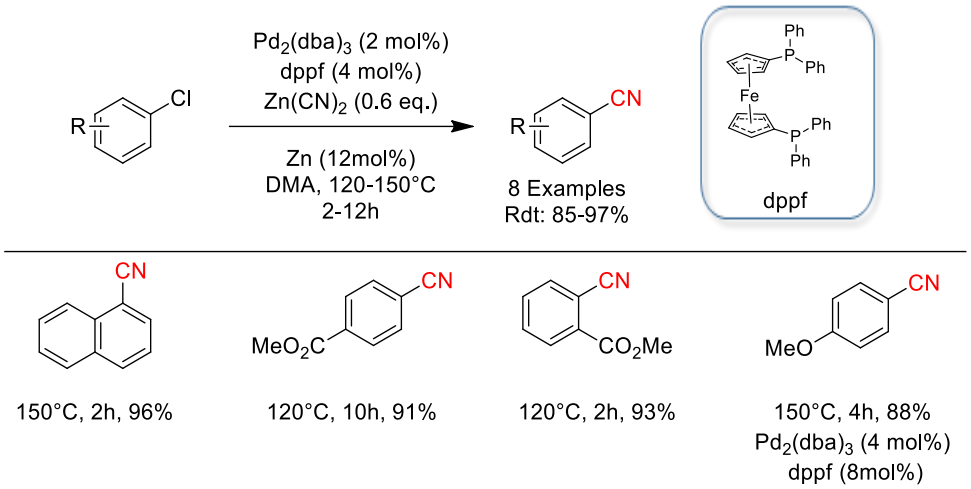

Scheme 58. Cyanation of aryl chlorides using $Pd_2(dba)_3$ and dppf in the presence of zinc.

Thus, milder conditions (≈ 95°C) were achieved in 2007 by employing the racemic ligand di-tert-butylphosphino-1,10-binapththyl by Buchwald.[14] With these new conditions, electron-rich aryl chlorides led to an efficient cyanation reaction in dimethylacetamide (DMAc) (Scheme 59).

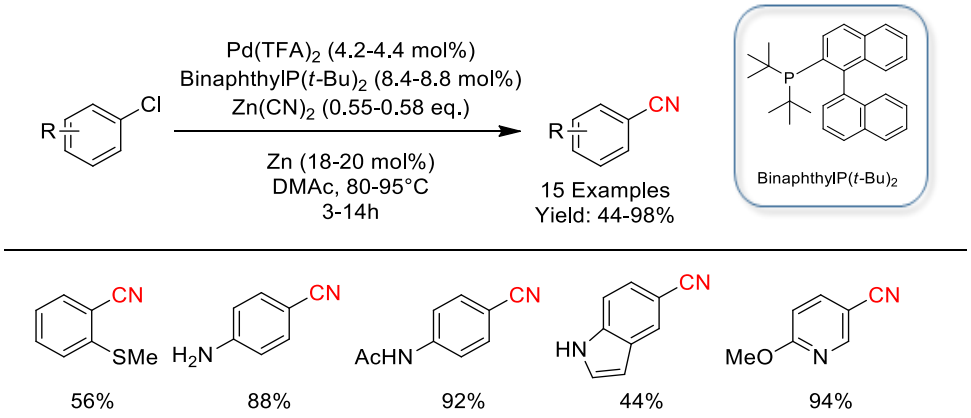

Scheme 59. Cyanation of aryl chlorides using $Pd(TFA)_2$ and binaphthylP(t-Bu)$_2$ in the presence of Zn as a reducing agent.

However, the most challenging obstacle to overcome in metal-catalyzed cyanation is likely the high affinity of cyanide for the metal center, leading to the formation of stable cyanide complexes in the catalytic system, thereby terminating the catalytic cycle.[15] Thus, a plethora of efforts has been deployed to address this issue. For example, the use of aprotic solvents to reduce the solubility of cyanide ions, or controlling the dosage of the cyanide source (cyanohydrin, TMSCN),[16] the addition of a co-catalyst (TMEDA, DABCO, or MDP),[17] or inorganic additives (Zn or Zn salts)[18] to regenerate an active catalyst. Other developments include microwave activation[19] or the study of new catalytic systems.[20]

In particular, in 2015, Buchwald et al. described a general and efficient cyanation at low temperature (25 - 40°C) of aromatic chlorides, bromides, or triflates catalyzed by palladium with $Zn(CN)_2$ in aqueous medium (Scheme 60). This reaction does not require vigorous drying of glassware or grinding of $Zn(CN)_2$. This method has been extended to various 5 or 6-membered heterocyclic halides/triflates, allowing for the synthesis of natural product derivatives and the advanced-stage synthesis of the non-nucleoside reverse transcriptase inhibitor, lersivirine.[21]

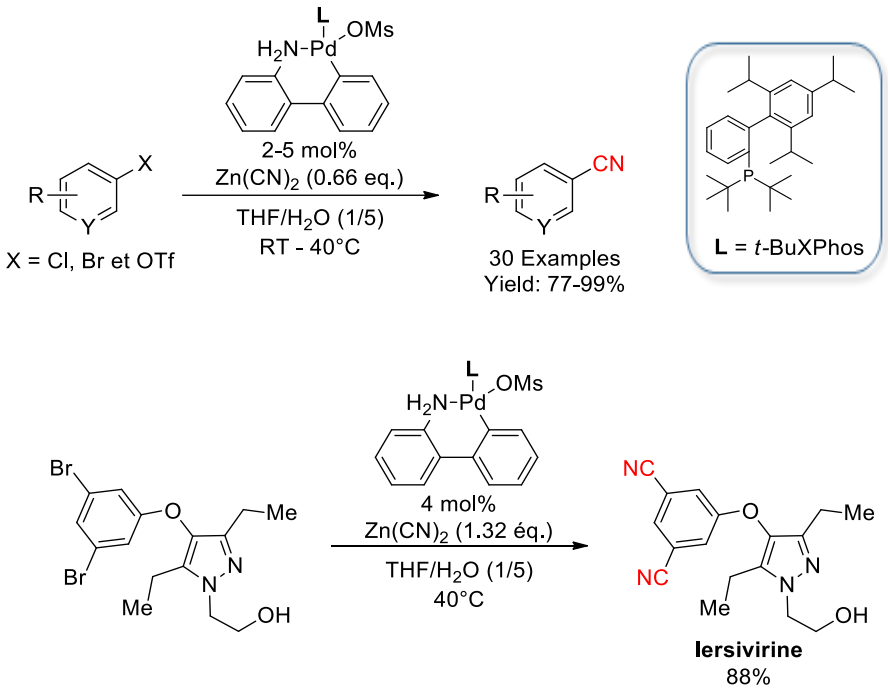

Scheme 60. Palladium-catalyzed cyanation at low temperature in aqueous medium using $Zn(CN)_2$.

1.1.2. Use of potassium ferrocyanide(II)

The easy release of cyanide anion is responsible for the high toxicity of the majority of cyanide sources, which poses significant safety issues for both academic and industrial

applications. To address these safety concerns, $K_4[Fe(CN)_6]$, a non-toxic food additive, was introduced by the groups of Beller[22] and Weissman[23] as a reagent for palladium-catalyzed cyanation of aryl halides. $K_4[Fe(CN)_6]$ is commercially available on a ton scale, it is inexpensive, non-toxic, and can release its six CN molecules for cyanation.

The cyanide ion is strongly bound to potassium ferrocyanide(II), justifying a substantially slow release of cyanide ions which can be beneficial to reduce catalyst deactivation.[24] However, harsh conditions (120-160°C) are necessary for most metal-catalyzed cyanations with $K_4[Fe(CN)_6]$ as the cyanide source. This paradox can be attributed to the difficult release of cyanide from $K_4Fe(CN)_6$ below 120°C. Recently, Grossman and Gelman demonstrated that this drawback could be overcome by developing a new "trans-spanning" palladium complex capable of promoting the cyanation of aryl bromides under milder conditions (Scheme 61).[25]

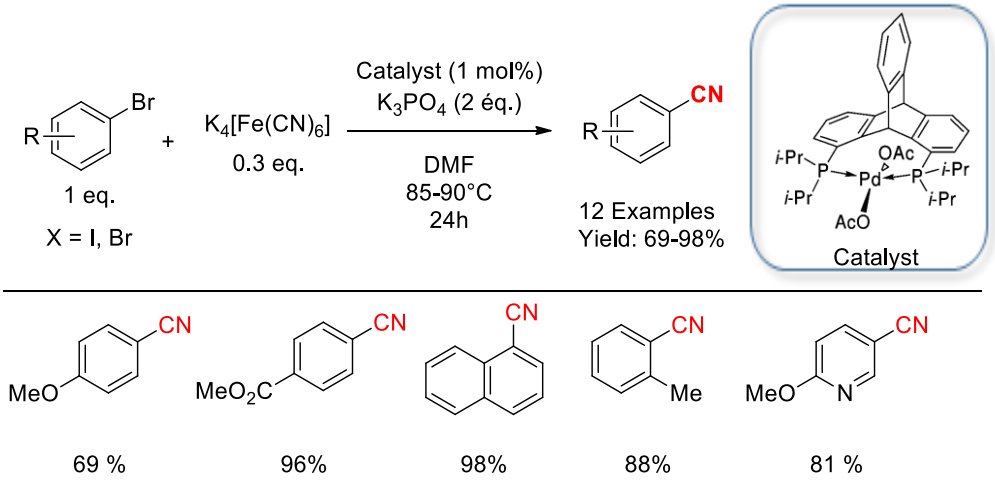

Scheme 61. Development of a "trans-spanning" palladium complex for the cyanation of aryl bromides using $K_4[Fe(CN)_6]$.

More recently, Kwong et al. employed $Pd(OAc)_2$/CM-phos complexes (ratio 1:4) to catalyze the cyanation of aromatic mesylates or tosylates under mild conditions (80°C) in water or in a water-butanol mixture (Scheme 62a).[26] Water is beneficial for Pd-catalyzed cyanation, likely due to its ability to enhance the solubility of the hydrated reagent $K_4[Fe(CN)_6]$. This reaction was subsequently efficiently extended to aryl chlorides using the same catalytic system but by reducing the ligand loading (ratio 1:2) and temperature (70°C) (Scheme 62b).[27]

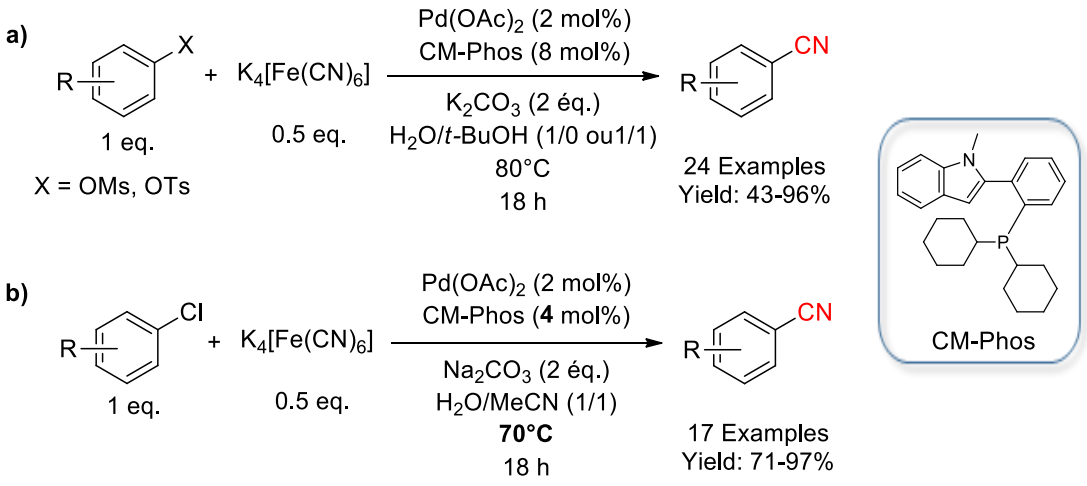

Scheme 62. Palladium-catalyzed cyanation in aqueous medium of aryl mesylates/tosylates (OMs/OTs) and aryl chlorides in the presence of $Pd(OAc)_2$/CM-Phos.

Despite these advancements, most of the cited examples suffer from the use of phosphine ligands that are either not readily available or sensitive to air. To address these issues, Hong Liu et al. developed a rapid synthesis of aryl bromide cyanation using Pd tetrakis to perform the reaction under mild conditions using a readily available palladium catalyst without additional additives.[28] The use of 1,8-diazabicyclo[5.4.0]undec-7-ene (DBU) helped enhance the release of cyanide ion as a promoter and reduce Pd inactivation as a co-catalyst (Scheme 63). This catalytic system $Pd(PPh_3)_4$/DBU proved effective for the synthesis of aminopyridine intermediates functionalized with a nitrile as pharmaceutically relevant intermediates.

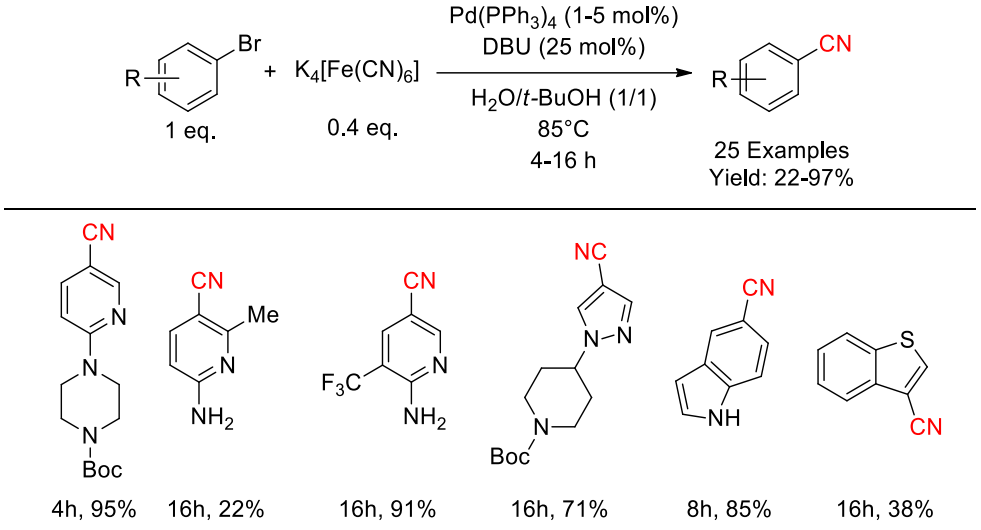

Scheme 63. Rapid cyanation mediated by Pd/DBU of aryl/heteroaryl bromides with $K_4[Fe(CN)_6]$.

1.2. Copper-Catalyzed Cyanation Reactions

1.2.1. Use of Metal Cyanides

It is clear that for a long time palladium complexes have largely dominated as catalysts in cyanation reactions because they tolerate a greater variety of functional groups and are more reactive than copper catalysts. Nevertheless, palladium is less abundant than copper and often requires the use of phosphine ligands, which are known for their high costs and toxicities. Therefore, the use of less expensive catalysts is of constant interest, and thus, copper-catalyzed reaction remains the most used method in the industry.

Interestingly, the addition of copper salts has been found beneficial in some palladium-catalyzed cyanation reactions. Indeed, during the preparation of a tricyclic intermediate bearing a nitrile group intended for obtaining a drug candidate against ergot alkaloid, Anderson et al. developed a cyanation procedure with a co-catalysis involving palladium and copper.[29] They achieved this transformation using a combination of $Pd(PPh_3)_4$ and CuI with NaCN in acetonitrile (MeCN) at 65°C in a short reaction time (0.5h). This protocol could be extended to aryl/heteroaryl bromides and triflates as well as vinyl bromides. Optimization studies showed that the cooperation between copper and palladium was essential for the reaction. However, the reaction provided poor yields when NaCN was used in solubilizing solvents (MeOH, DMF) and also when the highly soluble cyanation agent, Bu_4NCN, was used. In contrast, the reaction gave good yields in solvents such as EtCN, THF, and EtOAc, in which alkali metal cyanides are only slightly soluble. These results are consistent with the studies by Takagi cited previously, which revealed the formation of catalytically inert palladium cyanide complexes due to the presence of an excess of cyanide ion in solubilizing solvents.[8] A plausible cyanation mechanism involves the initial oxidative addition of an aryl halide to Pd(0) followed by subsequent transmetalation and reductive elimination to form an aryl nitrile, regenerating Pd(0). The copper co-catalyst reacts with NaCN to form a covalently bound cyanide species that interacts with the Pd(II) intermediate in the transmetalation step, thus regenerating the CuX co-catalyst (Scheme 64).

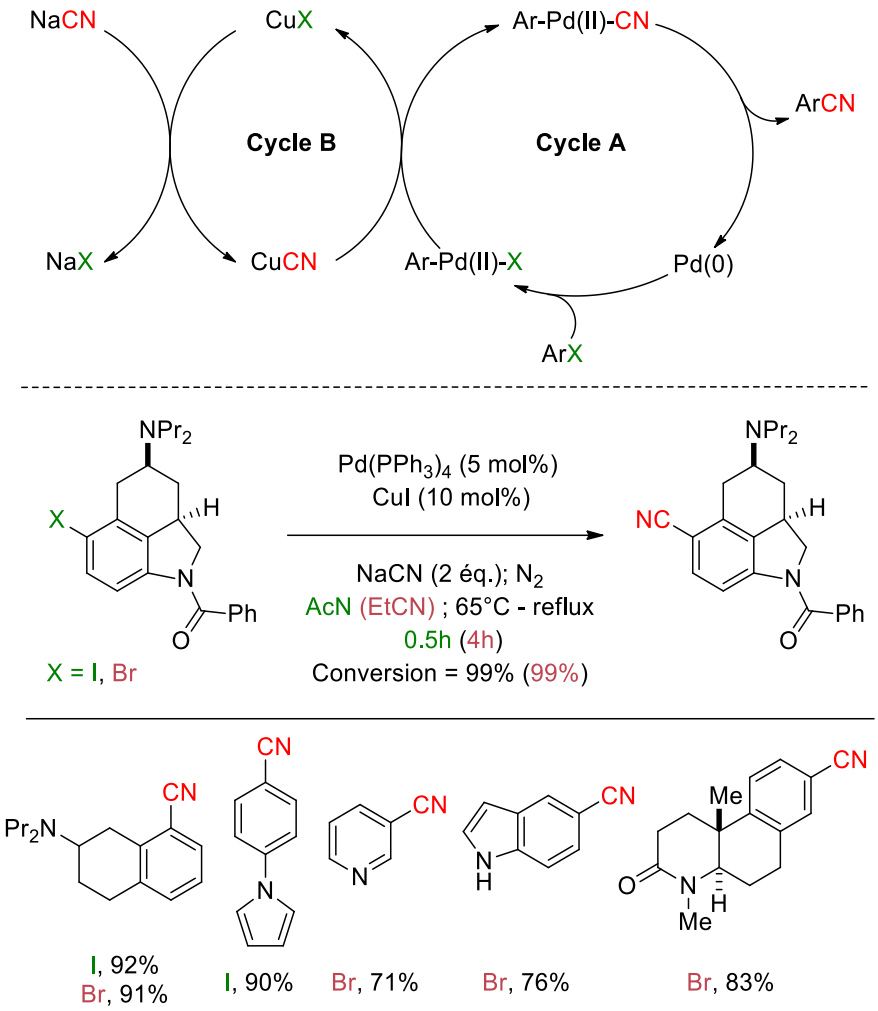

Scheme 64. Cyanation reaction with Pd/Cu and associated mechanism.

1.2.2. Activation of the catalytic system by introduction of ligands

However, it was in 2003 that significant progress was made when Buchwald and colleagues reported the development of an aryl bromide cyanation reaction based on the use of sub-stoichiometric amounts of copper (10 mol% copper(I) iodide) in the absence of additional metal catalyst. In this work, Buchwald demonstrated that the accelerating effect of 1,2-diamine ligands could be exploited in the copper-catalyzed halide exchange domino cyanation of aryl/heteroaryl bromides.[30] They particularly highlighted that CuI worked much better than CuBr or CuCN in the cyanation of aryl bromides. This result can be explained by the copper-catalyzed conversion of aryl bromide to aryl iodide, which is more reactive in the cyanation reaction. Thus, by adding KI (20 mol%), the efficiency of this cyanation reaction was improved. This reaction requires heating in toluene at 110-130°C and led to a wide range of substrates

with high tolerance of functional groups. Thus, the cyanation of a broad set of heterocycle bromides was achieved with very good yields, as illustrated in Scheme 65.

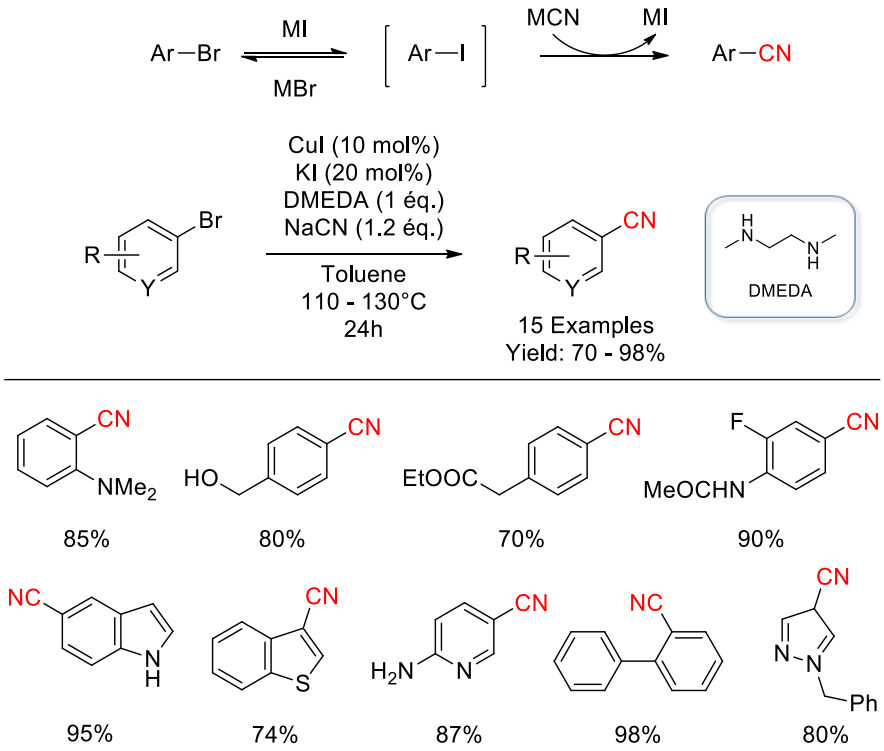

Scheme 65. Cyanation by halide exchange domino of aromatic bromides and use of DMEDA as an additive.

In 2005, Taillefer and colleagues described the cyanation of aryl iodides/bromides catalyzed by CuI/1,10-phenanthroline (phen) in DMF at 110°C.[31] The reaction of PhI with KCN in the presence of catalytic amounts of CuI and phen in DMF led to benzonitrile with a yield of 94% (Scheme 66a), while the same reaction starting from PhBr failed. However, the reaction of PhBr conducted with KI instead of KCN under identical conditions led to the rapid formation of iodobenzene with good yields. Furthermore, kinetic studies conducted by reacting an equimolar mixture of PhBr and KI or PhI and KBr both yielded a mixture of identical composition (20% PhBr and 80% PhI), indicating the existence of thermodynamic equilibrium between PhI and PhBr (Scheme 66b). Not surprisingly, their initial strategy of converting PhBr to PhCN under in situ conditions via the formation of PhI failed, probably due to the well-known deactivation effect of the catalyst by cyanide ion in polar solvents.

However, the delayed introduction of KCN into the reaction medium after sufficient formation of PhI (6h time) led to the desired product. Similarly, by adopting the acetone cyanohydrin/tributylamine combination instead of KCN, benzonitrile was obtained with a yield

of 80% (Scheme 66c). This protocol shows good yield but requires an extended reaction time (48-70h) and 50 mol% of KI. Subsequently, Beller and his collaborators also demonstrated the potential of acetone cyanohydrin for CuI-catalyzed cyanation of aryl bromides in the presence of Na_2CO_3 in o-xylene at 150°C.[32]

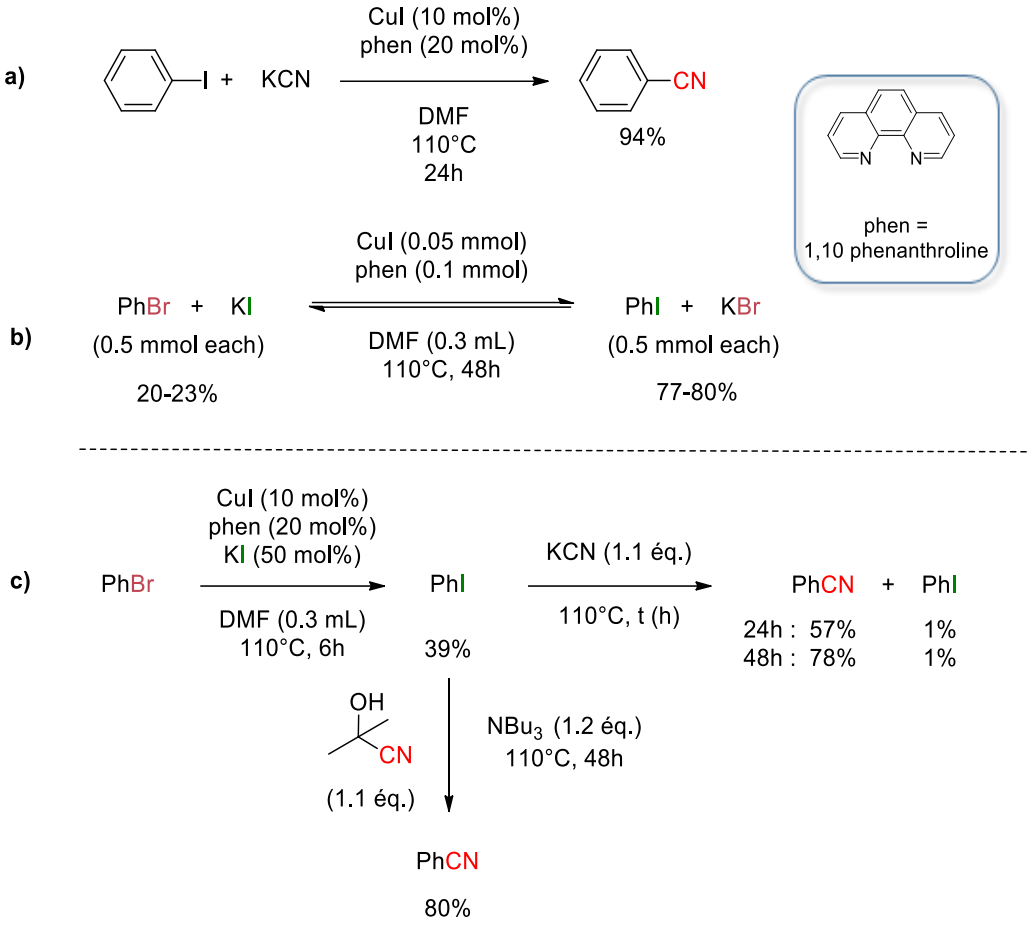

Scheme 66. Copper-catalyzed halide exchange reaction and cyanation in the presence of 1-10 phenanthroline.

CuCN can serve both as a copper catalyst and as a cyanation reagent, as in the Rosenmund-von Braun reaction, which nonetheless occurs at a high temperature (150-250°C). Ding et al. reported in 2008 a CuCN-mediated cyanation promoted by the ligand L-proline.[33] The reaction takes place in DMF at a lower temperature (80°C for ArI and 120°C for ArBr), but still requires the use of 2 equiv. of CuCN and 1 equiv. of L-proline (Scheme 67).

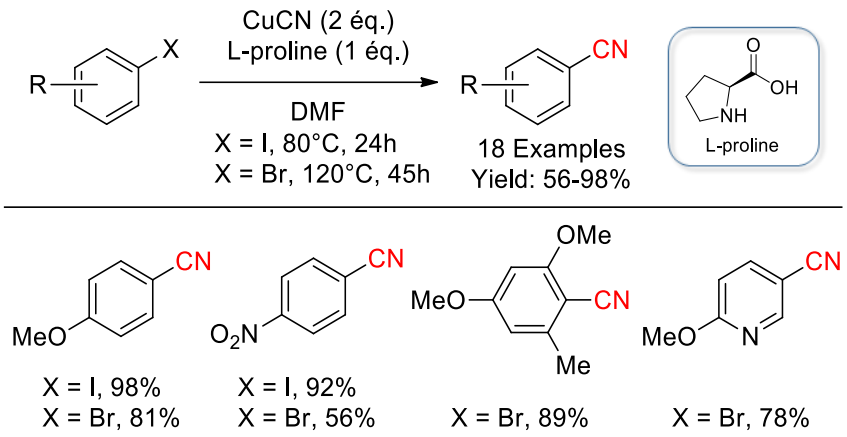

Scheme 67. Cyanation catalyzed by CuCN in the presence of L-proline.

Finally, a methodology for microwave-assisted domino catalysis catalyzed by copper was developed in 2013 for the cyanation of aryl chlorides.[34] The aryl chloride is first converted to aryl iodide through halogen exchange, and the obtained aryl iodide is then transformed into aryl nitrile. Various aryl chlorides were converted to aryl nitriles with satisfactory yields using KCN in the presence of a catalytic amount of CuI and N,N'-cyclohexane-1,2-diamine in acetonitrile at 200°C (1 to 2 hours). However, the reaction is sensitive to steric hindrance (as observed with 2-chlorotoluene, where a trace amount of product is formed), but 1-chloronaphthalene was converted to the corresponding product with a yield of 44%. The same copper/ligand system served as a multifunctional catalyst for both steps of the simultaneous catalytic process, as illustrated in Scheme 68.

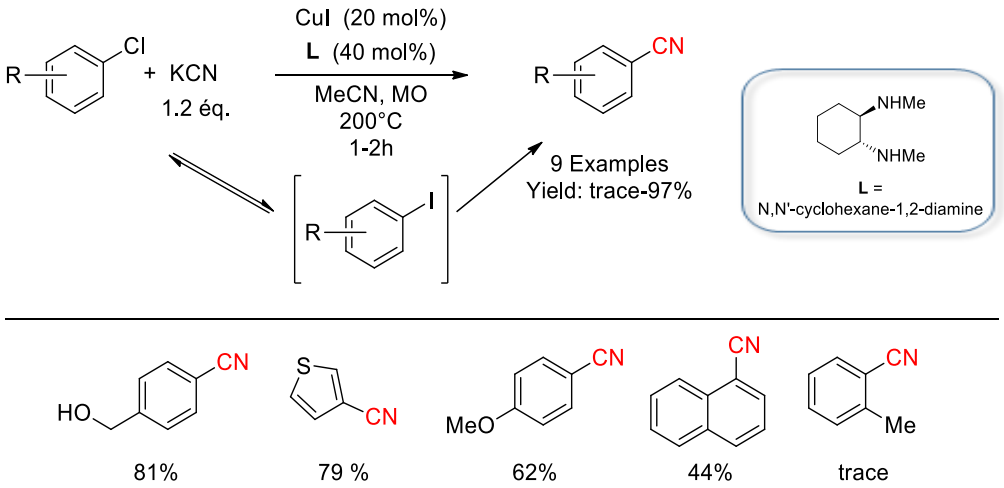

Scheme 68. Cyanation catalyzed by CuI of aryl chlorides assisted by microwave irradiation in the presence of N,N'-cyclohexane-1,2-diamine.

In 2013, Vantikommu et al. developed an efficient pathway for the synthesis of benzonitriles from aryl iodides through cyanation catalyzed by copper oxide nanoparticles.[35] Moreover, this reaction can be coupled with a copper-catalyzed [2+3] cycloaddition to generate 5-phenyl-1H-tetrazoles in a unique sequential process without isolating the cyanated intermediate. This new coupling reaction highlights the potential of CuO nanoparticles as efficient and recyclable coupling agents. However, this reaction requires heating at 100°C in DMF (Scheme 69).

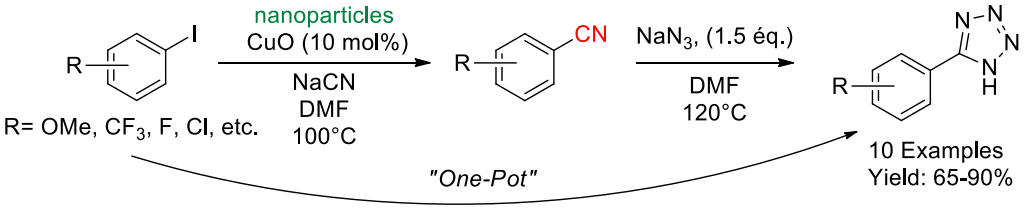

Erro! Indicador não definido.

Scheme 69. Sequential synthesis of 5-substituted 1H-tetrazoles from aryl iodides via CuO nanoparticle-catalyzed cyanation.

Finally, very recently, the first photoinduced Cu(I)-catalyzed cyanation of aromatic halides has been reported.[36] CuI(bisimine-CN) was used as an efficient photocatalytic material at room temperature using acetonitrile as the solvent (Scheme 70). The catalytic system tolerates a wide range of aromatic halides with exceptional functional group tolerance, including primary amines and carboxylic acids. Mechanistic studies indicate that the reaction proceeds via single-electron transfer (SET) between the aryl halide and an excited cyanide Cu(I) catalytic intermediate.

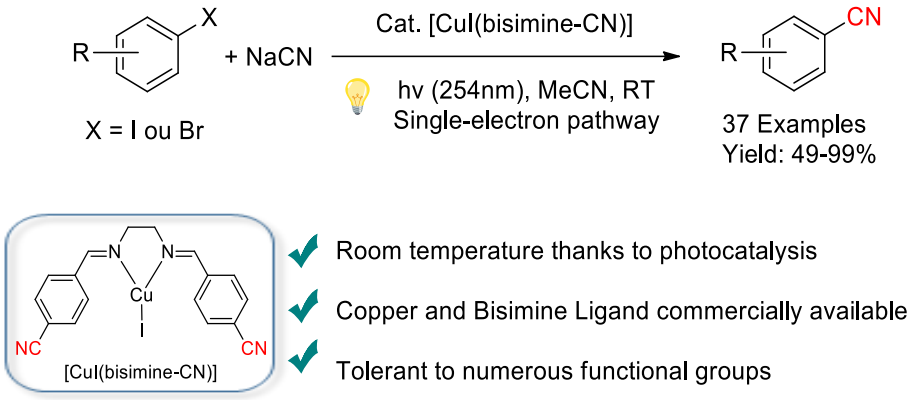

Scheme 70. Photoinduced cyanation at room temperature by CuI(bisimine-CN) hν.

1.2.3. Use of Potassium Ferrocyanide(II) in Copper-Catalyzed Cyanation Reactions

It was in 2005 that Beller combined the advantages of inexpensive copper catalysts with potassium ferrocyanide(II) ($K_4[Fe(CN)_6]$) as a non-toxic cyanide source to improve and extend the tools for cyanation of aryl halides.[37] In this regard, the team demonstrated the effectiveness of the $Cu(BF_4)_2 \cdot 6H_2O$ / N,N-dimethylethylenediamine (DMEDA) pair as a catalyst and ligand, respectively, for the cyanation of variously substituted aryl bromides (Scheme 71) with good yields. This new procedure represents a more environmentally friendly and less hazardous protocol by using non-toxic $K_4[Fe(CN)_6$ instead of highly toxic alkali cyanides. However, this reaction still requires high temperatures (140°C) in dimethylacetamide (DMAc) and an expensive ligand, DMEDA, in stoichiometric amounts.

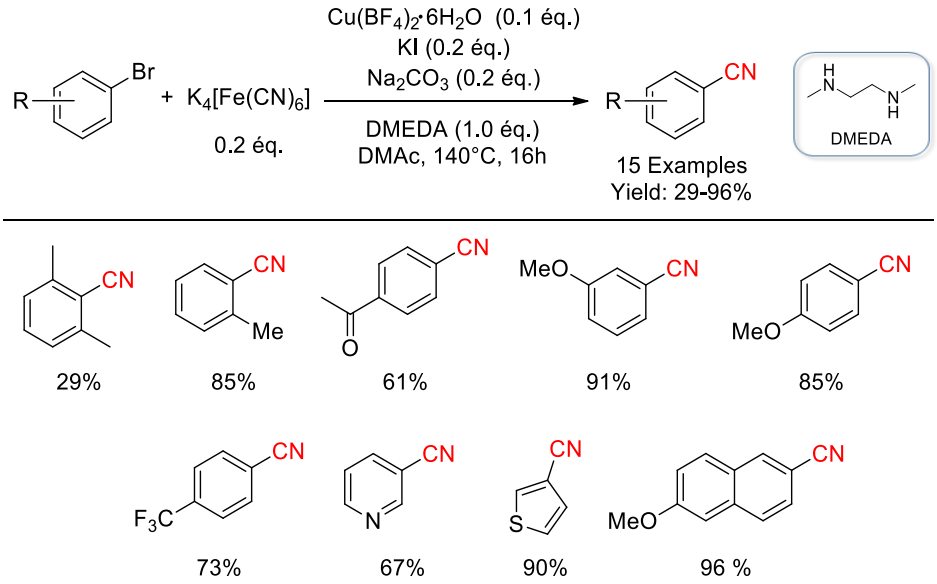

Scheme 71. Scope of the $Cu(BF_4)_2$-Catalyzed Cyanation Reaction of Aryl Bromides with DMEDA.

Subsequently, only a few other efficient catalytic systems have been developed, such as N,N'-dimethylethylenediamine (DMEDA)/CuI, ethylenediamine (EDA)/$Cu(OAc)_2$-H_2O,[38] 1,10-phenanthroline/CuI,[39] 1-alkylimidazoles/CuI,[40] 1,2-bis(5-tetrazolyl)benzene/@CuI.[41] However, all the procedures used required the use of almost stoichiometric amounts of ligands and high boiling point organic solvents (DMAc, NMP, DMF, o-xylene, etc.). Furthermore, the reactions were quite slow and required high temperatures.

From an environmental and economic perspective, the use of ligand-free or catalytic amount catalytic systems, and the replacement of organic solvents with water, remain highly desirable goals. In this context, Chen et al. demonstrated the application of microwaves for the

cyanation of aryl halides in the presence of $Cu(OAc)_2$ (10 mol%).[42] Their study showed that the presence of an equimolar amount of a phase transfer agent, TBAB, is essential for the success of the reaction.

Subsequently, Leadbeater reported a similar methodology for the cyanation of aryl iodides with $K_4[Fe(CN)_6]$ using water and a mixture of tetraethylene glycol as a solvent (Scheme 72).[43] However, under the same reaction conditions, the cyanation of aryl bromides did not succeed; it requires the use of a significant amount of DMEDA, a rather expensive ligand compared to the copper salt, to first carry out the Finkelstein reaction (ArBr→ArI).[44] This characteristic is therefore less attractive for large-scale applications.

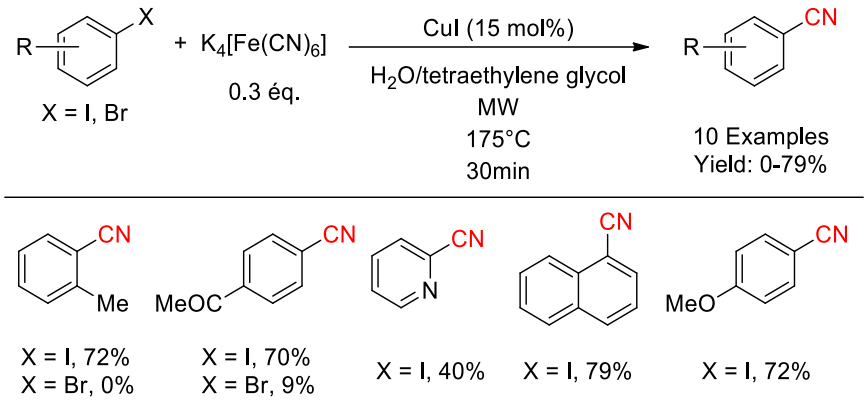

Scheme 72. Cyanation of aryl halides catalyzed by CuI with $K_4[Fe(CN)_6]$ in aqueous medium using microwave heating.

Some poly(ethylene glycols) (PEG 3400 to PEG-10000) have also been used as solvents for the cyanation of aryl halides using $K_4[Fe(CN)_6]$ and a catalytic amount of CuI (20 mol%). These reactions are carried out using sonochemical methods at 80°C, a temperature at which the polymer melts. The conversion of the substrate to the cyano compound depends on the viscosity of the melted PEG and gives the highest substrate conversion for PEG-5600. Increasing the viscosity of the molten mass (which strongly depends on the molecular weight) plays a major role in enhancing the absorption of acoustic energy, thereby allowing more efficient energy transfer to the substrates. Beyond PEG6000, yields decrease and fluctuate, which can be explained by excessive viscosity limiting the diffusion of reactants.

1.2.4. Use of bimetallic nanoparticles

Nowadays, bimetallic nanoparticles are known as efficient catalysts for various catalytic reactions. The synergistic combination of two metals can enhance their catalytic performance, activity, selectivity, and stability compared to corresponding monometallic catalysts.[45] Additionally, the reduction in bimetallic catalyst loading compared to the individual use of metals in reactions such as the Sonogashira reaction, where a second metal is usually required, is another advantage of bimetallic catalysts.

Ferrite nanoparticles are important magnetic materials used for various applications such as drug delivery, magneto-thermal therapy, microwave-absorbing sensors, and as catalysts for many organic transformations. In recent years, the application of copper ferrite nanoparticles as recyclable catalysts in various copper-catalyzed organic reactions has gained increasing interest. Particularly in 2015, palladium was supported on copper ferrite nanoparticles modified with (3-aminopropyl) triethoxysilane. The resulting heterogeneous catalyst is an efficient and recyclable catalyst in the cyanation of aryl iodides and bromides with a low palladium loading (Scheme 73).[46] It is more effective compared to palladium nanoparticles supported by Fe_3O_4, or homogeneous nanoparticles of $Pd(OAc)_2$, CuI, $CuCl_2$, Fe_3O_4, and $CuFe_2O_4$. It can be concluded that the synergistic effect between palladium and copper species is responsible for the observed reactivity. The catalyst showed good recyclability using an external magnet and could be used four times without a significant decrease in catalytic activity. However, this reaction requires high temperatures (120°C) in DMF.

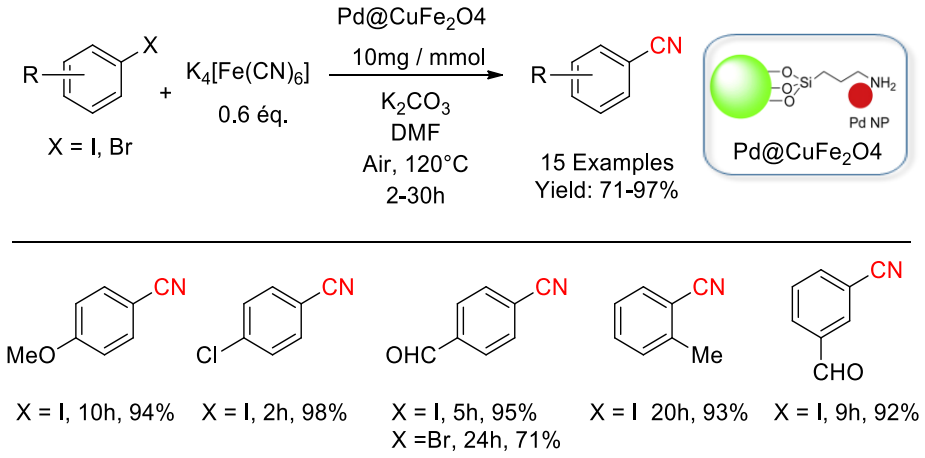

Scheme 73. Synergistic Effect of Palladium and Copper Nanoparticles for the Cyanation of Aryl Halides with $K_4[Fe(CN)_6]$.

1.2.5. Non-Metallic Organic Sources of Cyanide

In recent years, particular attention has been given to the use of non-metallic organic sources of cyanide. A few examples are provided below:

Hu, Cheng, et al. utilized a stoichiometric amount of $Cu(OAc)_2$ in combination with TMEDA (20 mol%) to generate CN from $(NH_4)HCO_3$ and DMF at a reaction temperature of 150°C (Scheme 74). The protocol tolerated the use of aryl iodides bearing various sensitive functional groups (OBn, COOMe, $N(Bu)_2$, NHAc, OH, COMe, etc.). However, cyanation of aryl bromides yielded moderate yields.[47]

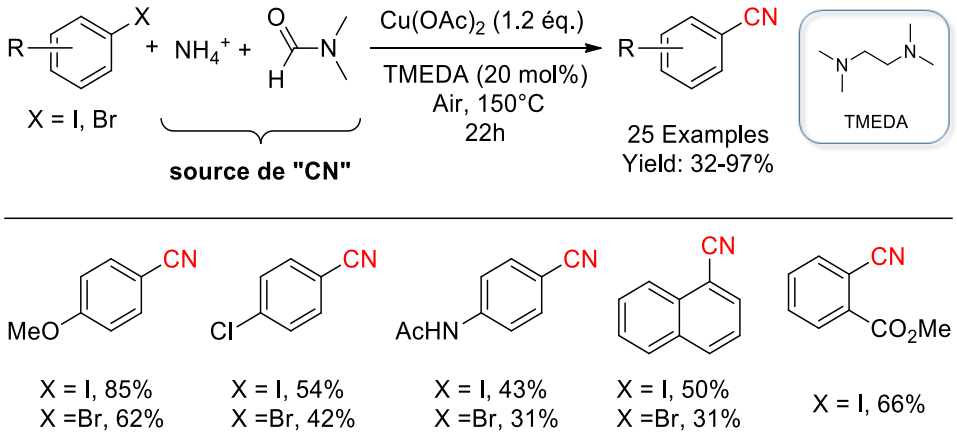

Scheme 74. DMF and $(NH_4)HCO_3$ as a combined source of "CN" for the cyanation of aryl halides.

In 2015, Pawar and Chang succeeded in making this catalytic process ($Cu(NO_3)_2 \cdot 3H_2O$, 20 mol%) work, although two equivalents of Ag_2CO_3 are required as an oxidant to maintain the efficient catalytic cycle (Scheme 75).[48] This procedure, like before, requires high temperatures and is effective starting from electron-rich iodinated aryls. For electron-deficient iodinated heteroaryls, this strategy required the use of an additive, 2-aminopyridine (20 mol%).

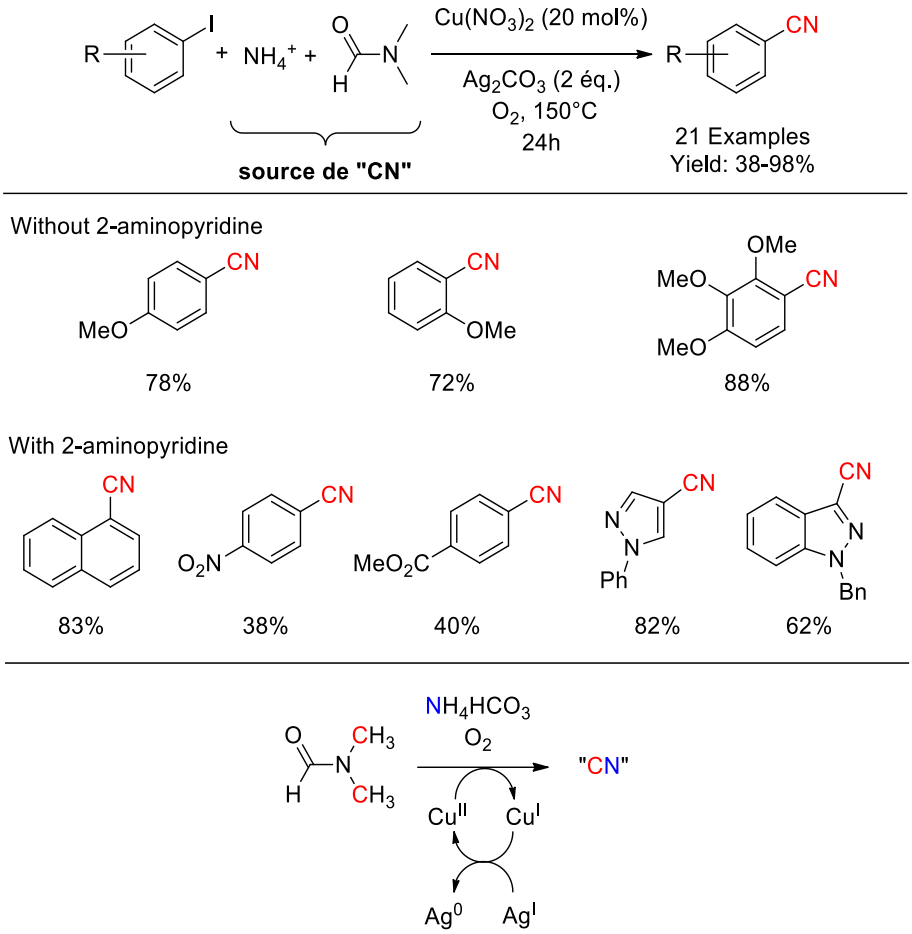

Scheme 75. Catalytic cyanation of aryl iodides using DMF and $(NH_4)HCO_3$ as a combined cyanide source.

Finally, aryl nitriles were prepared by cyanation of aryl iodides and bromides using DMF as the sole cyanide substitute (Scheme 76). Copper nitrate/acetic acid effectively facilitated the synthesis of aryl nitriles from aryl bromides or iodides using DMF under aerobic conditions and TBHP (*tert*-butyl hydroperoxide) as the oxidant.[49] However, the reaction requires equimolar amounts of copper, high temperatures (140°C), and long reaction time (48h).

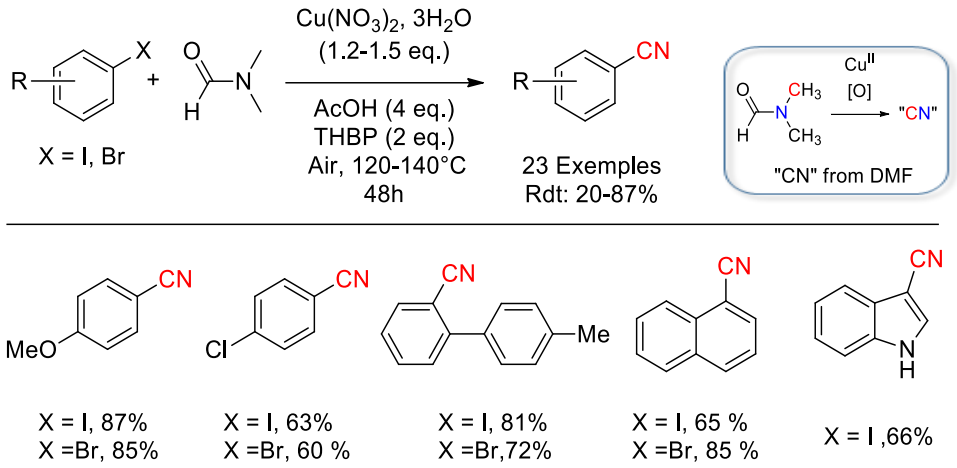

Scheme 76. DMF as a Sole Cyanide Substitute: Scope of Cyanation Reaction.

1.2.6. Use of DMSO and Urea as Cyanide Substitute

Chen et al. exploited a combination of DMSO and urea to generate the "CN" fraction in the cyanation of aryl iodides catalyzed by CuF_2 in the presence of phenanthroline (phen), (Scheme 77).[50] Studies conducted with ^{13}C-labeled DMSO confirmed that the carbon in the cyano group originated from DMSO. Importantly, a temperature of 150°C and 3 equiv. of Li_2CO_3 are required for the reaction.

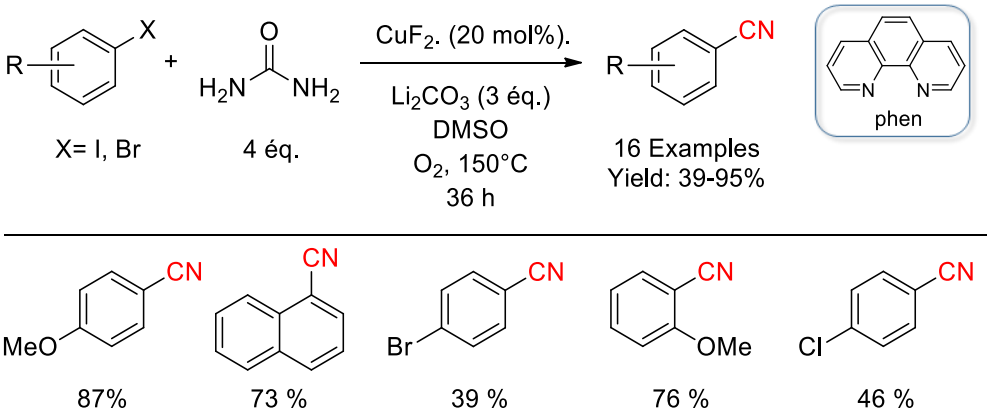

Scheme 77. DMSO as Cyanide Substitute for CuF_2/phen Catalyzed Cyanation.

1.2.7. Use of Malonitrile as Cyanide Substitute

In 2012, Zhou et al. utilized malonitrile as a cyanide substitute. In the presence of $Cu(OAc)_2$, phen, NaO*t*Bu, and KF in DMF at 120°C, iodinated aryls were cyanated with yields

ranging from 40-86%. They successfully isolated the reactive species from their reaction medium: [Cu(phen)$(CN)_2$], which is obtained via copper-catalyzed cleavage of C-CN bonds assisted by KF.[51] This complex, when reacted with 4-iodoanisole in the presence of NaOt-Bu in DMF at 120°C, yielded the corresponding cyanation product with a yield of 86% (Scheme 78).

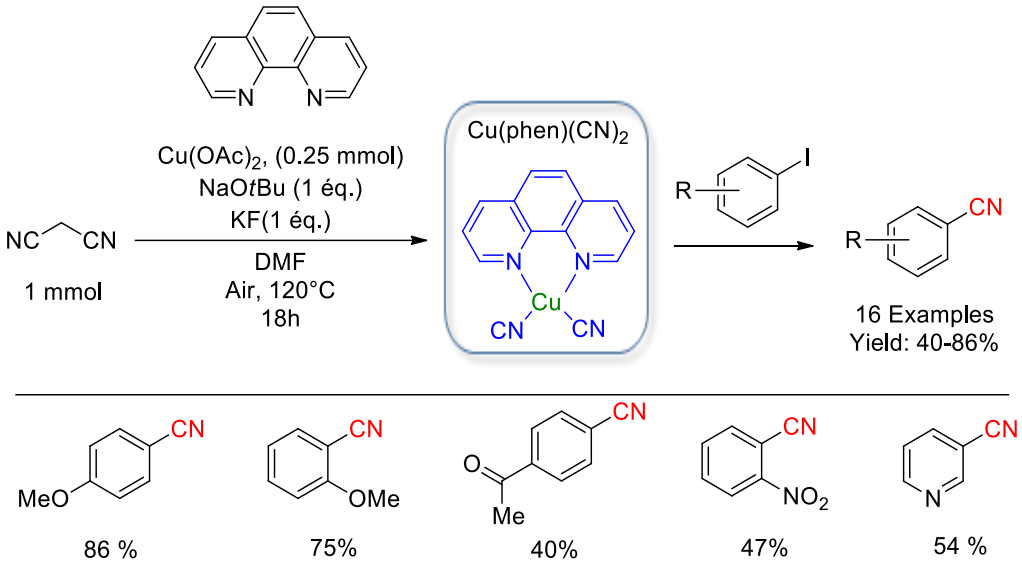

Scheme 78. Cyanation Catalyzed by [Cu(phen)$(CN)_2$] from Aryl Iodides in DMF.

Alternatives have been described more recently. In particular, Zhang and Huang demonstrated the scope of various α-cyanoacetate derivatives as CN precursors for cyanation reactions under aerobic conditions in NMP at 130°C.[52] In this work, $AgNO_3$ was used as an additive to enhance the activity of the Cu_2O/PPh_3 catalytic system. In a separate study, Qi et al. utilized ethyl (ethoxymethylene)cyanoacetate as a CN source for the cyanation of aryl iodides in the presence of CuI and THBP under aerobic conditions.[53] Unlike the two previous examples, this reaction requires an equimolar amount of copper at 130°C for 24 hours.

1.2.8. Use of benzonitrile or equivalent as a cyanide substitute

In 2013, Wang et al. reported the Cu_2O-mediated cyanation of aryl iodides/bromides in stoichiometric amounts in DMF at 130°C, using benzyl cyanide as the cyanation agent.[54] The procedure yielded good yields with aryl iodides, while aryl bromides provided moderate yields under the same conditions. Sensitive functional groups such as NO_2, COMe, COOMe, NMe_2, NHAc, and NH_2 were tolerated (Scheme 79). Subsequently, Chin et al. expanded the scope of

this reaction by using benzoyl cyanide as the cyanation agent for aryl bromides with $Cu(OAc)_2$ (10 mol%) /DMEDA (1 eq.) and KI.[55]

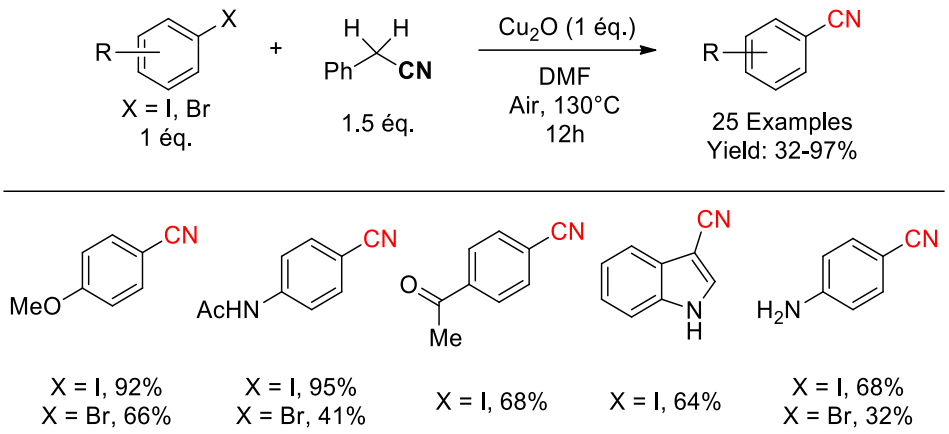

Scheme 79. Scope of the cyanation reaction with Cu_2O using benzonitrile as a cyanide substitute.

1.3. Palladium-catalyzed cyanation in micellar medium

The work of Lipshutz since 2008 has demonstrated the interest of catalysis in micellar medium, particularly palladium catalysis. He has recently published a palladium-catalyzed cyanation reaction.[56] His team carried out the cyanation reaction in an aqueous micellar medium as illustrated in Scheme 80. The use of a low-cost surfactant, Brij-30, in the presence of $Zn(CN)_2$, a low loading of palladacycle P8 (5000 ppm), and polymethylhydrosiloxane (PMHS) led to highly complex and functionalized substrates under mild conditions (45°-65°C). The presence of PMHS is essential for this reaction and likely assists in reducing Pd(II) to Pd(0), thereby minimizing the impact of excess cyanide and/or oxygen that may be present in the reaction mixture.

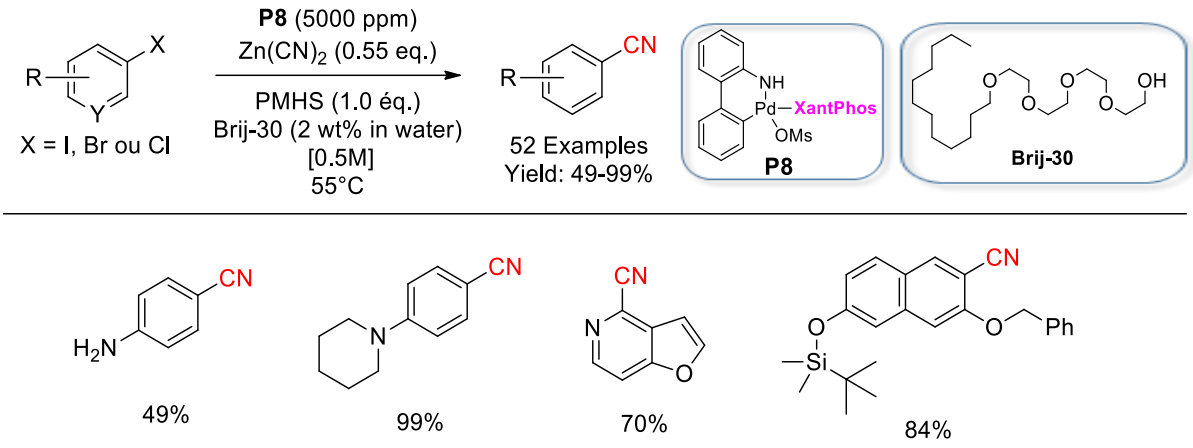

Scheme 80. Palladium-catalyzed cyanation in micellar medium.

1.4. Contribution to Copper-catalyzed Ullmann reaction by the Laboratory for Therapeutic Innovation (LIT)

Our team in the LIT also contributed to the emergence of these reactions in micellar media with palladium-[57] or copper-catalyzed[58] amination reactions. This on the Ullmann reaction has shown a simple, sustainable, efficient, mild, and low-cost protocol for D-glucose-assisted Cu-catalyzed Ullmann reactions in water for amides, carbamates, and nitrogen-containing heterocycles. The reaction was compatible with diverse aryl/heteroaryl iodides, giving highly substituted pyridine, indole or indazole rings. This method offers an attractive alternative to existing protocols, in particular because i) we use a simple and abundant reducant such as D-glucose (D-glc) to facilitate the reduction of Cu(II) to Cu(I) in aqueous media, ii) the reaction, occurs at or near ambient temperature, and iii) it provides the N-arylated products in good to high yields (Scheme 81).[58]

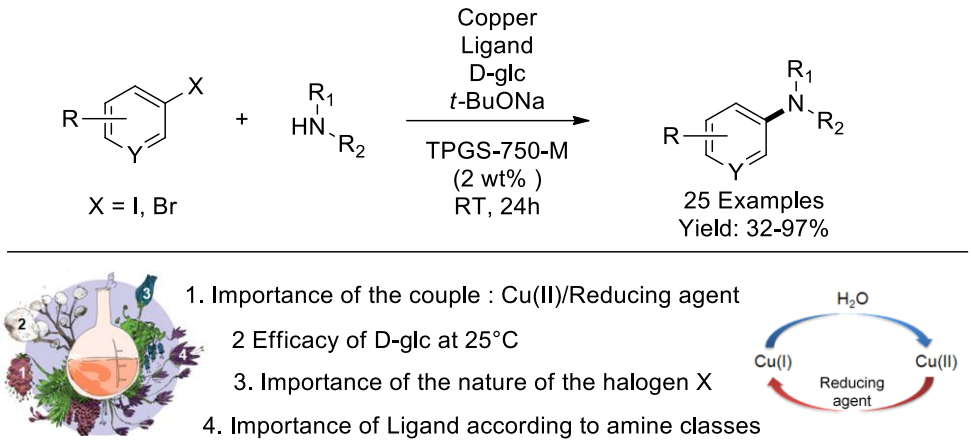

Scheme 81. Optimization and Scope of copper-catalyzed Ullmann-type reaction.[58]

2. OBJECTIVES

2.1. General objective

Various methods for the formation of aromatic nitriles were discussed in the introduction of this chapter. Many conditions have transitioned from ancestral methods using stoichiometric quantities to modern methods using catalytic amounts of transition metals. The sources have also evolved significantly from simple and highly toxic cyanide salts to less hazardous organic sources or those derived from stable complexes. Overall, reaction conditions mostly remain harsh, involving the use of high-boiling solvents at elevated reaction temperatures.

Our goal is to propose an environmentally friendly method for the synthesis of aromatic nitriles. This method should adhere to as many green chemistry criteria as possible, particularly focusing on the use of catalysis, green solvents, mild reaction temperatures, while minimizing the use of non-renewable resources.

2.2. Specific objectives

The aim is to develop a methodology of cyanation reaction in water applicable to industrial conditions.

3. RESULTS AND DICUSSION

The objective of this project is to carry out a cyanation reaction consistent with the principles of green chemistry. Thus, our strategy consisted of adopting the general conditions of the Ullmann-type reaction developed in our group[58] to perform a cyanation reaction in an aqueous medium via copper catalysis in the presence of D-glucose at low temperature.

During Dr. Philippe Steinsoultz's thesis an effective method for the preparation of aromatic nitriles from iodinated aromatics following the principles of green chemistry was developed. To do this, sodium nitroprusside ($Na_2Fe(II)(CN)_5NO$) was chosen as the cyanide donor due to its low toxicity. Starting from 4-iodoanisole used as a model reaction, various parameters were studied to develop a new efficient catalytic system in aqueous medium. This optimization work involved screening a large number of reaction conditions (surfactants, copper sources, nature of the ligand, optimal catalytic loading, base and influence of counter-ions, temperature, concentration, etc.). These experiments allowed us to obtain 4-methoxybenzonitrile with nearly quantitative yield. The reaction is conducted in pure water at ~70°C, using the catalytic system $CuBr_2$/(R,R)-N,N'-dimethyl-1,2-cyclohexanediamine (L_{14}) in a 1:1 ratio, low catalytic loading (5%), and NaOH as a base (Scheme 82). Additionally, these studies highlighted the effectiveness of D-glc as a bio-sourced additive, as the reaction yield drastically decreases in its absence. However, it is worth noting that during this work, reproducibility issues with significant yield fluctuations were encountered, especially in the absence of degassing. This suggests that perhaps not all reaction parameters are fully understood, and further efforts are needed to better understand the reaction mechanism (Scheme 82).

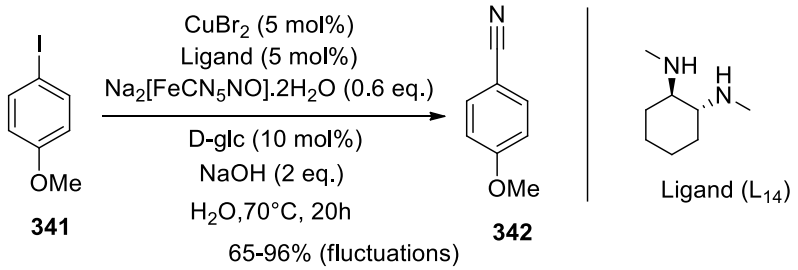

Scheme 82. Cyanation reaction in water.

Therefore, the main objective of this work was to simplify the reaction protocol and reduce or eliminate the reproducibility issues.

3.1. Optimization of the cyanation reaction in aqueous medium

For this reaction, we have used D-glucose as a reducing agent. The presence of this bio-sourced additive has allowed, in the studies on the Ullmann-type reaction, the reduction of inactive copper(II) to an active Cu(I) form. In this work, we sought to determine if the presence of this reducing agent is necessary for our reaction conditions (Table 20). We have shown that in the presence of D-glucose, the product is formed only to the extent of 30% (Table 20, entry 1), while in the absence of this reducing agent the product formation showed a increase in the reaction yield contradicting the previous findings (Table 20, entry 2).

The reduction in reaction time resulted in a 90% conversion and surprisingly the yield for the expected anisonitrile was only 40% (Table 20, entry 3); however, increasing the ratio between the ligand and the metal to 2:1 showed a better profile: 64% of formation of anisonitrile but only 73% of conversion (Table 20, entry 4).

Table 20. Influence of glucose, reaction time and $CuBr_2$/Ligand ratio.

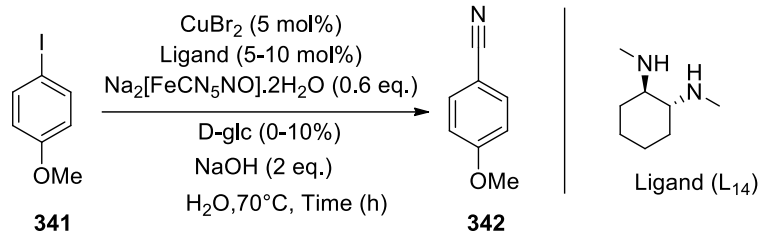

Entry	D-Glc (mol%)[a]	Time (h)	Conversion %[b]	Yield %[b]
1	10	20	54	30
2	0	20	96	59
3	0	10	90	45
4*	0	10	73	64

[a] Reaction conditions: 4-Iodoanisole (1 equiv., 0.42 mmol), $CuBr_2$ (5 mol%), L_{14} (R,R)-N,N'-dimethyl-1,2-cyclohexanediamine (5 mol%), $Na_2[Fe(CN)_5NO]$ (0.6 equiv.), NaOH (2 equiv.), D-Glc (0-100 mol%), H_2O (0.9 M), 70°C, 1200 rpm, 10 - 20h; [b] Conversion and yield determined by HPLC/UV analysis with caffeine as an internal standard.* use of Ligand (L_{14}) (10 mol%).

Nevertheless, the methodology still faces reproducibility issues, with fluctuations in reaction yields. Therefore, aiming to further simplify the reaction procedure we decided 1) to eliminate the D-glc and 2) to prepare properly the the copper pre-catalyst.

3.1.1. Preparation of the pre-catalyst

For the pre-catalyst preparation, we have followed the methodology described by Meek and Ehrhardt.[59] Independent solutions of $CuBr_2.H_2O$ and ligand (**L_{14}**) were prepared in ethanol and then, the metallic solution was slowly added to the ligand solution under stirring, and the reaction mixture was maintained at room temperature overnight. The precipitate formed was filtered to provide complex **C_1** in 85% yield. A small portion of the solid was re-dissolved in methanol and subjected to slow evaporation at low temperature to give blue crystals (Scheme 83C). The product was characterized by x-ray crystallography by the Crystallography Service of the University of Strasbourg. It was observed that one of the bromides is directly linked to the metal while the other acts as a counterion of the complex. Additionally, the presence of a molecule of H_2O was observed (Scheme 83).

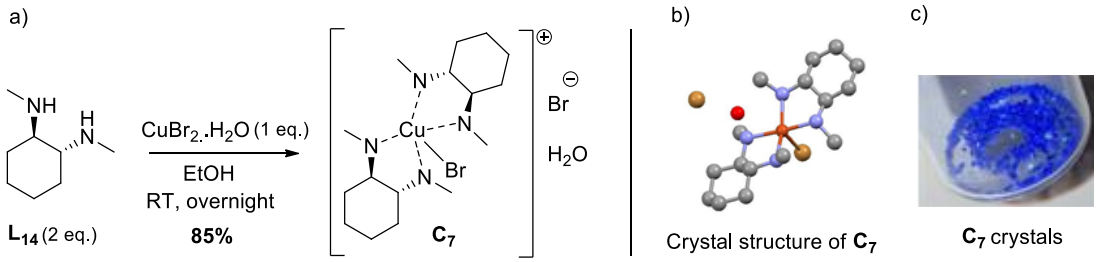

Scheme 83. a) Synthesis of the pre-catalyst; b) Crystal structure of **C_7**; c) **C_7** crystals.

The use of the pre-catalyst enables the simplification of the reaction protocol due to the hygroscopic nature of the ligand and the absence of the need for prior agitation of the ligand with the copper source. In the presence of **C_7** at different reaction times, it was observed that after 1 hour, the reaction yield was only 6% with low conversion of the reagent (10%, Table 21, entry 1). Increasing the reaction time to 4-6 hours showed higher reaction yields and increased reagent conversion of 71% and 85 % respectively (Table 21, entries 2 and 3). When subjected to a 15-hour reaction, complete consumption of the reagent was observed, but a significative reduction in reaction yield (40%) due the more important formation of the amide in the ration of 1/2 by HPLC with the anisonitrile (**342**) (Table 21, entry 4).

Table 21. Influence of pre-catalyst

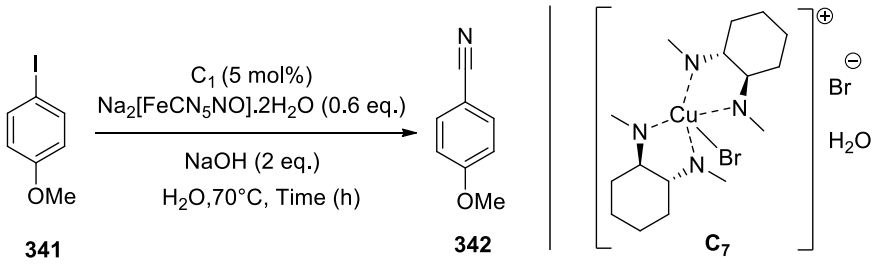

Entry	Time (h)	Conversion %[b]	Yield %[b]
1	1	10	6
2	4	71	63
3	6	85	65
4	15	100	40[c]

[a] Reaction conditions: 4-Iodoanisole (**341**) (1 equiv., 0.42 mmol), C_7 (5 mol%), $Na_2[Fe(CN)_5NO]$ (0.6 equiv.), NaOH (2 equiv.), H_2O (0.9 M), 70°C, 1200 rpm, 1 – 15 h; [b] Conversion and yield determined by HPLC/UV analysis with caffeine as an internal standard. [c] Presence of amide (R.F.= 3.3 min.) (ratio: **342**/**343** (1/1)).

c

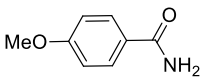

(**343**)

3.1.2. Amount of pre-catalyst and grain size influence: use of mechanochemistry

With the aim of further reducing fluctuations and achieving more homogeneous results, we chose to grind the solids using a mechanochemical reactor. Additionally, we conducted a scan of the ideal pre-catalyst quantity for the reaction (Tabela 22). Maintaining the pre-catalyst quantity at 5 mol% resulted in the preservation of the previously obtained yield of 65% after 6h (Table 22, entry 1). Increasing the catalytic load resulted in an increase in reaction yield (78-85%) and reagent conversion (92-100%), leading to improved outcomes (Table 22, entries 2 and 3).

Table 22. Quantity of pre-catalyst.

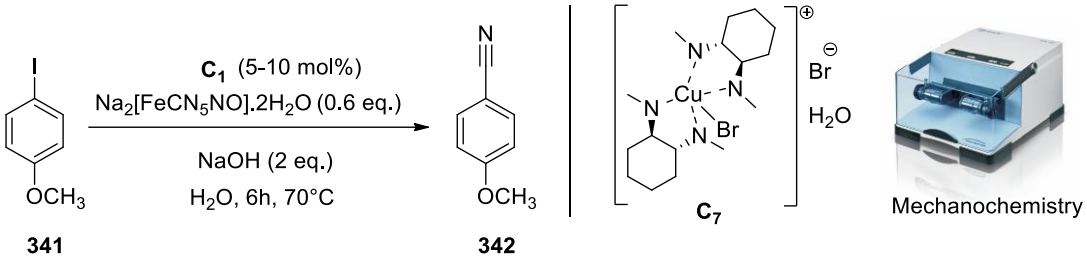

Entry	C_1 (mol%)[a]	Conversion %[b]	Yield%[b]
1	5	86	65
2	7	92	78
3	10	100	85

[a] Reaction conditions: 4-Iodoanisole (1 equiv., 0.42 mmol), C_7 (5-10 mol%), $Na_2[Fe(CN)_5NO].2H_2O$ (0.6 equiv.), NaOH (2 equiv.), H_2O (0.9 M), 70°C, 1200 rpm, 6h; [b] Conversion and yield determined by HPLC/UV analysis with caffeine as an internal standard.

3.1.3. Influence of the amount of NaOH

During our optimization study, we also investigated the influence of the number of equivalents of NaOH (Table 23). Starting with 2 equivalents of NaOH the yield of anisonitrile was 75%, albeit with a total conversion of the reaction (Table 23, Entry 1). We observed, via HPLC, the formation of the corresponding amide derivative in the ration of 1/5 with benzonitrile (**342**). Reducing the base from 2 eq. to 1.7 eq. kept the reaction conversion (100%) with a cyanide derivative yield of 86% (Table 23, Entry 2) and the presence of amide (**343**) in ratio of 1/17 with benzonitrile (**342**). The further reduction in the quantity of base led to a decrease in reaction conversion and reaction yield (Table 23, Entries 3-4).

Table 23. Quantity of base.

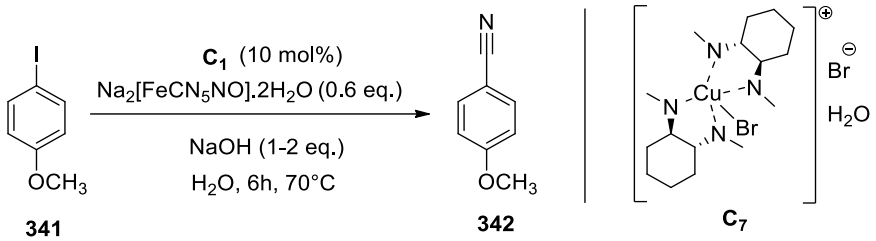

Entry	Eq. of NaOH[a]	Conversion %[b]	Yield%[b]
1	2	100	75[c]
2	1.7	100	86[c]
3	1.5	73	65
4	1	64	57

[a] Reaction conditions: 4-Iodoanisole (1 equiv., 0.42 mmol), C_7 (10 mol%), $Na_2[Fe(CN)_5NO].2H_2O$ (0.6 equiv.), NaOH (1-2 equiv.), H_2O (0.9 M), 70°C, 1200 rpm, 6h; [b] Conversion and yield determined by HPLC/UV analysis with caffeine as an internal standard.[c] Presence of amide (R.F.= 3.3 min.)

3.1.4. Influence of the type of Copper complex

We also investigated other types of copper catalys in particular monodentate ligands. For the synthesis of these new pre-catalysts, we followed another methodology also described by Meedk and Ehrhardt.[59] For the synthesis of the monodentate Cu(II) complex, independent solutions of $CuBr_2.H_2O$ and ligand (**L_1**) were prepared in ethanol. Subsequently, the ligand solution was slowly added to the metallic solution under stirring. The reaction mixture was left at room temperature overnight. The precipitate formed was filtered to yield **C_8** in 88% yield (Scheme 84a). For the synthesis of the monodentate Cu(I) complex (**C_9**), we followed the same protocol. However, using inert atmosphere and due to the lack of solubility of CuBr in ethanol, we used dry acetonitrile as solvent. The precipitate formed was isolated in 70% yield (Scheme 84b).

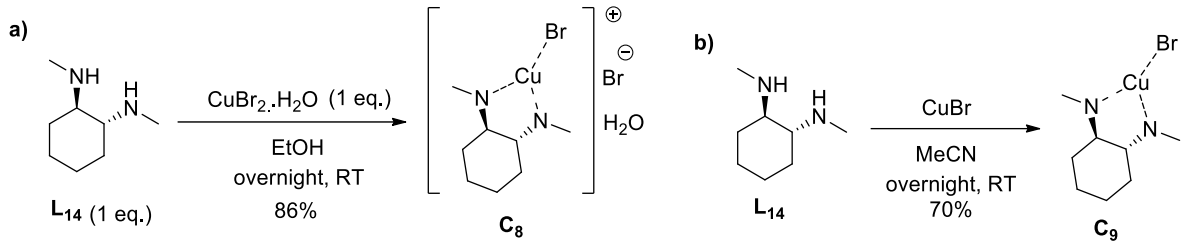

Scheme 84. a) Synthesis and proposed structure of $\mathbf{C_8}$; b) Synthesis and proposed structure of $\mathbf{C_9}$.

Despite several attempts at crystallization, it was not possible to determine the structure of complexes $\mathbf{C_8}$ and $\mathbf{C_9}$. Nevertheless, we proceeded with the investigation of the reaction protocol by comparing the three synthesized complexes using lower quantity of NaOH (1.3 eq.), in order to observe better the improvements. We observed lower reaction conversion using $\mathbf{C_7}$ compared to $\mathbf{C_8}$ and $\mathbf{C_9}$; however, the reaction yields did not show differences (77-80%) (Table 24).

Table 24. Influence of the type of pre-catalyst.

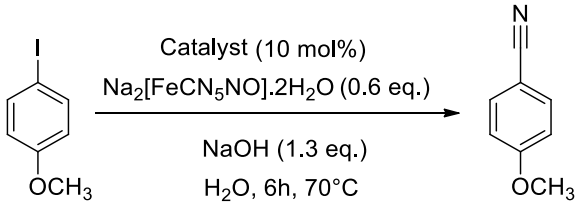

Entry	Catalyst	Conversion %[b]	Yield%[b]
1	$\mathbf{C_7}$	84	80
2	$\mathbf{C_8}$	93	78
3	$\mathbf{C_9}$	95	77

[a] Reaction conditions: 4-Iodoanisole (1 equiv., 0.42 mmol), Catalyst (10 mol%), $Na_2[Fe(CN)_5NO].2H_2O$ (0.6 equiv.), NaOH (1.3 equiv.), H_2O (0.9 M), 70°C, 1200 rpm, 6h; [b] Conversion and yield determined by HPLC/UV analysis with caffeine as an internal standard.

4. CONCLUSION AND PERSPECTIVES

Throughout this work, we were led to optimize the reaction protocol for the copper catalyzed cyanation in water using a non-toxic source of cyanide. To achieve this, we investigated various parameters: the influence of D-glucose (D-glc), the quantity of NaOH, the size of the solid (application of mechanochemistry) and the type of copper complex. After conducting all the tests, the best reaction condition found was **C_7** (10 mol%), Na_2FeCN_5NO (0.6 eq.), NaOH (1.7 eq.), H_2O, 6h, 70°C. As results of the employed tests, it was demonstrated that i) there is no need for the use of D-glc, ii) a substantial reduction in the reaction preparation time, iii) simplification of the methodological protocol due to the hygroscopic nature of the previously used ligand (**L_{14}**), and iv) a slight decrease in observed fluctuations in reaction yields. We particularly demonstrated the effectiveness of the copper complex (**C_7**), its preparation, crystallization, and the X-ray diffraction data. The use of the crystallized complex greatly facilitated the implementation of the reaction, and we initially obtained a yield of 85% from a model reaction. Even with the optimizations and simplification of the reaction procedure, it is worth noting that we still have encountered issues during the isolation. Finally, the scope and limitations of the reaction are currently being investigated in the laboratory.

5. EXPERIMENTAL

5.1. Materials and instruments

All commercial reagents were used without purification. Analytical TLC was performed using Merck 60 F254 silica gel plates, and visualized by exposure to ultraviolet light (254 and 365 nm). Compounds were purified on silica gel Merck 60 (particle size 0.040−0.063 nm). NMR spectra were recorded on Bruker Avance III spectrometers. Operating at 500, 400, or 300 MHz for ^{1}H, 125, 101, or 75 MHz for ^{13}C. All chemical shift values δ and coupling constants J are quoted in ppm and in Hz, respectively, multiplicity (s= singlet, d= doublet, t= triplet, q= quartet, m= multiplet, and br = broad). Analytical RP-HPLC-MS was performed using a LC 1200 Agilent with quadrupole-time-of-flight (QTOF) (Agilent Accurate Mass QToF 6520) with a ZORBAX Agilent C18-column (C18, 50 mm × 2.1 mm; 1.8 μm) using the following parameters: (1) the solvent system: A (0.05% of formic acid in acetonitrile) and B (0.05% of formic acid in H_2O); (2) a linear gradient: t = 0 min, 98% B; t = 8 min, 0% B; t = 12.5 min, 0% B; t = 12.6 min, 98% B; t = 13 min, 98% B; (3) flow rate of 0.5 mL/min; (4) column temperature: 35 °C; (5) DAD scan from 190 to 700 nm; and (6) ionization mode: ESI+. HPLC were performed using a Dionex UltiMate 3000 using the following parameters: column temperature: 40°C, from t = 0 min to t = 3.80 min the flow rate goes from 0.650 mL/min to 0.900 ml/min with the solvent system: A (0.05% of TFA in H_2O) and B (MeCN) with 5 to 100% of B, then after t = 3.80 min to the end of the run t = 5.50 min: 100% of B at 0.900 ml/min.

5.2. Synthetic Methodology

5.2.1. Synthesis of the copper complex (C_7)

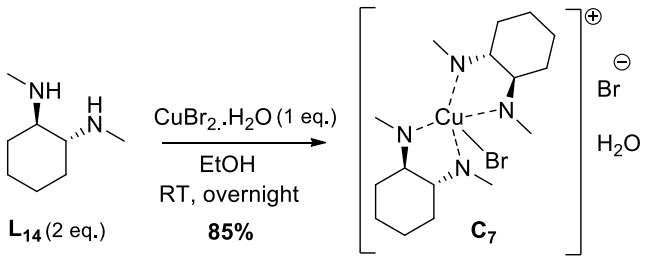

A 250 mL round bottom flask containing a Teflon stirrer bar was charged with (1R,2R)-N,N'-dimethyl-1,2-cyclohexanediamine (**L_{14}**) (2 eq., 1 g, 7.03 mmol) and 40 mL of absolute ethanol. A 100 mL beaker was charged with $CuBr_2.H_2O$ (1 eq., 0.78 g, 3.52 mmol) and solubilized in 20 mL of absolute ethanol. This solution was filtered with cotton and added

dropwise over the stirred solution of **L_{14}**. The reaction mixture was maintained under stirring at room temperature overnight. The precipitate formed in solution was filtered off under reduced pressure to afford the desired product as a violet solid (1.56 g, 2.97 mmol, 85%)

5.2.2. Crystallization of C_7

A 10 mL beaker was charged with small amount of **C_7** and solubilized with anhydrous methanol. This beaker was covered with parafilm containing small holes to allow evaporation. After few days and complete evaporation, blue crystals were observed.

5.2.3. Synthesis of the copper complex (C_8)

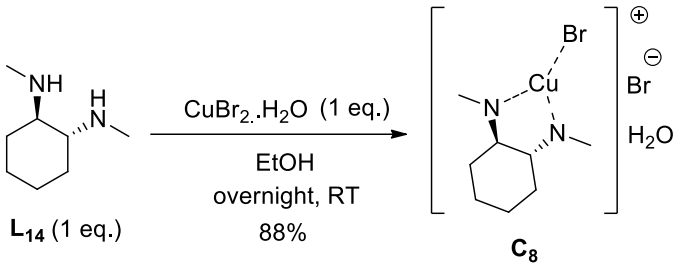

A 100 mL round bottom flask containing a Teflon stirrer bar was charged with $CuBr_2.H_2O$ (1 eq., 0.31 g, 1.4 mmol) and solubilized in 13 mL of absolute ethanol. A 50 mL beaker was charged with (1R,2R)-N,N'-dimethyl-1,2-cyclohexanediamine (**L_{14}**) (1 eq., 0.2 g, 1.4 mmol) and 13 mL of absolute ethanol. This solution was added dropwise over the stirred metallic solution. The reaction mixture was maintained under stirring at room temperature overnight. The precipitate formed in solution was filtered off under reduced pressure to give a dark green solid (0.45 g, 1.23 mmol, 88%). Efforts to crystallize **C_8** proved to be unsuccessful.

5.2.4. Synthesis of the copper complex (C_9)

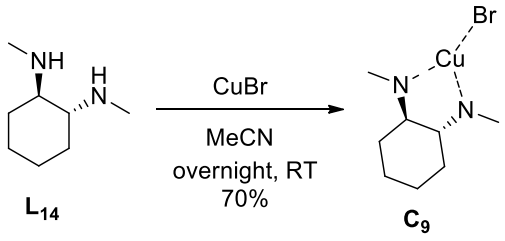

A 50 mL round bottom flask containing a Teflon stirrer bar was charged with CuBr (1 eq., 0.1 g, 0.7 mmol) and solubilized in 10 mL of anhydrous acetonitrile. A 50 mL beaker was charged with (1R,2R)-N,N'-dimethyl-1,2-cyclohexanediamine (**L_{14}**) (1 eq., 0.1 g, 0.7 mmol) and 10 mL of anhydrous acetonitrile. This solution was added dropwise over the stirred metallic solution. The reaction was then capped properly, evacuated and backfilled with argon (this process was repeated a total of three times) and then maintained under stirring at room temperature overnight. The precipitate formed in solution was filtered off under reduced pressure to give a pale blue solid in 70%. Efforts to crystallize **C_9** proved to be unsuccessful.

5.2.5. General procedure for the calibration

During the optimization of the procedure for the model reaction, yields were calculated by HPLC analysis. To determine the reaction yield we had to prepare standard curves for the reagent, the desired product and for the caffeine (external standard). They were prepared from known concentrations in MeCN at 202nm.

After the reaction time (6h), a known quantity of caffeine (~5-10 mg) was added to the reaction medium and the mixture diluted in EtOH (~ 3 mL). After homogenization, 10µL was diluted in 1 mL of MeCN and 1µL of this solution was injected in HPLC.

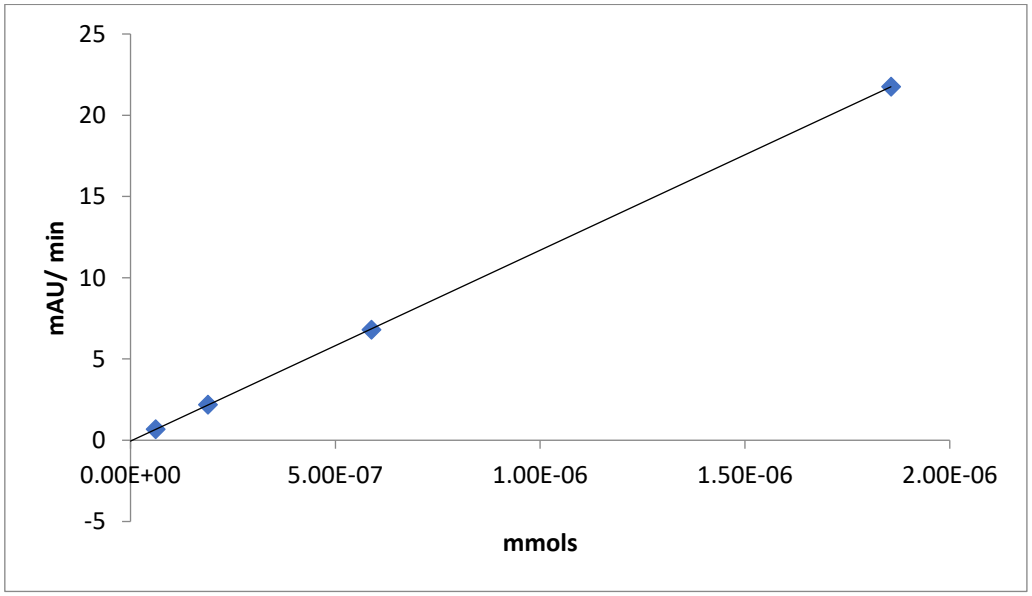

Graphic 1. Calibration curve for anisonitrile (**342**) at 202nm

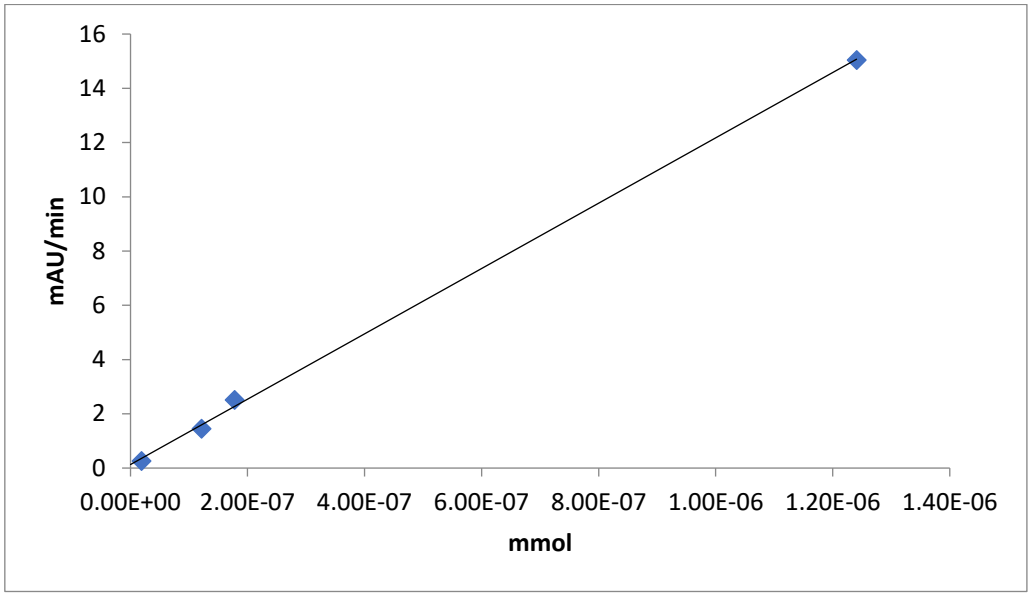

Graphic 2. Calibration curve for caffeine at 202nm

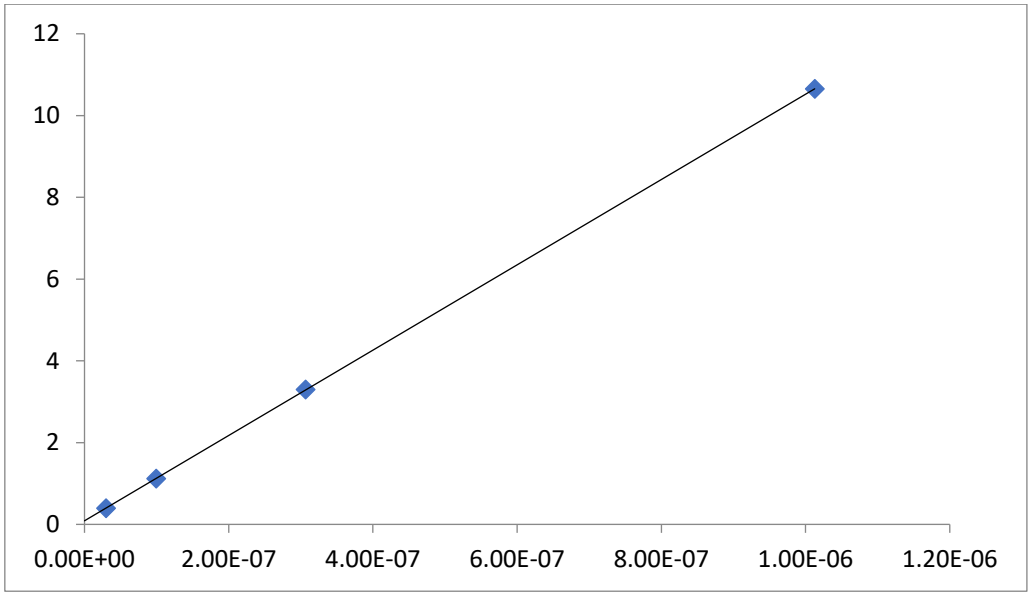

Graphic 3. Calibration curve for iodoanisol (**341**) at 202nm

5.2.6. Copper-catalized cyanation reaction

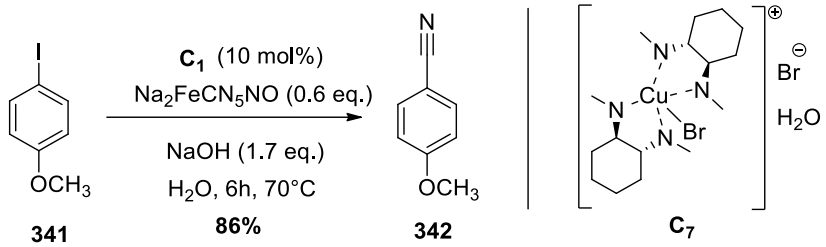

1. A microwave vessel containing a Teflon stirrer bar was charged with water and then caped properly, evacuated and backfilled with argon under stirring for 1 minute (this process was repeated a total of three times).

2. A microwave vessel containing a Teflon stirrer bar was charged with 1.6 g of NaOH and then capped properly, evacuated and backfilled with argon (this process was repeated a total of three times. Then, 10 mL of water was added.

3. The reagents 4-iodoanisole and disodium pentacyanonitrosylferrate(iii) were crushed separately by using the mechanochemistry reactor.

4. A bioshake IQ reaction vessel was charged with 4-iodoanisole (**341**) (1 eq., 0.1 g, 0.406 mmol), (3aR,3'aR,7aR,7'aR)-1,1',3,3'-tetramethyl-hexadecahydro-2,2'-spirobi[cyclohexa[d]-1,3-diaza-2-cupracyclopentane]-2,2-bis(ylium) hydrate dibromide (**C_7**) (0.1 eq., 0.021 g, 0.0406 mmol) and disodium pentacyanonitrosylferrate(iii) (0.6 eq., 0.072 g, 0.24 mmol). The mixture was then capped properly, evacuated and backfilled with argon (this process was repeated a total of three times). Then, 0.33 mL of water and 0.17 mL of NaOH solutions previously prepared were added. The reaction mixture was then placed in a preheated bioshake IQ at 70°C for 6h at 1200 rpm. The progress of the reaction was evaluated by HPLC.

5.2.7. X-ray crystallographic analysis

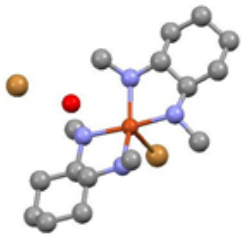

C_7

A specimen of $C_{16}H_{38}Br_2CuN_4O$ (**C_7**), approximate dimensions 0.120 mm x 0.130 mm x 0.200 mm, was used for the X-ray crystallographic analysis. The X-ray intensity data were measured (λ = 0.71073 Å).

The integration of the data using an orthorhombic unit cell yielded a total of 24320 reflections to a maximum θ angle of 27.94° (0.76 Å resolution), of which 5215 were independent (average redundancy 4.663, completeness = 99.6%, Rint = 7.51%, Rsig = 7.15%) and 3880 (74.40%) were greater than 2σ(F2). The final cell constants of a = 8.9017(5) Å, b = 11.2778(6) Å, c = 22.1952(12) Å, volume = 2228.2(2) Å3, are based upon the refinement of the XYZ-centroids of reflections above 20 σ(I). The calculated minimum and maximum transmission coefficients (based on crystal size) are 0.6043 and 0.7456.

The structure was solved and refined using the Bruker SHELXTL Software Package, using the space group P 21 21 21, with Z = 4 for the formula unit, $C_{16}H_{38}Br_2CuN_4O$. The final anisotropic full-matrix least-squares refinement on F2 with 239 variables converged at R1 = 4.88%, for the observed data and wR2 = 11.20% for all data. The goodness-of-fit was 1.045. The largest peak in the final difference electron density synthesis was 0.944 e-/Å3 and the largest hole was -1.176 e-/Å3 with an RMS deviation of 0.137 e-/Å3. On the basis of the final model, the calculated density was 1.568 g/cm3 and F(000), 1076 e-.

6. BIBLIOGRAPHY

1. a) Liu, K. C.; Howe, R. K. 3'-Arylspiro[Isobenzofuran-1(3H),5'(4'H)-Isoxazol]-3-Ones and Their Conversion to 2-(3-Arylisoxazol-5-Yl)Benzoates. *J. Org. Chem.* **1983**, *48* (24), 4590–4592. https://doi.org/10.1021/jo00172a030. b) Robertson, D. W.; Beedle, E. E.; Swartzendruber, J. K.; Jones, N. D.; Elzey, T. K.; Kauffman, R. F.; Wilson, H.; Hayes, J. S. Bipyridine Cardiotonics: The Three-Dimensional Structures of Amrinone and Milrinone. *J. Med. Chem.* **1986**, *29* (5), 635–640. https://doi.org/10.1021/jm00155a009. c) Harris, T. M.; Harris, C. M.; Oster, T. A.; Brown, L. E.; Lee, J. Y. C. Biomimetic Syntheses of Pretetramides. 2. A Synthetic Route Based on a Preformed D Ring. *J. Am. Chem. Soc.* **1988**, *110* (18), 6180–6186. https://doi.org/10.1021/ja00226a037.

2. a) Patterson, A. W.; Wood, W. J. L.; Hornsby, M.; Lesley, S.; Spraggon, G.; Ellman, J. A. Identification of Selective, Nonpeptidic Nitrile Inhibitors of Cathepsin S Using the Substrate Activity Screening Method. *J. Med. Chem.* **2006**, *49* (21), 6298–6307. https://doi.org/10.1021/jm060701s. b) Boyd, M. J.; Crane, S. N.; Robichaud, J.; Scheigetz, J.; Black, W. C.; Chauret, N.; Wang, Q.; Massé, F.; Oballa, R. Investigation of ketone warheads as alternatives to the nitrile for preparation of potent and selective cathepsin K inhibitors. *Bioorg. Med. Chem. Lett.*, **2009**, *19*, 675−679. - https://doi.org/10.1016/j.bmcl.2008.12.053

3. Larock, R. C.; Comprehensive Organic Transformations. A Guide to Functional Group Preparations; VCH Publishers: New York. **1989**.

4. a) Rosenmund, K. W.; Struck, E. Das am Ringkohlenstoff gebundene Halogen und sein Ersatz durch andere Substituenten. I. Mitteilung: Ersatz des Halogens durch die Carboxylgruppe. *Ber. Dtsch. Chem. Ges.* **1919** , *52* (8), 1749 – 1756. https://doi.org/10.1002/cber.19190520840. b) V. Braun, J.; Manz, G. Fluoranthen Und Seine Derivate. III. Mitteilung. *Liebigs Ann.* **1931**, *488* (1), 111–126. https://doi.org/10.1002/jlac.19314880107.

5. a) Anbarasan, P.; Schareina, T.; Beller, M. Recent Developments and Perspectives in Palladium-Catalyzed Cyanation of Aryl Halides: Synthesis of Benzonitriles. *Chem. Soc. Rev.* **2011**, *40* (10), 5049–5067. https://doi.org/10.1039/C1CS15004A. b) Sundermeier, M.; Zapf, A.; Beller, M. Palladium-Catalyzed Cyanation of Aryl Halides: Recent Developments and

Perspectives. *Eur. J. Inorg. Chem.* **2003**, *2003* (19), 3513–3526. https://doi.org/10.1002/ejic.200300162. c) Ellis, G. P.; Romney-Alexander, T. M. Cyanation of Aromatic Halides. *Chem. Rev.* **1987**, *87* (4), 779–794. https://doi.org/10.1021/cr00080a006. d) Lindley, J. Tetrahedron Report Number 163: Copper Assisted Nucleophilic Substitution of Aryl Halogen. *Tetrahedron* **1984**, *40* (9), 1433–1456. https://doi.org/10.1016/S0040-4020(01)91791-0.

6. Sandmeyer, T. Ueber Die Ersetzung Der Amidgruppe Durch Chlor in Den Aromatischen Substanzen. *Ber. Dtsch. Chem. Ges.* **1884**, *17* (2), 1633–1635. https://doi.org/10.1002/cber.18840170219.

7. a) Martin, A.; Kalevaru, N. V.; Lücke, B.; Sans, J. Eco-Friendly Synthesis of p-Nitrobenzonitrile by Heterogeneously Catalysed Gas Phase Ammoxidation. *Green Chem.* **2002**, *4* (5), 481–485. https://doi.org/10.1039/B204244B. b) Liu, Y.; Zhong, M.; Yu, W.; Ma, Y.-L. One-Step Synthesis of Tolunitriles by Heterogeneously Catalyzed Liquid-Phase Ammoxidation. *Synth. Commun.* **2005**, *35* (23), 2951–2954. https://doi.org/10.1080/00397910500278214. c) Rombi, E.; Ferino, I.; Monaci, R.; Picciau, C.; Solinas, V.; Buzzoni, R. Toluene Ammoxidation on α-Fe2O3-Based Catalysts. *Appl. Catal. A: Gen.* **2004**, *266* (1), 73–79. https://doi.org/10.1016/j.apcata.2004.01.028. d) Lücke, B.; Narayana, K. V.; Martin, A.; Jähnisch, K. Oxidation and Ammoxidation of Aromatics. *Adv. Synth. Catal.* **2004**, *346* (12), 1407–1424. https://doi.org/10.1002/adsc.200404027.

8. Takagi, K.; Okamoto, T.; Sakakibara, Y.; Ohno, A.; Oka, S.; Hayama, N. Nucleophilic Displacement Catalyzed by Transition Metal. I. General Consideration of the Cyanation of Aryl Halides Catalyzed by Palladium(II). *Bull. Chem. Soc. Jpn.* **1975**, *48* (11), 3298–3301. https://doi.org/10.1246/bcsj.48.3298.

9. a)Takagi, K.; Okamoto, T.; Sakakibara, Y.; Oka, S. Palladium(II) Catalyzed Synthesis of Aryl Cyanides from Aryl Halides. *Chem. Lett.* **1973**, *2* (5), 471–474. https://doi.org/10.1246/cl.1973.471. b) Akita, Y.; Shimazaki, M.; Ohta, A. Einführung der Cyano-Gruppe in Pyrazine. *Synthesis* **1981**, *12* (12), 974–975. https://doi.org/10.1055/s-1981-29665. c) Anderson, B. A.; Bell, E. C.; Ginah, F. O.; Harn, N. K.; Pagh, L. M.; Wepsiec, J. P. Cooperative Catalyst Effects in Palladium-Mediated Cyanation Reactions of Aryl Halides and Triflates. *J. Org. Chem.* **1998**, *63* (23), 8224–8228. https://doi.org/10.1021/jo9808674.

d) Sundermeier, M.; Zapf, A.; Mutyala, S.; Baumann, W.; Sans, J.; Weiss, S.; Beller, M. Progress in the Palladium-Catalyzed Cyanation of Aryl Chlorides. *Chem. Eur. J.* **2003**, *9* (8), 1828–1836. https://doi.org/10.1002/chem.200390210. e) Yang, C.; Williams, J. M. Palladium-Catalyzed Cyanation of Aryl Bromides Promoted by Low-Level Organotin Compounds. *Org. Lett.* **2004**, *6* (17), 2837–2840. https://doi.org/10.1021/ol049621d. f) Cristau, H.-J.; Ouali, A.; Spindler, J.-F.; Taillefer, M. Mild and Efficient Copper-Catalyzed Cyanation of Aryl Iodides and Bromides. *Chem. Eur. J.* **2005**, *11* (8), 2483–2492. https://doi.org/10.1002/chem.200400979.

10. a) Cassar, L. A New Nickel-Catalyzed Synthesis of Aromatic Nitriles. *J. Organomet. Chem.* **1973**, *54*, C57–C58. https://doi.org/10.1016/S0022-328X(00)84982-7. b) Cassar, L.; Ferrara, S.; Foá, M. Nickel-Catalyzed Cyanation of Aromatic Halides. In *Homogeneous Catalysis—II*; *Adv. Chem. Ser.*, **1974**; *132*, 252–273. https://doi.org/10.1021/ba-1974-0132.ch017. c) L. Cassar, M. Foa, F.Montanari, G. P. Marinelli. Phase-Transfer Catalysis in the Nickel-Catalyzed Cyanation of Aryl Halides. *J. Organomet. Chem.* **1979**, *173* (3), 335–339. https://doi.org/10.1016/S0022-328X(00)84788-9. d)Okano, T.; Iwahara, M.; Kiji, J. Catalytic Cyanation of Aryl Halides with NaCN in the Presence of Crowned Phosphine Complexes of Palladium under Solid-Liquid Two-Phase Conditions. *Synlett* **1998**, *09* (03), 243–244. https://doi.org/10.1055/s-1998-1651. e) Dalton, J. R.; Regen, S. L. Alumina Assisted Aryl Cyanation. *J. Org. Chem.* **1979**, *44* (24), 4443–4444. https://doi.org/10.1021/jo01338a042. f) Zanon, J.; Klapars, A.; Buchwald, S. L. Copper-Catalyzed Domino Halide Exchange-Cyanation of Aryl Bromides. *J. Am. Chem. Soc.* **2003**, *125* (10), 2890–2891. https://doi.org/10.1021/ja0299708. g) Ushkov, A. V.; Grushin, V. V. Rational Catalysis Design on the Basis of Mechanistic Understanding: Highly Efficient Pd-Catalyzed Cyanation of Aryl Bromides with NaCN in Recyclable Solvents. *J. Am. Chem. Soc.* **2011**, *133* (28), 10999–11005. https://doi.org/10.1021/ja2042035.

11. a) Chatani, N.; Hanafusa, T. Transition-Metal-Catalyzed Reactions of Trimethylsilyl Cyanide. 4. Palladium-Catalyzed Cyanation of Aryl Halides by Trimethylsilyl Cyanide. *J. Org. Chem.* **1986**, *51* (24), 4714–4716. https://doi.org/10.1021/jo00374a041. b) Sundermeier, M.; Mutyala, S.; Zapf, A.; Spannenberg, A.; Beller, M. A Convenient and Efficient Procedure for the Palladium-Catalyzed Cyanation of Aryl Halides Using Trimethylsilylcyanide. *J. Organomet. Chem.* **2003**, *684* (1–2), 50–55. https://doi.org/10.1016/S0022-328X(03)00503-5.

12. a) Tschaen, D. M.; Desmond, R.; King, A. O.; Fortin, M. C.; Pipik, B.; King, S.; Verhoeven, T. R. An Improved Procedure for Aromatic Cyanation. *Synth. Commun.* **1994**, *24* (6), 887–890. https://doi.org/10.1080/00397919408011310. b) Alterman, M.; Hallberg, A. Fast Microwave-Assisted Preparation of Aryl and Vinyl Nitriles and the Corresponding Tetrazoles from Organo-Halides. *J. Org. Chem.* **2000**, *65* (23), 7984–7989. https://doi.org/10.1021/jo0009954. c) Jin, F.; Confalone, P. N. Palladium-Catalyzed Cyanation Reactions of Aryl Chlorides. *Tetrahedron Lett.* **2000**, *41* (18), 3271–3273. https://doi.org/10.1016/S0040-4039(00)00384-1. d) Littke, A.; Soumeillant, M.; Kaltenbach, R. F.; Cherney, R. J.; Tarby, C. M.; Kiau, S. Mild and General Methods for the Palladium-Catalyzed Cyanation of Aryl and Heteroaryl Chlorides. *Org. Lett.* **2007**, *9* (9), 1711–1714. https://doi.org/10.1021/ol070372d. e) Cohen, D. T.; Buchwald, S. L. Mild Palladium-Catalyzed Cyanation of (Hetero)Aryl Halides and Triflates in Aqueous Media. *Org. Lett.* **2015**, *17* (2), 202–205. https://doi.org/10.1021/ol5032359. f) Zhang, X.; Xia, A.; Chen, H.; Liu, Y. General and Mild Nickel-Catalyzed Cyanation of Aryl/Heteroaryl Chlorides with $Zn(CN)_2$: Key Roles of DMAP. *Org. Lett.* **2017**, *19* (8), 2118–2121. https://doi.org/10.1021/acs.orglett.7b00732.

[1]3. Jin, F.; Confalone, P. N. Palladium-Catalyzed Cyanation Reactions of Aryl Chlorides. *Tetrahedron Lett.* **2000**, *41* (18), 3271–3273. https://doi.org/10.1016/S0040-4039(00)00384-1

[1]4. Littke, A.; Soumeillant, M.; Kaltenbach, R. F.; Cherney, R. J.; Tarby, C. M.; Kiau, S. Mild and General Methods for the Palladium-Catalyzed Cyanation of Aryl and Heteroaryl Chlorides. *Org. Lett.* **2007**, *9* (9), 1711–1714. https://doi.org/10.1021/ol070372d.

15. Dobbs, K. D.; Marshall, W. J.; Grushin, V. V. Why Excess Cyanide Can Be Detrimental to Pd-Catalyzed Cyanation of Haloarenes. Facile Formation and Characterization of $[Pd(CN)_3(H)]_2$- and $[Pd(CN)_3(Ph)]_2$. *J. Am. Chem. Soc.* **2007**, *129* (1), 30–31. https://doi.org/10.1021/ja066931d.

[1]6. Sundermeier, M.; Zapf, A.; Beller, M. A Convenient Procedure for the Palladium-Catalyzed Cyanation of Aryl Halides. *Angew. Chem. Int. Ed.* **2003**, *42* (14), 1661–1664. https://doi.org/10.1002/anie.200250778.

[1]7. a) Sundermeier, M.; Zapf, A.; Mutyala, S.; Baumann, W.; Sans, J.; Weiss, S.; Beller, M. Progress in the Palladium-Catalyzed Cyanation of Aryl Chlorides. *Chem. Eur. J.* **2003**, *9* (8), 1828–1836. https://doi.org/10.1002/chem.200390210. b) Zanon, J.; Klapars, A.; Buchwald, S. L. Copper-Catalyzed Domino Halide Exchange-Cyanation of Aryl Bromides. *J. Am. Chem. Soc.* **2003**, *125* (10), 2890–2891. https://doi.org/10.1021/ja0299708.http://doi.org/10.1021/ja0299708.

18. Ramnauth, J.; Bhardwaj, N.; Renton, P.; Rakhit, S.; Maddaford, S. P. The Room-Temperature Palladium-Catalyzed Cyanation of Aryl Bromides and Iodides with Tri-t-Butylphosphine as Ligand. *Synlett* **2003**, *2003* (14), 2237–2239. https://doi.org/10.1055/s-2003-42069.

19. a) Chobanian, H. R.; Fors, B. P.; Lin, L. A Facile Microwave-Assisted Palladium-Catalyzed Cyanation of Aryl Chlorides. *Tetrahedron Lett.* **2006**, *47* (19), 3303–3305. https://doi.org/10.1016/j.tetlet.2006.03.026. b) Srivastava, R. R.; Zych, A. J.; Jenkins, D. M.; Wang, H.-J.; Zhen-Jia Chen; Fairfax, D. J. Application of Polymer-Supported Triphenylphosphine and Microwave Irradiation to the Palladium-Catalyzed Cyanation of Aryl Triflates. *Synth. Commun.* **2007**, *37*(3), 431–438. https://doi.org/10.1080/00397910601039044.

20. Giachi, G.; Frediani, M.; Oberhauser, W.; Lamaty, F.; Martinez, J.; Colacino, E. Ultrasounds in Melted Poly(Ethylene Glycol) Promote Copper-Catalyzed Cyanation of Aryl Halides with K4[Fe(CN)6]. *ChemSusChem* **2014**, *7* (3), 919–924. https://doi.org/10.1002/cssc.201300997.

21. Cohen, D. T.; Buchwald, S. L. Mild Palladium-Catalyzed Cyanation of (Hetero)Aryl Halides and Triflates in Aqueous Media. *Org. Lett.* **2015**, *17* (2), 202–205. https://doi.org/10.1021/ol5032359.

22. a) Schareina, T.; Zapf, A.; Beller, M. Potassium Hexacyanoferrate(II)—a New Cyanating Agent for the Palladium-Catalyzed Cyanation of Aryl Halides. *Chem. Commun.* **2004**, *12*, 1388–1389. https://doi.org/10.1039/B400562G. b) Schareina, T.; Zapf, A.; Beller, M. An Environmentally Benign Procedure for the Cu-Catalyzed Cyanation of Aryl Bromides. *Tetrahedron Lett.* **2005**, *46* (15), 2585–2588. https://doi.org/10.1016/j.tetlet.2005.02.106.

23. Weissman, S. A.; Zewge, D.; Chen, C. Ligand-Free Palladium-Catalyzed Cyanation of Aryl Halides. *J. Org. Chem.* **2005**, *70* (4), 1508–1510. https://doi.org/10.1021/jo0481250.

24. Schareina, T.; Zapf, A.; Cotté, A.; Müller, N.; Beller, M. A Bio-Inspired Copper Catalyst System for Practical Catalytic Cyanation of Aryl Bromides. *Synthesis* **2008**, *2008* (20), 3351–3355. https://doi.org/10.1055/s-0028-1083161.

25. Grossman, O.; Gelman, D. Novel Trans-Spanned Palladium Complexes as Efficient Catalysts in Mild and Amine-Free Cyanation of Aryl Bromides under Air. *Org. Lett.* **2006**, *8* (6), 1189–1191. https://doi.org/10.1021/ol0601038.

26. Yeung, P. Y.; So, C. M.; Lau, C. P.; Kwong, F. Y. A Mild and Efficient Palladium-Catalyzed Cyanation of Aryl Mesylates in Water or *t*BuOH/Water. *Angew. Chem. Int. Ed.* **2010**, *49* (47), 8918–8922. https://doi.org/10.1002/anie.201005121.

27. Yeung, P. Y.; So, C. M.; Lau, C. P.; Kwong, F. Y. A Mild and Efficient Palladium-Catalyzed Cyanation of Aryl Chlorides with $K_4[Fe(CN)_6]$. *Org. Lett.* **2011**, *13* (4), 648–651. https://doi.org/10.1021/ol1028892.

28. Zhang, D.; Sun, H.; Zhang, L.; Zhou, Y.; Li, C.; Jiang, H.; Chen, K.; Liu, H. An Expedient Pd/DBU Mediated Cyanation of Aryl/Heteroaryl Bromides with K4[Fe(CN)6]. *Chem. Commun.* **2012**, *48* (23), 2909–2911. https://doi.org/10.1039/C2CC17468E.

29. Anderson, B. A.; Bell, E. C.; Ginah, F. O.; Harn, N. K.; Pagh, L. M.; Wepsiec, J. P. Cooperative Catalyst Effects in Palladium-Mediated Cyanation Reactions of Aryl Halides and Triflates. *J. Org. Chem.* **1998**, *63* (23), 8224–8228. https://doi.org/10.1021/jo9808674.

30. Zanon, J.; Klapars, A.; Buchwald, S. L. Copper-Catalyzed Domino Halide Exchange-Cyanation of Aryl Bromides. *J. Am. Chem. Soc.* **2003**, *125* (10), 2890–2891. https://doi.org/10.1021/ja0299708.

31. Cristau, H.-J.; Ouali, A.; Spindler, J.-F.; Taillefer, M. Mild and Efficient Copper-Catalyzed Cyanation of Aryl Iodides and Bromides. *Chem. Eur. J.* **2005**, *11* (8), 2483–2492. https://doi.org/10.1002/chem.200400979.

32. Schareina, T.; Zapf, A.; Cotté, A.; Gotta, M.; Beller, M. A Versatile Protocol for Copper-Catalyzed Cyanation of Aryl and Heteroaryl Bromides with Acetone Cyanohydrin. *Adv. Synth. Catal.* **2011**, *353* (5), 777–780. https://doi.org/10.1002/adsc.201000200.

33. Wang, D.; Kuang, L.; Li, Z.; Ding, K. L-Proline-Promoted Rosenmund-von Braun Reaction. *Synlett* **2008**, *2008* (01), 69–72. https://doi.org/10.1055/s-2007-992409.

34. Coughlin, M. M.; Kelly, C. K.; Lin, S.; MacArthur, A. H. R. Cyanation of Aryl Chlorides Using a Microwave-Assisted, Copper-Catalyzed Concurrent Tandem Catalysis Methodology. *Organometallics* **2013**, *32* (12), 3537–3543. https://doi.org/10.1021/om4004253.

35. Yapuri, U.; Palle, S.; Gudaparthi, O.; Narahari, S. R.; Rawat, D; K.; Mukkanti, K.; Vantikommu, J. Ligand-Free Nano Copper Oxide Catalyzed Cyanation of Aryl Halides and Sequential One-Pot Synthesis of 5-Substituted-1H-Tetrazoles. *Tetrahedron Lett.* **2013**, *54* (35), 4732–4734. https://doi.org/10.1016/j.tetlet.2013.06.107.

36. Kim, K.; Hong, S. H. Photoinduced Copper(I)-Catalyzed Cyanation of Aromatic Halides at Room Temperature. *Adv. Synth. Catal.* **2017**, *359* (14), 2345–2351. https://doi.org/10.1002/adsc.201700213.

37. Schareina, T.; Zapf, A.; Beller M. An Environmentally Benign Procedure for the Cu-Catalyzed Cyanation of Aryl Bromides. *Tetrahedron Lett.* **2005**, *46* (15), 2585–2588. https://doi.org/10.1016/j.tetlet.2005.02.106.

38. Ren, Y.; Liu, Z.; Zhao, S.; Tian, X.; Wang, J.; Yin, W.; He, S. Ethylenediamine/$Cu(OAc)_2 \cdot H_2O$-Catalyzed Cyanation of Aryl Halides with $K_4[Fe(CN)_6]$. *Catal. Commun.* **2009**, *10* (6), 768–771. https://doi.org/10.1016/j.catcom.2008.11.034.

39. Zhu, Y.-Z .; Cai, C. CuI/1,10-phenanthroline: An efficient catalyst system for the cyanation of aryl halides. *J. Chem. Res.* **2007**, *2007* (8), 484-485. https://doi.org/10.3184/030823407X237812.

40. a) Schareina, T.; Zapf, A.; Cotté, A.; Müller, N.; Beller, M. A Bio-Inspired Copper Catalyst System for Practical Catalytic Cyanation of Aryl Bromides. *Synthesis* **2008**, *2008* (20), 3351–3355. https://doi.org/10.1055/s-0028-1083161. b) Schareina, T.; Zapf, A.; Mägerlein, W.; Müller, N.; Beller, M. A State-of-the-Art Cyanation of Aryl Bromides: A Novel and Versatile Copper Catalyst System Inspired by Nature. *Chem. Eur. J.* **2007**, *13* (21), 6249–6254. https://doi.org/10.1002/chem.200700079. c) Schareina, T.; Zapf, A.; Mägerlein, W.; Müller, N.; Beller, M. Copper-Catalyzed Cyanation of Heteroaryl Bromides: A Novel and Versatile Catalyst System Inspired by Nature. *Synlett* **2007**, *4*, 555-558. https://doi.org/10.1055/s-2007-967979.

41. Maham, M.; Bahari, S. Copper iodide nanoparticles-catalysed cyanation of aryl halides using non-toxic $K_4[Fe(CN)_6]$ in the presence of 1,2-bis(5-tetrazolyl)benzene as an efficient ligand. *J. Chem. Res.* **2014**, 38 (5), 291-294. https://doi.org/10.3184/174751914X13966206828910.

42. Ren, Y.; Wang, W.; Zhao, S.; Tian, X.; Wang, J.; Yin, W.; Cheng, L. Microwave-Enhanced and Ligand-Free Copper-Catalyzed Cyanation of Aryl Halides with $K_4[Fe(CN)_6]$ in Water. *Tetrahedron Lett.* **2009**, *50* (32), 4595–4597. https://doi.org/10.1016/j.tetlet.2009.05.073.

43. DeBlase, C.; Leadbeater, N. E. Ligand-Free CuI-Catalyzed Cyanation of Aryl Halides Using $K_4[Fe(CN)_6]$ as Cyanide Source and Water as Solvent. *Tetrahedron* **2010**, *66* (5), 1098–1101. https://doi.org/10.1016/j.tet.2009.11.016.

44. Klapars, A.; Buchwald, S. L. Copper-Catalyzed Halogen Exchange in Aryl Halides: An Aromatic Finkelstein Reaction. *J. Am. Chem. Soc.* **2002**, *124* (50), 14844–14845. https://doi.org/10.1021/ja028865v.

45. Shi, J. On the Synergetic Catalytic Effect in Heterogeneous Nanocomposite Catalysts. *Chem. Rev*. **2013**, *113* (3), 2139-2181. https://doi.org/10.1021/cr3002752.

46. Gholinejad, M.; Aminianfar, A. Palladium Nanoparticles Supported on Magnetic Copper Ferrite Nanoparticles: The Synergistic Effect of Palladium and Copper for Cyanation of Aryl Halides with K4[Fe(CN)6]. *J. Mol. Catal. A: Chem.* **2015**, *397*, 106–113. https://doi.org/10.1016/j.molcata.2014.10.029.

47. Zhang, G.; Ren, X.; Chen, J.; Hu, M.; Cheng, J. Copper-Mediated Cyanation of Aryl Halide with the Combined Cyanide Source. *Org. Lett.* **2011**, *13* (19), 5004–5007. https://doi.org/10.1021/ol201713b.

48. Pawar, A. B.; Chang, S. Catalytic Cyanation of Aryl Iodides Using DMF and Ammonium Bicarbonate as the Combined Source of Cyanide: A Dual Role of Copper Catalysts. *Chem. Commun.* **2014**, *50* (4), 448–450. https://doi.org/10.1039/C3CC47926A.

49. Zhang, L.; Lu, P.; Wang, Y. Cu(NO3)2·3H2O-Mediated Cyanation of Aryl Iodides and Bromides Using DMF as a Single Surrogate of Cyanide. *Chem. Commun.* **2015**, *51* (14), 2840–2843. https://doi.org/10.1039/C4CC08579E.

50. Zheng, K.; Liu, B.; Chen, S.; Chen, F. Copper-Catalyzed Cyanation of Aryl Iodide with the Combined Cyanide Source of Urea and DMSO. *Tetrahedron Lett.* **2013**, *54* (38), 5250–5252. https://doi.org/10.1016/j.tetlet.2013.07.090.

51. a) Marlin, D. S.; Olmstead, M. M.; Mascharak, P. K. Heterolytic Cleavage of the C−C Bond of Acetonitrile with Simple Monomeric CuII Complexes: Melding Old Copper Chemistry with New Reactivity. *Angewandte Chemie International Edition* **2001**, *40* (24), 4752–4754. https://doi.org/10.1002/1521-3773(20011217)40:24<4752::AID-ANIE4752>3.0.CO;2-L. b) Lu, T.; Zhuang, X.; Li, Y.; Chen, S. C−C Bond Cleavage of Acetonitrile by a Dinuclear Copper(II) Cryptate. *J. Am. Chem. Soc.* **2004**, *126* (15), 4760–4761. https://doi.org/10.1021/ja031874z.

52. Zhang, S.-L.; Huang, L. Copper-Catalyzed Cyanation of Aryl Iodides with α-Cyanoacetates via C–CN Bond Activation. *Org. Biomol. Chem.* **2015**, *13* (39), 9963–9968. https://doi.org/10.1039/C5OB01675D.

53. Qi, C.; Hu, X.; He, H. Copper Iodide Mediated Cyanation of Arylboronic Acids and Aryl Iodides with Ethyl (Ethoxymethylene)cyanoacetate as Cyanating Agent. *Synlett* **2016**, *27* (13), 1979–1982. https://doi.org/10.1055/s-0035-1562112.

54. Wen, Q.; Jin, J.; Mei, Y.; Lu, P.; Wang, Y. Copper-Mediated Cyanation of Aryl Halides by Activation of Benzyl Cyanide as the Cyanide Source. *Eur. J. Org. Chem.* **2013**, *2013* (19), 4032–4036. https://doi.org/10.1002/ejoc.201300052.

55. Wang, L.; Pan, L.; Chen, Q.; He, M. Copper-Catalyzed Cyanations of Aromatic Bromides with Benzoyl Cyanide. *Chin. J. Chem.* **2014**, *32* (12), 1221–1224. https://doi.org/10.1002/cjoc.201400637.

56. Thakore, R. R.; Takale, B. S.; Singhania, V.; Gallou, F.; Lipshutz, B. H. Late-Stage Pd-Catalyzed Cyanations of Aryl/Heteroaryl Halides in Aqueous Micellar Media. *ChemCatChem* **2021**, *13* (1), 212–216. https://doi.org/10.1002/cctc.202001742.

57. a) Salomé, C.; Wagner, P.; Bollenbach, M.; Bihel, F.; Bourguignon, J.-J.; Schmitt, M. Buchwald–Hartwig Reactions in Water Using Surfactants. *Tetrahedron* **2014**, *70* (21), 3413–3421. https://doi.org/10.1016/j.tet.2014.03.083. b) Wagner, P.; Bollenbach, M.; Doebelin, C.; Bihel, F.; Bourguignon, J.-J.; Salomé, C.; Schmitt, M. *t*-BuXPhos: A Highly Efficient Ligand for Buchwald–Hartwig Coupling in Water. *Green Chem.* **2014**, *16* (9), 4170–4178. https://doi.org/10.1039/C4GC00853G.

58. a) Bollenbach, M.; Wagner, P.; Aquino, P. G. V.; Bourguignon, J.-J.; Bihel, F.; Salomé, C.; Schmitt, M. D-Glucose: An Efficient Reducing Agent for a Copper(II)-Mediated Arylation of Primary Amines in Water. *ChemSusChem* **2016**, *9* (22), 3244–3249. https://doi.org/10.1002/cssc.201600801. b) Bollenbach, M.; Aquino, P. G. V.; de Araújo-Júnior, J. X.; Bourguignon, J.-J.; Bihel, F.; Salomé, C.; Wagner, P.; Schmitt, M. Efficient and Mild Ullmann-Type N-Arylation of Amides, Carbamates, and Azoles in Water. *Chem. Eur. J.* **2017**, *23* (55), 13676–13683. https://doi.org/10.1002/chem.201700832.

59. Meek, D. W.; Ehrhardt, S. A. Copper(II) Complexes of Secondary and Tertiary N-Substituted Ethylenediamines. *Inorg. Chem.* **1965**, *4* (4), 584–587. https://doi.org/10.1021/ic50026a032.

ANNEX I

SPECTROSCOPIC CHARACTERIZATION

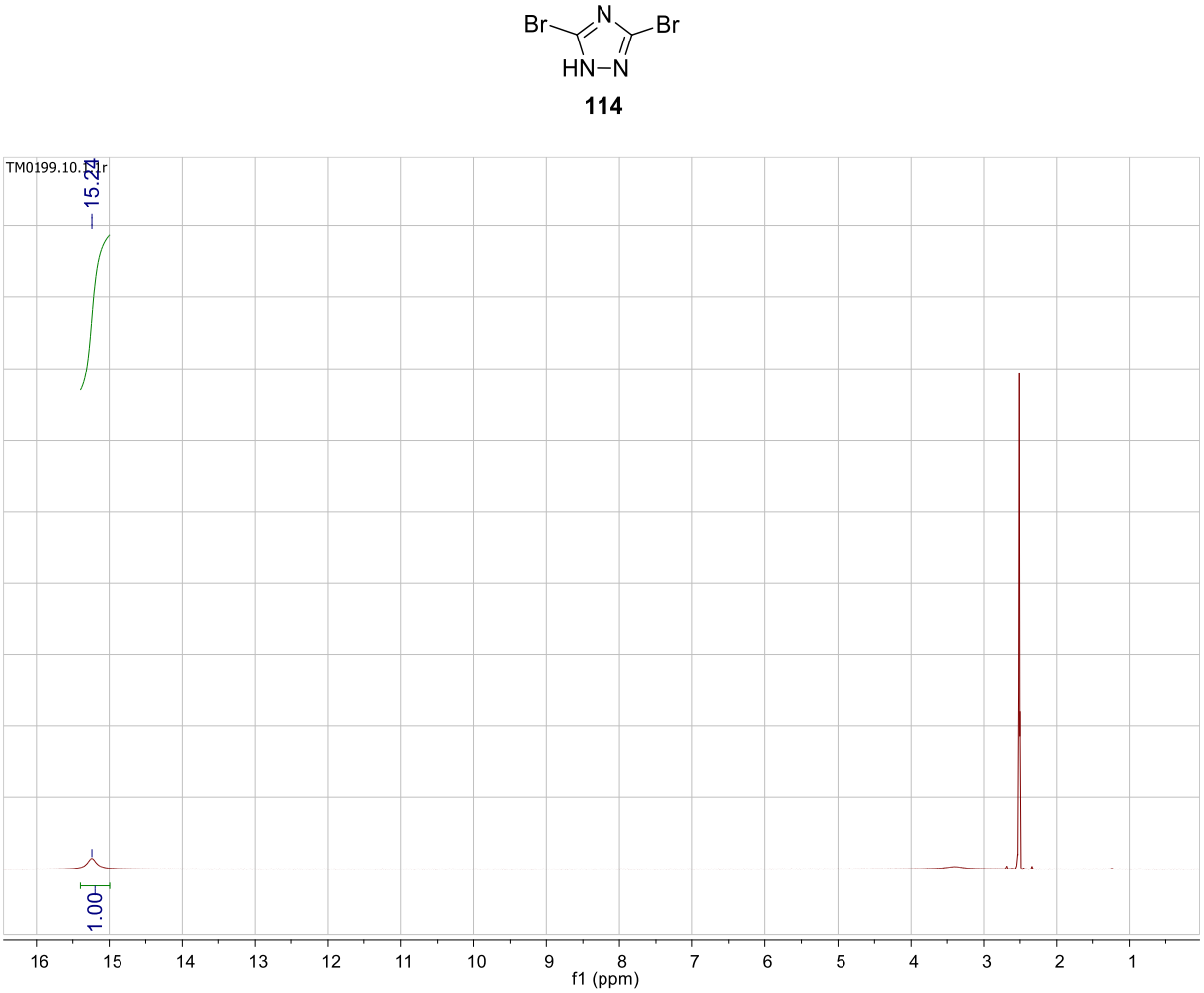

^{1}H NMR spectra of compound **114** in DMSO.

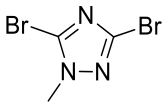

115a

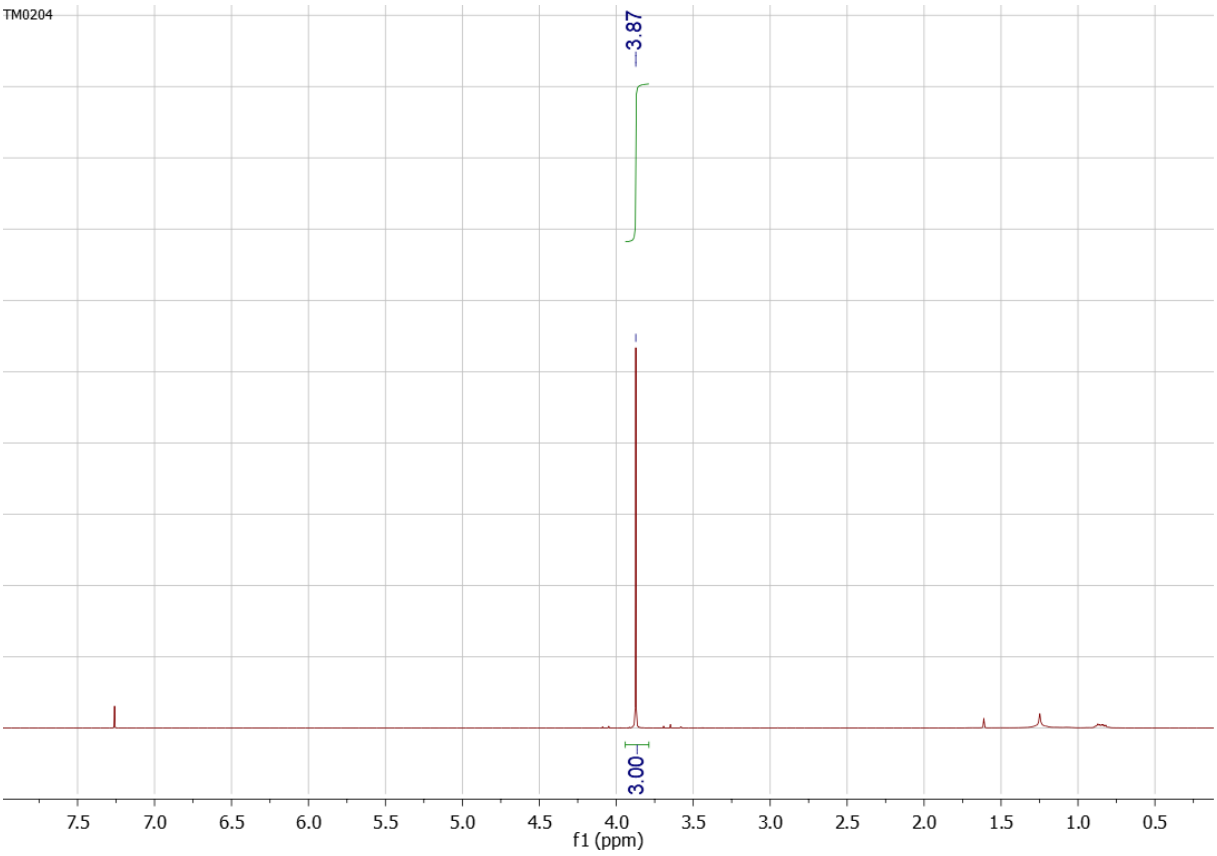

^{1}H NMR spectra of compound **115a** in $CDCl_3$.

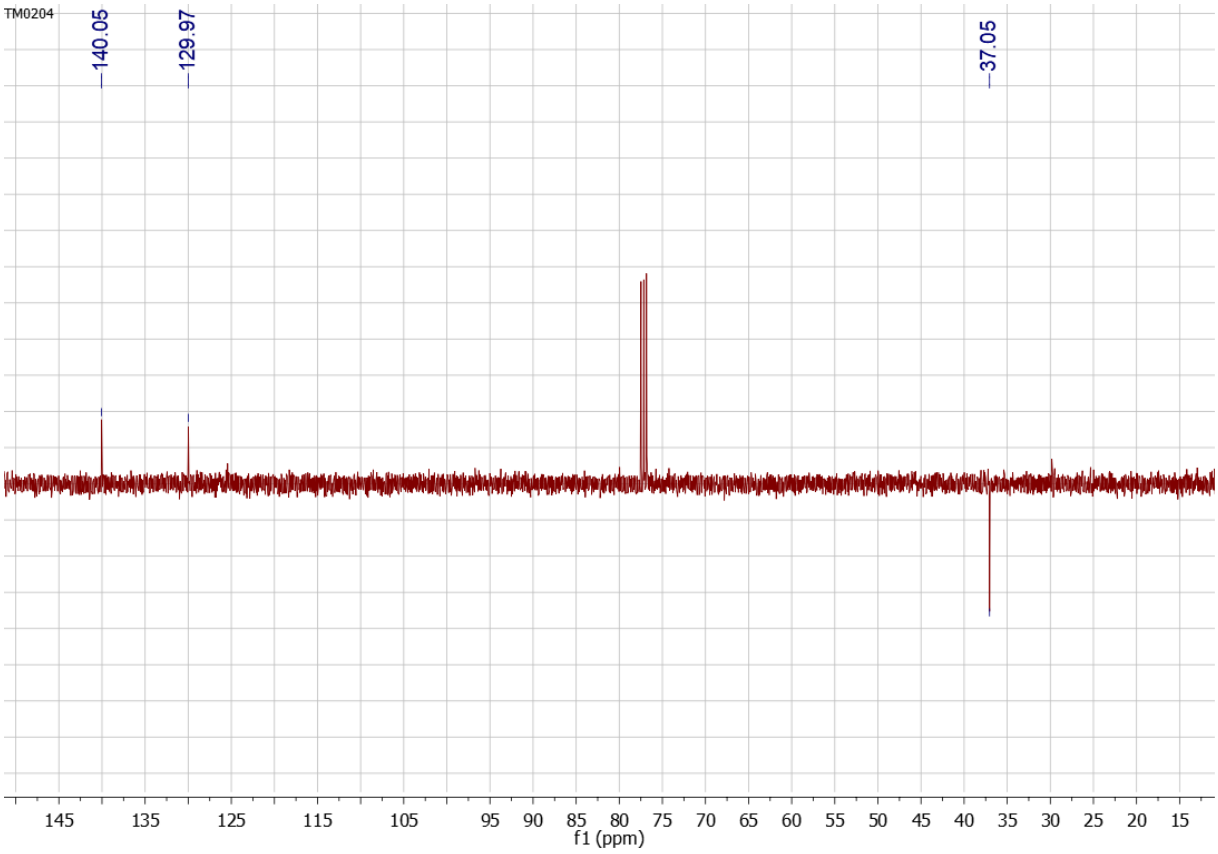

^{13}C NMR spectra of compound **115a** in $CDCl_3$.

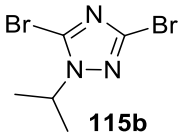

115b

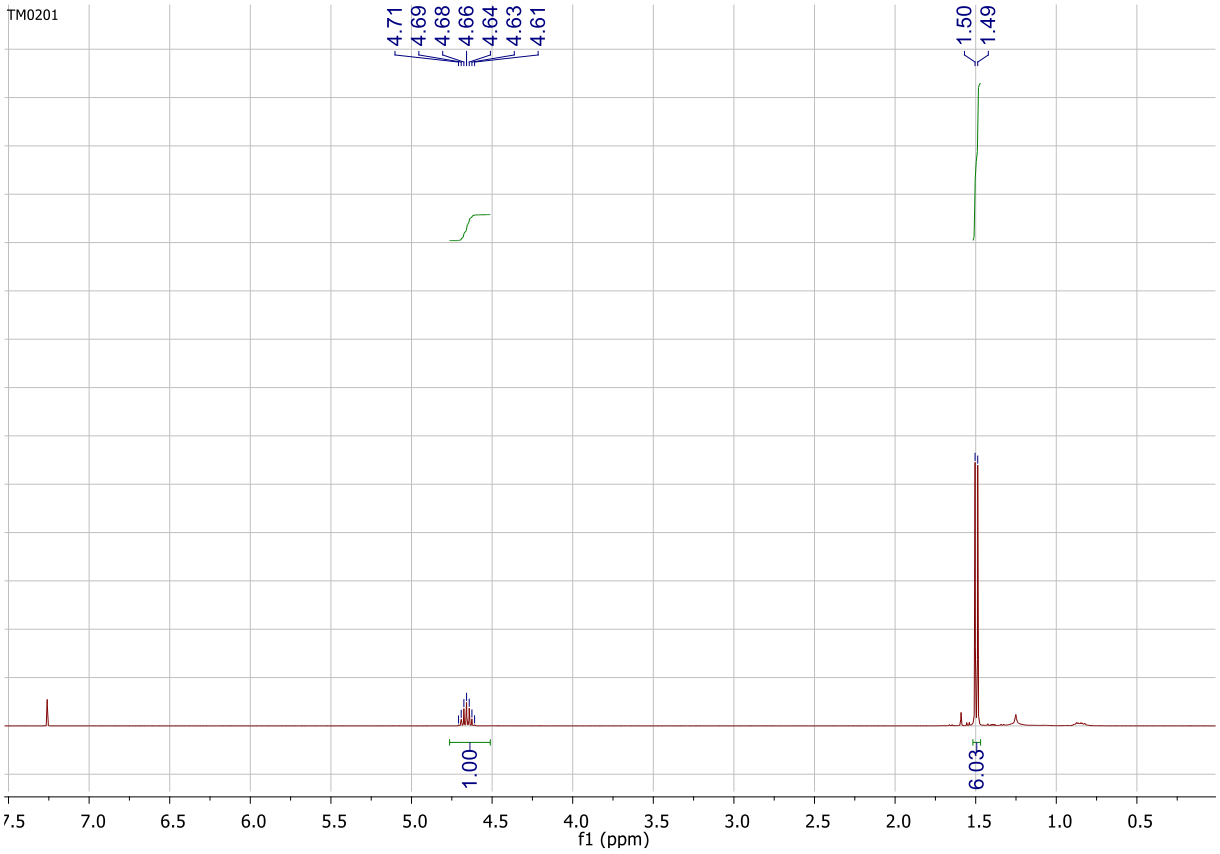

^{1}H NMR spectra of compound **115b** in $CDCl_3$.

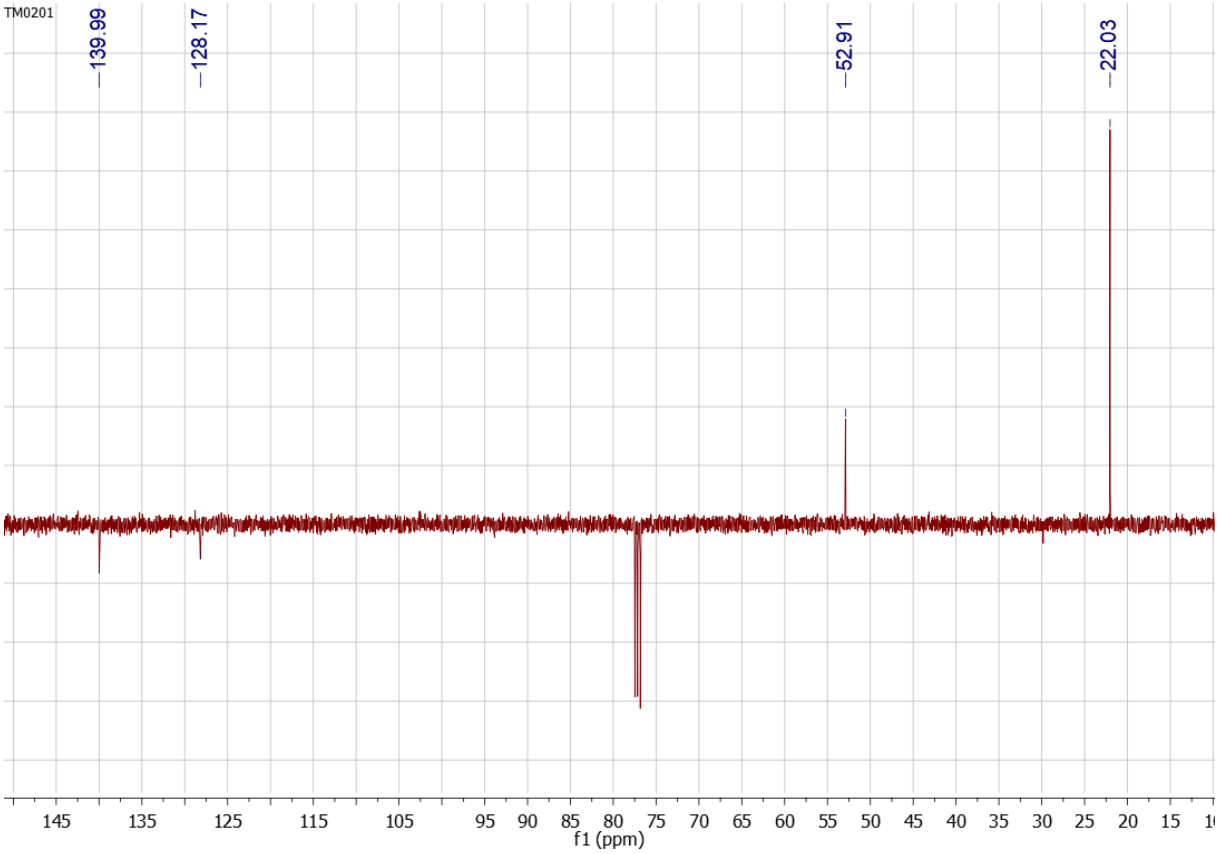

^{13}C NMR spectra of compound **115b** in $CDCl_3$.

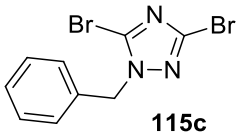

115c

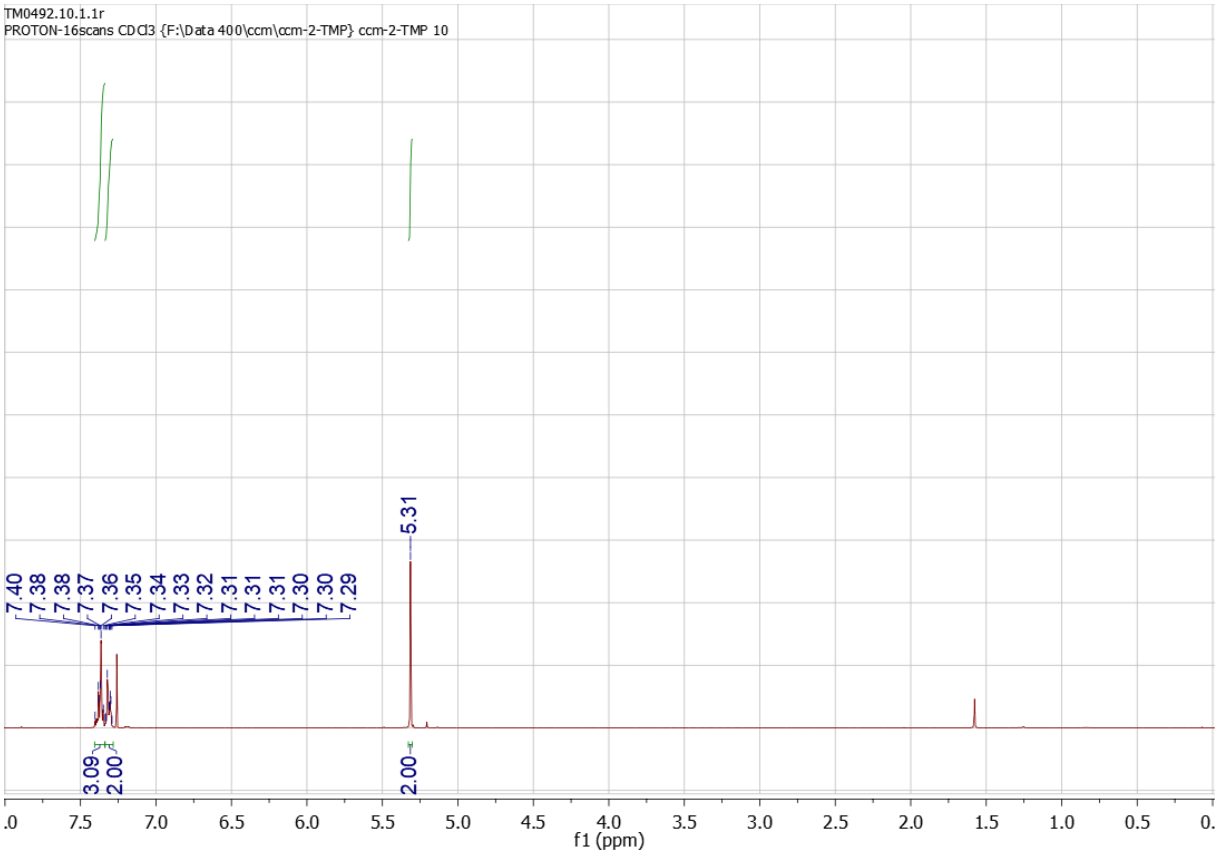

^{1}H NMR spectra of compound **115c** in $CDCl_3$.

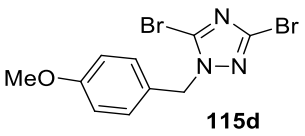

115d

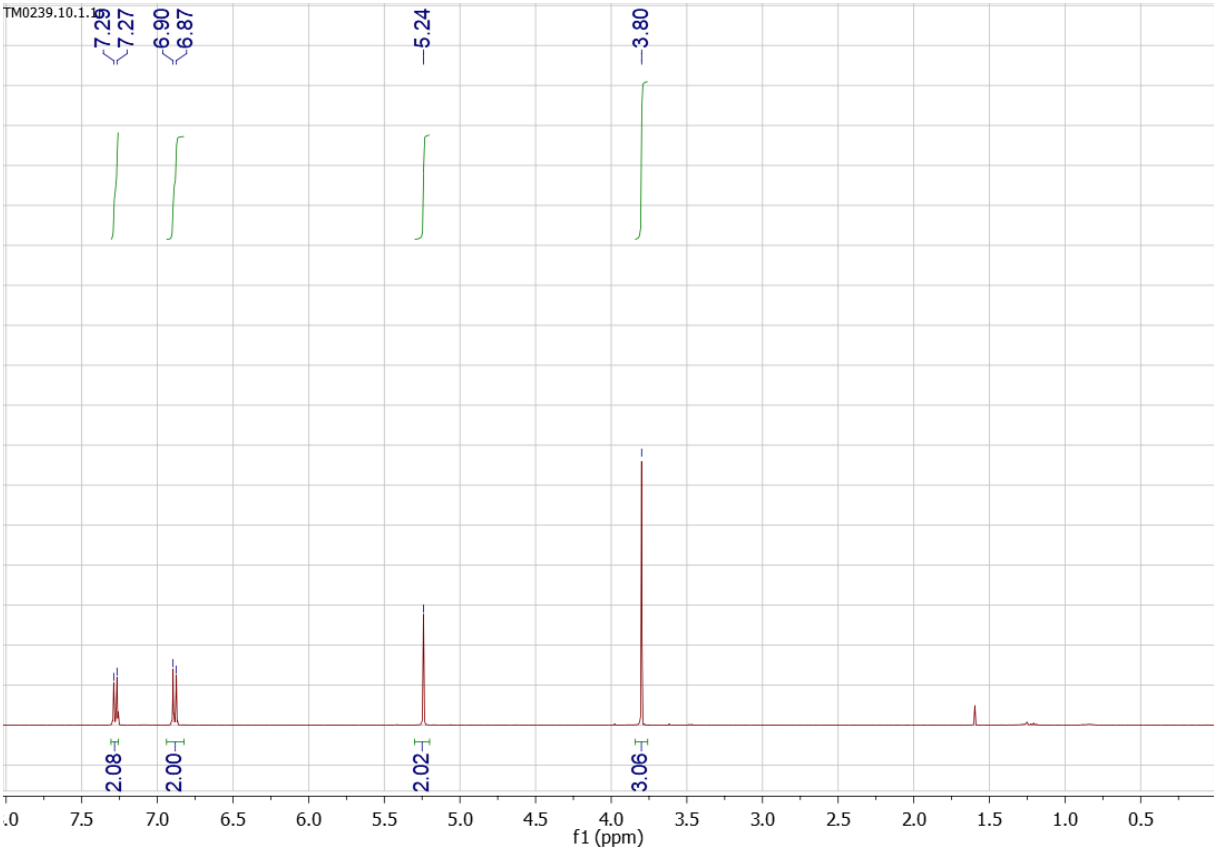

^{1}H NMR spectra of compound **115d** in $CDCl_3$.

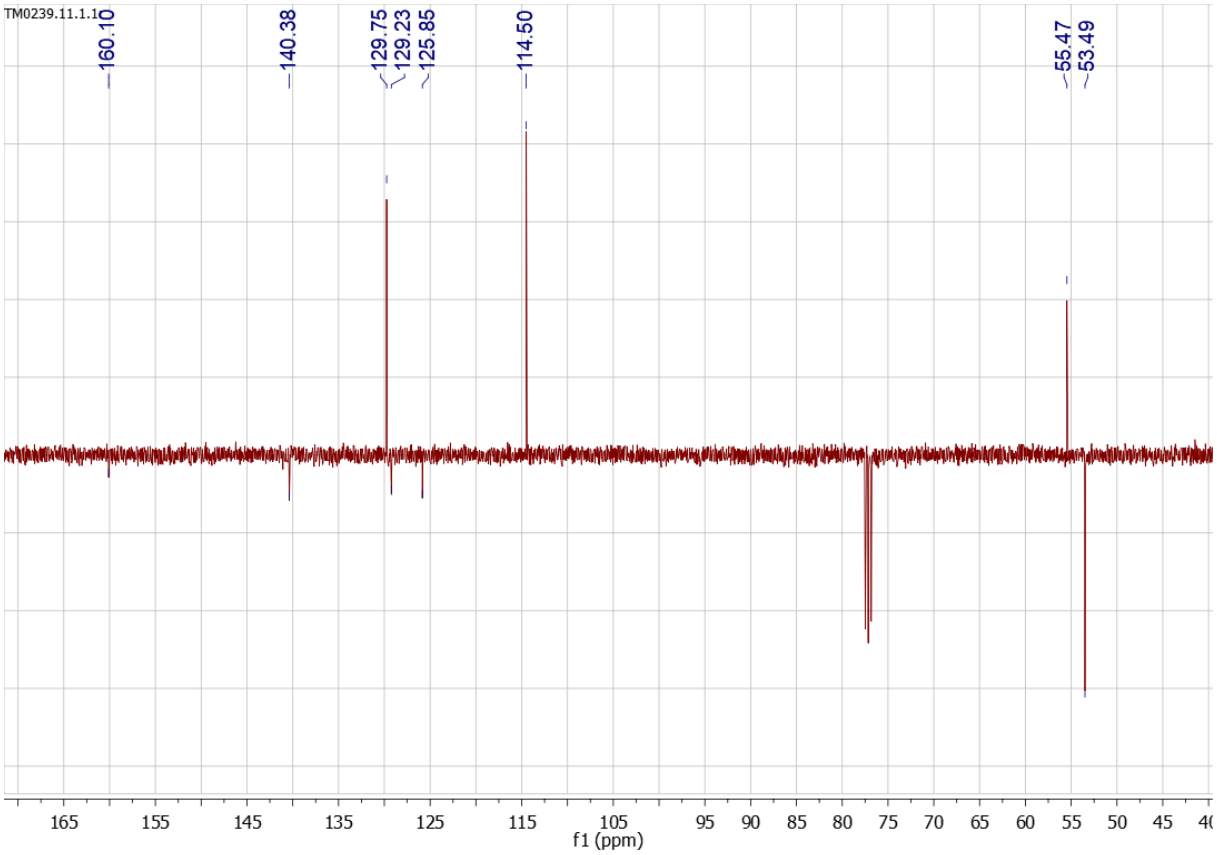

^{13}C NMR spectra of compound **115d** in $CDCl_3$.

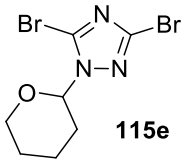

115e

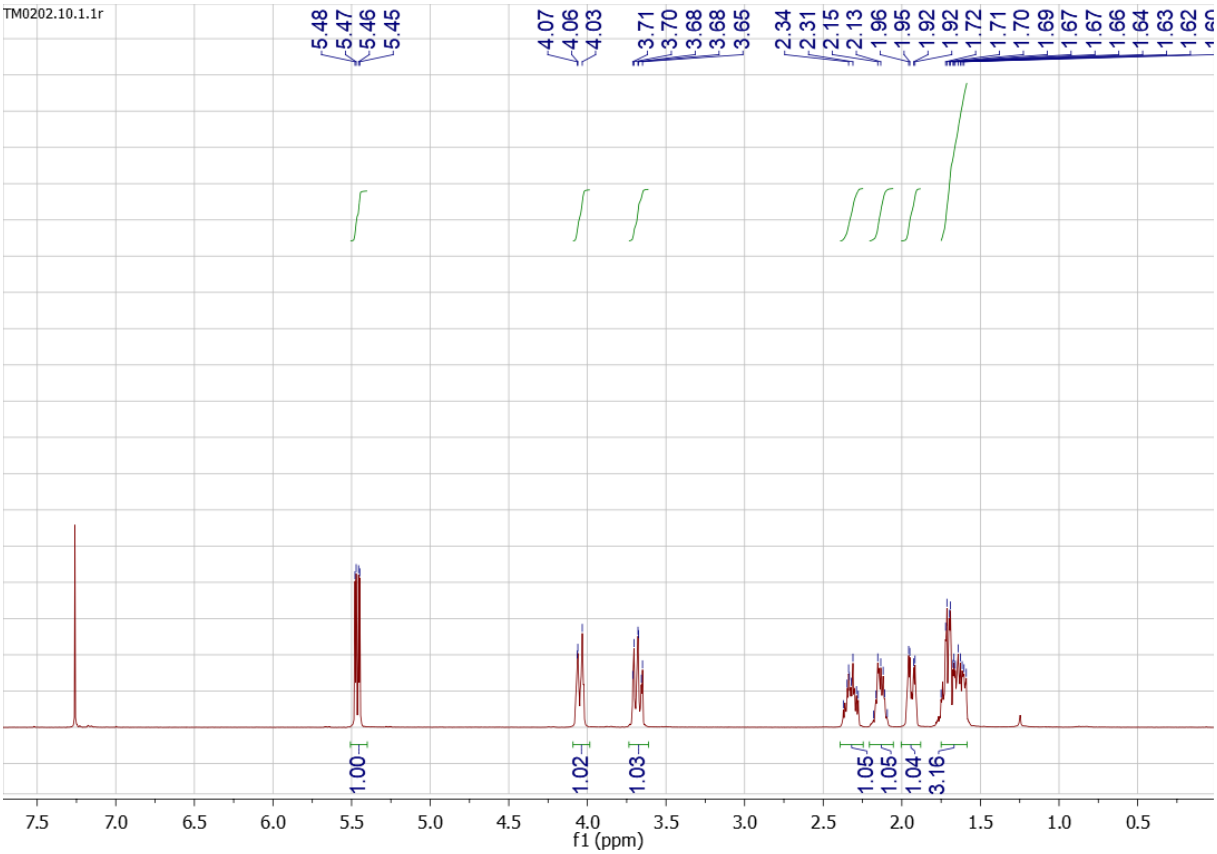

^{1}H NMR spectra of compound **115e** in $CDCl_3$.

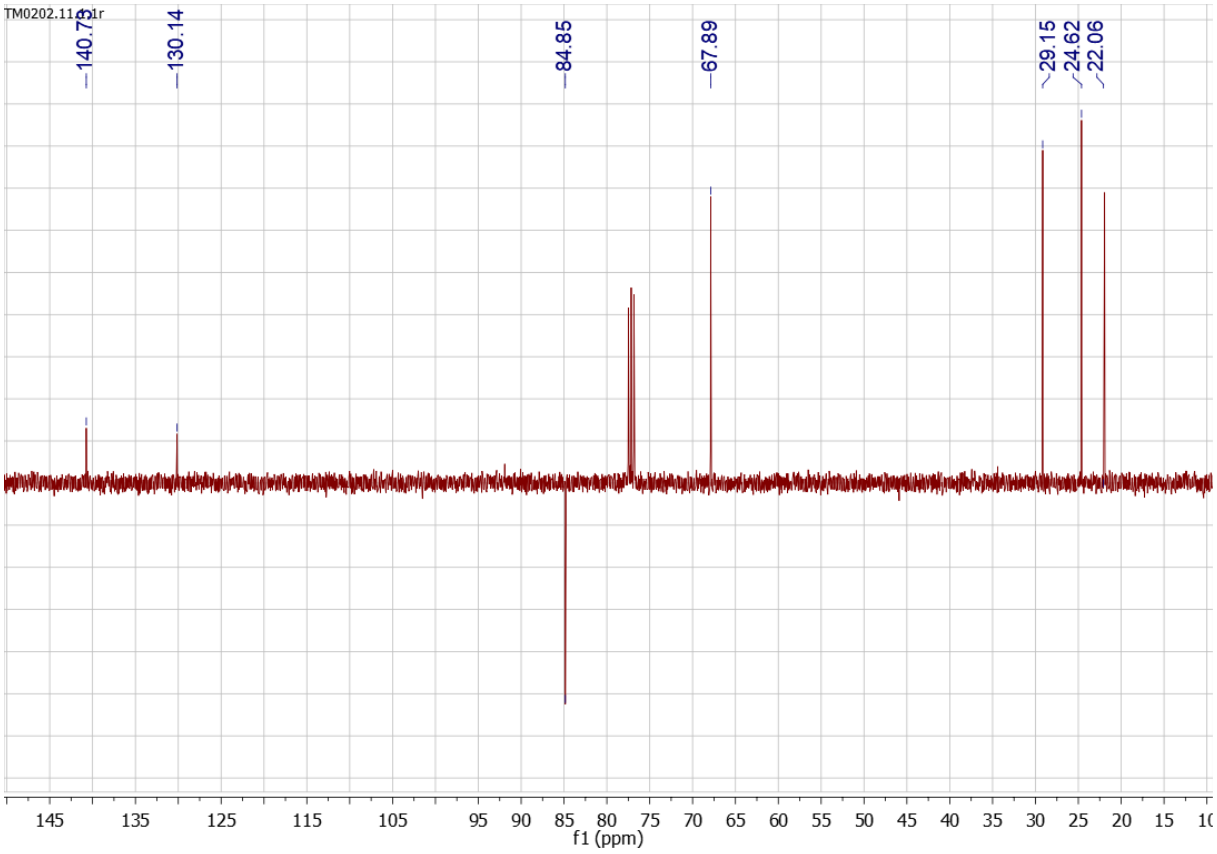

^{13}C NMR spectra of compound **115e** in $CDCl_3$.

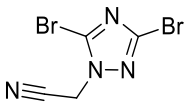

115h

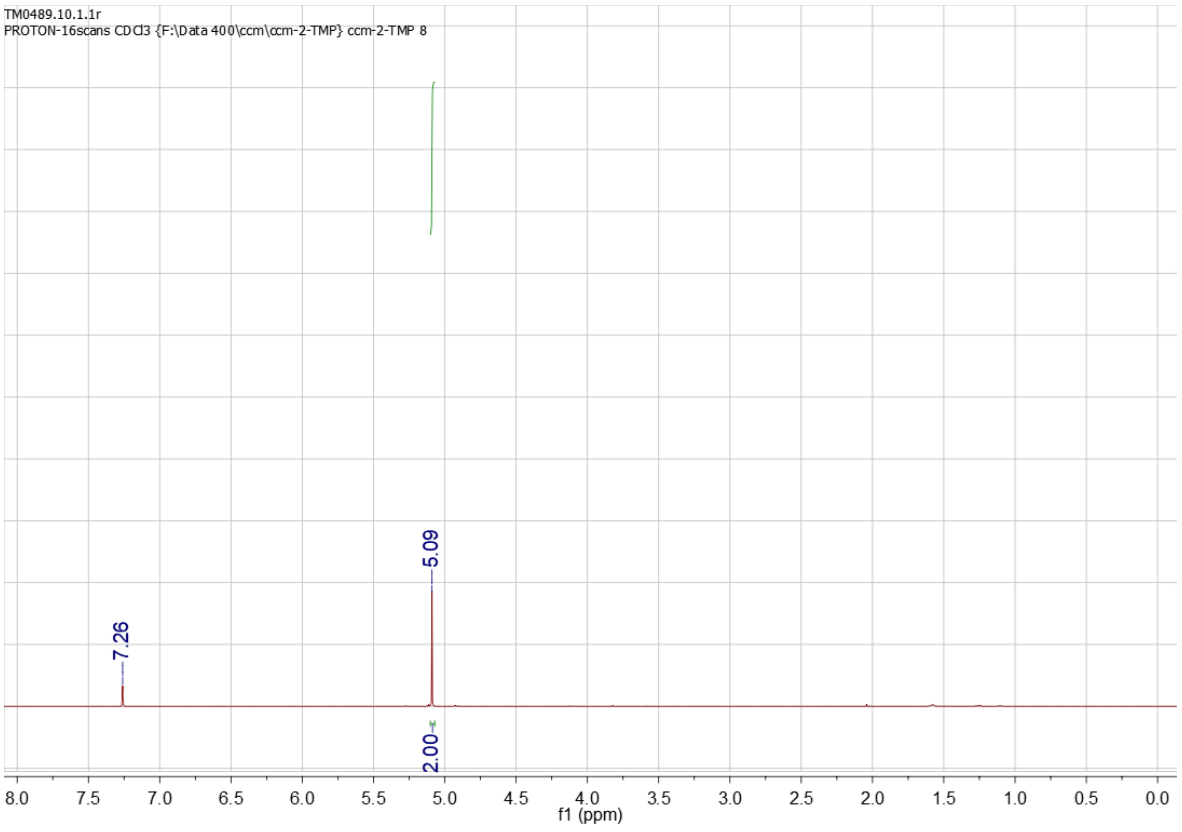

^{1}H NMR spectra of compound **115h** in $CDCl_3$.

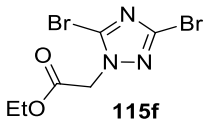

115f

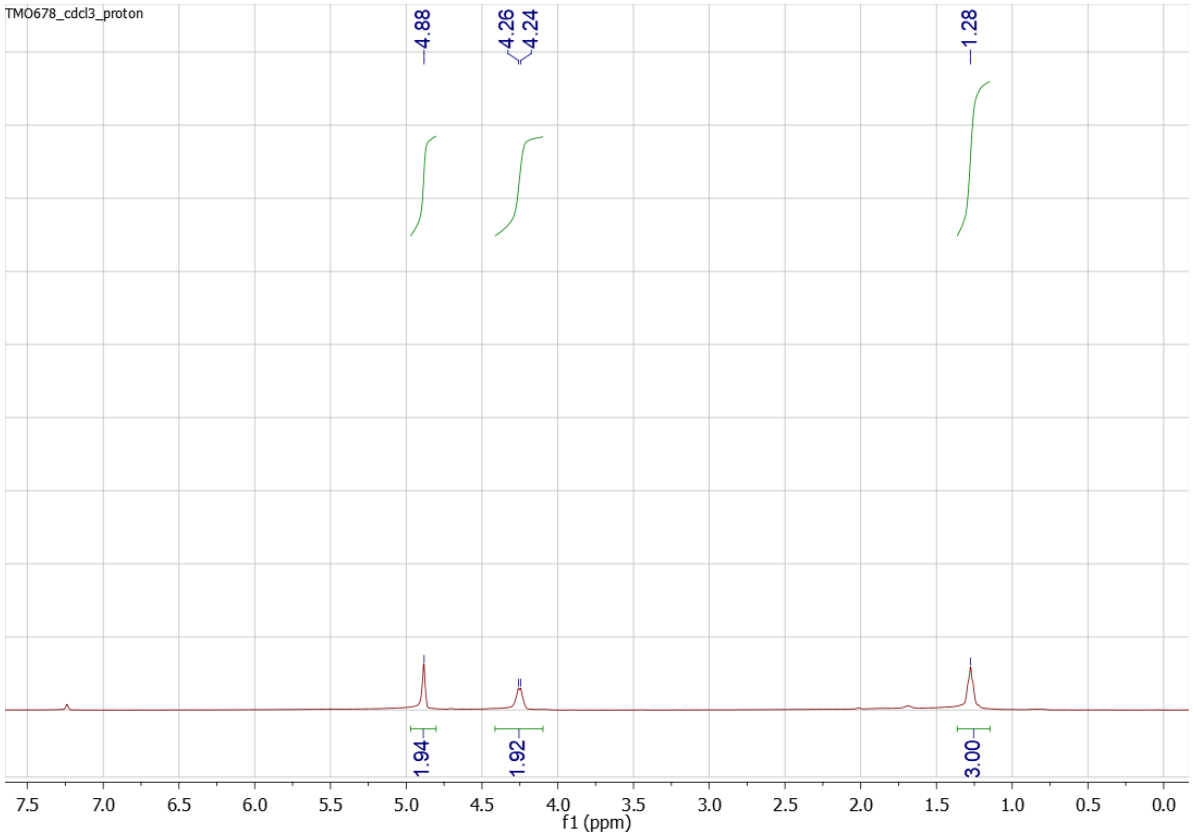

^{1}H NMR spectra of compound **115f** in $CDCl_3$.

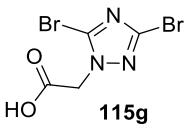

115g

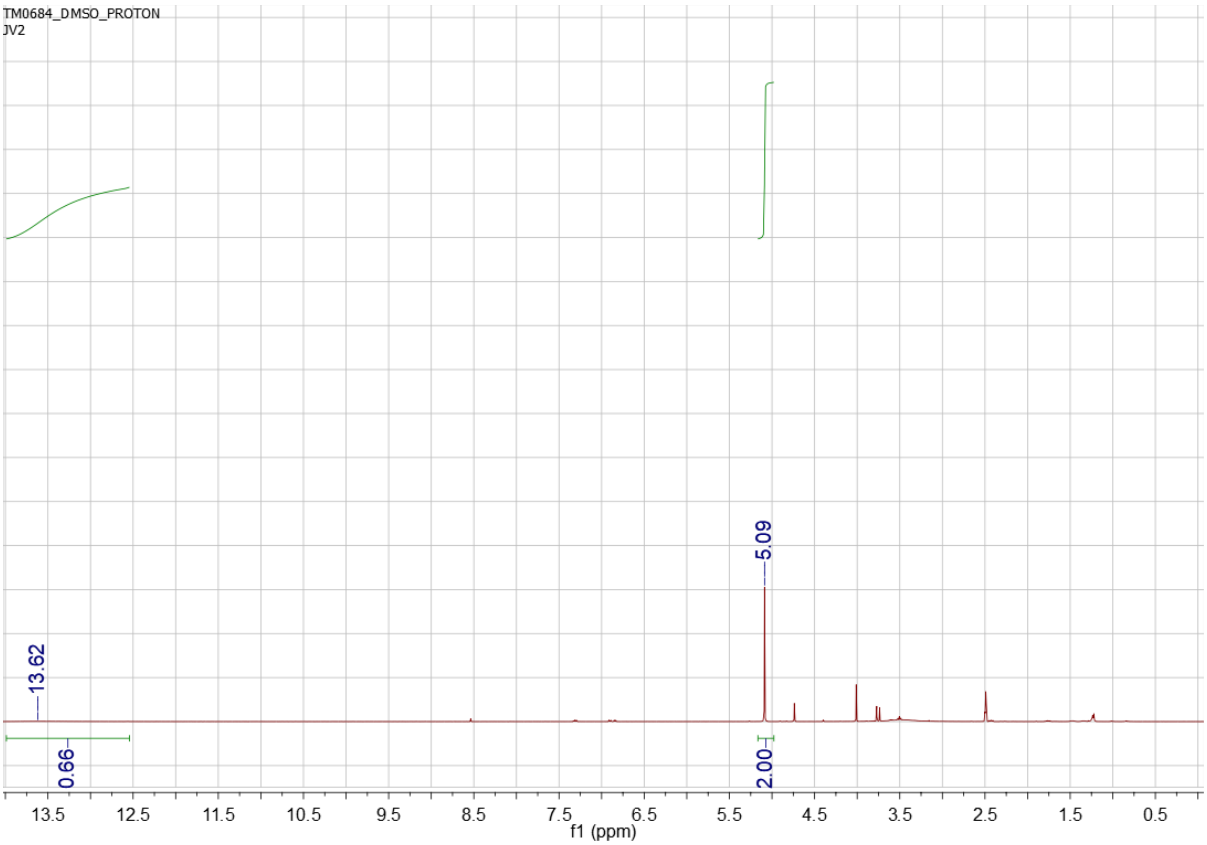

^{1}H NMR spectra of compound **115g** in DMSO.

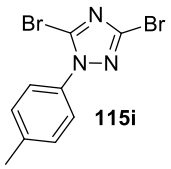

115i

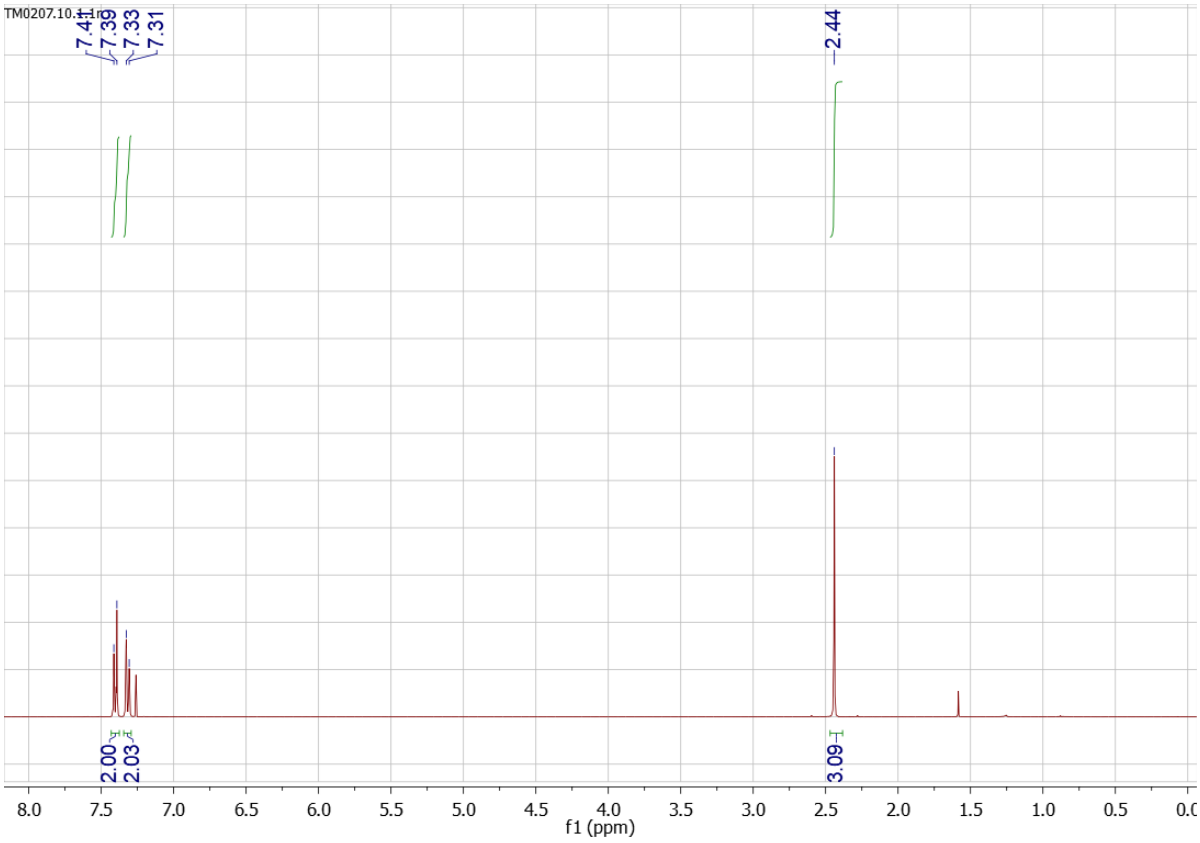

^{1}H NMR spectra of compound **115i** in $CDCl_3$.

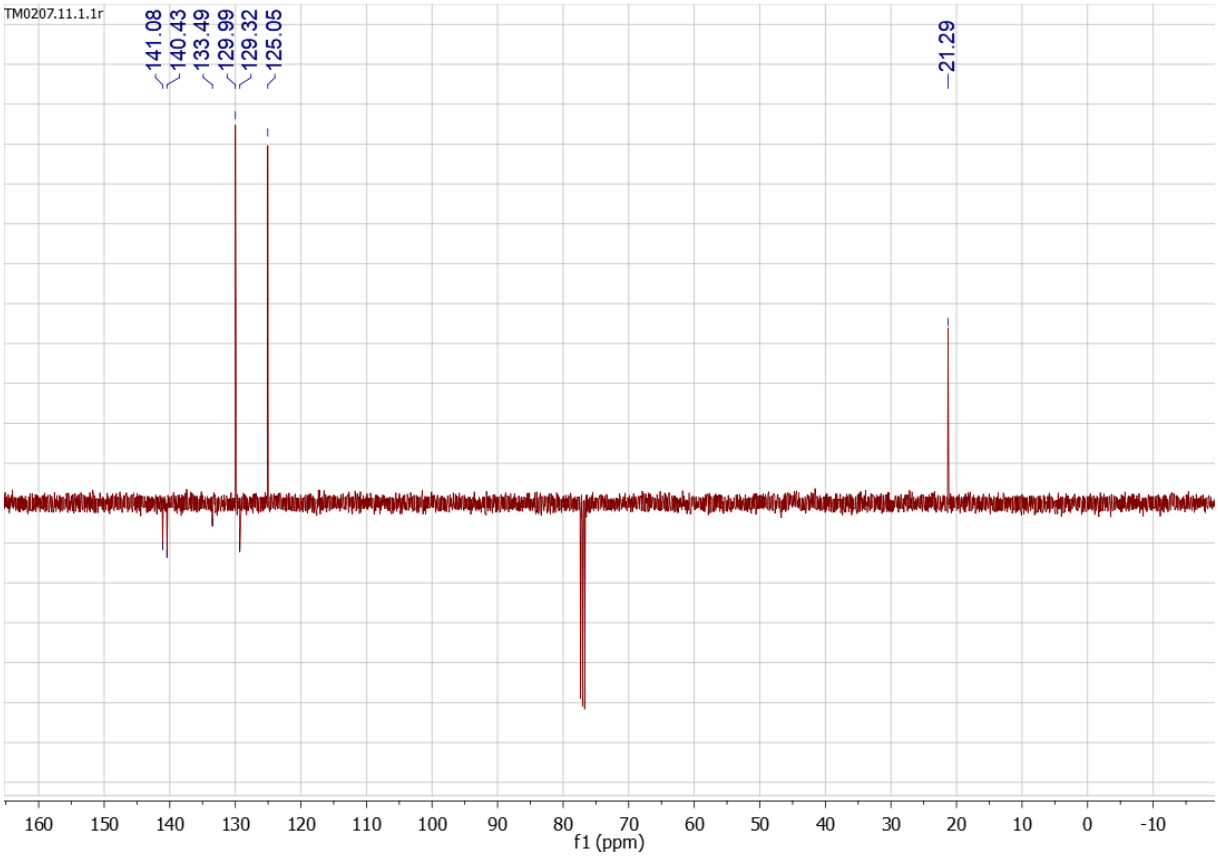

^{13}C NMR spectra of compound **115i** in $CDCl_3$.

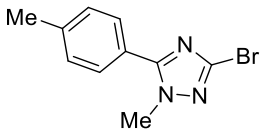

116a

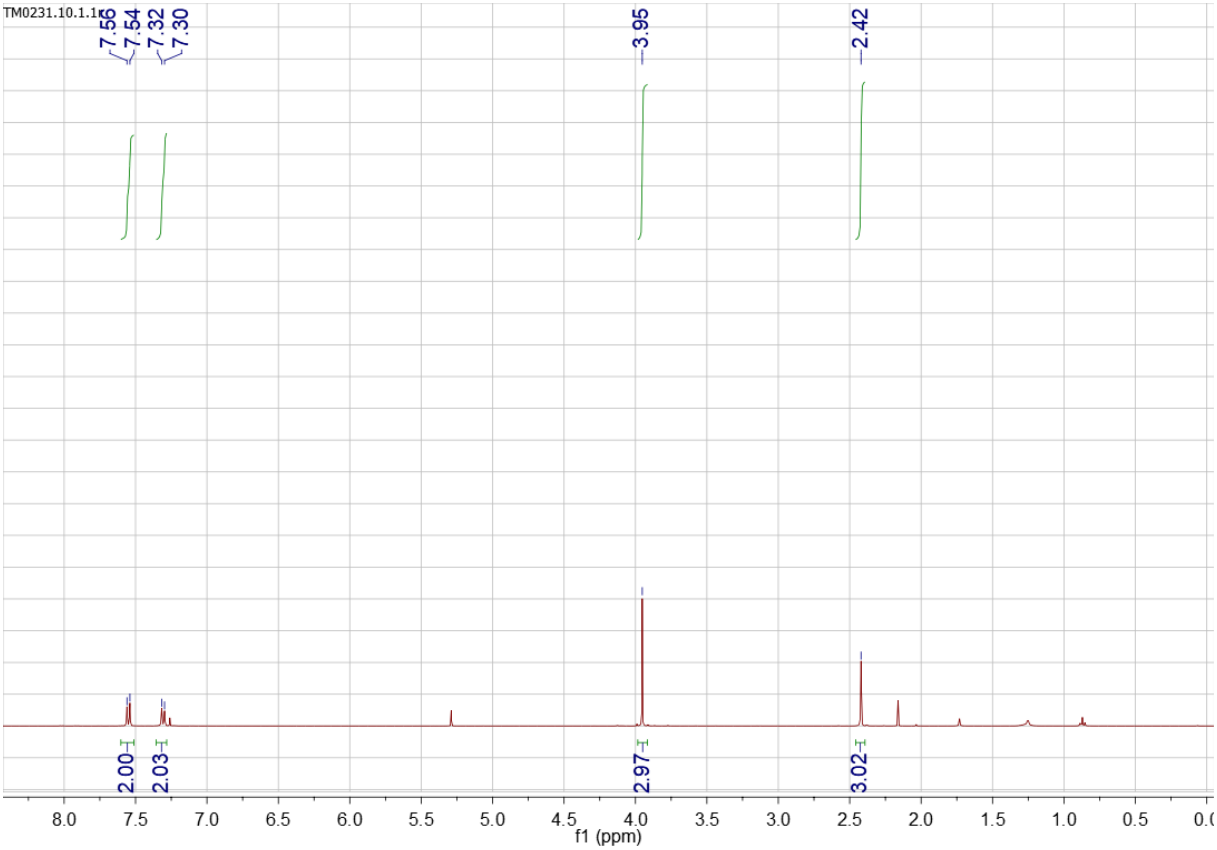

^{1}H NMR spectra of compound **116a** in $CDCl_3$.

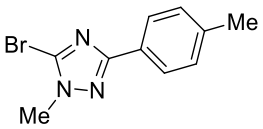

135a

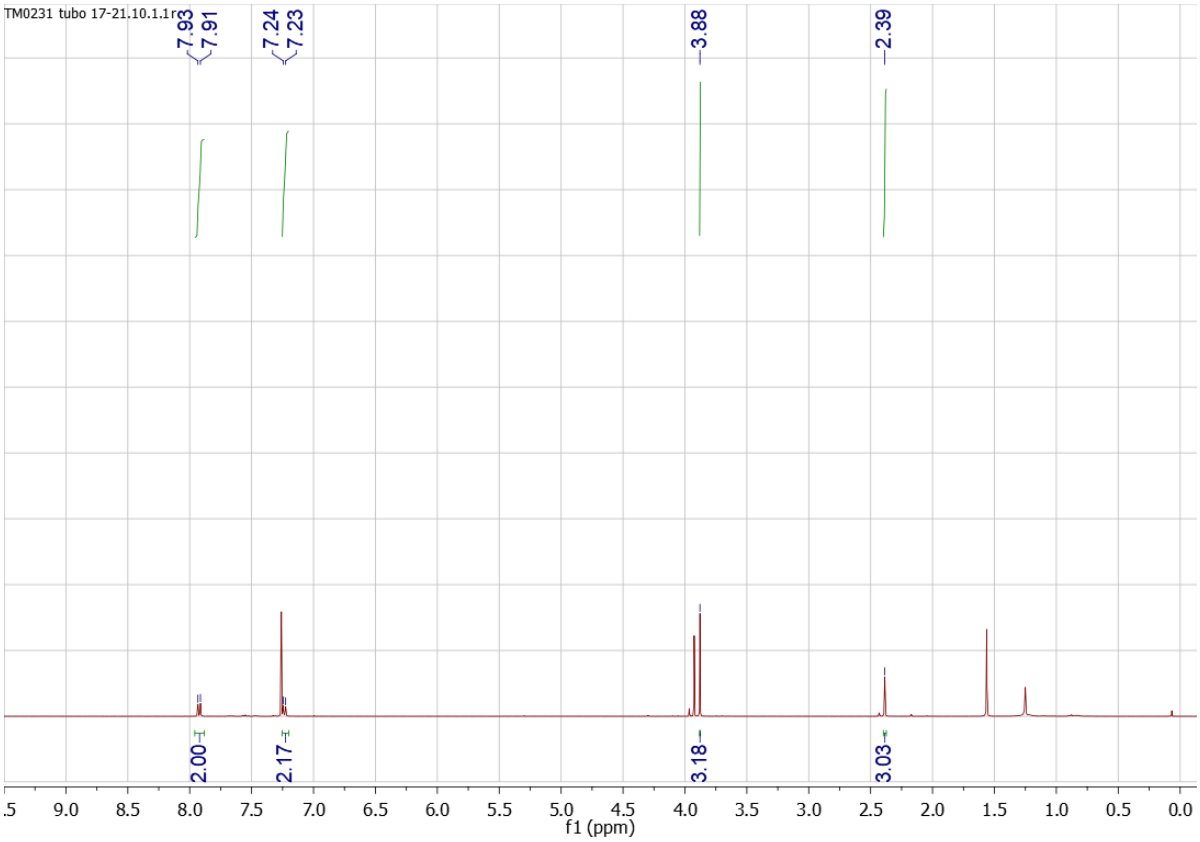

^{1}H NMR spectra of compound **135a** in $CDCl_3$.

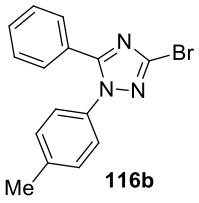

116b

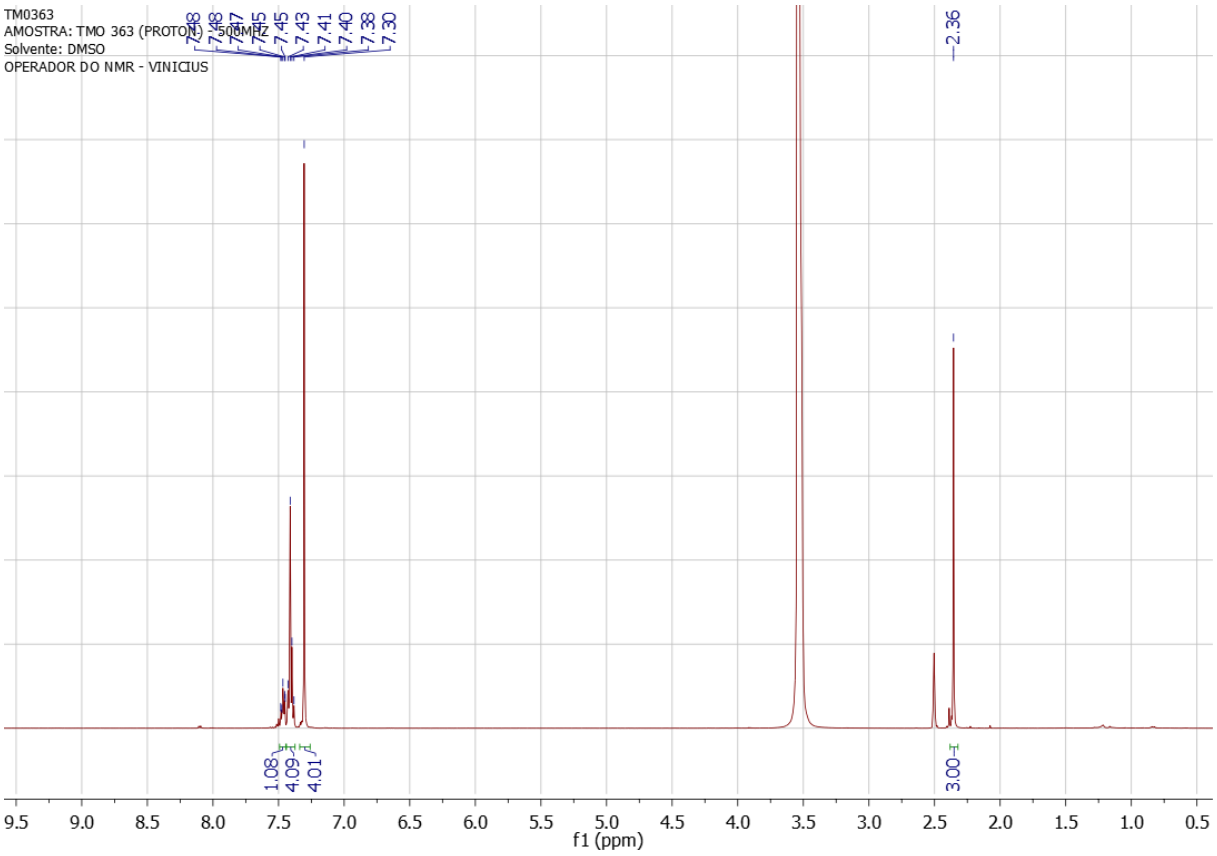

^{1}H NMR spectra of compound **116b** in DMSO.

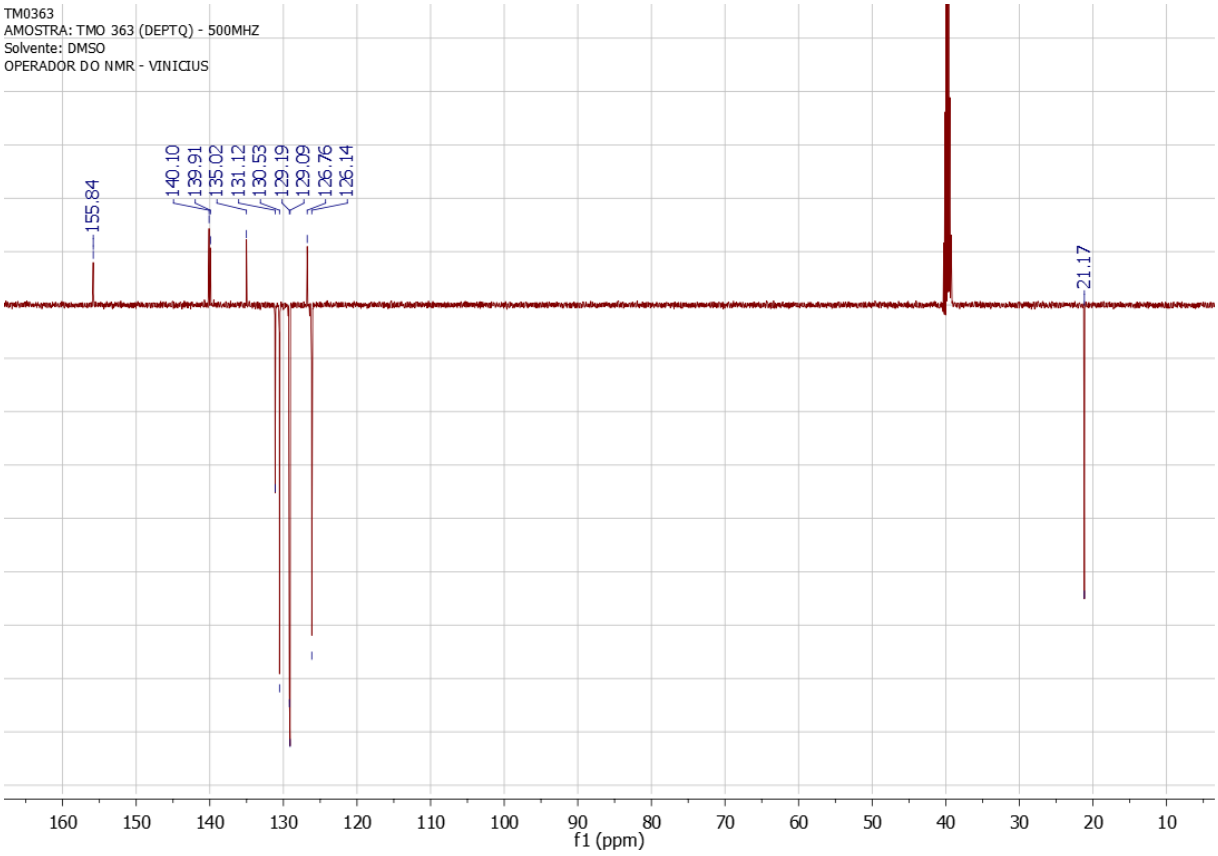

^{13}C NMR spectra of compound **116b** in DMSO.

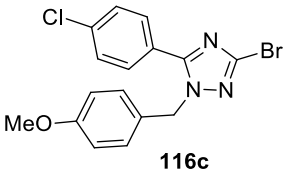

116c

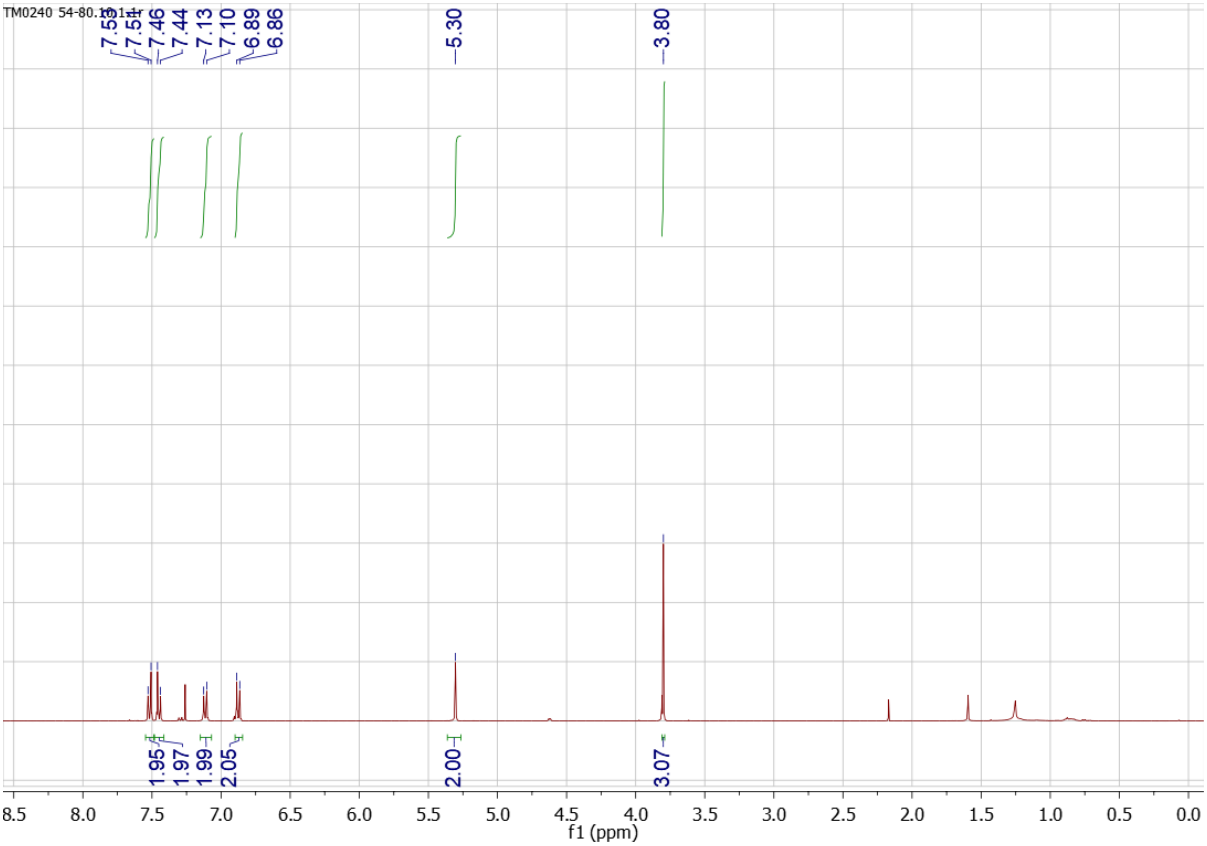

^{1}H NMR spectra of compound **116c** in $CDCl_3$.

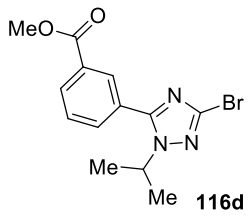

116d

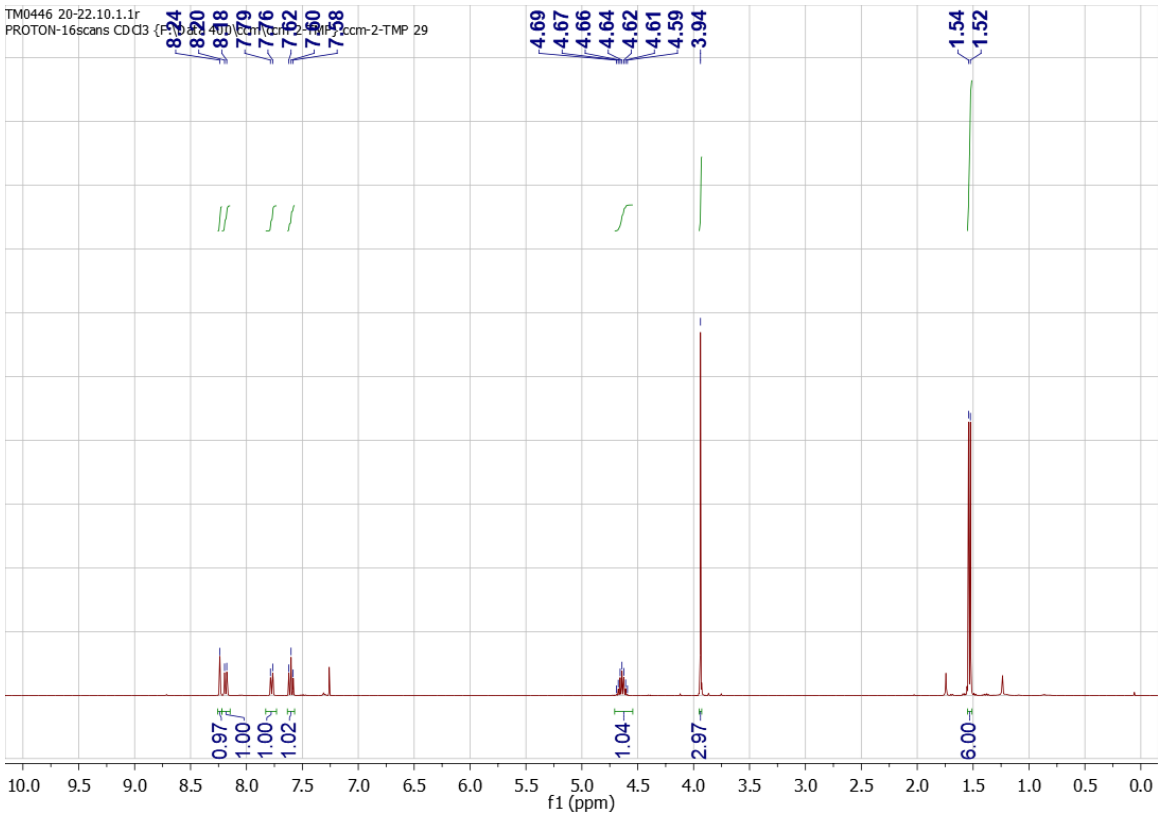

^{1}H NMR spectra of compound **116d** in $CDCl_3$.

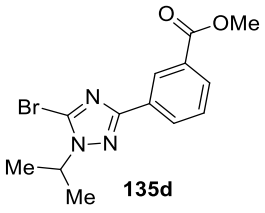

135d

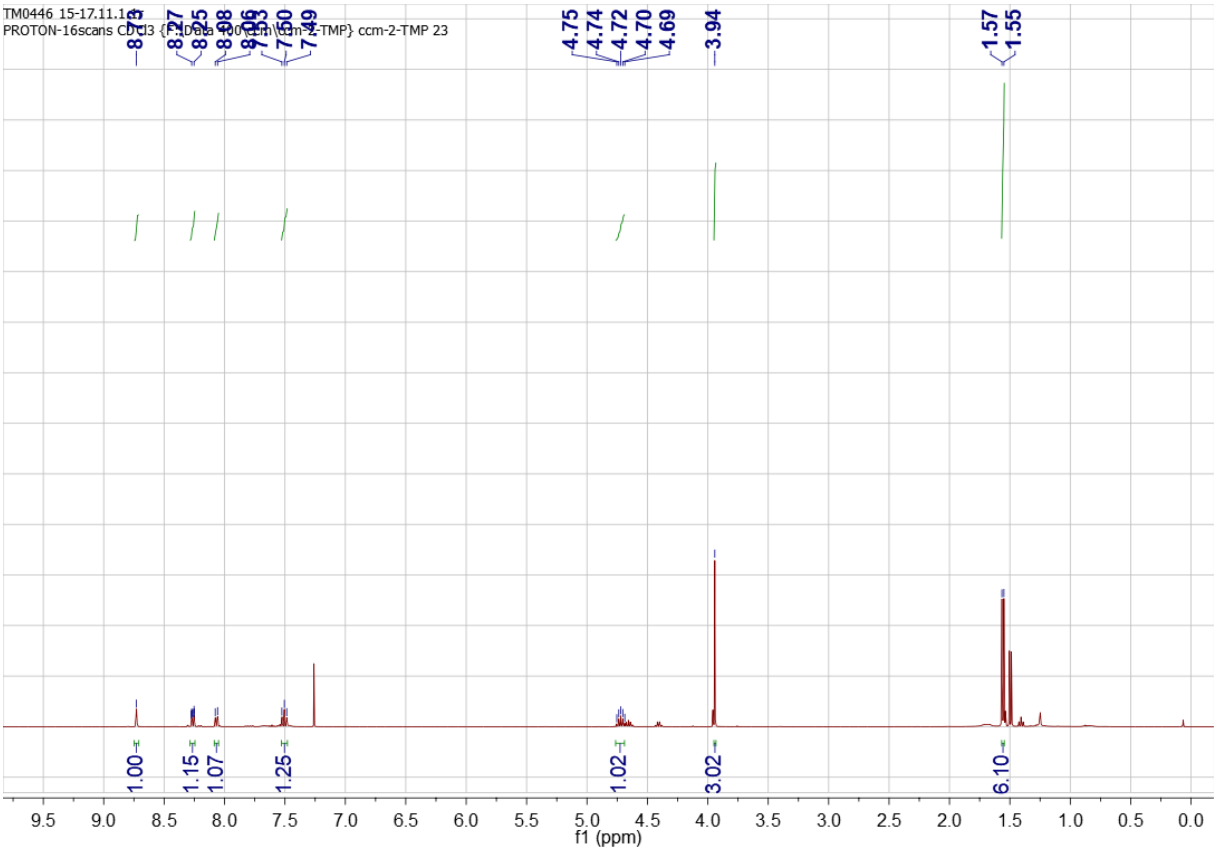

^{1}H NMR spectra of compound **135d** in $CDCl_3$.

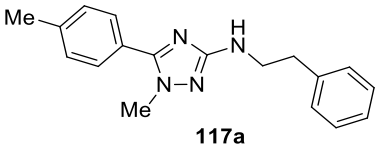

117a

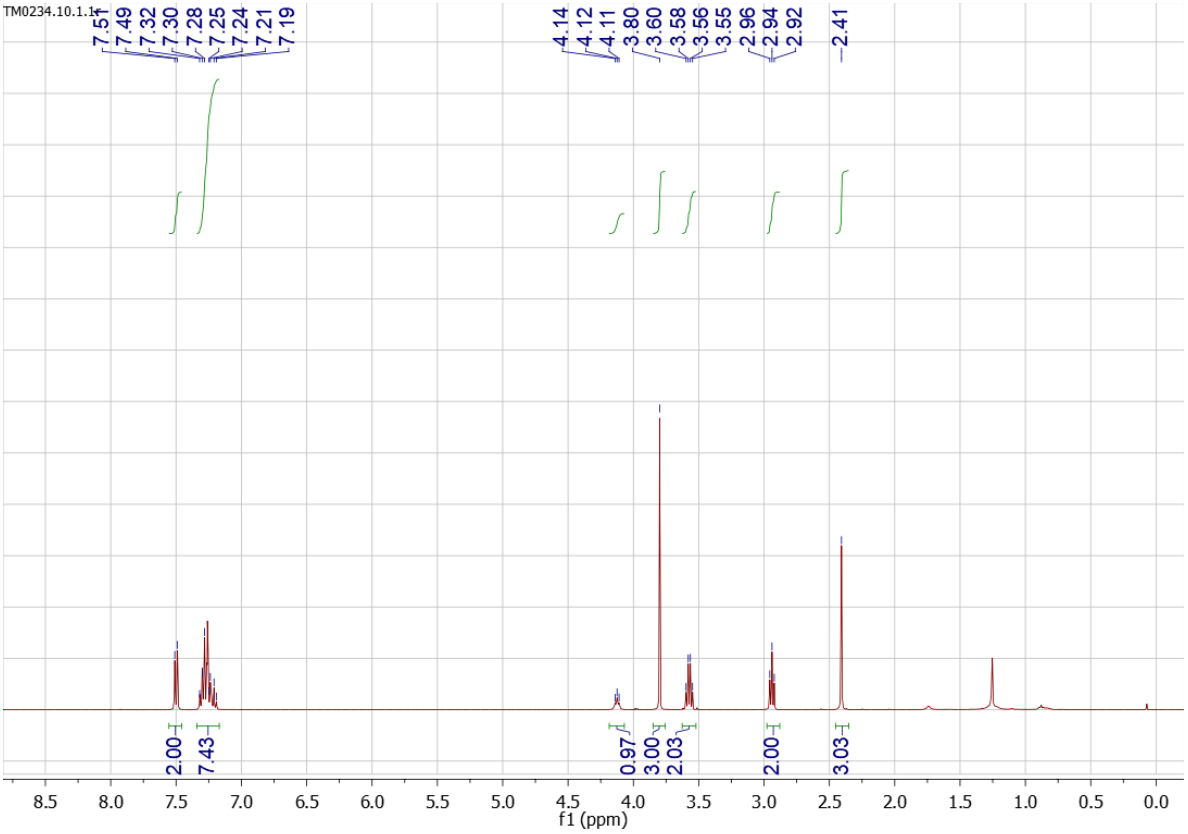

^{1}H NMR spectra of compound **117a** in $CDCl_3$.

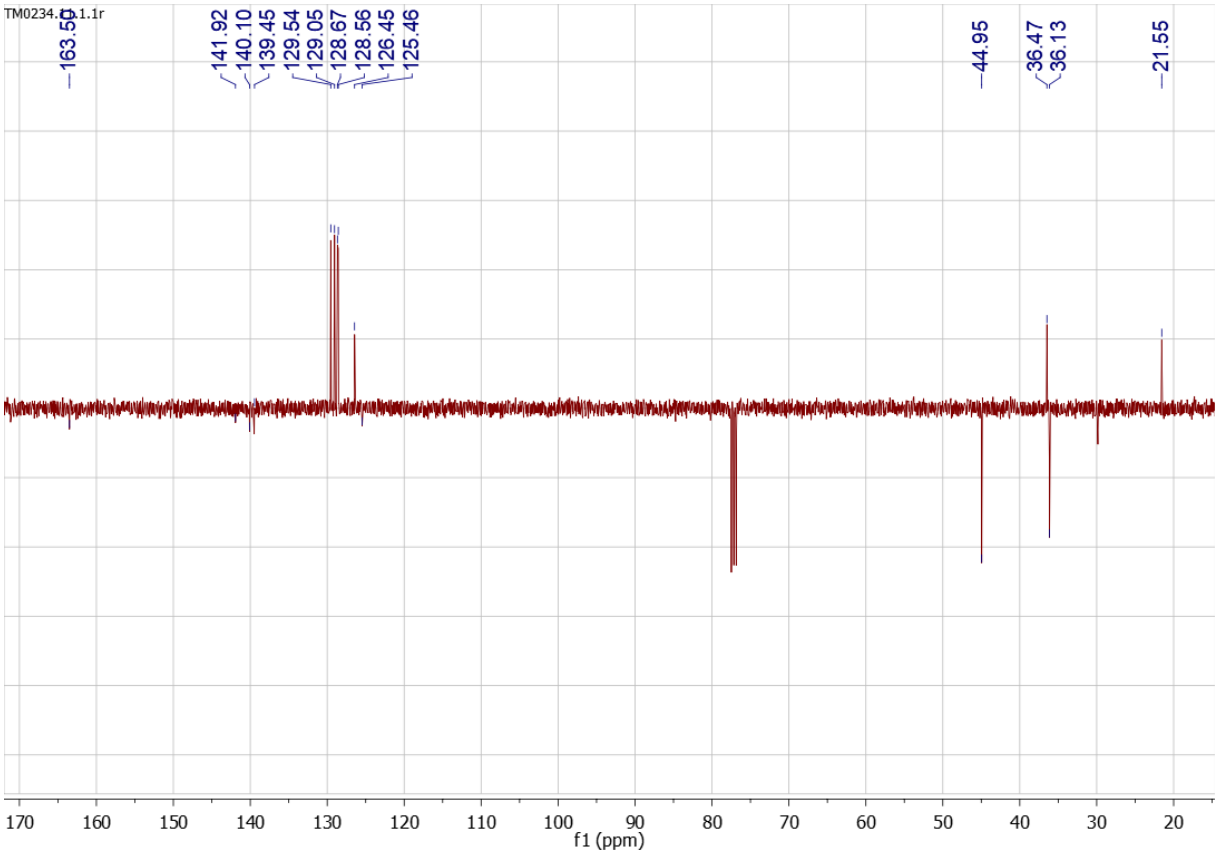

^{13}C NMR spectra of compound **117a** in $CDCl_3$.

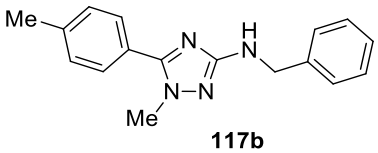

117b

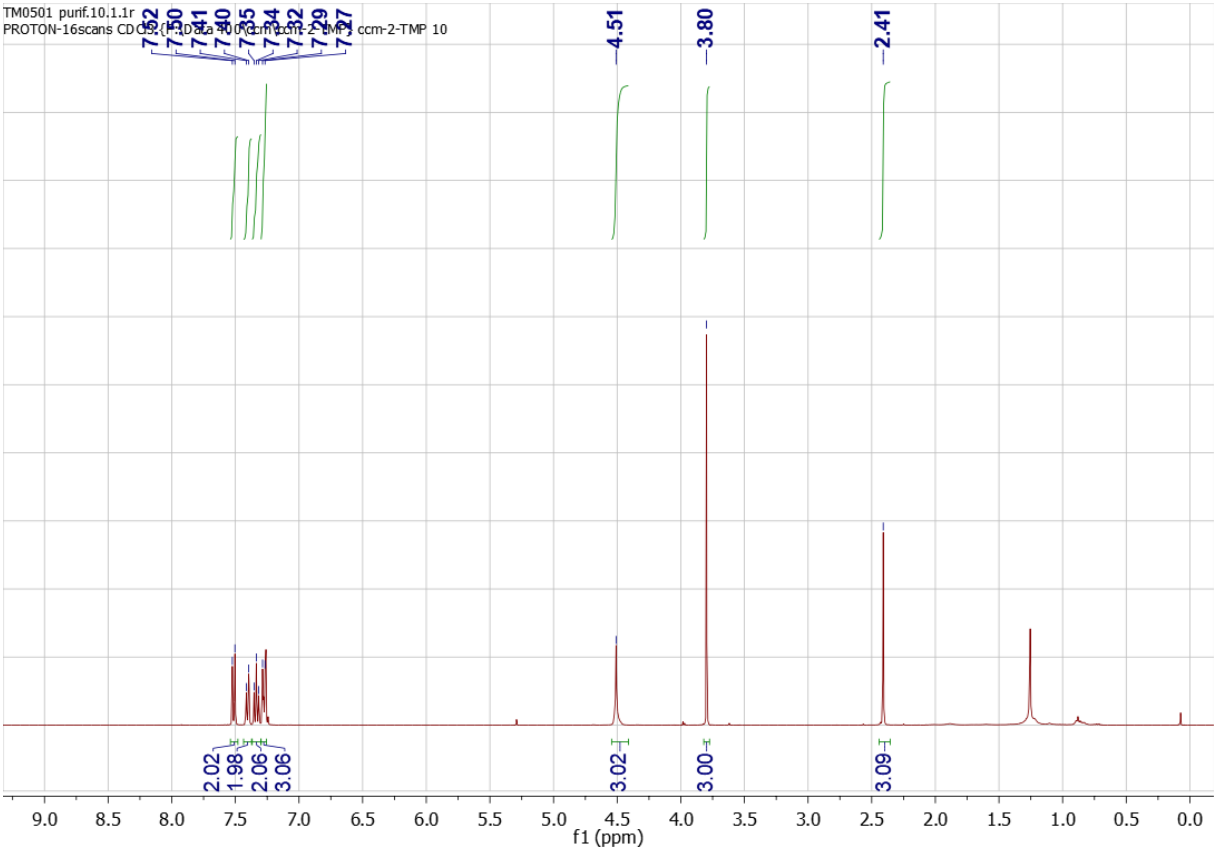

^{1}H NMR spectra of compound **117b** in $CDCl_3$.

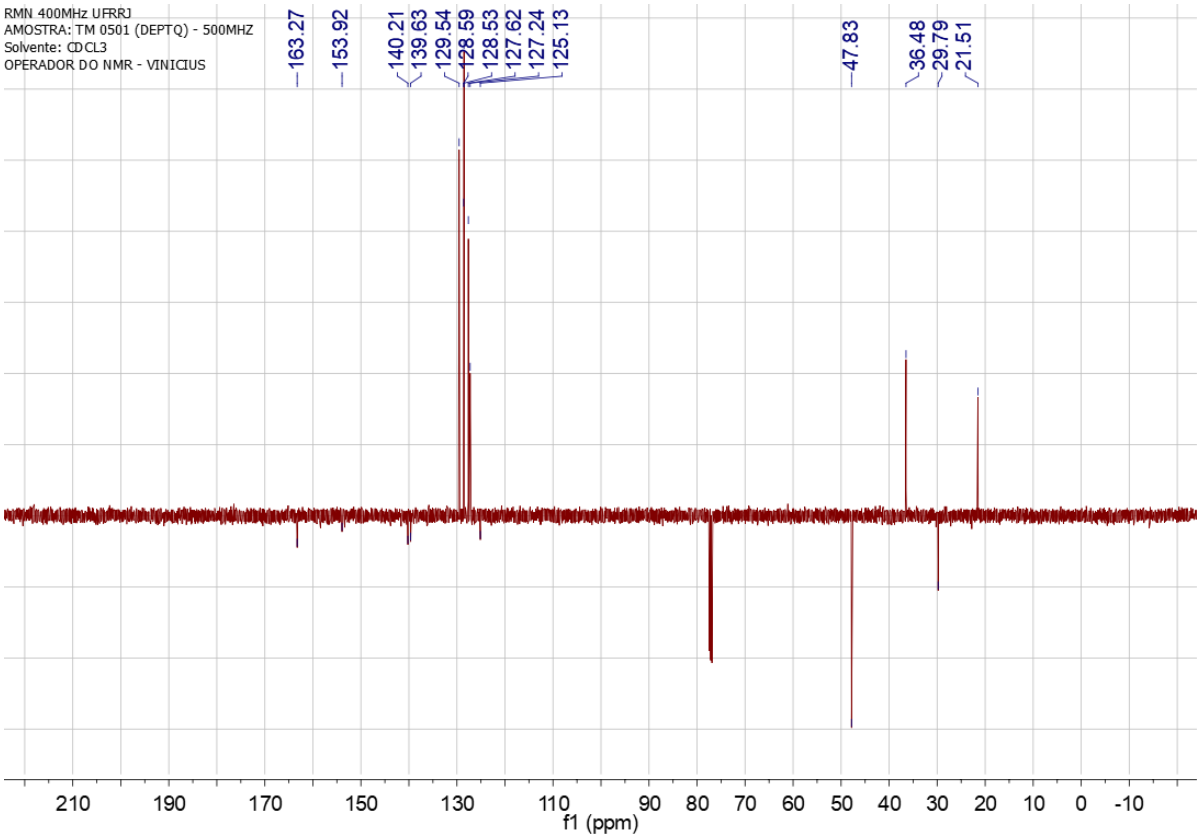

^{13}C NMR spectra of compound **117b** in $CDCl_3$.

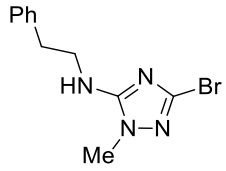

118a

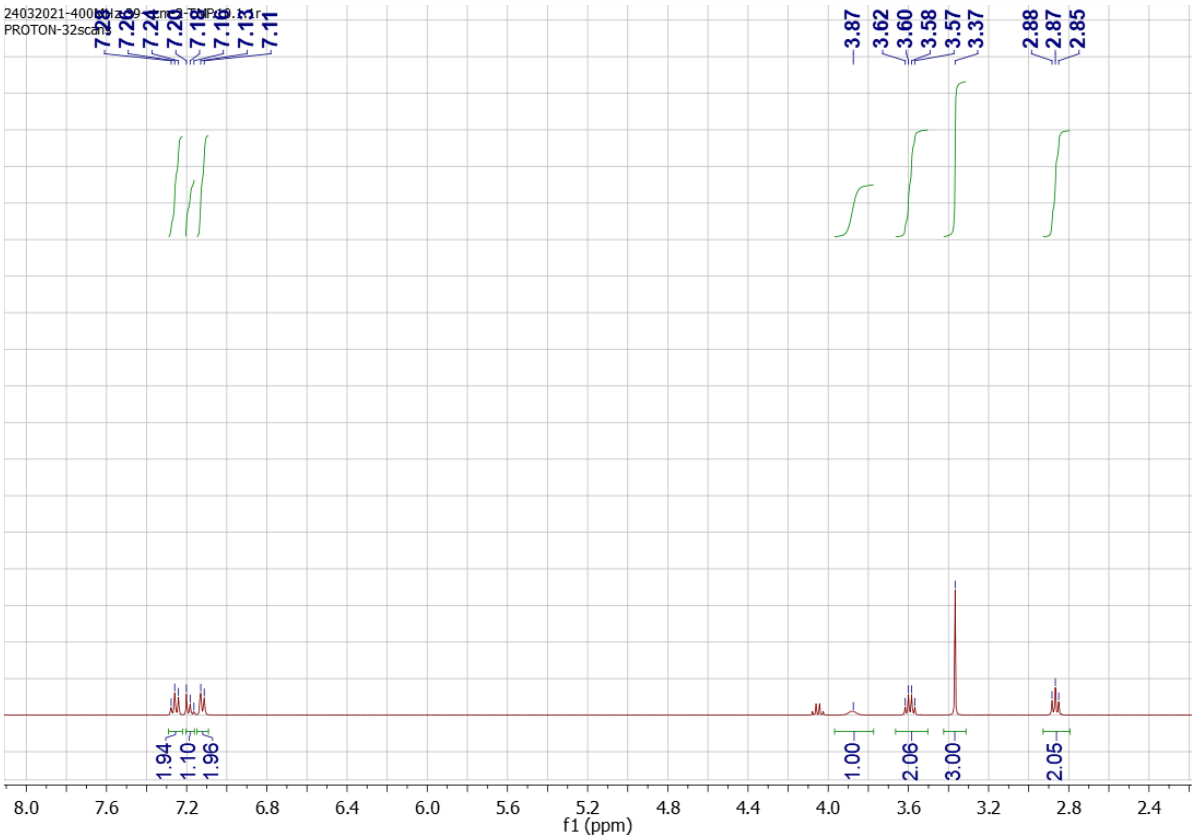

^{1}H NMR spectra of compound **118a** in $CDCl_3$.

.

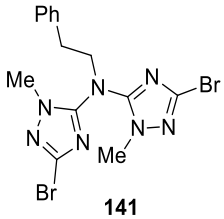

141

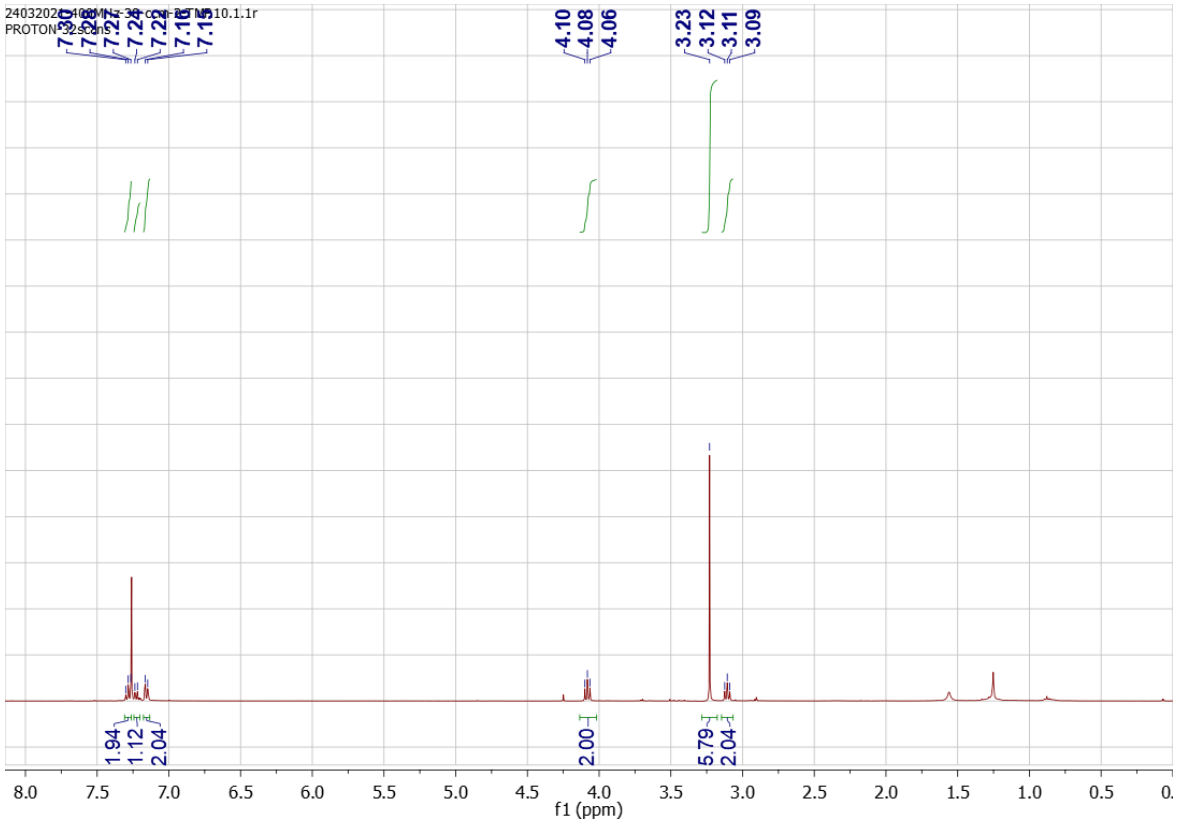

^{1}H NMR spectra of compound **141** in $CDCl_3$.

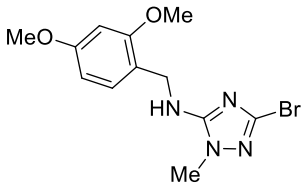

118c

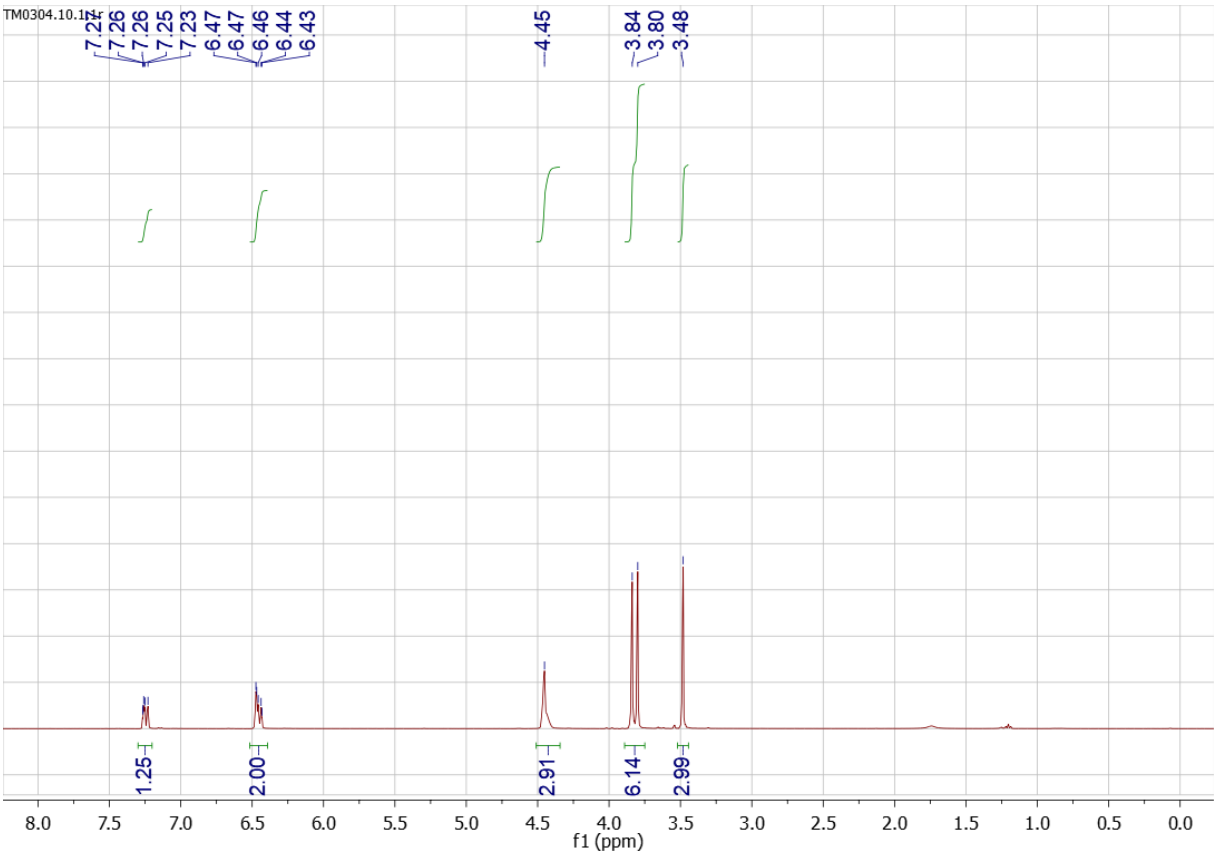

^{1}H NMR spectra of compound **118c** in $CDCl_3$.

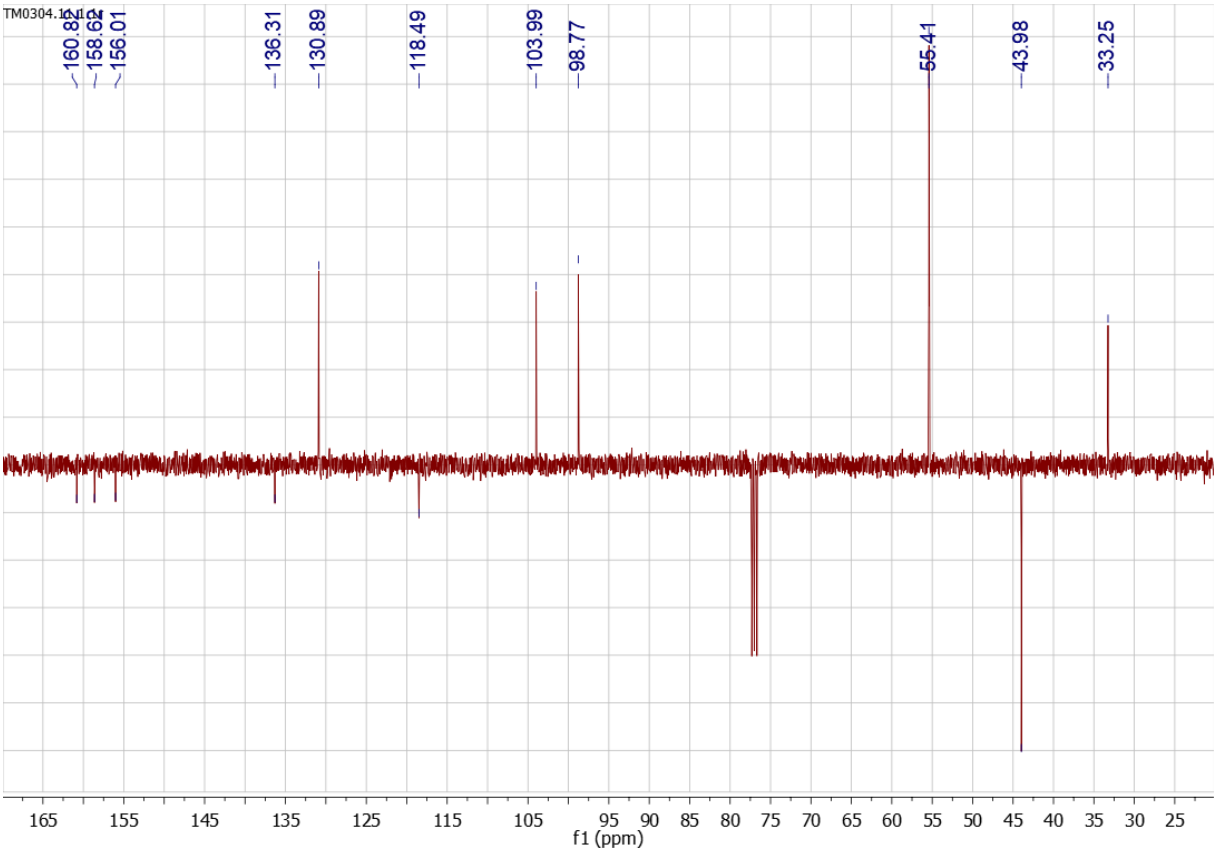

^{13}C NMR spectra of compound **118c** in $CDCl_3$.

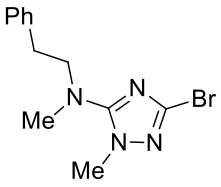

118e

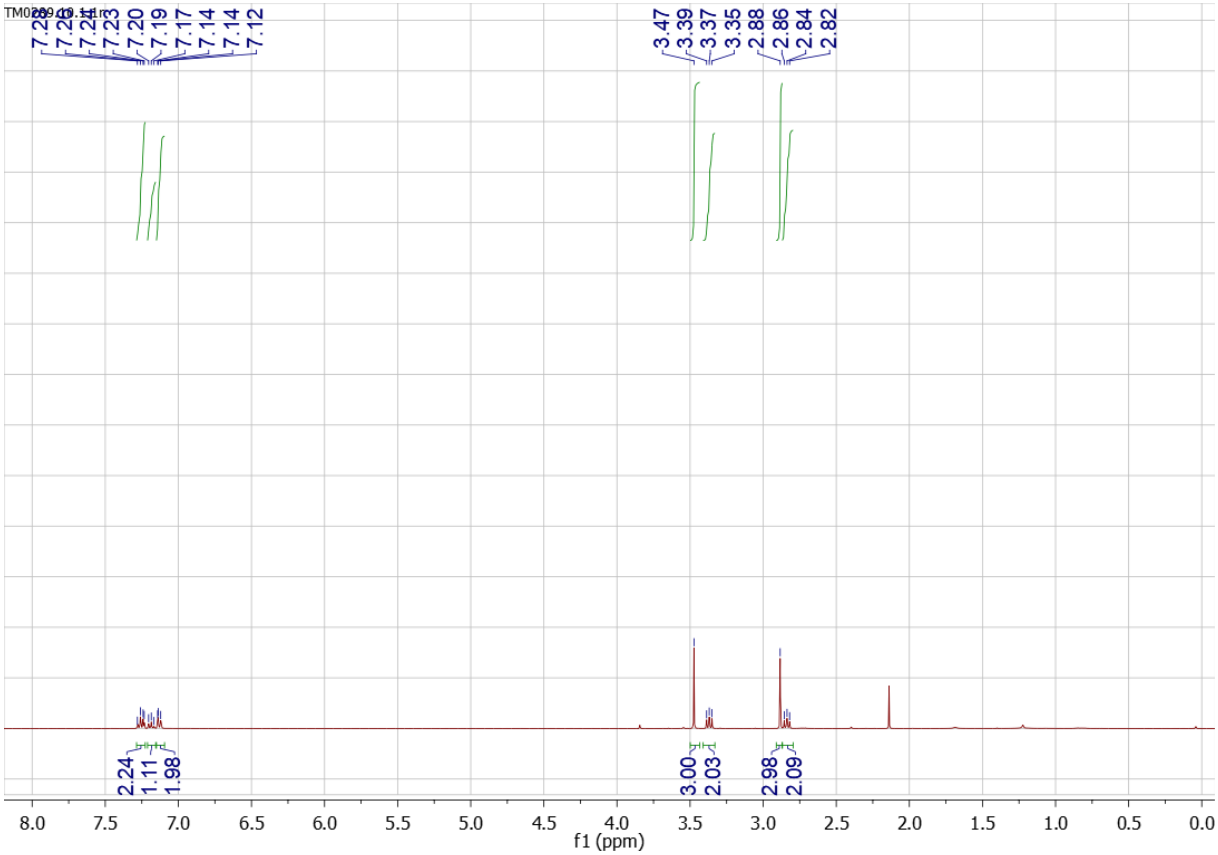

^{1}H NMR spectra of compound **118e** in $CDCl_3$.

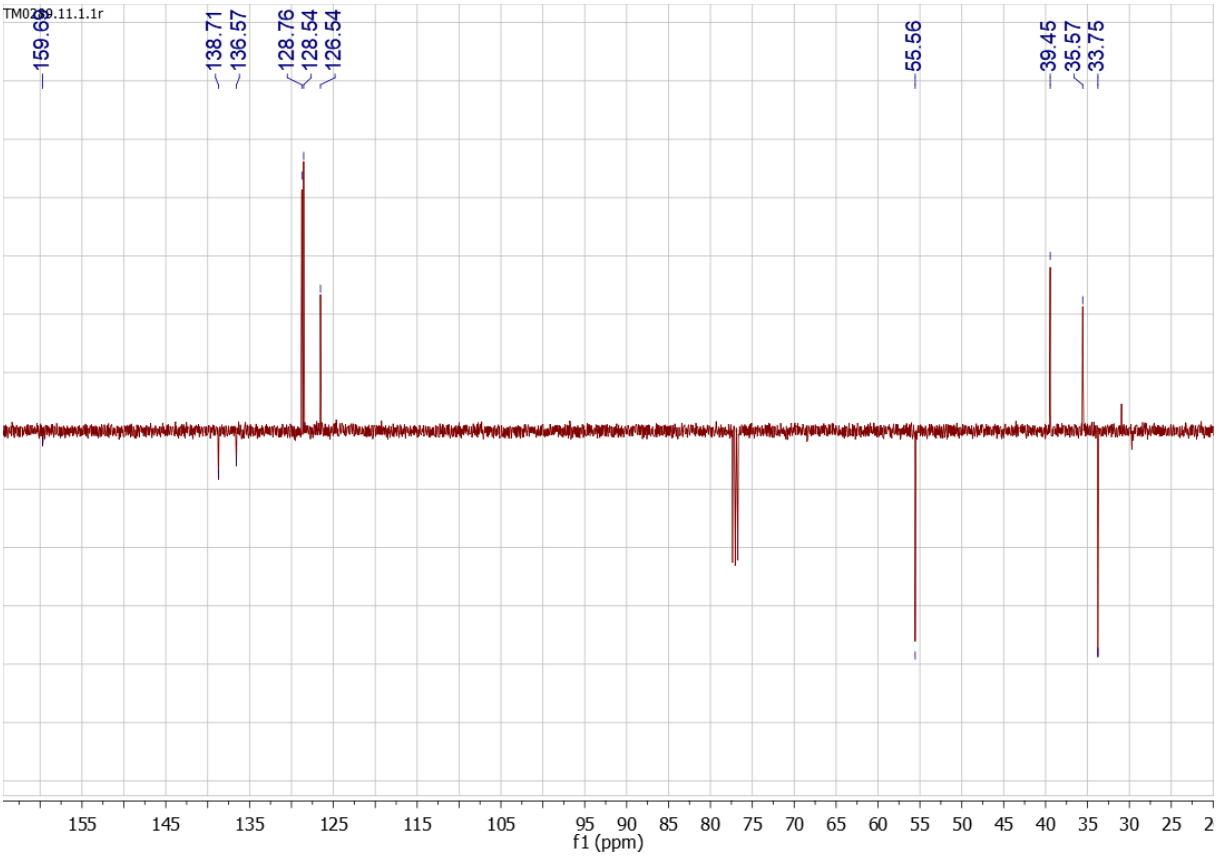

^{13}C NMR spectra of compound **118e** in $CDCl_3$.

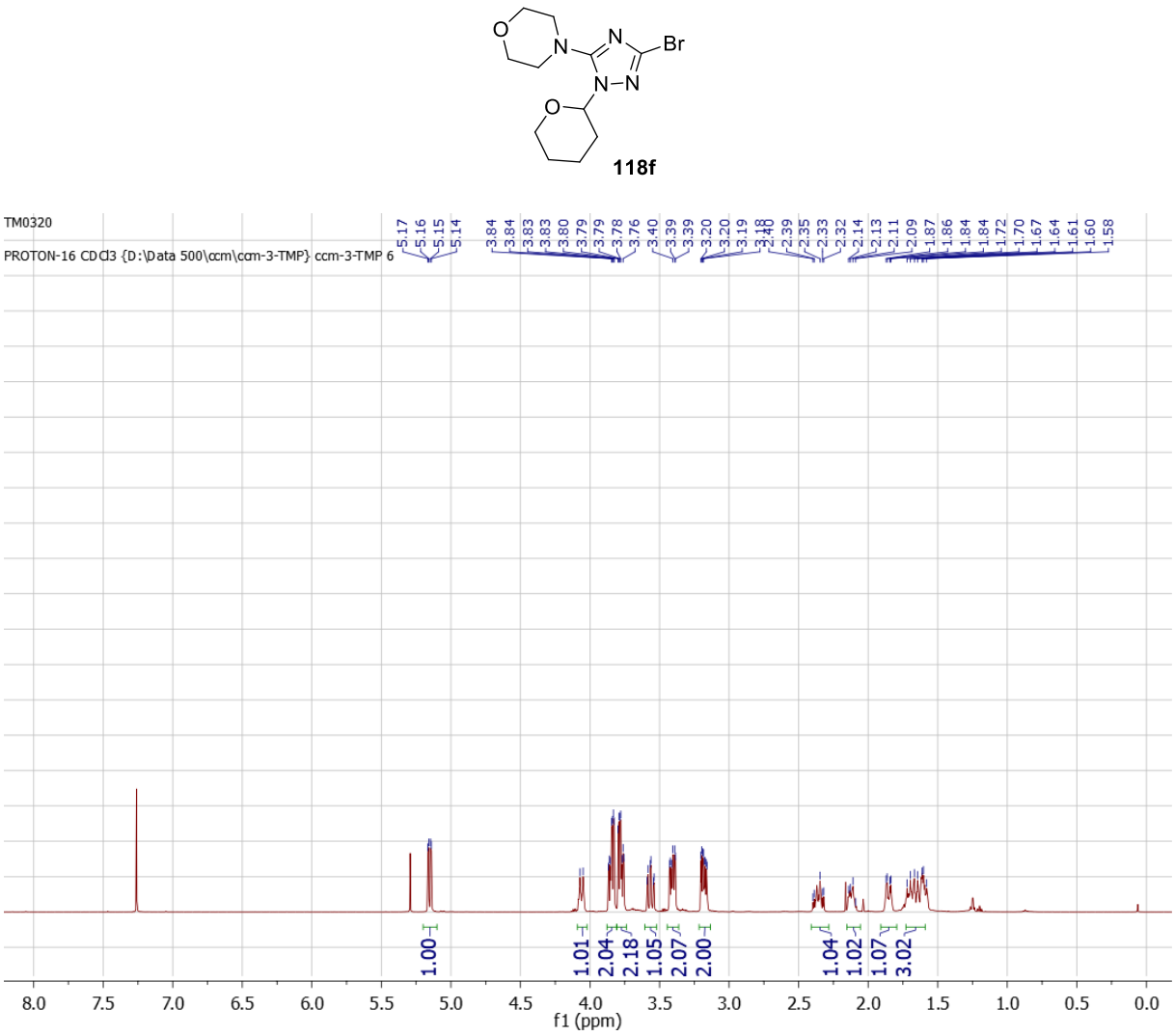

^{1}H NMR spectra of compound **118f** in $CDCl_3$.

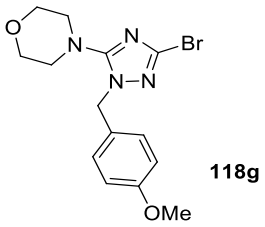

118g

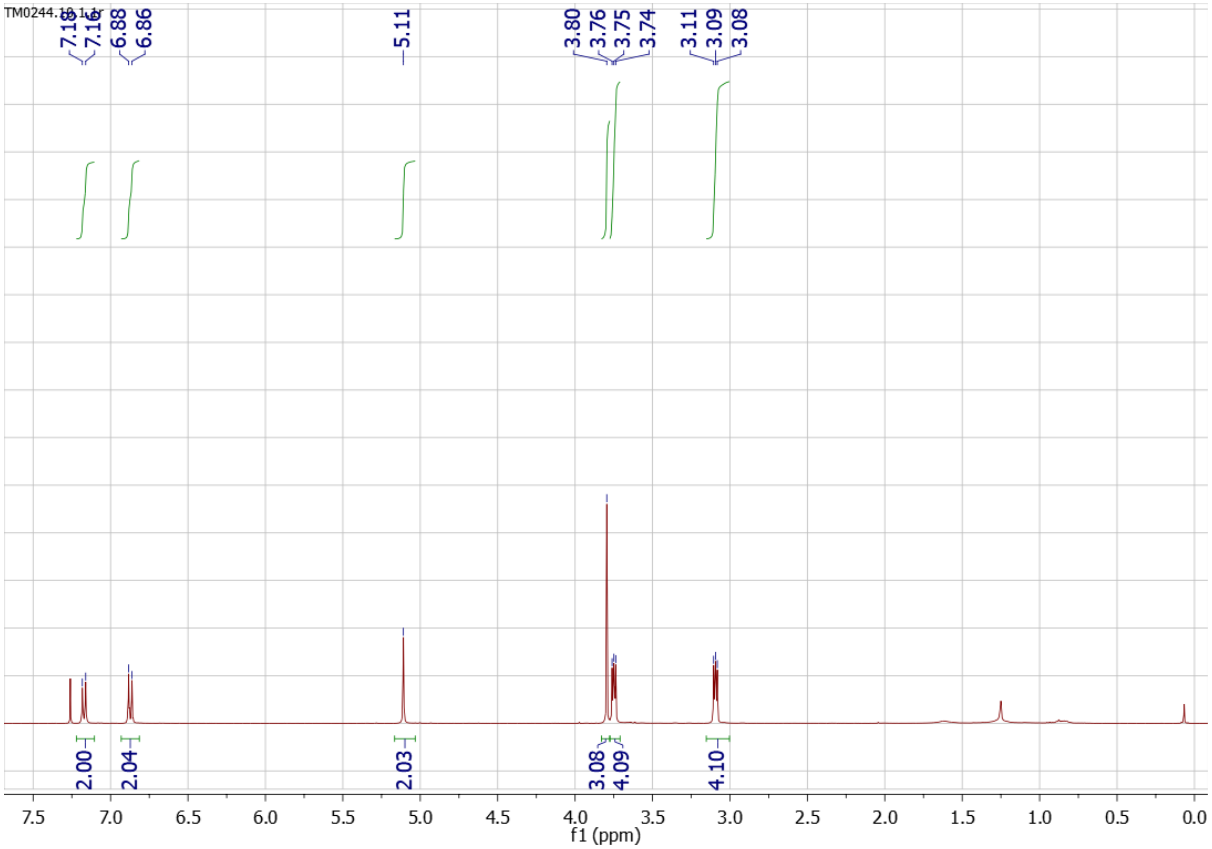

^{1}H NMR spectra of compound **118g** in $CDCl_3$.

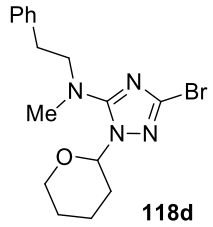

118d

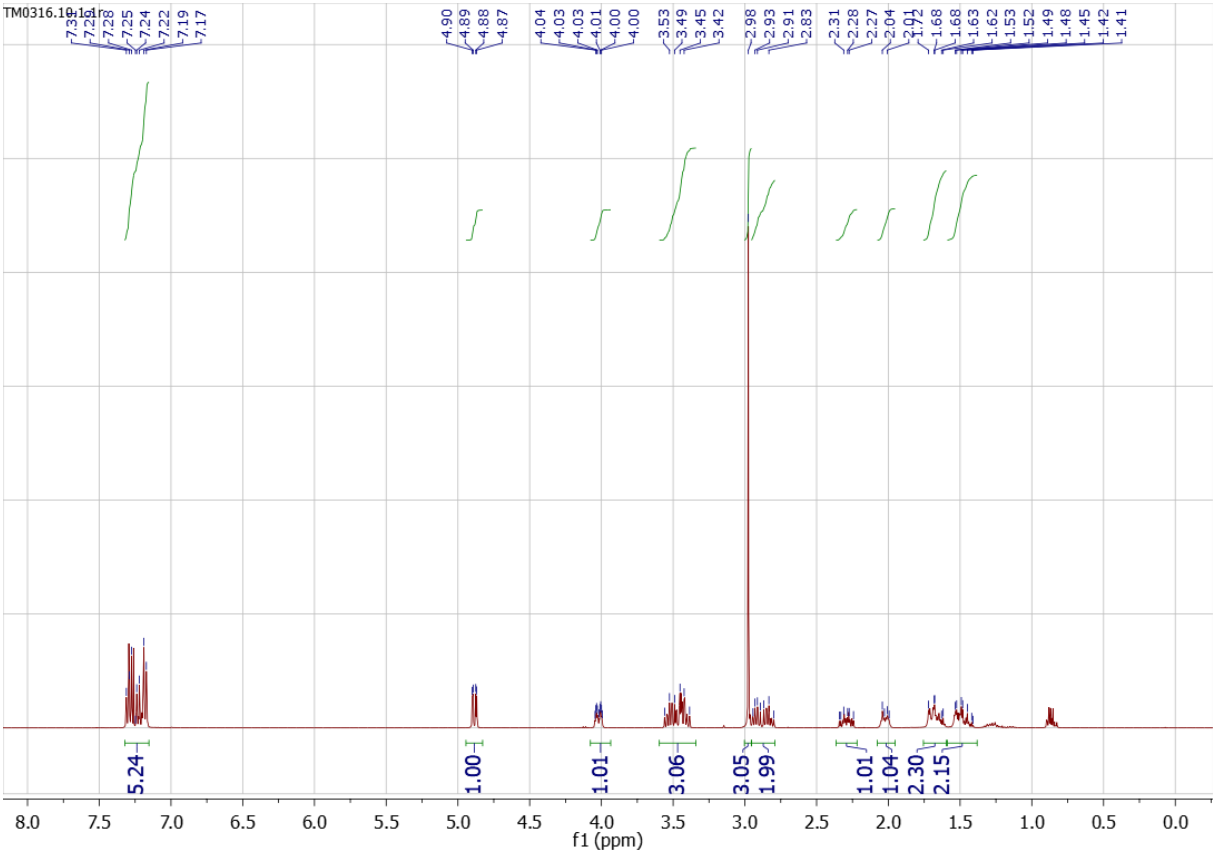

^{1}H NMR spectra of compound **118d** in $CDCl_3$.

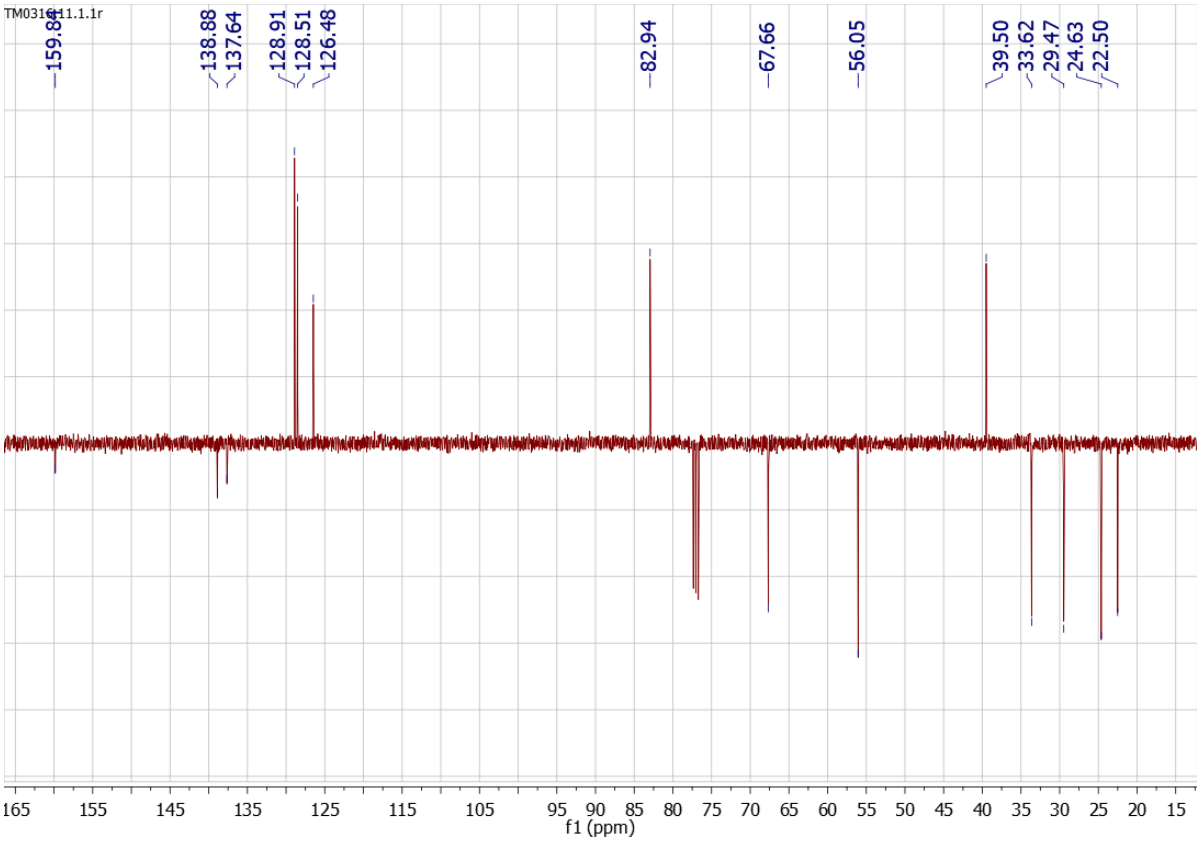

^{13}C NMR spectra of compound **118d** in $CDCl_3$.

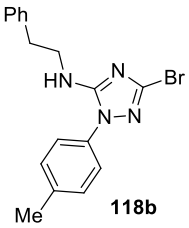

118b

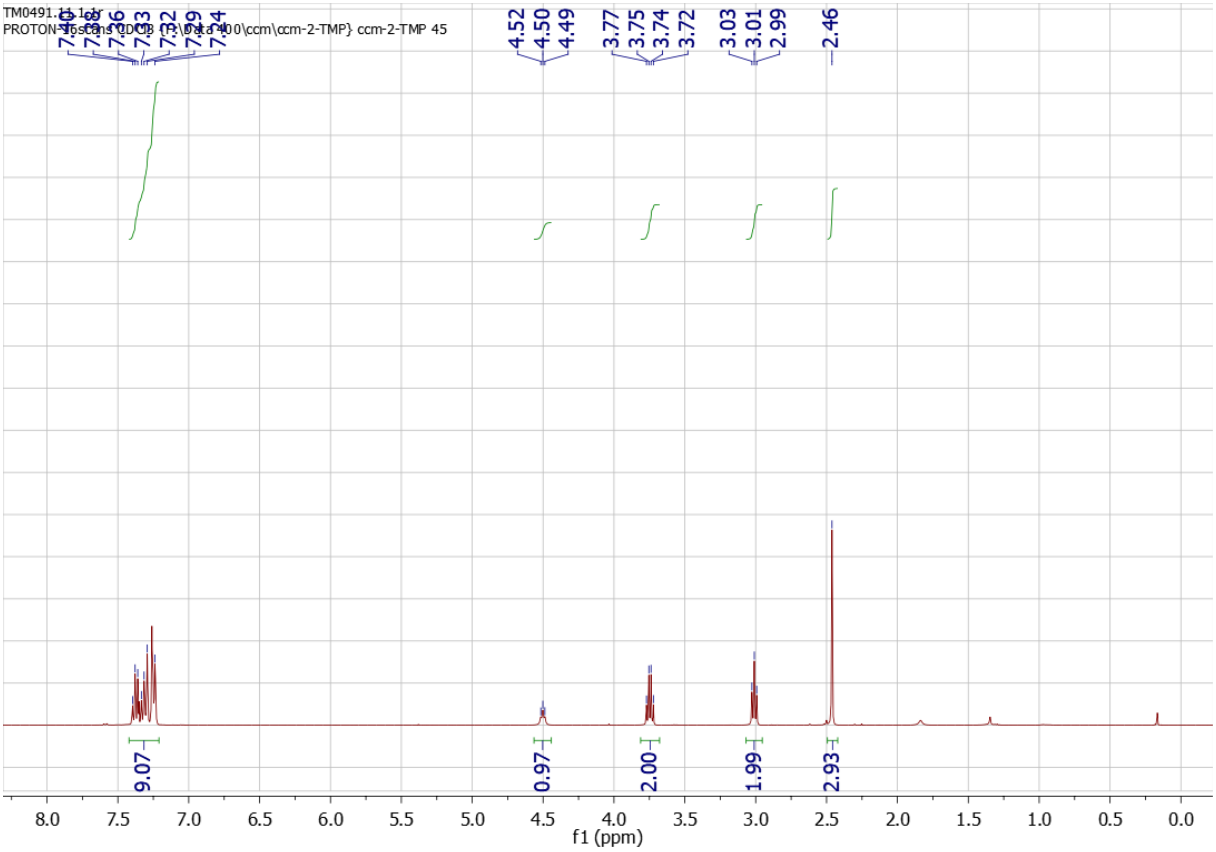

^{1}H NMR spectra of compound **118b** in $CDCl_3$.

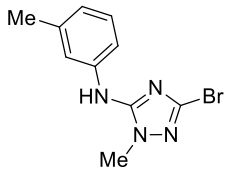

118h

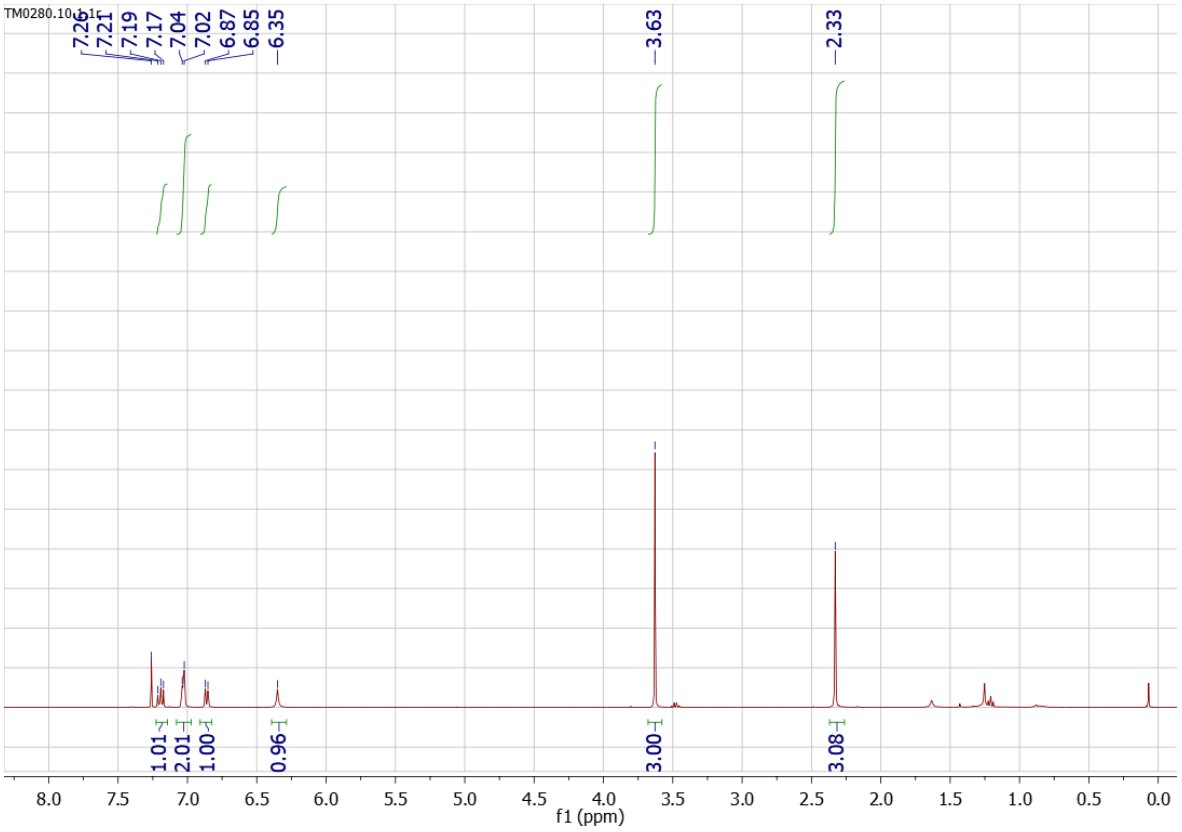

^{1}H NMR spectra of compound **118h** in $CDCl_3$.

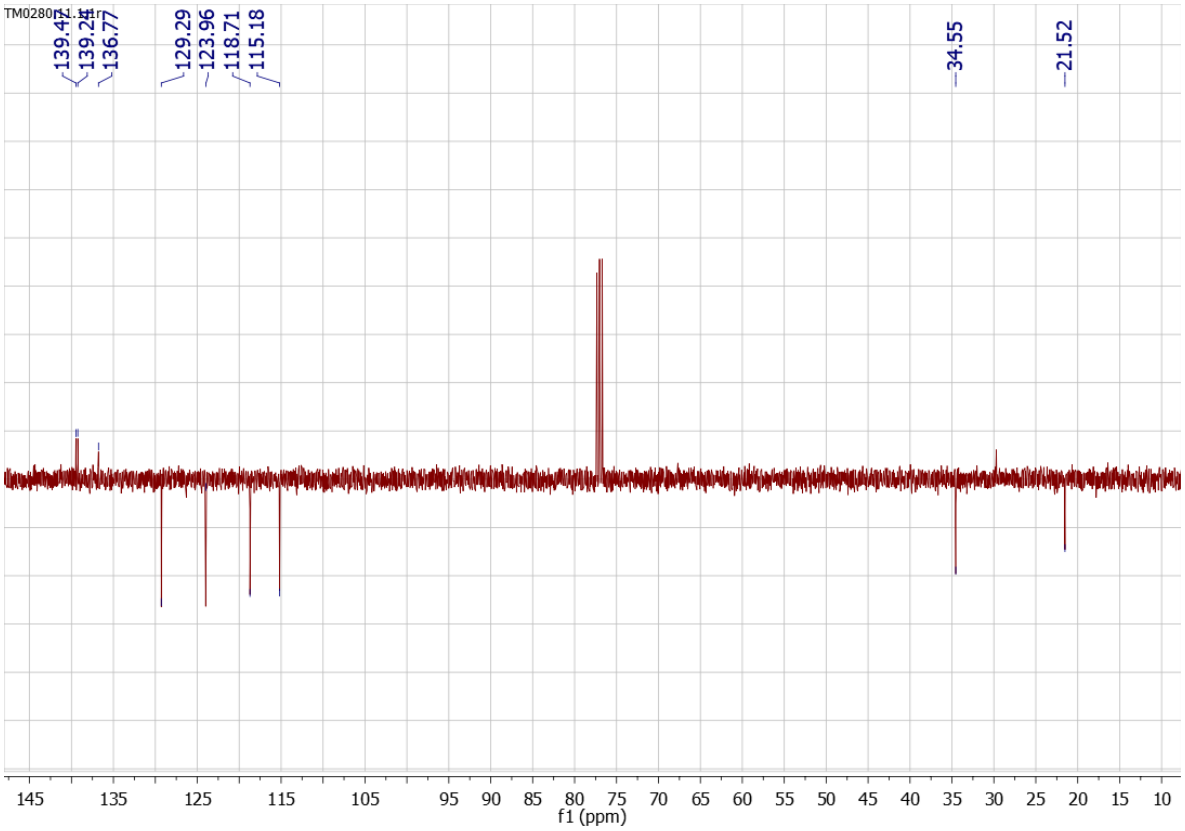

^{13}C NMR spectra of compound **118h** in $CDCl_3$.

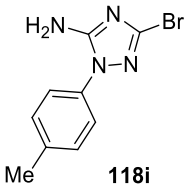

118i

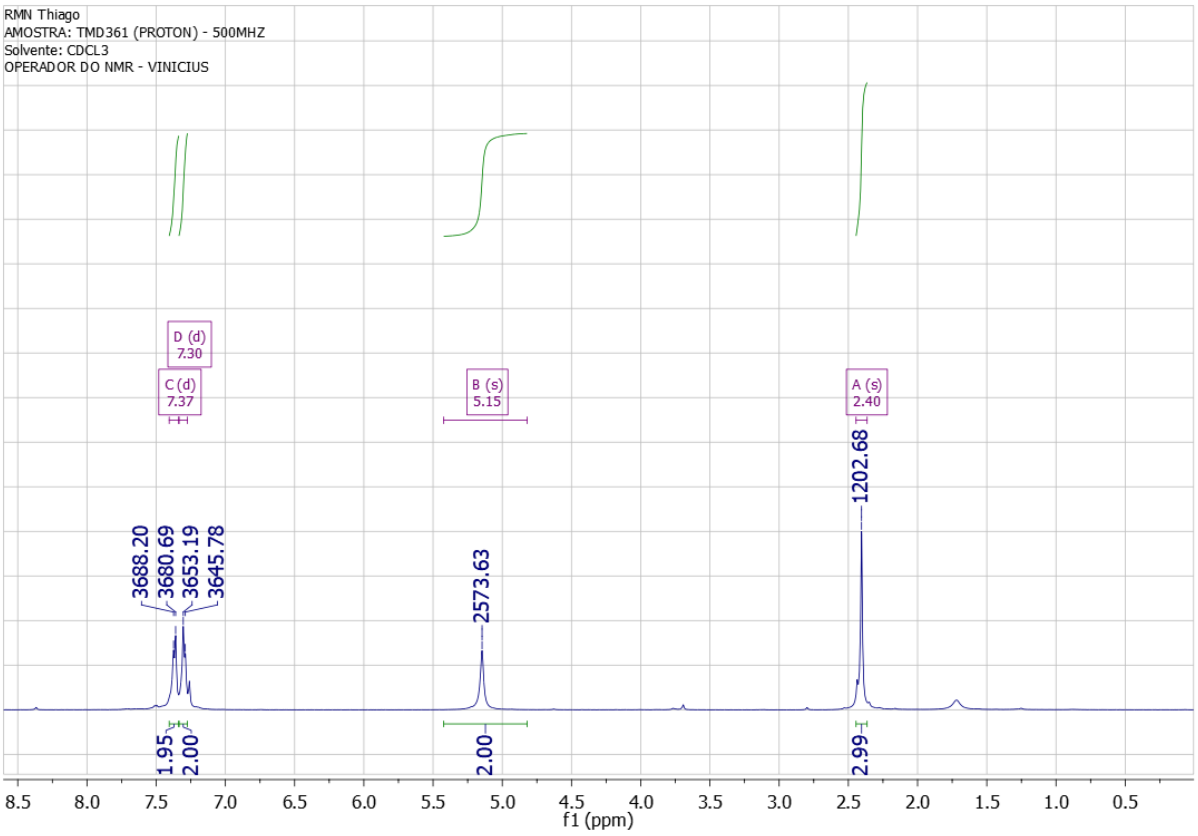

^{1}H NMR spectra of compound **118i** in $CDCl_3$.

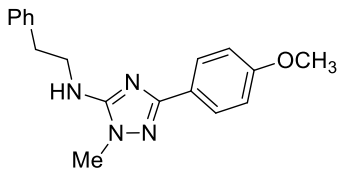

119a

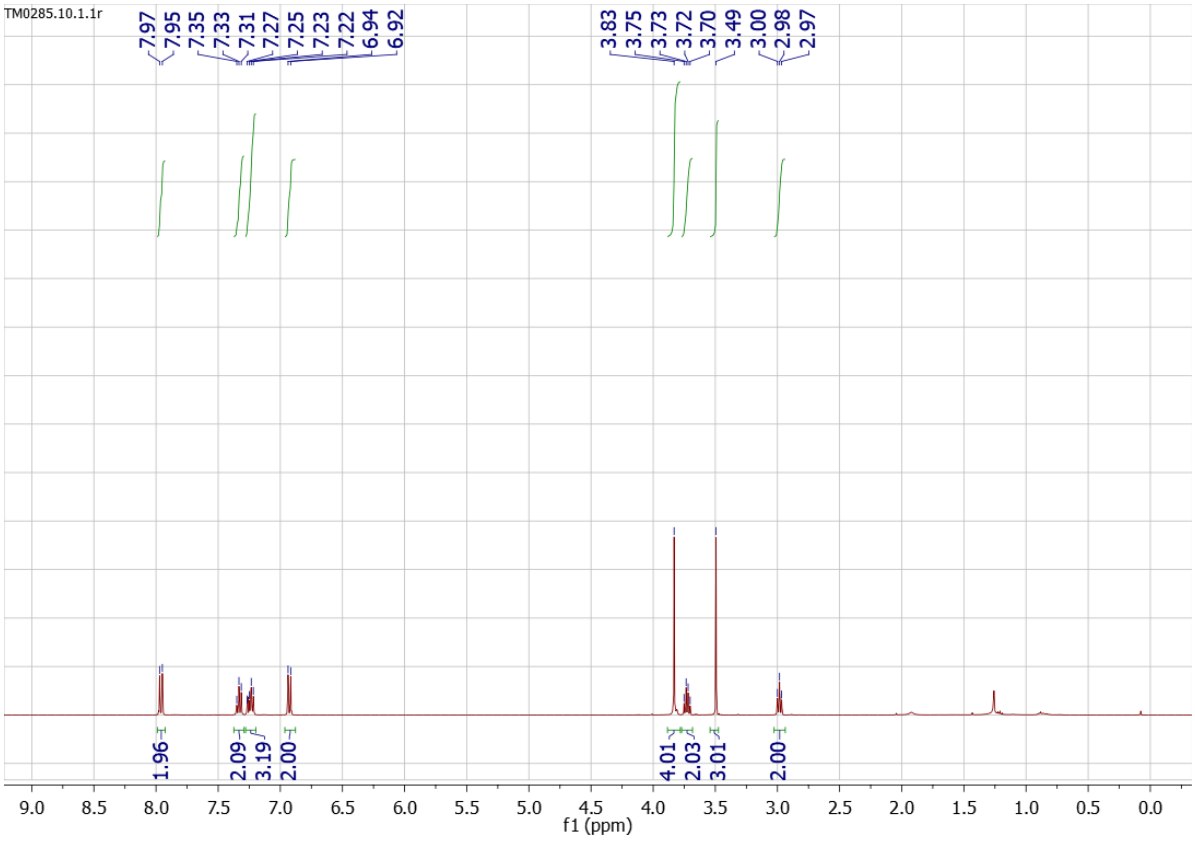

^{1}H NMR spectra of compound **119a** in $CDCl_3$.

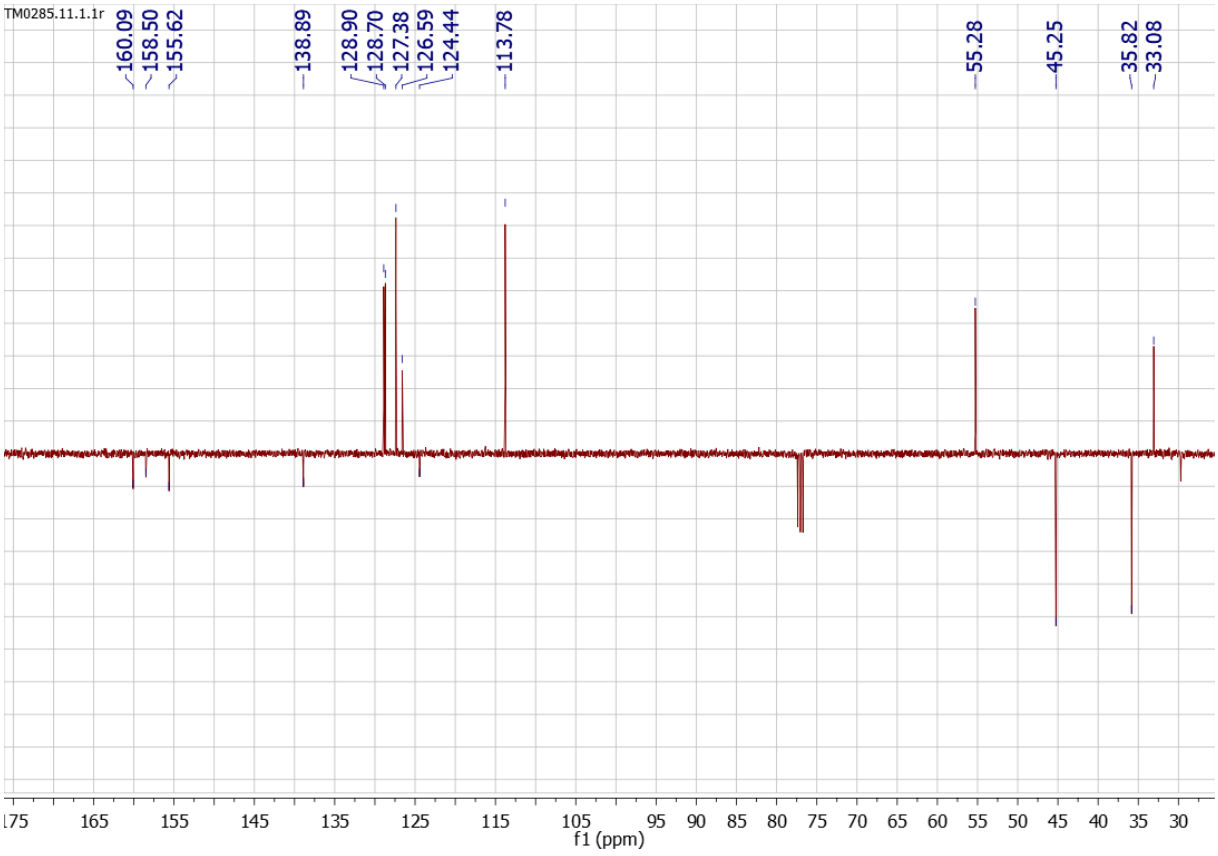

^{13}C NMR spectra of compound **119a** in $CDCl_3$.

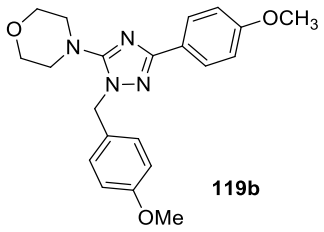

119b

Exact Mass: 380.18

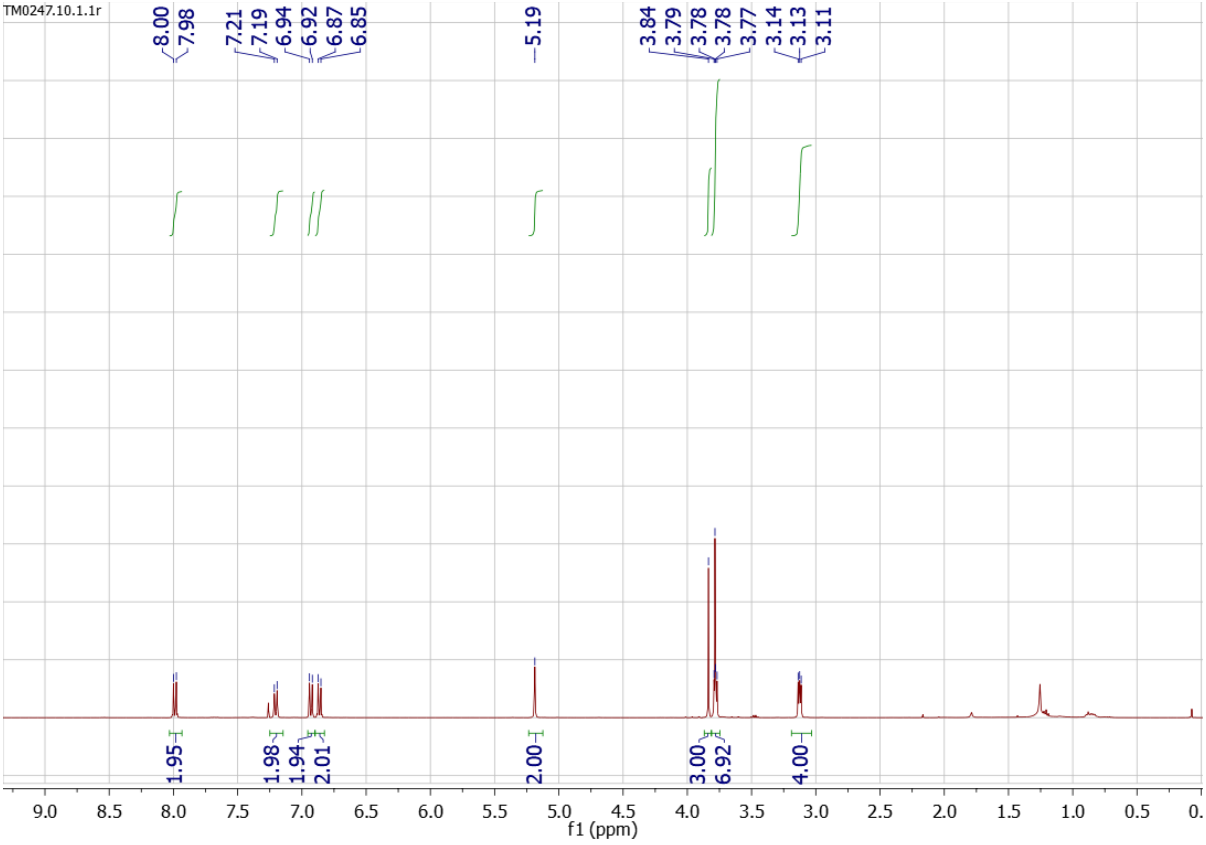

^{1}H NMR spectra of compound **119b** in $CDCl_3$.

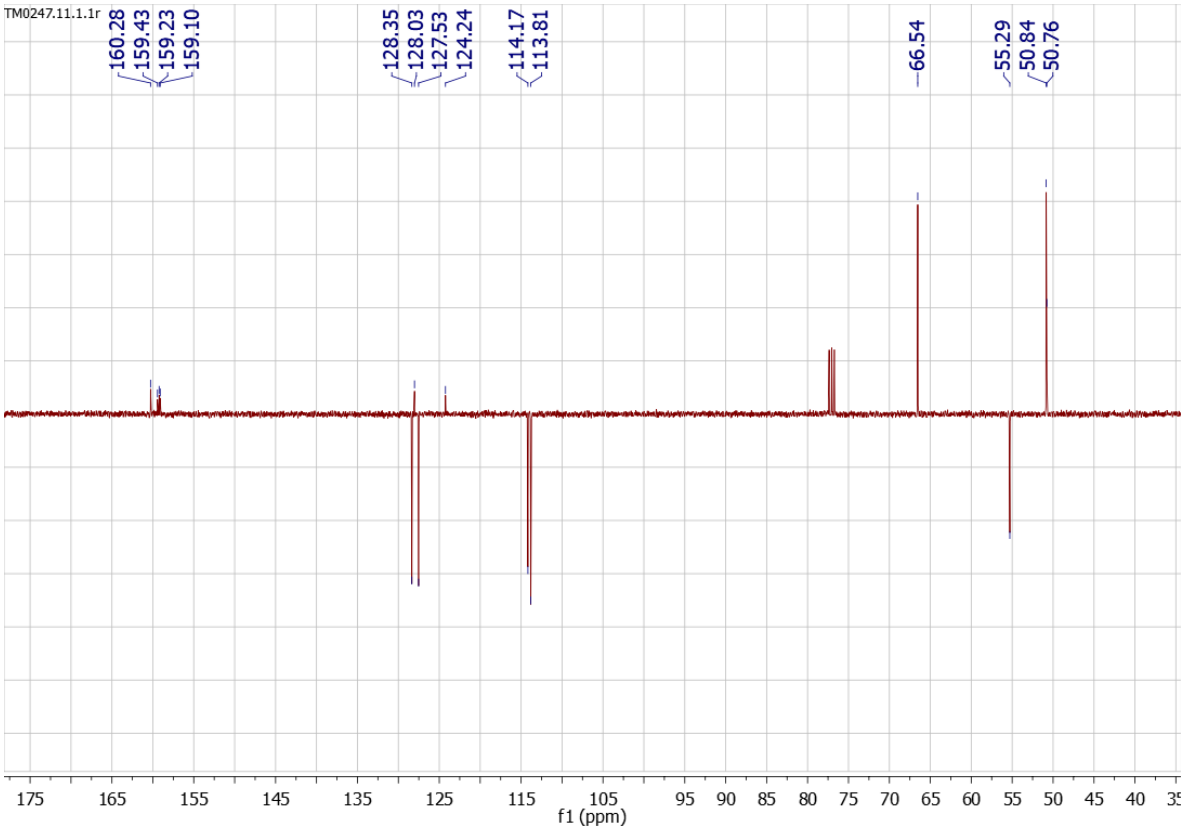

^{13}C NMR spectra of compound **119b** in $CDCl_3$.

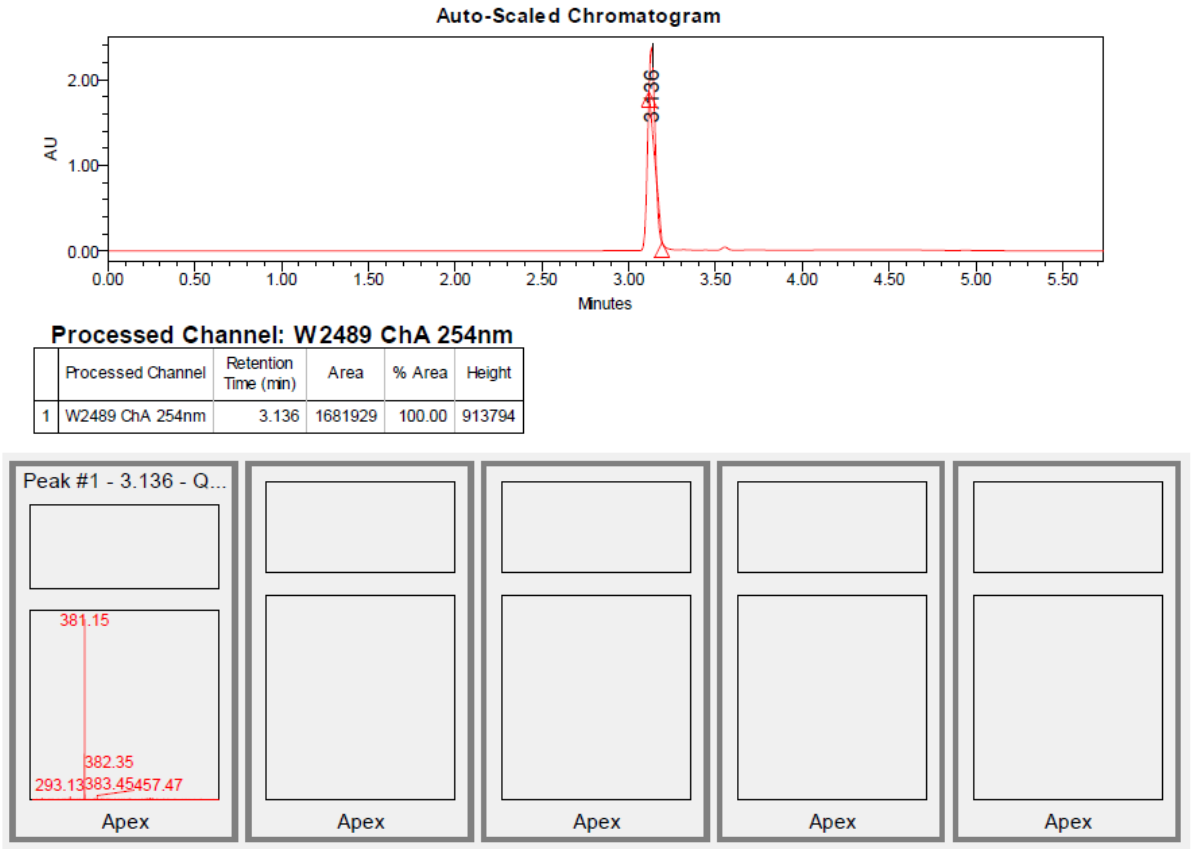

LC/MS of compound **119b**.

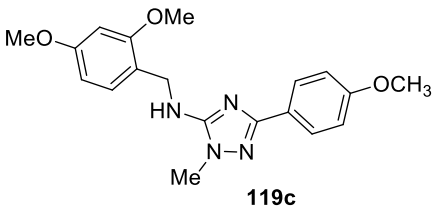

119c

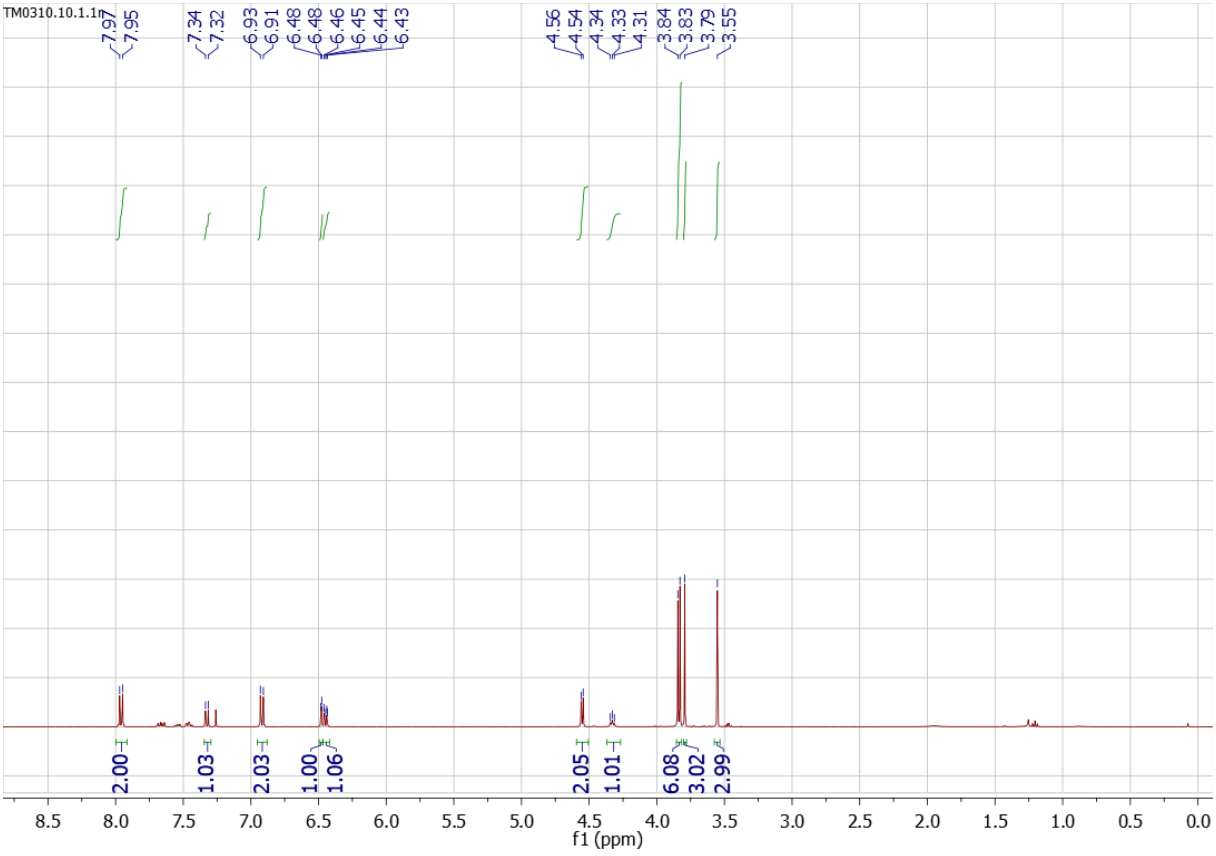

^{1}H NMR spectra of compound **119c** in $CDCl_3$.

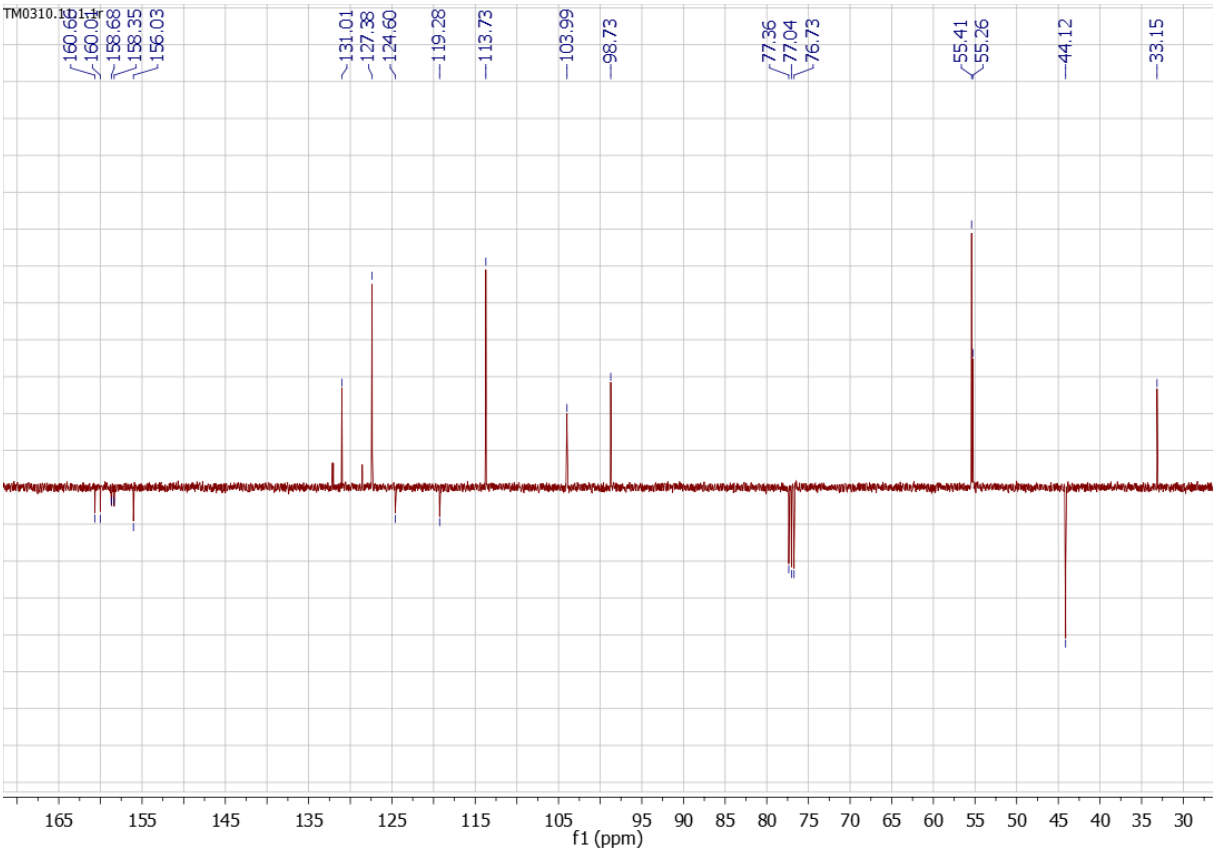

^{13}C NMR spectra of compound **119c** in $CDCl_3$.

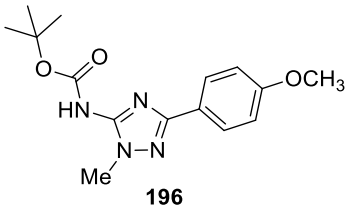

196

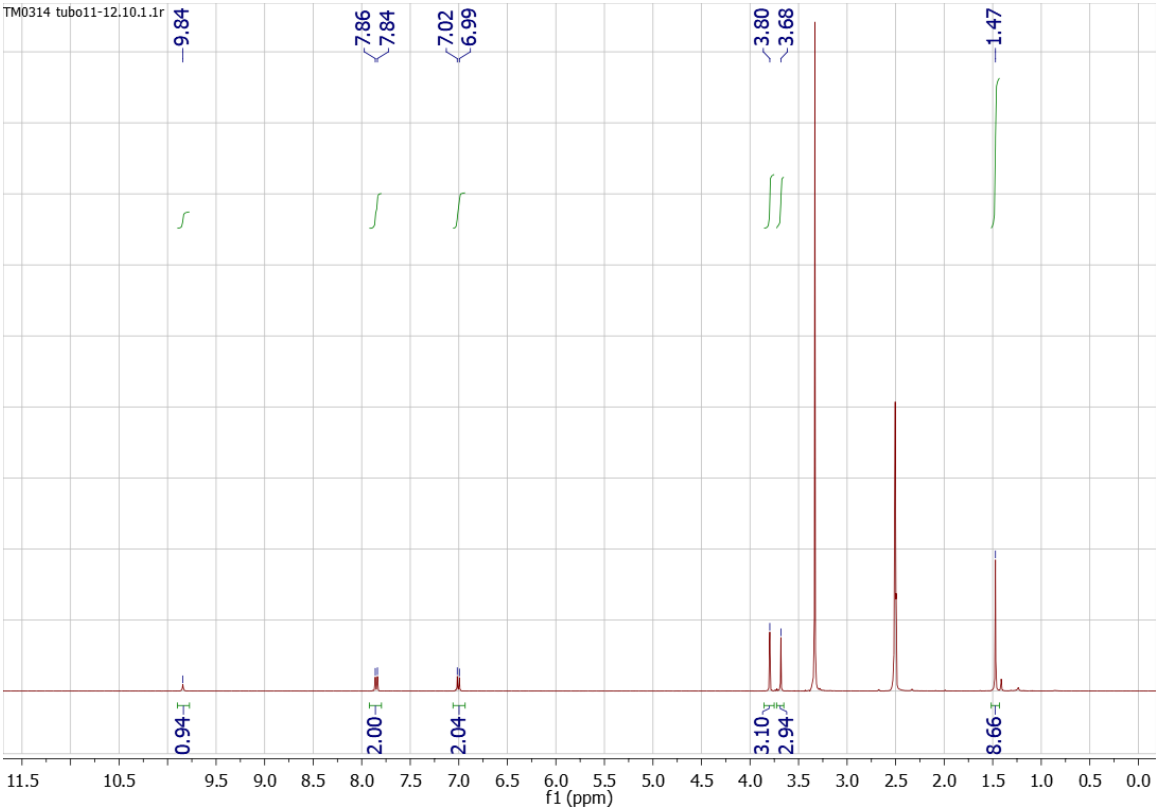

^{1}H NMR spectra of compound **196** in DMSO.

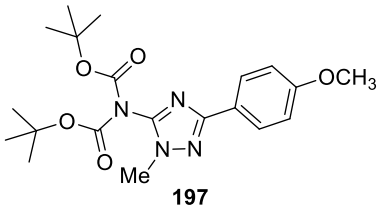

197

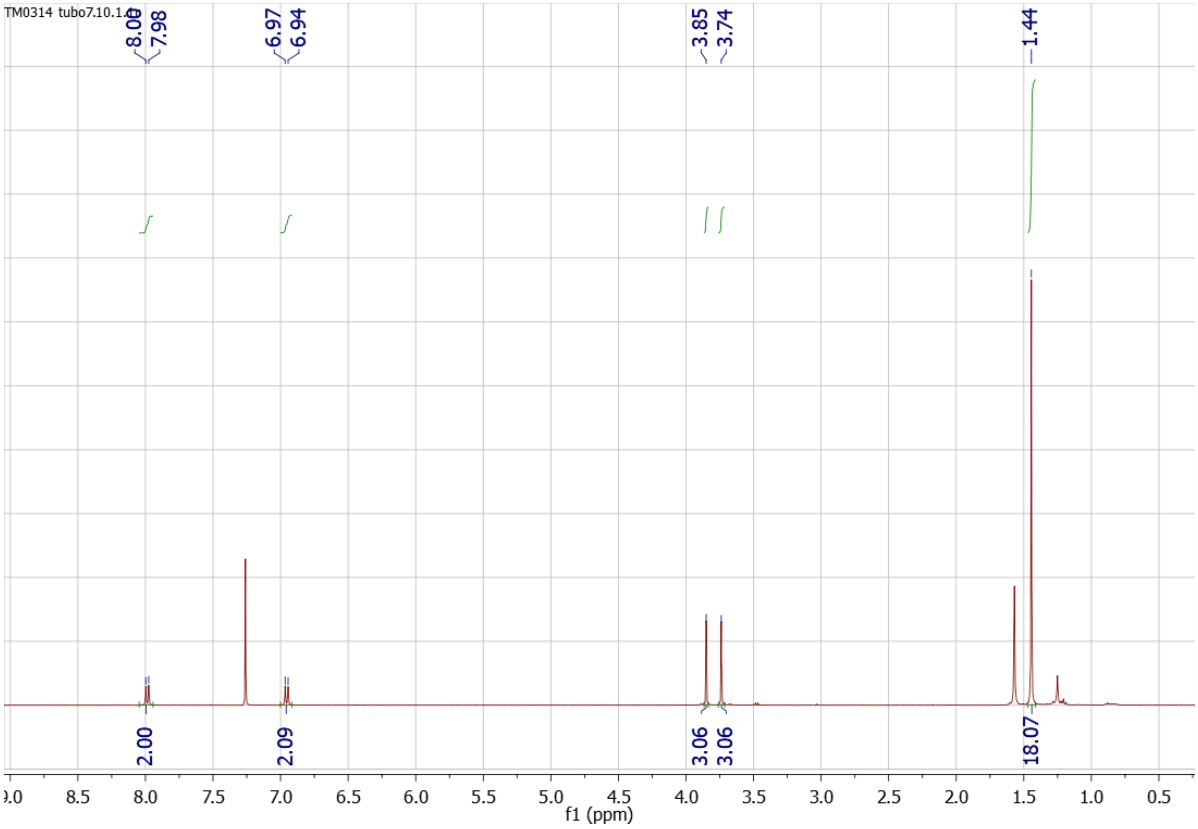

^{1}H NMR spectra of compound **197** in $CDCl_3$.

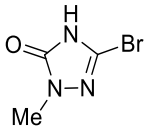

143a

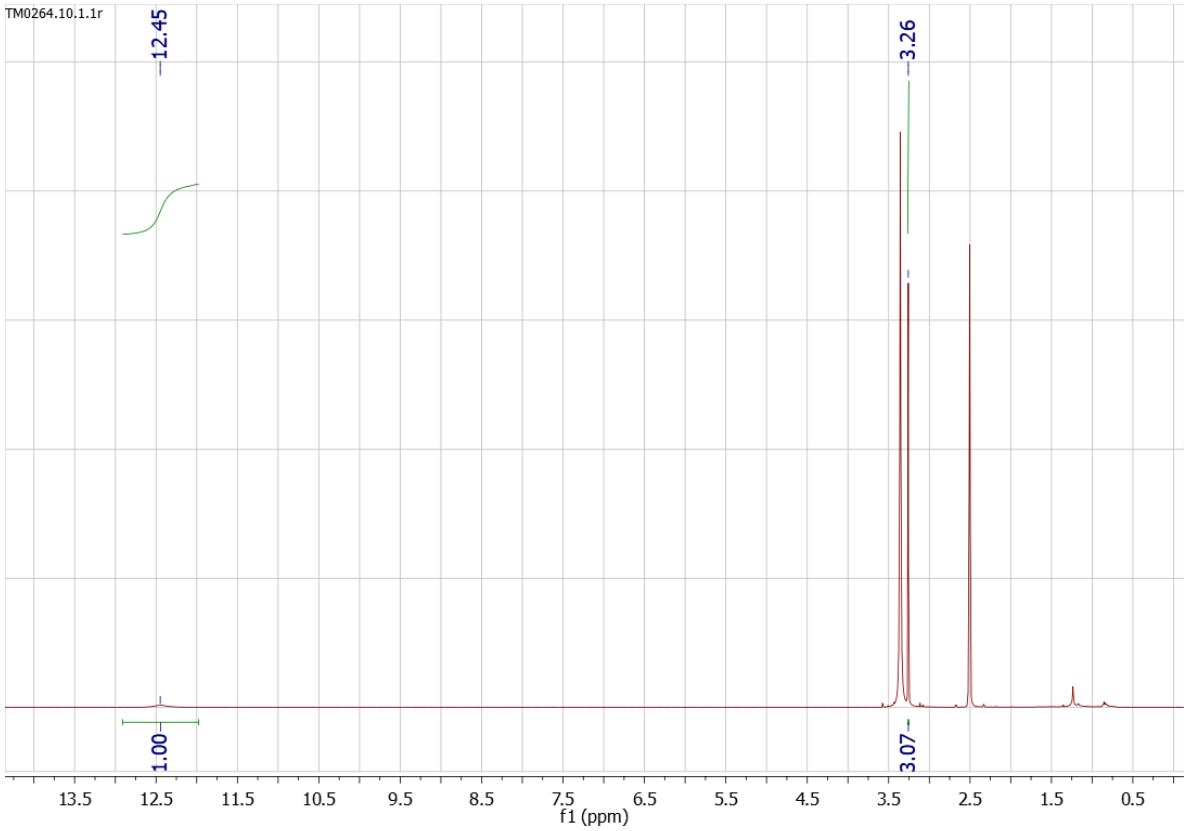

^{1}H NMR spectra of compound **143a** in DMSO.

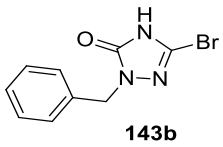

143b

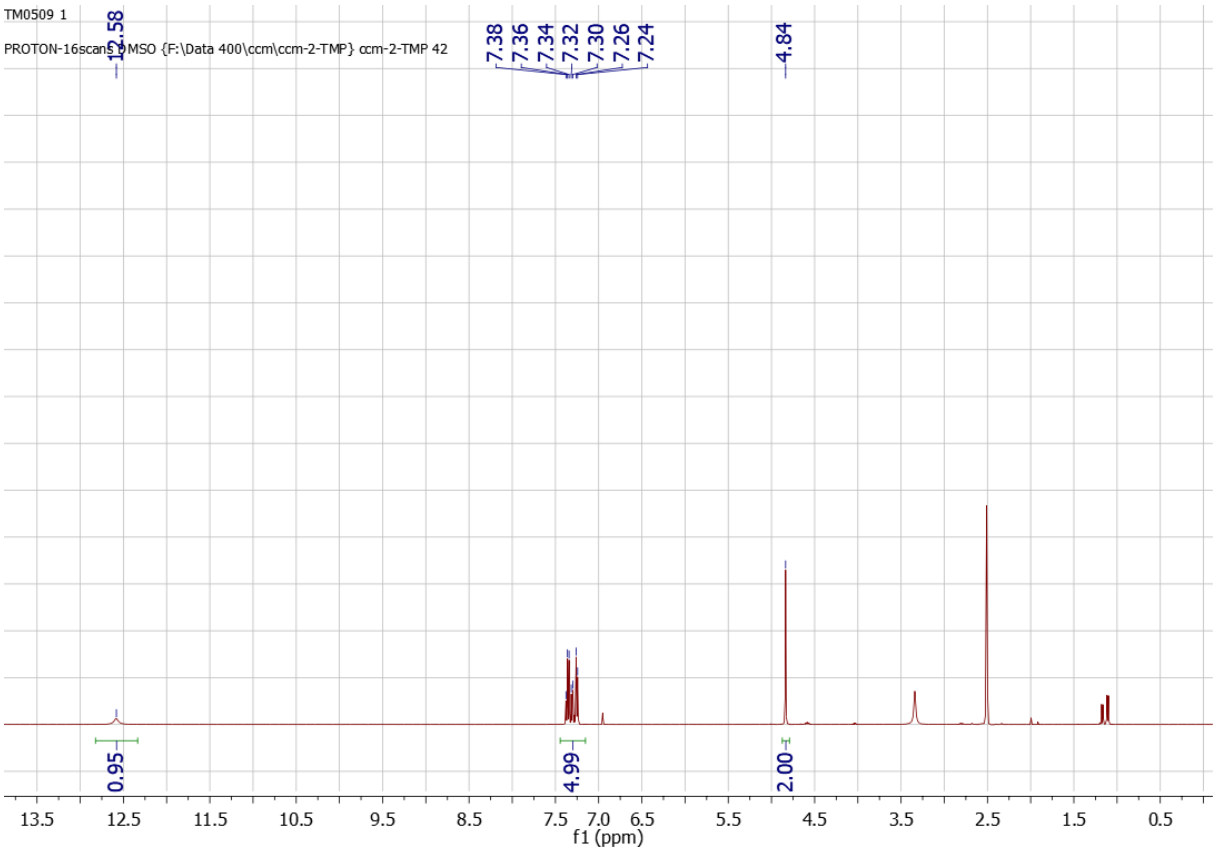

^{1}H NMR spectra of compound **143b** in DMSO.

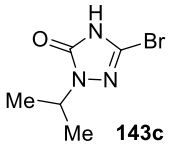

143c

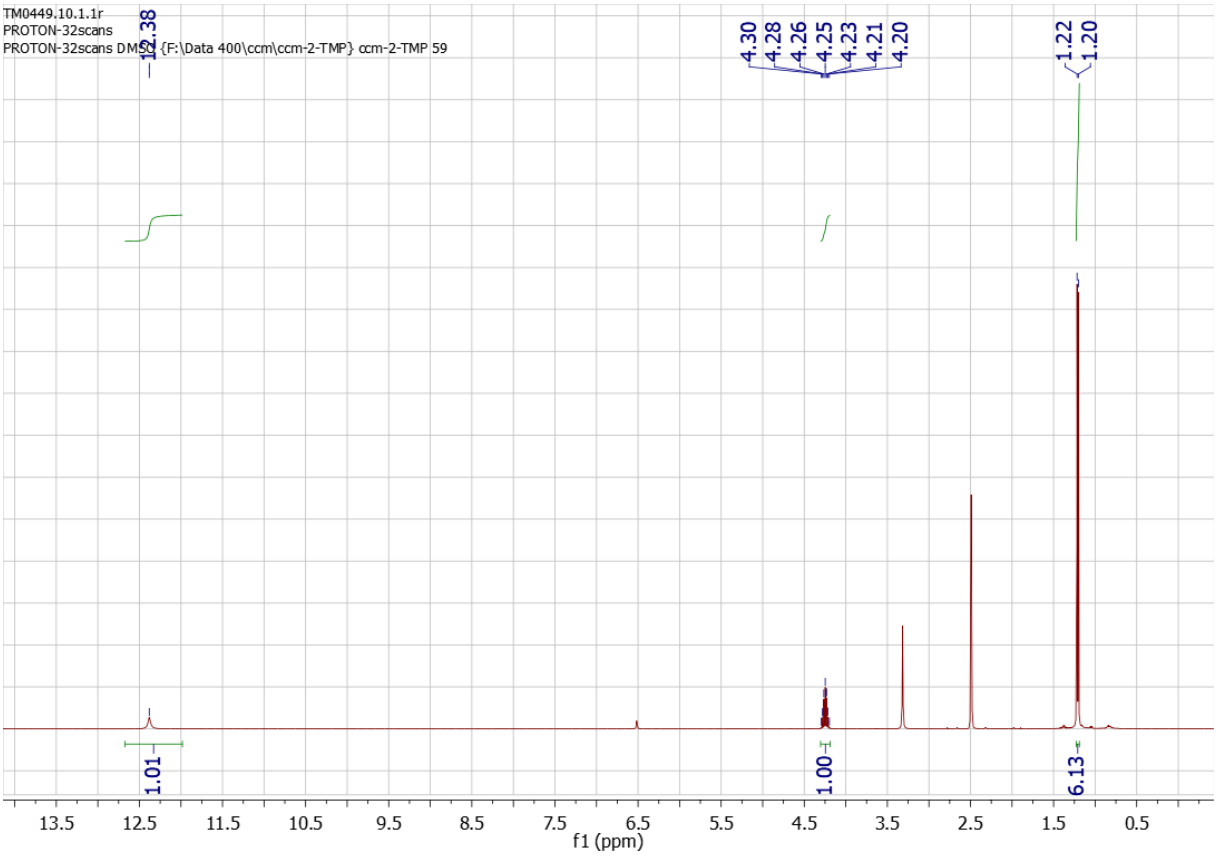

^{1}H NMR spectra of compound **143c** in DMSO.

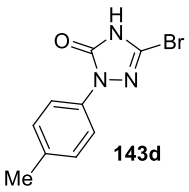

143d

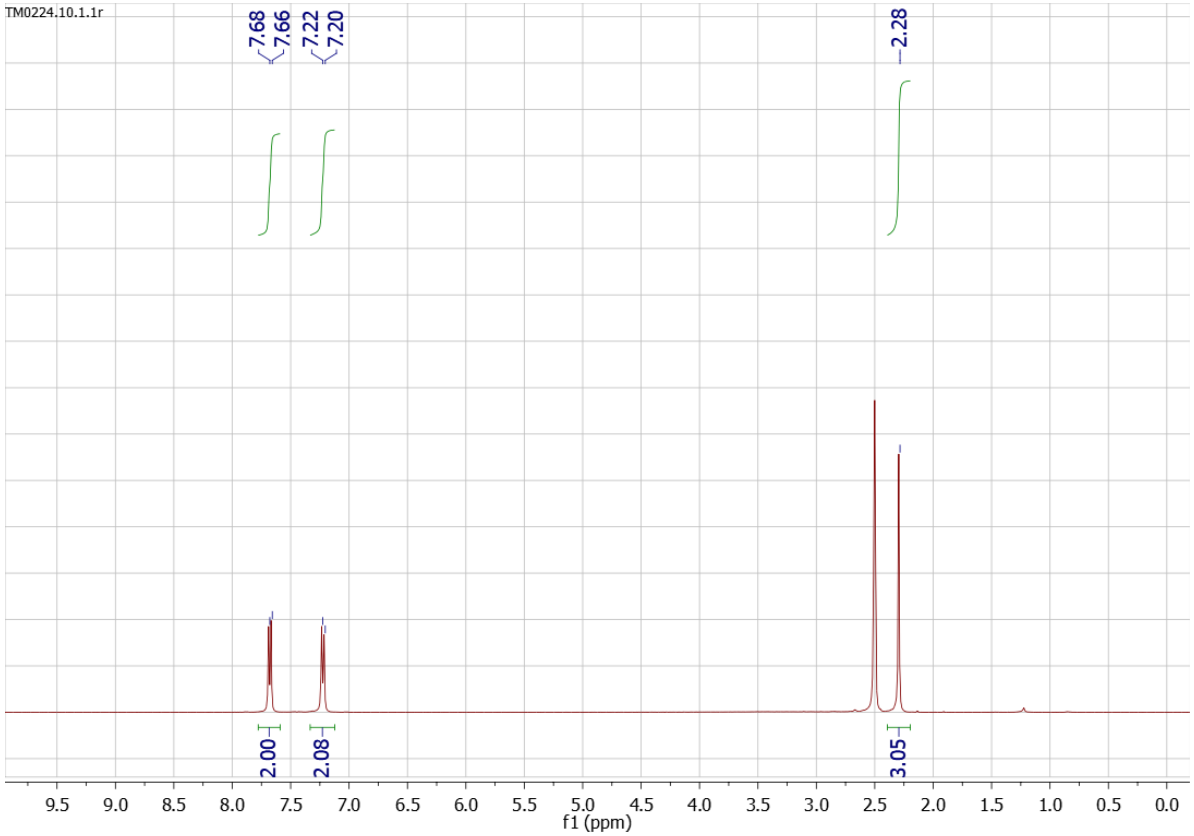

^{1}H NMR spectra of compound **143d** in DMSO.

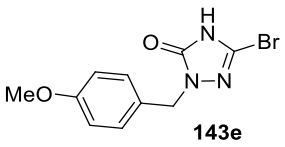

143e

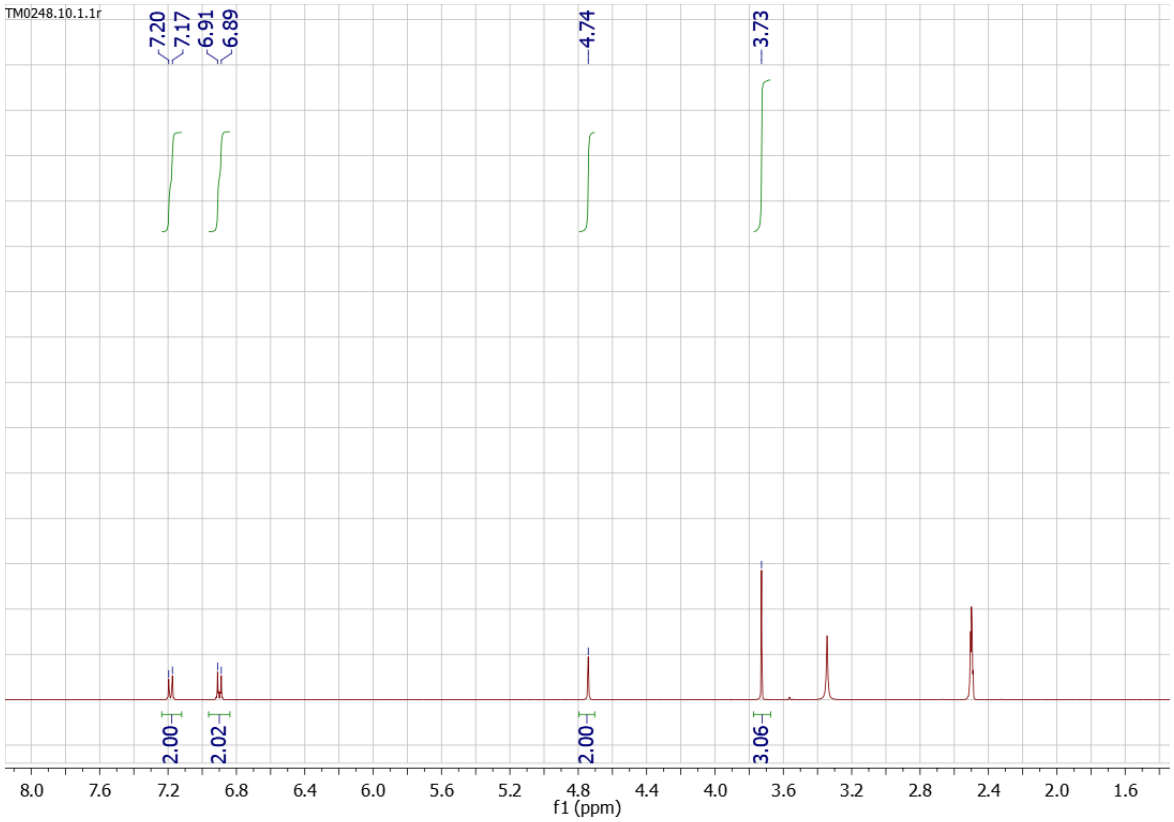

^{1}H NMR spectra of compound **143e** in DMSO.

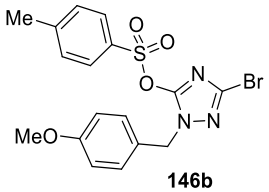

146b

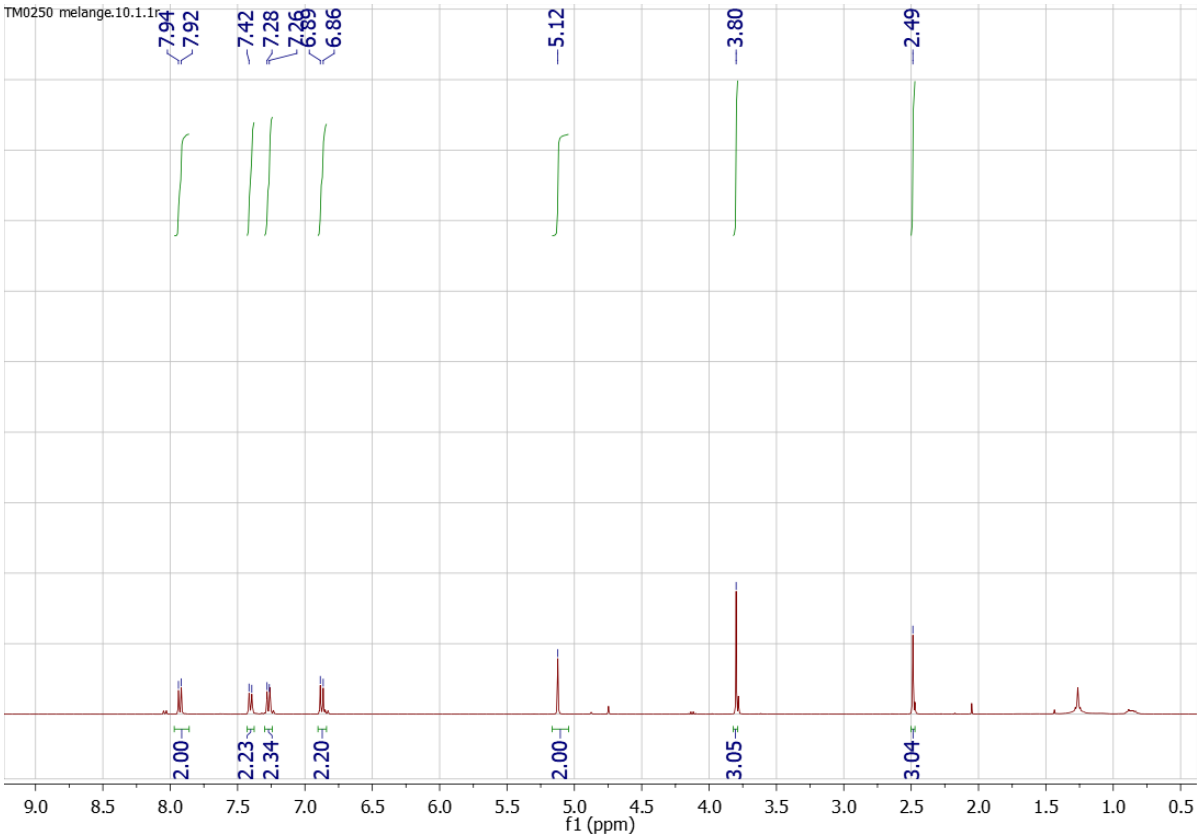

^{1}H NMR spectra of compound **146b** in $CDCl_3$.

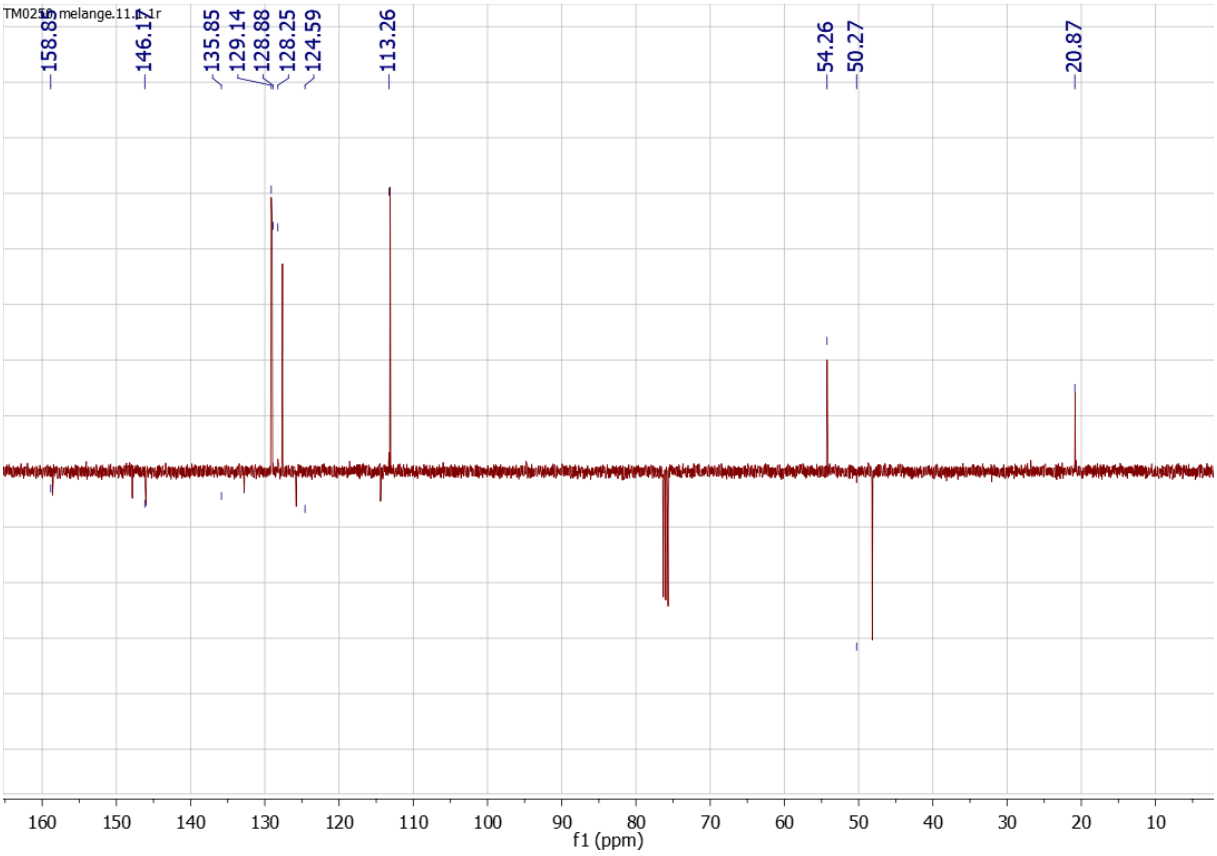

^{13}C NMR spectra of compound **146b** in $CDCl_3$.

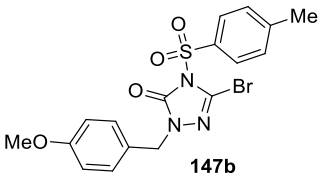

147b

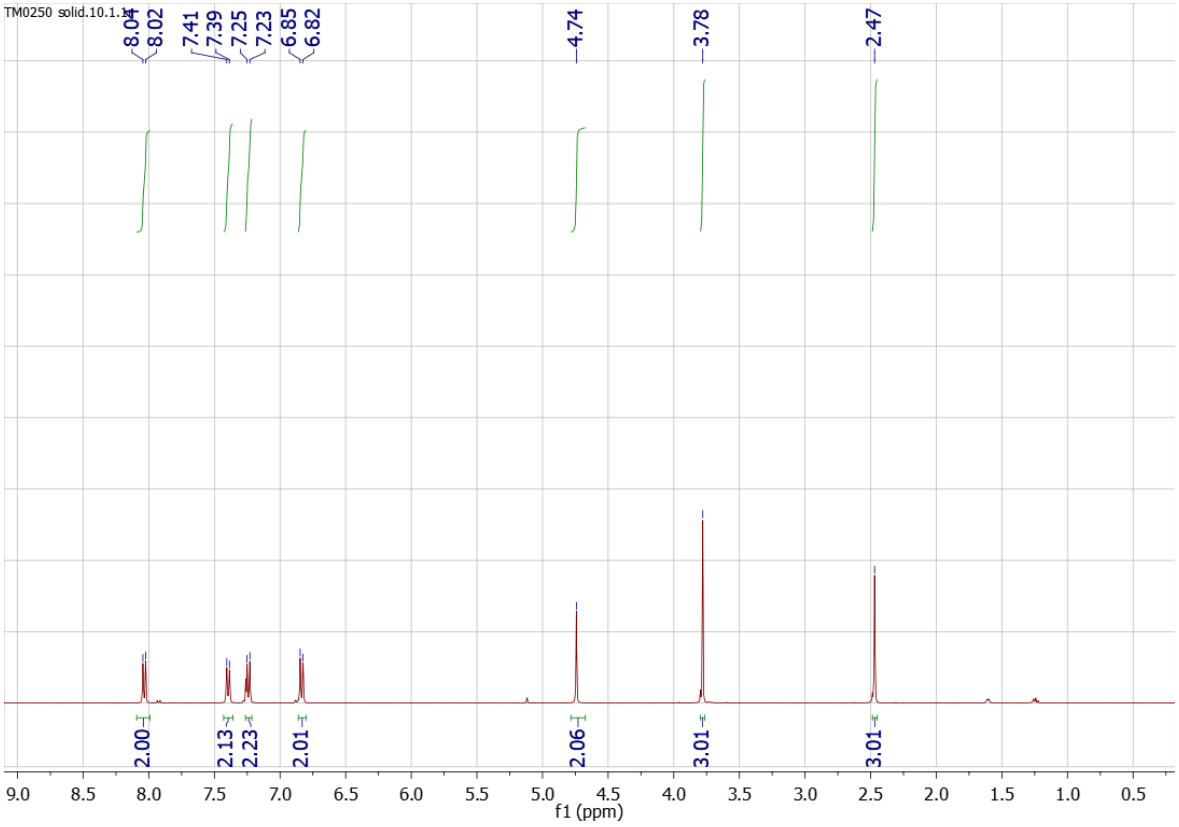

^{1}H NMR spectra of compound **147b** in $CDCl_3$.

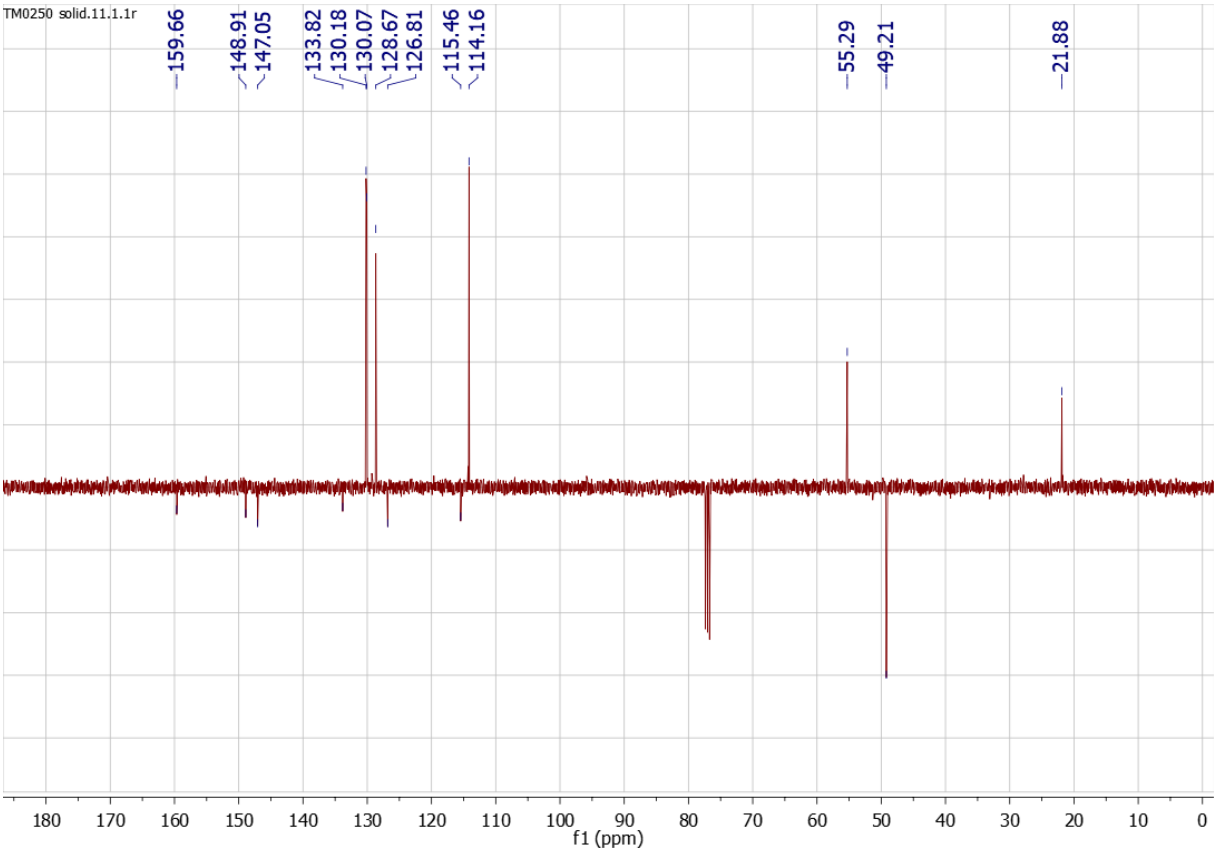

^{13}C NMR spectra of compound **147b** in $CDCl_3$.

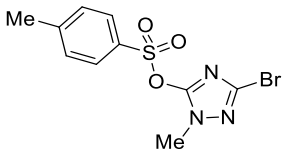

146a

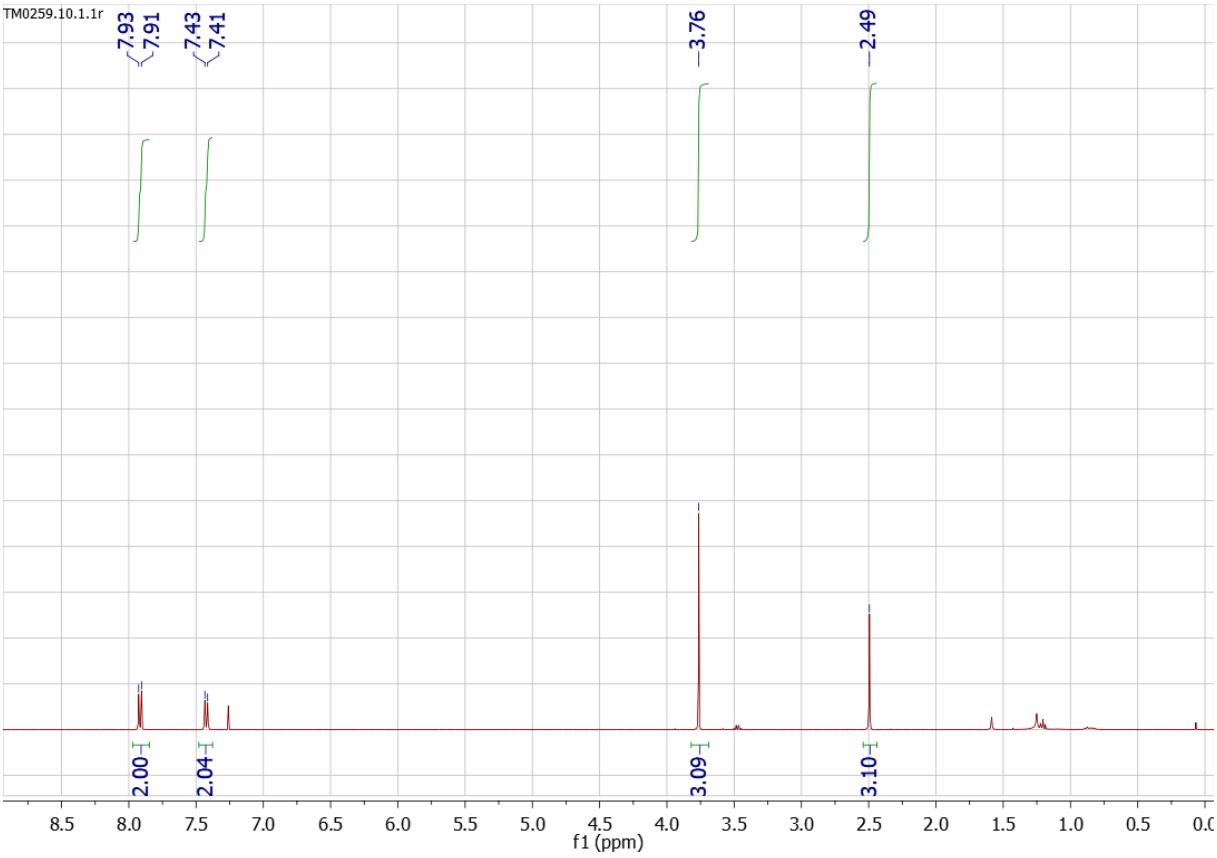

^{1}H NMR spectra of compound **146a** in $CDCl_3$.

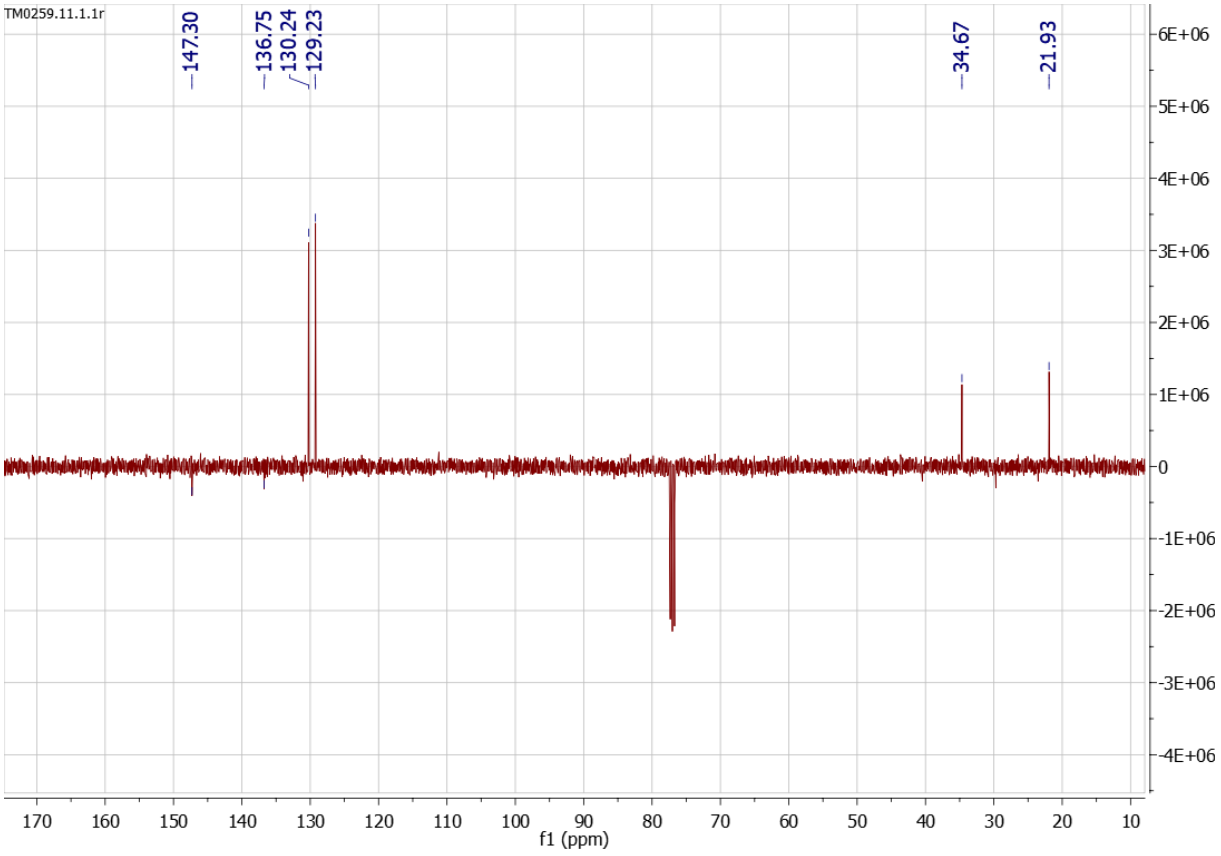

^{13}C NMR spectra of compound **146a** in $CDCl_3$.

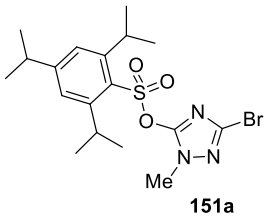

151a

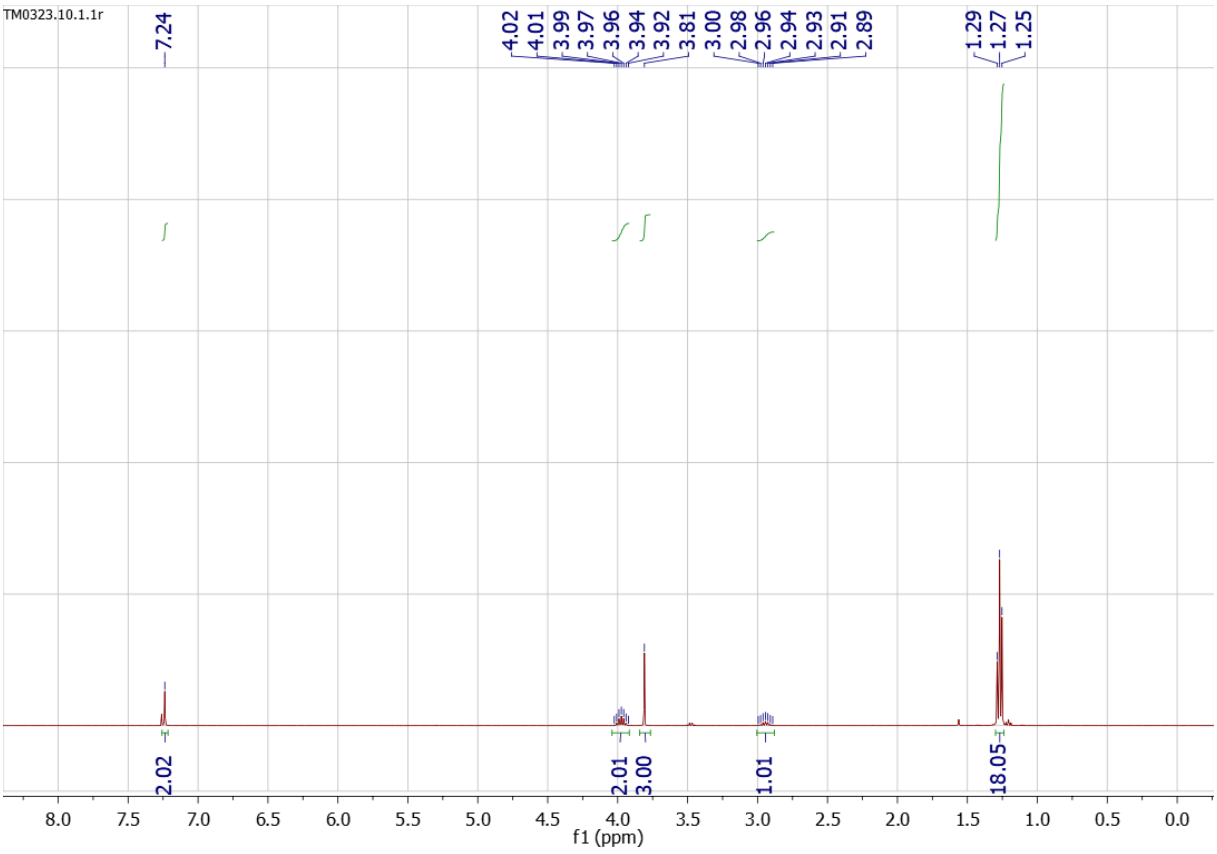

^{1}H NMR spectra of compound **151a** in $CDCl_3$.

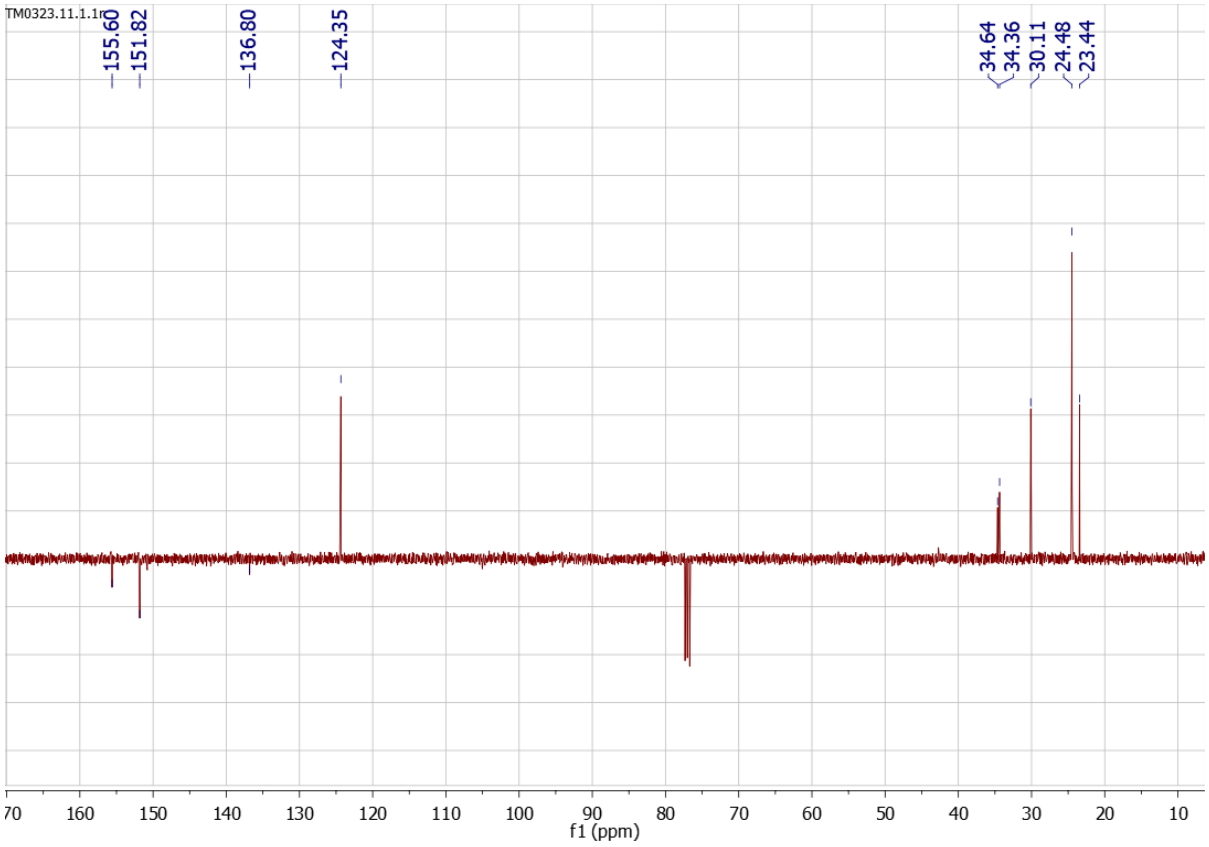

^{13}C NMR spectra of compound **151a** in $CDCl_3$.

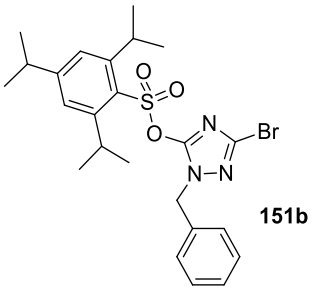

151b

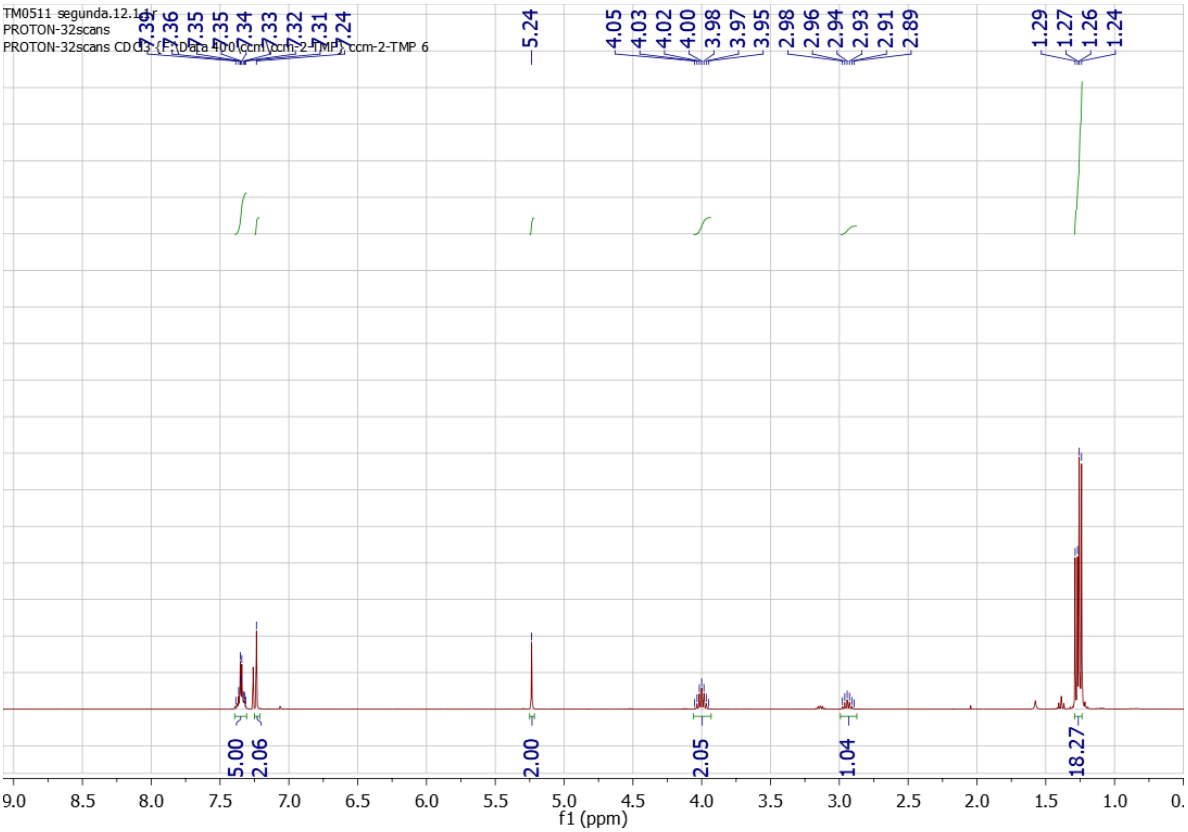

^{1}H NMR spectra of compound **151b** in $CDCl_3$.

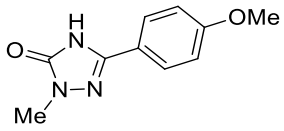

149

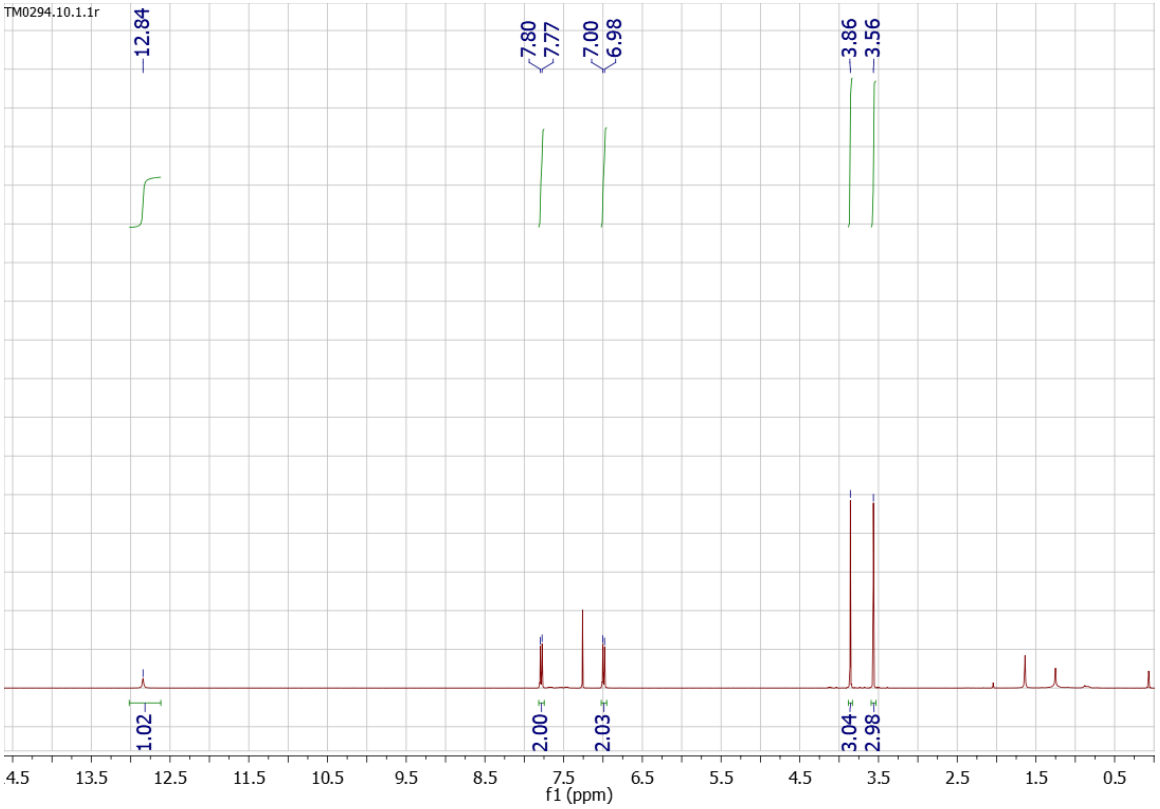

^{1}H NMR spectra of compound **149** in $CDCl_3$.

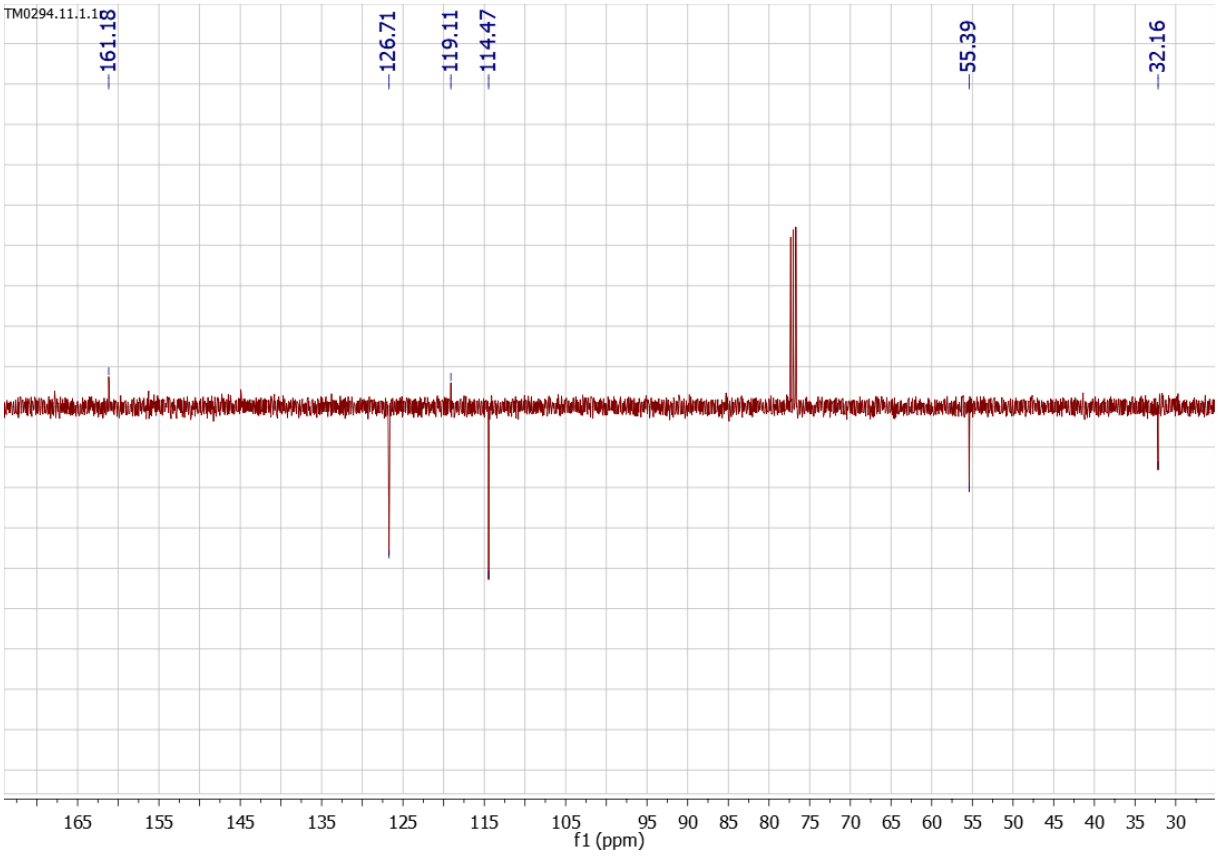

^{13}C NMR spectra of compound **149** in $CDCl_3$.

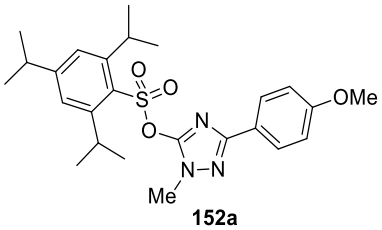

152a

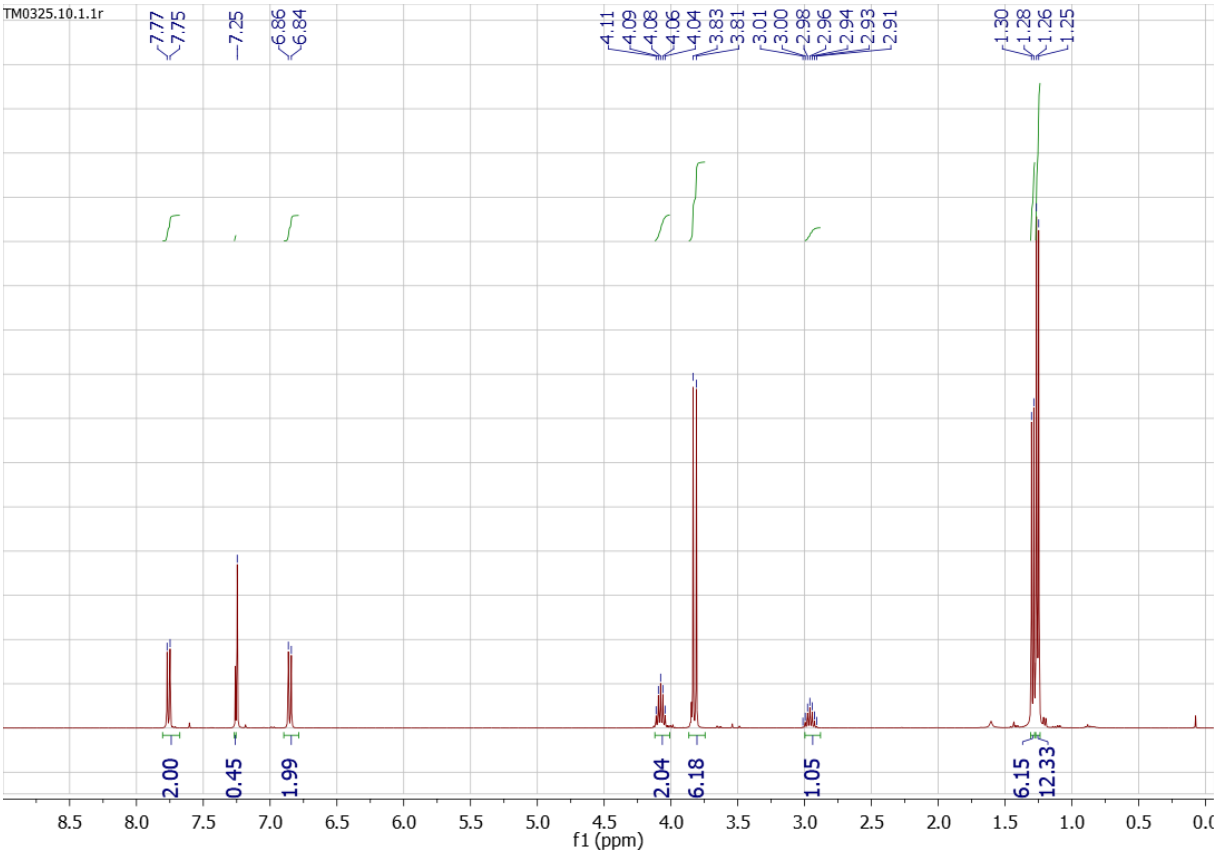

^{1}H NMR spectra of compound **152a** in $CDCl_3$.

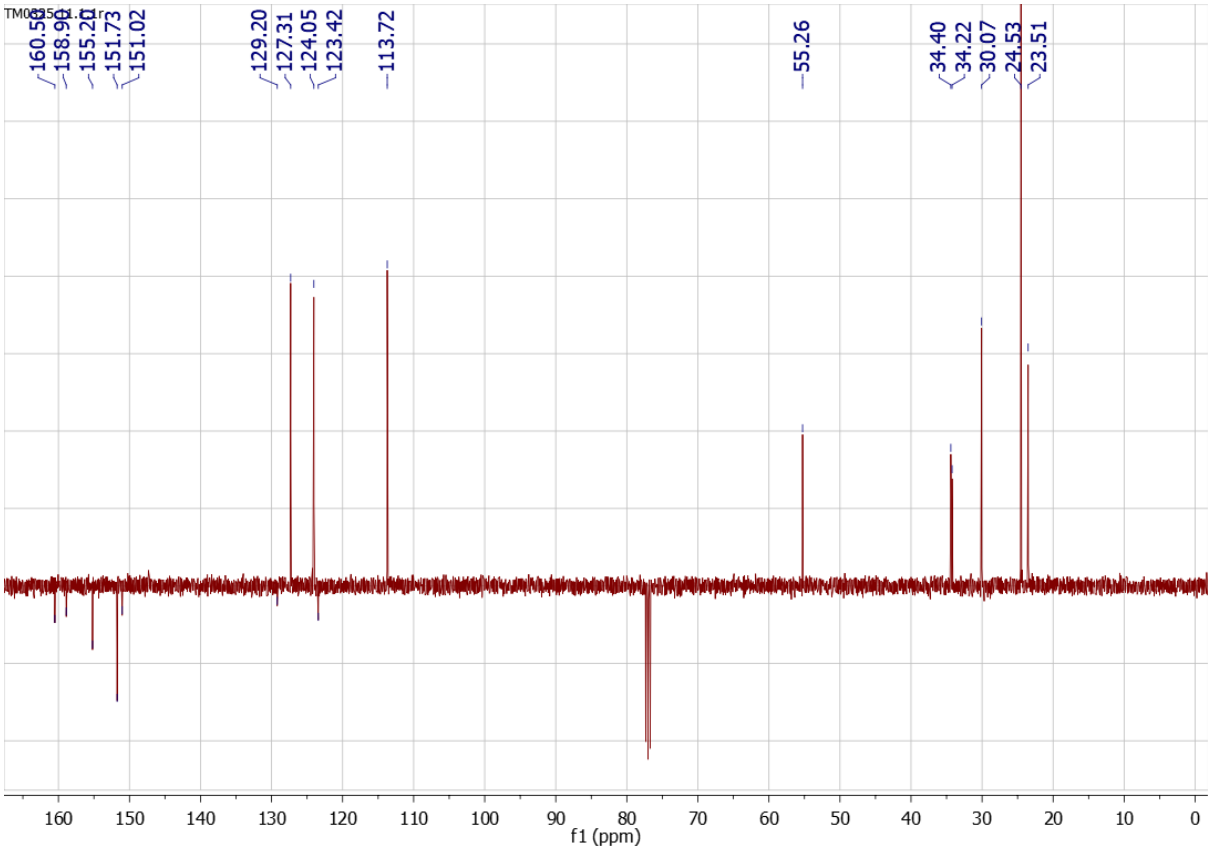

^{13}C NMR spectra of compound **152a** in $CDCl_3$.

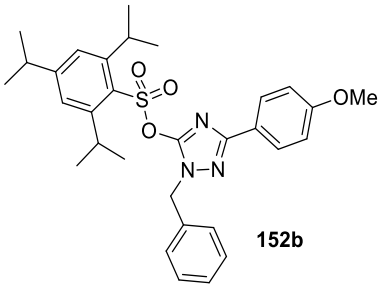

152b

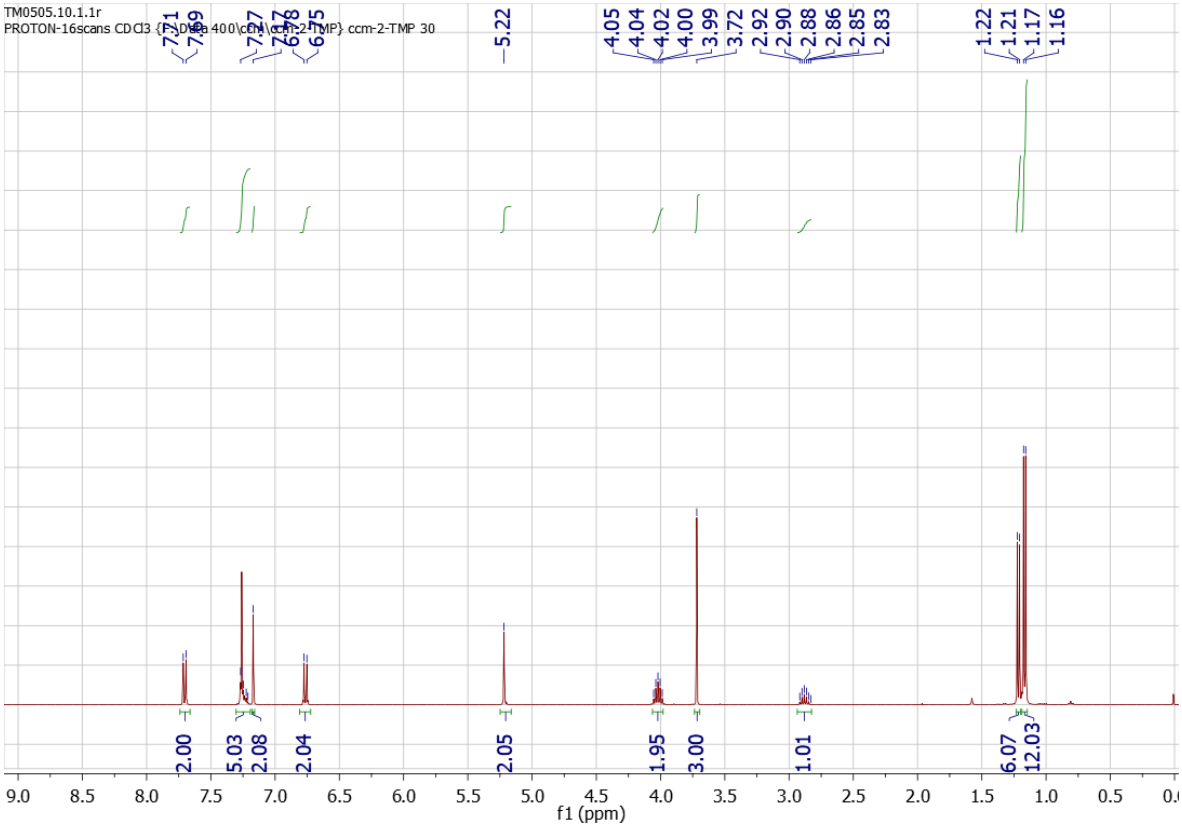

^{1}H NMR spectra of compound **152b** in $CDCl_3$.

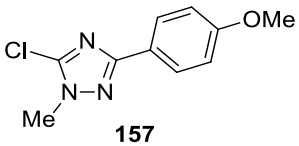

157

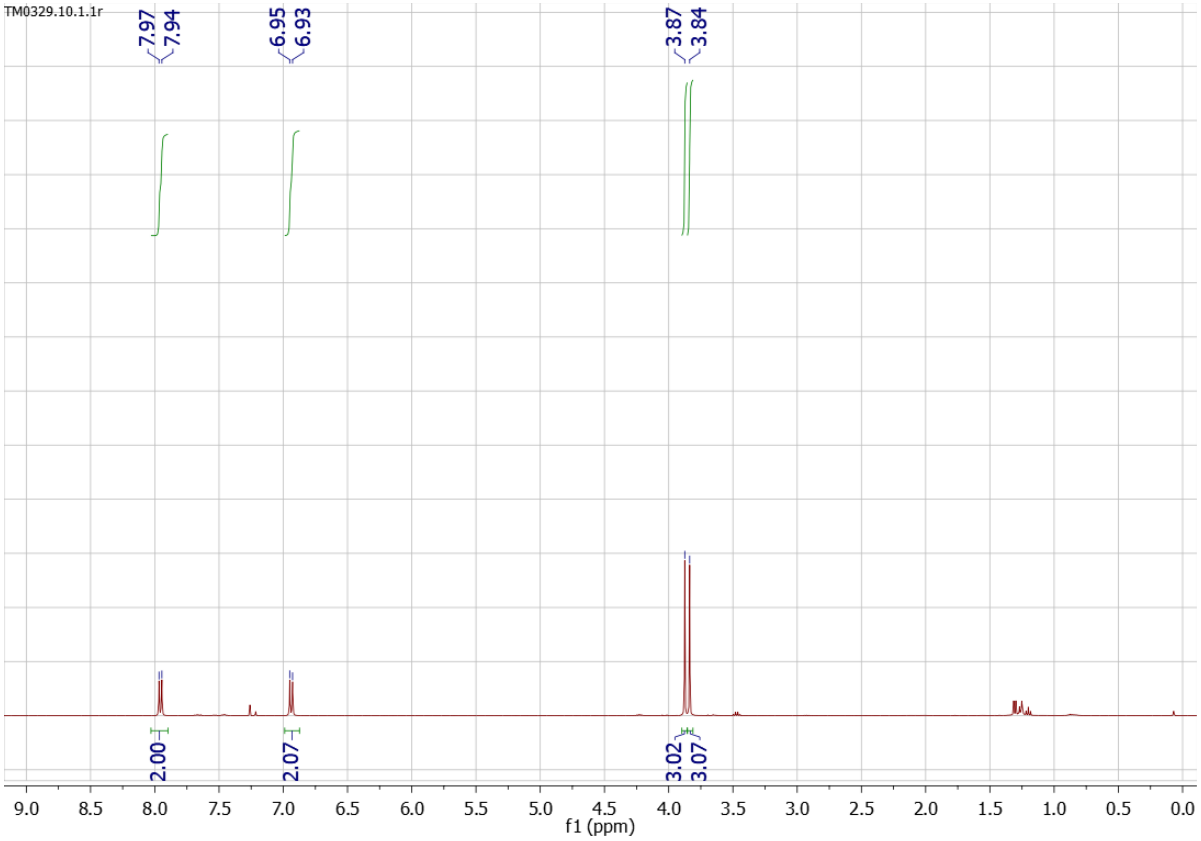

^{1}H NMR spectra of compound **157** in $CDCl_3$.

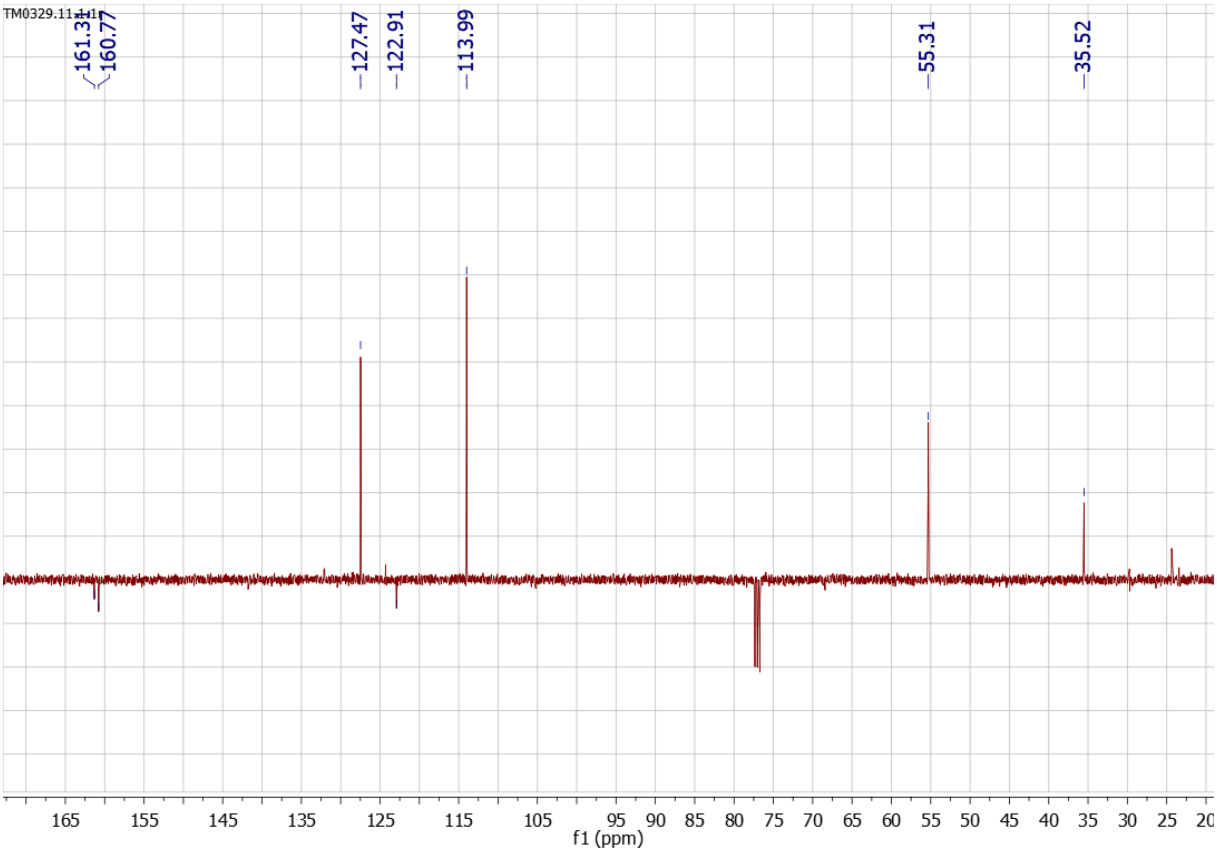

^{13}C NMR spectra of compound **157** in $CDCl_3$.

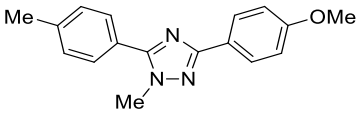

153

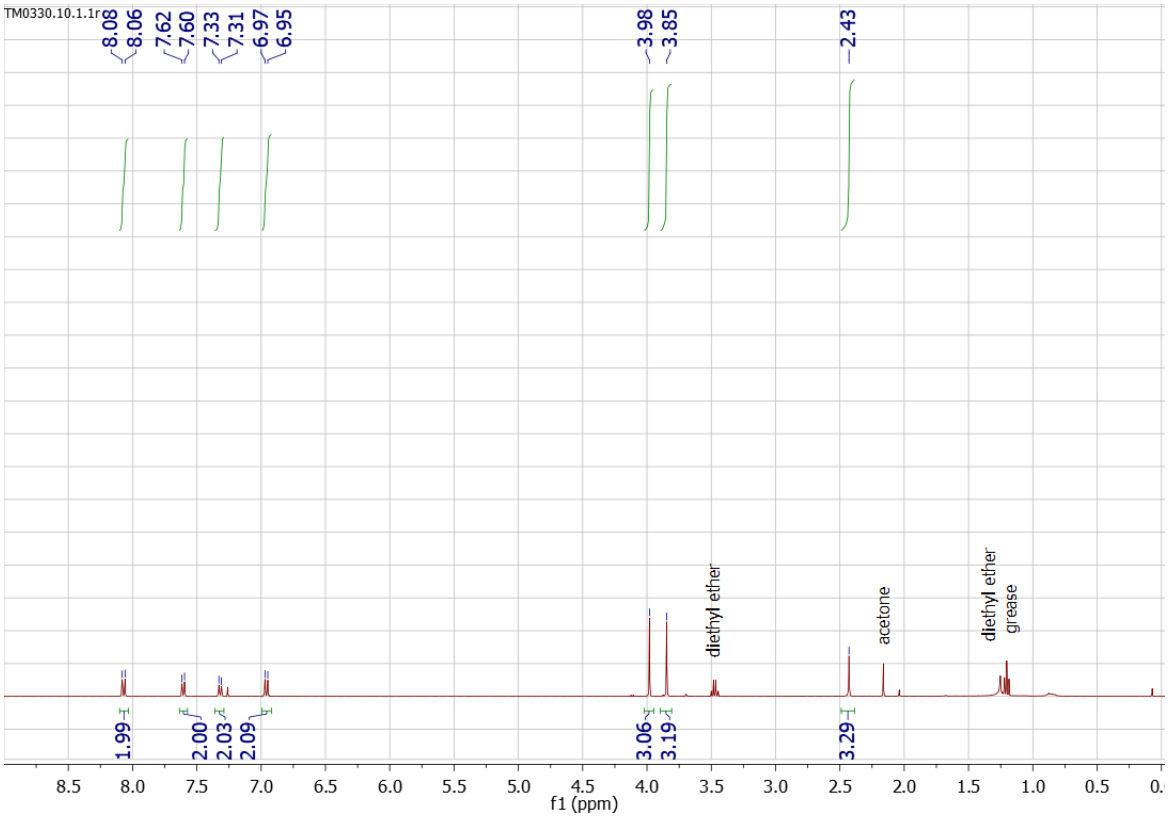

^{1}H NMR spectra of compound **153** in $CDCl_3$.

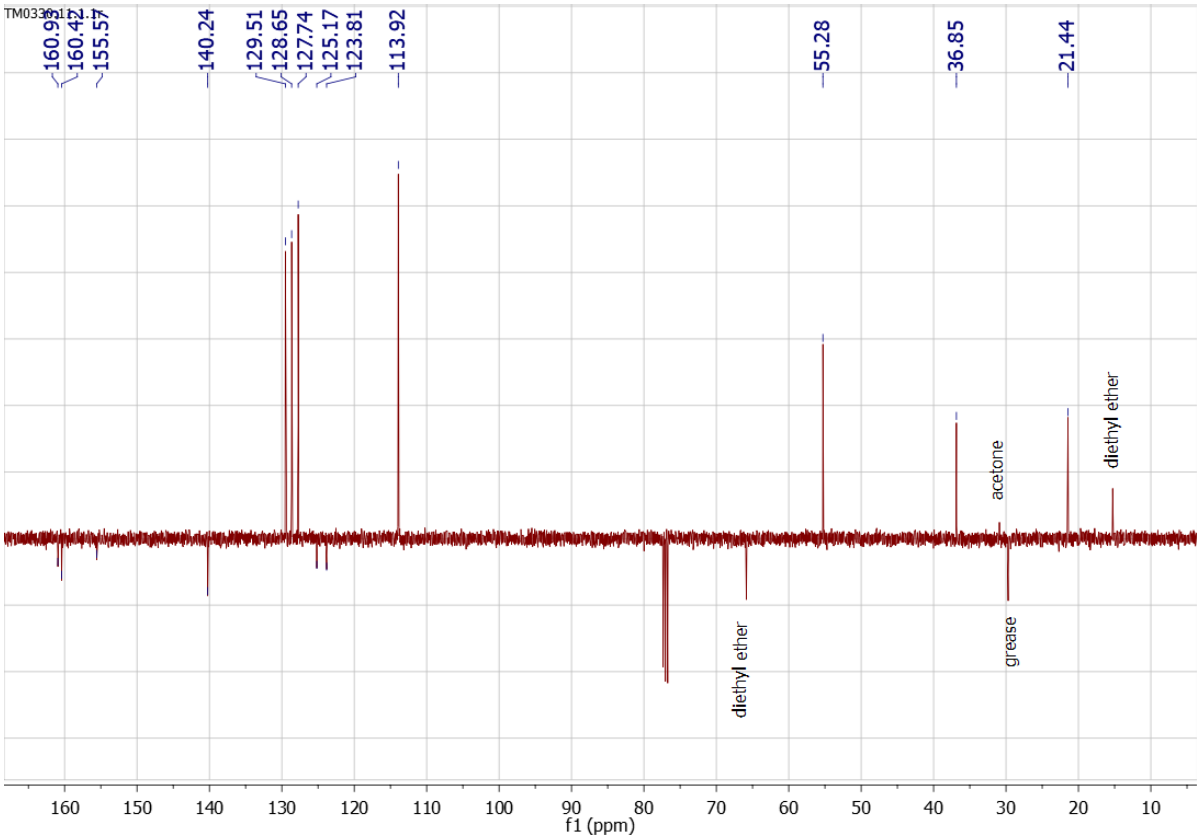

^{13}C NMR spectra of compound **153** in $CDCl_3$.

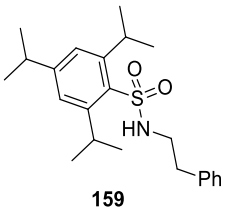

159

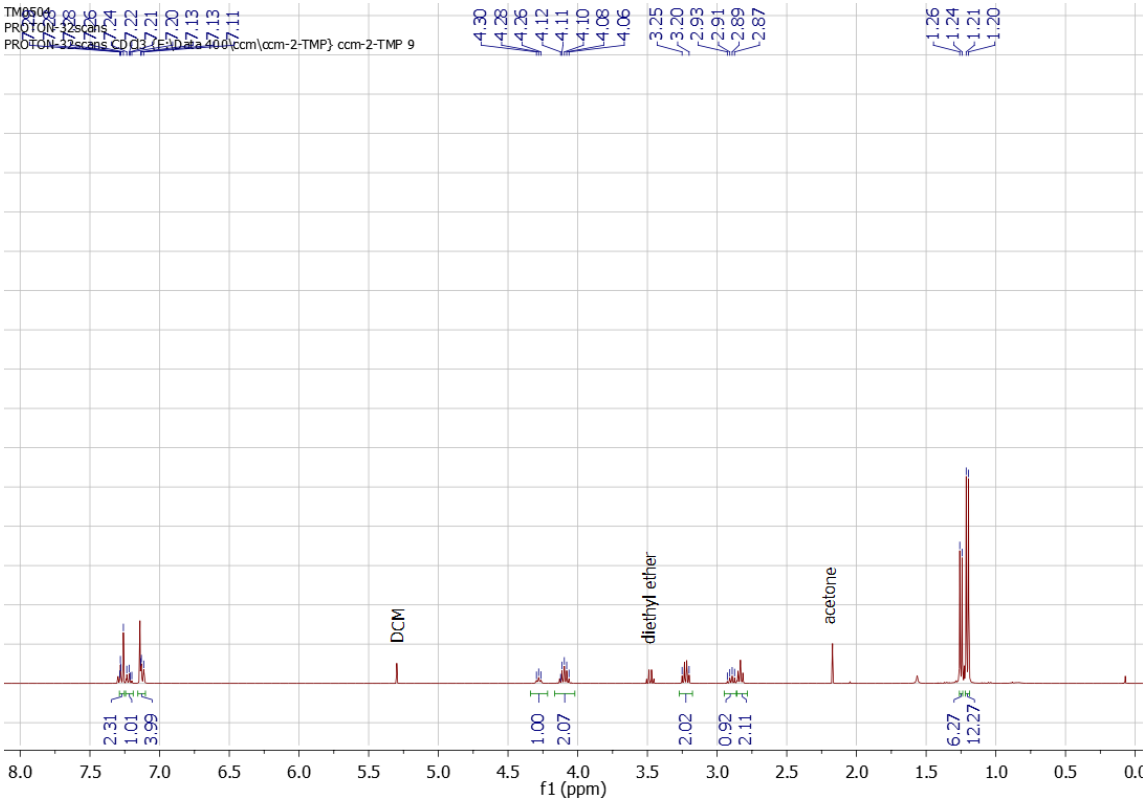

^{1}H NMR spectra of compound **159** in $CDCl_3$.

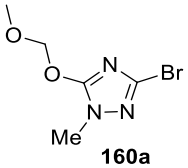

160a

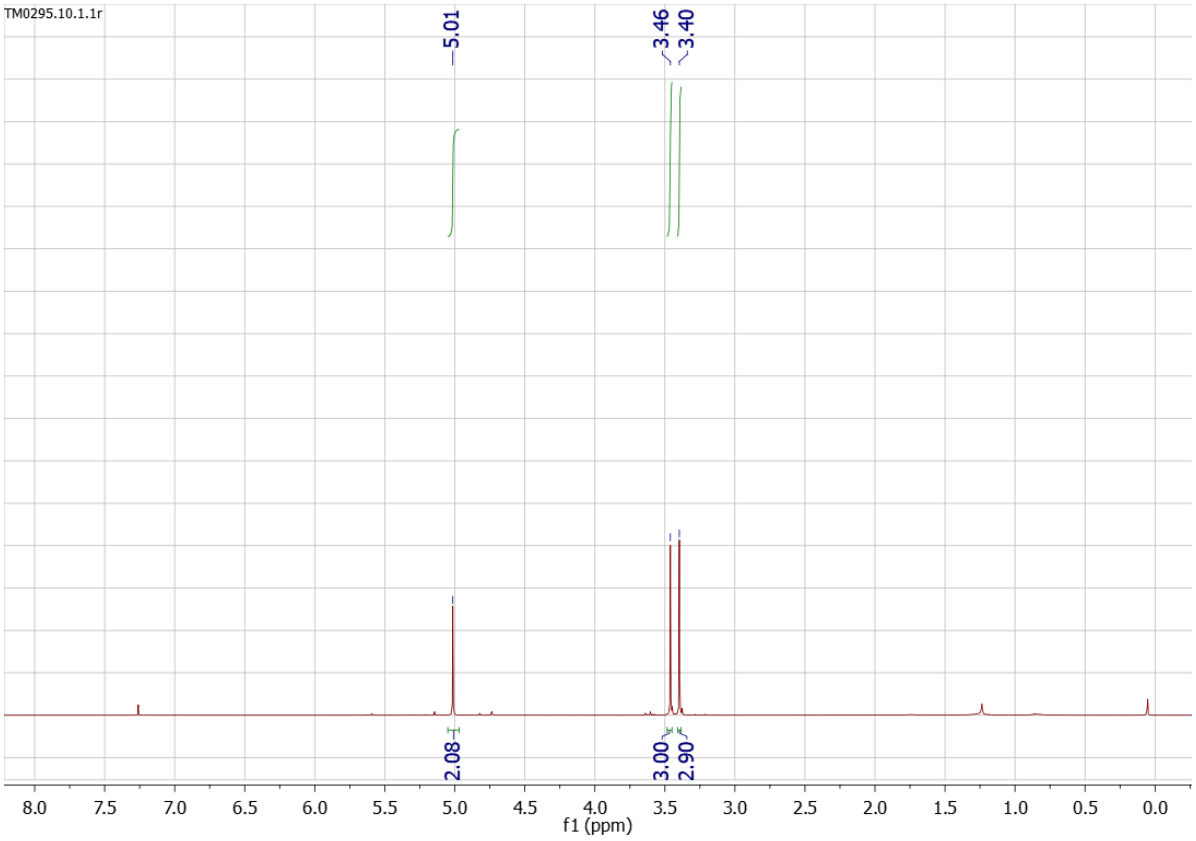

^{1}H NMR spectra of compound **160a** in $CDCl_3$.

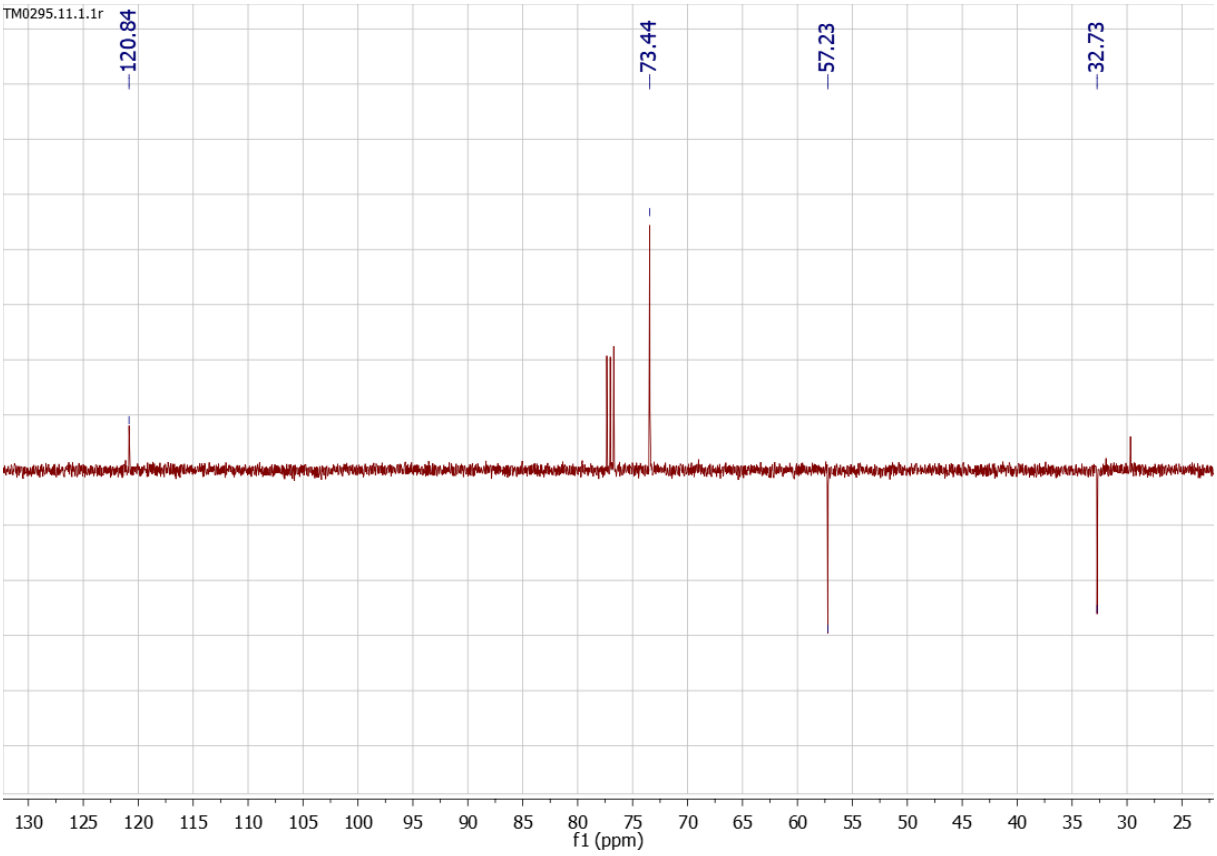

^{13}C NMR spectra of compound **160a** in $CDCl_3$.

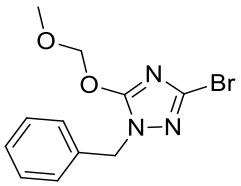

160b

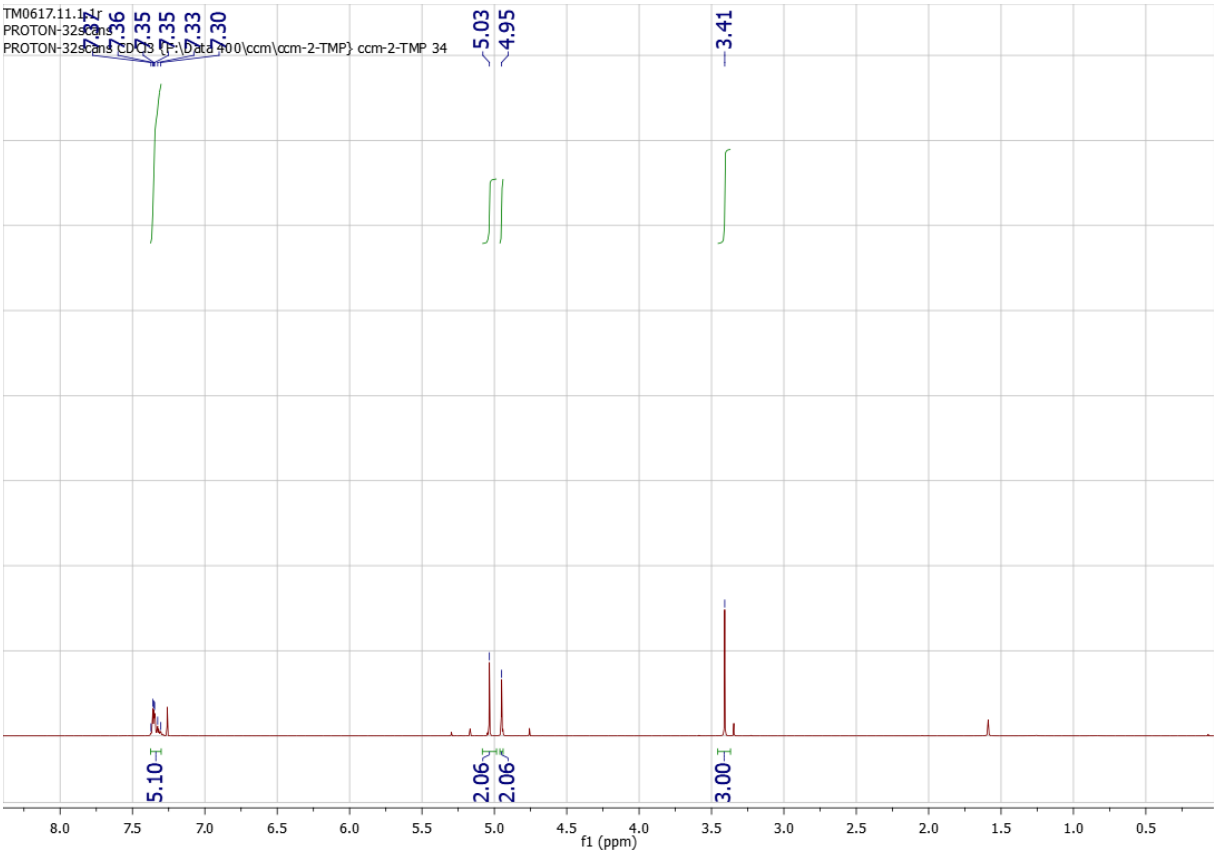

^{1}H NMR spectra of compound **160b** in $CDCl_3$.

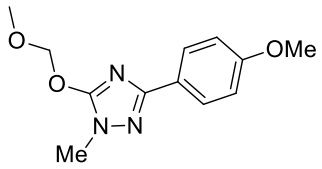

161

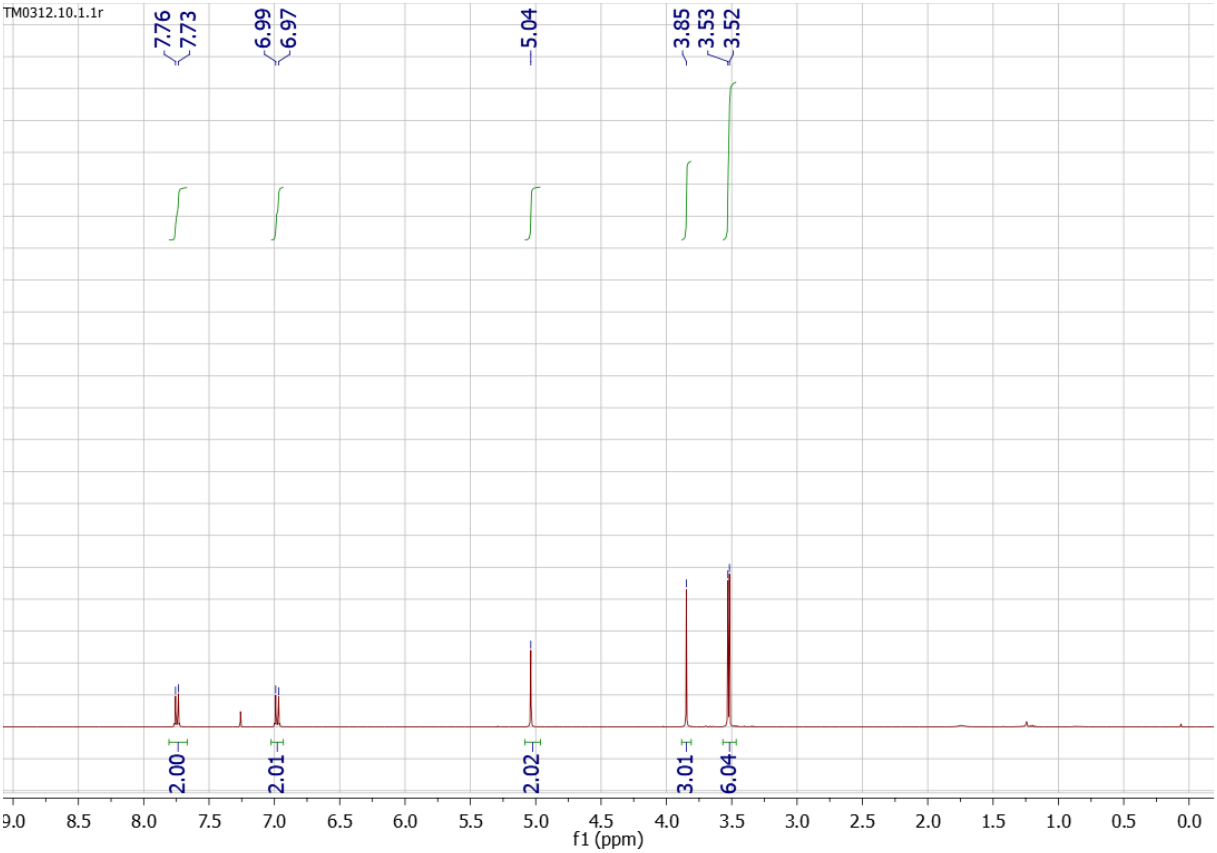

^{1}H NMR spectra of compound **161** in $CDCl_3$.

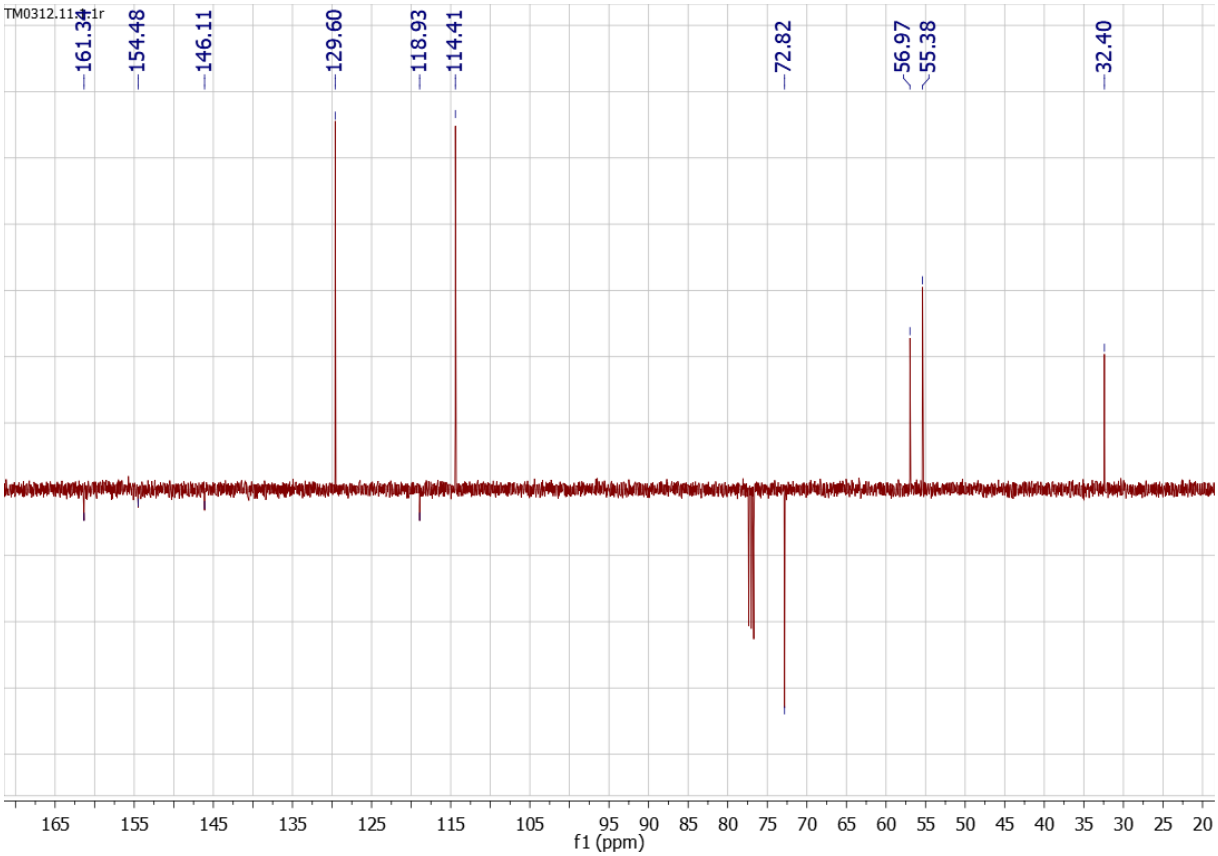

^{13}C NMR spectra of compound **161** in $CDCl_3$.

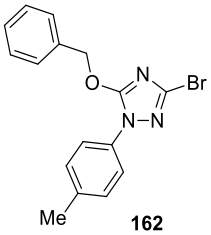

162

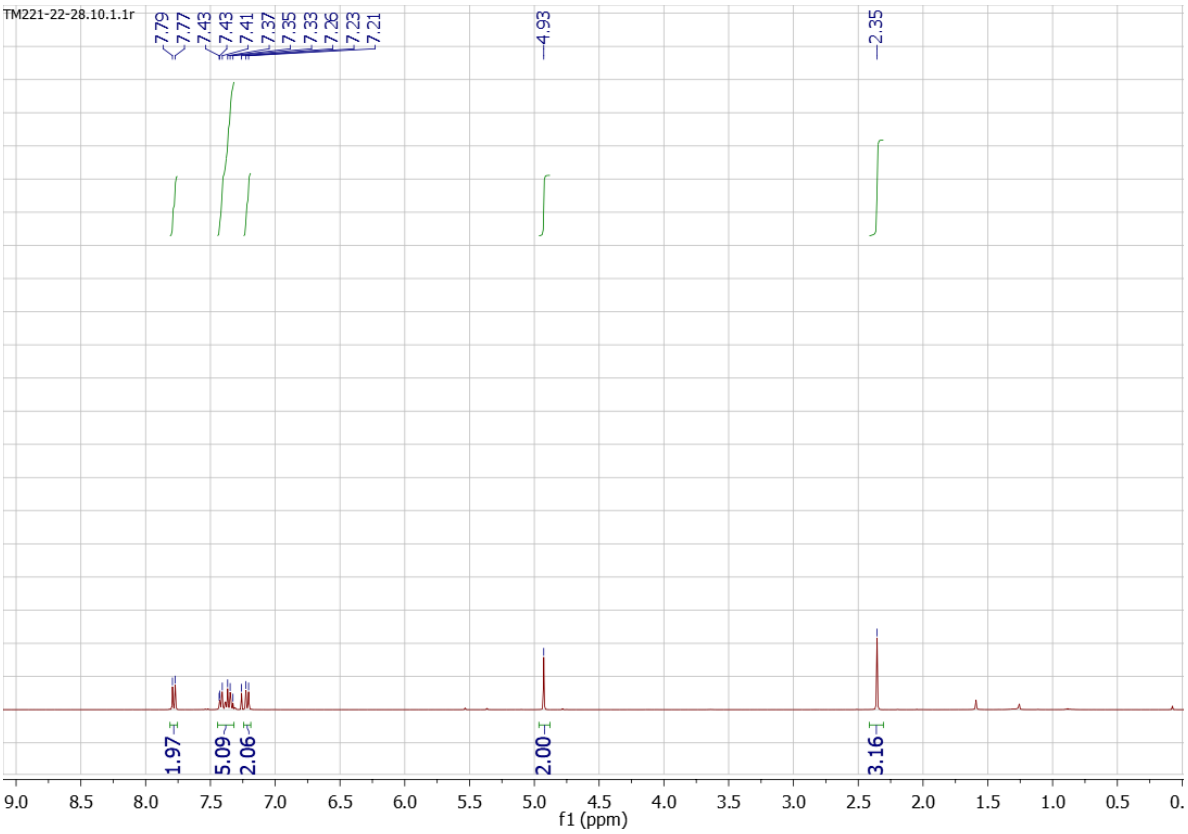

^{1}H NMR spectra of compound **162** in $CDCl_3$.

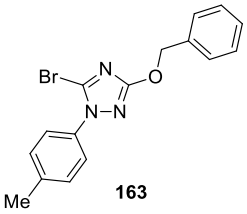

163

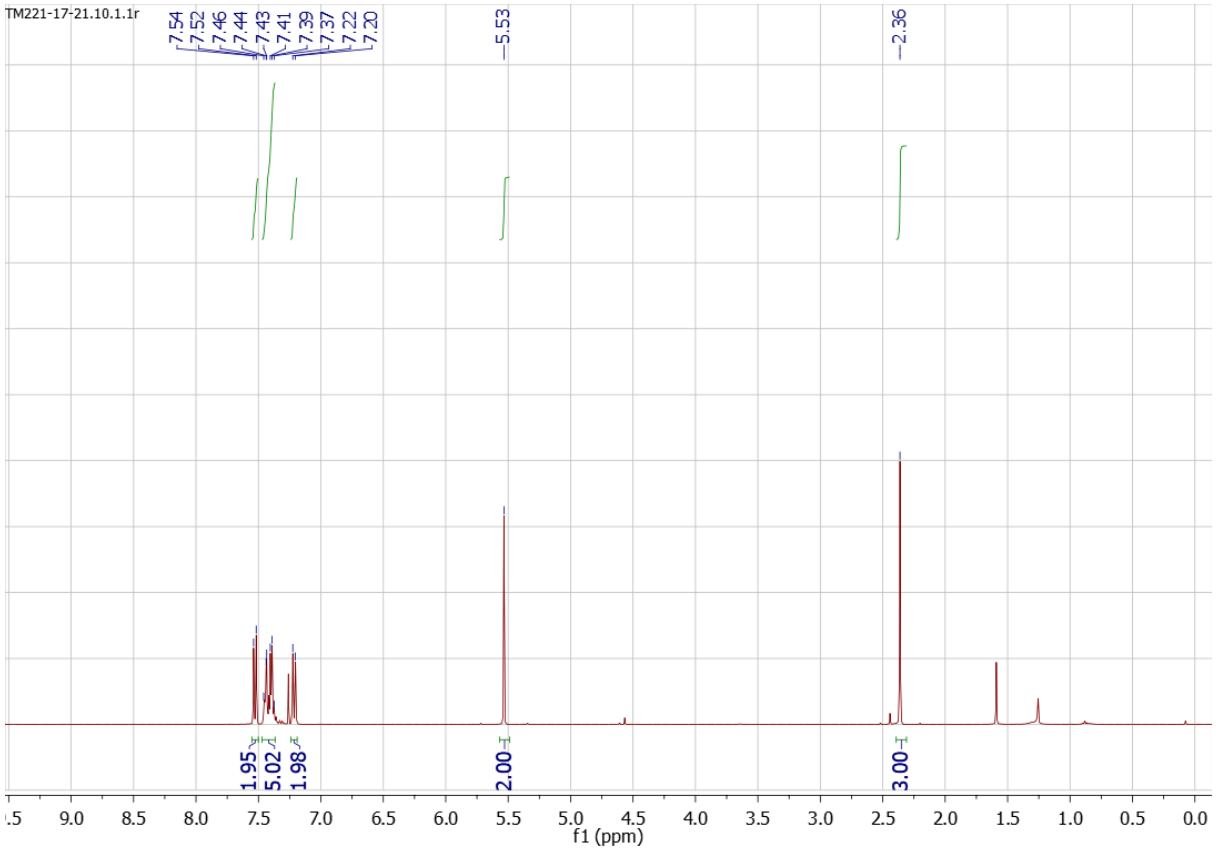

^{1}H NMR spectra of compound **163** in $CDCl_3$.

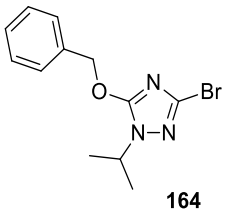

164

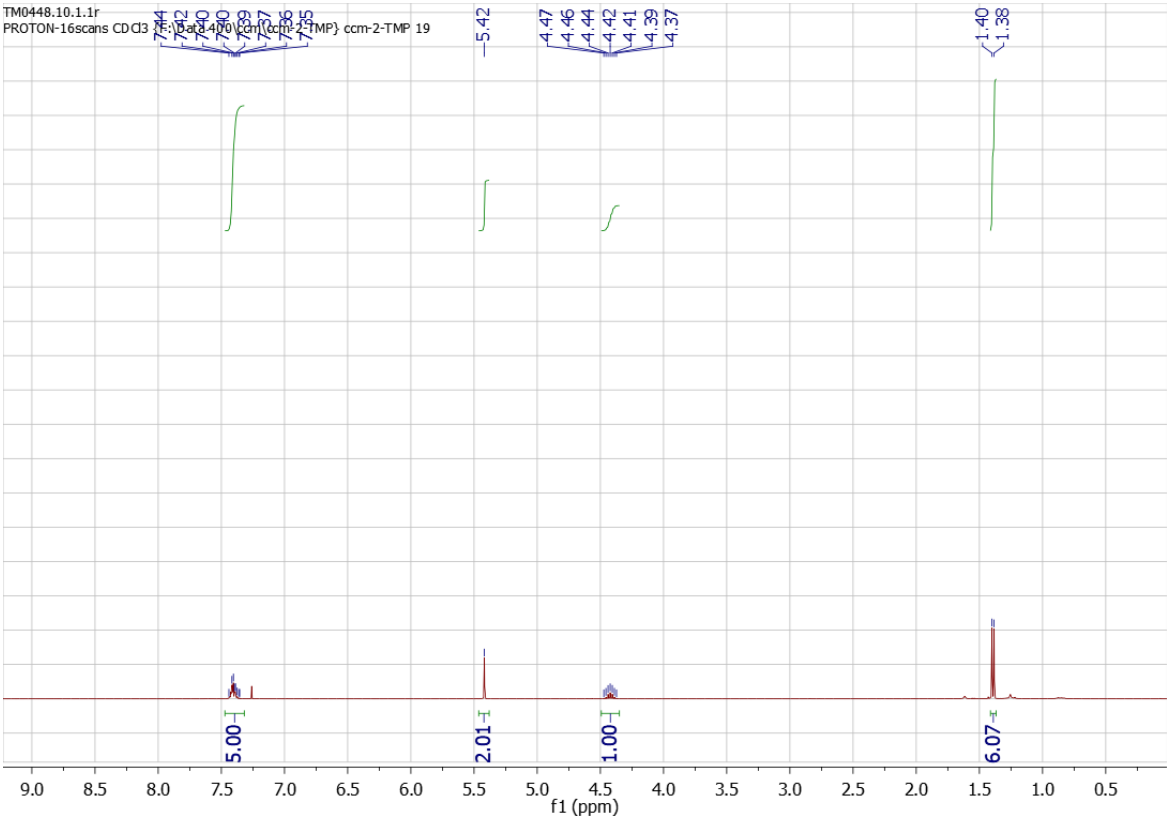

^{1}H NMR spectra of compound **164** in $CDCl_3$.

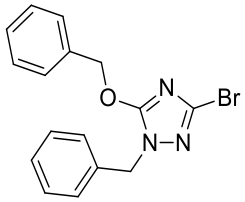

165

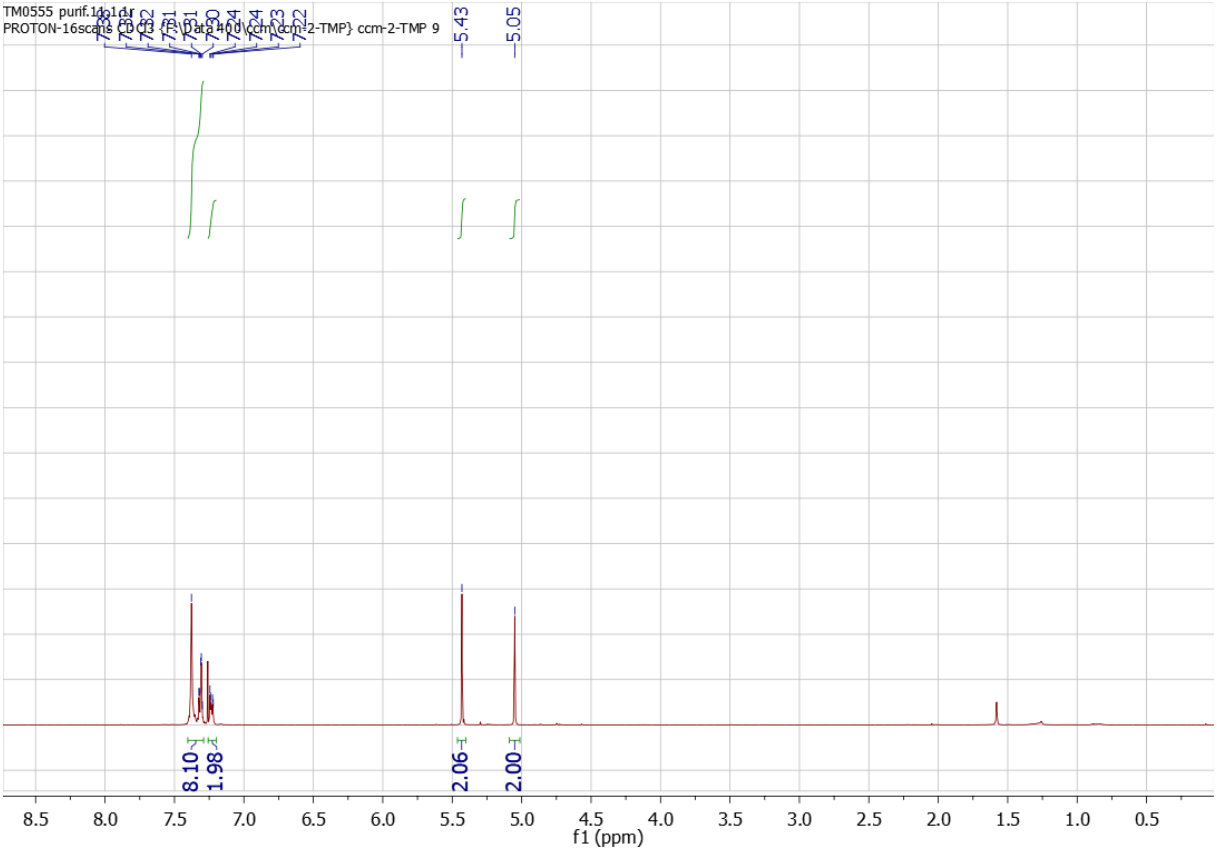

^{1}H NMR spectra of compound **165** in $CDCl_3$.

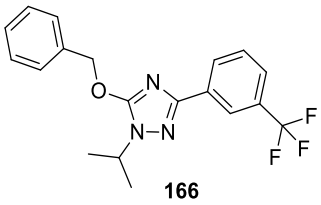

166

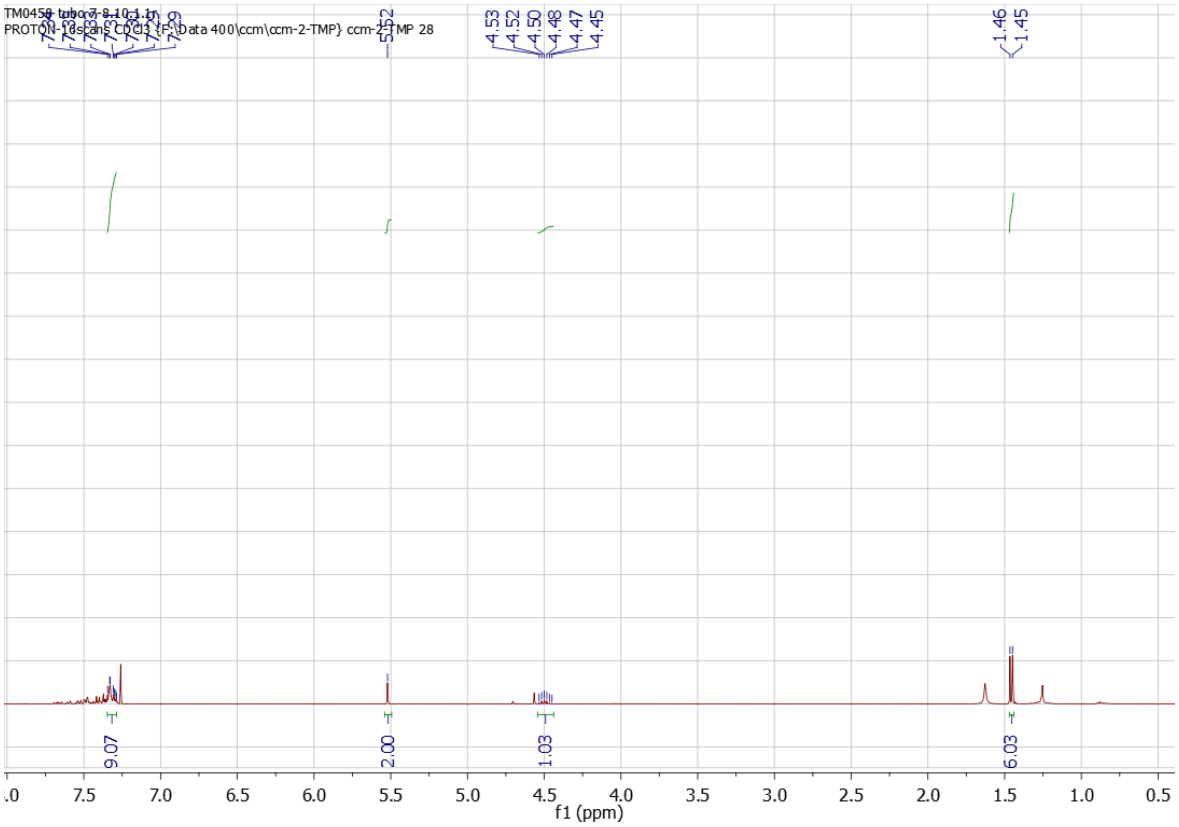

^{1}H NMR spectra of compound **166** in $CDCl_3$.

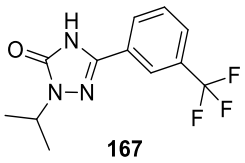

167

Exact Mass: 271.09

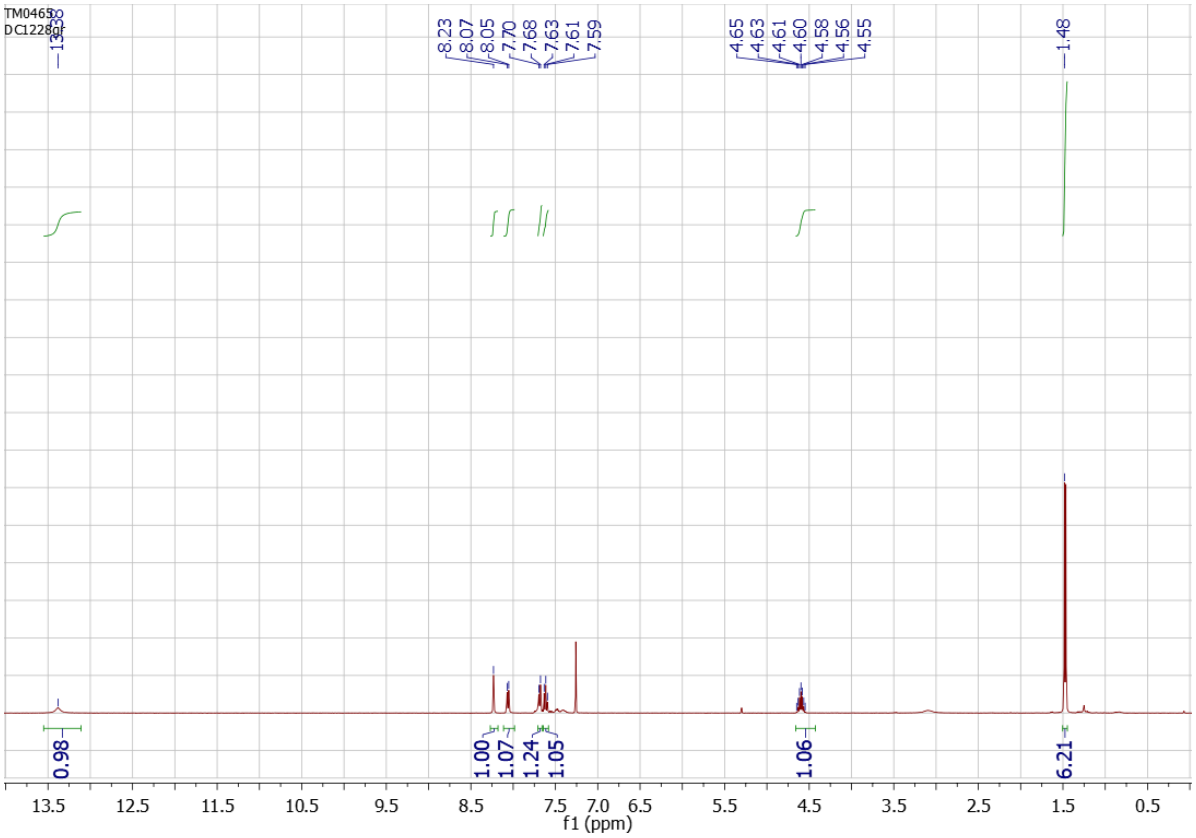

^{1}H NMR spectra of compound **167** in $CDCl_3$.

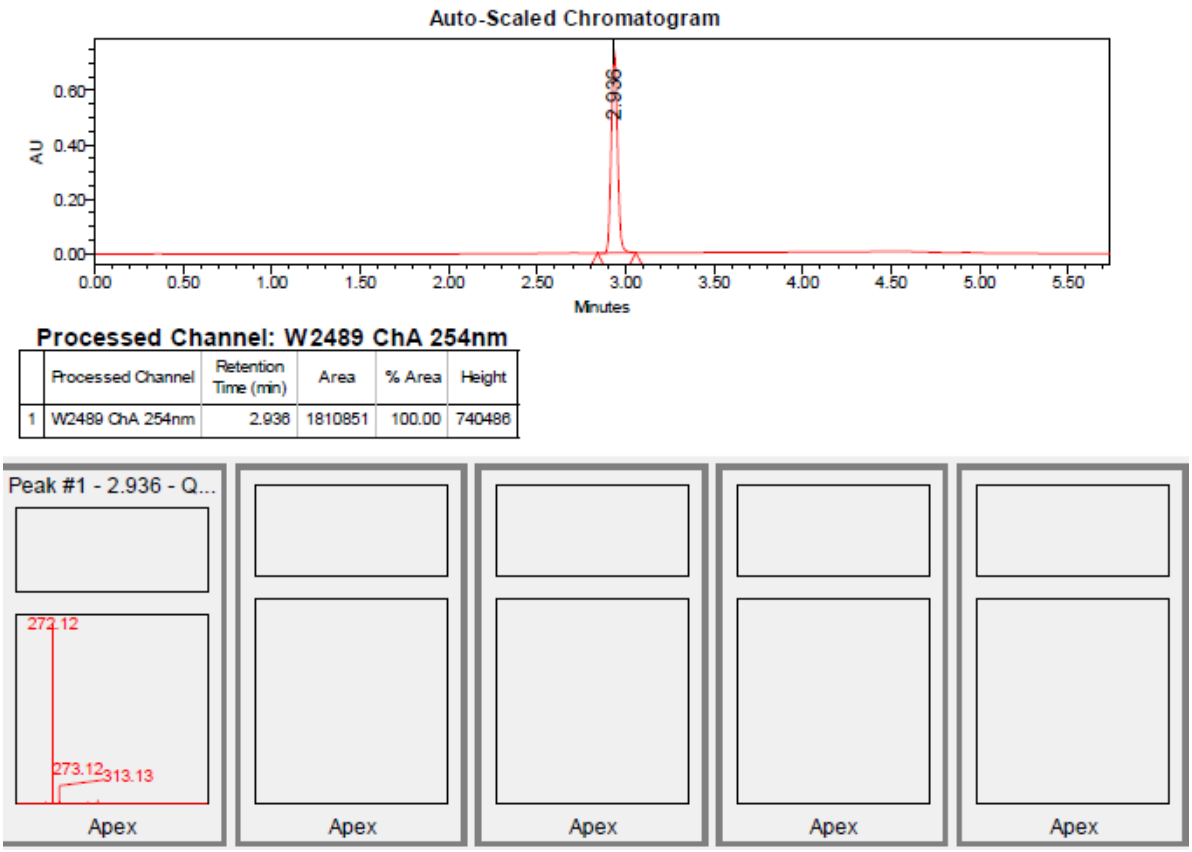

LC/MS of compound **167**.

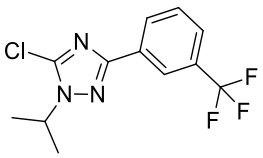

168

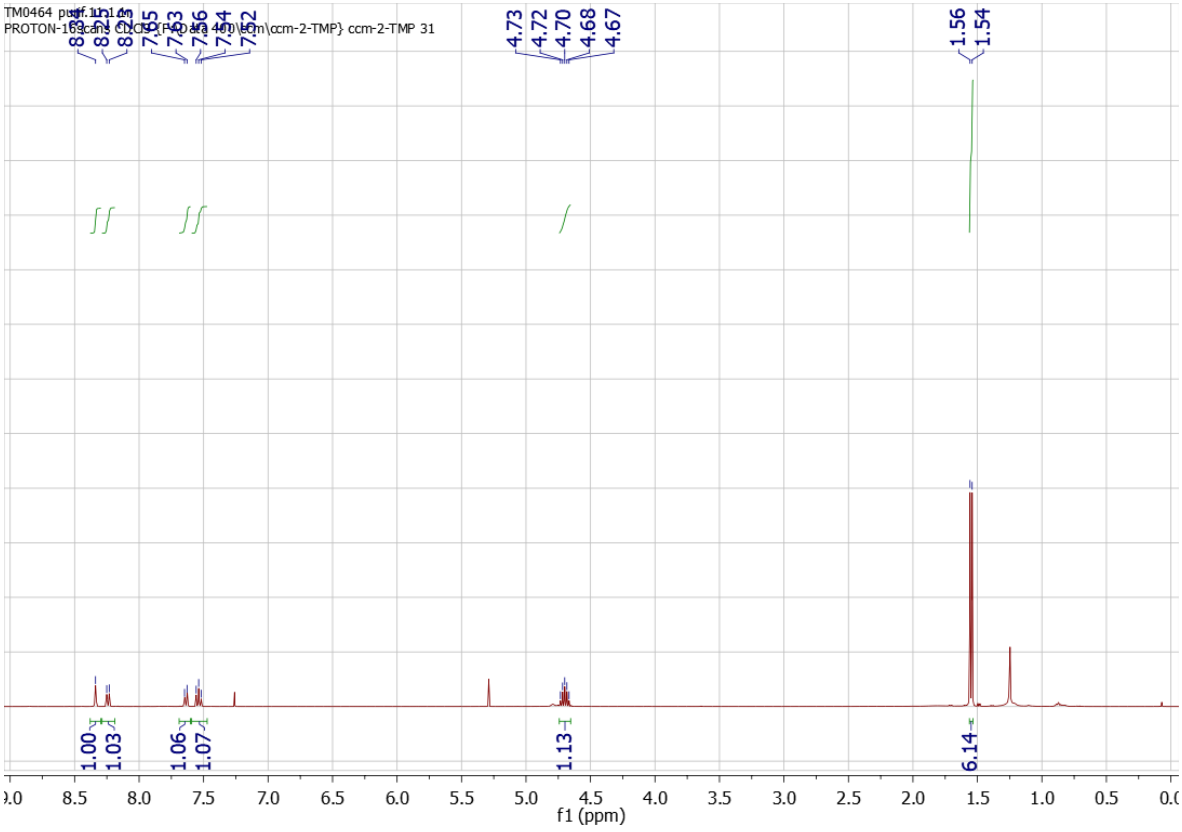

^{1}H NMR spectra of compound **168** in $CDCl_3$.

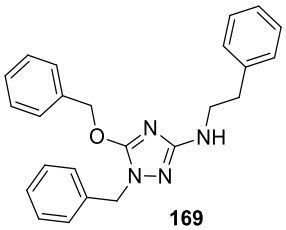

169

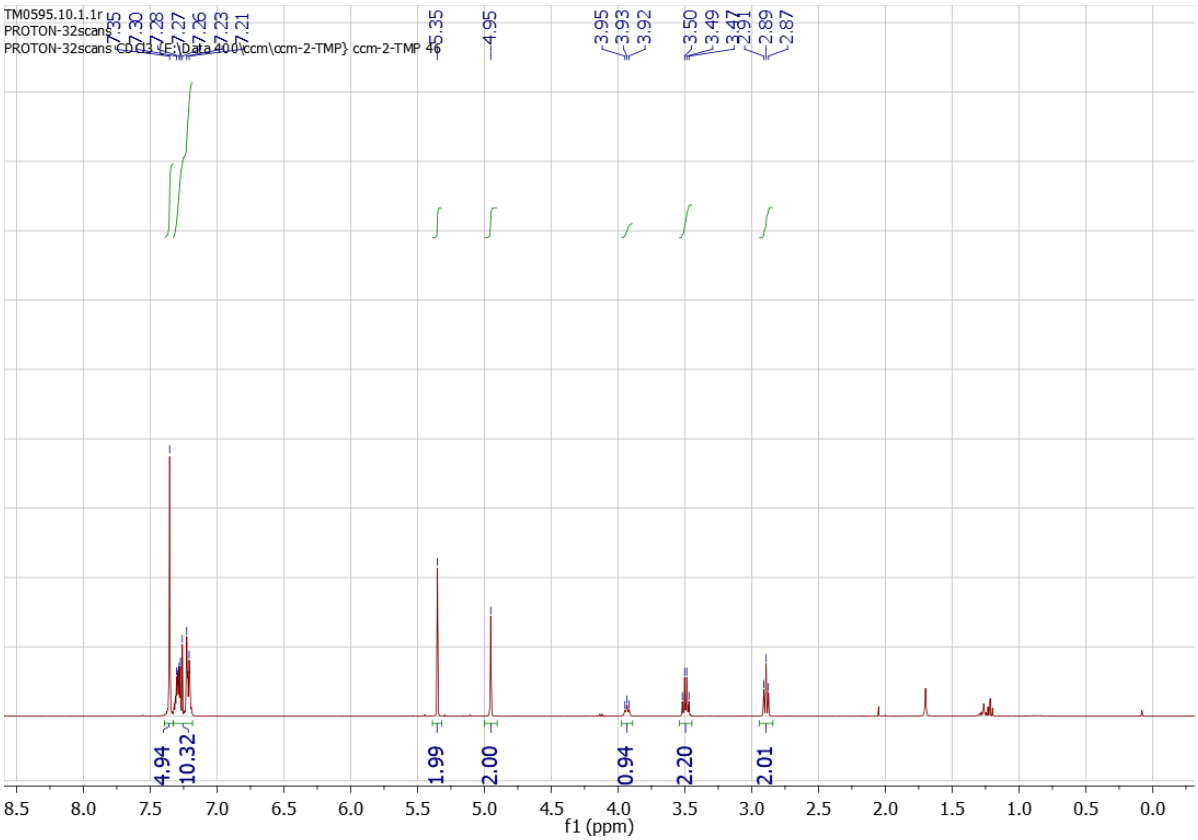

^{1}H NMR spectra of compound **169** in $CDCl_3$.

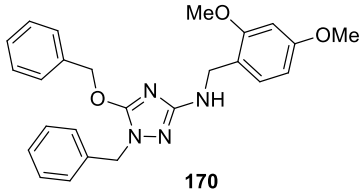

170

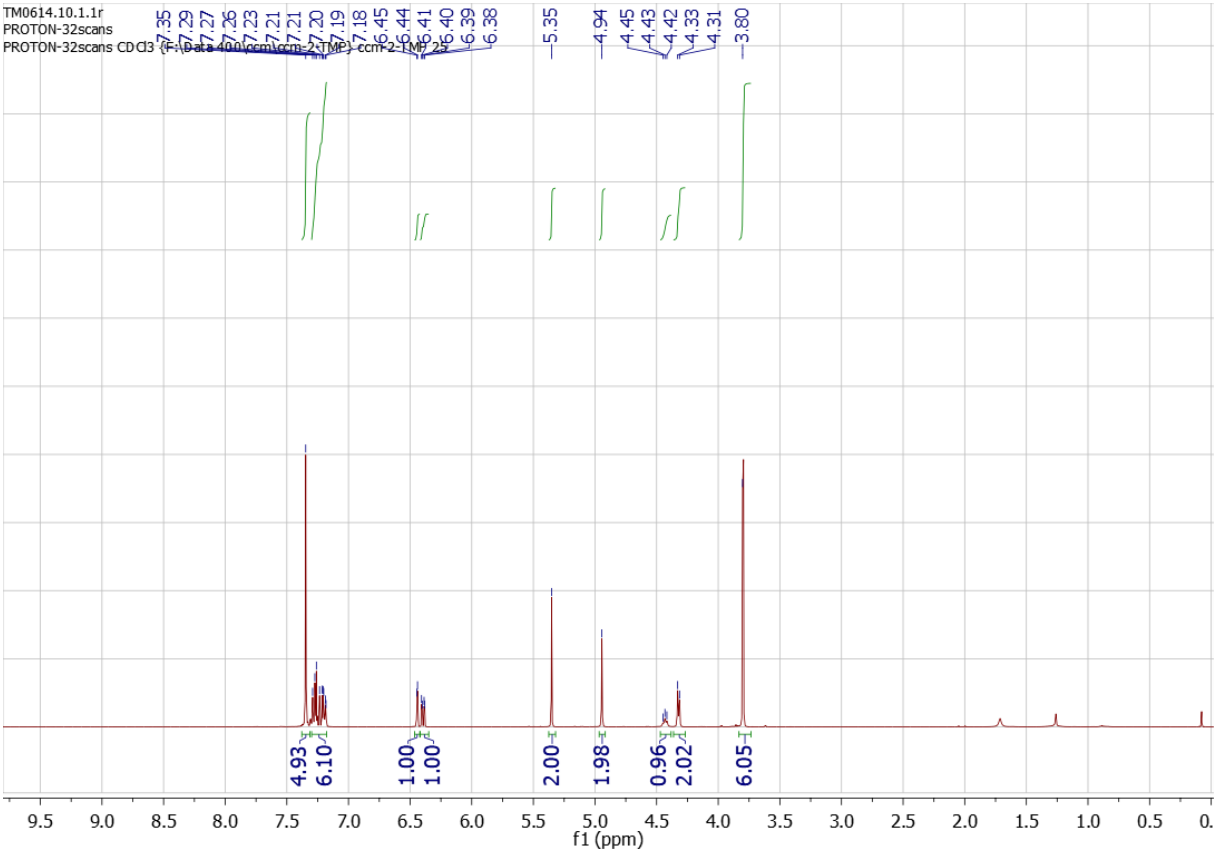

^{1}H NMR spectra of compound **170** in $CDCl_3$.

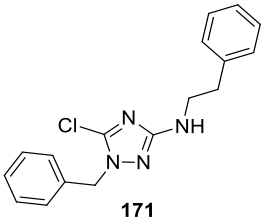

171

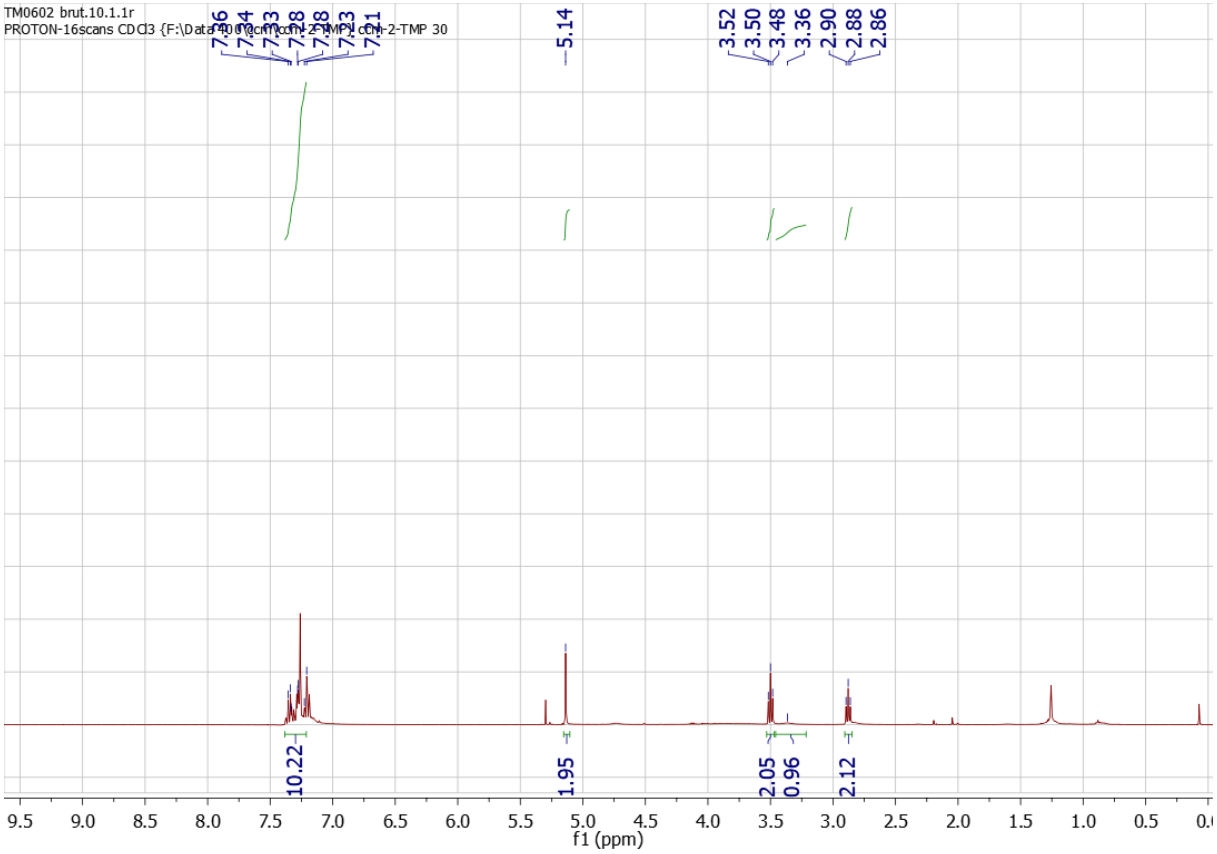

^{1}H NMR spectra of compound **171** in $CDCl_3$.

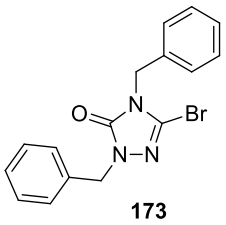

173

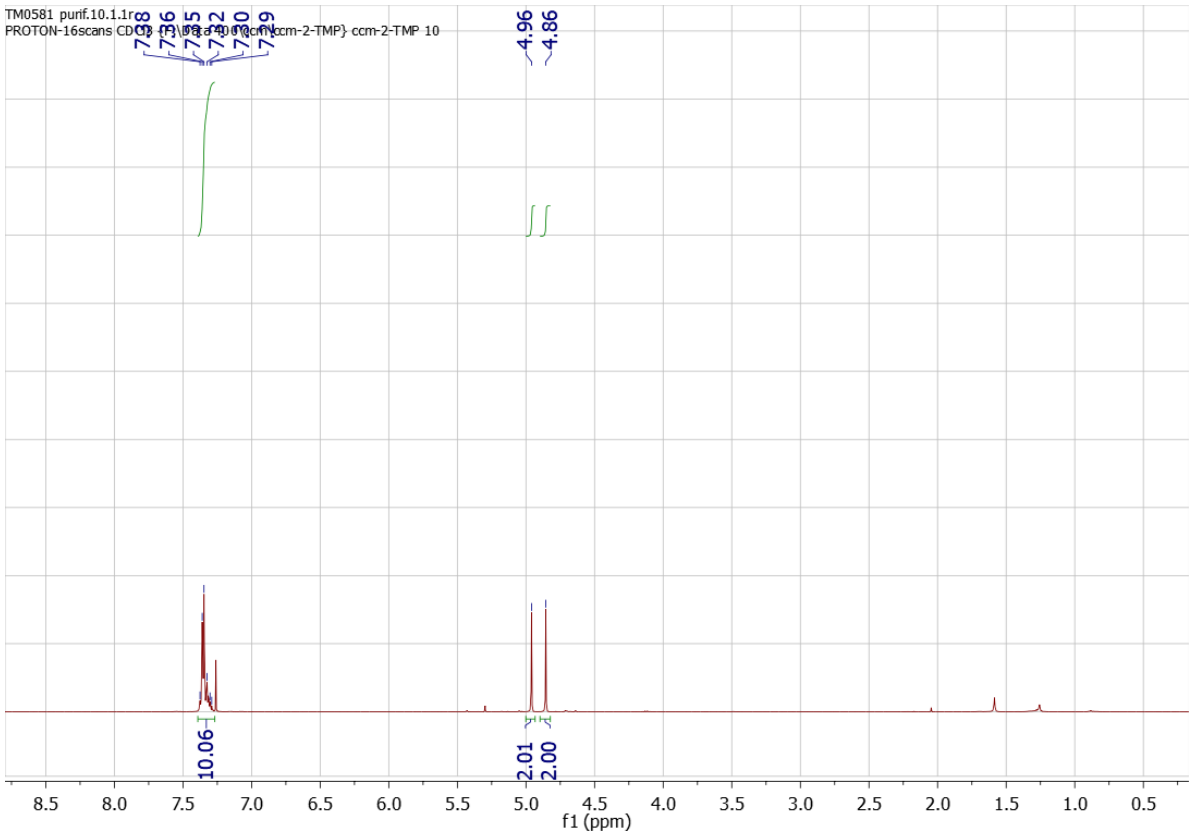

^{1}H NMR spectra of compound **173** in $CDCl_3$.

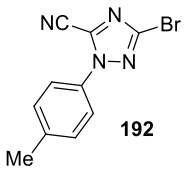

192

Exact Mass: 261.99

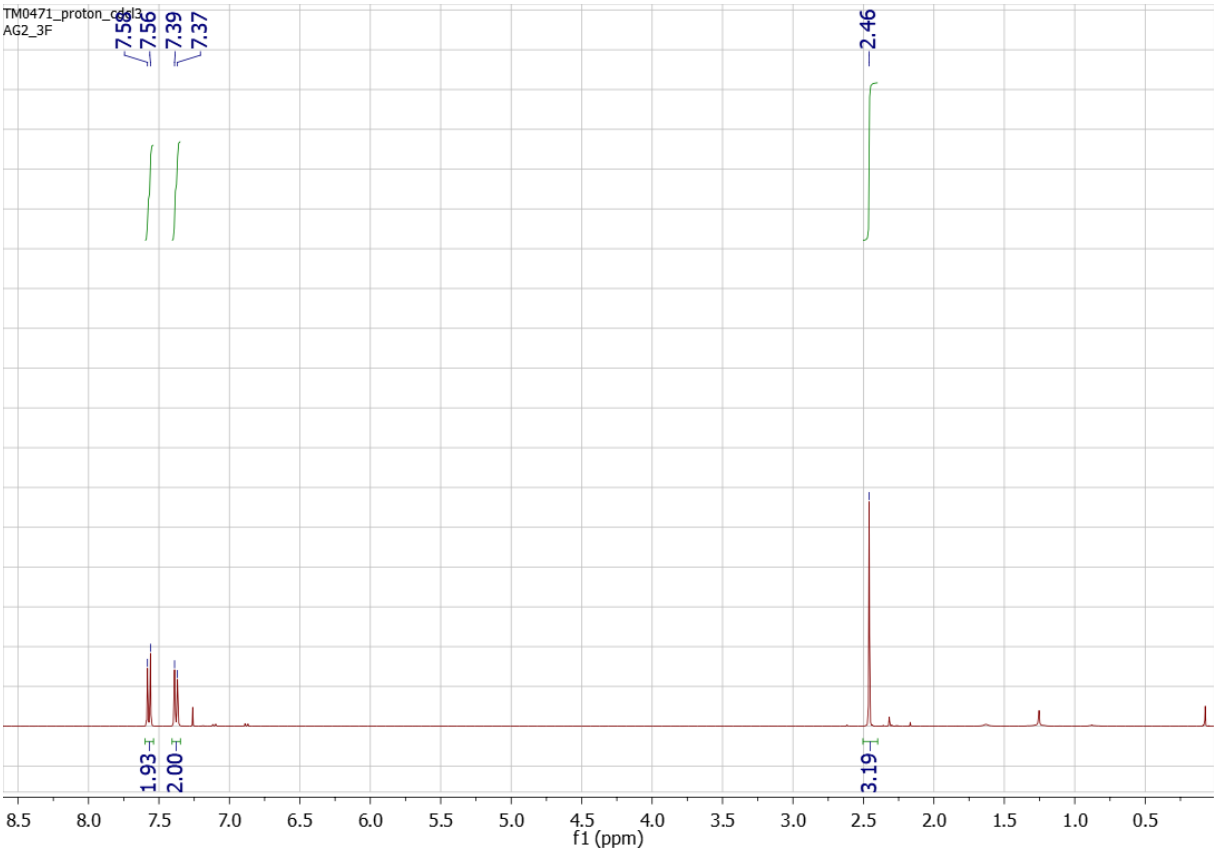

^{1}H NMR spectra of compound **192** in $CDCl_3$.

,

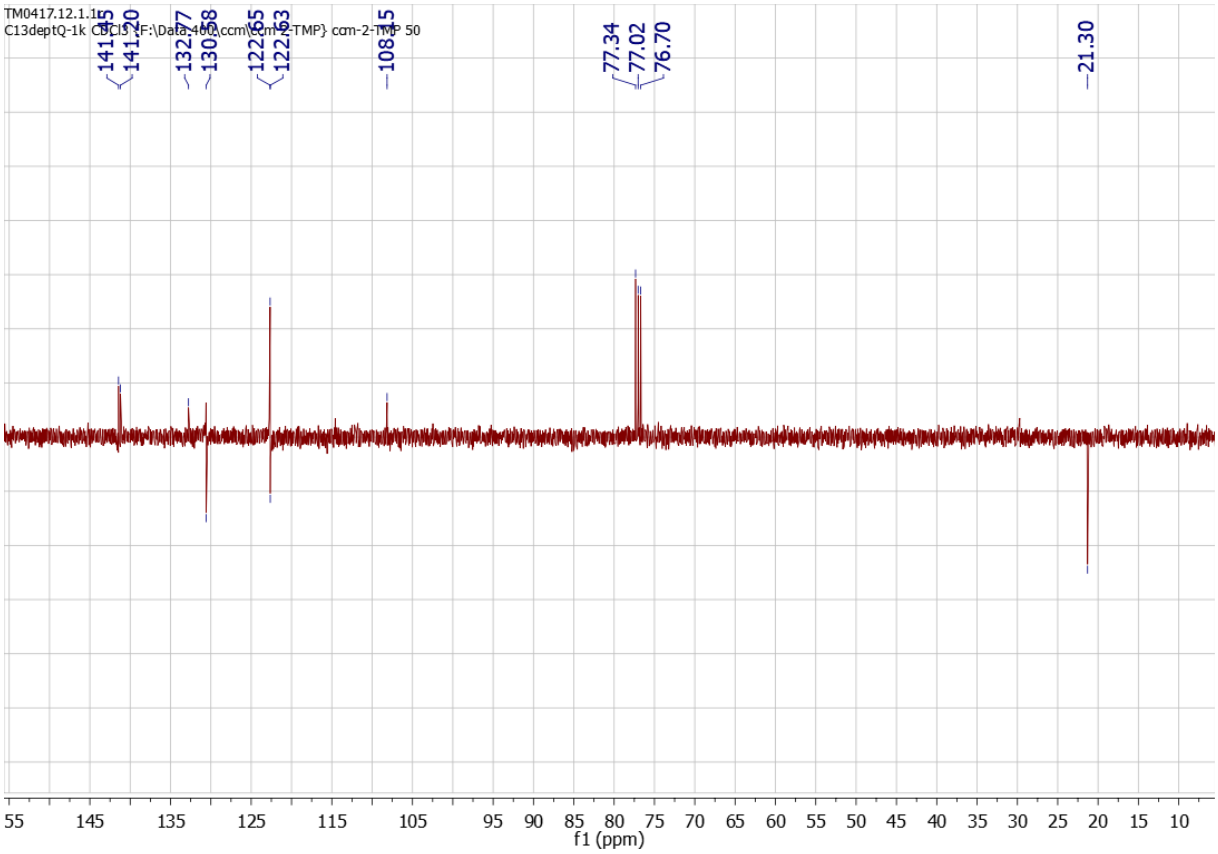

^{13}C NMR spectra of compound **192** in $CDCl_3$.

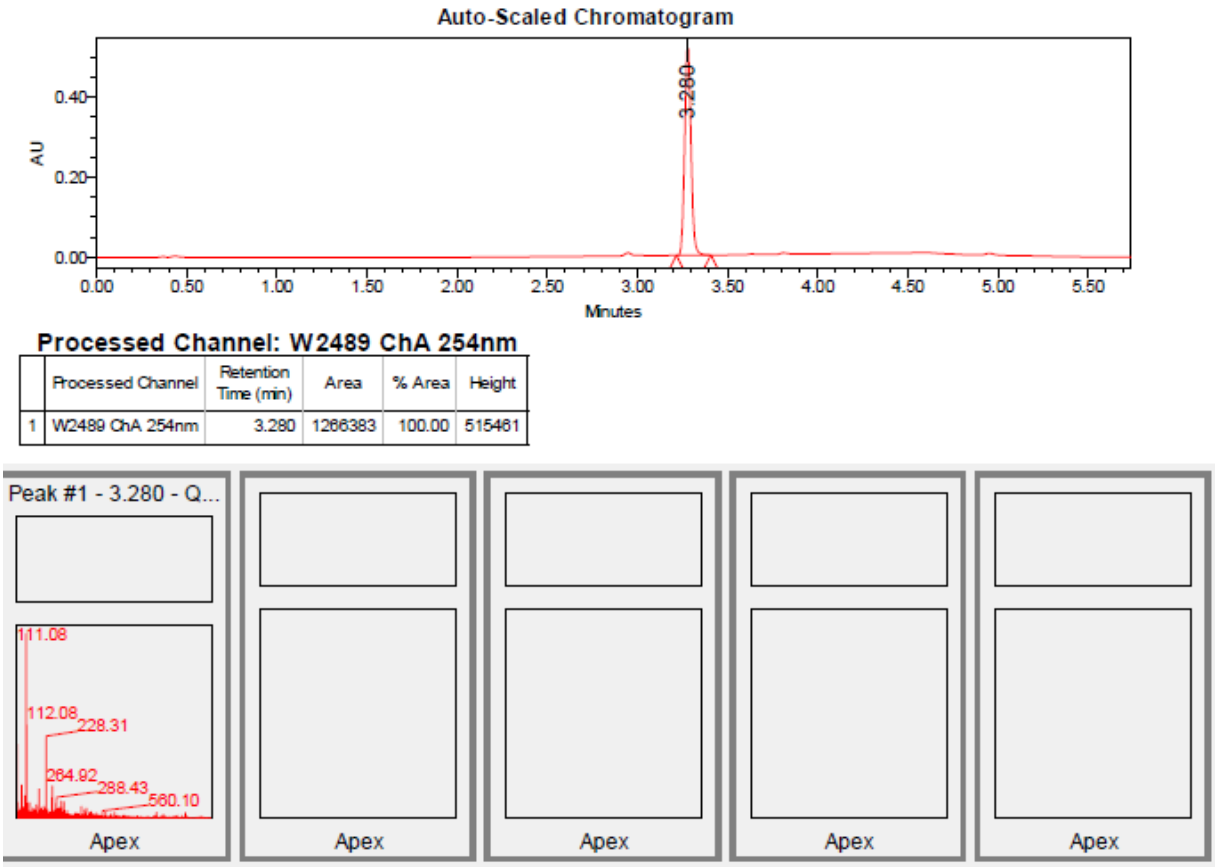

LC/MS of compound **192**.

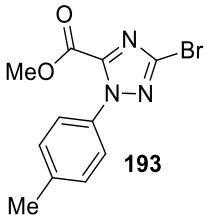

193

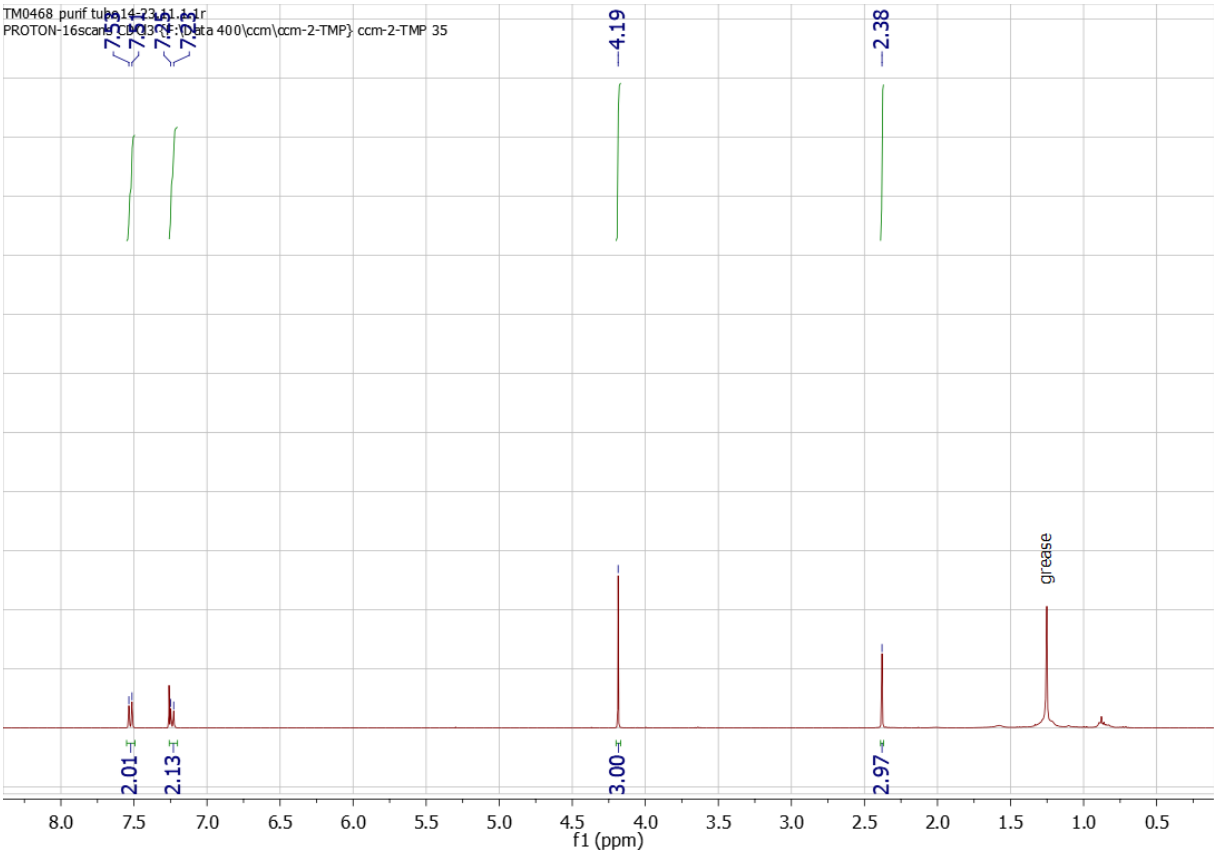

^{1}H NMR spectra of compound **193** in $CDCl_3$.

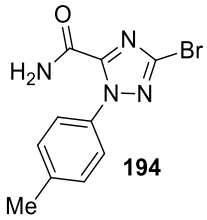

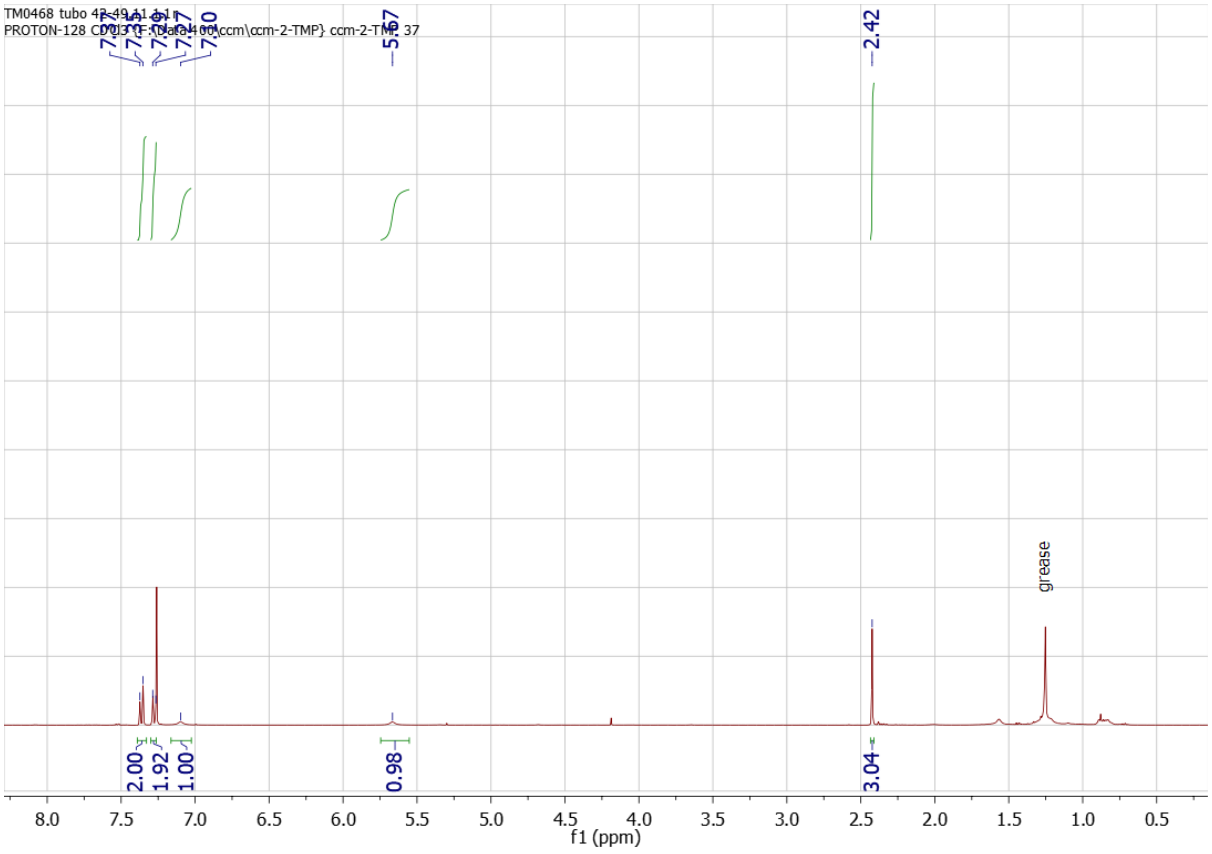

^{1}H NMR spectra of compound **194** in $CDCl_3$.

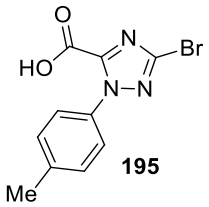

195

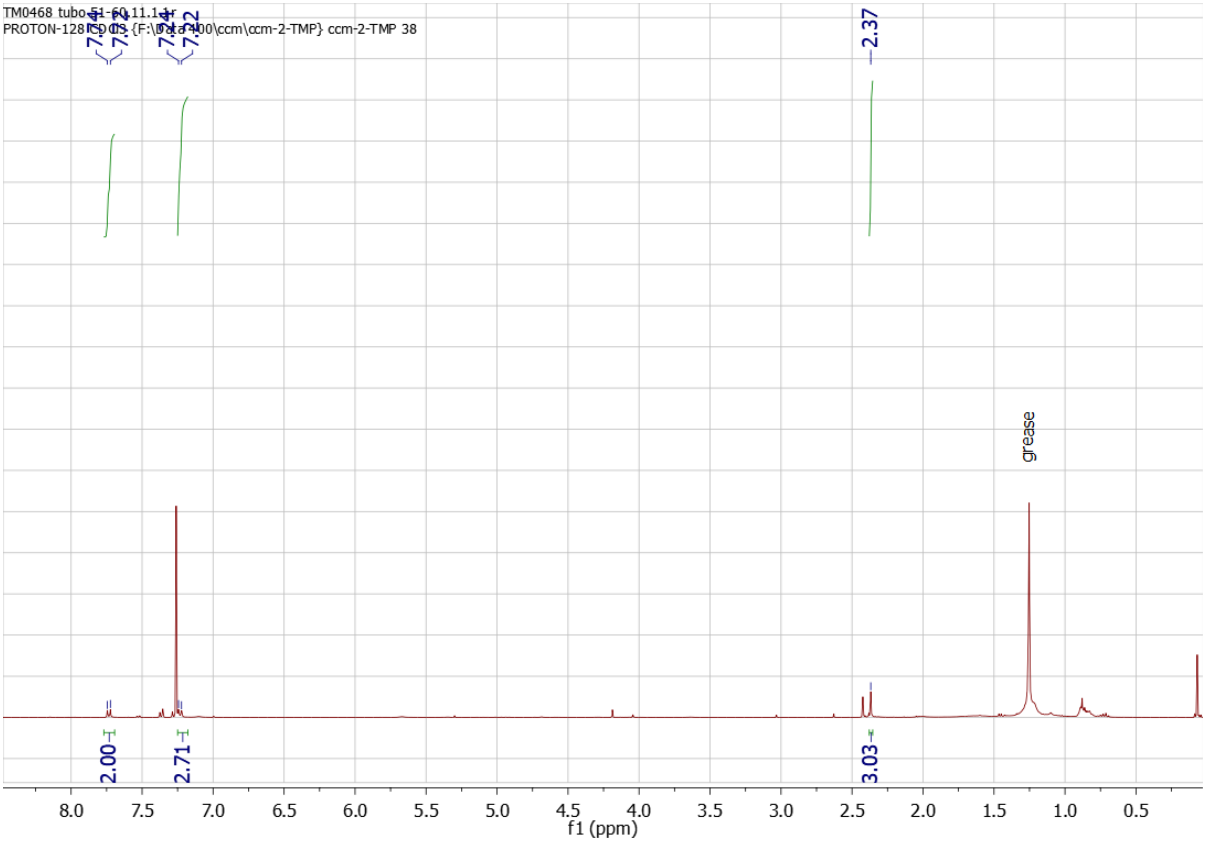

^{1}H NMR spectra of compound **195** in $CDCl_3$.

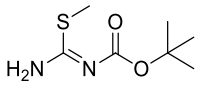

227

Exact Mass: 190.08

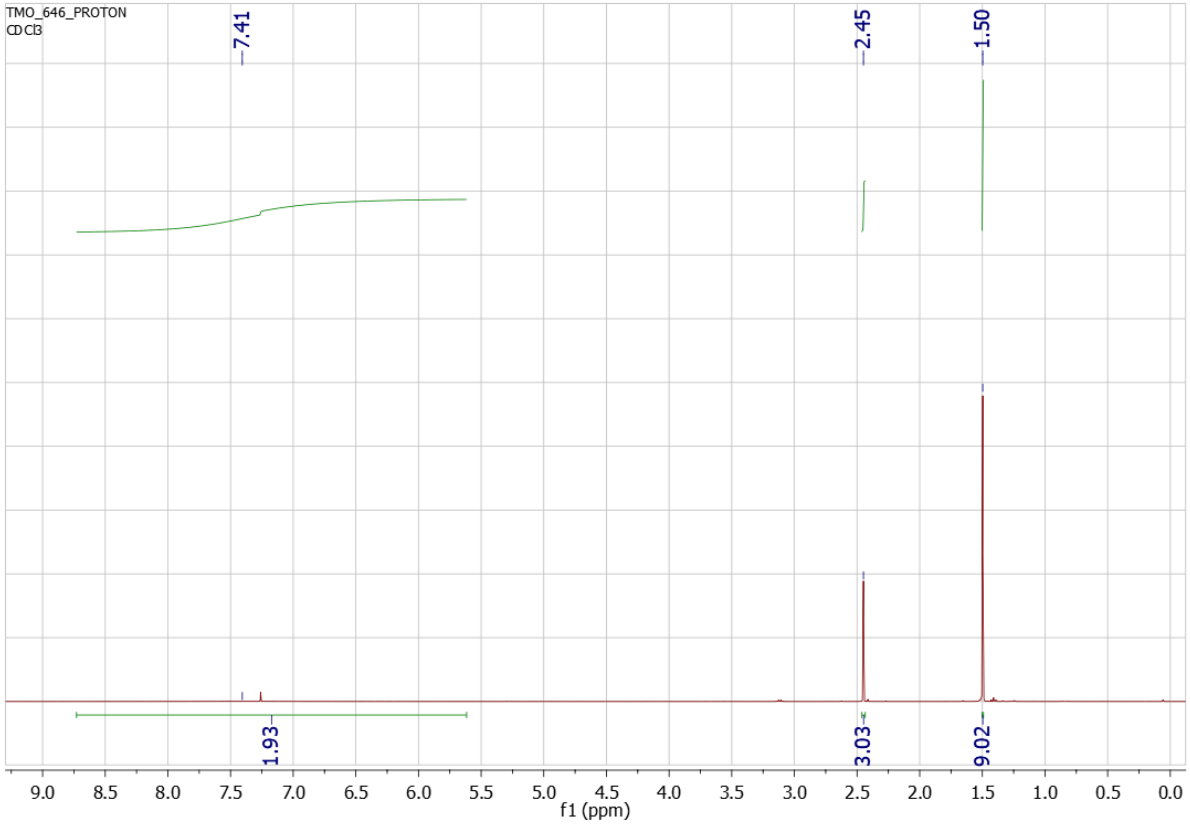

^{1}H NMR spectra of compound **227** in $CDCl_3$.

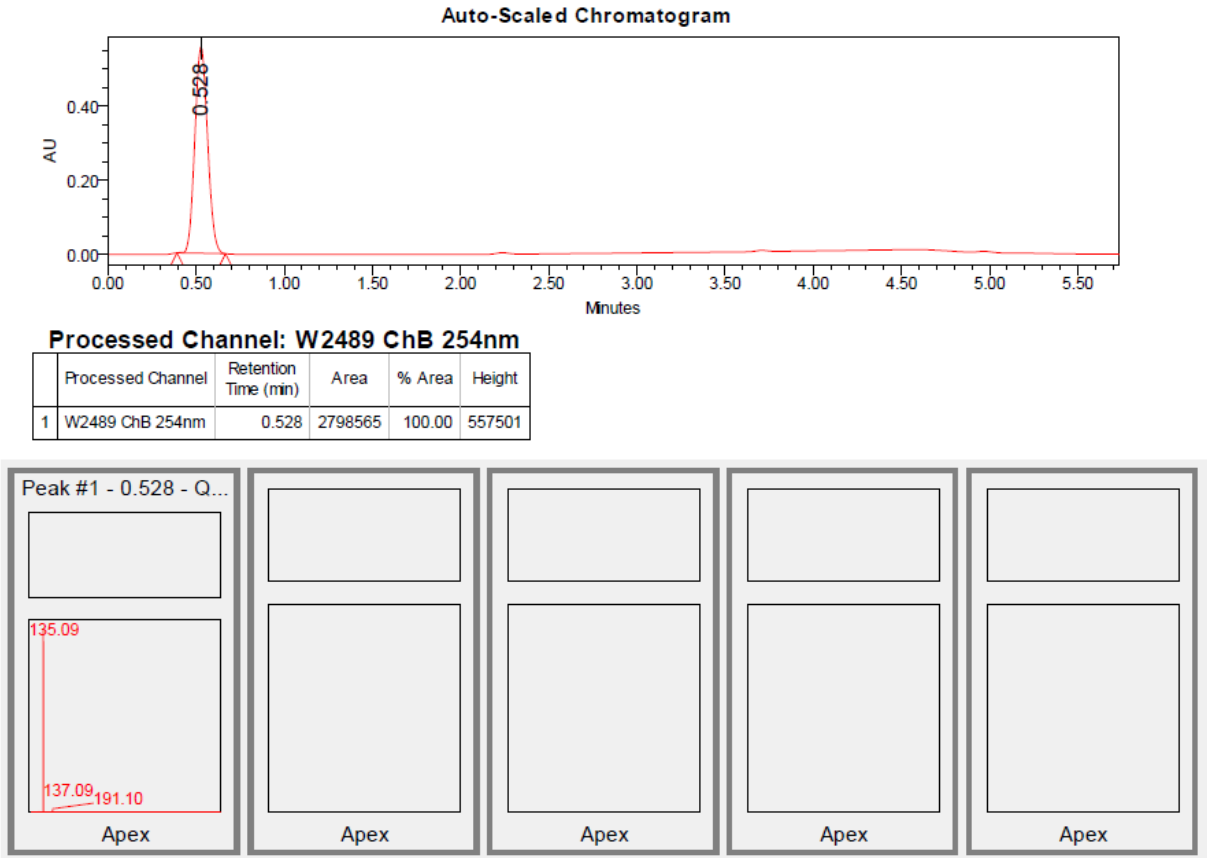

LC/MS of compound **227**.

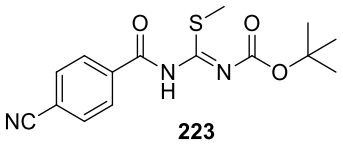

223

Exact Mass: 319.10

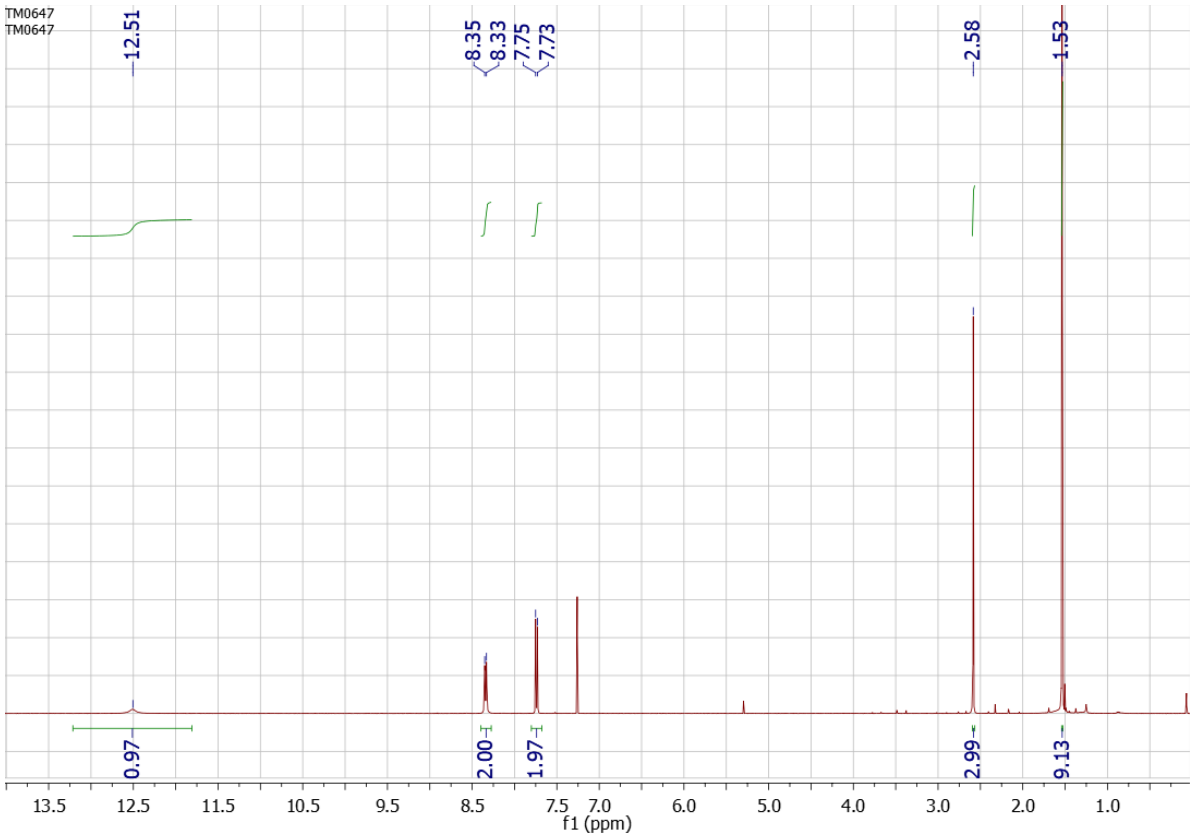

^{1}H NMR spectra of compound **223** in $CDCl_3$.

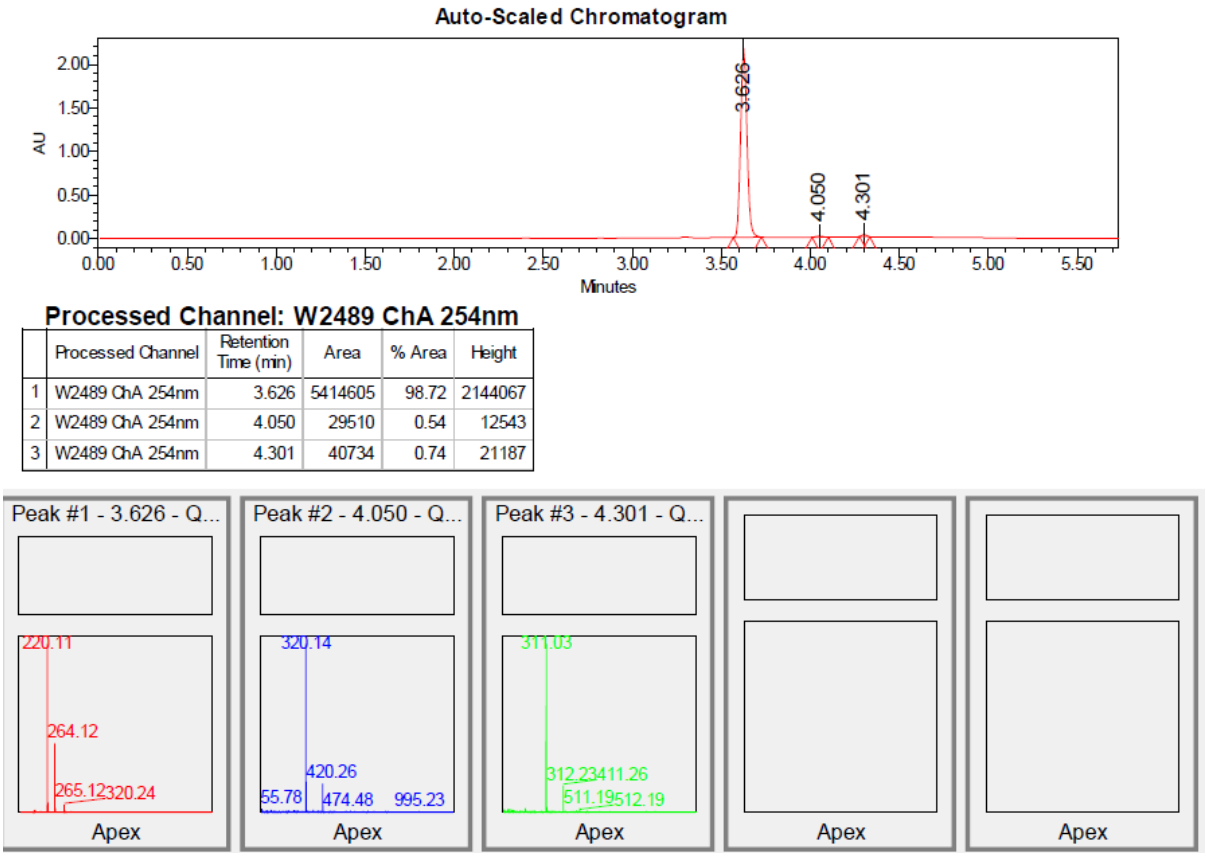

	Processed Channel	Retention Time (min)	Area	% Area	Height
1	W2489 ChA 254nm	3.626	5414605	98.72	2144067
2	W2489 ChA 254nm	4.050	29510	0.54	12543
3	W2489 ChA 254nm	4.301	40734	0.74	21187

LC/MS of compound **223**.

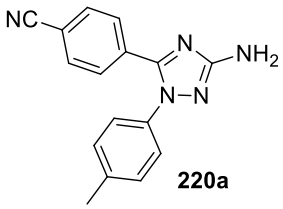

220a

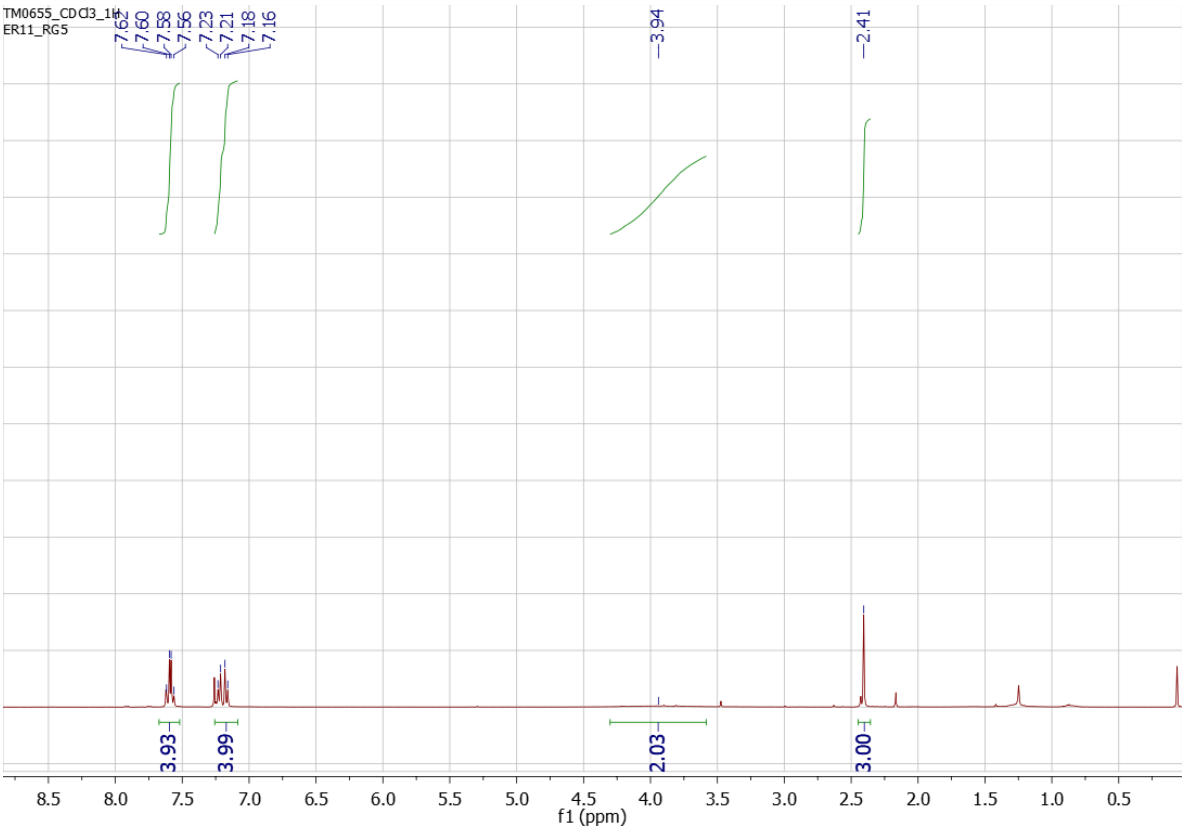

^{1}H NMR spectra of compound **220a** in $CDCl_3$.

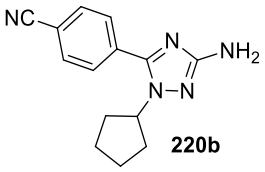

220b

Exact Mass: 253.13

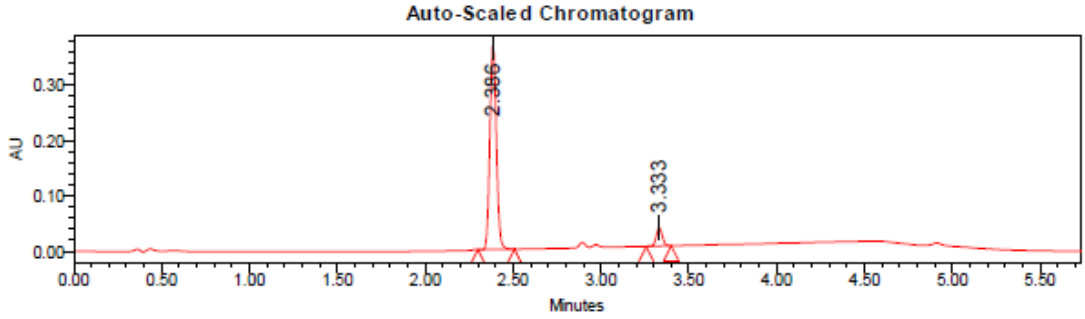

Processed Channel: W2489 ChA 254nm

	Processed Channel	Retention Time (min)	Area	% Area	Height
1	W2489 ChA 254nm	2.386	940203	92.29	365366
2	W2489 ChA 254nm	3.333	78526	7.71	32859

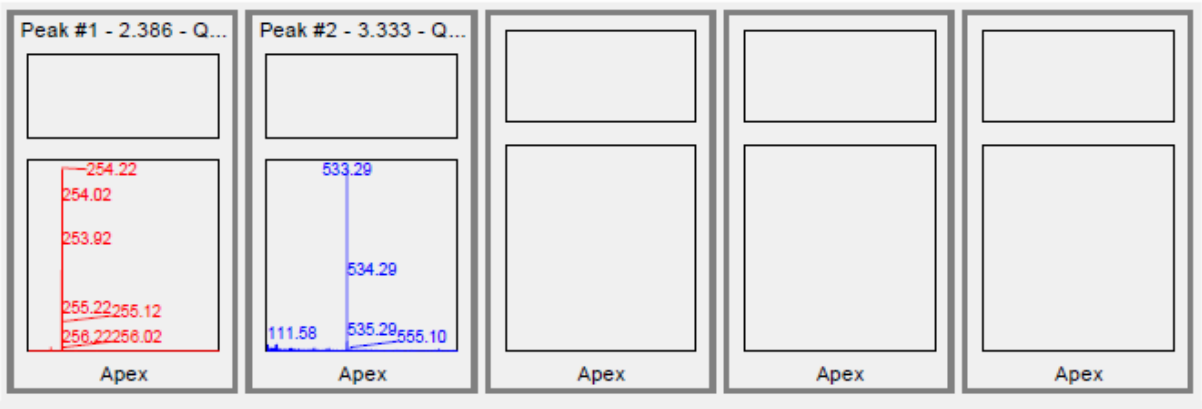

LC/MS of compound **220b**.

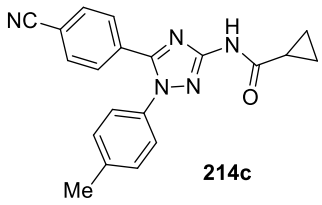

214c

Exact Mass: 343.14

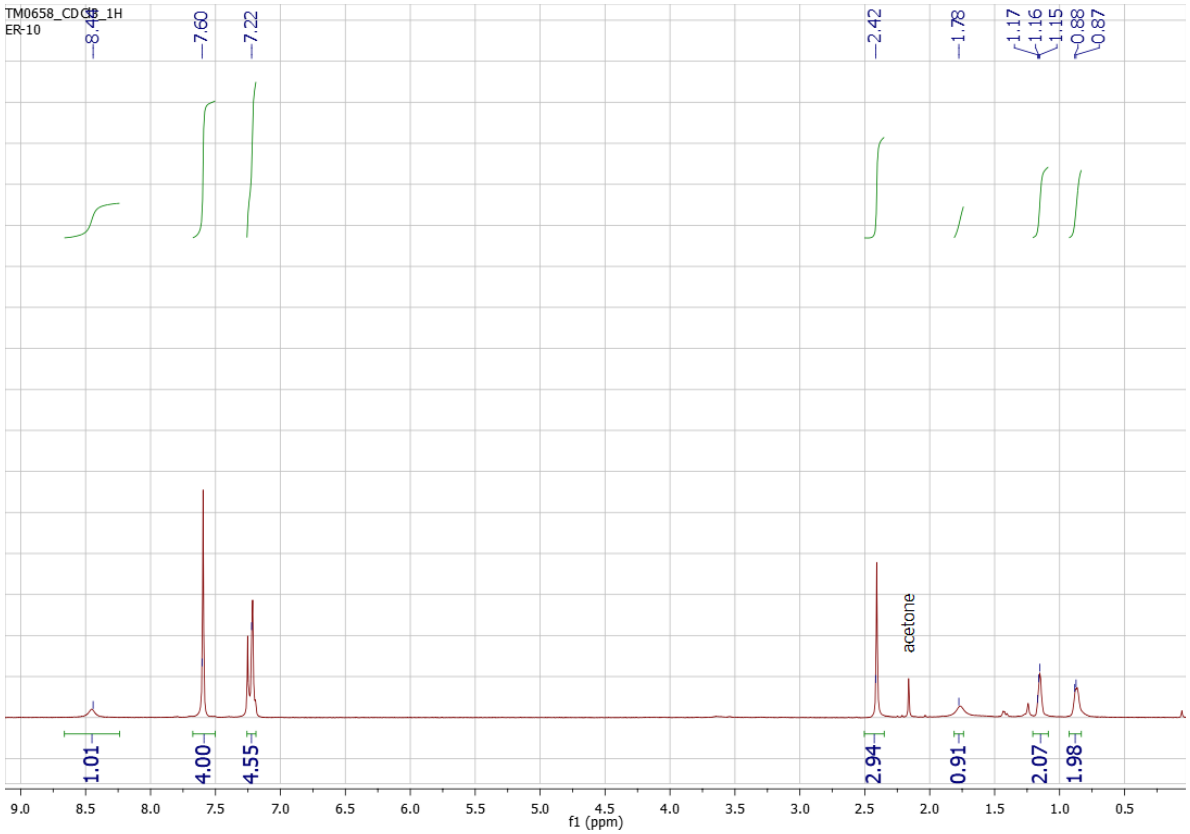

^{1}H NMR spectra of compound **214c** in $CDCl_3$.

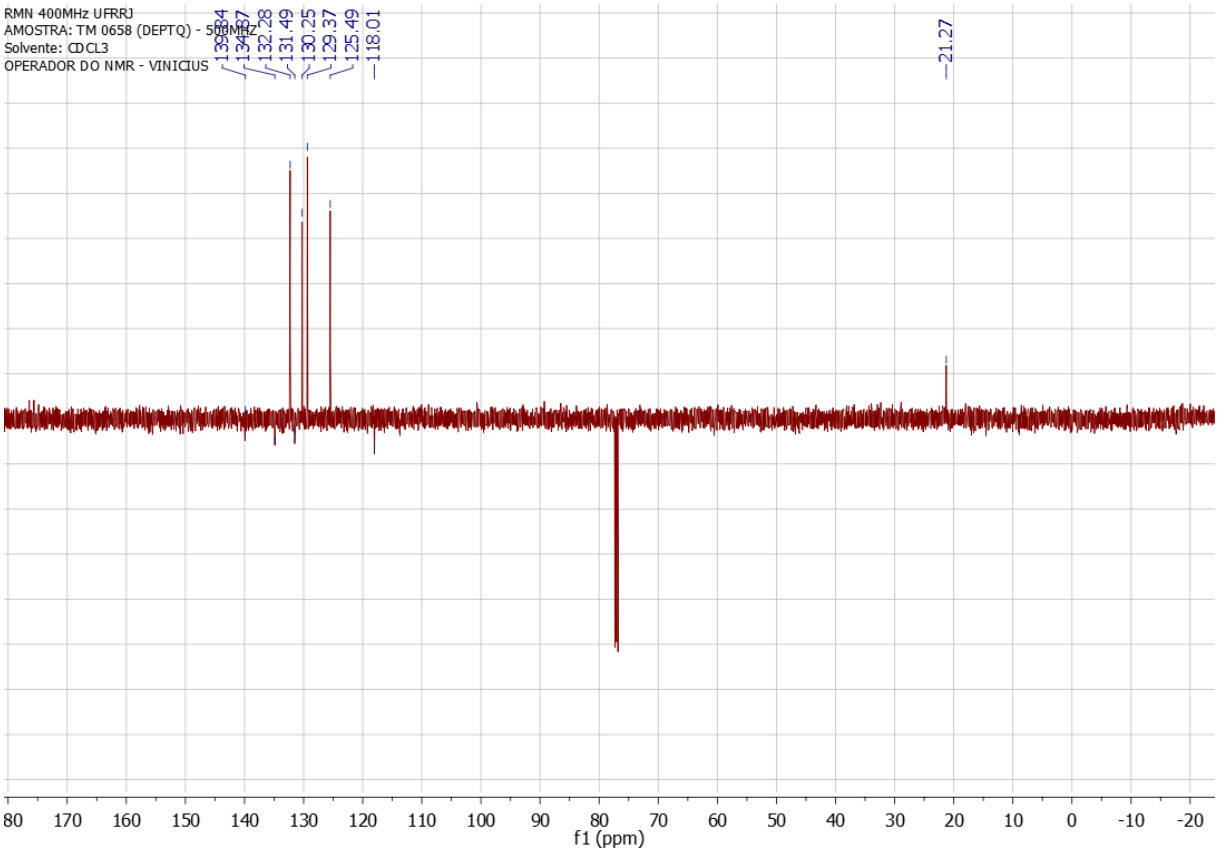

^{13}C NMR spectra of compound **214c** in $CDCl_3$.

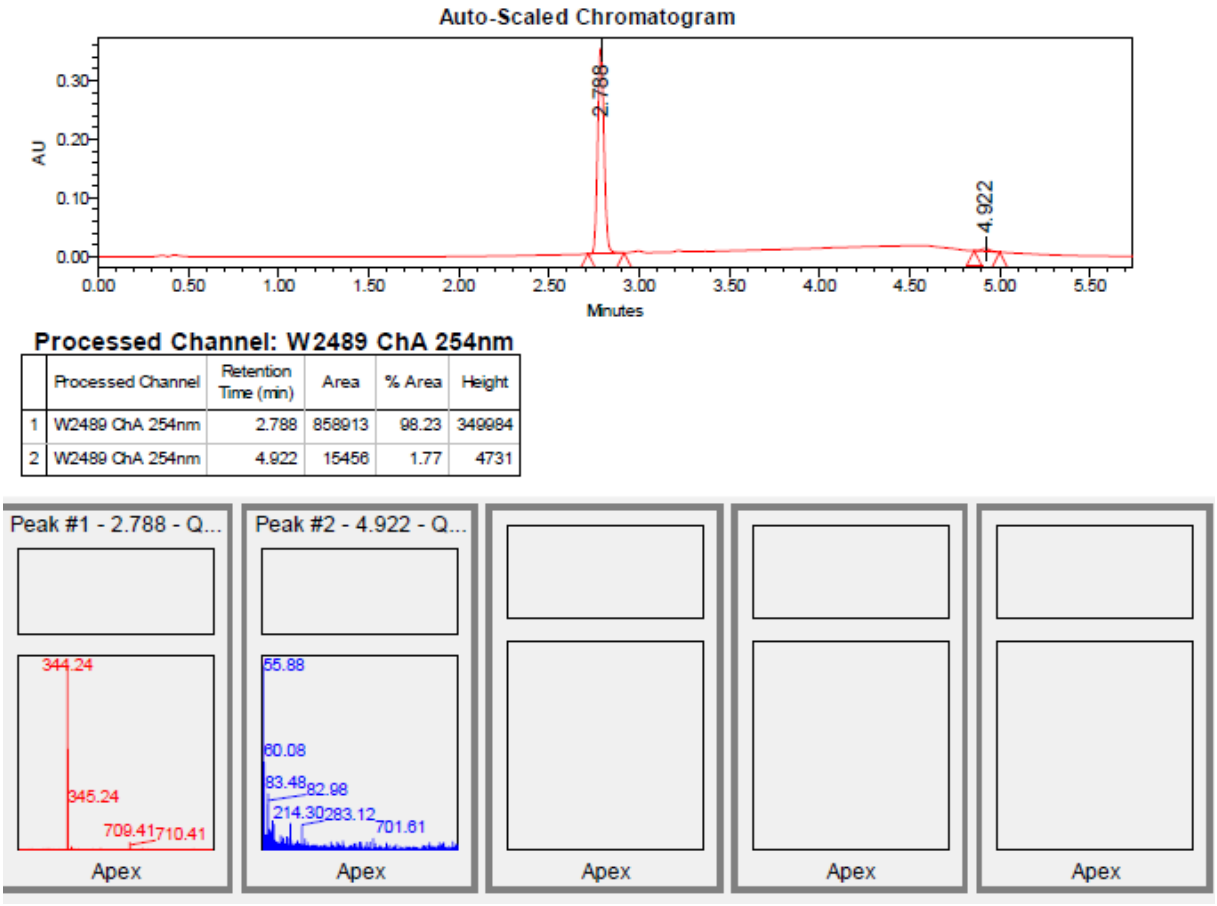

	Processed Channel	Retention Time (min)	Area	% Area	Height
1	W2489 ChA 254nm	2.788	858913	98.23	349984
2	W2489 ChA 254nm	4.922	15456	1.77	4731

LC/MS of compound **214c**.

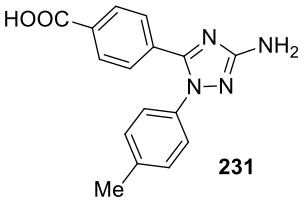

231

Exact Mass: 294.11

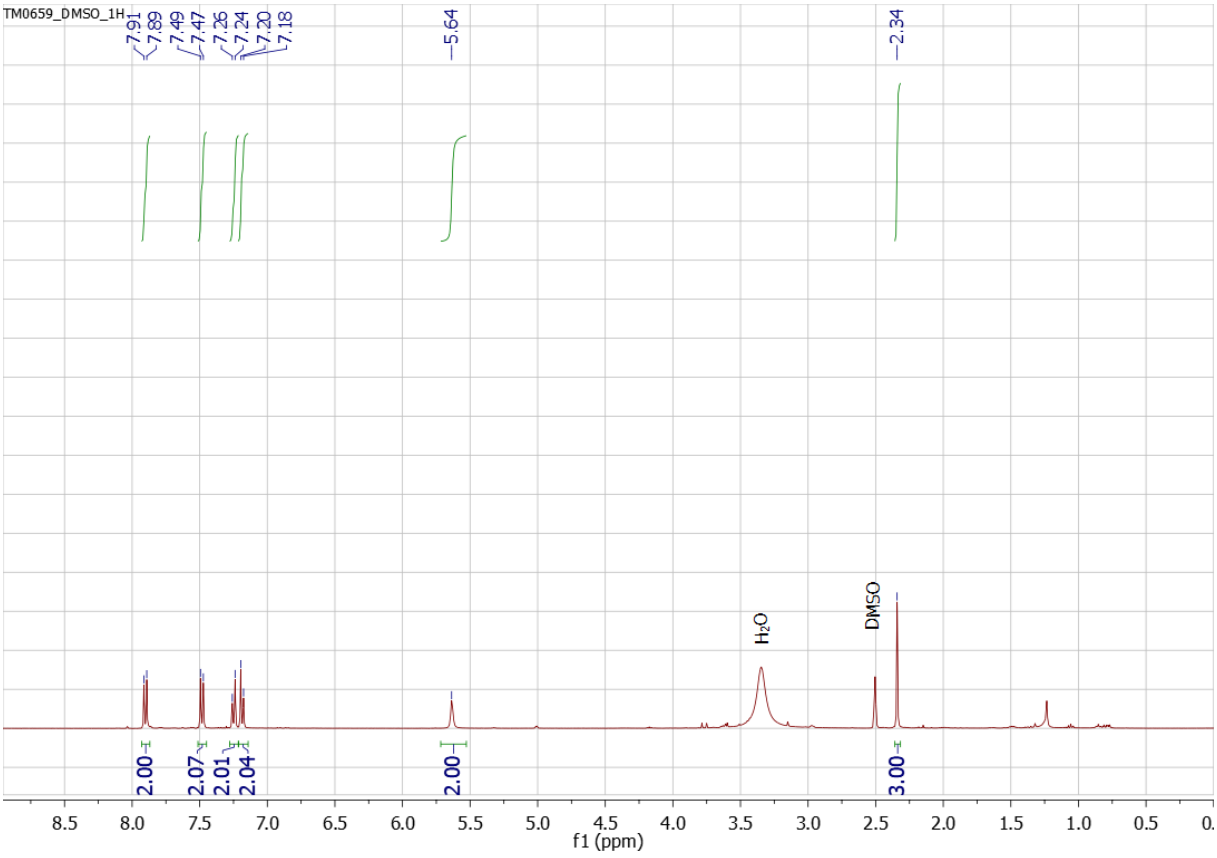

^{1}H NMR spectra of compound **231** in DMSO.

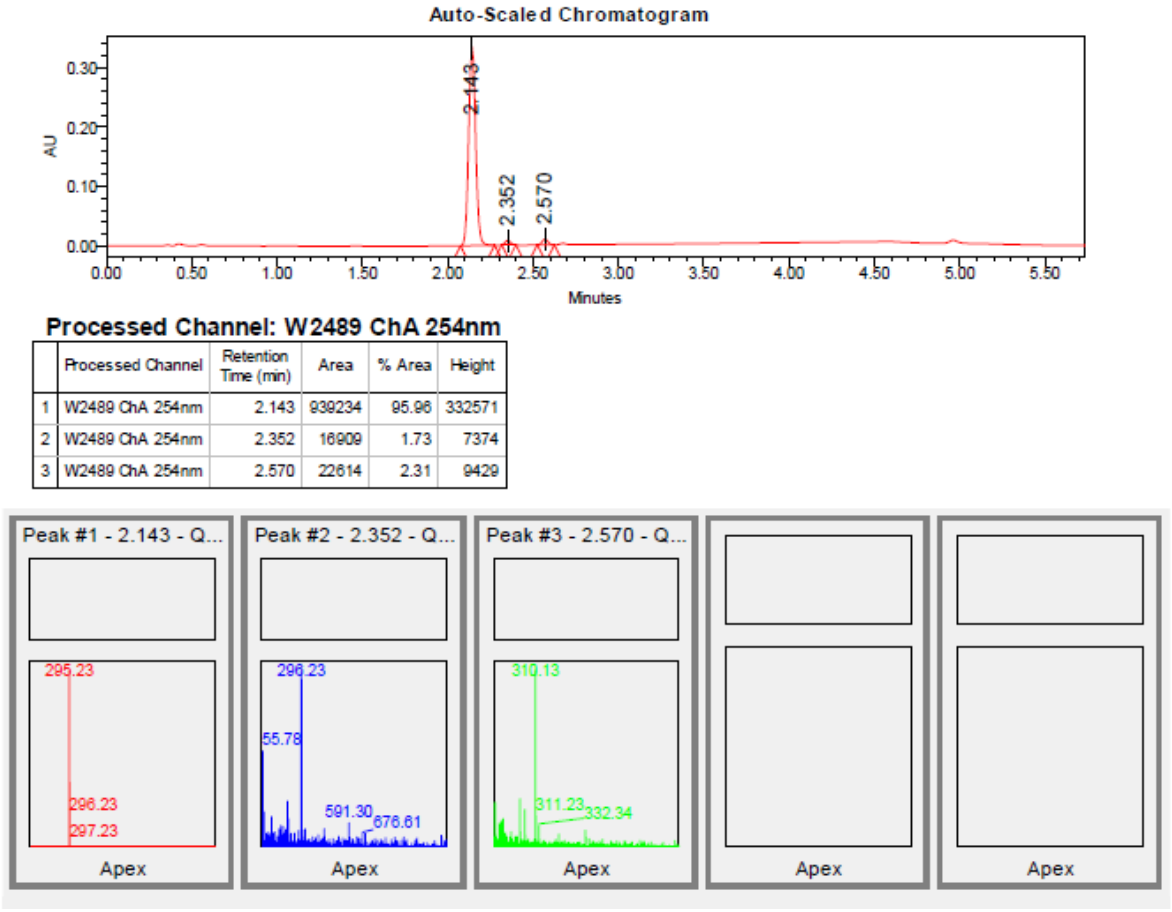

LC/MS of compound **231**.

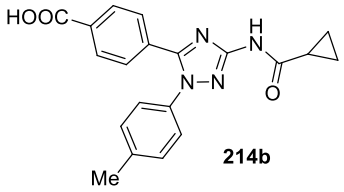

214b

Exact Mass: 362.14

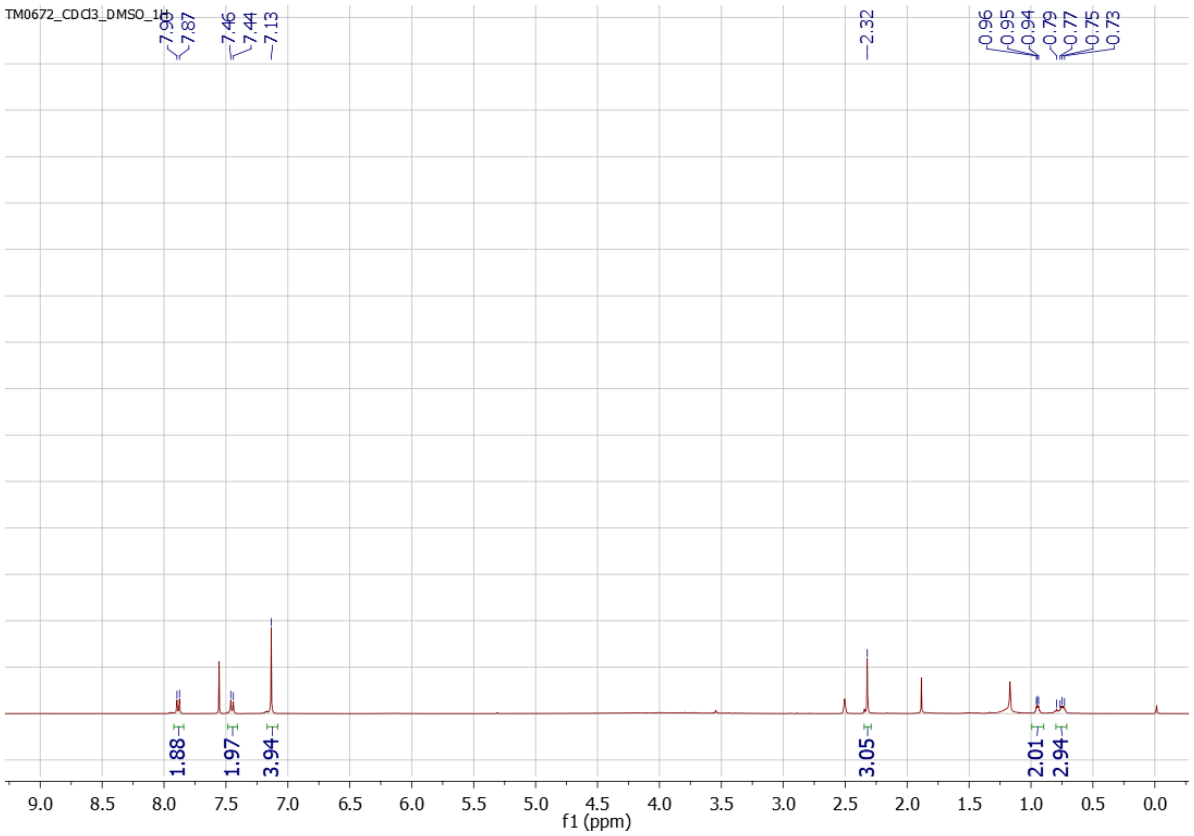

^{1}H NMR spectra of compound **214b** in DMSO + $CDCl_3$.

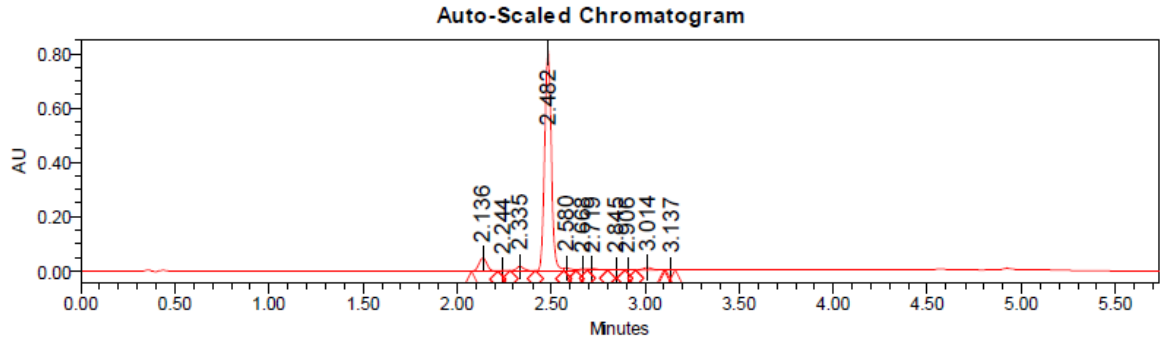

Peak Results

	Name	RT	Area	Height	% Area
1		2.136	136142	47360	6.01
2		2.244	3920	1286	0.17
3		2.335	41516	15545	1.83
4		2.482	1989490	798212	87.79
5		2.580	22963	8492	1.01
6		2.668	13833	4920	0.61
7		2.719	21925	5963	0.97
8		2.845	7310	1721	0.32
9		2.906	2942	1158	0.13
10		3.014	25911	8073	1.14
11		3.137	335	206	0.01

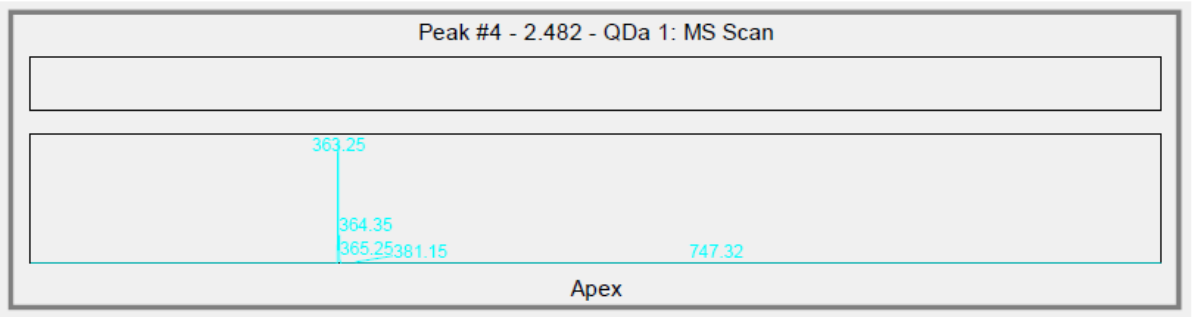

LC/MS of compound **214b**.

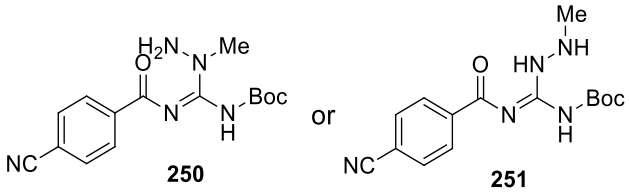

Exact Mass: 317.15

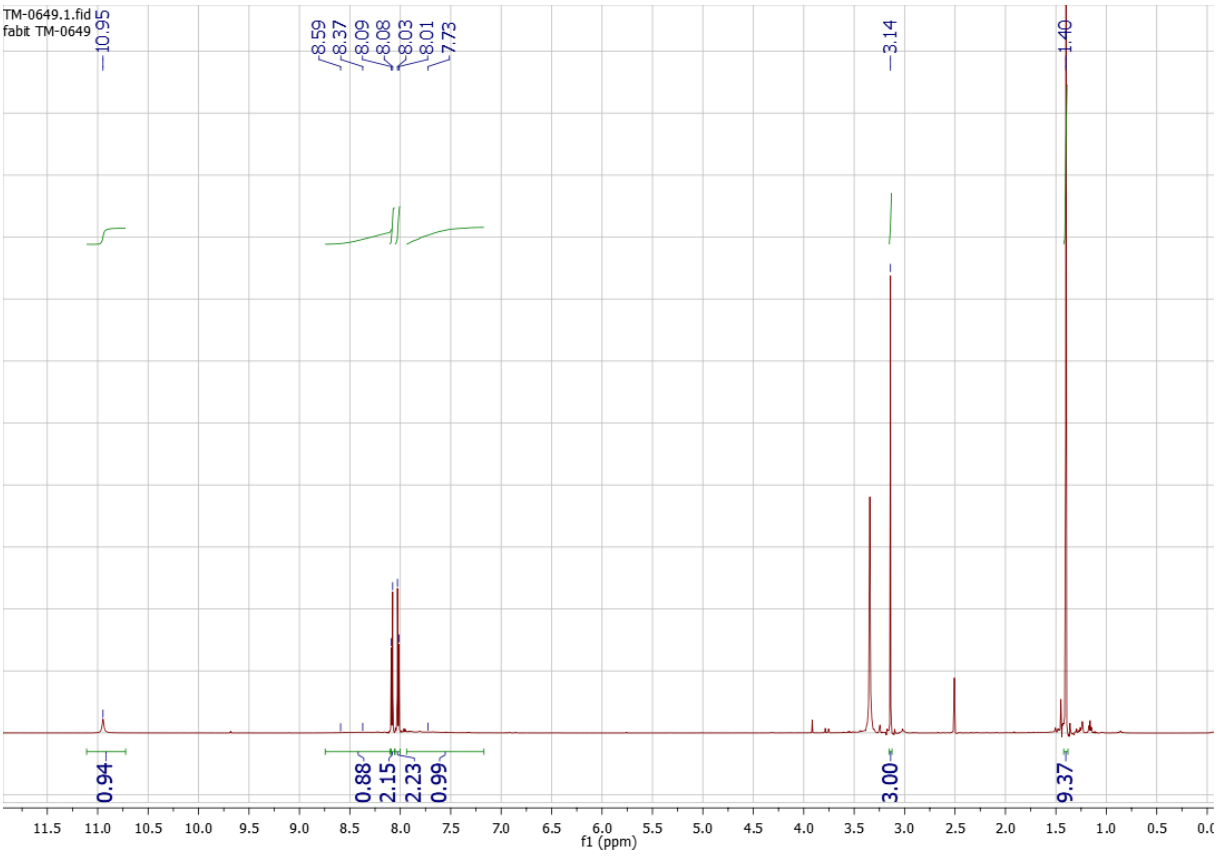

^{1}H NMR spectra of compound **250** or **251** in DMSO.

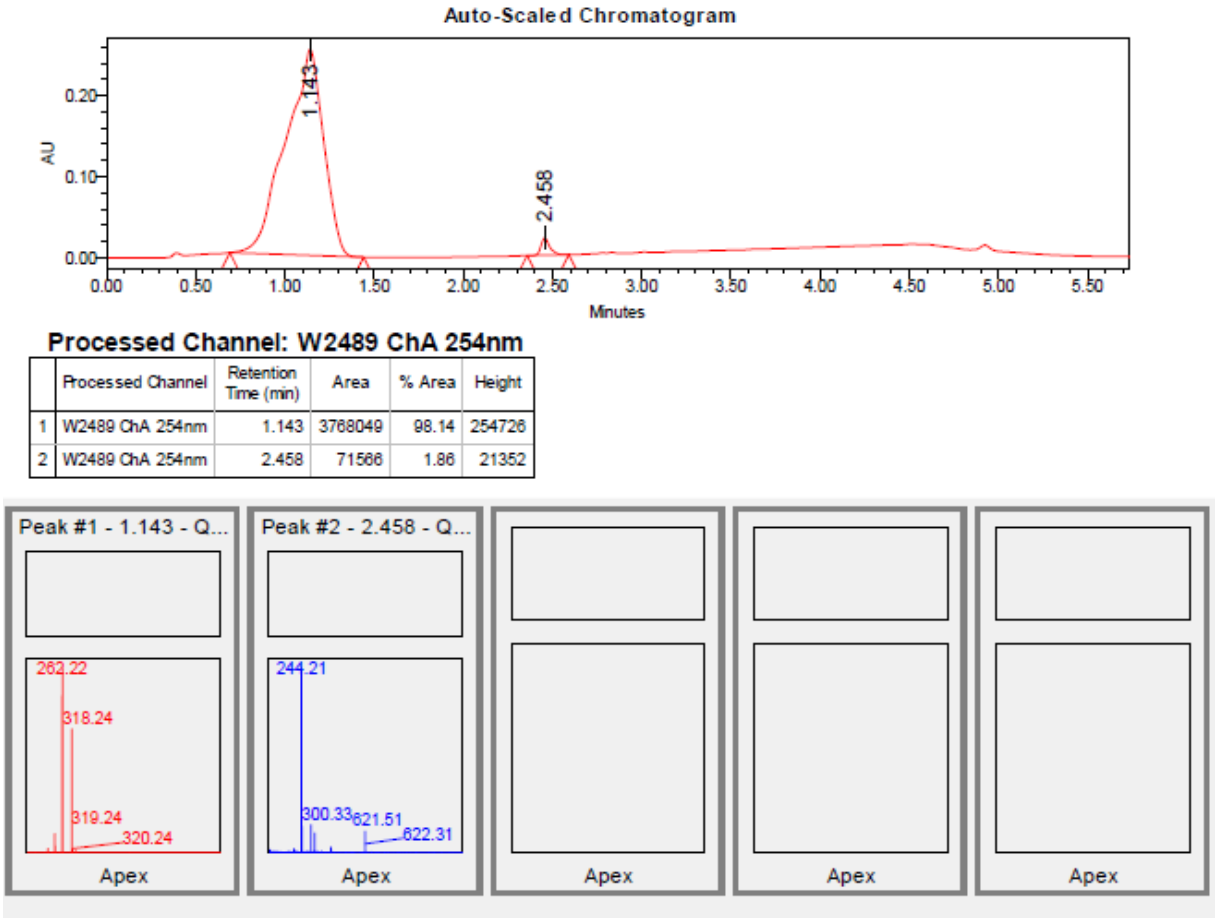

LC/MS of compound **250** or **251**.

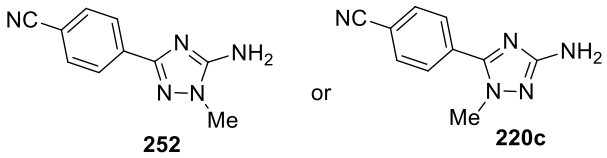

Exact Mass: 199.09

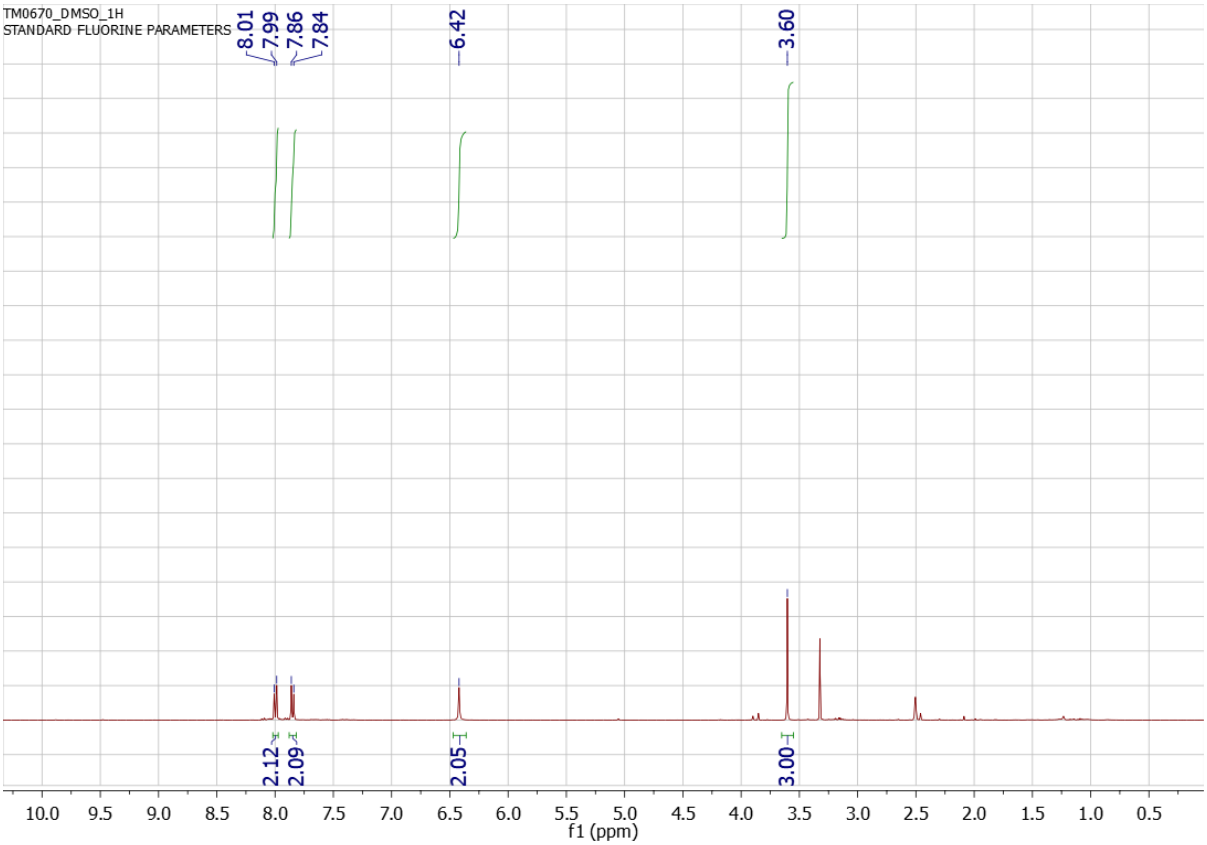

^{1}H NMR spectra of compound **252** or **220c** in DMSO.

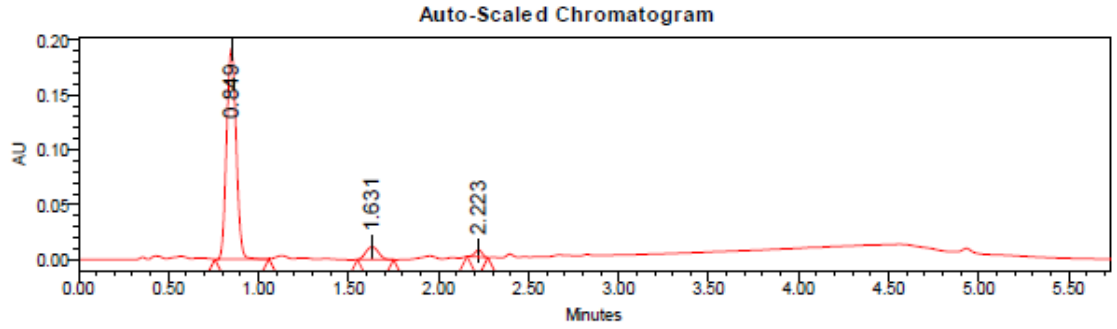

Processed Channel: W2489 ChA 254nm

	Processed Channel	Retention Time (min)	Area	% Area	Height
1	W2489 ChA 254nm	0.849	708199	90.55	191822
2	W2489 ChA 254nm	1.631	56329	7.20	11638
3	W2489 ChA 254nm	2.223	17571	2.25	6398

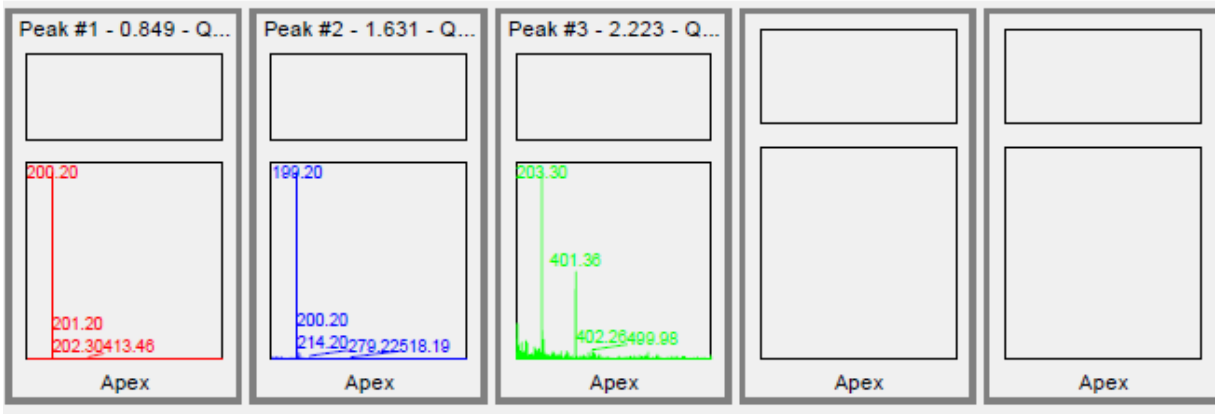

LC/MS of compound **252** or **220c**.

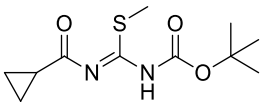

254

Exact Mass: 258.10

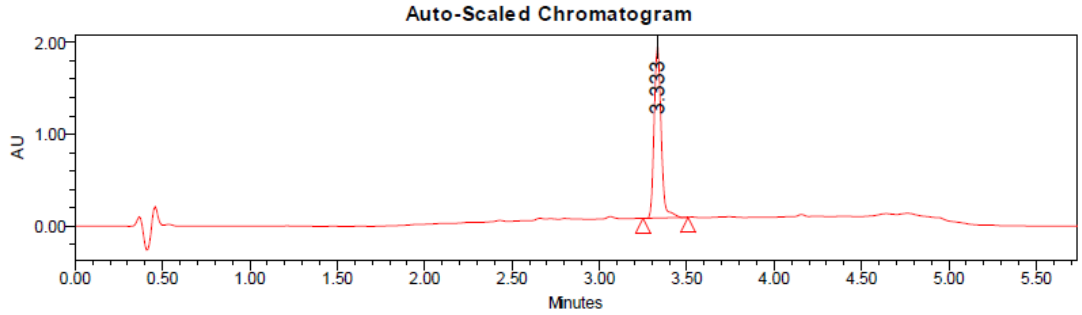

Processed Channel: W2489 ChA 202nm

	Processed Channel	Retention Time (min)	Area	% Area	Height
1	W2489 ChA 202nm	3.333	5185510	100.00	1858449

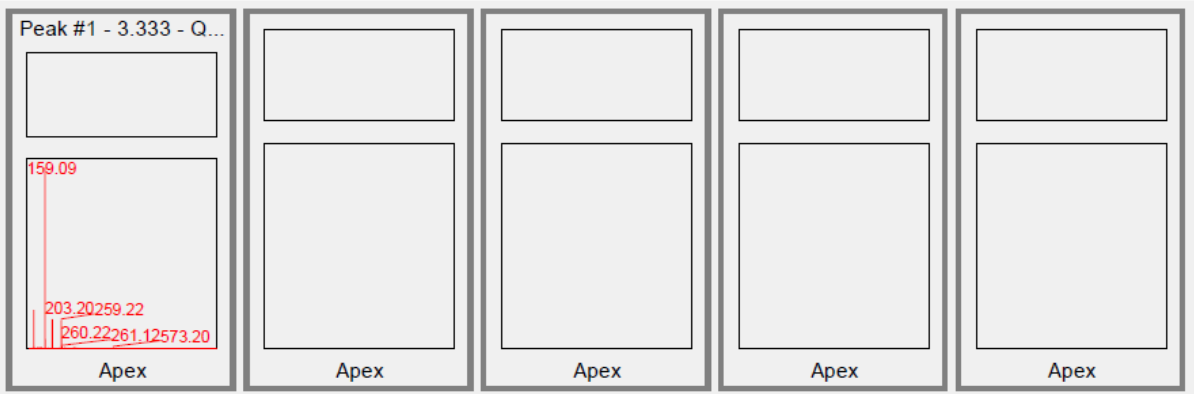

LC/MS of compound **254.**

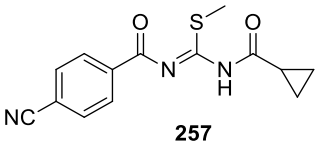

257

Exact Mass: 287.07

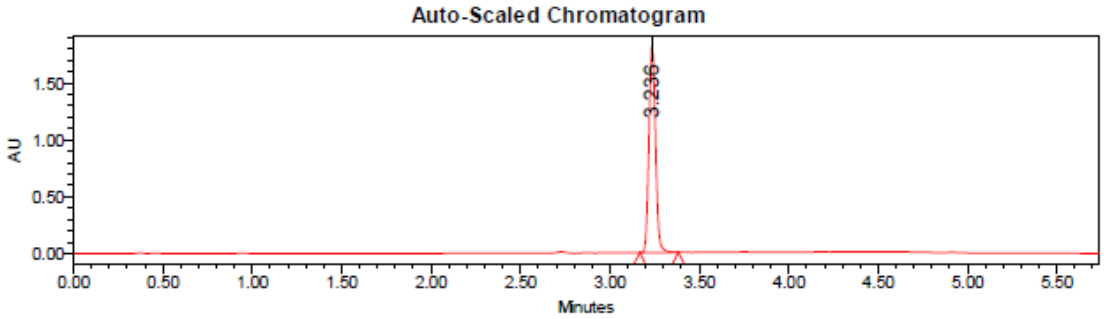

Processed Channel: W2489 ChA 254nm

	Processed Channel	Retention Time (min)	Area	% Area	Height
1	W2489 ChA 254nm	3.236	4622620	100.00	1803497

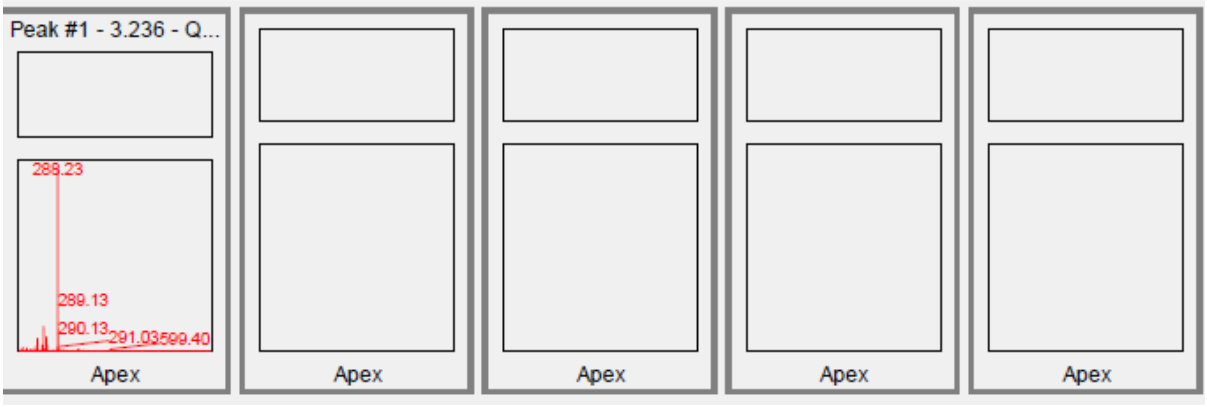

LC/MS of compound **257**.

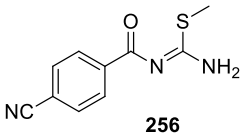

256

Exact Mass: 219.05

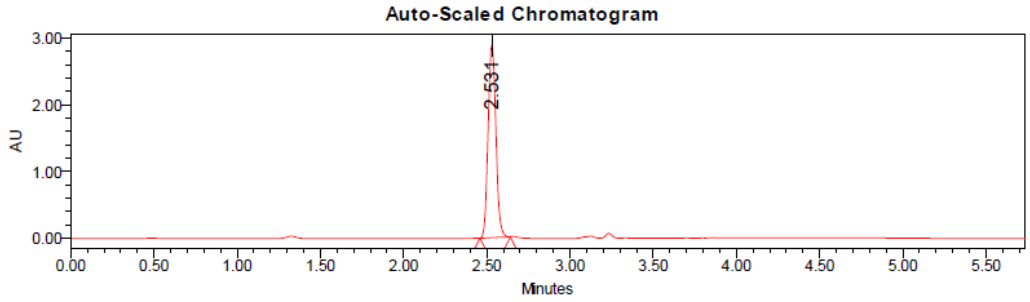

Processed Channel: W2489 ChA 254nm

	Processed Channel	Retention Time (min)	Area	% Area	Height
1	W2489 ChA 254nm	2.531	9383101	100.00	2904210

LC/MS of compound **256**.

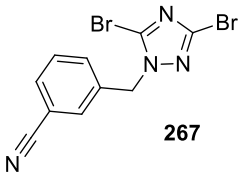

267

^{1}H NMR spectra of compound **267** in $CDCl_3$.

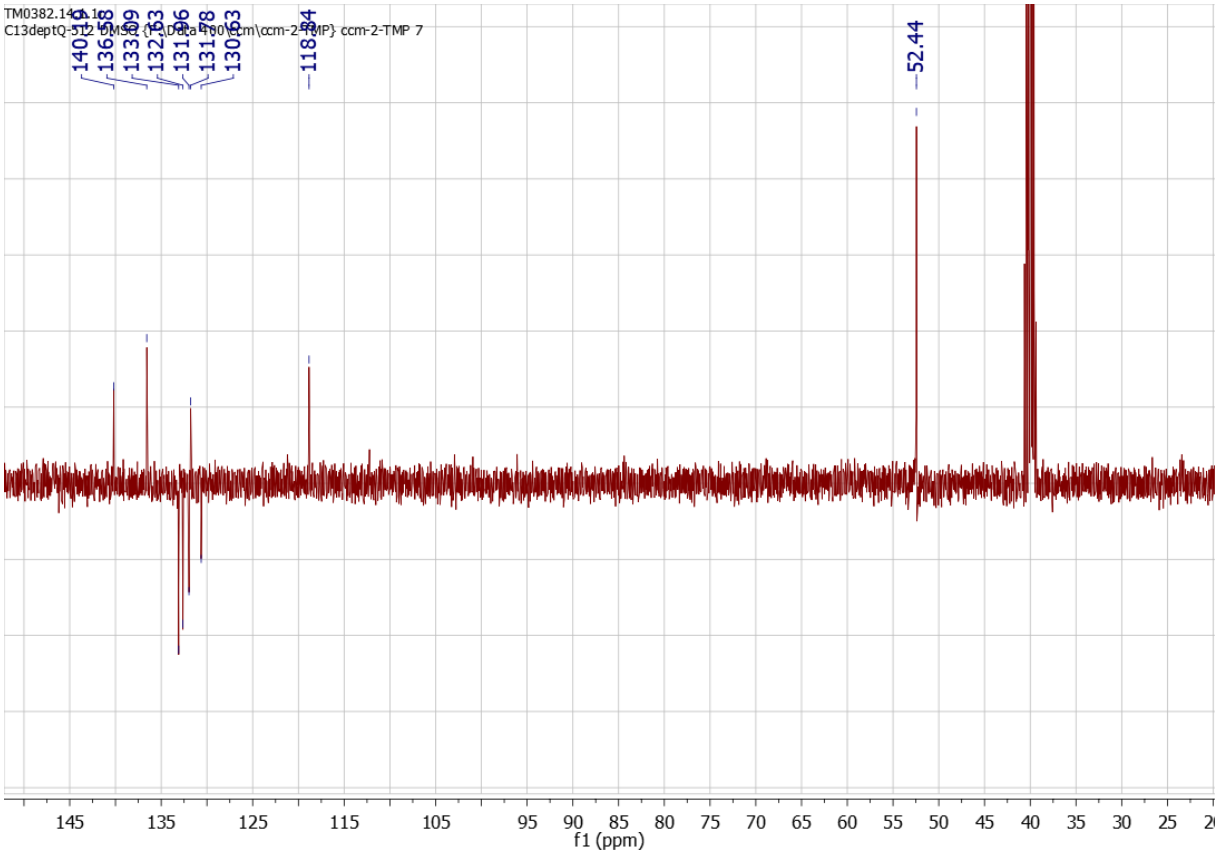

^{13}C NMR spectra of compound **267** in $CDCl_3$.

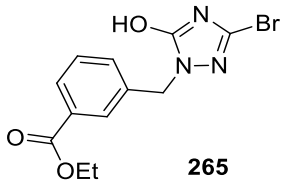

265

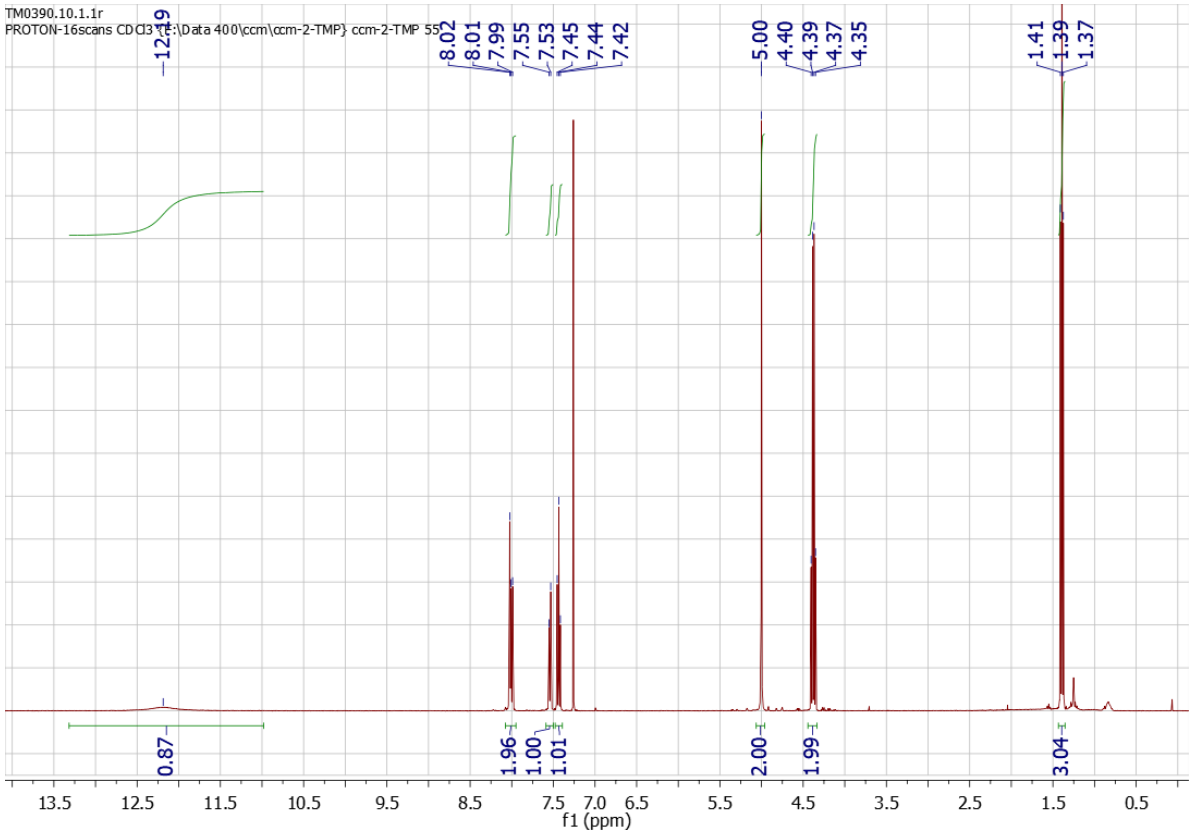

^{1}H NMR spectra of compound **265** in $CDCl_3$.

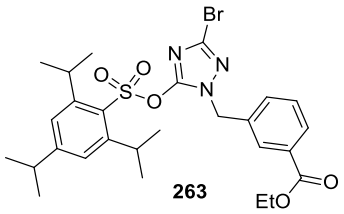

263

Exact Mass: 591.14

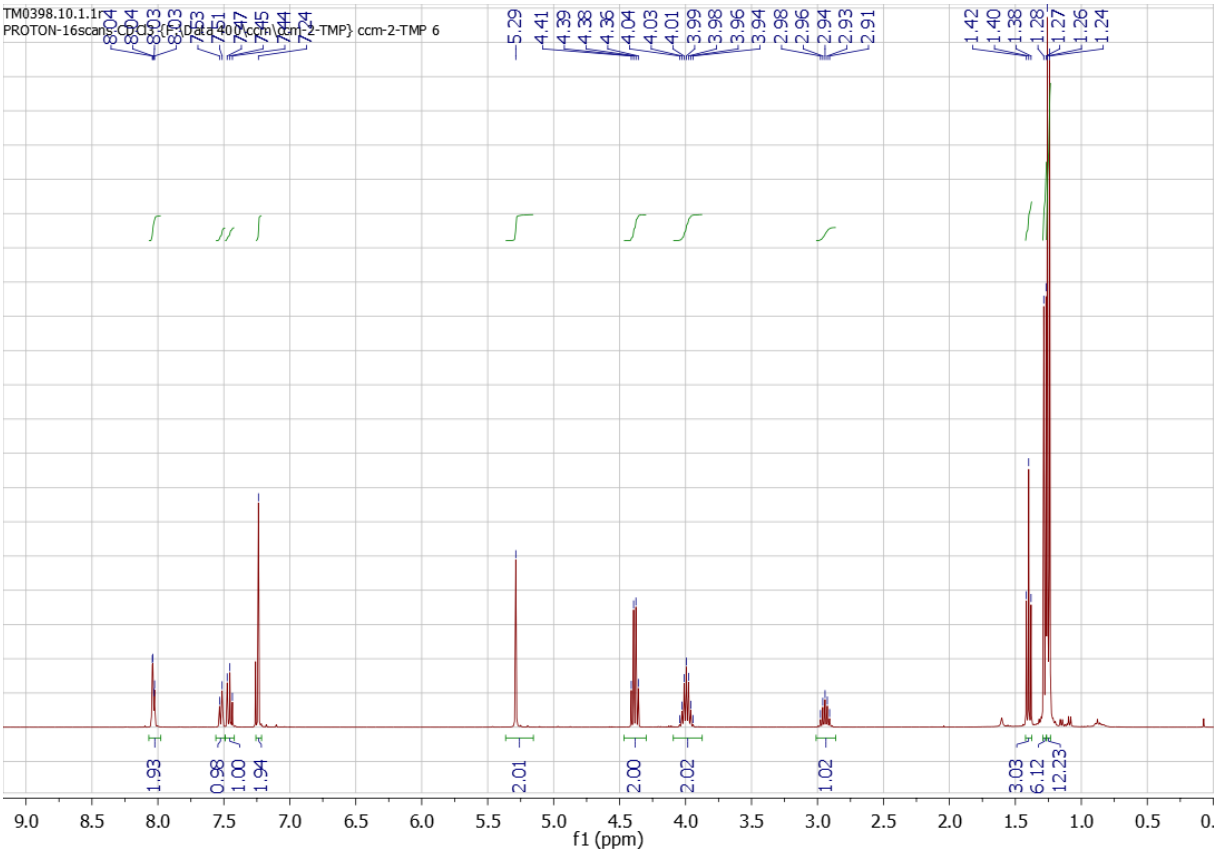

^{1}H NMR spectra of compound **263** in $CDCl_3$.

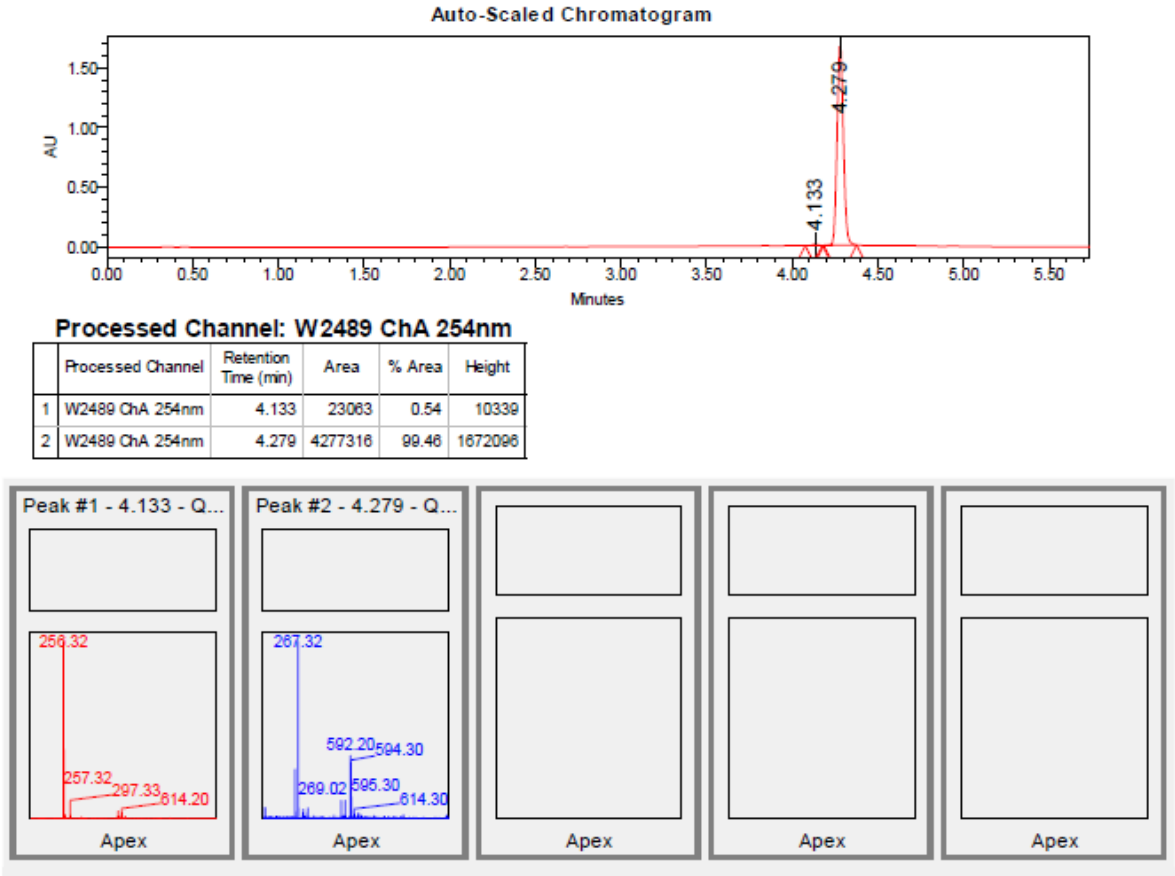

	Processed Channel	Retention Time (min)	Area	% Area	Height
1	W2489 ChA 254nm	4.133	23063	0.54	10339
2	W2489 ChA 254nm	4.279	4277316	99.46	1672096

LC/MS of compound **263**.

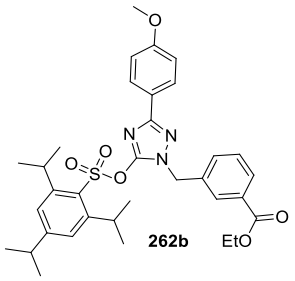

Exact Mass: 619.27

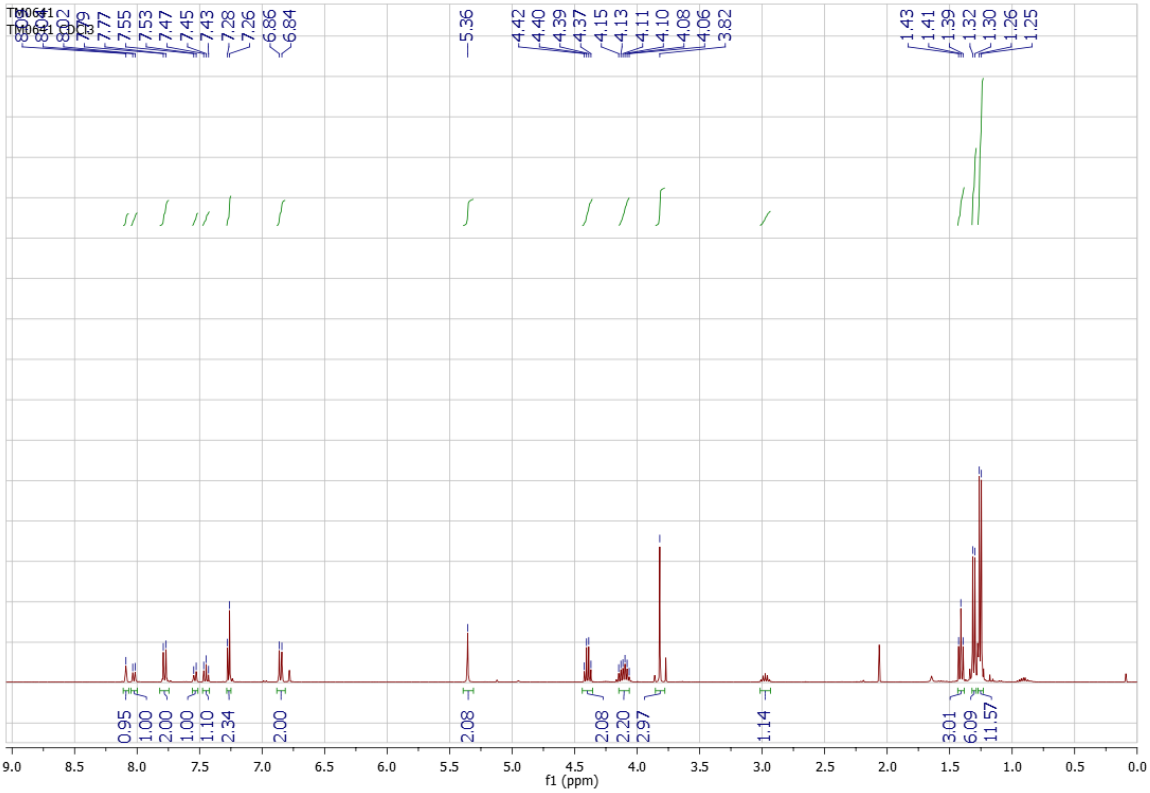

^{1}H NMR spectra of compound **262b** in $CDCl_3$.

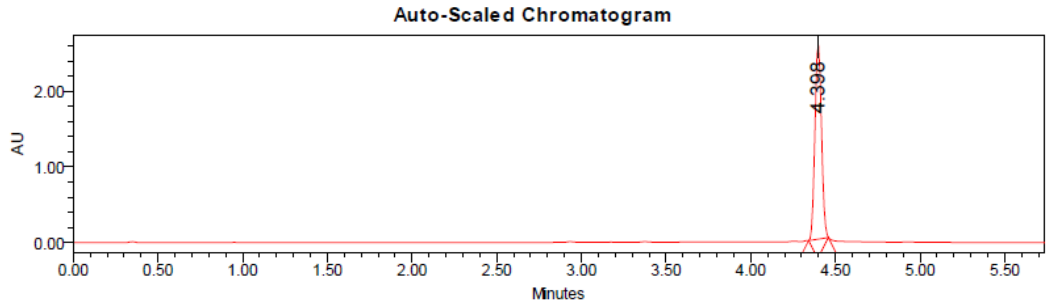

Processed Channel: W2489 ChA 254nm

	Processed Channel	Retention Time (min)	Area	% Area	Height
1	W2489 ChA 254nm	4.398	6914996	100.00	2548163

LC/MS of compound **262b**.

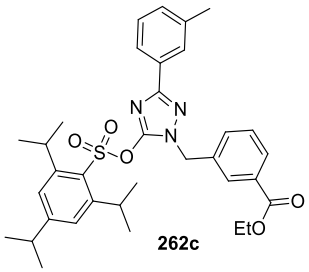

262c

Exact Mass: 603.28

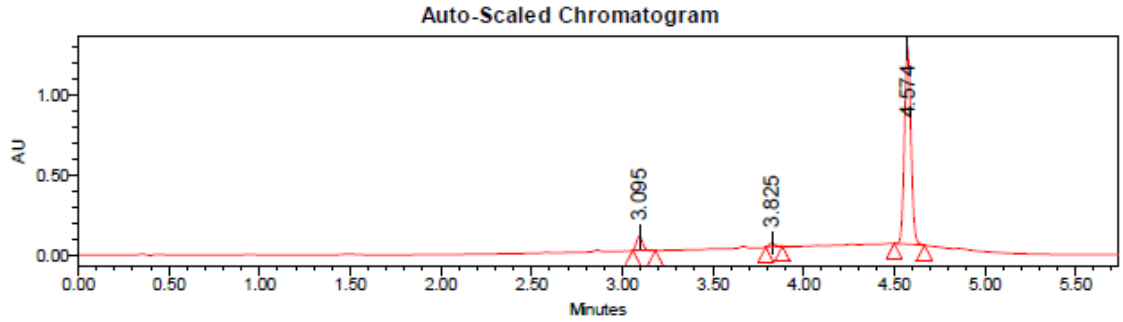

Processed Channel: W2489 ChA 254nm

	Processed Channel	Retention Time (min)	Area	% Area	Height
1	W2489 ChA 254nm	3.095	199716	6.07	86428
2	W2489 ChA 254nm	3.825	52731	1.60	23666
3	W2489 ChA 254nm	4.574	3039732	92.33	1212502

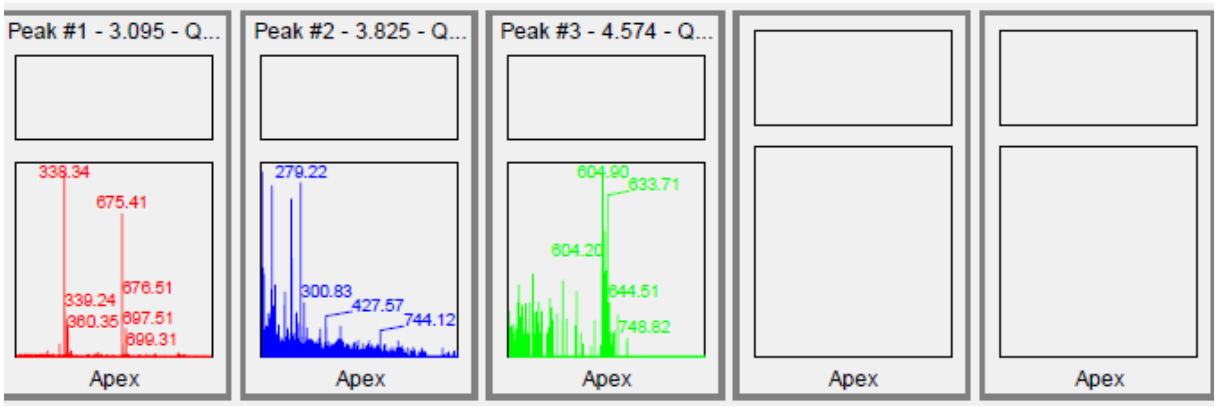

LC/MS of compound **262c**.

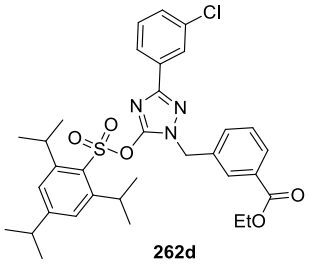

262d

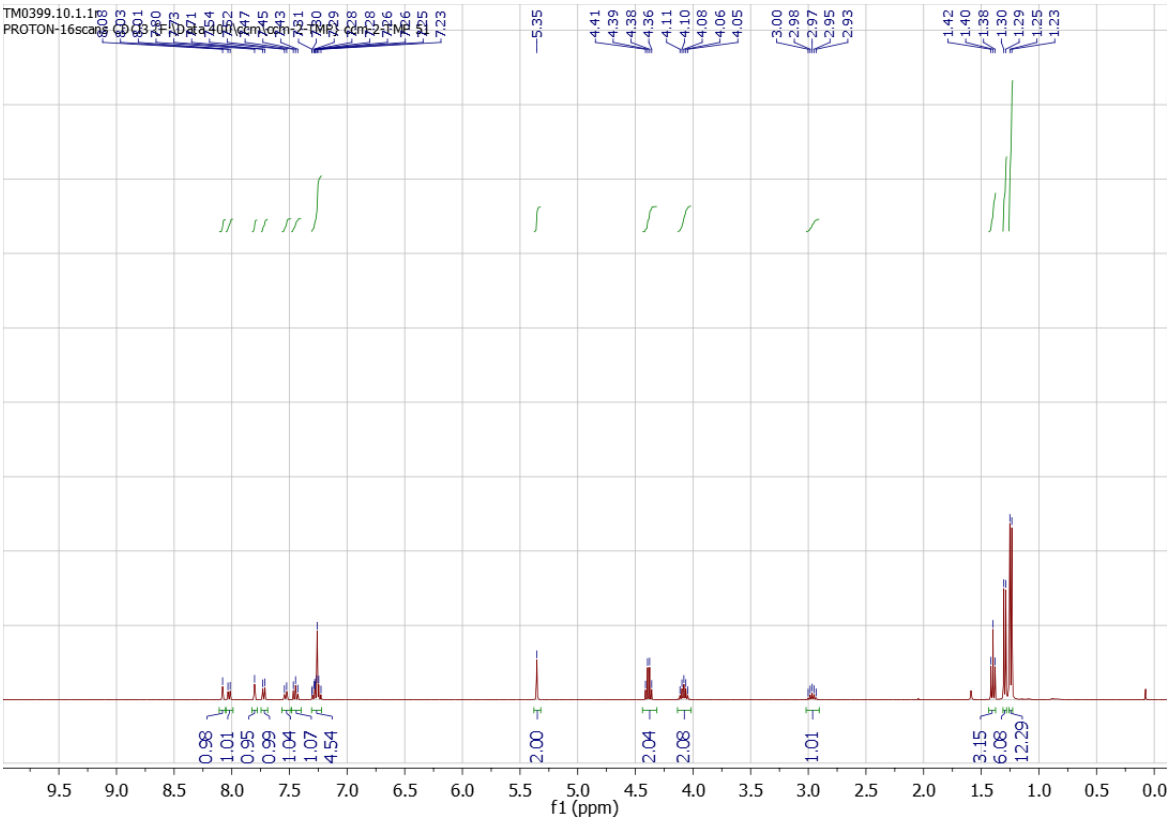

^{1}H NMR spectra of compound **262d** in $CDCl_3$.

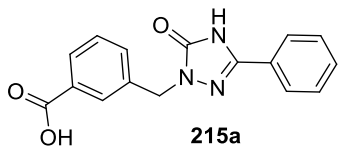

215a

Exact Mass: 295.10

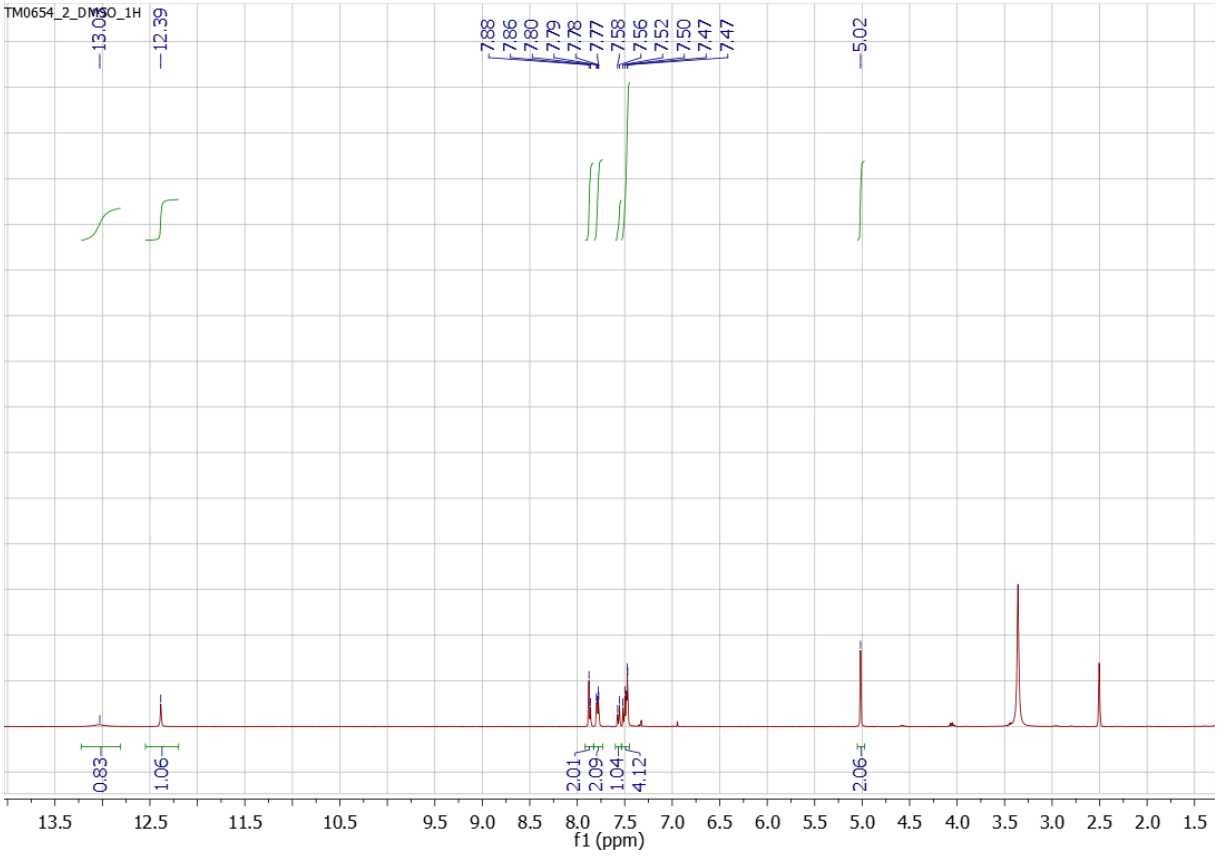

^{1}H NMR spectra of compound **215a** in DMSO.

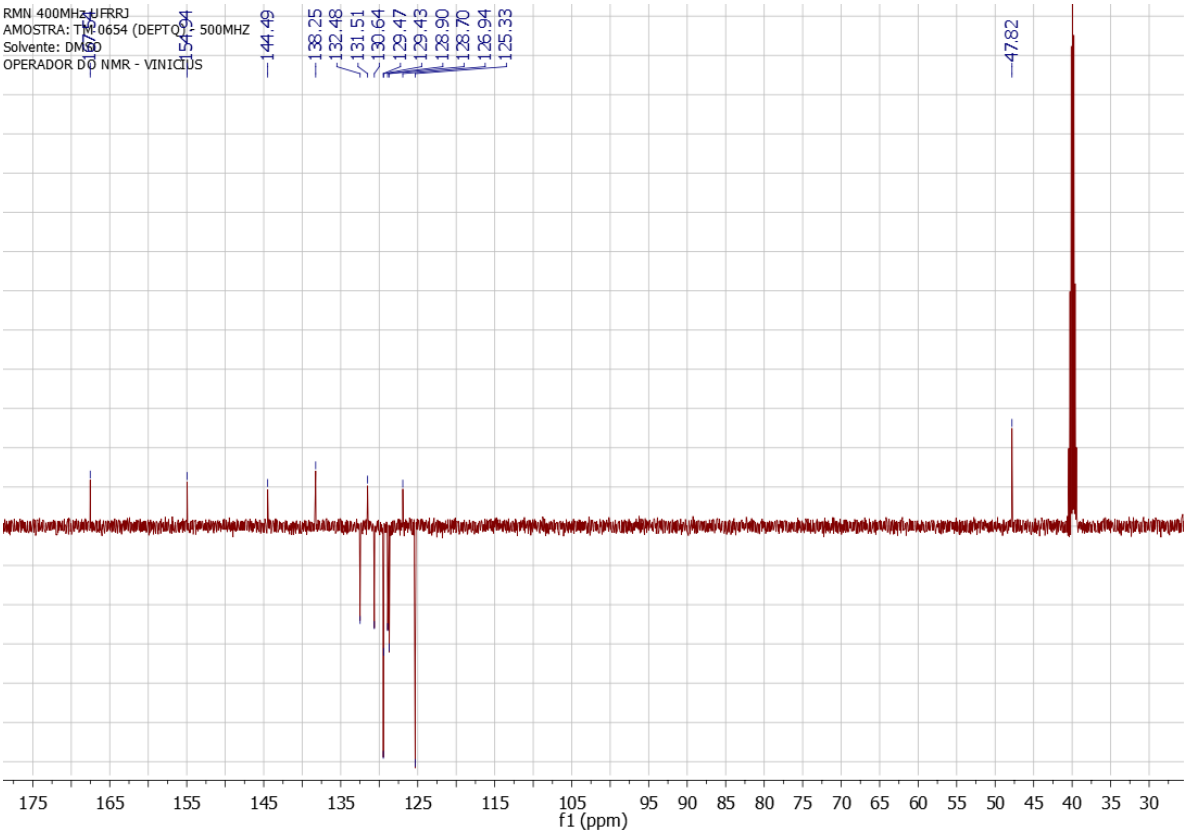

^{13}C NMR spectra of compound **215a** in DMSO.

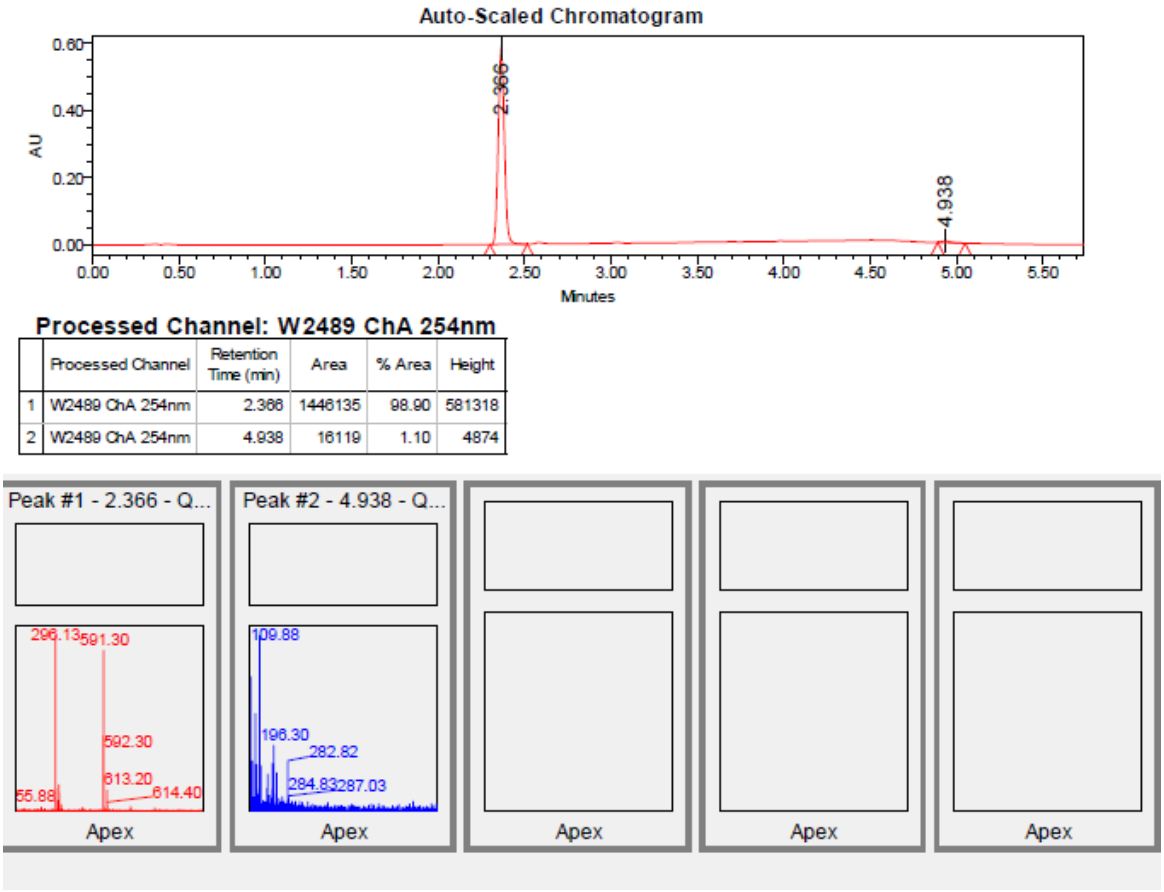

	Processed Channel	Retention Time (min)	Area	% Area	Height
1	W2489 ChA 254nm	2.366	1446135	98.90	581318
2	W2489 ChA 254nm	4.938	16119	1.10	4874

LC/MS of compound **215a**

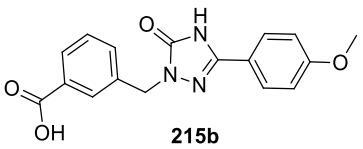

215b

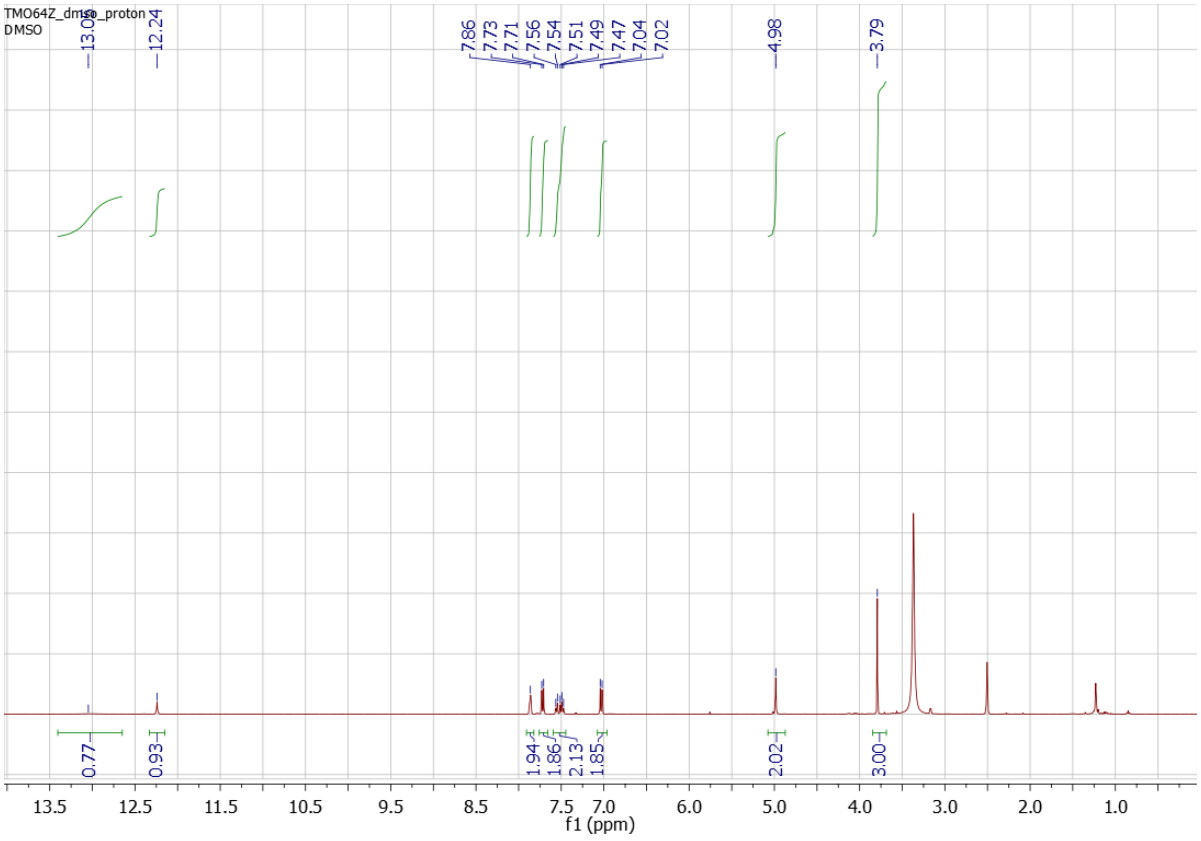

^{1}H NMR spectra of compound **215b** in DMSO.

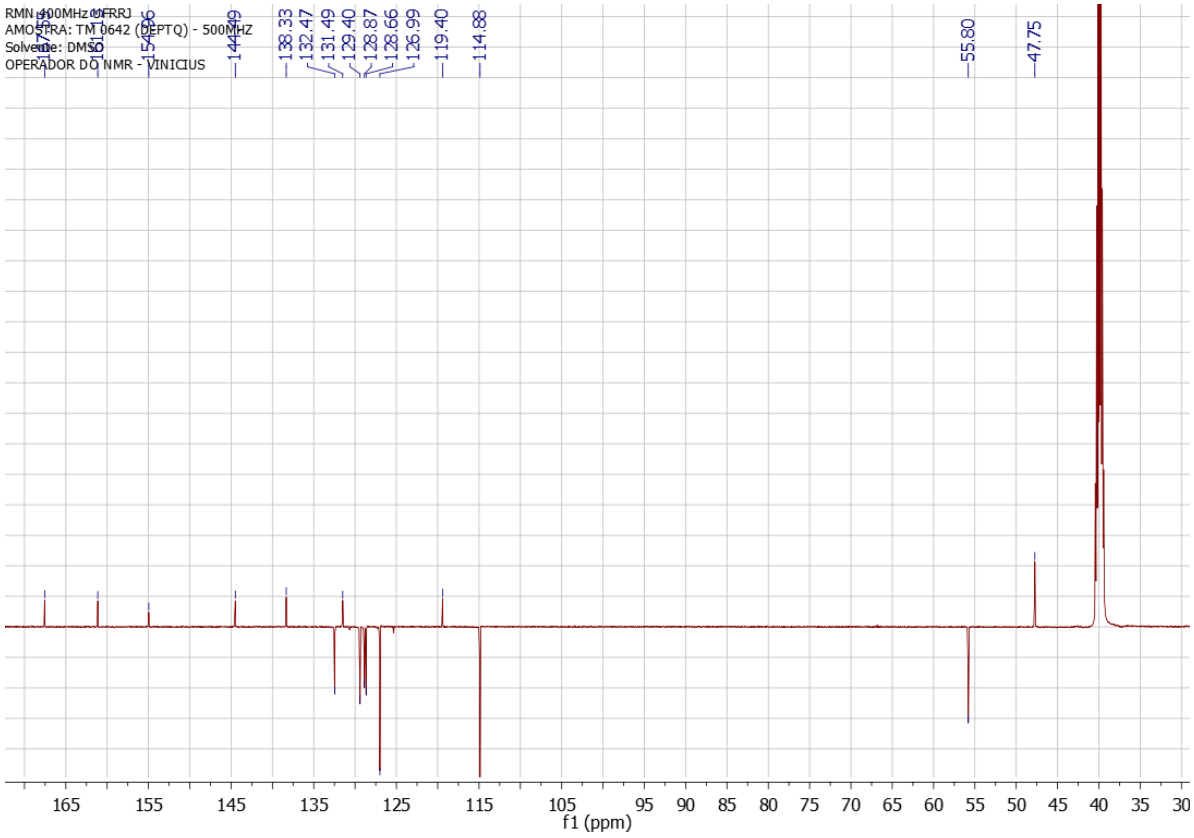

^{13}C NMR spectra of compound **215b** in DMSO.

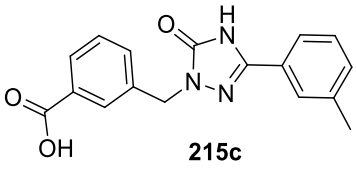

215c

Exact Mass: 309.11

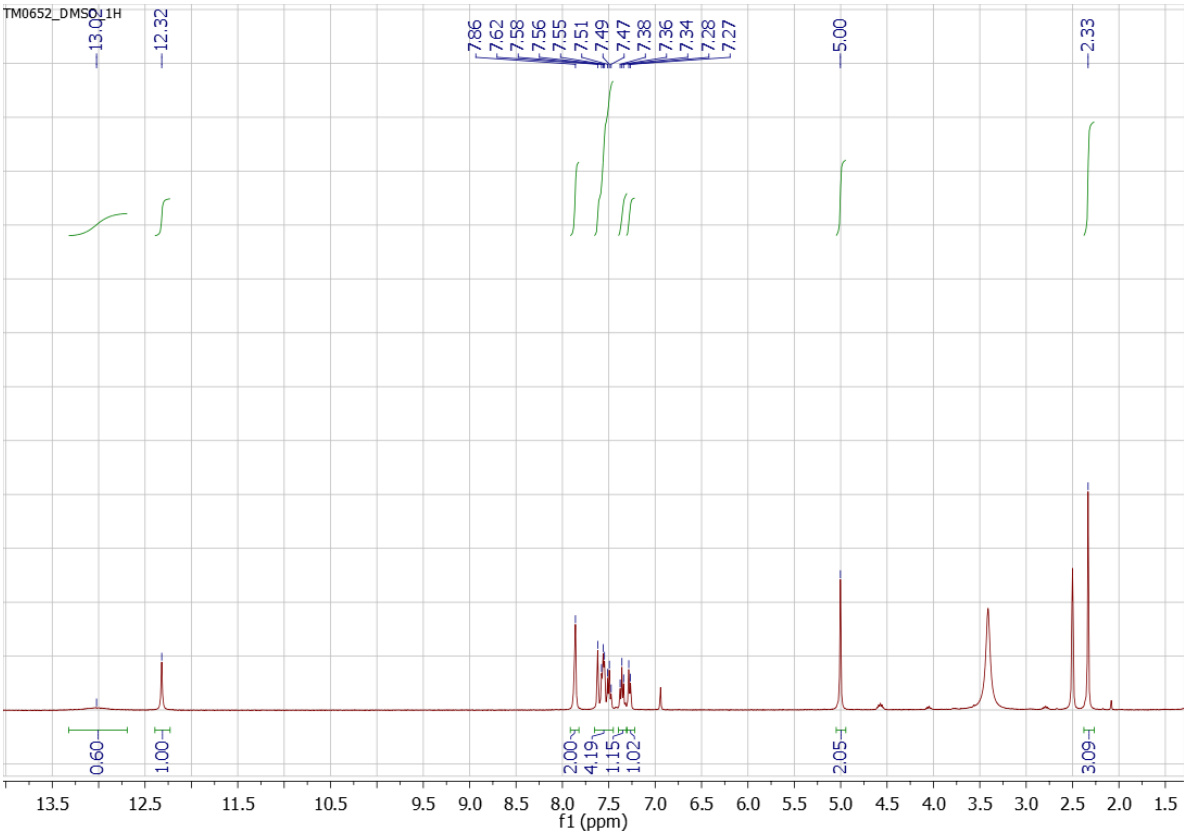

^{1}H NMR spectra of compound **215c** in DMSO.

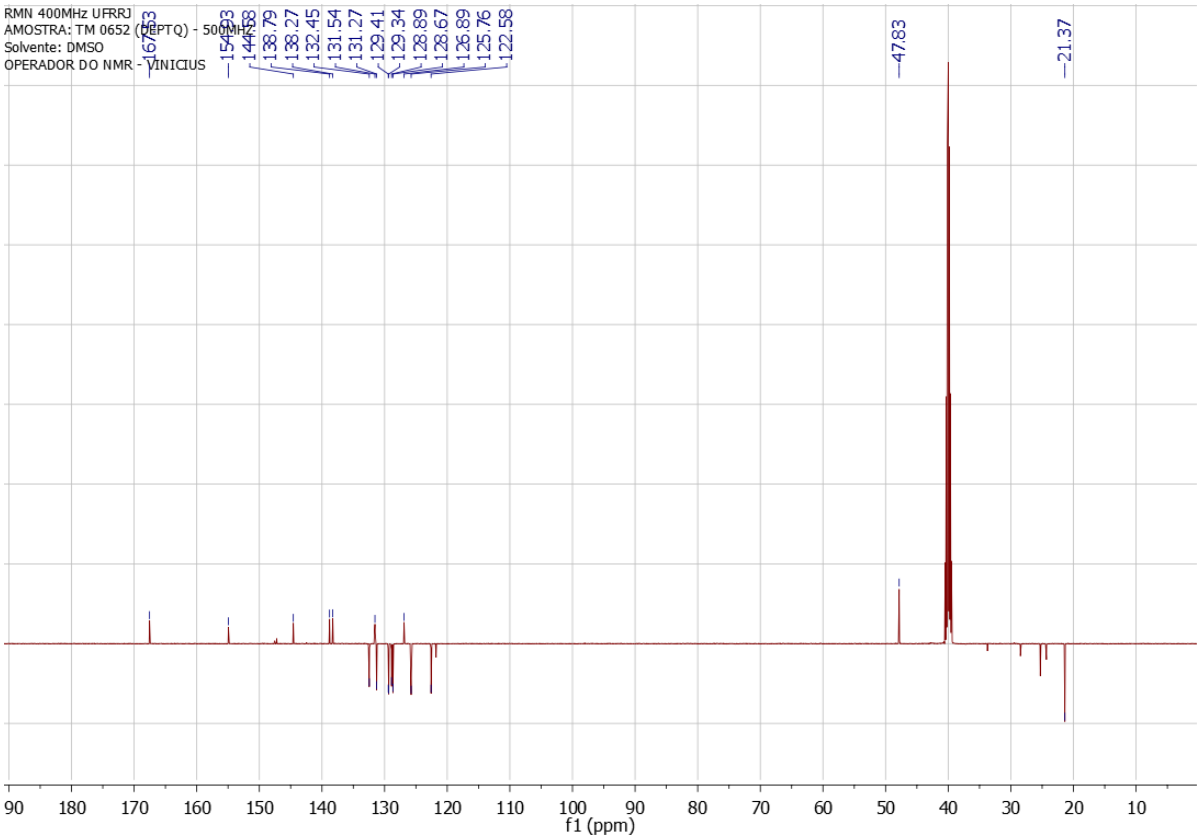

^{13}C NMR spectra of compound **215c** in DMSO.

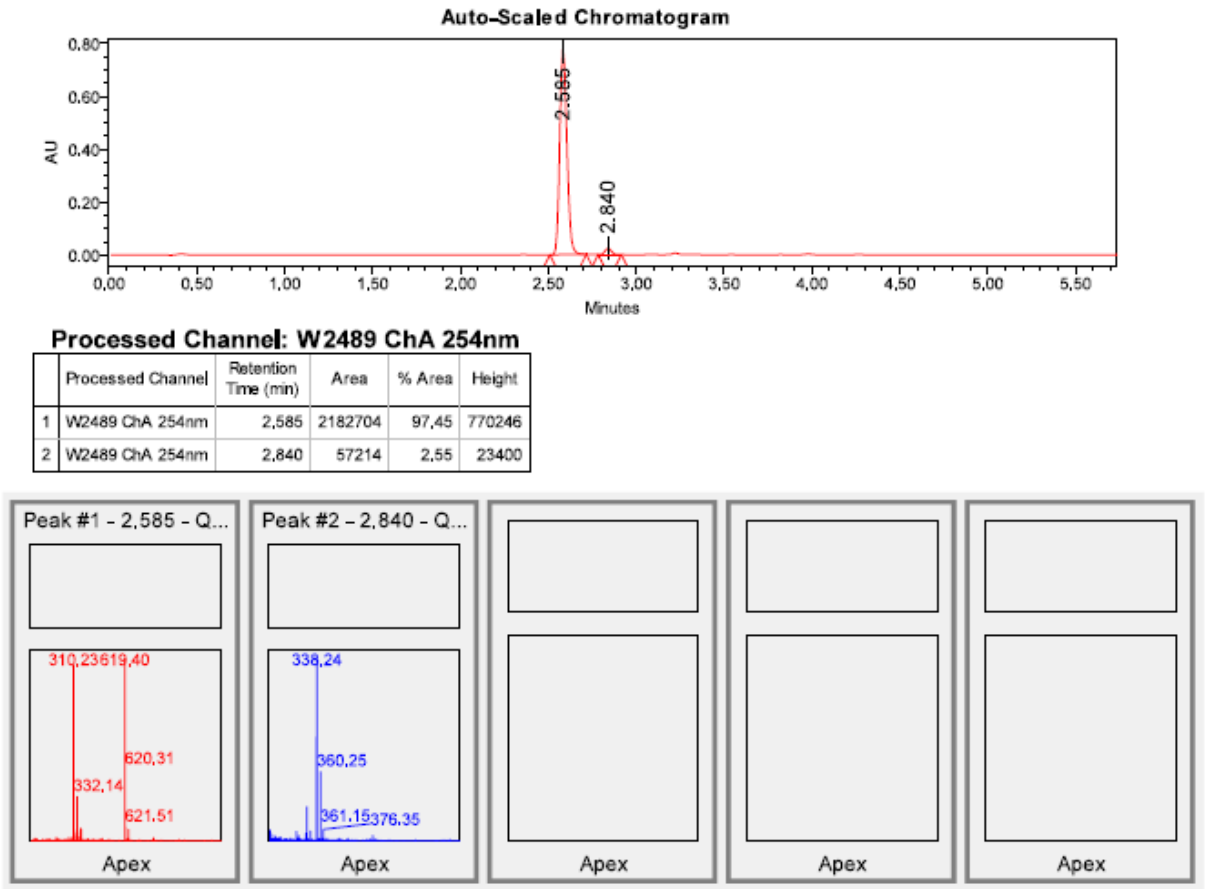

LC/MS of compound **215c**

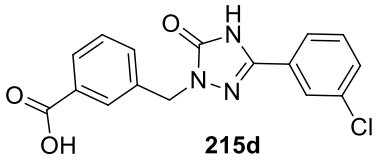

215d

Exact Mass: 329.06

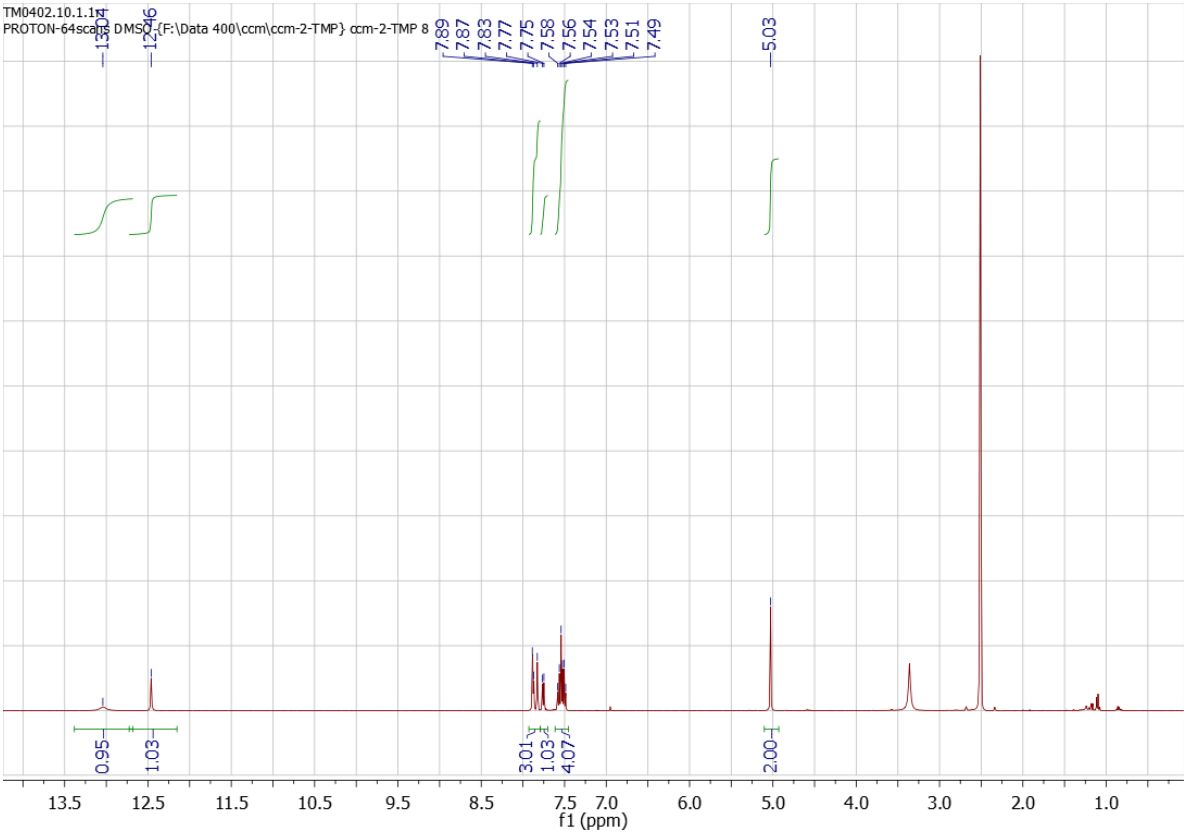

^{1}H NMR spectra of compound **215d** in DMSO.

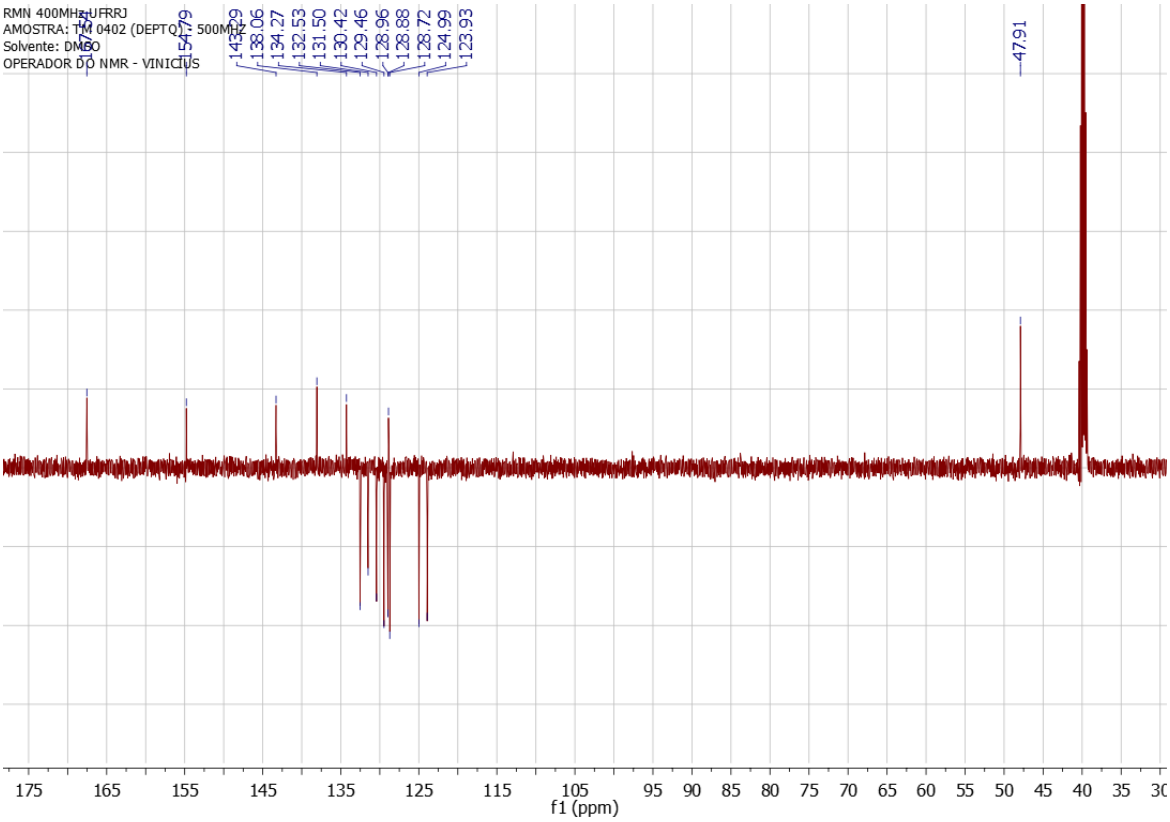

^{13}C NMR spectra of compound **215d** in DMSO.

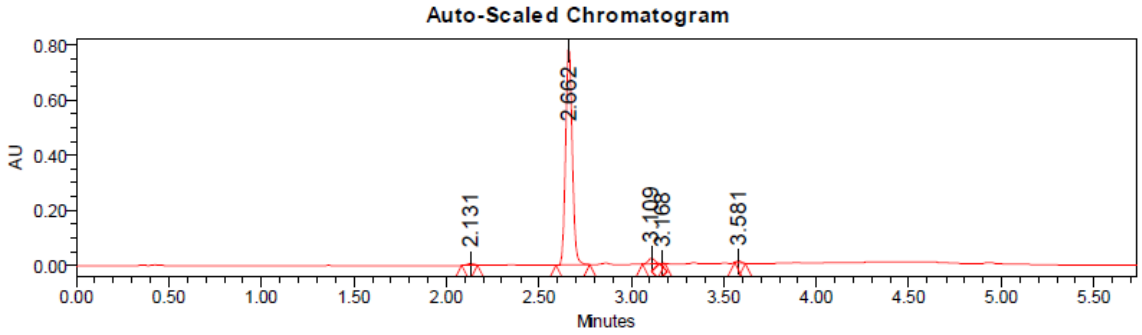

Peak Results

	Name	RT	Area	Height	% Area
1		2.131	13092	5143	0.66
2		2.662	1910614	783818	96.34
3		3.109	46662	20908	2.35
4		3.168	1209	914	0.06
5		3.581	11658	6356	0.59

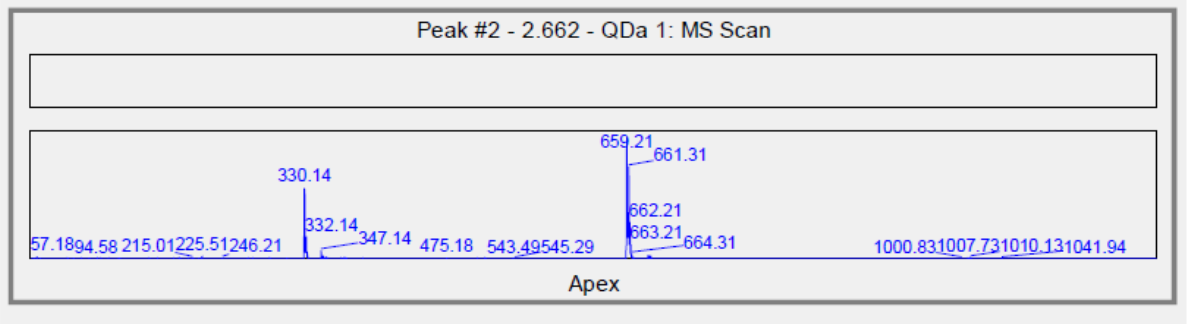

LC/MS of compound **215d**

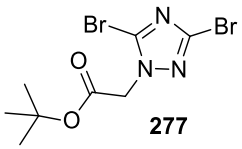

277

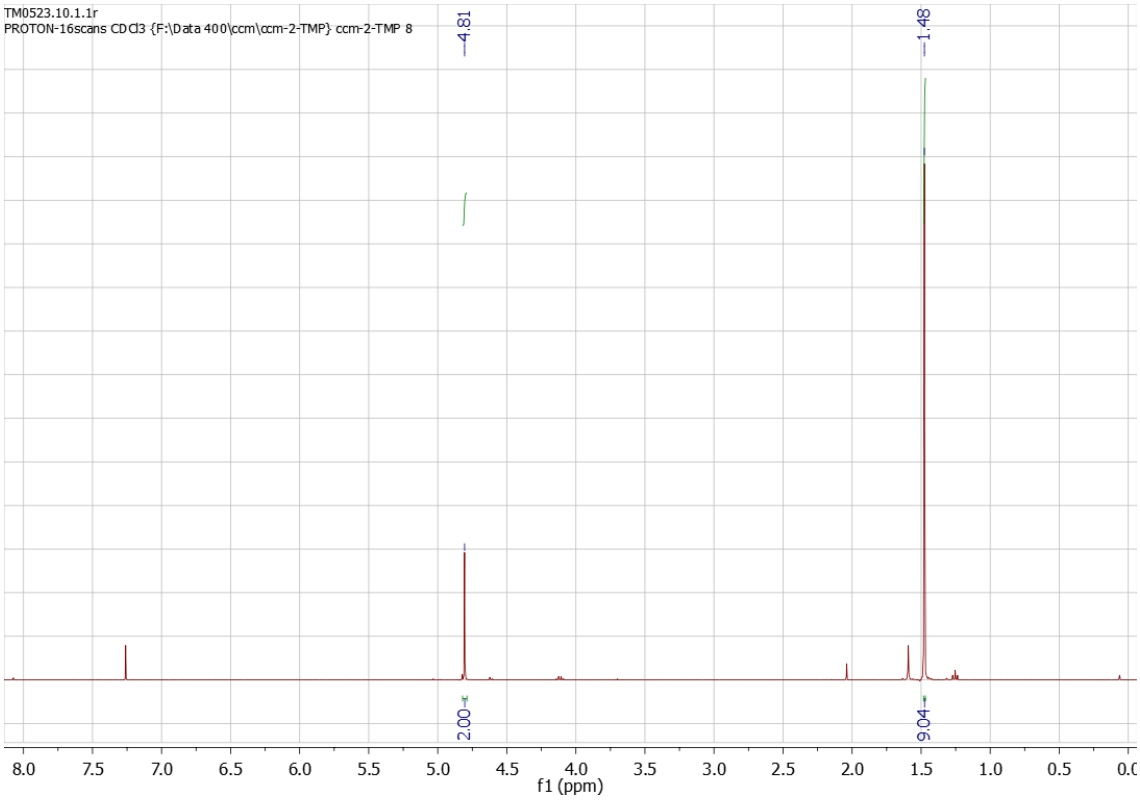

^{1}H NMR spectra of compound **277** in $CDCl_3$.

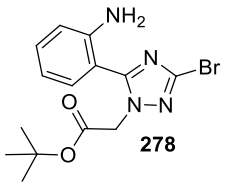

Exact Mass: 352.05

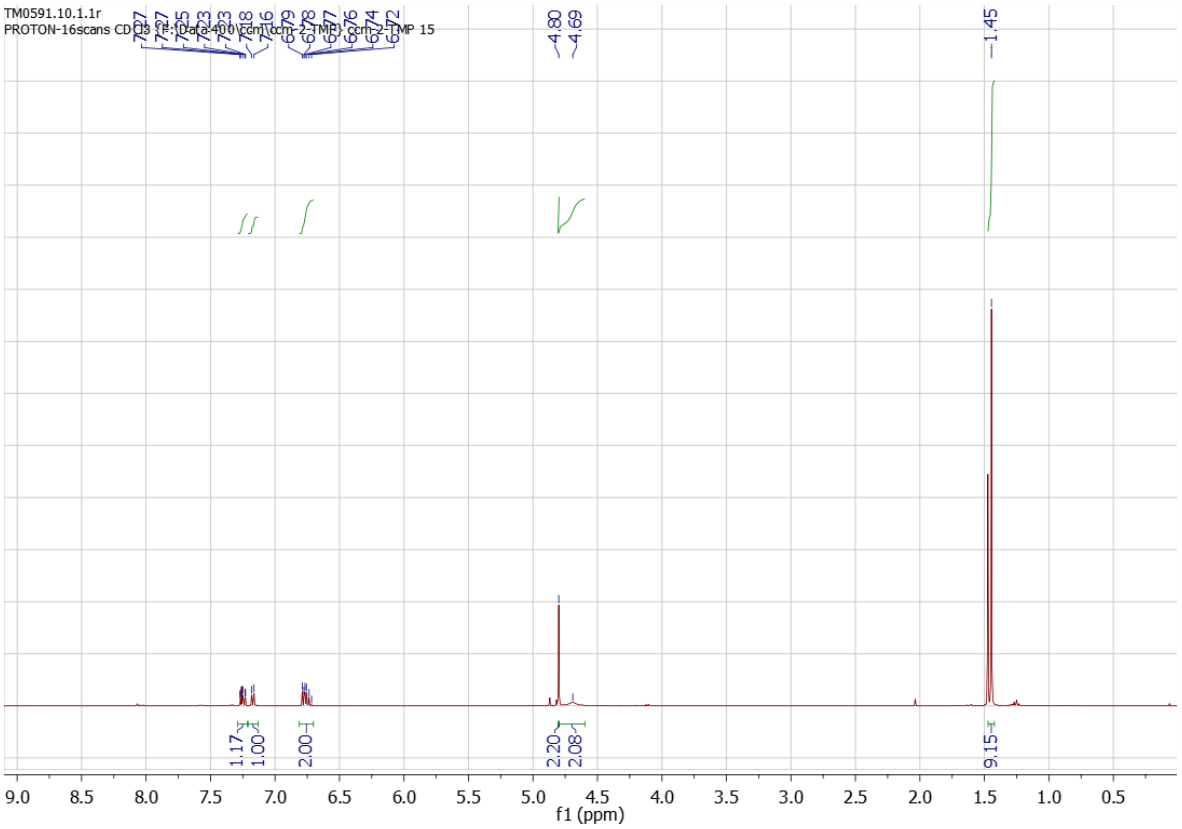

^{1}H NMR spectra of compound **278** in $CDCl_3$.

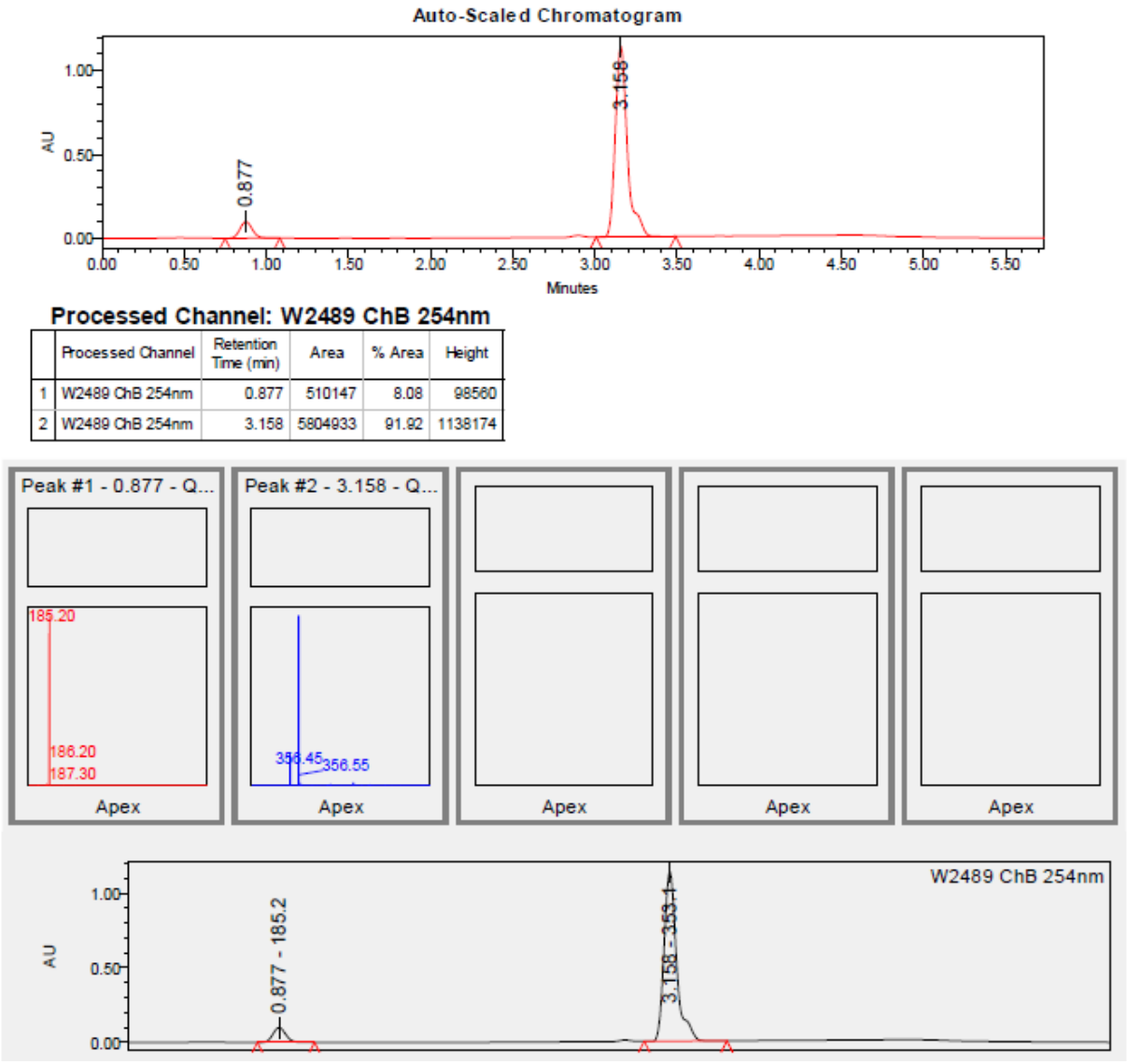

LC/MS of compound **278**

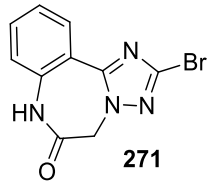

271

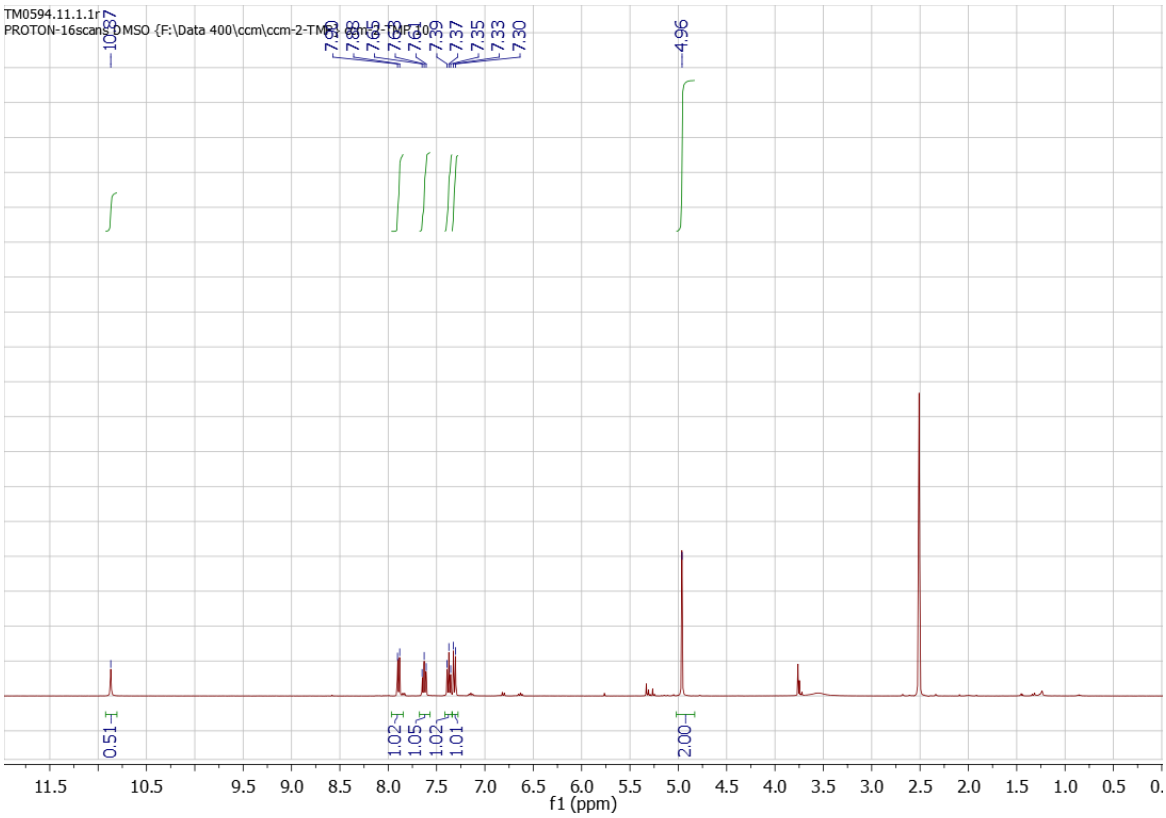

^{1}H NMR spectra of compound **271** in DMSO.

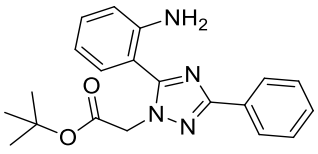

279a

Exact Mass: 350.17

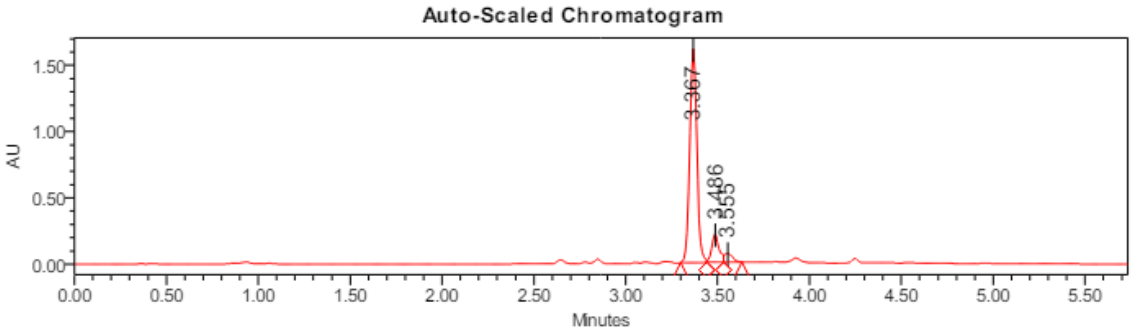

Peak Results

	Name	RT	Area	Height	% Area
1		3.367	4325756	1592795	84.64
2		3.486	583019	207181	11.41
3		3.555	201741	63723	3.95

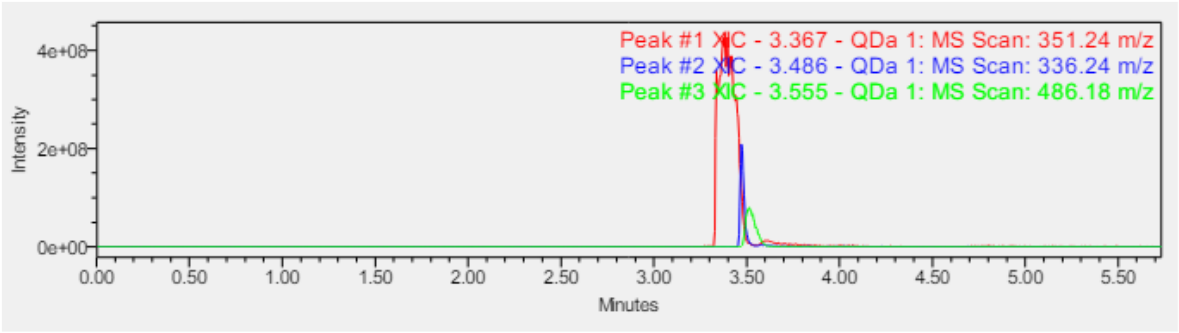

LC/MS of compound **279a**.

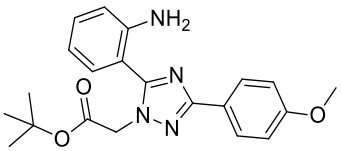

279b

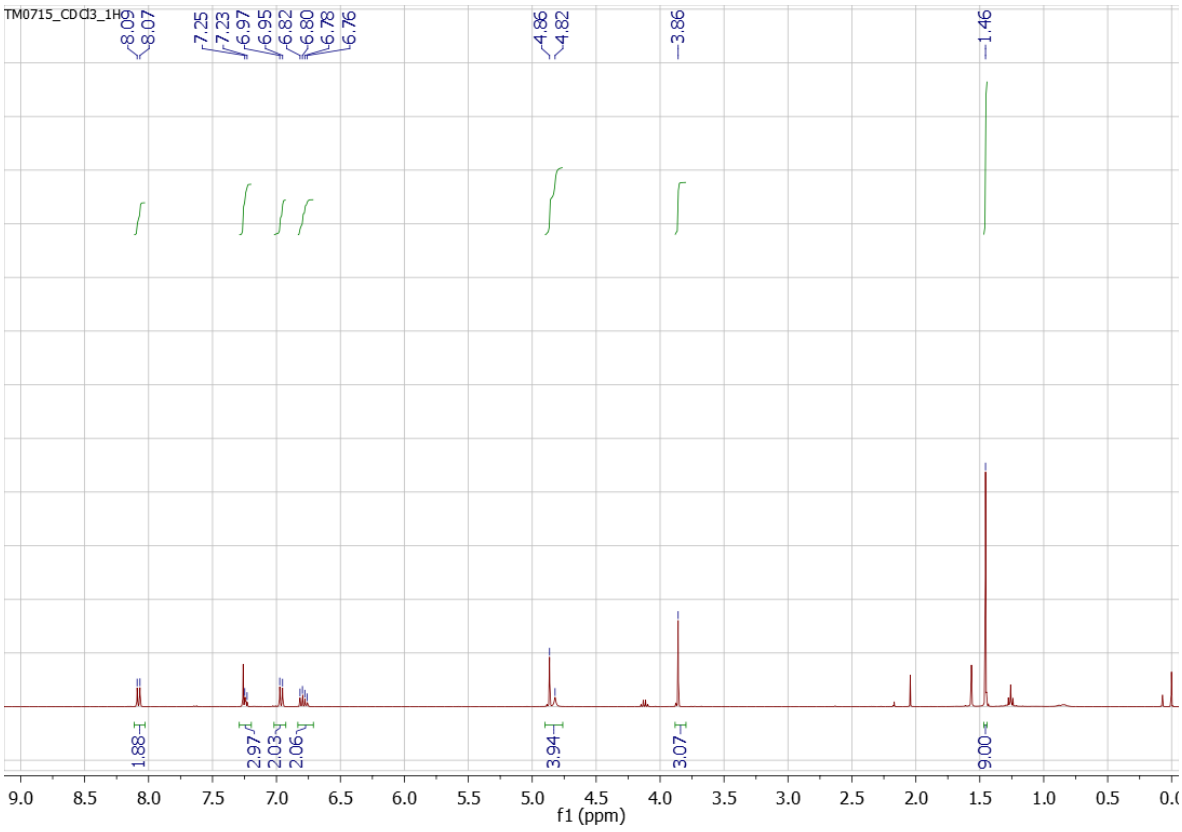

^{1}H NMR spectra of compound **279b** in $CDCl_3$.

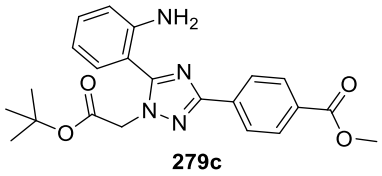

279c

Exact Mass: 408.18

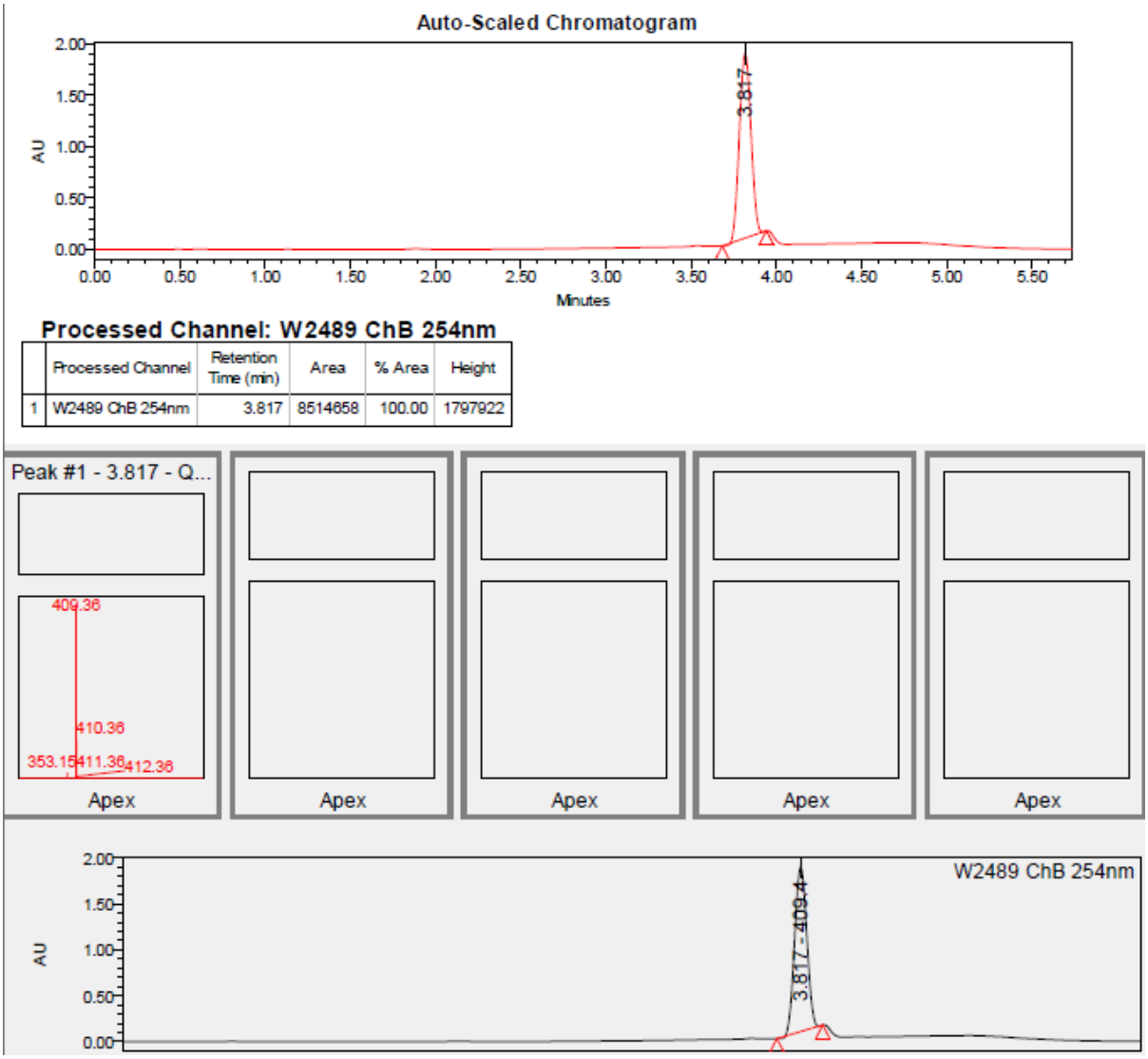

	Processed Channel	Retention Time (min)	Area	% Area	Height
1	W2489 ChB 254nm	3.817	8514658	100.00	1797922

LC/MS of compound **279c**

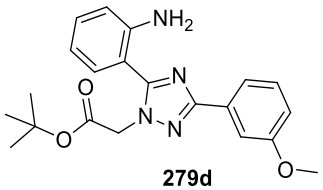

279d

Exact Mass: 380.18

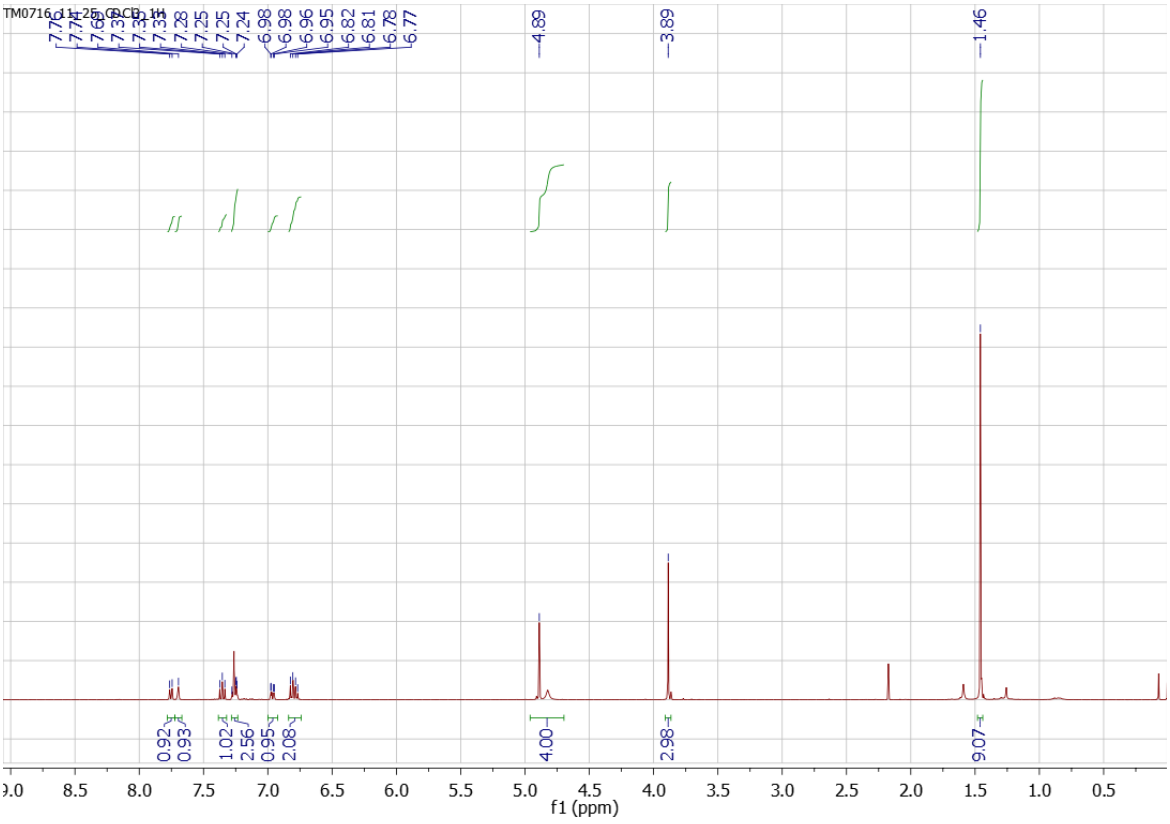

^{1}H NMR spectra of compound **279d** in $CDCl_3$.

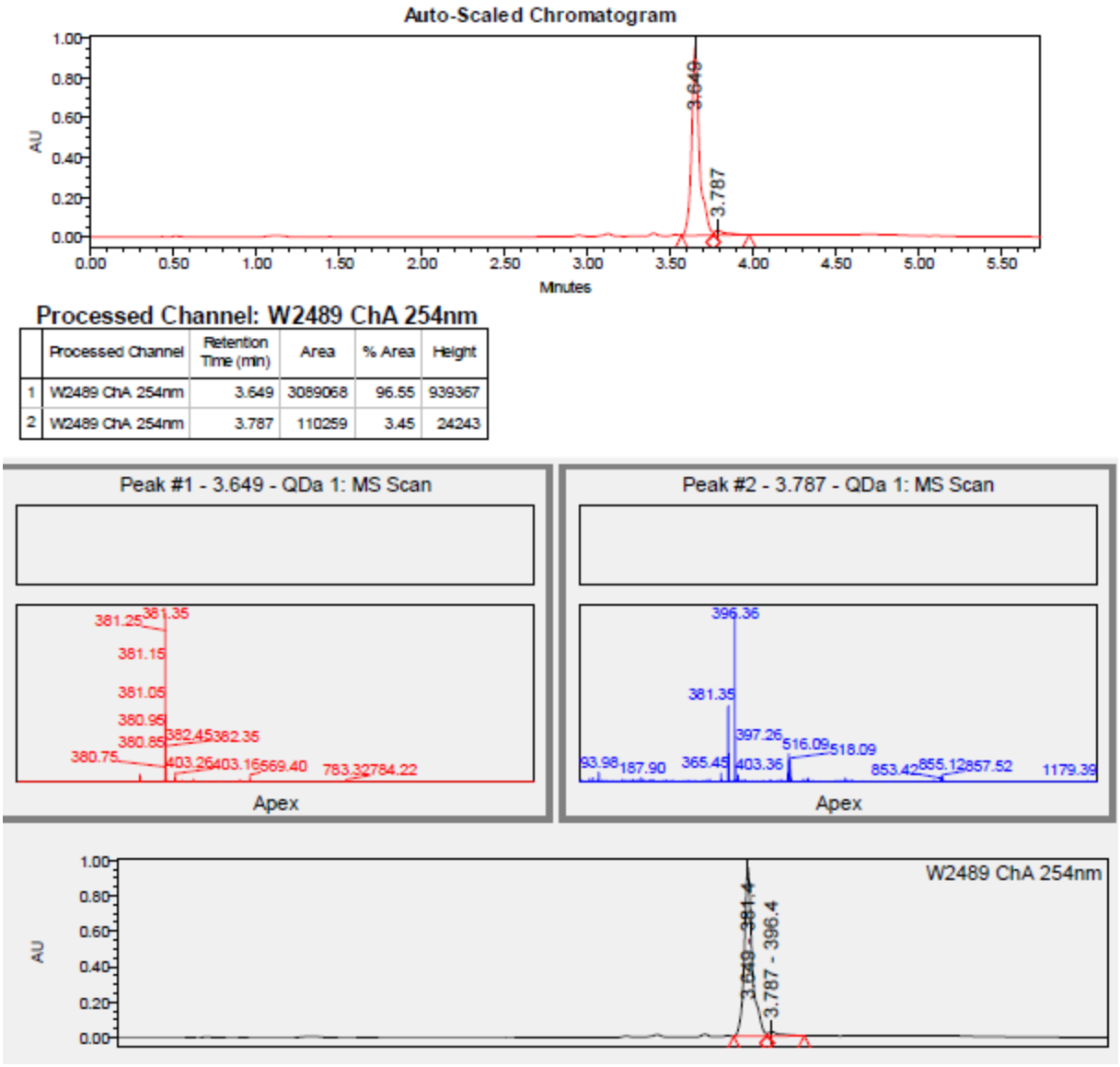

	Processed Channel	Retention Time (min)	Area	% Area	Height
1	W2489 ChA 254nm	3.649	3089068	96.55	939367
2	W2489 ChA 254nm	3.787	110259	3.45	24243

LC/MS of compound **279d**

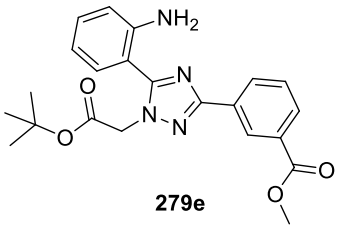

279e

Exact Mass: 408.18

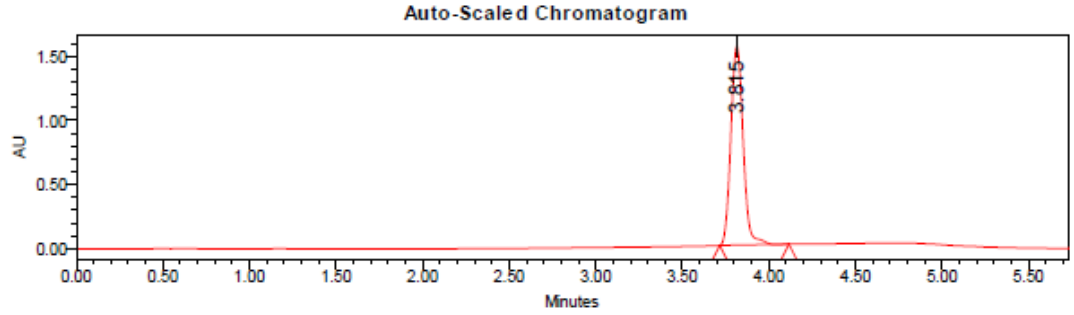

Processed Channel: W2489 ChB 254nm

	Processed Channel	Retention Time (min)	Area	% Area	Height
1	W2489 ChB 254nm	3.815	7631581	100.00	1555399

LC/MS of compound **279e**

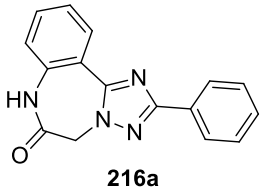

216a

Exact Mass: 276.10

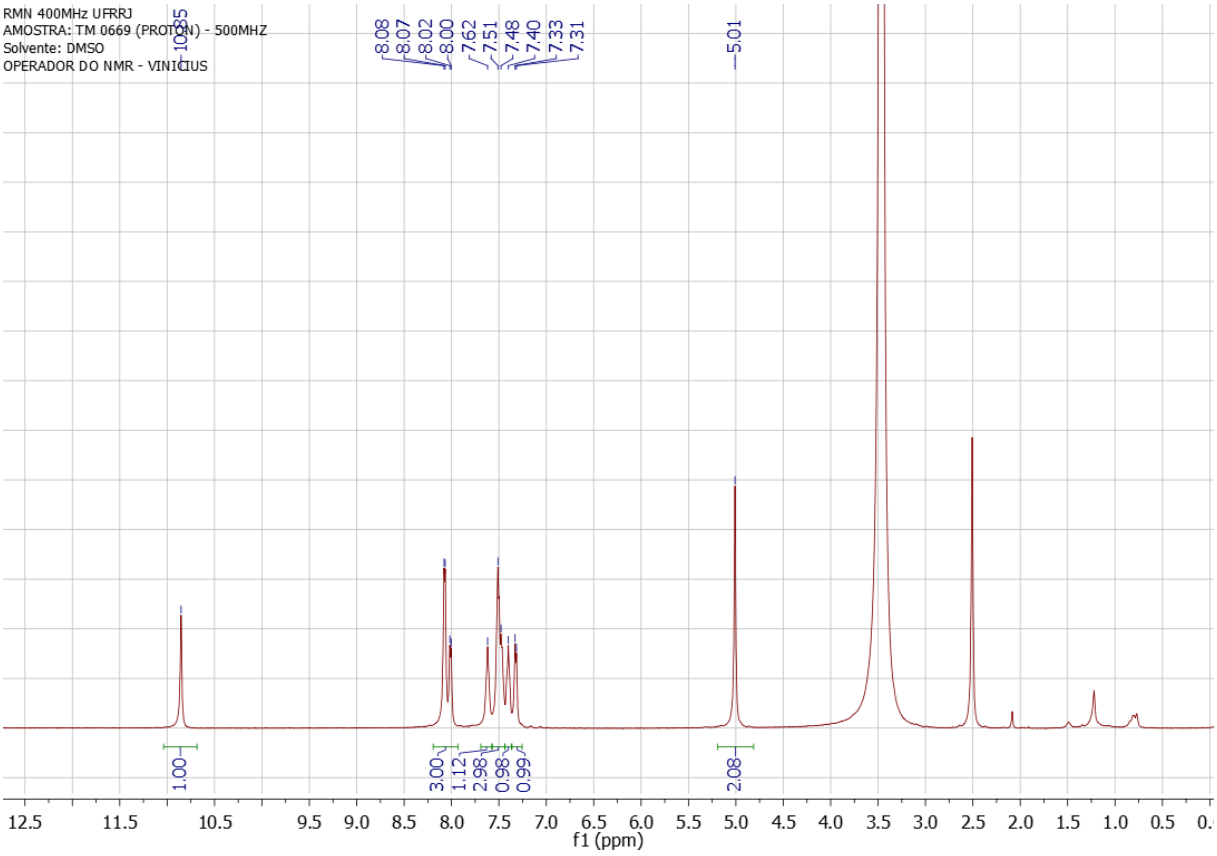

^{1}H NMR spectra of compound **216a** in DMSO.

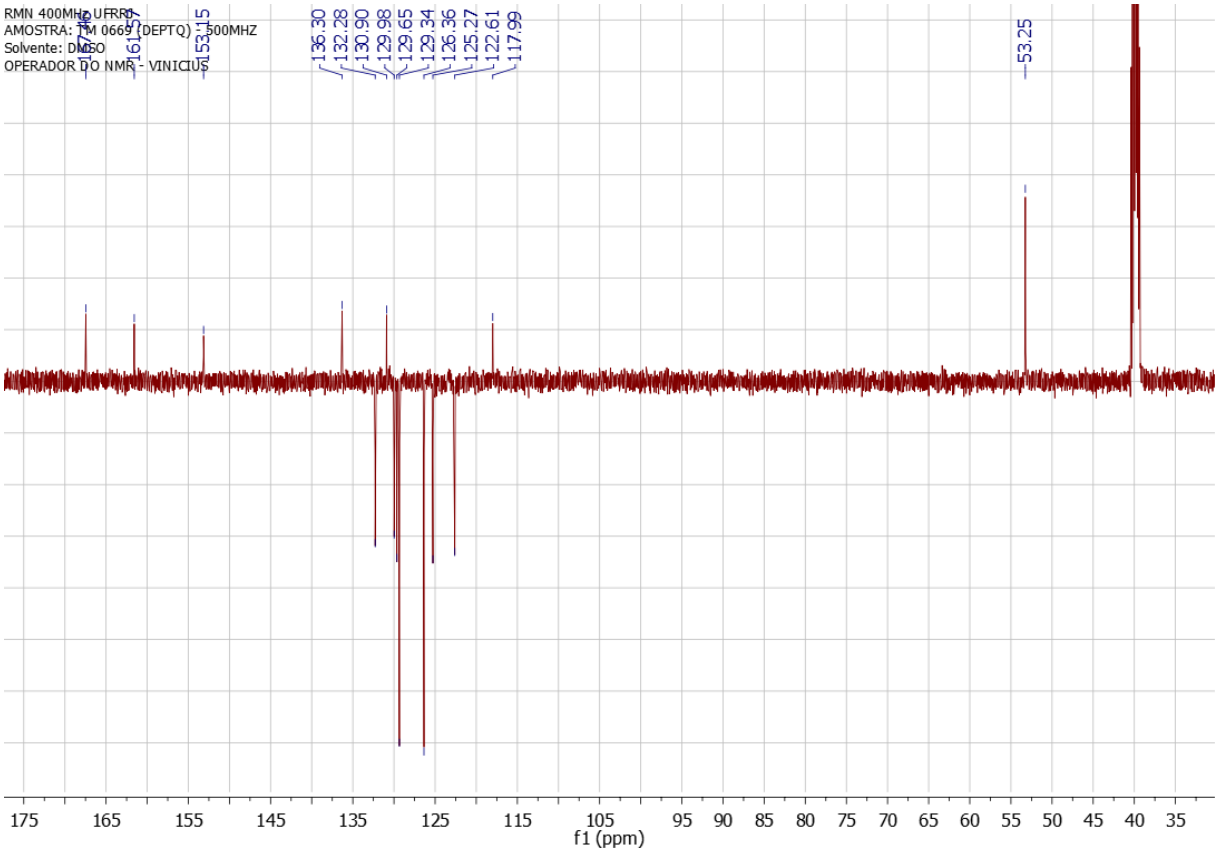

^{13}C NMR spectra of compound **216a** in DMSO.

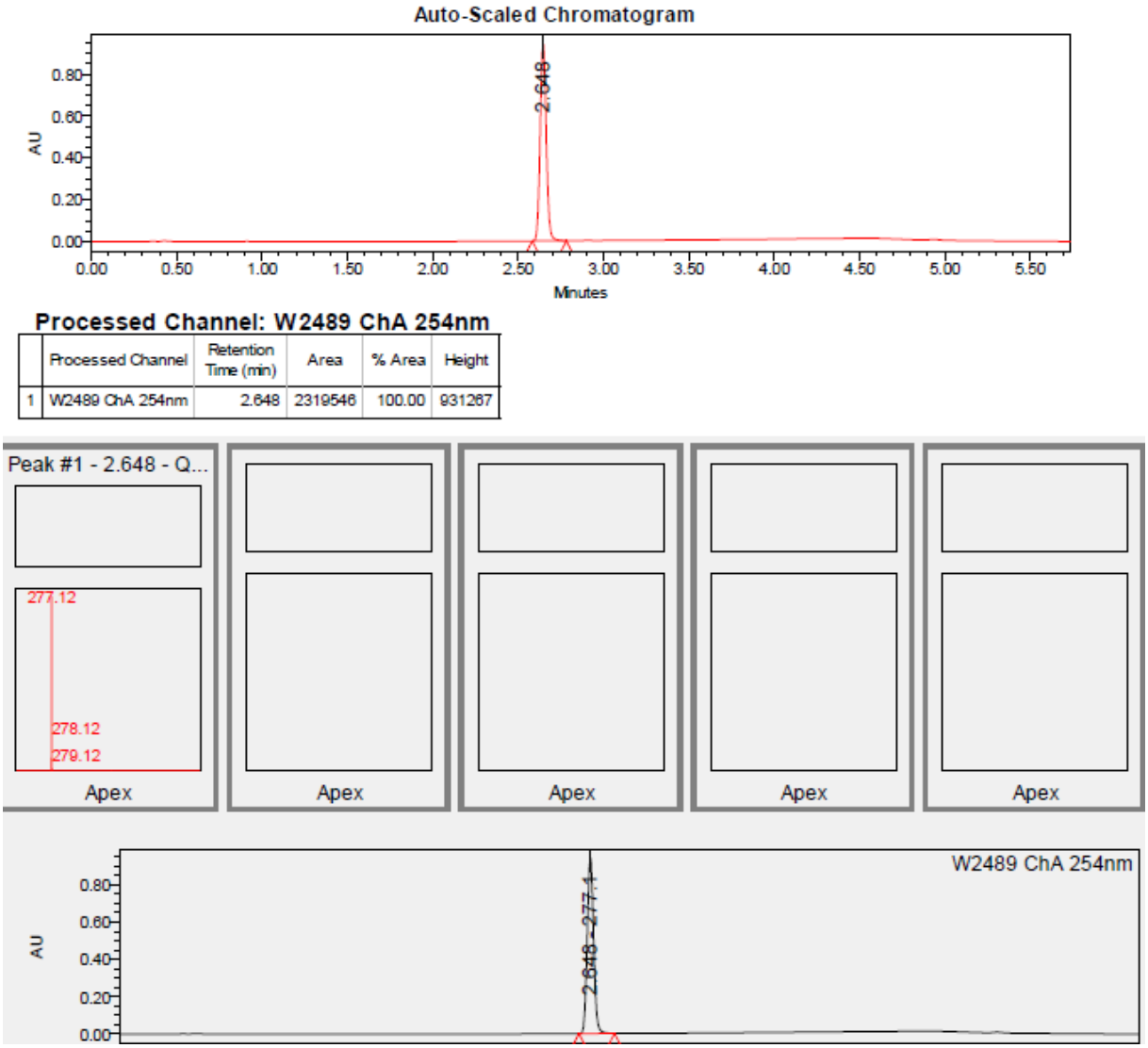

LC/MS of compound **216a**

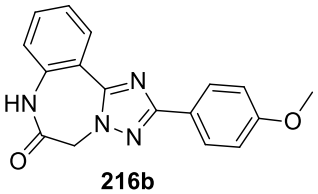

216b

Exact Mass: 306.11

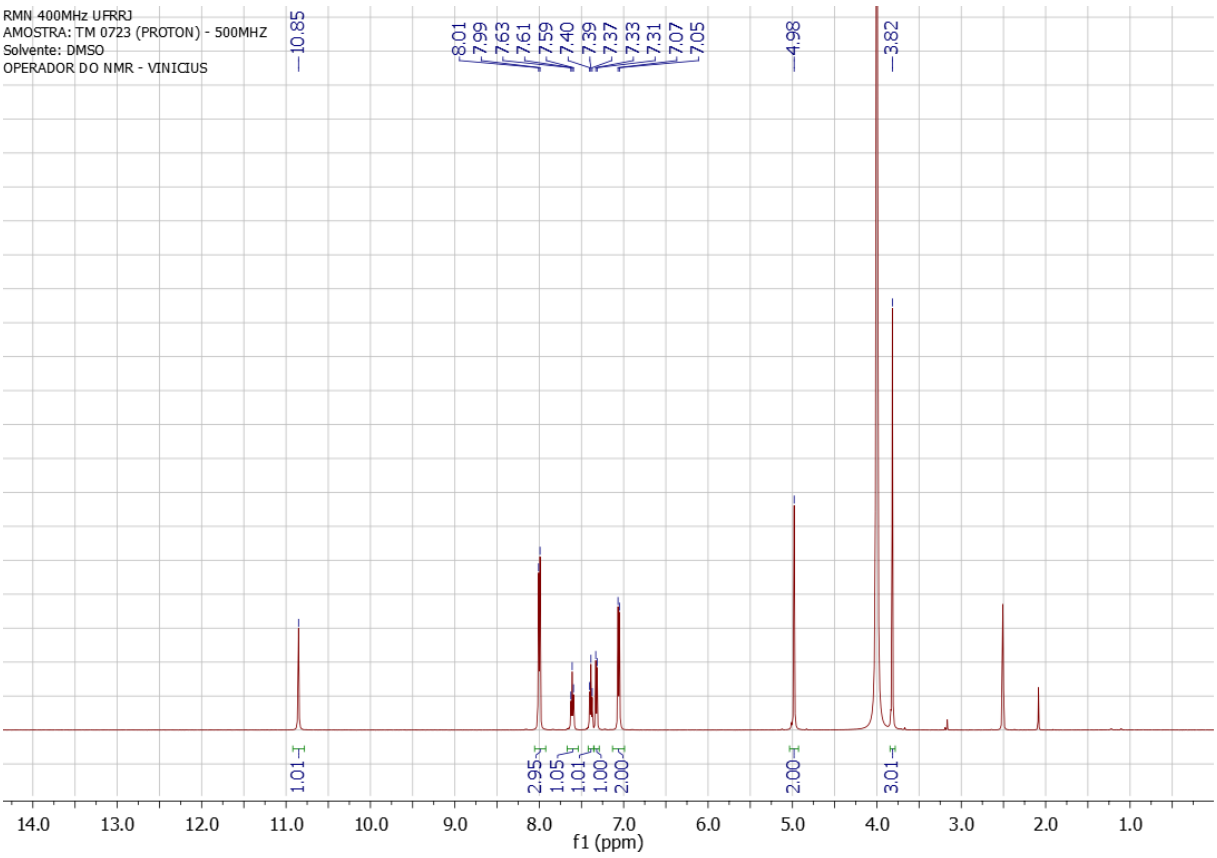

^{1}H NMR spectra of compound **216b** in DMSO.

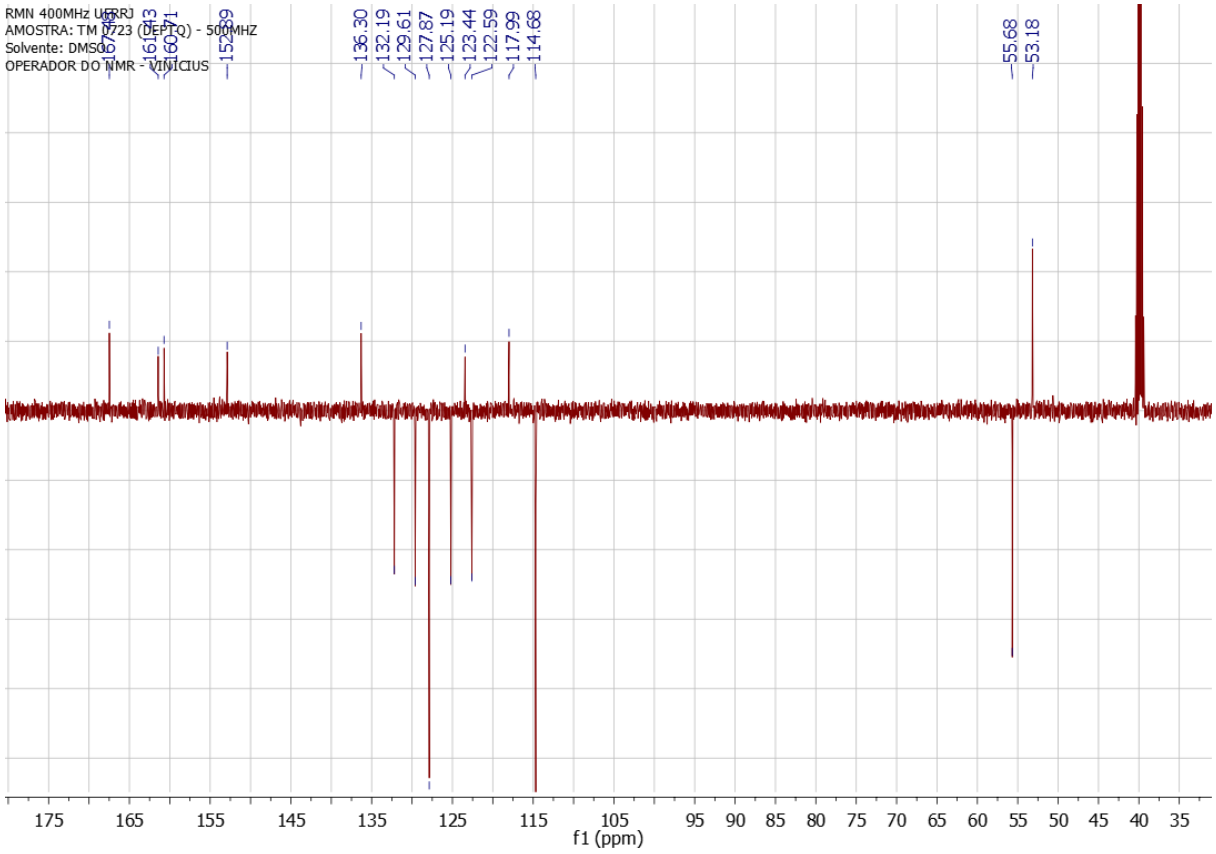

^{13}C NMR spectra of compound **216b** in DMSO.

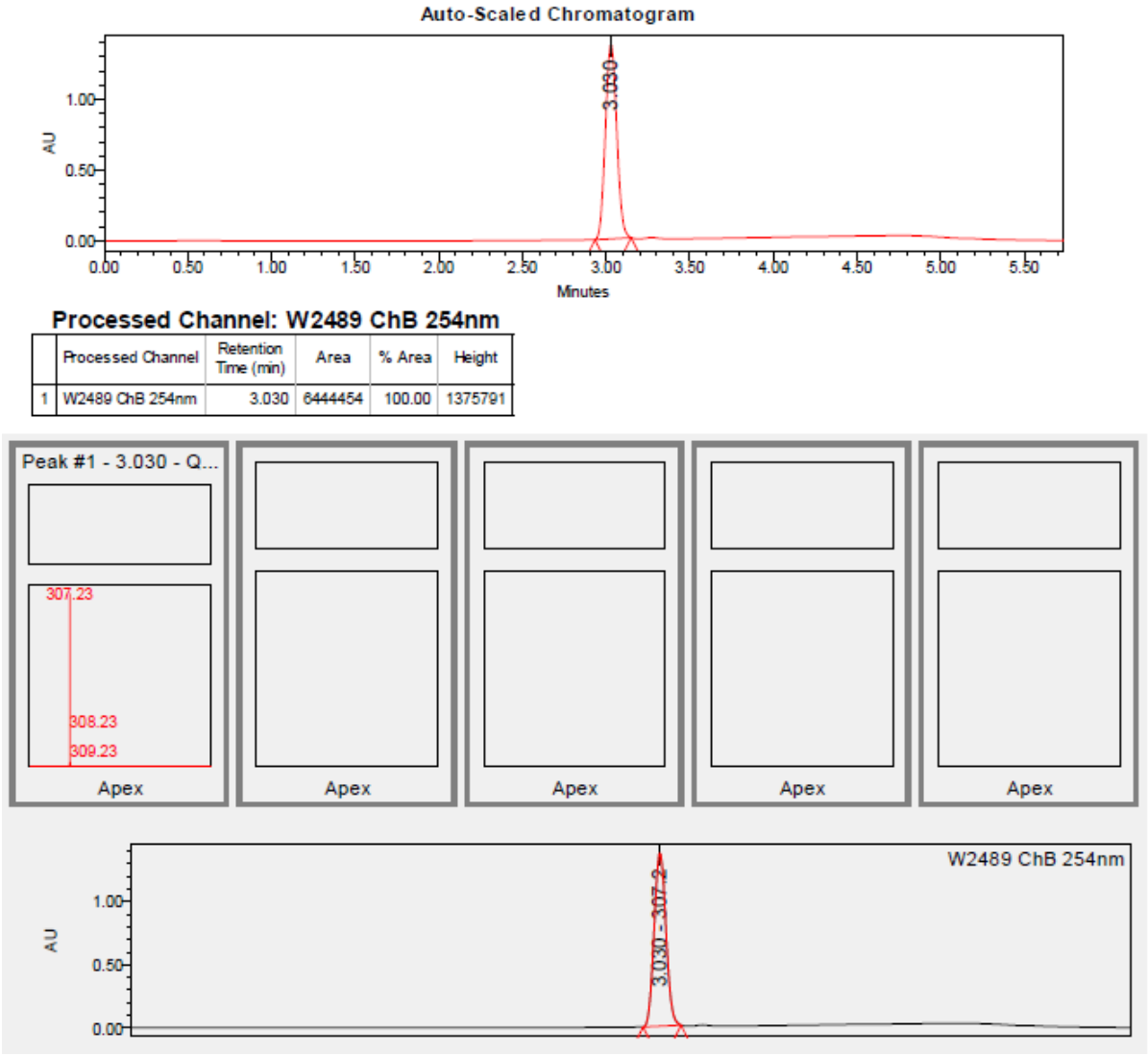

LC/MS of compound **216b**

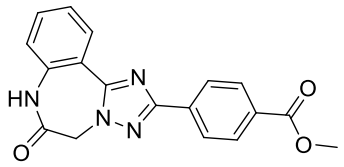

216c

Exact Mass: 334.11

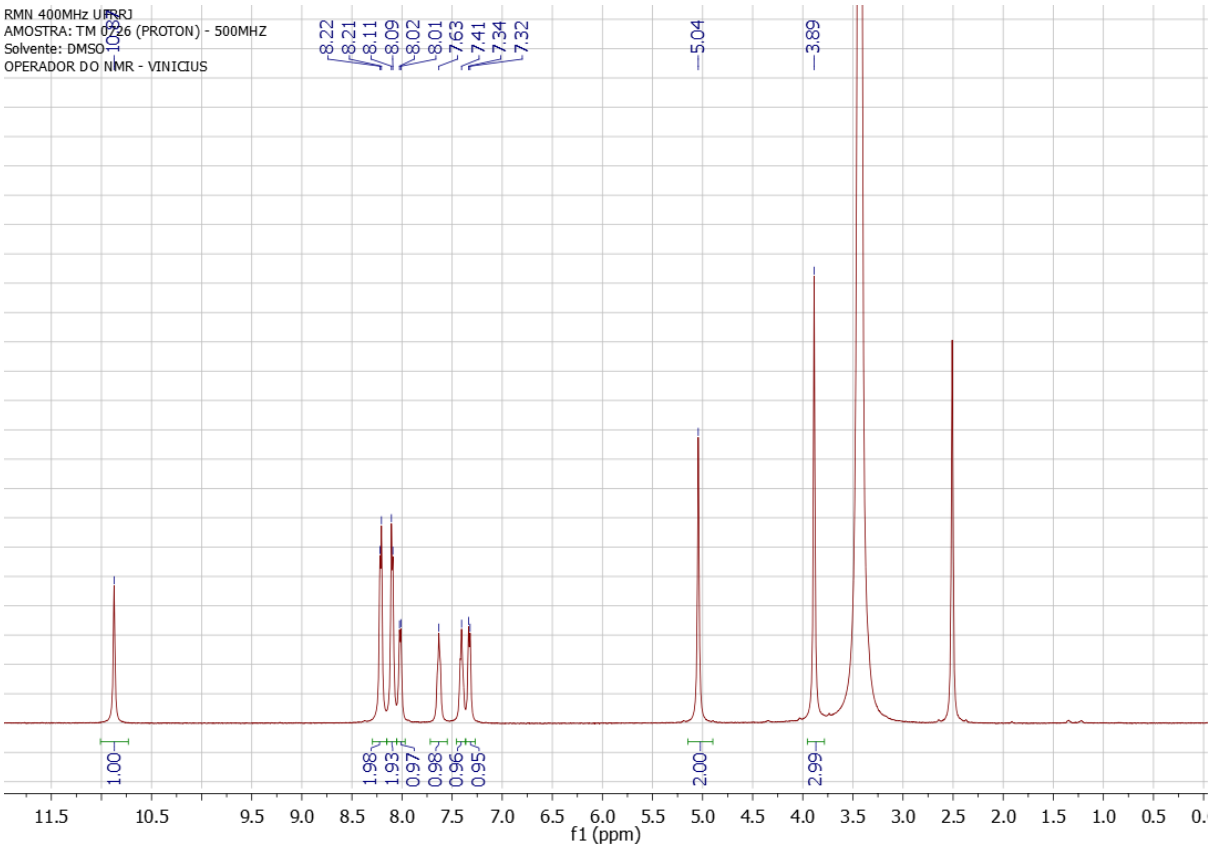

^{1}H NMR spectra of compound **216c** in DMSO.

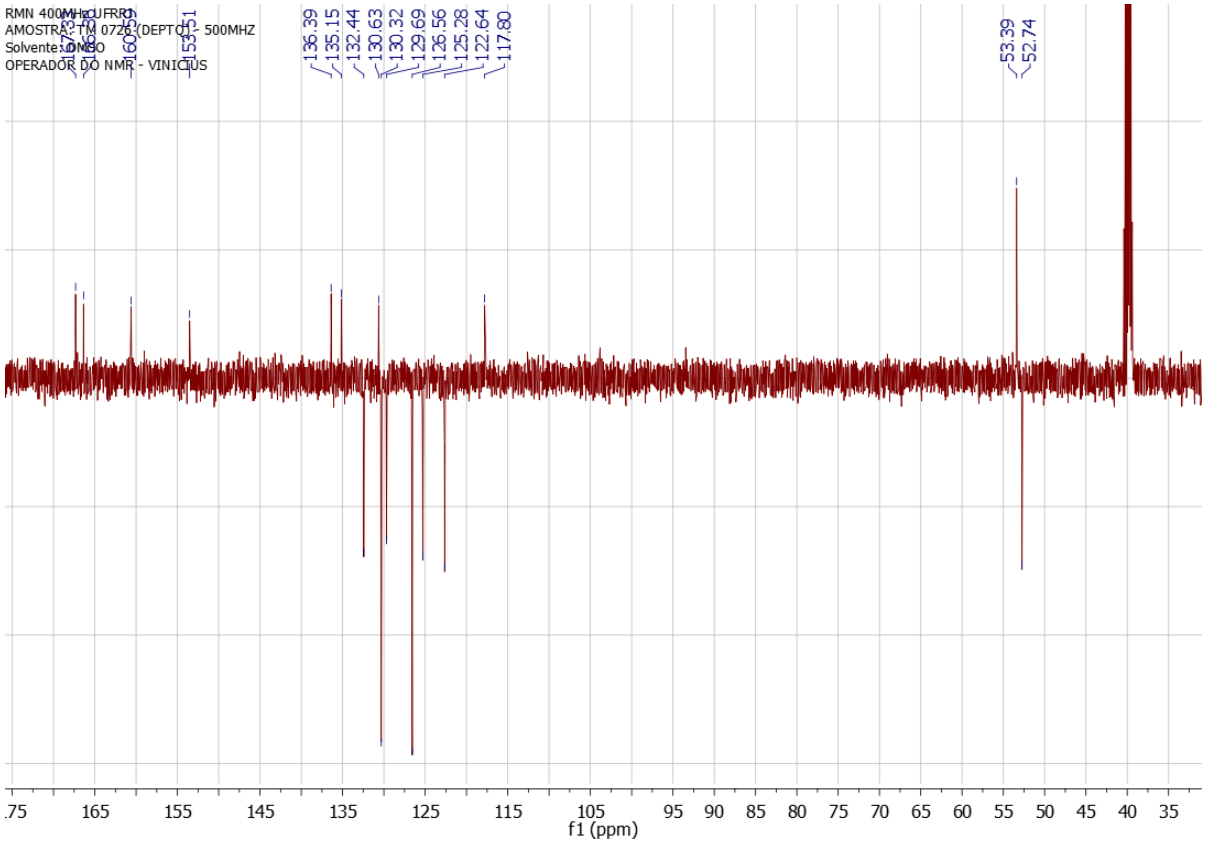

^{13}C NMR spectra of compound **216c** in DMSO.

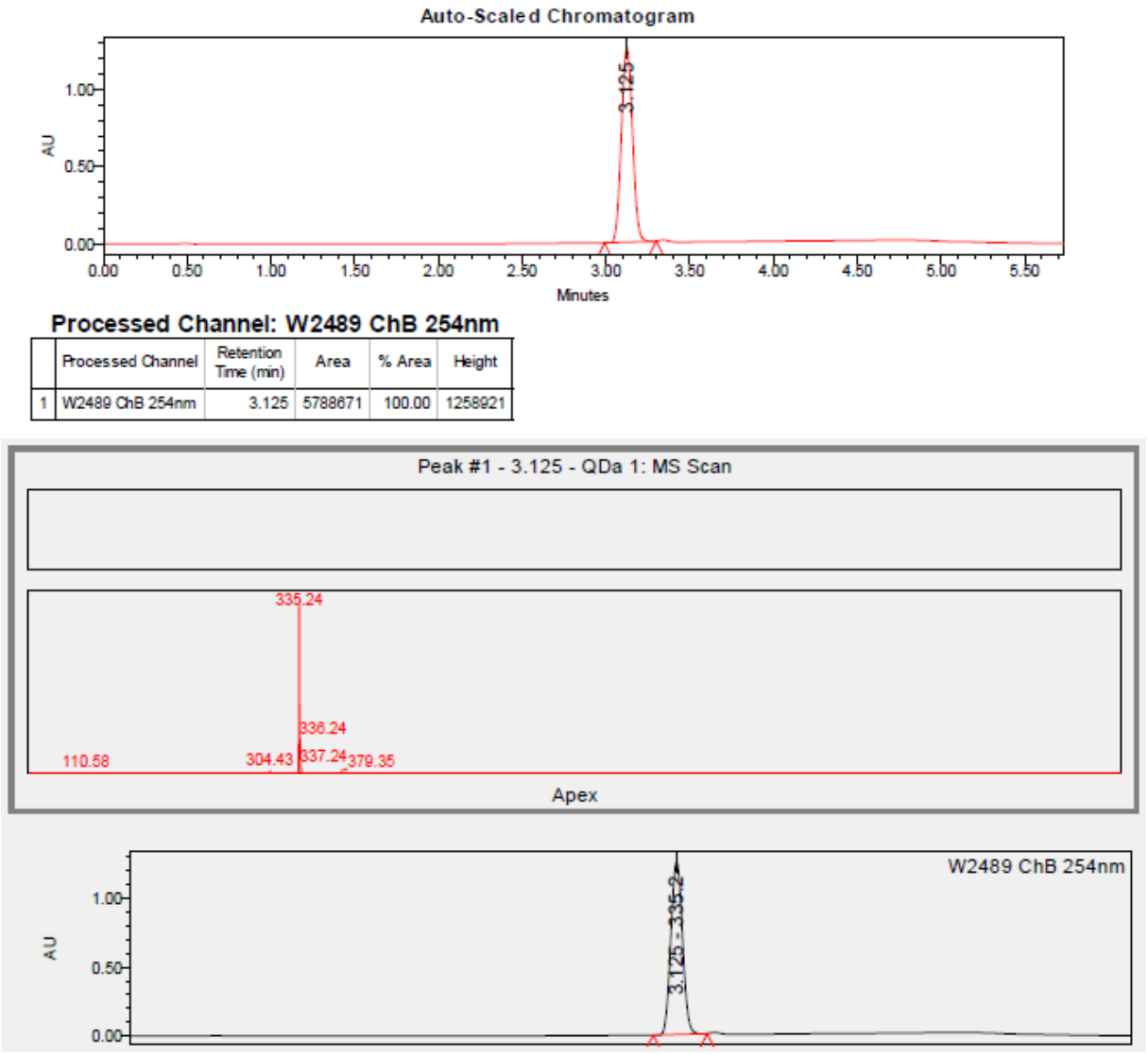

LC/MS of compound **216c**

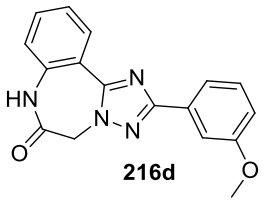

216d

Exact Mass: 306.11

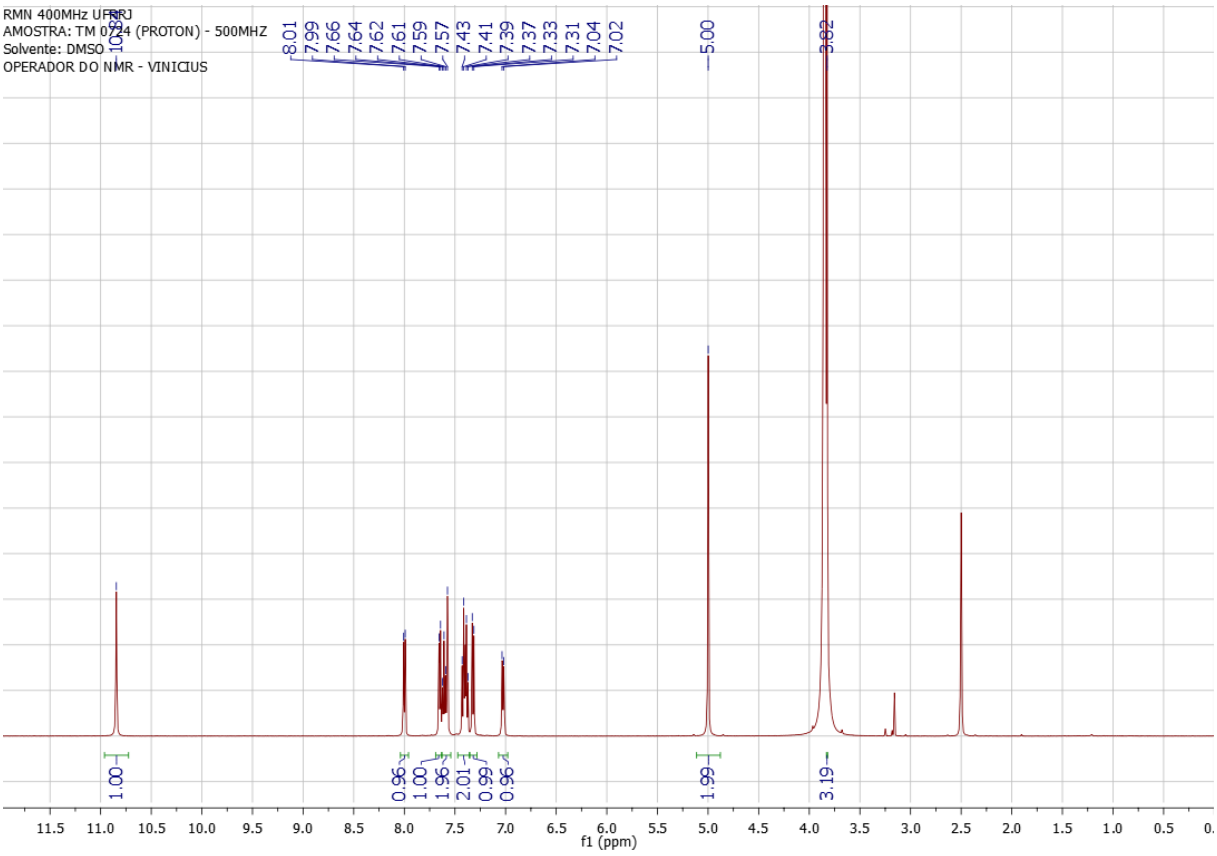

^{1}H NMR spectra of compound **216d** in DMSO.

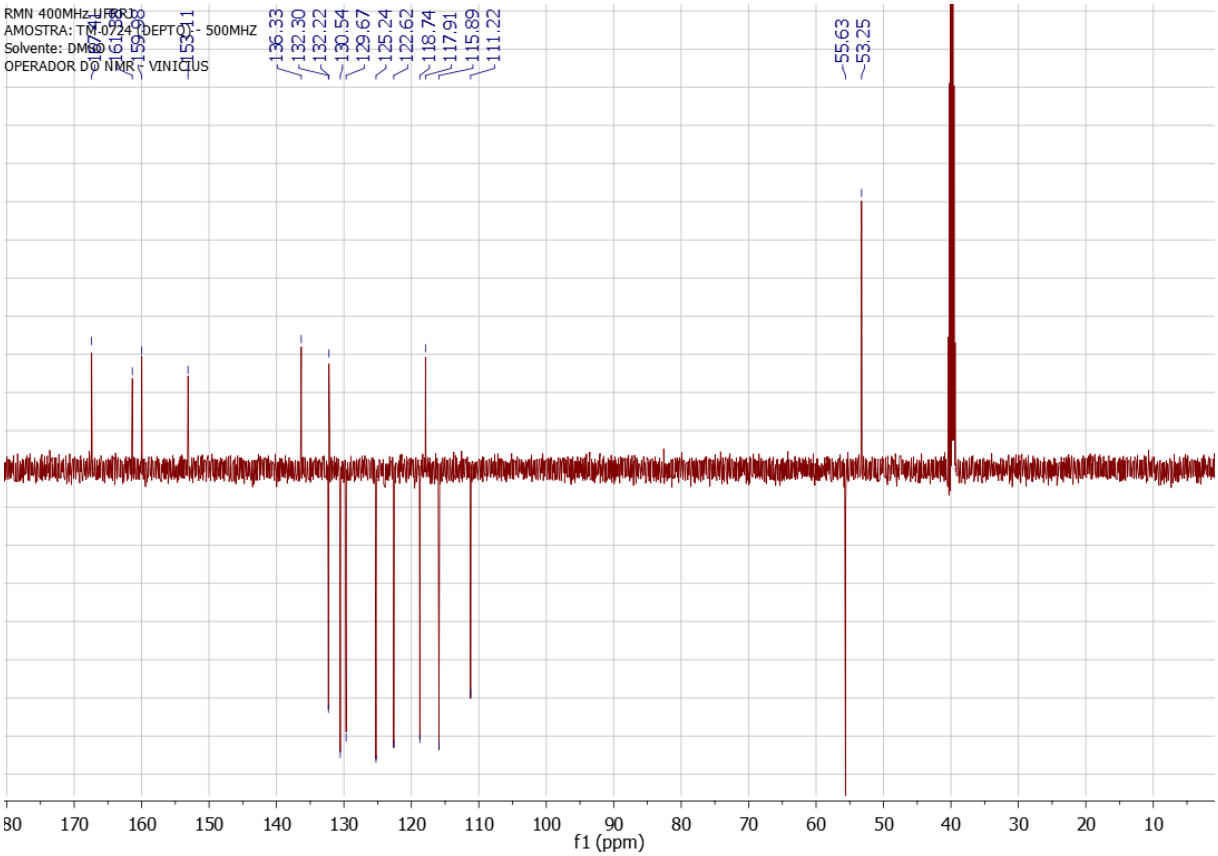

^{13}C NMR spectra of compound **216d** in DMSO.

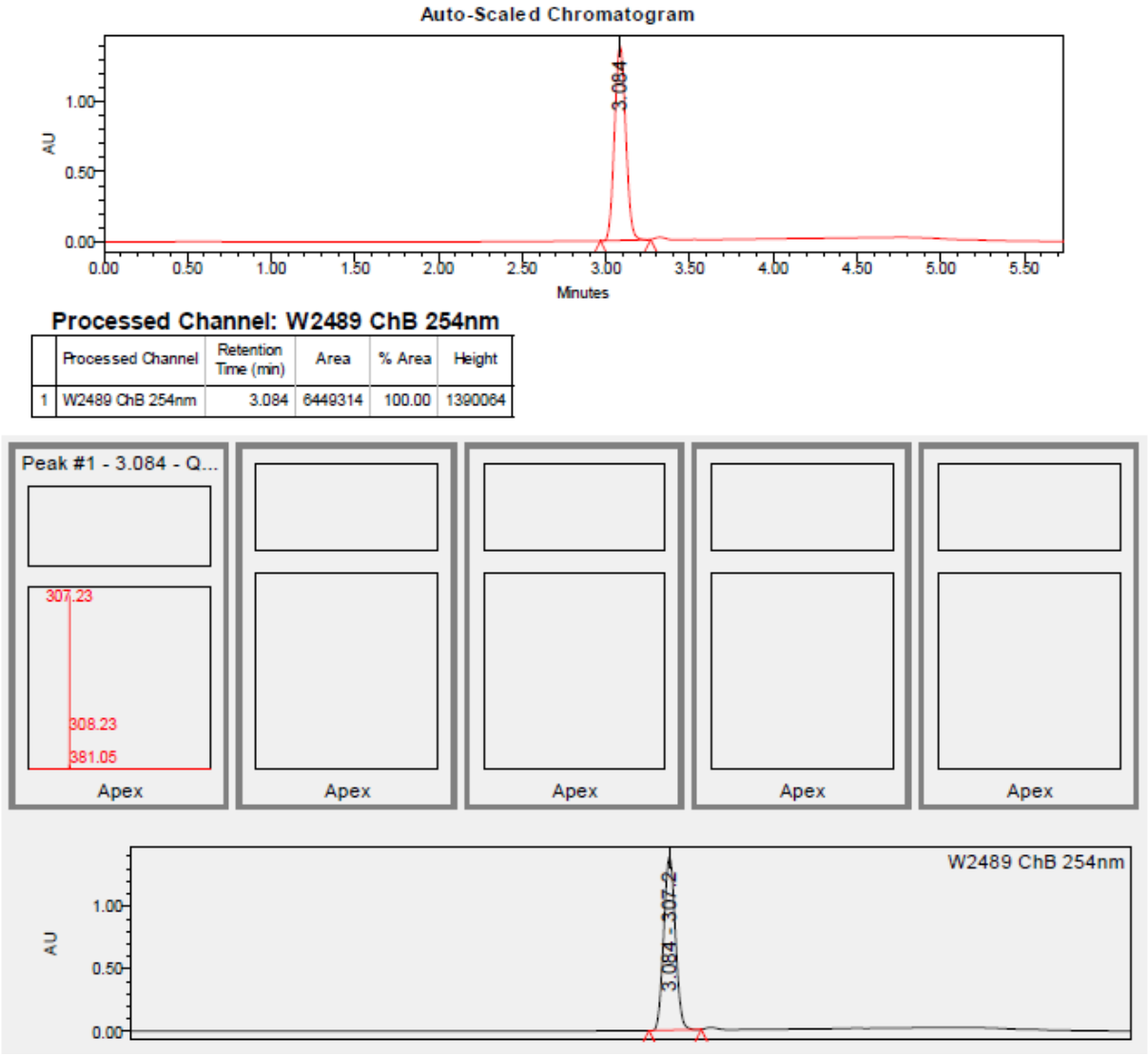

LC/MS of compound **216d**

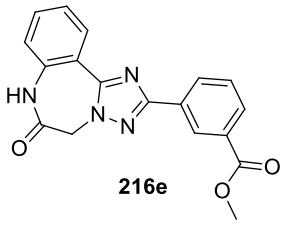

216e

Exact Mass: 334.11

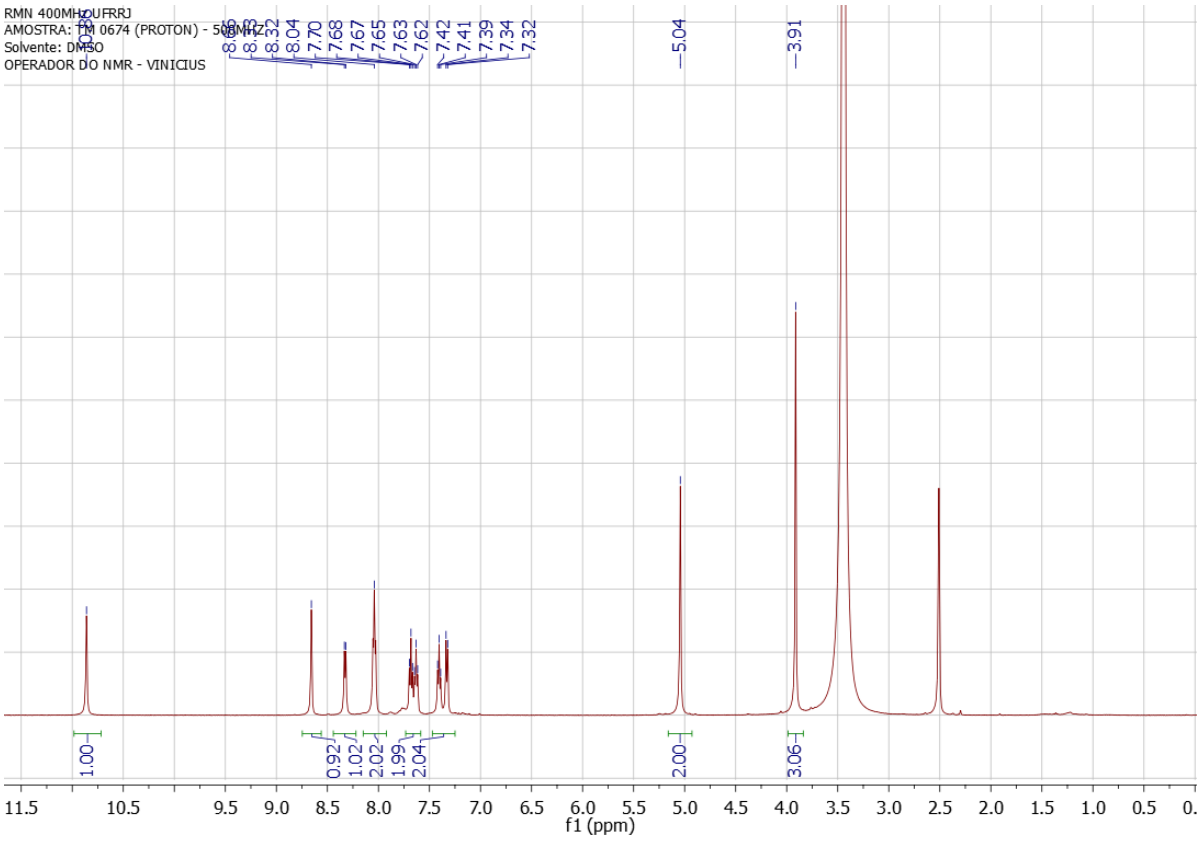

^{1}H NMR spectra of compound **216e** in DMSO.

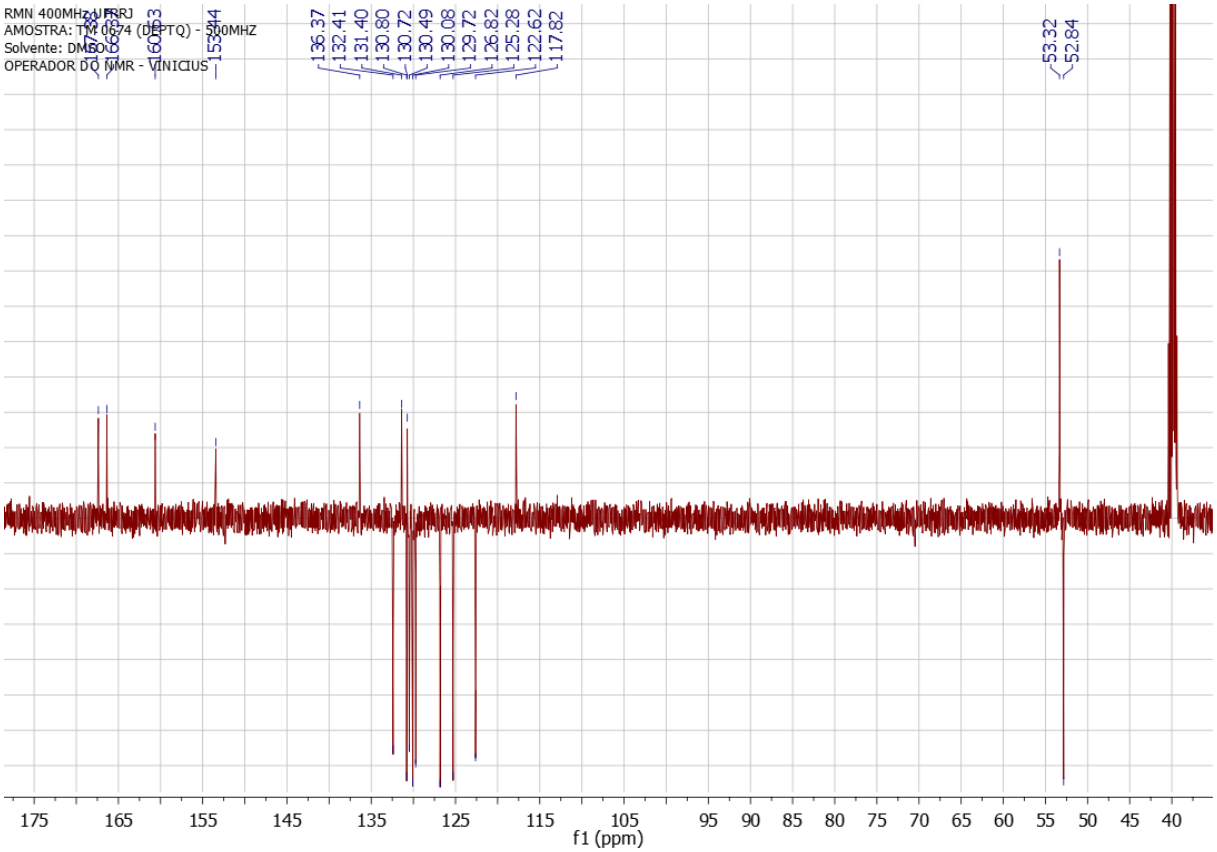

^{13}C NMR spectra of compound **216e** in DMSO.

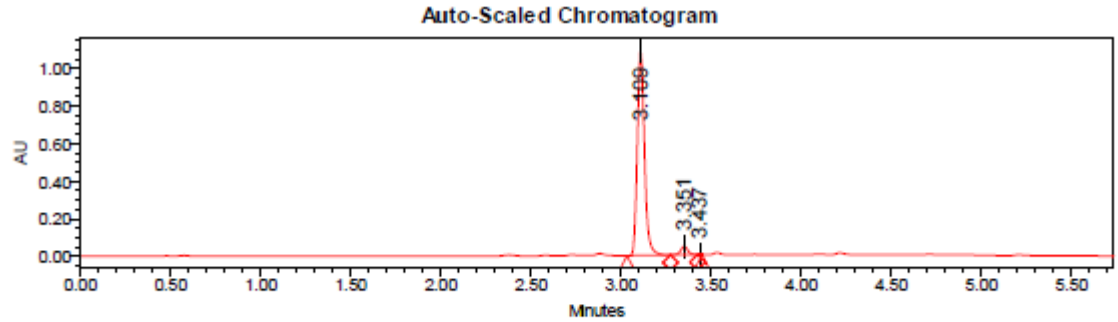

Processed Channel: W2489 ChA 254nm

	Processed Channel	Retention Time (min)	Area	% Area	Height
1	W2489 ChA 254nm	3.109	2999453	96.00	1085590
2	W2489 ChA 254nm	3.351	124407	3.98	44537
3	W2489 ChA 254nm	3.437	562	0.02	514

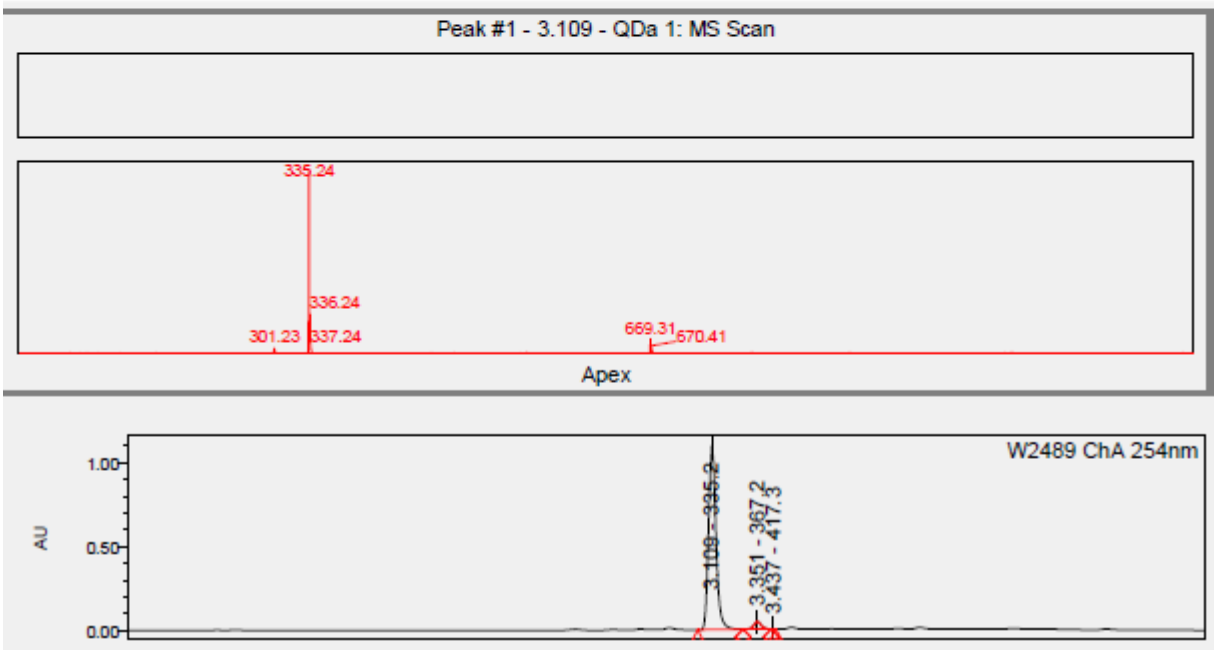

LC/MS of compound **216e**

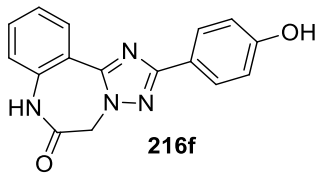

216f

Exact Mass: 292.10

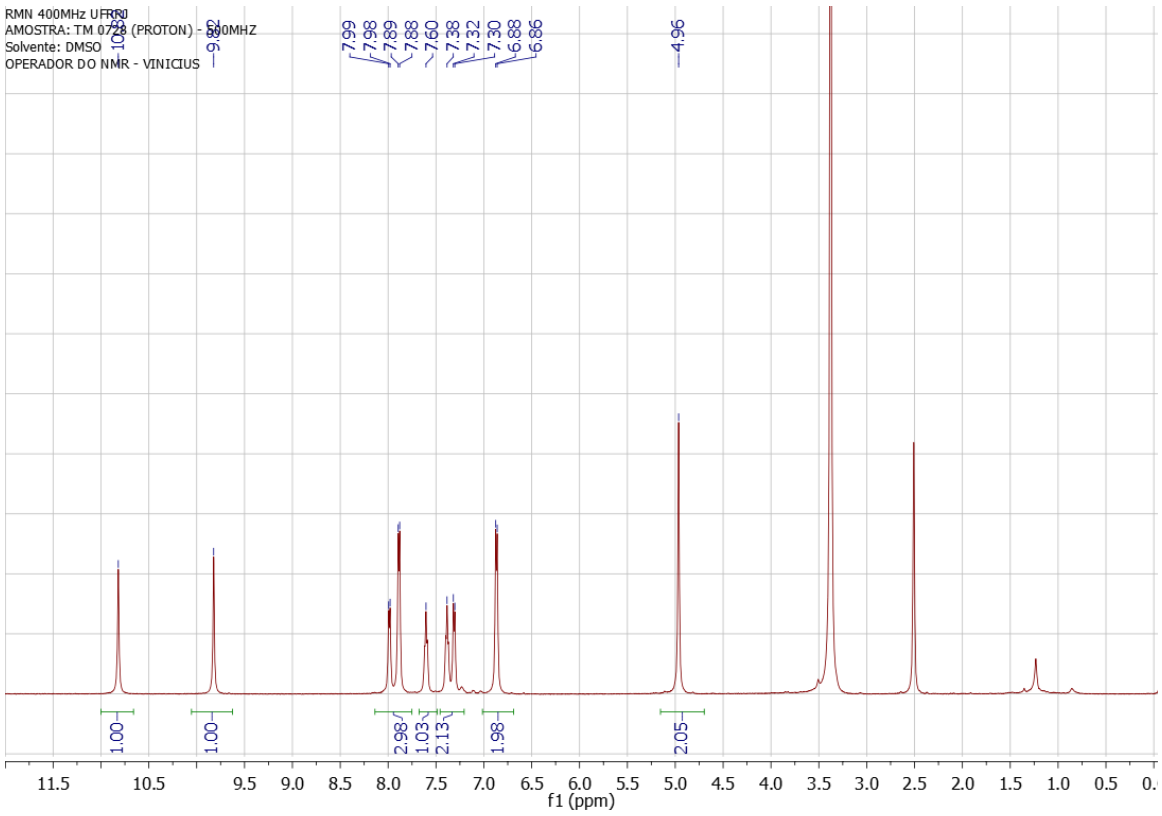

^{1}H NMR spectra of compound **216f** in DMSO.

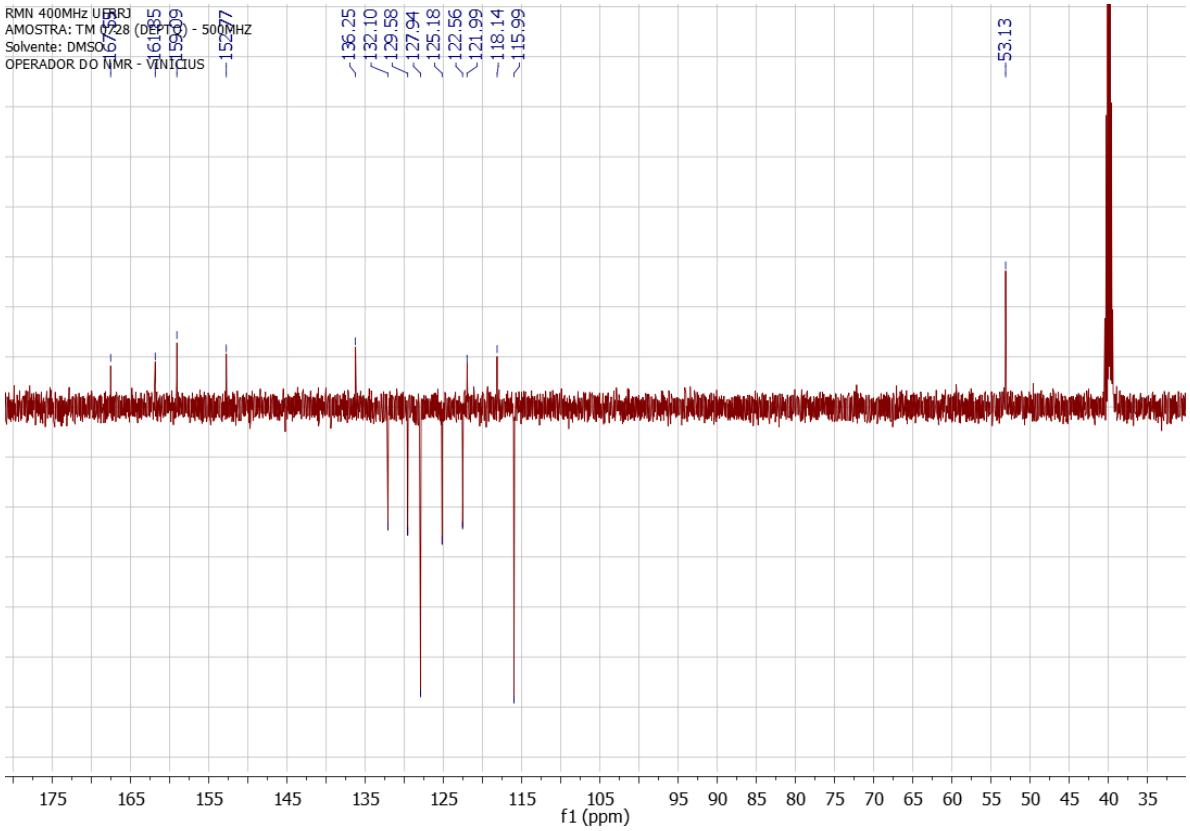

^{13}C NMR spectra of compound **216f** in DMSO.

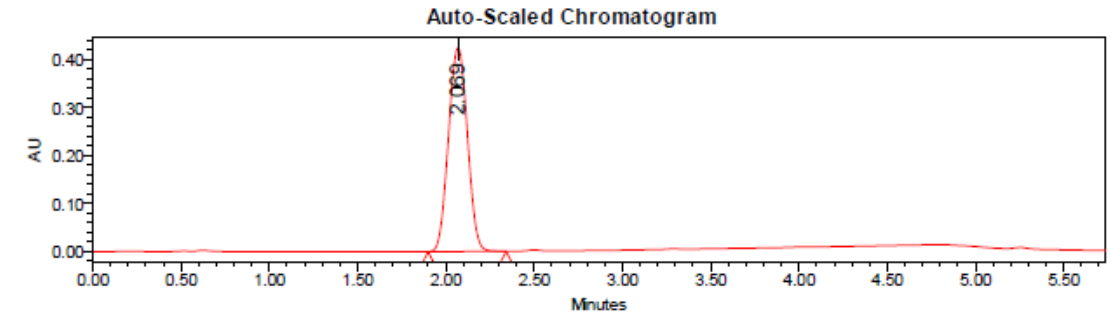

Processed Channel: W2489 ChB 254nm

	Processed Channel	Retention Time (min)	Area	% Area	Height
1	W2489 ChB 254nm	2.069	3170214	100.00	425035

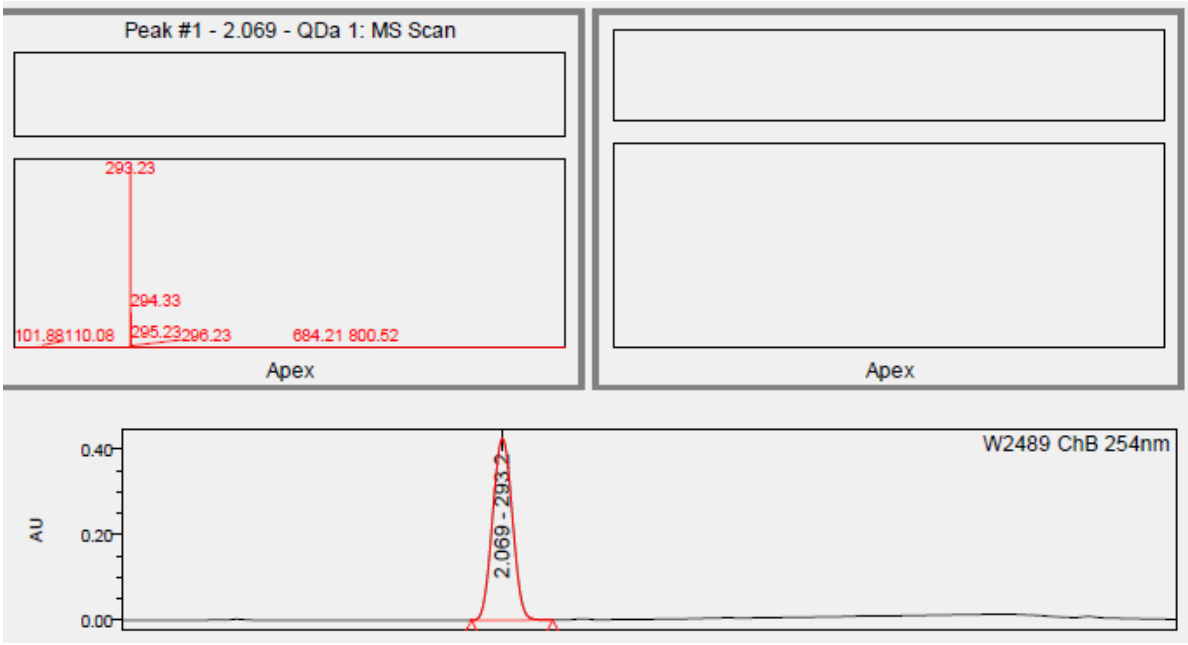

LC/MS of compound **216f**

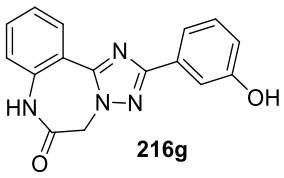

216g

Exact Mass: 292.10

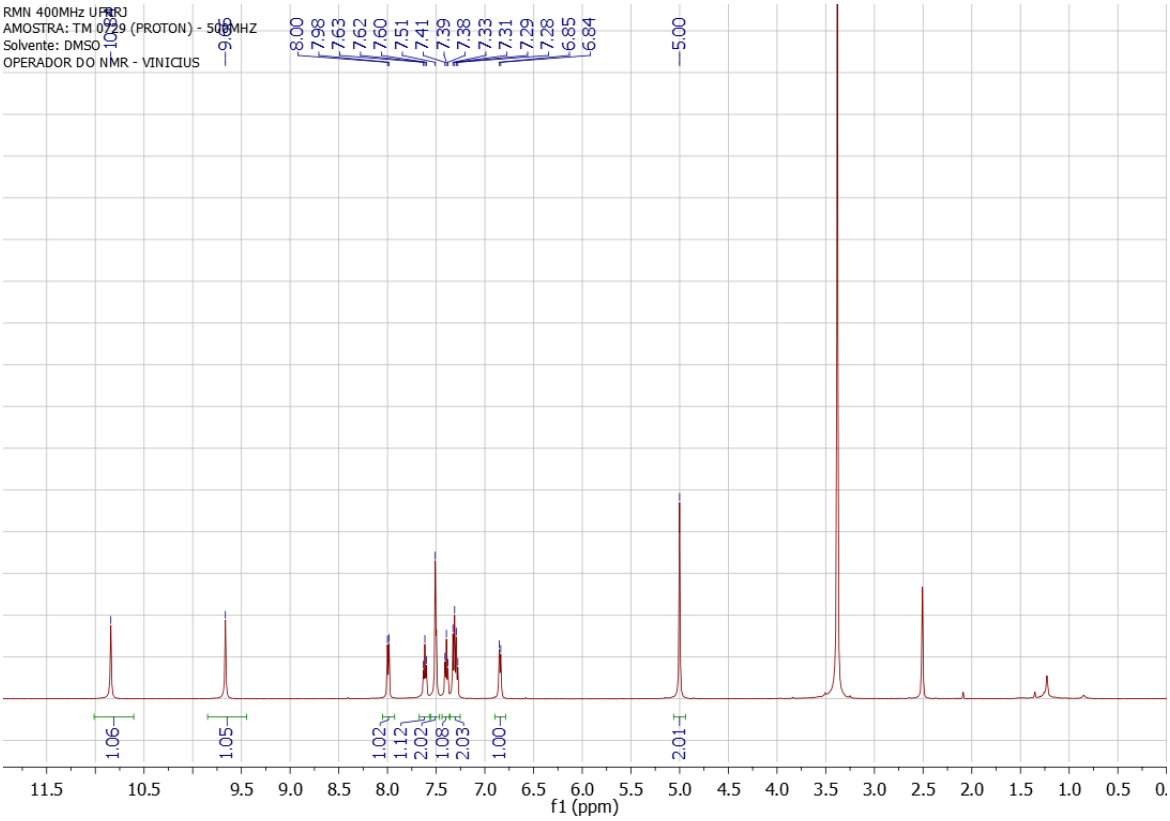

^{1}H NMR spectra of compound **216g** in DMSO.

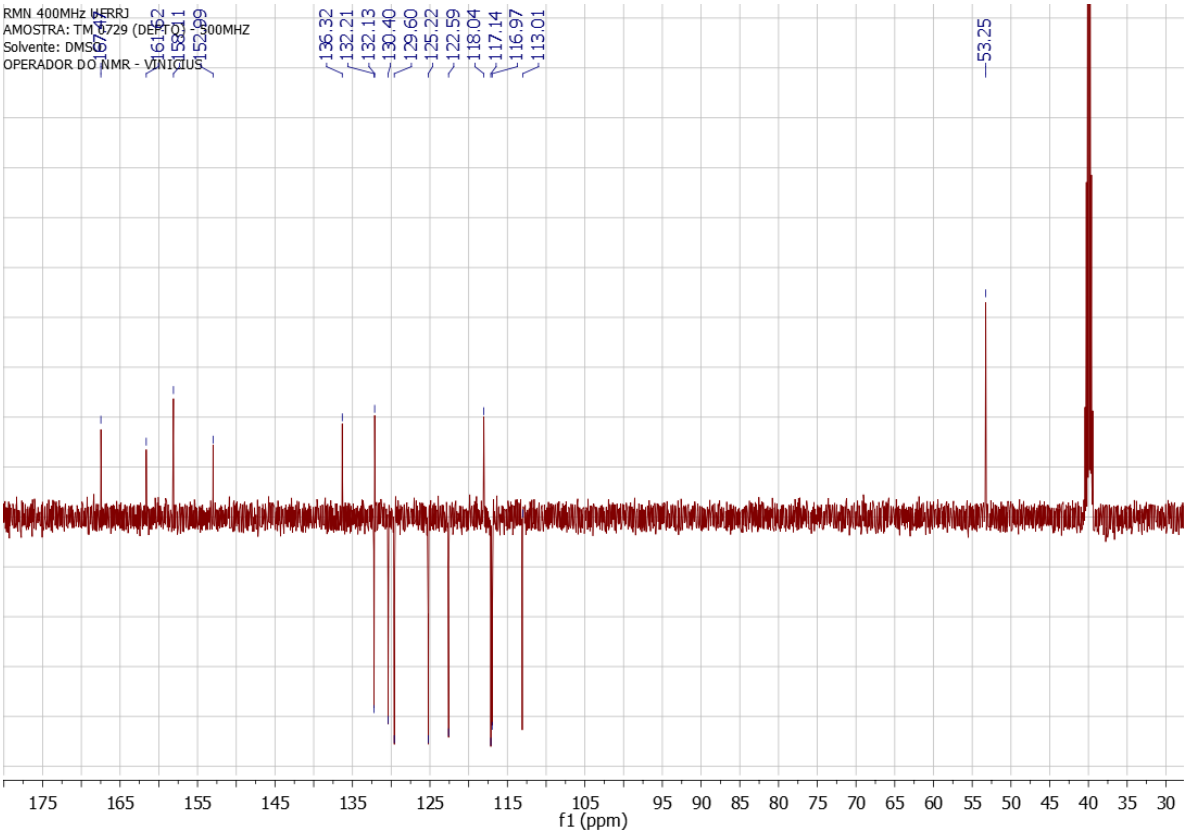

^{13}C NMR spectra of compound **216g** in DMSO.

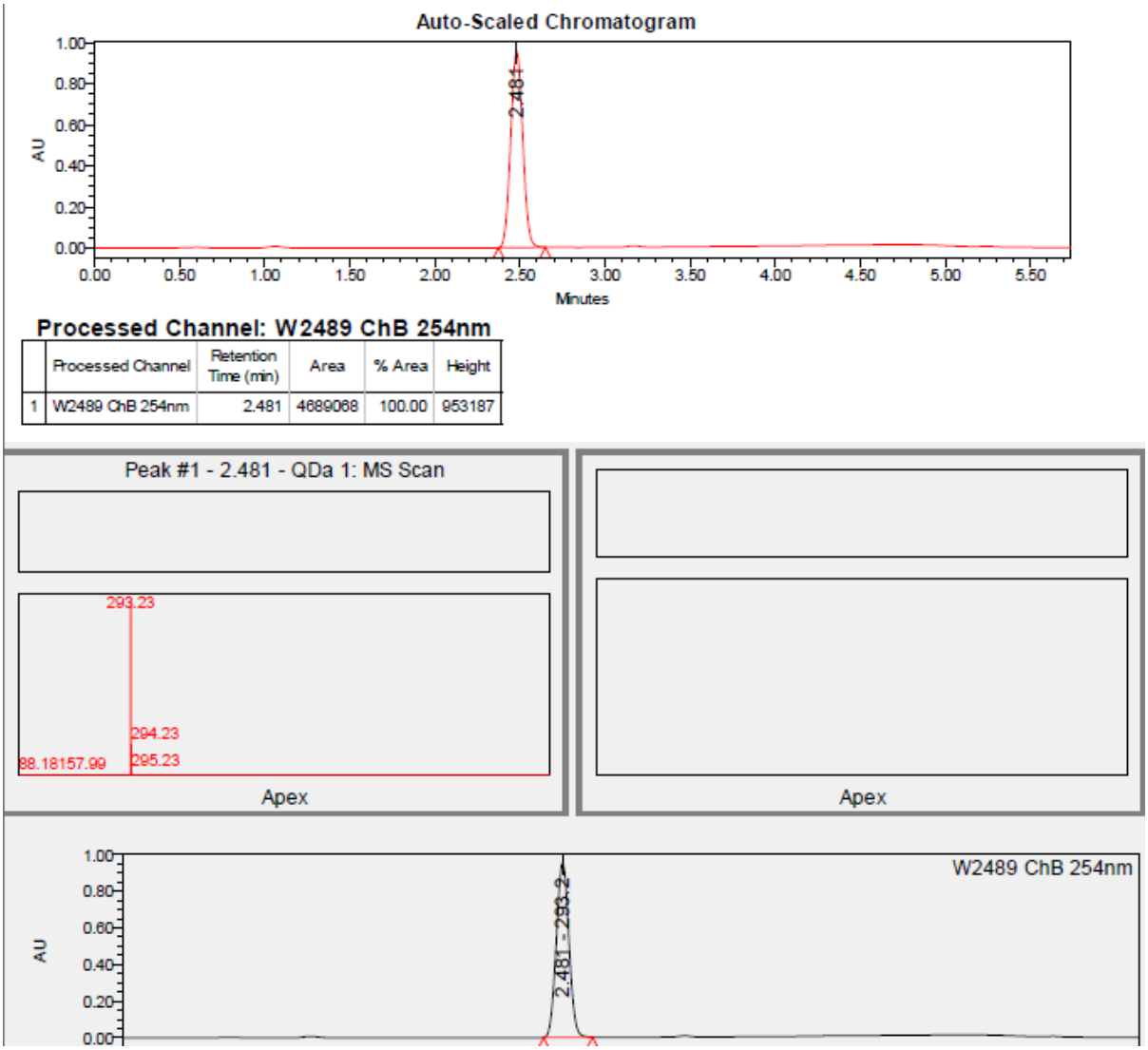

LC/MS of compound **216g**

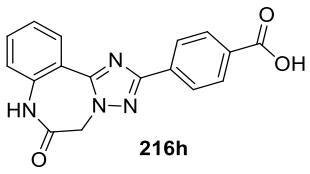

216h

Exact Mass: 320.09

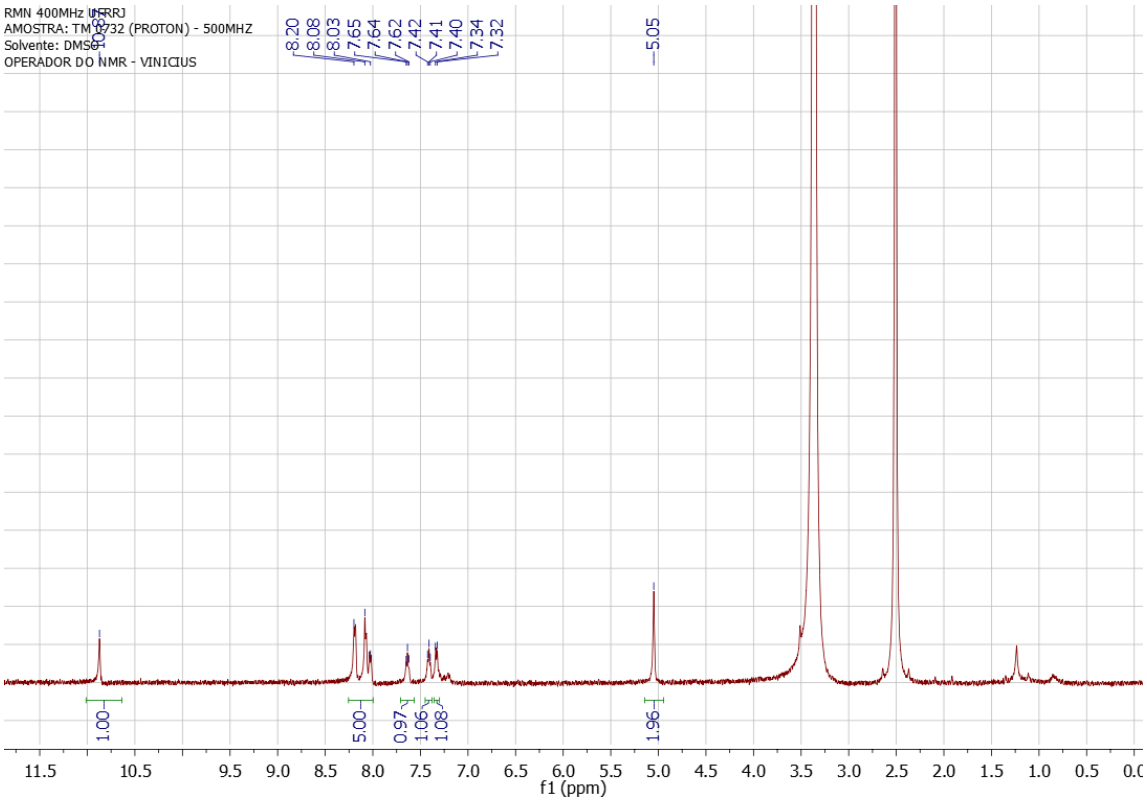

^{1}H NMR spectra of compound **216h** in DMSO.

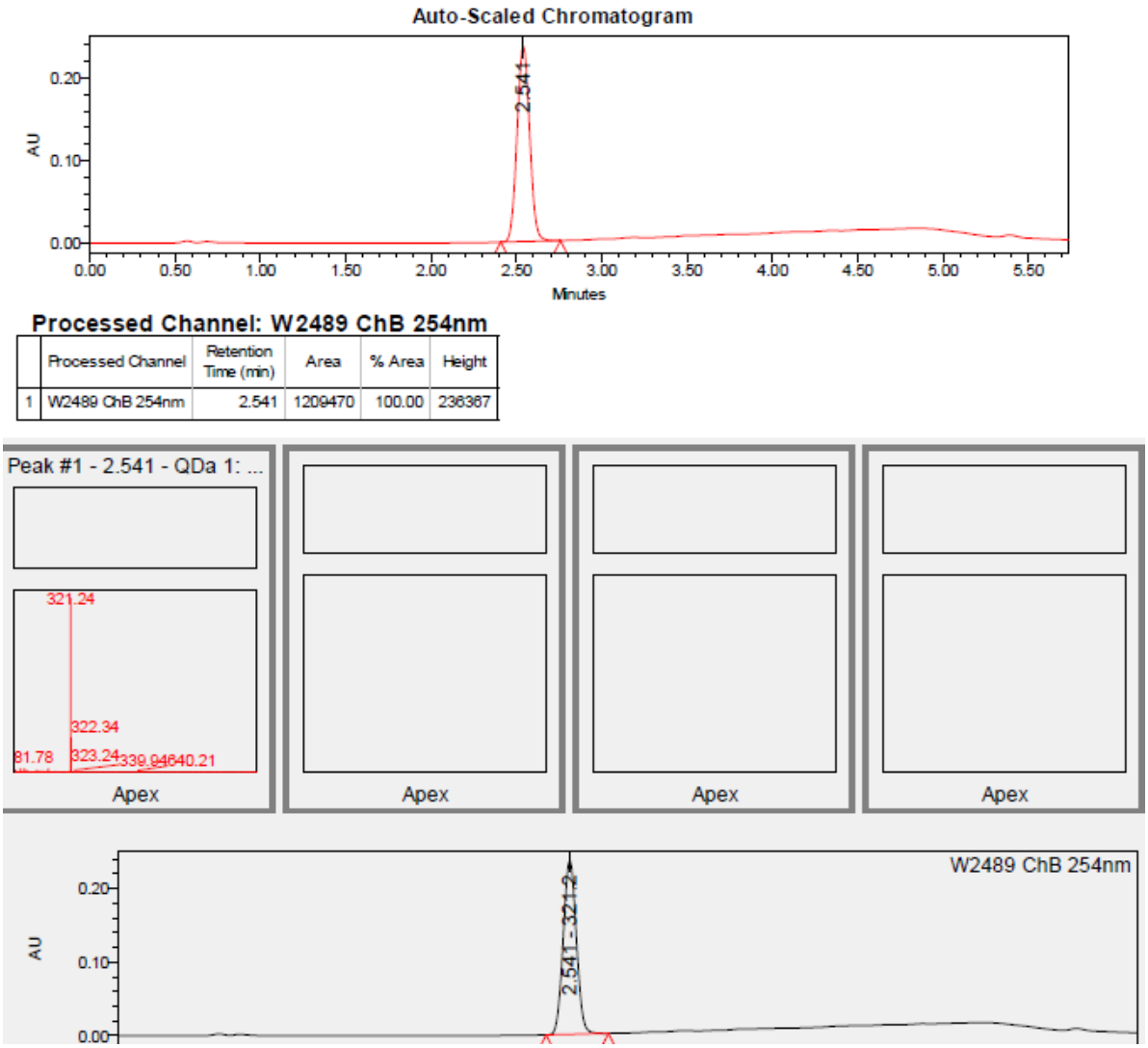

LC/MS of compound **216h**

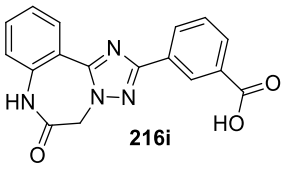

216i

Exact Mass: 320.09

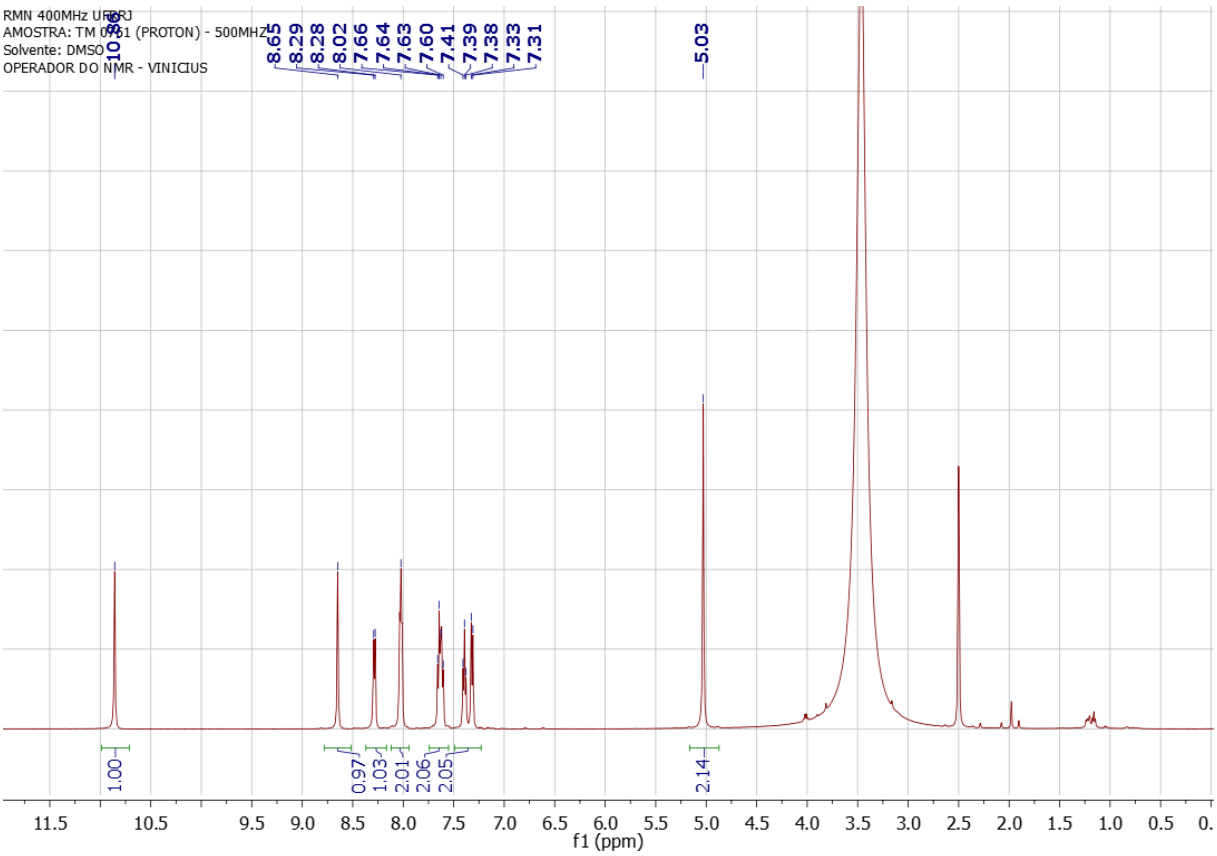

^{1}H NMR spectra of compound **216i** in DMSO.

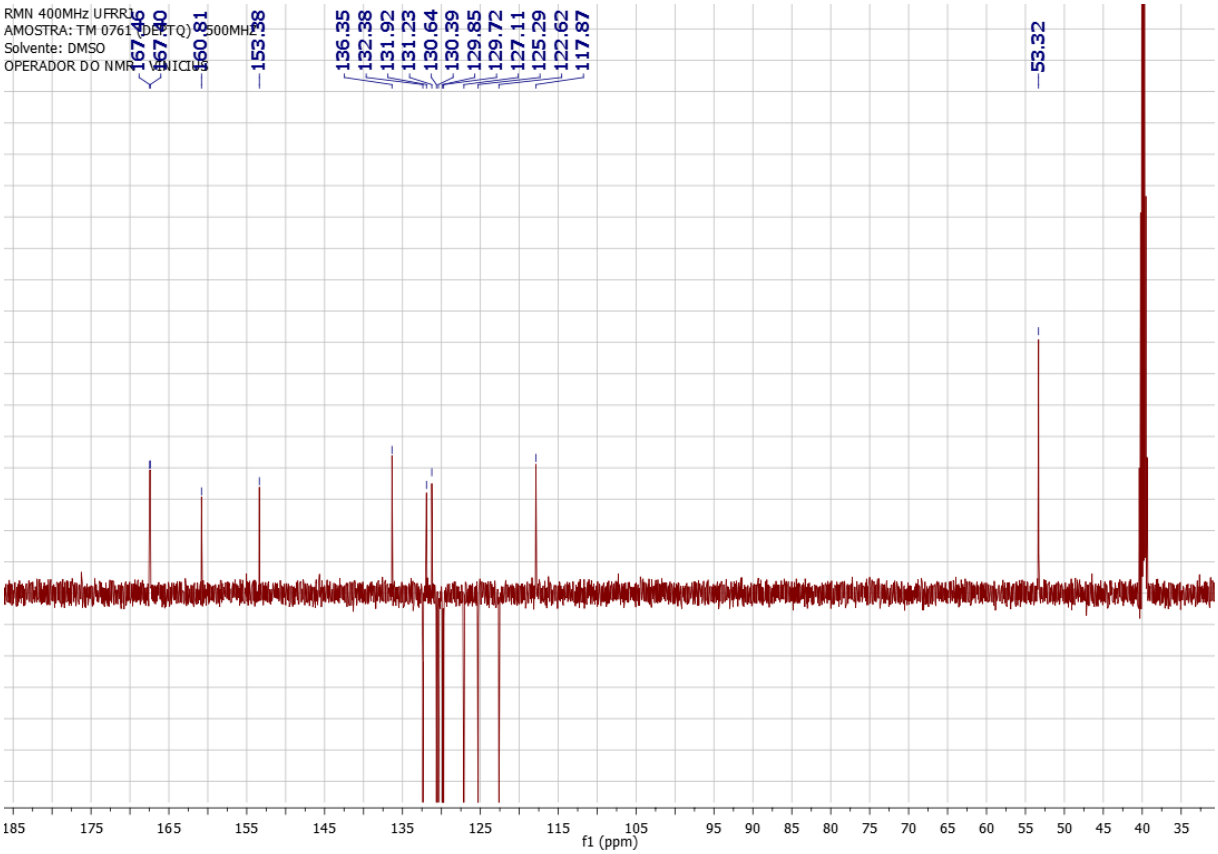

^{13}C NMR spectra of compound **216i** in DMSO.

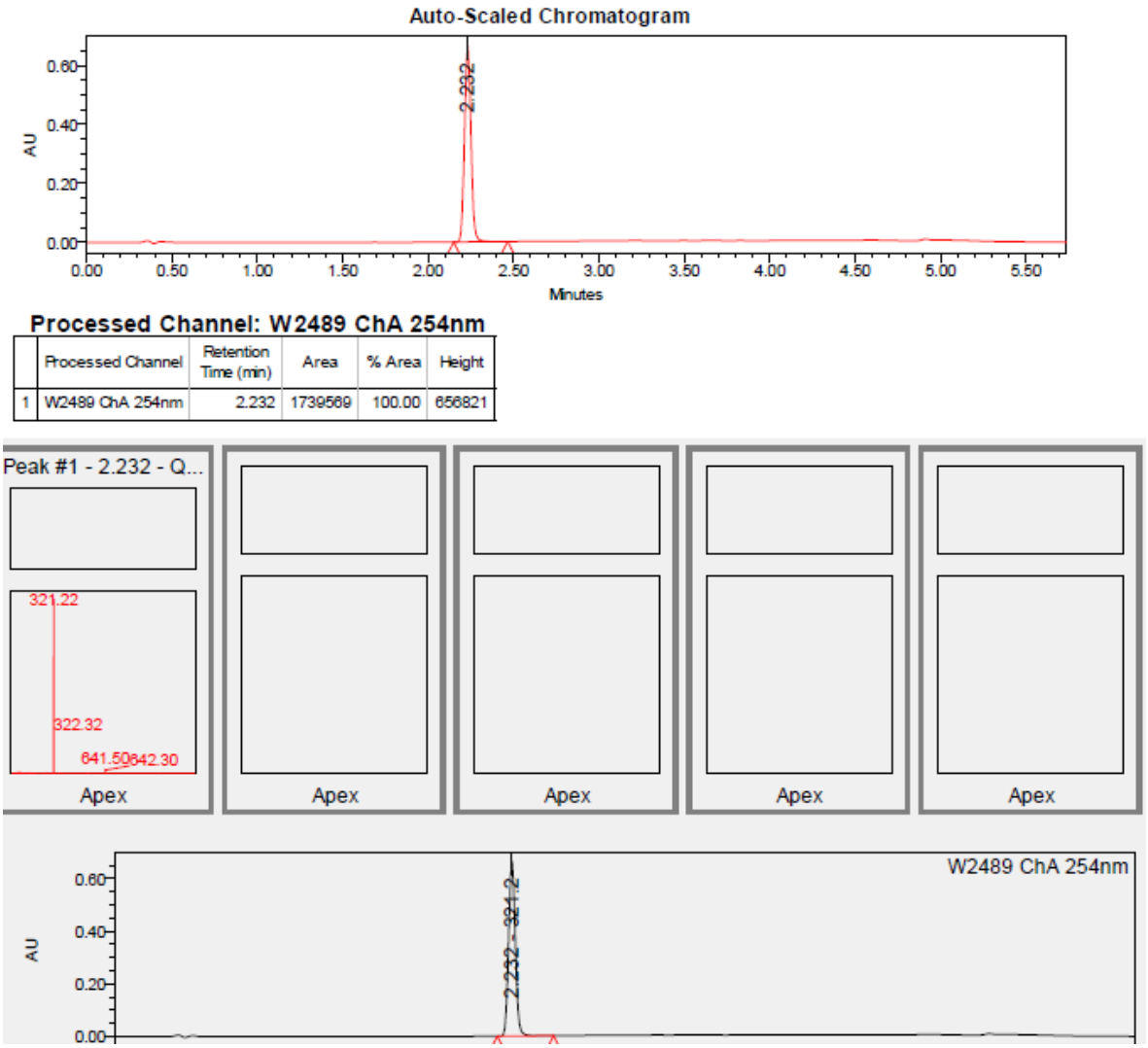

LC/MS of compound **216i**

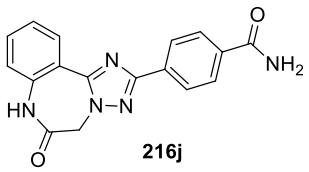

216j

Exact Mass: 319.11

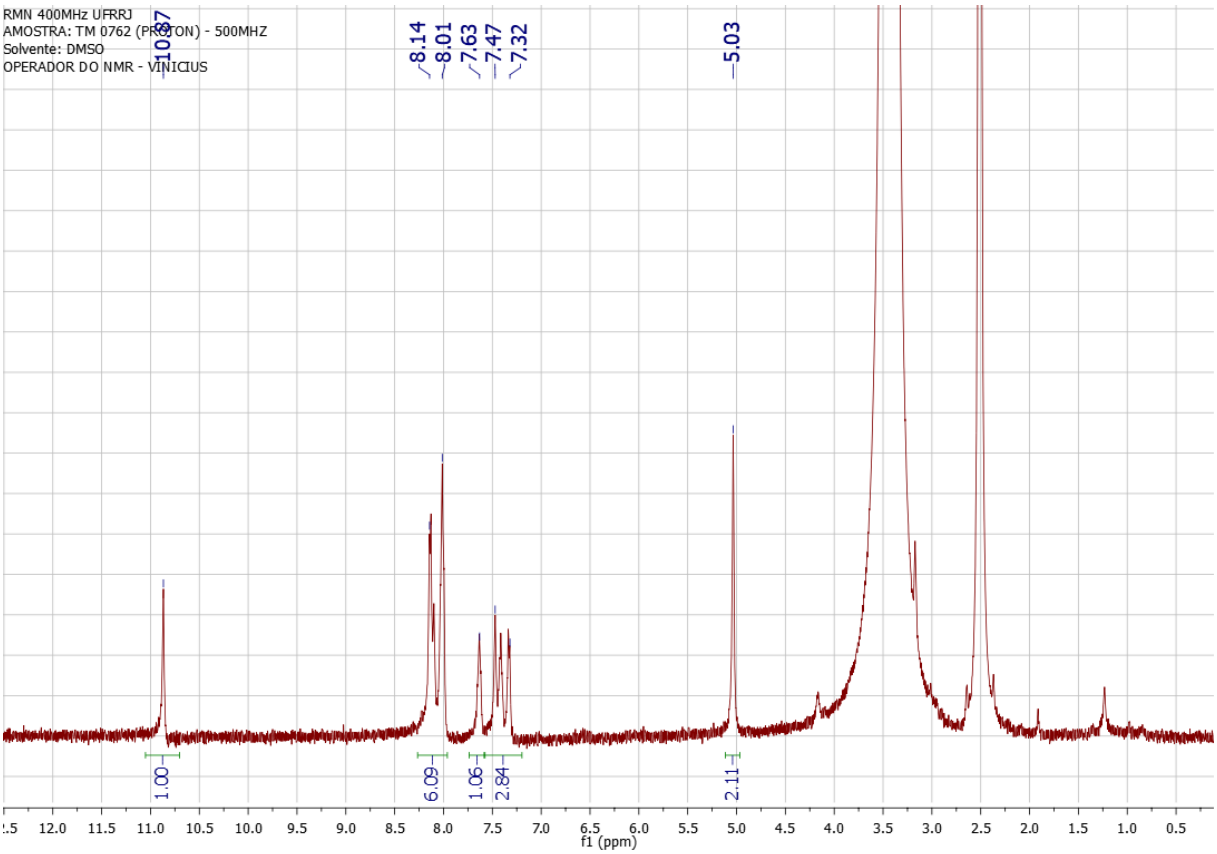

^{1}H NMR spectra of compound **216j** in DMSO.

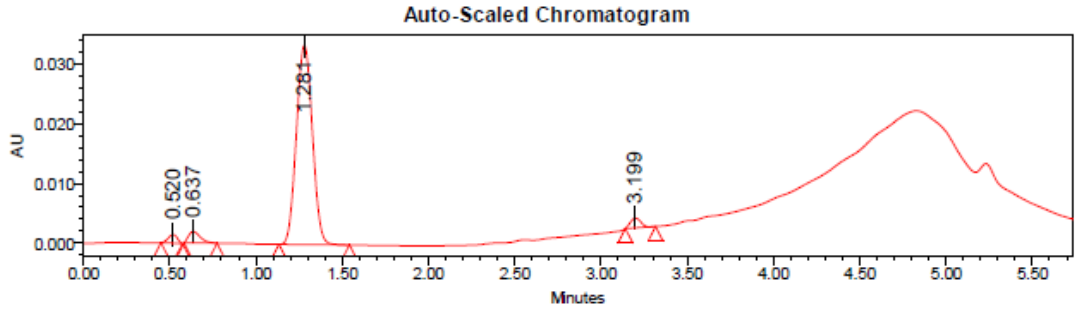

Processed Channel: W2489 ChB 254nm

	Processed Channel	Retention Time (min)	Area	% Area	Height
1	W2489 ChB 254nm	0.520	5213	2.22	1443
2	W2489 ChB 254nm	0.637	9071	3.86	1935
3	W2489 ChB 254nm	1.281	214269	91.08	33331
4	W2489 ChB 254nm	3.199	6706	2.85	1633

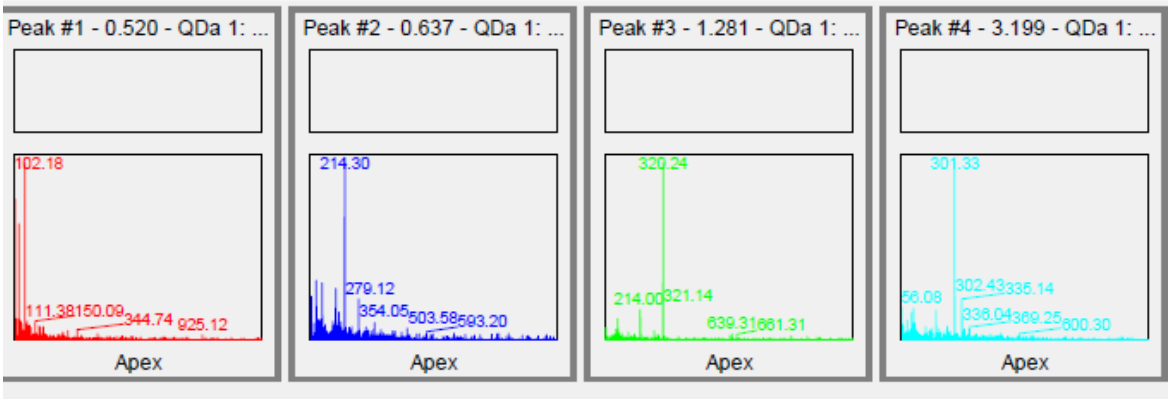

LC/MS of compound **216j**

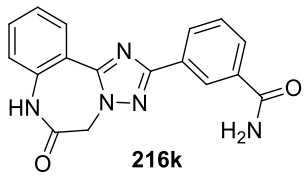

216k

Exact Mass: 319.11

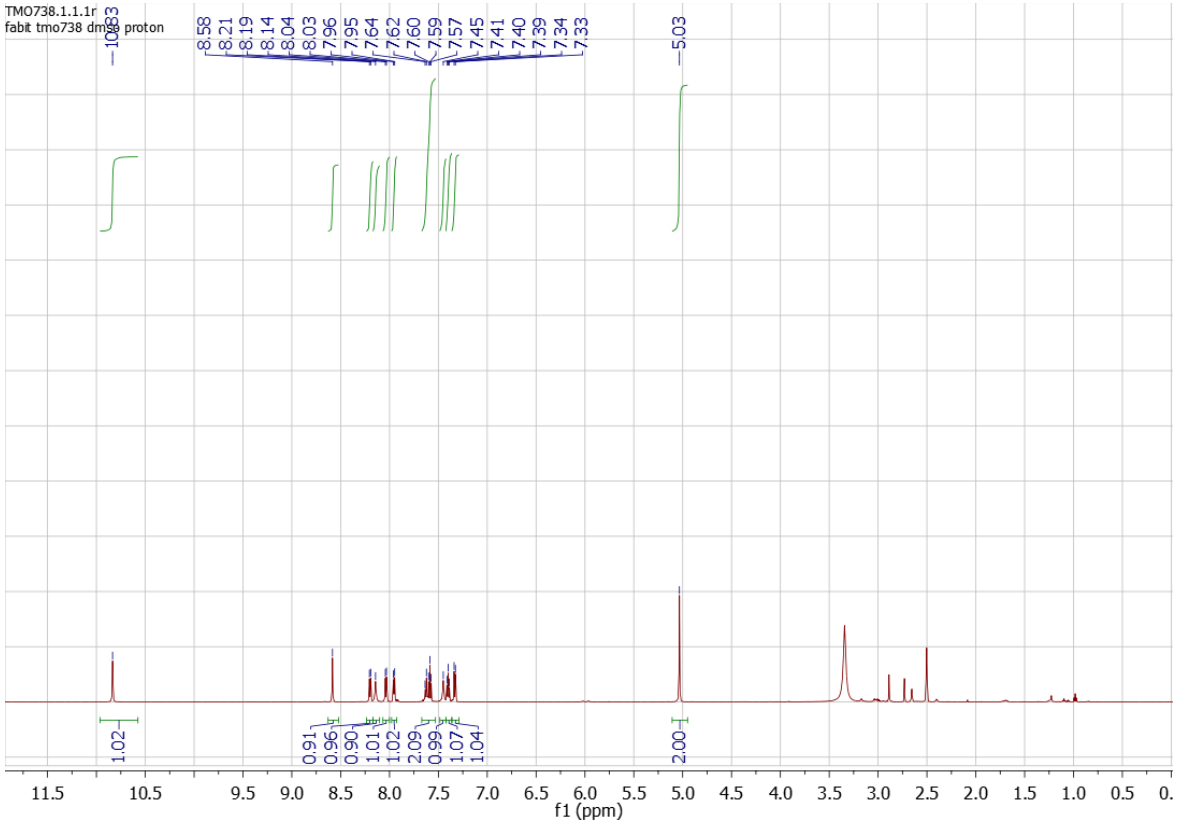

^{1}H NMR spectra of compound **216k** in DMSO.

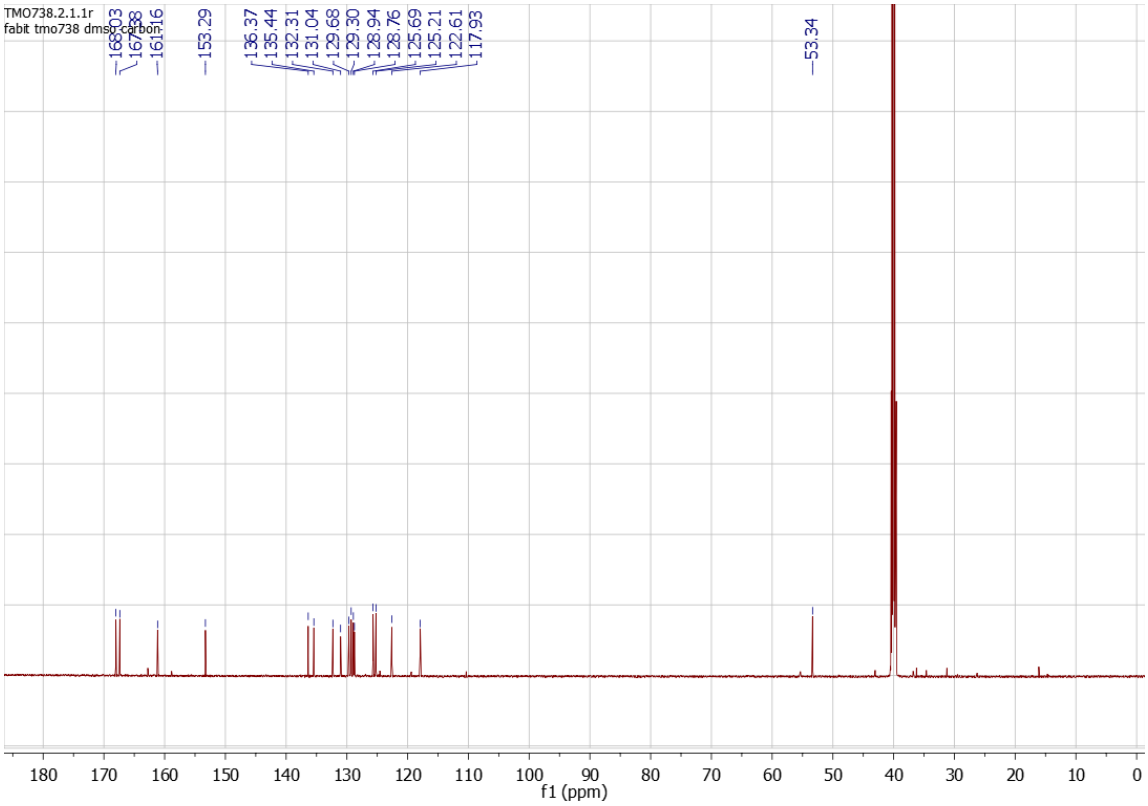

^{13}C NMR spectra of compound **216k** in DMSO.

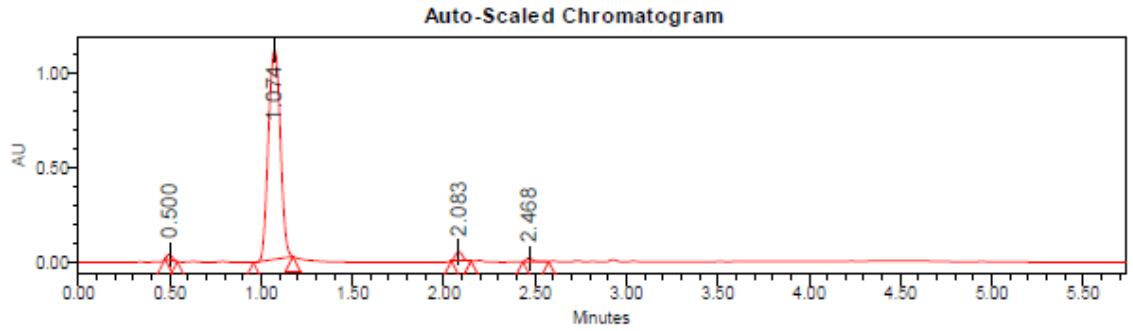

Peak Results

	Name	RT	Area	Height	% Area
1		0.500	58270	28778	1.10
2		1.074	5049518	1116720	95.51
3		2.083	133683	49639	2.53
4		2.468	45299	18683	0.86

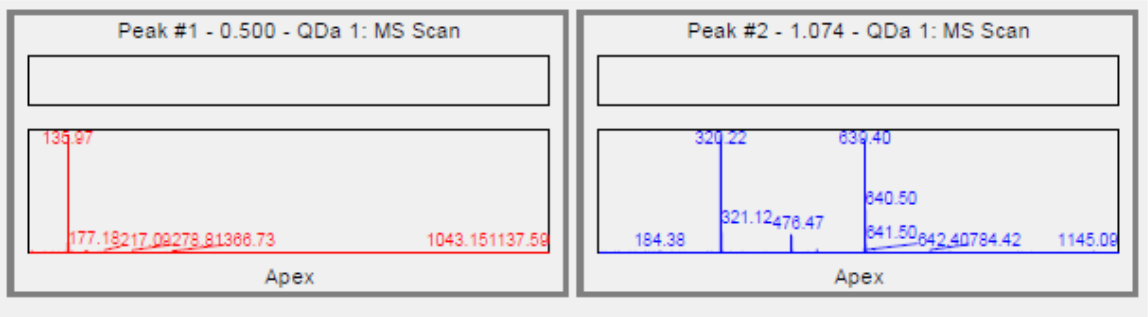

LC/MS of compound **216k**

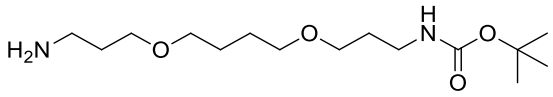

328

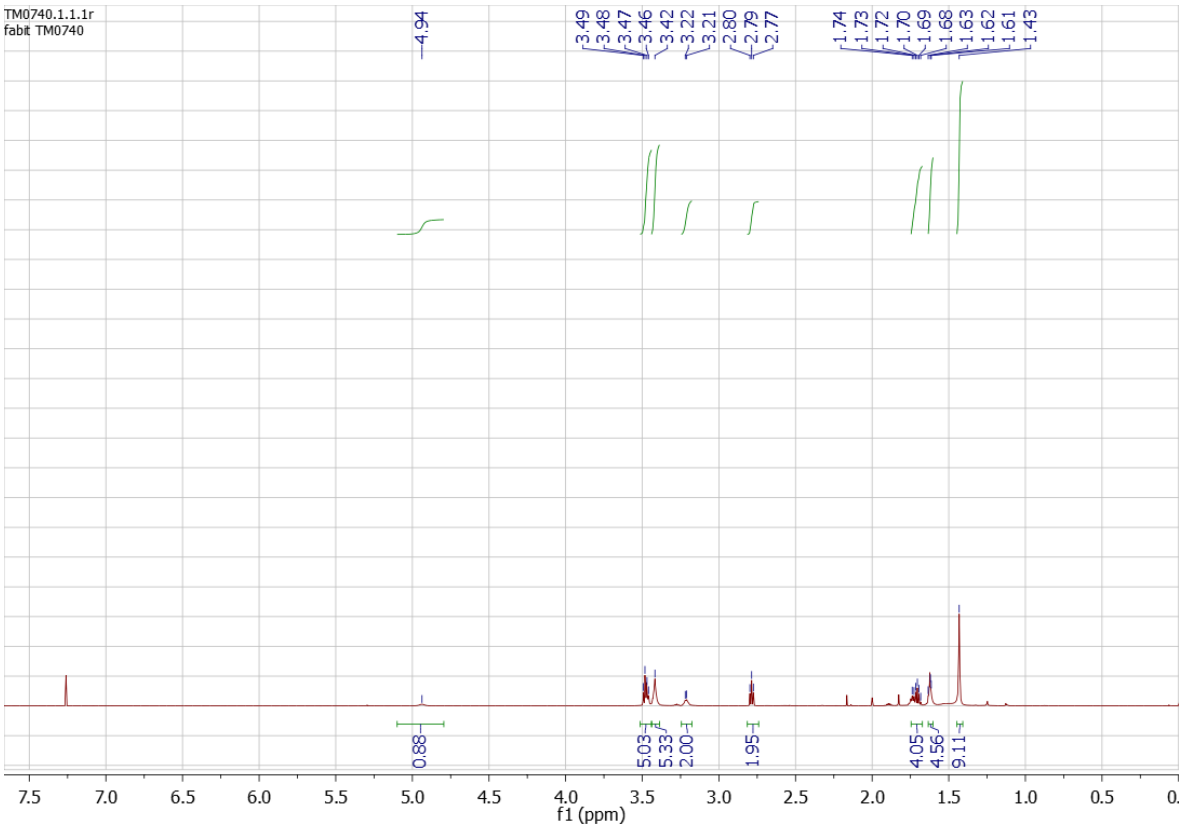

^{1}H NMR spectra of compound **328** in $CDCl_3$.

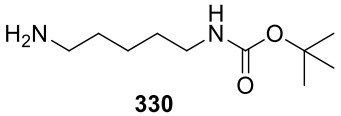

330

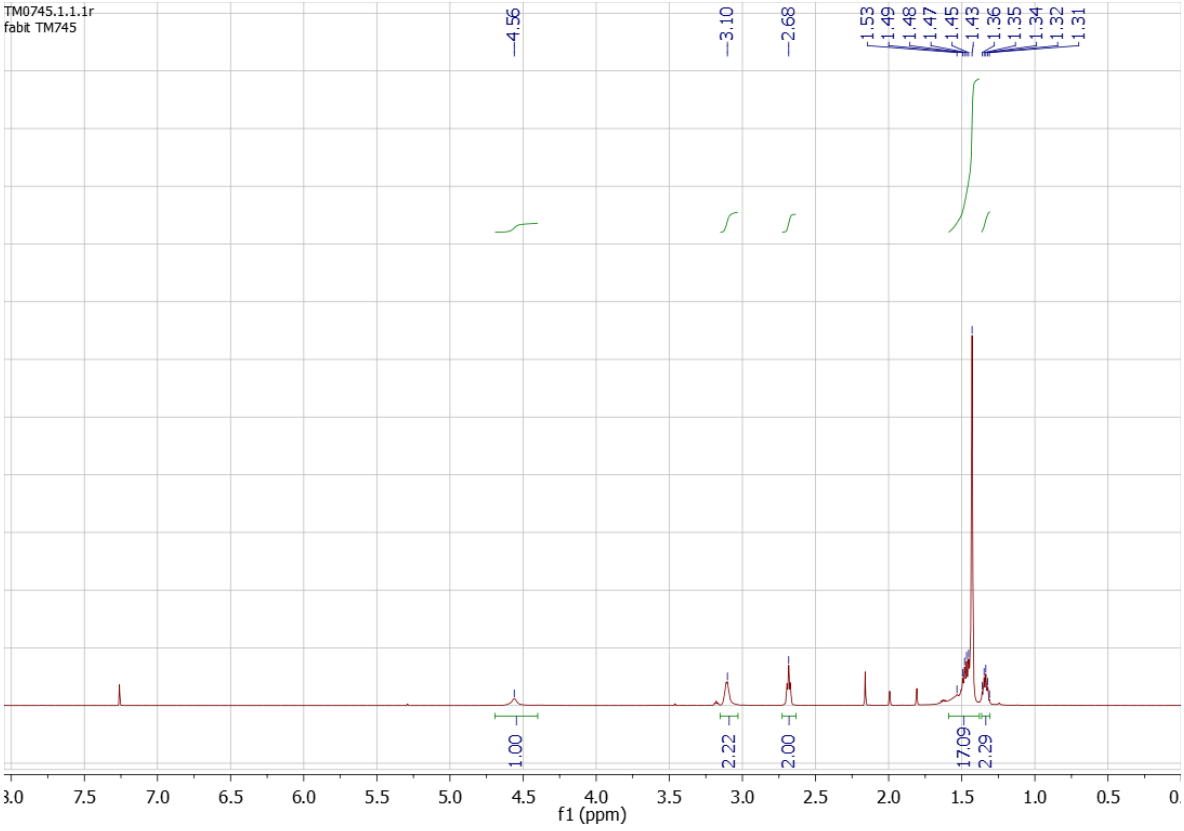

^{1}H NMR spectra of compound **330** in $CDCl_3$.

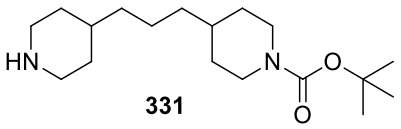

331

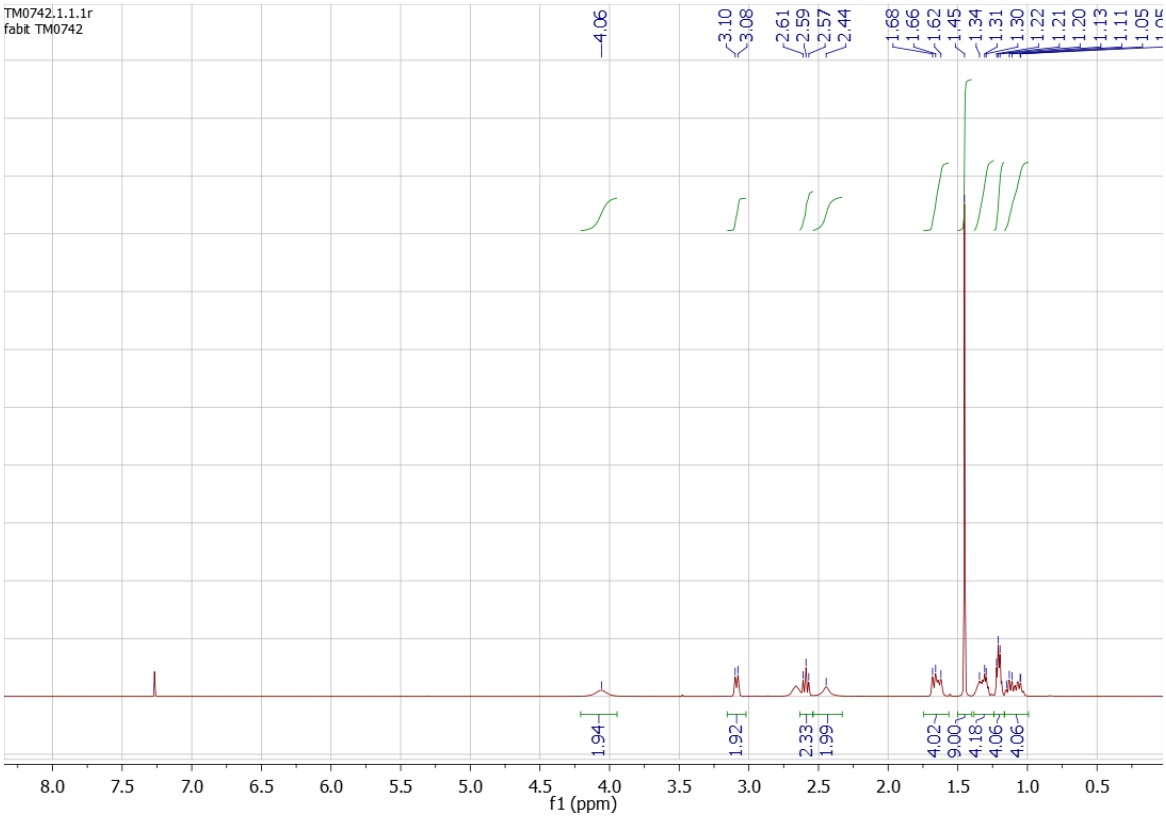

^{1}H NMR spectra of compound **331** in $CDCl_3$.

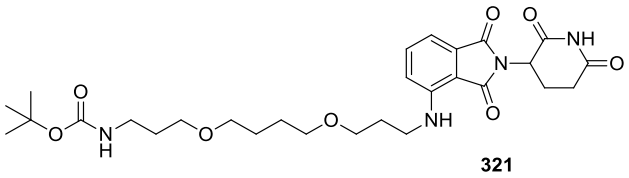

321

Exact Mass: 560.28

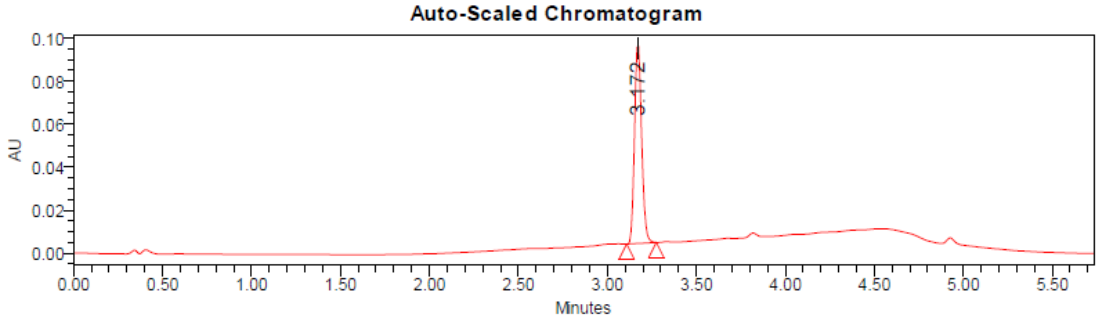

Peak Results

	Name	RT	Area	Height	% Area
1		3.172	257341	91972	100.00

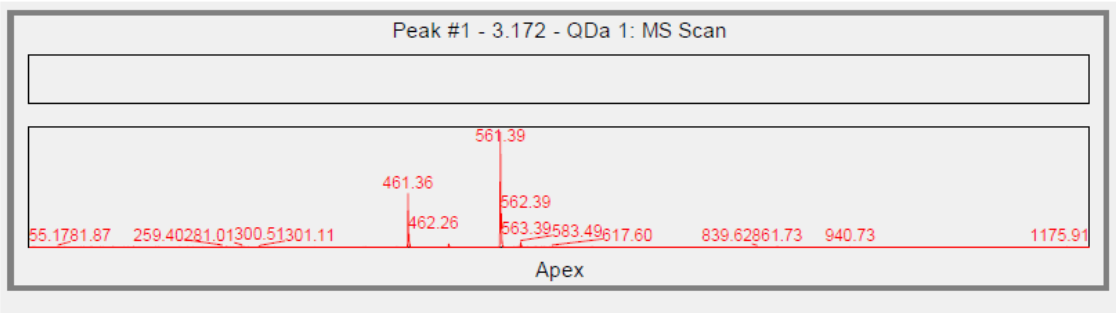

LC/MS of compound **321**

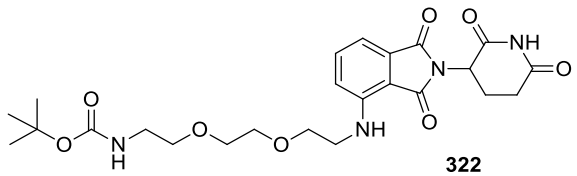

322

Exact Mass: 504.22

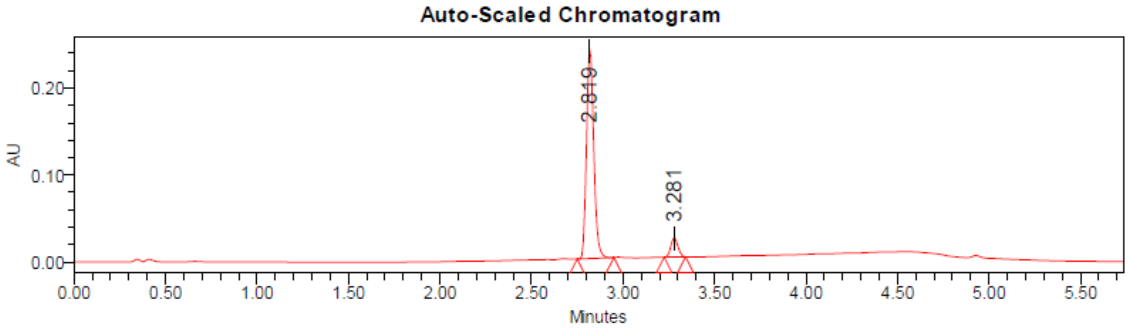

Peak Results

	Name	RT	Area	Height	% Area
1		2.819	661695	241026	91.84
2		3.281	58814	21632	8.16

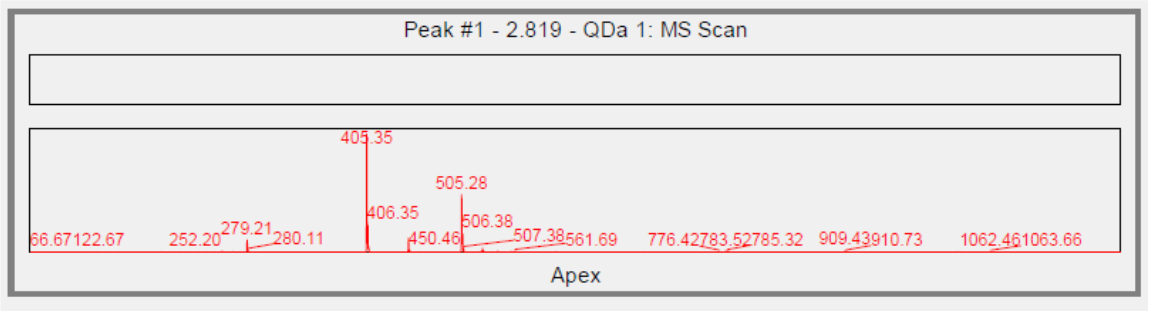

LC/MS of compound **322**

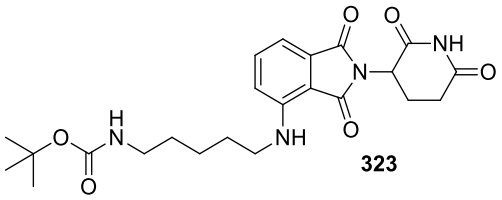

323

Exact Mass: 458.22

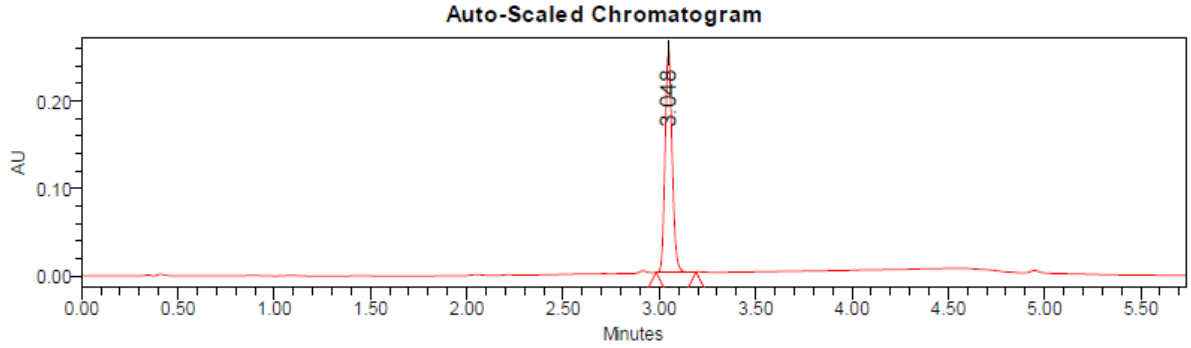

Peak Results

	Name	RT	Area	Height	% Area
1		3.048	641817	252184	100.00

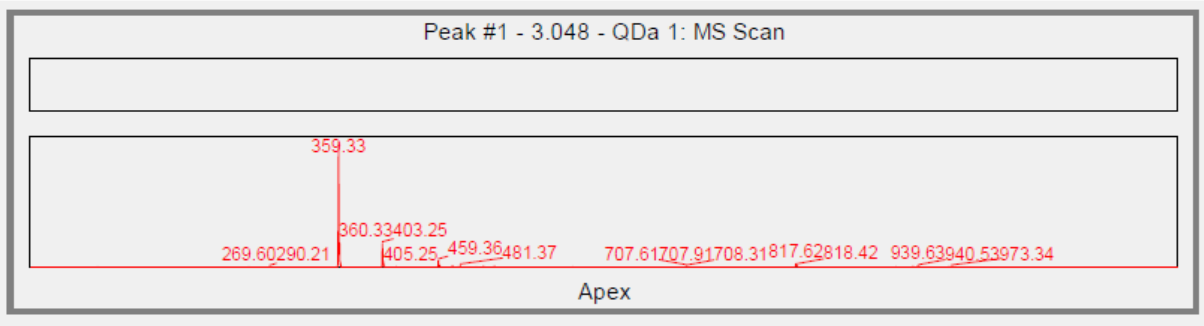

LC/MS of compound **323**

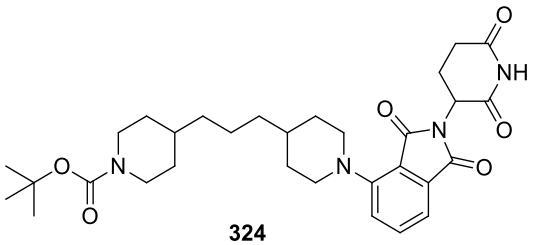

324

Exact Mass: 566.31

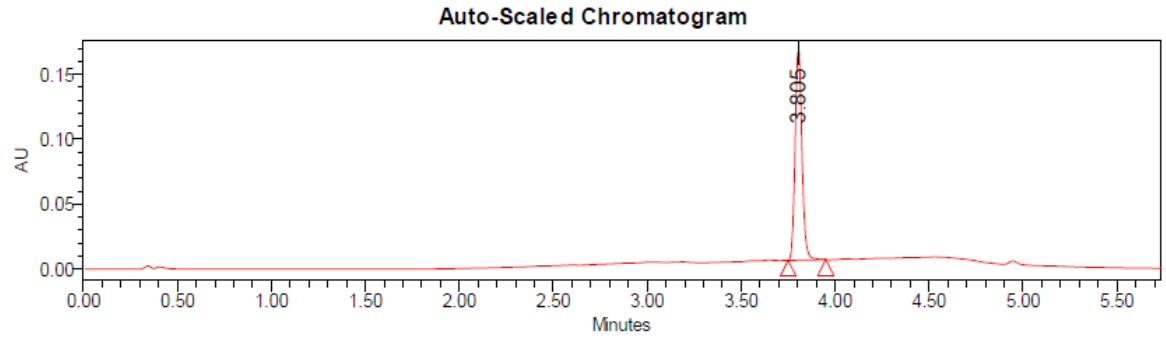

Peak Results

	Name	RT	Area	Height	% Area
1		3.805	411274	161072	100.00

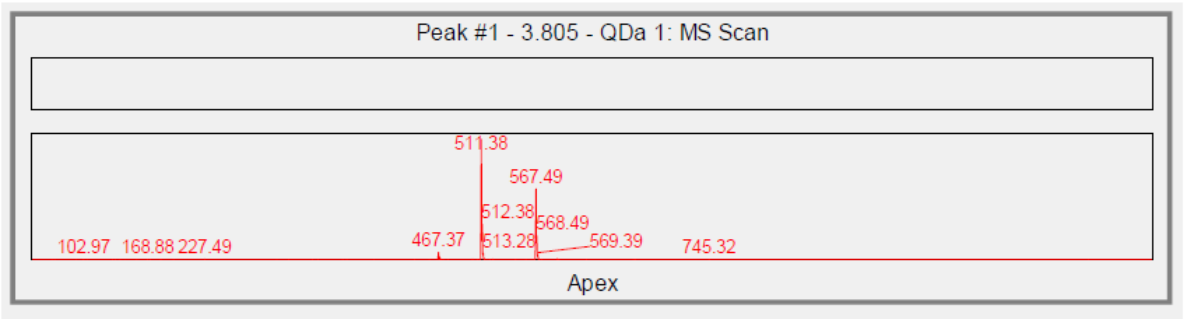

LC/MS of compound **324**

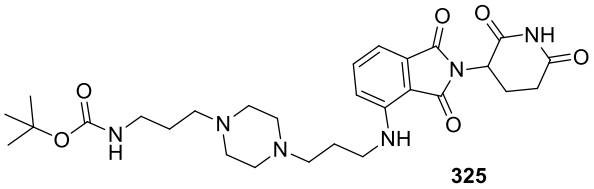

325

Exact Mass: 556.30

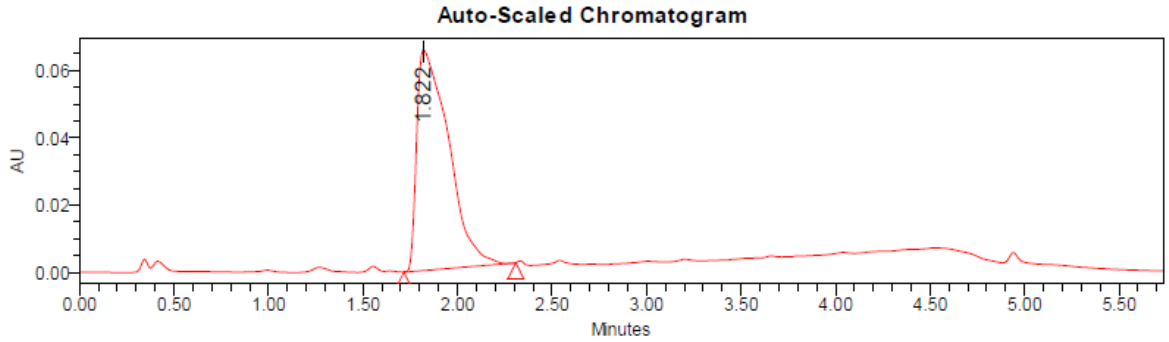

Peak Results

	Name	RT	Area	Height	% Area
1		1.822	764564	66035	100.00

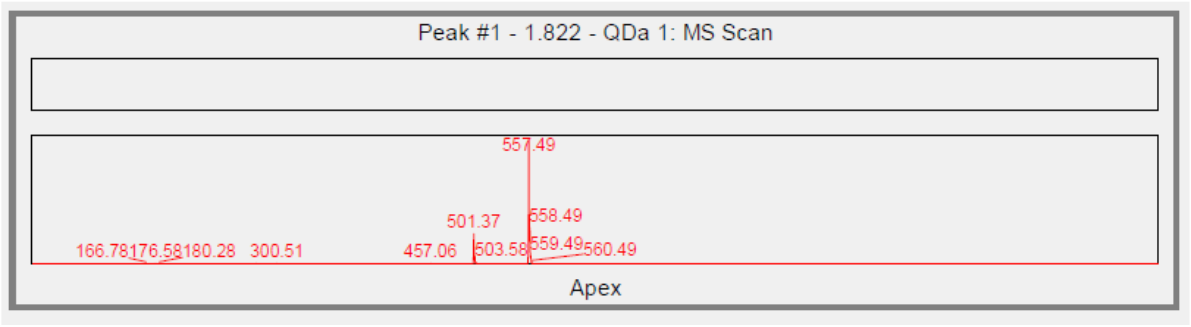

LC/MS of compound **325**

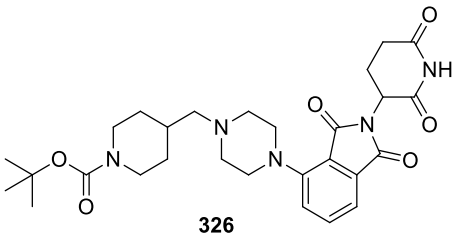

326

Exact Mass: 539.27

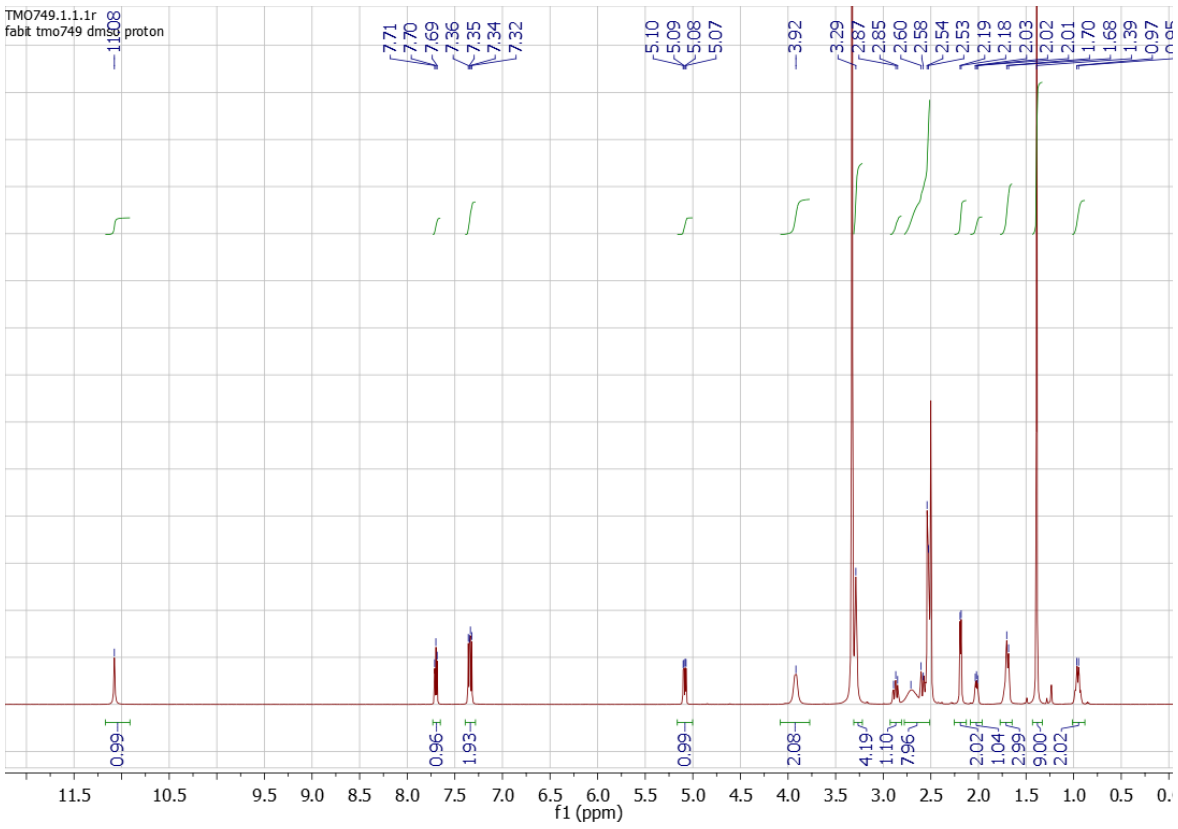

^{1}H NMR spectra of compound **326** in DMSO.

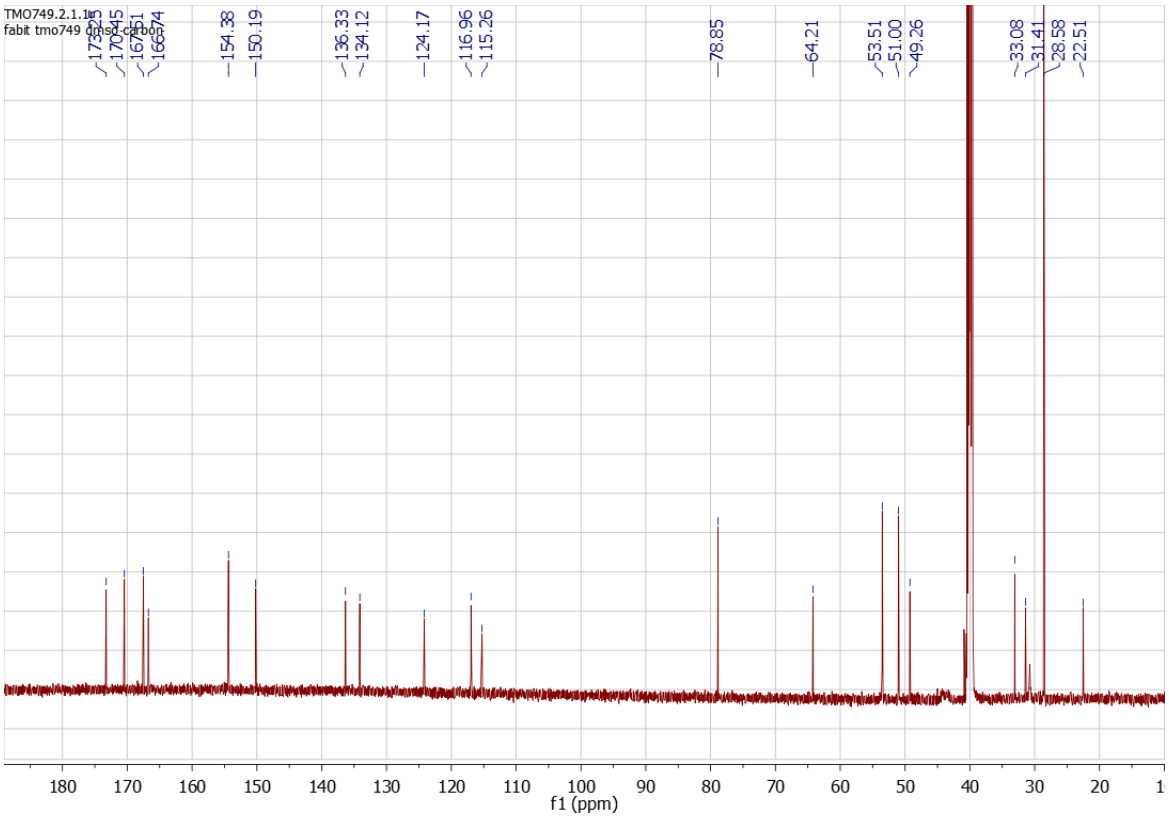

^{13}C NMR spectra of compound **326** in DMSO.

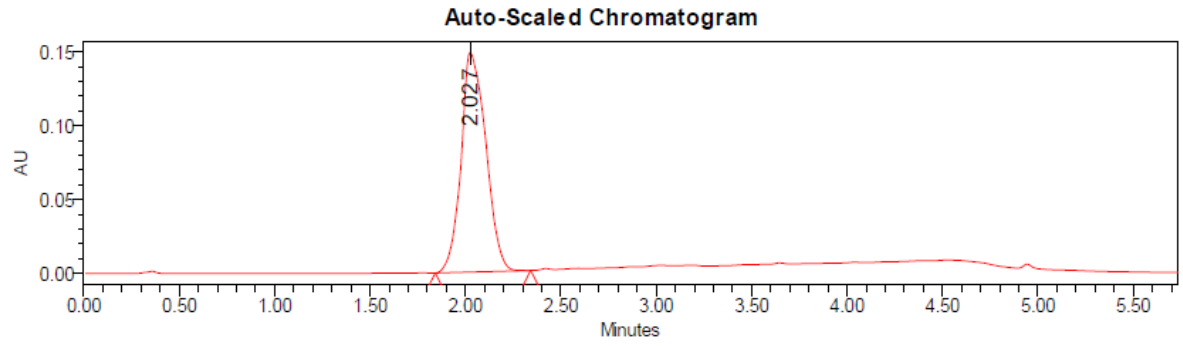

Peak Results

	Name	RT	Area	Height	% Area
1		2.027	1343561	148997	100.00

LC/MS of compound **326**

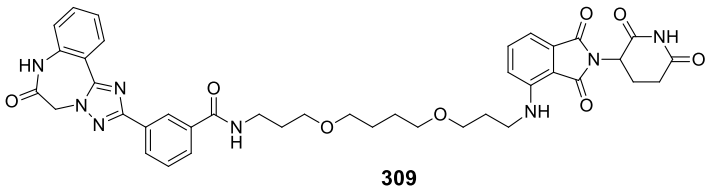

309

Exact Mass: 762.31

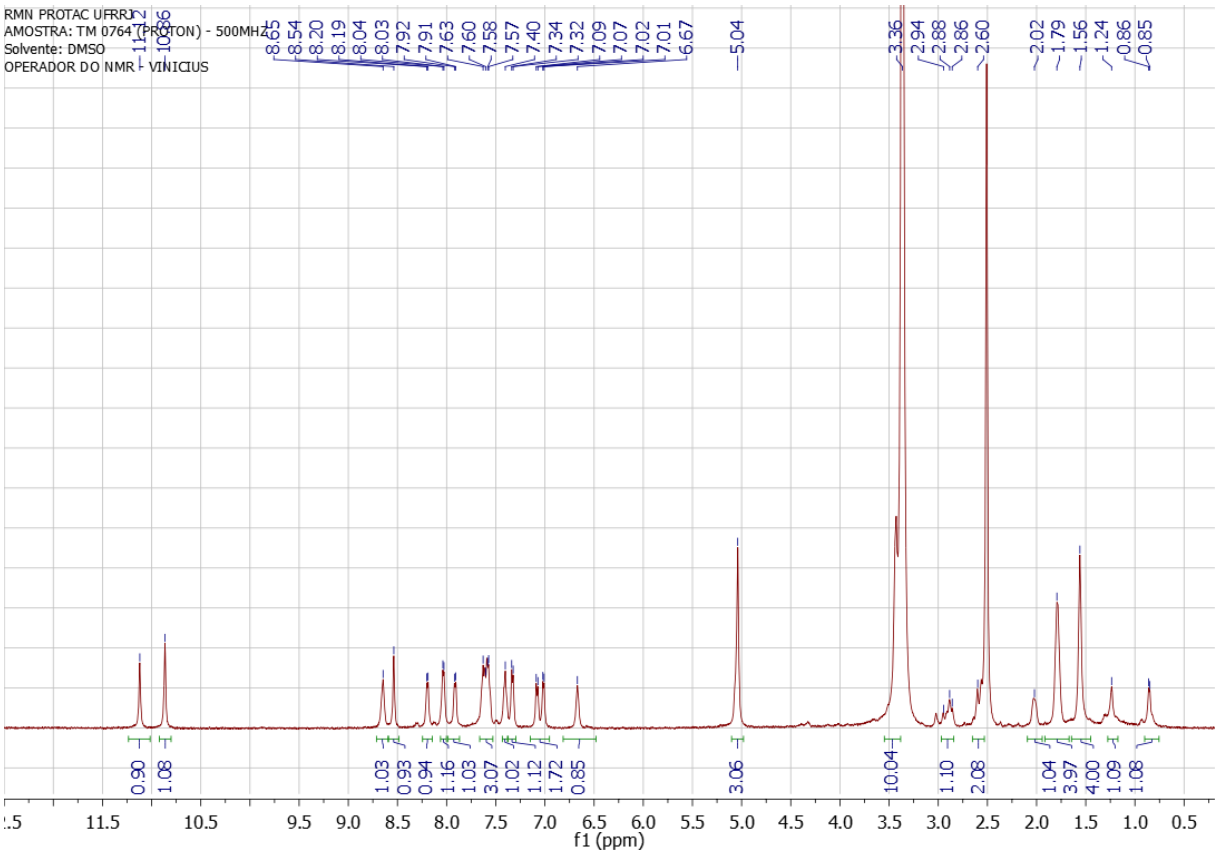

^{1}H NMR spectra of compound **309** in DMSO.

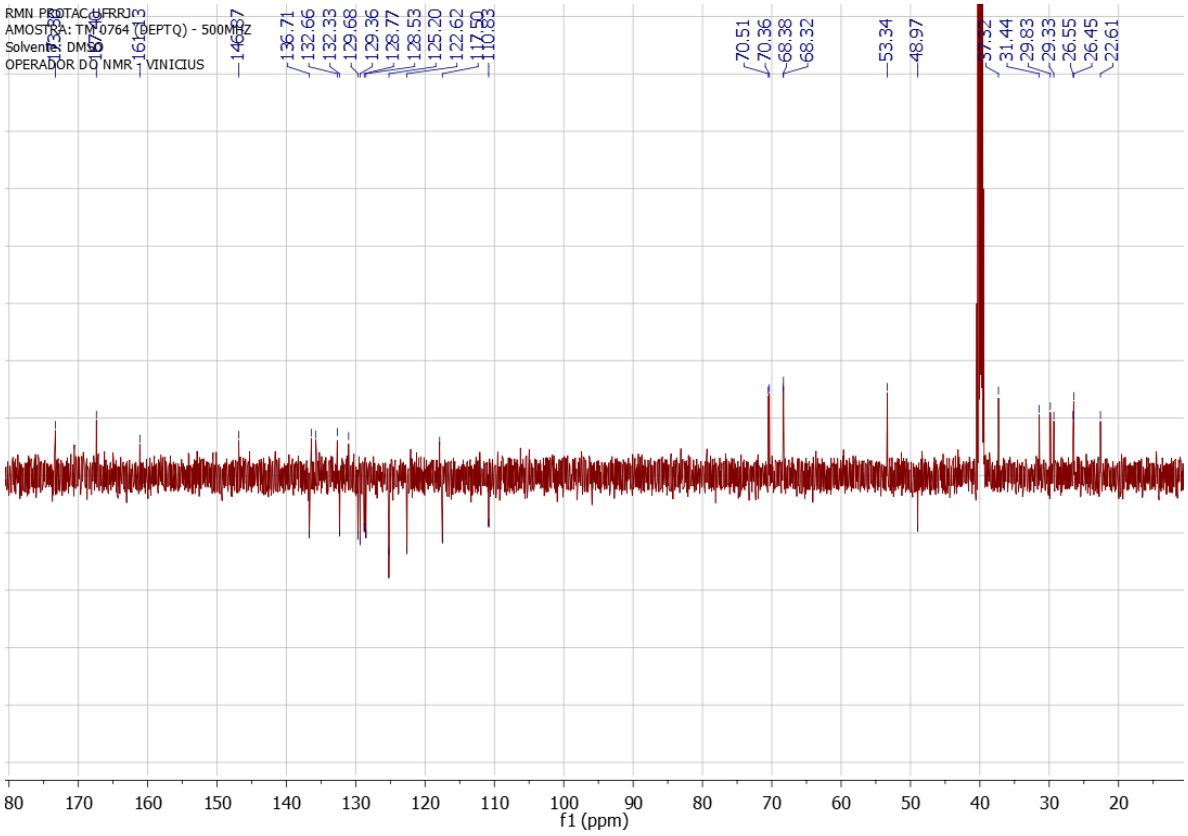

^{13}C NMR spectra of compound **309** in DMSO.

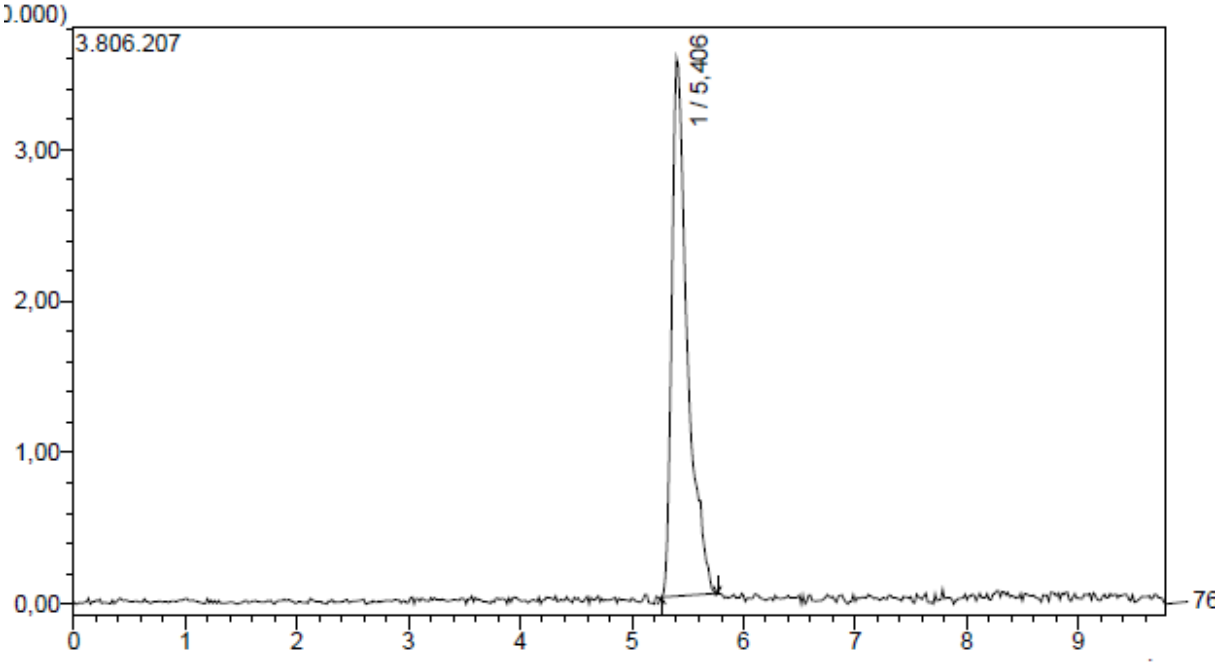

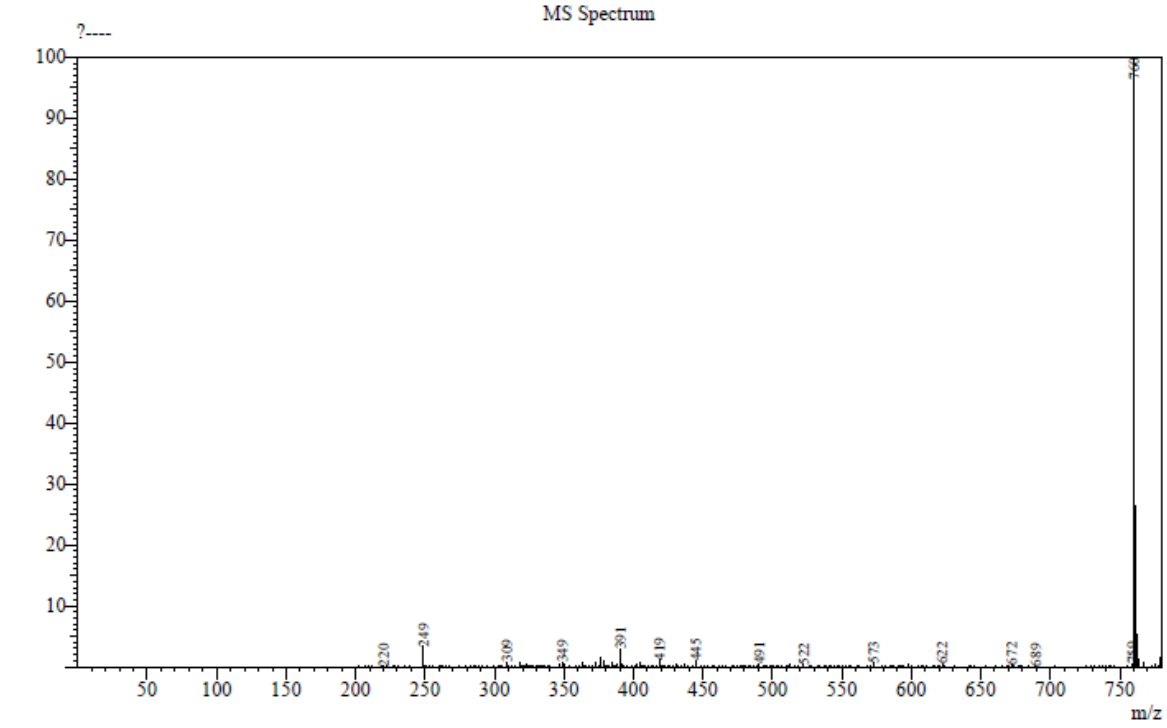

LC/MS of compound **309**.

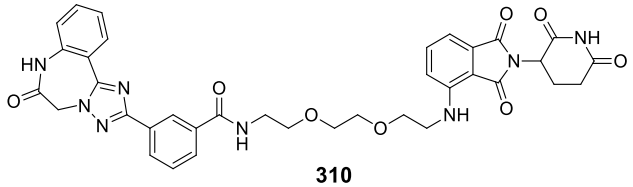

310

Exact Mass: 706.25

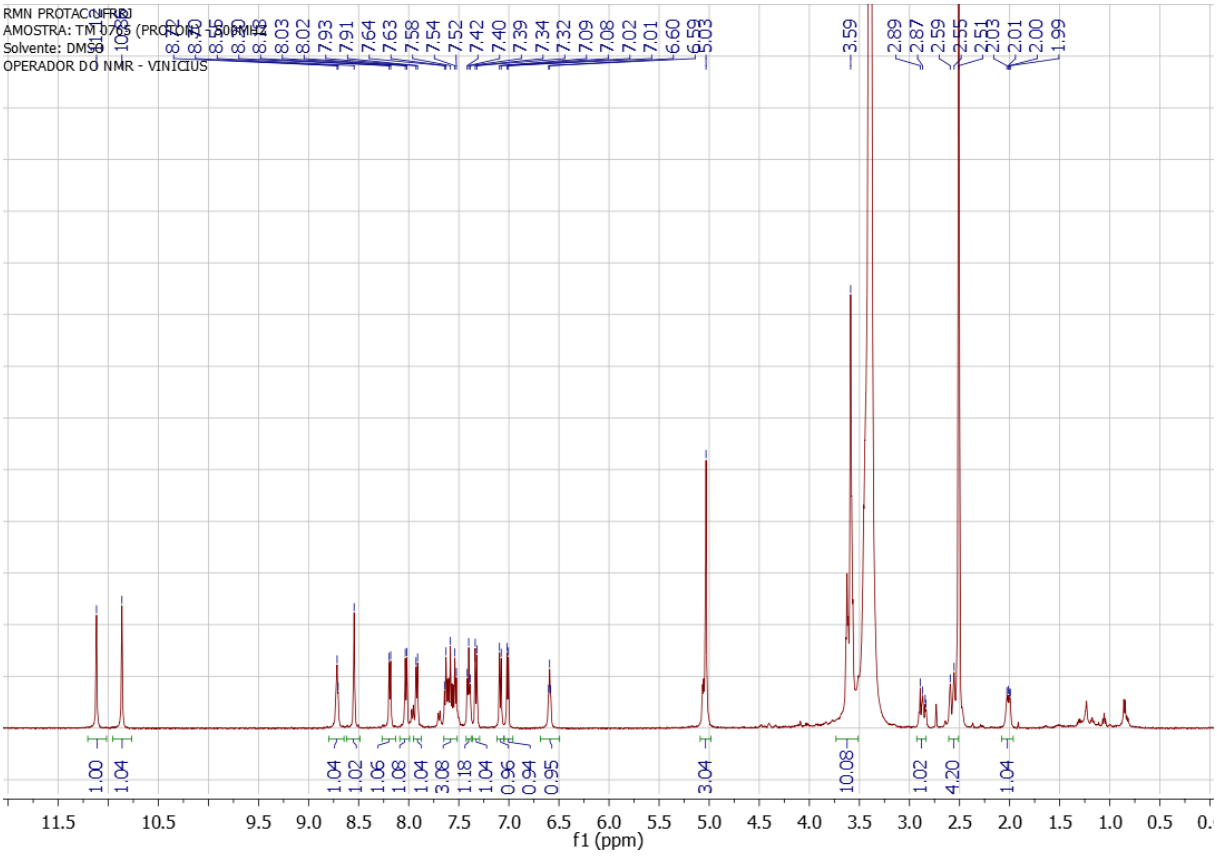

^{1}H NMR spectra of compound **310** in DMSO.

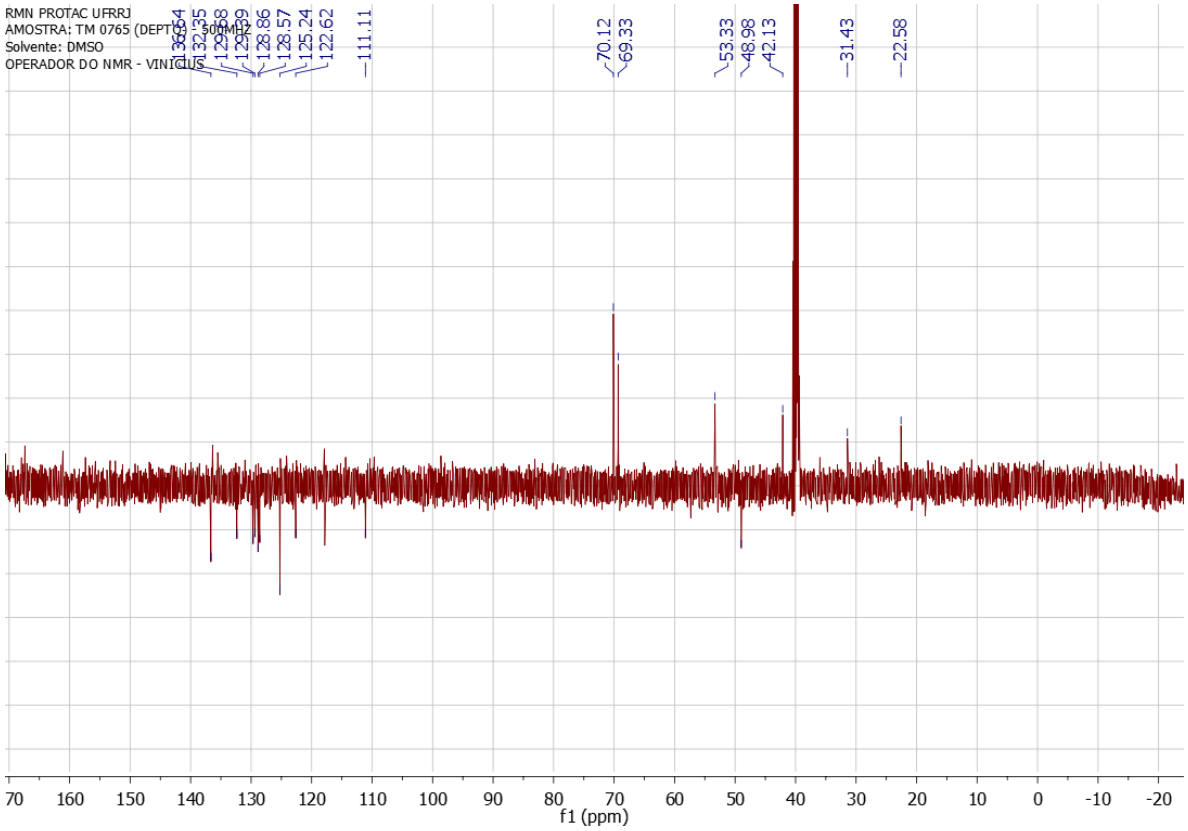

^{13}C NMR spectra of compound **310** in DMSO.

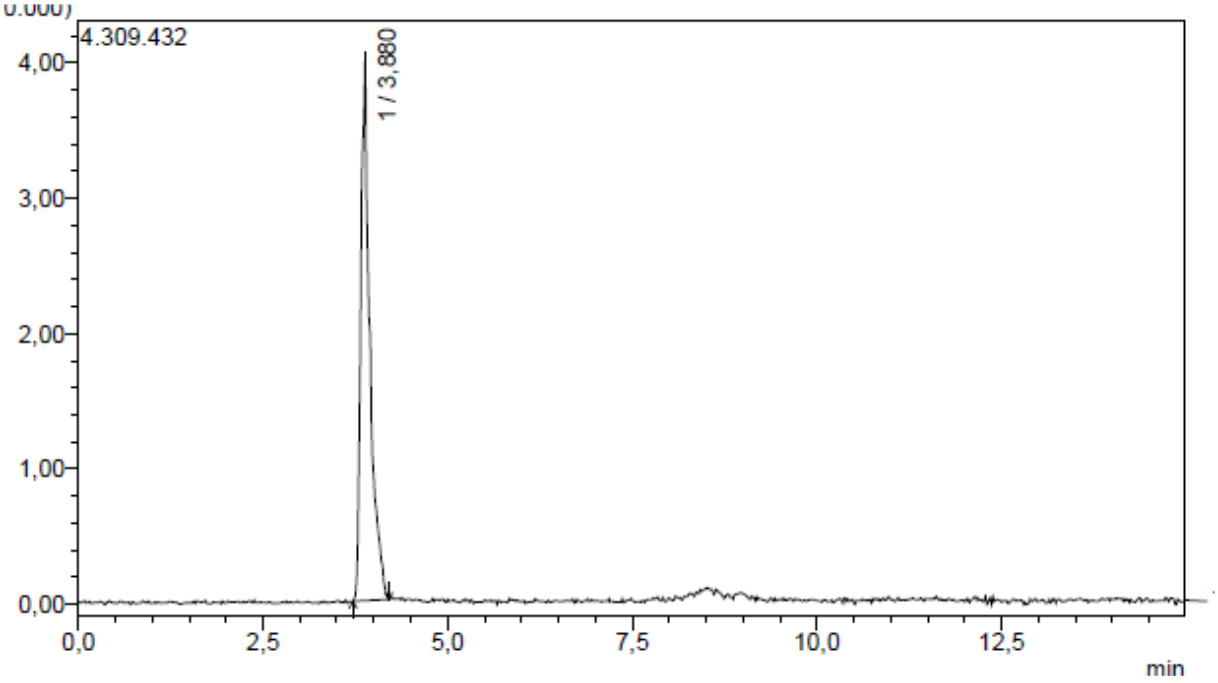

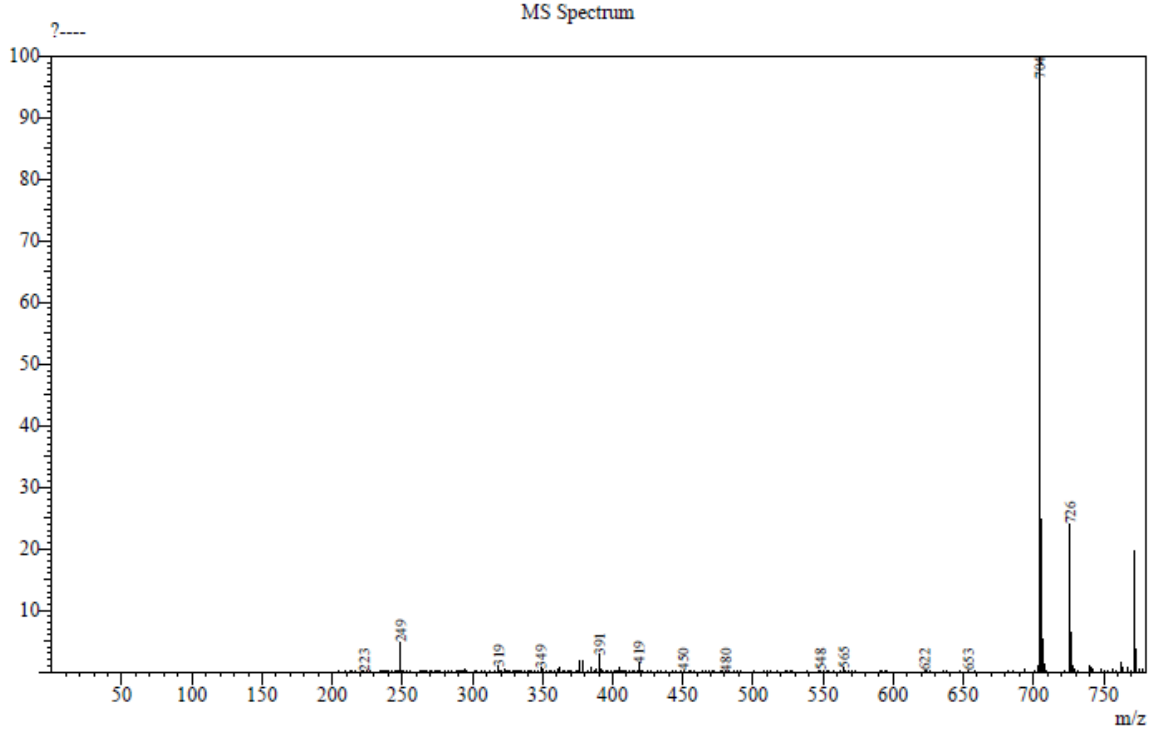

LC/MS of compound **310**.

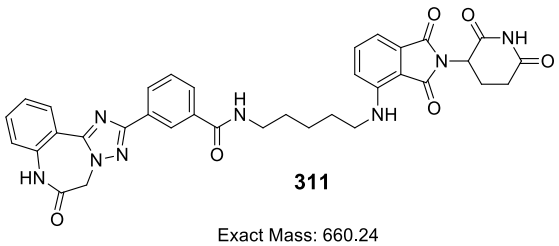

311

Exact Mass: 660.24

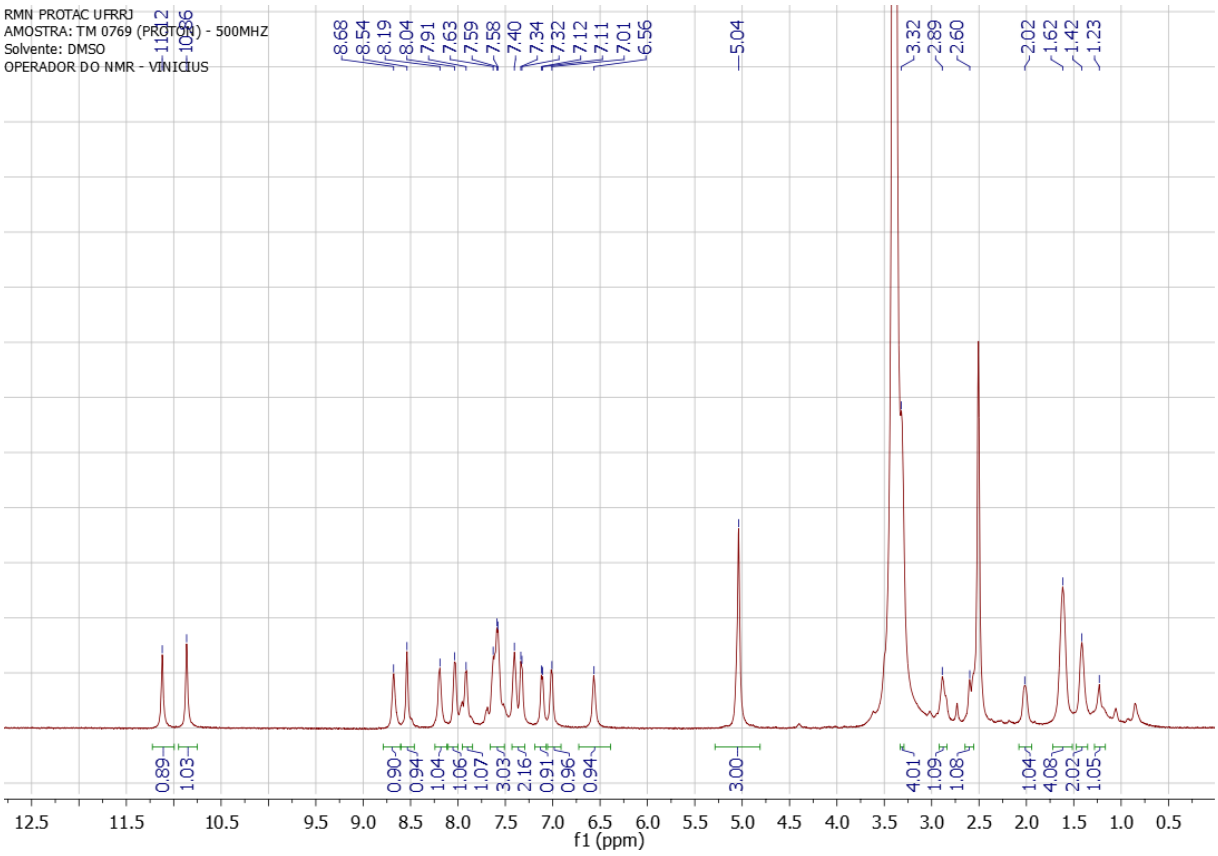

^{1}H NMR spectra of compound **311** in DMSO.

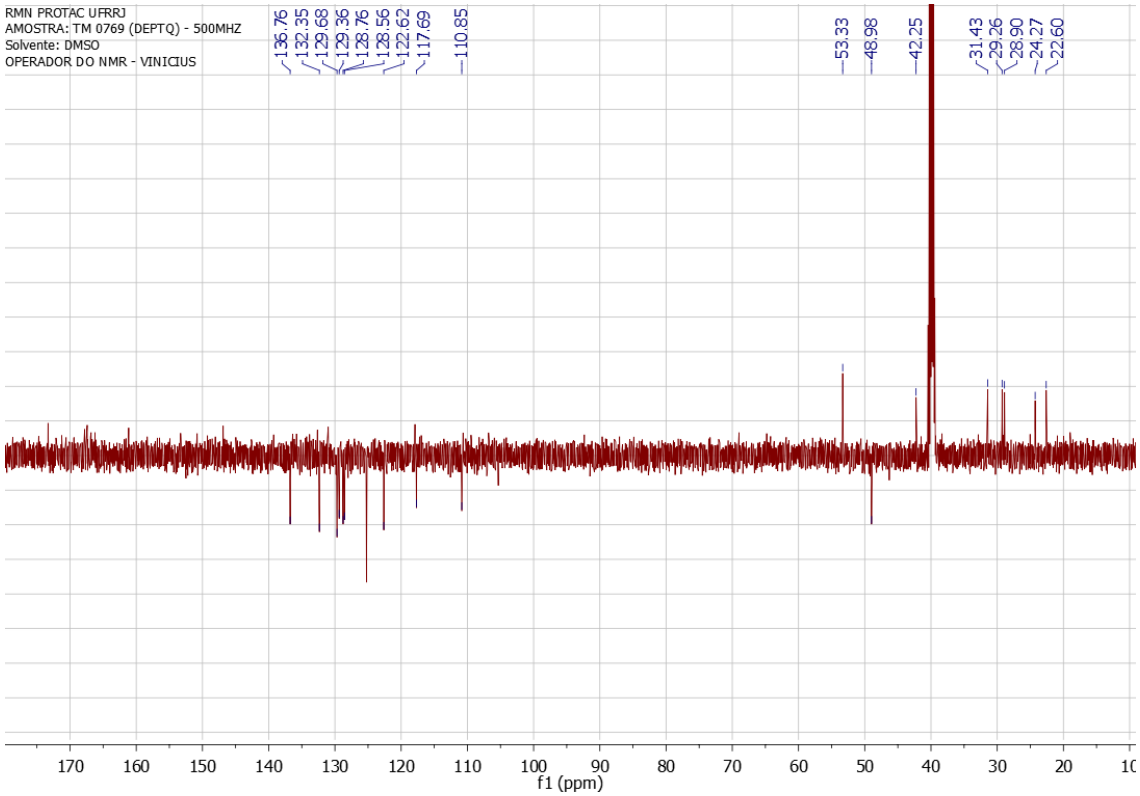

^{13}C NMR spectra of compound **311** in DMSO.

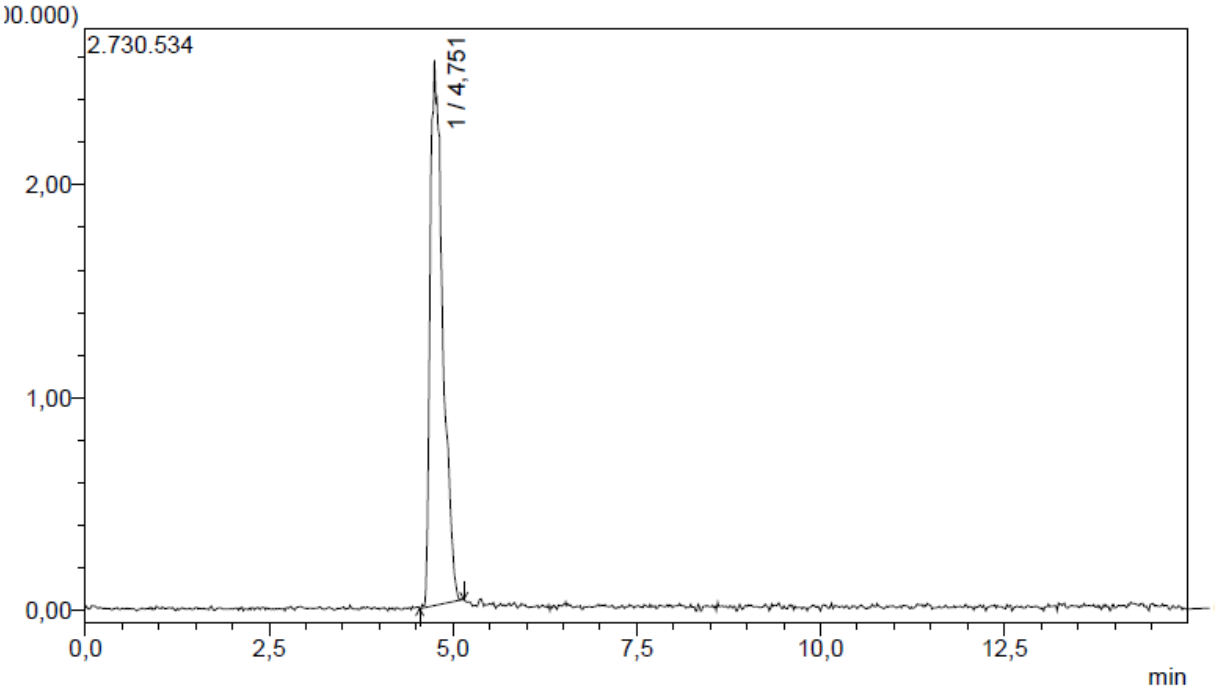

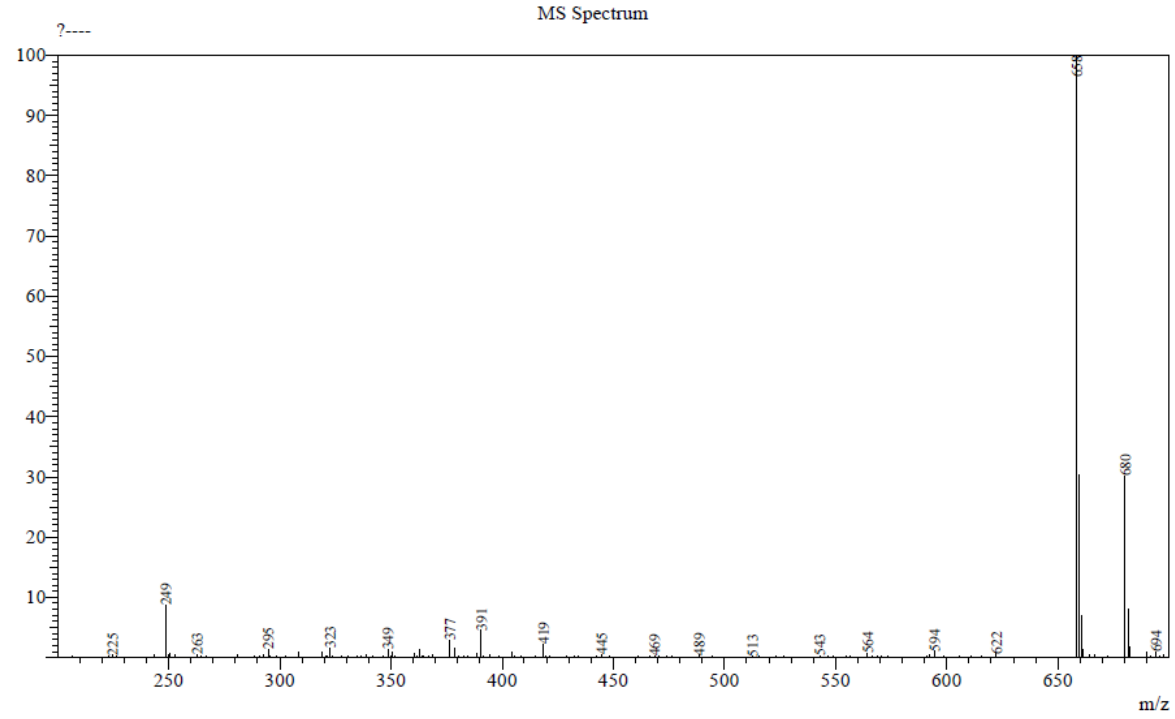

LC/MS of compound **311**.

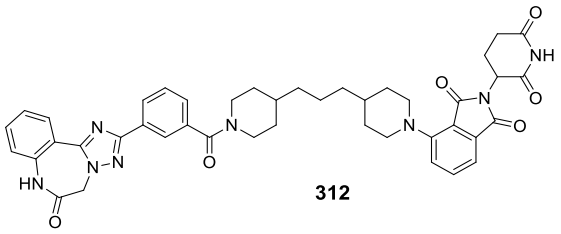

312

Exact Mass: 768.34

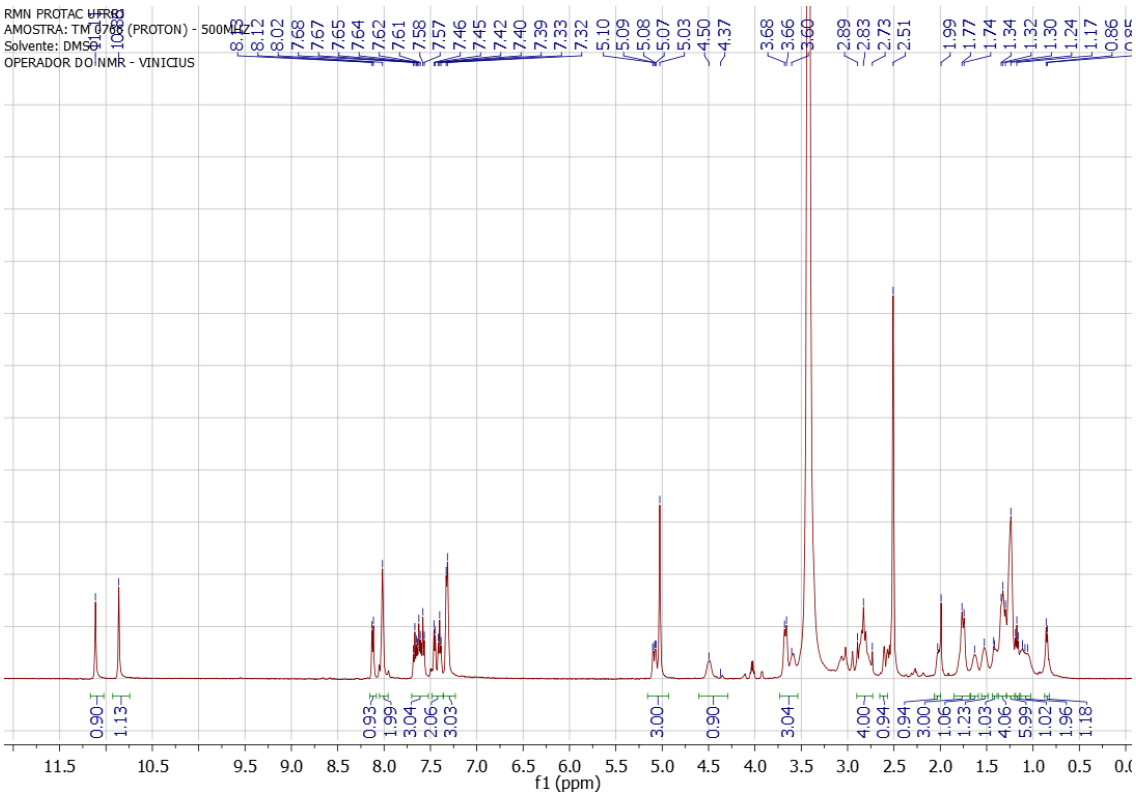

^{1}H NMR spectra of compound **312** in DMSO.

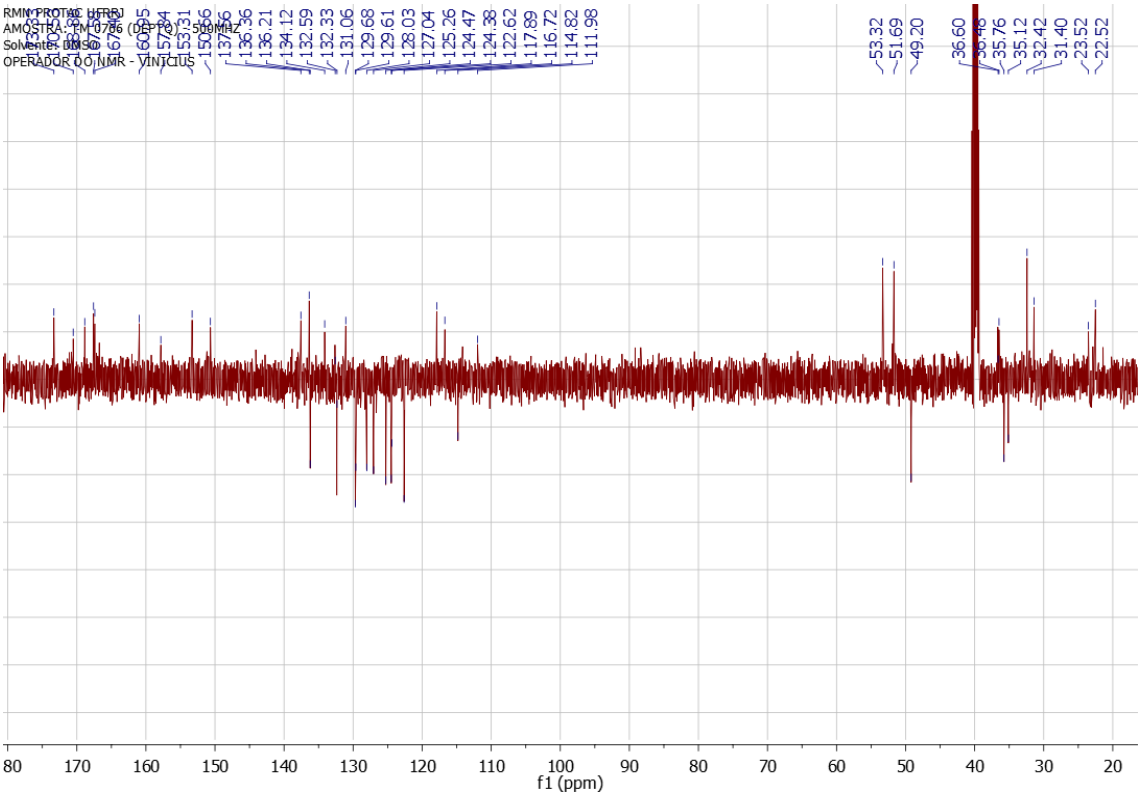

^{13}C NMR spectra of compound **312** in DMSO.

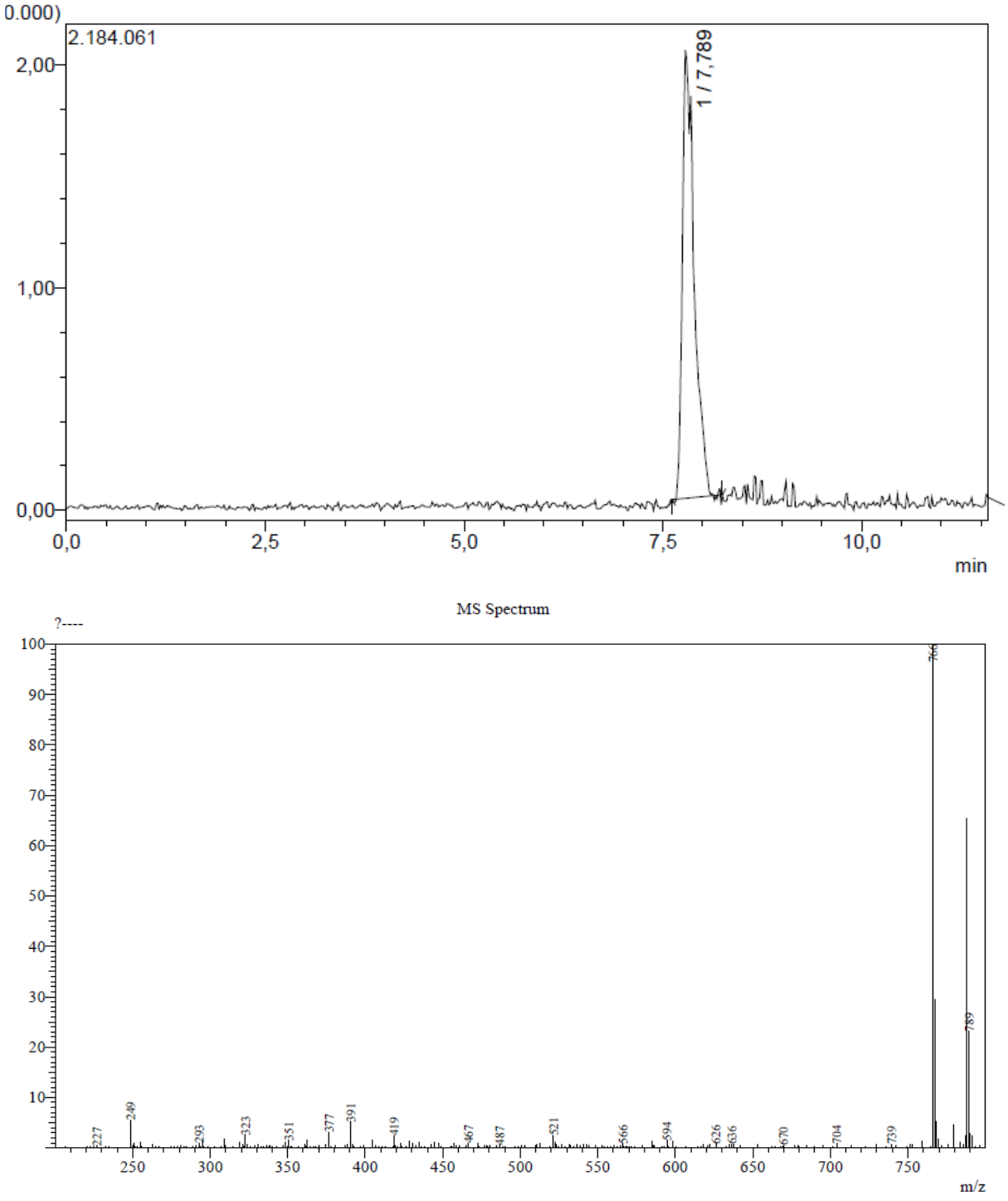

LC/MS of compound **312**.

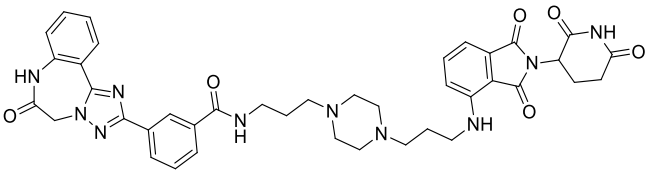

313

Exact Mass: 758.33

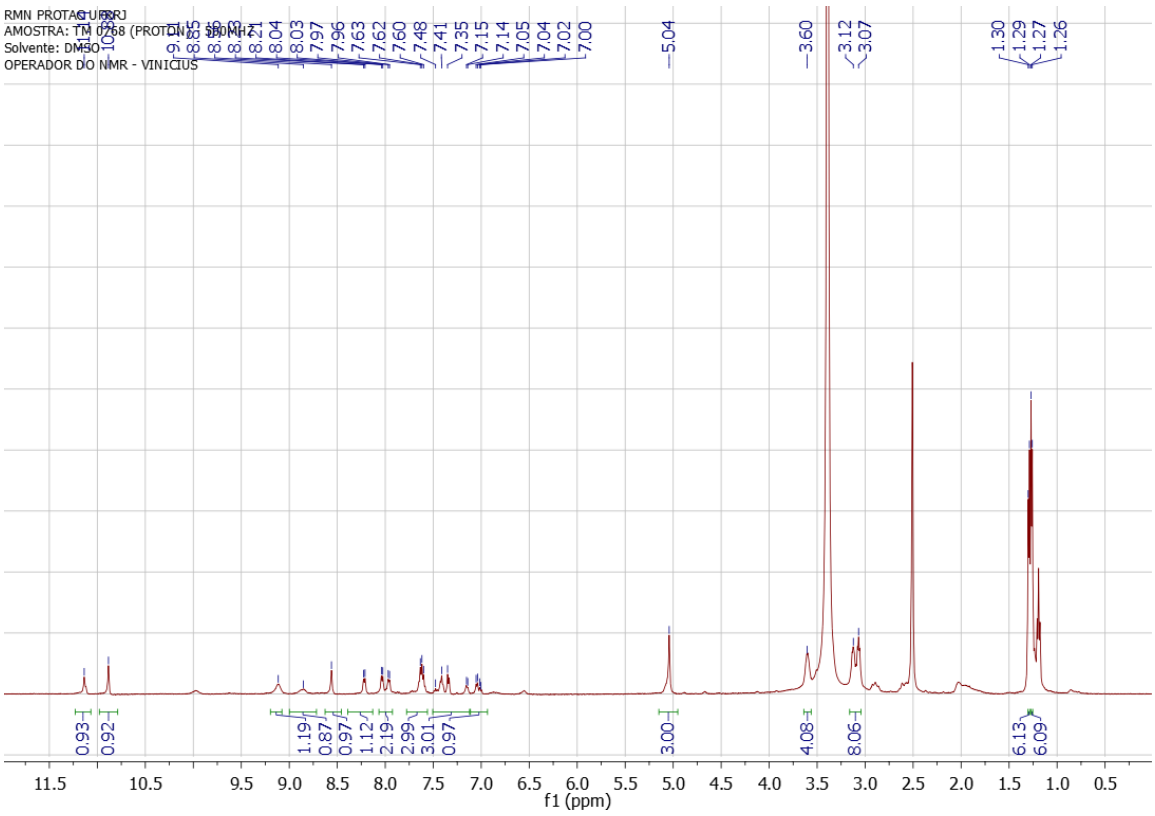

^{1}H NMR spectra of compound **313** in DMSO.

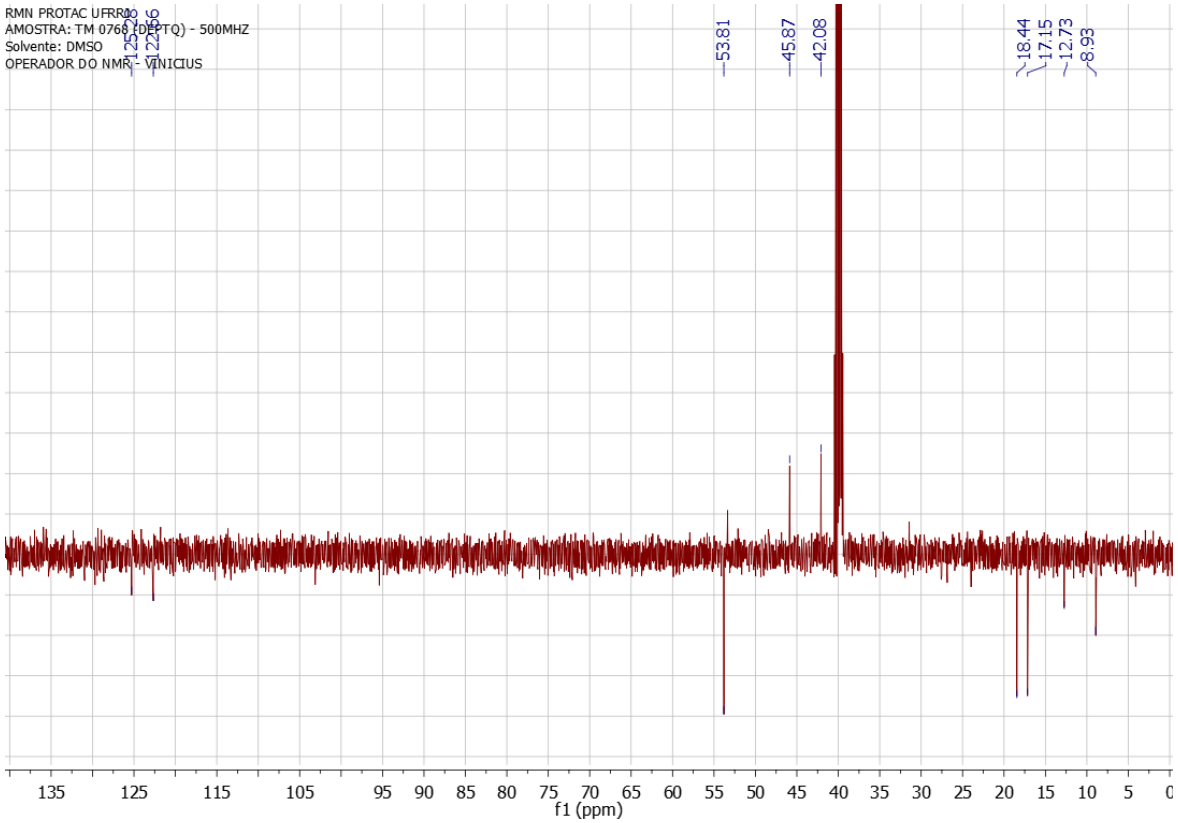

^{13}C NMR spectra of compound **313** in DMSO.

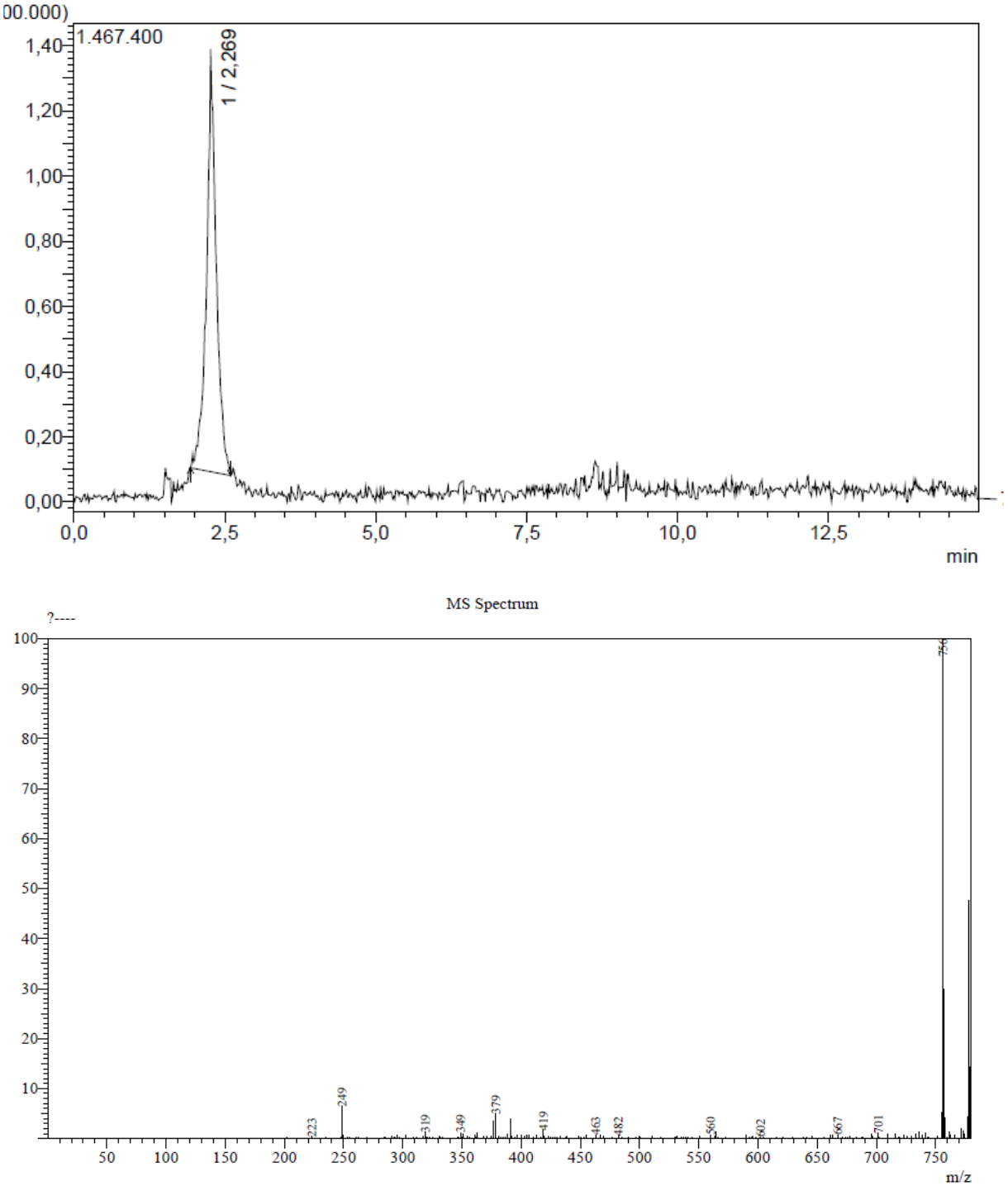

LC/MS of compound **313**.

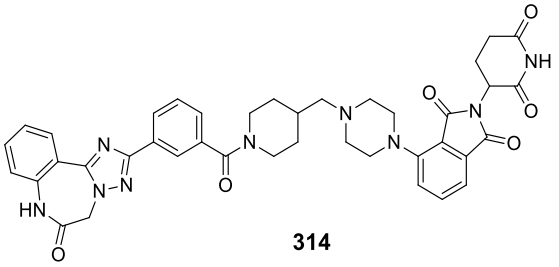

314

Exact Mass: 741.30

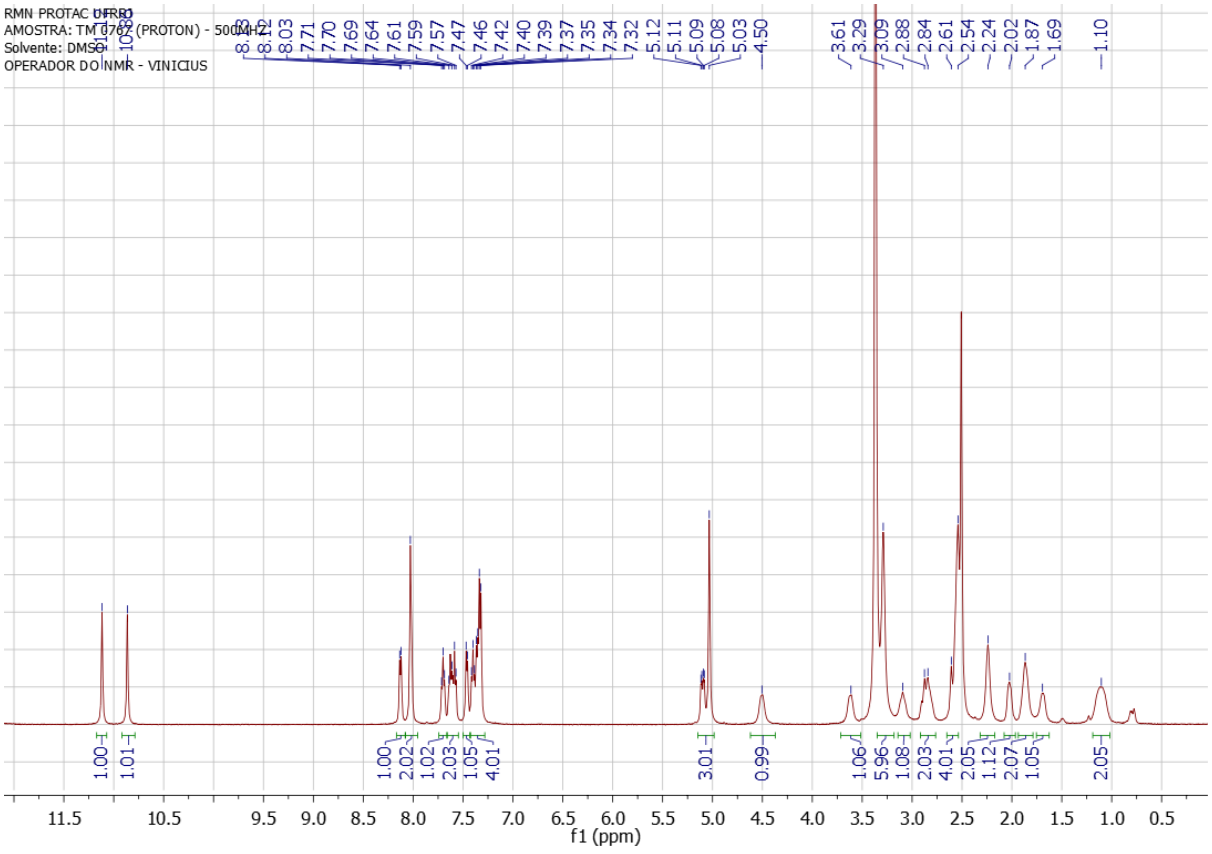

^{1}H NMR spectra of compound **314** in DMSO.

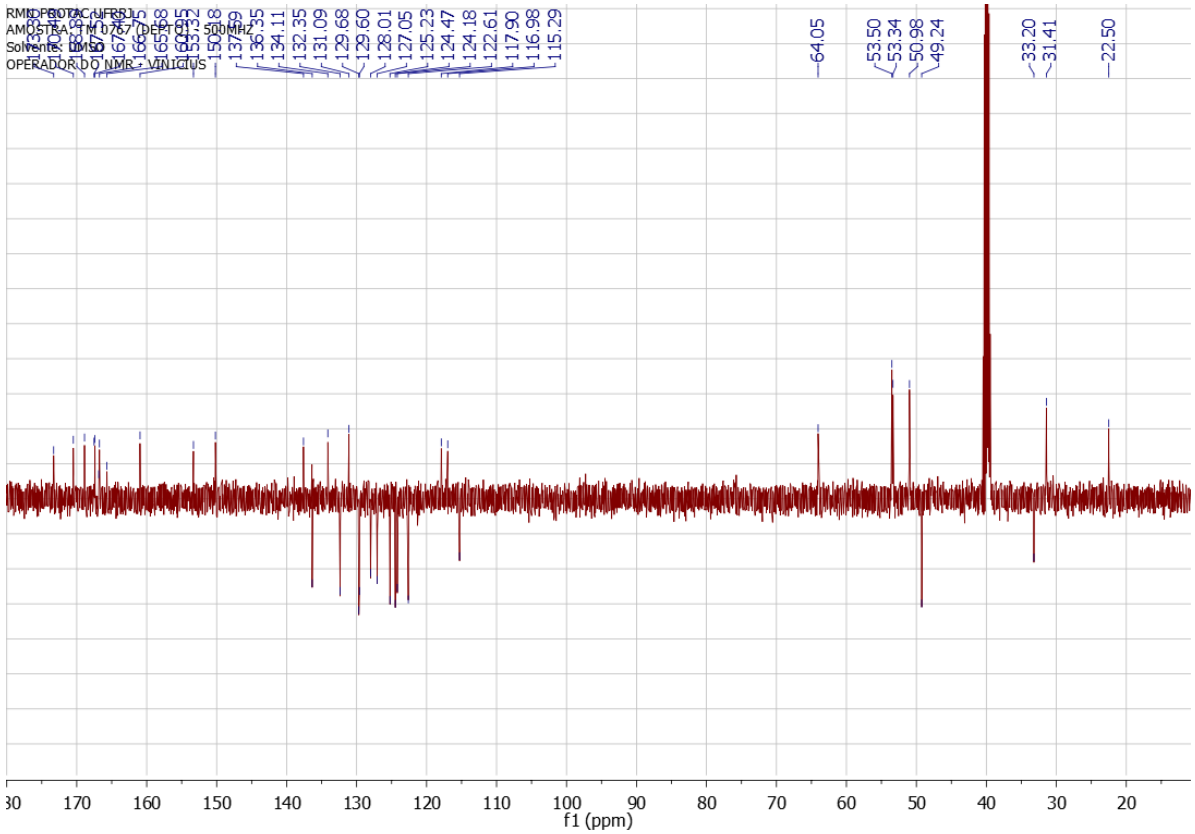

^{13}C NMR spectra of compound **314** in DMSO.

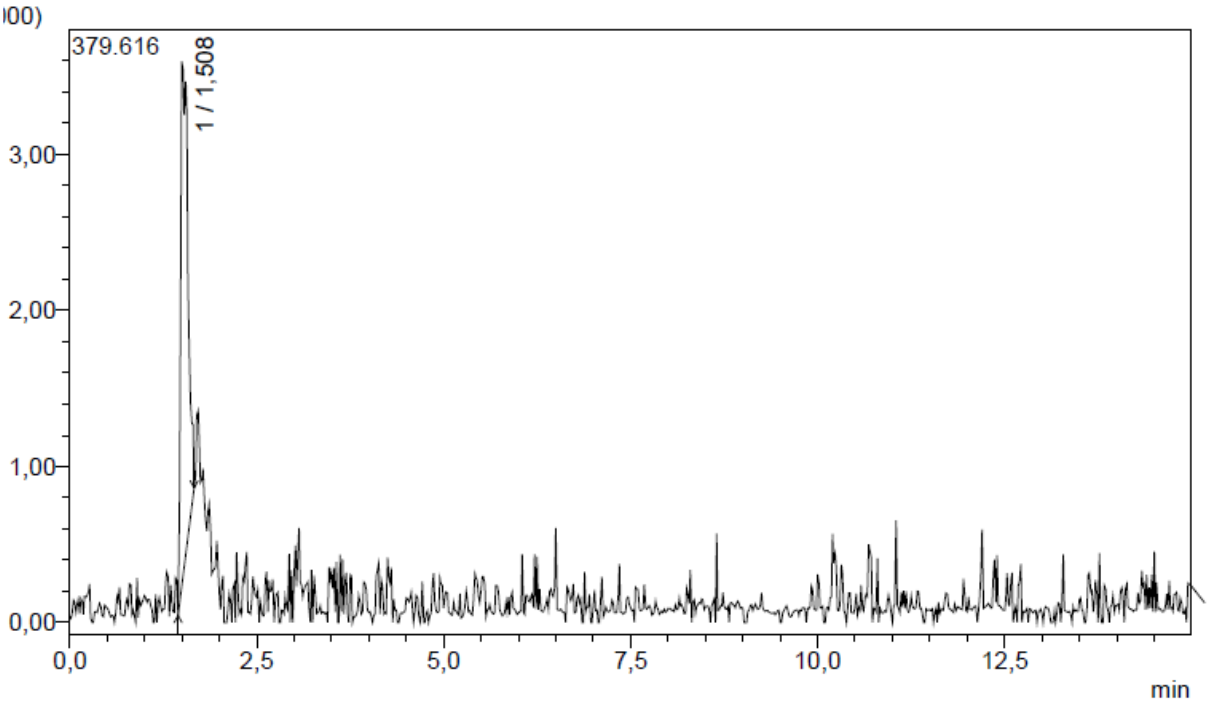

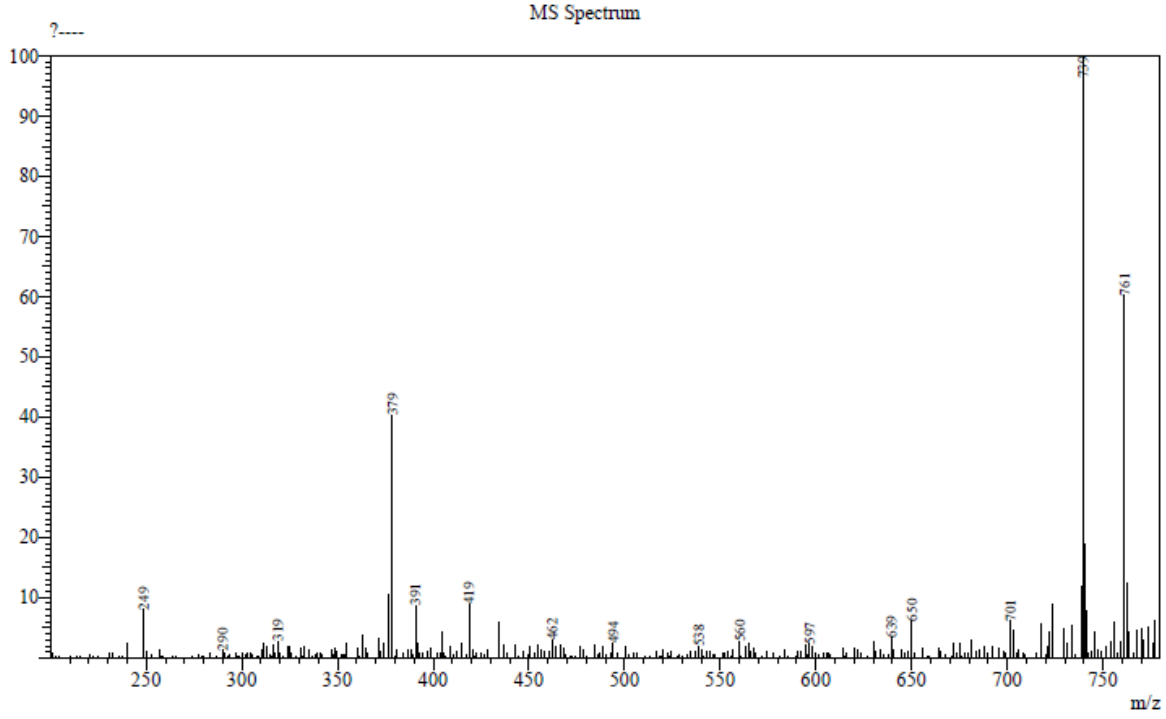

LC/MS of compound **314**.

ANNEX II

HONORS AND AWARDS

1. Best Poster Prize in "Organic Synthesis and natural products" of the 11th Brazilian Symposium on Medicinal Chemistry

Certificate

This is to certify that the abstract entitled:

Design and Synthesis of trisubstituted 1,2,4-triazoles: structural exploration in the inhibition of GSK-3β for the treatment of Alzheimer's Disease. **PEREIRA, T. M.; NADUR, N.; SIMONE, A.; ULIASSI, E.; BOLOGNESI, M. L.; SCHIMITT, M.; KUMMERLE, A.**

was awarded the **best poster prize in "organic synthesis and natural products"** of the 11th Brazilian Symposium on Medicinal Chemistry, which was held in Salvador, Bahia, Brazil, from October 24th to October 27th, 2023.

Marcelo Santos Castilho
Chair of BrazMedChem 2023

Gustavo H. G. Trossini
MED/BIO division of SBQ

@brazmedchem2023 www.brazmedchem.org/2023

2. European School of Medicinal Chemistry and European Federation for Medicinal Chemistry Fellowship winner

ESMEC and EFMC Fellowships

The European School of Medicinal Chemistry (ESMEC) and the European Federation for Medicinal Chemistry and Chemical Biology (EFMC) offer **13 (11 + 2) scholarships** for the participation to the 42nd edition of the school.
The scholarships, **covering the registration fee and the full board accommodation**, will be assigned to PhD students attending PhD courses in European Universities (excluding Italian Universities).
A Committee formed by members of the School's Scientific Committee, Dr Antoni Torrens (representative of EFMC), Prof. Tracey Pirali and Prof. Marco Macchia, will carry out the selection on the basis of the candidate scientific CV and research project.
APPLICATION CLOSED

Division of Medicinal Chemistry of the Italian Chemical Society fellowships
The Division of Medicinal chemistry of the italian chemical society offers 5 scholarships reserved to **Italian young researchers**, deadline **April 30th, 2023**
APPLICATION CLOSED

– FELLOWSHIP WINNERS –

ESMEC and EFMC Fellowships
AGUADO FERNANDEZ
CARDOSO JOANA
CARVALHAL FRANCISCA
CLARIANO MARTA
KIAKU CYRILLE
MAGDZIARZ SYLWIA
MARTINS MARCIA SILVA
MOREIRA PEREIRA THIAGO
SINGH PRAVEEN
TESINI ELEONORA
TRYBALA WOJCIECH
VILAçA PEREIRA DANIELA
WESTERVELD MARINDA

3. European School of Medicinal Chemistry Best Poster AWARD

ANNEX II

SCIENTIFIC PUBLICATIONS

Current Organic Chemistry, 2021, *25*, 2815-2839

REVIEW ARTICLE

Recent Advances in Microwave-Assisted Synthesis and Functionalization of 1,2,3- and 1,2,4-triazoles

Daiana Portella Franco[1,2], Lucas Caruso[1,2], Nathalia Fonseca Nadur[1,2], Thiago Moreira Pereira[1,2], Renata Barbosa Lacerda[2] and Arthur Eugen Kümmerle[1,2,*]

[1]*Laboratório de Diversidade Molecular e Química Medicinal (LaDMol-QM, Molecular Diversity and Medicinal Chemistry Laboratory), Chemistry Institute, Rural Federal University of Rio de Janeiro, Seropédica, 23897-000, Rio de Janeiro, Brazil;* [2]*Programa de Pós-Gradução em Química (PPGQ), Universidade Federal Rural do Rio de Janeiro, Seropédica, 23897-000, Rio de Janeiro, Brazil*

ARTICLE HISTORY

Received: June 25, 2021
Revised: August 25, 2021
Accepted: August 26, 2021

DOI:
10.2174/1385272825666211011111408

Abstract: Triazoles are five-membered aromatic heterocyclics, which exhibit two isosteric forms (1,2,3-triazoles and 1,2,4-triazoles), as well as multiple applications in medicinal, agricultural, supramolecular, and materials sciences. Famous examples of triazoles include drugs, such as fluconazole, ribavirin, cefatrizine, and tazobactam, as well as herbicides, such as cafenstrole and metosulam. This review aims to present the recent major examples of the application of microwave-assisted organic synthesis (MAOS) to the syntheses and end-functionalizations of 1,4- and 1,5-disubstituted 1,2,3-triazoles, 1,2,4-triazoles, 3-amino-1,2,4-triazoles, 1,2,4-triazol-3-one, and 1,2,4-triazol-3-thiol derivatives. Notably, the previous reviews on triazole syntheses have not exclusively elucidated the relevance of MAOS techniques in the obtention and derivatization of these compounds.

Arthur Eugen Kümmerle

Keywords: 1,2,3-triazoles, 1,2,4-triazoles, microwave-assisted synthesis, heterocycles, classical heating methods, microwave irradiation.

1. INTRODUCTION

Triazoles are aromatic heterocyclic compounds (molecular formula = $C_2H_3N_3$), which are characterized by a five-membered ring comprising three nitrogen and two carbon atoms [1]. Thus far, triazoles are exclusively obtained *via* synthesis because there are no indications of their natural occurrences [2].

These compounds exhibit two isosteric forms (1,2,3-triazoles and 1,2,4-triazoles) based on the position of the three nitrogen atoms [3]. Each isosteric form exhibits three tautomers that differ according to the position of the hydrogen atom; however, the structures of the proton of carbon-two (**3** and **6**) are non-aromatic and are rarely mentioned in the literature (Fig. **1**) [4, 5].

1,2,4-triazole derivatives exhibit a wide range of applications in medicinal, agricultural, supramolecular, and materials sciences. In medicinal chemistry, these derivatives exhibit extensive biological activities [6], such as anti-inflammatory [7-9], antibacterial [10-13], antifungal [14, 15], antiviral [16], anticancer [17], antioxidant [18-20], antitubercular [21], anticonvulsants [22], anti-nociceptive [9], as well as CNS-stimulating, antidepressants [23, 24], and antianxiety properties [25, 26]. To date, many drugs, including alprazolam (**7**), fluconazole (**8**), voriconazole (**9**), ribavirin (**10**), rizatriptan (**11**), estazolam (**12**), vorozole (**13**), anastrozole (**14**), and letrozole (**15**), containing the 1,2,4-triazole moiety have been extensively employed in clinics. In agriculture, 1,2,4-triazoles exhibit insecticidal and plant growth-regulating activities, as evidenced in cafenstrole (**16**), metosulam (**17**), azafenidin (**18**), carfentrazone-ethyl (**19**), and sulfentrazone (**20**) (Fig. **2**).

*Address correspondence to this author at the Department of Organic Chemistry, Rural Federal University of Rio de Janeiro, Seropédica, Brazil, 23897-000; Tel: ++55-21998576298; E-mails: akummerle@ufrrj.br; akummerle@hotmail.com

Similarly, 1,2,3-triazole-based compounds have been extensively employed as agrochemicals [27, 28], dyes [29, 30], corrosion inhibitors [31-33], photostabilizers [34], dendrimers [34-37], liquid crystals [38-40], and metal chelators [41, 42]. Additionally, 1,2,3-triazoles exist generally as the core structures of many compounds exhibiting broad biological activities [6], such as anti-HIV [43-45], anticancer [46, 47], antiprotozoal [48, 49], antimicrobial [50, 51], antifungal [52, 53], and neuroactive agents [54, 55]. However, only a few molecules contain 1,2,3-triazole moieties in the market or the last phase of clinical trials. Cefatrizine (**21**) and tazobactam (**22**) account for some of the already commercialized drugs exhibiting such a ring system (Fig. **2**).

A literature search performed in Scopus® on June 20, 2021, revealed that the 1,2,4-triazole system with 14,002 publications (containing the keywords "1,2,4-triazole") is the most studied compared with the 8,333 publications related to the other system (containing the keywords "1,2,3-triazole"). However, there has been significantly increased research on 1,2,3-triazoles since the past 20 years [56] probably owing to the advent of "click chemistry."

Among the organic synthesis techniques for preparing triazoles, Microwave-Assisted Organic Synthesis (MAOS) has attracted recent attention [57]. The utilization of microwave ovens for organic synthesis has been preferred to the classical heating method because it reduces the reaction time, ensures improved efficiency and product purity, as well as the possibility of eliminating the solvents [58]. Similar to MAOS, ultrasonic irradiation exhibits numerous advantages over other conventional methods (reduced cost, excellent yields, and improved purity). However, there is no well-established direct comparison between microwaves and ultrasound [59-61]. This review summarizes the most recent (since 2014) relevant microwave-assisted methods for synthesizing and deriving triazoles.

1875-5348/21 $65.00+.00

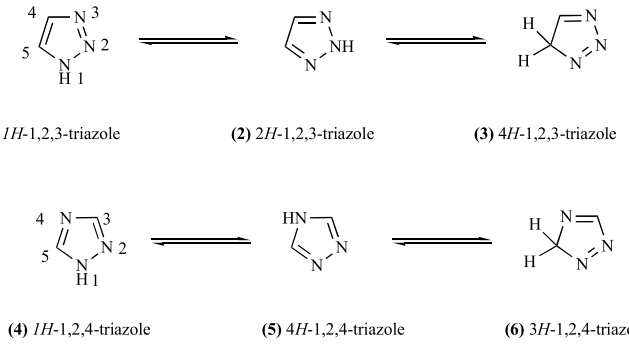

Fig. (1). Chemical structures of 1,2,3-triazoles and 1,2,4-triazoles and their tautomers (**1-6**).

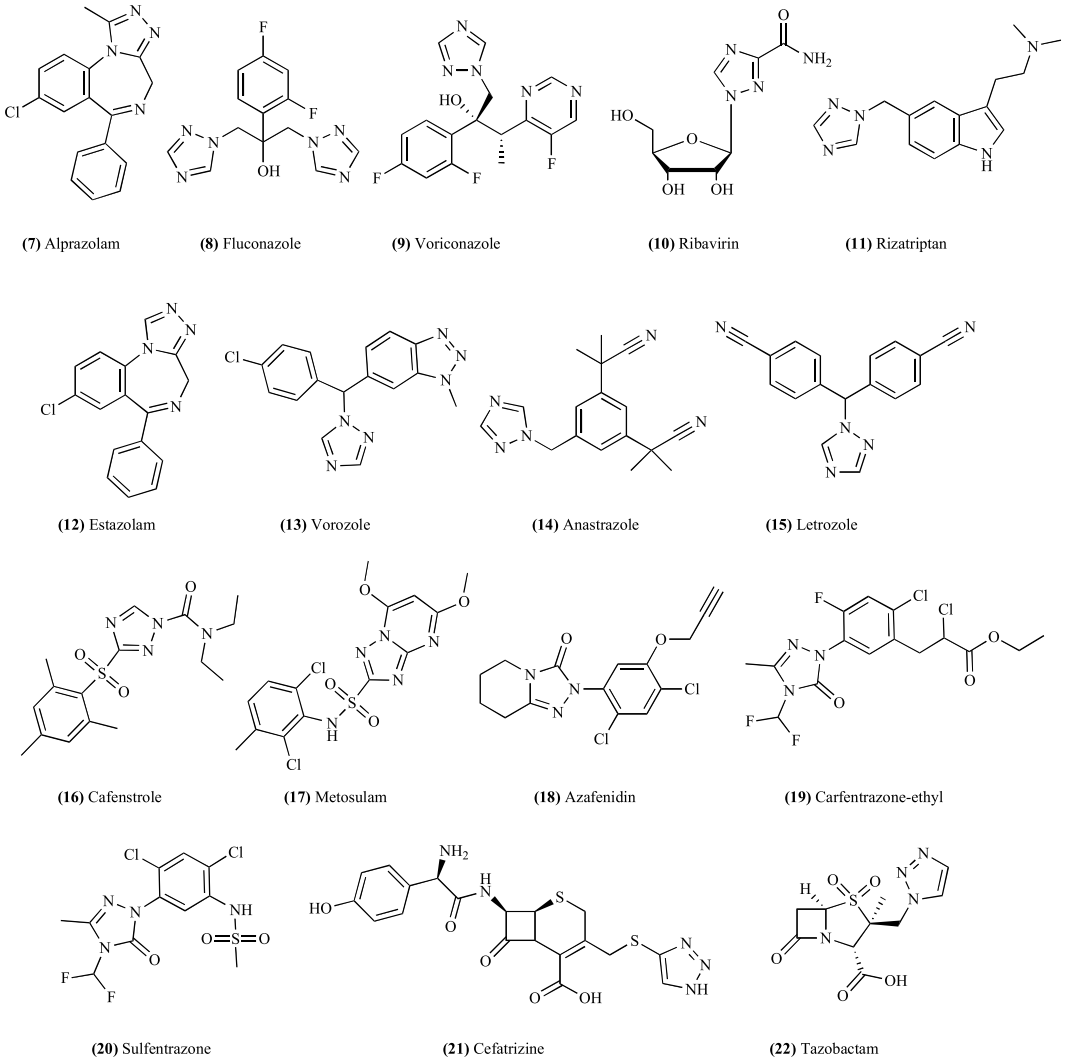

Fig. (2). Bioactive compounds containing triazole moiety (**7-22**).

2. 1,2,3-TRIAZOLE DERIVATIVES

The 1,2,3-triazole ring, which exhibits amphoterism (it is considered a weak acid (pKa = 9.40) and a weak base (pKaH = 1.17), has been extensively studied owing to its potential applications in different fields. This aromatic heterocycle has been widely employed to develop new drugs because of its pharmacological activities as a building block in molecular hybridization approaches [62]. Additionally, it has also been employed as a carbene precursor and a ligand to activate C-H [63].

Although 1,2,3-triazoles can be synthesized *via* different routes, the 1,3-dipolar cycloaddition reaction, which traditionally proceeds *via* azide-alkyne Huisgen [3 + 2]-cycloaddition, is the most significant [64]. This method generally yields a mixture of 1,4- and 1,5-disubstituted regioisomers, which require long reaction times and

that are largely challenging to separate *via* chromatography [65, 66]. However, based on the achievements recorded by different research groups, catalyzed 1,3-dipolar azide-alkyne cycloaddition (AAC), which is regarded as "click chemistry," was developed [67, 68]. This reaction exhibits several benefits, including a significant increase in the reaction speed, as well as the obtention of the specific regioisomers of 1,2,3-triazoles. Thus, the copper-catalyzed 1,3-dipolar cycloaddition reaction (copper-catalyzed AAC, CuAAC) exclusively yields 1,4-disubstituted 1,2,3-triazole, [69] while the ruthenium-catalyzed reactions (ruthenium-catalyzed AAC, RuAAC) mainly yield 1,5-disubstituted 1,2,3-triazoles (Fig. **3**) [70].

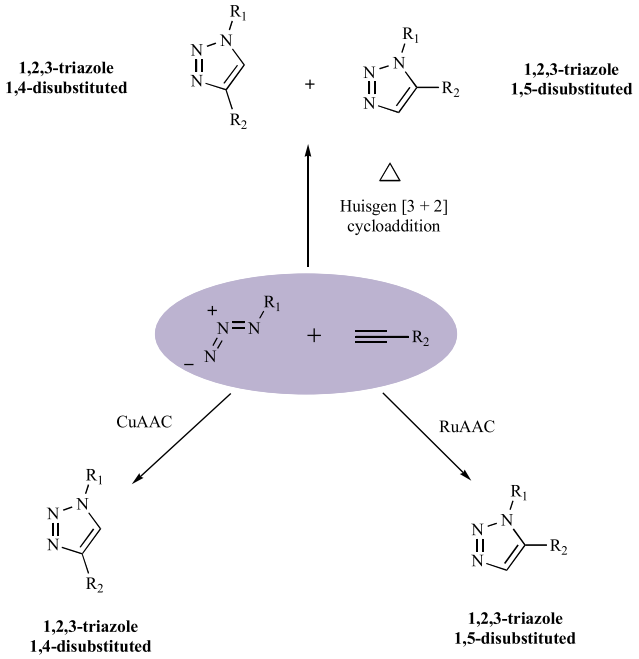

Fig. (3). General scheme for the synthesis of 1,2,3-triazoles.

2.1. Synthesis of 1,4-disubstituted 1,2,3-triazole Under Microwave Irradiation

Suresh and coworkers developed an efficient protocol for synthesizing the antibacterial, 1,2,3-triazole (**25**), *via* microwave irradiation. Further, previous protocols with poor yields (20-42%) required long reaction times (12 h) and high temperatures (100 °C) *via* conventional heating. A series of copper catalysts (CuI, CuOAc, CuCl, and $CuSO_4$/NaAsc) and different solvents (toluene, DMF, *t*-BuOH, and DMSO:H_2O), as well as the parameters, such as temperature, reaction time, and the irradiation power, were investigated, and the optimum conditions were thus: The copper sulfate-sodium ascorbate catalyst ($CuSO_4$/NaAsc) and sodium carbonate (Na_2CO_3) in DMSO:H_2O (3:1) under microwave irradiation for 30 min at 75 °C. These conditions also obtained the best yields (56-88%) for the syntheses of 1,4-disubstituted triazoles through α-azido chalcones (**23**) and different alkynes (**24**) without side products or degradation (Scheme **1**) [71].

Similarly, other antibacterials (**28**) could be obtained *via* the CuAAC reaction under conventional heating and microwave irradiation. Aarjane and colleagues compared the activities of different copper salts and solvents in the reaction of acridone (**26**) with phenylacetamide (**27**) to produce the antibacterial acridon-1,2,3-triazoles (**28**) (Scheme **2**). Employing microwave irradiation and $CuSO_4.5H_2O$/NaAsc in a DMF system, the reaction time could be reduced from 24 h to 10 min to obtain the final products in yields of 69-86% [72].

As following the above examples, the classical method (CuAAC reactions) employing the $Cu_2SO_4.5H_2O$/NaAsc system was adopted for the microwave syntheses of many 1,2,3-triazole derivatives; it only required the selection of a better solvent for each reaction. Further, Dürüst and Karakus, synthesized 1,2,4-oxadiazol-5-ylmethyl-1,2,3-triazole derivatives (**31**) in a mixture of EtOH:H_2O in only 2.5 min [73]; Souza and colleagues synthesized novel imine-1,2,3-triazoles (**35**) through the one-pot three-component reaction in acetonitrile for 3 h [74]. Moreover, Subhashini and coworkers synthesized a new series of pyrazole-based 1,2,3-triazoles (**38**) in 4-6 min (Scheme **3**) [75].

As illustrated in Scheme **3B**, one-pot reactions are common in the synthess of 1,2,3-triazoles. Kumar and coworkers synthesized triazole-linked thiazolidinones *via* the reaction of propargyloxybenzaldehyde (**39**) and aryl azide (**37**) employing the $CuSO_4.5H_2O$/D-glucose system in a THF:H_2O mixture under microwave irradiation for 15 min. Further, several anilines and thioglycolic acids were added and reacted for an additional 40-50 min to yield the desired thiazolidinones-1,2,3-triazoles (**40**) in excellent yields (Scheme **4A**) [76].

Srinivas and colleagues described optimized microwave syntheses of new 1,4-substituted 1,2,3-triazolo-quinazolin-4(3*H*)-one derivatives (**43a-z**) exhibiting anticancer activities. The reaction of the intermediates, quinazolinones (**41**), with different alkynes (**42**) in the presence of NaN_3, CuI, and DMF at 100 °C for 3 min ensured the obtentions of 1,2,3-triazolo-quinazolin-4(3*H*)-ones (**43a-z**) with yields of 70-80% (Scheme **4B**). Compounds **43a** (R_1 = H, R_2 = CH_3, R_3 = CH_3) and **43b** (R_1 = H, R_2 = CH_3, R_3 = Br) exhibited high cytotoxicity against the human cancer cell line, HL-60, particularly inhibiting the PI3Kγ isoform [77].

Ashok and his group optimized the syntheses of hybrid coumarin-1,2,3-triazoles (**46**) *via* microwave irradiation (Scheme **4C**), as well as the *in situ* formation of diazidoalkanes *via* the nucleophilic substitution reaction between dibromoalkanes (**45**) and sodium azide, which in turn reacts with Compound **44**. After testing various solvent mixtures (EtOH:H_2O, THF:H_2O, DMF:H_2O), two copper salts ($CuSO_4.5H_2O$/NaAsc and CuI), and conventional and microwave heating, the optimum conditions were determined thus: CuI in DMF:H_2O (1:3) at 180 W; these conditions reduced the reaction time from 24 h to 10 min and increased the yields from 43-53% to 75-86% [78].

Although many published studies employed $CuSO_4.5H_2O$ in the presence of a reducing agent (NaAsc), many others adopted different copper salts with or without the reducing agent. Schumacher's group proposed clean nonclassical methods for synthesizing 3-(1*H*-1,2,3-triazol-1-yl)-2-(arylselanyl) pyridine derivatives (**48**) from 2-(arylselanyl)-3-azido pyridines (**47**) and terminal alkynes (**42**) in the presence of $Cu(OAc)_2$ and NaAsc (Scheme **5**). These compounds had been previously synthesized in good yields by conventional heating, it the syntheses required long periods (5-24 h). The syntheses *via* microwave irradiation revealed that the same compounds could be obtained in excellent yields in only 10 min [79].

To synthesize indole-triazoles that can act as chemosensors for Ni^{+2} and Cu^{+2}, Singh conducted a comparative study between the conventional heating and microwave irradiation methods for coupling the indole acetylenic derivatives (**49**) and azide (**50**). The utilization of microwaves reduced the reaction time for coupling the acetylenic indole-appended Schiff base (**49**) and 3-azidopropyl-

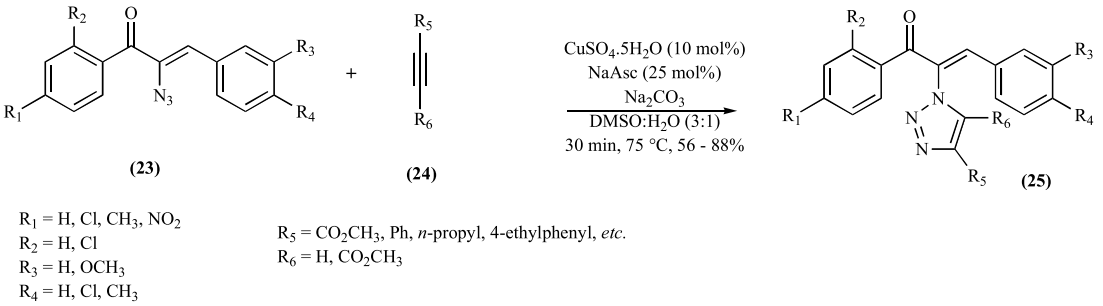

Scheme 1. Synthesis of antibacterial (*Z*)-1,3-diaryl-2-(4-substituted-1H-1,2,3-triazol-1-yl)prop-2-en-1-ones (**25**).

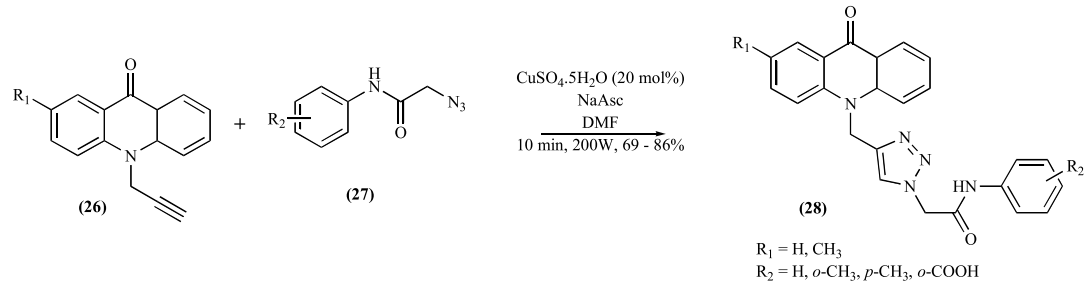

Scheme 2. Microwave-assisted synthesis of antibacterial acridon-1,2,3-triazole derivatives (**28**).

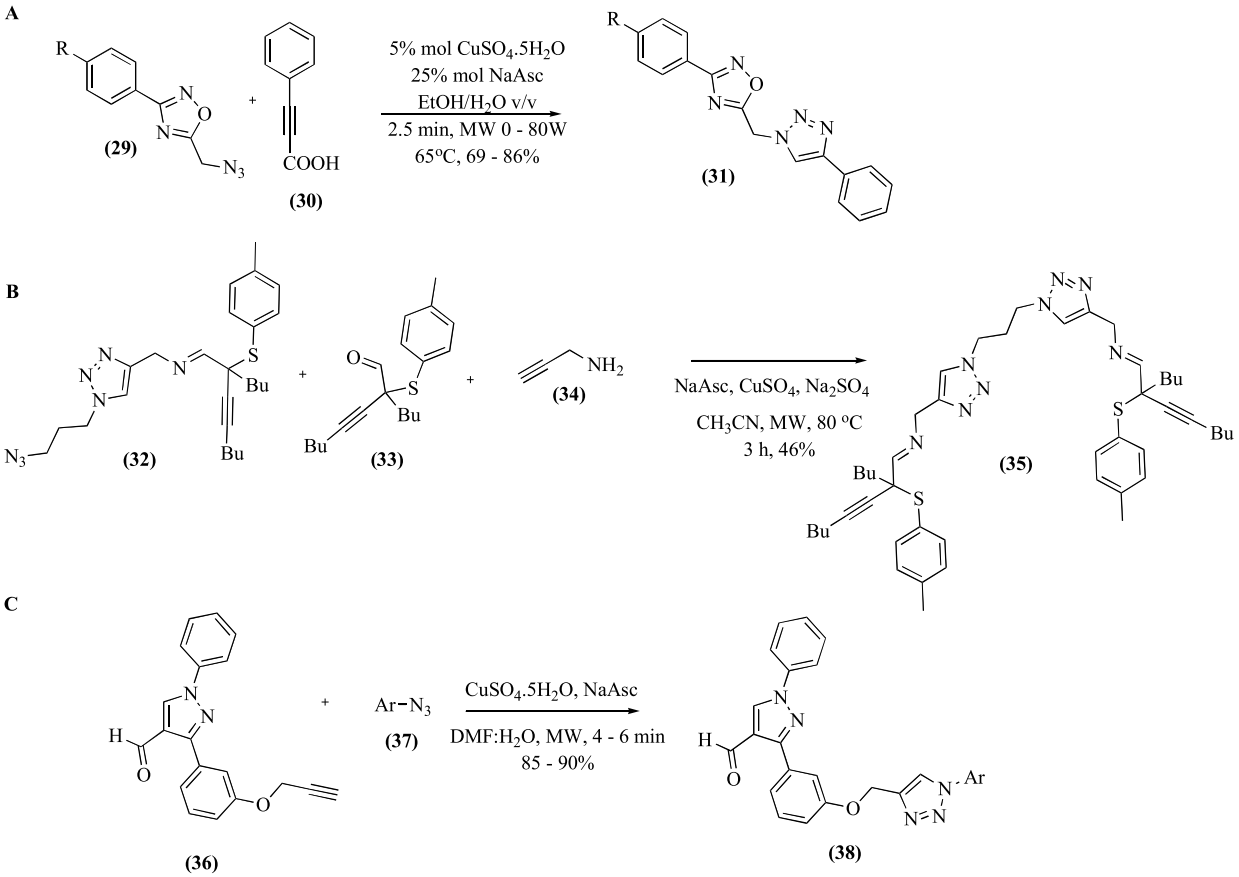

Scheme 3. A - Microwave-assisted synthesis of oxadiazole-1,2,3-triazoles (**31**); **B -** One-pot microwave three-component synthesis of imine 1,2,3-triazoles (**35**); **C -** Microwave synthesis of pyrazole-based 1,2,3-triazoles (**38**).

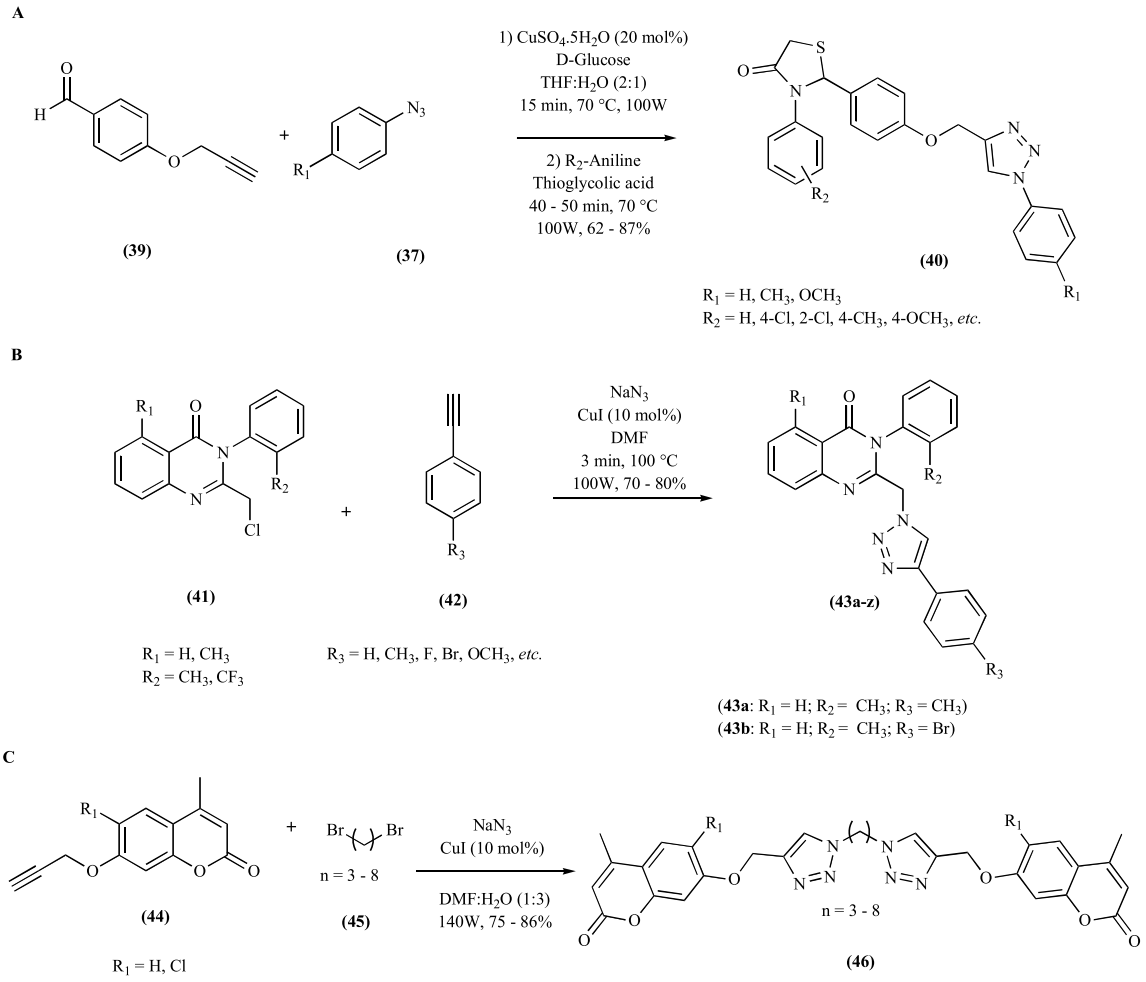

Scheme 4. One-pot microwave synthesis of triazole compounds. **A -** Synthesis of thiazolidinones-triazoles (**40**); **B -** Synthesis of 1,2,3-triazolo-quinazolin-4(3H)-ones (**43a-z**); **C -** Synthesis of coumarin-1,2,3-triazoles dimers (**46**).

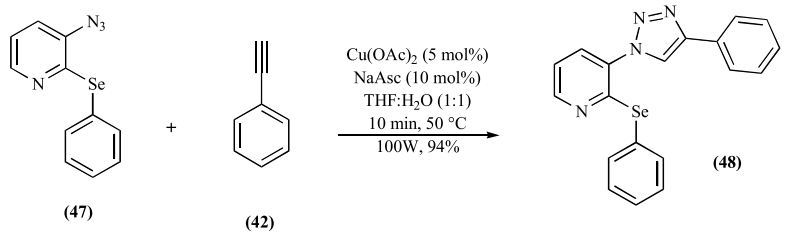

Scheme 5. Synthesis of 3-(1*H*-1,2,3-triazol-1-yl)-2-(arylselanyl) pyridines (**48**).

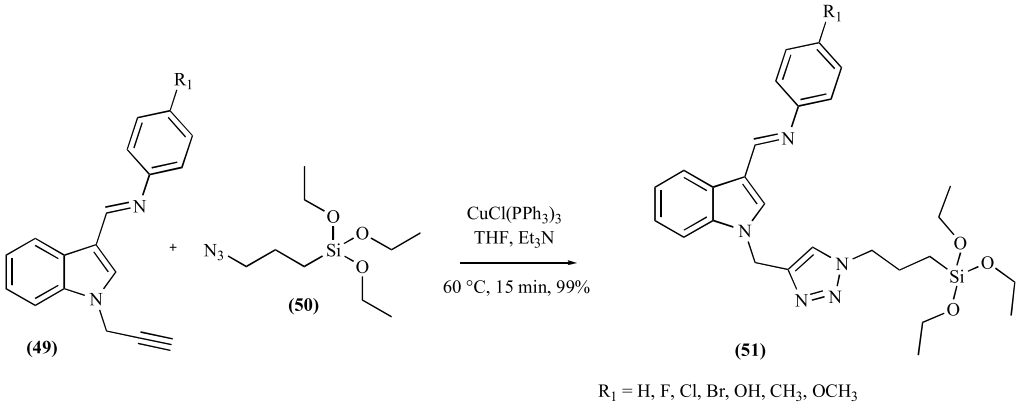

Scheme 6. Microwave-assisted synthesis of chemo sensors indole triazole pendant siloxy framework (**51**).

triethoxysilane (**50**) from 240 min (under conventional heating) to only 15 min. Further, in this coupling, which was conducted employing $CuCl(PPh_3)_3$ as the catalyst (without a reducing agent owing to the nature of Cu(I)), THF, and Et_3N at 60 °C, the indole-1,2,3-triazoles (**51**) products were obtained in excellent yields (Scheme **6**). Thereafter, spectroscopic studies, which revealed that the synthesized compounds could selectively detect Cu^{+2} and Ni^{+2} in the presence of other metals, were performed [80].

The utilization of nanoparticles (NPs) has emerged as a sustainable alternative to conventional homogenous catalysis in the syntheses of triazoles since these materials exhibit a significantly higher exposed surface area and can be recovered or easily separated after the reaction.

Dias and coworkers investigated several NPs for the 1,3-dipolar cycloaddition reaction between dicarbonyl compounds (**52**) and aryl azides (**37**) under microwave irradiation to yield 1,4,5-trisubstituted-1,2,3-triazoles, **55** (Scheme **7A**). Although Fe_2O_4 (30 mol%, 85%) and $Fe_2O_4Nb_2O_5$ (30 mol%, 89%) nanocatalysts exhibited excellent performances in DMSO; copper oxide NPs as a catalyst (CuO 30 mol%) exhibited the highest efficiency with 97% yield each in 24 h at room temperature and 15 min at 80 °C. Additionally, only a yield of 7% was obtained without the catalyst. Different dicarbonyl compounds and azides have been investigated for the obtention of a wide range of substituted 1,2,3-triazoles; they demonstrated that the developed method was versatile and regioselective [81].

Bhuyan and coworkers applied reusable $CuFe_2O_4$ NPs to the one-pot syntheses of 4-aryl-1-*H*-1,2,3-triazole compounds (**57**) by reacting sodium azide (**56**) with *in situ*-originated (nitrovinyl)-benzene intermediates (from the reaction between benzaldehydes (**54**) and nitro-methane (**55**)) (Scheme **7B**). After testing different solvents (H_2O, CH_3CN, EtOH, $CHCl_3$, DMF, and DMSO), catalyst concentrations (5-30 mol%), as well as comparing the conventional and microwave heating methods, they concluded that microwave irradiation was exceedingly valuable and afforded much higher yields and consumed shorter reaction times than conventional heating. The utilization of $CuFe_2O_4$ (5 mol%) in DMSO for 5-10 min at 120 °C employing microwave represented the most satisfactory method, and the copper NPs remained catalytically active even after six reuses [82].

Further, in the field of green chemistry, Radatz and colleagues reported a recoverable Cu/SiO_2 catalyst for the syntheses of 1,2,3-triazole compounds (**60**). The one-pot reaction proceeded by mixing organic halides (**58**) and sodium azide (**56**) to achieve the *in situ* formations of the respective organic azides, which subsequently reacted with alkyne (**59**) in an aqueous medium (Scheme **7C**). This method demonstrated effectiveness in conventional and microwave heating, delivering excellent yields although with a dramatic reduction in the reaction time from 12 h to 10 min regarding microwave irradiation [83].

Narsimha's group explored the utilization of ionic liquids (ILs) to synthesize fused benzothiazino[1,2,3]triazolo[4,5-*c*]quinolinone derivatives (**62**), which exhibited *in vitro* activity against different

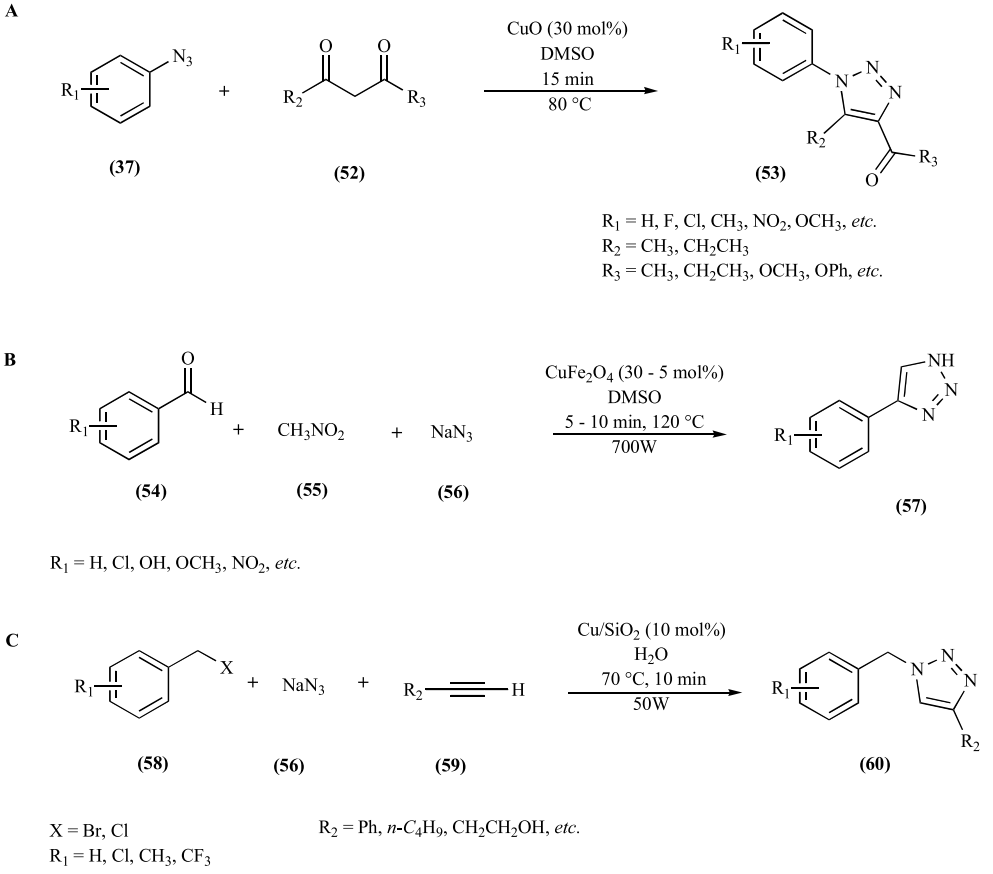

Scheme 7. Microwave-assisted synthesis of 1,2,3-triazoles using NPs. **A -** CuO NPs catalyzed synthesis of 1,4,5-trisubstituted 1,2,3-triazoles (**53**); **B -** $CuFe_2O_4$ catalyzed synthesis of 4-substituted-1*H*-1,2,3-triazoles (**57**); **C -** Syntheses of 1,4-disubstituted-1,2,3-triazoles (**60**) with Cu/SiO_2.

cancer cell lines. Employing conventional heating, as well as different catalysts and charges, temperatures, and different ILs as the solvent did not deliver yields of >47% even after 24 h of reaction; the adoption of microwave irradiation significantly improved the yields and reaction times. Furthermore, several derivatives were synthesized in good yields from iodine alkynes (**61**) and aryl azides (**37**) employing CuI (10 mol%) as the catalyst, $[Bmim]PF_6$ as the solvent, and *t*-BuOK (2 eq) for 30-40 min at 150 °C (Scheme **8**) [84].

Bruyat described the utilization of an air-stable Cu(I)-NHC complex as the catalyst for the solid-phase syntheses of peptidotriazoles (**65**) employing microwave irradiation (Scheme **9**). This approach was more efficient than the classic CuAAC methods employing $CuSO_4$/NaAsc or CuI. Compounds **65** were obtained in high purity from the reaction of azide (**63**) and alkyne (**64**) in the presence of 10 mol% Cu(I)-NHC in methanol under microwave irradiation at 50 °C, followed by the cleavage of the supported resin (ChemMatrix) [85].

Carreiro and coworkers synthesized novel 1,4-disubstituted-1,2,3-triazole dihydropyrimidinones (**69a-e**) under microwave irradiation to demonstrate a fascinating multicomponent one-pot synthesis protocol (Scheme **10**). First, they synthesized the compounds through a two-step reaction, *i.e.,* the click protocol, followed by the multicomponent Biginelli reaction. Although the first step obtained good yields (99%) in short reaction times (10 min under microwave), the Biginelli reaction required up to four days employing conventional heating and 24 h under microwave irradiation. Based on these results, the researchers conducted a sequential one-pot click-Biginelli process with the four components: 1-azidopropan-2-one (**67**), phenylacetylene (**42**), urea (**68**), and benzaldehyde (**54**). The best results were obtained in the presence of CuI, DIPEA/AcOH, and acetonitrile under microwave irradiation for 24 h. Additionally, some of these hybrids functioned as potent cell-proliferation inhibitors against non-small-cell lung, cervical, breast, and colon cancers [86].

2.2. Synthesis of 1,5-disubstituted 1,2,3-triazole Under Microwave Irradiation

Although most microwave irradiation protocols are demonstrated through the syntheses of 1,4-disubstituted triazole compounds, some fascinating 1,5-disubstituted class examples are available. For example, Ruthenium-Catalyzed Azide-Alkyne Cycloadditions (RuAAC) are the most common reactions for selectively producing 1,5-disubstituted isomers.

As a first example, de Andrade and colleagues applied RuAAC under microwave-assisted irradiation to synthesized 1,5-disubstituted 1,2,3-triazoles derivatives (**71**), which exhibited activity against *Trypanosoma cruzi*, from *N*-benzyl-2-azidoacetamide (**70**) and commercial alkynes (**59**) in the presence of $Cp^*RuCl(PPh_3)_2$ (pentamethylcyclopentadienyl bis(triphenylphosphine)ruthenium(II) chloride) as the catalyst in dioxane (Scheme **11A**) [87].

Similarly, Chouaïb and coworkers achieved the regiospecific synthesis of 1,5-disubstituted 1,2,3-triazoles (**73**) from oleanolic acid-alkyne derivative (**72**) and aromatic azides (**37**) under microwave irradiation. After optimizing the parameters, the best results were obtained in the presence of the ruthenium catalyst, $Cp^*RuCl(PPh_3)_2$ (5 mol%), in DMF. The optimized conditions afforded the desired new compounds after 3-6 min of reaction with 84-96% yields. Furthermore, the derivatives of 1,5-disubstituted 1,2,3-triazoles (**73**) were cytotoxic against murine EMT-6 (breast) and human SW480 (colon) cancer cell lines; they also exhibited anti-inflammatory properties in an LPS-stimulated human Peripheral Blood Mononuclear Cell (PBMC) test (Scheme **11B**) [88].

Kracker and his group developed a synthesis route for triazole-peptidotriazolamer hybrid molecules, which combined the features of peptides and triazolamers, thus exhibiting peptidomimetic structures. The obtained peptidotriazolamers (**79**) contained chiral 1,5-disubstituted 1,2,3-triazoles moieties in an alternating fashion with amide bonds. Microwave-assisted RuAAC from chiral propargy-

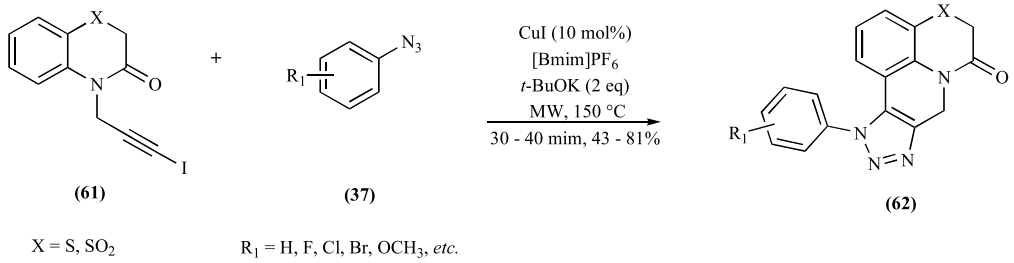

Scheme 8. Synthesis of fused benzothiazino[1,2,3]triazolo[4,5-*c*]quinolinone derivatives (**62**).

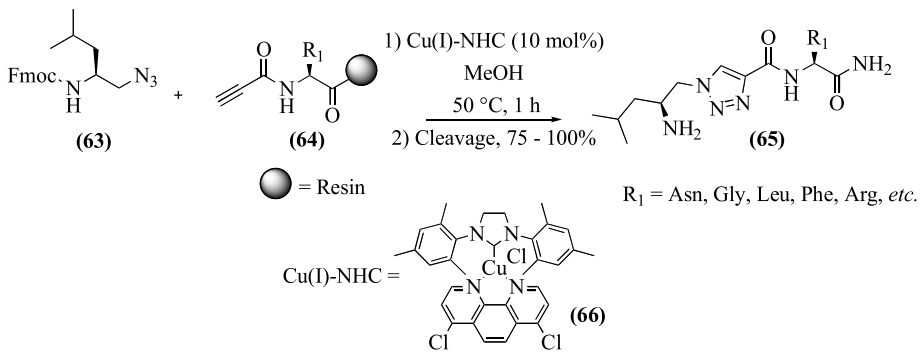

Scheme 9. Microwave-assisted solid-phase synthesis of peptidotriazoles (**65**).

lamines (**74**) and α -azide acids (**75**) in the presence of Cp*RuCl(COD) and THF as the catalyst and solvent, respectively, were employed as 1,5-disubstituted 1,2,3-triazole building blocks (**76**) in excellent yields within 1-2 h. The obtained homochiral and heterochiral triazole dipeptide building blocks (**77-79**) were further employed to assemble larger peptidotriazolamers *via* solution-phase peptide synthesis (Scheme **11C**) [89].

Conversely, some related reactions do not require catalysts to yield the 1,5-disubstituted isomers. For example, Rungta and colleagues performed the regiospecific and stereospecific syntheses of C-4′-(1,5-disubstituted)-triazole-spiro-α-L-arabinofuranosyl (**81**) nucleosides *via* the intramolecular Huisgen 1,3-dipolar cycloaddition reaction. Microwave irradiation ensured an increase in the yields, as well as a decrease in the reaction time (Scheme **12A**). According to the authors, prolonging the Huisgen cycloaddition reaction under conventional heating will cause the decomposition of the nucleoside precursor, and this explains the increased yields that were obtained *via* microwave-assisted Huisgen 1,3-dipolar cycloaddition reaction [90].

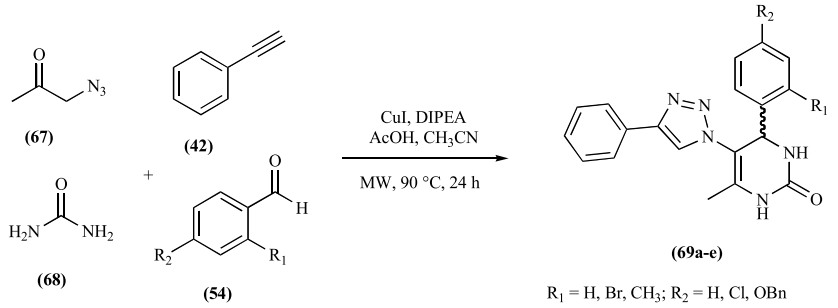

Scheme 10. One-pot synthesis of 1,2,3-triazole-dihydropyrimidinone hybrids (**69a-e**).

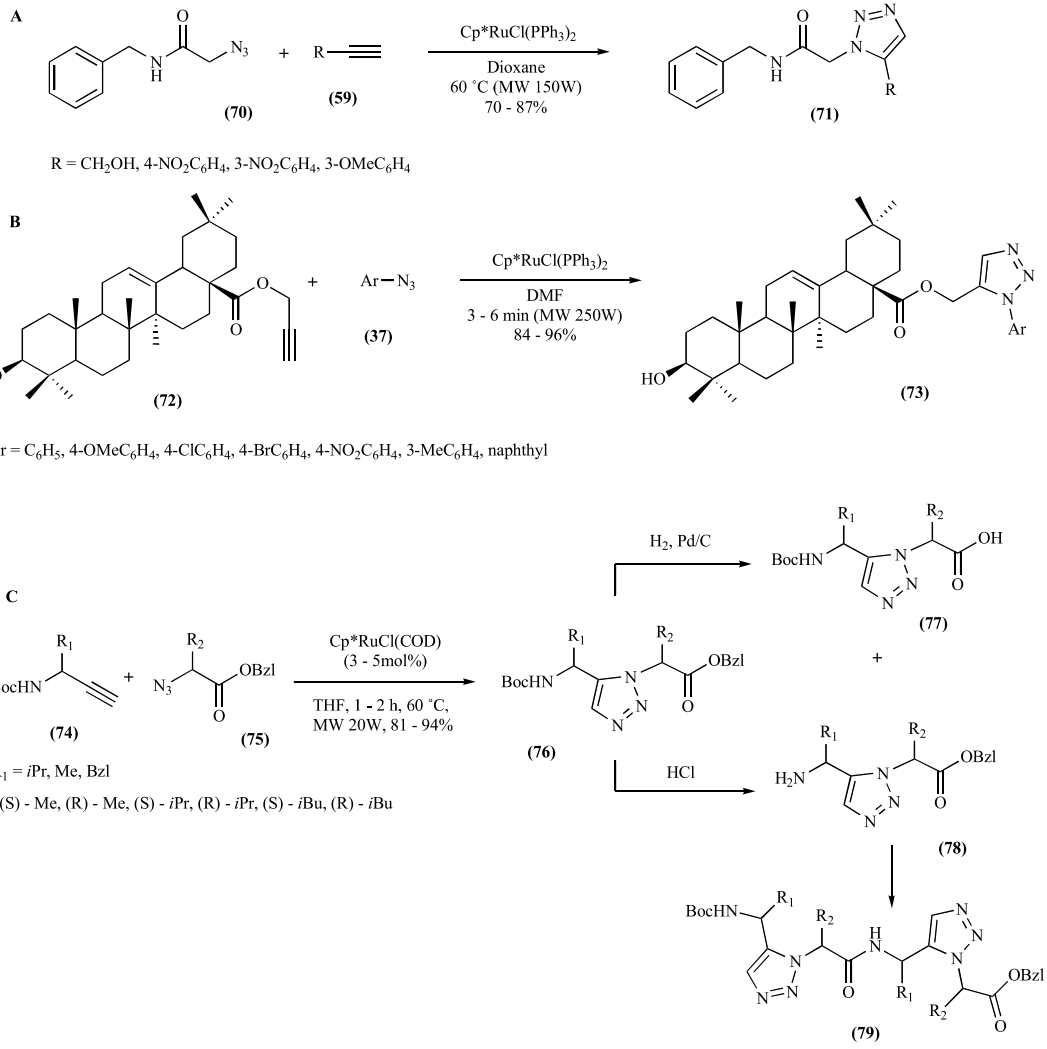

Scheme 11. Microwave-assisted RuAAC synthesis of 1,5-disubstituted 1,2,3-triazole building blocks. **A -** Synthesis of 1,5-disubstituted 1,2,3-triazoles (**71**); **B -** Synthesis of 1,5-disubstituted 1,2,3-triazoles (**73**); **C -** Synthesis of 1,5-disubstituted 1,2,3-triazoles (**76**) and derivatives (**77-79**).

As a final example, Medvedeva and coworkers proposed different synthesis routes for 1,2,3-triazole-5-carbaldehyde oxime (**85**) and observed that the most suitable route was the multicomponent reaction between trimethylsilylpropynal (**82**), trimethylsilyl azide (**83**), and hydroxylamine (**84**) in aqueous methanol under microwave irradiation. It achieved increased yields, reduced reaction time, and did not require any metal catalyst (Scheme **12B**) [91].

2.3. Microwave-assisted Synthesis in the Derivatization of 1,2,3-triazole Compounds

Microwave synthesis is valuable to the construction of 1,2,3-triazoles, as well as their derivatization and modification. Many reactions, such as alkylation, alkenylation, C-H activation, transannulation, and multicomponent reactions, as well as the Buchwald, Ullmann, and Suzuki cross-coupling reactions, involving microwave irradiation, have been described for this heterocycle.

The alkylation of the triazole N3 atom is quite common. Bulman Page and colleagues developed an efficient microwave-assisted method for converting 1-benzyl-4-phenyl-1,2,3-triazoles into 1-alkyl-5-phenyl 1,2,3-triazoles. The authors demonstrated the selective *N*-alkylation reaction of 1,4-disubstituted triazoles (**86**) to yield 1,3,4-trisubstituted-1,2,3-triazolium salts (**87**). A further debenzylation of **87** by treating it with potassium *tert*-butoxide yielded 1,5-disubstituted triazoles (**88**) *via* an inexpensive alternative ruthenium-free synthetic route (Scheme **13A**). The application of microwave irradiation to the *N*-alkylation of 1,4-disubstituted triazoles (**86**) obtained a higher yield of salts in much-reduced reaction times compared with the applications of conventional methods [92].

Similarly, Malekdar employed the alkenylation process to synthesize *N*-alkenyl-1,2,3-triazole derivatives (**91** and **92**) in good yields *via* a fast one-pot microwave-assisted solvent-free reaction of 1,2,3-benzotriazole (**89**) or 1*H*-triazole-4-carboxylic acid methyl ester (**90**) with alkyl-propiolates (**59**) (Scheme **13B**) [93].

C(5)-H activation is an interesting and existing method for deriving 1,2,3-triazoles. Targeting these modifications, Zhao and coworkers proposed the microwave-assisted $Pd(OAc)_2$-catalyzed C(5)-H arylation of 1,4-disubstituted 1,2,3-triazoles (**93**) without ligands obtain trisubstituted triazoles (**95**) (Scheme **14A**). The reaction conditions were optimized by varying the solvents, catalysts,

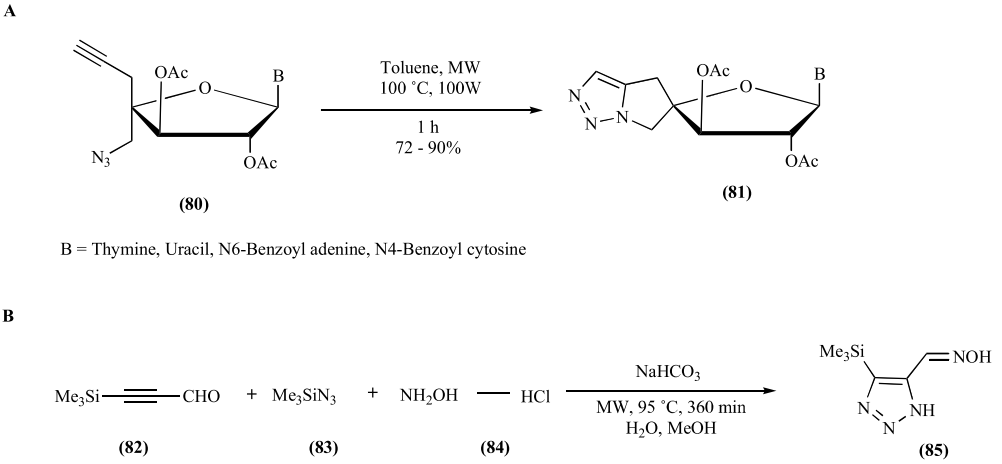

Scheme 12. A - Microwave-assisted synthesis of C-4'-(1,5-disubstituted)-triazole-spiro-α-L-arabinofuranosyl (**81**); **B -** Microwave-assisted multicomponent reaction for 4-trialkylsilyl (germyl)-1*H*-1,2,3-triazole-5-carbaldehyde oximes (**85**) synthesis.

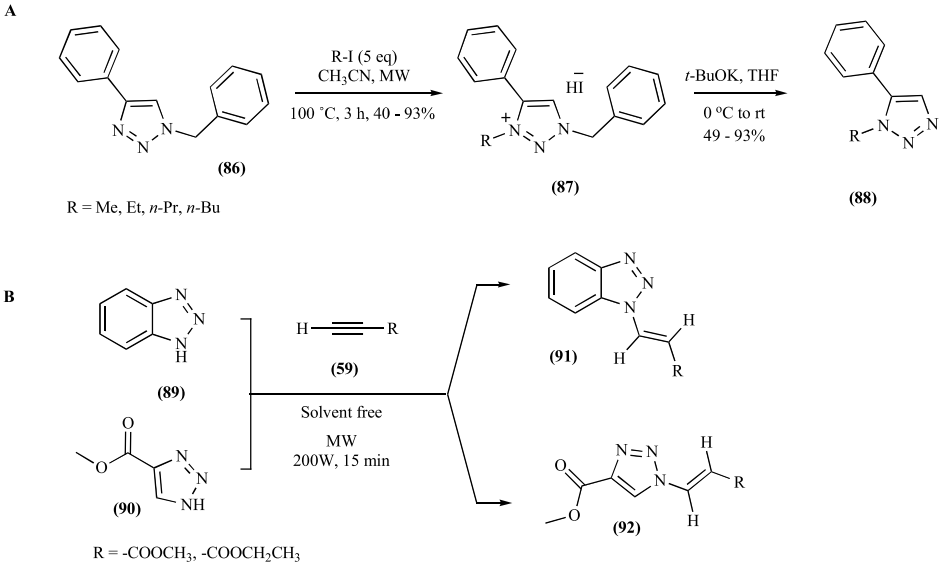

Scheme 13. A - Preparation of 1,3,4-trisubstituted 1,2,3-triazolium salts (**87**) by a microwave-assisted selective *N*-alkylation reaction with further obtaining of 1,5 disubstituted triazoles (**88**); **B -** Solvent-free, fast microwave-assisted one-pot synthesis of *N*-alkenyl 1,2,3-benzotriazoles (**91**) and triazoles (**92**).

bases, and additives, and the optimum conditions comprised the utilization of DMA with a $Pd(OAc)_2$ catalyst, Cs_2CO_3 as the base, and *t*-$BuCO_2H$ as the additive. Further, different microwave irradiation power levels were compared with their conventional heating levels; the microwave conditions exhibited better yields at 10 W for 1 h. Additionally, the trisubstituted triazoles (**95**) could be transformed into 4,5-disubstituted-1,2,3-triazoles (**96**) through debenzylation employing the one-pot microwave method [94].

There are only a few examples in the literature regarding the direct and selective C5 arylations of monosubstituted 1-benzyl-1,2,3-triazole derivatives; this is due to the intrinsic reactivity challenges. However, Liu and collaborators recently reported a simple and efficient method for obtaining a 1,2,3-triazole-1,5-disubstituted scaffold (**99a-r**) through the microwave-assisted C5 regioselective arylation of 1-benzyl-1,2,3-triazoles (**97a-e**) with aryl bromides (**98a-j**) (Scheme **14B**). The results indicated that ligand P(*t*-$Bu)_3$-HBF_4 exhibited the best performance compared with PPh_3 and PCy_3. Moreover, it was determined that K_2CO_3 was more effective than DBU, pyridine, and Et_3N in DMF. The results in which the phenyl bromides containing electron-withdrawing groups exhibited higher yields, also indicated that the different phenyl bromides achieved good to excellent yields [95].

Transannulation, which is a highly efficient atom-economical method for synthesizing other five-membered heterocycles, is a very common derivatization reaction route for 1,2,3-triazoles. Motornov and coworkers reported the several rhodium-catalyzed transannulation reactions of *N*-(per)-fluoroalkyl-1,2,3-triazoles to produce a range of structurally diverse five-membered nitrogen heterocycles. The authors applied the opening of the ring of *N*-(per)-fluoroalkyl-substituted 1,2,3-triazoles (**100**), followed by nitrogen elimination and microwave-assisted cycloaddition employing different enol ethers (**101**), silyl ketene acetals (**102**), nitriles (**103**), and isocyanates (**104**) to demonstrate the formations of *N*-(per)-fluoroalkyl-substituted pyrroles (**105**), pyrrolones (**106**), imidazoles (**107**), and imidazolones (**108**), respectively (Scheme **15**). The best conditions were established, following a study to optimize the transannulation reaction, indicating that microwave heating with a rhodium(II)octanoate dimer catalyst in chloroform was optimal [96].

In the same year (2018), Motornov also reported the microwave-assisted rhodium-catalyzed transannulation of *N*-perfluoroalkylated 1,2,3-triazoles (**100**) with 1- or 2-substituted 1,3-dienes (**109**) *via* the aza-[4 + 3] pathway to yield the *N*-perfluoroalkylated azepine derivatives (**110**) (Scheme **15**). The reaction conditions of the transannulation were optimized to increase the yields, and the best results were obtained with the rhodium(II)octanoate dimer catalyst in DCE [97].

Multicomponent reactions are very valuable tools in organic synthesis, and 5-amino-1,2,3-triazole is an interesting synthon for this purpose [98]. Gladkov proposed a three-component synthesis route for a new spiro derivative (**114**) from 5-amino-1,2,3-triazole-4-carboxamide (**111**), malononitrile (**112**), and cyclohexanone (**113**) in ethanol and triethylamine *via* microwave activation or conventional heating (Scheme **16A**). The authors revealed that employing both heating methods, a single product was formed without major differences in the yields, although the reaction times decreased considerably from the conventional heating reaction (5 h) to microwave activation (1 h) [99].

Analogously, Tkachenko and colleagues proposed the three-component reaction of 5-amino-2*H*-1,2,3-triazole derivatives (**111**) with acetaldehyde (**115**) and 1,3-dicarbonyl (**116**) compounds in an aqueous medium under microwave irradiation and achieved the regioselective formation of 4,7-dihydro[1,2,3]triazolo[1,5-a]pyrimidines (**117**). The authors also reported that the utilization of ethyl 4,4,4-trifluoro-3-oxobutanoate (**118**) as a 1,3-dicarbonyl compound under the same reaction conditions yielded the 5-hydroxy-4,5,6,7-tetrahydro derivatives (**119a-b**), which were not dehydrated by the reaction medium (Scheme **16 B**) [100].

Cross-coupling reactions are a convergent method for deriving 1,2,3-triazoles in the last synthesis step. De Nascimento and coworkers reported the synthesis of 1,2,3-triazolo-1,3,6-triazonines, **122**, from 5-iodo-1,2,3-triazoyl benzaldehydes (**120**) and substituted diaminobenzenes (**121**) *via* a copper-catalyzed intramolecular Ullmann cross-coupling reaction in DMSO in the presence of a 5 mol% CuI catalyst at 100 °C under microwave irradiation (Scheme **17A**). The results demonstrated that microwave irradiation reduced the reaction time and increased the yield compared with conventional heating. Thereafter, parameters, such as the time, temperature, solvent, and catalyst, were also optimized [101].

Jung and colleagues employed a structure-based drug design approach to develop novel resorcinolyl triazole derivatives (**125a-v**) as Hsp90 inhibitors. The click chemistry between the iodoethynyl resorcinol derivative and an azido was employed to synthesize a new family of 5-iodo-1,2,3-triazoles (**123**). The palladium-catalyzed Suzuki couplings of (**123**) with various arylboronic acids (**124**) were performed under microwave irradiation employing $Pd(dppf)Cl_2$ with Cs_2CO_3 in DMF and H_2O for 30 min at 100 °C (Scheme **17 B**). Subsequently, the methyl and benzyl groups were deprotected by BBr_3 or Pd/C, affording the 4-resorcinolyl-5-aryl-1,2,3-triazoles (**125a-v**) (Scheme **17B**). The IC_{50} values of the Hsp90 inhibitors [**125e** (R_1 = *i*Pr, R_3 = 4-SO_2-CH_3, R_4 = OCH_3), **125f** (R_1 = *i*Pr, R_3 = 3-SO_2-CH_3, R_4 = OCH_3), and **125q** (R_1 = *i*Pr, R_3 = 4-SO_2-CH_3, R_4 = OCH_2CH_3) were ~45 nM, and they displayed >350-fold selectivity for Hsp90 over TRAP1. Therefore, these Hsp90 inhibitors exhibited potentials for further development as antitumor agents [102].

3. 1,2,4-TRIAZOLES

Further, 1,2,4-triazoles are heterocycles that have been increasingly considered owing to their potential applications in different chemistry fields, mainly medicinal chemistry. Similar to the 1,2,3-triazole isomer, these heterocycles are amphoteric (they are considered weak bases and acids (pK_a = 10.26 and pK_aH = 2.19) [103].

The 1,2,4-triazole ring can be synthesized *via* different routes, including the Einhorn-Brunner and Pellizzari reactions. The Einhorn-Brunner reaction occurs between hydrazines and diacylamines to yield two isomers of 1,2,4-triazole, while the Pellizzari reaction occurs between amides and hydrazides [104].

Furthermore, 3-amino-1,2,4-triazoles and 1,2,4-triazole-3-thiones derivatives are very promising and can be obtained *via* several routes. For example, 1,5-disubstituted-3-amino-1,2,4-triazole can be obtained *via* the reaction of *N*-acyl-*S*-methylisothiourea derivatives with arylhydrazines. Another possible route toward 1,5-disubstituted derivatives comprises the reaction between 1,3,4-oxadiazolium perchlorate and cyanamide. The 1,2,4-triazole-3-thiones nucleus can be obtained *via* the intramolecular cyclization of acylthiosemicarbazide derivatives [35, 105-107] (Fig. **4**).

3.1. Synthesis and Derivatization of 1,2,4-triazole Under Microwave Irradiation

For this first set of 1,2,4-triazoles, we consider only those in which C3 and C5 are attached to the aryl, alkyl, or hydrogen sub-

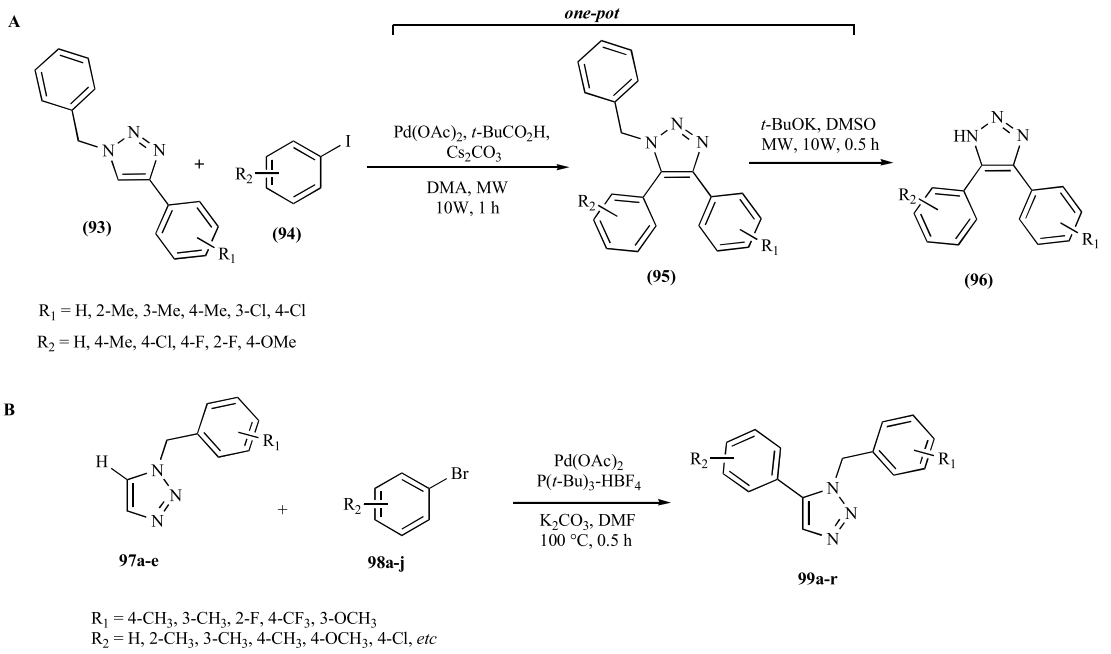

Scheme 14. A - Synthesis of 1,4,5-trisubstituted 1,2,3-triazoles (**95**) through C(5)–H activation of 1,4-disubstituted 1,2,3-triazoles (**93**); **B -** C-5 arylation of 1-benzyl-1,2,3-triazoles (**97a-e**).

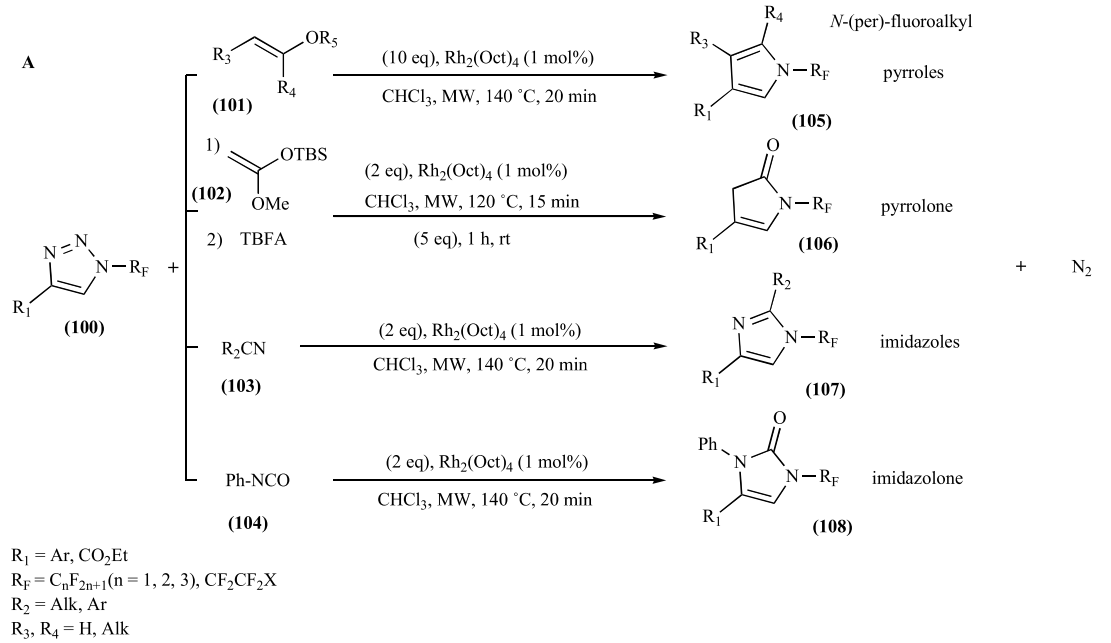

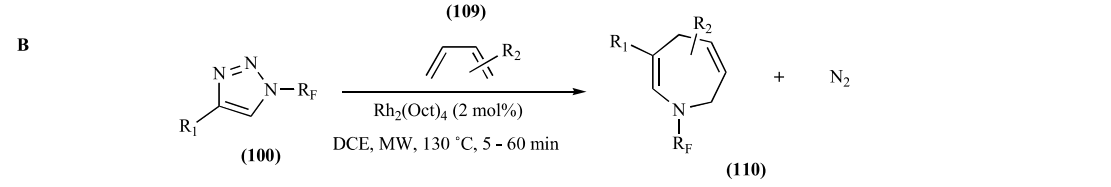

Scheme 15. A - Transannulation reactions with 1,2,3-triazoles (**100**) leading to structurally diverse five membered nitrogen heterocycles (**105-108**); **B -** Synthesis of *N*-perfluoroalkyl-2,5-dihydroazepines (**110**) derived from 2-substituted 1,3-dienes (**109**) and triazoles (**100**).

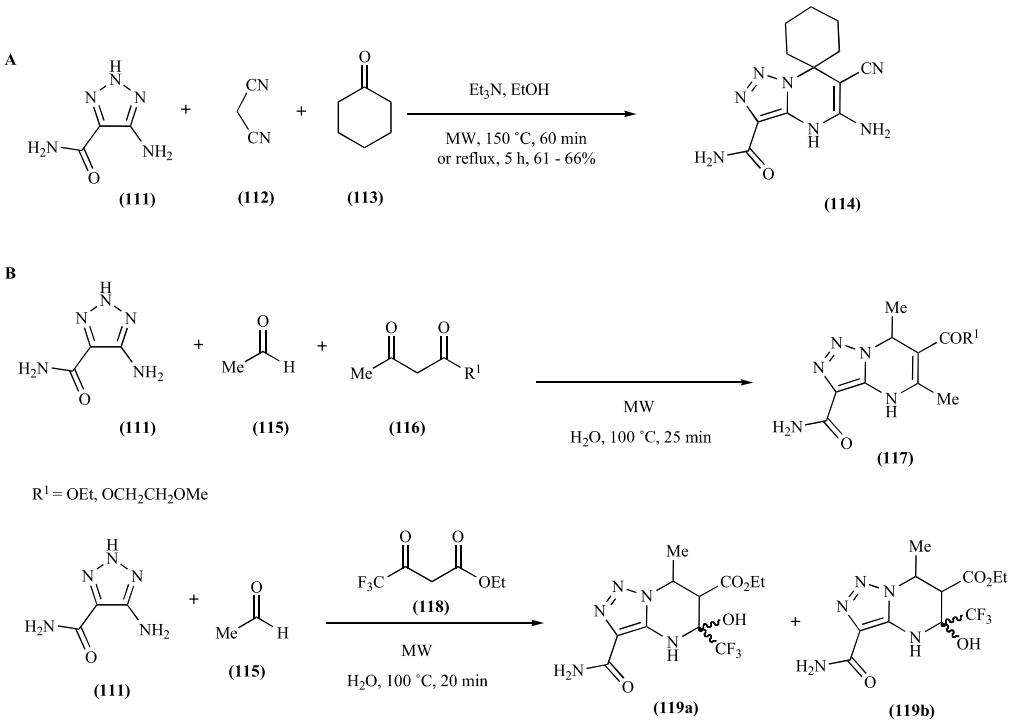

Scheme 16. A - Three-component synthesis of a new spiro derivative (**114**); **B -** Multicomponent microwave-assisted synthesis of azolopyrimidine derivatives (**117**) and (**119a-b**).

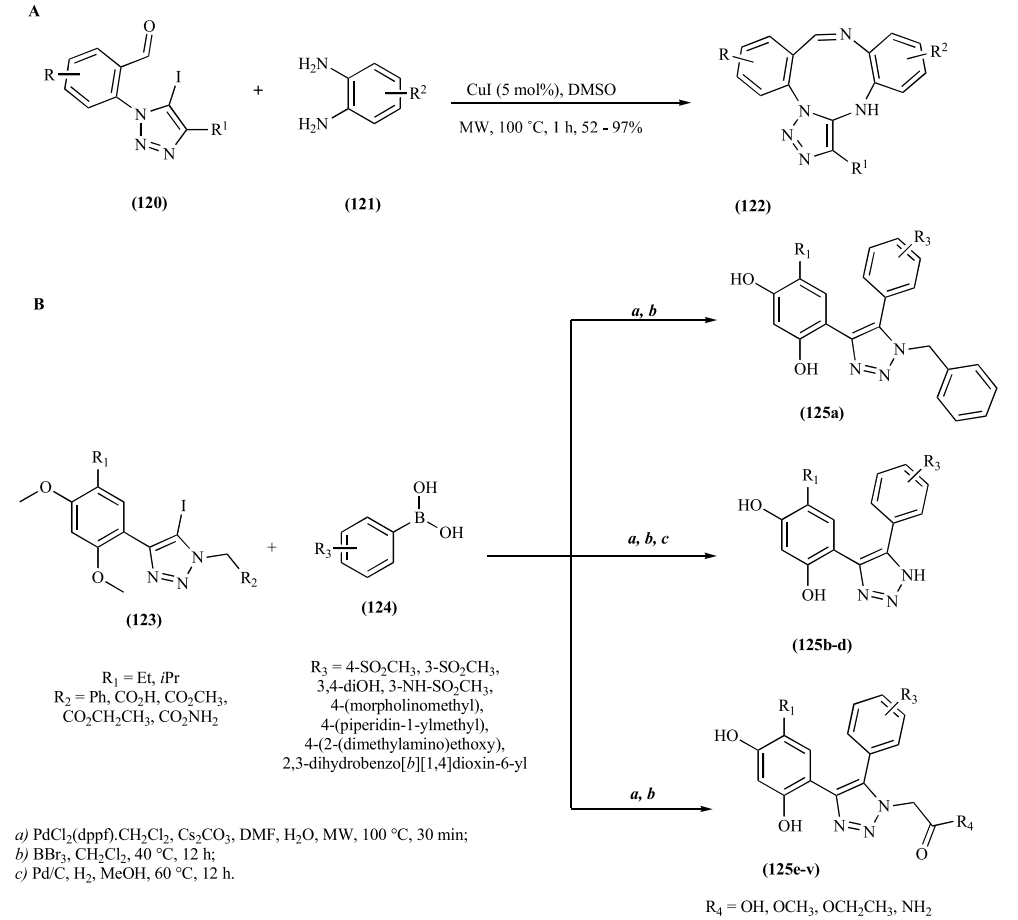

Scheme 17. A - Ullmann cross-coupling in the synthesis of 1,2,3-triazolo-1,3,6-triazonines (**122**); **B -** Preparation of 4-resorcinolyl-5-aryl-1,2,3-triazoles (**125a-v**) HSP90 inhibitors by Suzuki cross-coupling reaction.

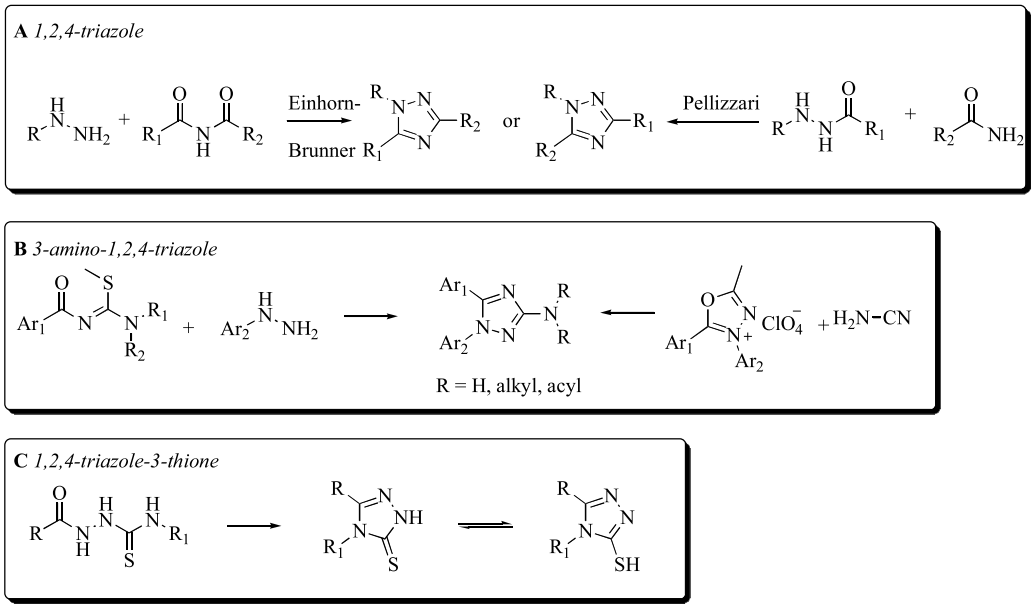

Fig. (4). General scheme for synthesis of (**A**) 1,2,4-triazoles, (**B**) 3-amino-1,2,4-triazoles and (**C**) 1,2,4-triazole-thiones.

stituents. This class of compounds usually contains hydrazides as reactants. In the first example demonstrated below, Sangshetti and colleagues synthesized a series of 5-((5-substituted-1*H*-1,2,4-triazol-3-yl)methyl)-4,5,6,7-tetrahydrothieno[3,2-*c*]pyridines (**127a-i**) from thienopyridine hydrazide (**126**) and substituted aromatic nitriles in the presence of 4-dimethylaminopyridine (DMAP) as the catalyst under microwave irradiation. To obtain the 1,2,4-triazole core, they optimized the reaction conditions with different bases, solvents, and catalysts. Thus, the best yield (91%) was obtained with 30 mol% DMAP and ethanol for 20 min under microwave irradiation (700 W). Additionally, the reaction scope was expanded to include different substituted aromatic nitrites under optimized conditions to furnish compounds exhibiting *in vitro* antifungal activities, thus revealing the potential and drug-like properties of the newly synthesized 1,2,4-triazoles (**127a-i**) (Scheme **18A**) [108].

A more substituted 1,2,4-triazole (3,4,5-trisubstituted) series (**130**) was obtained *via* one-pot synthesis from secondary amides (**128**) and hydrazides (**129**) employing triflic anhydride activation, followed by microwave-induced cyclodehydration (Scheme **18B**). Bechara and co-workers demonstrated the optimization process by varying the presence or absence of a base, as well as varying the time and temperature. Consequently, the highest yield (85%) was observed from cyclodehydration at 140 °C after 2 h. Moreover, the reaction scope was expanded, and the results demonstrated that these optimized conditions were favored the syntheses of many 3,4,5-trisubstituted 1,2,4-triazoles (**130**) exhibiting different alkyl/aryl substitution patterns in moderate to good yields (40-89%) [109].

Single N1-substituted 1,2,4-triazoles (**133a-q**) were obtained *via* a simple, efficient, and catalyst-free method from substituted hydrazines (**131a-q**) and formamide (**132**) under microwave irradiation (Scheme **19A**). The reaction conditions were optimized by varying the formamide equivalents, solvents, temperatures, and times under microwave irradiation (230 W) to obtain the 1,2,4-triazoles moieties (**133a-q**). The best conditions were observed upon irradiating the hydrazines (**131a-q**) with 20 equivalents of formamide (**132**) for 10 min at 160 °C to obtain substituted 1,2,4-triazoles (**133a-q**) in 54-81% yields [110].

The regioselective alkylation of 1,2,4-triazole (**4**) in potassium carbonate, ionic liquid (IL) (hexylpyridinium bromide), and alkyl bromides (**134**) is another method for synthesizing N1-substituted 1,2,4-triazoles (**135**). It was demonstrated by Kaur and coworkers as a green and environmentally sustainable method. They employed a microwave apparatus for 10 min at 110 °C (Scheme **19B**) to afford the products in an 88% yield. Compared with conventional heating, microwave irradiation accelerated the reaction and afforded the products with improved yields. Additionally, the base-IL system could be successfully reused for five cycles [111].

3.2. Synthesis and Derivatization of 3-amino-1,2,4-triazole Under Microwave Irradiation

Additionally, 3-amino-1,2,4-triazoles are fascinating compounds, which are similar to cyclic guanidines. Recently, Santos and colleagues described an efficient one-pot regioselective route for synthesizing *N*-protected or *N*-deprotected 1,5-diaryl-3-amino-1,2,4-triazoles (**137a-b**) from *N*-acyl-*N*-Boc-carbamidothioates (**136**) and phenylhydrazines (**131**) under microwave irradiation. The cyclization reaction to synthesize the 3-amino-1,2,4-triazole moiety was performed in two different solvents, heating sources, and times. During the optimization, it was observed that the introduction of an electron-withdrawing group at the -C=NH(S-CH_3) moiety employing a labile *tert*-butyloxycarbonyl group (-BOC) was necessary to increase the reactivity and ensure selectivity. The best conditions for the regioselective syntheses of 3-amino-1,2,4-triazole derivatives (**137a-b**) were microwave heating with acetonitrile for 40 min at 100 °C (to form the protected 1,5-diphenyl-3-amino-1,2,4-triazoles (**137a**) in an 87% yield). Conversely, to obtain the deprotected 1,5-diphenyl-3-amino-1,2,4-triazole (**137b**), DMF was utilized for 60 min at 150 °C, obtaining yields of up to 84%. Furthermore, derivatization of the amino groups yielded Compounds **138a-d**, which could inhibit cholinesterases with good IC_{50} values of up to 1 μM, thereby exhibiting the potentials of this class of compounds as new scaffolds for anticholinesterase activity (Scheme **20**) [112].

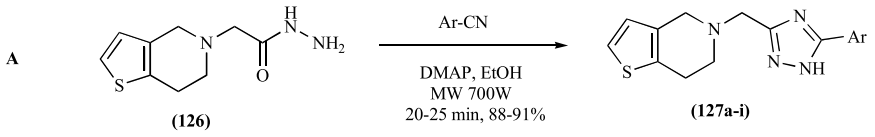

127a: Ar = Ph; **127b**: Ar = 4-Cl-Ph; **127c**: Ar = $CHPh_2$; **127d**: Ar = 3-Cl-Ph; **127e**: Ar = 2-Cl-Ph.
127f: Ar = 2-NH_2-Bn; **127g**: Ar = 4-F-Bn; **127h**: Ar = 4-MeO-Bn; **127i**: Ar = Bn.

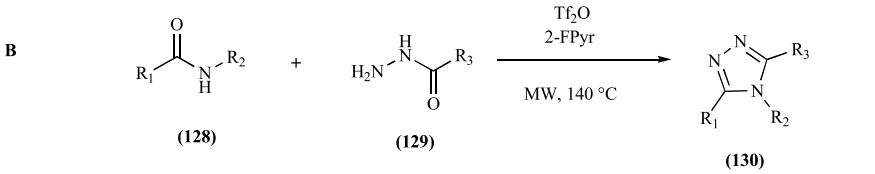

Scheme 18. Synthesis of 1,2,4-triazoles from hydrazides. **A -** Synthesis of novel 5-((5-substituted-1-*H*-1,2,4-triazol-3-yl) methyl)-4,5,6,7-tetrahydrothieno[3,2-*c*]pyridine (**127a-i**); **B -** One-pot synthesis of 3,4,5-trisubstituted 1,2,4-triazoles derivatives (**130**).

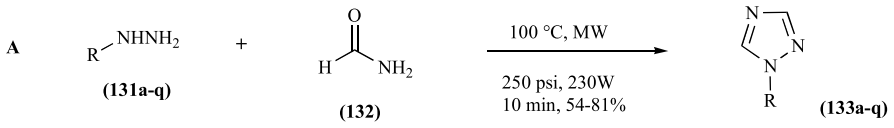

a: R = Ph; b: R = 4-MeO-C_6H_4; c: R = 2-Me-C_6H_4; d: R = 3-Me-C_6H_4; e: R = 3,4-Me_2-C_6H_3; f: R = 4-*t*-Bu-C_6H_4; g: R = 3-F-C_6H_4; h: R = 2-Cl-C_6H_4; i: R = 3-Cl-C_6H_4; j: R = 4-Cl-C_6H_4; k: R = 2,4-Cl_2-C_6H_3; l: R = 3,4-Cl_2-C_6H_3; m: R = 3-Cl-4-Me-C_6H_4; n: R = 4-Br-C_6H_4; o: R = 4-NC-C_6H_4; p: R = *t*-Bu; q: R = C_6H_{10}

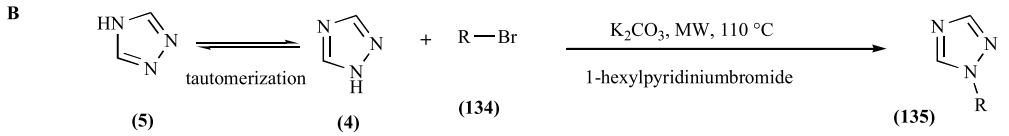

R = -C_4H_9; -C_5H_{11}; -C_6H_{13}; -C_8H_{17}; -$C_{10}H_{21}$; -$CH_2CH{=}CH_2$; -$CH_2C_6H_5$

Scheme 19. Synthesis of single N1-substituted 1,2,4-triazoles. **A -** Catalyst-free synthesis of substituted *N*-alkyl or aryl-1,2,4-triazoles (**133a-q**) from hydrazines; **B -** Alkylation of 1,2,4-triazole (**4**) using different alkyl halides (**134**).

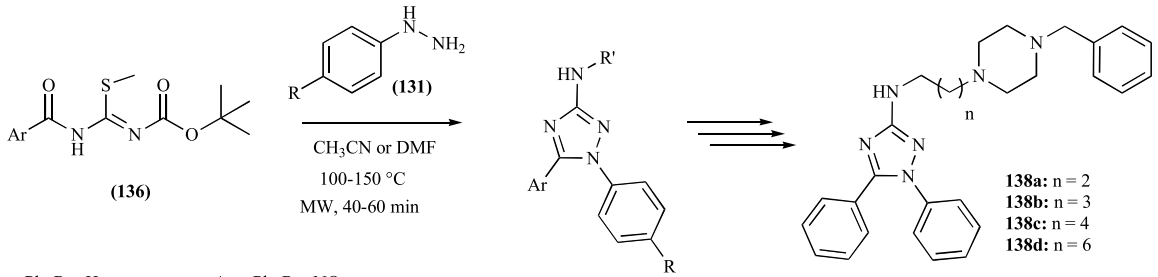

Ar = Ph; R = H
Ar = 4-OCH_3; R = H
Ar = 4-Cl-Ph; R = H
Ar = 4-NO_2-Ph; R = H
Ar = Ph; R = NO_2
Ar = Ph; R = SO_2CH_3
Ar = 4,5-di-Br-2-pyrrol; R = H
Ar = 2-Pyrrol; R = H

137a (R' = Boc)
137b (R' = H)

Scheme 20. One-pot regioselective synthesis of 1,5-diaryl-3-amino-1,2,4-triazoles (**137a-b**) and derivatives (**138a-d**) with anticholinesterase activity.

Aminoguanidines are particularly valuable reactants for synthesizing 3-amino-1,2,4-triazoles. Further, 3,3′-(5,5′)-polymethylene-bis-(1*H*-1,2,4-triazol-5(3)-amines) (**141**) was selectively and efficiently synthesized from dicarboxylic acids (**139**) and aminoguanidines (**140**) in an aqueous medium (Scheme **21A**). It has been reported that the condensation of succinic acid with aminoguanidine from which pure ethylene-bis(1*H*-1,2,4-triazol-5-amine) (**141**, n = 0) was isolated in 8-11% yields employing conventional heating, without selectivity. However, this limitation was resolved *via* microwave heating. Therefore, variations in the reaction pa-

rameters revealed that **141** was obtained in good yields and purities by heating succinic acid (**139**, n = 0) and aminoguanidine hydrochloride (**140**) in water for 15 min at 220 °C, followed by the addition of an aqueous solution of sodium hydroxide and further microwave irradiation for 5 min at 200 °C. The scope of the method was successfully explored in the preparation of a small library of polymethylene-bis(1*H*-1,2,4-triazol-5(3)-amines) exhibiting different alkyl chain linkers [113].

Similarly, Lim and coworkers demonstrated two pathways for synthesizing *N*-substituted 3-(5-amino-1*H*-1,2,4-triazol-3-yl) propanamides (**146** and **147**). The first began with the synthesis of *N*-guanidinosuccinimide (**144**) from succinic anhydride (**142**) and aminoguanidine hydrochloride (**140**), followed by its reaction with amines (**145**) and the cyclocondensation and cyclization of the 1,2,4-triazole ring under microwave irradiation (Scheme **21B**, Pathway B1). Thus, the desired product (**146**) was obtained in high purity after simple filtration, and the best results were achieved in acetonitrile for 25 min at 170 °C. This methodology was successful with aliphatic amines; however, it failed when less-nucleophilic aromatic amines were utilized. Therefore, an alternative pathway was applied; it involved the initial preparation of *N*-arylsuccinimides (**145**), followed by their reaction with aminoguanidine hydrochloride (**140**) under microwave irradiation (Scheme **21B**, Pathway B2). The most efficient condition was observed in ethanol for 50 min at 170 °C, followed by the addition of a potassium hydroxide solution in ethanol and heating for 15 min at 180 °C to produce **147** in a 58% yield [114].

Employing the microwave-assisted Fries rearrangement, 2-fluoro-*N*-(3-methylsulfanyl-1*H*-1,2,4-triazol-5-yl)benzamide (**151**) was prepared under catalyst and solvent-free conditions (Scheme **22**) from a tertiary amide (**150**), which was previously synthesized *via* the *N*-acylation of 3-amino-5-methylsulfanyl-1*H*-1,2,4-triazole (**148**). The authors tested many conditions by varying the temperatures and solvents, and compared microwave irradiation with conventional heating. The classical reaction protocols employing THF or toluene under reflux for 6 h afforded the desired product but with low yields (15% or 31%, respectively). Moreover, it was observed that high temperatures favored the Fries rearrangement. In the modified method, the microwave-assisted reaction under solvent and catalyst-free conditions at 413-453 K improved the reaction time to 20 min with the highest yield (84%). X-Ray Crystallography (XRC) and the theoretical studies (DFT) of the formation of an intimate ion pair were performed as the key step and analysis to investigate the mechanistic pathway of the Fries rearrangement [115].

3.3. Synthesis and Derivatization of 1,2,4-triazol-3-one and 1,2,4-triazol-3-thiol Under Microwave Irradiation

Certainly, 1,2,4-triazol-3-one and 1,2,4-triazole-3-thiol (or 1,2,4-triazole-3-thione) are the most described and explored classes of 1,2,4-triazoles. Xu and colleagues described the design, synthesis, and antifungal activities of novel 1,2,4-triazole thioether derivatives (**156a-m**) exhibiting a pyrimidine moiety. The synthesis proceeded with the preparation of 2-((4,6-dimethylpyrimidin-2-yl)thio)acetohydrazide (**153**) from ethyl-2-(4,6-dimethylpyrimidin-2-ylthio)acetate (**152**) and hydrazine hydrate under microwave irradiation at 80 °C for 10 min. Subsequently, 2-((4,6-dimethylpyrimidin-2-yl)thio)acetohydrazide (**153**) (the hydrazides were the precursors of almost all the 1,2,4-triazol-3-thiols) reacted with PhNCS (**154**) under microwave irradiation for 15 min at 80 °C to yield the 1,2,4-triazol-3-thiol derivative (**155**) in an 88% yield (Scheme **23**). The results demonstrated that the synthesis of the intermediate, **155**, *via* the conventional method expended more reaction time than the microwave-assisted method, which expended only 10 min, with a comparable yield. Additionally, **156a-m** demonstrated moderate to good inhibitory activities against *C. orbiculare* and *R. solani* and could be further optimized as potential fungicides [116].

Dengale and coworkers synthesized 1,2,4-triazoles derivatives under conventional and microwave heating conditions from the precursor, 2-{[2-(3-fluorophenyl)-4-methyl-1,3-thiazol-5-yl]carbonyl}-*N*-phenylhydrazinecarbothioamides (**158**). The cyclization products, 5-[2-(3-fluorophenyl)-4-methylthiazol-5-yl]-4-phenyl-

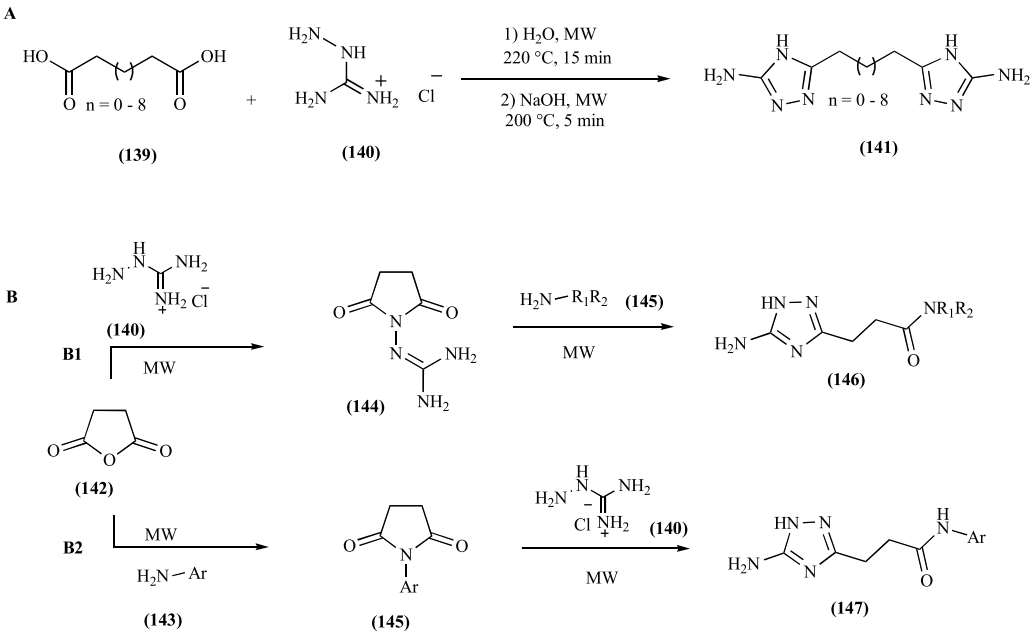

Scheme 21. A - One-pot synthesis of polymethylene-bridged bis (1H-1,2,4-triazol-5(3)-amines) (**141**); **B -** Synthesis of 3-(5-amino-1H-1,2,4-triazol-3-yl)propanamides (**146** and **147**).

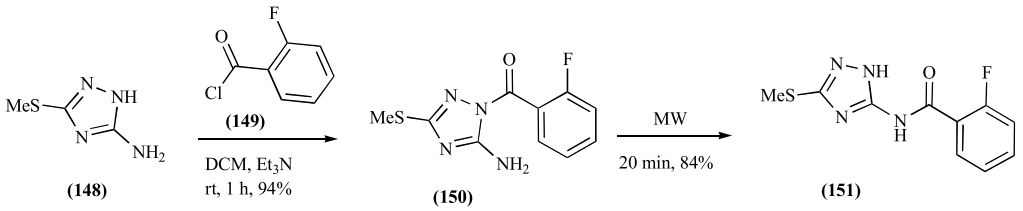

Scheme 22. Synthesis of 2-fluoro-*N*-(3-methylsulfanyl-1H-1,2,4-triazol-5-yl)benzamide (**151**) through microwave-assisted Fries rearrangement.

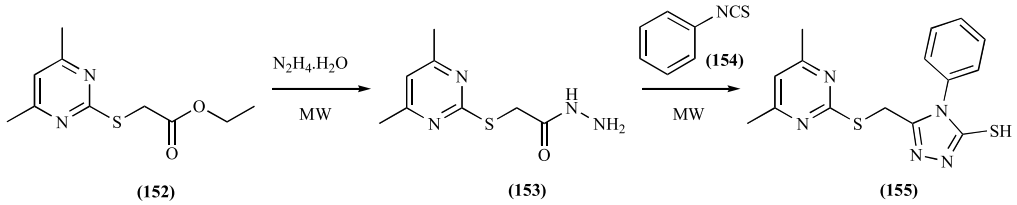

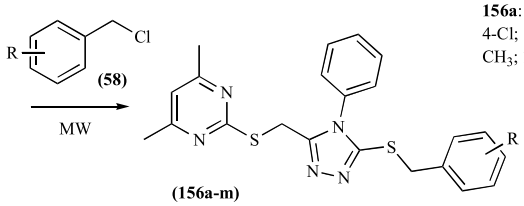

156a: R = 2-F; **156b**: R = 3-F; **156c**: R = 4-F; **156d**: R = 2-Cl; **156e**: R = 3-Cl; **156f**: R = 4-Cl; **156g**: R = 2,4-Cl_2; **156h**: R = 3,5-Cl_2; **156i**: R = 4-Br; **156j**: R = 4-CN; **156k**: R = 3-CH_3; **156l**: R = 3-*t*-Bu; **156m**: R = 4-OCH_3

Scheme 23. Novel series of 1,2,4-triazole thioether derivatives (**156a-m**).

4H-1,2,4-triazole-3-thiol (**159a-e**), were obtained from thiosemicarbazides (**158**) *via* conventional heating in NaOH after 2-3.5 h (yield = 60-69%). The microwave irradiation (200 W) of a mixture of thiosemicarbazide (**158**) and NaOH at 70 °C for 3 min obtained the same products (**159a-e**) in 70-77% yields (Scheme **24A**). All the products were tested for their *in vitro* antibacterial and antifungal activities, and they exhibited moderate to weak activities [117]. Under almost the same conditions, Reddy also obtained coumarin-based triazoles (**161a-e**, 70-84%) from 1-(2-(4-methyl-2-oxo-2-coumarin-7-yloxy)acetyl)-4-aryl thiosemicarbazides (**160**) under microwave irradiation (200 W) at 70 °C for 3 min (Scheme **24B**) [118].

Franklim and coworkers reported a novel series of 1,2,4-triazoles from natural piperine. Additionally, the trypanocidal agent and human serum albumin (HSA) interactions were evaluated. The cyclization step was performed employing thiosemicarbazides (**162a-e**) through the addition of an aqueous solution of NaOH under microwave irradiation (100 W) for 0.5 h to produce the corresponding triazoles (**163a-e**) in good yields (Scheme **24C**). The results revealed that the triazole derivatives (**163a-e**) displayed trypanocidal activities on the proliferative forms of *T. cruzi*, and a low level of toxicity on the host cells (murine macrophages) [119].

Similar to the previous example, several studies have demonstrated the syntheses and biological activities of 1,2,4-triazole derivatives that were obtained *via* the intramolecular cyclizations of semicarbazides or thiosemicarbazides in basic media employing the conventional and microwave-mediated methods. Some of these studies demonstrated new piperazine-azole-fluoroquinolone hybrids (**166**), which were synthesized and screened for antimicrobial and antioxidant activities. The results revealed that the reaction time for synthesizing 1,2,4-triazole was reduced from 3 h (under conventional heating) to 5-7 min (under microwave irradiation at 200 W) (Scheme **25A**) [120-122]. Demirci and colleagues reported the syntheses of 1,2,4-triazole thiomorpholine derivatives (**168**) containing piperidine, β-lactam, fluoroquinolone, and piperazine units (in the R_2 position); most of them demonstrated good to moderate antibacterial and/or antifungal activities. In this study, higher yields (88%-98%) and reduced reaction time [from 3 h (conventional heating) to 5-7 min (microwave heating at 200 W)] were achieved for the microwave-assisted syntheses of 1,2,4-triazole (Scheme **25B**) [123]. Mentese and coworkers demonstrated the synthesis of new hetero-functionalized norfloxacin derivatives comprising a 1,2,4-triazole core (**170**) and their antimicrobial activities; most of them exhibited moderate antimicrobial activities. Microwave irradiation ensures shorter reaction times for the syntheses of 1,2,4-triazole (15-30 min at 200 W) compared with conventional heating (25-40 h) (Scheme **25C**) [124]. Further, the same authors reported the syntheses of new quinolone-1,2,4-triazole hybrids (**172**), as well as their antimicrobial, antioxidant, and anticholinesterase activities. Similarly, microwave irradiation decreased the reaction time from 6 to 16 h (reflux) to 4-20 min (microwave irradiation at 200 W) (Scheme **25D**) [125, 126].

Recently, Balaydın, Özil, and Şentürk reported the syntheses of *N*-aryl-5-methyl-2,4-dihydro-3*H*-1,2,4-triazol-3-one Schiff base derivatives (**179a-j**) in two distinct scientific articles. In both articles, the triazole nucleus was synthesized by treating Compound **173** with ethyl-4-aminobenzoate (**174**) under microwave-assisted, solvent-free conditions to form the corresponding ethyl-4-(3-methyl-5-oxo-1,5-dihydro-4*H*-1,2,4-triazol-4-yl)benzoate (**175**) (Scheme **26A**). Six 1,2,4-triazol-3-one aryl derivatives (**179a-f**) exhibited carbonic anhydrase and cholinesterase (AChE and BuChE) inhibitory properties. Moreover, the synthesized compounds (**179g-j**) exhibited good inhibitory activities against glutathione reductase [126-128].

Liu and colleagues synthesized a series of novel 1,2,4-triazolo[4,3-*a*]pyridin-3(2*H*)-one derivatives (**183a-n**) exhibiting herbicidal activities. The three synthetic steps were performed under microwave irradiation. Cyclization was performed with hydraz-

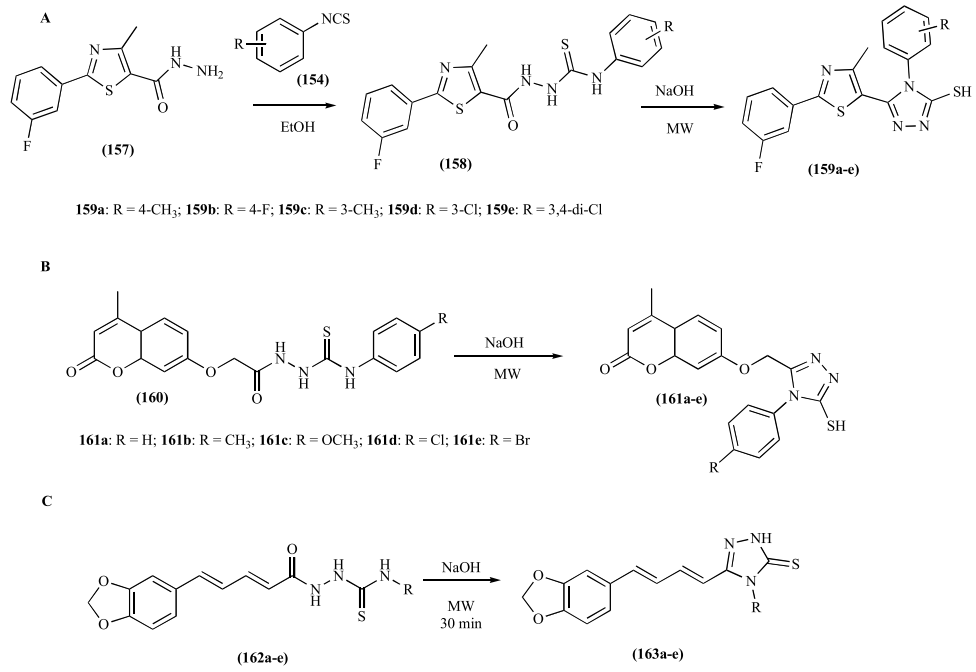

Scheme 24. A - Synthesis of novel 5-[2-(3-fluorophenyl)-4-methylthiazol- 5-yl]-4-phenyl-4*H*-1,2,4-triazole-3-thiol (**159a-e**); **B -** Synthesis of triazole substituted coumarins (**161a-e**); **C -** Synthesis of a novel series of 1,2,4-triazoles (**163a-e**) from natural piperine.

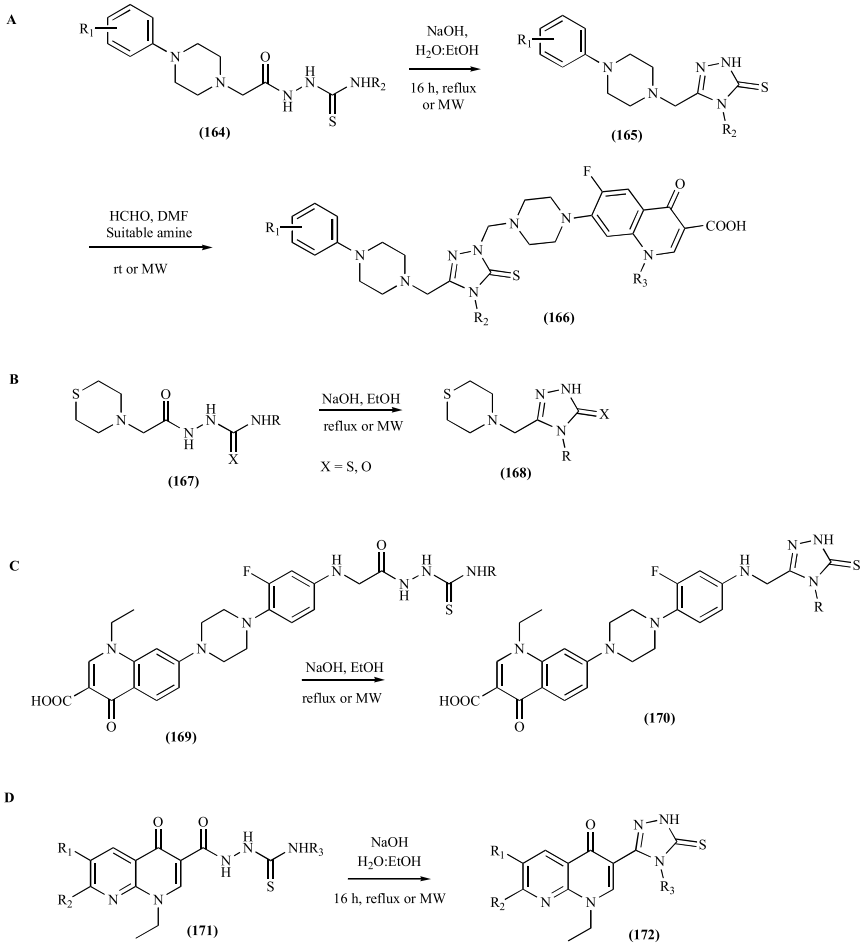

Scheme 25. Examples of different 1,2,4-triazolothione derivatives (**166**, **168**, **170** and **172**) synthesized from cyclization of semicarbazides or thiosemicarbazides under microwave irradiation.

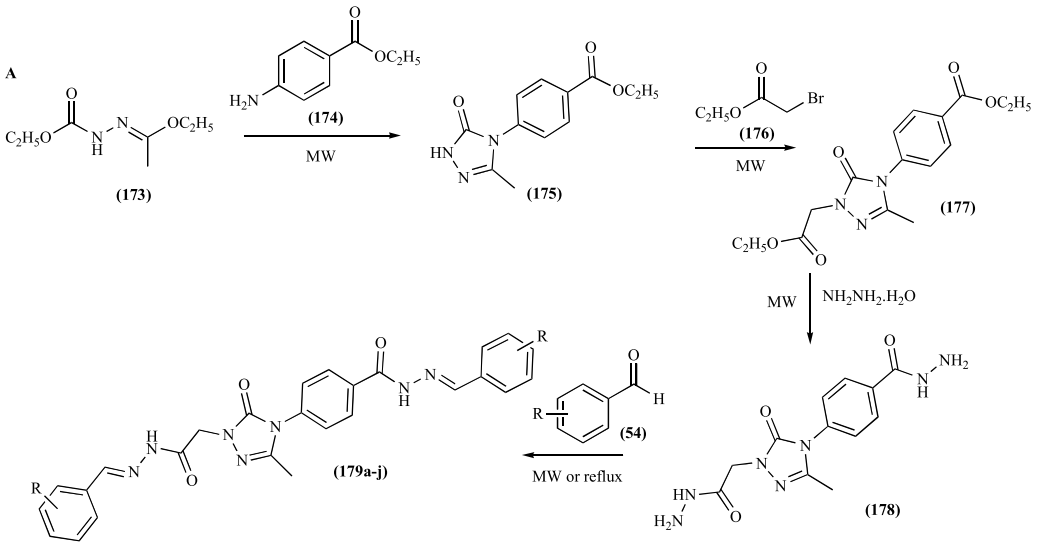

179a: R = H; **179b**: R = 4-Cl; **179c**: R = 4-Br; **179d**: R = 3-Br; **179e**: R = 3-OCH_3; **179f**: R = 2-OH, 4-Br; **179g**: R = 4-OH; **179h**: R = 3-OCH_3, 4-OH; **179i**: R = 4-NO_2; **179j**: R = 4-NO_2

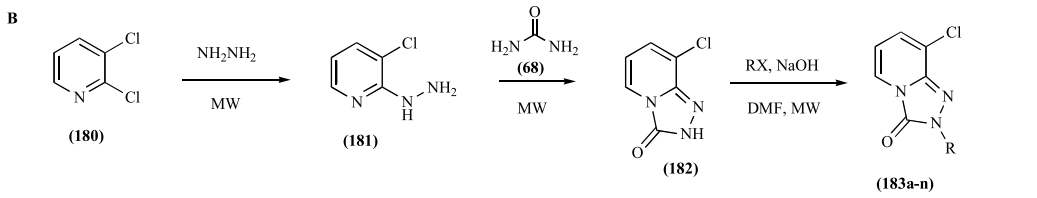

183a: R = 4-CN $PhCH_2$; **183b**: R = 4-Cl $PhCH_2$;**183c**: R = 4-OMe $PhCH_2$; **183d**: R = 3-Cl $PhCH_2$; **183e**: R = $PhCH_2$; **183f**: R = 2-Cl $PhCH_2$; **183g**: R = 2-F $PhCH_2$;**183h**: R = 4-*t*-Bu $PhCH_2$; **183i**: R = 4-Br $PhCH_2$; **183j:** R = CH_2CN; **183k**: R = propyl; **183l:** R = undecyl; **183m**: R = butyl; **183n**: R = allyl

Scheme 26. A - Synthesis of 5-methyl-2,4-dihydro-3*H*-1,2,4-triazol-3-one aryl Schiff base derivatives (**179a-j**); **B -** Synthesis of novel 1,2,4-triazolo[4,3-a]pyridin-3(2*H*)-one derivatives (**183a-n**).

ide and urea under microwave irradiation to yield the novel 8-chloro-[1,2,4]triazolo[4,3-*a*]pyridin-3(2*H*)-one (**182**) (Scheme **26B**) [129].

Shaikh reported the synthesis and evaluation of Schiff bases, 4-((1,3-diphenyl-1*H*-pyrazol-4-yl)methyleneamino)-5-(pyridin-4-yl)-4*H*-1,2,4-triazole-3-thiol (**197**), *via* the condensation of pyrazolyl carbaldehyde (**186**) and 4-amino-5-(pyridin-4yl)-1,2,4-triazole-3-thiol (**185**) under microwave irradiation. The 4-amino-1,2,4-triazole-3-thiol nucleus (**185**) was obtained through the reaction between isoniazid (**184**), hydrazine hydrate, and CS_2 in a basic medium under microwave irradiation for 20-25 min at 70-75 °C (Scheme **27A**) [130].

A series of new 4-amino-1,2,4-triazole-3-one derivatives bearing the salicyl moiety (**192**) was synthesized *via* microwave irradiation, and their anticonvulsant activities were evaluated. The 4-amino-1,2,4-triazole-3-one core (**189**) was synthesized *via* the reaction of ethoxycarbonylhydrazones (**188**) with hydrazine hydrate in water *via* microwave heating (300 W) for 5 min at 125 °C (Scheme **27B**). The final 4-amino-1,2,4-triazole-3-one derivatives (**192**) exhibited moderate anticonvulsant activities in the maximum electroshock-induced and minimal chronic seizure models of mice without neurotoxic effects [131].

The synthesis of Schiff bases from 4-amino-[1,2,4]triazoles is a common reaction involving this class of compounds. Recently, a fluorogenic Schiff base probe (**195**) for the selective detection of Fe^{3+} in a mixed aqueous organic medium was synthesized from 4-amino-3-(2-fluorobenzyl)-1*H*-1,2,4-triazole-5(4*H*)-thione (**193**) and thiophene-2-carbaldehyde (**194**) in methanol under microwave irradiation (Scheme **28A**). Both reactants were dissolved separately and mixed before they were exposed to microwave radiation for 10 min. The photophysical analysis demonstrated that (*Z*)-3-(2-fluorobenzyl)-4-[(thiophen-2-ylmethylene) amino]-1*H*-1,2,4-triazole-5(4*H*)-thione (**195**) could be employed as an optical sensing platform for selective detections in organic and mixed organic-aqueous solutions [132].

The same idea was applied to the synthesis of a Schiff base fluorescent probe from 4-amino-5-(1*H*-indol-3-yl)-4*H*-[1,2,4]triazole-3-thiol (**196**) and salicylaldehyde (**190**) in ethanol and drops of concentrated HCl for the detection of for Al^{3+}. The reactants were mixed and irradiated in a microwave apparatus for 5 min at 350 W (90 °C) (Scheme **28B**). The chemosensor (**197**) demonstrated excellent selectivity toward Al^{3+} over the other metal cations under weakly acidic and neutral conditions, and this could be observed with the naked eye under UV-lamp irradiation. The spectroscopic analyses (fluorescence, ESI-MS, and ^{1}H NMR) revealed that the limit of detection, stoichiometric ratio, and association constant (K_a) were 29.9 nM, 1:1, and 9.31×10^4 M^{-1}, respectively [133].

The key intermediates (**200** and **202**) in the syntheses of zinc phthalocyanines containing morpholine and 1,2,4-triazole were synthesized under microwave irradiation, as well as conventional methods. Compound **200** was obtained in a 31% yield from 1,2,4-

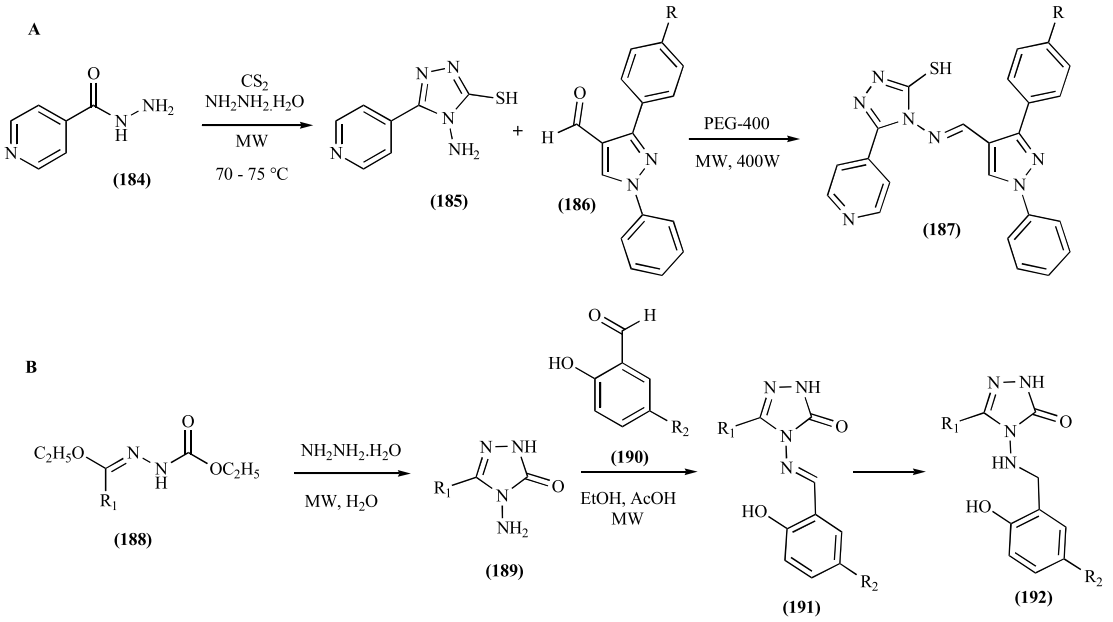

Scheme 27. A - Synthesis of novel Schiff Bases of 1,2,4-triazole (**186**) in PEG-400; **B -** Synthesis of novel 1,2,4-triazol-3-one derivatives (**192**) containing salicyl moiety.

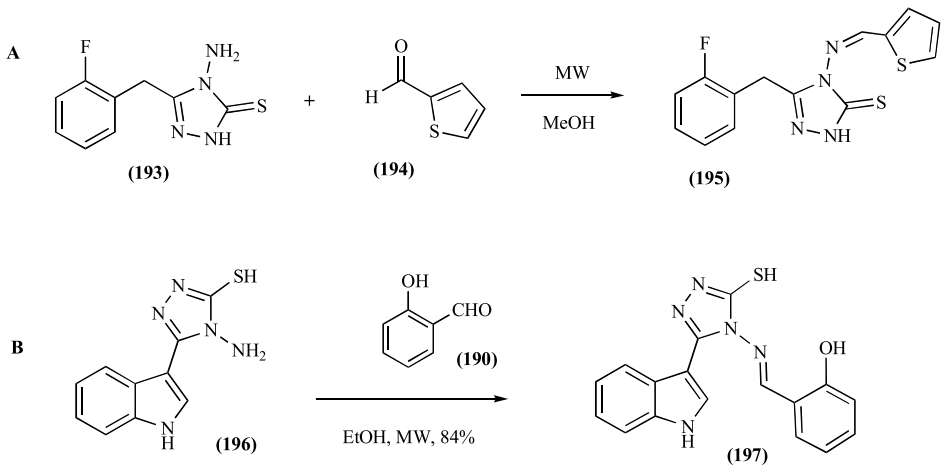

Scheme 28. Microwave-assisted synthesis of **A -** Fe^{3+} Schiff base fluorogenic probe (**195**); **B -** Al^{3+} fluorescent probe (**197**).

triazole derivative (**198**) and 4-nitro-1,2-dicyanobenzene (**199**) in dry DMF, and anhydrous K_2CO_3 under conventional heating for 48 h at 60 °C. The same reaction obtained an 80% yield under microwave irradiation (800 W) for 10 min. Derivative **202** was obtained from 1,2,4-triazole (**198**) and 4,5-dichloro-1,2-dicyanobenzene (**201**) in dry DMF and anhydrous K_2CO_3. For the conventional method, the reaction mixture was stirred for 48 h at 60 °C to obtain the product in a 42% yield. In the microwave method, the reaction flask was irradiated in a microwave apparatus at 800 W for 10 min to afford the same product in a 75% yield (Scheme **29**) [134].

A series of thioether derivatives containing the 1,2,4-triazole moiety (**204**), which exhibited moderate antifungal activity, were synthesized from thiol ether (**203**), RCH_2Cl, DMF, and NaOH under microwave irradiation. The microwave synthesis in a CEM Discover Focused Synthesizer (150 W, 90 °C, 200 psi) for 15 min afforded higher yields and shorter reaction times than that, which proceeded *via* the conventional method (Scheme **30**) [135].

3.4. Microwave Assisted Multicomponent Synthesis using 1,2,4 Triazole Derivatives

As previously described, multicomponent reactions are very essential to organic and medicinal chemistry syntheses [98]. Further, 3-amino-1,2,4-triazoles are synthons with many applications in this regard, acting as single (in $-NH_2$) or double nucleophiles (in $-NH_2$ and N2). In Biginelli multicomponent reactions, 3-amino-1,2,4-triazoles are utilized as a pseudo-guanidine. Based on this characteristic, Farahi and co-workers demonstrated a green regioselective method for obtaining 9-aryl-5,9-dihydropyrimido[4,5-*d*][1,2,4]triazolo[1,5-*a*]pyrimidine-6,8(4*H*,7*H*)-dione derivatives (**207**) from an equimolar mixture of barbituric acids (**206**), aromatic aldehydes (**54**), and 3-amino-1*H*-1,2,4-triazoles (**205**) *via* Biginelli microwave-assisted synthesis (Scheme **31A**). The synthetic protocol was evaluated in a domestic microwave oven, irradiated at 300 W for 10-15 min under solvent and catalyst-free conditions, obtaining good yields (85-97%) after recrystallization [136].

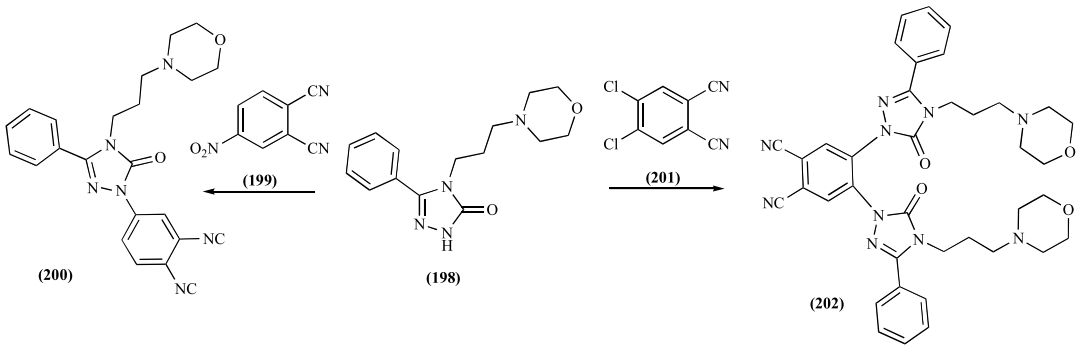

Scheme 29. *N*-arylation of 1,2,4-triazole derivatives.

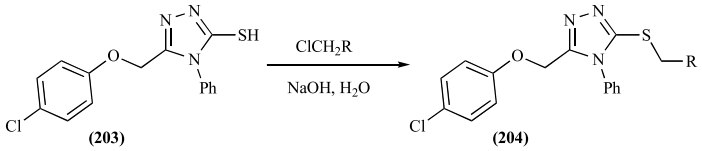

Scheme 30. General procedure for 1,2,4-triazoles thioether derivatives (**204**) synthesis.

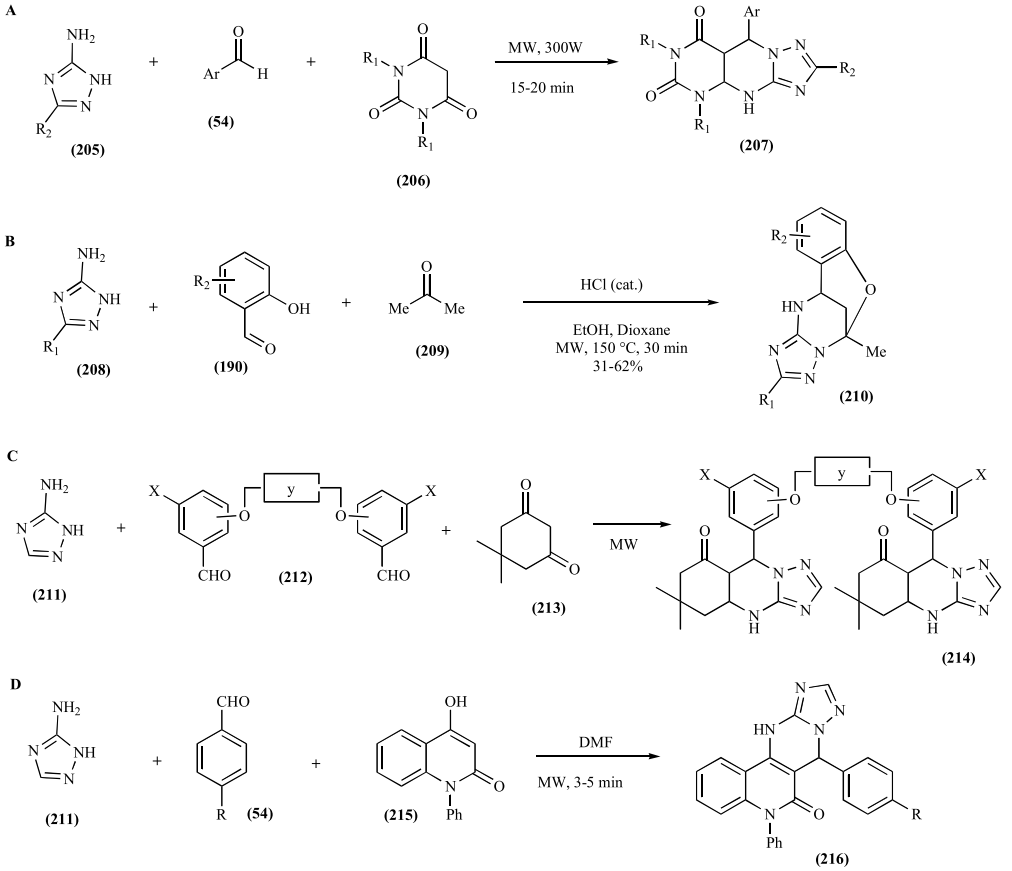

Scheme 31. Microwave-assisted Biginelli-like three-component reaction of. **A** - 9-aryl-5,9-dihydropyrimido[4,5-*d*][1,2,4]triazolo[1,5-*a*]pyrimidine-6,8(4*H*,7*H*)-diones (**207**); **B** - tetrahydrotriazolopyrimidine (**210**) compounds; **C** - bis(tetrahydro[1,2,4]triazolo[5,1-*b*]quinazolin-8(4*H*)-ones) (**214**); **D** - pyrimidoquinoline (**216**) compounds.

Microwave-assisted Biginelli-like three-component reactions have also been employed to synthesize several oxygen-bridged tetrahydrotriazolopyrimidine (**210**) compounds from 5-substituted 3-amino-1,2,4-triazoles (**208**), salicylaldehydes (**190**), and acetone (**209**) in good yields (Scheme **31B**). This reaction utilized acetone instead of β-dicarbonyl compounds, thus enlarging the scope of this multicomponent reaction. The authors proposed that the reaction mechanism includes the formation of the Schiff bases toward 3-amino-1,2,4-triazole and salicylaldehydes, followed by the reaction with acetone to form the intermediate, which suffered a cascade of transformations until the final product [137].

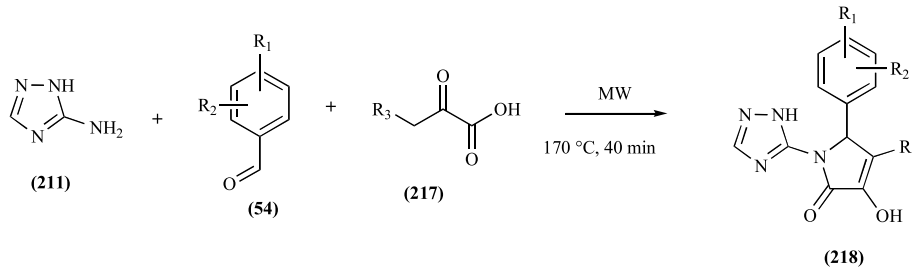

(211) (54) (217) (218)

Scheme 32. Synthesis of pyrrolones (**218**) by three-component reaction.

Compared with conventional heating methods, microwave irradiation has been proven as a powerful technique for preparing a series of bis(tetrahydro[1,2,4]triazolo[5,1-b]quinazolin-8(4*H*)-ones) (**214**) in a Biginelli three-component regioselective reaction involving bis-aldehydes (**212**), 5-amino-1,2,4-triazole (**211**), and 5,5-dimethyl-1,3-cyclohexanedione (**213**) (dimedone) (Scheme **31C**). The best results were achieved under microwave irradiation with ZnO NPs (10 mol%) as the heterogeneous catalyst, which improved the reaction yield and decreased the reaction times [138].

Mourad and coworkers performed the Biginelli-like condensations of 4-hydroxy-1-phenylquinolin-2(1*H*)-one (**215**), 5-amino-1*H*-1,2,4-triazole (**211**), and benzaldehydes (**54**) were performed under microwave irradiation. To synthesize several novel condensed heterocycles from pyrimido quinoline with biological properties, this group utilized the fascinating binuclear active methylene scaffold (4-hydroxy-1-phenylquinolin-2(1*H*)-one, **215**. Both techniques, *i.e.,* conventional heating and microwave irradiation, were applied to synthesize pyrimidoquinolines (**216**) (Scheme **31D**), but microwave irradiation achieved better results with higher yields (microwave: 77-84% and conventional heating: 31-61%) and very fast reaction times (microwave: 3-5 min, conventional heating 17-21 h) [139].

Another multicomponent reaction involving 3-amino-1,2,4-triazole (**211**), aldehydes (**54**), and pyruvic acids (**217**) was reported by Murlykina and colleagues. This three-component reaction afforded different products depending on the reaction parameters. The modification of pyruvic acid, including a β-aryl substituent, caused the formation of different types of heterocyclic compounds compared with those formed with unsubstituted pyruvic acid. This study compared the microwave-assisted synthesis (170 °C for 40 min) of an equimolar mixture of aminotriazole (**211**), aldehydes (**54**), and β-arylpyruvic acids (**217**) in AcOH with the conventional heating (130 °C for 3 h) method; pyrrolones (**218**) were obtained (Scheme **32**), and some of them demonstrated anti-influenza activity [140].

CONCLUSION

Triazole derivatives are particularly valuable aza-heterocycle compounds because of their applications in medicinal, agricultural, supramolecular, and materials science, as demonstrated in the text examples. In this review, we demonstrated that the Microwave-Assisted Organic Synthesis Technique (MAOS), which was recently applied to synthesize triazoles, as well as their derivatives, was welcomed by the scientific community because of its advantages. As demonstrated in many cases, microwave irradiation ensured significant improvements regarding the reaction yields and reduced reaction times compared with classical heating methods. Additionally, in some cases, this technique ensured the regioselective formation of triazole nuclei, as well as their derivatives. Furthermore, the utilization of polar solvents to synthesize triazoles was mostly observed probably because of their capacity to generate heat mainly *via* dielectric polarization and conduction [141]. The challenges associated with this technique were mainly the costs of acquiring the equipment, as well as maintenance and scale-up limitations. However, to reflect the increasing diffusion of MAOS, it is expected that this method would become more accessible, thus increasing its application in new triazoles and other heterocycles. It is hoped that the obtained knowledge regarding MAOS in the syntheses reported herein could be aid the design of new methods, as well as innovative triazoles.

CONSENT FOR PUBLICATION

Not applicable.

FUNDING

None.

CONFLICT OF INTEREST

The authors declare no conflict of interest, financial or otherwise.

ACKNOWLEDGEMENTS

Declared none.

REFERENCES

[1] Gilchrist, T.L. *Heterocyclic Chemistry,* 3rd ed; Pearson College Div: Harlow, **1997**.
[2] Hudson, J., Ed.; *The History of Chemistry*; Springer US, **1992**.
[3] Joule, J.A.; Mills, K. *Heterocyclic Chemistry,* 5th ed; Wiley-Blackwell, **2013**.
[4] Balaban, A.T.; Oniciu, D.C.; Katritzky, A.R. Aromaticity as a cornerstone of heterocyclic chemistry. *Chem. Rev.,* **2004**, *104*(5), 2777-2812. http://dx.doi.org/10.1021/cr0306790 PMID: 15137807
[5] Bean, G.P. Application of natural bond orbital analysis and natural resonance theory to delocalization and aromaticity in five-membered heteroaromatic compounds. *J. Org. Chem.,* **1998**, *63*(8), 2497-2506. http://dx.doi.org/10.1021/jo971725x PMID: 11672111
[6] Morais, P.A.B.; Francisco, C.S.; de Paula, H.; Ribeiro, R.; Eloy, M.A.; Javarini, C.L.; Neto, Á.C.; Júnior, V.L. semisynthetic triazoles as an approach in the discovery of novel lead compounds. *Curr. Org. Chem.,* **2021**, *25*, 1097-1179. http://dx.doi.org/10.2174/1385272825666210126100227
[7] Palaska, E.; Şahin, G.; Kelicen, P.; Durlu, N.T.; Altinok, G. Synthesis and anti-inflammatory activity of 1-acylthiosemicarbazides, 1,3,4-oxadiazoles, 1,3,4-thiadiazoles and 1,2,4-triazole-3-thiones. *Farmaco,* **2002**, *57*(2), 101-107. http://dx.doi.org/10.1016/S0014-827X(01)01176-4 PMID: 11902651
[8] Amir, M.; Kumar, S. Anti-inflammatory and gastro sparing activity of some new indomethacin derivatives. *Arch. Pharm. (Weinheim),* **2005**, *338*, 24-31. http://dx.doi.org/10.1002/ardp.200400891 PMID: 15674801
[9] Upmanyu, N.; Gupta, J.K.; Shah, K.; Mishra, P. Anti-inflammatory and antinociceptive evaluation of newly synthesized 4-(substituted ethanoyl) amino-3-mercapto-5-(4-methoxy) phenyl-1,2,4-triazoles. *J. Pharm. Bioallied Sci.,* **2011**, *3*(2), 259-265. http://dx.doi.org/10.4103/0975-7406.80783 PMID: 21687356
[10] Demirbas, N.; Karaoglu, S.A.; Demirbas, A.; Sancak, K. Synthesis and antimicrobial activities of some new 1-(5-phenylamino-[1,3,4]thiadiazol-2-yl)methyl-5-oxo-[1,2,4]triazole and 1-(4-phenyl-5-thioxo-[1,2,4]triazol-3-yl)methyl-5-oxo- [1,2,4]triazole derivatives. *Eur. J. Med. Chem.,* **2004**, *39*(9), 793-804. http://dx.doi.org/10.1016/j.ejmech.2004.06.007 PMID: 15337292
[11] Atia, A.J.Kh. Synthesis and antibacterial activities of new metronidazole and imidazole derivatives. *Molecules,* **2009**, *14*(7), 2431-2446. http://dx.doi.org/10.3390/molecules14072431 PMID: 19633614

[12] Sahoo, P.K.; Sharma, R.; Pattanayak, P. Synthesis and evaluation of 4-amino-5-phenyl-4H-[1,2,4]-triazole-3-thiol derivatives as antimicrobial agents. *Med. Chem. Res.,* **2010**, *19*, 127-135. http://dx.doi.org/10.1007/s00044-009-9178-8

[13] Sumangala, V.; Poojary, B.; Chidananda, N.; Arulmoli, T.; Shenoy, S. Synthesis and biological evaluation of some schiff bases of 4-amino-5-(4-methylsulfonyl)benzyl-2,4-dihydro-3H-[1,2,4]-triazole-3-thione. *Med. Chem. Res.,* **2013**, *22*, 2921-2928. http://dx.doi.org/10.1007/s00044-012-0294-5

[14] Shalini, K.; Kumar, N.; Drabu, S.; Sharma, P.K. Advances in synthetic approach to and antifungal activity of triazoles. *Beilstein J. Org. Chem.,* **2011**, *7*, 668-677. http://dx.doi.org/10.3762/bjoc.7.79 PMID: 21804864

[15] Kocyigit-Kaymakcioglu, B.; Celen, A.O.; Tabanca, N.; Ali, A.; Khan, S.I.; Khan, I.A.; Wedge, D.E. Synthesis and biological activity of substituted urea and thiourea derivatives containing 1,2,4-triazole moieties. *Molecules,* **2013**, *18*(3), 3562-3576. http://dx.doi.org/10.3390/molecules18033562 PMID: 23519199

[16] Küçükgüzel, I.; Tatar, E.; Küçükgüzel, Ş.G.; Rollas, S.; De Clercq, E. Synthesis of some novel thiourea derivatives obtained from 5-[(4-aminophenoxy)methyl]-4-alkyl/aryl-2,4-dihydro-3H-1,2,4-triazole-3-thiones and evaluation as antiviral/anti-HIV and anti-tuberculosis agents. *Eur. J. Med. Chem.,* **2008**, *43*(2), 381-392. http://dx.doi.org/10.1016/j.ejmech.2007.04.010 PMID: 17583388

[17] Li, Y-H.; Zhang, B.; Yang, H-K.; Li, Q.; Diao, P-C.; You, W-W.; Zhao, P-L. Design, synthesis, and biological evaluation of novel alkylsulfanyl-1,2,4-triazoles as cis-restricted combretastatin A-4 analogues. *Eur. J. Med. Chem.,* **2017**, *125*, 1098-1106. http://dx.doi.org/10.1016/j.ejmech.2016.10.051 PMID: 27810596

[18] Aswathanarayanappa, C.; Bheemappa, E.; Bodke, Y.D.; Krishnegowda, P.S.; Venkata, S.P.; Ningegowda, R. Synthesis and evaluation of antioxidant properties of novel 1,2,4-triazole-based schiff base heterocycles. *Arch. Pharm. (Weinheim),* **2013**, *346*(12), 922-930. http://dx.doi.org/10.1002/ardp.201300202 PMID: 24301964

[19] Khan, I.; Ali, S.; Hameed, S.; Rama, N.H.; Hussain, M.T.; Wadood, A.; Uddin, R.; Ul-Haq, Z.; Khan, A.; Ali, S.; Choudhary, M.I. Synthesis, antioxidant activities and urease inhibition of some new 1,2,4-triazole and 1,3,4-thiadiazole derivatives. *Eur. J. Med. Chem.,* **2010**, *45*(11), 5200-5207. http://dx.doi.org/10.1016/j.ejmech.2010.08.034 PMID: 20828889

[20] Karayel, A.; Özbey, S.; Ayhan-Kılcıgil, G.; Kuş, C. Crystal structures and intermolecular interactions of two novel antioxidant triazolyl-benzimidazole compounds. *Crystallogr. Rep.,* **2015**, *60*, 1084-1088. http://dx.doi.org/10.1134/S1063774515070111

[21] Nandikolla, A.; Srinivasarao, S.; Karan Kumar, B.; Murugesan, S.; Aggarwal, H.; Major, L.L.; Smith, T.K.; Chandra Sekhar, K.V.G. Synthesis, study of antileishmanial and antitrypanosomal activity of imidazo pyridine fused triazole analogues. *RSC Adv.,* **2020**, *10*, 38328-38343. http://dx.doi.org/10.1039/D0RA07881F

[22] Siddiqui, N.; Ahsan, W. Triazole incorporated thiazoles as a new class of anticonvulsants: Design, synthesis and *in vivo* screening. *Eur. J. Med. Chem.,* **2010**, *45*(4), 1536-1543. http://dx.doi.org/10.1016/j.ejmech.2009.12.062 PMID: 20116140

[23] Khan, I.; Tantray, M.A.; Hamid, H.; Alam, M.S.; Kalam, A.; Hussain, F.; Dhulap, A. Synthesis of pyrimidin-4-one-1,2,3-triazole conjugates as glycogen synthase kinase-3β inhibitors with anti-depressant activity. *Bioorg. Chem.,* **2016**, *68*, 41-55. http://dx.doi.org/10.1016/j.bioorg.2016.07.007 PMID: 27454617

[24] Chelamalla, R.; Akena, V.; Manda, S. Synthesis of N′-arylidene-2-(5-Aryl-1H-1, 2, 4-triazol-3-ylthio) acetohydrazides as antidepressants. *Med. Chem. Res.,* **2017**, *26*, 1359-1366. http://dx.doi.org/10.1007/s00044-017-1854-5

[25] Reed, C.W.; Yohn, S.E.; Washecheck, J.P.; Roenfanz, H.F.; Quitalig, M.C.; Luscombe, V.B.; Jenkins, M.T.; Rodriguez, A.L.; Engers, D.W.; Blobaum, A.L.; Conn, P.J.; Niswender, C.M.; Lindsley, C.W. Discovery of an orally bioavailable and Central Nervous System (CNS) penetrant $mGlu_7$ Negative Allosteric Modulator (NAM) *in vivo* tool compound: N-(2-(1 H-1,2,4-triazol-1-yl)-5-(trifluoromethoxy)phenyl)-4-(cyclopropylmethoxy)-3-methoxybenzamide (VU6012962). *J. Med. Chem.,* **2019**, *62*(3), 1690-1695. http://dx.doi.org/10.1021/acs.jmedchem.8b01810 PMID: 30608678

[26] Reed, C.W.; McGowan, K.M.; Spearing, P.K.; Stansley, B.J.; Roenfanz, H.F.; Engers, D.W.; Rodriguez, A.L.; Engelberg, E.M.; Luscombe, V.B.; Loch, M.T.; Remke, D.H.; Rook, J.M.; Blobaum, A.L.; Conn, P.J.; Niswender, C.M.; Lindsley, C.W. VU6010608, a novel $mGlu_7$ NAM from a series of *N*-(2-(1*H*-1,2,4-triazol-1-yl)-5-(trifluoromethoxy)phenyl)benzamides. *ACS Med. Chem. Lett.,* **2017**, *8*(12), 1326-1330. http://dx.doi.org/10.1021/acsmedchemlett.7b00429 PMID: 29259756

[27] da Silva, R.A.; Quintela, E.D.; Mascarin, G.M.; Barrigossi, J.A.F.; Lião, L.M. Compatibility of conventional agrochemicals used in rice crops with the entomopathogenic fungus Metarhizium Anisopliae. *Sci. Agric.,* **2013**, *70*, 152-160. http://dx.doi.org/10.1590/S0103-90162013000300003

[28] Borgati, T.F.; Alves, R.B.; Teixeira, R.R.; de Freitas, R.P.; Perdigão, T.G.; da Silva, S.F.; dos Santos, A.A.; Bastidas, A. Synthesis and phytotoxic activity of 1,2,3-triazole derivatives. *J. Braz. Chem. Soc.,* **2013**, *24*(6), 953-961. http://dx.doi.org/10.5935/0103-5053.20130121

[29] Kishorekumar, A.; Jaleel, C.A.; Manivannan, P.; Sankar, B.; Sridharan, R.; Panneerselvam, R. Comparative effects of different triazole compounds on growth, photosynthetic pigments and carbohydrate metabolism of *Solenostemon rotundifolius*. *Colloids Surf. B Biointerfaces,* **2007**, *60*(2), 207-212. http://dx.doi.org/10.1016/j.colsurfb.2007.06.008 PMID: 17669636

[30] Yen, Y-S.; Hsu, J-L.; Ni, J-S.; Lin, J.T. Influence of various dithienoheterocycles as conjugated linker in naphtho[2,3-d] [1,2,3]triazole-based organic dyes for dye-sensitized solar cells. *Dyes Pigments,* **2021**, *188*, 109220. http://dx.doi.org/10.1016/j.dyepig.2021.109220

[31] Mostafa, M.A.; Ashmawy, A.M.; Reheim, M.A.M.A.; Bedair, M.A.; Abuelela, A.M. Molecular structure aspects and molecular reactivity of some triazole derivatives for corrosion inhibition of aluminum in 1 M HCl solution. *J. Mol. Struct.,* **2021**, *1236*, 130292. http://dx.doi.org/10.1016/j.molstruc.2021.130292

[32] Hrimla, M.; Bahsis, L.; Boutouil, A.; Laamari, M.R.; Julve, M.; Stiriba, S-E. Corrosion inhibition performance of a structurally well-defined 1,2,3-triazole derivative on mild steel-hydrochloric acid interface. *J. Mol. Struct.,* **2021**, *1231*, 129895. http://dx.doi.org/10.1016/j.molstruc.2021.129895

[33] Finšgar, M. The influence of the amino group in 3-amino-1,2,4-triazole corrosion inhibitor on the interface properties for brass studied by ToF-SIMS. *Rapid Commun. Mass Spectrom.,* **2021**, *35*(7), e9056. http://dx.doi.org/10.1002/rcm.9056 PMID: 33522034

[34] Ali, G.Q.; El-Hiti, G.A.; Tomi, I.H.; Haddad, R.; Al-Qaisi, A.J.; Yousif, E. Photostability and performance of polystyrene films containing 1,2,4-triazole-3-thiol ring system schiff bases. *Molecules,* **2016**, *21*(12), 1699. http://dx.doi.org/10.3390/molecules21121699 PMID: 27941675

[35] Katritzky, A.R.; Song, Y.; Sakhuja, R.; Gyanda, R.; Meher, N.K.; Wang, L.; Duran, R.S.; Ciaramitaro, D.A.; Bedford, C.D. Synthesis of boltorn 1,2,3-triazole dendrimers by click chemistry. *J. Polym. Sci. Part Polym. Chem.,* **2009**, *47*, 3748-3756. http://dx.doi.org/10.1002/pola.23427

[36] Arseneault, M.; Wafer, C.; Morin, J-F. Recent advances in click chemistry applied to dendrimer synthesis. *Molecules,* **2015**, *20*(5), 9263-9294. http://dx.doi.org/10.3390/molecules20059263 PMID: 26007183

[37] Johnson, J.A.; Finn, M.G.; Koberstein, J.T.; Turro, N.J. Construction of linear polymers, dendrimers, networks, and other polymeric architectures by copper‐catalyzed azide‐alkyne cycloaddition "click" chemistry. *Macromol. Rapid Commun.,* **2008**, *29*, 1052-1072. http://dx.doi.org/10.1002/marc.200800208

[38] Tsuei, M.; Shivrayan, M.; Kim, Y-K.; Thayumanavan, S.; Abbott, N.L. Optical "blinking" triggered by collisions of single supramolecular assemblies of amphiphilic molecules with interfaces of liquid crystals. *J. Am. Chem. Soc.,* **2020**, *142*(13), 6139-6148. http://dx.doi.org/10.1021/jacs.9b13360 PMID: 32085676

[39] Al-shargabi, A.; Yeap, G-Y.; Mahmood, W.A.K.; Han, C-C.; Lin, H-C.; Ito, M.M. Liquid crystal dimers containing cholesteryl and triazole-containing mesogenic units. *Liq. Cryst.,* **2020**, *47*, 219-230. http://dx.doi.org/10.1080/02678292.2019.1641637

[40] Srividhya, D.; Manjunathan, S.; Thirumaran, S.; Saravanan, C.; Senthil, S. Synthesis and characterization of [1,2,3]-triazole containing liquid crystals through click reaction. *J. Mol. Struct.,* **2009**, *927*, 7-13. http://dx.doi.org/10.1016/j.molstruc.2009.01.035

[41] Xiao, D.; Do, L.H. Triazolecarboxamidate donors as supporting ligands for nickel olefin polymerization catalysts. *Organometallics,* **2018**, *37*, 254-260. http://dx.doi.org/10.1021/acs.organomet.7b00807

[42] McCarney, E.P.; Hawes, C.S.; Blasco, S.; Gunnlaugsson, T. Synthesis and structural studies of 1,4-di(2-pyridyl)-1,2,3-triazole and its transition metal complexes; a versatile and subtly unsymmetric ligand. *Dalton Trans.,* **2016**, *45*(25), 10209-10221. http://dx.doi.org/10.1039/C6DT01416J PMID: 27231030

[43] Feng, L.S.; Zheng, M.J.; Zhao, F.; Liu, D. 1,2,3-Triazole hybrids with anti-HIV-1 activity. *Arch. Pharm. (Weinheim),* **2021**, *354*(1), e2000163. http://dx.doi.org/10.1002/ardp.202000163 PMID: 32960467

[44] Brai, A.; Riva, V.; Saladini, F.; Zamperini, C.; Trivisani, C.I.; Garbelli, A.; Pennisi, C.; Giannini, A.; Boccuto, A.; Bugli, F.; Martini, M.; Sanguinetti, M.; Zazzi, M.; Dreassi, E.; Botta, M.; Maga, G. DDX3X inhibitors, an effective way to overcome HIV-1 resistance targeting host proteins. *Eur. J. Med. Chem.,* **2020**, *200*, 112319. http://dx.doi.org/10.1016/j.ejmech.2020.112319 PMID: 32446036

[45] Sun, L.; Huang, T.; Dick, A.; Meuser, M.E.; Zalloum, W.A.; Chen, C-H.; Ding, X.; Gao, P.; Cocklin, S.; Lee, K-H.; Zhan, P.; Liu, X. Design, synthesis and structure-activity relationships of 4-phenyl-1H-1,2,3-triazole phenylalanine derivatives as novel HIV-1 capsid inhibitors with promising antiviral activities. *Eur. J. Med. Chem.,* **2020**, *190*, 112085. http://dx.doi.org/10.1016/j.ejmech.2020.112085 PMID: 32066010

[46] Li, N.; Chen, C.; Zhu, H.; Shi, Z.; Sun, J.; Chen, L. Discovery of novel celastrol-triazole derivatives with Hsp90-Cdc37 disruption to induce tumor cell apoptosis. *Bioorg. Chem.,* **2021**, *111*, 104867. http://dx.doi.org/10.1016/j.bioorg.2021.104867 PMID: 33845380

[47] Zhang, X-H.; Kang, H-Q.; Tao, Y-Y.; Li, Y-H.; Zhao, J-R.; Ya-Gao, ; Ma, L.Y.; Liu, H.M. Identification of novel 1,3-diaryl-1,2,4-triazole-capped histone deacetylase 6 inhibitors with potential anti-gastric cancer activity. *Eur. J. Med. Chem.,* **2021**, *218*, 113392.

http://dx.doi.org/10.1016/j.ejmech.2021.113392 PMID: 33831778

[48] Pertino, M.W.; F de la Torre, A.; Schmeda-Hirschmann, G.; Vega, C.; Rolón, M.; Coronel, C.; Rojas de Arias, A.; Leal López, K.; Carranza-Rosales, P.; Viveros Valdez, E. Synthesis, trypanocidal and anti-leishmania activity of new triazole-lapachol and nor-lapachol hybrids. *Bioorg. Chem.,* **2020**, *103*, 104122.
http://dx.doi.org/10.1016/j.bioorg.2020.104122 PMID: 32745754

[49] Sahu, A.; Agrawal, R.K.; Pandey, R. Synthesis and systemic toxicity assessment of quinine-triazole scaffold with antiprotozoal potency. *Bioorg. Chem.,* **2019**, *88*, 102939.
http://dx.doi.org/10.1016/j.bioorg.2019.102939 PMID: 31028993

[50] Phatak, P.S.; Bakale, R.D.; Kulkarni, R.S.; Dhumal, S.T.; Dixit, P.P.; Krishna, V.S.; Sriram, D.; Khedkar, V.M.; Haval, K.P. Design and synthesis of new indanol-1,2,3-triazole derivatives as potent antitubercular and antimicrobial agents. *Bioorg. Med. Chem. Lett.,* **2020**, *30*(22), 127579.
http://dx.doi.org/10.1016/j.bmcl.2020.127579 PMID: 32987135

[51] Gondru, R.; Kanugala, S.; Raj, S.; Ganesh Kumar, C.; Pasupuleti, M.; Banothu, J.; Bavantula, R. 1,2,3-triazole-thiazole hybrids: Synthesis, *in vitro* antimicrobial activity and antibiofilm studies. *Bioorg. Med. Chem. Lett.,* **2021**, *33*, 127746.
http://dx.doi.org/10.1016/j.bmcl.2020.127746 PMID: 33333162

[52] Blokhina, S.V.; Sharapova, A.V.; Ol'khovich, M.V.; Doroshenko, I.A.; Levshin, I.B.; Perlovich, G.L. Synthesis and antifungal activity of new hybrids thiazolo[4,5-d]pyrimidines with (1H-1,2,4)triazole. *Bioorg. Med. Chem. Lett.,* **2021**, *40*, 127944.
http://dx.doi.org/10.1016/j.bmcl.2021.127944 PMID: 33713781

[53] Zoidis, G.; Kritsi, E.; Lecinska, P.; Ivanov, M.; Zoumpoulakis, P.; Sokovic, M.; Catto, M. The triazole ring as a privileged scaffold for putative antifungals: synthesis and evaluation of a series of new analogues. *ChemMedChem,* **2021**, *16*(1), 134-144.
http://dx.doi.org/10.1002/cmdc.202000312 PMID: 33428335

[54] Jahani, R.; Reza Abtahi, S.; Nematpour, M.; Fasihi Dastjerdi, H.; Chamanara, M.; Hami, Z.; Paknejad, B. Design, synthesis, and pharmacological evaluation of novel 1,2,4-triazol-3-amine derivatives as potential agonists of $GABA_A$ subtype receptors with anticonvulsant and hypnotic effects. *Bioorg. Chem.,* **2020**, *104*, 104212.
http://dx.doi.org/10.1016/j.bioorg.2020.104212 PMID: 32916390

[55] Ouach, A.; Pin, F.; Bertrand, E.; Vercouillie, J.; Gulhan, Z.; Mothes, C.; Deloye, J-B.; Guilloteau, D.; Suzenet, F.; Chalon, S.; Routier, S. Design of α7 nicotinic acetylcholine receptor ligands using the (het)Aryl-1,2,3-triazole core: Synthesis, *in vitro* evaluation and SAR studies. *Eur. J. Med. Chem.,* **2016**, *107*, 153-164.
http://dx.doi.org/10.1016/j.ejmech.2015.11.001 PMID: 26580980

[56] Scopus preview - Scopus - Welcome to Scopus. Available from: https://www.scopus.com/home.uri (Accessed Jun 20, **2021**).

[57] Russell, C.B.; Mason, J.D.; Bean, T.G.; Murphree, S.S. A student-centered first-semester introductory organic laboratory curriculum facilitated by Microwave-Assisted Synthesis (MAOS). *J. Chem. Educ.,* **2014**, *91*, 511-517.
http://dx.doi.org/10.1021/ed400064f

[58] Crouch, R.D.; Howard, J.L.; Zile, J.L.; Barker, K.H. Microwave-mediated synthesis of lophine: developing a mechanism to explain a product. *J. Chem. Educ.,* **2006**, *83*, 1658.
http://dx.doi.org/10.1021/ed083p1658

[59] Banerjee, B. Recent developments on ultrasound assisted catalyst-free organic synthesis. *Ultrason. Sonochem.,* **2017**, *35*(Pt A), 1-14.
http://dx.doi.org/10.1016/j.ultsonch.2016.09.023 PMID: 27771266

[60] Barge, A.; Tagliapietra, S.; Binello, A.; Cravotto, G. Click chemistry under microwave or ultrasound irradiation. *Curr. Org. Chem.,* **2011**, *15*, 189-203.
http://dx.doi.org/10.2174/138527211793979826

[61] Mohammadi Ziarani, G.; Kheilkordi, Z.; Gholamzadeh, P. Ultrasound-assisted synthesis of heterocyclic compounds. *Mol. Divers.,* **2020**, *24*(3), 771-820.
http://dx.doi.org/10.1007/s11030-019-09964-1 PMID: 31165431

[62] Agalave, S.G.; Maujan, S.R.; Pore, V.S. Click chemistry: 1,2,3-triazoles as pharmacophores. *Chem. Asian J.,* **2011**, *6*(10), 2696-2718.
http://dx.doi.org/10.1002/asia.201100432 PMID: 21954075

[63] Fokin, V.V.; Matyjaszewski, K. CuAAC: The Quintessential Click Reaction. In: *Organic Chemistry - Breakthroughs and Perspectives*; Ding, K.; Dai, L.-X. Wiley-VCH Verlag GmbH & Co. KGaA: Weinheim, Germany, **2012**; pp. 247-277.

[64] Barluenga, J., Ed.; *Modern Heterocyclic Chemistry, 4 Volume Set; Alvarez-Builla, J.; Vaquero, J.J,* 1st ed; Wiley-VCH: Weinheim, Germany, **2011**.

[65] Talekar, R.R.; Wightman, R.H. Synthesis of some pyrrolo[2,3-d]pyrimidine and 1,2,3-triazole isonucleosides. *Tetrahedron,* **1997**, *53*, 3831-3842.
http://dx.doi.org/10.1016/S0040-4020(97)00102-6

[66] Landge, K.P.; Seo, Y-W.; Kwak, J-M.; Park, W-K.; Gong, J-Y.; Lee, H-Y.; Koh, H-Y. Versatile synthesis of disubstituted triazole library for dopamine and serotonin receptor ligands. *Bull. Korean Chem. Soc.,* **2011**, *32*, 3101-3104.
http://dx.doi.org/10.5012/bkcs.2011.32.8.3101

[67] Meldal, M.; Tornøe, C.W. Cu-catalyzed azide-alkyne cycloaddition. *Chem. Rev.,* **2008**, *108*(8), 2952-3015.
http://dx.doi.org/10.1021/cr0783479 PMID: 18698735

[68] Rostovtsev, V.V.; Green, L.G.; Fokin, V.V.; Sharpless, K.B. A stepwise huisgen cycloaddition process: copper(I)-catalyzed regioselective "ligation" of azides and terminal alkynes. *Angew. Chem. Int. Ed.,* **2002**, *41*(14), 2596-2599.
http://dx.doi.org/10.1002/1521-3773(20020715)41:14<2596::AID-ANIE2596>3.0.CO;2-4 PMID: 12203546

[69] Kumar, D.; Reddy, V.B.; Varma, R.S. A Facile and regioselective synthesis of 1,4-disubstituted 1,2,3-triazoles using click chemistry. *Tetrahedron Lett.,* **2009**, *50*, 2065-2068.
http://dx.doi.org/10.1016/j.tetlet.2009.02.107

[70] Takasu, K.; Azuma, T.; Takemoto, Y. Synthesis of trifunctional thioureas bearing 1,5-disubstituted triazole tether by Ru-catalyzed huisgen cycloaddition. *Tetrahedron Lett.,* **2010**, *51*, 2737-2740.
http://dx.doi.org/10.1016/j.tetlet.2010.03.053

[71] Suresh, R.; Muthusubramanian, S.; Paul, N.; Kalidhasan, N.; Shanmugaiah, V. Synthesis of (Z)-1,3-diaryl-2-(4-aryl-1h-1,2,3-triazol-1-yl)prop-2-En-1-ones and their antibacterial studies. *Med. Chem. Res.,* **2014**, *23*, 4367-4375.
http://dx.doi.org/10.1007/s00044-014-1004-2

[72] Aarjane, M.; Slassi, S.; Tazi, B.; Maouloua, M.; Amine, A. Novel series of acridone-1,2,3-triazole derivatives: Microwave-assisted synthesis, DFT study and antibacterial activities. *J. Chem. Sci.,* **2019**, *131*, 85.
http://dx.doi.org/10.1007/s12039-019-1653-2

[73] Dürüst, Y.; Karakuş, H. Microwave-Assisted synthesis and crystal structure of some novel 1,2,4-oxadiazol-5-ylmethyl-1,2,3-triazoles. *Synth. Commun.,* **2017**, *47*, 907-912.
http://dx.doi.org/10.1080/00397911.2017.1296158

[74] Souza, F.B.; Pimenta, D.C.; Stefani, H.A. Microwave-assisted one-pot three-component synthesis of imine 1,2,3-triazoles. *Tetrahedron Lett.,* **2016**, *57*, 1592-1596.
http://dx.doi.org/10.1016/j.tetlet.2016.02.105

[75] Subhashini, N.J.P.; Sravanthi, K.; Sravanthi, Ch.; Reddy, M.S. Microwave-assisted synthesis of pyrazole-based 1,2,3-triazole derivatives and evaluation of their antimicrobial activity. *Russ. J. Gen. Chem.,* **2016**, *86*, 2777-2784.
http://dx.doi.org/10.1134/S1070363216120392

[76] Kumar, Y.; Matta, A.; Kumar, P.; Parmar, V.S.; Van der Eycken, E.V.; Singh, B.K. Cu(I)-catalyzed microwave-assisted synthesis of 1,2,3-triazole linked with 4-thiazolidinones: a one-pot sequential approach. *RSC Adv.,* **2015**, *5*, 1628-1639.
http://dx.doi.org/10.1039/C4RA12592D

[77] Srinivas, M.; Singh Pathania, A.; Mahajan, P.; Verma, P.K.; Chobe, S.S.; Malik, F.A.; Nargotra, A.; Vishwakarma, R.A.; Sawant, S.D. Design and synthesis of 1,4-substituted 1H-1,2,3-triazolo-quinazolin-4(3H)-ones by Huisgen 1,3-dipolar cycloaddition with PI3Kγ isoform selective activity. *Bioorg. Med. Chem. Lett.,* **2018**, *28*(6), 1005-1010.
http://dx.doi.org/10.1016/j.bmcl.2018.02.032 PMID: 29486969

[78] Ashok, D.; Gundu, S.; Aamate, V.K.; Devulapally, M.G.; Bathini, R.; Manga, V. Dimers of coumarin-1,2,3-triazole hybrids bearing alkyl spacer: design, microwave-assisted synthesis, molecular docking and evaluation as antimycobacterial and antimicrobial agents. *J. Mol. Struct.,* **2018**, *1157*, 312-321.
http://dx.doi.org/10.1016/j.molstruc.2017.12.080

[79] Schumacher, R.F.; Laer, P.B.V.; Betin, E.S.; Cargnelutti, R.; Perin, G.; Alves, D. Synthesis of 3-(1 *H* -1,2,3-triazol-1-yl)-2-(arylselanyl)pyridines by copper-catalyzed 1,3-dipolar cycloaddition of 2-(arylselanyl)-3-azidopyridines with terminal alkynes. *J. Braz. Chem. Soc.,* **2015**, *26*(11), 2298-2306.
http://dx.doi.org/10.5935/0103-5053.20150221

[80] Singh, G.; Kalra, P.; Arora, A.; Sanchita, ; Sharma, G.; Singh, A.; Verma, V. Design and synthesis of indole triazole pendant siloxy framework as a chemo sensor for sensing of Cu^{2+} and Ni^{2+}: A comparison between traditional and microwave method. *Inorg. Chim. Acta,* **2018**, *473*, 186-193.
http://dx.doi.org/10.1016/j.ica.2018.01.003

[81] da S. Dias, C.; de M. Lima, T.; Lima, C.G.S.; Zuekrman-Schpector, J.; Schwab, R.S. CuO Nanoparticles as an efficient heterogeneous catalyst for the 1,3-dipolar cycloaddition of dicarbonyl compounds to azides. *ChemistrySelect,* **2018**, *3*, 6195-6202.
http://dx.doi.org/10.1002/slct.201800816

[82] Bhuyan, P.; Bhorali, P.; Islam, I.; Bhuyan, A.J.; Saikia, L. Magnetically recoverable copper ferrite catalyzed cascade synthesis of 4-aryl-1h-1,2,3-triazoles under microwave irradiation. *Tetrahedron Lett.,* **2018**, *59*, 1587-1591.
http://dx.doi.org/10.1016/j.tetlet.2018.03.032

[83] Radatz, C.S.; Soares, L.do A.; Vieira, E.R.; Alves, D.; Russowsky, D.; Schneider, P.H. Recoverable Cu/SiO_2 composite-catalysed click synthesis of 1,2,3-triazoles in water media. *New J. Chem.,* **2014**, *38*, 1410-1417.
http://dx.doi.org/10.1039/C3NJ01167D

[84] Narsimha, S.; Battula, K.S.; Reddy, Y.N.; Nagavelli, V.R. Microwave-assisted Cu-catalyzed C–C bond formation: one-pot synthesis of fully substituted 1,2,3-triazoles using nonsymmetrical iodoalkynes and their biological evaluation. *Chem. Heterocycl. Compd.,* **2018**, *54*, 1161-1167.
http://dx.doi.org/10.1007/s10593-019-02408-6

[85] Bruyat, P.; Gautier, A.; Jean, L.; Renard, P-Y. Use of an air-stable Cu(I)-NHC catalyst for the synthesis of peptidotriazoles. *J. Org. Chem.,* **2018**, *83*(21), 13515-13522.
http://dx.doi.org/10.1021/acs.joc.8b01490 PMID: 30280899

[86] Carreiro, E.P.; Sena, A.M.; Puerta, A.; Padrón, J.M.; Burke, A.J. Synthesis of novel 1,2,3-triazole-dihydropyrimidinone hybrids using multicomponent 1,3-

dipolar cycloaddition (click)–biginelli reactions: anticancer activity. *Synlett,* **2020**, *31*, 615-621.
http://dx.doi.org/10.1055/s-0039-1690781

[87] de Andrade, P.; Galo, O.A.; Carvalho, M.R.; Lopes, C.D.; Carneiro, Z.A.; Sesti-Costa, R.; de Melo, E.B.; Silva, J.S.; Carvalho, I. 1,2,3-Triazole-based analogue of benznidazole displays remarkable activity against *Trypanosoma cruzi*. *Bioorg. Med. Chem.,* **2015**, *23*(21), 6815-6826.
http://dx.doi.org/10.1016/j.bmc.2015.10.008 PMID: 26476667

[88] Chouaïb, K.; Romdhane, A.; Delemasure, S.; Dutartre, P.; Elie, N.; Touboul, D.; Ben Jannet, H. Regiospecific synthesis by copper- and ruthenium-catalyzed azide–alkyne 1,3-dipolar cycloaddition, anticancer and anti-inflammatory activities of oleanolic acid triazole derivatives. *Arab. J. Chem.,* **2019**, *12*, 3732-3742.
http://dx.doi.org/10.1016/j.arabjc.2015.12.013

[89] Kracker, O.; Góra, J.; Krzciuk-Gula, J.; Marion, A.; Neumann, B.; Stammler, H-G.; Nieß, A.; Antes, I.; Latajka, R.; Sewald, N. 1,5-disubstituted 1,2,3-triazole-containing peptidotriazolamers: design principles for a class of versatile peptidomimetics. *Chemistry,* **2018**, *24*(4), 953-961.
http://dx.doi.org/10.1002/chem.201704583 PMID: 29160605

[90] Rungta, P.; Mangla, P.; Maikhuri, V.K.; Singh, S.K.; Prasad, A.K. Microwave-assisted synthesis of C-4′-(1,5-disubstituted)-triazole-spiro-α-l-arabinofuranosyl nucleosides. *ChemistrySelect,* **2017**, *2*, 7808-7812.
http://dx.doi.org/10.1002/slct.201701111

[91] Medvedeva, A.S.; Demina, M.M.; Konkova, T.V.; Vu, T.D.; Larina, L.I. Synthesis of 4-trialkylsilyl(germyl)-1H-1,2,3-triazolecarbaldehyde oximes. *Chem. Heterocycl. Compd.,* **2014**, *50*, 967-971.
http://dx.doi.org/10.1007/s10593-014-1551-y

[92] Bulman Page, P.; Stephenson, G.; Harvey, J.; Slawin, A. Ruthenium-free preparation of 1,5-disubstituted triazoles by alkylative debenzylation of 1,4-disubstituted triazoles. *Synlett,* **2016**, *27*, 2500-2504.
http://dx.doi.org/10.1055/s-0035-1562603

[93] Malekdar, M.; Taherpour, A.A.; Yavari, I.; Larijani, K. One-pot microwave-assisted solvent-free synthesis, theoretical and experimental studies on barrier rotation of C–N bond of N-alkenyl-1,2,3-triazoles. *Struct. Chem.,* **2014**, *25*, 1483-1493.
http://dx.doi.org/10.1007/s11224-014-0422-6

[94] Zhao, F.; Tian, W-H.; Luo, F.; Cheng, H-L.; Jiang, Y-B.; Chen, Z. Pd-catalyzed ligand-free C(5)–H arylation of 1,4-disubstituted 1,2,3-triazoles promoted by microwaves. *Synth. Commun.,* **2016**, *46*, 1678-1686.
http://dx.doi.org/10.1080/00397911.2016.1222441

[95] Liu, W.; Li, Y.; Wang, R.; Jiang, Y.; Kuang, C. Microwave assisted direct arylation of 1-benzyl-1,2,3-triazole. *Tetrahedron Lett.,* **2020**, *61*, 151390.
http://dx.doi.org/10.1016/j.tetlet.2019.151390

[96] Motornov, V.; Markos, A.; Beier, P. A rhodium-catalyzed transannulation of *N*-(per)fluoroalkyl-1,2,3-triazoles under microwave conditions-a general route to *N*-(per)fluoroalkyl-substituted five-membered heterocycles. *Chem. Commun. (Camb.),* **2018**, *54*(26), 3258-3261.
http://dx.doi.org/10.1039/C8CC01446A PMID: 29537032

[97] Motornov, V.; Beier, P. Chemoselective aza-[4+3]-annulation of *N*-perfluoroalkyl-1,2,3-triazoles with 1,3-dienes: access to *N*-perfluoroalkyl-substituted azepines. *J. Org. Chem.,* **2018**, *83*(24), 15195-15201.
http://dx.doi.org/10.1021/acs.joc.8b02472 PMID: 30516987

[98] Graebin, C.S.; Ribeiro, F.V.; Rogério, K.R.; Kümmerle, A.E. Multicomponent reactions for the synthesis of bioactive compounds: A review. *Curr. Org. Synth.,* **2019**, *16*(6), 855-899.
http://dx.doi.org/10.2174/1570179416666190718153703 PMID: 31984910

[99] Gladkov, E.S.; Sirko, S.M.; Musatov, V.I.; Shishkina, S.V.; Tkachenko, I.G.; Komykhov, S.A.; Desenko, S.M. New spiro derivative of dihydro-1,2,3-triazolo[1,5-a]pyrimidine as a product of multicomponent reaction. *Chem. Heterocycl. Compd.,* **2018**, *54*, 1139-1144.
http://dx.doi.org/10.1007/s10593-019-02405-9

[100] Tkachenko, I.G.; Komykhov, S.A.; Gladkov, E.S.; Musatov, V.I.; Chebanov, V.A.; Desenko, S.M. Acetic aldehyde in multicomponent synthesis of azolopyrimidine derivatives in water. *Chem. Heterocycl. Compd.,* **2019**, *55*, 392-396.
http://dx.doi.org/10.1007/s10593-019-02470-0

[101] do Nascimento, J.E.R.; Gonçalves, L.C.C.; Hooyberghs, G.; Van der Eycken, E.V.; Alves, D.; Lenardão, E.J.; Perin, G.; Jacob, R.G. Synthesis of fused 1,2,3-triazolo-1,3,6-triazonines through copper-catalyzed intramolecular ullmann cross-coupling reaction. *Tetrahedron Lett.,* **2016**, *57*, 4885-4889.
http://dx.doi.org/10.1016/j.tetlet.2016.09.027

[102] Jung, S.; Yoon, N.G.; Yang, S.; Kim, D.; Lee, W.S.; Hong, K.B.; Lee, C.; Kang, B.H.; Lee, J.H.; Kang, S. Discovery of 2-((4-resorcinolyl)-5-aryl-1,2,3-triazol-1-yl)acetates as potent Hsp90 inhibitors with selectivity over TRAP1. *Bioorg. Med. Chem. Lett.,* **2020**, *30*(2), 126809.
http://dx.doi.org/10.1016/j.bmcl.2019.126809 PMID: 31839539

[103] Eicher, T.; Hauptmann, S.; Speicher, A.; Suschitzky, H. *The Chemistry of Heterocycles: Structure, Reactions, Syntheses, and Applicationscompletely rev. and enl. ed*; Wiley-VCH: Weinheim, **2008**.

[104] Wang, Z., Ed.; *Comprehensive Organic Name Reactions and Reagents*; Wiley-Interscience: Hoboken, N.J, **2009**.

[105] Küçükgüzel, Ş.G.; Çıkla-Süzgün, P. Recent advances bioactive 1,2,4-triazole-3-thiones. *Eur. J. Med. Chem.,* **2015**, *97*, 830-870.
http://dx.doi.org/10.1016/j.ejmech.2014.11.033 PMID: 25563511

[106] Nasri, S.; Bayat, M.; Kochia, K. Strategies for synthesis of 1,2,4-triazole-containing scaffolds using 3-amino-1,2,4-triazole. *Mol. Divers.,* **2021**.
http://dx.doi.org/10.1007/s11030-021-10197-4 PMID: 33608844

[107] Bozó, E.; Szilágyi, G.; Janáky, J. 1,2,4-triazoles, III: New 1,5-diaryl-3-(substituted amino)-1H-1,2,4-triazoles as anti-inflammatory agents. *Arch. Pharm. (Weinheim),* **1989**, *322*(10), 583-587.
http://dx.doi.org/10.1002/ardp.19893221003 PMID: 2624521

[108] Sangshetti, J.N.; Kalam Khan, F.A.; Chouthe, R.S.; Damale, M.G.; Shinde, D.B. Synthesis, docking and ADMET prediction of novel 5-((5-substituted-1-H-1,2,4-triazol-3-yl) methyl)-4,5,6,7-tetrahydrothieno[3,2-c]pyridine as antifungal agents. *Chin. Chem. Lett.,* **2014**, *25*, 1033-1038.
http://dx.doi.org/10.1016/j.cclet.2014.04.003

[109] Bechara, W.S.; Khazhieva, I.S.; Rodriguez, E.; Charette, A.B. One-pot synthesis of 3,4,5-trisubstituted 1,2,4-triazoles *via* the addition of hydrazides to activated secondary amides. *Org. Lett.,* **2015**, *17*(5), 1184-1187.
http://dx.doi.org/10.1021/acs.orglett.5b00128 PMID: 25700199

[110] Shelke, G.; Rao, V.; Jha, M.; Cameron, T.; Kumar, A. Microwave-assisted catalyst-free synthesis of substituted 1,2,4-triazoles. *Synlett,* **2015**, *26*, 404-407.
http://dx.doi.org/10.1055/s-0034-1379734

[111] Kaur, R.; Kumar, B.; Dwivedi, A.R.; Kumar, V. *Regioselective Alkylation of 1,2,4-Triazole Using Ionic Liquids under Microwave Conditions*; Green Process. Synth, **2016**, p5.

[112] Santos, S.N.; Alves de Souza, G.; Pereira, T.M.; Franco, D.P.; de Nigris Del Cistia, C.; Sant'Anna, C.M.R.; Lacerda, R.B.; Kümmerle, A.E. Regioselective microwave synthesis and derivatization of 1,5-diaryl-3-amino-1,2,4-triazoles and a study of their cholinesterase inhibition properties. *RSC Adv.,* **2019**, *9*, 20356-20369.
http://dx.doi.org/10.1039/C9RA04105B

[113] Lim, F.P.L.; Hu, L.M.; Tiekink, E.R.T.; Dolzhenko, A.V. One-pot, microwave-assisted synthesis of polymethylene-bridged bis(1H-1,2,4-triazol-5(3)-amines) and their tautomerism. *Tetrahedron Lett.,* **2018**, *59*, 3792-3796.
http://dx.doi.org/10.1016/j.tetlet.2018.09.018

[114] Lim, F.P.L.; Tan, L.Y.; Tiekink, E.R.T.; Dolzhenko, A.V. Synthesis of 3-(5-amino-1 *h* -1,2,4-triazol-3-yl)propanamides and their tautomerism. *RSC Adv.,* **2018**, *8*, 22351-22360.
http://dx.doi.org/10.1039/C8RA04576C

[115] Moreno-Fuquen, R.; Arango-Daraviña, K.; Becerra, D.; Castillo, J-C.; Kennedy, A.R.; Macías, M.A. Catalyst- and solvent-free synthesis of 2-fluoro-*N*-(3-methylsulfanyl-1*H*-1,2,4-triazol-5-yl)benzamide through a microwave-assisted fries rearrangement: X-ray structural and theoretical studies. *Acta Crystallogr. C Struct. Chem.,* **2019**, *75*(Pt 3), 359-371.
http://dx.doi.org/10.1107/S2053229619002572 PMID: 30833533

[116] Xu, M.; Zhu, Y-B.; Wang, M.; Khan, I.A.; Liu, X-H.; Weng, J-Q. Microwave-assisted synthesis and antifungal activity of novel 1,2,4- triazole thioether derivatives containing pyrimidine moiety. *Lett. Drug Des. Discov.,* **2018**, *15*, 347-352.
http://dx.doi.org/10.2174/1570180814666170602082440

[117] Dengale, S.G.; Karale, B.K.; Akolkar, H.N.; Darekar, N.R.; Deshmukh, K.K. Microwave assisted synthesis and antimicrobial activity of novel 1,3,4-thiadiazoles and 1,2,4-triazoles derived from 2-(3-fluorophenyl)-4-methylthiazole-5-carbohydrazide. *Russ. J. Gen. Chem.,* **2019**, *89*, 1535-1540.
http://dx.doi.org/10.1134/S1070363219070259

[118] Reddy, K.R.; Mamatha, R.; Babu, M.S.S.; Shiva Kumar, K.; Jayaveera, K.N.; Narayanaswamy, G. Synthesis and antimicrobial activities of some triazole, thiadiazole, and oxadiazole substituted coumarins: synthesis and antimicrobial activities of some triazole, thiadiazole, and oxadiazole substituted coumarins. *J. Heterocycl. Chem.,* **2014**, *51*, 132-137.
http://dx.doi.org/10.1002/jhet.1745

[119] Franklim, T.N.; Freire-de-Lima, L.; de Nazareth Sá Diniz, J.; Previato, J.O.; Castro, R.N.; Mendonça-Previato, L.; de Lima, M.E.F. Design, synthesis and trypanocidal evaluation of novel 1,2,4-triazoles-3-thiones derived from natural piperine. *Molecules,* **2013**, *18*(6), 6366-6382.
http://dx.doi.org/10.3390/molecules18066366 PMID: 23760033

[120] Mermer, A.; Faiz, O.; Demirbas, A.; Demirbas, N.; Alagumuthu, M.; Arumugam, S. Piperazine-azole-fluoroquinolone hybrids: conventional and microwave irradiated synthesis, biological activity screening and molecular docking studies. *Bioorg. Chem.,* **2019**, *85*, 308-318.
http://dx.doi.org/10.1016/j.bioorg.2019.01.009 PMID: 30654222

[121] Basoglu Ozdemir, S.; Demirbas, N.; Demirbas, A.; Ayaz, F.A.; Çolak, N. Microwave-assisted synthesis, antioxidant, and antimicrobial evaluation of piperazine-azole-fluoroquinolone based 1,2,4-triazole derivatives. *J. Heterocycl. Chem.,* **2018**, *55*, 2744-2759.
http://dx.doi.org/10.1002/jhet.3336

[122] Mentese, M.; Demirbas, N.; Mermer, A.; Demirci, S.; Demirbas, A.; Ayaz, F.A. Novel azole-functionalited flouroquinolone hybrids: design, conventional and microwave irradiated synthesis, evaluation as antibacterial and antioxidant agents. Available from: https://www.ingentaconnect-com.ez30.periodicos.capes.gov.br/content/ben/lddd/2018/00000015/00000001/art00009# (Accessed April 17, **2021**).

[123] Demirci, S.; Mermer, A.; Ak, G.; Aksakal, F.; Colak, N.; Demirbas, A.; Ayaz, F.A.; Demirbas, N. Conventional and microwave-assisted total synthesis, antioxidant capacity, biological activity, and molecular docking studies of new hybrid compounds. *J. Heterocycl. Chem.,* **2017**, *54*, 1785-1805.

http://dx.doi.org/10.1002/jhet.2760

[124] Mentese, M.; Demirci, S.; Ozdemir, B.; Demirbas, A.; Ulker, S.; Demirbas, N. Microwave assisted synthesis and antimicrobial activity evaluation of new heterofunctionalized norfloxacine derivatives. Available from: https://www.ingentaconnect-com.ez30.periodicos.capes.gov.br/content/ben/lddd/2016/00000013/00000010/art00012 (Accessed April 17, **2021**).

[125] Mermer, A.; Demirbaş, N.; Şirin, Y.; Uslu, H.; Özdemir, Z.; Demirbaş, A. Conventional and microwave prompted synthesis, antioxidant, anticholinesterase activity screening and molecular docking studies of new quinolone-triazole hybrids. *Bioorg. Chem.,* **2018**, *78*, 236-248. http://dx.doi.org/10.1016/j.bioorg.2018.03.017 PMID: 29614435

[126] Ceylan, S.; Bayrak, H.; Basoglu Ozdemir, S.; Uygun, Y.; Mermer, A.; Demirbas, N.; Ulker, S. Microwave-assisted and conventional synthesis of novel antimicrobial 1,2,4-triazole derivatives containing nalidixic acid skeleton. *Heterocycl. Commun.,* **2016**, *22*(4), http://dx.doi.org/10.1515/hc-2016-0019

[127] Balaydın, H.T.; Özil, M.; Şentürk, M. Synthesis and glutathione reductase inhibitory properties of 5-methyl-2,4-dihydro-3H-1,2,4-triazol-3-one's aryl schiff base derivatives. *Arch. Pharm. (Weinheim),* **2018**, *351*, e1800086. http://dx.doi.org/10.1002/ardp.201800086 PMID: 29882995

[128] Özil, M.; Balaydın, H.T.; Şentürk, M. Synthesis of 5-methyl-2,4-dihydro-3H-1,2,4-triazole-3-one's aryl Schiff base derivatives and investigation of carbonic anhydrase and cholinesterase (AChE, BuChE) inhibitory properties. *Bioorg. Chem.,* **2019**, *86*, 705-713. http://dx.doi.org/10.1016/j.bioorg.2019.02.045 PMID: 30836234

[129] Liu, X-H.; Xu, X-Y.; Tan, C-X.; Weng, J-Q.; Xin, J-H.; Chen, J. Synthesis, crystal structure, herbicidal activities and 3D-QSAR study of some novel 1,2,4-triazolo[4,3-a]pyridine derivatives. *Pest. Manag. Sci.,* **2015**, *71*(2), 292-301. http://dx.doi.org/10.1002/ps.3804 PMID: 24753294

[130] Shaikh, M.; Wagare, D.; Farooqui, M.; Durrani, A. Microwave assisted synthesis of novel schiff bases of pyrazolyl carbaldehyde and triazole in PEG-400. *Polycycl. Aromat. Compd.,* **2020**, *40*, 1315-1320. http://dx.doi.org/10.1080/10406638.2018.1544154

[131] Kahveci, B.; Menteşe, E.; Akkaya, E.; Yılmaz, F.; Doğan, İ.S.; Özel, A. Synthesis of some novel 1,2,4-triazol-3-one derivatives bearing the salicyl moiety and their anticonvulsant activities: 1,2,4-triazol-3-ones and their anticonvulsant activities. *Arch. Pharm. (Weinheim),* **2014**, *347*, 449-455. http://dx.doi.org/10.1002/ardp.201300427 PMID: 24623369

[132] Saleem, M.; Kang, S.K.; Lee, K.H. Microwave assisted synthesis of a novel Optical chemosensor for selective Fe^{3+} detection. *J. Lumin.,* **2015**, *162*, 14-24. http://dx.doi.org/10.1016/j.jlumin.2015.02.004

[133] Shi, Z.; Zhao, Z. Microwave irradiation synthesis of novel indole triazole schiff base fluorescent probe for Al^{3+} ion. *Inorg. Chim. Acta,* **2019**, *498*, 119135. http://dx.doi.org/10.1016/j.ica.2019.119135

[134] Kantar, G.K.; Baltaş, N.; Menteşe, E.; Şaşmaz, S. Microwave-assisted synthesis and investigation of xanthine oxidase inhibition of new phthalonitrile and phthalocyanines containing morpholino substituted 1,2,4-triazole-3-one. *J. Organomet. Chem.,* **2015**, *787*, 8-13. http://dx.doi.org/10.1016/j.jorganchem.2015.03.033

[135] Min, L.-J.; Shi, Y.-X.; Wu, H.-K.; Sun, Z.-H.; Liu, X.-H.; Li, B.-J.; Zhang, Y.-G. Microwave-assisted synthesis and antifungal activity of some novel thioethers containing 1,2,4-triazole moiety. *Appl. Sci. (Basel),* **2015**, *5*, 1211-1220. http://dx.doi.org/10.3390/app5041211

[136] Farahi, M.; Karami, B.; Banaki, Z. Improved microwave-assisted catalyst-free synthesis of 9-aryl-5,9-dihydropyrimido[4,5-d][1,2,4]triazolo[1,5-a]pyrimidine-6,8(4h,7h)-dione derivatives. *Chin. Chem. Lett.,* **2015**, *26*, 1065-1067. http://dx.doi.org/10.1016/j.cclet.2015.05.035

[137] Gümüş, M.K.; Gorobets, N.Yu.; Sedash, Y.V.; Chebanov, V.A.; Desenko, S.M. A modified biginelli reaction toward oxygen-bridged tetrahydropyrimidines fused with substituted 1,2,4-triazole ring. *Chem. Heterocycl. Compd.,* **2017**, *53*, 1261-1267. http://dx.doi.org/10.1007/s10593-018-2204-3

[138] El-Fatah, N.A.A.; Darweesh, A.F.; Mohamed, A.A.; Abdelhamid, I.A.; Elwahy, A.H.M. Regioselective synthesis and theoretical studies of novel bis(tetrahydro[1,2,4]triazolo[5,1-b]quinazolin-8(4H)-ones) catalyzed by ZnO nanoparticles. *Monatshefte Für Chem. - Chem. Mon.,* **2017**, *148*, 2107-2122. http://dx.doi.org/10.1007/s00706-017-2040-7

[139] Mourad, A-F.E.; Amer, A.A.; El-Shaieb, K.M.; Ali, A.M.; Aly, A.A. 4-Hydroxy-1-phenylquinolin-2(1 *H*)-one in one-pot synthesis of pyrimidoquinolines and related compounds under microwave irradiation and conventional conditions: 4-hydroxy-1-phenylquinolin-2(1h)-one in one-pot synthesis of pyrimidoquinolines and related compounds under microwave irradiation and conventional con. *J. Heterocycl. Chem.,* **2016**, *53*, 383-388. http://dx.doi.org/10.1002/jhet.2286

[140] Murlykina, M.V.; Sakhno, Y.I.; Desenko, S.M.; Shishkina, S.V.; Shishkin, O.V.; Sysoiev, D.O.; Kornet, M.N.; Schols, D.; Goeman, J.L.; Van der Eycken, J.; Van der Eycken, E.V.; Chebanov, V.A. Study of the chemoselectivity of multicomponent heterocyclizations involving 3-amino-1,2,4-triazole and pyruvic acids as key reagents, and biological activity of the reaction products: chemoselectivity of multicomponent heterocyclizations. *Eur. J. Org. Chem.,* **2015**, *2015*, 4481-4492. http://dx.doi.org/10.1002/ejoc.201500469

[141] Berrino, E.; Supuran, C.T. Advances in microwave-assisted synthesis and the impact of novel drug discovery. *Expert Opin. Drug Discov.,* **2018**, *13*(9), 861-873. http://dx.doi.org/10.1080/17460441.2018.1494721 PMID: 30010444

Review

Journal of the Brazilian Chemical Society

https://dx.doi.org/10.21577/0103-5053.20240160

J. Braz. Chem. Soc. **2024**, *35*, 10, e-20240160, 1-31

The Discovery of Protheolysis Targeting Chimeras (PROTACs), Evolution, Design and Perspectives in Modulating Inflammatory Diseases

Lucas Caruso, [a,b] ***Thiago M. Pereira*** [a,b,c] ***and Arthur E. Kümmerle*** [*,a,b]

[a]*Instituto de Química, Universidade Federal Rural do Rio de Janeiro, 23897-000 Seropédica-RJ, Brazil*

[b]*Laboratório de Diversidade Molecular e Química Medicinal (LaDMol-QM), Instituto de Química, Universidade Federal Rural do Rio de Janeiro, 23897-000 Seropédica-RJ, Brazil*

[c]*Medicinal Chemistry Department, University of Strasbourg, 67200 Strasbourg, France*

Currently, most drugs have their mode of action based on occupation-oriented pharmacology (proteins modulation through temporary inhibition by association and dissociation). Alternative modes of actions are welcome to exploit current known targets (in a more selective way, for example) as well as those known as "undruggable". PROTAC (protheolysis targeting chimera) technology provides a compelling new approach that is based on an event-driven mode of action, exploring simultaneous binding to a protein and an E3 ligase, leading to targeted protein degradation, modulating the proteins levels. After all progress over the past two decades and the recent level of interest, clearly targeted protein degradation mode of action could become a therapeutic modality in the future. Furthermore, several PROTACs are under clinical trials, even already progressing to phase 3 (i.e., ARV-471). In this review we addressed the PROTACs discovery process, mode of action, evolution, current stage, their design, applications to modulating inflammatory conditions and the future directions of this promising drug discovery modality, including problems that still need to be overcome.

Keywords: PROTAC, event-driven mode of action, undruggable targets, hybrid compounds, E3 ligase

1. Introduction

In the last 20 years, the drug discovery process has seen a groundbreaking paradigm shift with the discovery of targeted protein degradation (TPD), a therapeutical strategy of inducing the depletion and/or reduction of a disease-causing protein via hijacking the endogenous protein degradation machineries.[1-3] During this period, the focus has changed from complete attention to the classical targets of traditional therapies (e.g., enzymes, ion channels, protein kinases, G protein-coupled receptors (GPCRs)), to also include those "unreachable" of high biological function interests, such as targets considered "undruggable".[4]

These "undruggable" targets are molecular entities that have proven challenging to modulate with traditional small-molecule therapies but that remained of great therapeutic interest.[1,5] Generally, they include proteins without enzymatic function, such as scaffolding proteins and transcription factors,[6,7] and play crucial roles in various diseases, such as cancer, neurodegenerative disorders, and inflammatory and infectious diseases. Estimative counts that nearly 400 human "undruggable" proteins are disease-related.[8,9] As characteristics, these targets have broad active sites and functional interfaces that are flat and lacking defined pockets, which are challenging for small molecules to bind to.[8]

The traditional and well-succeeded design of occupancy-driven small molecule compounds, for single or multitarget compounds, has been used during the last several decades in drug discovery.[10,11] This strategy is focused on modulating target proteins' function by occupying their active, orthosteric or allosteric sites. However, occupancy-driven drug discovery, despite having beautiful exceptions, is not always feasible and efficient for all drug targets, several times needing well-defined binding sites and preferentially high affinity.[1] From this point, the TPD approach emerged

*e-mail: akummerle@ufrrj.br
Editor handled this article: Carlos Maurício R. de Sant'Anna (guest)

Prof Eliezer Barreiro, thanks for all your groundbreaking and enthusiastic contributions to Brazilian Medicinal Chemistry. It is a great honor for us, your scientific son and your grandsons, having you as part of our histories.

as innovative and a key therapeutic modality to exploit current known targets (in a more selective way or overcoming potential resistances, for example) as well as those called "undruggables" by means of an event-driven new mode of action (MOA).[5,12,13]

Probably the main class of small molecules acting as TPD are proteolysis-targeting chimeras (PROTACs), first described in 2001 by Crews and co-workers.[14] Since many protein levels are regulated by ubiquitin-dependent proteasome system (UPS), they designed these compounds as TPD aiming at hijacking the cellular machinery to degrade a protein of interest (POI), as an effective way to modulate the protein abundance of normal and/or diseased cells. Indeed, the PROTACs were designed to be hetero-bifunctional compounds able to bring together a POI and the UPS degradation machinery, which do not usually form such a complex.

In this review, we will briefly address the PROTACs discovery process, MOA, evolution, current stage, their design, applications to modulating inflammatory conditions and the future directions of this promising drug discovery modality, including problems that still need to be overcome.

1.1. The UPS system behind the discovery of PROTACs

The proteostasis process, which is indeed protein homeostasis, denotes the intricate and interrelated cellular processes employed to control the concentration, conformation, and subcellular localization of proteins.[15] This complex system encompasses a wide array of pathways governing protein synthesis, folding, transport, and disposal.[16] In eukaryotic cells, damaged proteins or organelles can be effectively eliminated through proteasomes,[17] which manage the degradation of short-lived proteins and soluble misfolded proteins through the UPS,[18] a major pathway that degrades intracellular proteins.

In this pathway (Figure 1), proteins are targeted for degradation by the proteasome in a three-step process involving ubiquitin-activating enzymes (E1), ubiquitin-conjugating enzymes (E2) and ubiquitin protein ligases (E3), which coordinate the transfer of ubiquitin (Ub) molecules to the target protein (substrate) with high specificity through formation of isopeptide linkages between the C-terminal carboxyl group of a Ub moiety and an ε-NH_2 group on a lysine on the protein substrate.[19] Ub is a small eukaryotic regulatory molecule (76-amino acid), which is responsible for marking proteins (through polyubiquitination) for degradation via the above described proteasome system. After the linkage of first Ub to the protein, the next Ub molecules are always linked to one of the seven lysine residues (K6, K11, K27, K29, K33, K48, K63) or the N-terminal methionine of the previous Ub molecule.[20] Poly-ubiquitinated proteins in K48 (one of the most abundant) are often targeted to proteasome for degradation (Figure 1). Poly-ubiquitinated proteins in K48 (one of the most abundant) are often targeted to proteasome for degradation. The human genome is estimated to encode more than 600 E3 ligase,[21,22] each one with high selectivity for different subsets of proteins.

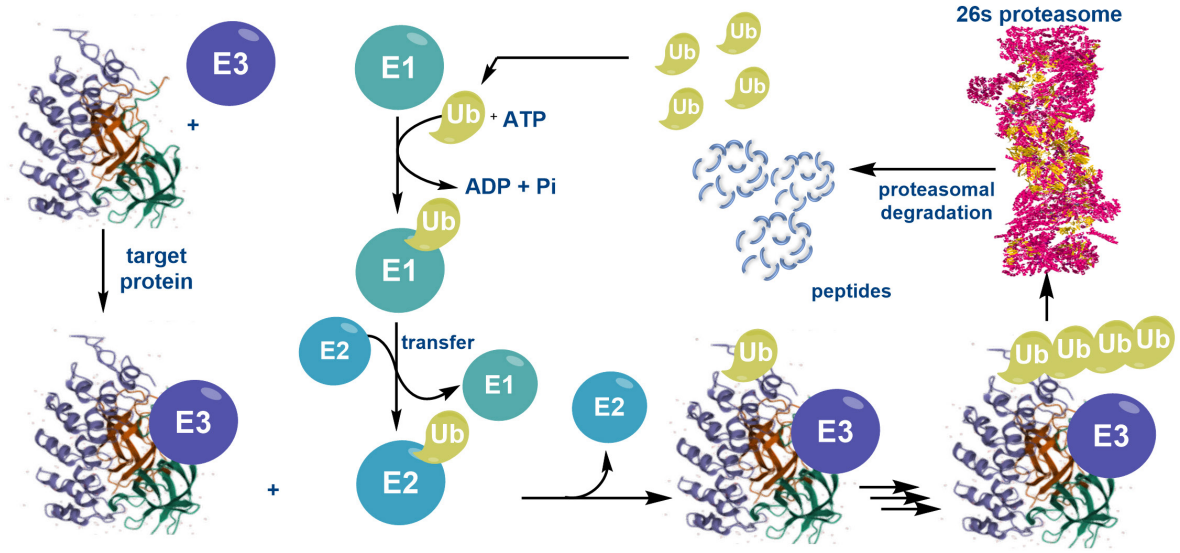

Figure 1. Schematic representation of ubiquitin-proteasome system (UPS) process of protein degradation. The ubiquitin molecule (Ub) is linked to ubiquitin-activating enzymes (E1) (EC:6.2.1.45) through an ATP-dependent process that is subsequently transferred to ubiquitin-conjugating enzymes (E2) (EC:2.3.2.23) through interaction with E2. In a parallel process, ubiquitin protein ligases (E3) (EC:2.3.2.26) recognize and binds to the target protein (depicted in cartoon form). After, the complexed E3 catalyzes the transfer of the ubiquitin molecule from E2 to the target protein. Thus, a sequential process results in the polyubiquitination of the substrate, targeting it for the subsequent proteasome degradation.

The utilization of this protein degradation system for therapeutic applications drew inspiration from researches conducted on viruses and plants. More than 20 different viruses can hijack the human UPS system to promote their own survival and replication.[23] For example, human papillomavirus types 16 (HPV-16) and 18 (HPV-18) possess the E6 protein that recruits the human E3 ligase to ubiquitylate p53, resulting in its degradation.[24] Due to the fast degradation of ubiquitinated proteins within cells and nature inspiration, Craig M. Crews and Raymond J. Deshaies[14] raised the idea that manipulating the UPS pathway could serve as an effective method for regulating the protein levels in both healthy and diseased cells. This approach led to the discovery of PROTACs.

1.2. Discovery and mode of action of PROTACs

Despite the occupancy-driven pharmacology MOA has been successful for many biological targets, this MOA can be challenging for modulating all kinds of targets. Specifically, it can be less effective for proteins lacking enzymatic activity, such as scaffolding proteins or those that rely on protein-protein interactions (PPIs).[25] Drugs that work by occupying a target site are most effective when the target site remains occupied. Those with low potencies often require high drug doses that can lead to unwanted side effects due to off-target binding at higher drug concentrations.[26] Additionally, resistance to inhibition by occupancy-driven therapies can be developed in many diseases, including cancer and bacterial infections.[27,28] As a result, many researchers have been exploring new drug classes that use alternatives MOA.

Under this perspective, in the early 2000s, PROTACs were developed as a novel class of small molecules with a new MOA, being designed to harness the cellular machinery responsible for protein degradation. The first PROTAC (named Protac-1), synthesized in 2001,[14] was the *in vitro* proof of concept for the biological application of this class of compounds, and confirmed the expectations for its MOA. Protac-1 was specifically designed to target methionyl aminopeptidase 2 (MetAp-2), identified as the potential target of the potent angiogenesis inhibitors ovalicin and fumagillin. Protac-1 comprised two different components attached by a linker: ovalicin (ligand for the POI) and a 10-amino acid phosphopeptide DRHDSGLDSM derived from nuclear factor-κB inhibitor-α (NF-κBIα, also known as IκBα), which is recognized by the E3 ligase β-transducin repeat-containing E3 ubiquitin-protein ligase (β-TRCP) (Figure 2a). Protac-1 acted as a molecular bridge, promoting the interaction between MetAp-2 and β-TRCP, allowing the ligase to ubiquitylate METAP2 and inducing its degradation.[14]

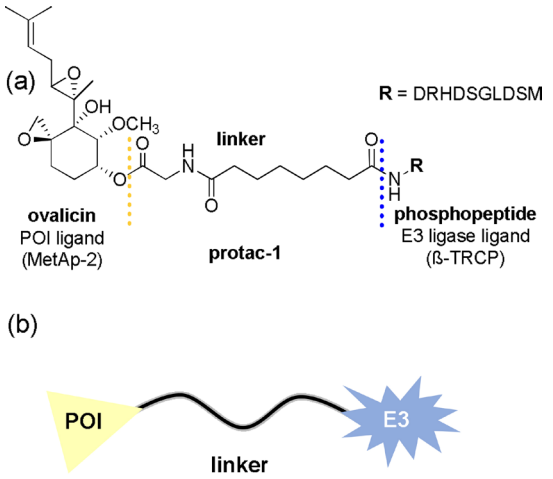

Figure 2. (a) Structure of first described PROTAC (Protac-1); (b) PROTACs hetero-bifunctional nature including POI ligand, a linker, and a ligand for E3 ligase.

As for Protac-1, the development of PROTAC technology was based on its hetero-bifunctional nature, which includes a ligand for the POI, a ligand for recruiting ubiquitin E3 ligase, and a linker (Figure 2b).[2,29] This unique heterobifunctional character allows simultaneously binding to both the POI and a ubiquitin E3 ligase, forming a ternary complex that activates the UPS for the degradation of the POI (Figure 2).[2,29,30]

The event-driven nature of PROTACs allows them to act catalytically (considered sub-stoichiometric and an innovative pharmacodynamic modality), triggering the degradation of multiple molecules of the POI with just one PROTAC molecule (Figure 3). This distinctive ability to induce protein degradation and the event-driven MOA distinguish PROTACs as having unique therapeutic potential when compared to classical occupancy-driven therapeutics (Figure 3).[31,32]

Indeed, while both inhibitors and degraders share the common objective of diminishing functional proteins, their mechanisms differ: inhibition governs protein function, while degradation manages protein abundance. The main advantage of PROTACs MOA, like in Protac-1, is the depletion of the entire target and thereby disrupts both enzymatic activity and nonenzymatic functions. This comprehensive approach enables PROTACs to tackle potential resistance encountered in current therapeutic treatments.[33-36] Moreover, PROTACs are also less affected by increases in target expression and mutations in the target protein, as their catalytic action requires only low doses.[37,38]

1.3. PROTACs mechanistic highlights

The main point of PROTAC-induced degradation MOA resides in the ternary complex (POI-PROTAC-E3)

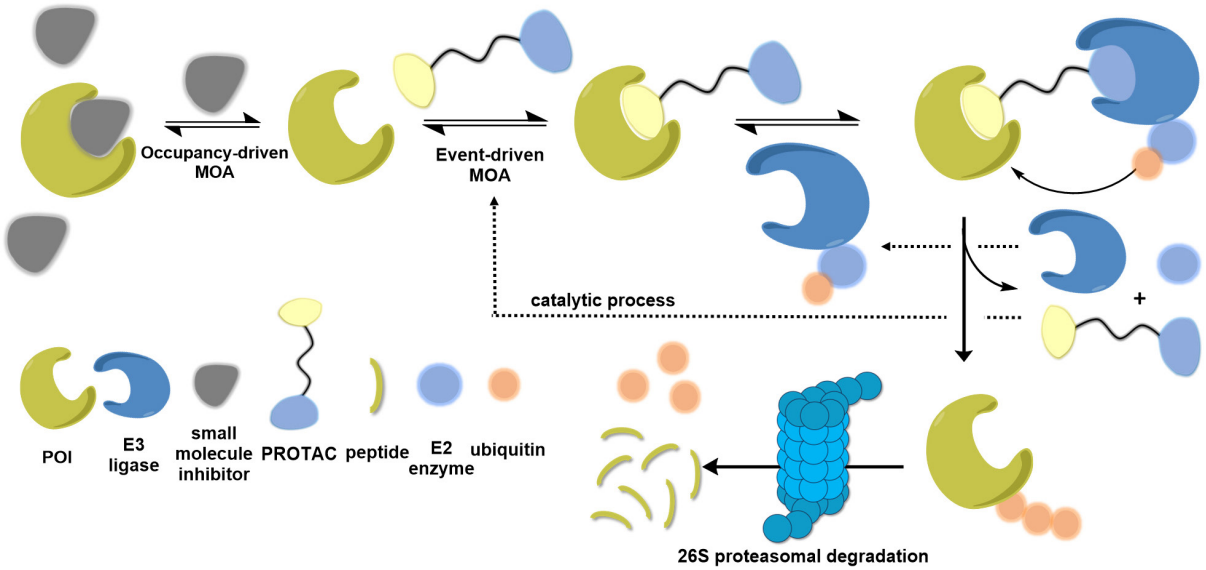

Figure 3. Illustration comparing occupancy- and event-driven MOA. In occupancy-driven MOA the small molecule modulates the POI by means of an association-dissociation occupancy of active site (non-catalytic). In event-driven MOA (catalytic), protein function is modulated by degradation, with PROTAC initiating a degradation cascade involving POI ubiquitination followed by its 26S proteasomal degradation.

formation, enabling POI polyubiquitination and subsequent proteasomal degradation (Figure 3). Established mathematical models applied to this ternary complex formation[39,40] predict a bell-shaped dependency on PROTAC concentration (Figure 4a).[41] In the classical occupancy-driven MOA, the amount of effect increases depending on how many of the targets the compound can bind to, ultimately generating a response. As receptor occupancy approaches 100%, the observed effect is diminished (S-shape of concentration-response). For PROTACs, the increase in concentration leads to augmentation of the ternary complex, activating the protein degradation. Differently from the occupancy-driven MOA, exceeding the ideal dose can generate a phenomenon called "hook effect" occurs, diminishing degradation activity due to the formation of an unproductive binary complex (Figure 4a).[42] Furthermore, interactions between the POI and E3 may stabilize or destabilize ternary complex formation (Figure 4b). A cooperative factor ($\alpha = K_{d\ binary}/K_{d\ ternary}$) provides a measure of susceptibility to ternary complex formation and can be positive or negative. Positive cooperativity ($\alpha > 1$) occurs when stabilizing PPIs between the POI and E3 promote the ternary complex formation, in which the hook effect can be effectively minimized, which ultimately leads to an amplified production of ternary complex. On the other hand, negative values ($\alpha < 1$) mean that destabilizing factors are abrogating the ternary complex formation.[43]

The first experimental demonstration of the ternary complex was only described in 2017 by Ciulli and co-workers[44] laboratory from a complex involving MZ1

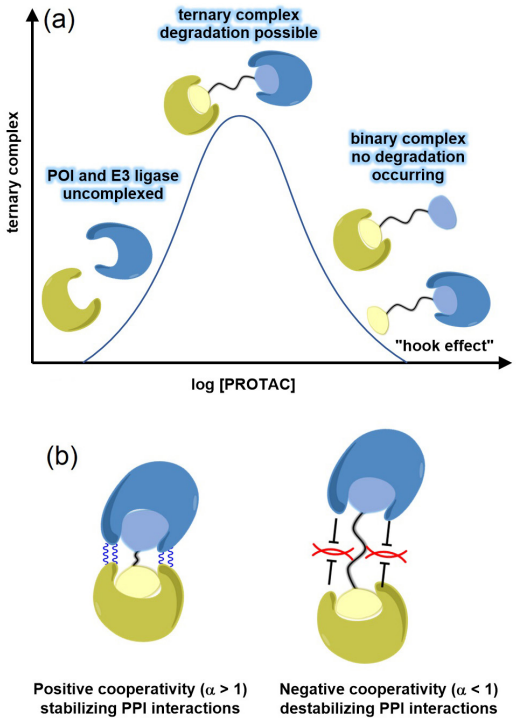

Figure 4. (a) Increasing concentration of PROTAC leading to formation of ternary complex (ideal concentration), and the binary complex and "hook effect" (when concentration is too high). PROTAC compound; POI ligand (yellow), E3 ligase (blue); (b) positive and negative cooperativity working on stabilizing or destabilizing, respectively, PPIs interactions. Favorable interactions (blue wave line), unfavorable interactions like charge repulsion and/or steric clashes (red curves).

(PROTAC) and both the bromodomain of $Brd4^{BD2}$ (POI) and VHL (Von Hippel-Lindau disease tumor-suppressor protein, E3 ligase). The crystal structure revealed valuable insights into the interactions among BRD4, VHL, and

the PROTAC linker. Through assessments using diverse biophysical methods, the study demonstrated positive cooperativity. This cooperative effect was found to enhance the potency and selectivity of PROTAC MZ1, leading to the induced degradation of specific members within the BRD family (Figure 5).[44]

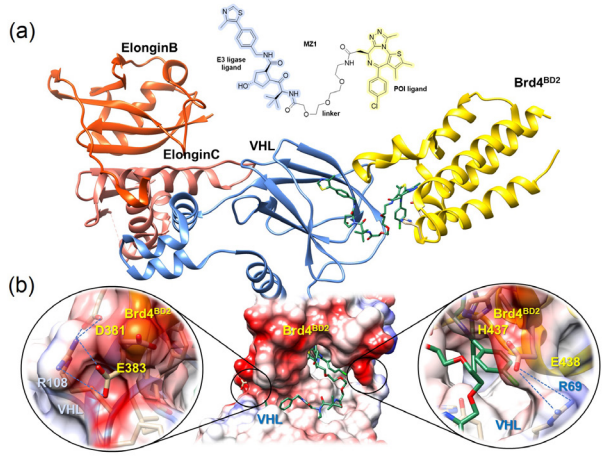

Figure 5. (a) Crystal structure of the complex PROTAC MZ1 (POI ligand–linker–E3 ligase ligand), $Brd4^{BD2}$ and VHL (PDB 5T35); (b) electrostatic potential map showing the charged zipper contacts between $Brd4^{BD2}$ residues D381 and E383 with E3 VHL residue R108; and E438 from $Brd4^{BD2}$ with E3 VHL residue R69. Blue dashed lines indicate hydrogen bonds. The image and the electrostatic potential were generated in UCSF Chimera alfa version 1.17.[45] Red surfaces represent negative electrostatic potentials and blue surfaces represent positive electrostatic potentials.

Many times, one can hear that the good affinity of a given PROTAC for its POI is not the most important point for a good degradation. Indeed, because of occupancy-driven MOA, Medicinal Chemists are used to thinking that good affinities can be converted into good activities. However, the event-driven nature of PROTACs is completely associated with the ternary complex formation. As described above, its formation can occur with positive cooperativity due to favorable/stabilizing PPIs,[44] which can ultimately lead to better activities and potencies. Indeed, Wurz *et al.*[46] showed that degradation potency and initial rates of degradation correlate well with the ternary complex binding affinity and cooperativity, not depending only on binary affinities (i.e., POI ligand - POI or E3 ligase ligand - E3 ligase). For example, an ibrutinib PROTAC derivative (**1**) exhibiting a low binary binding affinity (K_d = 11 μM) towards the Bruton's tyrosine kinase (BTK) demonstrated potent induction of its degradation, with a half-maximal degradation concentration (DC_{50}) of 1.1 nM and a maximum degradation efficacy (Dmax) of 87% (Figure 6). Many efforts are still needed to understand the ternary complex and cooperativity effects. It is important to bear in mind that due to the catalytic MOA, positive cooperativity is not a perfect rule for good PROTACs, as demonstrated in some examples in which cooperativity was not a main factor for efficient degradation.[47]

2. Evolution of PROTACs until the Present

Since the discovery and first description of PROTACs by Crews group,[14] the technology has hugely expanded from molecules studied in cell lysates and cell culture to studies in animals and animal disease models, finally reaching clinical trials in humans. PROTACs have also spread from an exclusive academic universe at the beginning to the pharmaceutical and biotechnological industries (Figure 7).

Regarding publications in PROTACs and based on the Scopus database, we analyzed the period from 2001 to the end of 2023. Curiously, the entry "PROTAC" was not the most precise since some articles described this acronym for fields other than the proteolysis target chimeras. Thus, our analysis was made with the entries "PROTAC" or "PROTACs" and "proteolysis" or "E3".

After the discovery of Protac-1 in 2001, a clear gap with minor publications was observed until 2015, when an inflection point started, with an impressive increase from 2017. This first period was marked by peptidic PROTACs (e.g., **2**) targeting the degradation of the androgen and estrogen nuclear receptors (AR and ER, respectively), expanding the target scope.[48] A proof of concept that PROTACs could modulate protein degradation

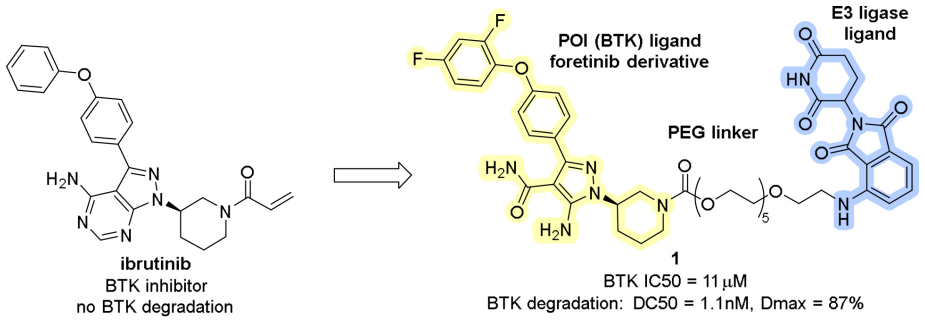

Figure 6. Ibrutinib and PROTAC **1** structures. Comparison between binary (half-maximal inhibitory concentration, IC_{50}) and ternary (half-maximal degradation concentration, DC_{50}) potencies of PROTAC **1**.

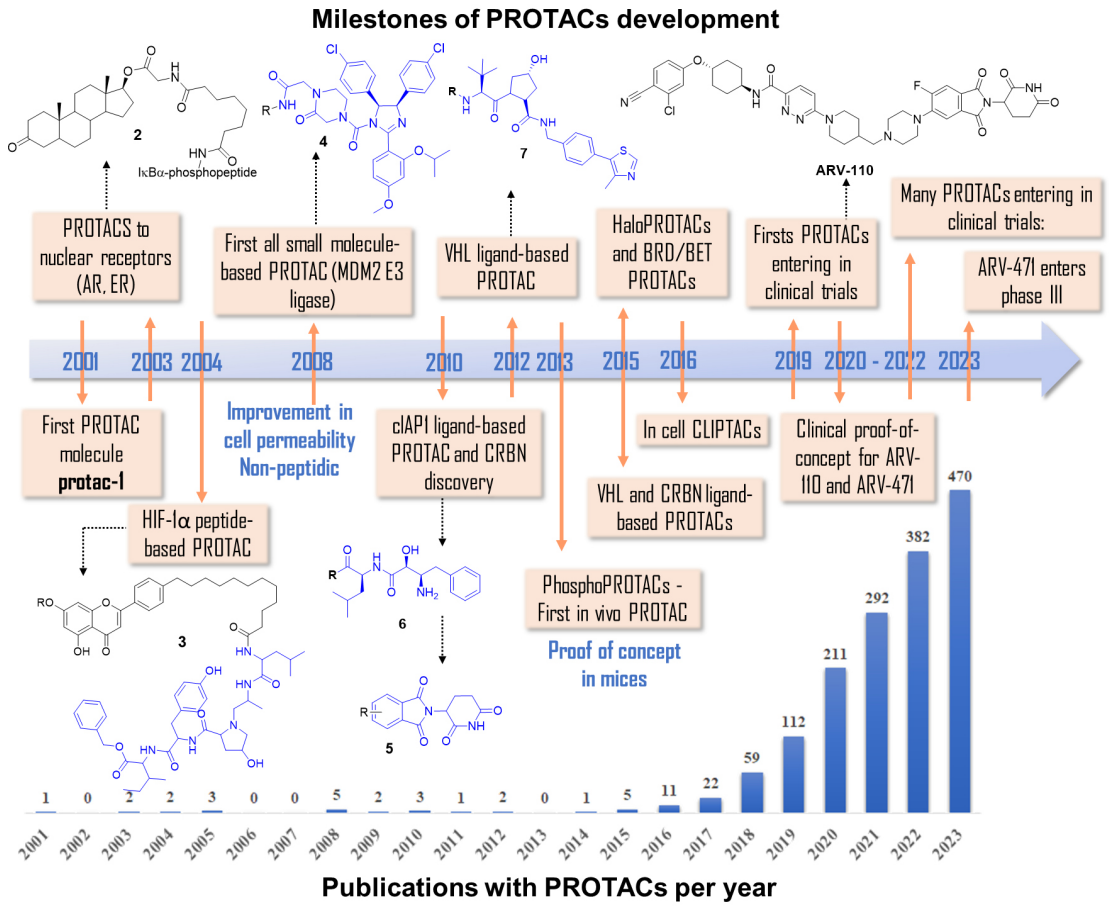

Figure 7. Milestones of the PROTACs' discovery and development and publications about PROTACs since the first relate in 2001.

intracellularly was achieved when microinjections of these AR and ER targeting PROTACs demonstrated that they could function in an intact cell. However, these PROTACs lacked good cell permeability (Figure 7).

The subsequent development of PROTACs involved incorporating a peptide from hypoxia-inducible factor 1 subunit-α (HIF1α), a fragment able to recruit the VHL E3 ligase in intact cells, eliminating the need for microinjection.[49] A shorter peptide fragment of HIF-1α was later incorporated into a PROTAC targeting aryl hydrocarbon receptor nuclear trans20240160 (ARNT).[50] Despite this PROTAC's "first generation" (indeed considered "bioPROTACs" today) confirmed promising applications inducing specific degradation of desired targets, the peptide nature of these compounds led to poor cell permeability that summed to the low micromolecular activities, hampered their use as therapeutic products (Figure 7).[7]

The undesirable cell penetration parameters led to efforts to overcome this problem and, in 2008, Crew and co-workers[51] developed the first small-molecule PROTAC targeting AR (**4**), increasing dramatically the targets reported[52] to be degraded by PROTACs, consisting of nonsteroidal AR ligand (SARM), a ligand targeting E3 ligase from murine double minute 2 (MDM2-p53 PPI inhibitor, nutlin), and a polyethylene glycol (PEG)-based linker.[51] These compounds were more readily taken up by cells than previous peptide-based PROTACs and more likely to be developed into drugs (Figure 7).[29]

During the next years, the discovery of multiple other E3 ligases, including cereblon (CRBN) (**5**),[53,54] cell inhibitor of apoptosis protein (cIAP) (**6**),[54,55] and later the VHL (**7**),[56,57] led to a significant advancement of the PROTAC technology. Special attention and development have been made to VHL and CRBN ligands. While many peptidomimetics of VHL ligand class, with high affinity for the homonym E3 ligase, were developed,[58-60] as well as further structure-activity relationship (SAR) performed to improve physical-chemical properties maintaining similar affinities towards VHL E3 ligase, the immunomodulatory drugs (IMiDs), including thalidomide, pomalidomide, and lenalidomide, were found to target the E3 CRBN at the molecular level (Figure 7).[61-66]

Despite promising applications for PROTACs have been demonstrated until the beginning of 2010s,[1,7] no *in vivo* activity evidence was reported until 2013, when PhosphoPROTACs were described as the first *in vivo* proof

of concept of PROTACs, being able of inhibiting tumor growth in murine models.[67] Moreover, PhosphoPROTACs have distinguished between receptor tyrosine kinase (RTK) signaling pathways by incorporating different peptide sequencers as POI recruiting moiety (Figure 7).

The following years experienced an increase on PROTACs interest and development. In 2014, the first peptide based antiviral PROTACs against HBV was developed;[68] and in 2015, CRBN and VHL E3 recruiting ligands were used to develop CRBN- and VHL-based PROTACs such as the Halo-PROTACs,[69] and PROTACs targeting the bromodomain and extra-terminal (BRD/BET) family of epigenetic proteins.[70] In 2016, a new PROTAC class was discovered by Astex Pharmaceuticals,[71] the CLIPTACs (in cell clickformed proteolysis targeting chimeras). These PROTACs could be formed intracellularly by biocompatible reactions such as an inverse electron demand Diels-Alder reaction after treating cells, sequentially, with cell permeable compounds.

Probably, 2019 was a landmark year in which PROTACs shifted from laboratory proof of concepts to a translational exploration when compounds ARV-110 (NCT03888612) and ARV-471 (NCT04072952) entered in clinical trial phase 1 targeting the androgen receptor (AR) and estrogen receptor (ER), respectively (Figure 7). The interest for PROTACs as pharmaceutical products also had a considerable increase after 2019 when the number of patents with the term "PROTAC" was analyzed in Scifinder database. For instance, the number of patents since the first Crews patent in 2002 until 2019 was 57. Only in 2020, 48 patents were registered while this number grew to 176 registers last year. Worth of note, antitumoral and anti-inflammatory compounds correspond to the major applications described inside the patents, with anticancer responding to 61%, though.

The increasing interest of pharmaceutical companies accelerated the translation process of PROTACs from the basic research to the clinical trials and as reflected in the increase in patents number. Furthermore, the clinical significance of the PROTAC approach became evident through the initiation of many clinical trials with PROTAC-based molecules until today (data shown in section 2.1.1).

2.1. Present

The total number of 470 publications in PROTACs last year and 1467 in a 5-years period (2019-2023) shows how this field has grown since its first description in 2001 (Figure 7). The importance of PROTACs is measured not only by the number of publications, but also the high-impact journals in which we can find these publications: Journal of Medicinal Chemistry (149), European Journal of Medicinal Chemistry (110), Cell Chemical Biology (46), ACS Medicinal Chemistry Letters (36), and Journal of the American Chemical Society (36).

Regarding targets reached, in 2019, a review from Sun *et al*.[37] described that around 40 proteins could be degraded by PROTACs at that time. The same group updated this number for about 130 degradable targets in 2021,[38] showing an impressive increase of 90 targets in two years. Currently, consulting the PROTAC-DB (an electronic repository of structural and experimental data about PROTACs with POI and chemical structures of POI ligands, along with biological activities and physicochemical properties),[72] the number of these targeted proteins has increased to 323 (an increase of 70% in degradable targets in only 2 years),[72] indicating that the era of protein degradation has indeed arrived.

Maybe one of the main appeals to PROTACs is the possibility of reaching "undruggable" targets. Indeed, some compounds were developed as degraders of proteins lacking a catalytic site or a small-molecule binding site like aberrant Tau, present in frontotemporal dementia.[73-75] The most frequently mutated gene family in cancers,[76-79] rat sarcoma virus (RAS) (Kirsten (KRAS), neuroblastoma (NRAS) and Harvey (HRAS)), was at one time termed as "undruggable" and was a model for the development of many PROTACs. Today, modulating RAS using PROTACs is still an open avenue for discovering RAS therapies and understanding its basic cell biology.[80] Nevertheless, the use of PROTAC for degrading these proteins, particularly those engaged in PPIs, remains somehow restricted due to challenges in identifying small-molecule binders for these proteins.[81] New techniques are welcome to identify new chemical entities that bind to these "undruggable" POI, like the recently described site-specific and fragment-based covalent ligand screening using liquid chromatography-tandem mass spectrometry (LC-MS/MS).[81]

In contrast, PROTACs are widely used for targeting kinases (n = 195 kinases), today representing around 60% of all described PROTACs' targeted proteins. At first sight, it appears to be countersense since kinases are already an explored target by the classical occupancy-driven pharmacology MOA. The main point here is that many kinases possess well-established and potent inhibitors or high affinity ligands. These compounds can be readily modified to incorporate linkers, keeping adequate binding affinity. Furthermore, kinases exhibit deep binding pockets, facilitating the binding of PROTACs, and prompting interaction between the kinases and the E3 ligases, leading to ubiquitination and eventual degradation.

Additionally, PROTACs may solve one of the main problems of adenosine 5'-triphosphate (ATP)-competitive kinase inhibitors, the lack of selectivity due to the high degree of homology of ATP binding sites between kinases.[38] When nonselective inhibitors are used as POI ligands for designing new PROTACs, both the protein ligands and the degraders can bind to the corresponding kinases. However, in the case of PROTACs this recognition induces specific protein-protein interactions between the POI and E3 ligase, forming a ternary complex that can be very specific. This two-step recognition mechanism contributes to the selective degradation of targets.[38] This curious characteristic is because functional residues in proteins tend to be highly conserved over evolutionary time. Jack *et al.*[82] described an analysis with 524 distinct enzymes, demonstrating a highly evolutionary conservation of amino acid residues near the catalytic site, while in contrast, sites in protein-protein interfaces are only weakly conserved. The lack of selectivity for ATP-competitive kinase inhibitors resides in the interaction of these compounds with the highly conservative sites of the enzymes, while in PROTACs, the ternary complex conduct the E3 ligase to a lesser conservative region of enzymes, i.e., the protein-protein interfaces, possibly giving completely different modes of interactions.

An interesting example was described by Bondeson *et al.*[83] From a high-throughput competitive binding assay, they discovered that foretinib at 10 μM could bind to more than 130 different kinases (Figure 8). Taking foretinib as model for the POI ligand, they designed and synthesized two PROTACs (**8** and **9**) using different E3 ligase ligands (CRBN (**8**) and VHL (**9**)). PROTACs **8** and **9**, at the same concentration, significantly changed the binding profile, in which **8** retained binding to 52 kinases while **9** bonded 62 kinases and were able to only degrade less than 10 kinases. Additionally, they demonstrated that PROTAC **8** effectively degraded the therapeutically relevant protein p38a/MAPK14, despite weak binding affinity (Figure 8).[83]

Common observed drug resistance via mutations (close to the inhibitor binding pockets), gain of scaffolding function or overexpression of drug targets in long term treatments with traditional kinase inhibitors are explanations to the current option for new PROTACs. The event-driven MOA of PROTACs, resulting in catalytic removal of POI, can evade drug resistance from long-term selection pressure by degrading target proteins.[84] Furthermore, studies have revealed that PROTACs can induce the degradation of many mutated kinases like BTK. This highlights the potential of TPD for treating diseases, e.g., chronic lymphocytic leukemia (CLL), resulting from kinase resistance to ibrutinib due to mutations.[85-87] While the ibrutinib MOA is to covalently bind to cysteine in the ATP binding pocket of BTK, exactly where the mutation occurs (C481S), PROTAC derivatives were not designed to covalently bind to BTK, inducing the degradation of both wildtype and mutant (C418S) forms.[34,46,46,85,88]

2.1.1. Clinical proof-of-concept

All the attractive characteristics of PROTACs described herein had their clinical validation when ARV-110 (AR) and ARV-471 (ER) entered in clinical trials in 2019. The oral efficacy and safety of ARV-110 have been proven in managing metastatic castrated prostate cancer (mCRPC),[89-91] while ARV-471 has demonstrated promising results in treating breast cancer.[92] Since them, an increasing number of protein targets have emerged to develop clinical degraders and 21 new PROTACs entering in clinical trials as single chemical entities or as pharmaceutical combination with other drugs, and nowadays, 20 clinical trials are still running. These PROTACs degraders are based on different E3 ligands, but mainly on CRBN-based ligands.

While the first two PROTACs modulated androgen (AR) and estrogen (ER) receptors, many other targets raised such as B-cell lymphoma-extra large (BCL-X_L), bromodomain-containing protein 9 (BRD9), signal transducer and activator of transcription 3 (STAT3) (Table 1

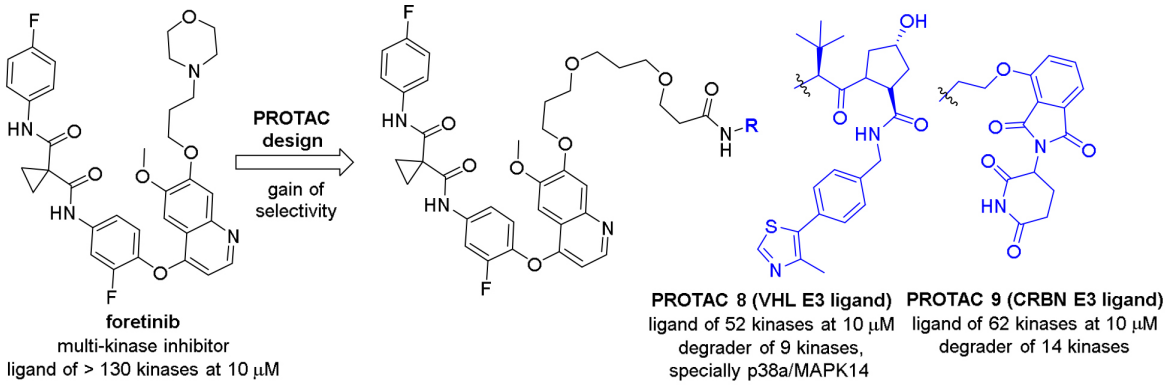

Figure 8. Use of non-selective inhibitor foretinib as POI ligand for designing new selective PROTACs.

and disclosed structures in Figure 9). Currently, almost all clinical trials are focused on research for anticancer PROTACs. However, recently (in 2021) the first clinical degrader of interleukin-1 receptor associated kinase 4 (IRAK-4) for autoimmune inflammation-diseases entered in clinical trials, the KYMERA's degrader KT-474.[93] Worth of note, KT-474 is already in phase 2 clinical trials and is showing that degraders for inflammatory conditions might be an interesting and promising field.

2.1.2. Current drawbacks of PROTACs and possible avenues to improvements

Despite many advantages discussed above in this review, PROTACs still have space for improvement in some

Table 1. Status and characteristics of PROTACs currently under clinical trial evaluations

Year	Comp	PROTAC	ROA	Target	Main indications	E3	CP	NCT number	Status
2019	Arvinas	ARV-110	oral	AR	metastatic castration resistant prostate cancer	CRBN	I/II, Ib	NCT03888612	A, NR
							Ib	NCT05177042	A, NR
2019	Arvinas / Pfizer	ARV-471	oral	ER	ER+/HER2- locally advanced or metastatic breast cancer	CRBN	I	NCT05538312 NCT05930925 NCT05652660 NCT05673889 NCT06005688	C
								NCT05463952 NCT05501769 NCT05732428	A, NR
							I/II	NCT05548127 NCT04072952	R
								NCT06206837	NYR
							II	NCT05549505	A, NR
								NCT06125522 NCT05573555 NCT01042379	R
							III	NCT05909397 NCT05654623	R
2020	Bristol Myers Squibb	CC-94676	oral	AR	metastatic castration-resistant prostate cancer	CRBN	I	NCT03554993 NCT04958291	C
2021	BeiGene	BGB-16673		BTK	B-cell malignancies	CRBN	I	NCT05294731 NCT05006716	R
2021	Nurix Therap.	NX-2127	oral	BTK	relapsed/refractory B-cell malignancies	CRBN	I	NCT04830137	A, NR
2021	Nurix Therap.	NX-5948	oral	BTK	relapsed/refractory B-cell malignancies	CRBN	I	NCT05131022	R
2021	Haisco	HSK29116		BTK	relapsed/refractory B-cell malignancies	CRBN	I	NCT04861779	R
2021	Lynk	LNK-01002		Ras GTP-ase	myelofibrosis (PV-MF, ET-MF) or acute myeloid leukemia	CRBN	I	NCT04896112	W
2021	Accutar Biotech	AC682	oral	ER	locally advanced or metastatic ER+ breast cancer	CRBN	I	NCT05489679	T
							I	NCT05080842	A, NR
2021	Arvinas	ARV-766	oral	AR	metastatic castration-resistant prostate cancer	undisclosed	I/II	NCT05067140	R
2021	Dialectic Therap.	DT2216	i.v.	BCL-XL	solid tumor, hematologic malignancy	VHL	I	NCT04886622	C
2021	Foghorn Therap.	FHD-609	i.v.	BRD9	advanced synovial sarcoma	undisclosed	I	NCT04965753	A, NR
2021	Kymera / Sanofi	KT-474	oral	IRAK-4	autoimmune diseases, atopic dermatitis (AD) or hidradenitis suppurativa (HS)	CRBN-based	I	NCT04772885	C
							II	NCT06058156, NCT06028230	R

Table 1. Status and characteristics of PROTACs currently under clinical trial evaluations (cont.)

Year	Comp	PROTAC	ROA	Target	Main indications	E3	CP	NCT number	Status
2022	Hinova	HP518		AR	metastatic castration-resistant prostate cancer	CRBN	I	NCT05252364	C
							I	NCT06155084	NYR
2022	Kintor	GT-20029		AR	prostate cancer	CRBN	I	NCT05428449	C
2022	Arvinas	ARV-110		AR	ARV-110 in combination with abiraterone	CRBN	I	NCT05177042	A, NR
							I/II	NCT03888612	A, NR
2022	Kymera	KT-413	i.v.	IRAK-4	relapsed or refractory B-cell NHL	CRBN	I	NCT05233033	S
2022	Kymera	KT-333	ND	STAT3	lymphoma, large granular lymphocytic leukemia, solid tumors	undisclosed	I	NCT05225584	R
2022	C4 Therap.	CFT8634	oral	BRD9	synovial sarcoma	CRBN	I/II	NCT05355753	T
2022	C4 Therap.	CFT8919	oral	EGFR-L858R	non-small-cell lung cancer	CRBN	I	FDA permission, not yet started	–
2022	Accutar Biotech	AC176	oral	AR	prostate cancer	undisclosed	I	NCT05241613	A, NR
2022	Cullgen	CG 001419	oral	TRK	cancer and other indications	CRBN	I/II	FDA permission, not yet started	–
2022	Astellas Pharma	ASP3082	i.v.	KRAS G12D	solid tumor	undisclosed	I	NCT05382559	R

PROTAC: protheolysis targeting chimera; ROA: route of administration; CP: clinical phase; NCT numbers: National Clinical Trial (NCT) identifier number; AR: androgen receptor; CRBN: cereblon; A: active; NR: not recruiting; ER: estrogen receptor; C: completed; R: recruiting; NYR: not yet recruiting; BTK: Bruton's tyrosine kinase; PV-MF: polycythemia vera myelofibrosis; ET-MF: essential thrombocythemia myelofibrosis; W: withdrawal; T: terminated; i.v.: intravenous; VHL: Von-Hippel-Lindau; BRD9: bromodomain-containing protein 9; IRAK-4: interleukin-1 receptor associated kinase 4; NHL: non-Hodgkin lymphoma; S: suspended; STAT3: signal transducer and activator of transcription 3; EGFR-L858R: L858R mutant form of the epidermal growth factor receptor; FDA: Food and Drug Administration; TRK: tropomyosin receptor kinase; KRAS G12D: Kirsten rat sarcoma virus gene mutation G12D.

areas that can be considered disadvantageous,[94] such as:

(*i*) PROTACs have some drawbacks in terms of potential toxicities, stemming from either on-target or off-target protein degradation. PROTACs may lack selectivity, leading to the degradation of other proteins (off-target effect) or causing unselective degradation of the POIs in undesired tissues (on-target effect). This challenge can be partially addressed using other administration ways, like topical PROTACs that have proven to mitigate systemic exposure and associated side effects. A recent illustration is compound GT20029 (structure not yet disclosed), targeting AR and currently undergoing phase I clinical trials in China.[95] However, in cases where systemic administration is necessary, targeted delivery systems can potentially overcome issues related to poor selectivity. In contrast to conventional small molecules, PROTACs typically present greater complexities in terms of drug metabolism and pharmacokinetics (DMPK) and need more comprehensive safety evaluations.[96] The metabolites of PROTACs, particularly those formed through linker cleavage, have the potential to competitively bind to the POI or the E3 ligase. This competitive binding may "antagonize" the degradation of the POI, consequently diminishing the efficacy of the original PROTAC. Hence, there is a need to develop innovative approaches for characterizing pharmacokinetics and metabolite profiling.[96]

(*ii*) PROTACs are molecules with properties laying outside Lipinsk's rule of five that can negatively affect their pharmaceutical effects.[97-99] As an illustration, PROTACs possess a higher molecular weight (MW) in comparison to conventional small-molecule inhibitors, potentially posing a pharmacokinetic challenge to their cellular permeability.[100] However, upon oral administration, PROTACs have demonstrated the ability to induce degradation of the POIs in any accessible cells as proved in clinical trials. Recent studies[101,102] reveal an intriguing aspect of PROTACs, indicating that their properties can somehow contribute to their cell-permeability. An example from a PEG-linker PROTAC demonstrated varying conformations in different environments. In aqueous solvents like extra- and intra-cellular compartments, the PROTAC assumed elongated and polar conformations. Conversely, in apolar solvents such as chloroform, simulating the cell membrane interior, the PROTAC adopted conformations with a smaller polar surface area. It suggests that the flexibility of PROTACs could facilitate a kind of chameleonic behavior, allowing the PROTAC surface to adapt to the solvent, ensuring

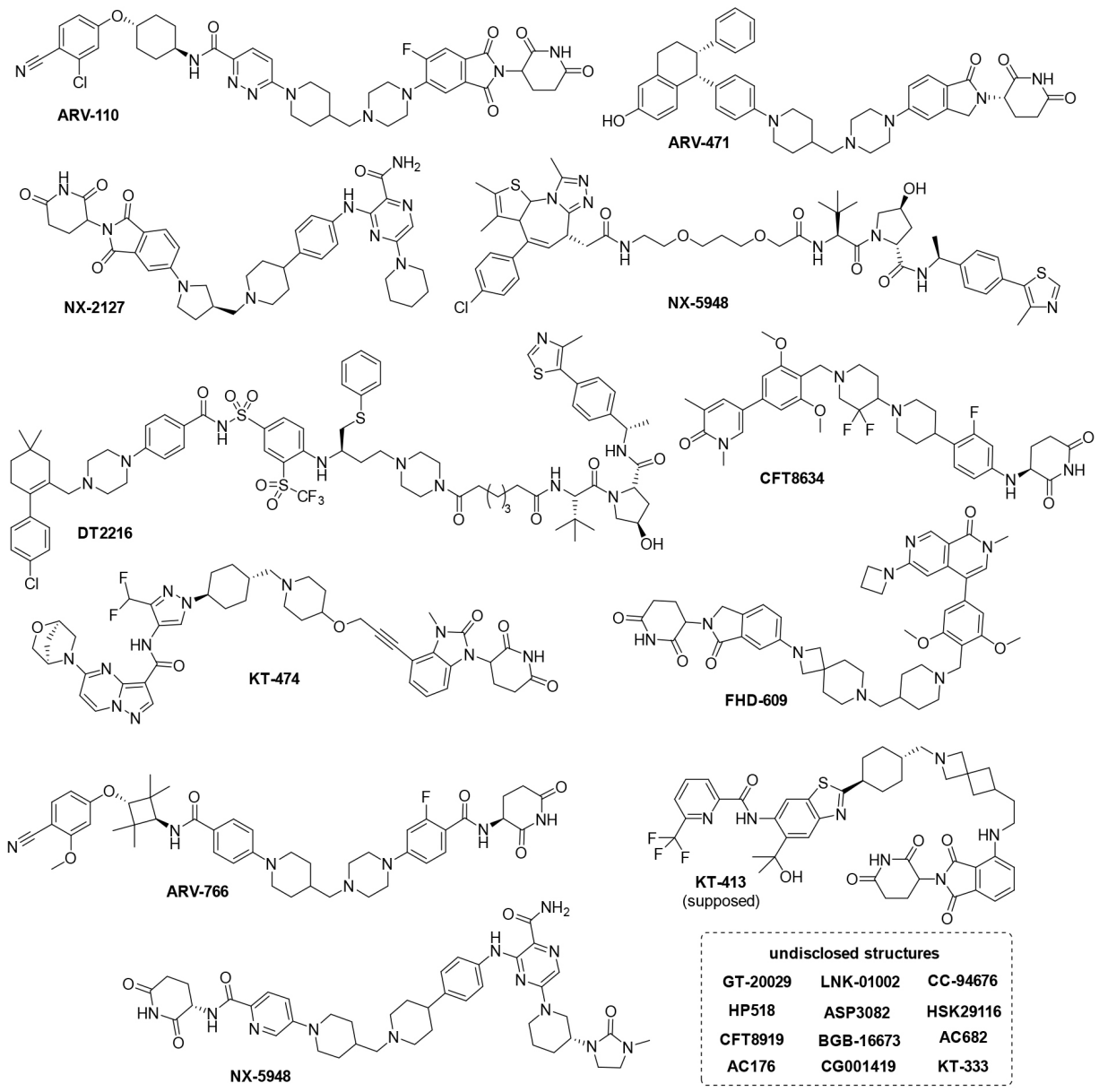

Figure 9. All disclosed structures of PROTACs under clinical evaluations.

good solubility in both polar and apolar compartments and, consequently, enabling cellular permeability.[101,102]

(*iii*) A current obstacle in advancing proteolysis targeting chimeras (PROTACs) lies in the empirical nature of structure-activity relationships (SARs) associated with linker length as well as the flexibility, that is a crucial parameter to be considered during design and development. More than only influencing PK properties,[103,104] length and flexibility "play important roles in inducing the ternary complex formation. In this context, employing macrocyclization or conformational restriction strategies to rigidify the linkers, and so fixing POI and E3 ligands in the bioactive conformation, may promote the formation of ternary complexes and improve the degradation profile of the PROTAC.[96]

(*iv*) At elevated concentrations, PROTACs exhibit "hook effects", wherein the competitive formation of a target POI-PROTAC or E3 ligase-PROTAC binary complex occurs, leading to diminished efficacy. This phenomenon has been observed in various studies[94,97,105] and can lead to problems regarding differences in metabolic capabilities between populations.

(*v*) Despite previous theories, it is already possible to identify PROTACs' resistance emerging through genomic alterations in the core components of E3 ligase complexes.[106] This is an additional challenge for PROTAC development arising from the potential development of resistance in cells treated with degraders containing CRBN and VHL E3 ligase recruiters.[106] Thus far, a limited number

of E3 ligases (e.g., CRBN, VHL, MDM2, IAP) are used for PROTAC development (discussed in section 3.2). CRBN and VHL E3 ligases are generally considered to be ubiquitously expressed in humans, showing limited selectivity of PROTACs in cancer cells over normal cells. There are some exceptions when tumor enrichment of an E3 ligase coincides with the dependence of the tumor on expression of that ligase. An analysis with CERES scores in DepMap of E3 ligases across multiple tumor cell lines indicated these correlations.[107] This discovery has enabled the recognition of E3 ligases and other genes associated with the UPS, with some better-characterized than others (e.g., WD repeat-containing protein 82 (WDR82) and cell division cycle 20 (CDC20)), that demonstrate significant tumor essentiality across various cancer cell types.[108] Ligases exhibiting these profiles offer the advantage of reducing the likelihood of tumor cells developing resistance to PROTACs through ligase-based mechanisms.

(*vi*) New E3 ligase scaffolds must be developed. CRBN-based structures (the most used scaffold) are thalidomide like derivatives that are known as possible degradation inducer of Structural Design of PROTACs. From this optics, PROTACs must be as selective as possible to prevent the degradation of proteins caused by the CRBN ligands themselves.[64,109]

(*vii*) As explained before, the number of targets that can be degraded by PROTACs has greatly expanded. However, most of them are "druggable" targets while some others are still challenge to tackle via small-molecule degraders.[1] For instance, modulation of targets lacking well defined binding sites and hydrophobic pockets have received growing attention with the use of new potential strategies as oligonucleotide-based PROTACs.[1,96,110,111]

3. Design of PROTACs

From a structural perspective, the success of designing PROTACs for targeting different proteins, as quickly discussed above, depends on integrating three distinct chemical moieties: a ligand for POI, an E3 ligase binder, and a linker connecting these two components.[12,37,105] In a Medicinal Chemistry point of view, the design strategy of PROTACs is not different from the so called "Molecular Hybridization", which is a strategy that aims to combine two or more molecules (or parts of them) in a new, single chemical entity.[112,113] Identifying the proper combination of these three elements is the first and pivotal step, needing a thorough examination of the structural features of both the E3 ligase and the POI. The formation of a ternary complex is completely dependent on the spatial orientation and alignment of both elements (POI and E3 ligase ligands), which plays a pivotal role in conducting the ubiquitin-protein knockdown process. As so, the design is specially influenced by the attachment position used to link the E3 ligase and POI ligands, a parameter that can be anticipated based, for example, on the binding mode of the POI and its ligand from a co-crystallized structure or by using computational tools. Additionally, the length and flexibility of the linker connecting the two moieties, i.e., POI and E3 ligase, can markedly impact potency and selectivity.[56,83,105,114,115]

3.1. The POI ligand requirements

The structural requirements for the POI ligand choice/exploration always depends on which target is supposed to be used. Regarding these ligands, a diverse range of warheads has been documented,[116] encompassing non-covalent, irreversible, and reversible covalent ligands, as well as allosteric variants.[117] Good consultation sources of POI ligands are the PROTAC-DB[64,109] database and PROTACpedia.[72,118] Both serve as valuable resources for PROTAC development by gathering the chemical structures, biological activities, and physicochemical properties of POI ligands.

As described within topic "2.1. Present", most of the current proteins targeted by PROTACs are "druggable" targets. For these POI, structural information can many times be found, such as crystal structures with bounded ligands or their SAR, guiding the design of new degraders. Based on these data, it is feasible to identify optimal linker attachment points in solvent-exposed regions that do not interact with the POI. Two examples of degraders starting from co-crystallized ligands are described in Figure 10. The potent IRAK-4 (enzyme involved in inflammatory processes) degrader **10** was designed based on the crystal structure of PF-06650833 (a phase II IRAK-4 inhibitor) inside the IRAK-4 kinase domain, showing solvent exposed vector at 4-position of isoquinoline scaffold. This position was selected to the linker attachment and led to the PROTAC **10** with a DC_{50} of 151 nM (Figure 10a).[119] The second example describes a similar approach for the discovery of the GPX4 degrader, the GDC-11. From the covalent inhibitor ML 162, crystallized with GPX4, three sites that were observed turned to the solvent and able to be modified. To the original anisole moiety, an amide linker and a pomalidomide based E3 ligase ligand were attached giving the PROTAC GDC-11, which presented a moderate GPX4 degradation efficacy of 33% at 10 μM (Figure 10b).[120]

Nevertheless, the absence of a well-defined ligand capable of engaging the intended target limits early-stage drug discovery initiatives, particularly those focused on

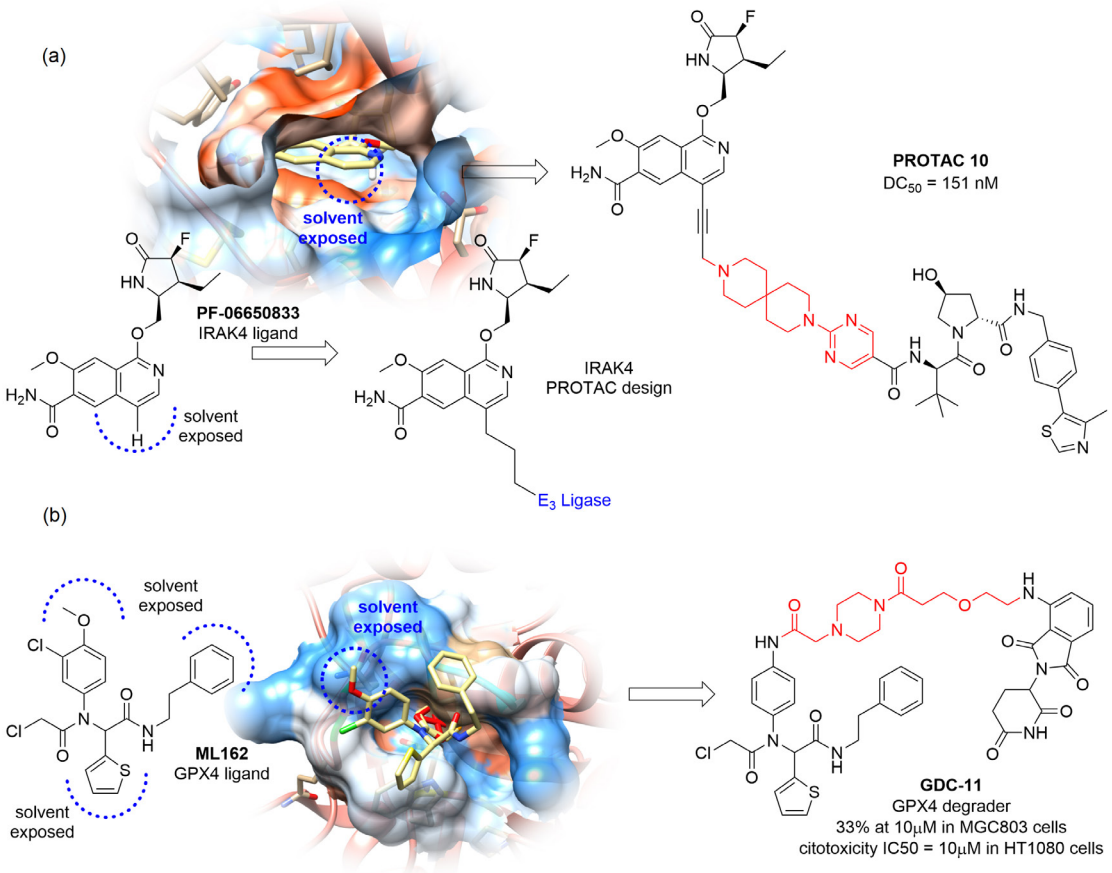

Figure 10. (a) Design of PROTAC **10** based on the crystal structure (PDB 5UIU) of phase II IRAK-4 inhibitor PF-06650833; (b) discovery of the GPX4 degrader GDC-11 from the co-crystallized covalent inhibitor ML 162 (PDEB 6HKQ). The image and the hydrophobic surfaces were generated in UCSF Chimera alfa version 1.17.[45] Red surfaces represent hydrophobic regions and blue surfaces represent hydrophilic surfaces.

novel biological targets characterized by poorly understood pharmacology. These "undruggable targets" need more technologies helping the discovery of new compounds useful as POI ligands. However, it is important to remember that the affinity of the ligand to the POI is not the main focus on PROTACs, since their mechanism of action is based on an event-driven sub-stoichiometric catalytic MOA (Figure 3).[5,12,13] Thus, techniques like fragment based drug discovery (FBDD), which is frequently used to discover new ligands (usually with low affinities) can be a valuable starting point for the discovery of new POI ligands moieties.[121] Indeed, many successful examples of PROTACs used the FBDD at the beginning of their discovery process including CST905 ($BRAF^{V600E}$-PROTAC), SIAIS100 (BCR-ABL-PROTAC) and **11** (CDK9-PROTAC) (Figure 11).[122-124]

Maybe the most successful example of FBDD in the drug discovery process is the BCL-X_L-PROTAC DT2216, that is currently in phase 1 clinical trials (Table 1 and Figures 9 and 12).[125] This PROTAC was developed from a nuclear magnetic resonance (NMR)-based screening that furnished two active fragments (**12** (300 μM) and **13** (4300

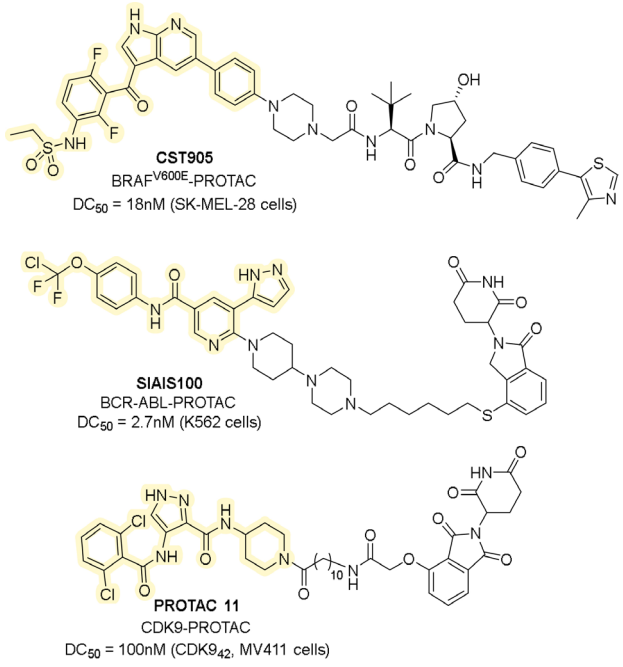

Figure 11. Discovered PROTACs in which the FBDD process was applied at the discovery of the POI ligand moiety (yellow).

μM)) binding in adjacent sites. Both fragments were linked by the sulfonamide group, leading to compound **14** (half-maximal inhibitory concentration (IC_{50}) = 93 nM) (Figure 12). A lead optimization process was carried out with further modifications in this structure, specifically outside the active pocket, aiming at improving hydrophobic interaction and the π-π stacking with BCL-X_L resulted in compound ABT-737 (**15**) (IC_{50} = 83 pM). Due to its low solubility and high lipophilicity, which resulted in poor pharmacokinetic properties, optimization of compound **15** continued by replacing the hydrophobic groups with hydrophilic ones. Furthermore, the crystal structure of compound **15** (PDB 2YXJ) indicated that the tertiary amine was turned to an open space, and to this group, the linker and VHL E3 ligase were attached, giving the compound DT2216 (Figure 12).

3.2. The linkers as fundamental moieties

Linkers play a crucial role in the activities of PROTACs. The adaptability of the linkers significantly influences the overall degradation efficiency of a specific PROTAC. Parameters such as the distance between the POI and the UPS, and the presentation and accessibility of reactive lysine residues on the POI to the E2 are vital factors, ultimately determined by the characteristics of the linker unit. Nonetheless, the connection between the spatial arrangement of lysine residues on the POI surface, the structure, and interconnection of poly-Ub chains, and the effectiveness of degradation remains inadequately comprehended.[114,126] Guidelines for formulating potent PROTAC linker designs, from scratch, are regrettably absent and, to date, studies on the SAR of linkers are predominantly empirical, and the design of linkers still poses a bottleneck.

The appropriate combination of length, hydrophilicity, and rigidity in ligand-connecting linkers has been demonstrated to influence various properties of PROTACs such as pharmacodynamic (PD), and pharmacokinetic (PK) characteristics such as cellular permeability, metabolic stability, solubility, and, of course, biological activity.[114,127,128] This combination forms the basis for the successful design of effective PROTACs. Optimization of linker composition is crucial for each ligand pair (POI and E3 ligase), especially concerning the length and conjugation sites on each ligand.[46,114] A commonly employed strategy involves creating a library of PROTACs incorporating linear unsaturated aliphatic linkers of variable lengths, typically ranging from a few atoms to 29 atoms. This process continues until a suitable spatial orientation is identified, proving productive for ternary complex formation between the target POI and the E3 ubiquitin ligase.[1,103,114] The most potent PROTAC linkers are selected through systematic and extensive iterations, incorporating different chemical motifs.

Typically, longer aliphatic linkers, including polyethylene glycol and other glycol chains, have produced substantial contributions to protein-ligand

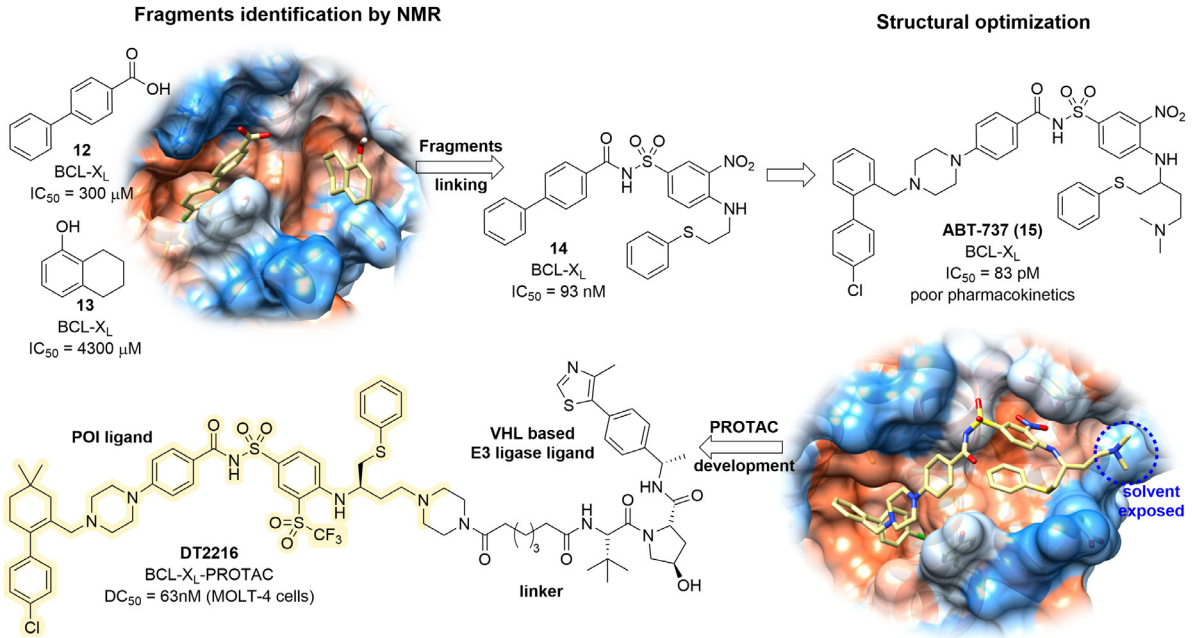

Figure 12. FBDD applied to the discovery of the BCL-X_L-PROTAC DT2216 (phase 1 clinical trials) from the two fragment hits (**12** and **13**) identified by NMR (PDB 1YSG). The image and the hydrophobic surfaces were generated in UCSF Chimera alfa version 1.17.[45] Red surfaces represent hydrophobic regions and blue surfaces represent hydrophilic surfaces.

interactions within the ternary complex.[129-132] They have played a role in stabilizing the orientation of the complex through cooperative binding. However, there are cases where the energy gained in the ternary complex from new PPIs is counteracted by the entropic cost associated with reduced PROTAC flexibility.[103] Recently, there has been a shift from flexible, linear alkyl- and PEG linkers to more rigid structures, including alkyne, and cyclic scaffolds like piperazine, piperidine, and triazole (Figure 13). This sentence is particularly true if we have a look to the disclosed structures from compounds in clinical trials in Figure 9, in which nine of eleven PROTACs have more rigid linkers.

One prevalent approach to combine POI and an E3 ligase binders involves the utilization of click chemistry, such as the copper-catalyzed Huisgen 1,3-dipolar cycloaddition reaction described by Sharpless and co-workers,[133] Meldal and co-workers,[134] and Bertozzi and co-workers,[135] which incorporates an azide and an alkyne moiety given an 1,2,3-triazol. An extensive and insightful review on this technique applied to PROTACs was provided by Pasieka *et al.*,[136] covering a wide range of aspects related to the topic. Beyond the broad applicability and excellent compatibility of this linking strategy, the resultant triazole ring may offer a metabolic advantage compared to linear linkers being more susceptible to oxidative metabolism *in vivo*, as highlighted by Xia *et al.*[137] Furthermore, improving linker rigidification can potentially reduce entropy loss within the system.

The first two articles introducing the utilization of cu-catalyzed azide-alkyne cycloaddition (CuAAC) to PROTAC synthesis were concurrently published in a special issue of the Journal of Medicinal Chemistry. The research conducted by Jung and co-workers[138] focused on the synthesis of triazole-base (Sirt), a family of histone deacetylases implicated in the pathogenesis of various diseases, including inflammation.[138,139] A Sirt2-selective and potent compound (SirReal) was chosen as the ligand for the POI, while the well-established CRBN ligand thalidomide was selected as the E3 ligase binder. For the first time the use of a triazole linker led to novel degraders and induced the degradation process of Sirt by facilitating the formation of a ternary complex (Figure 14).[138] In the second work, Wurz *et al.*[140] developed PROTACs targeting BRD4 utilizing the well-known JQ-1 moiety,[141] which binds to BRD4, along with E3 ligase binders from both the VHL and CRBN classes, connected by PEG linkers. Proximity and protein degradation assays confirmed the capability of the triazole-based PROTACs **16**-**18** to form the ternary complex, thus inducing proteasome-mediated degradation (Figure 14).[140]

Another interesting feature involved with linkers is the possible photochemical modulation of PROTACs activity, enabling spatiotemporal control of PROTAC-mediated protein degradation, which has potential to avoid side effects.[142] Two possible photochemically controllable PROTACs (PHOTACs) are known: (*i*) photocaged, that is a modified PROTAC designed by caging the PROTAC, thus leading to an inactive degrader, in which the light irradiation can remove the substituent leading to an active PROTAC able to conduct the protein degradation.[143] This approach, despite applied to linkers, can be also used in POI and E3 ligase binders; and (*ii*) photoswitchable PROTACs, that is applied specially to linkers. This photochemical modulation is an alternative approach to locally activate PROTACs by means of a photoisomerization.

Pfaff *et al.*[144] designed the photoswitchable PROTAC **19** by integrating a bistable *ortho*-tetrafluoroazobenzenes (*ortho*-F_4-azobenzenes) linker between the POI ligand and the E3 ligase ligand. So far, azobenzenes are the most

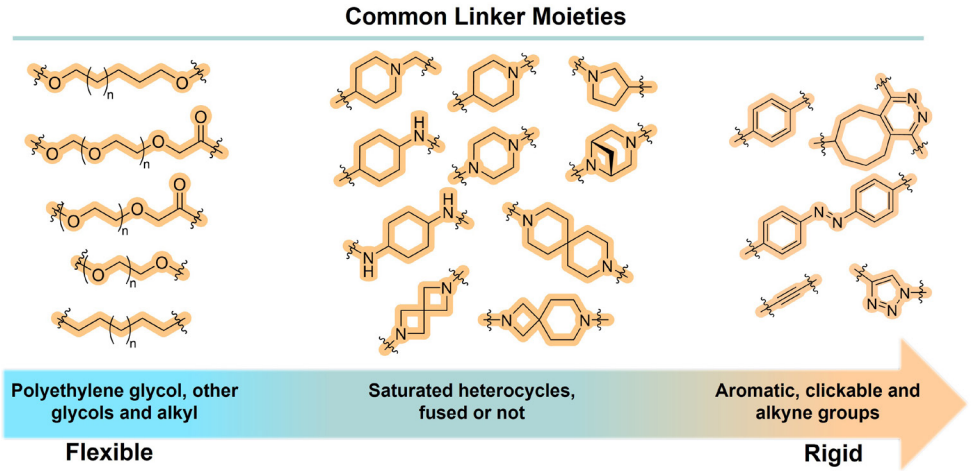

Figure 13. The most common linker moieties used in PROTAC design according to chain flexibility.

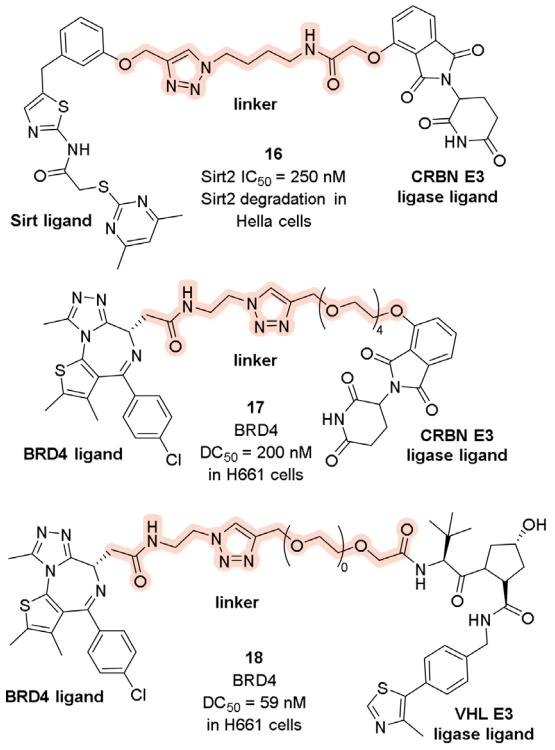

Figure 14. Synthesis of first-in-class 1,2,3-triazole-based PROTACs **16** as Sirt2 degraders and **17** and **18**, as BRD4 degraders.

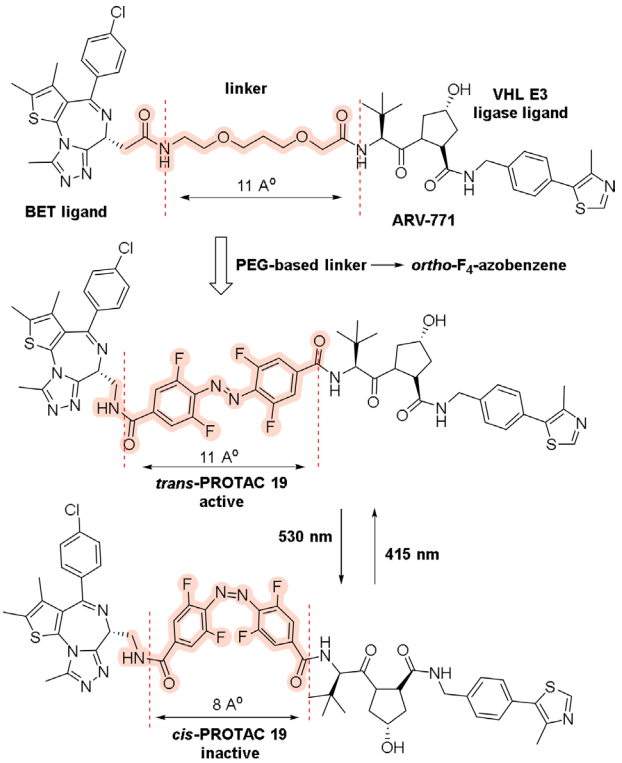

Figure 15. Photoswitchable BET PROTAC design: substitution of the PEG linker in ARV-771 by an *ortho*-F_4-azobenzene generating anisomeric photo-PROTAC **19** pair of isomers with considerable changing in the distance between POI ligand and E3 ligase binder moieties.

common class of photoswitches used for the photo-control of biomolecules.[145] The lead PROTAC structure chosen was ARV-771, where the linker's length between the POI ligand and the E3 ligase ligand is approximately 11 Å. As illustrated in Figure 15, substituting the PEG-based linker in ARV-771 with *ortho*-F_4-azobenzene resulted in an anisomeric photo PROTAC pair.[144] The *trans*-PROTAC **19** (active form) maintained an optimal distance of 11 Å between both ligands, while *cis*-PROTAC **19** (inactive form) presented a shorter distance of only 8 Å. Photoswitch occurred upon exposure to 530 nm irradiation (visible light), in which *trans*-PROTAC **19** could be converted into *cis*-PROTAC **19**. Conversely, under 415 nm irradiation, *cis*-PROTAC **19** could be transformed into *trans*-PROTAC **19**. Intriguingly, *trans*-PROTAC **19** induced the degradation of BRD2 but not BRD4 in Ramos cells after 18 h, while no apparent degradation was observed with *cis*-PROTAC **19**. In contrast to photocaged PROTACs, photoswitchable PROTACs provide a reversible on/off switch for targeted protein degradation.[144]

3.3. The E3 ligase universe in expansion

The selection of the E3 ligase ligand plays a crucial role in determining the ultimate success of PROTACs, since they are the "responsible moiety" to recruit the degrader machinery.

The human genome contains two members of the E1 enzyme family, approximately 40 E2, and over 600 E3 ubiquitin ligases.[146] While our comprehension of substrate recognition and the regulation of ubiquitination remains incomplete, the genome's choice of approximately 600 E3 ligases demonstrates the capacity to ubiquitinate a significantly larger number of protein substrates in a controlled manner, exhibiting considerable specificity.[147] Playing a vital role in protein ubiquitination, E3 ligases contribute to substrate selection and influence the efficiency of the ubiquitin cascade.[22] The success of a protein knockdown depends directly on the selection of the best E3 ligase. Different degradation profiles can be observed on a specific target based on the recruited E3 ligase.[148]

A beautiful example of this specificity was demonstrated by Ciulli and co-workers,[149] when they reported the development of a leucine-rich repeat kinase 2 (LRRK2) (implicated in Parkinson's disease and inflammatory processes) PROTAC XL01126,[150] as an alternative LRRK2-targeting strategy. Initial design and screenings of PROTACs based on ligands for the E3 ligases VHL, CRBN, and cIAP identified the best degraders, always containing a thioether-conjugated VHL ligand, while other E3 ligase ligands presented none or insipient activity (Figure 16). A structural optimization in a second step led to the discovery

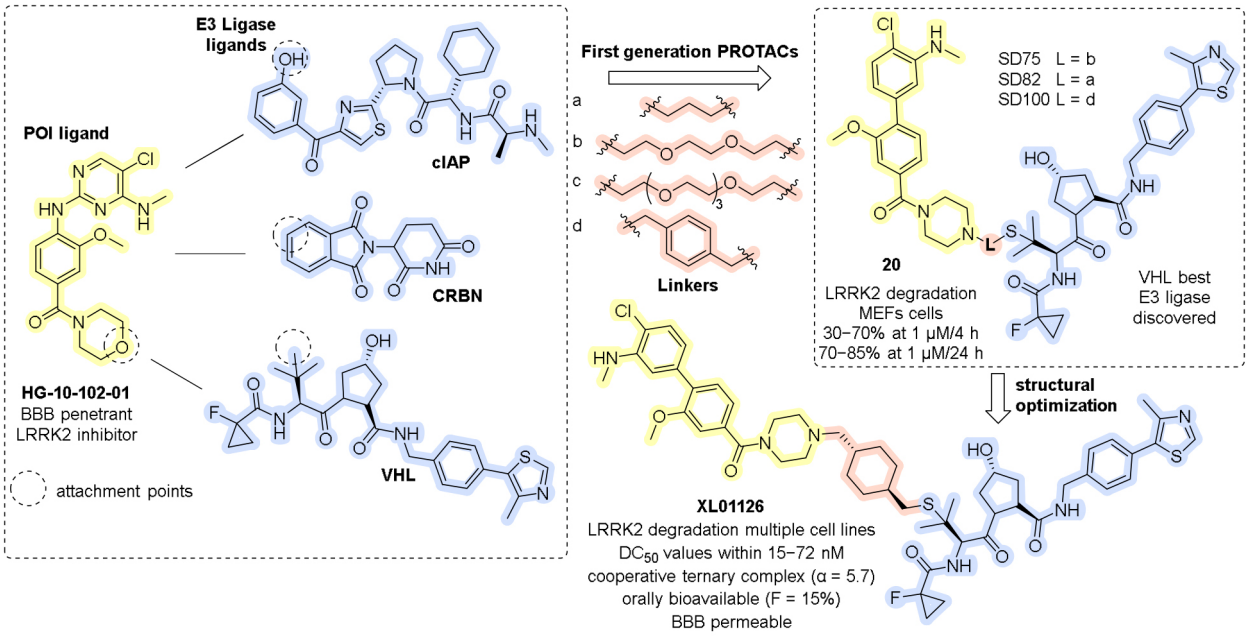

Figure 16. Development of the LRRK2 PROTAC XL01126 by screening different ligands for the E3 ligases: von VHL, CRBN, and cIAP.

of XL01126 as a fast and potent degrader of LRRK2 in multiple cell lines, with DC_{50} varying within 15-72 nM, high cell permeability, positively cooperative ternary complex with VHL and LRRK2 (α = 5.7) (Figure 16). It also presented interesting PK properties being orally bioavailable (F = 15%) and penetrating to the blood-brain barrier (BBB) after either oral or parenteral dosing in mice.[149]

Each E3 ligase has its own specificities and, despite the vast number of known E3 ligases, until now not many of them have been successfully used as PROTACs' targets, as exemplified until here, in this review: e.g., VHL, MDM2, cIAP, and CRBN. Thus, a substantial universe of E3 ligases is still unexplored, holding promise for targeted protein degradation. Consequently, E3 ubiquitin ligases are garnering attention as appealing drug targets, given their implication and dysregulation in various diseases.[53,96] A significant amount of the initial efforts has focused on pairing VHL or CRBN with various target proteins to optimize resource utilization and accelerate advancement of PROTACs and indeed, these are the most common E3 ligase ligands found in "PROTACs' world".

We proceeded with an analysis on PROTAC-DB[72] for mapping the relevance of each E3 ligase ligand to the PROTACs' development until today. CRBN (65%, n = 3530) is so far the most used ligand, followed by VHL (29%, n = 1578), the IAP family (XIAP, cIAP, and IAPs; 4%, n = 190) and MDM2 (1%, n = 56) (Figure 17). Main representants of these E3 ligase ligand families are illustrated in Figure 18. The most used E3 ligases explored (CRBN and VHL) are considered to have low

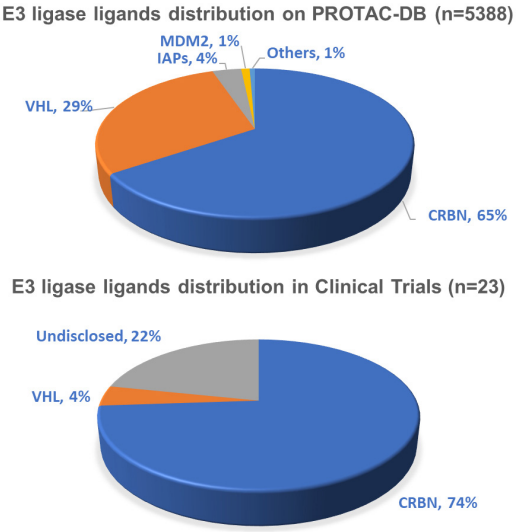

Figure 17. Representative analysis of E3 ligase ligand families described on PROTAC-DB[72] (accessed on 02-19-2024) and under current clinical trials.

tissue-specific expression and already presented reports of punctual mutations in cancer models. This demonstrates the importance of developing new ligands for E3 ligase and some are already ongoing, like DCAF11, DCAF15, DCAF16, FEM1B, RNF114, RNF4,[151-155] that are depicted as "others" in Figure 19, still representing an incipient 1% of total examples, within 34 PROTACs. Despite a few examples, the main structures of these new E3 ligase ligands are disclosed in Figure 19. The analysis of PROTACs undergoing clinical trials was impacted by five compounds (22%) for which the structures have not yet been disclosed. Within the disclosed structures, again CRBN is for sure

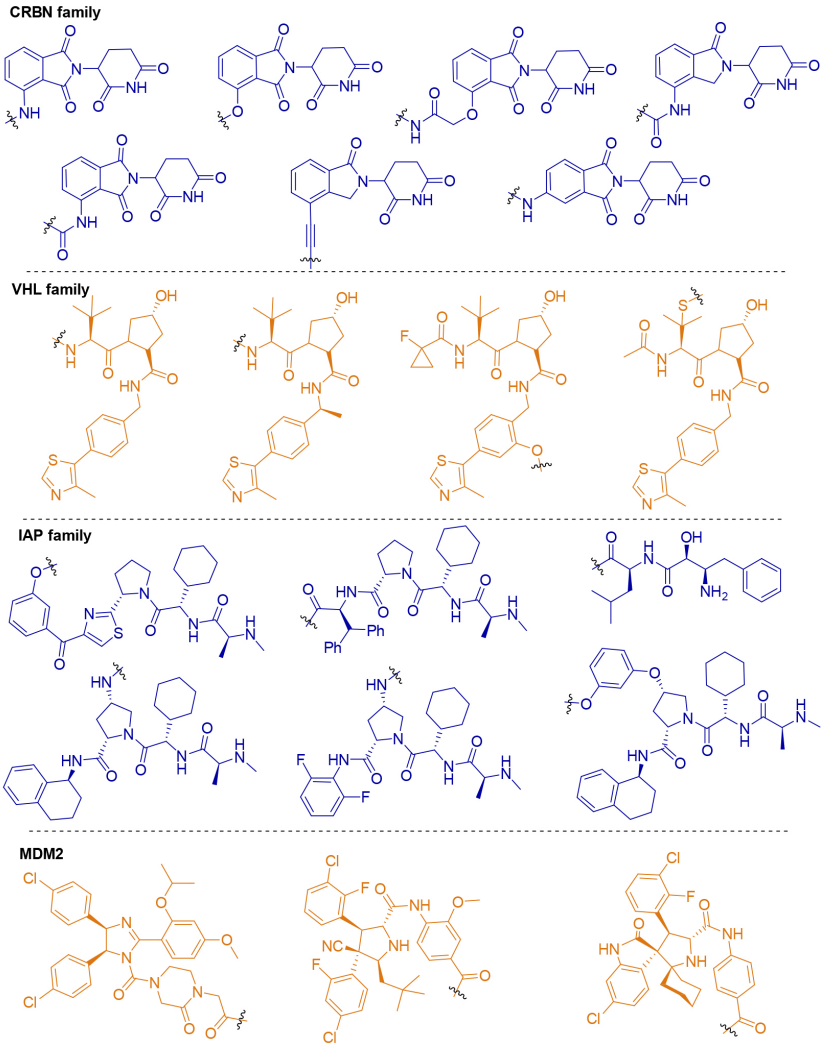

Figure 18. Main representants of the most used E3 ligase ligands families according to the correspondent E3 ligase. The black wave line represents the point of attachment to the linker.

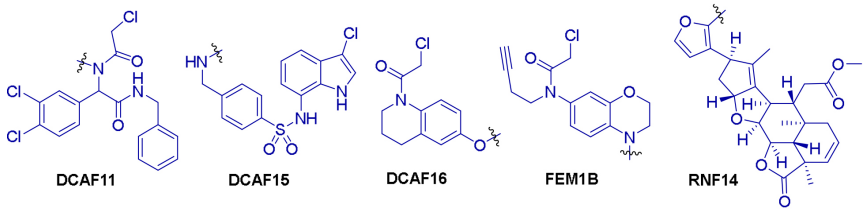

Figure 19. Representants of the "other" used E3 ligase ligands families according to the correspondent E3 ligase.

the most applied (74%, n = 17), with VHL presenting only 1 compound (4%) (Figure 17).

Nowadays there is increasing interest in academia and industry for identifying E3 ligases with unique expression profiles to enable tissue- and cell-type-specific target degradation.[1] Recent discoveries[156] suggested that E3 ligases with tissue-selective expression profiles may present unique therapeutic opportunities, even though their mechanisms have not yet been fully elucidated. For example, specific E3 ligases from the central nervous system (CNS) have emerged, including ring finger protein 182 (RNF182) and tripartite motif-containing protein 9 (TRIM9).[157,158] These ligases are particularly noteworthy for addressing targets associated with neuronal diseases, possibly allowing CNS-specific therapeutic targeting, and avoiding systemic off-target and toxicity effects, despite no PROTAC has been developed until now for these ligases. The same idea can be used to treatments focusing on degrading specific proteins in cells with improvement of a determined E3 ligase, such as

the F-box protein 44 (FBXO44) that is enriched in some tissues but not specific to any.[159,160]

4. PROTACs Developed for Inflammation Processes

4.1. PROTACs developed for histone deacetylases (HDACs)

After their introduction in cancer therapy, histone deacetylases (HDACs) inhibitors (HDACi) gained attention for application in other diseases as well. HDACs play crucial roles in inflammatory diseases such as asthma, rheumatoid arthritis (RA), and chronic obstructive pulmonary disease (COPD).[161-164] Understanding and intervening in the functions of specific isoforms that contribute to inflammation provide opportunities for the development of novel therapeutics. In RA, specifically, HDAC3i significantly suppressed most interleukin (IL)-1β-inducible genes targeted by pan-HDACi. The same result was reproduced by silencing HDAC3 expression. These results identify HDAC3 as a potential therapeutic target in the treatment of inflammatory and autoimmune diseases and indicated that the degradation of HDAC3 would be an interesting approach for this purpose.[162,163,165]

Cao *et al.*[165] described the development of PROTACs targeting HDAC3 for degradation, containing pomalidomide (**21**) as CRBN-based E3 ligase recruiter, linked to a class of I HDAC inhibitors (**22**) with the *ortho*-aminoanilide subunit (Figure 20a). The nucleus *ortho*-aminoanilide was chosen because derivatives of this class exhibited specific slow-tight binding to the active site of class I HDACs 1, 2, and 3, a feature that could be advantageous in the development of PROTACs.[166,167] Moreover, two notable inhibitors from this class, entinostat and CI994, are currently undergoing clinical trials.

The authors[165] synthesized a series of PROTACs varying the linker length between pomalidomide and the HDAC inhibitor subunit. PROTAC **23a** was capable of degrading HDAC3 at a concentration of 10 μM in murine macrophage cell line RAW 264.7 macrophages, while HDAC1 and HDAC2 were also degraded at higher concentrations though. Curiously, it was observed that the efficacy of PROTAC-mediated degradation was somehow cell selective depending on the type of cell line used, as no degradation of HDAC3 was observed in A549 cells. The presence of the *para*-fluoro *ortho*-aminoanilide group in **3b** provided increased selectivity for HDAC3. Despite compound **23a** has been more potent as HDACs inhibitor, compound **23b** exhibited higher potency and enhanced selectivity for HDAC3 degradation compared to **23a**, with a DC_{50} value of 0.32 μM in RAW 264.7 macrophages.[165]

A novel PROTAC (**25**) that links the HDAC inhibitor ligand (**24**) to VHL E3 ligase recruiter, instead of pomalidomide (**21**), was able to induce the degradation of HDAC3 in THP-1 and HeLa cells, with a DC_{50} value of 0.6 nM and a Dmax of approximately 90% in THP-1 cells (Figure 20b). While degradation of HDAC8 was observed at much higher concentrations, HDACs 1, 2, 4, and 6 remained unchanged. PROTAC **25** caused a decrease in HDAC3 levels at low micromolar concentrations in

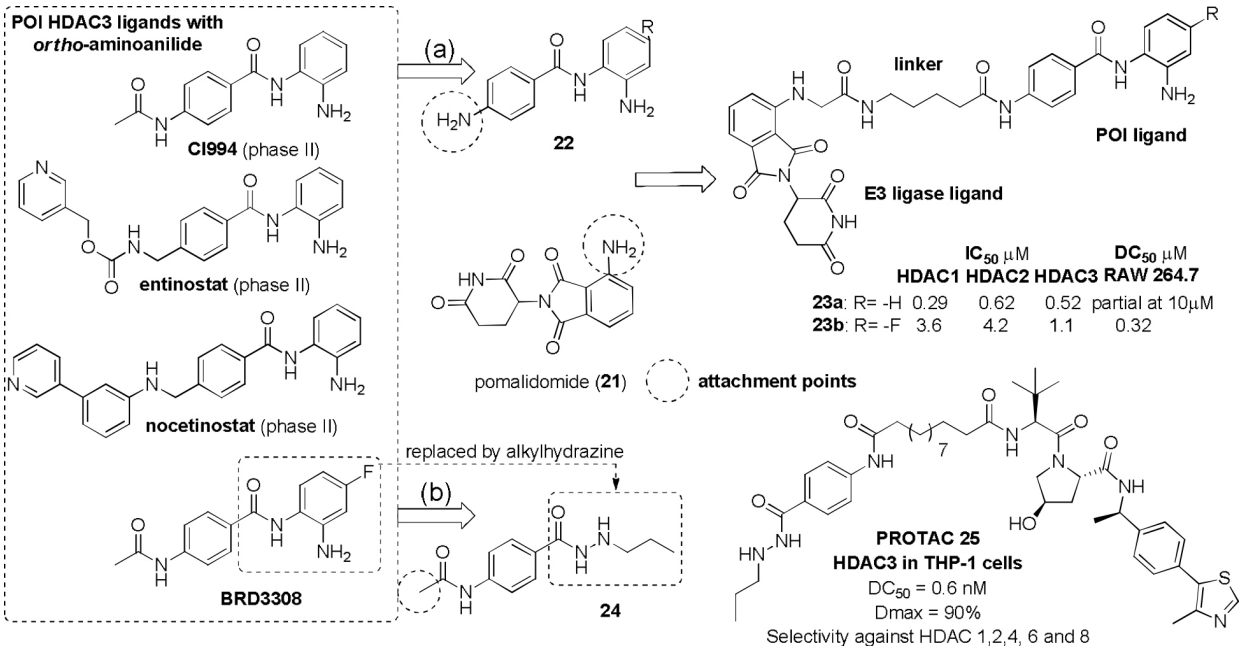

Figure 20. New PROTACs based on *ortho*-aminoanilide compounds. (a) Design and evaluation of PROTACs **23a** and **23b** using CRBN E3 ligase ligand; (b) design and evaluation of PROTAC **23a** and **23b** using VHL E3 ligase ligand.

primary human macrophages. Additionally, **25** was able to reduce the secretion of pro-inflammatory cytokines such as TNF-α and IL-6, in levels notably superior to that observed for the HDAC3 inhibitor prototype **24** in the same assay. Macrophage polarization, that is crucial in the inflammatory process, was also evaluated. In this context, compound **25** was able to prevent the polarization of M0 to M1-like macrophages in response to stimulation in a cell culture of primary human macrophages. Overall, the results obtained are good evidences suggesting that PROTACs targeting HDAC3, such as PROTAC **25**, have interesting anti-inflammatory potential.[163]

Histone deacetylase 6 (HDAC6) emerged as a promising therapeutic target for treating various diseases.[168,169] A recent investigation[164] demonstrated the significance of HDAC6 in the activation of the nucleotide oligomerization domain-like receptors family pyrin domain containing 3 (NLRP3) inflammasome, indicating that modulating HDAC6 activity holds potential for the treatment of numerous inflammatory disorders. In 2021, the PROTAC **27** was described demonstrating low toxicity and the ability to efficiently and selectively degrade HDAC6 in different cell lines, including activated THP-1. The PROTAC **27** was designed using the E3 ligase ligand pomalidomide (**21**) (CRBN-based), and the potent HDAC6 inhibitor (**26**) (IC_{50} = 128.6 μM), a compound designed by combining structures from the natural product indirubin and the pharmacophore for HDACi: hydroxamic acid group (ZBG)-linker-cap (Figure 21a).[170,171] The authors demonstrated, for the first time, that using PROTACs to selectively degrade HDAC6 is a good and efficient strategy to block NLRP3 inflammasome activation in lipopolysaccharide (LPS)-induced mice model. Moreover, PROTAC **25** was able to produce an anti-inflammatory activity *in vivo* attenuating NLRP3 inflammasome activation in LPS-induced mice, suggesting that *in vivo* NLRP3 inflammasome activation depends on HDAC6 (Figure 21a).[172]

Following the idea of NLRP3 modulation by HDAC6, two new PROTACs (**27** and **28**) were described recently[173] with the aim of investigating the effect of HDAC6 deficiency on NLRP3-mediated IL-1β release. The design of PROTAC **27** was based on the pan-HDAC inhibitor suberoylanilide hydroxamic acid (SAHA) and the CRBN-based E3 ligase recruiter, thalidomide (Figure 21b). PROTAC **28** was designed as a negative (non-degrading) control, being able to bind to HDAC6 but lacking the ability to induce degradation. The strategy of CRBN-moiety methylation is quite common to negative controls because the free N–H in glutarimide ring is essential for recruiting the E3 ligase. PROTAC **27** significantly reduced HDAC6 levels in THP-1 macrophages at low concentrations of 0.1 μM and with maximum degradation at 10 μM, without affecting cell viability at same concentrations (Figure 21a). On the other hand, PROTAC **28**, as expected, could not degrade HDAC6. The biological evaluations indicated that both PROTACs (**27** and **28**) significantly reduced IL-1β release in a concentration-dependent manner, suggesting that HDAC6 degradation is not necessary to inhibit NLRP3 inflammasome-mediated IL-1β release.[173]

The next example is about sirtuin 2 (Sirt2) degraders. Sirt2 is a nicotinamide adenine dinucleotide (NAD^+)-dependent histone deacetylases, classified as HDAC class III[174,175]

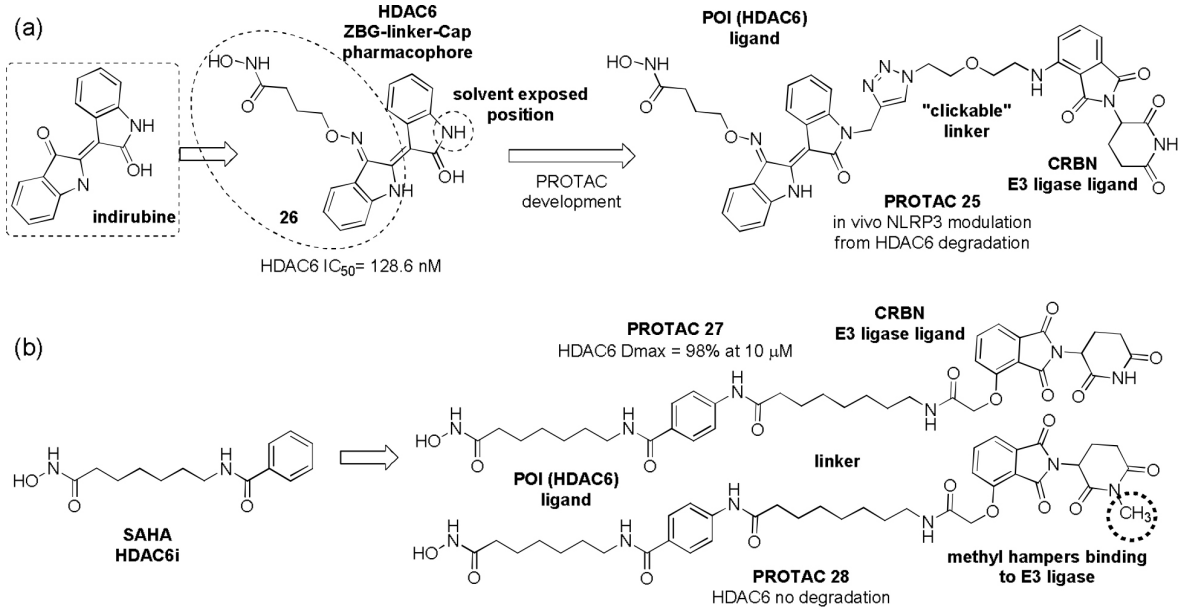

Figure 21. Structures and activities of HDAC6 PROTACs. (a) Design and evaluation of PROTAC **25** using CRBN E3 ligase ligand; (b) design and evaluation of CRBN E3 ligase derivatives PROTAC **27** and PROTAC **28** (with methylated CRBN E3 ligase ligand as negative control).

In 2018, Schiedel *et al.*[138] described the development of PROTAC **16** combining, as POI ligand, an interesting and selective inhibitor (**29**) for Sirt2, which is implicated with the anti-inflammatory response,[176] with thalidomide, as E3 ligase ligand. The attachment position (*meta* or *para*) came from observation of crystal structure of **29** with Sirt2 (PDB4RMI) (Figure 22b). In this work, for the first time, the construction of the PROTAC linker used the Cu^{I}-catalyzed azide-alkyne cycloaddition to joint an azide derivative of thalidomide to the Sirt inhibitor **29**. PROTAC **16** was able to chemically induce the Sirt2 degradation potently and selectively, resulting in hyperacetylation of the microtubule network, accompanied by an increase in process elongation (Figure 22b).[138]

4.2. PROTACs developed for miscellaneous inflammation-related targets

The IRAK-4 is a member of serine-threonine kinase family, playing a significant role in the regulation

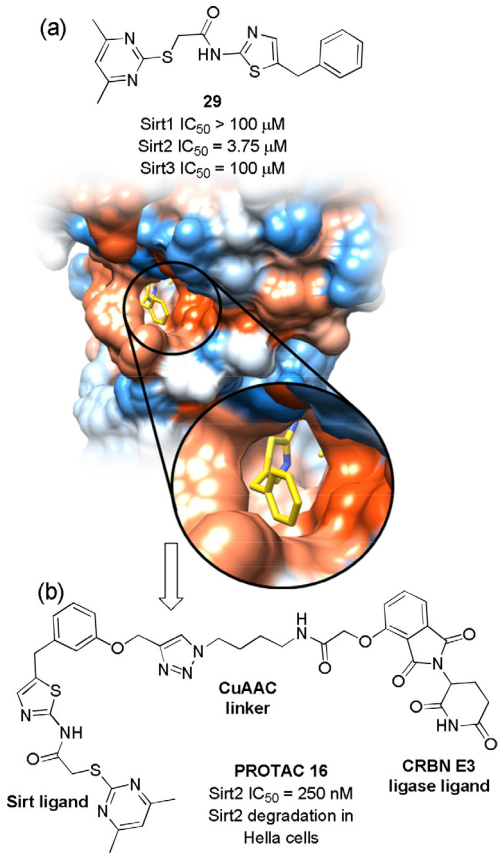

Figure 22. (a) Selective ligand of Sirt2 chosen as POI ligand and its binding mode to the enzyme evidencing the benzyl ring turned to the solvent. Positions *meta* and *para* as attachment points; (b) PROTAC **16** structure with the triazole link and CRBN E3 ligase recruiter. The image and the hydrophobic surfaces were generated in UCSF Chimera alfa version 1.17.[45] Red surfaces represent hydrophobic regions and blue surfaces represent hydrophilic surfaces.

of interleukin-1 receptors (IL-1R) and Toll-like receptors (TLRs) related signaling pathways.[177] Recognition of foreign pathogens and inflammatory signals by these receptors promotes activation that leads to the production of pro-inflammatory cytokines via the NF-κB pathway. The IRAK-4 mediated inflammation and related signaling pathways contribute to inflammation in autoimmune diseases and cancers. Therefore, targeting IRAK-4 to develop single-target, multi-target inhibitors and PROTAC degraders is an important direction for the treatment of inflammation and related diseases.[119,178,179]

GlaxoSmithKline researchers developed a PROTAC with potential to inhibit multiple pro-inflammatory cytokines in peripheral blood mononuclear cells (PBMCs).[119] From the analysis of the IRAK-4 co-crystallized with an inhibitor, the researchers verified that the position 4 of the isoquinoline ring was exposed to the solvent, being an optimal position for modifications. PROTAC design started by choosing the ideal E3 ligase recruiter. Firstly, compounds containing the IRAK-4 ligand subunit, flexible linkers and VHL (PROTAC **29**), CRBN (PROTAC **30**) and IAP (PROTAC **31**) as E3 ligase ligands were synthesized (Figure 23).

The authors identified that the majority of synthesized compounds could bind to IRAK-4 (IC_{50} ranging from 0.022 to 21 nM), but only the VHL-PROTACs (PROTAC **29**) were effective to degrade IRAK-4 (50% degradation at 3 μM). Once found the best match structure (IRAK-4 ligand-linker-E3 ligase ligand), they tried to optimize the IRAK-4 ligand. The authors hypothesized that a more potent IRAK-4 ligand could result in a more effective IRAK-4 degradation, reason why they optimized the ligand using PF-06650833 as a prototype, altering the lactam ring. This modification resulted in a PROTAC **32** with DC_{50} = 259 nM in PBMC. After, aiming to improve the activity of PROTAC **32**, efforts were directed to linker optimization focusing on modulating polarity and flexibility of the chain. The best combined result was obtained by changing the aliphatic chain by a spirocyclic pyrimidine linker, resulting in the PROTAC **10** with DC_{50} = 151 nM in PBMC (Figure 23). To confirm that the real degradation mechanism was proteasome dependent, assays were performed in the presence of epoxomycin (a proteasome inhibitor), observing a non-existent change regarding the IRAK-4 levels in the tests with epoxomycin. Next, they sought to investigate the IRAK-4 potential kinase independent role in TLR mediated signaling. The PROTAC was monitored for cytokine inhibition upon TLR7/8 stimulation in PBMCs and were capable of completely blocking IL-6 secretion as well as a wider panel of cytokines.

Cyclic adenosine monophosphate (cAMP) response element-binding protein (CREB) is a transcription factor

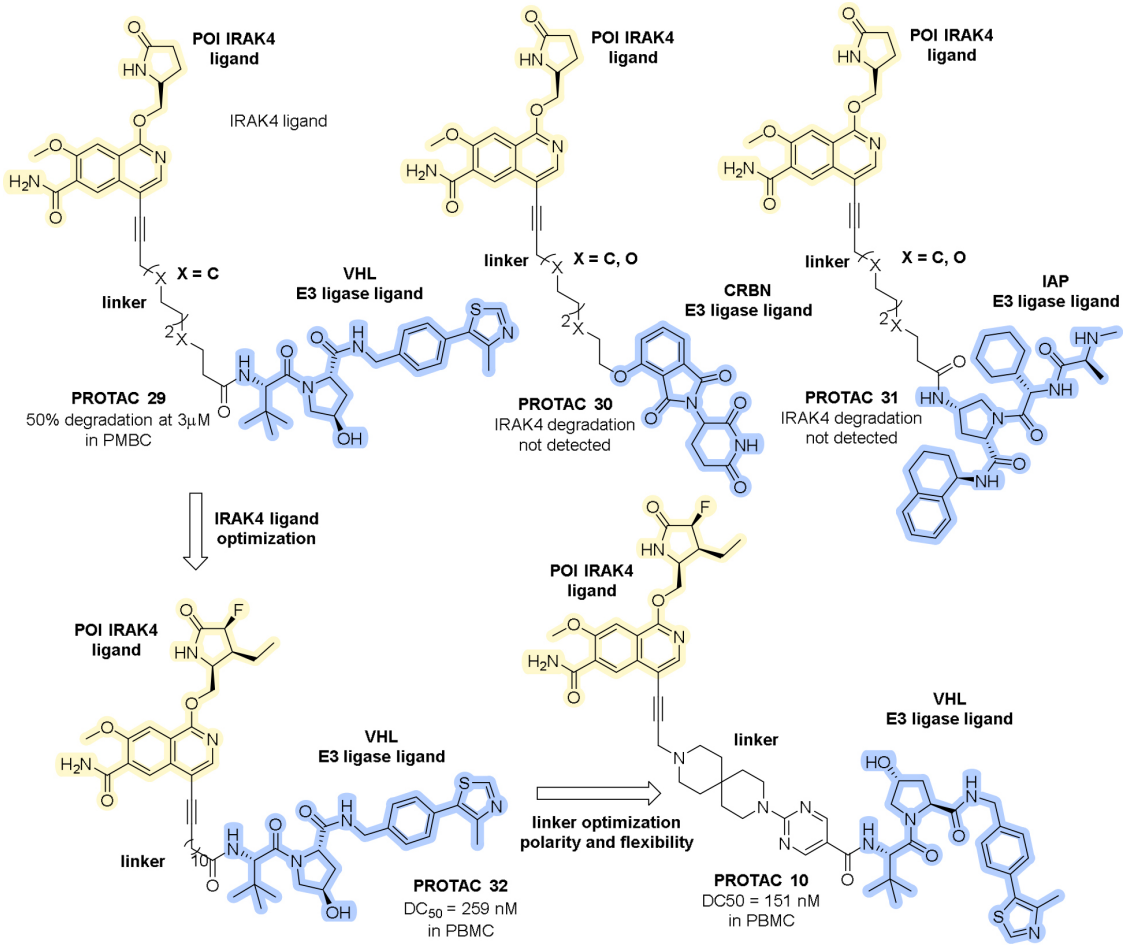

Figure 23. Discovery process of IRAK-4 PROTAC **10** from the initial screening of different E3 ligase ligands, followed by optimization of IRAK-4 ligand moiety and linker optimization.

responsible for regulating multiple cellular responses, including proliferation, survival and differentiation. CREB is induced by a variety of growth factors and inflammatory signals and subsequently mediates the transcription of genes containing a cAMP-responsive element. Several immune-related genes possess this cAMP-responsive element, including IL-2, IL-6, IL-10, and TNF-α. In addition, phosphorylated CREB has been proposed to directly inhibit NF-κB activation by blocking the binding of CREB binding protein to the NF-κB complex, thereby limiting pro-inflammatory responses. EP300 (E1A-binding protein P300) is defined as an acetyltransferase that can acetylate histone and has been broadly studied in several chronic diseases, including cancer and inflammation.[180-182]

Following the same strategy of the GlaxoSmithKline group cited above, Cheng-Sánchez *et al.*[183] used a crystallographic structure of CREB-binding protein (CBP)/EP300 with a co-crystallized ligand (CPI-1612) as a starting point for the development of PROTACs. Analysis of this X-ray structure (PDB 6V8N) showed that the methyl group on the pyrazole moiety pointed outside the pocket, thus revealing an optimal attachment position to add the linker and E3 ligase ligands. Firstly, they evaluated the most used E3 ligase recruiters (VHL, IAP and CRBN) and aliphatic/PEG short linkers (n = 2 and 3). In the first moment, the PROTACs did not degrade CBP/EP300 and the authors hypothesized that maybe the sizes of the linkers were not ideal. New PROTACs were synthesized with larger linkers (n = 4-7). The authors assessed if the compounds were able to form a ternary complex between CRBN and the CBP catalytic core using fluorescent-based technology for detecting protein-protein interactions (FluoPPI). Using FluoPPI technology, it was possible to detect that compounds with larger linkers were able of forming a ternary complex between CBP/EP300 and CRBN. Moreover, western blotting in LP1 cells demonstrated that compounds with longer linkers were able to degrade CBP/EP300, suggesting that the absence of ternary complex formation was responsible for the inactivity of PROTACs with shorter linkers. The results showed that CRBN-recruiting was better than VHL/IAP and increased linker length led to active

CBP/EP300 degraders and the main representant of the series as the PROTAC dCE-1 (Figure 24).

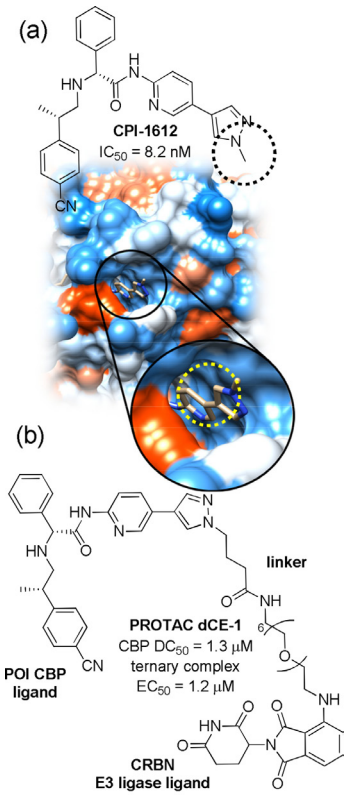

Figure 24. Discovery of PROTAC dCE-1. (a) Selective and potent ligand of CBP, CPI-1612, was chosen as POI ligand and its binding mode to the enzyme (PDB 6V8N) evidenced the methylpyrazole ring turned to the solvent; (b) PROTAC dCE-1 structure with the linker and CRBN E3 ligase recruiter. The image and the hydrophobic surfaces were generated in UCSF Chimera alfa version 1.17.[45] Red surfaces represent hydrophobic regions and blue surfaces represent hydrophilic surfaces.

Receptor-interacting serine/threonine protein kinase 2 (RIPK2) sits downstream of the pattern recognition of the nucleotide-binding oligomerization domain (NOD) receptors NOD1 and NOD2. Stimulated NOD1 and NOD2 interact with RIPK2 and lead to the activation of NF-κB and mitogen-activated protein kinases (MAPK), followed by the production of pro-inflammatory cytokines such as TNF-α, IL-6, and IL-12/23. Defects in NOD/RIPK2 signaling pathway are associated with numerous inflammatory diseases, including asthma, sarcoidosis, inflammatory bowel disease and multiple sclerosis.[184-186]

Initially, Mares *et al.*[186] planned the new PROTACs through the combination of a RIPK2 ligand and E3 ligase recruiters (VHL, CRBN and IAP) by a PEG linker. All synthesized PROTACs were effective in degrading RIPK2, so the authors focused their efforts on IAP-recruiting E3 ligase. PROTAC **33** proved to be a potent degrader of RIPK2 in THP-1 cells, also inhibiting TNF-α release in a human whole blood assay (Figure 25). Despite the good results, the physicochemical and pharmacokinetic properties were not adequate, so researchers have focused efforts on optimizing these factors. Using medicinal chemistry optimization strategies, the researchers modified RIPK2 binder, IAP ligase binder and linker, obtaining PROTAC **34** (Figure 25). Even with the physical-chemical and pharmacokinetic improvements and the capacity to degrade RIPK2, their cellular degradation potency was modest, impacting the dose required to deliver high levels of *in vivo* degradation of RIPK2. One more time, the authors attempted to optimize the linker and IAP binder regions through structural modifications. The additional methylene group in PROTAC **35** increased the RIPK2 inhibitory potency in more than 10-fold, which translated into significantly improved cellular degradation potency in human PBMCs, besides completely inhibiting the release of TNFα, IL1β, IL-6, and IL-10 (Figure 25).

NF-κB represents a family of inducible transcription factors, regulating a large array of genes involved in different processes of the inflammatory responses. In macrophages, excessive or chronic activation of NF-κB regulates the expression of genes for inflammatory responses and mediates the release of pro-inflammatory factors and chemokines, thus contributing to the pathogenesis of many inflammatory diseases. Inhibition of NF-κB activation in macrophages is a promising strategy to prevent or treat these conditions. BTK is a nonreceptor cytoplasmic tyrosine kinase in the Tec family of protein tyrosine kinases. Aberrant activation of B-cells is demonstrated to play a central role in the pathogenesis of B-cell malignancies, autoimmune diseases and inflammation.[187-189]

Using computational molecular modeling tools, Buhimschi *et al.*[190] developed new PROTACs based on ibrutinib. Docking the crystal structures of BTK and cereblon ternary complex showed that the eight-atoms linker is nearing the minimal length needed to bridge the two binding sites. Afterwards, the researchers synthesized MT-802, a PROTAC that degrades BTK with a DC_{50} of 9.1 nM in Namalwa cell line (Figure 26).

Based on studies by Buhimschi *et al.*,[190] Huang *et al.*[191] evaluated the influence of a new linkers on PROTAC based ibrutinib-CRBN. Initially, ligands containing a piperazine ring attached to PEGs of different lengths were synthesized, but neither of the compounds with a semi-rigid linker proved to be better than the flexible MT-802 prototype. The semi-rigid piperidine PROTACs reduced BTK levels in Ramos cells in the range of 28-61% at 100 nM, while MT-802 reduced 75% at 100 nM. PROTACs with an even more conformationally constrained linkers were synthesized. These new PROTACs containing two cycles linkers reduced BTK levels in the range of 31-99% at 100 nM, with PROTAC **36** being the most active, containing a piperazine

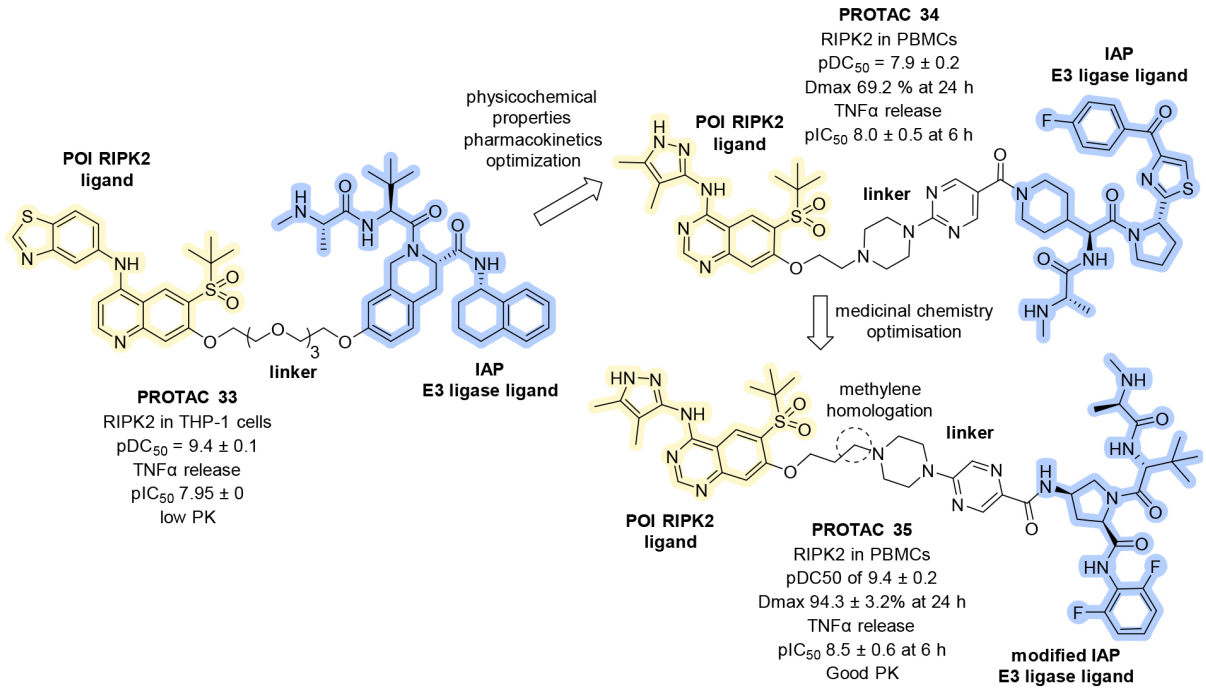

Figure 25. Design and optimization of PROTACs for RIPK2 degradation.

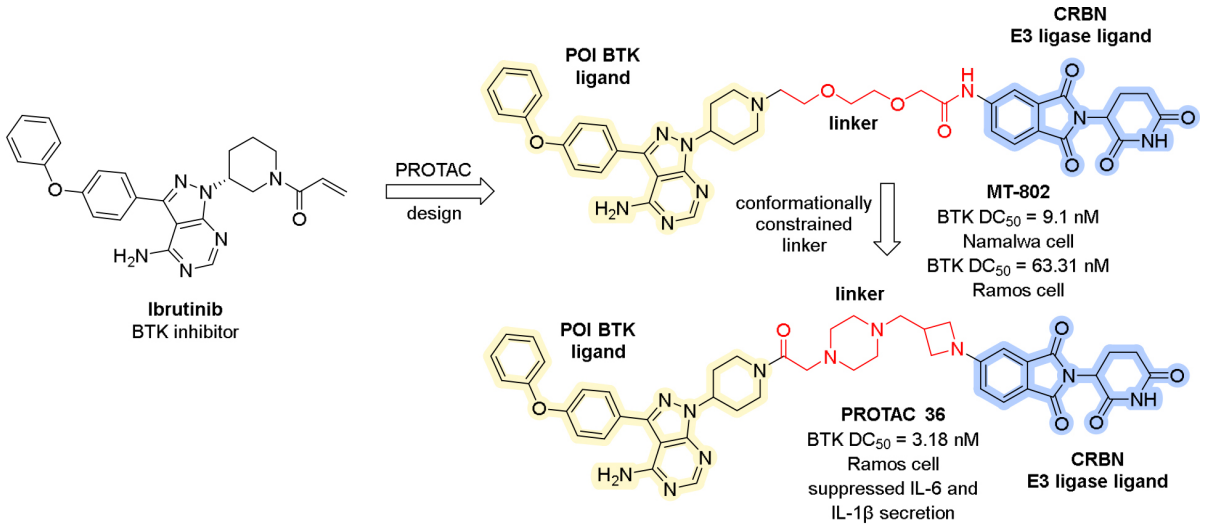

Figure 26. Design of conformational constrained linkers in the development of new BTK PROTACs based on ibrutinib.

and an azetidine linker. The authors evaluated the time and concentration-dependent degradation effects against BTK in Ramos cells and PROTAC **36** degraded BTK with DC_{50} = 3.18 nM, while MT-802 showed DC_{50} = 63.31 nM in the same cell. PROTAC **36** degraded BTK in Mino cells with DC_{50} = 7.07 nM and MT-802 DC_{50} = 35.55 nM. PROTAC **36** suppressed IL-6 and IL-1β secretion (protein levels) in LPS-stimulated RAW 264.7 cells as measured by enzyme-linked immunosorbent assay. PROTAC **36** also decreased the IL-1β and IL-6 levels in the ZIP animal model. These results suggest that PROTAC **36** effectively inhibited NF-κB-mediated production of pro-inflammatory chemokines, indicating its therapeutic potential for inflammatory diseases (Figure 26).

5. Conclusions

In this review, we summarize the discovery, development, design, and importance of PROTACs. Since the first report, when Protac-1 was developed, many advances have been done. Today the interest for PROTACs is well spread in both academic and industry fields with high level of investments. Despite having only 23 years since its discovery, PROTACs are hugely impacting the drug discovery process

due to their special event-driven mode of action. For sure, during this time many advances have improved the technique as the strong development on new linkers, E3 ligase ligands, PD and PK improvements, etc. However, as discussed, some drawbacks still need to be overcome for the complete success of PROTACs like potential toxicities, high molecular weights, difficulties with PK (like crossing barriers), better understanding of SAR, etc. With all the current success of PROTACs, the event-driven mode of action is moving around being applied to other classes of TPDs like the AUTAC,[192] LYTAC,[193] "molecular glues",[194] RIBOTAC,[195] HomoPROTAC,[196] multitargetPROTACs,[96] etc.

But will PROTACs and derivatives indeed become a new major class of pharmacological treatments or only continuing an excellent pharmacological tool? Maybe in a couple of years we can come back through this text with the answer and see what else happened.

Acknowledgments

First, the authors would like to thank Prof Eliezer Barreiro for all his commitment over the years disseminating knowledge and defending good practices in Medicinal Chemistry in Brazil. Authors would also like to thank the National Council for Scientific and Technological Development (CNPq, 314723/2021-8), and Fundação de Amparo à Pesquisa do Estado do Rio de Janeiro (FAPERJ, No. E-26/210.134/2018 and 210.018/2020) for the financial support. This study was also financed in part by the Coordenação de Aperfeiçoamento de Pessoal de Nível Superior - Brasil (CAPES), finance code 001.

Autor Contributions

Lucas Caruso was responsible for conceptualization, formal analysis, writing (original draft); Thiago M. Pereira was responsible for conceptualization, formal analysis, writing (original draft); Arthur E. Kümmerle for conceptualization, writing (original draft, review and editing), supervision, project administration, funding acquisition.

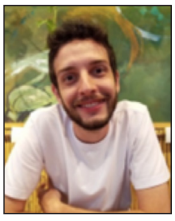

Lucas Caruso *is currently a PhD candidate in Chemistry at Laboratório de Diversidadade Molecular e Química Medicinal (LaDMol-QM, Molecular Diversity and Medicinal Chemistry Laboratory) at Federal Rural University of Rio de Janeiro and has a master's degree in chemistry from the same university. He has experience in organic synthesis, cross-coupling reactions catalyzed by transition metals and development of bioactive compounds for neurodegenerative diseases.*

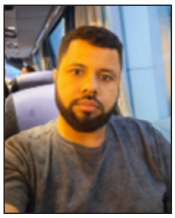

Thiago M. Pereira *is currently a PhD candidate in Chemistry at the University of Strasbourg and the Federal Rural University of Rio de Janeiro (UFRRJ), with a sandwich period at the University of Bologna. He holds master's and bachelor's degrees in Chemistry from the UFRRJ. His research focuses on the field of Organic and Medicinal Chemistry, with a specific emphasis on the synthesis of heterocyclic compounds with potential bioactivity for the treatment of Alzheimer's disease, and the development of more convergent synthetic procedures through metal catalyzed cross-coupling reactions.*

Arthur E. Kümmerle *is PhD in Chemistry from the Institute of Chemistry at the Federal University of Rio de Janeiro, under supervision of Prof Eliezer Barreiro, with a sandwich period at the University of Strasbourg (France). Currently is Associate Professor III at the Federal Rural University of Rio de Janeiro. He is CNPq level 2 tiers (since 2013) and was visiting professor at the University of Strasbourg and Uppsala University (Sweden), Young Scientist of Our State FAPERJ (2015-2022), Director of the Medicinal Chemistry Division of SBQ (2020-2022). He coordinates the LaDMol-QM laboratory, and is engaged in drug design for treating neurodegenerative, inflammatory and tumoral diseases. Recently he is also focusing on obtaining theranostic compounds, as well as the development of PROTACs.*

References

1. Békés, M.; Langley, D. R.; Crews, C. M.; *Nat. Rev. Drug Discovery* **2022**, *21*, 181. [Crossref]
2. Luh, L. M.; Scheib, U.; Juenemann, K.; Wortmann, L.; Brands, M.; Cromm, P. M.; *Angew. Chem., Int. Ed.* **2020**, *59*, 15448. [Crossref]
3. Dale, B.; Cheng, M.; Park, K.-S.; Kaniskan, H. Ü.; Xiong, Y.; Jin, J.; *Nat. Rev. Cancer* **2021**, *21*, 638. [Crossref]
4. Valeur, E.; Guéret, S. M.; Adihou, H.; Gopalakrishnan, R.; Lemurell, M.; Waldmann, H.; Grossmann, T. N.; Plowright, A. T.; *Angew. Chem., Int. Ed.* **2017**, *56*, 10294. [Crossref]
5. Samarasinghe, K. T. G.; Crews, C. M.; *Cell Chem. Biol.* **2021**, *28*, 934. [Crossref]

6. Hopkins, A. L.; Groom, C. R.; *Nat. Rev. Drug Discovery* **2002**, *1*, 727. [Crossref]
7. Pettersson, M.; Crews, C. M.; *Drug Discovery Today: Technol.* **2019**, *31*, 15. [Crossref]
8. Dang, C. V.; Reddy, E. P.; Shokat, K. M.; Soucek, L.; *Nat. Rev. Cancer* **2017**, *17*, 502. [Crossref]
9. Xie, X.; Yu, T.; Li, X.; Zhang, N.; Foster, L. J.; Peng, C.; Huang, W.; He, G.; *Signal Transduction Targeted Ther.* **2023**, *8*, 335. [Crossref]
10. Pedreira, J. G. B.; Franco, L. S.; Barreiro, E. J.; *Curr. Top. Med. Chem.* **2019**, *19*, 1679. [Crossref]
11. Bolognesi, M. L.; *ACS Med. Chem. Lett.* **2019**, *10*, 273. [Crossref]
12. Paiva, S.-L.; Crews, C. M.; *Curr. Opin. Chem. Biol.* **2019**, *50*, 111. [Crossref]
13. Zhao, L.; Zhao, J.; Zhong, K.; Tong, A.; Jia, D.; *Signal Transduction Targeted Ther.* **2022**, *7*, 113. [Crossref]
14. Sakamoto, K. M.; Kim, K. B.; Kumagai, A.; Mercurio, F.; Crews, C. M.; Deshaies, R. J.; *Proc. Natl. Acad. Sci.* **2001**, *98*, 8554. [Crossref]
15. Anfinsen, C. B.; *Science* **1973**, *181*, 223. [Crossref]
16. Hanley, S. E.; Cooper, K. F.; *Cells* **2021**, *10*, 17. [Crossref]
17. Dikic, I.; *Annu. Rev. Biochem.* **2017**, *86*, 193. [Crossref]
18. Pohl, C.; Dikic, I.; *Science* **2019**, *366*, 818. [Crossref]
19. Ciechanover, A.; Orian, A.; Schwartz, A. L.; *BioEssays* **2000**, *22*, 442. [Crossref]
20. Tracz, M.; Bialek, W.; *Cell. Mol. Biol. Lett.* **2021**, *26*, 1. [Crossref]
21. Jeong, Y.; Oh, A.-R.; Jung, Y. H.; Gi, H.; Kim, Y. U.; Kim, K.; *Exp. Mol. Med.* **2023**, *55*, 2097. [Crossref]
22. Zheng, N.; Shabek, N.; *Annu. Rev. Biochem.* **2017**, *86*, 129. [Crossref]
23. Verma, R.; Mohl, D.; Deshaies, R. J.; *Mol. Cell* **2020**, *77*, 446. [Crossref]
24. Lou, Z.; Wang, S.; *J. Int. Med. Res.* **2014**, *42*, 247. [Crossref]
25. Fuller, J. C.; Burgoyne, N. J.; Jackson, R. M.; *Drug Discovery Today* **2009**, *14*, 155. [Crossref]
26. Adjei, A. A.; *J. Clin. Oncol.* **2006**, *24*, 4054. [Crossref]
27. Holohan, C.; Van Schaeybroeck, S.; Longley, D. B.; Johnston, P. G.; *Nat. Rev. Cancer* **2013**, *13*, 714. [Crossref]
28. Blair, J. M. A.; Webber, M. A.; Baylay, A. J.; Ogbolu, D. O.; Piddock, L. J. V.; *Nat. Rev. Microbiol.* **2015**, *13*, 42. [Crossref]
29. Toure, M.; Crews, C. M.; *Angew. Chem., Int. Ed.* **2016**, *55*, 1966. [Crossref]
30. Hershko, A.; *Angew. Chem., Int. Ed.* **2005**, *44*, 5932. [Crossref]
31. Bondeson, D. P.; Mares, A.; Smith, I. E. D.; Ko, E.; Campos, S.; Miah, A. H.; Mulholland, K. E.; Routly, N.; Buckley, D. L.; Gustafson, J. L.; Zinn, N.; Grandi, P.; Shimamura, S.; Bergamini, G.; Faelth-Savitski, M.; Bantscheff, M.; Cox, C.; Gordon, D. A.; Willard, R. R.; Flanagan, J. J.; Casillas, L. N.; Votta, B. J.; den Besten, W.; Famm, K.; Kruidenier, L.; Carter, P. S.; Harling, J. D.; Churcher, I.; Crews, C. M.; *Nat. Chem. Biol.* **2015**, *11*, 611. [Crossref]
32. Burslem, G. M.; Smith, B. E.; Lai, A. C.; Jaime-Figueroa, S.; McQuaid, D. C.; Bondeson, D. P.; Toure, M.; Dong, H.; Qian, Y.; Wang, J.; Crew, A. P.; Hines, J.; Crews, C. M.; *Cell Chem. Biol.* **2018**, *25*, 67.e3. [Crossref]
33. Yang, Y.; Gao, H.; Sun, X.; Sun, Y.; Qiu, Y.; Weng, Q.; Rao, Y.; *J. Med. Chem.* **2020**, *63*, 8567. [Crossref]
34. Sun, Y.; Zhao, X.; Ding, N.; Gao, H.; Wu, Y.; Yang, Y.; Zhao, M.; Hwang, J.; Song, Y.; Liu, W.; Rao, Y.; *Cell Res.* **2018**, *28*, 779. [Crossref]
35. Sun, X.; Rao, Y.; *Biochemistry* **2020**, *59*, 240. [Crossref]
36. Martín-Acosta, P.; Xiao, X.; *Eur. J. Med. Chem.* **2021**, *210*, 112993. [Crossref]
37. Sun, X.; Gao, H.; Yang, Y.; He, M.; Wu, Y.; Song, Y.; Tong, Y.; Rao, Y.; *Signal Transduction Targeted Ther.* **2019**, *4*, 64. [Crossref]
38. He, M.; Cao, C.; Ni, Z.; Liu, Y.; Song, P.; Hao, S.; He, Y.; Sun, X.; Rao, Y.; *Signal Transduction Targeted Ther.* **2022**, *7*, 181. [Crossref]
39. Douglass Jr., E. F.; Miller, C. J.; Sparer, G.; Shapiro, H.; Spiegel, D. A.; *J. Am. Chem. Soc.* **2013**, *135*, 6092. [Crossref]
40. Lu, C.; Wang, Z.-X.; *Anal. Chem.* **2017**, *89*, 6926. [Crossref]
41. Hughes, S. J.; Ciulli, A.; *Essays Biochem.* **2017**, *61*, 505. [Crossref]
42. Tate, J.; Ward, G.; *Clin. Biochem. Rev.* **2004**, *25*, 105. [Crossref] accessed in July 2024
43. Roy, R. D.; Rosenmund, C.; Stefan, M. I.; *BMC Syst. Biol.* **2017**, *11*, 74. [Crossref]
44. Gadd, M. S.; Testa, A.; Lucas, X.; Chan, K.-H.; Chen, W.; Lamont, D. J.; Zengerle, M.; Ciulli, A.; *Nat. Chem. Biol.* **2017**, *13*, 514. [Crossref]
45. Pettersen, E. F.; Goddard, T. D.; Huang, C. C.; Couch, G. S.; Greenblatt, D. M.; Meng, E. C.; Ferrin, T. E.; *J. Comput. Chem.* **2004**, *25*, 16051612. [Crossref]
46. Wurz, R. P.; Rui, H.; Dellamaggiore, K.; Ghimire-Rijal, S.; Choi, K.; Smither, K.; Amegadzie, A.; Chen, N.; Li, X.; Banerjee, A.; Chen, Q.; Mohl, D.; Vaish, A.; *Nat. Commun.* **2023**, *14*, 4177. [Crossref]
47. Zorba, A.; Nguyen, C.; Xu, Y.; Starr, J.; Borzilleri, K.; Smith, J.; Zhu, H.; Farley, K. A.; Ding, W.; Schiemer, J.; Feng, X.; Chang, J. S.; Uccello, D. P.; Young, J. A.; Garcia-Irrizary, C. N.; Czabaniuk, L.; Schuff, B.; Oliver, R.; Montgomery, J.; Hayward, M. M.; Coe, J.; Chen, J.; Niosi, M.; Luthra, S.; Shah, J. C.; El-Kattan, A.; Qiu, X.; West, G. M.; Noe, M. C.; Shanmugasundaram, V.; Gilbert, A. M.; Brown, M. F.; Calabrese, M. F.; *Proc. Natl. Acad. Sci. U. S. A.* **2018**, *115*, E7285. [Crossref]
48. Sakamoto, K. M.; Kim, K. B.; Verma, R.; Ransick, A.; Stein, B.; Crews, C. M.; Deshaies, R. J.; *Mol. Cell. Proteomics* **2003**, *2*, 1350. [Crossref]
49. Schneekloth Jr., J. S.; Fonseca, F. N.; Koldobskiy, M.; Mandal, A.; Deshaies, R.; Sakamoto, K.; Crews, C. M.; *J. Am. Chem. Soc.* **2004**, *126*, 3748. [Crossref]

50. Lee, H.; Puppala, D.; Choi, E.-Y.; Swanson, H.; Kim, K.-B.; *ChemBioChem* **2007**, *8*, 2058. [Crossref]
51. Schneekloth, A. R.; Pucheault, M.; Tae, H. S.; Crews, C. M.; *Bioorg. Med. Chem. Lett.* **2008**, *18*, 5904. [Crossref]
52. Zou, Y.; Ma, D.; Wang, Y.; *Cell Biochem. Funct.* **2019**, *37*, 21. [Crossref]
53. Wang, C.; Zhang, Y.; Wu, Y.; Xing, D.; *Eur. J. Med. Chem.* **2021**, *225*, 113749. [Crossref]
54. Bricelj, A.; Steinebach, C.; Kuchta, R.; Gütschow, M.; Sosič, I.; *Front. Chem.* **2021**, *9*, 707317. [Crossref]
55. Yang, X.-D.; Sun, S.-C.; *Immunol. Rev.* **2015**, *266*, 56. [Crossref]
56. Diehl, C. J.; Ciulli, A.; *Chem. Soc. Rev.* **2022**, *51*, 8216. [Crossref]
57. Setia, N.; Almuqdadi, H. T. A.; Abid, M.; *Eur. J. Med. Chem.* **2024**, *265*, 116041. [Crossref]
58. Buckley, D. L.; Gustafson, J. L.; Van Molle, I.; Roth, A. G.; Tae, H. S.; Gareiss, P. C.; Jorgensen, W. L.; Ciulli, A.; Crews, C. M.; *Angew. Chem., Int. Ed.* **2012**, *51*, 11463. [Crossref]
59. Buckley, D. L.; Van Molle, I.; Gareiss, P. C.; Tae, H. S.; Michel, J.; Noblin, D. J.; Jorgensen, W. L.; Ciulli, A.; Crews, C. M.; *J. Am. Chem. Soc.* **2012**, *134*, 4465. [Crossref]
60. Van Molle, I.; Thomann, A.; Buckley, D. L.; So, E. C.; Lang, S.; Crews, C. M.; Ciulli, A.; *Chem. Biol.* **2012**, *19*, 1300. [Crossref]
61. Ito, T.; Ando, H.; Suzuki, T.; Ogura, T.; Hotta, K.; Imamura, Y.; Yamaguchi, Y.; Handa, H.; *Science* **2010**, *327*, 1345. [Crossref]
62. Lopez-Girona, A.; Mendy, D.; Ito, T.; Miller, K.; Gandhi, A. K.; Kang, J.; Karasawa, S.; Carmel, G.; Jackson, P.; Abbasian, M.; Mahmoudi, A.; Cathers, B.; Rychak, E.; Gaidarova, S.; Chen, R.; Schafer, P. H.; Handa, H.; Daniel, T. O.; Evans, J. F.; Chopra, R.; *Leukemia* **2012**, *26*, 2326. [Crossref]
63. Fischer, E. S.; Böhm, K.; Lydeard, J. R.; Yang, H.; Stadler, M. B.; Cavadini, S.; Nagel, J.; Serluca, F.; Acker, V.; Lingaraju, G. M.; Tichkule, R. B.; Schebesta, M.; Forrester, W. C.; Schirle, M.; Hassiepen, U.; Ottl, J.; Hild, M.; Beckwith, R. E. J.; Harper, J. W.; Jenkins, J. L.; Thomä, N. H.; *Nature* **2014**, *512*, 49. [Crossref]
64. Krönke, J.; Udeshi, N. D.; Narla, A.; Grauman, P.; Hurst, S. N.; McConkey, M.; Svinkina, T.; Heckl, D.; Comer, E.; Li, X.; Ciarlo, C.; Hartman, E.; Munshi, N.; Schenone, M.; Schreiber, S. L.; Carr, S. A.; Ebert, B. L.; *Science* **2014**, *343*, 301. [Crossref]
65. Petzold, G.; Fischer, E. S.; Thomä, N. H.; *Nature* **2016**, *532*, 127. [Crossref]
66. Gandhi, A. K.; Kang, J.; Havens, C. G.; Conklin, T.; Ning, Y.; Wu, L.; Ito, T.; Ando, H.; Waldman, M. F.; Thakurta, A.; Klippel, A.; Handa, H.; Daniel, T. O.; Schafer, P. H.; Chopra, R.; *Br. J. Haematol.* **2014**, *164*, 811. [Crossref]
67. Hines, J.; Gough, J. D.; Corson, T. W.; Crews, C. M.; *Proc. Natl. Acad. Sci.* **2013**, *110*, 8942. [Crossref]
68. Montrose, K.; Krissansen, G. W.; *Biochem. Biophys. Res. Commun.* **2014**, *453*, 735. [Crossref]
69. Buckley, D. L.; Raina, K.; Darricarrere, N.; Hines, J.; Gustafson, J. L.; Smith, I. E.; Miah, A. H.; Harling, J. D.; Crews, C. M.; *ACS Chem. Biol.* **2015**, *10*, 1831. [Crossref]
70. Zengerle, M.; Chan, K.-H.; Ciulli, A.; *ACS Chem. Biol.* **2015**, *10*, 1770. [Crossref]
71. Lebraud, H.; Wright, D. J.; Johnson, C. N.; Heightman, T. D.; *ACS Cent. Sci.* **2016**, *2*, 927. [Crossref]
72. Weng, G.; Cai, X.; Cao, D.; Du, H.; Shen, C.; Deng, Y.; He, Q.; Yang, B.; Li, D.; Hou, T.; *Nucleic Acids Res.* **2023**, *51*, D1367. [Crossref]; PROTAC-DB, http://cadd.zju.edu.cn/protacdb/, accessed in July 2024.
73. Silva, M. C.; Ferguson, F. M.; Cai, Q.; Donovan, K. A.; Nandi, G.; Patnaik, D.; Zhang, T.; Huang, H.-T.; Lucente, D. E.; Dickerson, B. C.; Mitchison, T. J.; Fischer, E. S.; Gray, N. S.; Haggarty, S. J.; *eLife* **2019**, *8*, e45457. [Crossref]
74. Silva, M. C.; Nandi, G.; Donovan, K. A.; Cai, Q.; Berry, B. C.; Nowak, R. P.; Fischer, E. S.; Gray, N. S.; Ferguson, F. M.; Haggarty, S. J.; *Front. Cell. Neurosci.* **2022**, *16*, 801179. [Crossref]
75. Wang, W.; Zhou, Q.; Jiang, T.; Li, S.; Ye, J.; Zheng, J.; Wang, X.; Liu, Y.; Deng, M.; Ke, D.; Wang, Q.; Wang, Y.; Wang, J.-Z.; *Theranostics* **2021**, *11*, 5279. [Crossref]
76. Moore, A. R.; Rosenberg, S. C.; McCormick, F.; Malek, S.; *Nat. Rev. Drug Discovery* **2020**, *19*, 533. [Crossref]
77. Yang, F.; Wen, Y.; Wang, C.; Zhou, Y.; Zhou, Y.; Zhang, Z.-M.; Liu, T.; Lu, X.; *Eur. J. Med. Chem.* **2022**, *230*, 114088. [Crossref]
78. Bond, M. J.; Chu, L.; Nalawansha, D. A.; Li, K.; Crews, C. M.; *ACS Cent. Sci.* **2020**, *6*, 1367. [Crossref]
79. Li, L.; Wu, Y.; Yang, Z.; Xu, C.; Zhao, H.; Liu, J.; Chen, J.; Chen, J.; *Bioorg. Chem.* **2021**, *117*, 105447. [Crossref]
80. Escher, T. E.; Satchell, K. J. F.; *Mol. Ther.* **2023**, *31*, 1904. [Crossref]
81. Lee, H.; Lee, J. Y.; Jang, H.; Cho, H. Y.; Kang, M.; Bae, S. H.; Kim, S.; Kim, E.; Jang, J.; Kim, J. Y.; Jeon, Y. H.; *Eur. J. Med. Chem.* **2024**, *263*, 115929. [Crossref]
82. Jack, B. R.; Meyer, A. G.; Echave, J.; Wilke, C. O.; *PLoS Biol.* **2016**, *14*, e1002452. [Crossref]
83. Bondeson, D. P.; Smith, B. E.; Burslem, G. M.; Buhimschi, A. D.; Hines, J.; Jaime-Figueroa, S.; Wang, J.; Hamman, B. D.; Ishchenko, A.; Crews, C. M.; *Cell Chem. Biol.* **2018**, *25*, 78.e5. [Crossref]
84. Burke, M. R.; Smith, A. R.; Zheng, G.; *Front. Cell Dev. Biol.* **2022**, *10*, 872729. [Crossref]
85. Lim, Y. S.; Yoo, S.-M.; Patil, V.; Kim, H. W.; Kim, H.-H.; Suh, B.; Park, J. Y.; Jeong, N.; Park, C. H.; Ryu, J. H.; Lee, B.-H.; Kim, P.; Lee, S. H.; *Blood Adv.* **2023**, *7*, 92105. [Crossref]
86. Bueno, C.; Velasco-Hernandez, T.; Gutiérrez-Agüera, F.; Zanetti, S. R.; Baroni, M. L.; Sánchez-Martínez, D.; Molina, O.; Closa, A.; Agraz-Doblás, A.; Marín, P.; Eyras, E.; Varela, I.; Menéndez, P.; *Leukemia* **2019**, *33*, 2090. [Crossref]

87. Woyach, J. A.; Furman, R. R.; Liu, T.-M.; Ozer, H. G.; Zapatka, M.; Ruppert, A. S.; Xue, L.; Li, D. H.-H.; Steggerda, S. M.; Versele, M.; Dave, S. S.; Zhang, J.; Yilmaz, A. S.; Jaglowski, S. M.; Blum, K. A.; Lozanski, A.; Lozanski, G.; James, D. F.; Barrientos, J. C.; Lichter, P.; Stilgenbauer, S.; Buggy, J. J.; Chang, B. Y.; Johnson, A. J.; Byrd, J. C.; *N. Engl. J. Med.* **2014**, *370*, 2286. [Crossref]
88. Huang, H.-T.; Dobrovolsky, D.; Paulk, J.; Yang, G.; Weisberg, E. L.; Doctor, Z. M.; Buckley, D. L.; Cho, J.-H.; Ko, E.; Jang, J.; Shi, K.; Choi, H. G.; Griffin, J. D.; Li, Y.; Treon, S. P.; Fischer, E. S.; Bradner, J. E.; Tan, L.; Gray, N. S.; *Cell Chem. Biol.* **2018**, *25*, 88.e6. [Crossref]
89. Neklesa, T.; Snyder, L. B.; Willard, R. R.; Vitale, N.; Pizzano, J.; Gordon, D. A.; Bookbinder, M.; Macaluso, J.; Dong, H.; Ferraro, C.; Wang, G.; Wang, J.; Crews, C. M.; Houston, J.; Crew, A. P.; Taylor, I.; *J. Clin. Oncol.* **2019**, *37*, 259. [Crossref]
90. Neklesa, T.; Snyder, L. B.; Willard, R. R.; Vitale, N.; Raina, K.; Pizzano, J.; Gordon, D.; Bookbinder, M.; Macaluso, J.; Dong, H.; Liu, Z.; Ferraro, C.; Wang, G.; Wang, J.; Crews, C. M.; Houston, J.; Crew, A. P.; Taylor, I.; *Cancer Res.* **2018**, *78*, 5236. [Crossref]
91. Gao, X.; Burris III, H. A.; Vuky, J.; Dreicer, R.; Sartor, A. O.; Sternberg, C. N.; Percent, I. J.; Hussain, M. H. A.; Kalebasty, A. R.; Shen, J.; Heath, E. I.; Abesada-Terk, G.; Gandhi, S. G.; McKean, M.; Lu, H.; Berghorn, E.; Gedrich, R.; Chirnomas, S. D.; Vogelzang, N. J.; Petrylak, D. P.; *J. Clin. Oncol.* **2022**, *40*, 17. [Crossref]
92. Snyder, L. B.; Flanagan, J. J.; Qian, Y.; Gough, S. M.; Andreoli, M.; Bookbinder, M.; Cadelina, G.; Bradley, J.; Rousseau, E.; Chandler, J.; Willard, R.; Pizzano, J.; Crews, C. M.; Crew, A. P.; Houston, J.; Moore, M. D.; Peck, R.; Taylor, I.; *Cancer Res.* **2021**, *81*, 44. [Crossref]
93. Ackerman, L.; Acloque, G.; Bacchelli, S.; Schwartz, H.; Feinstein, B. J.; La Stella, P.; Alavi, A.; Gollerkeri, A.; Davis, J.; Campbell, V.; McDonald, A.; Agarwal, S.; Karnik, R.; Shi, K.; Mishkin, A.; Culbertson, J.; Klaus, C.; Enerson, B.; Massa, V.; Kuhn, E.; Sharma, K.; Keaney, E.; Barnes, R.; Chen, D.; Zheng, X.; Rong, H.; Sabesan, V.; Ho, C.; Mainolfi, N.; Slavin, A.; Gollob, J. A.; *Nat. Med.* **2023**, *29*, 3127. [Crossref]
94. Moreau, K.; Coen, M.; Zhang, A. X.; Pachl, F.; Castaldi, M. P.; Dahl, G.; Boyd, H.; Scott, C.; Newham, P.; *Br. J. Pharmacol.* **2020**, *177*, 1709. [Crossref]
95. Kintor, *Kintor Pharmaceutical Announces AR-PROTAC (GT20029) Approved for Acne and Androgenic Alopecia Clinical Trials in China*, https://en.kintor.com.cn/news/171.html, accessed in July 2024.
96. Salerno, A.; Seghetti, F.; Caciolla, J.; Uliassi, E.; Testi, E.; Guardigni, M.; Roberti, M.; Milelli, A.; Bolognesi, M. L.; *J. Med. Chem.* **2022**, *65*, 9507. [Crossref]
97. Kostic, M.; Jones, L. H.; *Trends Pharmacol. Sci.* **2020**, *41*, 305. [Crossref]
98. Edmondson, S. D.; Yang, B.; Fallan, C.; *Bioorg. Med. Chem. Lett.* **2019**, *29*, 1555. [Crossref]
99. Lipinski, C. A.; Lombardo, F.; Dominy, B. W.; Feeney, P. J.; *Adv. Drug Delivery Rev.* **1997**, *23*, 3. [Crossref]
100. Matsson, P.; Kihlberg, J.; *J. Med. Chem.* **2017**, *60*, 1662. [Crossref]
101. Jimenez, D. G.; Sebastiano, M. R.; Caron, G.; Ermondi, G.; *ADMET DMPK* **2021**, *9*, 243. [Crossref]
102. Atilaw, Y.; Poongavanam, V.; Nilsson, C. S.; Nguyen, D.; Giese, A.; Meibom, D.; Erdelyi, M.; Kihlberg, J.; *ACS Med. Chem. Lett.* **2021**, *12*, 107. [Crossref]
103. Bemis, T. A.; La Clair, J. J.; Burkart, M. D.; *J. Med. Chem.* **2021**, *64*, 8042. [Crossref]
104. Chen, S.; Chen, Z.; Lu, L.; Zhao, Y.; Zhou, R.; Xie, Q.; Shu, Y.; Lin, J.; Yu, X.; Wang, Y.; *Eur. J. Med. Chem.* **2023**, *255*, 115403. [Crossref]
105. Cecchini, C.; Pannilunghi, S.; Tardy, S.; Scapozza, L.; *Front. Chem.* **2021**, *9*, 672267. [Crossref]
106. Zhang, L.; Riley-Gillis, B.; Vijay, P.; Shen, Y.; *Mol. Cancer Ther.* **2019**, *18*, 1302. [Crossref]
107. Pacini, C.; Dempster, J. M.; Boyle, I.; Gonçalves, E.; Najgebauer, H.; Karakoc, E.; van der Meer, D.; Barthorpe, A.; Lightfoot, H.; Jaaks, P.; McFarland, J. M.; Garnett, M. J.; Tsherniak, A.; Iorio, F.; *Nat. Commun.* **2021**, *12*, 1661. [Crossref]
108. Shirasaki, R.; Matthews, G. M.; Gandolfi, S.; Simoes, R. M.; Buckley, D. L.; Vora, J. R.; Sievers, Q. L.; Brüggenthies, J. B.; Dashevsky, O.; Poarch, H.; Tang, H.; Bariteau, M. A.; Sheffer, M.; Hu, Y.; Downey-Kopyscinski, S. L.; Hengeveld, P. J.; Glassner, B. J.; Dhimolea, E.; Ott, C. J.; Zhang, T.; Kwiatkowski, N. P.; Laubach, J. P.; Schlossman, R. L.; Richardson, P. G.; Culhane, A. C.; Groen, R. W. J.; Fischer, E. S.; Vazquez, F.; Tsherniak, A.; Hahn, W. C.; Levy, J.; Auclair, D.; Licht, J. D.; Keats, J. J.; Boise, L. H.; Ebert, B. L.; Bradner, J. E.; Gray, N. S.; Mitsiades, C. S.; *Cell Rep.* **2021**, *34*, 108532. [Crossref]
109. Matyskiela, M. E.; Lu, G.; Ito, T.; Pagarigan, B.; Lu, C.-C.; Miller, K.; Fang, W.; Wang, N.-Y.; Nguyen, D.; Houston, J.; Carmel, G.; Tran, T.; Riley, M.; Nosaka, L.; Lander, G. C.; Gaidarova, S.; Xu, S.; Ruchelman, A. L.; Handa, H.; Carmichael, J.; Daniel, T. O.; Cathers, B. E.; Lopez-Girona, A.; Chamberlain, P. P.; *Nature* **2016**, *535*, 252. [Crossref]
110. Zhong, Y.; Chi, F.; Wu, H.; Liu, Y.; Xie, Z.; Huang, W.; Shi, W.; Qian, H.; *Eur. J. Med. Chem.* **2022**, *231*, 114142. [Crossref]
111. Ghidini, A.; Cléry, A.; Halloy, F.; Allain, F. H. T.; Hall, J.; *Angew. Chem., Int. Ed.* **2021**, *60*, 3163. [Crossref]
112. Viegas-Junior, C.; Danuello, A.; Bolzani, V. S.; Barreiro, E. J.; Fraga, C. A. M.; *Curr. Med. Chem.* **2007**, *14*, 1829. [Crossref]
113. Ivasiv, V.; Albertini, C.; Gonçalves, A. E.; Rossi, M.; Bolognesi, M. L.; *Curr. Top. Med. Chem.* **2019**, *19*, 1694. [Crossref]
114. Troup, R. I.; Fallan, C.; Baud, M. G. J.; *Explor. Targeted Anti-Tumor Ther.* **2020**, *1*, 273. [Crossref]

115. Zheng, S.; Tan, Y.; Wang, Z.; Li, C.; Zhang, Z.; Sang, X.; Chen, H.; Yang, Y.; *Nat. Mach. Intell.* **2022**, *4*, 739. [Crossref]
116. Fisher, S. L.; Phillips, A. J.; *Curr. Opin. Chem. Biol.* **2018**, *44*, 47. [Crossref]
117. Nalawansha, D. A.; Crews, C. M.; *Cell Chem. Biol.* **2020**, *27*, 998. [Crossref]
118. PROTACpedia, https://protacpedia.weizmann.ac.il/ptcb/main, accessed in July 2024.
119. Nunes, J.; McGonagle, G. A.; Eden, J.; Kiritharan, G.; Touzet, M.; Lewell, X.; Emery, J.; Eidam, H.; Harling, J. D.; Anderson, N. A.; *ACS Med. Chem. Lett.* **2019**, *10*, 1081. [Crossref]
120. Cai, M.; Ma, F.; Hu, C.; Li, H.; Cao, F.; Li, Y.; Dong, J.; Qin, J.-J.; *Bioorg. Med. Chem.* **2023**, *90*, 117352. [Crossref]
121. Chen, P.; Li, Q.; Lei, X.; *TrAC, Trends Anal. Chem.* **2024**, *171*, 117539. [Crossref]
122. Miller, D. S. J.; Voell, S. A.; Sosič, I.; Proj, M.; Rossanese, O. W.; Schnakenburg, G.; Gütschow, M.; Collins, I.; Steinebach, C.; *RSC Med. Chem.* **2022**, *13*, 731. [Crossref]
123. Liu, H.; Mi, Q.; Ding, X.; Lin, C.; Liu, L.; Ren, C.; Shen, S.; Shao, Y.; Chen, J.; Zhou, Y.; Ji, L.; Zhang, H.; Bai, F.; Yang, X.; Yin, Q.; Jiang, B.; *Eur. J. Med. Chem.* **2022**, *244*, 114810. [Crossref]
124. Tokarski II, R. J.; Sharpe, C. M.; Huntsman, A. C.; Mize, B. K.; Ayinde, O. R.; Stahl, E. H.; Lerma, J. R.; Reed, A.; Carmichael, B.; Muthusamy, N.; Byrd, J. C.; Fuchs, J. R.; *Eur. J. Med. Chem.* **2023**, *254*, 115342. [Crossref]
125. Khan, S.; Zhang, X.; Lv, D.; Zhang, Q.; He, Y.; Zhang, P.; Liu, X.; Thummuri, D.; Yuan, Y.; Wiegand, J. S.; Pei, J.; Zhang, W.; Sharma, A.; McCurdy, C. R.; Kuruvilla, V. M.; Baran, N.; Ferrando, A. A.; Kim, Y.; Rogojina, A.; Houghton, P. J.; Huang, G.; Hromas, R.; Konopleva, M.; Zheng, G.; Zhou, D.; *Nat. Med.* **2019**, *25*, 1938. [Crossref]
126. Churcher, I.; *J. Med. Chem.* **2018**, *61*, 444. [Crossref]
127. Zografou-Barredo, N. A.; Hallatt, A. J.; Goujon-Ricci, J.; Cano, C.; *Bioorg. Med. Chem.* **2023**, *88*, 117334. [Crossref]
128. Dong, Y.; Ma, T.; Xu, T.; Feng, Z.; Li, Y.; Song, L.; Yao, X.; Ashby Jr., C. R.; Hao, G.-F.; *Acta Pharm. Sin. B* **2024**, *in press*. [Crossref]
129. Zhang, X.; Xu, F.; Tong, L.; Zhang, T.; Xie, H.; Lu, X.; Ren, X.; Ding, K.; *Eur. J. Med. Chem.* **2020**, *192*, 112199. [Crossref]
130. Cyrus, K.; Wehenkel, M.; Choi, E.-Y.; Han, H.-J.; Lee, H.; Swanson, H.; Kim, K.-B.; *Mol. BioSyst.* **2011**, *7*, 359. [Crossref]
131. Cyrus, K.; Wehenkel, M.; Choi, E.-Y.; Lee, H.; Swanson, H.; Kim, K.-B.; *ChemMedChem* **2010**, *5*, 979. [Crossref]
132. Rana, S.; Bendjennat, M.; Kour, S.; King, H. M.; Kizhake, S.; Zahid, M.; Natarajan, A.; *Bioorg. Med. Chem. Lett.* **2019**, *29*, 1375. [Crossref]
133. Rostovtsev, V. V.; Green, L. G.; Fokin, V. V.; Sharpless, K. B.; *Angew. Chem., Int. Ed.* **2002**, *41*, 2596. [Crossref]
134. Tornøe, C. W.; Christensen, C.; Meldal, M.; *J. Org. Chem.* **2002**, *67*, 3057. [Crossref]
135. Agard, N. J.; Prescher, J. A.; Bertozzi, C. R.; *J. Am. Chem. Soc.* **2004**, *126*, 15046. [Crossref]
136. Pasieka, A.; Diamanti, E.; Uliassi, E.; Bolognesi, M. L.; *ChemMedChem* **2023**, *18*, e202300422. [Crossref]
137. Xia, L.-W.; Ba, M.-Y.; Liu, W.; Cheng, W.; Hu, C.-P.; Zhao, Q.; Yao, Y.-F.; Sun, M.-R.; Duan, Y.-T.; *Future Med. Chem.* **2019**, *11*, 2919. [Crossref]
138. Schiedel, M.; Herp, D.; Hammelmann, S.; Swyter, S.; Lehotzky, A.; Robaa, D.; Oláh, J.; Ovádi, J.; Sippl, W.; Jung, M.; *J. Med. Chem.* **2018**, *61*, 482. [Crossref]
139. Wu, Q.-J.; Zhang, T.-N.; Chen, H.-H.; Yu, X.-F.; Lv, J.-L.; Liu, Y.-Y.; Liu, Y.-S.; Zheng, G.; Zhao, J.-Q.; Wei, Y.-F.; Guo, J.-Y.; Liu, F.-H.; Chang, Q.; Zhang, Y.-X.; Liu, C.-G.; Zhao, Y.-H.; *Signal Transduction Targeted Ther.* **2022**, *7*, 402. [Crossref]
140. Wurz, R. P.; Dellamaggiore, K.; Dou, H.; Javier, N.; Lo, M.-C.; McCarter, J. D.; Mohl, D.; Sastri, C.; Lipford, J. R.; Cee, V. J.; *J. Med. Chem.* **2018**, *61*, 453. [Crossref]
141. Filippakopoulos, P.; Qi, J.; Picaud, S.; Shen, Y.; Smith, W. B.; Fedorov, O.; Morse, E. M.; Keates, T.; Hickman, T. T.; Felletar, I.; Philpott, M.; Munro, S.; McKeown, M. R.; Wang, Y.; Christie, A. L.; West, N.; Cameron, M. J.; Schwartz, B.; Heightman, T. D.; La Thangue, N.; French, C. A.; Wiest, O.; Kung, A. L.; Knapp, S.; Bradner, J. E.; *Nature* **2010**, *468*, 1067. [Crossref]
142. Reynders, M.; Trauner, D.; *Cell Chem. Biol.* **2021**, *28*, 969. [Crossref]
143. Li, W.; Elhassan, R. M.; Fang, H.; Hou, X.; *Future Med. Chem.* **2020**, *12*, 1991. [Crossref]
144. Pfaff, P.; Samarasinghe, K. T. G.; Crews, C. M.; Carreira, E. M.; *ACS Cent. Sci.* **2019**, *5*, 1682. [Crossref]
145. Bléger, D.; Schwarz, J.; Brouwer, A. M.; Hecht, S.; *J. Am. Chem. Soc.* **2012**, *134*, 20597. [Crossref]
146. Kleiger, G.; Mayor, T.; *Trends Cell Biol.* **2014**, *24*, 352. [Crossref]
147. Belcher, B. P.; Ward, C. C.; Nomura, D. K.; *Biochemistry* **2023**, *62*, 588600. [Crossref]
148. Steinebach, C.; Ng, Y. L. D.; Sosič, I.; Lee, C.-S.; Chen, S.; Lindner, S.; Vu, L. P.; Bricelj, A.; Haschemi, R.; Monschke, M.; Steinwarz, E.; Wagner, K. G.; Bendas, G.; Luo, J.; Gütschow, M.; Krönke, J.; *Chem. Sci.* **2020**, *11*, 3474. [Crossref]
149. Liu, X.; Kalogeropulou, A. F.; Domingos, S.; Makukhin, N.; Nirujogi, R. S.; Singh, F.; Shpiro, N.; Saalfrank, A.; Sammler, E.; Ganley, I. G.; Moreira, R.; Alessi, D. R.; Ciulli, A.; *J. Am. Chem. Soc.* **2022**, *144*, 16930. [Crossref]
150. Dwyer, Z.; Rudyk, C.; Thompson, A.; Farmer, K.; Fenner, B.; Fortin, T.; Derksen, A.; Sun, H.; Hayley, S.; *Neurobiol. Aging* **2020**, *91*, 45. [Crossref]
151. Tong, B.; Spradlin, J. N.; Novaes, L. F. T.; Zhang, E.; Hu, X.; Moeller, M.; Brittain, S. M.; McGregor, L. M.; McKenna, J. M.; Tallarico, J. A.; Schirle, M.; Maimone, T. J.; Nomura, D. K.; *ACS Chem. Biol.* **2020**, *15*, 1788. [Crossref]

152. Henning, N. J.; Manford, A. G.; Spradlin, J. N.; Brittain, S. M.; Zhang, E.; McKenna, J. M.; Tallarico, J. A.; Schirle, M.; Rape, M.; Nomura, D. K.; *J. Am. Chem. Soc.* **2022**, *144*, 701. [Crossref]
153. Zhang, X.; Crowley, V. M.; Wucherpfennig, T. G.; Dix, M. M.; Cravatt, B. F.; *Nat. Chem. Biol.* **2019**, *15*, 737. [Crossref]
154. Zhang, X.; Luukkonen, L. M.; Eissler, C. L.; Crowley, V. M.; Yamashita, Y.; Schafroth, M. A.; Kikuchi, S.; Weinstein, D. S.; Symons, K. T.; Nordin, B. E.; Rodriguez, J. L.; Wucherpfennig, T. G.; Bauer, L. G.; Dix, M. M.; Stamos, D.; Kinsella, T. M.; Simon, G. M.; Baltgalvis, K. A.; Cravatt, B. F.; *J. Am. Chem. Soc.* **2021**, *143*, 5141. [Crossref]
155. Zoppi, V.; Hughes, S. J.; Maniaci, C.; Testa, A.; Gmaschitz, T.; Wieshofer, C.; Koegl, M.; Riching, K. M.; Daniels, D. L.; Spallarossa, A.; Ciulli, A.; *J. Med. Chem.* **2019**, *62*, 699. [Crossref]
156. Schapira, M.; Calabrese, M. F.; Bullock, A. N.; Crews, C. M.; *Nat. Rev. Drug Discovery* **2019**, *18*, 949. [Crossref]
157. Liu, Q. Y.; Lei, J. X.; Sikorska, M.; Liu, R.; *Mol. Neurodegener.* **2008**, *3*, 4. [Crossref]
158. Menon, S.; Goldfarb, D.; Ho, C. T.; Cloer, E. W.; Boyer, N. P.; Hardie, C.; Bock, A. J.; Johnson, E. C.; Anil, J.; Major, M. B.; Gupton, S. L.; *Mol. Biol. Cell* **2021**, *32*, 311. [Crossref]
159. Kumanomidou, T.; Nishio, K.; Takagi, K.; Nakagawa, T.; Suzuki, A.; Yamane, T.; Tokunaga, F.; Iwai, K.; Murakami, A.; Yoshida, Y.; Tanaka, K.; Mizushima, T.; *PLoS One* **2015**, *10*, e0140366. [Crossref]
160. Glenn, K. A.; Nelson, R. F.; Wen, H. M.; Mallinger, A. J.; Paulson, H. L.; *J. Biol. Chem.* **2008**, *283*, 12717. [Crossref]
161. Angiolilli, C.; Kabala, P. A.; Grabiec, A. M.; Van Baarsen, I. M.; Ferguson, B. S.; García, S.; Malvar Fernandez, B.; McKinsey, T. A.; Tak, P. P.; Fossati, G.; Mascagni, P.; Baeten, D. L.; Reedquist, K. A.; *Ann. Rheum. Dis.* **2017**, *76*, 277. [Crossref]
162. Leus, N. G.; Zwinderman, M. R.; Dekker, F. J.; *Curr. Opin. Chem. Biol.* **2016**, *33*, 160. [Crossref]
163. Zhao, C.; Chen, S.; Chen, D.; Río-Bergé, C.; Zhang, J.; Van Der Wouden, P. E.; Daemen, T.; Dekker, F. J.; *Angew. Chem., Int. Ed.* **2023**, *62*, e202310059. [Crossref]
164. Magupalli, V. G.; Negro, R.; Tian, Y.; Hauenstein, A. V.; Di Caprio, G.; Skillern, W.; Deng, Q.; Orning, P.; Alam, H. B.; Maliga, Z.; Sharif, H.; Hu, J. J.; Evavold, C. L.; Kagan, J. C.; Schmidt, F. I.; Fitzgerald, K. A.; Kirchhausen, T.; Li, Y.; Wu, H.; *Science* **2020**, *369*, eaas8995. [Crossref]
165. Cao, F.; de Weerd, S.; Chen, D.; Zwinderman, M. R. H.; van der Wouden, P. E.; Dekker, F. J.; *Eur. J. Med. Chem.* **2020**, *208*, 112800. [Crossref]
166. Wagner, F. F.; Lundh, M.; Kaya, T.; McCarren, P.; Zhang, Y.-L.; Chattopadhyay, S.; Gale, J. P.; Galbo, T.; Fisher, S. L.; Meier, B. C.; Vetere, A.; Richardson, S.; Morgan, N. G.; Christensen, D. P.; Gilbert, T. J.; Hooker, J. M.; Leroy, M.; Walpita, D.; Mandrup-Poulsen, T.; Wagner, B. K.; Holson, E. B.; *ACS Chem. Biol.* **2016**, *11*, 363. [Crossref]
167. Chou, C. J.; Herman, D.; Gottesfeld, J. M.; *J. Biol. Chem.* **2008**, *283*, 35402. [Crossref]
168. Zhang, X.-H.; Qin-Ma; Wu, H.-P.; Khamis, M. Y.; Li, Y.-H.; Ma, L.-Y.; Liu, H.-M.; *J. Med. Chem.* **2021**, *64*, 1362. [Crossref]
169. Rodrigues, D. A.; Thota, S.; Fraga, C. A. M.; *Mini-Rev. Med. Chem.* **2016**, *16*, 1175. [Crossref]
170. Cao, Z.; Yang, F.; Wang, J.; Gu, Z.; Lin, S.; Wang, P.; An, J.; Liu, T.; Li, Y.; Li, Y.; Lin, H.; Zhao, Y.; He, B.; *J. Med. Chem.* **2021**, *64*, 15280. [Crossref]
171. Zhang, L.; Zhang, J.; Jiang, Q.; Zhang, L.; Song, W.; *J. Enzyme Inhib. Med. Chem.* **2018**, *33*, 714. [Crossref]
172. Cao, Z.; Gu, Z.; Lin, S.; Chen, D.; Wang, J.; Zhao, Y.; Li, Y.; Liu, T.; Li, Y.; Wang, Y.; Lin, H.; He, B.; *ACS Chem. Biol.* **2021**, *16*, 2746. [Crossref]
173. Bockstiegel, J.; Wurnig, S. L.; Engelhardt, J.; Enns, J.; Hansen, F. K.; Weindl, G.; *Biochem. Pharmacol.* **2023**, *215*, 115693. [Crossref]
174. North, B. J.; Verdin, E.; *Genome Biol.* **2004**, *5*, 224. [Crossref]
175. Park, S.-Y.; Kim, J.-S. A Short Guide to Histone Deacetylases Including Recent Progress on Class II Enzymes. *Exp. Mol. Med.* **2020**, *52*, 204212. [Crossref]
176. Pais, T. F.; Szegő, É. M.; Marques, O.; Miller-Fleming, L.; Antas, P.; Guerreiro, P.; de Oliveira, R. M.; Kasapoglu, B.; Outeiro, T. F.; *EMBO J.* **2013**, *32*, 26032616. [Crossref]
177. Bai, Y.-R.; Yang, W.-G.; Hou, X.-H.; Shen, D.-D.; Zhang, S.-N.; Li, Y.; Qiao, Y.-Y.; Wang, S.-Q.; Yuan, S.; Liu, H.-M.; *Eur. J. Med. Chem.* **2023**, *258*, 115606. [Crossref]
178. Wang, Z.; Wesche, H.; Stevens, T.; Walker, N.; Yeh, W.-C.; *Curr. Top. Med. Chem.* **2009**, *9*, 724. [Crossref]
179. Mullard, A.; *Nat. Biotechnol.* **2020**, *38*, 12211223. [Crossref]
180. Ghizzoni, M.; Haisma, H. J.; Maarsingh, H.; Dekker, F. J.; *Drug Discovery Today* **2011**, *16*, 504. [Crossref]
181. Wen, A. Y.; Sakamoto, K. M.; Miller, L. S.; *J. Immunol.* **2010**, *185*, 6413. [Crossref]
182. Tao, J.; Zhang, M.; Wen, Z.; Wang, B.; Zhang, L.; Ou, Y.; Tang, X.; Yu, X.; Jiang, Q.; *Biomed. Pharmacother.* **2018**, *106*, 1727. [Crossref]
183. Cheng-Sánchez, I.; Gosselé, K. A.; Palaferri, L.; Kirillova, M. S.; Nevado, C.; *ACS Med. Chem. Lett.* **2024**, *15*, 355. [Crossref]
184. Miah, A. H.; Smith, I. E. D.; Rackham, M.; Mares, A.; Thawani, A. R.; Nagilla, R.; Haile, P. A.; Votta, B. J.; Gordon, L. J.; Watt, G.; Denyer, J.; Fisher, D. T.; Dace, P.; Giffen, P.; Goncalves, A.; Churcher, I.; Scott-Stevens, P.; Harling, J. D.; *J. Med. Chem.* **2021**, *64*, 12978. [Crossref]
185. Pham, A.-T.; Ghilardi, A. F.; Sun, L.; *Front. Pharmacol.* **2023**, *14*, 1127722. [Crossref]
186. Mares, A.; Miah, A. H.; Smith, I. E. D.; Rackham, M.; Thawani, A. R.; Cryan, J.; Haile, P. A.; Votta, B. J.; Beal, A. M.; Capriotti, C.; Reilly, M. A.; Fisher, D. T.; Zinn, N.; Bantscheff, M.; MacDonald, T. T.; Vossenkamper, A.; Dace, P.; Churcher, I.;

Benowitz, A. B.; Watt, G.; Denyer, J.; Scott-Stevens, P.; Harling, J. D.; *Commun. Biol.* **2020**, *3*, 140. [Crossref]

187. Liu, T.; Zhang, L.; Joo, D.; Sun, S.-C.; *Signal Transduction Targeted Ther.* **2017**, *2*, 17023. [Crossref]
188. Zhang, D.; Gong, H.; Meng, F.; *Molecules* **2021**, *26*, 4907. [Crossref]
189. Neys, S. F. H.; Hendriks, R. W.; Corneth, O. B. J.; *Front. Cell Dev. Biol.* **2021**, *9*, 668131. [Crossref]
190. Lim, Y. S.; Yoo, S.-M.; Patil, V.; Kim, H. W.; Kim, H.-H.; Suh, B.; Park, J. Y.; Jeong, N.; Park, C. H.; Ryu, J. H.; Lee, B.-H.; Kim, P.; Lee, S. H.; *Blood Adv.* **2023**, *7*, 92105. [Crossref]
191. Huang, J.; Ma, Z.; Yang, Z.; He, Z.; Bao, J.; Peng, X.; Liu, Y.; Chen, T.; Cai, S.; Chen, J.; Zeng, Z.; *Eur. J. Med. Chem.* **2023**, *259*, 115664. [Crossref]
192. Takahashi, D.; Moriyama, J.; Nakamura, T.; Miki, E.; Takahashi, E.; Sato, A.; Akaike, T.; Itto-Nakama, K.; Arimoto, H.; *Mol. Cell* **2019**, *76*, 797.e10. [Crossref]
193. Banik, S. M.; Pedram, K.; Wisnovsky, S.; Ahn, G.; Riley, N. M.; Bertozzi, C. R.; *Nature* **2020**, *584*, 291. [Crossref]
194. Yang, J.; Li, Y.; Aguilar, A.; Liu, Z.; Yang, C.-Y.; Wang, S.; *J. Med. Chem.* **2019**, *62*, 9471. [Crossref]
195. Dey, S. K.; Jaffrey, S. R.; *Cell Chem. Biol.* **2019**, *26*, 1047. [Crossref]
196. Maniaci, C.; Hughes, S. J.; Testa, A.; Chen, W.; Lamont, D. J.; Rocha, S.; Alessi, D. R.; Romeo, R.; Ciulli, A.; *Nat. Commun.* **2017**, *8*, 830. [Crossref]

Submitted: February 27, 2024
Published online: August 13, 2024

RÉSUMÉ

CONCEPTION ET SYNTHÈSE DE DERIVES 1,2,4-TRIAZOLES TRISUBSTITUÉS: EXPLORATION STRUCTURALE DE L'INHIBITION DE GSK-3β POUR LE TRAITEMENT DE LA MALADIE D'ALZHEIMER

Ce travail de thèse en cotutelle France -Brésil a été réalisé d'une part entre le laboratoire d'Innovation Thérapeutique (LIT, UMR 7200) à Strasbourg dans l'équipe Chémogénomique et Chimie médicinale (CCM) sous la direction du Dr SCHMITT Martine, et le laboratoire de diversité Moléculaire et chimie Médicinale de l'université Fédérale de Rio de Janeiro sous la direction du Professeur EUGEN KUMMERLE Arthur. L'objectif principal de cette thèse s'articule autour de la conception et la synthèse de dérivés 1,2,4-triazoles trisubstitués: exploration structurale de l'inhibition de GSK-3β pour le traitement de la maladie d'Alzheimer. Ce manuscrit comporte 4 chapitres. Le premier chapitre concerne la synthèse et l'exploration de la diversité moléculaire des triazoles 1, 2, 4 trisubstitués avec comme objectif principal la mise au point de méthodes convergentes. Le chapitre 2 concerne la conception, la synthèse et l'évaluation pharmacologique des dérivés de triazoles diversement fonctionnalisés comme inhibiteurs de GSK-3β. Le Chapitre 3 met en avant la synthèse de chimères (PROTACs) pour moduler la dégradation de la GSK-3β. Compte-tenu de l' impact important de la chimie sur l' environnement, le laboratoire à Strasbourg est impliqué dans la mise au point de réaction métallo-catalysées en milieu aqueux. J'ai ainsi eu l'opportunité de participer à un projet de méthodologie totalement indépendant des 3 chapitres précédents et qui concerne la réaction de cyanation dans des conditions éco-compatibles . Ceci à fait l'objet de mon 4eme Chapitre de Thèse .

INTRODUCTION

Selon l'Organisation mondiale de la santé (OMS), actuellement 55 millions de personnes vivent avec la démence dans le monde et près de 10 millions de nouveaux cas sont enregistrés chaque année. En 2019, le coût sociétal mondial estimé de la démence s'élevait à 1,3 billion de dollars américains et ces coûts devraient dépasser 2,8 billions de dollars américains d'ici 2030. La démence résulte d'une variété de maladies et de blessures qui affectent le cerveau, et sa forme la plus courante est la maladie d'Alzheimer (MA), qui contribue à 60 à 70 % des cas.[1] La MA est une maladie hétérogène causée par de multiples facteurs délétères. Parmi eux, l'accumulation de peptides bêta-amyloïdes et la présence de filaments insolubles associés à la protéine Tau (p-Tau) favorisent la dégénérescence cellulaire et le déficit en neurotransmetteurs tels que l'acétylcholine dans des régions spécifiques du cerveau responsables des fonctions cognitives.[2,3] Actuellement, seuls des médicaments pour le traitement symptomatique de la MA sont disponibles.[4] Les approches thérapeutiques centrées sur la théorie de l'amyloïde se sont

révélées inefficaces ces dernières années,[5] en revanche, les inhibiteurs de Glycogène Synthase Kinase (GSK-3β), liés à la p-Tau, ont montré des résultats prometteurs in vivo, émergeant comme une classe thérapeutique potentiellement modifiante de la maladie, valide pour la MA.[6]

Les inhibiteurs de GSK-3β peuvent avoir une origine naturelle ou synthétique et, en général, présentent des structures très différentes, couvrant une large gamme d'espaces chimiques.[7,8] En fonction de leurs mécanismes d'inhibition, ils sont généralement classés comme compétitifs ou non compétitifs vis-à-vis de l'ATP. La plupart des inhibiteurs appartiennent au premier groupe et agissent en bloquant l'enzyme en concurrençant l'ATP pour son site de liaison. En particulier, la classe des amino/amido-azahétérocycles est largement décrite. Parmi ceux-ci, les acyl-aminopyridines ont vu leur espace chimique systématiquement exploité autour de l'espacement central, conduisant à des inhibiteurs de GSK-3β puissants à une ou plusieurs concentrations inférieures au nanomolaire.[9] Lorsqu'ils sont administrés par voie orale à un modèle murin transgénique de la maladie d'Alzheimer (MA), le composé **1** (voir Fig. 1, IC_{50} = 1,1 nM) a montré une réduction significative de la phosphorylation de Tau. Cette caractéristique repose sur la capacité des aminopyridines à mimer la liaison de l'adénine de l'ATP au site catalytique de GSK-3β par des liaisons hydrogène avec Val135 et Asp133, tandis que leurs substituants cherchent à interagir avec Lys85 et Glu185, région d'interaction triphosphate (Fig. 1). D'autres classes telles que les maléimides (**2**) ont également été largement explorées en tant qu'inhibiteurs de GSK-3β.[7] La structure de base des maléimides peut former des liaisons hydrogène clés avec des acides aminés situés dans la région de charnière enzymatique (même site d'interaction de l'adénine de l'ATP). En particulier, l'atome d'azote interagit avec l'oxygène carbonyle de l'Asp133, tandis que l'un des deux oxygènes carbonyle interagit avec l'azote de la chaîne primaire de Val135 (Fig. 1).[10] Les produits naturels de la classe des Paullones, tels que l'alsterpaullone (**3**), constituent une autre classe intéressante d'inhibiteurs compétitifs de l'ATP.[11] La structure cristalline a révélé que l'alsterpaullone est également capable d'établir des liaisons hydrogène avec Val135, tandis que le groupe nitro établit des interactions de liaison hydrogène avec Lys85 (Fig. 1).

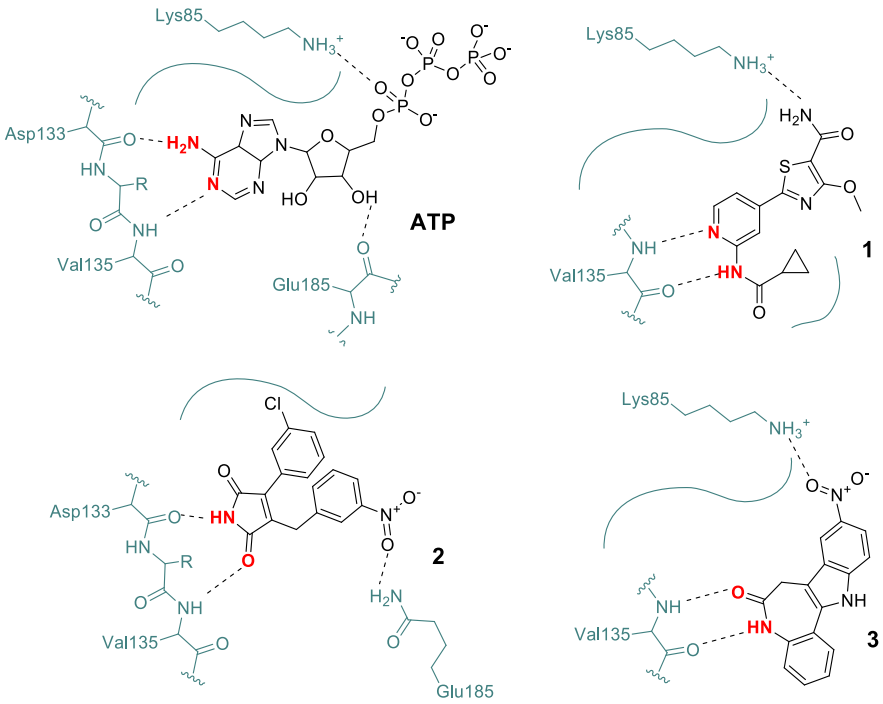

Figure 1. ATP, inhibiteurs compétitifs de GSK-3β (**1-3**) et leurs modes d'interactions sur le site de GSK-3β.

Notre groupe de recherche à l'université Fédérale Rurale de Rio de Janeiro (LadMol-QM, Laboratório de Diversidade Molecular e Química Medicinal) s'est consacré au développement synthétique et à la conception de dérivés du 1,2,4-triazole en tant qu'inhibiteurs d'enzymes impliquées dans la maladie d'Alzheimer.[12] Les dérivés du 1,2,4-triazole ont de nombreuses applications en médecine, en agriculture, en sciences supramoléculaires et des matériaux. En chimie médicinale, ces cycles démontrent un large éventail d'activités biologiques telles que anti-inflammatoires,[13] antibactériennes,[14] antifongiques,[15] antivirales,[16] anticancéreuses,[17] antioxydantes,[18] antituberculeuses,[19] anticonvulsivantes,[20] antinociceptives,[21] antidépressives[22] et anxiolytiques.[23] Un grand nombre de médicaments contenant des 1,2,4-triazoles ont été largement utilisés en clinique, y compris l'alprazolam, le fluconazole, le voriconazole, la ribavirine, le rizatriptan, l'estazolam, le vorozole, l'anastrozole et le létrozole. En agriculture, les 1,2,4-triazoles présentent des activités insecticides et de régulation de la croissance des plantes, comme dans les exemples du cafenstrole, du métosulam, de l'azafénidin, du carfentrazone-éthyl et du sulfentrazone.

Étant donné l'importance du noyau 1,2,4-triazole et l'expertise de notre groupe de recherche dans les réactions de couplage catalysées par les métaux,[24] l'un de nos principaux objectifs récents a été la synthèse chimio et la dérivatisation régiosélective des 1,2,4-triazoles

trisubstitués en utilisant une stratégie pertinente à partir du 3,5-dibromo-1H-1,2,4-triazole facilement disponible. De plus, nous envisageons que nos amino-triazoles pourraient, d'une certaine manière, imiter la liaison de l'anneau adénosine de l'ATP avec les sites catalytiques des kinases. Ainsi, soutenus par des calculs de modélisation moléculaire, nous avons conçu de nouvelles classes de composés iGSK-3β basées sur 3 inhibiteurs compétitifs connus.

RÉSULTATS ET DISCUSSION

En 2019, nous avons décrit l'importance des dérivés du 1,2,4-triazole en tant qu'inhibiteurs de la cholinestérase.[12] Cette série de composés a été synthétisée en six étapes en utilisant une méthode conventionelle avec la fonctionnalisation du noyau triazole dans les premières étapes.

Par la suite, notre objectif principal a été de préparer des dérivés du 1,2,4-triazole selon une méthode plus convergente à partir du dérivé 3,5-dibromo-1H-1,2,4-triazole (**4**) comme intermédiaire clé (Schéma 1). Tout d'abord, cet intermédiaire a été fonctionnalisé par i) alkylation en $\mathbf{N_1}$ avec des différents groupes : méthyle (94%), isopropyle (83%), THP (71%), p-méthoxybenzyle (84%) et ii) N-arylation (60%) mettant en jeu le 4-méthylphényle à l'aide de la réaction de couplage de Chan-Lam catalysée par le cuivre. Nos objectifs généraux portent sur l'introduction facile de divers substituants en position 3 et 5 en combinant à la fois des réactions d'amination et de Suzuki-Miyaura, comme illustré dans le schéma 1. Cependant, en démarrant par une réaction de Suzuki-type prototypique (Na_2CO_3 (2 éq.), $Pd(PPh_3)_4$ (5 mol%), PhMe:EtOH:H_2O (5:1:1), 105°C, 1 h), la haute réactivité des 3,5-dibromotriazoles a conduit à un mélange de mono et di-adduits. Bien que les mono-adduits **6** sont obtenus majoritairement, la purification n'était pas aisée. Dans un deuxième temps, la liaison C-N a été introduite par une réaction de Buchwald-Hartwig (t-BuONa (1,5 éq.), $PdCl(cinnamyl)]_2$ (5 mol%), tBuXPhos (10 mol%), PhMe, 100°C, 16h) avec des amines primaires (68%) et secondaires (13%) (Schéma 1). Le faible rendement obtenu avec les amines secondaires n'a pas encore été optimisé. Au cours de ce travail nous avons inversé l'ordre de réactivité en introduisant le reste amino dans une première étape. Cependant, nous avons observé dans le milieu au départ de **5** un mélange de produits difficilement séparables par chromatographie. La forte réactivité de **5** dans les réactions métallocatalysées nous a conduit étudié la substitution nucléophile aromatique (SNAr) avec des amines primaires (phényléthylamine (48-82%), 4-diméthoxybenzylamine (48%), aniline (36%) et amines secondaires (N-méthylphényléthylamine (69%) et morpholine (84%)), conduisant aux composé mono-aminé **8** respectifs. Enfin, la nouvelle liaison C-C sp2

a été introduite au moyen d'une réaction de Suzuki-Miyaura avec d'excellents rendements (cpsés **9**, 89-90%) (Schéma 1).

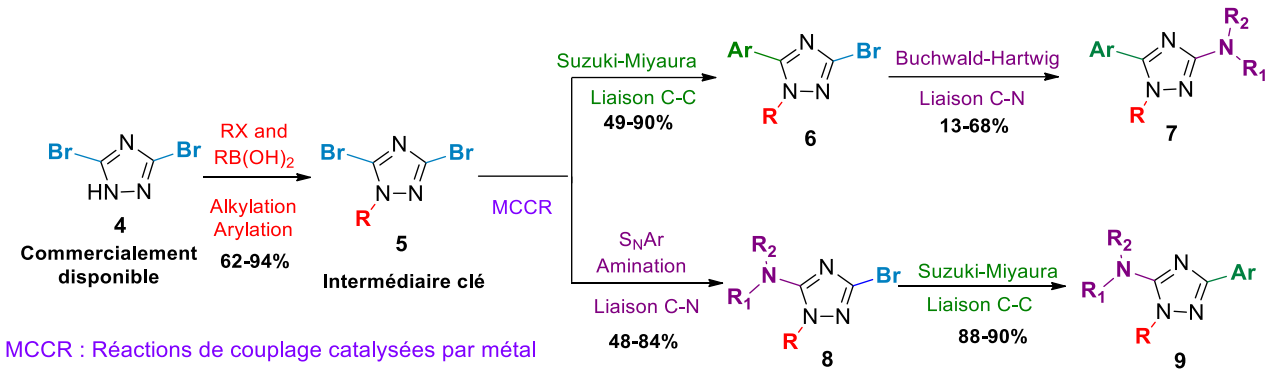

Schéma 1. Méthode convergente pour obtenir des dérivés fonctionnalisés du 1,2,4-triazole.

Afin de différencier la réactivité des deux bromures du composé **5**, nous avons étudié l'introduction d'un groupe O-Tri-O-4,6-triisopropylbenzènesulfonyle (TIPSO, Schéma 2), qui est connu pour être moins réactif dans la réaction de couplage au Palladium (PCCR). Par conséquent, l'intermédiaire clé **5** a d'abord été porté sous reflux dans une solution de soude aqueuse pour donner le composé **10** avec un rendement quantitatif. Ensuite, le dérivé TIPSO **11** a été obtenu avec un rendement de 89% en utilisant le TIPSCl avec la NEt_3 dans le dichlorométhane (DCM). La procédure de Suzuki a été appliquée avec succès pour donner **12** avec un rendement quantitatif, cependant, malgré de nombreuses tentatives pour fonctionnaliser le groupe sulfonate à l'aide de la réaction de Suzuki, tous les efforts se sont révélés infructueux. Par conséquent, nous avons opté pour une étape d' hydrolyse ultérieure dans un milieu d'hydroxyde de sodium (NaOH), conduisant à la formation des dérivés de triazolone (**17**). Pour mieux appréhender la réactivité des iminobromures, nous avons choisi une approche alternative impliquant l'introduction du groupe protecteur méthoxyméthyléther. Le composé **10** a été protégé avec du chlorure de 2-méthoxyéthoxyméthyle en présence de NEt_3 dans le DCM à température ambiante, fournissant **13** avec un rendement de 82%. Ensuite, le produit arylé **14** a été obtenu avec succès en utilisant le protocole de Suzuki avec un rendement de 82%, suivi de la déprotection dans des conditions acides pour produire la triazolone (**17**) (Schéma 2A). **17** a ensuite été activé par de l'oxychlorure de phosphore ($POCl_3$) et la réactivité de l'iminochlorure formé **18** est abordée par l'utilisation de différentes réactions PCCR (Suzuki-Miyaura et Buchwald-Hartwig). L'utilisation de l'acide 4-méthylphénylboronique a conduit au composé **19**

avec un rendement de 72%. En partant de la 2-phényléthylamine, la réaction de Buchwald-Hartwig nous a permis d'obtenir **9** avec un rendement de 80% après purification (Schéma 2B).

Nous avons également étudié la benzylation du triazole comme autre stratégie de protection. Le composé **10** a été traité avec du bromure de benzyle et du carbonate de potassium (K_2CO_3) dans l'acétonitrile (MeCN) pendant 3 heures. Le composé N-arylé (**15**) a été obtenu avec un rendement de 63%, et nous étudions actuellement au laboratoire la réactivité **15** vis-à-vis de la réaction de Buchwald-Hartwig (Schéma 2).

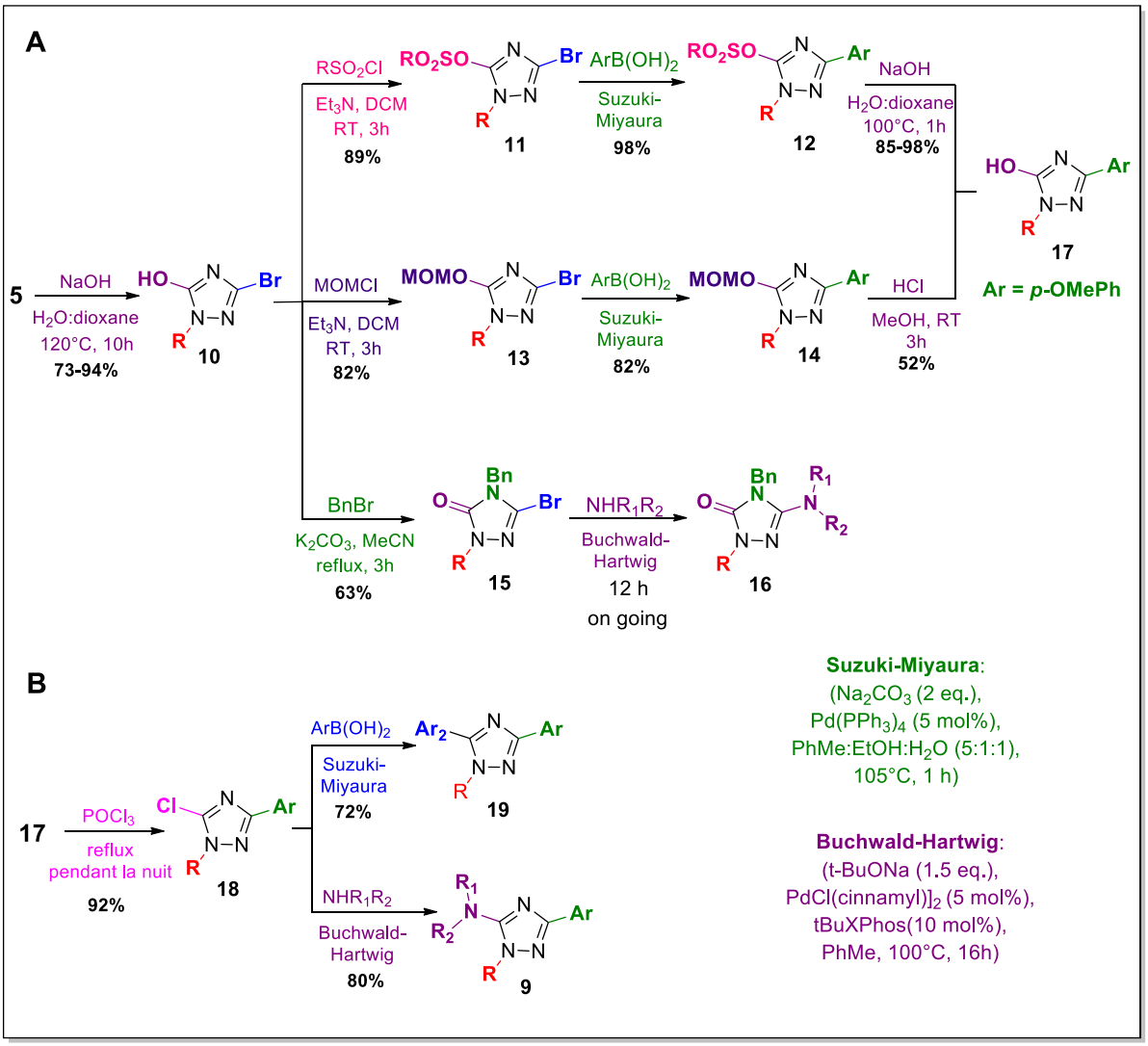

Schéma 2. Désymétrisation des dérivés du 1,2,4-triazole.

Nous avons également préparé le dérivé O-Bn triazole **20** au départ de **5** par action de benzylate de sodium dans le THF. Le composé **20** a été obtenu avec un rendement quantitatif. et a été soumis à une réaction de Suzuki-Miyaura . De manière surprenante un mélange de

produits a été observé, comprenant le produit désiré **21** mais aussi la triazolone **22** dans un rapport de 1:3,5 après purification. D'autre part, le dérivé OBn **20** a également été soumis à une réaction d'amination de type Buchwald-Hartwig, ne produisant que le produit protégé désiré **23**, qui a ensuite été activé avec $POCl_3$ sous reflux, conduisant à l'iminochlorure **24** avec un rendement de 89%. Le comportement de **24** sous les conditions de Suzuki-Miyaura est actuellement en cours au laboratoire, (Schéma 3). Enfin, nous avons voulu étudier la possibilité d'introduire un groupe cyano au départ du composé **5** via une substitution nucléophile aromatique. En utilisant NaCN dans le DMF à 110°C, le triazole cyano **25** a été obtenu en rendement quantitatif et a conduit au dérivé ester correspondant **26** par méthanolyse avec $SOCl_2$ à température ambiante (**26**) (Schéma 3).

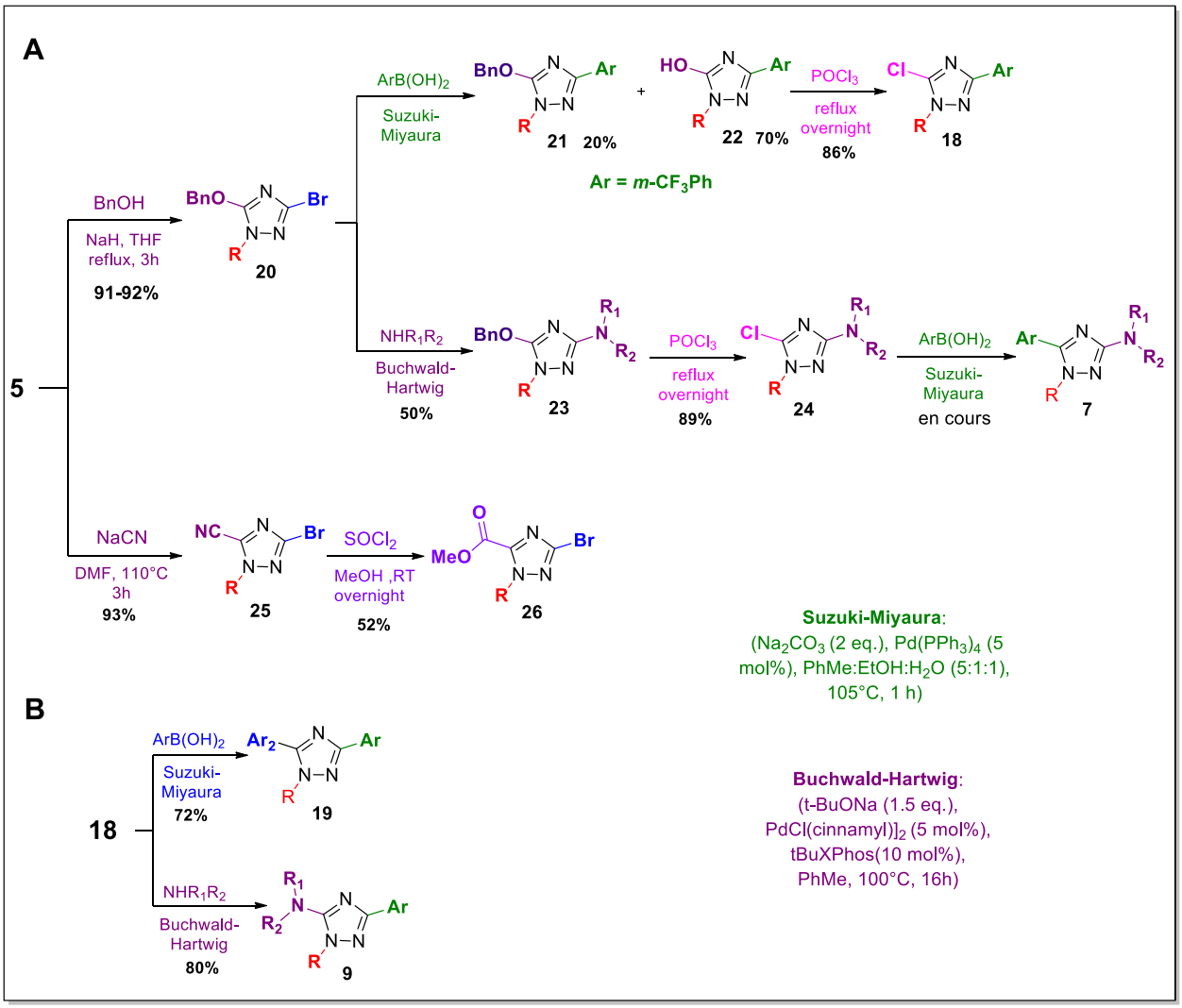

Schéma 3. Désymétrisation des dérivés du 1,2,4-triazole.

Dans une deuxième partie, nous avons entrepris une étude théorique dans le but de concevoir de nouvelles classes de composés iGSK-3β. Cette conception structurale était basée sur trois séries (amino-pyridines - **1** et **27**, paullones - **3** et maléimides - **2**), comme illustré dans le schéma 4. La première classe conçue (**28**) (Schéma 4A) était basée sur un bioisostérisme classique (**a**) de l'amino-pyridine 1 (pyridine → 1,2,4-triazole). Dans ce cas, les 3-amino-1,2,4-triazoles pourraient imiter les interactions avec le site de l'adénine, tout comme les amino-pyridines. En rouge sont mis en évidence les sites possibles d'interaction avec Val135. La transposition du groupe fonctionnel en b avait comme principe la voie de synthèse et le maintien de l'exploration d'une cavité hydrophobe dans la région. Le groupe R dans ce cas pourrait être des groupes alkyles et aromatiques. La deuxième série (**29**) a été proposée à partir de l'alsterpaullone (**3**), à travers les échanges bioisostériques classiques du pyrrole par le 1,2,4-triazole en **c**, et l'ouverture non classique de l'anneau en d. Avec la possible différence spatiale entre les anneaux en d, des groupes fonctionnels tels que les amides, les nitro et les acides carboxyliques peuvent être explorés aux positions 2, 3 et 4 du noyau, visant des interactions par liaisons hydrogène avec Lys85 (Schéma 4B). Enfin, la troisième série (**30**) était basée sur la classe des maléimides **2** qui montrent des interactions au site de l'adénine avec Val135 et Asp133 par des liaisons hydrogène. Pour la **série 2**, la modification du maléimide par le 1,2,4-triazolol a été envisagée, en maintenant exactement les mêmes interactions mises en évidence par les atomes en rouge avec Val135 et Asp133. De plus, la transposition du groupe fonctionnel en e maintiendrait les interactions avec la même cavité hydrophobe du prototype **2** (Schéma 4C).

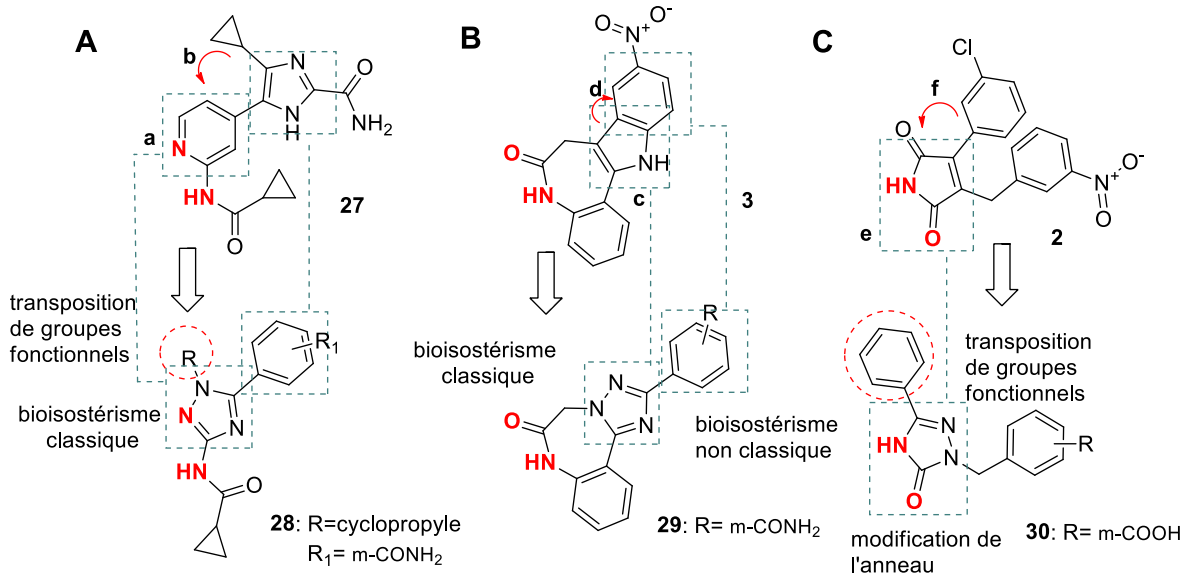

Schéma 4. Séries de 1,2,4-triazoles trisubstitués conçues.

Pour étayer la conception structurale, des analyses de docking moléculaire ont été utilisées pour vérifier théoriquement si les prérequis d'interaction avec le site actif de GSK-3β, discutés ci-dessus, pouvaient être observés. Pour l'analyse, les composés **28a**, **29a** et **30a** ont été utilisés, en plus des prototypes correspondants **27**, **3** et **2**. Les résultats de docking ont indiqué que les composés planifiés pourraient réaliser les principales interactions de leurs prototypes, comme prédit par la planification structurale. De plus, les valeurs de score obtenues pour les composés **29a** (score= 31.05) et **30a** (score= 71.10) étaient assez similaires à celles de leurs prototypes directs (3 (score= 32.39) et **2** (score= 73.39)), tandis que le composé **28a** (score= 57.32) présentait une valeur beaucoup plus élevée que **27** (score= 48.44), indiquant peut-être que la transposition du groupe fonctionnel peut conduire à de meilleures interactions dans la cavité hydrophobe (Figure 2).

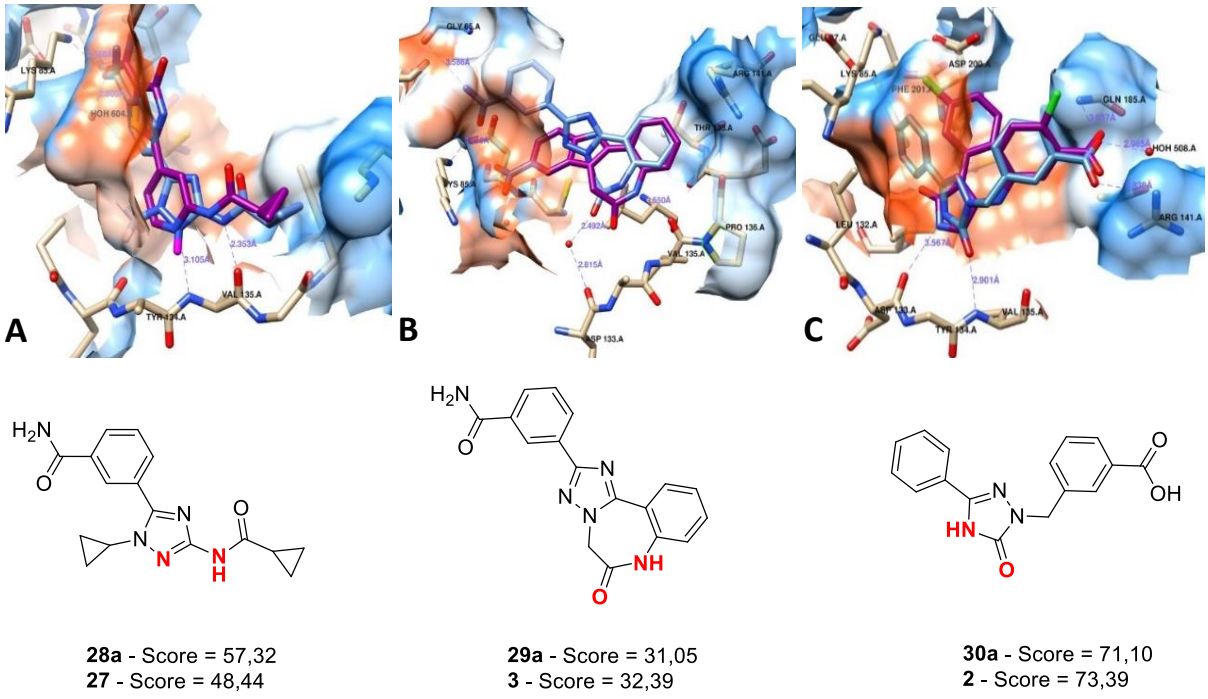

Figure 2. Comparaison des dockings moléculaires dans le site actif de la GSK-3β entre les prototypes d'amino-pyridine **27**, l'alsterspaullone **3** et le maléimide **2** avec les composés **28a** (**A**), **29a** (**B**) et **30a** (**C**). Résultats obtenus à l'aide du logiciel Gold et des PDBs 4PTC (**A**), 1Q3L (**B**) et 1Q4L (**C**).

La synthèse de la troisième série avec le composé **30** comme représentant a commencé par la N-alkylation de **4** avec du 3-(bromométhyl)benzonitrile pour donner **31** avec un

rendement de 79%. Sous reflux dans une solution aqueuse de NaOH, le composé **31** subit 2 transformations simultanées: l'hydrolyse de l'imino-bromure et la conversion du groupe cyano en acide carboxylique pour donner **32** en rendement quantitatif. Ensuite, l'estérification de Fischer-Speier a été appliquée pour obtenir **33** avec un rendement de 94%. Le dérivé TIPSO **34** a été obtenu avec un rendement de 84% en utilisant la même procédure que celle décrite précédemment (TIPSCl et NEt_3 dans le DCM à température ambiante, voir Schéma 2). La procédure de Suzuki a été appliquée avec succès pour fournir **35a-d** avec des rendements de 55 à 98%, suivie d'une étape d'hydrolyse subséquente qui a conduit aux composés **30a-d** avec des rendements bons à excellents (83-99%) (Schéma 5).

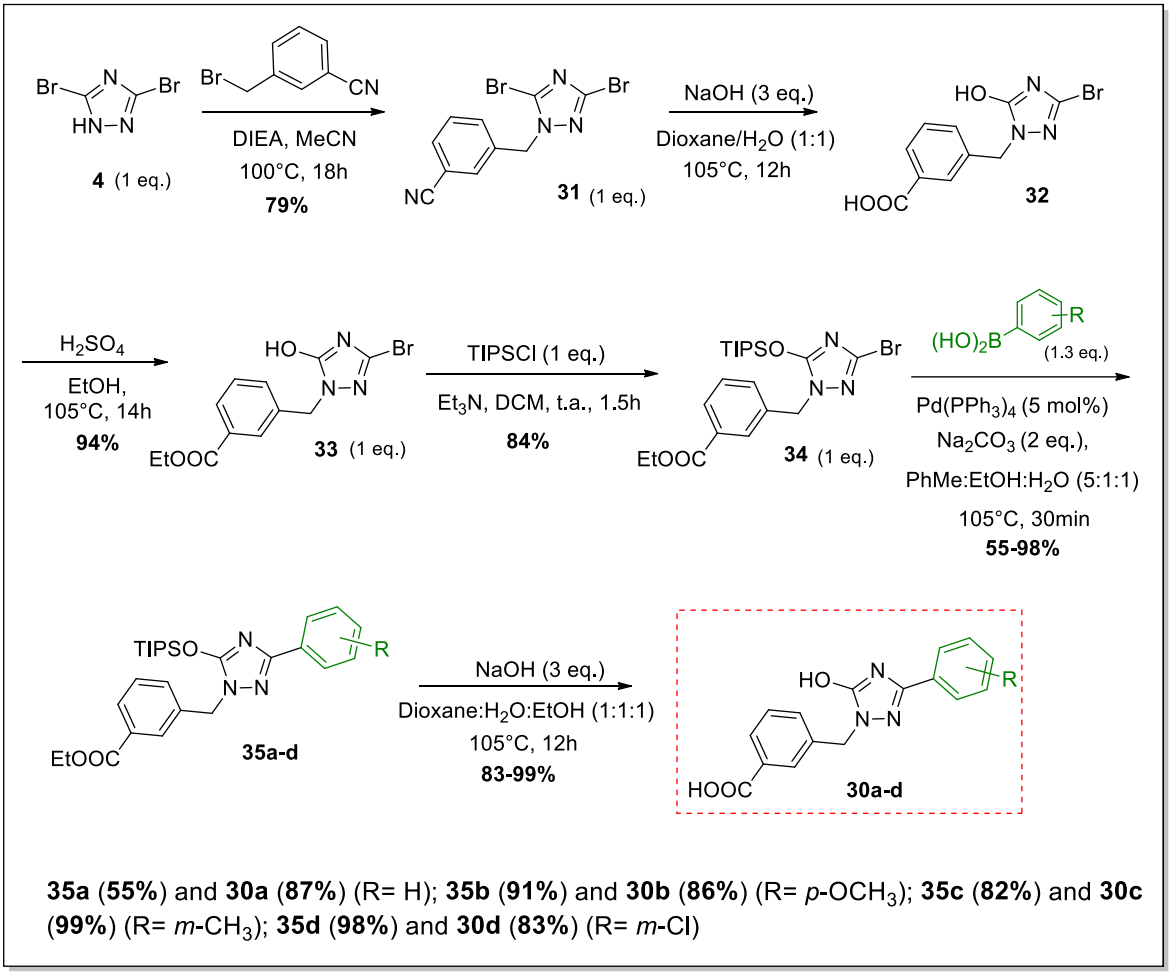

Schéma 5. Synthèse de la série C.

La voie de synthèse pour obtenir la deuxième série avec le composé **29** comme représentant a commencé par la N-alkylation du 3,5-dibromo-1H-1,2,4-triazole avec le tert-butyl-2-bromoacétate pour donner **36** avec un rendement quantitatif. Pour éviter le mélange de

mono et di-adduits dans la procédure de Suzuki, un excès (2 équivalents) de l'intermédiaire alkylé **36** par rapport à l'acide boronique a été appliqué avec succès pour obtenir le mono-adduit **37** comme principal produit avec un rendement de 80%. Ensuite, une réaction de Suzuki-Miyaura a permis l'introduction d'un fragment aromatique en position 3 du noyau triazolique conduisant aux composés **38a-e** avec des rendements modérés à excellents variant de 49 à 94%. Enfin, lors de la dernière étape, les composés **29a-e** ont été obtenus avec des rendements variant entre 67et 91% après conversion de l'ester tert-butylique en ester méthylique à l'aide de $SOCl_2$ dans du MeOH suivi de la cyclisation subséquente dans du toluène à 120°Ct (Schéma 6).

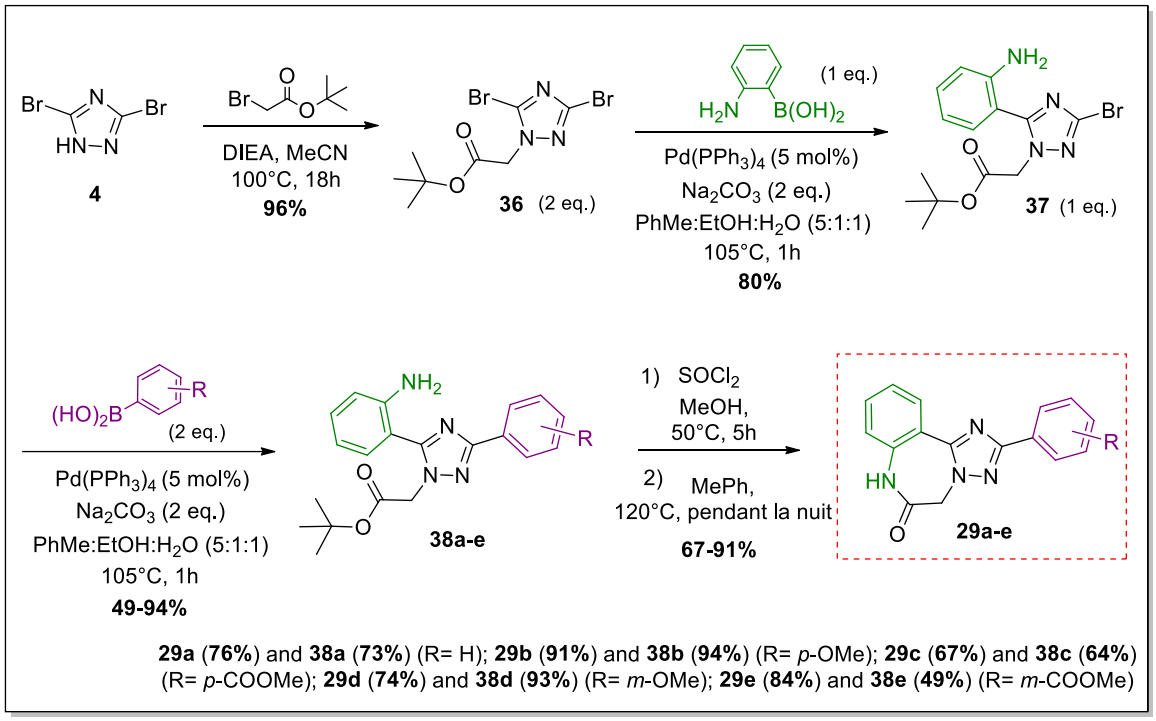

Schéma 6. Synthèse de la **série B** (**29a-e**).

Les composés **29b** et **29d** ont été déméthylés en présence de BBr_3 (6,5 équivalents) dans du DCM sous reflux comme illustré dans le Schéma 7A. Les dérivés p- et m-OH (**29f-g**) ont été obtenus avec des rendements de 83 et 76 %, respectivement, après purification. La saponification des composés **29c** et **29e** avec LiOH a conduit après hydrolyse aux acides carboxyliques attendus **29h-i**. Cependant, nous avons observé par LC/MS la formation d'un sous-produit résultant de l'ouverture du cycle δ-lactame. Le mélange brut a finalement été mis sous reflux dans du toluène pour fournir **29h** (90%) et **29i** (91%). Les dérivés amides m- et p- (**29j-k**) ont été obtenus avec succès en utilisant une solution de NH_3 (7M dans MeOH) avec un

intermédiaire de benzotriazole activé, précédemment obtenu à partir de la réaction in situ du dérivé acide benzoïque (**29i**) avec le chlorhydrate de N-(3-diméthylaminopropyl)-N'-éthylcarbodiimide (EDC.HCl) et de l'hydroxybenzotriazole (HOBt) (Schéma 7B).

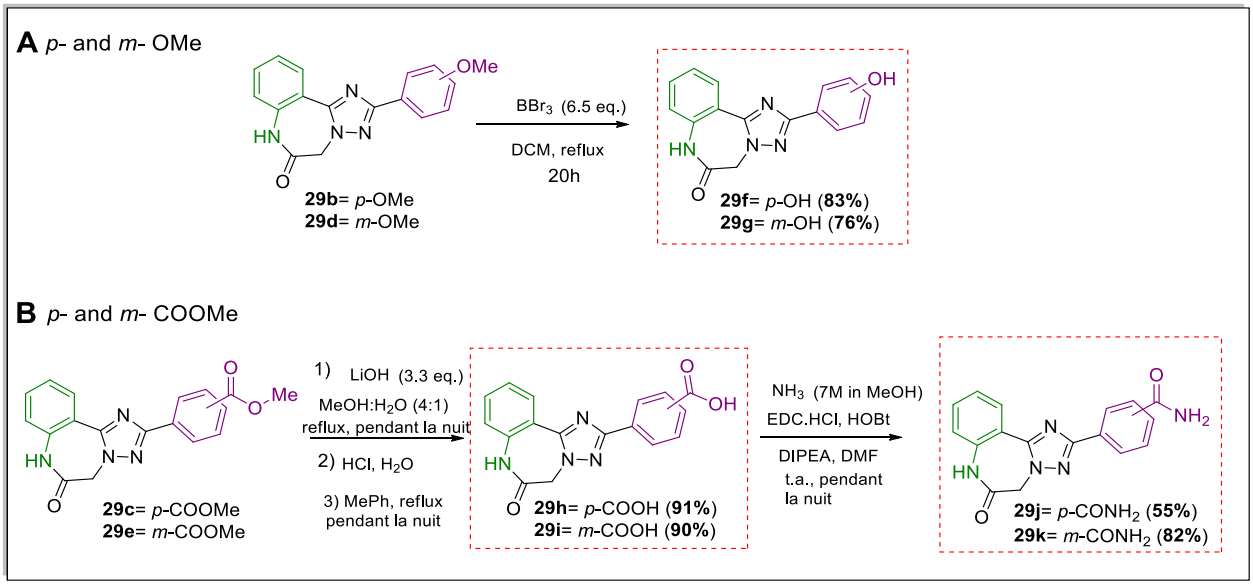

Schéma 7. Synthèse de la **série B** (**29f-k**)

Pour obtenir la première série avec le composé **28** comme représentant, nous avons envisagé les réactions de Buchwald-Hartwig ou d'Ullmann comme moyen efficace d'introduire des amides en position 3 de l'intermédiaire clé **39** (Schéma 8). La réaction de Buchwald-Hartwig ([(cinnamyl)PdCl]$_2$, t-BuXPhos, t-BuONa dans le toluène ou [Pd(allyl)Cl]$_2$, AdBrettPhos, $CsCO_3$ dans le 2-Méthyl-2-Butanol à 100°C pendant 20h) n'a pas donné le produit désiré, tandis que la procédure d'Ullmann (CuI, trans-N,N -Diméthylcyclohexane-1,2-diamine (DMCyDA), K_3PO_4 et ascorbate de sodium dans le toluène ou H_2O:EtOH à 100°C pendant 5h) a montré la formation par LC/MS du composé attendu **40** mais avec plusieurs autres produits, rendant la purification difficile.

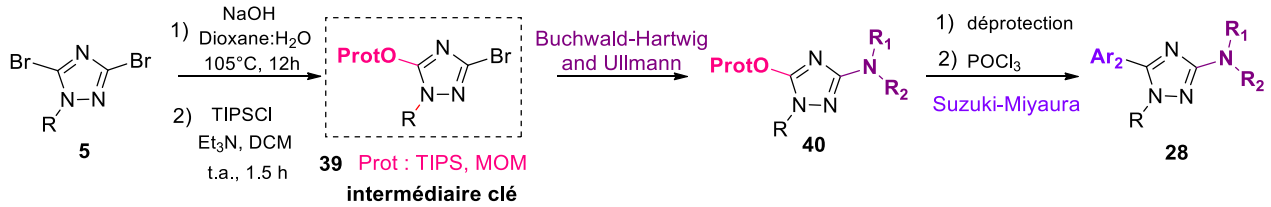

Schéma 8. Synthèse prévue de la **série A**.

En raison de la nécessité d'améliorer la procédure de couplage croisé pour obtenir le composé **28**, mais face au manque de catalyseurs et de conditions appropriées pour travailler avec ce type de réaction lors du stage en Italie, nous avons décidé d'utiliser une voie synthétique conventionelle et non convergente pour obtenir la série A.[12] La première étape a été la synthèse de la S-méthylisothiourée **42** comme décrit précédemment,[25] par alkylation de la thiourée **41**avec de l'iodure de méthyle suivie de précipitation et de filtration (rendement de 99 %). La deuxième étape a été la synthèse de la N-Boc-S-méthylisothiourée en faisant réagir **42** avec du dicarbonate de di-tert-butyle (Boc_2O) dans le DCM à température ambiante. Le composé attendu **43** a été obtenu avec un rendement de 83% puis mis en réaction avec le chlorure de 4-cyanobenzoyle dans le DCM à température ambiante pendant 24 heures, conduisant à l'intermédiaire désiré **44** avec un rendement de 82 % (Schéma 9). Nous avons commencé l'étape de cyclocondensation avec des dérivés d'hydrazine appropriés (c-Pentyl-hydrazine et tolyl-hydrazine) en utilisant la procédure de la littérature (même température: 100°C; et solvant: par exemple MeCN, même durée : 2h). Ces conditions ne se sont pas montrées efficaces. En plus d'une grande quantité du matériel de départ, nous avons observé la formation du triazole Boc attendu mais aussi du triazole déprotégé (**45**). Afin de consommer entièrement **44**, le temps de réaction a été prolongé de 14 heures supplémentaires, conduisant aux produits déprotégés **45** (79 %) et **46** (40 %). L'acylation de **45** a été réalisée en utilisant le chlorure de cyclopropanecarbonyle, avec la pyridine comme base et du DCM à température ambiante. Après 4 heures, la consommation complète de **30** a été observée, fournissant **47** avec un rendement de 46 %. Dans une première tentative de conversion du groupe nitrile en acide carboxylique, le cpd **47** a été traité avec un excès important de NaOH. Ces conditions de réactions ont permis d'hydrolyser quantitativement le nitrile mais ont conduit aussi à la déacetylation du reste cyclopropanecarboxamide, fournissant **48** avec un rendement de 89%. Enfin, en raison de la faible solubilité de **48**, la réaction d'acétylation a été réalisée avec du chlorure de cyclopropane-carbonyle au reflux de la pyridine, conduisant à **49** avec un rendement de 35% après purification (Schéma 9). Le rendement n'a pas encore été optimisé.

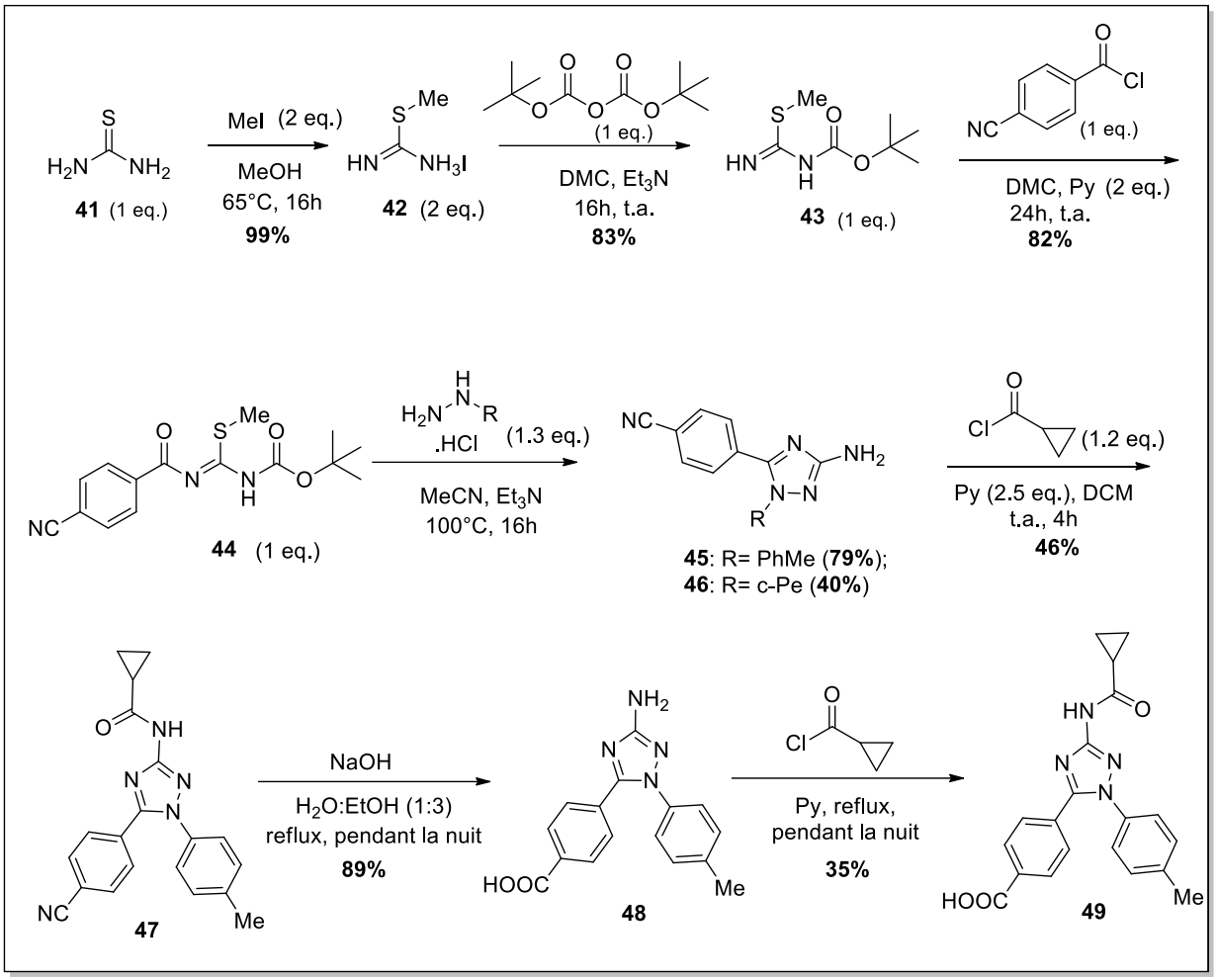

Schéma 9. Synthèse de la **série A**.

Grâce à notre collaboration avec le professeur Angela de Simone (Université de Turin), une évaluation préliminaire de l'activité inhibitrice des composés **29a-j**, **30a-d** et **47** contre la GSK-3β humaine recombinante a été réalisée en utilisant la méthode de Baki.[26] 10 µL de solutions des composés (20 µM - concentration finale) et d'ATP (1 µM) dans un tampon phosphate (pH 7,5) ont été ajoutés séquentiellement à chaque puits dans une plaque de 96 puits de couleur blanche. Après 1 minute, 10 µL de substrat polypeptidique (25 µM) et d'enzyme (GSK-3β) (20 ng) ont été ajoutés et la plaque d'essai a été incubée à 30°C pendant 30 min. Ensuite, le réactif de détection Kinase-Glo a été ajouté et la quantité de luminescence a été enregistrée après 10 minutes dans un lecteur de plaque à plusieurs puits Victor X3 PerkinElmer. L'activité inhibitrice a été calculée en fonction de la valeur de luminescence (Tableau 1).[26]

Tableau 1. Effets des composés **29a-j**, **30a-d** et **47** sur l'activité de la GSK-3β.

Composé	R	%Inhibition @10 µM	IC_{50} [µM]
29a	H	42.3	-
29b	*p*-OMe	9	-
29c	*p*-COOMe	14.3	-
29d	*m*-OMe	15.2	-
29[e]	*m*-COOMe	52	44
29f	*p*-OH	49.7	15
29g	*m*-OH	71.2	2.5
29h	*p*-COOH	4	-
29i	*m*-COOH	42	21
29j	*p*-$CONH_2$	15.7	-
30a	H	n.i.	-
30b	*p*-OMe	n.i.	-
30c	*m*-Me	n.i.	-
30d	*m*-Cl	n.i.	-
47	-	n.i.	-

n.i. – pas d'inhibition

Les résultats de l'activité inhibitrice ont montré que la série conçue **30a-d** n'a montré aucune inhibition contre la GSK-3β. Nous attribuons ce résultat au tautomère iminol (-N=C-OH) prédominant en solution plutôt qu'à l'amide (-NH-C=O) qui est essentiel pour l'interaction avec les acides aminés environnants (valine et acide aspartique). D'autre part, afin d'expliquer l'inactivité du composé **47** nous émettons l' hypothèse suivante : contrairement à la première série (composés **28)**, la présence du groupe p-tolyle, un substituant plus volumineux que les groupes -méthyle ou -cyclopropyle, n'autorise pas le composé **47** à s'adapter dans le site catalytique de la GSK-3β. Enfin, de manière très encourageante, les résultats obtenus pour la deuxième série conçue (composés **29**) sont prometteurs et le motif de substitution des fractions aromatiques semble jouer un rôle important pour l'inhibition de la GSK-3β, avec le composé **29g** montrant le meilleur profil inhibiteur. Une évaluation plus poussée du profil inhibiteur de la GSK-3β est en cours.

Nous avons effectué des calculs de modélisation moléculaire pour vérifier si les résultats de l'activité inhibitrice sont conformes au modèle théorique précédemment utilisé. Pour cela, les composés méta-substitués ont été comparés et selon les calculs de docking, **29g** a également

montré le meilleur profil avec un score plus élevé (Figure 3B). Ce résultat nous inspire, nous incitant à poursuivre les investigations sur les relations structure-activité et les optimisations, actuellement en cours.

A

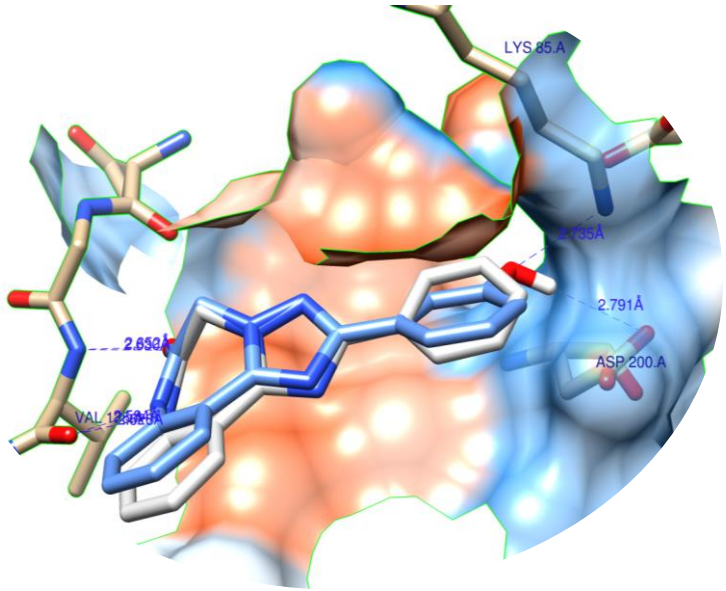

B

Composé	Score
29a	29.1
29g	32.2
29d	32.0
29k	31.5
Alsterpaullone	32.4

Figure 3. A - Analyse de docking; **B** - Tableau des calculs de mécanique moléculaire

La technologie PROTAC

Récemment, un nouveau paradigme dans la conception de médicaments est apparu, appelé chimières de ciblage de protéolyse (PROTAC).[27] Cette modalité révolutionnaire vise à contrôler le niveau des protéines plutôt que leur fonction. En effet, les PROTACs n'inhibent pas une protéine d'intérêt donnée (POI) mais induisent sa dégradation en se liant à elle et en exploitant le système de dégradation cellulaire ubiquitine-protéasome (UPS). Sur la base de ce mécanisme, les PROTACs peuvent éliminer différentes quantités de protéines même à faible dose et, en même temps, éviter de nombreux problèmes associés aux petites molécules inhibitrices classiques des protéines, tels que les effets secondaires et la résistance aux médicaments.[27–29] Plus de 1000 PROTACs différents ont été décrits depuis le premier rapport il y a 20 ans et certains d'entre eux ont été approuvés pour des essais cliniques.[30]

Depuis ces dernières années, trois groupes de recherche indépendants ont publié des études sur les PROTACs ciblant la GSK-3β.[29,31,32] Ces trois PROTACs ont été capables

d'induire la dégradation de la GSK-3β dans les cellules, et l'un d'entre eux s'est également révélé efficace dans un modèle murin de la maladie d'Alzheimer.[32]

En raison de la disponibilité d'une nouvelle série d'inhibiteurs de la GSK-3β (**29a-j**), nous avons cherché à développer de nouveaux PROTACs caractérisés par différents types de liaisons et notre recruteur de GSK-3β non exploré. Particulièrement, nous étions intéressés à évaluer s'il y avait une différence entre les différents types de liaisons et les éléments de recrutement de ligases E3 (Figure 4B). En analysant le modèle théorique, il est apparu que les positions **a**, **b** et **c** de **29a** pourraient être de bons candidats pour des modifications afin de construire les PROTACs. Ces positions ne présentent pas de groupes fonctionnels essentiels pour l'activité de la GSK-3β face à la région solvant de cette kinase. Ensuite, différents types de liaisons pourraient être attachés à **a**, **b** ou **c** pour relier le 1,2,4-triazole (**29a**) aux éléments de recrutement de ligases E3 (pomalidomide et 5-aminotthalidomide) (Figure 4A). Étant donné que le potentiel de dégradation des PROTACs dépend de leur capacité à former un complexe ternaire avec le POI et la ligase E3, nous avons émis l'hypothèse d'utiliser six liaisons de différentes longueurs et formes. Nous avons sélectionné des motifs communs (PEG et alkyle) incorporés dans les PROTACs en raison de leurs propriétés favorables en termes de flexibilité, de disponibilité et de profil physico-chimique. À la recherche d'une plus grande rigidité, nous avons également sélectionné des liaisons avec des composés cycliques tels que la pipéridine et la pipérazine. Les structures proposées à construire sont représentées dans la figure 4.

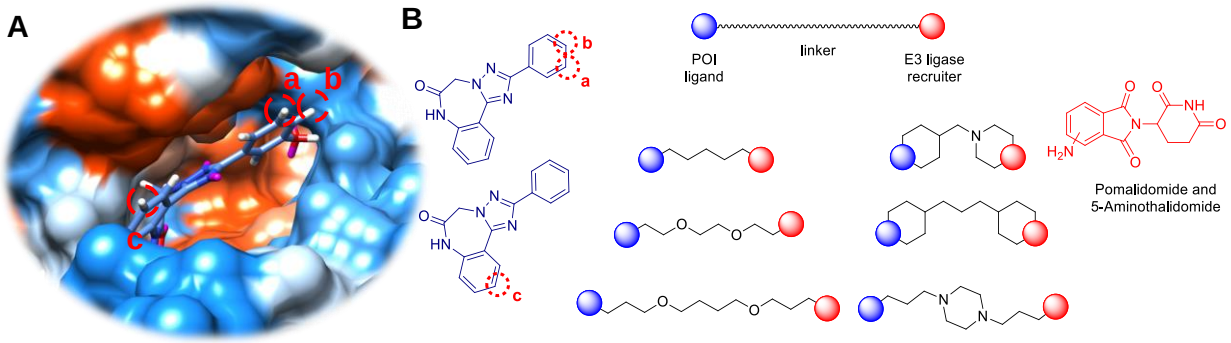

Figure 4. A - Docking moléculaire de 29a et du site catalytique de la GSK-3β. **B** - PROTACs proposés à construire.

La synthèse des PROTAC a commencé par une monoprotection N-Boc des diamines **50-54**. La protection a été réalisée avec du Boc_2O dans du DCM à température ambiante pendant

3 heures, produisant respectivement les composés **56-60** avec des rendements de 68 à 95% (Schéma 10A). Par substitution nucléophile (S_N2), le N-Boc-4-(bromométhyl)pipéridine (**55**) a réagi avec un excès important de pipérazine (10 éq.) à reflux pendant 16 heures, donnant **61** avec un rendement de 88% après précipitation et filtration (Schéma 10B).

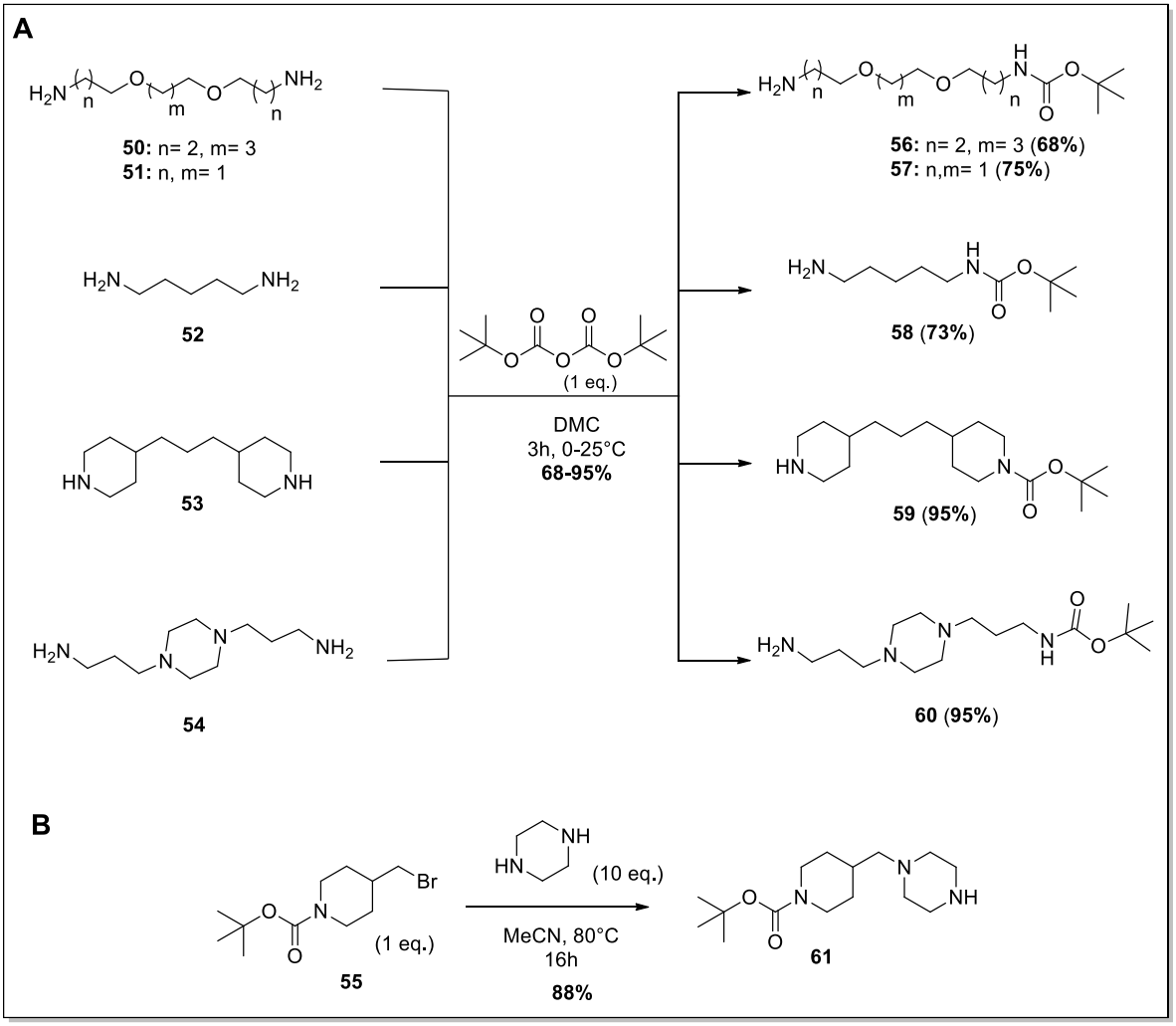

Schéma 10. Synthèse des dérivés N-Boc **56-61**.

Les dérivés de pomalidomide **62-67** ont été synthétisés par des réactions SNAr impliquant le 5-Fluorothalidomide et les amines précédemment synthétisées **56-61**. Les réactions ont suivi un protocole standardisé utilisant le diméthylsulfoxyde (DMSO) comme solvant, avec du diisopropyléthylamine (DIPEA) comme base à 90°C pendant 16 heures. Les procédures de purification (chromatographie sur gel de silice) ont permis d'obtenir les composés avec des rendements allant de 33 à 92% (Schéma 13).

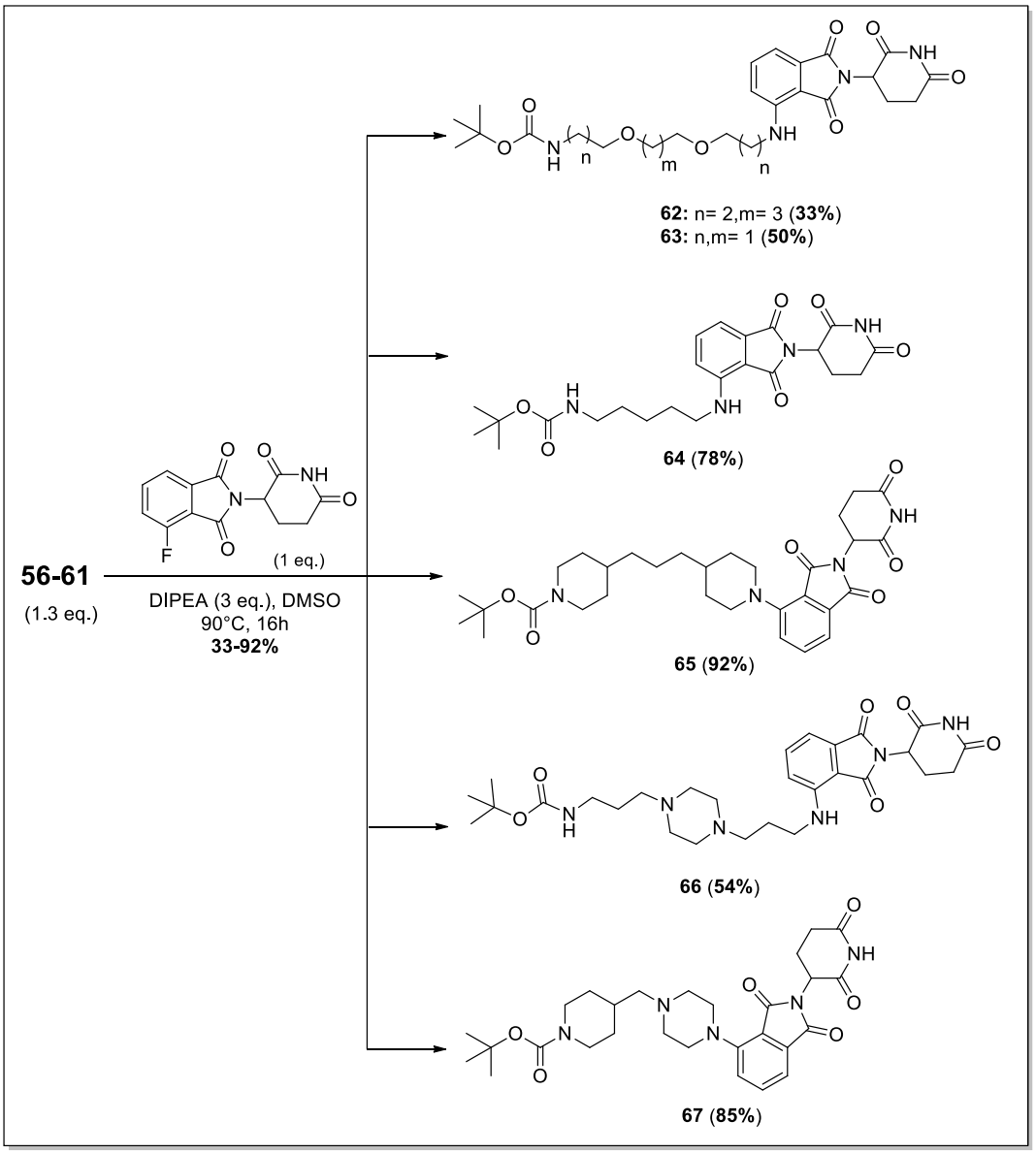

Schéma 13. Synthèse des dérivés de pomalidomide.

Les composés de pomalidomide (**62-67**) ont été déprotégés à l'aide de l'acide trifluoroacétique (TFA) puis utilisés directement dans l'étape de couplage avec le composé **29i** sans étape de purification supplémentaire. L'utilisation de l'EDC.HCl à l'aide de HOBT et de la DIPEA a permis d'obtenir les PROTACs désirés 68-73 avec des rendements variant de 37 à 66% après purification (Schéma 14). Actuellement, les PROTACs conçus **68-73** sont en cours d'évaluation pour l'inhibition et la dégradation de GSK-3β.

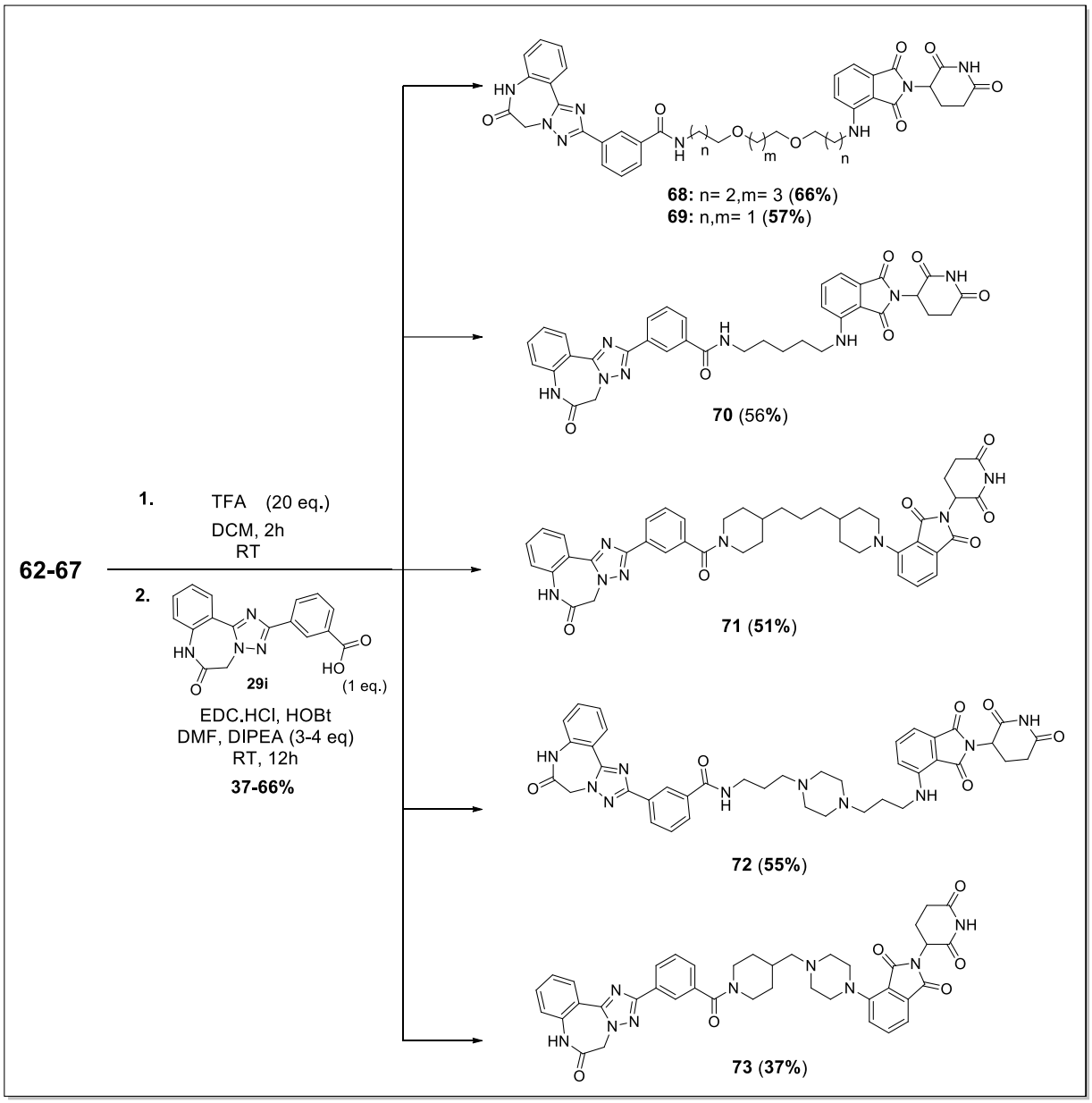

Schéma 14. Conception et Synthèse des PROTACs .

Réaction de cyanation catalysée par le cuivre dans l'eau

Les nitriles aryles sont des éléments de construction importants pour de nombreux médicaments, herbicides, produits naturels et colorants.[33] La compacité du groupe nitrile, ainsi que sa capacité à accepter l'hydrogène et sa stabilité métabolique in vivo, en ont fait un groupe fonctionnel significatif pour la recherche en chimie médicinale.[34] Actuellement, il existe plus de 30 médicaments approuvés, ainsi que 20 candidats médicamenteux en phases d'essais cliniques, contenant un ou plusieurs substituants nitrile dans leur composition chimique. La

fonction nitrile sert de précurseur synthétique excellent pour une variété de groupes fonctionnels, tels que les amides, les cétones, les amines et les alcools. Pour ces raisons, une attention significative a été accordée au développement de méthodologies efficaces et pratiques pour la synthèse de nitriles aryles.

Historiquement, la stratégie de synthèse la plus populaire est la réaction classique de Rosenmund-von Braun.[35] En raison des quantités stoichiométriques de résidus métalliques générés, ce processus ne répond pas aux critères actuels de la synthèse durable. Les procédures à base de cuivre utilisent généralement des sources toxiques de cyanure (KCN, NaCN, CuCN, $Zn(CN)_2$, TMSCN), en plus de températures élevées. L'utilisation de sources de cyanure moins toxiques telles que K4[$Fe(CN)_6$ s'est avérée efficace mais uniquement dans des solvants amides hautement polaires (DMF, NMP) et à des températures élevées (130-155°C).[36] La cyanation aryle a également été rapportée dans l'eau, en utilisant $K_4[Fe(CN)_6$ comme source de cyanure, catalysée par le cuivre à des températures élevées (175°C).[37–39] Néanmoins, le manque de tolérance pour de nombreux groupes fonctionnels et les conditions de réaction sévères rendent ce protocole moins adapté à la synthèse de benzonitriles fonctionnalisés. (Schéma 15). Dans ce contexte, l'équipe a développé une méthode de cyanation plus respectueuse de l'environnement en utilisant le nitroprussiate de sodium comme source de nitrile non toxique, le $CuBr_2$ comme catalyseur, la trans-N,N′-Dimethylcyclohexane-1,2-diamine (DmcHexDA, L1)comme ligand et NaOH comme Base, de l'eau comme solvant vert et une température de réaction inférieure à 80°C (Schéma 15). Cette réaction a été conduite en présence de D-Glucose (D-glc) afin d'éviter l'oxydation du Cu(I) en Cu(II) dans l'eau. Ce réducteur avait montré son efficacité dans la N-arylation de type Ullmann des amines primaires des amides et azoles dans l'eau.[40,41]

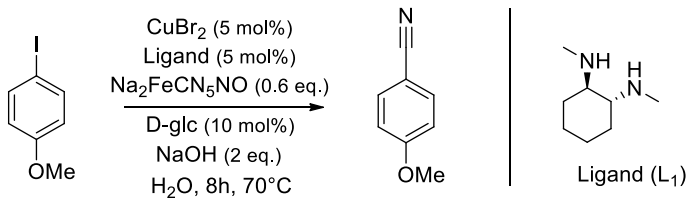

Schéma 15. Réaction de cyanation dans l'eau.

Cependant, ce protocole de réaction présentait des problèmes de reproductibilité avec des fluctuations constantes dans les rendements de réaction. Par conséquent, l'objectif de ce travail était de simplifier le protocole de réaction et de réduire ou d'éliminer les problèmes de

reproductibilité. Une des manières de simplifier le protocole a été de préparer au préalable le complexe Cu-L1 (Complexe C1).

Pour la synthèse du complexe de cuivre, des solutions indépendantes de $CuBr_2.H_2O$ et de ligand (**L_1**) ont été préparées dans de l'éthanol. La solution métallique a été ajoutée lentement à la solution de ligand sous agitation, et le mélange de réaction a été maintenu à température ambiante pendant toute une nuit. Le précipité formé a été filtré pour fournir le complexe **C_1** avec un rendement de 85 % (Schéma 16). Une petite portion du solide a été redissoute dans du méthanol et soumise à une évaporation lente à basse température pour former des cristaux qui ont été étudiés par cristallographie. (schéma 16)

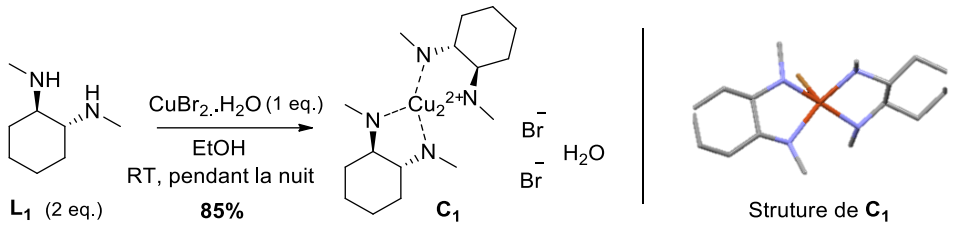

Schéma 16. Synthèse du pré-catalyseur et sa structure cristalline.

Pour l'optimisation des conditions de réaction de la cyanation, nous avons étudié divers paramètres : l'influence du D-glucose (D-glc), la nature de la base, la présence d'un co-solvant, d'un piège à radicaux, la taille du solide (application de la mécano-chimie), la quantité de base, **C_1** et Na_2FeCN_5NO. Après avoir réalisé tous les tests, les meilleures conditions de réaction trouvées sont résumées ici : **C_1** (10 mol%), Na_2FeCN_5NO (0,6 eq.), NaOH (1,7 eq.), H_2O, 6 h, 70°C (Schéma 17).

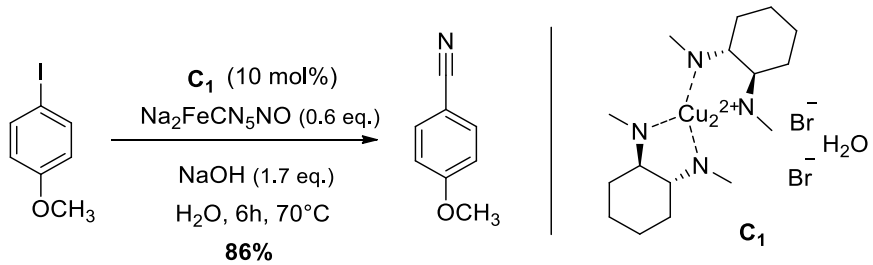

Scheme 17. Réaction de cyanation optimisée dans l'eau.

Les tests effectués ont montré que i) il n'est pas nécessaire d'utiliser du D-glc, ii) une réduction substantielle du temps de préparation de la réaction, iii) une simplification du

protocole méthodologique en raison de la nature hygroscopique du ligand précédemment utilisé (**L_1**), et iv) une diminution des fluctuations observées dans les rendements de réaction.

Actuellement une approche statistique (Design of Experiment,DoE) est utilisée par le Dr Kevin Brugemann pour déterminer les quantités idéales de réactifs utilisées, et l'étude de la portée et des limitations de la réaction en vue d'une publication est en cours.

CONCLUSIONS

Le 3,5-dibromo-1H-1,2,4-triazole disponible commercialement s'est révélé être un matériel de départ polyvalent, garantissant une exploration directe de la diversité structurale.

Les voies de synthèse pour obtenir les séries et les PROTACs conçus ont été développées avec succès. À noter, les composés **29a-j** appartiennent à une nouvelle classe d'hétérocycles et à une nouvelle structure pour l'inhibition de GSK-3β. De manière encourageante, les résultats de l'activité inhibitrice sont prometteurs, incitant à de nouvelles optimisations.

Le protocole de réaction pour la cyanation catalysée par le cuivre dans l'eau en utilisant une source non toxique de cyanure a été avec succès optimisé. Actuellement, la synthèse d'une série de nitriles aryles est en cours pour publication scientifique.

BIBLIOGRAPHIE

(1) *Dementia*. https://www.who.int/news-room/fact-sheets/detail/dementia (accessed 2024-02-06).

(2) Nichols, E.; Szoeke, C. E. I.; Vollset, S. E.; Abbasi, N.; Abd-Allah, F.; Abdela, J.; Aichour, M. T. E.; Akinyemi, R. O.; Alahdab, F.; Asgedom, S. W.; Awasthi, A.; Barker-Collo, S. L.; Baune, B. T.; Béjot, Y.; Belachew, A. B.; Bennett, D. A.; Biadgo, B.; Bijani, A.; Sayeed, M. S. B.; Brayne, C.; Carpenter, D. O.; Carvalho, F.; Catalá-López, F.; Cerin, E.; Choi, J.-Y. J.; Dang, A. K.; Degefa, M. G.; Djalalinia, S.; Dubey, M.; Duken, E. E.; Edvardsson, D.; Endres, M.; Eskandarieh, S.; Faro, A.; Farzadfar, F.; Fereshtehnejad, S.-M.; Fernandes, E.; Filip, I.; Fischer, F.; Gebre, A. K.; Geremew, D.; Ghasemi-Kasman, M.; Gnedovskaya, E. V.; Gupta, R.; Hachinski, V.; Hagos, T. B.; Hamidi, S.; Hankey, G. J.; Haro, J. M.; Hay, S. I.; Irvani, S. S. N.; Jha, R. P.; Jonas, J. B.; Kalani, R.; Karch, A.; Kasaeian, A.; Khader, Y. S.; Khalil, I. A.; Khan, E. A.; Khanna, T.; Khoja, T. A. M.; Khubchandani, J.; Kisa, A.; Kissimova-Skarbek, K.; Kivimäki, M.; Koyanagi, A.; Krohn, K. J.; Logroscino, G.; Lorkowski, S.; Majdan, M.; Malekzadeh, R.; März, W.; Massano, J.; Mengistu, G.; Meretoja, A.; Mohammadi, M.; Mohammadi-Khanaposhtani, M.; Mokdad, A. H.; Mondello, S.; Moradi, G.; Nagel, G.;

Naghavi, M.; Naik, G.; Nguyen, L. H.; Nguyen, T. H.; Nirayo, Y. L.; Nixon, M. R.; Ofori-Asenso, R.; Ogbo, F. A.; Olagunju, A. T.; Owolabi, M. O.; Panda-Jonas, S.; Passos, V. M. de A.; Pereira, D. M.; Pinilla-Monsalve, G. D.; Piradov, M. A.; Pond, C. D.; Poustchi, H.; Qorbani, M.; Radfar, A.; Reiner, R. C.; Robinson, S. R.; Roshandel, G.; Rostami, A.; Russ, T. C.; Sachdev, P. S.; Safari, H.; Safiri, S.; Sahathevan, R.; Salimi, Y.; Satpathy, M.; Sawhney, M.; Saylan, M.; Sepanlou, S. G.; Shafieesabet, A.; Shaikh, M. A.; Sahraian, M. A.; Shigematsu, M.; Shiri, R.; Shiue, I.; Silva, J. P.; Smith, M.; Sobhani, S.; Stein, D. J.; Tabarés-Seisdedos, R.; Tovani-Palone, M. R.; Tran, B. X.; Tran, T. T.; Tsegay, A. T.; Ullah, I.; Venketasubramanian, N.; Vlassov, V.; Wang, Y.-P.; Weiss, J.; Westerman, R.; Wijeratne, T.; Wyper, G. M. A.; Yano, Y.; Yimer, E. M.; Yonemoto, N.; Yousefifard, M.; Zaidi, Z.; Zare, Z.; Vos, T.; Feigin, V. L.; Murray, C. J. L. Global, Regional, and National Burden of Alzheimer's Disease and Other Dementias, 1990–2016: A Systematic Analysis for the Global Burden of Disease Study 2016. *The Lancet Neurology* **2019**, *18* (1), 88–106. https://doi.org/10.1016/S1474-4422(18)30403-4.

(3) 2020 Alzheimer's Disease Facts and Figures. *Alzheimers Dement* **2020**. https://doi.org/10.1002/alz.12068.

(4) *Divulgação anual | IBGE*. https://www.ibge.gov.br/estatisticas/sociais/populacao/17270-pnad-continua.html?edicao=20915&t=sobre (accessed 2024-05-12).

(5) Hardy, J. Testing Times for the "Amyloid Cascade Hypothesis." *Neurobiol Aging* **2002**, *23* (6), 1073–1074. https://doi.org/10.1016/s0197-4580(02)00042-8.

(6) Goedert, M. Tau Protein and Neurodegeneration. *Semin Cell Dev Biol* **2004**, *15* (1), 45–49. https://doi.org/10.1016/j.semcdb.2003.12.015.

(7) Kramer, T.; Schmidt, B.; Lo Monte, F. Small-Molecule Inhibitors of GSK-3: Structural Insights and Their Application to Alzheimer's Disease Models. *Int J Alzheimers Dis* **2012**, *2012*, 381029. https://doi.org/10.1155/2012/381029.

(8) Xu, M.; Wang, S. L.; Zhu, L.; Wu, P. Y.; Dai, W. B.; Rakesh, K. P. Structure-Activity Relationship (SAR) Studies of Synthetic Glycogen Synthase Kinase-3β Inhibitors: A Critical Review. *Eur J Med Chem* **2019**, *164*, 448–470. https://doi.org/10.1016/j.ejmech.2018.12.073.

(9) Sivaprakasam, P.; Han, X.; Civiello, R. L.; Jacutin-Porte, S.; Kish, K.; Pokross, M.; Lewis, H. A.; Ahmed, N.; Szapiel, N.; Newitt, J. A.; Baldwin, E. T.; Xiao, H.; Krause, C. M.; Park, H.; Nophsker, M.; Lippy, J. S.; Burton, C. R.; Langley, D. R.; Macor, J. E.; Dubowchik, G. M. Discovery of New Acylaminopyridines as GSK-3 Inhibitors by a Structure Guided in-Depth Exploration of Chemical Space around a Pyrrolopyridinone Core. *Bioorg Med Chem Lett* **2015**, *25* (9), 1856–1863. https://doi.org/10.1016/j.bmcl.2015.03.046.

(10) Bertrand, J. A.; Thieffine, S.; Vulpetti, A.; Cristiani, C.; Valsasina, B.; Knapp, S.; Kalisz, H. M.; Flocco, M. Structural Characterization of the GSK-3beta Active Site Using Selective and Non-Selective ATP-Mimetic Inhibitors. *J Mol Biol* **2003**, *333* (2), 393–407. https://doi.org/10.1016/j.jmb.2003.08.031.

(11) Leost, M.; Schultz, C.; Link, A.; Wu, Y. Z.; Biernat, J.; Mandelkow, E. M.; Bibb, J. A.; Snyder, G. L.; Greengard, P.; Zaharevitz, D. W.; Gussio, R.; Senderowicz, A. M.; Sausville, E. A.; Kunick, C.; Meijer, L. Paullones Are Potent Inhibitors of Glycogen Synthase Kinase-3beta and Cyclin-Dependent Kinase 5/P25. *Eur J Biochem* **2000**, *267* (19), 5983–5994. https://doi.org/10.1046/j.1432-1327.2000.01673.x.

(12) Santos, S. N.; Souza, G. A. de; Pereira, T. M.; Franco, D. P.; Cistia, C. de N. D.; Sant'Anna, C. M. R.; Lacerda, R. B.; Kümmerle, A. E. Regioselective Microwave Synthesis and Derivatization of 1,5-Diaryl-3-Amino-1,2,4-Triazoles and a Study of

Their Cholinesterase Inhibition Properties. *RSC Adv.* **2019**, *9* (35), 20356–20369. https://doi.org/10.1039/C9RA04105B.
(13) Palaska, E.; Sahin, G.; Kelicen, P.; Durlu, N. T.; Altinok, G. Synthesis and Anti-Inflammatory Activity of 1-Acylthiosemicarbazides, 1,3,4-Oxadiazoles, 1,3,4-Thiadiazoles and 1,2,4-Triazole-3-Thiones. *Farmaco* **2002**, *57* (2), 101–107. https://doi.org/10.1016/s0014-827x(01)01176-4.
(14) Demirbas, N.; Karaoglu, S. A.; Demirbas, A.; Sancak, K. Synthesis and Antimicrobial Activities of Some New 1-(5-Phenylamino-[1,3,4]Thiadiazol-2-Yl)Methyl-5-Oxo-[1,2,4]Triazole and 1-(4-Phenyl-5-Thioxo-[1,2,4]Triazol-3-Yl)Methyl-5-Oxo-[1,2,4]Triazole Derivatives. *European Journal of Medicinal Chemistry* **2004**, *39* (9), 793–804. https://doi.org/10.1016/j.ejmech.2004.06.007.
(15) Shalini, K.; Kumar, N.; Drabu, S.; Sharma, P. K. Advances in Synthetic Approach to and Antifungal Activity of Triazoles. *Beilstein J Org Chem* **2011**, *7*, 668–677. https://doi.org/10.3762/bjoc.7.79.
(16) Küçükgüzel, İ.; Tatar, E.; Küçükgüzel, Ş. G.; Rollas, S.; De Clercq, E. Synthesis of Some Novel Thiourea Derivatives Obtained from 5-[(4-Aminophenoxy)Methyl]-4-Alkyl/Aryl-2,4-Dihydro-3H-1,2,4-Triazole-3-Thiones and Evaluation as Antiviral/Anti-HIV and Anti-Tuberculosis Agents. *European Journal of Medicinal Chemistry* **2008**, *43* (2), 381–392. https://doi.org/10.1016/j.ejmech.2007.04.010.
(17) Li, Y.-H.; Zhang, B.; Yang, H.-K.; Li, Q.; Diao, P.-C.; You, W.-W.; Zhao, P.-L. Design, Synthesis, and Biological Evaluation of Novel Alkylsulfanyl-1,2,4-Triazoles as Cis-Restricted Combretastatin A-4 Analogues. *Eur J Med Chem* **2017**, *125*, 1098–1106. https://doi.org/10.1016/j.ejmech.2016.10.051.
(18) Aswathanarayanappa, C.; Bheemappa, E.; Bodke, Y. D.; Krishnegowda, P. S.; Venkata, S. P.; Ningegowda, R. Synthesis and Evaluation of Antioxidant Properties of Novel 1,2,4-Triazole-Based Schiff Base Heterocycles. *Arch Pharm (Weinheim)* **2013**, *346* (12), 922–930. https://doi.org/10.1002/ardp.201300202.
(19) Nandikolla, A.; Srinivasarao, S.; Kumar, B. K.; Murugesan, S.; Aggarwal, H.; Major, L. L.; Smith, T. K.; Sekhar, K. V. G. C. Synthesis, Study of Antileishmanial and Antitrypanosomal Activity of Imidazo Pyridine Fused Triazole Analogues. *RSC Adv.* **2020**, *10* (63), 38328–38343. https://doi.org/10.1039/D0RA07881F.
(20) Siddiqui, N.; Ahsan, W. Triazole Incorporated Thiazoles as a New Class of Anticonvulsants: Design, Synthesis and in Vivo Screening. *European Journal of Medicinal Chemistry* **2010**, *45* (4), 1536–1543. https://doi.org/10.1016/j.ejmech.2009.12.062.
(21) Upmanyu, N.; Gupta, J. K.; Shah, K.; Mishra, P. Anti-Inflammatory and Antinociceptive Evaluation of Newly Synthesized 4-(Substituted Ethanoyl) Amino-3-Mercapto-5-(4-Methoxy) Phenyl-1,2,4-Triazoles. *J Pharm Bioallied Sci* **2011**, *3* (2), 259–265. https://doi.org/10.4103/0975-7406.80783.
(22) Khan, I.; Tantray, M. A.; Hamid, H.; Alam, M. S.; Kalam, A.; Hussain, F.; Dhulap, A. Synthesis of Pyrimidin-4-One-1,2,3-Triazole Conjugates as Glycogen Synthase Kinase-3β Inhibitors with Anti-Depressant Activity. *Bioorganic Chemistry* **2016**, *68*, 41–55. https://doi.org/10.1016/j.bioorg.2016.07.007.
(23) Reed, C. W.; Yohn, S. E.; Washecheck, J. P.; Roenfanz, H. F.; Quitalig, M. C.; Luscombe, V. B.; Jenkins, M. T.; Rodriguez, A. L.; Engers, D. W.; Blobaum, A. L.; Conn, P. J.; Niswender, C. M.; Lindsley, C. W. Discovery of an Orally Bioavailable and Central Nervous System (CNS) Penetrant mGlu7 Negative Allosteric Modulator (NAM) in Vivo Tool Compound: N-(2-(1H-1,2,4-Triazol-1-Yl)-5-(Trifluoromethoxy)Phenyl)-4-(Cyclopropylmethoxy)-3-Methoxybenzamide (VU6012962). *J. Med. Chem.* **2019**, *62* (3), 1690–1695. https://doi.org/10.1021/acs.jmedchem.8b01810.

(24) Benderitter, P.; de Araújo Júnior, J. X.; Schmitt, M.; Bourguignon, J.-J. 2-Amino-6-Iodo-4-Tosyloxypyrimidine: A Versatile Key Intermediate for Regioselective Functionalization of 2-Aminopyrimidines in 4- and 6-Positions. *Tetrahedron* **2007**, *63* (50), 12465–12470. https://doi.org/10.1016/j.tet.2007.07.100.
(25) Hickey, S. M.; Ashton, T. D.; Khosa, S. K.; Pfeffer, F. M. An Optimised Synthesis of 2-[2,3-Bis(Tert-Butoxycarbonyl)Guanidino]Ethylamine. *Synlett* **2012**, *23* (12), 1779–1782. https://doi.org/10.1055/s-0031-1290698.
(26) Baki, A.; Bielik, A.; Molnár, L.; Szendrei, G.; Keserü, G. M. A High Throughput Luminescent Assay for Glycogen Synthase Kinase-3beta Inhibitors. *Assay Drug Dev Technol* **2007**, *5* (1), 75–83. https://doi.org/10.1089/adt.2006.029.
(27) Burslem, G. M.; Crews, C. M. Proteolysis-Targeting Chimeras as Therapeutics and Tools for Biological Discovery. *Cell* **2020**, *181* (1), 102–114. https://doi.org/10.1016/j.cell.2019.11.031.
(28) Burslem, G. M.; Smith, B. E.; Lai, A. C.; Jaime-Figueroa, S.; McQuaid, D. C.; Bondeson, D. P.; Toure, M.; Dong, H.; Qian, Y.; Wang, J.; Crew, A. P.; Hines, J.; Crews, C. M. The Advantages of Targeted Protein Degradation Over Inhibition: An RTK Case Study. *Cell Chem Biol* **2018**, *25* (1), 67-77.e3. https://doi.org/10.1016/j.chembiol.2017.09.009.
(29) Churcher, I. Protac-Induced Protein Degradation in Drug Discovery: Breaking the Rules or Just Making New Ones? *J. Med. Chem.* **2018**, *61* (2), 444–452. https://doi.org/10.1021/acs.jmedchem.7b01272.
(30) Békés, M.; Langley, D. R.; Crews, C. M. PROTAC Targeted Protein Degraders: The Past Is Prologue. *Nat Rev Drug Discov* **2022**, *21* (3), 181–200. https://doi.org/10.1038/s41573-021-00371-6.
(31) Qu, L.; Li, S.; Ji, L.; Luo, S.; Ding, M.; Yin, F.; Wang, C.; Luo, H.; Lu, D.; Liu, X.; Peng, W.; Kong, L.; Wang, X. Discovery of PT-65 as a Highly Potent and Selective Proteolysis-Targeting Chimera Degrader of GSK3 for Treating Alzheimer's Disease. *Eur J Med Chem* **2021**, *226*, 113889. https://doi.org/10.1016/j.ejmech.2021.113889.
(32) Guardigni, M.; Pruccoli, L.; Santini, A.; Simone, A. D.; Bersani, M.; Spyrakis, F.; Frabetti, F.; Uliassi, E.; Andrisano, V.; Pagliarani, B.; Fernández-Gómez, P.; Palomo, V.; Bolognesi, M. L.; Tarozzi, A.; Milelli, A. PROTAC-Induced Glycogen Synthase Kinase 3β Degradation as a Potential Therapeutic Strategy for Alzheimer's Disease. *ACS Chem. Neurosci.* **2023**, *14* (11), 1963–1970. https://doi.org/10.1021/acschemneuro.3c00096.
(33) Chanda, A.; Fokin, V. V. Organic Synthesis "On Water." *Chem. Rev.* **2009**, *109* (2), 725–748. https://doi.org/10.1021/cr800448q.
(34) Lipshutz, B.; Ghorai, S. Transition-Metal-Catalyzed Cross-Couplings Going Green: In Water at Room Temperature. *Aldrichimica Acta* **2008**, *41*.
(35) Rosenmund, K. W.; Struck, E. Das am Ringkohlenstoff gebundene Halogen und sein Ersatz durch andere Substituenten. I. Mitteilung: Ersatz des Halogens durch die Carboxylgruppe. *Ber. dtsch. Chem. Ges. A/B* **1919**, *52* (8), 1749–1756. https://doi.org/10.1002/cber.19190520840.
(36) Ren, Y.; Dong, C.; Zhao, S.; Sun, Y.; Wang, J.; Ma, J.; Hou, C. Copper-Catalyzed Cyanation of Benzyl Chlorides with Non-Toxic K4[Fe(CN)6]. *Tetrahedron Letters* **2012**, *53* (23), 2825–2827. https://doi.org/10.1016/j.tetlet.2012.03.109.
(37) Ren, Y.; Wang, W.; Zhao, S.; Tian, X.; Wang, J.; Yin, W.; Cheng, L. Microwave-Enhanced and Ligand-Free Copper-Catalyzed Cyanation of Aryl Halides with K4[Fe(CN)6] in Water. *Tetrahedron Letters* **2009**, *50* (32), 4595–4597. https://doi.org/10.1016/j.tetlet.2009.05.073.

(38) Mehmood, A.; Devine, W. G.; Leadbeater, N. E. Development of Methodologies for Copper-Catalyzed C–O Bond Formation and Direct Cyanation of Aryl Iodides. *Top Catal* **2010**, *53* (15), 1073–1080. https://doi.org/10.1007/s11244-010-9535-3.
(39) DeBlase, C.; Leadbeater, N. E. Ligand-Free CuI-Catalyzed Cyanation of Aryl Halides Using K4[Fe(CN)6] as Cyanide Source and Water as Solvent. *Tetrahedron* **2010**, *66* (5), 1098–1101. https://doi.org/10.1016/j.tet.2009.11.016.
(40) Bollenbach, M.; Wagner, P.; Aquino, P. G. V.; Bourguignon, J.-J.; Bihel, F.; Salomé, C.; Schmitt, M. D-Glucose: An Efficient Reducing Agent for a Copper(II)-Mediated Arylation of Primary Amines in Water. *ChemSusChem* **2016**, *9* (22), 3244–3249. https://doi.org/10.1002/cssc.201600801.
(41) Bollenbach, M.; Aquino, P. G. V.; de Araújo-Júnior, J. X.; Bourguignon, J.-J.; Bihel, F.; Salomé, C.; Wagner, P.; Schmitt, M. Efficient and Mild Ullmann-Type N-Arylation of Amides, Carbamates, and Azoles in Water. *Chemistry – A European Journal* **2017**, *23* (55), 13676–13683. https://doi.org/10.1002/chem.201700832.